Benicia - Martinez Bridge

for

California Department of Transportation

I-680 in Solano and Contra Costa Counties

Bridge No. 28 - 0153R
Contract No. 59S742
Project No. 1130/137499

Materials Handout

Prepared by

T·Y·LIN INTERNATIONAL / CH2M HILL
A JOINT VENTURE

825 Battery Street
San Francisco, CA 94111

Date: Mar 31, 1998

8. Materials Handout

- Evaluation of Pile Drivability

FUGRO - McCLELLAND MARINE GEOSCIENCES, INC.

6100 Hillcroft (77081)
P.O. Box 740010
Houston, TX 77274
Phone : 713-778-5500
Fax : 713-778-5573

CH2M HILL
Sacramento
OCT 28 1999
RECEIVED

Report No. 0201-3933
October 22, 1999

Earth Mechanics
17660 Newhope Street, Suite E
Fountain Valley, California 92708

Attention: Dr. Hubert Law

Evaluation of Pile Drivability
Benicia-Martinez Bridge
Suison Bay, California

This report presents the results of our drivability study for 2500-mm-diameter permanent steel casings to be driven at the above location. The study was authorized by your letter dated September 9, 1999. Preliminary results were submitted on September 17 and September 24, 1999.

Principal Findings

Our evaluation of pile drivability indicates that the 2500-mm-ID casing should be driven 10 m into the rock with a Delmag D-100 hammer if the lower bound resistance is applicable, but an IHC S-500 hammer would be required if the upper bound resistance is applicable. The required penetration could also be obtained for the upper bound resistance with a Delmag D-100 hammer and center relief drilling. The maximum driving stresses are acceptable for all hammers, as the permanent casing has a minimum yield strength of 50 ksi (345 MPa).

General Soil Conditions

Our evaluation of pile drivability is based on a soil boring drilled by others. Boring 97-1 was drilled at 5.0 m Rt. Sta. 39+10. Soil conditions are tabulated below to the depth of interest.

Stratum	Depth, m From	Depth, m To	Description
I	0	9	Very loose clayey silt
II	9	14	Very loose silt and fine sandy silt with clay
III	14	16	Very loose fine sand with silt
IV	16	17.5	Medium dense fine sand with silt
V	17.5	20	Very loose fine sand with silt
VI	20	21	Very soft to firm clay with silt
VII	21	22.5	Very soft decomposed siltstone
VIII	22.5	23	Moderately soft to soft, moderately weathered sandstone
IX	23	25	Hard to moderately hard, moderately to slightly weathered sandstone
X	25	27	Moderately soft, moderately weathered claystone, siltstone, and sandstone
XI	27	32	Moderately hard, slightly weathered sandstone and siltstone

A Roman numeral representing each stratum is shown in the above tabulation, as well as on the resistance to driving and predicted blow count plates. Soils are naturally formed materials, and their properties are likely to be variable, controlled by nonuniform geologic depositional processes and post-depositional events. Layered strata, in particular, may change in thickness, density, and soil type within relatively short horizontal and vertical distances. Because soil borings provide information at discrete intervals, some soil property variations may not be detected. Subsequent recommendations contained in this report were developed assuming that soil conditions as revealed by the borings are continuous throughout the general area. Consideration of possible stratigraphic changes, faulting, or other differences in soil conditions that could influence pile drivability is beyond the scope of this investigation.

Evaluation of Pile Drivability

Soil Resistance to Driving. Curves of soil resistance to driving were computed for coring conditions using procedures recommended by Stevens, Wiltsie, and Turton (1982), and are presented on Plate 1 for a 2500-mm-diameter permanent steel casing without a driving shoe. When a pile cores, relative movement between pile and soil occurs both on the outside and inside of the pile wall. The end bearing area is only the cross-sectional area of steel at the driving shoe. When a pile plugs, the soil plug moves with the pile during driving. Shaft resistance is mobilized only on the outer wall. The end bearing area is the gross area of the pile.

The soil resistance to driving in rock is based on the RQD (Rock Quality Designation), the percent recovery, and the compressive strength of the rock. The RQD is defined as the percent ratio of the cumulative length of core samples 4 in. long or longer to the length of the core run. The percent recovery is defined as the percent ratio of the length of sample recovered to the length of core run. Very poor to poor quality rock is considered to have an RQD of less than 50 percent. Rock having a compressive strength of less than 5 MPa is considered to be weak.

Driving piles into rock is anticipated to severely fracture the rock layers and reduce the rock to a granular material. Therefore, unit skin friction for piles driven in rock layers is computed assuming sand parameters. Silty sand parameters are assigned to rock layers that are interbedded with silt or clay seams and layers.

For poor to fair quality rock, unit end bearing is limited to values given for granular soils. For more competent rock, unit end bearing is computed using the following equation:

$$q = u N_u$$

where: u = compressive strength of rock, and

N_u = dimensionless bearing capacity factor.

A value of 3 is used for N_u. Rock end bearing acts only on the area of steel at the pile tip. Unit end bearing for the soil plug is computed assuming sand parameters, or silty sand parameters for rock layers interbedded with silt or clay.

Qualitatively, refusal in rock layers is likely when the RQD is greater than 50 percent, the percent recovery is greater than 85 percent, and the unconfined compressive strength of the rock is greater than 5 MPa.

Wave Equation Analyses. Wave equation analyses were performed using the hammer, pile, and soil parameters given on Plate 2. The GRLWEAP computer program developed by Goble and Rausche (1986) was used to model the Delmag D-100 diesel hammer and the IHC S-200 and S-500 hydraulic hammers. GRLWEAP differs from other diesel hammer simulations in two respects: (1) a thermodynamic analysis determines the gas pressure in the combustion chamber during compression, combustion delay,

ignition, and expansion, rather than assuming a constant pressure; and (2) the hammer stroke is calculated rather than using a prescribed value. For hydraulic hammers, the ram impacts directly on the pile cap. A cushion is not used. A follower is required because the largest pile diameter driven with the IHC S-200 and D-100 hammers is 48 inches (1219 mm).

The GRLWEAP computer program was also used to model the Vulcan 560 and Menck 3000 hammers. For air/steam hammers, the rated hammer energy, hammer efficiency, ram weight, pile cap weight, and cushion properties are required. Driving system performance parameters were determined from our data base. A follower is required because the largest pile diameter driven with the Vulcan 560 and Menck 3000 hammers is 72 inches (1829 mm).

The soil quake and damping parameters recommended by Roussel (1979) were used in our wave equation analyses. These parameters were determined form a comprehensive correlation study performed for large-diameter offshore piles in which the driving records of 58 piles at 15 offshore sites in the Gulf of Mexico were analyzed. The side and point quake are assumed equal, with a magnitude of 0.10 in. (2.5 mm) for stiff to hard clay, silt, and sand. Side damping in clay decreases with increasing shear strength, which is in agreement with the laboratory test results of Coyle and Gibson (1970) and Heerema (1979). For silt and sand, side damping is 0.07 and 0.08 sec/ft (0.23 and 0.26 sec/m), respectively. Point damping of 0.15 sec/ft (0.49 sec/m) is recommended for firm to hard clay, silt, and sand. The quake and damping parameters recommended for silt are also recommended for rock.

Results of Wave Equation Analyses

Our experience with driving large-diameter piles has shown that blow counts predicted for the coring case will generally give the best estimate of the field blow counts. Predicted blow counts are presented on Plates 3 through 5 for the Delmag D-100 diesel hammer.

Results are presented for the 2500-mm-ID casing without a driving shoe on Plate 3. For the lower bound resistances, blow counts are expected to be less than 100 blows per 0.25 m to 27-m penetration, but greater than 200 blows per 0.25 m in the underlying moderately hard sandstone and siltstone.

The use of a driving shoe can prevent damage to the pile toe during hard driving. The inside clearance provided by the driving shoe also acts to reduce skin friction on the inside of the pile, and may delay plugging by reducing lateral stresses developed in the soil plug. Wave equation analyses were also performed for the 2500-mm-ID casing with a driving shoe having the same outside diameter, a wall thickness of 54 mm, and a length of 1.5 m. The results presented on Plate 4 indicate that the reduction in internal friction is offset by the increase in end bearing, and the predicted blow counts are similar.

Drivability can be improved by center relief drilling. Results are presented on Plate 5 assuming drilling extends 1 m ahead of the pile toe. Because both the internal friction and the end bearing are reduced, the driving is much easier. Blow counts are expected to be less than about 80 blows per 0.25 m for the lower bound resistance, and less than 300 blows per 0.25 m for the upper bound resistance.

Wave equation analyses were also performed for several hammers to compare the maximum resistance overcome by each hammer at 200 blows per 0.25 m, and the maximum driving stresses. Results are tabulated below:

Hammer	Driving Resistance, MN	Maximum Driving Stress, MPa
Delmag D-100-13	20.21	112
IHC S-200	29.89	142
Vulcan 560	33.81	164
Menck MRBS 3000	34.88	158
IHC S-500	54.32	257

These results indicate that a Delmag D-100 hammer should drive the 2500-mm-ID casing 10 m into the rock if the lower bound resistance is applicable, but an IHC S-500 hammer would be required if the upper bound resistance is applicable. The required penetration could also be obtained for the upper bound resistance with a Delmag D-100 hammer and center relief drilling. The maximum driving stresses are acceptable for all hammers, as the special provisions for this project call for AASHTO M270, Grade 345 plate for the permanent casing, which has a minimum yield strength of 50 ksi (345 MPa).

Warranty

The results presented in this report are based on soil conditions revealed by a single boring obtained by others at the boring location only. Lateral variation in subsurface conditions across the site could result in variable blow counts. Deviations between the observed and predicted blow counts may indicate soil conditions, which are different from those assumed for this study, and may require further investigation.

Fugro-McClelland warrants that its services with respect to this study were performed with a degree of care and skill equal to that ordinarily exercised under similar conditions by reputable members of our profession practicing in the same or similar locality. No other warranty, express or implied, is made or intended.

The following illustrations are attached and complete this report:

Plate 1	Estimated Soil Resistance to Driving
Plate 2	Summary of Wave Equation Parameters
Plates 3 thru 5	Predicted Blow Counts

We are pleased to be of assistance on this project. Please contact us if you have any questions or need additional information.

Sincerely,

FUGRO-McCLELLAND
MARINE GEOSCIENCES, INC.

Robert F. Stevens

Robert F. Stevens, Ph.D., P.E.
Senior Consultant

RFS/dka(3933lrpt)
Copies Submitted: (3)

REFERENCES

Coyle, H.M. and Gibson, G.C. (1970), "Empirical Damping Constants for Sands and Clays," Journal, Soil Mechanics and Foundations Division, ASCE, Vol. 96, No. SM3, pp. 949-965.

Goble, G.G. and Rausche, F. (1986), Wave Equation Analysis of Pile Foundations, WEAP 86 Program, U.S. Department of Transportation, Federal Highway Administration.

Heerema, E.P. (1979), "Relationships Between Wall Friction, Displacement Velocity and Horizontal Stress in Clays and in Sand, for Pile Drivability Analysis," Ground Engineering, Vol. 12, No. 1, pp. 55-61, 65.

Roussel, H.J. (1979), Pile Driving Analysis of Large Diameter High Capacity Offshore Pipe Piles, Ph.D. Thesis, Department of Civil Engineering, Tulane University, New Orleans.

Stevens, R.F., Wiltsie, E.A., and Turton, T.H. (1982), "Evaluating Pile Drivability for Hard Clay, Very Dense Sand, and Rock," Proceedings, 14th Offshore Technology Conference, Houston, Vol. 1, pp. 465-481.

Date: 10/19/

Drawn By: RFS

Date: 10/20/99
Date: 10/21/99

Checked By: DR
Approved By:

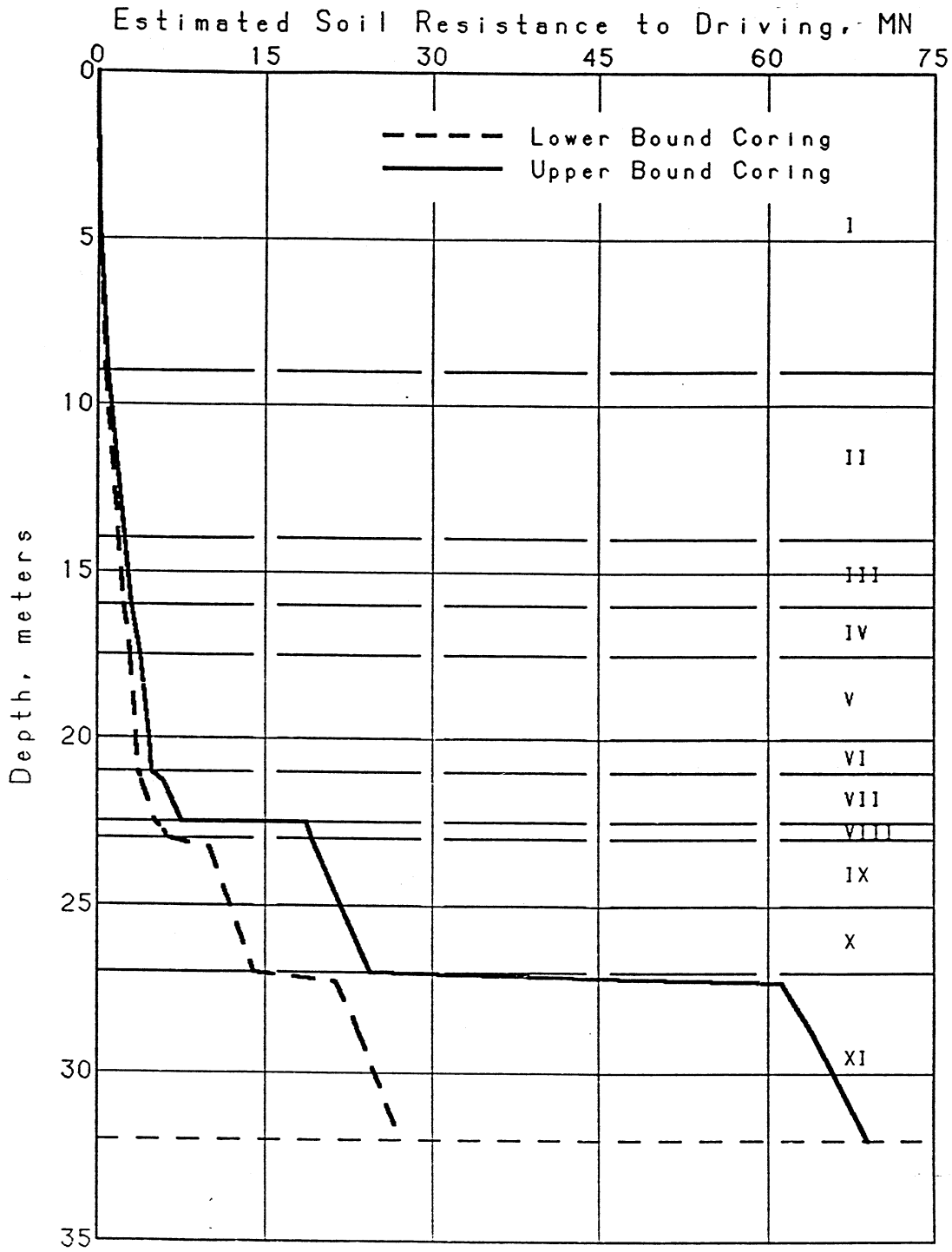

ESTIMATED SOIL RESISTANCE TO DRIVING
2500-mm-ID Permanent Steel Casing
Benicia-Martinez Bridge

Date: 10/19/

Drawn By: RF

Date: 10/20/95

Date: 10/21/96

Checked By: DIC

Approved By:

HAMMER PROPERTIES

	IHC-S-200	IHC-S-500	Vulcan 560	Menck 3000
Rated Energy, ft-lb	147,180	368,300	312,500	325,480
Hammer Efficiency, %	95	95	67	67
Weight of Ram, lb	22,000	55,300	62,500	66,100
Weight of Pile Cap, lb	7,700	12,300	45,900	34,800
Cushion Stiffness, lb/in.	--	--	9.0×10^7	5.5×10^7
Coefficient of Restitution				
Cushion	0.98	0.98	0.70	0.70
Pile Cap on Follower	0.95	0.95	0.95	0.95

PILE PROPERTIES

Inside Diameter, mm	2500
Length, m	36
Wall Thickness, mm	41
Unit Weight, pcf	492
Modulus, psi	29.6×10^6

SOIL PROPERTIES

Quake, in.	
Side	0.10
Tip	0.10
Damping, sec/ft	
Side	0.07
Tip	0.15
Tip Resistance	1 to 95

SUMMARY OF WAVE EQUATION PARAMETERS

Benicia-Martinez Bridge

Date: 10/19/

Drawn By: RF

Date: 10/20/99
Date: 10/21/99

Checked By: DR
Approved By: [illegible]

HAMMER PROPERTIES

	Delmag D-100-13
Rated Energy, ft-kips	158 to 246
Blow Rate, blows per minute	34 to 45
Weight of Ram, lb	22,030
Ram Springs, lb/in.	3.83×10^8
Weight of Impact Block, lb	5,000
Ram-Impact Block Spring, lb	1.78×10^8
Stiffness of Cushion, lb/in.	1.64×10^8
Weight of Pile Cap, lb	4,220
Coefficient of Restitution,	
Ram on Impact Block	0.90
Cushion (Aluminum-Micarta)	0.80
Pile Cap on Pile	0.95
Maximum Stroke, ft	11.16
Maximum Combustion Pressure, psi	1,275
Minimum Combustion Pressure, psi	929
Combustion Chamber Volume, $in.^3$	1080
Combustion Delay, sec	.0005
Duration of Fuel Ignition, sec	.002
Area of Cylinder, $in.^2$	483.0
Exponent for Expansion Process	1.25
Compressive Stroke	28.35

SUMMARY OF WAVE EQUATION PARAMETERS
Benicia-Martinez Bridge

Date: 10/19/

Drawn By: RF

Date: 10/20/95

Date: 10/21/95

Checked By: DA

Approved By:

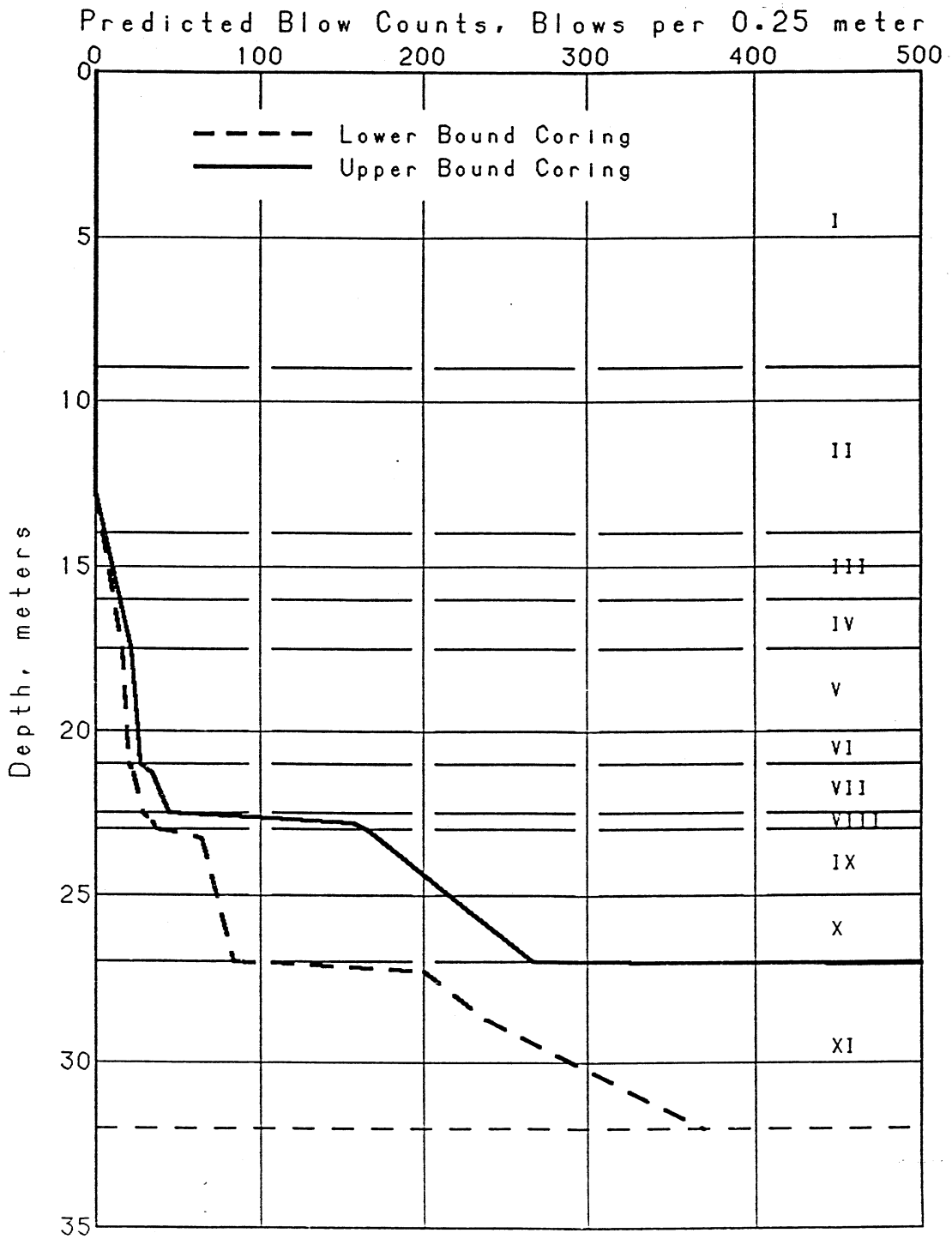

PREDICTED BLOW COUNTS
2500-mm-ID Permanent Steel Casing
Delmag D-100-13 Diesel Hammer
Benicia-Martinez Bridge

Date: 10/19/

Drawn By: RF

Date: 10/20/95
Date: 10/21/95

Checked By: DVL
Approved By:

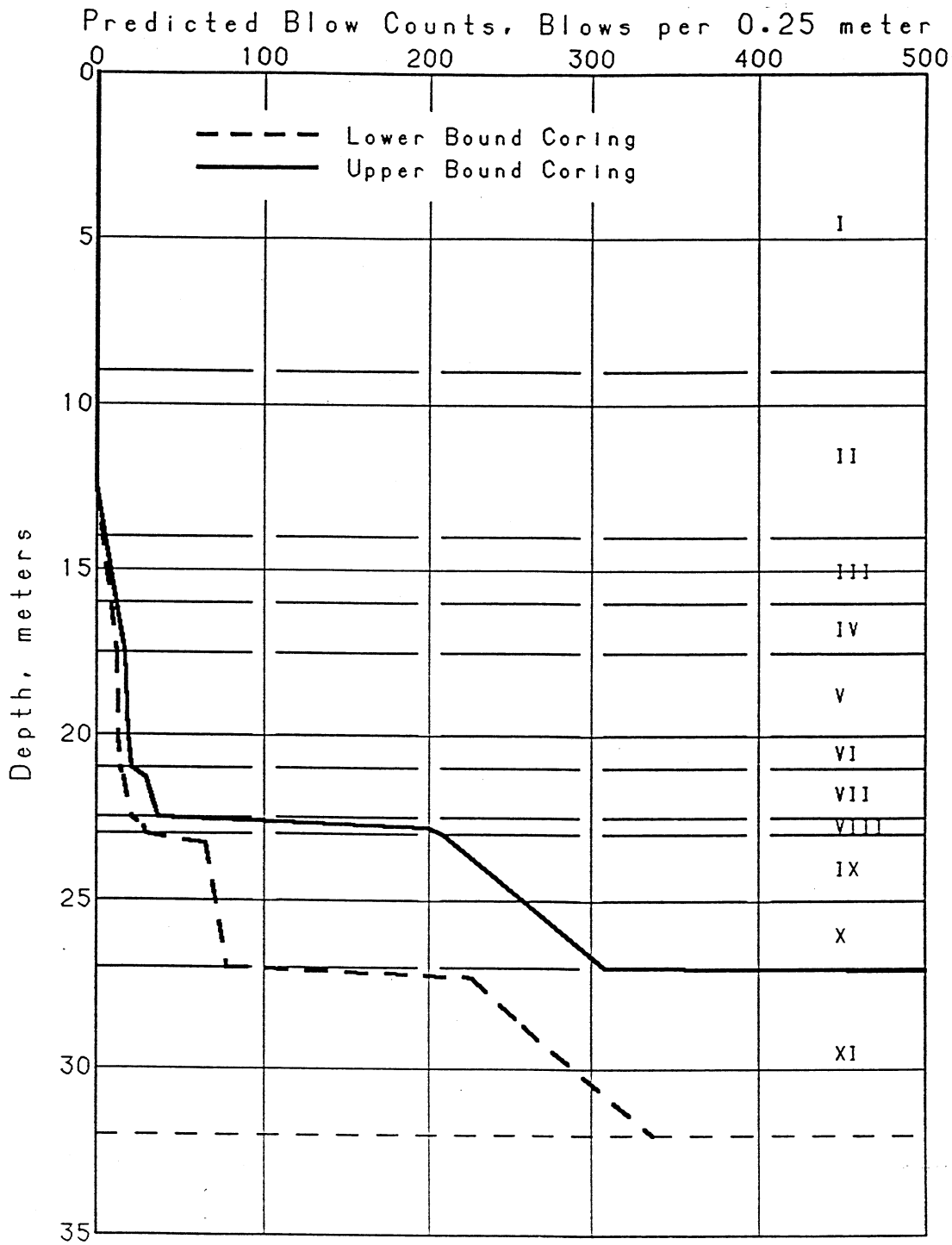

PREDICTED BLOW COUNTS
2500-mm-ID Permanent Steel Casing with Driving Shoe
Delmag D-100-13 Diesel Hammer
Benicia-Martinez Bridge

Date: 10/19

Drawn By: RF

Date: 10/20/99
Date: 10/21/99

Checked By: DN
Approved By: [illegible]

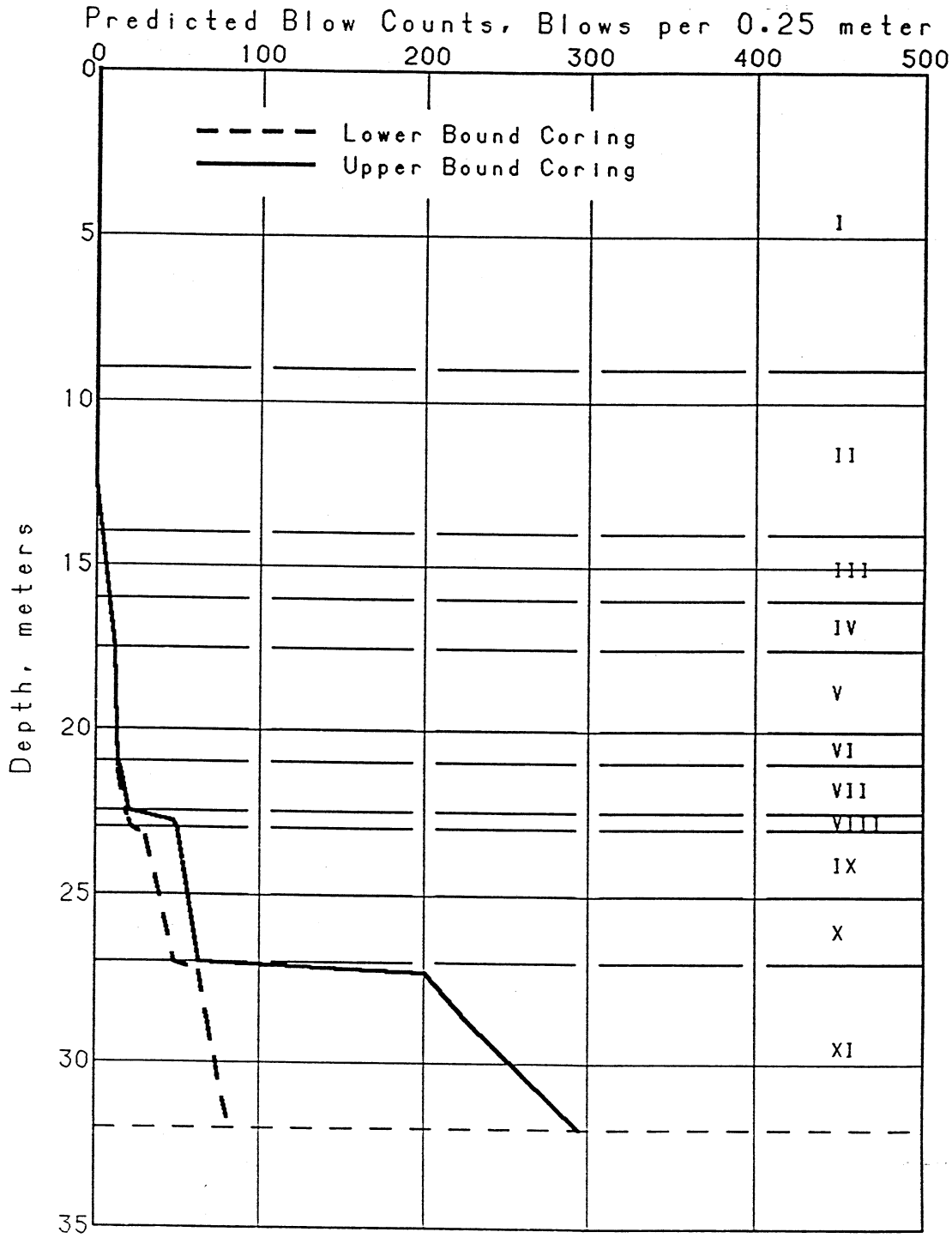

PREDICTED BLOW COUNTS
2500-mm-ID Permanent Steel Casing
Delmag D-100-13 Diesel Hammer
Center Relief Drilling
Benicia-Martinez Bridge

Creep & Shrinkage
Test Report

- Creep and Shrinkage Test Reports

CTL **Structural/Architectural Engineering, Testing and Materials Technology**

5420 Old Orchard Road, Skokie, Illinois 60077-1030
847/965-7500 **800/522-2CTL** Fax: 847/965-6541

October 21, 1999

Mr. Steve Thoman
CH2M Hill
2485 Natomas Drive, Suite 600
Sacramento, CA 95833

Re: *Lightweight Concrete Creep and Shrinkage Tests for the Benicia-Martinez Bridge*

Dear Mr. Thoman:

As authorized by a CH2M Hill/T.Y. Lin International Subconsultants Services Agreement, CTL has performed compressive strength, modulus of elasticity, and creep tests on concrete samples submitted and identified others. We understand the samples were fabricated from three sanded-lightweight concrete mixes, each containing a different lightweight coarse aggregate. Target 28-day compressive strength was 6500 psi.

Modulus of elasticity was determined in accordance with ASTM C 469-94, "Standard Test Method for Static Modulus of Elasticity and Poisson's Ratio of Concrete in Compression. Compressive strength was determined in accordance with ASTM C 39-96, "Standard Test Method for Compressive Strength of Cylindrical Concrete Specimens." Creep tests were performed in accordance with ASTM C 512-87 (Reapproved 1997), "Standard Test Method for Creep of Concrete in Compression." All tests were conducted on specimens fabricated, submitted, and identified by others. Creep was determined for each concrete mix at three ages of loading: 3, 28 and 91 days. Creep specimens were maintained under load for at least 91 days.

Test results are summarized in the attached tables and graphs. The "Realite" concrete mix loaded at 7 days was not required by the agreement, however, by the time this was discovered the test was well underway. Results are presented for your information. Interestingly, the results for this concrete loaded at 7 days fit well with the other data for this concrete. In some cases, creep and shrinkage tests were continued past the required 91 days of loading because other tests were still in progress.

Creep data are presented both as specific creep (creep strain/applied creep load) and creep coefficient (creep deformation as a ratio to initial elastic deformation) for your convenience. The performance of the three mixes, with respect to creep and shrinkage, can be compared by evaluating test data for a similar age of loading after a specific time under load. The creep

CTL

and shrinkage test data can also be used to refine creep models used to predict field deformations.

If you have any questions on this matter, please call me.

Sincerely,
CONSTRUCTION TECHNOLOGY LABORATORIES, INC.

Ronald G. Burg

Ronald G. Burg, P.E.
Principal Engineer

RGB/tp

109061

Compressive Strength and Modulus of Elasticity Test Results
"Realite" Aggregate Concrete

Test	Age	Specimen No. 1	2	3	Average
Compressive Strength, psi	4	6370	6280	6360	6340
Modulus of Elasticity, ksi	4	—	3360	3300	3330
Compressive Strength, psi	7	6590	7800	6920	7100
Modulus of Elasticity, ksi	7	—	3680	—	3680
Compressive Strength, psi	28	8670	8720	8530	8640
Modulus of Elasticity, ksi	28	—	3080	3100	3090
Compressive Strength, psi	91	9500	10,180	9010	9560
Modulus of Elasticity, ksi	91	—	3410	3740	3580

Notes:

1. All specimens provided and identified by others.
2. Specimens tested at an age of three days were cured in molds prior to test.
3. Specimes tested at 7 days cured in molds for 3 days, moist cured until test.
4. Specimens tested at an age of 28 and 91 days were cured in molds for three days, moist cured until an age of 14 days and then air cured until test.

ASTM C 512 Creep and Shrinkage of Realite
(Load Applied and Drying Started at an Age of 4 Days)

Days Loaded	Drying shrinkage (millionths)	Load induced deformation* (millionths)	Specific creep (μstrain/psi)	Creep coefficient	Condition
0	0	951	0	0.00	Instantaneous strain
1	36	1307	0.14	0.37	Additional strain due to creep
2	73	1482	0.21	0.56	" "
3	100	1552	0.24	0.63	" "
4	108	1627	0.27	0.71	" "
5	126	1725	0.31	0.81	" "
6	130	1739	0.32	0.83	" "
7	133	1778	0.33	0.87	" "
14	162	1910	0.38	1.01	" "
21	165	1950	0.40	1.05	" "
28	204	2015	0.43	1.12	" "
59	231	2127	0.47	1.24	" "
91	237	2153	0.48	1.26	" "
121	300	2248	0.52	1.36	" "
151	343	2318	0.55	1.44	" "
183	376	2362	0.56	1.48	" "
214	413	2400	0.58	1.52	" "
245	419	2412	0.58	1.54	" "

Notes:

*Adjusted for drying shrinkage

Test specimens are 6x12-in. cylinders and were indentified and provided by others.

Applied stress during creep test:	2500 psi
Compressive strength at time of loading:	6340 psi (ASTM C 39)
Modulus of elasticity at time of loading:	3330 ksi (ASTM 469)
Age at loading:	4 days
Preload environment:	in molds
Loaded environment:	50% ±4 relative humidity

ASTM C 512 Creep and Shrinkage of Realite
(Load Applied and Drying Started at an Age of 4 Days)

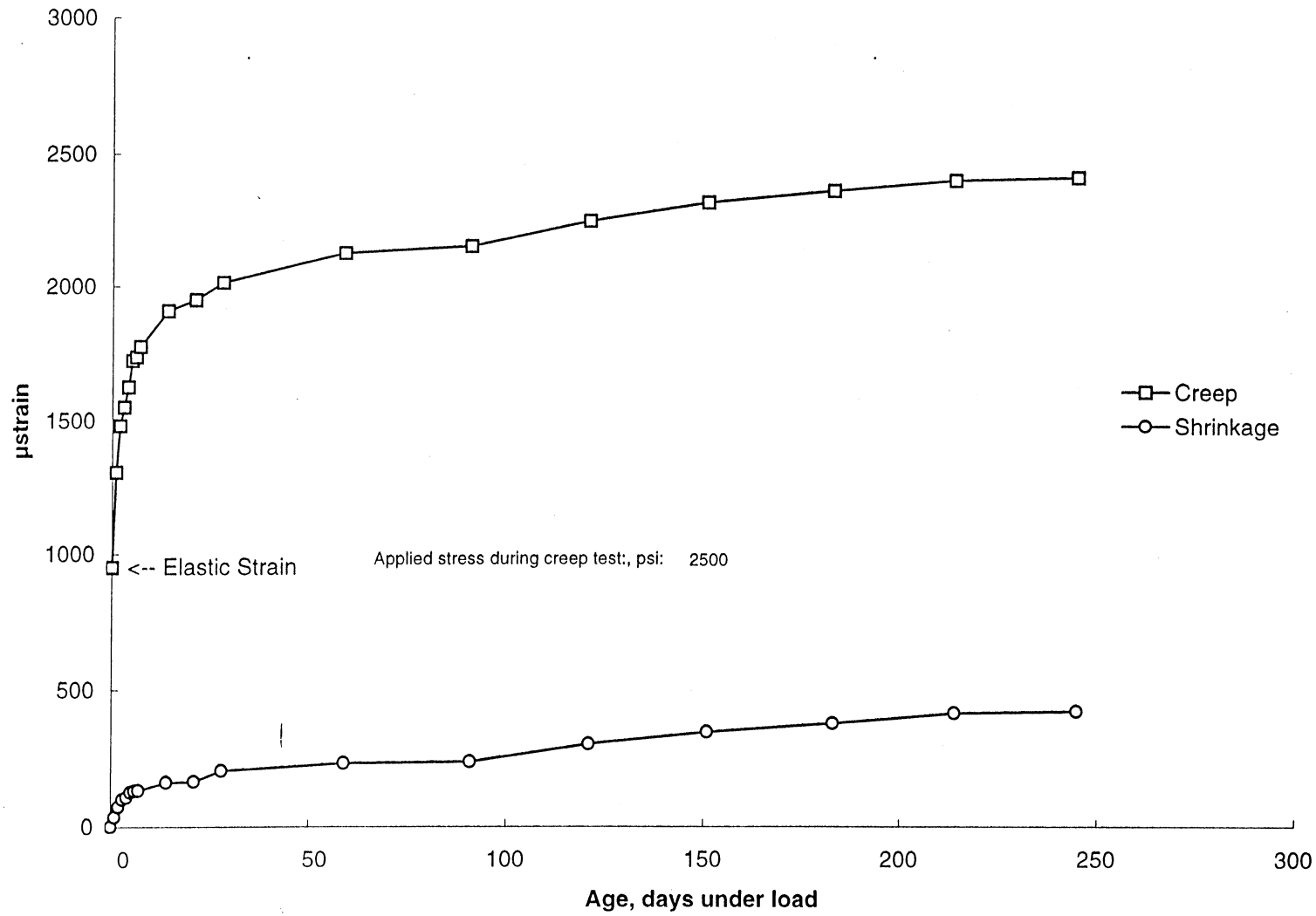

ASTM C 512 Creep and Shrinkage of Realite
(Load Applied and Drying Started at an Age of 7 Days)

Days Loaded	Drying shrinkage (millionths)	Load induced deformation* (millionths)	Specific creep (μstrain/psi)	Creep coefficient	Condition
0	0	863	0	0.00	Instantaneous strain
1	3	1107	0.10	0.28	Additional strain due to creep
2	45	1222	0.14	0.42	" "
3	46	1263	0.16	0.46	" "
4	53	1302	0.18	0.51	" "
5	45	1328	0.19	0.54	" "
6	47	1365	0.20	0.58	" "
7	54	1400	0.22	0.62	" "
14	69	1516	0.26	0.76	" "
21	68	1531	0.27	0.77	" "
28	68	1603	0.30	0.86	" "
60	98	1740	0.35	1.02	" "
90	121	1783	0.37	1.07	" "
120	147	1863	0.40	1.16	" "
152	197	1965	0.44	1.28	" "
183	242	2016	0.46	1.34	" "
214	254	2026	0.47	1.35	" "
245	292	2085	0.49	1.42	" "

Notes:

*Adjusted for drying shrinkage

Test specimens are 6x12-in. cylinders and were provided and indentified by others.

Applied stress during creep test:	2500 psi
Compressive strength at time of loading:	7100 psi (ASTM C 39)
Modulus of elasticity at time of loading:	3680 ksi (ASTM 469)
Age at loading:	7 days
Preload environment:	3 days in mold, 4 days moist
Loaded environment:	50% ±4 relative humidity

ASTM C 512 Creep and Shrinkage of Realite
(Load Applied and Drying Started at an Age of 7 Days)

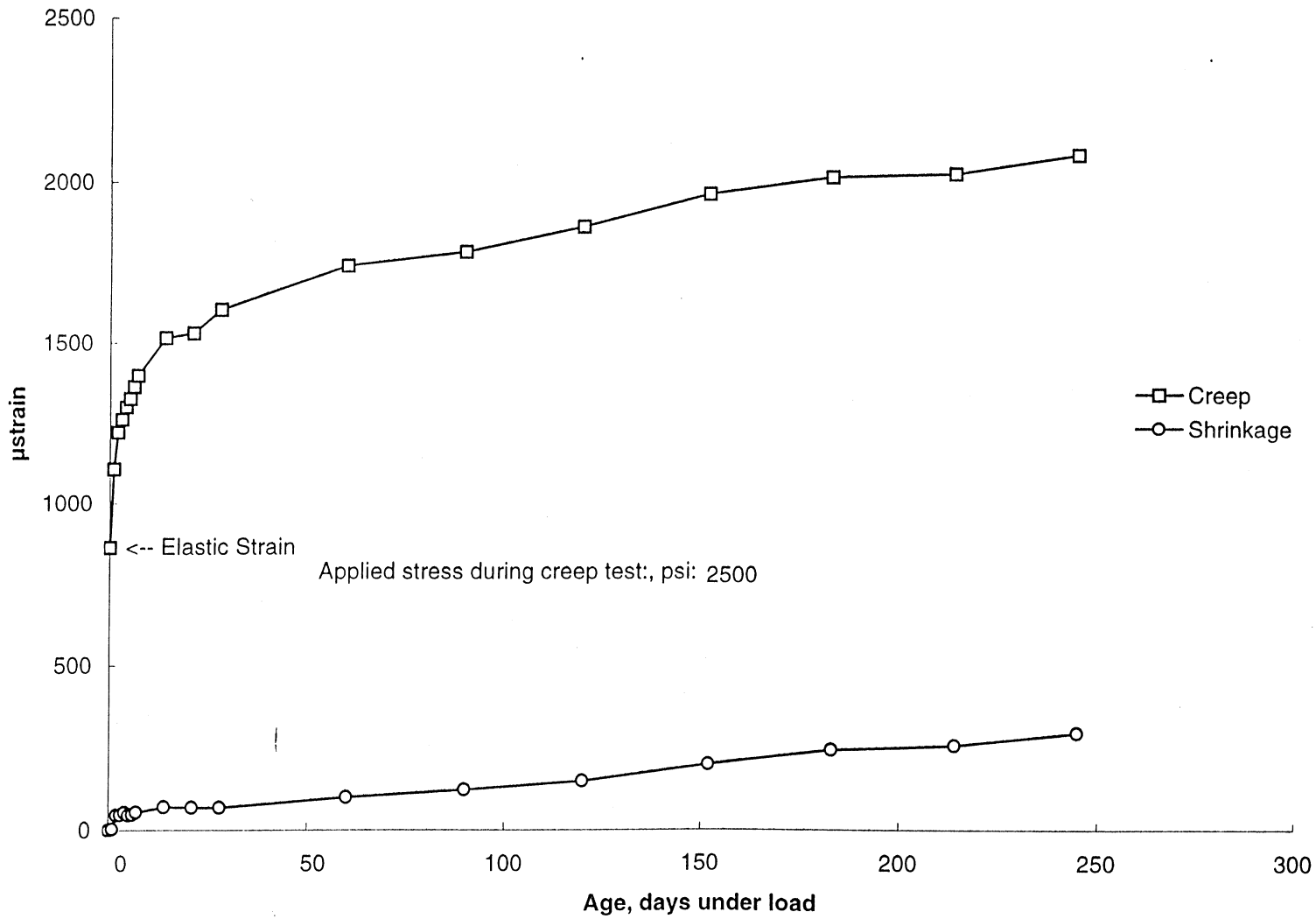

ASTM C 512 Creep and Shrinkage of Realite Concrete
(Drying Started at an Age 14 days, Load Applied at an Age of 28 Days)

Days Loaded	Drying shrinkage (millionths)	Load induced deformation* (millionths)	Specific creep (μstrain/psi)	Creep coefficient	Condition
0	0	748	0	0.00	Instantaneous strain
1	- 11	885	0.05	0.18	Additional strain due to creep
2	0	903	0.06	0.21	" "
3	- 8	924	0.07	0.23	" "
4	- 23	924	0.07	0.23	" "
5	- 15	943	0.08	0.26	" "
6	- 13	953	0.08	0.27	" "
7	- 54	970	0.09	0.30	" "
14	- 60	1061	0.13	0.42	" "
21	- 47	1053	0.12	0.41	" "
28	- 59	1088	0.14	0.45	" "
59	- 38	1197	0.18	0.60	" "
90	- 37	1243	0.20	0.66	" "

Notes:

*Adjusted for drying shrinkage

Test specimens are 6x12-in. cylinders and were provided and indentified by others.

Applied stress during creep test:	2500 psi
Compressive strength at time of loading:	8640 psi (ASTM C 39)
Modulus of elasticity at time of loading:	3090 ksi (ASTM 469)
Age at loading:	28 days
Preload environment:	14 days moist, 14 days in air
Loaded environment:	50% ±4 relative humidity

ASTM C 512 Creep and Shrinkage of Realite Concrete
(Drying Started at an Age 14 days, Load Applied at an Age of 28 Days)

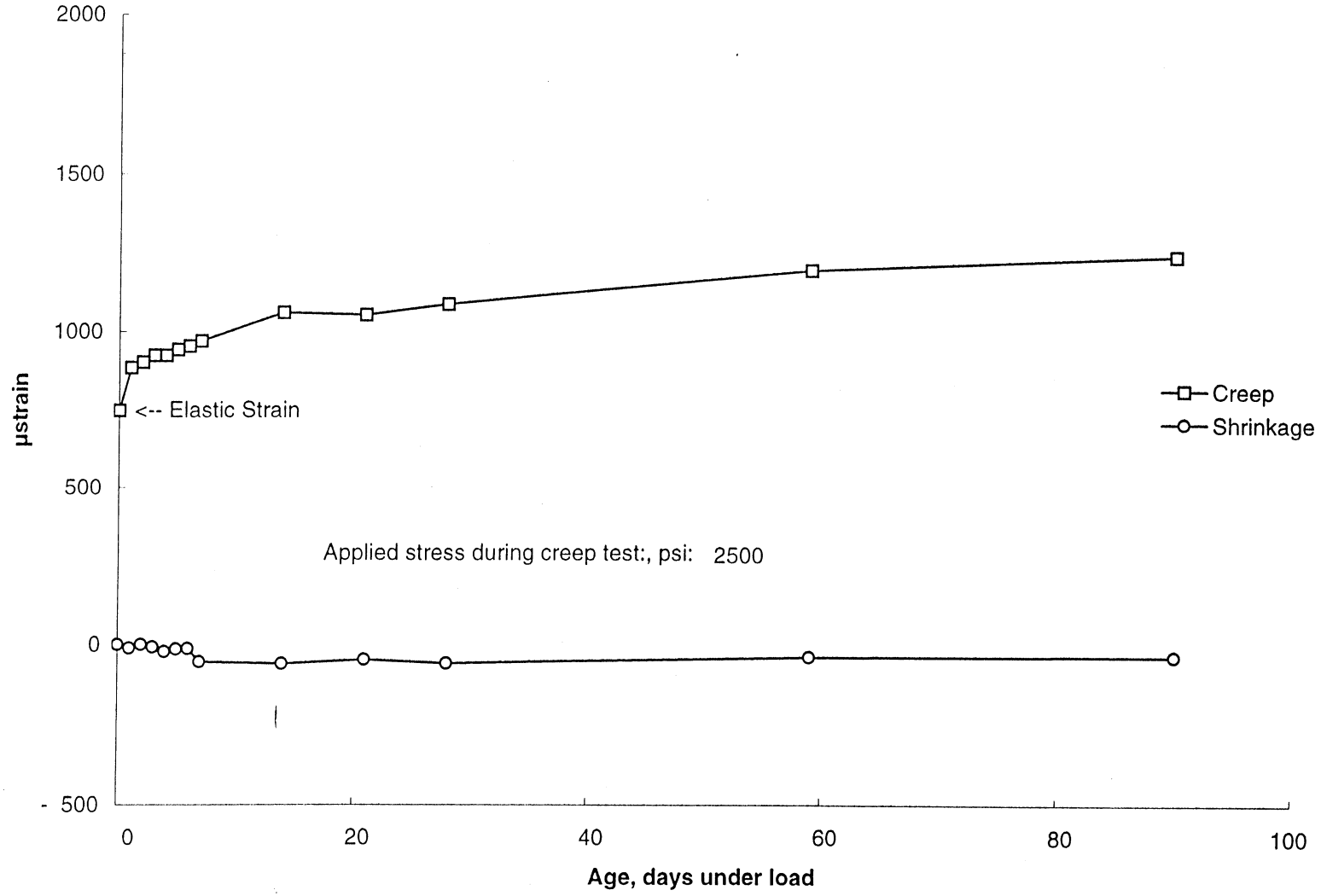

ASTM C 512 Creep and Shrinkage of Realite Concrete
(Drying Started at an Age 14 days, Load Applied at an Age of 91 Days)

Days Loaded	Drying shrinkage (millionths)	Load induced deformation* (millionths)	Specific creep (μstrain/psi)	Creep coefficient	Condition
0	0	789	0	0.00	Instantaneous strain
1	- 8	842	0.02	0.07	Additional strain due to creep
2	- 3	884	0.04	0.12	" "
3	5	931	0.06	0.18	" "
4	4	945	0.06	0.20	" "
5	4	946	0.06	0.20	" "
6	4	948	0.06	0.20	" "
7	8	966	0.07	0.22	" "
14	15	994	0.08	0.26	" "
21	15	1028	0.10	0.30	" "
28	17	1067	0.11	0.35	" "
58	66	1159	0.15	0.47	" "
90	122	1275	0.19	0.62	" "
121	144	1324	0.21	0.68	" "
152	176	1374	0.23	0.74	" "

Notes:

*Adjusted for drying shrinkage

Test specimens are 6x12-in. cylinders and were provided and indentified by others.

Applied stress during creep test:	2500 psi
Compressive strength at time of loading:	9570 psi (ASTM C 39)
Modulus of elasticity at time of loading:	3680 ksi (ASTM 469)
Age at loading:	91 days
Preload environment:	14 days moist, 77 days in air
Loaded environment:	50% ±4 relative humidity

ASTM C 512 Creep and Shrinkage of Realite Concrete
(Drying Started at an Age 14 days, Load Applied at an Age of 91 Days)

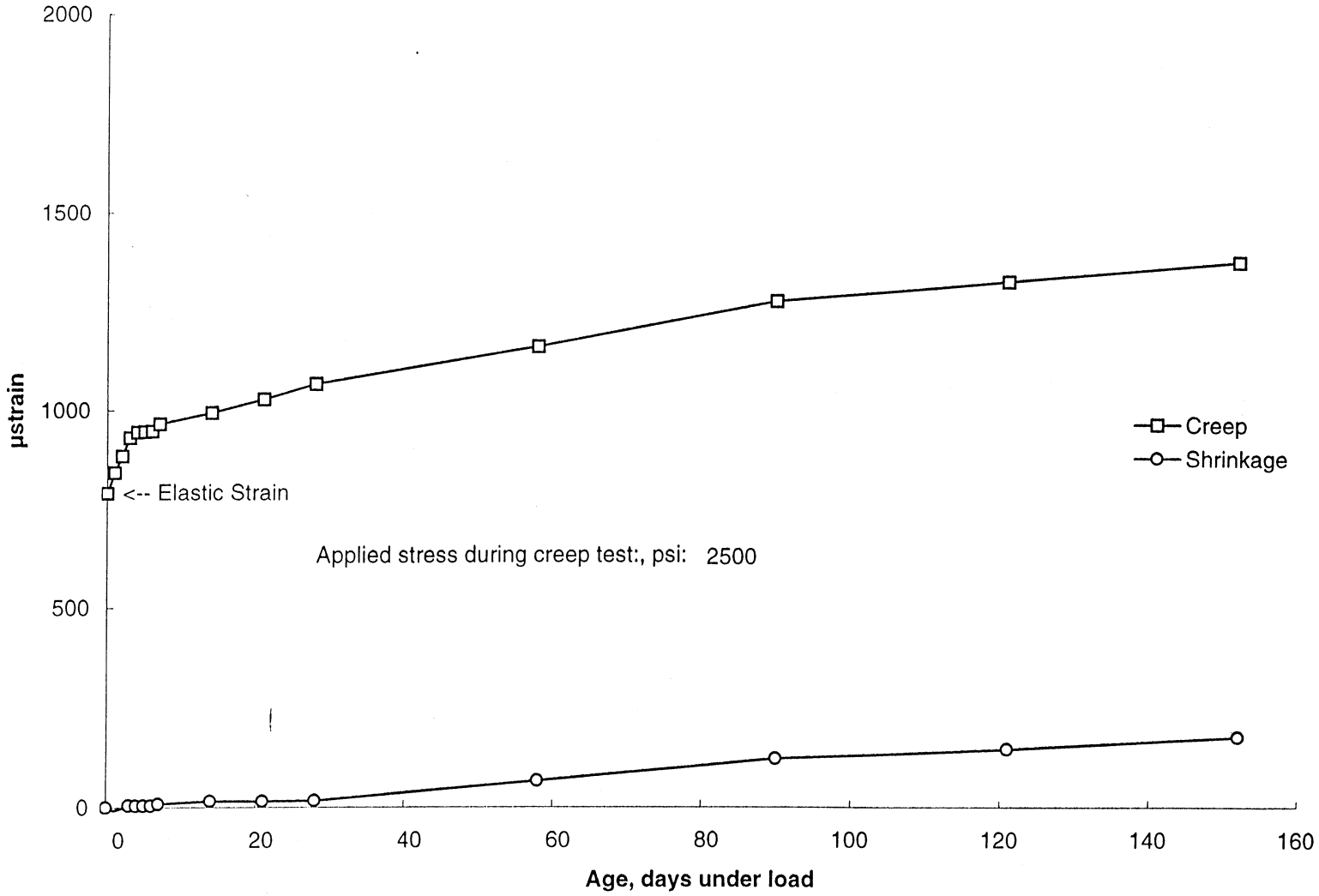

Compressive Strength and Modulus of Elasticity Test Results
"Utelite" Aggregate Concrete

Test	Age	Specimen No. 1	Specimen No. 2	Specimen No. 3	Average
Compressive Strength, psi	3	4450	5060	4820	4780
Modulus of Elasticity, ksi	3	—	2640	2520	2580
Compressive Strength, psi	28	7310	7360	6650	7110
Modulus of Elasticity, ksi	28	—	3190	2870	3030
Compressive Strength, psi	91	8970	7950	7940	8290
Modulus of Elasticity, ksi	91	—	3210	2950	3080

Notes:

1. All specimens provided and identified by others.
2. Specimens tested at an age of three days were cured in molds prior to test.
3. Specimens tested at an age of 28 and 91 days were cured in molds for three days, moist cured until an age of 14 days and then air cured until test.

ASTM C 512 Creep and Shrinkage of Utelite Concrete
(Load Applied and Drying Started at an Age of 3 Days)

Days Loaded	Drying shrinkage (millionths)	Load induced deformation* (millionths)	Specific creep (μstrain/psi)	Creep coefficient	Condition
0	0	863	0	0.00	Instantaneous strain
1	0	1124	0.12	0.30	Additional strain due to creep
2	25	1223	0.16	0.42	" "
3	28	1305	0.20	0.51	" "
4	32	1382	0.23	0.60	" "
5	30	1422	0.25	0.65	" "
6	30	1442	0.26	0.67	" "
7	45	1491	0.28	0.73	" "
14	46	1592	0.33	0.84	" "
21	53	1624	0.34	0.88	" "
28	57	1685	0.37	0.95	" "
59	33	1741	0.40	1.02	" "
90	36	1784	0.41	1.07	" "
122	42	1835	0.44	1.13	" "
152	70	1915	0.47	1.22	" "
182	135	1974	0.50	1.29	" "
214	136	1983	0.50	1.30	" "

Notes:

*Adjusted for drying shrinkage

Test specimens are 6x12-in. cylinders and were provided and indentified by others.

Applied stress during creep test:	2220 psi
Compressive strength at time of loading	4780 psi (ASTM C 39)
Modulus of elasticity at time of loading:	2580 ksi (ASTM 469)
Age at loading:	3 days
Preload environment:	in molds
Loaded environment:	50% ±4 relative humidity

ASTM C 512 Creep and Shrinkage of Utelite Concrete
(Load Applied and Drying Started at an Age of 3 Days)

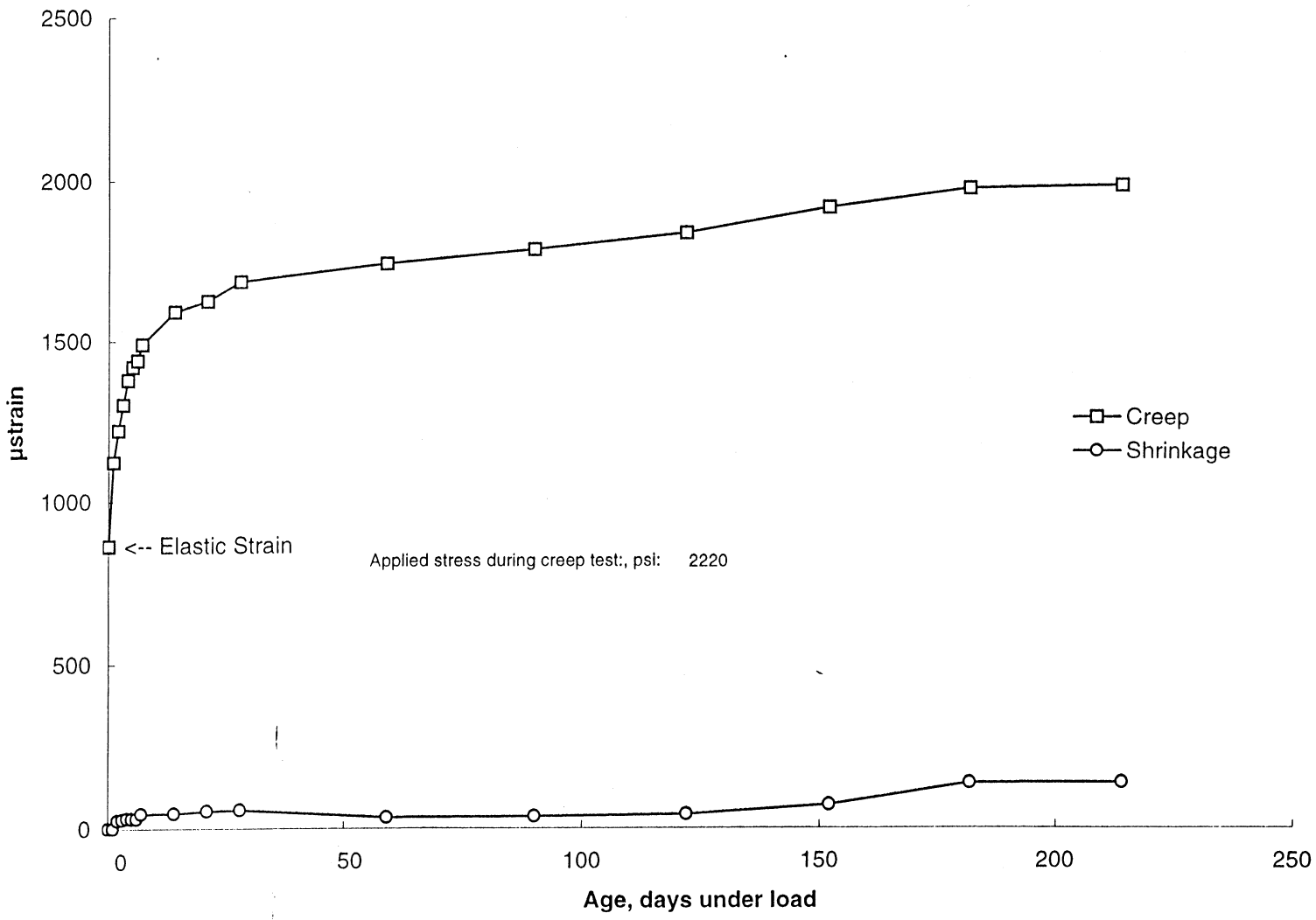

ASTM C 512 Creep and Shrinkage of Utelite
Drying Started at an Age of 14 Days, Load Applied at an Age of 28 Days

Days Loaded	Drying shrinkage (millionths)	Load induced deformation* (millionths)	Specific creep (μstrain/psi)	Creep coefficient	Condition
0	0	793	0	0.00	Instantaneous strain
1	25	913	0.05	0.15	Additional strain due to creep
2	11	916	0.05	0.16	" "
3	11	953	0.06	0.20	" "
4	12	968	0.07	0.22	" "
5	13	979	0.07	0.24	" "
6	15	999	0.08	0.26	" "
7	18	1000	0.08	0.26	" "
14	30	1087	0.12	0.37	" "
21	37	1144	0.14	0.44	" "
28	37	1140	0.14	0.44	" "
59	25	1196	0.16	0.51	" "
90	38	1261	0.19	0.59	" "
121	74	1337	0.22	0.69	" "
153	73	1373	0.23	0.73	" "
183	81	1409	0.25	0.78	" "

Notes:

*Adjusted for drying shrinkage

Test specimens are 6x12-in. cylinders and were provided and indentified by others.

Applied stress during creep test:	2500 psi
Compressive strength at time of loading	7110 psi (ASTM C 39)
Modulus of elasticity at time of loading:	3030 ksi (ASTM 469)
Age at loading:	28 days
Preload environment:	14 days moist, 14 days air dry
Loaded environment:	50% ±4 relative humidity

ASTM C 512 Creep and Shrinkage of Utelite

Drying Started at an Age of 14 Days, Load Applied at an Age of 28 Days

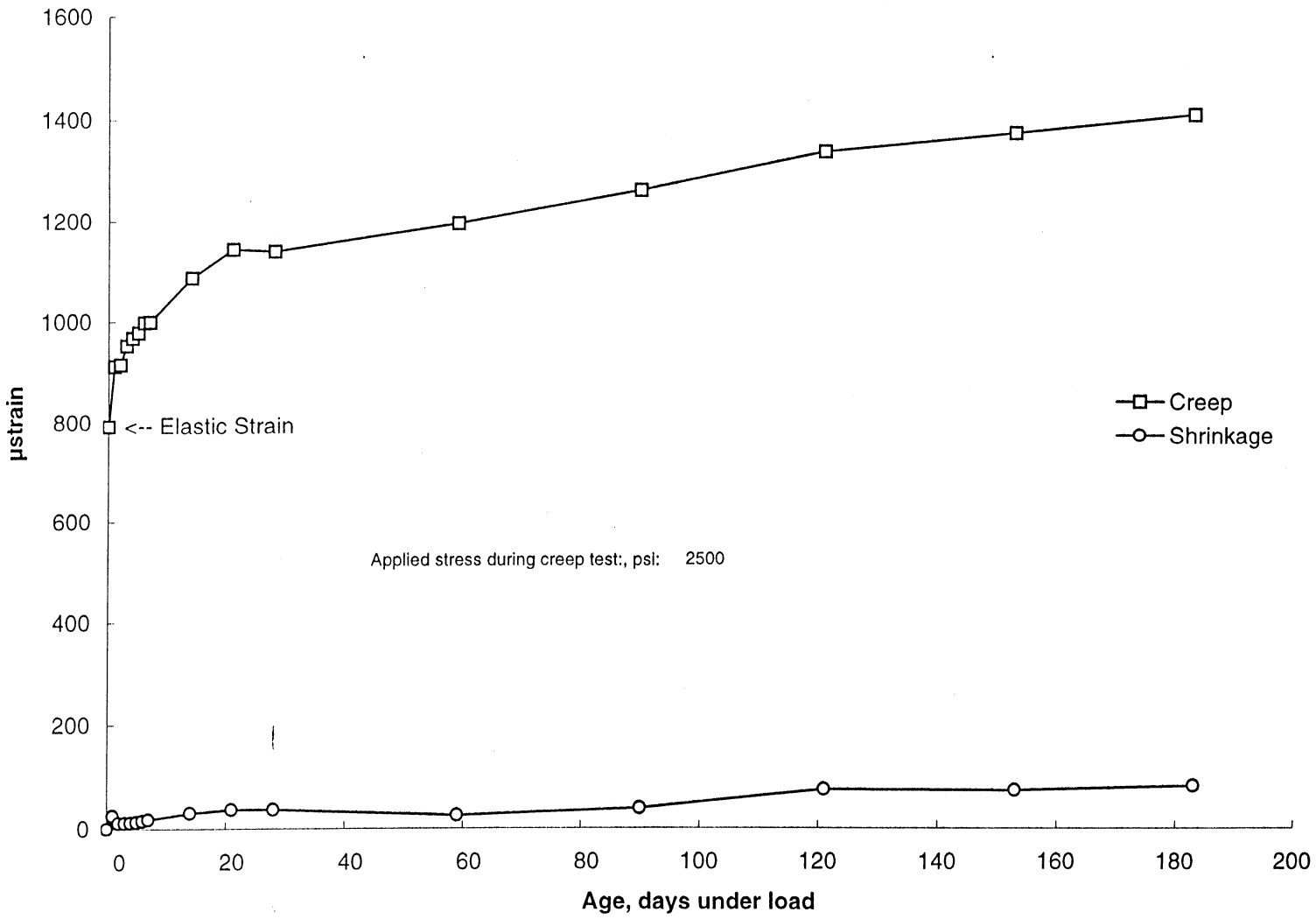

ASTM C 512 Creep and Shrinkage of Utelite Concrete
Drying Started at an Age of 14 Days, Load Applied at an Age of 91 Days

Days Loaded	Drying shrinkage (millionths)	Load induced deformation* (millionths)	Specific creep (µstrain/psi)	Creep coefficient	Condition
0	0	859	0	0.00	Instantaneous strain
1	14	916	0.02	0.07	Additional strain due to creep
2	16	928	0.03	0.08	" "
3	15	940	0.03	0.09	" "
4	18	970	0.04	0.13	" "
5	27	988	0.05	0.15	" "
6	28	998	0.06	0.16	" "
7	29	1006	0.06	0.17	" "
14	34	1034	0.07	0.20	" "
21	41	1055	0.08	0.23	" "
28	41	1086	0.09	0.26	" "
59	102	1174	0.13	0.37	" "
90	104	1234	0.15	0.44	" "
121	121	1268	0.16	0.48	" "

Notes:

*Adjusted for drying shrinkage

Test specimens are 6x12-in. cylinders and were provided and indentified by others.

Applied stress during creep test:	2500 psi
Compressive strength at time of loading	8280 psi (ASTM C 39)
Modulus of elasticity at time of loading:	3030 ksi (ASTM 469)
Age at loading:	91 days
Preload environment:	14 days moist, 77 days air dry.
Loaded environment:	50% ±4 relative humidity

ASTM C 512 Creep and Shrinkage of Utelite Concrete
Drying Started at an Age of 14 Days, Load Applied at an Age of 91 Days

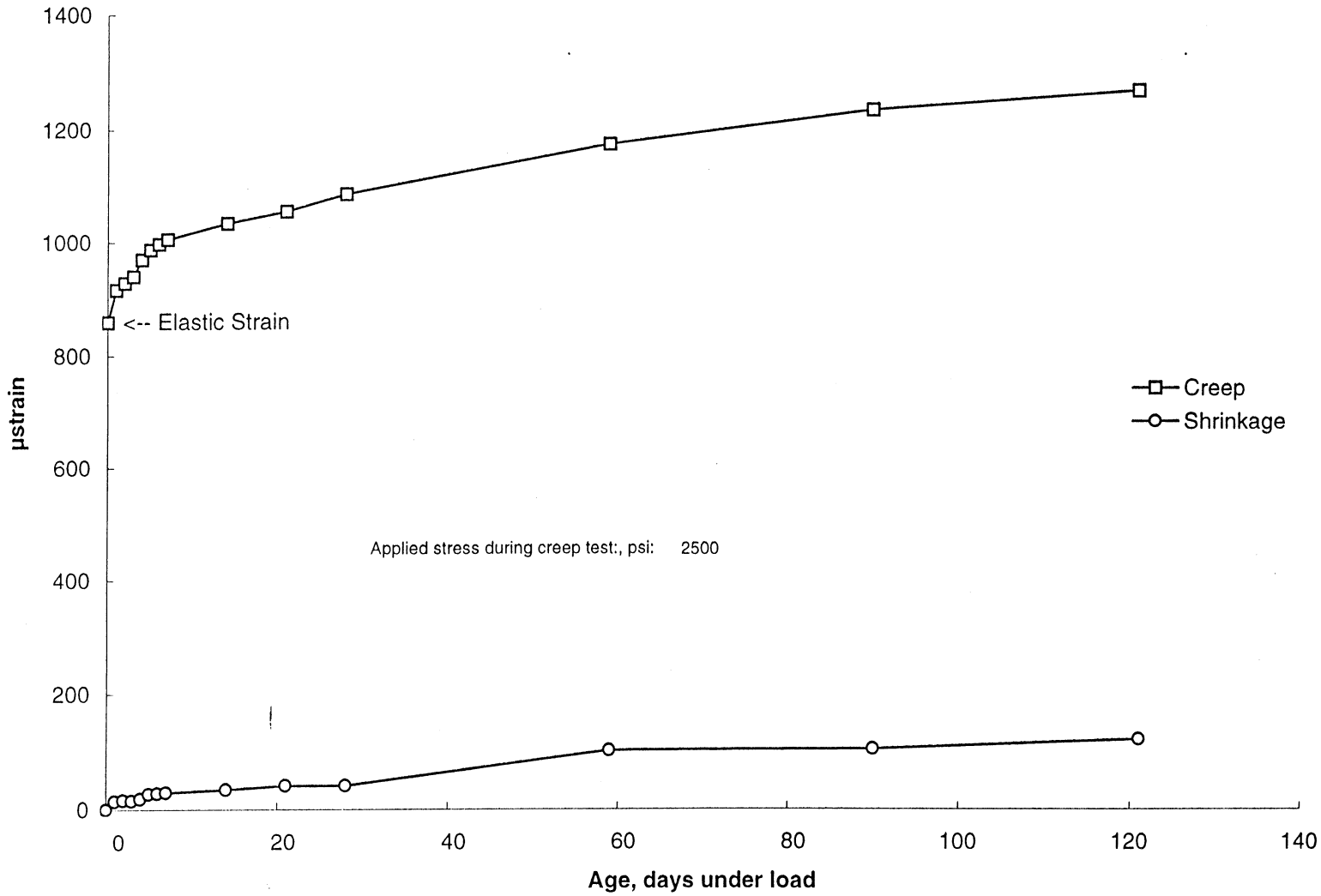

Compressive Strength and Modulus of Elasticity Test Results
"Stalite" Aggregate Concrete

Test	Age	Specimen No. 1	Specimen No. 2	Specimen No. 3	Average
Compressive Strength, psi	3	3980	4040	3970	4000
Modulus of Elasticity, ksi	3	—	3000	3000	3000
Compressive Strength, psi	28	8760	8320	8030	8370
Modulus of Elasticity, ksi	28	—	3940	3760	3850
Compressive Strength, psi	91	9550	9460	8380	9130
Modulus of Elasticity, ksi	91	—	3910	3900	3910

Notes:

1. All specimens provided and identified by others.
2. Specimens tested at an age of three days were cured in molds prior to test.
3. Specimens tested at an age of 28 and 91 days were cured in molds for three days, moist cured until an age of 14 days and then air cured until test.

ASTM C 512 Creep and Shrinkage of Statlite Concrete
(Load Applied and Drying Started at an Age of 3 Days)

Days Loaded	Drying shrinkage (millionths)	Load induced deformation* (millionths)	Specific creep (µstrain/psi)	Creep coefficient	Condition
0	0	619	0	0.00	Instantaneous strain
1	30	909	0.18	0.47	Additional strain due to creep
2	58	1011	0.24	0.63	" "
3	63	1082	0.29	0.75	" "
4	61	1108	0.31	0.79	" "
5	80	1181	0.35	0.91	" "
6	98	1229	0.38	0.99	" "
7	142	1286	0.42	1.08	" "
14	199	1402	0.49	1.26	" "
21	257	1454	0.52	1.35	" "
28	262	1481	0.54	1.39	" "
59	302	1566	0.59	1.53	" "
90	333	1600	0.61	1.58	" "

Notes:

*Adjusted for drying shrinkage

Test specimens are 6x12-in. cylinders and were provided and indentified by others.

Applied stress during creep test:	1600 psi
Compressive strength at time of loading	4000 psi (ASTM C 39)
Modulus of elasticity at time of loading:	3000 ksi (ASTM 469)
Age at loading:	3 days
Preload environment:	in molds
Loaded environment:	50% ±4 relative humidity

ASTM C 512 Creep and Shrinkage of Statlite Concrete
(Load Applied and Drying Started at an Age of 3 Days)

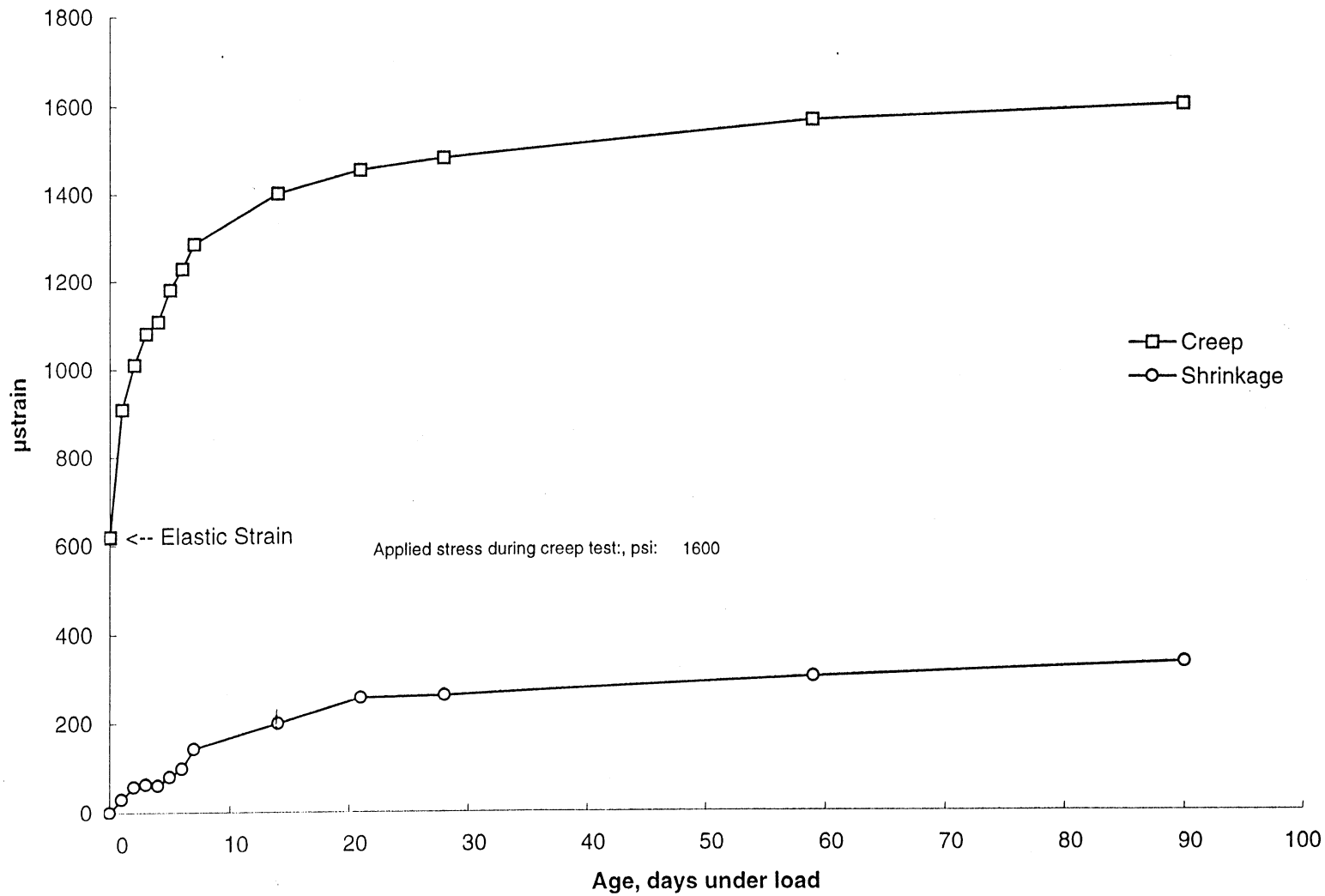

ASTM C 512 Creep and Shrinkage of Statlite Concrete
(Load Applied at 28 Days, Drying Started at an Age of 14 Days)

Days Loaded	Drying shrinkage (millionths)	Load induced deformation* (millionths)	Specific creep (μstrain/psi)	Creep coefficient	Condition
0	0	643	0	0.00	Instantaneous strain
1	0	787	0.06	0.22	Additional strain due to creep
2	4	829	0.07	0.29	" "
3	16	865	0.09	0.35	" "
4	23	887	0.10	0.38	" "
5	25	903	0.10	0.40	" "
6	28	918	0.11	0.43	" "
7	37	954	0.12	0.49	" "
14	75	1027	0.15	0.60	" "
21	97	1099	0.18	0.71	" "
28	105	1108	0.19	0.73	" "
59	173	1262	0.25	0.96	" "
90	174	1258	0.25	0.96	" "

Notes:

*Adjusted for drying shrinkage

Test specimens are 6x12-in. cylinders and were provided and indentified by others.

Applied stress during creep test:	2500 psi
Compressive strength at time of loading	8370 psi (ASTM C 39)
Modulus of elasticity at time of loading:	3850 ksi (ASTM 469)
Age at loading:	28 days
Preload environment:	14 days moist, 14 days air dry
Loaded environment:	50% ±4 relative humidity

ASTM C 512 Creep and Shrinkage of Statlite Concrete
(Load Applied at 28 Days, Drying Started at an Age of 14 Days)

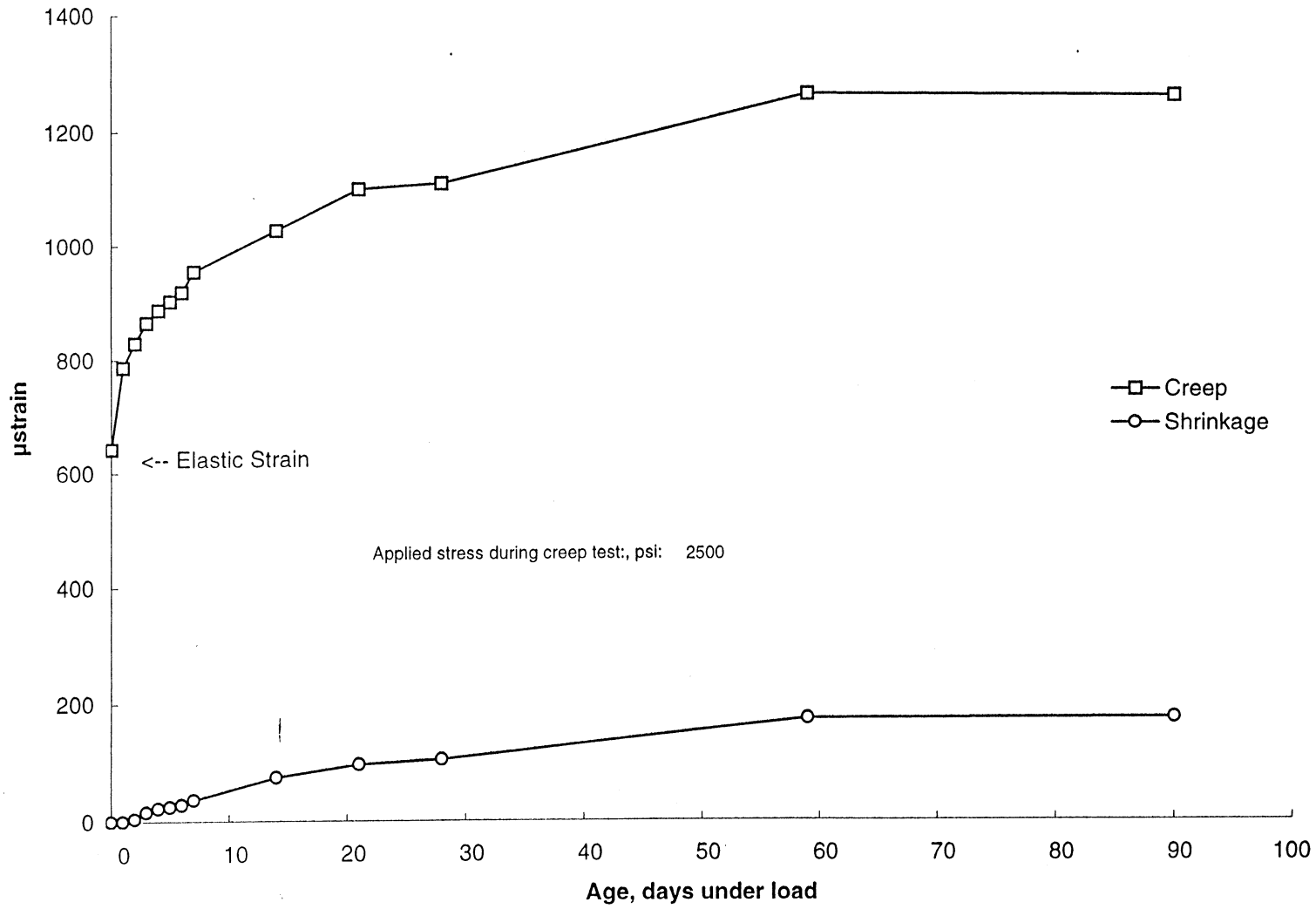

ASTM C 512 Creep and Shrinkage of Statlite Concrete
(Load Applied at 91 Days, Drying Started at an Age of 14 Days)

Days Loaded	Drying shrinkage (millionths)	Load induced deformation* (millionths)	Specific creep (μstrain/psi)	Creep coefficient	Condition
0	0	673	0	0.00	Instantaneous strain
1	38	753	0.03	0.12	Additional strain due to creep
2	35	783	0.04	0.16	" "
3	39	794	0.05	0.18	" "
4	33	809	0.05	0.20	" "
5	30	837	0.07	0.24	" "
6	34	843	0.07	0.25	" "
7	33	847	0.07	0.26	" "
14	35	886	0.09	0.32	" "
21	19	890	0.09	0.32	" "
28	28	911	0.10	0.35	" "
58	104	1065	0.16	0.58	" "
92	114	1117	0.18	0.66	" "

Notes:

*Adjusted for drying shrinkage

Test specimens are 6x12-in. cylinders and were provided and indentified by others.

Applied stress during creep test:	2500 psi
Compressive strength at time of loading	9130 psi (ASTM C 39)
Modulus of elasticity at time of loading:	3910 ksi (ASTM 469)
Age at loading:	91 days
Preload environment:	14 days moist, 77 days air dry
Loaded environment:	50% ±4 relative humidity

ASTM C 512 Creep and Shrinkage of Statlite Concrete
(Load Applied at 91 Days, Drying Started at an Age of 14 Days)

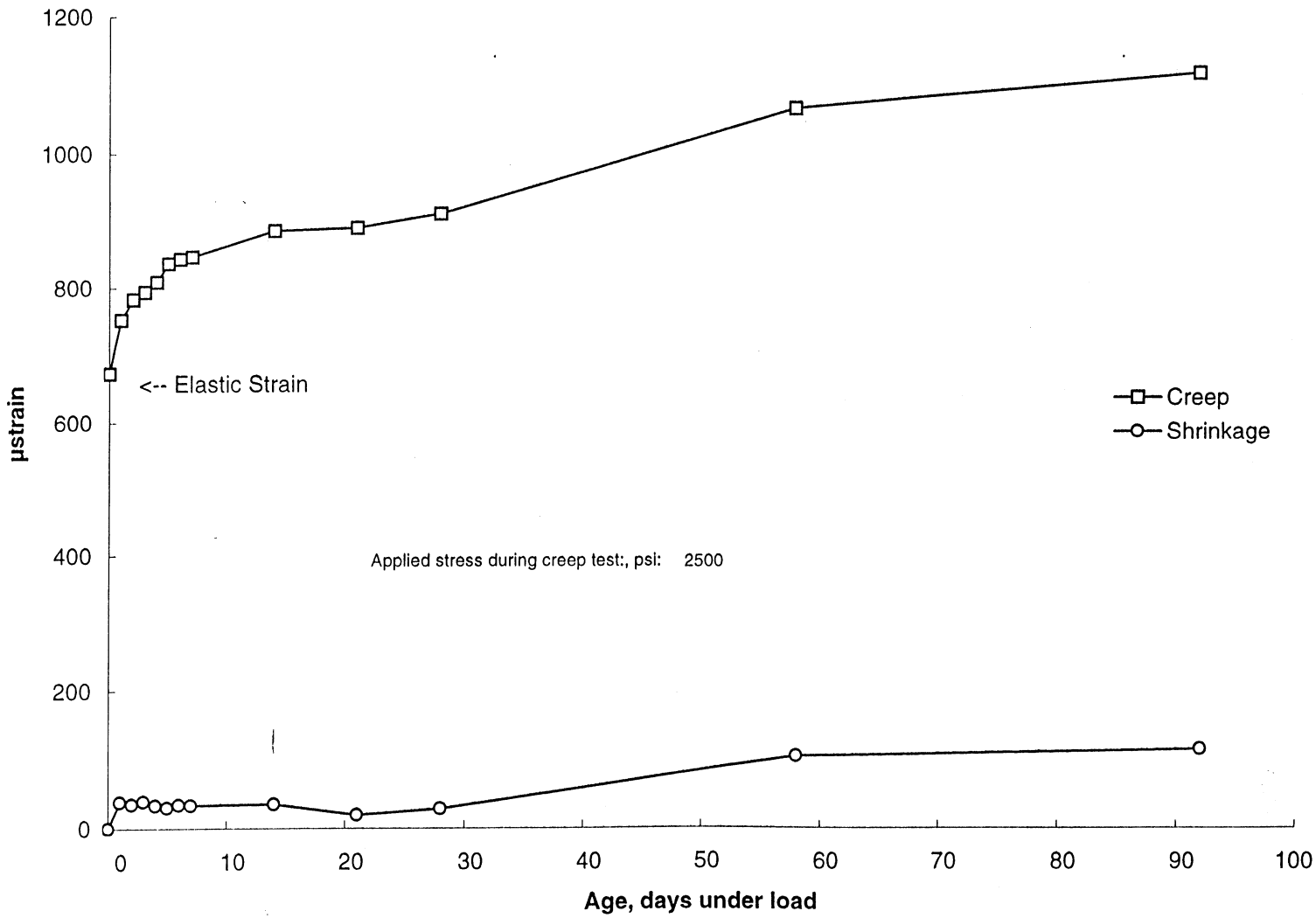

Construction for
Mass Concrete

Construction Guidelines for Mass Concrete and Thermal Effects

Guidelines for Successful Construction of the Benicia-Martinez Bridge

Thermal Considerations for Mass Concrete Elements

May 14, 1999

John Gajda
Senior Engineer
Construction Technology Laboratories, Inc.
5420 Old Orchard Road
Skokie, IL 60077

Signature: _____

Seal:

Cautionary Statement: This report was prepared from in-progress designs, plans, and special provisions dated December 14, 1998. The structural elements and concrete mixes used in this report may vary from the final contract plans and special provisions, but in general should be similar. The reader is advised to understand the implications of the assumptions in this report and any variations between the in-progress and final designs, plans, and contract documents.

TABLE OF CONTENTS

BACKGROUND **1**

INTRODUCTION **1**

MASS CONCRETE ELEMENTS **2**

CONCRETE SECTIONS 2
CONCRETE MIXES 3

ANALYSES **3**

MAXIMUM ALLOWABLE TEMPERATURE DIFFERENCES TO PREVENT THERMAL CRACKING ... 3
PREDICTED MAXIMUM TEMPERATURE AND TEMPERATURE DIFFERENCES 5
Cementitious Materials 5
Concrete Temperature 6
Surface Insulation 6
Maximum Temperature 6
Internal Cooling 6

POTENTIAL SOLUTIONS **7**

CEMENTITIOUS MATERIALS 7
CONCRETE MIX 7
INITIAL CONCRETE TEMPERATURE 9
SURFACE INSULATION 10
INTERNAL COOLING PIPES 11
LIMITING LIFT HEIGHTS 12
TEMPERATURE LOGGING 12

IMPORTANCE OF ASSUMPTIONS **12**

BACKGROUND

This report is the second of two reports that discusses thermal analyses of the referenced project. This generalized report provides guidelines for the constructability of the mass concrete elements of the referenced project. The first report, entitled "Thermal Analyses and Recommendations Regarding the Specifications and Constructability of Typical Mass Concrete Structural Elements of the Benicia-Martinez Bridge" is a technical report, which discusses the results of thermal analyses and provides recommendations regarding the specifications and constructability of typical mass concrete structural elements of the referenced project. Recommendations presented in the first report were based on thermal analyses performed in accordance with calculation procedures described in ACI 207, "Mass Concrete".

INTRODUCTION

Mass concrete is defined as any cast concrete section with a minimum dimension greater than 1 m (3 ft) or any cast concrete section with high cement content. Many sections of the Benicia-Martinez Bridge are considered to be mass concrete.

Placement of mass concrete requires special considerations because large increases in concrete temperature routinely occur as a result of hydration of the cementitious materials. Figure 1 presents a typical time - temperature plot for a massive concrete element. Note this plot may not be representative of any specific element in the Benicia-Martinez Bridge.

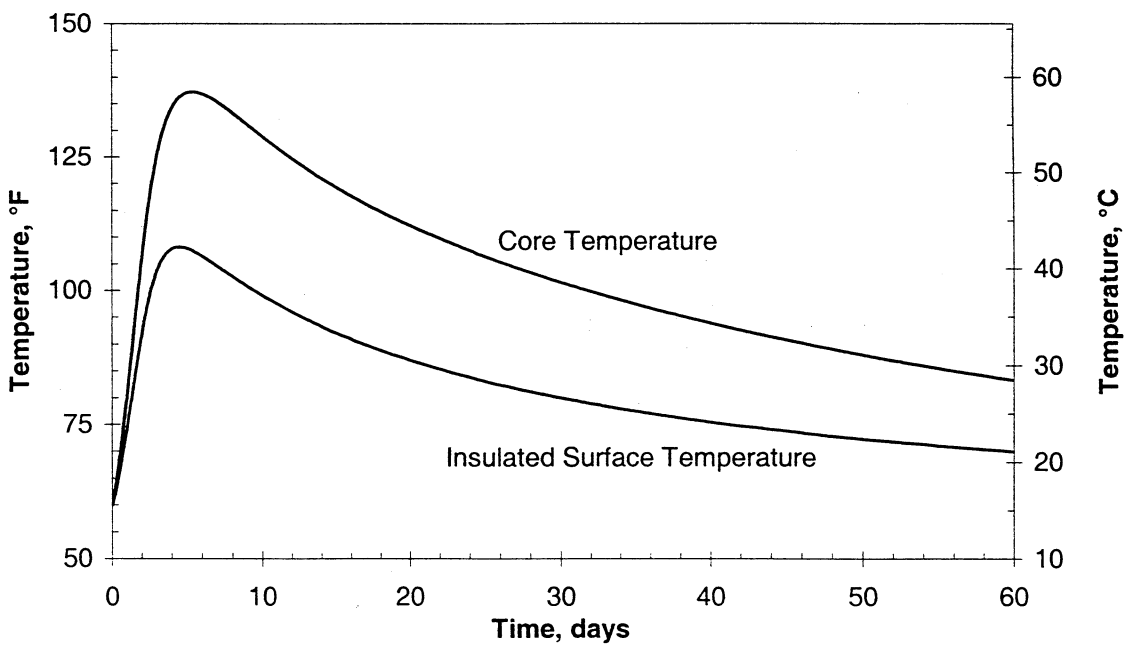

Figure 1 – Hypothetical Temperatures within a Massive Concrete Element

Problems related to mass concrete include thermal cracking and long-term durability of the concrete. Thermal cracking of the concrete results from high internal concrete temperatures and a relatively cool surface temperature. Extensive thermal cracking of the structures can occur if special precautions are not followed. Long-term durability of the concrete can be compromised

if the temperature of the concrete exceeds 70°C (158°F). Specific durability concerns are related to delayed ettringite formation (DEF). DEF can result in expansion and cracking of hardened concrete during exposure to moisture. The deterioration can begin months or years after construction and may continue for several years.

MASS CONCRETE ELEMENTS

The Benicia-Martinez Bridge is compromised of five distinct mass concrete elements. These elements include piles, pile caps, pier shafts, pier tables, and box girder bottom slabs. The concrete elements are described below along with potential problems. A range of solutions are discussed in later sections.

Concrete Sections

The concrete piles consist of reinforced concrete elements cast into 2.5-m diameter steel shafts. Piles extend from the bedrock to a height of approximately 2 m (6.6 ft) above the bay water. Without precautions, thermal cracking may occur on the top surface of the concrete piles.

Pile caps consist of reinforced post-tensioned concrete cast into a precast reinforced concrete shell. Nine piles extend approximately 4 m (13.1 ft) into the pile caps. The overall dimensions of the pile caps are approximately 19 by 21.5 by 5.25 m high (62.3 by 70.5 by 17.2 ft). The precast shell has a wall thickness of approximately 400 mm (15.7 in.) and a floor thickness of 1375 mm (54.1 in.). The bottom of the precast shell is planned to be approximately 2 m (6.6 ft) below water level. Within the precast shell, an 18.2 by 20.7 x 3.9-m (59.7 by 67.9 by 12.8 ft) block of concrete must be cast. Without precautions, thermal cracking is likely to occur on the top surface of the pile cap. In extreme cases, cracking may also occur on the side faces. Due to the size of the mass concrete, maximum concrete temperatures may easily exceed 70°C (158°F) which can result in long-term durability (DEF) concerns.

Pier shafts consist of integrally cast reinforced concrete pier "lobes" and walls with overall plan dimensions of 6.6 by 8.5 m (21.7 by 27.9 ft). The maximum wall thickness is 1600 mm (63 in.). The minimum wall thickness is 775 mm (29.7 in.). Pier shafts range in height up to 40 m (131.2 ft). The potential for thermal cracking of the concrete can be controlled with precautions. The maximum temperature of the concrete may also be problematic.

Pier tables and box girder bottom slabs require concrete with a high modulus of elasticity. The easiest way to achieve a high modulus of elasticity is with a low water to cement ratio, likely resulting in high cement contents. Although many of the box girder bottom slab sections are less than 1 m (3 ft) thick, the required high cement content forces the box girder bottom slabs to be considered as mass concrete. The concrete bottom slab width and thickness at the pier shaft were taken to be 8500 and 1700 mm (334.6 and 66.9 in.), respectively. The concrete bottom slab width and thickness at station "1N" were taken to be 8653 and 1485 mm (340.6 and 58.5 in.), respectively. The concrete bottom slab width and thickness at station "7N" were taken to be 9612 and 761 mm (378.4 and 30.0 in.), respectively.

Concrete Mixes

In general, each concrete element requires a different concrete mix design. Specifications describe the mix designs by the 28-day compressive strength and the unit weight of the concrete. Compressive strengths of the piles, pile caps, pier shafts, pier tables, and box girder bottom slabs are 25, 35, 35, 45, and 45 MPa (3600, 5100, 5100, 6500, and 6500 psi), respectively. Box girder bottom slabs consist of lightweight concrete, while all other mass elements consist of normal weight concrete.

Project specifications require cementitious contents of the piles, pile caps, pier shafts range from 350 to 475 kg/m^3 (590 to 800 pcy). Cementitious content of the pier tables and box girder bottom slabs are required to range from 400 to 550 kg/m^3 (675 to 925 pcy). The use of fly ash is suggested in the project specifications.

ANALYSES

Analyses were performed to determine 1) the maximum allowable temperature difference[i] between the interior of the concrete and the exterior surface to prevent thermal cracking and 2) the maximum concrete temperature and temperature difference[ii] due the hydration of cementitious materials. Analyses were performed for all of the typical mass concrete elements.

Maximum Allowable Temperature Differences to Prevent Thermal Cracking

Analyses to determine the maximum allowable temperature difference for each typical concrete element indicated that precautions are required for all concrete elements. Concrete piles and pile caps will crack unless some minimal precautions are followed. Potential solutions such as insulating the concrete surface and precooling concrete are discussed in later sections.

Maximum allowable temperature differences are presented in Table 1. These temperatures represent the maximum allowable temperature differences between the highest temperature within the concrete, usually at or near the center, and the outside surface. Surface cracking of the concrete can be anticipated if these temperature differences are exceeded. Results in Table 1 indicate that the faster the concrete develops strength, the higher the allowable temperature difference, and the sooner insulation can be removed.

Calculations assumed a coefficient of thermal expansion for concrete of 3.3 x 10^{-6} mm/mm/°C (5.9 x 10^{-6} in/in/°F). Thermal expansion is based on the type of aggregate used. The effect of the thermal expansion is significant on the maximum allowable temperature difference. Lower thermal expansions result in higher allowable temperature differences. Higher thermal expansions result in lower allowable temperature differences. Table 2 shows the effect of thermal expansion on the allowable temperature difference for the pile caps. As shown in the table, selection of aggregates has a significant effect on the allowable temperature rise and the required precautions.

---

[i] Analyses outlined in sections 4.2 and 4.4 of ACI 207.2R-95, "Effect of Restraint, Volume Change, and Reinforcement on Cracking of Mass Concrete".

[ii] Analyses used a 2-dimensional finite difference model as outlined in ACI 207.1R-87, "Mass Concrete".

Table 1 – Maximum Allowable Temperature Differences to Prevent Thermal Cracking

Concrete Compressive Strength*, MPa		Allowable Temperature Difference					
		Piles, Pier Tables, and Box Girder Bottom Slabs		Piers		Pile Caps	
MPa	psi	°C	°F	°C	°F	°C	°F
5	720	10.6	19	5.0	9	3.9	7
10	1450	15.0	27	7.2	13	5.6	10
15	2170	18.3	33	8.9	16	7.2	13
20	2900	21.1	38	10.6	19	8.3	15
25	3620	23.3	42	11.7	21	8.9	16
30	4350	25.6	46	12.8	23	10.0	18
35	5070	27.8	50	13.9	25	10.6	19
40	5800	29.4	53	15.0	27	11.7	21
45	6520	31.7	57	15.6	28	12.2	22
50	7250	33.3	60	16.7	30	12.8	23

* Compressive strength of the concrete surface at any time after casting.

Table 2 – Effect of Thermal Expansion (Aggregate Type) on the Maximum Allowable Temperature Differences for Concrete Pile Caps.

In-Place Concrete Compressive Strength*		Aggregate Type and Thermal Expansion**					
		Limestone 2.2×10^{-6} mm/mm/°C (4.0×10^{-6} in/in/°F)		Gravel 3.3×10^{-6} mm/mm/°C (5.9×10^{-6} in/in/°F)		Quartz 3.9×10^{-6} mm/mm/°C (7.0×10^{-6} in/in/°F)	
MPa	psi	°C	°F	°C	°F	°C	°F
10	1450	8.9	16	5.6	10	5.0	9
20	2900	12.2	22	8.3	15	7.2	13
30	4350	15.0	27	10.0	18	8.3	15
40	5800	17.2	31	11.7	21	10.0	18
50	7250	19.4	35	12.8	23	11.1	20

* This is the actual concrete strength, not the design strength

** Typical values of thermal expansion.

Predicted Maximum Temperature and Temperature Differences

Analyses to determine the maximum concrete temperature due to hydration of the cementitious materials considered:

1. Initial concrete temperature
2. Average air temperature (during the curing of the concrete)
3. Water temperature (for elements in contact with water)
4. Effects of insulation
5. Cementitious (cement and fly ash) content
6. Type II and Type V cement
7. Internal cooling pipes on the pile caps

To simplify this report, results of the analyses are summarized below. Specific results for a variety of conditions can be found in the referenced technical report.

Cementitious Materials

The use of fly ash, as a partial replacement to cement can significantly reduce the maximum concrete temperature. Class "F" fly ash generates approximately half as much heat as the cement that it replaces. Fly ash should be used at the maximum level allowed.

Cement type has a significant effect on the maximum concrete temperature. In general, cements with the lowest heat of hydration should be used. Figure 2 shows the typical heat generation of various cement types.

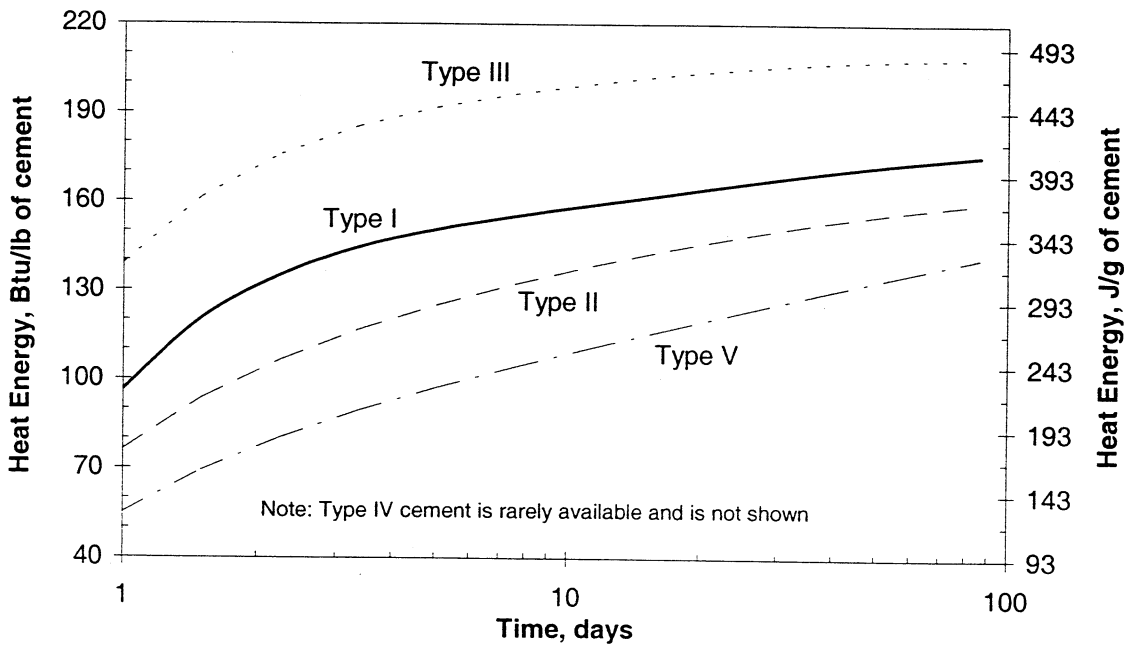

Figure 2 – Typical Heat of Hydration Curves for Common Cement Types (REF: PCA[iii] Publication EB001, "Design and Control of Concrete Mixtures)

[iii] Portland Cement Association, 5420 Old Orchard Road, Skokie, Illinois, 60077

Concrete Temperature

The initial concrete temperature is the most influential factor in the resulting maximum concrete temperature from hydration of cementitious materials. In most cases, reducing the initial concrete temperature by 5.6°C (10°F) reduced the resulting maximum concrete temperature by a similar amount. Initial concrete temperatures are significantly affected by practices of the concrete supplier. Keeping the aggregate in the shade, or frequently sprinkling the aggregate stockpile will keep the aggregate temperature near or possibly below that of the average air temperature. To further reduce concrete temperatures, ice can be substituted for water in the concrete mix. Liquid nitrogen can be used to cool the concrete mix to 1.7°C (35°F), if required.

Surface Insulation

Adding insulation to the exterior surface of the concrete does not significantly increase the maximum concrete temperature. However, insulation does result in lower temperature differences by increasing the surface temperature. Additional benefits of insulation and increased surface temperatures are discussed in a late section. In most cases, surface insulation is required to prevent thermal cracking.

Maximum Temperature

In many cases, the maximum concrete temperature exceeded 70°C (158°F). It is CTL's opinion that long-term durability of the concrete, in regard to delayed ettringite formation (DEF), may be compromised at temperature in excess of 70°C (158°F). Data regarding the long-term ability of supplementary cementitious materials, such as fly ash and slag, to prevent DEF in concrete that has been exposed to high temperatures does not currently exist.

Internal Cooling

Analyses were performed to determine the effect of internal cooling on the concrete pile caps. Pile caps are massive concrete elements that, due to their geometry, contact with water, and precast concrete shell, cannot tolerate large temperature differences. Analyses were performed with and without internal cooling pipes. Analyses indicated that, even with internal cooling, surface insulation is required to minimize or prevent thermal cracking.

Analyses without concrete cooling pipes indicated that concrete temperatures readily exceeded 70°C (158°F). Temperature rises ranged from 25.0 to 62.8°C (45°F to 113°F), depending on the cementitious content and cement type. For a concrete mix without internal cooling, a low thermal expansion concrete with a minimum cementitious content and a low heat of hydration cement is required. Maximum concrete temperatures are predicted to occur between 10 and 20 days after casting, depending on the concrete mix, water temperature, and average air temperature. Removal of the insulation, although not calculated, may be allowed at a time of 60 or more days after casting. Removal of the insulation can occur when the concrete core temperature is within the allowable temperature difference as indicated in Table 1.

Analyses assumed concrete with surface insulation and internal cooling pipes placed at 610-mm (24 in.) on-center, in one direction. Bay water was assumed to be pumped through the cooling pipes. Analyses indicated that cooling pipes decreases the maximum concrete temperature by 10 to 52°F, depending on the initial concrete temperature, the bay water temperature, and the cementitious materials. In all cases, the maximum concrete temperature was below 70°C (158°F). Temperature rises were reduced to 18 to 80°F, and time of maximum temperature was

reduced significantly to 1 to 4 days after casting. Removal of the insulation, although not calculated, is likely to occur much sooner in piles with internal cooling than piles without internal cooling. This implies that the construction schedule can proceed with fewer delays.

The use of internal cooling is likely to have similar effects on other mass concrete elements.

POTENTIAL SOLUTIONS

Many potential solutions exist to minimize thermal problems in mass concrete. Many options for dealing with thermal problems are discussed below.

Cementitious Materials

Proper selection of the cementitious materials is essential in designing a mix for mass concrete applications. The cement type and use of pozzolans should be selected to minimize the heat of hydration. Type II and Type V cements, in general, have the lowest heat of hydration (Figure 2). Many cement manufacturers do not provide heat of hydration data in normal documentation. Cements should be sought with the lowest heat of hydration. If measured in accordance with ASTM C186, early age heat of hydration at 3 and 7 days should be measured in addition to the typical 28-day heat of hydration. Maximum concrete temperatures typically occur in less than 7 days. Fly ash typically generates half of the amount of heat of the cement that it replaces. The use of fly ash also can increase the strength of concrete; therefore, fly ash content should be maximized.

Concrete Mix

The concrete mix can significantly influence the potential for thermal problems. Selection of a low thermal expansion aggregate, as previously discussed can significantly affect the potential for thermal cracking. If a low thermal expansion aggregate is used, allowable temperature differences are increased, thus minimizing the amount of time that the concrete surface must be insulated.

Cementitious contents have a significant effect on the maximum concrete temperature as illustrated in Figure 3. Cementitious contents should be minimized. If allowed by specifications, or by the project engineer, concrete mixes should be designed to meet compressive strength requirements at 56 days, rather than 28 days. This may allow for a significant reduction in the cementitious content.

Maximizing the aggregate size will also allow for a reduction of cementitious content, while maintaining the compressive strength requirement. Figure 4 illustrates the effect of aggregate size on the optimum cementitious content. The maximum aggregate size should be no greater than allowed by applicable codes.

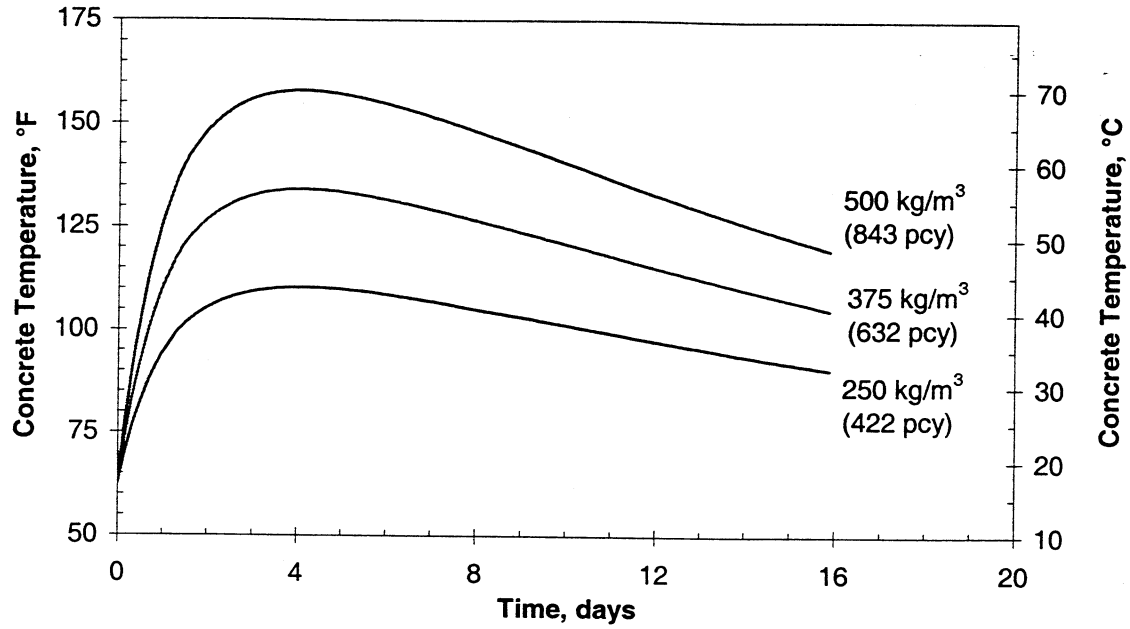

Figure 3 – Effect of Cementitious Content on the Maximum Concrete Temperature

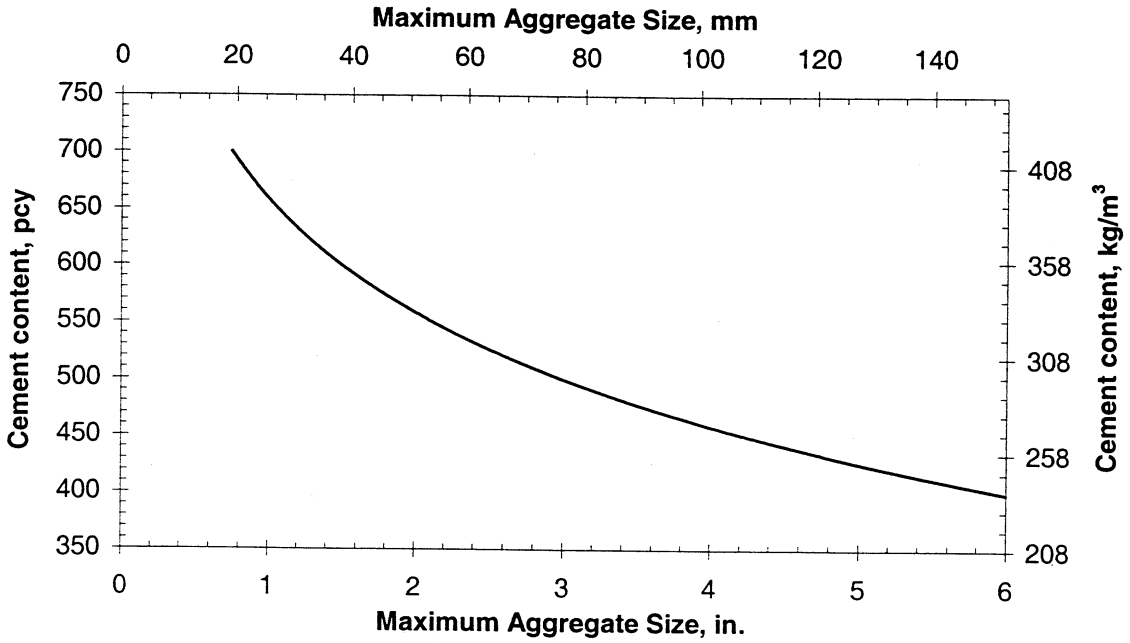

Figure 4 – Effect of Aggregate Size on the Optimum Cementitious Content (REF: PCA Publication IS128, "Concrete for Massive Structures")

Minimizing the water-to-cementitious ratio will maximize the compressive strength, and minimize the required cementitious content as shown in Figure 5. The minimum practical water to cementitious ratio is on the order of 0.35. Achieving a workable mix at this low water content requires the use of admixtures. Care should be taken to minimize the air content of the concrete.

A typical rule of thumb is that compressive strength is reduced by 5% by every 1% of entrained air. Entrained air can significantly decrease the compressive strength, thus increasing the required cementitious content to meet a specified compressive strength.

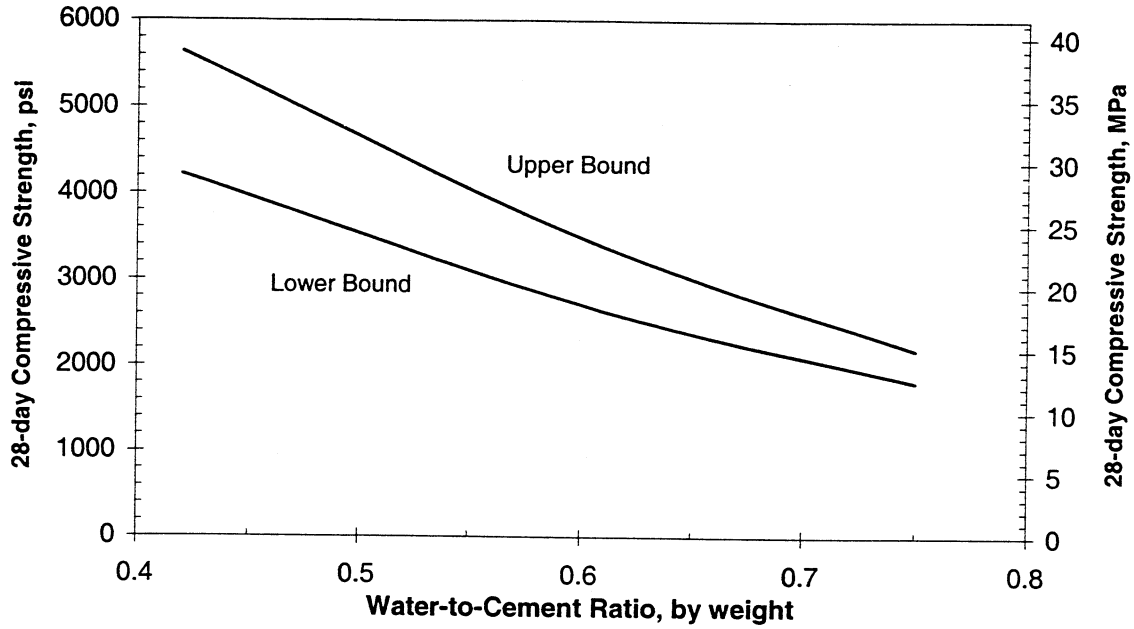

Figure 5 – Relationship between Water to Cement Ratio and Compressive Strength (REF: PCA Publication IS128, "Concrete for Massive Structures")

As a note, compressive strength development of concrete in massive structures is typically considerably more rapid than that of lab-cured cylinders due to the higher temperatures in the concrete structure. Curing at elevated temperatures increases the compressive strength development, as seen in Figure 6.

It is advantageous to measure or estimate the compressive strength of the concrete surface, or concrete cylinders cured at the surface temperature. If removal of insulation, based on allowable temperature differences, is determined by the compressive strength of the concrete surface (assuming the surface is insulated), insulation can be removed sooner than if the allowable temperature difference is based on compressive strength of lab cured cylinders.

Initial Concrete Temperature

The initial concrete temperature is the most influential factor in the resulting maximum concrete temperature from hydration of cementitious materials. In most cases, reducing the initial concrete temperature by 5.6°C (10°F) reduced the resulting maximum concrete temperature by a similar amount.

Initial concrete temperatures are significantly affected by practices of the concrete supplier. Keeping the aggregate in the shade, or frequently sprinkling the aggregate stockpile will keep the aggregate temperature near that of the average air temperature.

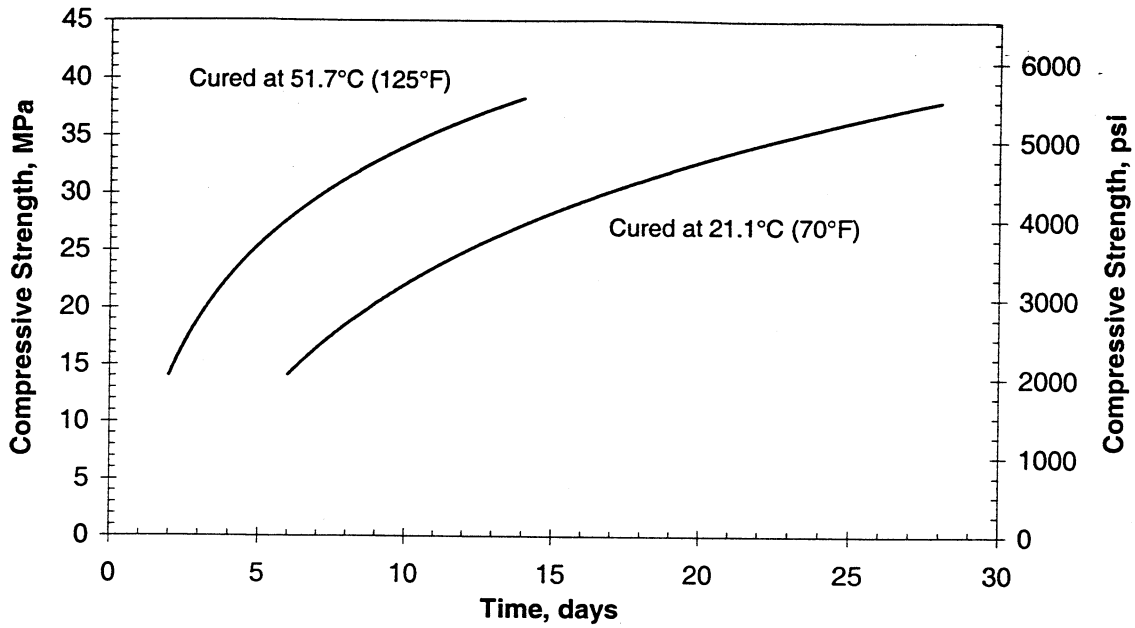

Figure 6 – Effect of Temperature on Compressive Strength Development

To further reduce concrete temperatures, ice must be substituted for water in the concrete mix. Liquid nitrogen can be used to cool the concrete mix to 1.7°C (35°F), if required. Project specifications and ACI practices must be followed if either practice is used.

Simple practices to cool aggregates at the batch plant by shading and sprinkling are much more cost effective than the use of ice and liquid nitrogen.

Surface Insulation

Analyses indicate that insulation is required on the formwork and exposed concrete surfaces to prevent thermal cracking. Insulation is only required to prevent the temperature differential between the exterior and interior from exceeding allowable temperature differences presented in Table 1.

Good practice is to place the insulation on the concrete after it has set, so the concrete surface is not damaged, but before the first night when colder temperatures may cause a decrease in exterior surface temperatures.

Insulating the surface of large concrete elements increases the concrete surface temperature, which in turn decreases the temperature difference between the interior and surface. The insulation also slows the rate of cooling of the concrete interior. The use of insulation to minimize thermal cracking can negatively impact the construction schedule. This can be inferred from Figure 7.

Removing insulation periodically while maintaining a temperature differential between the surface and interior of less than the allowable temperature difference will allow the concrete interior to cool at a faster rate. This will allow an earlier permanent removal of insulation.

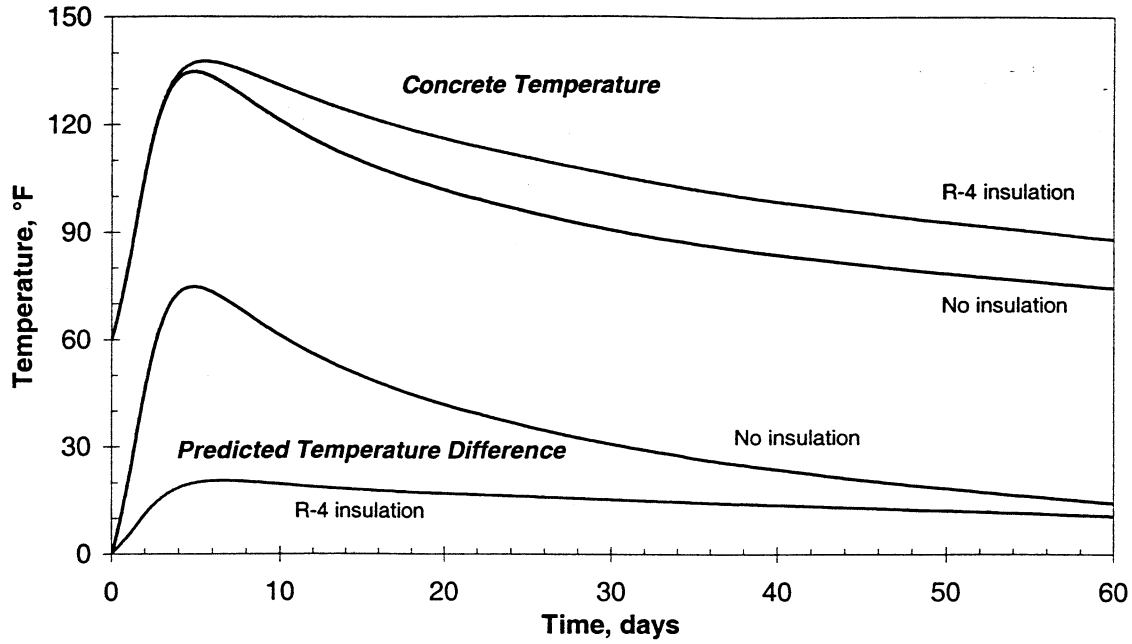

Figure 7 – Effect of Insulation on Concrete Temperature and Temperature Difference

Except as explained below, insulation must be kept in contact with all exposed concrete surfaces, including forms, until the difference between the interior concrete and the anticipated night time (low daily) air temperature is less than the allowable. If it is not possible to have direct contact between the insulation and concrete, the air space between the concrete or forms and insulation should be enclosed so that it is a dead air space and not subjected to infiltration of exterior air. Insulation may be removed periodically to remove formwork, perform other work, or allow the concrete to cool if done in the following manner. Thermocouples must be available to read concrete surface and interior concrete temperatures. The maximum interior concrete temperature is generally at the center of the thickest portion of the element. Insulation may be removed from a concrete surface as long as the allowable temperature difference is not exceeded. Insulation should be replaced every evening so the concrete surface does not cool beyond these limits overnight. Removal sequencing should be performed so that the critical sections such as the ends are exposed to air for the least amount of time.

When the concrete interior temperature is within the allowable temperature difference of the coldest anticipated nighttime air temperature for the next several days, the insulation may be permanently removed.

Internal Cooling Pipes

The use of internal cooling pipes within the pile caps was shown to significantly reduce the maximum concrete temperature and time of maximum temperature. Cooling pipes can be effectively used to speed the construction and the potential for thermal problems.

In the concrete pile cap, cooling pipes were assumed to be spaced at 610 mm (24 in.), on center in one direction. Bay water was assumed to be pumped through the cooling pipes. Cooling pipes will remain in the concrete after the concrete has hardened, therefore, must not be deleterious to

the concrete. PVC or flexible plastic pipes may be acceptable, unless rigidity of the structure is questioned. Copper pipes may cause problems with the corrosion of reinforcing steel. Steel or iron pipes may be a better alternative, however, the time associated with fabrication and installation should be considered.

Limiting Lift Heights

Limiting the height of concrete pours to 1 m (3 ft) or less can be a successful method to minimize the potential for thermal problems. Mass concrete is defined as any concrete pour with a minimum dimension less than 1 m (3 ft), or any concrete mix with a high cementitious content. It may be possible to construct such elements as the concrete pile cap in several pours without the use of insulation or other precautions.

If concrete is placed in lifts, several days should be allowed between pours to dissipate excessive heat. Because the amount of time required dissipate excessive heat is dependent on the concrete temperature, average air temperature, concrete element size and surface insulation, a specific time cannot be provided. Concrete placed on existing concrete that has not cooled sufficiently will reduce the ability of the new concrete to cool downwards. This will increase internal concrete temperatures of the new concrete, and therefore increase the temperature differential between the top surface and interior of the new concrete.

Concrete surfaces and penetrating rebar will need to be water blasted and wetted (at a minimum) to ensure a good bond between concrete pours.

Temperature Logging

Thermocouples should be used to measure concrete core and surface temperatures and ambient air temperatures. Teflon sheathed Type "K" thermocouples are recommended. Temperature logging equipment should be capable of printing, data storage and downloading to a computer. Additional thermocouples should be incorporated into concrete elements in case critical thermocouples are defective or are damaged during or after concrete placement. The referenced technical report indicates recommended locations for thermocouple placement.

The use of thermocouples along with the proper development of concrete maturity data in many cases can allow compressive strengths to be accurately predicted. In-place concrete compressive strength is important because warm (or hot) concrete develops strength more rapidly than lab cured concrete. The use of in-place concrete compressive strengths will allow for quicker removal of surface insulation.

IMPORTANCE OF ASSUMPTIONS

CTL has exercised engineering judgment to make reasonable assumptions in the analyses and resulting recommendations presented in this report and the referenced technical report. Calculation assumptions may not replicate field conditions. Data in tables and figures of this report are hypothetical and may not be applicable to this project.

Analysis for Mass
Concrete

- Analysis and Recommendations for Mass Concrete and Thermal Effects

Thermal Analyses and Recommendations Regarding the Specifications and Constructability of Typical Mass Concrete Structural Elements of the Benicia-Martinez Bridge

May 14, 1999

John Gajda
Senior Engineer
Construction Technology Laboratories, Inc.
5420 Old Orchard Road
Skokie, IL 60077

Signature: _____

Seal:

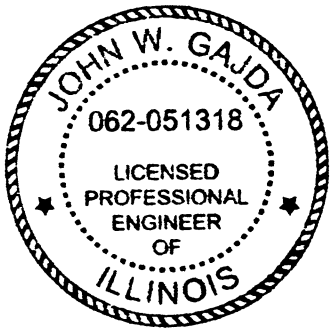

Cautionary Statement: This report was prepared from in-progress designs, plans, and special provisions dated December 14, 1998. The structural elements and concrete mixes used in this report may vary from the final contract plans and special provisions, but in general should be similar. The reader is advised to understand the implications of the assumptions in this report and any variations between the in-progress and final designs, plans, and contract documents.

TABLE OF CONTENTS

INTRODUCTION **1**

BACKGROUND **1**

DIMENSIONS 1
CONCRETE 1

ANALYSES AND ASSUMPTIONS **2**

MAXIMUM ALLOWABLE TEMPERATURE DIFFERENCES 2
PREDICTED MAXIMUM TEMPERATURE AND TEMPERATURE DIFFERENCES 2

RESULTS **5**

MAXIMUM ALLOWABLE TEMPERATURE DIFFERENCES 5
PREDICTED MAXIMUM TEMPERATURE AND TEMPERATURE DIFFERENCES 6

RECOMMENDATIONS **7**

CEMENTITIOUS CONTENT 7
DELAYED ETTRINGITE FORMATION 8
TEMPERATURE MEASUREMENT 9
PILE CAPS 9
INSULATION 9

APPENDIX A – EXAMPLES **15**

EXAMPLE 1 – DETERMINE THE MAXIMUM INITIAL CONCRETE TEMPERATURE FOR A PILE CAP 15
EXAMPLE 2 – DETERMINE THE REQUIRED LEVEL OF INSULATION FOR A PIER TABLE 16

APPENDIX B – RESULTS OF ANALYSES **17**

INTRODUCTION

This report is the first of two reports that discusses thermal analyses of the referenced project. This report is a technical report, which discusses the results of thermal analyses and provides recommendations regarding the specifications and constructability of typical mass concrete structural elements of the referenced project. A second report, entitled "Guidelines for Successful Construction of the Benicia-Martinez Bridge – Thermal Considerations for Mass Concrete Elements" is a generalized report provides guidelines for the constructability of the mass concrete elements of the referenced project.

BACKGROUND

Dimensions

Typical concrete pile, pile cap, pier shafts, pier table, and box girder bottom slab sections for the referenced project were taken from reduced-size set of drawings entitled "Benicia Martinez Bridge & OH". Drawings were stamped "In-progress 90% checked details". Page T009 of the drawings presented the typical concrete sections for analyses.

The concrete pile and pile cap dimensions were taken from details presented on pages T022 and T031. As shown, piles consist of reinforced concrete elements cast into 2.5-m (8.2-ft) diameter steel shafts. Steel shafts extend from air through brackish water, mud and bedrock. Pile caps were indicated to consist of reinforced concrete cast into a precast reinforced and post-tensioned concrete shell. The overall dimensions of the pile caps were 19 by 21.5 by 5.25 m (62.3 by 70.5 by 17.2 ft). The precast shell had a wall thickness of approximately 400 mm (15.7 in.) and a floor thickness of 1375 mm (54.1 in.). The bottom the precast shell was indicated to be approximately 2-m (6.6 ft) below water level.

Pier shaft dimensions were taken from page T049. Pier shafts consist of integrally cast reinforced concrete pier "lobes" and walls with overall plan dimensions of 6.6 by 8.5 m (21.7 by 27.9 ft). The maximum wall thickness is 1600 mm (63 in.). The minimum wall thickness is 775 mm (29.7 in.).

Pier table and box girder bottom slab dimensions were taken from page T063. The pier table width and thickness (concrete bottom slab at the pier shaft) were taken to be 8500 and 1700 mm (334.6 and 66.9 in.), respectively. The concrete box girder bottom slab width and thickness at location "1N" were taken to be 8653 and 1485 mm (340.6 and 58.5 in.), respectively. The concrete bottom box girder slab width and thickness at location "7N" were taken to be 9612 and 761 mm (378.4 and 30.0 in.), respectively.

Concrete

Five concrete mixes were considered for this project. Exact mix designs were not specified. Provided information that indicated 28-day design compressive strengths were 25, 35, 35, and 45 MPa (3600, 5100, 5100, and 6500 psi) for the piles, pile caps, pier shafts, and pier tables, respectively. Normal weight concrete was specified for the piles, pile caps, and pier shafts. Page T063 of the referenced drawings indicated that the pier tables were to be constructed of normal weight concrete, with adjoining box girder bottom slabs sections (including sections "1N" and "7N") to be constructed of lightweight 1920 kg/m^3 (120 pcf) concrete.

Section 90-1.01 of the referenced project specifications indicated that the cementitious content of the piles, pile caps, pier shafts should be in the range of 350 to 475 kg/m^3 (590 to 800 pcy). Cementitious content of the pier tables should be in the range of 400 to 550 kg/m^3 (675 to 925 pcy). Cement types and the use of fly ash were suggested in the CalTrans and project specifications.

ANALYSES AND ASSUMPTIONS

Maximum Allowable Temperature Differences

The maximum allowable temperature differences between the interior of the concrete and the exterior surface were calculated according to Sections 4.2 and 4.4 of ACI 207.2R-95, "Effect of Restraint, Volume Change, and Reinforcement on Cracking of Mass Concrete". The calculated values are the predicted maximum allowable temperature differences to prevent thermal cracking due to heat generation from hydration of cementitious material and the subsequent heat dissipation. Concrete will crack as a result of a warm interior and large tensile stress on a relatively cool exterior surface.

The maximum allowable temperature differences to prevent thermal cracking for the four typical concrete elements were calculated based on the geometry of the element, the restraint, compressive strength, and coefficient of thermal expansion. The coefficient of thermal expansion of the concrete was assumed to be 3.3×10^{-6} mm/mm/°C (5.9×10^{-6} in./in./°F). Elastic modulus and tensile strength were estimated based on the compressive strength. The restraint of the piles, pile caps, piers, pier tables, and box girder bottom slabs was assumed to be 0.35, 0.9, 0.7, 0.35, and 0.35, respectively (Reference: "Mass Concrete", *Concrete Society Digest No. 2*, The Concrete Society, London.).

Although the piles are cast into a steel shell, the thermal expansion of the shell, in comparison to the concrete, is such that the external restraint is assumed to be minimal. The restraint of the pile caps is high because of the restraint provided by the precast concrete shell. The restraint of the piers is relatively high because the piers are tall and significantly less massive than the pile caps on which the piers are cast. The external restraint of the pier tables and box girder bottom slabs was assumed to be minimal.

Predicted Maximum Temperature and Temperature Differences

Two dimensional finite-difference analyses were performed according to ACI 207.1R-87, "Mass Concrete" to calculate the maximum predicted temperature difference within the described concrete sections. The analyses were performed using 45-minute time increments until a period of 24 hours after the maximum concrete temperature was achieved. The thermal diffusivity of the concrete was assumed to be 39 and 65 mm^2/min (0.6 and 1.0 ft^2/day) for the lightweight and normal weight concrete sections, respectively. Assumptions resulted in a modeling resolution of 46 and 76 mm (1.8 and 3 in.), respectively.

To simplify thermal analyses, all concrete sections were modeled using twelve different concrete mix designs. Concrete mix designs consisted of either Type II or Type V cement with 20 percent class "F" fly ash replacement. Type II and Type V cements, with their low heats of hydration are often used in mass concrete. Type V cement typically has a lower heat of hydration than Type II

cement. Fly ash was incorporated because its heat of hydration is approximately half that of the cement that it replaces.

Typical heat of hydration data was taken from PCA Publication EB001, "Design and Control of Concrete Mixtures". Analyses considered total cementitious contents of 300, 350, 400, 450, 500, and 550 kg/m^3, (506, 590, 674, 758, 843, 927 pcy), as presented in Table 1. Fly ash was assumed to generate 60% less heat than cement. The coefficient of thermal expansion of the concrete was assumed to be 3.3×10^{-6} mm/mm/°C (5.9×10^{-6} in./in./°F). Initial concrete temperatures were assumed to range from 7.2 to 23.9°C (45 to 75°F) in 5.6°C (10°F) increments. Concrete temperatures at the lower end of the assumed range may require the use of ice in the mix water or other supplementary cooling such as liquid nitrogen.

Analyses were performed using average ambient air temperatures of 1.7, 27.8, 8.9, 12.8, 17.2, and 16.1°C (35, 82, 48, 55, 63, and 61°F). These temperatures represent winter design, summer design and historical average January, April, July, and September conditions in San Francisco, California. For purposes of this project, the average ambient air temperature can be calculated by averaging hourly job-site air temperatures over a period of several days before and after a specific concrete placement.

Table 1 – Concrete Mix Summary

Mix No.	Cement Type	Cementitious Content,		Cement Content,		Fly Ash Content,	
		kg/m^3	pcy	kg/m^3	pcy	kg/m^3	pcy
1	II	300	506	240	405	60	101
2	V						
3	II	350	590	280	472	70	118
4	V						
5	II	400	674	320	539	80	135
6	V						
7	II	450	758	360	606	90	152
8	V						
9	II	500	843	400	674	100	169
10	V						
11	II	550	927	440	742	110	185
12	V						

Water temperatures use in the analyses were supplied by Mr. Steve Lyles of the NOAA National Ocean Service's San Francisco Bay Physical Oceanographic Real-time Monitoring System (PORTS) project, in an Email on March 3, 1999. Mr. Lyles indicated that historic surface water temperature data are not available at Benicia. He noted that historic surface water temperature data at San Francisco typically range "in the low 50's (°F) during the winter months and up to the 70's (°F) during the summer months". He also indicated that at San Francisco, the lowest and highest recorded surface water temperatures were 6.7 and 23.3°C (44 and 74°F), respectively. The exact location of the recording station was not provided. Air and water temperature assumptions used in the analyses are presented in Table 2.

Table 2 – Assumed Air and Water Temperatures

Case	Average Air Temperature,		Water Temperature,	
	°C	°F	°C	°F
1	8.9	48	10.0	50
2	12.8	55	12.8	55
3	17.2	63	18.3	65
4	16.1	61	15.6	60
5	1.7	35	6.7	44
6	27.8	82	23.3	74

Insulating the concrete surfaces was selected as a means of maintaining the temperature difference between the interior and surface of the analyzed concrete sections. No insulation and insulation with R-values of 2 and 4 hr·ft^2·°F/Btu were used in the analyses. Insulation, if present, was assumed to be placed on all exposed surfaces after initial set of the concrete. Insulation materials are discussed in a later section of this report.

The effects of hourly temperature changes, wind, humidity, formwork, and rebar placement do not significantly affect the temperatures within mass concrete, and are generally not included in heat generation and dissipation analyses. Mass concrete temperatures are affected more by average daily temperatures than by hourly temperatures. Constant average daily temperatures, denoted ambient temperatures in this report, have been used in the analyses. Calculations assume concrete sections will not be directly exposed to high winds for long periods and ambient conditions (during the time of concrete placement) will remain relatively constant while the concrete cures.

Calculations in this report are for concrete placed on existing concrete that has cooled to approximately average ambient temperatures. The required time for cooling is a function of the maximum concrete temperature, average ambient air temperature, surface insulation, and concrete geometry. Concrete placed on existing concrete that has not cooled sufficiently will reduce the ability of the new concrete to cool downwards. This will increase internal concrete temperatures of the new concrete, and therefore increase the temperature differential between the top surface and interior of the new concrete.

Three sets of analyses were performed for concrete pile caps. The first set assumed that the steel shell of the pile caps acted a perfect heat sink. The temperature of the steel shell was set to that of the bay water temperature. The second set of analyses assumed that the steel shell of the pile caps acted like the concrete of the precast concrete shell. This resulted in conservative analyses, where the concrete of the pile cap did not dissipate heat as quickly. The third set of analyses assumed cooling pipes were cast into the concrete. This set of analyses is discussed in a later section of this report.

RESULTS

Maximum Allowable Temperature Differences

Results of the analyses to determine the maximum allowable temperature difference for each typical concrete element are presented in Table 3. These temperatures represent the maximum allowable temperature differences between the highest temperature within the concrete (usually at or near the center) and the outside surface based on the compressive strength of the surface concrete. Surface cracking of the concrete can be anticipated if these temperatures are exceeded.

It is important to note that the compressive strength development of concrete in massive structures is typically considerably more rapid than that of lab-cured cylinders due to the higher temperatures in the concrete structure. Because of this, it is not practical to present the allowable temperature difference on a time scale. The allowable temperature difference is presented in Table 3 as a function of the in-place compressive strength of the concrete surface.

It is also important to note that the allowable temperature differences listed in Table 3 are somewhat dependent on the actual concrete mix design and physical properties. Values presented assume typical relationships between the elastic modulus, tensile strength, tensile strain capacity, and compressive strength. If an aggregate with a higher coefficient of thermal expansion is used, the allowable temperature differences will be reduced.

Table 3 – Maximum Allowable Temperature Differences to Prevent Thermal Cracking

Concrete Compressive Strength*, Mpa		Allowable Temperature Difference					
		Piles, Pier Tables, and Box Girder Bottom Slabs		Piers		Pile Caps	
MPa	psi	°C	°F	°C	°F	°C	°F
5	720	10.6	19	5.0	9	3.9	7
10	1450	15.0	27	7.2	13	5.6	10
15	2170	18.3	33	8.9	16	7.2	13
20	2900	21.1	38	10.6	19	8.3	15
25	3620	23.3	42	11.7	21	8.9	16
30	4350	25.6	46	12.8	23	10.0	18
35	5070	27.8	50	13.9	25	10.6	19
40	5800	29.4	53	15.0	27	11.7	21
45	6520	31.7	57	15.6	28	12.2	22
50	7250	33.3	60	16.7	30	12.8	23

* Compressive strength of the concrete surface at any time after casting.

The typical "rule-of-thumb" for the maximum allowable temperature difference is 20°C (36°F). Calculations show that the compressive strength development significantly affects the allowable temperature difference. Calculations also show that use of the typical "rule-of-thumb" will lead to thermal cracking in many cases.

As indicated in Table 3, the allowable temperature difference of the pile caps is reduced in comparison to that of the other structures. This is due to the high restraint provided by the precast concrete shell of the pile cap. If the allowable temperature difference is exceeded, thermal cracking is likely to occur on the top surface of the pile cap. Insulation is required on the top surface to minimize or eliminate the potential for thermal cracking. The analyses indicated that it is not practical to insulate the sides of the precast concrete shell. The walls of the precast concrete shell have an approximate R-value of 1 $hr \cdot ft^2 \cdot °F/Btu$. Additional surface insulation on the walls would likely increase the internal concrete temperatures, resulting in increased thermal expansion and increased stresses in the precast concrete shell.

Thermal cracking of the top surface of the pile caps is likely to be uniformly spaced and parallel to the edges, in both directions. The spacing and width of the thermal cracking is dependent on the difference between the actual and allowable temperature difference. Unless the reinforcing steel has yielded, cracking will extend only to the surface of the reinforcing steel. Thermal cracking is often mistaken for drying shrinkage; however, the width of drying shrinkage cracks typically increases over time, while thermal cracks typically close as the structure cools.

The restraint due to casting of the tall, thin, and complex shape of the pier shafts on the pile caps also significantly reduces the allowable temperature difference. If the allowable temperature difference is exceeded, thermal cracking is likely occur near the bottom of the pier shaft. Thermal cracking is likely to be vertically oriented and uniformly spaced, extending upwards from the base of the pier. The spacing, width, and height of the thermal cracking is dependent on the difference between the actual and allowable temperature difference. Insulation is required on the formwork to minimize or eliminate the potential for thermal cracking. Insulation should also be placed on the surface of the pile caps immediately surrounding the piers.

Predicted Maximum Temperature and Temperature Differences

Results of the analyses to predict the maximum concrete temperature and temperature differences for each typical concrete element are presented in Tables B1 through B4 in Appendix B. Table B1 considers the portion of the concrete pile above water. Table B2 considers the pile cap. Two cases are presented; one with concrete, and one with internal cooling pipes spaced at 610 mm (24 in.) on-center in one direction. Analyses considering the cooling potential of the steel shell of the piles indicated little difference in the maximum concrete temperature and temperature difference; however, the time of maximum temperature occurred 15 percent sooner (on average) in the analyses assuming that the steel acted as a perfect heat sink. Table B2 presents the more conservative of the analyses. Table B3 considers the concrete pier shaft. Table B4 considers the pier table and the box girder bottom slabs at locations "1N" and "7N". In all tables, maximum predicted temperatures in excess 70°C (158°F) are presented in bold typeface. Use of the tables is illustrated in examples provided in Appendix A.

In summary, the initial concrete temperature is the most influential factor in the resulting maximum concrete temperature from hydration of cementitious materials. Adding insulation to the exterior surface of the concrete does not significantly increase the maximum concrete temperature due to hydration of cementitious materials but does significantly reduce the maximum temperature difference. In most cases, surface insulation is required to prevent thermal cracking.

Analyses show that maximum concrete temperatures can exceeded 70°C (158°F). It is well known that the long-term durability of concrete can be compromised at temperatures in excess of 70°C (158°F). CTL recommends that concrete be limited to a maximum temperature of 70°C (158°F) to alleviate potential durability concerns, as described below.

RECOMMENDATIONS

The analyses presented in this report assumed that thermal cracking is not desirable or allowable. Results of the analyses indicate that for all elements considered, it is possible to construct the elements without thermal cracking. ACI 224R-90 "Control of Cracking in Concrete Structures", does allow for limited thermal cracking of prescribed widths. Table 4.1 of ACI 224-90 indicates that maximum tolerable crack widths of 0.15 and 0.30 mm (0.006 and 0.012-in.) are allowed for concrete exposed to "seawater and seawater spray" and "humidity, moist air, and soil", respectively. Allowing thermal cracks up to these limits will typically increase the maximum allowable temperature difference. This may speed the construction schedule, and reduce construction costs.

Calculations to predict the width and spacing are based on the geometry of the element, early age concrete properties, restraint, and reinforcing steel layout. If thermal cracking is allowed, it is important to note that unless the reinforcing steel is yielded, thermal cracks typically extends to the depth of the reinforcing steel and may close ("heal") as the element cools. Additionally, thermal crack may also close as the structure is loaded.

Although this report indicates that constructing a structure free of thermal cracks is possible with reasonable effort, it may be desirable for the contract documents to allow thermal cracking to "acceptable" widths. Allowing acceptable cracking may allow for a quicker construction schedule and deceased costs to the owner. If allowed, CTL recommends that ACI 207 calculations to predict the maximum allowable temperature rise for each element be required and that measured early age properties including the compressive strength, elastic modulus, and tensile strength be required in the analyses. Early age properties are key because it is often at early ages when the temperature rise of the element exceeds the allowable temperature rise.

If thermal cracking is allowed, it is important to note that additional stresses from drying shrinkage or other mechanisms may increase the size of the thermal cracks beyond the acceptable limits. Therefore, CTL recommends a specified crack repair procedure be included in the contract documents.

Cementitious Content

The best strategy for reducing the cracking potential due to thermal gradients is to keep the cementitious content of the concrete mix design to a minimum. We recommend using a concrete mix that achieves the required compressive strength for the structure at a time greater than 28 days, without excessive over-design. Often, ultimate strengths lower than 30 MPa (4,350 psi) are adequate for large mass structures. High compressive strengths are often specified as a factor of safety against durability issues. High cementitious contents are often specified as a means of meeting low water/cement ratios. Both these practices contribute to excessive heat generation within the concrete, and increase the potential for thermal cracking.

Concrete mix designs for use in this project are currently specified by compressive strength, minimum cementitious content, and maximum cement replacement by supplementary cementitious materials. CalTrans specifies 28-day compressive strengths for concretes less than 31 MPa (4,490 psi) and 35-day compressive strengths for concretes greater than 31 MPa (4,490 psi).

CTL recommends the minimum cementitious contents be significantly reduced if the contractor or supplier can demonstrate compliance with the compressive strength specification. The maximum supplementary material replacement level should be increased to allow for unique mixes with low heats of hydration. Additionally, the 28- and 35-day specification should be increased to a 56-day specification to further reduce the required cementitious content or allow for low heat of hydration concrete mix designs with slow initial strength development assuming the elements are not subjected to full design loading until they are at least 56 days old. The impact of using 28-day, rather than 56-day compressive strengths, regarding the factor of safety for the design compressive strength is not considered. Concrete mixes should be evaluated on a case-by-case basis through pretesting.

Additionally, it is well known that compressive strength development is increased with increased temperatures. Considerations should be made for the use of reliable in-place concrete strength measurements, rather than that of lab-cured cylinders. CTL can provide assistance if required.

Delayed Ettringite Formation

In many cases, the maximum concrete temperature are predicted to exceed 70°C (158°F). It is CTL's opinion that long-term durability of the concrete, with regard to delayed ettringite formation (DEF), may be compromised at temperatures in excess of 70°C (158°F).

DEF may occur in hardened concrete that has been subjected to high-temperature at early ages. The resulting deterioration is manifested as expansion and cracking of the concrete during subsequent exposure to moisture. The deterioration can begin after months or years and may continue for several years.

It is important to note that not all ettringite is harmful. Ettringite is a normal and healthy hydration product, formed during setting and hardening of concrete as a result of the reaction between the gypsum and the tricalcium aluminate of the cement. In concrete exposed to varying moisture conditions, ettringite tends to re-crystallize in pores and cracks as so-called secondary ettringite.

Ettringite is unstable above a certain critical temperature and is therefore decomposed and not formed in concrete heat cured above that critical temperature. The location of the components of the decomposed ettringite at this stage is highly debated, but one school of thought indicates, that the sulfate is taken up in the hydrated calcium silicates from where it later is slowly released when the hardened concrete reaches ambient temperature. Ettringite will form at various rates depending on the permeability and moisture condition of the concrete. Whether the concrete will expand and crack as a result of this ettringite formation depends on the chemical composition of the cement, the aggregate, and exposure conditions. As of now, the fundamental reactions and mechanisms are highly debated amongst researchers.

Concrete mixes with supplementary cementitious materials have shown moderate-term resistance to DEF at temperatures well above 70°C (158°F). Long-term studies are now underway; however, results are not available. Therefore, CTL recommends a maximum allowable concrete temperature of 70°C (158°F).

Temperature Measurement

Thermocouples should be used to log concrete core and surface temperatures and ambient air temperatures. Duplicate thermocouples should be incorporated into concrete elements in case critical thermocouples are defective or are damaged during concrete placement. Figures 1 through 4 present suggested locations for thermocouple placement. The thermocouples should be connected to a data acquisition system capable of printing, data storage and downloading to a computer. Temperatures should be recorded on an hourly basis. Teflon sheathed Type K thermocouples are recommended.

The use of thermocouples along with the proper development of concrete maturity data, in many cases, can allow for compressive strengths to be accurately predicted and reduce the number of field cured quality control cylinders. CTL can provide additional assistance, if requested.

Pile Caps

The pile caps, as proposed, have unique problems relating to heat generation and thermal expansion. Mass concrete is cast into a precast concrete shell. The walls of the precast shell are relatively thin in comparison to the base and the overall plan dimensions of the shell. Nine rigid concrete piles restrain the base of the shell, and the bottom 2 m (6.6 ft) of the shell is below the water surface. Analyses, which do not consider special precautions, indicate a concrete temperature rise of 25.0 to 62.8°C (45°F to 113°F). A simplified calculation considering the temperature rise and the previously described concrete property assumptions (and not the effects of reinforcing steel or crack control joints) indicates the potential unrestrained volumetric thermal expansion of the pile cap ranges from 5 to 13 mm (0.2 to 0.5 in.). Although not in our scope of work, these expansions may generate significant stresses on the shell walls. CTL recommends that a structural engineer calculate the potential for cracking in the shell walls.

If the potential for structural cracking is real and significant, many strategies are available to minimize any potential thermal expansion problems. The maximum and allowable temperature difference can be limited, however this may place additional burdens on the contractor. Other measures include casting of the mass concrete of the pile caps in four equal lifts with significant time to allow for cooling of the concrete to ambient temperatures. Alternatively, cooling pipes can be cast into the concrete. Table B2 provides this strategy as an alternative. In the analyses, pipes were spaced at 610 mm (24 in.) on-center in one direction. The water temperature within the cooling pipes was assumed to be constant (along the length of the cooling pipes) and at the temperature of the surrounding water. Pipes should not be of a material that is deleterious to concrete or causes corrosion of the reinforcing steel.

Insulation

Insulating the surface of large concrete elements increases the concrete surface temperature, which in turn decreases the temperature difference between the interior and surface. The insulation also slows the rate of cooling of the concrete interior.

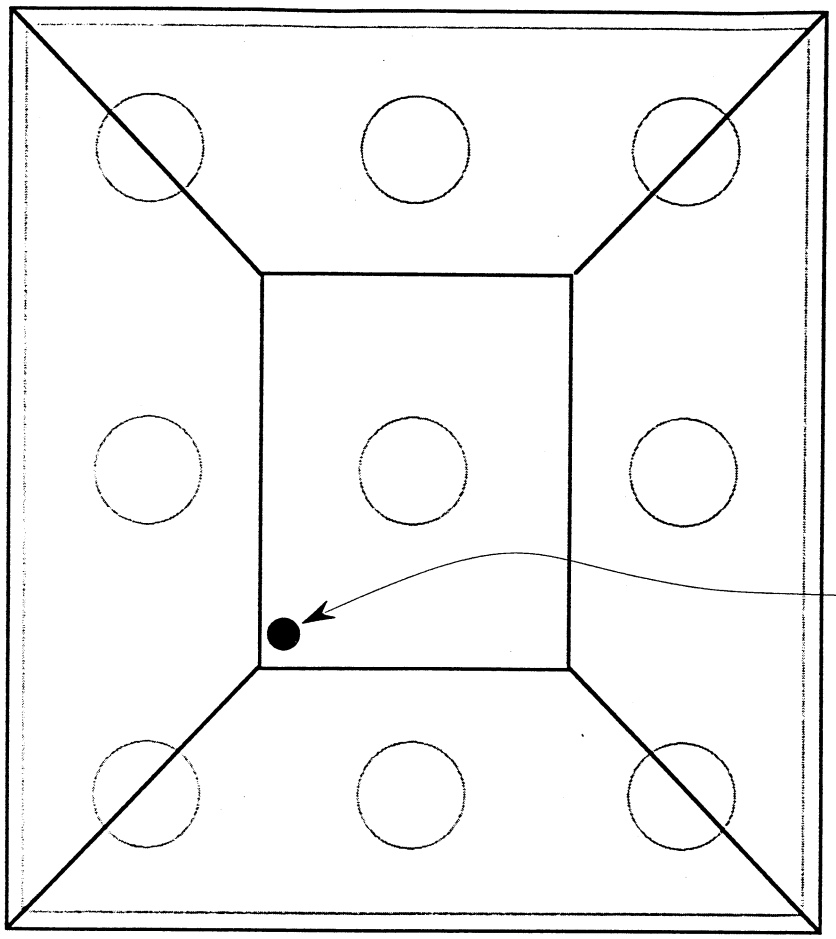

Recommended location for a thermocouple tree (equidistant from piles). It is recommended that a second thermocouple tree be installed as a backup. Only one tree needs to be monitored.

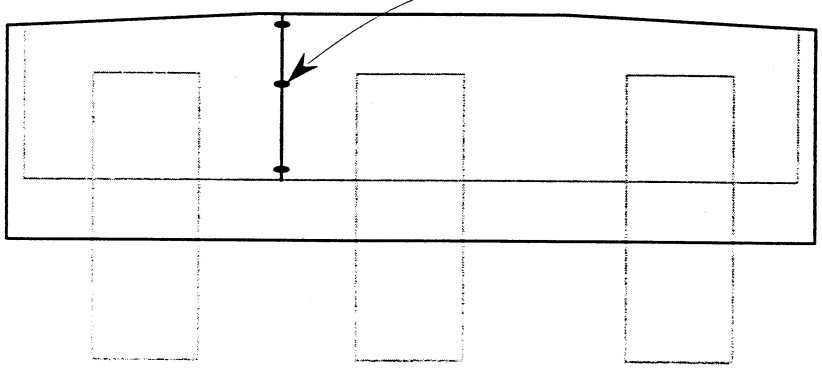

Thermocouples should be placed 50 mm (2 in.) from the top and bottom surfaces. An additional thermocouple should be placed 100 mm (4 in.) below the top surface of the piles. Thermocouples should be supported by plastic or wood and should be kept away from reinforcing steel.

FIGURE 1 - Recommended Location of Thermocouples in the Pile Caps

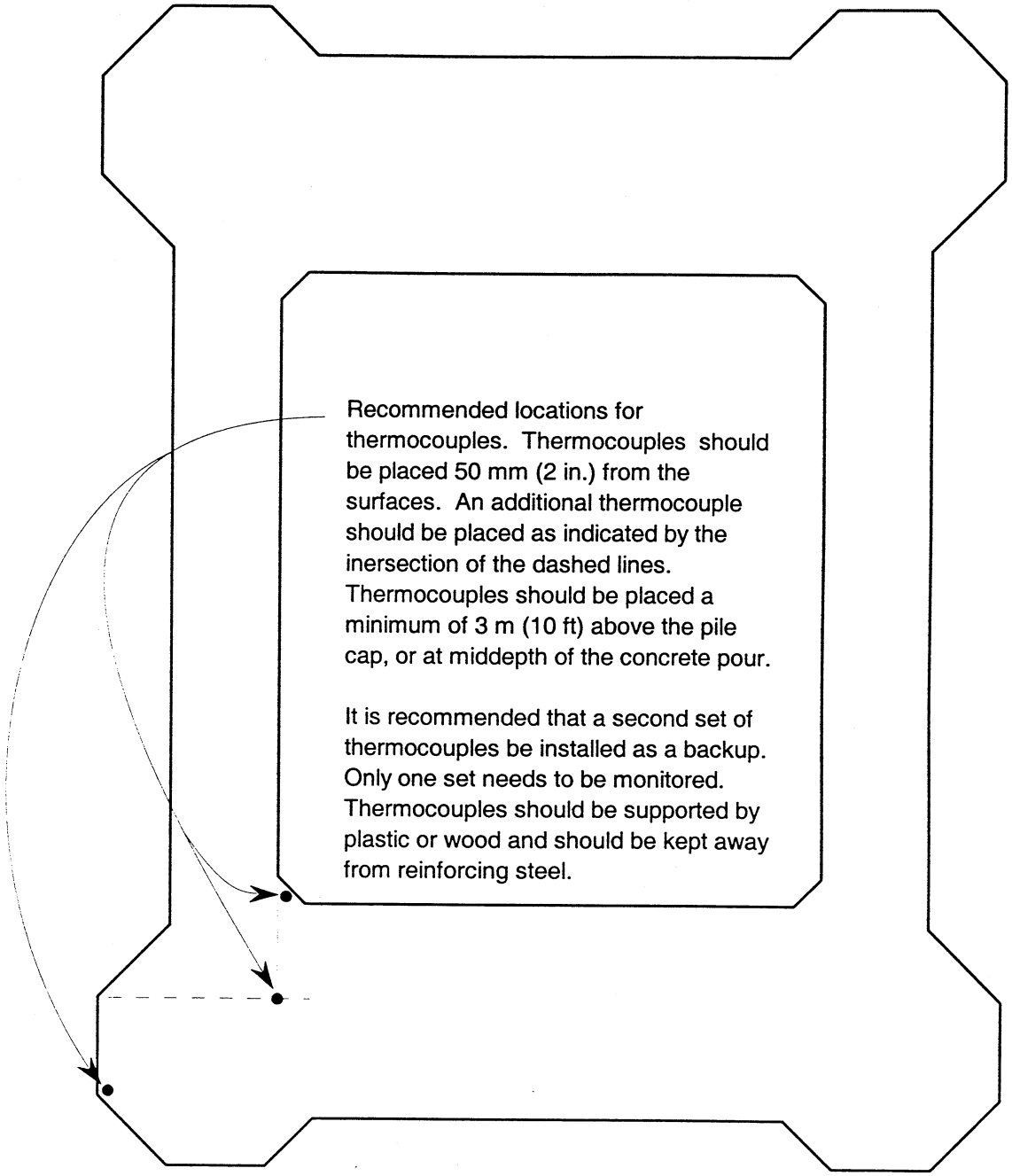

FIGURE 2 - Recommended Location of Thermocouples in the Piers

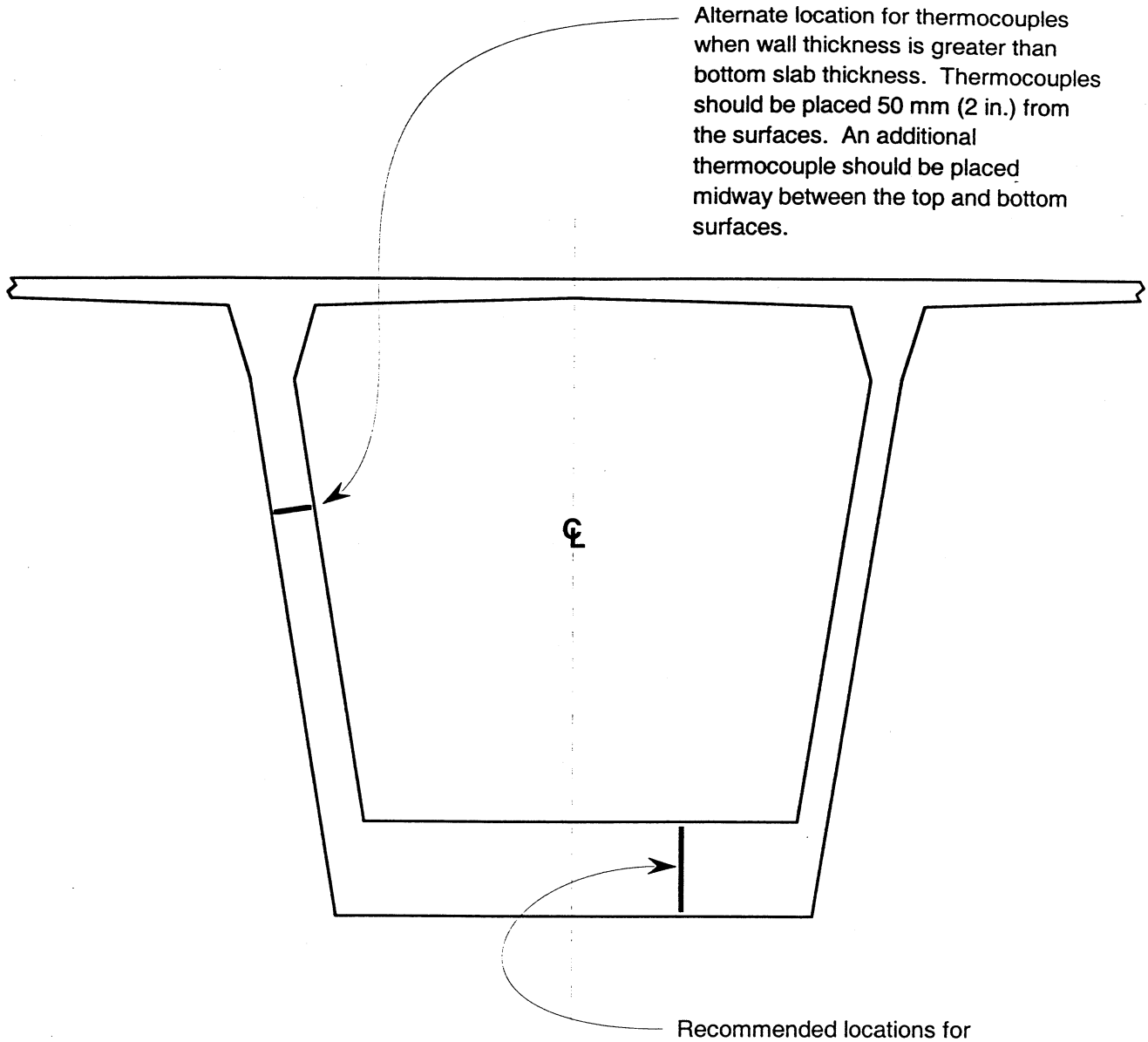

It is recommended that a second set of thermocouples be installed as a backup. Only one set needs to be monitored. Thermocouples should be supported by plastic or wood and should be kept away from reinforcing steel.

NOTE: Simplified Drawing

FIGURE 3 - Recommended Location of Thermocouples in the Pier Tables and Box Girder Bottom Slabs

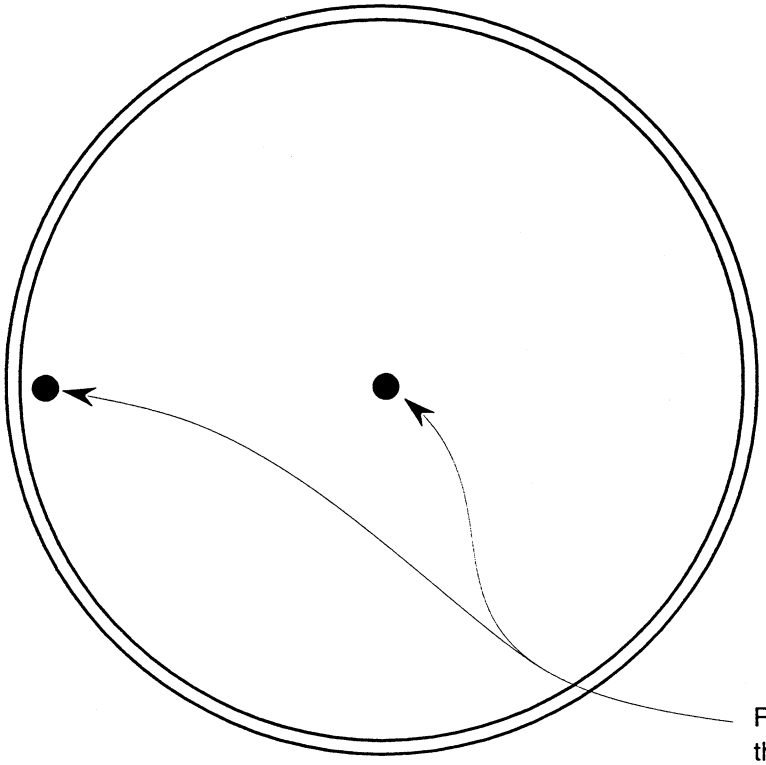

Recommended locations for thermocouples. Thermocouples should be placed 50 mm (2 in.) from the outer surface. An additional thermocouple should be at the pile centerline.

Themocouple should be placed at mid-depth of the pour.

It is recommended that a second set of thermocouples be installed as a backup. Only one set needs to be monitored. Thermocouples should be supported by plastic or wood and should be kept away from reinforcing steel.

FIGURE 4 - Recommended Location of Thermocouples in the Piles

Insulation can consist of almost any material. Table 4 describes the insulating properties of various materials. CTL typically recommends that polystyrene insulation covered with plywood be used wherever the insulation must be used a working surface. In other locations, commercially available insulating blankets for concrete construction or any other insulating material can be used.

Table 4 – Typical R-Values of Various Insulating Materials

Material	Thickness		R-Value
	mm	in.	$hr \cdot ft^2 \cdot °F/Btu$
Polystyrene (pink)	10	⅜	2
Polystyrene (white)	25	1	4
Plywood	13	½	0.6
Insulating Blanket	—	—	2.8
Sand (estimated)	400	16	1
Wood Shavings (dry)	25	1	2.2

NOTE: Metric units are not typically provided for insulation.

Removing insulation periodically while maintaining a temperature differential between the surface and interior of less than the allowable temperature difference will allow the concrete interior to cool at a faster rate. This will allow an earlier permanent removal of insulation.

Except as explained below, insulation must be kept in contact with all exposed concrete surfaces, including forms, until the difference between the interior concrete and the anticipated night time (low daily) air temperature is less than the allowable. If it is not possible to have direct contact between the insulation and concrete, the air space between the concrete or forms and insulation should be enclosed so that it is a dead air space and not subjected to infiltration of exterior air.

Insulation may be removed periodically to remove formwork, perform other work, or allow the concrete to cool if done in the following manner. Thermocouples must be available to read concrete surface and interior concrete temperatures. The maximum interior concrete temperature is generally at the center of the thickest portion of the element. Insulation may be removed from a concrete surface as long as the allowable temperature difference is not exceeded. Insulation should be replaced every evening so the concrete surface does not cool beyond these limits overnight. Removal sequencing should be performed so that the critical sections such as the ends are exposed to air for the least amount of time.

Good practice is to place insulation on the concrete after it has set, so the concrete surface is not damaged, but before the first night when colder temperatures may cause a decrease in exterior surface temperatures. Calculations that assume immediate placement of insulation are not adversely affected by placing the insulation on the concrete after the concrete has set, before the first night, and before the temperature differential exceeds the allowable.

Insulation may be permanently removed when the concrete interior temperature is within the allowable temperature difference of the coldest anticipated nighttime air temperature for the next several days.

APPENDIX A – EXAMPLES

Example 1 – Determine the Maximum Initial Concrete Temperature for a Pile Cap

Assume:

1. Mix 5 - Normal weight concrete with 400 kg/m^3 (674 pcy) of cementitious material (80% Type II cement and 20% fly ash).
2. Average water temperature is 15.6°C (60°F).
3. Average air temperature is 16.1°C (61°F).
4. R-4 insulation will be used.
5. Internal cooling pipes will not be used.

Procedure:

Determine the relevant data. Columns 8, 9, and 10 of Table B2 contain data for pile caps without cooling pipes. Cases 340, 346, 352, and 358 consider the appropriate air and water temperatures. Calculated concrete temperatures are presented below.

Initial Concrete Temp.	Max Concrete Temp.
7.2°C (45°F)	53.9°C (129°F)
12.8°C (55°F)	58.9°C (138°F)
18.3°C (65°F)	63.9°C (147°F)
23.9°C (75°F)	69.4°C (157°F)

Data indicates that an initial concrete temperature of 23.9°C (75°F) will result in a temperature just below the maximum allowable temperature of 70°C (158°F) recommended by CTL. In practice, the concrete temperature should be measured as it is placed in the formwork because concrete can heat by 5.6°C (10°F) during pumping and placement. Because of this, the initial concrete temperature as delivered to the jobsite should be 18.3°C (65°F) or less.

Example 2 – Determine the Required Level of Insulation for a Pier Table

Assume:

1. Mix 6 - Normal weight concrete with 400 kg/m^3 (674 pcy) of cementitious material (80% Type II cement and 20% fly ash).
2. Compressive strengths based on lab testing are 10, 25, 30, 40, and 50 MPa (1450, 3630, 4350, 5800, and 7250 psi) at 1, 3, 6, 14, and 28 days, respectively.
3. Average air temperature is 16.1°C (61°F)
4. Initial concrete temperature is 12.8°C (55°F)
5. The compressive strength development of the concrete structure is similar to that determined in the laboratory. *Note this is typically incorrect for mass concrete with insulating blankets.*

Procedure:

Determine the allowable temperature difference. Table 3 indicates the following allowable temperature differences (dT):

Day	Compressive Strength	dT
1	10 MPa (1450 psi)	15.0°C (27°F)
3	25 MPa (3630 psi)	23.3°C (42°F)
6	30 MPa (4350 psi)	25.6°C (46°F)
14	40 MPa (5800 psi)	29.4°C (53°F)
28	50 MPa (7250 psi)	33.3°C (60°F)

Determine the level of insulation. Columns 6 though 8 of Table B4 contains data regarding pier tabless With normal weight concrete. Cases 370, 394, 418 consider no insulation, R-2 and R-4 insulation on the pier table, as indicated below:

Insulation	Max Temp.	dT	Time, days
None	41.1°C (106°F)	24.4°C (44°F)	3.3
R-2	43.9°C (111°F)	17.2°C (31°F)	5.3
R-4	45.6°C (114°F)	13.9°C (25°F)	7.5

Note because the maximum temperatures are below 70°C (158°F), none of the insulation levels are deleterious to the long-term durability of the concrete. Although the predicted temperature difference of the case with no insulation is marginally acceptable (24.4°C (44°F) predicted at 3.3 days versus 23.3°C (42°F) allowed at 3 days), good practice is to insulate the formwork and concrete surface with R-2 insulation.

APPENDIX B – RESULTS OF ANALYSES

This section of the report presents results of the thermal analyses in tabular format. Results are presented for a twelve different concrete mix designs and range of initial concrete, ambient air, and water (if applicable) temperatures. Due to space limitations, data is presented in inch-pound units only. For conversions to SI units use the following conversions:

Temperature: °C = (°F – 31) / 1.8

Temperature Difference: °C = °F / 1.8

Table B1 considers the portion of the concrete pile above water. Table B2 considers the pile cap. Two cases are presented; one with concrete, and one with internal cooling pipes at 610 mm (24 in.) on-center in one direction. Table B3 considers the concrete pier shaft. Table B4 considers the pier table and the box girder bottom slab at locations "1N" and "7N".

In all tables, maximum predicted temperatures in excess 70°C (158°F) are presented in bold typeface.

Table B1 - Predicted Temperatures and Temperature Differences for Concrete Piles

Case	Concrete Mix No.	Insulation R-Value	Average Air Temp., °F	Initial Concrete Temp., °F	Maximum Concrete Temp., °F	Maximum Temperature Difference, °F	Time of Maximum Temp. Diff., days
1	1	0	48	45	96	44	3.3
2	1	0	55	45	97	39	3.4
3	1	0	63	45	98	33	3.8
4	1	0	61	45	98	34	3.7
5	1	0	35	45	95	55	2.9
6	1	0	82	45	103	19	5.1
7	1	0	48	55	105	53	3.0
8	1	0	55	55	105	47	3.2
9	1	0	63	55	106	40	3.4
10	1	0	61	55	106	42	3.3
11	1	0	35	55	104	64	2.7
12	1	0	82	55	110	26	4.3
13	1	0	48	65	114	61	2.8
14	1	0	55	65	115	55	2.9
15	1	0	63	65	115	48	3.1
16	1	0	61	65	115	50	3.0
17	1	0	35	65	113	72	2.6
18	1	0	82	65	118	33	3.8
19	1	0	48	75	123	70	2.7
20	1	0	55	75	124	64	2.7
21	1	0	63	75	124	57	2.8
22	1	0	61	75	124	59	2.8
23	1	0	35	75	122	81	2.5
24	1	0	82	75	126	41	3.4

Table B1 - Predicted Temperatures and Temperature Differences for Concrete Piles

Case	Concrete Mix No.	Insulation R-Value	Average Air Temp., °F	Initial Concrete Temp., °F	Maximum Concrete Temp., °F	Maximum Temperature Difference, °F	Time of Maximum Temp. Diff., days
25	1	2	48	45	99	24	4.6
26	1	2	55	45	100	21	4.9
27	1	2	63	45	101	18	5.4
28	1	2	61	45	101	19	5.3
29	1	2	35	45	98	30	4.2
30	1	2	82	45	104	11	7.3
31	1	2	48	55	108	28	4.2
32	1	2	55	55	109	26	4.5
33	1	2	63	55	110	22	4.8
34	1	2	61	55	110	23	4.7
35	1	2	35	55	108	34	3.9
36	1	2	82	55	112	15	6.1
37	1	2	48	65	118	33	4.0
38	1	2	55	65	118	30	4.2
39	1	2	63	65	119	26	4.4
40	1	2	61	65	119	27	4.3
41	1	2	35	65	117	38	3.7
42	1	2	82	65	121	19	5.3
43	1	2	48	75	127	37	3.7
44	1	2	55	75	128	34	3.9
45	1	2	63	75	128	30	4.1
46	1	2	61	75	128	31	4.0
47	1	2	35	75	127	42	3.5
48	1	2	82	75	130	23	4.8

Table B1 - Predicted Temperatures and Temperature Differences for Concrete Piles

Case	Concrete Mix No.	Insulation R-Value	Average Air Temp., °F	Initial Concrete Temp., °F	Maximum Concrete Temp., °F	Maximum Temperature Difference, °F	Time of Maximum Temp. Diff., days
49	1	4	48	45	101	16	5.6
50	1	4	55	45	102	15	6.0
51	1	4	63	45	102	12	6.6
52	1	4	61	45	102	13	6.4
53	1	4	35	45	100	20	5.0
54	1	4	82	45	105	8	9.1
55	1	4	48	55	110	19	5.1
56	1	4	55	55	111	17	5.4
57	1	4	63	55	111	15	5.9
58	1	4	61	55	111	16	5.8
59	1	4	35	55	109	23	4.7
60	1	4	82	55	114	10	7.5
61	1	4	48	65	119	22	4.8
62	1	4	55	65	120	20	5.0
63	1	4	63	65	120	18	5.3
64	1	4	61	65	120	18	5.3
65	1	4	35	65	119	25	4.4
66	1	4	82	65	122	13	6.5
67	1	4	48	75	129	25	4.5
68	1	4	55	75	129	23	4.7
69	1	4	63	75	130	21	5.0
70	1	4	61	75	130	21	4.9
71	1	4	35	75	128	28	4.2
72	1	4	82	75	131	15	5.8

Table B1 - Predicted Temperatures and Temperature Differences for Concrete Piles

Case	Concrete Mix No.	Insulation R-Value	Average Air Temp., °F	Initial Concrete Temp., °F	Maximum Concrete Temp., °F	Maximum Temperature Difference, °F	Time of Maximum Temp. Diff., days
73	2	0	48	45	84	34	3.5
74	2	0	55	45	85	28	3.8
75	2	0	63	45	87	22	4.4
76	2	0	61	45	87	24	4.3
77	2	0	35	45	83	44	3.0
78	2	0	82	45	94	11	6.9
79	2	0	48	55	93	42	3.1
80	2	0	55	55	94	36	3.3
81	2	0	63	55	95	30	3.8
82	2	0	61	55	95	31	3.6
83	2	0	35	55	92	53	2.8
84	2	0	82	55	100	16	5.3
85	2	0	48	65	102	50	2.8
86	2	0	55	65	103	44	3.0
87	2	0	63	65	104	38	3.3
88	2	0	61	65	103	39	3.2
89	2	0	35	65	101	61	2.6
90	2	0	82	65	107	23	4.3
91	2	0	48	75	111	59	2.7
92	2	0	55	75	112	53	2.8
93	2	0	63	75	112	46	3.0
94	2	0	61	75	112	48	2.9
95	2	0	35	75	111	70	2.5
96	2	0	82	75	115	31	3.7

Table B1 - Predicted Temperatures and Temperature Differences for Concrete Piles

Case	Concrete Mix No.	Insulation R-Value	Average Air Temp., °F	Initial Concrete Temp., °F	Maximum Concrete Temp., °F	Maximum Temperature Difference, °F	Time of Maximum Temp. Diff., days
97	2	2	48	45	87	19	5.0
98	2	2	55	45	88	16	5.6
99	2	2	63	45	90	13	6.4
100	2	2	61	45	89	14	6.1
101	2	2	35	45	86	24	4.4
102	2	2	82	45	95	6	10.7
103	2	2	48	55	96	23	4.5
104	2	2	55	55	97	20	4.9
105	2	2	63	55	98	17	5.4
106	2	2	61	55	98	18	5.3
107	2	2	35	55	95	28	4.0
108	2	2	82	55	102	10	7.8
109	2	2	48	65	106	27	4.2
110	2	2	55	65	106	24	4.4
111	2	2	63	65	107	21	4.8
112	2	2	61	65	107	22	4.7
113	2	2	35	65	105	33	3.8
114	2	2	82	65	109	13	6.3
115	2	2	48	75	115	31	3.8
116	2	2	55	75	115	28	4.0
117	2	2	63	75	116	25	4.3
118	2	2	61	75	116	26	4.2
119	2	2	35	75	114	37	3.5
120	2	2	82	75	118	17	5.3

Table B1 - Predicted Temperatures and Temperature Differences for Concrete Piles

Case	Concrete Mix No.	Insulation R-Value	Average Air Temp., °F	Initial Concrete Temp., °F	Maximum Concrete Temp., °F	Maximum Temperature Difference, °F	Time of Maximum Temp. Diff., days
121	2	4	48	45	89	13	6.3
122	2	4	55	45	90	11	7.0
123	2	4	63	45	91	9	8.1
124	2	4	61	45	91	10	7.8
125	2	4	35	45	88	16	5.4
126	2	4	82	45	96	5	14.1
127	2	4	48	55	98	16	5.6
128	2	4	55	55	99	14	6.1
129	2	4	63	55	100	12	6.8
130	2	4	61	55	99	12	6.6
131	2	4	35	55	97	19	5.0
132	2	4	82	55	103	7	10.1
133	2	4	48	65	107	18	5.1
134	2	4	55	65	108	16	5.4
135	2	4	63	65	108	14	5.9
136	2	4	61	65	108	15	5.8
137	2	4	35	65	106	22	4.6
138	2	4	82	65	111	9	7.9
139	2	4	48	75	117	21	4.7
140	2	4	55	75	117	19	5.0
141	2	4	63	75	118	17	5.3
142	2	4	61	75	117	18	5.2
143	2	4	35	75	116	25	4.3
144	2	4	82	75	119	12	6.7

Table B1 - Predicted Temperatures and Temperature Differences for Concrete Piles

Case	Concrete Mix No.	Insulation R-Value	Average Air Temp., °F	Initial Concrete Temp., °F	Maximum Concrete Temp., °F	Maximum Temperature Difference, °F	Time of Maximum Temp. Diff., days
145	3	0	48	45	104	52	3.2
146	3	0	55	45	105	47	3.4
147	3	0	63	45	106	40	3.7
148	3	0	61	45	106	42	3.6
149	3	0	35	45	103	63	3.0
150	3	0	82	45	110	26	4.6
151	3	0	48	55	113	60	3.0
152	3	0	55	55	114	55	3.2
153	3	0	63	55	115	48	3.4
154	3	0	61	55	115	50	3.3
155	3	0	35	55	112	71	2.8
156	3	0	82	55	118	33	4.1
157	3	0	48	65	122	69	2.8
158	3	0	55	65	123	63	3.0
159	3	0	63	65	124	56	3.1
160	3	0	61	65	123	58	3.0
161	3	0	35	65	121	80	2.7
162	3	0	82	65	126	41	3.6
163	3	0	48	75	132	77	2.7
164	3	0	55	75	132	71	2.8
165	3	0	63	75	133	65	2.9
166	3	0	61	75	133	66	2.8
167	3	0	35	75	131	89	2.5
168	3	0	82	75	135	49	3.3

Table B1 - Predicted Temperatures and Temperature Differences for Concrete Piles

Case	Concrete Mix No.	Insulation R-Value	Average Air Temp., °F	Initial Concrete Temp., °F	Maximum Concrete Temp., °F	Maximum Temperature Difference, °F	Time of Maximum Temp. Diff., days
169	3	2	48	45	108	29	4.6
170	3	2	55	45	109	26	4.8
171	3	2	63	45	110	22	5.2
172	3	2	61	45	110	23	5.1
173	3	2	35	45	107	34	4.2
174	3	2	82	45	113	15	6.6
175	3	2	48	55	117	33	4.3
176	3	2	55	55	118	30	4.5
177	3	2	63	55	119	26	4.8
178	3	2	61	55	119	27	4.7
179	3	2	35	55	117	38	4.0
180	3	2	82	55	121	19	5.8
181	3	2	48	65	127	37	4.0
182	3	2	55	65	127	34	4.2
183	3	2	63	65	128	31	4.4
184	3	2	61	65	128	31	4.3
185	3	2	35	65	126	42	3.8
186	3	2	82	65	130	23	5.1
187	3	2	48	75	136	41	3.8
188	3	2	55	75	137	38	4.0
189	3	2	63	75	137	35	4.1
190	3	2	61	75	137	36	4.1
191	3	2	35	75	135	46	3.6
192	3	2	82	75	139	27	4.7

Table B1 - Predicted Temperatures and Temperature Differences for Concrete Piles

Case	Concrete Mix No.	Insulation R-Value	Average Air Temp., °F	Initial Concrete Temp., °F	Maximum Concrete Temp., °F	Maximum Temperature Difference, °F	Time of Maximum Temp. Diff., days
193	3	4	48	45	110	19	5.6
194	3	4	55	45	111	17	5.9
195	3	4	63	45	112	15	6.4
196	3	4	61	45	111	16	6.3
197	3	4	35	45	109	23	5.1
198	3	4	82	45	114	10	8.1
199	3	4	48	55	119	22	5.2
200	3	4	55	55	120	20	5.4
201	3	4	63	55	121	18	5.8
202	3	4	61	55	120	19	5.7
203	3	4	35	55	118	26	4.8
204	3	4	82	55	123	13	7.1
205	3	4	48	65	129	25	4.8
206	3	4	55	65	129	23	5.1
207	3	4	63	65	130	21	5.3
208	3	4	61	65	130	21	5.3
209	3	4	35	65	128	28	4.5
210	3	4	82	65	131	16	6.3
211	3	4	48	75	138	27	4.6
212	3	4	55	75	138	26	4.8
213	3	4	63	75	139	23	5.0
214	3	4	61	75	139	24	5.0
215	3	4	35	75	137	31	4.3
216	3	4	82	75	140	18	5.8

Table B1 - Predicted Temperatures and Temperature Differences for Concrete Piles

Case	Concrete Mix No.	Insulation R-Value	Average Air Temp., °F	Initial Concrete Temp., °F	Maximum Concrete Temp., °F	Maximum Temperature Difference, °F	Time of Maximum Temp. Diff., days
217	4	0	48	45	91	40	3.4
218	4	0	55	45	92	34	3.8
219	4	0	63	45	93	28	4.2
220	4	0	61	45	93	30	4.1
221	4	0	35	45	89	50	3.1
222	4	0	82	45	99	16	5.9
223	4	0	48	55	99	48	3.2
224	4	0	55	55	100	42	3.3
225	4	0	63	55	101	36	3.7
226	4	0	61	55	101	37	3.6
227	4	0	35	55	98	59	2.8
228	4	0	82	55	106	22	4.9
229	4	0	48	65	108	56	2.9
230	4	0	55	65	109	50	3.1
231	4	0	63	65	110	44	3.3
232	4	0	61	65	110	45	3.2
233	4	0	35	65	107	67	2.7
234	4	0	82	65	113	29	4.1
235	4	0	48	75	118	65	2.7
236	4	0	55	75	118	59	2.8
237	4	0	63	75	119	52	3.0
238	4	0	61	75	119	54	3.0
239	4	0	35	75	117	76	2.5
240	4	0	82	75	121	36	3.6

Table B1 - Predicted Temperatures and Temperature Differences for Concrete Piles

Case	Concrete Mix No.	Insulation R-Value	Average Air Temp., °F	Initial Concrete Temp., °F	Maximum Concrete Temp., °F	Maximum Temperature Difference, °F	Time of Maximum Temp. Diff., days
241	4	2	48	45	94	22	5.0
242	4	2	55	45	95	19	5.4
243	4	2	63	45	96	16	6.1
244	4	2	61	45	96	17	5.9
245	4	2	35	45	93	28	4.4
246	4	2	82	45	101	9	8.9
247	4	2	48	55	103	26	4.5
248	4	2	55	55	104	23	4.9
249	4	2	63	55	105	20	5.3
250	4	2	61	55	105	21	5.2
251	4	2	35	55	102	32	4.1
252	4	2	82	55	108	13	7.1
253	4	2	48	65	113	30	4.2
254	4	2	55	65	113	28	4.4
255	4	2	63	65	114	24	4.8
256	4	2	61	65	114	25	4.7
257	4	2	35	65	112	36	3.8
258	4	2	82	65	116	17	6.0
259	4	2	48	75	122	35	4.0
260	4	2	55	75	122	32	4.1
261	4	2	63	75	123	28	4.3
262	4	2	61	75	123	29	4.3
263	4	2	35	75	121	40	3.7
264	4	2	82	75	125	21	5.3

Table B1 - Predicted Temperatures and Temperature Differences for Concrete Piles

Case	Concrete Mix No.	Insulation R-Value	Average Air Temp., °F	Initial Concrete Temp., °F	Maximum Concrete Temp., °F	Maximum Temperature Difference, °F	Time of Maximum Temp. Diff., days
265	4	4	48	45	96	15	6.3
266	4	4	55	45	97	13	6.8
267	4	4	63	45	98	11	7.7
268	4	4	61	45	98	12	7.4
269	4	4	35	45	95	19	5.5
270	4	4	82	45	102	7	11.6
271	4	4	48	55	105	18	5.7
272	4	4	55	55	106	16	6.1
273	4	4	63	55	107	14	6.7
274	4	4	61	55	107	14	6.5
275	4	4	35	55	104	21	5.1
276	4	4	82	55	110	9	9.1
277	4	4	48	65	114	21	5.2
278	4	4	55	65	115	19	5.5
279	4	4	63	65	116	17	5.9
280	4	4	61	65	115	17	5.8
281	4	4	35	65	114	24	4.8
282	4	4	82	65	118	12	7.6
283	4	4	48	75	124	23	4.8
284	4	4	55	75	124	21	5.1
285	4	4	63	75	125	19	5.4
286	4	4	61	75	125	20	5.3
287	4	4	35	75	123	27	4.5
288	4	4	82	75	127	14	6.6

Table B1 - Predicted Temperatures and Temperature Differences for Concrete Piles

Case	Concrete Mix No.	Insulation R-Value	Average Air Temp., °F	Initial Concrete Temp., °F	Maximum Concrete Temp., °F	Maximum Temperature Difference, °F	Time of Maximum Temp. Diff., days
289	5	0	48	45	113	60	3.2
290	5	0	55	45	114	54	3.4
291	5	0	63	45	115	48	3.6
292	5	0	61	45	114	50	3.6
293	5	0	35	45	111	71	3.0
294	5	0	82	45	118	34	4.3
295	5	0	48	55	122	68	3.0
296	5	0	55	55	122	62	3.2
297	5	0	63	55	123	56	3.3
298	5	0	61	55	123	57	3.3
299	5	0	35	55	120	79	2.8
300	5	0	82	55	126	41	3.9
301	5	0	48	65	131	77	2.8
302	5	0	55	65	131	71	3.0
303	5	0	63	65	132	64	3.1
304	5	0	61	65	132	66	3.1
305	5	0	35	65	130	88	2.7
306	5	0	82	65	135	49	3.6
307	5	0	48	75	140	85	2.7
308	5	0	55	75	140	79	2.8
309	5	0	63	75	141	72	2.9
310	5	0	61	75	141	74	2.9
311	5	0	35	75	139	96	2.6
312	5	0	82	75	143	57	3.3

Table B1 - Predicted Temperatures and Temperature Differences for Concrete Piles

Case	Concrete Mix No.	Insulation R-Value	Average Air Temp., °F	Initial Concrete Temp., °F	Maximum Concrete Temp., °F	Maximum Temperature Difference, °F	Time of Maximum Temp. Diff., days
313	5	2	48	45	117	33	4.5
314	5	2	55	45	118	30	4.8
315	5	2	63	45	119	27	5.1
316	5	2	61	45	119	27	5.0
317	5	2	35	45	116	38	4.2
318	5	2	82	45	122	19	6.1
319	5	2	48	55	126	37	4.3
320	5	2	55	55	127	34	4.5
321	5	2	63	55	128	31	4.7
322	5	2	61	55	128	31	4.6
323	5	2	35	55	125	42	4.0
324	5	2	82	55	130	23	5.5
325	5	2	48	65	136	41	4.0
326	5	2	55	65	136	38	4.2
327	5	2	63	65	137	35	4.4
328	5	2	61	65	137	36	4.3
329	5	2	35	65	135	46	3.8
330	5	2	82	65	139	27	5.1
331	5	2	48	75	145	45	3.8
332	5	2	55	75	145	42	4.0
333	5	2	63	75	146	39	4.2
334	5	2	61	75	146	40	4.1
335	5	2	35	75	144	51	3.7
336	5	2	82	75	148	31	4.7

Table B1 - Predicted Temperatures and Temperature Differences for Concrete Piles

Case	Concrete Mix No.	Insulation R-Value	Average Air Temp., °F	Initial Concrete Temp., °F	Maximum Concrete Temp., °F	Maximum Temperature Difference, °F	Time of Maximum Temp. Diff., days
337	5	4	48	45	119	22	5.5
338	5	4	55	45	120	20	5.8
339	5	4	63	45	121	18	6.2
340	5	4	61	45	121	19	6.1
341	5	4	35	45	118	26	5.1
342	5	4	82	45	123	13	7.6
343	5	4	48	55	129	25	5.2
344	5	4	55	55	129	23	5.4
345	5	4	63	55	130	21	5.8
346	5	4	61	55	130	21	5.7
347	5	4	35	55	128	28	4.8
348	5	4	82	55	132	16	6.8
349	5	4	48	65	138	28	4.9
350	5	4	55	65	138	26	5.1
351	5	4	63	65	139	24	5.3
352	5	4	61	65	139	24	5.3
353	5	4	35	65	137	31	4.6
354	5	4	82	65	141	19	6.2
355	5	4	48	75	147	30	4.7
356	5	4	55	75	148	28	4.8
357	5	4	63	75	148	26	5.0
358	5	4	61	75	148	27	5.0
359	5	4	35	75	147	34	4.4
360	5	4	82	75	150	21	5.7

Table B1 - Predicted Temperatures and Temperature Differences for Concrete Piles

Case	Concrete Mix No.	Insulation R-Value	Average Air Temp., °F	Initial Concrete Temp., °F	Maximum Concrete Temp., °F	Maximum Temperature Difference, °F	Time of Maximum Temp. Diff., days
361	6	0	48	45	97	46	3.4
362	6	0	55	45	98	40	3.7
363	6	0	63	45	100	34	4.1
364	6	0	61	45	99	36	3.9
365	6	0	35	45	96	56	3.1
366	6	0	82	45	105	21	5.4
367	6	0	48	55	106	54	3.2
368	6	0	55	55	107	48	3.3
369	6	0	63	55	108	42	3.6
370	6	0	61	55	108	43	3.6
371	6	0	35	55	105	65	2.9
372	6	0	82	55	112	28	4.6
373	6	0	48	65	115	62	3.0
374	6	0	55	65	116	56	3.1
375	6	0	63	65	116	50	3.3
376	6	0	61	65	116	51	3.2
377	6	0	35	65	114	73	2.7
378	6	0	82	65	120	35	4.0
379	6	0	48	75	124	70	2.8
380	6	0	55	75	125	65	2.9
381	6	0	63	75	125	58	3.0
382	6	0	61	75	125	59	3.0
383	6	0	35	75	123	82	2.6
384	6	0	82	75	128	42	3.6

Table B1 - Predicted Temperatures and Temperature Differences for Concrete Piles

Case	Concrete Mix No.	Insulation R-Value	Average Air Temp., °F	Initial Concrete Temp., °F	Maximum Concrete Temp., °F	Maximum Temperature Difference, °F	Time of Maximum Temp. Diff., days
385	6	2	48	45	101	26	5.0
386	6	2	55	45	102	23	5.4
387	6	2	63	45	103	20	5.9
388	6	2	61	45	103	20	5.8
389	6	2	35	45	100	31	4.5
390	6	2	82	45	107	12	8.0
391	6	2	48	55	110	30	4.6
392	6	2	55	55	111	27	4.9
393	6	2	63	55	112	24	5.3
394	6	2	61	55	112	24	5.1
395	6	2	35	55	109	35	4.2
396	6	2	82	55	115	16	6.7
397	6	2	48	65	119	34	4.3
398	6	2	55	65	120	31	4.5
399	6	2	63	65	121	28	4.8
400	6	2	61	65	121	28	4.7
401	6	2	35	65	119	39	4.0
402	6	2	82	65	123	20	5.8
403	6	2	48	75	129	38	4.0
404	6	2	55	75	129	35	4.2
405	6	2	63	75	130	32	4.4
406	6	2	61	75	130	32	4.3
407	6	2	35	75	128	43	3.8
408	6	2	82	75	132	24	5.2

Table B1 - Predicted Temperatures and Temperature Differences for Concrete Piles

Case	Concrete Mix No.	Insulation R-Value	Average Air Temp., °F	Initial Concrete Temp., °F	Maximum Concrete Temp., °F	Maximum Temperature Difference, °F	Time of Maximum Temp. Diff., days
409	6	4	48	45	103	18	6.3
410	6	4	55	45	104	16	6.7
411	6	4	63	45	105	14	7.4
412	6	4	61	45	105	14	7.3
413	6	4	35	45	102	21	5.6
414	6	4	82	45	109	9	10.3
415	6	4	48	55	112	20	5.7
416	6	4	55	55	113	18	6.1
417	6	4	63	55	114	16	6.6
418	6	4	61	55	114	17	6.4
419	6	4	35	55	111	24	5.2
420	6	4	82	55	117	11	8.5
421	6	4	48	65	122	23	5.3
422	6	4	55	65	122	21	5.6
423	6	4	63	65	123	19	5.9
424	6	4	61	65	123	19	5.8
425	6	4	35	65	121	26	4.8
426	6	4	82	65	125	14	7.3
427	6	4	48	75	131	26	5.0
428	6	4	55	75	131	24	5.2
429	6	4	63	75	132	22	5.5
430	6	4	61	75	132	22	5.4
431	6	4	35	75	130	29	4.6
432	6	4	82	75	134	17	6.5

Table B1 - Predicted Temperatures and Temperature Differences for Concrete Piles

Case	Concrete Mix No.	Insulation R-Value	Average Air Temp., °F	Initial Concrete Temp., °F	Maximum Concrete Temp., °F	Maximum Temperature Difference, °F	Time of Maximum Temp. Diff., days
433	7	0	48	45	121	68	3.2
434	7	0	55	45	122	62	3.4
435	7	0	63	45	123	56	3.6
436	7	0	61	45	123	57	3.5
437	7	0	35	45	120	78	3.0
438	7	0	82	45	126	41	4.1
439	7	0	48	55	130	76	3.0
440	7	0	55	55	131	70	3.2
441	7	0	63	55	132	64	3.3
442	7	0	61	55	131	65	3.3
443	7	0	35	55	129	87	2.8
444	7	0	82	55	135	49	3.8
445	7	0	48	65	139	84	2.9
446	7	0	55	65	140	78	3.0
447	7	0	63	65	140	72	3.1
448	7	0	61	65	140	74	3.1
449	7	0	35	65	138	95	2.7
450	7	0	82	65	143	56	3.5
451	7	0	48	75	148	93	2.8
452	7	0	55	75	149	87	2.8
453	7	0	63	75	149	80	3.0
454	7	0	61	75	149	82	2.9
455	7	0	35	75	147	104	2.7
456	7	0	82	75	152	64	3.3

Table B1 - Predicted Temperatures and Temperature Differences for Concrete Piles

Case	Concrete Mix No.	Insulation R-Value	Average Air Temp., °F	Initial Concrete Temp., °F	Maximum Concrete Temp., °F	Maximum Temperature Difference, °F	Time of Maximum Temp. Diff., days
457	7	2	48	45	126	37	4.5
458	7	2	55	45	127	34	4.8
459	7	2	63	45	128	31	5.0
460	7	2	61	45	128	32	4.9
461	7	2	35	45	125	42	4.2
462	7	2	82	45	130	23	5.9
463	7	2	48	55	135	41	4.3
464	7	2	55	55	136	38	4.5
465	7	2	63	55	137	35	4.7
466	7	2	61	55	137	36	4.6
467	7	2	35	55	134	46	4.0
468	7	2	82	55	139	27	5.4
469	7	2	48	65	145	45	4.1
470	7	2	55	65	145	42	4.2
471	7	2	63	65	146	39	4.4
472	7	2	61	65	146	40	4.3
473	7	2	35	65	144	51	3.9
474	7	2	82	65	148	31	4.9
475	7	2	48	75	154	49	3.9
476	7	2	55	75	154	46	4.0
477	7	2	63	75	155	43	4.2
478	7	2	61	75	155	44	4.2
479	7	2	35	75	153	55	3.7
480	7	2	82	75	157	35	4.6

Table B1 - Predicted Temperatures and Temperature Differences for Concrete Piles

Case	Concrete Mix No.	Insulation R-Value	Average Air Temp., °F	Initial Concrete Temp., °F	Maximum Concrete Temp., °F	Maximum Temperature Difference, °F	Time of Maximum Temp. Diff., days
481	7	4	48	45	129	25	5.5
482	7	4	55	45	129	23	5.8
483	7	4	63	45	130	21	6.1
484	7	4	61	45	130	22	6.0
485	7	4	35	45	128	29	5.2
486	7	4	82	45	132	16	7.3
487	7	4	48	55	138	28	5.2
488	7	4	55	55	138	26	5.4
489	7	4	63	55	139	24	5.7
490	7	4	61	55	139	24	5.6
491	7	4	35	55	137	31	4.9
492	7	4	82	55	141	19	6.6
493	7	4	48	65	147	31	5.0
494	7	4	55	65	148	29	5.2
495	7	4	63	65	148	26	5.4
496	7	4	61	65	148	27	5.3
497	7	4	35	65	146	34	4.7
498	7	4	82	65	150	21	6.1
499	7	4	48	75	157	33	4.8
500	7	4	55	75	157	31	4.9
501	7	4	63	75	157	29	5.1
502	7	4	61	75	157	30	5.0
503	7	4	35	75	156	37	4.5
504	7	4	82	75	**159**	24	5.7

Table B1 - Predicted Temperatures and Temperature Differences for Concrete Piles

Case	Concrete Mix No.	Insulation R-Value	Average Air Temp., °F	Initial Concrete Temp., °F	Maximum Concrete Temp., °F	Maximum Temperature Difference, °F	Time of Maximum Temp. Diff., days
505	8	0	48	45	104	52	3.4
506	8	0	55	45	105	46	3.7
507	8	0	63	45	106	40	3.9
508	8	0	61	45	106	42	3.9
509	8	0	35	45	102	62	3.1
510	8	0	82	45	111	27	5.1
511	8	0	48	55	112	60	3.2
512	8	0	55	55	113	54	3.3
513	8	0	63	55	114	48	3.6
514	8	0	61	55	114	49	3.5
515	8	0	35	55	111	70	3.0
516	8	0	82	55	118	34	4.4
517	8	0	48	65	121	68	3.0
518	8	0	55	65	122	62	3.1
519	8	0	63	65	123	56	3.3
520	8	0	61	65	123	57	3.3
521	8	0	35	65	120	79	2.8
522	8	0	82	65	126	41	3.9
523	8	0	48	75	130	76	2.8
524	8	0	55	75	131	70	3.0
525	8	0	63	75	132	64	3.1
526	8	0	61	75	132	65	3.0
527	8	0	35	75	129	87	2.7
528	8	0	82	75	134	48	3.6

Table B1 - Predicted Temperatures and Temperature Differences for Concrete Piles

Case	Concrete Mix No.	Insulation R-Value	Average Air Temp., °F	Initial Concrete Temp., °F	Maximum Concrete Temp., °F	Maximum Temperature Difference, °F	Time of Maximum Temp. Diff., days
529	8	2	48	45	108	29	5.0
530	8	2	55	45	109	26	5.3
531	8	2	63	45	110	23	5.8
532	8	2	61	45	110	24	5.6
533	8	2	35	45	107	34	4.5
534	8	2	82	45	114	16	7.4
535	8	2	48	55	117	33	4.6
536	8	2	55	55	118	30	4.9
537	8	2	63	55	119	27	5.2
538	8	2	61	55	119	28	5.1
539	8	2	35	55	116	38	4.3
540	8	2	82	55	122	19	6.4
541	8	2	48	65	126	37	4.3
542	8	2	55	65	127	34	4.5
543	8	2	63	65	128	31	4.8
544	8	2	61	65	128	32	4.7
545	8	2	35	65	125	42	4.0
546	8	2	82	65	130	23	5.7
547	8	2	48	75	136	41	4.1
548	8	2	55	75	136	38	4.3
549	8	2	63	75	137	35	4.5
550	8	2	61	75	137	36	4.4
551	8	2	35	75	135	47	3.8
552	8	2	82	75	139	27	5.2

Table B1 - Predicted Temperatures and Temperature Differences for Concrete Piles

Case	Concrete Mix No.	Insulation R-Value	Average Air Temp., °F	Initial Concrete Temp., °F	Maximum Concrete Temp., °F	Maximum Temperature Difference, °F	Time of Maximum Temp. Diff., days
553	8	4	48	45	111	20	6.2
554	8	4	55	45	111	18	6.6
555	8	4	63	45	113	16	7.3
556	8	4	61	45	112	16	7.1
557	8	4	35	45	109	23	5.6
558	8	4	82	45	116	11	9.5
559	8	4	48	55	120	23	5.7
560	8	4	55	55	120	21	6.1
561	8	4	63	55	121	19	6.5
562	8	4	61	55	121	19	6.4
563	8	4	35	55	119	26	5.3
564	8	4	82	55	124	14	8.1
565	8	4	48	65	129	25	5.3
566	8	4	55	65	129	23	5.6
567	8	4	63	65	130	21	6.0
568	8	4	61	65	130	22	5.9
569	8	4	35	65	128	29	5.0
570	8	4	82	65	132	16	7.1
571	8	4	48	75	138	28	5.0
572	8	4	55	75	139	26	5.3
573	8	4	63	75	139	24	5.5
574	8	4	61	75	139	24	5.5
575	8	4	35	75	137	31	4.7
576	8	4	82	75	141	19	6.4

Table B1 - Predicted Temperatures and Temperature Differences for Concrete Piles

Case	Concrete Mix No.	Insulation R-Value	Average Air Temp., °F	Initial Concrete Temp., °F	Maximum Concrete Temp., °F	Maximum Temperature Difference, °F	Time of Maximum Temp. Diff., days
577	9	0	48	45	130	76	3.2
578	9	0	55	45	130	70	3.3
579	9	0	63	45	132	64	3.5
580	9	0	61	45	131	65	3.4
581	9	0	35	45	128	86	3.0
582	9	0	82	45	135	49	4.0
583	9	0	48	55	138	84	3.0
584	9	0	55	55	139	78	3.2
585	9	0	63	55	140	72	3.3
586	9	0	61	55	140	73	3.3
587	9	0	35	55	137	95	2.8
588	9	0	82	55	143	57	3.7
589	9	0	48	65	148	92	2.9
590	9	0	55	65	148	86	3.0
591	9	0	63	65	149	80	3.1
592	9	0	61	65	149	81	3.1
593	9	0	35	65	146	103	2.8
594	9	0	82	65	151	64	3.4
595	9	0	48	75	157	101	2.8
596	9	0	55	75	157	95	2.8
597	9	0	63	75	158	88	3.0
598	9	0	61	75	158	90	3.0
599	9	0	35	75	156	112	2.7
600	9	0	82	75	**160**	72	3.3

Table B1 - Predicted Temperatures and Temperature Differences for Concrete Piles

Case	Concrete Mix No.	Insulation R-Value	Average Air Temp., °F	Initial Concrete Temp., °F	Maximum Concrete Temp., °F	Maximum Temperature Difference, °F	Time of Maximum Temp. Diff., days
601	9	2	48	45	135	41	4.5
602	9	2	55	45	136	38	4.7
603	9	2	63	45	137	35	4.9
604	9	2	61	45	137	36	4.9
605	9	2	35	45	134	47	4.3
606	9	2	82	45	139	27	5.6
607	9	2	48	55	144	45	4.3
608	9	2	55	55	145	43	4.5
609	9	2	63	55	146	39	4.7
610	9	2	61	55	146	40	4.6
611	9	2	35	55	144	51	4.1
612	9	2	82	55	148	32	5.3
613	9	2	48	65	154	50	4.1
614	9	2	55	65	154	47	4.3
615	9	2	63	65	155	43	4.4
616	9	2	61	65	155	44	4.4
617	9	2	35	65	153	55	3.9
618	9	2	82	65	157	35	4.9
619	9	2	48	75	**163**	54	4.0
620	9	2	55	75	**164**	51	4.1
621	9	2	63	75	**164**	47	4.2
622	9	2	61	75	**164**	48	4.2
623	9	2	35	75	**162**	59	3.8
624	9	2	82	75	**166**	40	4.6

Table B1 - Predicted Temperatures and Temperature Differences for Concrete Piles

Case	Concrete Mix No.	Insulation R-Value	Average Air Temp., °F	Initial Concrete Temp., °F	Maximum Concrete Temp., °F	Maximum Temperature Difference, °F	Time of Maximum Temp. Diff., days
625	9	4	48	45	138	28	5.5
626	9	4	55	45	139	26	5.8
627	9	4	63	45	139	24	6.0
628	9	4	61	45	139	25	5.9
629	9	4	35	45	137	32	5.2
630	9	4	82	45	142	19	6.9
631	9	4	48	55	147	31	5.3
632	9	4	55	55	148	29	5.4
633	9	4	63	55	148	27	5.7
634	9	4	61	55	148	27	5.6
635	9	4	35	55	146	34	5.0
636	9	4	82	55	150	22	6.4
637	9	4	48	65	156	33	5.0
638	9	4	55	65	157	32	5.2
639	9	4	63	65	158	29	5.4
640	9	4	61	65	157	30	5.3
641	9	4	35	65	156	37	4.8
642	9	4	82	65	**159**	24	6.0
643	9	4	48	75	**166**	36	4.8
644	9	4	55	75	**166**	34	5.0
645	9	4	63	75	**167**	32	5.1
646	9	4	61	75	**167**	33	5.1
647	9	4	35	75	**165**	40	4.6
648	9	4	82	75	**168**	27	5.6

Table B1 - Predicted Temperatures and Temperature Differences for Concrete Piles

Case	Concrete Mix No.	Insulation R-Value	Average Air Temp., °F	Initial Concrete Temp., °F	Maximum Concrete Temp., °F	Maximum Temperature Difference, °F	Time of Maximum Temp. Diff., days
649	10	0	48	45	110	58	3.4
650	10	0	55	45	111	52	3.6
651	10	0	63	45	113	46	3.9
652	10	0	61	45	112	48	3.8
653	10	0	35	45	108	68	3.2
654	10	0	82	45	117	33	4.8
655	10	0	48	55	119	66	3.2
656	10	0	55	55	120	60	3.3
657	10	0	63	55	121	54	3.6
658	10	0	61	55	121	55	3.5
659	10	0	35	55	117	76	3.0
660	10	0	82	55	124	39	4.3
661	10	0	48	65	128	74	3.0
662	10	0	55	65	128	68	3.2
663	10	0	63	65	129	62	3.3
664	10	0	61	65	129	63	3.3
665	10	0	35	65	127	85	2.8
666	10	0	82	65	132	47	3.9
667	10	0	48	75	137	82	2.8
668	10	0	55	75	137	76	3.0
669	10	0	63	75	138	70	3.1
670	10	0	61	75	138	72	3.1
671	10	0	35	75	136	93	2.7
672	10	0	82	75	141	55	3.6

Table B1 - Predicted Temperatures and Temperature Differences for Concrete Piles

Case	Concrete Mix No.	Insulation R-Value	Average Air Temp., °F	Initial Concrete Temp., °F	Maximum Concrete Temp., °F	Maximum Temperature Difference, °F	Time of Maximum Temp. Diff., days
673	10	2	48	45	115	32	5.0
674	10	2	55	45	116	29	5.3
675	10	2	63	45	117	26	5.6
676	10	2	61	45	117	27	5.5
677	10	2	35	45	114	38	4.5
678	10	2	82	45	121	19	7.0
679	10	2	48	55	124	36	4.7
680	10	2	55	55	125	33	4.9
681	10	2	63	55	126	30	5.2
682	10	2	61	55	126	31	5.1
683	10	2	35	55	123	42	4.3
684	10	2	82	55	129	23	6.2
685	10	2	48	65	133	40	4.4
686	10	2	55	65	134	38	4.5
687	10	2	63	65	135	34	4.8
688	10	2	61	65	135	35	4.7
689	10	2	35	65	133	46	4.1
690	10	2	82	65	137	27	5.6
691	10	2	48	75	143	45	4.2
692	10	2	55	75	143	42	4.3
693	10	2	63	75	144	38	4.5
694	10	2	61	75	144	39	4.5
695	10	2	35	75	142	50	3.9
696	10	2	82	75	146	31	5.1

Table B1 - Predicted Temperatures and Temperature Differences for Concrete Piles

Case	Concrete Mix No.	Insulation R-Value	Average Air Temp., °F	Initial Concrete Temp., °F	Maximum Concrete Temp., °F	Maximum Temperature Difference, °F	Time of Maximum Temp. Diff., days
697	10	4	48	45	118	22	6.2
698	10	4	55	45	119	20	6.6
699	10	4	63	45	120	18	7.1
700	10	4	61	45	120	19	6.9
701	10	4	35	45	117	26	5.7
702	10	4	82	45	123	13	8.9
703	10	4	48	55	127	25	5.8
704	10	4	55	55	128	23	6.1
705	10	4	63	55	129	21	6.4
706	10	4	61	55	128	21	6.3
707	10	4	35	55	126	28	5.3
708	10	4	82	55	131	16	7.8
709	10	4	48	65	136	28	5.4
710	10	4	55	65	137	26	5.7
711	10	4	63	65	137	24	6.0
712	10	4	61	65	137	24	5.9
713	10	4	35	65	135	31	5.0
714	10	4	82	65	140	18	7.0
715	10	4	48	75	145	30	5.1
716	10	4	55	75	146	28	5.3
717	10	4	63	75	147	26	5.6
718	10	4	61	75	146	27	5.5
719	10	4	35	75	145	34	4.8
720	10	4	82	75	148	21	6.4

Table B1 - Predicted Temperatures and Temperature Differences for Concrete Piles

Case	Concrete Mix No.	Insulation R-Value	Average Air Temp., °F	Initial Concrete Temp., °F	Maximum Concrete Temp., °F	Maximum Temperature Difference, °F	Time of Maximum Temp. Diff., days
721	11	0	48	45	138	83	3.2
722	11	0	55	45	139	78	3.3
723	11	0	63	45	140	71	3.4
724	11	0	61	45	140	73	3.4
725	11	0	35	45	137	94	3.0
726	11	0	82	45	143	57	3.9
727	11	0	48	55	147	92	3.0
728	11	0	55	55	148	86	3.2
729	11	0	63	55	149	79	3.3
730	11	0	61	55	148	81	3.3
731	11	0	35	55	146	103	2.9
732	11	0	82	55	151	64	3.6
733	11	0	48	65	156	100	2.9
734	11	0	55	65	157	94	3.0
735	11	0	63	65	157	87	3.1
736	11	0	61	65	157	89	3.1
737	11	0	35	65	155	111	2.8
738	11	0	82	65	**160**	72	3.4
739	11	0	48	75	**165**	109	2.8
740	11	0	55	75	**166**	103	2.9
741	11	0	63	75	**166**	96	3.0
742	11	0	61	75	**166**	98	3.0
743	11	0	35	75	**164**	120	2.7
744	11	0	82	75	**168**	80	3.3

Table B1 - Predicted Temperatures and Temperature Differences for Concrete Piles

Case	Concrete Mix No.	Insulation R-Value	Average Air Temp., °F	Initial Concrete Temp., °F	Maximum Concrete Temp., °F	Maximum Temperature Difference, °F	Time of Maximum Temp. Diff., days
745	11	2	48	45	144	46	4.5
746	11	2	55	45	145	43	4.7
747	11	2	63	45	146	39	4.9
748	11	2	61	45	146	40	4.8
749	11	2	35	45	143	51	4.3
750	11	2	82	45	148	32	5.5
751	11	2	48	55	153	50	4.3
752	11	2	55	55	154	47	4.5
753	11	2	63	55	155	43	4.6
754	11	2	61	55	155	44	4.6
755	11	2	35	55	152	55	4.1
756	11	2	82	55	157	36	5.1
757	11	2	48	65	**163**	54	4.2
758	11	2	55	65	**163**	51	4.3
759	11	2	63	65	**164**	48	4.4
760	11	2	61	65	**164**	48	4.4
761	11	2	35	65	**162**	59	4.0
762	11	2	82	65	**166**	40	4.9
763	11	2	48	75	**172**	58	4.0
764	11	2	55	75	**172**	55	4.1
765	11	2	63	75	**173**	52	4.2
766	11	2	61	75	**173**	53	4.2
767	11	2	35	75	**171**	63	3.8
768	11	2	82	75	**175**	44	4.6

Table B1 - Predicted Temperatures and Temperature Differences for Concrete Piles

Case	Concrete Mix No.	Insulation R-Value	Average Air Temp., °F	Initial Concrete Temp., °F	Maximum Concrete Temp., °F	Maximum Temperature Difference, °F	Time of Maximum Temp. Diff., days
769	11	4	48	45	147	31	5.5
770	11	4	55	45	148	29	5.7
771	11	4	63	45	149	27	6.0
772	11	4	61	45	148	27	5.9
773	11	4	35	45	146	34	5.2
774	11	4	82	45	151	22	6.8
775	11	4	48	55	156	34	5.3
776	11	4	55	55	157	32	5.4
777	11	4	63	55	158	30	5.7
778	11	4	61	55	157	30	5.6
779	11	4	35	55	156	37	5.0
780	11	4	82	55	**160**	24	6.3
781	11	4	48	65	**166**	36	5.0
782	11	4	55	65	**166**	34	5.2
783	11	4	63	65	**167**	32	5.4
784	11	4	61	65	**167**	33	5.3
785	11	4	35	65	**165**	40	4.8
786	11	4	82	65	**169**	27	5.9
787	11	4	48	75	**175**	39	4.8
788	11	4	55	75	**176**	37	5.0
789	11	4	63	75	**176**	35	5.2
790	11	4	61	75	**176**	35	5.1
791	11	4	35	75	**174**	43	4.7
792	11	4	82	75	**178**	30	5.6

Table B1 - Predicted Temperatures and Temperature Differences for Concrete Piles

Case	Concrete Mix No.	Insulation R-Value	Average Air Temp., °F	Initial Concrete Temp., °F	Maximum Concrete Temp., °F	Maximum Temperature Difference, °F	Time of Maximum Temp. Diff., days
793	12	0	48	45	117	64	3.4
794	12	0	55	45	118	58	3.6
795	12	0	63	45	119	52	3.8
796	12	0	61	45	119	53	3.8
797	12	0	35	45	115	74	3.2
798	12	0	82	45	123	38	4.6
799	12	0	48	55	125	72	3.2
800	12	0	55	55	126	66	3.3
801	12	0	63	55	127	60	3.6
802	12	0	61	55	127	61	3.5
803	12	0	35	55	124	82	3.0
804	12	0	82	55	131	45	4.1
805	12	0	48	65	134	80	3.0
806	12	0	55	65	135	74	3.2
807	12	0	63	65	136	68	3.3
808	12	0	61	65	136	69	3.3
809	12	0	35	65	133	91	2.8
810	12	0	82	65	139	53	3.8
811	12	0	48	75	143	88	2.9
812	12	0	55	75	144	82	3.0
813	12	0	63	75	145	76	3.2
814	12	0	61	75	145	77	3.1
815	12	0	35	75	142	99	2.8
816	12	0	82	75	147	60	3.5

Table B1 - Predicted Temperatures and Temperature Differences for Concrete Piles

Case	Concrete Mix No.	Insulation R-Value	Average Air Temp., °F	Initial Concrete Temp., °F	Maximum Concrete Temp., °F	Maximum Temperature Difference, °F	Time of Maximum Temp. Diff., days
817	12	2	48	45	122	36	5.0
818	12	2	55	45	123	33	5.2
819	12	2	63	45	124	30	5.6
820	12	2	61	45	124	30	5.4
821	12	2	35	45	121	41	4.6
822	12	2	82	45	128	22	6.7
823	12	2	48	55	131	40	4.7
824	12	2	55	55	132	37	4.9
825	12	2	63	55	133	34	5.1
826	12	2	61	55	133	34	5.1
827	12	2	35	55	130	45	4.3
828	12	2	82	55	136	26	6.0
829	12	2	48	65	140	44	4.4
830	12	2	55	65	141	41	4.6
831	12	2	63	65	142	38	4.8
832	12	2	61	65	142	38	4.8
833	12	2	35	65	139	49	4.2
834	12	2	82	65	144	30	5.5
835	12	2	48	75	150	48	4.2
836	12	2	55	75	150	45	4.3
837	12	2	63	75	151	42	4.5
838	12	2	61	75	151	43	4.5
839	12	2	35	75	149	53	4.0
840	12	2	82	75	153	34	5.1

Table B1 - Predicted Temperatures and Temperature Differences for Concrete Piles

Case	Concrete Mix No.	Insulation R-Value	Average Air Temp., °F	Initial Concrete Temp., °F	Maximum Concrete Temp., °F	Maximum Temperature Difference, °F	Time of Maximum Temp. Diff., days
841	12	4	48	45	125	24	6.2
842	12	4	55	45	126	23	6.5
843	12	4	63	45	127	21	7.0
844	12	4	61	45	127	21	6.9
845	12	4	35	45	124	28	5.7
846	12	4	82	45	130	16	8.5
847	12	4	48	55	134	27	5.8
848	12	4	55	55	135	25	6.1
849	12	4	63	55	136	23	6.4
850	12	4	61	55	136	24	6.3
851	12	4	35	55	133	31	5.4
852	12	4	82	55	138	18	7.6
853	12	4	48	65	143	30	5.5
854	12	4	55	65	144	28	5.7
855	12	4	63	65	145	26	6.0
856	12	4	61	65	145	26	5.9
857	12	4	35	65	142	33	5.1
858	12	4	82	65	147	21	6.9
859	12	4	48	75	153	33	5.2
860	12	4	55	75	153	31	5.4
861	12	4	63	75	154	29	5.6
862	12	4	61	75	154	29	5.5
863	12	4	35	75	152	36	4.9
864	12	4	82	75	156	23	6.4

Table B2 - Predicted Temperatures and Temperature Differences for Concrete Pile Caps Considering Concrete and Concrete with Internal Cooling

Case	Concrete Mix No.	Insulation R-Value	Average Air Temp., °F	Initial Concrete Temp., °F	Water and Precast Concrete Shell Temp., °F	Concrete Only			Cooling Pipes at 610-mm On-Center		
						Maximum Concrete Temp., °F	Maximum Temperature Difference, °F	Time of Maximum Temp. Diff., days	Maximum Concrete Temp., °F	Maximum Temeprature Difference, °F	Time of Maximum Temp. Diff., days
1	1	0	48	45	50	105	55	8.2	83	30	1.7
2	1	0	55	45	55	105	48	8.6	84	25	1.8
3	1	0	63	45	65	106	41	9.5	88	22	2.1
4	1	0	61	45	60	105	43	9.0	86	22	1.9
5	1	0	35	45	44	104	67	7.7	81	39	1.6
6	1	0	82	45	74	107	26	11.3	93	13	2.4
7	1	0	48	55	50	114	64	7.6	89	35	1.5
8	1	0	55	55	55	114	57	7.9	91	31	1.6
9	1	0	63	55	65	115	50	8.5	94	27	1.8
10	1	0	61	55	60	115	52	8.3	93	27	1.7
11	1	0	35	55	44	114	76	7.3	88	45	1.5
12	1	0	82	55	74	116	33	9.8	98	16	2.0
13	1	0	48	65	50	124	73	7.2	96	41	1.4
14	1	0	55	65	55	124	66	7.4	98	37	1.5
15	1	0	63	65	65	124	59	7.9	101	32	1.6
16	1	0	61	65	60	124	61	7.7	99	33	1.5
17	1	0	35	65	44	123	85	6.9	95	51	1.3
18	1	0	82	65	74	125	42	8.8	104	20	1.8
19	1	0	48	75	50	133	82	6.8	104	48	1.3
20	1	0	55	75	55	134	76	7.0	105	43	1.3
21	1	0	63	75	65	134	68	7.4	108	38	1.5
22	1	0	61	75	60	134	70	7.2	106	39	1.4
23	1	0	35	75	44	133	94	6.6	102	58	1.2
24	1	0	82	75	74	135	51	8.0	111	25	1.6

Table B2 - Predicted Temperatures and Temperature Differences for Concrete Pile Caps Considering Concrete and Concrete with Internal Cooling

Case	Concrete Mix No.	Insulation R-Value	Average Air Temp., °F	Initial Concrete Temp., °F	Water and Precast Concrete Shell Temp., °F	Concrete Only			Cooling Pipes at 610-mm On-Center		
						Maximum Concrete Temp., °F	Maximum Temperature Difference, °F	Time of Maximum Temp. Diff., days	Maximum Concrete Temp., °F	Maximum Temeprature Difference, °F	Time of Maximum Temp. Diff., days
25	1	2	48	45	50	105	45	9.2	83	22	1.7
26	1	2	55	45	55	106	41	9.7	84	20	1.8
27	1	2	63	45	65	106	35	10.7	88	16	2.1
28	1	2	61	45	60	106	38	10.3	86	18	1.9
29	1	2	35	45	44	105	55	8.7	81	25	1.6
30	1	2	82	45	74	108	27	12.9	94	14	2.6
31	1	2	48	55	50	115	53	8.5	89	26	1.5
32	1	2	55	55	55	115	49	8.9	91	24	1.6
33	1	2	63	55	65	116	42	9.6	94	20	1.8
34	1	2	61	55	60	115	45	9.3	93	22	1.7
35	1	2	35	55	44	115	62	8.1	88	29	1.5
36	1	2	82	55	74	117	35	11.0	99	17	2.2
37	1	2	48	65	50	124	60	8.0	96	31	1.4
38	1	2	55	65	55	125	56	8.3	98	29	1.5
39	1	2	63	65	65	125	49	8.8	101	24	1.6
40	1	2	61	65	60	125	53	8.6	99	26	1.5
41	1	2	35	65	44	124	69	7.7	95	34	1.3
42	1	2	82	65	74	126	42	9.8	105	21	1.9
43	1	2	48	75	50	134	68	7.6	104	36	1.3
44	1	2	55	75	55	134	64	7.8	105	34	1.3
45	1	2	63	75	65	135	56	8.3	108	29	1.5
46	1	2	61	75	60	134	60	8.0	106	31	1.4
47	1	2	35	75	44	134	76	7.3	102	39	1.2
48	1	2	82	75	74	135	49	9.0	111	25	1.7

Table B2 - Predicted Temperatures and Temperature Differences for Concrete Pile Caps Considering Concrete and Concrete with Internal Cooling

Case	Concrete Mix No.	Insulation R-Value	Average Air Temp., °F	Initial Concrete Temp., °F	Water and Precast Concrete Shell Temp., °F	Concrete Only			Cooling Pipes at 610-mm On-Center		
						Maximum Concrete Temp., °F	Maximum Temperature Difference, °F	Time of Maximum Temp. Diff., days	Maximum Concrete Temp., °F	Maximum Temeprature Difference, °F	Time of Maximum Temp. Diff., days
49	1	4	48	45	50	106	46	9.9	84	23	1.9
50	1	4	55	45	55	106	42	10.4	86	21	2.0
51	1	4	63	45	65	107	35	11.5	89	17	2.3
52	1	4	61	45	60	107	38	11.0	88	19	2.2
53	1	4	35	45	44	105	51	9.3	81	25	1.7
54	1	4	82	45	74	108	28	13.9	94	15	2.8
55	1	4	48	55	50	115	53	9.1	91	28	1.7
56	1	4	55	55	55	116	50	9.5	93	26	1.8
57	1	4	63	55	65	116	42	10.3	96	21	2.0
58	1	4	61	55	60	116	46	9.9	94	24	2.0
59	1	4	35	55	44	115	58	8.6	89	30	1.6
60	1	4	82	55	74	117	35	11.9	100	18	2.4
61	1	4	48	65	50	125	61	8.5	98	33	1.5
62	1	4	55	65	55	125	57	8.8	100	31	1.6
63	1	4	63	65	65	125	50	9.5	102	26	1.8
64	1	4	61	65	60	125	53	9.2	101	28	1.8
65	1	4	35	65	44	124	66	8.1	96	36	1.5
66	1	4	82	65	74	126	43	10.6	106	23	2.1
67	1	4	48	75	50	134	68	8.1	106	38	1.5
68	1	4	55	75	55	135	65	8.3	107	36	1.5
69	1	4	63	75	65	135	57	8.8	109	30	1.6
70	1	4	61	75	60	135	61	8.6	109	33	1.5
71	1	4	35	75	44	134	73	7.8	104	41	1.3
72	1	4	82	75	74	136	50	9.6	113	27	1.8

Table B2 - Predicted Temperatures and Temperature Differences for Concrete Pile Caps Considering Concrete and Concrete with Internal Cooling

Case	Concrete Mix No.	Insulation R-Value	Average Air Temp., °F	Initial Concrete Temp., °F	Water and Precast Concrete Shell Temp., °F	Concrete Only			Cooling Pipes at 610-mm On-Center		
						Maximum Concrete Temp., °F	Maximum Temperature Difference, °F	Time of Maximum Temp. Diff., days	Maximum Concrete Temp., °F	Maximum Temeprature Difference, °F	Time of Maximum Temp. Diff., days
73	2	0	48	45	50	93	43	9.3	74	22	1.9
74	2	0	55	45	55	93	37	10.1	76	18	2.1
75	2	0	63	45	65	94	30	11.8	80	15	2.5
76	2	0	61	45	60	94	32	11.0	78	15	2.3
77	2	0	35	45	44	92	55	8.6	72	32	1.7
78	2	0	82	45	74	97	18	16.3	87	9	2.2
79	2	0	48	55	50	102	52	8.4	80	28	1.6
80	2	0	55	55	55	102	46	8.9	82	23	1.7
81	2	0	63	55	65	103	39	10.0	86	20	2.1
82	2	0	61	55	60	103	40	9.5	84	20	1.9
83	2	0	35	55	44	101	64	7.8	78	37	1.5
84	2	0	82	55	74	105	25	12.5	90	11	2.4
85	2	0	48	65	50	111	61	7.8	87	34	1.5
86	2	0	55	65	55	112	55	8.1	89	29	1.5
87	2	0	63	65	65	112	47	8.8	92	25	1.7
88	2	0	61	65	60	112	49	8.5	90	25	1.6
89	2	0	35	65	44	111	73	7.3	85	43	1.3
90	2	0	82	65	74	113	31	10.4	95	14	2.0
91	2	0	48	75	50	121	70	7.3	94	40	1.3
92	2	0	55	75	55	121	64	7.5	96	35	1.4
93	2	0	63	75	65	121	56	8.1	99	31	1.5
94	2	0	61	75	60	121	58	7.8	97	31	1.5
95	2	0	35	75	44	120	82	6.9	93	50	1.2
96	2	0	82	75	74	122	39	9.1	102	18	1.7

Table B2 - Predicted Temperatures and Temperature Differences for Concrete Pile Caps Considering Concrete and Concrete with Internal Cooling

Case	Concrete Mix No.	Insulation R-Value	Average Air Temp., °F	Initial Concrete Temp., °F	Water and Precast Concrete Shell Temp., °F	Concrete Only			Cooling Pipes at 610-mm On-Center		
						Maximum Concrete Temp., °F	Maximum Temperature Difference, °F	Time of Maximum Temp. Diff., days	Maximum Concrete Temp., °F	Maximum Temeprature Difference, °F	Time of Maximum Temp. Diff., days
97	2	2	48	45	50	93	36	10.8	74	16	1.9
98	2	2	55	45	55	94	32	11.6	76	14	2.1
99	2	2	63	45	65	95	26	13.7	80	10	2.5
100	2	2	61	45	60	94	29	12.7	78	12	2.3
101	2	2	35	45	44	93	46	9.8	72	18	1.7
102	2	2	82	45	74	97	19	19.2	87	10	3.2
103	2	2	48	55	50	103	43	9.6	80	20	1.6
104	2	2	55	55	55	103	39	10.2	82	18	1.7
105	2	2	63	55	65	104	33	11.5	86	14	2.1
106	2	2	61	55	60	103	36	10.9	84	16	1.9
107	2	2	35	55	44	102	53	8.9	78	23	1.5
108	2	2	82	55	74	105	26	14.6	91	12	2.7
109	2	2	48	65	50	112	51	8.8	87	25	1.5
110	2	2	55	65	55	112	47	9.2	89	23	1.5
111	2	2	63	65	65	113	40	10.1	92	18	1.7
112	2	2	61	65	60	113	43	9.7	90	20	1.6
113	2	2	35	65	44	112	60	8.3	85	28	1.3
114	2	2	82	65	74	114	33	12.0	96	15	2.1
115	2	2	48	75	50	122	58	8.2	94	30	1.3
116	2	2	55	75	55	122	54	8.5	96	27	1.4
117	2	2	63	75	65	122	47	9.2	99	23	1.5
118	2	2	61	75	60	122	50	8.8	97	25	1.5
119	2	2	35	75	44	121	67	7.8	93	33	1.2
120	2	2	82	75	74	123	40	10.4	102	19	1.8

Table B2 - Predicted Temperatures and Temperature Differences for Concrete Pile Caps Considering Concrete and Concrete with Internal Cooling

Case	Concrete Mix No.	Insulation R-Value	Average Air Temp., °F	Initial Concrete Temp., °F	Water and Precast Concrete Shell Temp., °F	Concrete Only			Cooling Pipes at 610-mm On-Center		
						Maximum Concrete Temp., °F	Maximum Temperature Difference, °F	Time of Maximum Temp. Diff., days	Maximum Concrete Temp., °F	Maximum Temeprature Difference, °F	Time of Maximum Temp. Diff., days
121	2	4	48	45	50	94	37	11.7	75	17	2.1
122	2	4	55	45	55	94	33	12.7	77	15	2.3
123	2	4	63	45	65	95	26	15.1	81	11	2.8
124	2	4	61	45	60	95	29	14.0	79	13	2.6
125	2	4	35	45	44	93	43	10.6	72	19	1.8
126	2	4	82	45	74	98	20	20.0	87	10	3.5
127	2	4	48	55	50	103	44	10.4	82	22	1.8
128	2	4	55	55	55	103	40	11.0	83	19	2.0
129	2	4	63	55	65	104	33	12.6	87	15	2.3
130	2	4	61	55	60	104	36	11.9	85	17	2.2
131	2	4	35	55	44	103	50	9.6	79	24	1.7
132	2	4	82	55	74	106	26	16.1	92	13	2.9
133	2	4	48	65	50	112	51	9.5	89	26	1.6
134	2	4	55	65	55	113	47	9.9	90	24	1.8
135	2	4	63	65	65	113	40	11.0	93	19	1.9
136	2	4	61	65	60	113	44	10.5	92	22	1.9
137	2	4	35	65	44	112	56	8.9	87	29	1.5
138	2	4	82	65	74	114	33	13.2	98	17	2.3
139	2	4	48	75	50	122	59	8.8	96	32	1.5
140	2	4	55	75	55	122	55	9.2	98	29	1.5
141	2	4	63	75	65	123	48	9.9	100	24	1.7
142	2	4	61	75	60	122	51	9.5	99	27	1.6
143	2	4	35	75	44	122	64	8.3	94	34	1.3
144	2	4	82	75	74	124	41	11.3	104	21	2.0

Table B2 - Predicted Temperatures and Temperature Differences for Concrete Pile Caps Considering Concrete and Concrete with Internal Cooling

Case	Concrete Mix No.	Insulation R-Value	Average Air Temp., °F	Initial Concrete Temp., °F	Water and Precast Concrete Shell Temp., °F	Concrete Only			Cooling Pipes at 610-mm On-Center		
						Maximum Concrete Temp., °F	Maximum Temperature Difference, °F	Time of Maximum Temp. Diff., days	Maximum Concrete Temp., °F	Maximum Temeprature Difference, °F	Time of Maximum Temp. Diff., days
145	3	0	48	45	50	115	64	8.2	89	35	1.7
146	3	0	55	45	55	115	58	8.5	90	30	1.8
147	3	0	63	45	65	116	51	9.2	94	27	2.0
148	3	0	61	45	60	115	52	8.8	92	27	1.9
149	3	0	35	45	44	114	76	7.8	87	44	1.6
150	3	0	82	45	74	117	34	10.5	98	17	2.2
151	3	0	48	55	50	124	73	7.6	95	40	1.5
152	3	0	55	55	55	124	67	7.9	97	36	1.6
153	3	0	63	55	65	125	60	8.5	100	32	1.8
154	3	0	61	55	60	125	61	8.2	99	32	1.7
155	3	0	35	55	44	124	85	7.3	94	50	1.5
156	3	0	82	55	74	126	42	9.4	104	20	1.9
157	3	0	48	65	50	134	82	7.3	102	47	1.5
158	3	0	55	65	55	134	76	7.5	104	42	1.5
159	3	0	63	65	65	134	69	7.9	107	38	1.6
160	3	0	61	65	60	134	70	7.7	105	38	1.5
161	3	0	35	65	44	133	95	7.0	101	56	1.4
162	3	0	82	65	74	135	51	8.6	110	24	1.8
163	3	0	48	75	50	143	92	6.9	110	53	1.3
164	3	0	55	75	55	143	85	7.1	111	48	1.4
165	3	0	63	75	65	144	78	7.4	114	43	1.5
166	3	0	61	75	60	144	80	7.3	112	44	1.5
167	3	0	35	75	44	143	104	6.7	108	63	1.3
168	3	0	82	75	74	144	60	8.0	117	30	1.6

Table B2 - Predicted Temperatures and Temperature Differences for Concrete Pile Caps Considering Concrete and Concrete with Internal Cooling

Case	Concrete Mix No.	Insulation R-Value	Average Air Temp., °F	Initial Concrete Temp., °F	Water and Precast Concrete Shell Temp., °F	Concrete Only			Cooling Pipes at 610-mm On-Center		
						Maximum Concrete Temp., °F	Maximum Temperature Difference, °F	Time of Maximum Temp. Diff., days	Maximum Concrete Temp., °F	Maximum Temeprature Difference, °F	Time of Maximum Temp. Diff., days
169	3	2	48	45	50	115	53	9.2	89	26	1.7
170	3	2	55	45	55	116	50	9.6	90	24	1.8
171	3	2	63	45	65	116	43	10.4	94	20	2.0
172	3	2	61	45	60	116	46	10.0	92	22	1.9
173	3	2	35	45	44	115	63	8.7	87	29	1.6
174	3	2	82	45	74	118	35	11.9	99	17	2.4
175	3	2	48	55	50	125	61	8.6	95	30	1.5
176	3	2	55	55	55	125	57	8.9	97	28	1.6
177	3	2	63	55	65	126	50	9.5	100	24	1.8
178	3	2	61	55	60	125	53	9.3	99	26	1.7
179	3	2	35	55	44	125	70	8.2	94	33	1.5
180	3	2	82	55	74	127	43	10.7	105	21	2.1
181	3	2	48	65	50	134	68	8.1	102	35	1.5
182	3	2	55	65	55	135	64	8.3	104	33	1.5
183	3	2	63	65	65	135	57	8.8	107	28	1.6
184	3	2	61	65	60	135	61	8.7	105	30	1.5
185	3	2	35	65	44	134	77	7.8	101	38	1.4
186	3	2	82	65	74	136	50	9.7	111	25	1.9
187	3	2	48	75	50	144	76	7.7	110	40	1.3
188	3	2	55	75	55	144	72	8.0	111	38	1.4
189	3	2	63	75	65	145	64	8.3	114	33	1.5
190	3	2	61	75	60	144	68	8.2	112	35	1.5
191	3	2	35	75	44	144	84	7.5	108	43	1.3
192	3	2	82	75	74	145	57	9.0	117	29	1.7

Table B2 - Predicted Temperatures and Temperature Differences for Concrete Pile Caps Considering Concrete and Concrete with Internal Cooling

Case	Concrete Mix No.	Insulation R-Value	Average Air Temp., °F	Initial Concrete Temp., °F	Water and Precast Concrete Shell Temp., °F	Concrete Only			Cooling Pipes at 610-mm On-Center		
						Maximum Concrete Temp., °F	Maximum Temperature Difference, °F	Time of Maximum Temp. Diff., days	Maximum Concrete Temp., °F	Maximum Temeprature Difference, °F	Time of Maximum Temp. Diff., days
193	3	4	48	45	50	116	54	9.8	90	27	1.9
194	3	4	55	45	55	116	50	10.3	92	25	2.0
195	3	4	63	45	65	117	43	11.1	95	21	2.3
196	3	4	61	45	60	117	47	10.8	94	23	2.2
197	3	4	35	45	44	115	59	9.3	88	30	1.8
198	3	4	82	45	74	118	36	12.8	100	19	2.6
199	3	4	48	55	50	125	62	9.2	97	32	1.8
200	3	4	55	55	55	126	58	9.5	99	30	1.8
201	3	4	63	55	65	126	50	10.2	102	25	2.0
202	3	4	61	55	60	126	54	9.9	100	28	1.9
203	3	4	35	55	44	125	66	8.7	95	35	1.6
204	3	4	82	55	74	127	43	11.5	106	23	2.3
205	3	4	48	65	50	135	69	8.7	104	37	1.6
206	3	4	55	65	55	135	65	8.9	106	35	1.7
207	3	4	63	65	65	136	58	9.5	109	30	1.8
208	3	4	61	65	60	135	61	9.2	107	33	1.8
209	3	4	35	65	44	134	74	8.3	102	40	1.5
210	3	4	82	65	74	136	51	10.4	113	27	2.0
211	3	4	48	75	50	144	77	8.2	112	42	1.5
212	3	4	55	75	55	145	73	8.5	113	40	1.5
213	3	4	63	75	65	145	65	8.9	116	35	1.7
214	3	4	61	75	60	145	69	8.7	115	38	1.6
215	3	4	35	75	44	144	81	7.9	110	45	1.4
216	3	4	82	75	74	146	58	9.6	119	32	1.8

Table B2 - Predicted Temperatures and Temperature Differences for Concrete Pile Caps Considering Concrete and Concrete with Internal Cooling

Case	Concrete Mix No.	Insulation R-Value	Average Air Temp., °F	Initial Concrete Temp., °F	Water and Precast Concrete Shell Temp., °F	Concrete Only			Cooling Pipes at 610-mm On-Center		
						Maximum Concrete Temp., °F	Maximum Temperature Difference, °F	Time of Maximum Temp. Diff., days	Maximum Concrete Temp., °F	Maximum Temeprature Difference, °F	Time of Maximum Temp. Diff., days
217	4	0	48	45	50	100	51	9.3	78	26	1.9
218	4	0	55	45	55	101	44	9.9	80	22	2.0
219	4	0	63	45	65	102	38	11.3	85	19	2.4
220	4	0	61	45	60	101	39	10.6	82	18	2.2
221	4	0	35	45	44	100	63	8.6	76	36	1.7
222	4	0	82	45	74	104	24	14.3	90	11	2.6
223	4	0	48	55	50	110	60	8.4	85	32	1.7
224	4	0	55	55	55	110	53	8.9	86	27	1.7
225	4	0	63	55	65	111	46	9.8	90	23	2.0
226	4	0	61	55	60	110	48	9.4	88	23	1.9
227	4	0	35	55	44	109	72	7.9	83	41	1.5
228	4	0	82	55	74	112	31	11.7	94	14	2.3
229	4	0	48	65	50	119	69	7.9	92	37	1.5
230	4	0	55	65	55	119	62	8.2	93	33	1.5
231	4	0	63	65	65	120	55	8.8	96	29	1.7
232	4	0	61	65	60	120	57	8.6	95	29	1.7
233	4	0	35	65	44	119	81	7.4	90	47	1.4
234	4	0	82	65	74	121	38	10.1	100	17	2.0
235	4	0	48	75	50	129	78	7.4	99	44	1.3
236	4	0	55	75	55	129	71	7.6	100	39	1.4
237	4	0	63	75	65	129	64	8.1	103	34	1.5
238	4	0	61	75	60	129	66	7.9	102	35	1.5
239	4	0	35	75	44	128	90	7.1	97	53	1.3
240	4	0	82	75	74	130	47	9.0	106	21	1.7

Table B2 - Predicted Temperatures and Temperature Differences for Concrete Pile Caps Considering Concrete and Concrete with Internal Cooling

Case	Concrete Mix No.	Insulation R-Value	Average Air Temp., °F	Initial Concrete Temp., °F	Water and Precast Concrete Shell Temp., °F	Concrete Only			Cooling Pipes at 610-mm On-Center		
						Maximum Concrete Temp., °F	Maximum Temperature Difference, °F	Time of Maximum Temp. Diff., days	Maximum Concrete Temp., °F	Maximum Temeprature Difference, °F	Time of Maximum Temp. Diff., days
241	4	2	48	45	50	101	43	10.7	78	19	1.9
242	4	2	55	45	55	102	39	11.4	80	17	2.0
243	4	2	63	45	65	103	32	13.0	85	13	2.4
244	4	2	61	45	60	102	35	12.3	82	15	2.2
245	4	2	35	45	44	101	52	9.8	76	21	1.7
246	4	2	82	45	74	105	25	16.7	91	12	3.0
247	4	2	48	55	50	111	50	9.7	85	23	1.7
248	4	2	55	55	55	111	46	10.2	86	21	1.7
249	4	2	63	55	65	112	39	11.3	90	17	2.0
250	4	2	61	55	60	111	42	10.8	88	19	1.9
251	4	2	35	55	44	110	59	9.1	83	26	1.5
252	4	2	82	55	74	113	32	13.6	95	15	2.4
253	4	2	48	65	50	120	57	9.0	92	28	1.5
254	4	2	55	65	55	120	53	9.3	93	26	1.5
255	4	2	63	65	65	121	46	10.2	96	21	1.7
256	4	2	61	65	60	121	50	9.8	95	23	1.7
257	4	2	35	65	44	120	66	8.5	90	31	1.4
258	4	2	82	65	74	122	39	11.7	101	18	2.1
259	4	2	48	75	50	129	65	8.4	99	33	1.3
260	4	2	55	75	55	130	61	8.7	100	30	1.4
261	4	2	63	75	65	130	53	9.3	103	26	1.5
262	4	2	61	75	60	130	57	9.0	102	28	1.5
263	4	2	35	75	44	129	74	8.0	97	36	1.3
264	4	2	82	75	74	131	46	10.4	107	22	1.8

Table B2 - Predicted Temperatures and Temperature Differences for Concrete Pile Caps Considering Concrete and Concrete with Internal Cooling

Case	Concrete Mix No.	Insulation R-Value	Average Air Temp., °F	Initial Concrete Temp., °F	Water and Precast Concrete Shell Temp., °F	Concrete Only			Cooling Pipes at 610-mm On-Center		
						Maximum Concrete Temp., °F	Maximum Temperature Difference, °F	Time of Maximum Temp. Diff., days	Maximum Concrete Temp., °F	Maximum Temeprature Difference, °F	Time of Maximum Temp. Diff., days
265	4	4	48	45	50	102	43	11.6	79	20	2.1
266	4	4	55	45	55	102	40	12.4	82	18	2.3
267	4	4	63	45	65	103	32	14.3	85	14	2.6
268	4	4	61	45	60	103	36	13.4	84	16	2.5
269	4	4	35	45	44	101	49	10.6	77	22	1.9
270	4	4	82	45	74	105	26	18.6	91	12	3.3
271	4	4	48	55	50	111	51	10.5	86	25	1.9
272	4	4	55	55	55	111	47	11.0	88	23	2.0
273	4	4	63	55	65	112	40	12.3	91	18	2.3
274	4	4	61	55	60	112	43	11.8	90	21	2.1
275	4	4	35	55	44	111	56	9.8	84	27	1.7
276	4	4	82	55	74	114	33	15.0	96	16	2.7
277	4	4	48	65	50	120	58	9.7	93	30	1.6
278	4	4	55	65	55	121	54	10.1	95	27	1.8
279	4	4	63	65	65	121	47	11.0	98	22	2.0
280	4	4	61	65	60	121	50	10.5	97	25	1.9
281	4	4	35	65	44	120	63	9.1	91	32	1.5
282	4	4	82	65	74	122	40	12.8	102	20	2.3
283	4	4	48	75	50	130	65	9.0	101	35	1.5
284	4	4	55	75	55	130	62	9.3	102	32	1.6
285	4	4	63	75	65	131	54	10.0	105	27	1.8
286	4	4	61	75	60	130	58	9.7	104	30	1.7
287	4	4	35	75	44	130	70	8.6	99	37	1.4
288	4	4	82	75	74	132	47	11.3	109	24	2.0

Table B2 - Predicted Temperatures and Temperature Differences for Concrete Pile Caps Considering Concrete and Concrete with Internal Cooling

Case	Concrete Mix No.	Insulation R-Value	Average Air Temp., °F	Initial Concrete Temp., °F	Water and Precast Concrete Shell Temp., °F	Concrete Only			Cooling Pipes at 610-mm On-Center		
						Maximum Concrete Temp., °F	Maximum Temperature Difference, °F	Time of Maximum Temp. Diff., days	Maximum Concrete Temp., °F	Maximum Temeprature Difference, °F	Time of Maximum Temp. Diff., days
289	5	0	48	45	50	124	74	8.1	95	40	1.7
290	5	0	55	45	55	125	67	8.4	96	35	1.8
291	5	0	63	45	65	125	60	9.0	100	32	1.9
292	5	0	61	45	60	125	62	8.7	98	32	1.9
293	5	0	35	45	44	124	86	7.8	93	49	1.6
294	5	0	82	45	74	127	43	10.0	104	20	2.1
295	5	0	48	55	50	134	83	7.7	101	45	1.5
296	5	0	55	55	55	134	76	7.9	103	41	1.6
297	5	0	63	55	65	135	69	8.3	106	37	1.8
298	5	0	61	55	60	134	71	8.2	105	37	1.7
299	5	0	35	55	44	134	95	7.4	99	55	1.5
300	5	0	82	55	74	136	52	9.1	110	24	1.9
301	5	0	48	65	50	143	92	7.3	108	52	1.5
302	5	0	55	65	55	144	86	7.5	110	47	1.5
303	5	0	63	65	65	144	78	7.9	113	43	1.6
304	5	0	61	65	60	144	80	7.8	111	43	1.5
305	5	0	35	65	44	143	104	7.1	107	61	1.4
306	5	0	82	65	74	145	61	8.5	116	29	1.8
307	5	0	48	75	50	153	101	7.1	115	58	1.3
308	5	0	55	75	55	153	95	7.2	117	53	1.4
309	5	0	63	75	65	154	87	7.5	120	49	1.5
310	5	0	61	75	60	153	89	7.4	118	49	1.5
311	5	0	35	75	44	153	113	6.8	114	68	1.3
312	5	0	82	75	74	154	70	8.0	123	35	1.6

Table B2 - Predicted Temperatures and Temperature Differences for Concrete Pile Caps Considering Concrete and Concrete with Internal Cooling

Case	Concrete Mix No.	Insulation R-Value	Average Air Temp., °F	Initial Concrete Temp., °F	Water and Precast Concrete Shell Temp., °F	Concrete Only			Cooling Pipes at 610-mm On-Center		
						Maximum Concrete Temp., °F	Maximum Temperature Difference, °F	Time of Maximum Temp. Diff., days	Maximum Concrete Temp., °F	Maximum Temeprature Difference, °F	Time of Maximum Temp. Diff., days
313	5	2	48	45	50	125	61	9.1	95	30	1.7
314	5	2	55	45	55	126	58	9.4	96	28	1.8
315	5	2	63	45	65	126	50	10.1	100	24	1.9
316	5	2	61	45	60	126	54	9.8	98	26	1.9
317	5	2	35	45	44	125	71	8.7	93	33	1.6
318	5	2	82	45	74	127	43	11.3	105	21	2.3
319	5	2	48	55	50	135	69	8.6	101	34	1.5
320	5	2	55	55	55	135	65	8.9	103	32	1.6
321	5	2	63	55	65	136	58	9.4	106	28	1.8
322	5	2	61	55	60	135	61	9.2	105	30	1.7
323	5	2	35	55	44	134	78	8.3	99	37	1.5
324	5	2	82	55	74	137	51	10.3	110	25	2.0
325	5	2	48	65	50	144	76	8.2	108	39	1.5
326	5	2	55	65	55	145	72	8.4	110	37	1.5
327	5	2	63	65	65	145	65	8.8	113	32	1.6
328	5	2	61	65	60	145	69	8.7	111	34	1.5
329	5	2	35	65	44	144	85	7.9	107	42	1.4
330	5	2	82	65	74	146	58	9.6	117	29	1.8
331	5	2	48	75	50	154	84	7.8	115	44	1.3
332	5	2	55	75	55	154	80	8.0	117	42	1.4
333	5	2	63	75	65	155	73	8.4	120	37	1.5
334	5	2	61	75	60	154	76	8.2	118	39	1.5
335	5	2	35	75	44	154	92	7.6	114	47	1.3
336	5	2	82	75	74	155	65	9.0	123	33	1.7

Table B2 - Predicted Temperatures and Temperature Differences for Concrete Pile Caps Considering Concrete and Concrete with Internal Cooling

Case	Concrete Mix No.	Insulation R-Value	Average Air Temp., °F	Initial Concrete Temp., °F	Water and Precast Concrete Shell Temp., °F	Concrete Only			Cooling Pipes at 610-mm On-Center		
						Maximum Concrete Temp., °F	Maximum Temperature Difference, °F	Time of Maximum Temp. Diff., days	Maximum Concrete Temp., °F	Maximum Temeprature Difference, °F	Time of Maximum Temp. Diff., days
337	5	4	48	45	50	126	62	9.8	96	32	1.9
338	5	4	55	45	55	126	59	10.1	98	30	2.0
339	5	4	63	45	65	127	51	10.9	101	25	2.2
340	5	4	61	45	60	127	55	10.6	100	28	2.1
341	5	4	35	45	44	125	67	9.3	94	34	1.8
342	5	4	82	45	74	128	44	12.2	106	23	2.5
343	5	4	48	55	50	135	70	9.2	103	37	1.8
344	5	4	55	55	55	136	66	9.5	105	34	1.8
345	5	4	63	55	65	136	59	10.1	108	29	2.0
346	5	4	61	55	60	136	62	9.8	107	32	1.9
347	5	4	35	55	44	135	75	8.8	101	39	1.7
348	5	4	82	55	74	137	52	11.2	112	27	2.2
349	5	4	48	65	50	145	77	8.7	111	41	1.6
350	5	4	55	65	55	145	73	9.0	112	39	1.7
351	5	4	63	65	65	146	66	9.5	115	34	1.8
352	5	4	61	65	60	145	70	9.2	114	37	1.8
353	5	4	35	65	44	145	82	8.4	108	44	1.5
354	5	4	82	65	74	146	59	10.3	119	31	2.0
355	5	4	48	75	50	154	85	8.3	118	47	1.5
356	5	4	55	75	55	155	81	8.5	119	44	1.5
357	5	4	63	75	65	155	74	9.0	122	39	1.7
358	5	4	61	75	60	155	77	8.8	121	42	1.6
359	5	4	35	75	44	154	90	8.1	116	49	1.5
360	5	4	82	75	74	156	66	9.6	126	36	1.8

Table B2 - Predicted Temperatures and Temperature Differences for Concrete Pile Caps Considering Concrete and Concrete with Internal Cooling

Case	Concrete Mix No.	Insulation R-Value	Average Air Temp., °F	Initial Concrete Temp., °F	Water and Precast Concrete Shell Temp., °F	Concrete Only			Cooling Pipes at 610-mm On-Center		
						Maximum Concrete Temp., °F	Maximum Temperature Difference, °F	Time of Maximum Temp. Diff., days	Maximum Concrete Temp., °F	Maximum Temeprature Difference, °F	Time of Maximum Temp. Diff., days
361	6	0	48	45	50	108	58	9.2	83	30	1.9
362	6	0	55	45	55	109	52	9.7	85	25	1.9
363	6	0	63	45	65	110	45	10.8	89	22	2.3
364	6	0	61	45	60	109	47	10.3	87	22	2.1
365	6	0	35	45	44	108	70	8.7	81	39	1.7
366	6	0	82	45	74	111	30	13.1	94	14	2.5
367	6	0	48	55	50	117	67	8.5	89	35	1.7
368	6	0	55	55	55	118	61	8.9	91	31	1.7
369	6	0	63	55	65	119	54	9.7	95	27	1.9
370	6	0	61	55	60	118	55	9.3	93	27	1.9
371	6	0	35	55	44	117	79	8.1	87	45	1.5
372	6	0	82	55	74	120	37	11.2	99	17	2.2
373	6	0	48	65	50	127	76	7.9	96	41	1.5
374	6	0	55	65	55	127	70	8.3	98	37	1.6
375	6	0	63	65	65	128	63	8.8	101	33	1.7
376	6	0	61	65	60	128	64	8.6	99	33	1.7
377	6	0	35	65	44	126	88	7.6	94	51	1.5
378	6	0	82	65	74	129	45	9.9	104	20	1.9
379	6	0	48	75	50	136	85	7.6	103	47	1.4
380	6	0	55	75	55	137	79	7.8	105	43	1.5
381	6	0	63	75	65	137	72	8.3	108	38	1.6
382	6	0	61	75	60	137	73	8.0	106	39	1.5
383	6	0	35	75	44	136	97	7.3	101	57	1.3
384	6	0	82	75	74	138	54	9.1	111	25	1.7

Table B2 - Predicted Temperatures and Temperature Differences for Concrete Pile Caps Considering Concrete and Concrete with Internal Cooling

Case	Concrete Mix No.	Insulation R-Value	Average Air Temp., °F	Initial Concrete Temp., °F	Water and Precast Concrete Shell Temp., °F	Concrete Only			Cooling Pipes at 610-mm On-Center		
						Maximum Concrete Temp., °F	Maximum Temperature Difference, °F	Time of Maximum Temp. Diff., days	Maximum Concrete Temp., °F	Maximum Temeprature Difference, °F	Time of Maximum Temp. Diff., days
385	6	2	48	45	50	109	49	10.6	83	22	1.9
386	6	2	55	45	55	110	45	11.2	85	20	1.9
387	6	2	63	45	65	111	39	12.5	89	16	2.3
388	6	2	61	45	60	110	42	11.9	87	18	2.1
389	6	2	35	45	44	109	59	9.8	81	24	1.7
390	6	2	82	45	74	113	32	15.3	95	14	2.8
391	6	2	48	55	50	119	56	9.7	89	26	1.7
392	6	2	55	55	55	119	52	10.2	91	24	1.7
393	6	2	63	55	65	120	46	11.1	95	20	1.9
394	6	2	61	55	60	119	49	10.7	93	22	1.9
395	6	2	35	55	44	118	66	9.2	87	29	1.5
396	6	2	82	55	74	121	39	13.0	100	18	2.4
397	6	2	48	65	50	128	64	9.1	96	31	1.5
398	6	2	55	65	55	128	60	9.4	98	28	1.6
399	6	2	63	65	65	129	53	10.2	101	24	1.7
400	6	2	61	65	60	129	56	9.8	99	26	1.7
401	6	2	35	65	44	127	73	8.7	94	34	1.5
402	6	2	82	65	74	130	46	11.5	105	21	2.1
403	6	2	48	75	50	137	71	8.5	103	36	1.4
404	6	2	55	75	55	138	67	8.8	105	33	1.5
405	6	2	63	75	65	138	60	9.4	108	28	1.6
406	6	2	61	75	60	138	63	9.1	106	31	1.5
407	6	2	35	75	44	137	80	8.2	101	39	1.3
408	6	2	82	75	74	139	53	10.4	111	25	1.8

Table B2 - Predicted Temperatures and Temperature Differences for Concrete Pile Caps Considering Concrete and Concrete with Internal Cooling

Case	Concrete Mix No.	Insulation R-Value	Average Air Temp., °F	Initial Concrete Temp., °F	Water and Precast Concrete Shell Temp., °F	Concrete Only			Cooling Pipes at 610-mm On-Center		
						Maximum Concrete Temp., °F	Maximum Temperature Difference, °F	Time of Maximum Temp. Diff., days	Maximum Concrete Temp., °F	Maximum Temeprature Difference, °F	Time of Maximum Temp. Diff., days
409	6	4	48	45	50	110	50	11.5	84	23	2.1
410	6	4	55	45	55	110	46	12.3	86	21	2.2
411	6	4	63	45	65	111	39	13.8	90	17	2.5
412	6	4	61	45	60	111	43	13.0	88	20	2.4
413	6	4	35	45	44	109	55	10.7	81	25	1.9
414	6	4	82	45	74	113	33	16.9	96	15	3.0
415	6	4	48	55	50	119	57	10.5	91	28	1.9
416	6	4	55	55	55	119	53	11.0	93	26	2.0
417	6	4	63	55	65	120	46	12.1	96	21	2.2
418	6	4	61	55	60	120	50	11.6	95	24	2.1
419	6	4	35	55	44	119	62	9.9	88	30	1.7
420	6	4	82	55	74	122	40	14.3	101	19	2.6
421	6	4	48	65	50	128	65	9.8	98	33	1.7
422	6	4	55	65	55	129	61	10.2	100	31	1.8
423	6	4	63	65	65	129	54	11.0	102	26	2.0
424	6	4	61	65	60	129	57	10.6	101	28	1.9
425	6	4	35	65	44	128	69	9.3	96	35	1.5
426	6	4	82	65	74	131	47	12.5	107	23	2.3
427	6	4	48	75	50	138	72	9.2	105	38	1.5
428	6	4	55	75	55	138	68	9.5	107	36	1.6
429	6	4	63	75	65	139	61	10.2	109	30	1.8
430	6	4	61	75	60	138	65	9.8	108	33	1.7
431	6	4	35	75	44	138	77	8.8	103	41	1.5
432	6	4	82	75	74	140	54	11.3	113	27	2.0

Table B2 - Predicted Temperatures and Temperature Differences for Concrete Pile Caps Considering Concrete and Concrete with Internal Cooling

Case	Concrete Mix No.	Insulation R-Value	Average Air Temp., °F	Initial Concrete Temp., °F	Water and Precast Concrete Shell Temp., °F	Concrete Only			Cooling Pipes at 610-mm On-Center		
						Maximum Concrete Temp., °F	Maximum Temperature Difference, °F	Time of Maximum Temp. Diff., days	Maximum Concrete Temp., °F	Maximum Temeprature Difference, °F	Time of Maximum Temp. Diff., days
433	7	0	48	45	50	134	83	8.1	100	45	1.7
434	7	0	55	45	55	135	77	8.3	102	41	1.8
435	7	0	63	45	65	135	70	8.8	106	37	1.9
436	7	0	61	45	60	135	71	8.6	104	37	1.8
437	7	0	35	45	44	134	95	7.8	98	55	1.6
438	7	0	82	45	74	136	52	9.7	110	24	2.0
439	7	0	48	55	50	144	92	7.7	107	51	1.5
440	7	0	55	55	55	144	86	7.9	109	46	1.6
441	7	0	63	55	65	145	79	8.3	112	42	1.8
442	7	0	61	55	60	144	80	8.2	110	42	1.7
443	7	0	35	55	44	143	105	7.4	105	60	1.5
444	7	0	82	55	74	145	61	9.0	116	29	1.9
445	7	0	48	65	50	153	102	7.4	114	57	1.5
446	7	0	55	65	55	154	95	7.6	116	52	1.5
447	7	0	63	65	65	154	88	7.9	119	48	1.6
448	7	0	61	65	60	154	90	7.8	117	48	1.5
449	7	0	35	65	44	153	114	7.1	112	66	1.4
450	7	0	82	65	74	155	70	8.4	122	34	1.8
451	7	0	48	75	50	**163**	111	7.1	121	63	1.4
452	7	0	55	75	55	**163**	104	7.3	123	58	1.5
453	7	0	63	75	65	**164**	97	7.6	126	54	1.5
454	7	0	61	75	60	**163**	99	7.4	124	54	1.5
455	7	0	35	75	44	**163**	123	6.9	120	73	1.3
456	7	0	82	75	74	**164**	79	8.0	128	40	1.6

Table B2 - Predicted Temperatures and Temperature Differences for Concrete Pile Caps Considering Concrete and Concrete with Internal Cooling

Case	Concrete Mix No.	Insulation R-Value	Average Air Temp., °F	Initial Concrete Temp., °F	Water and Precast Concrete Shell Temp., °F	Concrete Only			Cooling Pipes at 610-mm On-Center		
						Maximum Concrete Temp., °F	Maximum Temperature Difference, °F	Time of Maximum Temp. Diff., days	Maximum Concrete Temp., °F	Maximum Temeprature Difference, °F	Time of Maximum Temp. Diff., days
457	7	2	48	45	50	135	70	9.1	100	34	1.7
458	7	2	55	45	55	136	66	9.4	102	32	1.8
459	7	2	63	45	65	136	58	10.0	106	28	1.9
460	7	2	61	45	60	136	62	9.7	104	30	1.8
461	7	2	35	45	44	135	79	8.7	98	37	1.6
462	7	2	82	45	74	137	52	11.0	110	25	2.2
463	7	2	48	55	50	145	77	8.7	107	38	1.5
464	7	2	55	55	55	145	73	8.9	109	36	1.6
465	7	2	63	55	65	146	66	9.4	112	32	1.8
466	7	2	61	55	60	145	69	9.1	110	34	1.7
467	7	2	35	55	44	144	86	8.3	105	41	1.5
468	7	2	82	55	74	147	59	10.2	116	29	1.9
469	7	2	48	65	50	154	84	8.3	114	43	1.5
470	7	2	55	65	55	155	81	8.5	116	41	1.5
471	7	2	63	65	65	155	73	8.8	119	36	1.6
472	7	2	61	65	60	155	77	8.7	117	38	1.5
473	7	2	35	65	44	154	93	8.0	112	46	1.4
474	7	2	82	65	74	156	66	9.5	122	33	1.8
475	7	2	48	75	50	**164**	92	8.0	121	48	1.4
476	7	2	55	75	55	**164**	88	8.2	123	45	1.5
477	7	2	63	75	65	**165**	81	8.5	126	41	1.5
478	7	2	61	75	60	**164**	84	8.3	124	43	1.5
479	7	2	35	75	44	**164**	100	7.7	120	51	1.3
480	7	2	82	75	74	**165**	74	9.0	129	37	1.7

Table B2 - Predicted Temperatures and Temperature Differences for Concrete Pile Caps Considering Concrete and Concrete with Internal Cooling

Case	Concrete Mix No.	Insulation R-Value	Average Air Temp., °F	Initial Concrete Temp., °F	Water and Precast Concrete Shell Temp., °F	Concrete Only			Cooling Pipes at 610-mm On-Center		
						Maximum Concrete Temp., °F	Maximum Temperature Difference, °F	Time of Maximum Temp. Diff., days	Maximum Concrete Temp., °F	Maximum Temeprature Difference, °F	Time of Maximum Temp. Diff., days
481	7	4	48	45	50	136	71	9.8	103	36	1.9
482	7	4	55	45	55	136	67	10.1	104	34	2.0
483	7	4	63	45	65	137	59	10.7	108	29	2.2
484	7	4	61	45	60	137	63	10.4	106	32	2.1
485	7	4	35	45	44	136	75	9.3	100	38	1.8
486	7	4	82	45	74	138	52	11.8	112	27	2.4
487	7	4	48	55	50	145	78	9.2	110	41	1.8
488	7	4	55	55	55	146	74	9.5	111	39	1.8
489	7	4	63	55	65	146	67	10.0	114	34	2.0
490	7	4	61	55	60	146	70	9.8	113	36	1.9
491	7	4	35	55	44	145	83	8.9	107	43	1.7
492	7	4	82	55	74	147	60	10.9	119	31	2.2
493	7	4	48	65	50	155	86	8.8	117	46	1.6
494	7	4	55	65	55	155	82	9.0	118	43	1.7
495	7	4	63	65	65	156	74	9.5	121	38	1.8
496	7	4	61	65	60	155	78	9.3	120	41	1.8
497	7	4	35	65	44	155	90	8.5	115	48	1.5
498	7	4	82	65	74	156	67	10.1	125	35	2.0
499	7	4	48	75	50	**164**	93	8.5	124	51	1.5
500	7	4	55	75	55	**165**	89	8.7	126	49	1.6
501	7	4	63	75	65	**165**	82	9.0	128	43	1.7
502	7	4	61	75	60	**165**	85	8.8	127	46	1.6
503	7	4	35	75	44	**164**	98	8.2	122	53	1.5
504	7	4	82	75	74	**166**	75	9.6	132	40	1.8

Table B2 - Predicted Temperatures and Temperature Differences for Concrete Pile Caps Considering Concrete and Concrete with Internal Cooling

Case	Concrete Mix No.	Insulation R-Value	Average Air Temp., °F	Initial Concrete Temp., °F	Water and Precast Concrete Shell Temp., °F	Concrete Only			Cooling Pipes at 610-mm On-Center		
						Maximum Concrete Temp., °F	Maximum Temperature Difference, °F	Time of Maximum Temp. Diff., days	Maximum Concrete Temp., °F	Maximum Temeprature Difference, °F	Time of Maximum Temp. Diff., days
505	8	0	48	45	50	116	66	9.2	87	34	1.8
506	8	0	55	45	55	117	60	9.7	89	29	1.9
507	8	0	63	45	65	117	53	10.5	93	26	2.2
508	8	0	61	45	60	117	54	10.1	91	26	2.1
509	8	0	35	45	44	115	78	8.7	85	43	1.7
510	8	0	82	45	74	119	36	12.3	98	16	2.4
511	8	0	48	55	50	125	75	8.6	94	39	1.7
512	8	0	55	55	55	126	68	8.9	95	35	1.7
513	8	0	63	55	65	126	61	9.6	99	31	1.9
514	8	0	61	55	60	126	63	9.3	97	31	1.8
515	8	0	35	55	44	125	87	8.1	92	49	1.6
516	8	0	82	55	74	128	44	10.8	103	19	2.1
517	8	0	48	65	50	135	84	8.1	100	45	1.5
518	8	0	55	65	55	135	77	8.3	102	40	1.6
519	8	0	63	65	65	136	70	8.8	105	36	1.7
520	8	0	61	65	60	135	72	8.6	104	37	1.7
521	8	0	35	65	44	134	96	7.7	99	55	1.5
522	8	0	82	65	74	137	53	9.8	109	24	1.9
523	8	0	48	75	50	144	93	7.6	107	51	1.4
524	8	0	55	75	55	144	86	7.9	109	46	1.5
525	8	0	63	75	65	145	79	8.3	112	42	1.6
526	8	0	61	75	60	145	81	8.1	110	42	1.5
527	8	0	35	75	44	144	105	7.4	106	61	1.3
528	8	0	82	75	74	146	62	9.0	115	28	1.7

Table B2 - Predicted Temperatures and Temperature Differences for Concrete Pile Caps Considering Concrete and Concrete with Internal Cooling

Case	Concrete Mix No.	Insulation R-Value	Average Air Temp., °F	Initial Concrete Temp., °F	Water and Precast Concrete Shell Temp., °F	Concrete Only			Cooling Pipes at 610-mm On-Center		
						Maximum Concrete Temp., °F	Maximum Temperature Difference, °F	Time of Maximum Temp. Diff., days	Maximum Concrete Temp., °F	Maximum Temeprature Difference, °F	Time of Maximum Temp. Diff., days
529	8	2	48	45	50	117	55	10.6	87	25	1.8
530	8	2	55	45	55	118	52	11.1	89	23	1.9
531	8	2	63	45	65	119	45	12.2	93	19	2.2
532	8	2	61	45	60	118	48	11.7	91	21	2.1
533	8	2	35	45	44	117	65	9.9	85	27	1.7
534	8	2	82	45	74	120	38	14.3	99	17	2.6
535	8	2	48	55	50	127	63	9.8	94	29	1.7
536	8	2	55	55	55	127	59	10.2	95	27	1.7
537	8	2	63	55	65	128	52	11.0	99	23	1.9
538	8	2	61	55	60	127	55	10.6	97	25	1.8
539	8	2	35	55	44	126	72	9.3	92	32	1.6
540	8	2	82	55	74	129	45	12.5	104	20	2.3
541	8	2	48	65	50	136	70	9.2	100	34	1.5
542	8	2	55	65	55	136	66	9.5	102	31	1.6
543	8	2	63	65	65	137	59	10.2	105	27	1.7
544	8	2	61	65	60	137	63	9.8	104	29	1.7
545	8	2	35	65	44	135	79	8.8	99	37	1.5
546	8	2	82	65	74	138	52	11.3	110	24	2.0
547	8	2	48	75	50	145	78	8.7	107	39	1.4
548	8	2	55	75	55	146	74	9.0	109	36	1.5
549	8	2	63	75	65	146	66	9.5	112	31	1.6
550	8	2	61	75	60	146	70	9.2	110	34	1.5
551	8	2	35	75	44	145	86	8.3	106	42	1.3
552	8	2	82	75	74	147	59	10.3	116	28	1.8

Table B2 - Predicted Temperatures and Temperature Differences for Concrete Pile Caps Considering Concrete and Concrete with Internal Cooling

Case	Concrete Mix No.	Insulation R-Value	Average Air Temp., °F	Initial Concrete Temp., °F	Water and Precast Concrete Shell Temp., °F	Concrete Only			Cooling Pipes at 610-mm On-Center		
						Maximum Concrete Temp., °F	Maximum Temperature Difference, °F	Time of Maximum Temp. Diff., days	Maximum Concrete Temp., °F	Maximum Temeprature Difference, °F	Time of Maximum Temp. Diff., days
553	8	4	48	45	50	118	57	11.5	89	27	2.1
554	8	4	55	45	55	118	53	12.1	91	25	2.2
555	8	4	63	45	65	119	46	13.3	95	20	2.5
556	8	4	61	45	60	119	49	12.8	93	23	2.3
557	8	4	35	45	44	117	61	10.7	86	29	1.9
558	8	4	82	45	74	121	39	15.9	100	18	2.9
559	8	4	48	55	50	127	64	10.6	96	31	1.9
560	8	4	55	55	55	128	60	11.0	97	29	2.0
561	8	4	63	55	65	128	53	12.0	101	24	2.2
562	8	4	61	55	60	128	56	11.6	99	27	2.1
563	8	4	35	55	44	127	69	10.0	93	33	1.7
564	8	4	82	55	74	130	46	13.8	106	22	2.5
565	8	4	48	65	50	136	71	9.9	103	36	1.7
566	8	4	55	65	55	137	68	10.3	104	34	1.8
567	8	4	63	65	65	137	60	11.0	107	29	2.0
568	8	4	61	65	60	137	64	10.7	106	32	1.9
569	8	4	35	65	44	136	76	9.5	100	38	1.6
570	8	4	82	65	74	139	53	12.3	112	26	2.2
571	8	4	48	75	50	146	79	9.3	110	41	1.6
572	8	4	55	75	55	146	75	9.7	111	39	1.6
573	8	4	63	75	65	147	68	10.2	114	34	1.8
574	8	4	61	75	60	147	71	10.0	113	36	1.8
575	8	4	35	75	44	146	84	9.0	108	44	1.5
576	8	4	82	75	74	148	61	11.3	118	31	2.0

Table B2 - Predicted Temperatures and Temperature Differences for Concrete Pile Caps Considering Concrete and Concrete with Internal Cooling

Case	Concrete Mix No.	Insulation R-Value	Average Air Temp., °F	Initial Concrete Temp., °F	Water and Precast Concrete Shell Temp., °F	Concrete Only			Cooling Pipes at 610-mm On-Center		
						Maximum Concrete Temp., °F	Maximum Temperature Difference, °F	Time of Maximum Temp. Diff., days	Maximum Concrete Temp., °F	Maximum Temeprature Difference, °F	Time of Maximum Temp. Diff., days
577	9	0	48	45	50	144	93	8.1	107	50	1.7
578	9	0	55	45	55	145	87	8.3	108	46	1.8
579	9	0	63	45	65	145	79	8.7	112	42	1.9
580	9	0	61	45	60	145	81	8.5	110	42	1.8
581	9	0	35	45	44	144	105	7.8	105	60	1.6
582	9	0	82	45	74	146	62	9.5	116	29	2.0
583	9	0	48	55	50	154	102	7.8	113	56	1.5
584	9	0	55	55	55	154	96	7.9	115	51	1.6
585	9	0	63	55	65	155	88	8.3	118	47	1.8
586	9	0	61	55	60	154	90	8.1	117	48	1.7
587	9	0	35	55	44	153	114	7.5	111	65	1.5
588	9	0	82	55	74	155	71	8.8	122	34	1.9
589	9	0	48	65	50	**163**	111	7.4	120	62	1.5
590	9	0	55	65	55	**164**	105	7.6	122	57	1.5
591	9	0	63	65	65	**164**	97	7.9	125	53	1.6
592	9	0	61	65	60	**164**	99	7.8	123	53	1.5
593	9	0	35	65	44	**163**	123	7.3	119	72	1.5
594	9	0	82	65	74	**165**	80	8.4	128	39	1.7
595	9	0	48	75	50	**173**	120	7.2	127	68	1.4
596	9	0	55	75	55	**173**	114	7.3	129	63	1.5
597	9	0	63	75	65	**174**	107	7.6	132	59	1.5
598	9	0	61	75	60	**173**	108	7.4	130	59	1.5
599	9	0	35	75	44	**173**	133	7.0	126	78	1.3
600	9	0	82	75	74	**174**	89	8.0	135	45	1.6

Table B2 - Predicted Temperatures and Temperature Differences for Concrete Pile Caps Considering Concrete and Concrete with Internal Cooling

Case	Concrete Mix No.	Insulation R-Value	Average Air Temp., °F	Initial Concrete Temp., °F	Water and Precast Concrete Shell Temp., °F	Concrete Only			Cooling Pipes at 610-mm On-Center		
						Maximum Concrete Temp., °F	Maximum Temperature Difference, °F	Time of Maximum Temp. Diff., days	Maximum Concrete Temp., °F	Maximum Temeprature Difference, °F	Time of Maximum Temp. Diff., days
601	9	2	48	45	50	146	78	9.1	107	38	1.7
602	9	2	55	45	55	146	74	9.3	108	36	1.8
603	9	2	63	45	65	147	67	9.8	112	32	1.9
604	9	2	61	45	60	146	70	9.6	110	34	1.8
605	9	2	35	45	44	145	87	8.7	105	41	1.6
606	9	2	82	45	74	147	60	10.7	116	29	2.1
607	9	2	48	55	50	155	85	8.7	113	42	1.5
608	9	2	55	55	55	155	81	8.9	115	40	1.6
609	9	2	63	55	65	156	74	9.3	118	36	1.8
610	9	2	61	55	60	156	78	9.1	117	38	1.7
611	9	2	35	55	44	155	94	8.4	111	45	1.5
612	9	2	82	55	74	157	67	10.0	122	33	1.9
613	9	2	48	65	50	**165**	93	8.3	120	47	1.5
614	9	2	55	65	55	**165**	89	8.5	122	45	1.5
615	9	2	63	65	65	**165**	81	8.8	125	40	1.6
616	9	2	61	65	60	**165**	85	8.7	123	42	1.5
617	9	2	35	65	44	**164**	101	8.1	119	50	1.5
618	9	2	82	65	74	**166**	74	9.4	128	37	1.8
619	9	2	48	75	50	**174**	100	8.0	127	52	1.4
620	9	2	55	75	55	**174**	96	8.2	129	50	1.5
621	9	2	63	75	65	**175**	89	8.5	132	45	1.5
622	9	2	61	75	60	**175**	93	8.3	130	47	1.5
623	9	2	35	75	44	**174**	108	7.8	126	55	1.3
624	9	2	82	75	74	**175**	82	9.0	135	41	1.7

Table B2 - Predicted Temperatures and Temperature Differences for Concrete Pile Caps Considering Concrete and Concrete with Internal Cooling

Case	Concrete Mix No.	Insulation R-Value	Average Air Temp., °F	Initial Concrete Temp., °F	Water and Precast Concrete Shell Temp., °F	Concrete Only			Cooling Pipes at 610-mm On-Center		
						Maximum Concrete Temp., °F	Maximum Temperature Difference, °F	Time of Maximum Temp. Diff., days	Maximum Concrete Temp., °F	Maximum Temeprature Difference, °F	Time of Maximum Temp. Diff., days
625	9	4	48	45	50	146	79	9.7	109	40	1.9
626	9	4	55	45	55	146	75	10.0	111	38	2.0
627	9	4	63	45	65	147	68	10.6	114	34	2.1
628	9	4	61	45	60	147	71	10.3	113	36	2.0
629	9	4	35	45	44	146	84	9.3	106	43	1.8
630	9	4	82	45	74	148	61	11.5	119	31	2.3
631	9	4	48	55	50	156	86	9.3	116	45	1.8
632	9	4	55	55	55	156	83	9.5	118	43	1.8
633	9	4	63	55	65	156	75	9.9	121	38	2.0
634	9	4	61	55	60	156	79	9.8	119	41	1.9
635	9	4	35	55	44	155	91	9.0	114	47	1.7
636	9	4	82	55	74	157	68	10.7	125	35	2.2
637	9	4	48	65	50	**165**	94	8.9	123	50	1.7
638	9	4	55	65	55	**165**	90	9.1	125	48	1.7
639	9	4	63	65	65	**166**	83	9.5	127	43	1.8
640	9	4	61	65	60	**166**	86	9.3	126	46	1.8
641	9	4	35	65	44	**165**	99	8.6	121	53	1.6
642	9	4	82	65	74	**167**	76	10.1	131	40	2.0
643	9	4	48	75	50	**175**	101	8.5	130	55	1.5
644	9	4	55	75	55	**175**	98	8.7	132	53	1.6
645	9	4	63	75	65	**175**	90	9.0	134	48	1.7
646	9	4	61	75	60	**175**	94	8.9	133	50	1.7
647	9	4	35	75	44	**174**	106	8.3	128	58	1.5
648	9	4	82	75	74	**176**	83	9.6	138	44	1.8

Table B2 - Predicted Temperatures and Temperature Differences for Concrete Pile Caps Considering Concrete and Concrete with Internal Cooling

Case	Concrete Mix No.	Insulation R-Value	Average Air Temp., °F	Initial Concrete Temp., °F	Water and Precast Concrete Shell Temp., °F	Concrete Only			Cooling Pipes at 610-mm On-Center		
						Maximum Concrete Temp., °F	Maximum Temperature Difference, °F	Time of Maximum Temp. Diff., days	Maximum Concrete Temp., °F	Maximum Temeprature Difference, °F	Time of Maximum Temp. Diff., days
649	10	0	48	45	50	124	73	9.2	92	38	1.8
650	10	0	55	45	55	124	67	9.5	94	33	1.9
651	10	0	63	45	65	125	60	10.3	98	30	2.1
652	10	0	61	45	60	125	62	10.0	96	30	2.0
653	10	0	35	45	44	123	85	8.7	90	47	1.7
654	10	0	82	45	74	127	43	11.8	102	19	2.3
655	10	0	48	55	50	133	82	8.6	98	43	1.7
656	10	0	55	55	55	134	76	8.9	100	39	1.7
657	10	0	63	55	65	134	69	9.5	104	35	1.9
658	10	0	61	55	60	134	71	9.2	102	35	1.8
659	10	0	35	55	44	133	94	8.2	96	53	1.6
660	10	0	82	55	74	136	52	10.6	107	23	2.1
661	10	0	48	65	50	143	91	8.1	105	49	1.5
662	10	0	55	65	55	143	85	8.4	107	44	1.6
663	10	0	63	65	65	144	78	8.9	110	40	1.7
664	10	0	61	65	60	143	80	8.6	108	40	1.7
665	10	0	35	65	44	142	103	7.8	103	59	1.5
666	10	0	82	65	74	145	61	9.7	113	27	1.9
667	10	0	48	75	50	152	100	7.8	112	55	1.5
668	10	0	55	75	55	152	94	7.9	113	50	1.5
669	10	0	63	75	65	153	87	8.3	117	46	1.6
670	10	0	61	75	60	153	89	8.2	115	46	1.5
671	10	0	35	75	44	152	113	7.5	110	65	1.4
672	10	0	82	75	74	154	69	9.0	120	32	1.7

Table B3 - Predicted Temperatures and Temperature Differences for Concrete Pier Shafts

Case	Concrete Mix No.	Insulation R-Value	Average Air Temp., °F	Initial Concrete Temp., °F	Maximum Concrete Temp., °F	Maximum Temeprature Difference, °F	Time of Maximum Temp. Diff., days
793	12	0	48	45	113	61	3.0
794	12	0	55	45	114	55	3.2
795	12	0	63	45	116	50	3.4
796	12	0	61	45	115	51	3.3
797	12	0	35	45	111	71	2.8
798	12	0	82	45	121	36	4.2
799	12	0	48	55	121	69	2.8
800	12	0	55	55	122	63	3.0
801	12	0	63	55	124	57	3.2
802	12	0	61	55	123	58	3.1
803	12	0	35	55	120	79	2.6
804	12	0	82	55	128	43	3.7
805	12	0	48	65	130	77	2.7
806	12	0	55	65	131	71	2.8
807	12	0	63	65	132	65	2.9
808	12	0	61	65	132	66	2.9
809	12	0	35	65	128	87	2.5
810	12	0	82	65	136	50	3.4
811	12	0	48	75	139	85	2.5
812	12	0	55	75	140	79	2.6
813	12	0	63	75	141	73	2.8
814	12	0	61	75	140	74	2.7
815	12	0	35	75	137	96	2.4
816	12	0	82	75	144	58	3.1

Table B2 - Predicted Temperatures and Temperature Differences for Concrete Pile Caps Considering Concrete and Concrete with Internal Cooling

Case	Concrete Mix No.	Insulation R-Value	Average Air Temp., °F	Initial Concrete Temp., °F	Water and Precast Concrete Shell Temp., °F	Concrete Only			Cooling Pipes at 610-mm On-Center		
						Maximum Concrete Temp., °F	Maximum Temperature Difference, °F	Time of Maximum Temp. Diff., days	Maximum Concrete Temp., °F	Maximum Temeprature Difference, °F	Time of Maximum Temp. Diff., days
697	10	4	48	45	50	126	63	11.4	94	30	2.1
698	10	4	55	45	55	127	60	11.9	96	28	2.2
699	10	4	63	45	65	127	53	13.1	99	23	2.4
700	10	4	61	45	60	127	56	12.6	98	26	2.3
701	10	4	35	45	44	125	68	10.8	91	32	1.9
702	10	4	82	45	74	129	46	15.0	104	21	2.8
703	10	4	48	55	50	135	71	10.7	100	35	1.9
704	10	4	55	55	55	136	67	11.0	102	32	2.0
705	10	4	63	55	65	136	60	11.9	105	28	2.2
706	10	4	61	55	60	136	63	11.5	104	30	2.1
707	10	4	35	55	44	135	75	10.1	98	37	1.7
708	10	4	82	55	74	138	53	13.4	110	25	2.5
709	10	4	48	65	50	145	78	10.0	107	39	1.8
710	10	4	55	65	55	145	74	10.3	109	37	1.8
711	10	4	63	65	65	146	67	11.0	112	32	2.0
712	10	4	61	65	60	145	71	10.7	111	35	1.9
713	10	4	35	65	44	144	83	9.6	105	42	1.6
714	10	4	82	65	74	147	60	12.2	116	29	2.2
715	10	4	48	75	50	154	85	9.5	115	44	1.6
716	10	4	55	75	55	154	82	9.8	116	42	1.7
717	10	4	63	75	65	155	74	10.3	119	37	1.8
718	10	4	61	75	60	155	78	10.0	118	40	1.8
719	10	4	35	75	44	154	90	9.1	112	47	1.5
720	10	4	82	75	74	156	67	11.3	123	34	2.0

Table B2 - Predicted Temperatures and Temperature Differences for Concrete Pile Caps Considering Concrete and Concrete with Internal Cooling

Case	Concrete Mix No.	Insulation R-Value	Average Air Temp., °F	Initial Concrete Temp., °F	Water and Precast Concrete Shell Temp., °F	Concrete Only			Cooling Pipes at 610-mm On-Center		
						Maximum Concrete Temp., °F	Maximum Temperature Difference, °F	Time of Maximum Temp. Diff., days	Maximum Concrete Temp., °F	Maximum Temeprature Difference, °F	Time of Maximum Temp. Diff., days
721	11	0	48	45	50	154	102	8.0	113	55	1.7
722	11	0	55	45	55	155	96	8.3	114	51	1.7
723	11	0	63	45	65	155	89	8.7	118	47	1.8
724	11	0	61	45	60	155	91	8.5	116	47	1.8
725	11	0	35	45	44	154	115	7.8	111	65	1.6
726	11	0	82	45	74	156	72	9.3	121	34	1.9
727	11	0	48	55	50	**164**	112	7.8	119	61	1.5
728	11	0	55	55	55	**164**	105	7.9	121	56	1.6
729	11	0	63	55	65	**165**	98	8.2	124	52	1.7
730	11	0	61	55	60	**164**	100	8.1	123	53	1.7
731	11	0	35	55	44	**163**	124	7.5	117	71	1.5
732	11	0	82	55	74	**165**	80	8.8	128	39	1.8
733	11	0	48	65	50	**173**	121	7.5	126	67	1.5
734	11	0	55	65	55	**173**	114	7.6	128	62	1.5
735	11	0	63	65	65	**174**	107	7.9	131	58	1.6
736	11	0	61	65	60	**174**	109	7.8	129	58	1.5
737	11	0	35	65	44	**173**	133	7.3	124	77	1.5
738	11	0	82	65	74	**175**	89	8.3	134	44	1.7
739	11	0	48	75	50	**183**	130	7.3	133	73	1.4
740	11	0	55	75	55	**183**	123	7.4	135	68	1.5
741	11	0	63	75	65	**183**	116	7.6	138	64	1.5
742	11	0	61	75	60	**183**	118	7.5	136	64	1.5
743	11	0	35	75	44	**182**	142	7.1	132	83	1.4
744	11	0	82	75	74	**184**	98	8.0	141	50	1.6

Table B2 - Predicted Temperatures and Temperature Differences for Concrete Pile Caps Considering Concrete and Concrete with Internal Cooling

Case	Concrete Mix No.	Insulation R-Value	Average Air Temp., °F	Initial Concrete Temp., °F	Water and Precast Concrete Shell Temp., °F	Concrete Only			Cooling Pipes at 610-mm On-Center		
						Maximum Concrete Temp., °F	Maximum Temperature Difference, °F	Time of Maximum Temp. Diff., days	Maximum Concrete Temp., °F	Maximum Temeprature Difference, °F	Time of Maximum Temp. Diff., days
745	11	2	48	45	50	156	86	9.1	113	42	1.7
746	11	2	55	45	55	156	82	9.3	114	40	1.7
747	11	2	63	45	65	156	75	9.8	118	36	1.8
748	11	2	61	45	60	156	78	9.6	116	38	1.8
749	11	2	35	45	44	155	94	8.8	111	45	1.6
750	11	2	82	45	74	157	68	10.5	122	32	2.1
751	11	2	48	55	50	**165**	93	8.7	119	46	1.5
752	11	2	55	55	55	**165**	90	8.9	121	44	1.6
753	11	2	63	55	65	**166**	82	9.3	124	40	1.7
754	11	2	61	55	60	**166**	86	9.1	123	42	1.7
755	11	2	35	55	44	**165**	101	8.4	117	49	1.5
756	11	2	82	55	74	**167**	75	9.8	128	36	1.9
757	11	2	48	65	50	**175**	101	8.3	126	51	1.5
758	11	2	55	65	55	**175**	97	8.5	128	49	1.5
759	11	2	63	65	65	**175**	90	8.8	131	44	1.6
760	11	2	61	65	60	**175**	93	8.7	129	46	1.5
761	11	2	35	65	44	**174**	109	8.2	124	54	1.5
762	11	2	82	65	74	**176**	83	9.4	134	40	1.8
763	11	2	48	75	50	**184**	108	8.1	133	56	1.4
764	11	2	55	75	55	**184**	104	8.2	135	53	1.5
765	11	2	63	75	65	**185**	97	8.5	138	49	1.5
766	11	2	61	75	60	**185**	101	8.4	136	51	1.5
767	11	2	35	75	44	**184**	116	7.9	132	59	1.4
768	11	2	82	75	74	**185**	90	9.0	141	45	1.7

Table B2 - Predicted Temperatures and Temperature Differences for Concrete Pile Caps Considering Concrete and Concrete with Internal Cooling

Case	Concrete Mix No.	Insulation R-Value	Average Air Temp., °F	Initial Concrete Temp., °F	Water and Precast Concrete Shell Temp., °F	Concrete Only			Cooling Pipes at 610-mm On-Center		
						Maximum Concrete Temp., °F	Maximum Temperature Difference, °F	Time of Maximum Temp. Diff., days	Maximum Concrete Temp., °F	Maximum Temeprature Difference, °F	Time of Maximum Temp. Diff., days
769	11	4	48	45	50	156	87	9.7	115	45	1.9
770	11	4	55	45	55	157	83	9.9	117	43	2.0
771	11	4	63	45	65	157	76	10.4	120	38	2.1
772	11	4	61	45	60	157	80	10.3	119	40	2.0
773	11	4	35	45	44	156	92	9.3	113	47	1.8
774	11	4	82	45	74	**158**	69	11.3	125	35	2.3
775	11	4	48	55	50	**166**	95	9.3	122	49	1.8
776	11	4	55	55	55	**166**	91	9.5	124	47	1.8
777	11	4	63	55	65	**167**	83	9.9	127	42	2.0
778	11	4	61	55	60	**166**	87	9.8	126	45	1.9
779	11	4	35	55	44	**165**	99	9.0	120	52	1.7
780	11	4	82	55	74	**167**	76	10.6	131	40	2.1
781	11	4	48	65	50	**175**	102	8.9	129	54	1.7
782	11	4	55	65	55	**175**	98	9.1	131	52	1.8
783	11	4	63	65	65	**176**	91	9.5	134	47	1.8
784	11	4	61	65	60	**176**	95	9.3	133	50	1.8
785	11	4	35	65	44	**175**	107	8.7	127	57	1.6
786	11	4	82	65	74	**177**	84	10.0	138	44	2.0
787	11	4	48	75	50	**185**	110	8.6	137	59	1.5
788	11	4	55	75	55	**185**	106	8.8	138	57	1.6
789	11	4	63	75	65	**185**	98	9.1	141	52	1.8
790	11	4	61	75	60	**185**	102	9.0	140	55	1.7
791	11	4	35	75	44	**184**	115	8.4	135	62	1.5
792	11	4	82	75	74	**186**	91	9.5	145	49	1.8

Table B2 - Predicted Temperatures and Temperature Differences for Concrete Pile Caps Considering Concrete and Concrete with Internal Cooling

Case	Concrete Mix No.	Insulation R-Value	Average Air Temp., °F	Initial Concrete Temp., °F	Water and Precast Concrete Shell Temp., °F	Concrete Only			Cooling Pipes at 610-mm On-Center		
						Maximum Concrete Temp., °F	Maximum Temperature Difference, °F	Time of Maximum Temp. Diff., days	Maximum Concrete Temp., °F	Maximum Temeprature Difference, °F	Time of Maximum Temp. Diff., days
793	12	0	48	45	50	132	81	9.2	96	41	1.8
794	12	0	55	45	55	132	75	9.5	98	37	1.9
795	12	0	63	45	65	133	68	10.2	102	34	2.1
796	12	0	61	45	60	133	69	9.8	100	34	2.0
797	12	0	35	45	44	131	93	8.7	94	51	1.7
798	12	0	82	45	74	135	51	11.4	106	22	2.3
799	12	0	48	55	50	141	90	8.6	103	47	1.7
800	12	0	55	55	55	142	84	8.9	104	42	1.7
801	12	0	63	55	65	142	77	9.4	108	39	1.9
802	12	0	61	55	60	142	78	9.2	106	39	1.8
803	12	0	35	55	44	141	102	8.3	101	57	1.6
804	12	0	82	55	74	143	59	10.4	112	26	2.1
805	12	0	48	65	50	150	99	8.2	109	53	1.5
806	12	0	55	65	55	151	93	8.4	111	48	1.6
807	12	0	63	65	65	151	86	8.9	114	44	1.7
808	12	0	61	65	60	151	87	8.7	113	44	1.7
809	12	0	35	65	44	150	111	7.9	108	62	1.5
810	12	0	82	65	74	152	68	9.6	118	31	1.9
811	12	0	48	75	50	**160**	108	7.8	116	59	1.5
812	12	0	55	75	55	**160**	102	8.0	118	54	1.5
813	12	0	63	75	65	**161**	94	8.4	121	50	1.6
814	12	0	61	75	60	**161**	96	8.3	119	50	1.5
815	12	0	35	75	44	**159**	120	7.6	115	68	1.4
816	12	0	82	75	74	**162**	77	9.0	124	36	1.7

Table B2 - Predicted Temperatures and Temperature Differences for Concrete Pile Caps Considering Concrete and Concrete with Internal Cooling

Case	Concrete Mix No.	Insulation R-Value	Average Air Temp., °F	Initial Concrete Temp., °F	Water and Precast Concrete Shell Temp., °F	Concrete Only			Cooling Pipes at 610-mm On-Center		
						Maximum Concrete Temp., °F	Maximum Temperature Difference, °F	Time of Maximum Temp. Diff., days	Maximum Concrete Temp., °F	Maximum Temeprature Difference, °F	Time of Maximum Temp. Diff., days
817	12	2	48	45	50	133	69	10.5	96	31	1.8
818	12	2	55	45	55	134	65	10.9	98	29	1.9
819	12	2	63	45	65	135	58	11.8	102	25	2.1
820	12	2	61	45	60	134	61	11.4	100	27	2.0
821	12	2	35	45	44	133	78	10.0	94	33	1.7
822	12	2	82	45	74	136	51	13.2	107	23	2.4
823	12	2	48	55	50	143	76	9.8	103	35	1.7
824	12	2	55	55	55	143	72	10.2	104	33	1.7
825	12	2	63	55	65	144	65	10.9	108	29	1.9
826	12	2	61	55	60	143	69	10.6	106	31	1.8
827	12	2	35	55	44	142	85	9.4	101	38	1.6
828	12	2	82	55	74	145	58	12.0	113	26	2.2
829	12	2	48	65	50	152	83	9.3	109	40	1.5
830	12	2	55	65	55	152	79	9.6	111	37	1.6
831	12	2	63	65	65	153	72	10.2	114	33	1.7
832	12	2	61	65	60	153	76	9.9	113	35	1.7
833	12	2	35	65	44	151	92	9.0	108	43	1.5
834	12	2	82	65	74	154	65	11.0	118	30	1.9
835	12	2	48	75	50	**161**	91	8.9	116	45	1.5
836	12	2	55	75	55	**162**	87	9.2	118	42	1.5
837	12	2	63	75	65	**162**	80	9.6	121	37	1.6
838	12	2	61	75	60	**162**	83	9.4	119	40	1.5
839	12	2	35	75	44	**161**	99	8.6	115	47	1.4
840	12	2	82	75	74	**163**	73	10.3	125	34	1.8

Table B2 - Predicted Temperatures and Temperature Differences for Concrete Pile Caps Considering Concrete and Concrete with Internal Cooling

Case	Concrete Mix No.	Insulation R-Value	Average Air Temp., °F	Initial Concrete Temp., °F	Water and Precast Concrete Shell Temp., °F	Concrete Only			Cooling Pipes at 610-mm On-Center		
						Maximum Concrete Temp., °F	Maximum Temperature Difference, °F	Time of Maximum Temp. Diff., days	Maximum Concrete Temp., °F	Maximum Temeprature Difference, °F	Time of Maximum Temp. Diff., days
841	12	4	48	45	50	134	70	11.4	98	33	2.0
842	12	4	55	45	55	135	66	11.9	100	31	2.2
843	12	4	63	45	65	136	59	12.8	104	27	2.3
844	12	4	61	45	60	135	63	12.4	102	29	2.3
845	12	4	35	45	44	133	75	10.8	96	35	1.9
846	12	4	82	45	74	137	52	14.5	109	25	2.7
847	12	4	48	55	50	143	77	10.7	105	38	1.9
848	12	4	55	55	55	144	74	11.0	107	36	2.0
849	12	4	63	55	65	145	66	11.8	110	31	2.2
850	12	4	61	55	60	144	70	11.4	109	34	2.1
851	12	4	35	55	44	143	82	10.2	103	40	1.8
852	12	4	82	55	74	146	60	13.2	115	28	2.4
853	12	4	48	65	50	153	85	10.1	112	43	1.8
854	12	4	55	65	55	153	81	10.4	114	40	1.8
855	12	4	63	65	65	154	74	11.0	117	35	2.0
856	12	4	61	65	60	153	77	10.7	115	38	1.9
857	12	4	35	65	44	152	89	9.7	110	45	1.7
858	12	4	82	65	74	155	67	12.1	121	33	2.2
859	12	4	48	75	50	**162**	92	9.6	119	47	1.6
860	12	4	55	75	55	**162**	88	9.8	121	45	1.7
861	12	4	63	75	65	**163**	81	10.3	124	40	1.8
862	12	4	61	75	60	**163**	85	10.2	122	43	1.8
863	12	4	35	75	44	**162**	97	9.2	117	50	1.5
864	12	4	82	75	74	**164**	74	11.2	128	37	2.0

Table B3 - Predicted Temperatures and Temperature Differences for Concrete Pier Shafts

Case	Concrete Mix No.	Insulation R-Value	Average Air Temp., °F	Initial Concrete Temp., °F	Maximum Concrete Temp., °F	Maximum Temeprature Difference, °F	Time of Maximum Temp. Diff., days
1	1	0	48	45	93	43	2.8
2	1	0	55	45	95	37	3.0
3	1	0	63	45	96	31	3.3
4	1	0	61	45	96	33	3.3
5	1	0	35	45	92	53	2.6
6	1	0	82	45	101	18	4.6
7	1	0	48	55	102	51	2.6
8	1	0	55	55	103	45	2.8
9	1	0	63	55	104	39	3.0
10	1	0	61	55	104	40	2.9
11	1	0	35	55	101	61	2.4
12	1	0	82	55	108	25	3.8
13	1	0	48	65	111	59	2.4
14	1	0	55	65	112	53	2.6
15	1	0	63	65	113	47	2.7
16	1	0	61	65	113	48	2.7
17	1	0	35	65	110	70	2.2
18	1	0	82	65	116	32	3.3
19	1	0	48	75	120	67	2.3
20	1	0	55	75	121	61	2.4
21	1	0	63	75	122	55	2.5
22	1	0	61	75	121	56	2.4
23	1	0	35	75	119	78	2.1
24	1	0	82	75	124	39	3.0

Table B3 - Predicted Temperatures and Temperature Differences for Concrete Pier Shafts

Case	Concrete Mix No.	Insulation R-Value	Average Air Temp., °F	Initial Concrete Temp., °F	Maximum Concrete Temp., °F	Maximum Temeprature Difference, °F	Time of Maximum Temp. Diff., days
25	1	2	48	45	98	24	4.5
26	1	2	55	45	99	22	4.9
27	1	2	63	45	100	18	5.4
28	1	2	61	45	100	19	5.3
29	1	2	35	45	97	30	4.0
30	1	2	82	45	104	11	7.5
31	1	2	48	55	107	28	4.1
32	1	2	55	55	108	26	4.4
33	1	2	63	55	109	22	4.8
34	1	2	61	55	109	23	4.7
35	1	2	35	55	106	34	3.8
36	1	2	82	55	112	15	6.2
37	1	2	48	65	117	32	3.8
38	1	2	55	65	117	30	4.0
39	1	2	63	65	118	26	4.3
40	1	2	61	65	118	27	4.2
41	1	2	35	65	116	38	3.5
42	1	2	82	65	120	19	5.3
43	1	2	48	75	126	36	3.6
44	1	2	55	75	126	34	3.8
45	1	2	63	75	127	30	4.0
46	1	2	61	75	127	31	3.9
47	1	2	35	75	125	42	3.3
48	1	2	82	75	129	23	4.7

Table B3 - Predicted Temperatures and Temperature Differences for Concrete Pier Shafts

Case	Concrete Mix No.	Insulation R-Value	Average Air Temp., °F	Initial Concrete Temp., °F	Maximum Concrete Temp., °F	Maximum Temeprature Difference, °F	Time of Maximum Temp. Diff., days
49	1	4	48	45	100	17	5.9
50	1	4	55	45	101	15	6.3
51	1	4	63	45	102	13	7.1
52	1	4	61	45	102	14	6.9
53	1	4	35	45	99	21	5.2
54	1	4	82	45	105	8	10.2
55	1	4	48	55	110	20	5.3
56	1	4	55	55	110	18	5.7
57	1	4	63	55	111	16	6.2
58	1	4	61	55	111	17	6.1
59	1	4	35	55	109	23	4.8
60	1	4	82	55	113	11	8.2
61	1	4	48	65	119	23	4.9
62	1	4	55	65	119	21	5.2
63	1	4	63	65	120	19	5.6
64	1	4	61	65	120	19	5.5
65	1	4	35	65	118	26	4.5
66	1	4	82	65	122	14	7.0
67	1	4	48	75	128	25	4.6
68	1	4	55	75	129	23	4.8
69	1	4	63	75	129	21	5.1
70	1	4	61	75	129	22	5.0
71	1	4	35	75	127	29	4.3
72	1	4	82	75	131	16	6.1

Table B3 - Predicted Temperatures and Temperature Differences for Concrete Pier Shafts

Case	Concrete Mix No.	Insulation R-Value	Average Air Temp., °F	Initial Concrete Temp., °F	Maximum Concrete Temp., °F	Maximum Temeprature Difference, °F	Time of Maximum Temp. Diff., days
73	2	0	48	45	82	32	3.1
74	2	0	55	45	84	27	3.4
75	2	0	63	45	86	21	4.0
76	2	0	61	45	85	23	3.8
77	2	0	35	45	80	42	2.6
78	2	0	82	45	93	10	6.4
79	2	0	48	55	91	40	2.8
80	2	0	55	55	92	34	3.0
81	2	0	63	55	93	28	3.3
82	2	0	61	55	93	30	3.2
83	2	0	35	55	89	51	2.4
84	2	0	82	55	99	16	4.8
85	2	0	48	65	99	48	2.4
86	2	0	55	65	100	42	2.6
87	2	0	63	65	101	36	2.9
88	2	0	61	65	101	38	2.8
89	2	0	35	65	98	59	2.3
90	2	0	82	65	105	22	3.9
91	2	0	48	75	108	56	2.3
92	2	0	55	75	109	51	2.4
93	2	0	63	75	110	44	2.6
94	2	0	61	75	110	46	2.6
95	2	0	35	75	107	68	2.1
96	2	0	82	75	113	29	3.3

Table B3 - Predicted Temperatures and Temperature Differences for Concrete Pier Shafts

Case	Concrete Mix No.	Insulation R-Value	Average Air Temp., °F	Initial Concrete Temp., °F	Maximum Concrete Temp., °F	Maximum Temeprature Difference, °F	Time of Maximum Temp. Diff., days
97	2	2	48	45	87	19	5.1
98	2	2	55	45	88	16	5.7
99	2	2	63	45	89	13	6.6
100	2	2	61	45	89	14	6.3
101	2	2	35	45	85	24	4.3
102	2	2	82	45	95	7	11.7
103	2	2	48	55	95	23	4.5
104	2	2	55	55	96	20	4.9
105	2	2	63	55	97	17	5.5
106	2	2	61	55	97	18	5.3
107	2	2	35	55	94	28	3.9
108	2	2	82	55	101	10	8.3
109	2	2	48	65	105	27	4.0
110	2	2	55	65	105	24	4.3
111	2	2	63	65	106	21	4.8
112	2	2	61	65	106	22	4.7
113	2	2	35	65	103	32	3.6
114	2	2	82	65	109	14	6.5
115	2	2	48	75	114	31	3.7
116	2	2	55	75	114	28	3.9
117	2	2	63	75	115	25	4.3
118	2	2	61	75	115	26	4.2
119	2	2	35	75	113	36	3.4
120	2	2	82	75	117	18	5.4

Table B3 - Predicted Temperatures and Temperature Differences for Concrete Pier Shafts

Case	Concrete Mix No.	Insulation R-Value	Average Air Temp., °F	Initial Concrete Temp., °F	Maximum Concrete Temp., °F	Maximum Temeprature Difference, °F	Time of Maximum Temp. Diff., days
121	2	4	48	45	89	14	6.8
122	2	4	55	45	90	12	7.8
123	2	4	63	45	91	10	9.2
124	2	4	61	45	91	11	8.8
125	2	4	35	45	87	17	5.8
126	2	4	82	45	96	6	17.4
127	2	4	48	55	98	17	5.9
128	2	4	55	55	98	15	6.6
129	2	4	63	55	99	13	7.4
130	2	4	61	55	99	13	7.2
131	2	4	35	55	96	20	5.2
132	2	4	82	55	103	8	11.9
133	2	4	48	65	107	19	5.3
134	2	4	55	65	107	17	5.8
135	2	4	63	65	108	15	6.3
136	2	4	61	65	108	16	6.2
137	2	4	35	65	106	23	4.7
138	2	4	82	65	111	10	9.0
139	2	4	48	75	116	22	4.8
140	2	4	55	75	116	20	5.2
141	2	4	63	75	117	18	5.6
142	2	4	61	75	117	18	5.5
143	2	4	35	75	115	25	4.4
144	2	4	82	75	119	13	7.3

Table B3 - Predicted Temperatures and Temperature Differences for Concrete Pier Shafts

Case	Concrete Mix No.	Insulation R-Value	Average Air Temp., °F	Initial Concrete Temp., °F	Maximum Concrete Temp., °F	Maximum Temeprature Difference, °F	Time of Maximum Temp. Diff., days
145	3	0	48	45	101	50	2.8
146	3	0	55	45	103	45	3.0
147	3	0	63	45	104	38	3.3
148	3	0	61	45	104	40	3.2
149	3	0	35	45	100	60	2.6
150	3	0	82	45	109	25	4.2
151	3	0	48	55	110	58	2.6
152	3	0	55	55	111	52	2.8
153	3	0	63	55	112	46	3.0
154	3	0	61	55	112	48	2.9
155	3	0	35	55	109	69	2.4
156	3	0	82	55	116	32	3.6
157	3	0	48	65	119	66	2.4
158	3	0	55	65	120	60	2.6
159	3	0	63	65	121	54	2.7
160	3	0	61	65	120	56	2.7
161	3	0	35	65	118	77	2.3
162	3	0	82	65	124	39	3.2
163	3	0	48	75	128	75	2.3
164	3	0	55	75	129	69	2.4
165	3	0	63	75	129	62	2.5
166	3	0	61	75	129	64	2.5
167	3	0	35	75	127	86	2.2
168	3	0	82	75	132	47	2.9

Table B3 - Predicted Temperatures and Temperature Differences for Concrete Pier Shafts

Case	Concrete Mix No.	Insulation R-Value	Average Air Temp., °F	Initial Concrete Temp., °F	Maximum Concrete Temp., °F	Maximum Temeprature Difference, °F	Time of Maximum Temp. Diff., days
169	3	2	48	45	107	29	4.5
170	3	2	55	45	108	26	4.8
171	3	2	63	45	109	23	5.2
172	3	2	61	45	109	23	5.1
173	3	2	35	45	106	34	4.1
174	3	2	82	45	112	15	6.7
175	3	2	48	55	116	33	4.2
176	3	2	55	55	117	30	4.4
177	3	2	63	55	118	27	4.7
178	3	2	61	55	118	27	4.6
179	3	2	35	55	115	38	3.8
180	3	2	82	55	120	19	5.8
181	3	2	48	65	125	37	3.9
182	3	2	55	65	126	34	4.1
183	3	2	63	65	127	31	4.3
184	3	2	61	65	126	31	4.3
185	3	2	35	65	124	42	3.6
186	3	2	82	65	129	23	5.2
187	3	2	48	75	135	41	3.7
188	3	2	55	75	135	38	3.8
189	3	2	63	75	136	35	4.0
190	3	2	61	75	136	35	4.0
191	3	2	35	75	134	46	3.4
192	3	2	82	75	138	27	4.7

Table B3 - Predicted Temperatures and Temperature Differences for Concrete Pier Shafts

Case	Concrete Mix No.	Insulation R-Value	Average Air Temp., °F	Initial Concrete Temp., °F	Maximum Concrete Temp., °F	Maximum Temeprature Difference, °F	Time of Maximum Temp. Diff., days
193	3	4	48	45	110	20	5.8
194	3	4	55	45	110	19	6.3
195	3	4	63	45	111	16	6.8
196	3	4	61	45	111	17	6.6
197	3	4	35	45	108	24	5.2
198	3	4	82	45	114	11	9.0
199	3	4	48	55	119	23	5.4
200	3	4	55	55	119	21	5.7
201	3	4	63	55	120	19	6.1
202	3	4	61	55	120	20	6.0
203	3	4	35	55	118	26	4.9
204	3	4	82	55	123	14	7.7
205	3	4	48	65	128	26	5.0
206	3	4	55	65	128	24	5.2
207	3	4	63	65	129	22	5.6
208	3	4	61	65	129	22	5.5
209	3	4	35	65	127	29	4.6
210	3	4	82	65	131	17	6.7
211	3	4	48	75	137	28	4.7
212	3	4	55	75	138	26	4.9
213	3	4	63	75	138	24	5.2
214	3	4	61	75	138	25	5.1
215	3	4	35	75	136	32	4.4
216	3	4	82	75	140	19	6.1

Table B3 - Predicted Temperatures and Temperature Differences for Concrete Pier Shafts

Case	Concrete Mix No.	Insulation R-Value	Average Air Temp., °F	Initial Concrete Temp., °F	Maximum Concrete Temp., °F	Maximum Temeprature Difference, °F	Time of Maximum Temp. Diff., days
217	4	0	48	45	88	38	3.1
218	4	0	55	45	90	33	3.3
219	4	0	63	45	92	27	3.8
220	4	0	61	45	91	28	3.7
221	4	0	35	45	86	48	2.7
222	4	0	82	45	98	15	5.5
223	4	0	48	55	97	46	2.8
224	4	0	55	55	98	40	3.0
225	4	0	63	55	99	34	3.3
226	4	0	61	55	99	36	3.2
227	4	0	35	55	95	56	2.4
228	4	0	82	55	104	21	4.4
229	4	0	48	65	106	54	2.5
230	4	0	55	65	106	48	2.7
231	4	0	63	65	108	42	2.9
232	4	0	61	65	107	43	2.8
233	4	0	35	65	104	65	2.3
234	4	0	82	65	111	28	3.7
235	4	0	48	75	114	62	2.3
236	4	0	55	75	115	56	2.4
237	4	0	63	75	116	50	2.6
238	4	0	61	75	116	51	2.6
239	4	0	35	75	113	73	2.2
240	4	0	82	75	119	35	3.2

Table B3 - Predicted Temperatures and Temperature Differences for Concrete Pier Shafts

Case	Concrete Mix No.	Insulation R-Value	Average Air Temp., °F	Initial Concrete Temp., °F	Maximum Concrete Temp., °F	Maximum Temeprature Difference, °F	Time of Maximum Temp. Diff., days
241	4	2	48	45	94	23	5.1
242	4	2	55	45	95	20	5.5
243	4	2	63	45	96	17	6.3
244	4	2	61	45	96	17	6.0
245	4	2	35	45	92	28	4.4
246	4	2	82	45	101	10	9.6
247	4	2	48	55	102	26	4.5
248	4	2	55	55	103	24	4.9
249	4	2	63	55	104	21	5.4
250	4	2	61	55	104	21	5.3
251	4	2	35	55	101	32	4.0
252	4	2	82	55	108	13	7.5
253	4	2	48	65	111	30	4.1
254	4	2	55	65	112	28	4.4
255	4	2	63	65	113	24	4.8
256	4	2	61	65	113	25	4.7
257	4	2	35	65	110	36	3.7
258	4	2	82	65	116	17	6.2
259	4	2	48	75	120	34	3.8
260	4	2	55	75	121	32	4.0
261	4	2	63	75	122	28	4.3
262	4	2	61	75	122	29	4.3
263	4	2	35	75	120	40	3.5
264	4	2	82	75	124	21	5.3

Table B3 - Predicted Temperatures and Temperature Differences for Concrete Pier Shafts

Case	Concrete Mix No.	Insulation R-Value	Average Air Temp., °F	Initial Concrete Temp., °F	Maximum Concrete Temp., °F	Maximum Temeprature Difference, °F	Time of Maximum Temp. Diff., days
265	4	4	48	45	96	16	6.8
266	4	4	55	45	97	15	7.5
267	4	4	63	45	98	13	8.6
268	4	4	61	45	98	13	8.3
269	4	4	35	45	94	20	5.8
270	4	4	82	45	103	8	14.1
271	4	4	48	55	105	19	6.0
272	4	4	55	55	106	17	6.6
273	4	4	63	55	107	15	7.3
274	4	4	61	55	106	16	7.1
275	4	4	35	55	104	22	5.3
276	4	4	82	55	110	10	10.6
277	4	4	48	65	114	22	5.5
278	4	4	55	65	114	20	5.8
279	4	4	63	65	115	18	6.3
280	4	4	61	65	115	18	6.2
281	4	4	35	65	113	25	4.9
282	4	4	82	65	118	13	8.5
283	4	4	48	75	123	24	5.0
284	4	4	55	75	124	22	5.3
285	4	4	63	75	124	20	5.7
286	4	4	61	75	124	21	5.6
287	4	4	35	75	122	28	4.6
288	4	4	82	75	126	15	7.2

Table B3 - Predicted Temperatures and Temperature Differences for Concrete Pier Shafts

Case	Concrete Mix No.	Insulation R-Value	Average Air Temp., °F	Initial Concrete Temp., °F	Maximum Concrete Temp., °F	Maximum Temeprature Difference, °F	Time of Maximum Temp. Diff., days
289	5	0	48	45	109	57	2.8
290	5	0	55	45	111	52	3.0
291	5	0	63	45	112	46	3.2
292	5	0	61	45	112	47	3.2
293	5	0	35	45	108	68	2.6
294	5	0	82	45	116	32	3.9
295	5	0	48	55	118	65	2.6
296	5	0	55	55	119	60	2.8
297	5	0	63	55	120	54	2.9
298	5	0	61	55	120	55	2.9
299	5	0	35	55	117	76	2.4
300	5	0	82	55	124	39	3.5
301	5	0	48	65	127	74	2.5
302	5	0	55	65	128	68	2.6
303	5	0	63	65	129	61	2.7
304	5	0	61	65	128	63	2.7
305	5	0	35	65	126	85	2.3
306	5	0	82	65	132	47	3.2
307	5	0	48	75	136	82	2.4
308	5	0	55	75	137	76	2.4
309	5	0	63	75	137	70	2.6
310	5	0	61	75	137	71	2.5
311	5	0	35	75	135	93	2.2
312	5	0	82	75	140	54	2.9

Table B3 - Predicted Temperatures and Temperature Differences for Concrete Pier Shafts

Case	Concrete Mix No.	Insulation R-Value	Average Air Temp., °F	Initial Concrete Temp., °F	Maximum Concrete Temp., °F	Maximum Temeprature Difference, °F	Time of Maximum Temp. Diff., days
313	5	2	48	45	116	33	4.5
314	5	2	55	45	117	30	4.8
315	5	2	63	45	118	27	5.1
316	5	2	61	45	118	28	5.0
317	5	2	35	45	115	38	4.1
318	5	2	82	45	121	19	6.3
319	5	2	48	55	125	37	4.2
320	5	2	55	55	126	34	4.4
321	5	2	63	55	127	31	4.7
322	5	2	61	55	126	32	4.6
323	5	2	35	55	124	42	3.9
324	5	2	82	55	129	23	5.6
325	5	2	48	65	134	41	3.9
326	5	2	55	65	135	38	4.1
327	5	2	63	65	135	35	4.3
328	5	2	61	65	135	36	4.3
329	5	2	35	65	133	46	3.7
330	5	2	82	65	138	27	5.0
331	5	2	48	75	143	45	3.7
332	5	2	55	75	144	42	3.9
333	5	2	63	75	145	39	4.0
334	5	2	61	75	144	40	4.0
335	5	2	35	75	142	50	3.5
336	5	2	82	75	146	31	4.6

Table B3 - Predicted Temperatures and Temperature Differences for Concrete Pier Shafts

Case	Concrete Mix No.	Insulation R-Value	Average Air Temp., °F	Initial Concrete Temp., °F	Maximum Concrete Temp., °F	Maximum Temeprature Difference, °F	Time of Maximum Temp. Diff., days
337	5	4	48	45	119	23	5.8
338	5	4	55	45	120	22	6.2
339	5	4	63	45	120	19	6.6
340	5	4	61	45	120	20	6.5
341	5	4	35	45	118	27	5.3
342	5	4	82	45	123	14	8.3
343	5	4	48	55	128	26	5.4
344	5	4	55	55	129	24	5.7
345	5	4	63	55	129	22	6.1
346	5	4	61	55	129	23	6.0
347	5	4	35	55	127	29	5.0
348	5	4	82	55	132	17	7.3
349	5	4	48	65	137	29	5.1
350	5	4	55	65	138	27	5.3
351	5	4	63	65	138	25	5.6
352	5	4	61	65	138	25	5.5
353	5	4	35	65	136	32	4.7
354	5	4	82	65	140	20	6.6
355	5	4	48	75	146	31	4.8
356	5	4	55	75	147	29	5.0
357	5	4	63	75	147	27	5.2
358	5	4	61	75	147	28	5.1
359	5	4	35	75	146	35	4.5
360	5	4	82	75	149	22	6.0

Table B3 - Predicted Temperatures and Temperature Differences for Concrete Pier Shafts

Case	Concrete Mix No.	Insulation R-Value	Average Air Temp., °F	Initial Concrete Temp., °F	Maximum Concrete Temp., °F	Maximum Temeprature Difference, °F	Time of Maximum Temp. Diff., days
361	6	0	48	45	95	44	3.0
362	6	0	55	45	96	38	3.3
363	6	0	63	45	98	32	3.7
364	6	0	61	45	97	34	3.5
365	6	0	35	45	92	54	2.7
366	6	0	82	45	103	20	4.9
367	6	0	48	55	103	51	2.8
368	6	0	55	55	104	46	3.0
369	6	0	63	55	105	40	3.2
370	6	0	61	55	105	41	3.2
371	6	0	35	55	101	62	2.5
372	6	0	82	55	110	26	4.2
373	6	0	48	65	112	59	2.6
374	6	0	55	65	112	54	2.7
375	6	0	63	65	114	47	2.9
376	6	0	61	65	113	49	2.9
377	6	0	35	65	110	70	2.4
378	6	0	82	65	117	33	3.6
379	6	0	48	75	120	68	2.4
380	6	0	55	75	121	62	2.5
381	6	0	63	75	122	55	2.7
382	6	0	61	75	122	57	2.6
383	6	0	35	75	119	79	2.3
384	6	0	82	75	125	40	3.2

Table B3 - Predicted Temperatures and Temperature Differences for Concrete Pier Shafts

Case	Concrete Mix No.	Insulation R-Value	Average Air Temp., °F	Initial Concrete Temp., °F	Maximum Concrete Temp., °F	Maximum Temeprature Difference, °F	Time of Maximum Temp. Diff., days
385	6	2	48	45	100	26	5.0
386	6	2	55	45	101	23	5.4
387	6	2	63	45	103	20	6.0
388	6	2	61	45	102	21	5.8
389	6	2	35	45	99	31	4.5
390	6	2	82	45	107	13	8.5
391	6	2	48	55	109	30	4.6
392	6	2	55	55	110	27	4.9
393	6	2	63	55	111	24	5.3
394	6	2	61	55	111	25	5.2
395	6	2	35	55	108	35	4.1
396	6	2	82	55	114	17	7.0
397	6	2	48	65	118	34	4.2
398	6	2	55	65	119	31	4.5
399	6	2	63	65	120	28	4.8
400	6	2	61	65	120	29	4.7
401	6	2	35	65	117	39	3.8
402	6	2	82	65	123	20	5.9
403	6	2	48	75	127	38	3.9
404	6	2	55	75	128	35	4.1
405	6	2	63	75	129	32	4.4
406	6	2	61	75	128	33	4.3
407	6	2	35	75	126	43	3.6
408	6	2	82	75	131	24	5.3

Table B3 - Predicted Temperatures and Temperature Differences for Concrete Pier Shafts

Case	Concrete Mix No.	Insulation R-Value	Average Air Temp., °F	Initial Concrete Temp., °F	Maximum Concrete Temp., °F	Maximum Temeprature Difference, °F	Time of Maximum Temp. Diff., days
409	6	4	48	45	103	19	6.8
410	6	4	55	45	104	17	7.4
411	6	4	63	45	105	15	8.3
412	6	4	61	45	105	16	8.1
413	6	4	35	45	102	22	5.9
414	6	4	82	45	109	10	12.2
415	6	4	48	55	112	21	6.1
416	6	4	55	55	113	20	6.6
417	6	4	63	55	114	18	7.2
418	6	4	61	55	113	18	7.0
419	6	4	35	55	111	25	5.4
420	6	4	82	55	117	13	9.7
421	6	4	48	65	121	24	5.6
422	6	4	55	65	122	22	5.9
423	6	4	63	65	123	20	6.4
424	6	4	61	65	122	21	6.3
425	6	4	35	65	120	27	5.0
426	6	4	82	65	125	15	8.2
427	6	4	48	75	130	27	5.2
428	6	4	55	75	131	25	5.4
429	6	4	63	75	131	23	5.8
430	6	4	61	75	131	23	5.7
431	6	4	35	75	129	30	4.7
432	6	4	82	75	134	18	7.1

Table B3 - Predicted Temperatures and Temperature Differences for Concrete Pier Shafts

Case	Concrete Mix No.	Insulation R-Value	Average Air Temp., °F	Initial Concrete Temp., °F	Maximum Concrete Temp., °F	Maximum Temeprature Difference, °F	Time of Maximum Temp. Diff., days
433	7	0	48	45	117	65	2.8
434	7	0	55	45	119	59	3.0
435	7	0	63	45	120	53	3.2
436	7	0	61	45	120	55	3.1
437	7	0	35	45	116	75	2.6
438	7	0	82	45	124	39	3.7
439	7	0	48	55	126	73	2.6
440	7	0	55	55	127	67	2.8
441	7	0	63	55	128	61	2.9
442	7	0	61	55	128	63	2.8
443	7	0	35	55	125	84	2.4
444	7	0	82	55	132	47	3.3
445	7	0	48	65	135	81	2.5
446	7	0	55	65	136	75	2.6
447	7	0	63	65	137	69	2.7
448	7	0	61	65	136	71	2.7
449	7	0	35	65	133	92	2.4
450	7	0	82	65	140	54	3.1
451	7	0	48	75	144	89	2.4
452	7	0	55	75	145	84	2.4
453	7	0	63	75	145	77	2.6
454	7	0	61	75	145	79	2.6
455	7	0	35	75	143	100	2.3
456	7	0	82	75	148	62	2.9

Table B3 - Predicted Temperatures and Temperature Differences for Concrete Pier Shafts

Case	Concrete Mix No.	Insulation R-Value	Average Air Temp., °F	Initial Concrete Temp., °F	Maximum Concrete Temp., °F	Maximum Temeprature Difference, °F	Time of Maximum Temp. Diff., days
457	7	2	48	45	125	37	4.5
458	7	2	55	45	126	34	4.7
459	7	2	63	45	127	31	5.0
460	7	2	61	45	126	32	4.9
461	7	2	35	45	124	42	4.1
462	7	2	82	45	129	24	6.0
463	7	2	48	55	134	41	4.2
464	7	2	55	55	134	38	4.4
465	7	2	63	55	135	35	4.7
466	7	2	61	55	135	36	4.6
467	7	2	35	55	133	46	3.9
468	7	2	82	55	138	28	5.4
469	7	2	48	65	143	45	4.0
470	7	2	55	65	144	42	4.1
471	7	2	63	65	144	39	4.3
472	7	2	61	65	144	40	4.3
473	7	2	35	65	142	50	3.8
474	7	2	82	65	146	32	5.0
475	7	2	48	75	152	49	3.8
476	7	2	55	75	153	46	3.9
477	7	2	63	75	153	43	4.1
478	7	2	61	75	153	44	4.0
479	7	2	35	75	151	54	3.6
480	7	2	82	75	155	36	4.6

Table B3 - Predicted Temperatures and Temperature Differences for Concrete Pier Shafts

Case	Concrete Mix No.	Insulation R-Value	Average Air Temp., °F	Initial Concrete Temp., °F	Maximum Concrete Temp., °F	Maximum Temeprature Difference, °F	Time of Maximum Temp. Diff., days
481	7	4	48	45	128	26	5.8
482	7	4	55	45	129	25	6.1
483	7	4	63	45	130	22	6.5
484	7	4	61	45	129	23	6.4
485	7	4	35	45	127	30	5.3
486	7	4	82	45	132	17	7.8
487	7	4	48	55	137	29	5.5
488	7	4	55	55	138	27	5.7
489	7	4	63	55	138	25	6.0
490	7	4	61	55	138	26	5.9
491	7	4	35	55	136	32	5.0
492	7	4	82	55	141	20	7.1
493	7	4	48	65	146	32	5.1
494	7	4	55	65	147	30	5.3
495	7	4	63	65	147	28	5.6
496	7	4	61	65	147	28	5.6
497	7	4	35	65	145	35	4.8
498	7	4	82	65	149	23	6.4
499	7	4	48	75	155	34	4.9
500	7	4	55	75	156	32	5.0
501	7	4	63	75	157	30	5.3
502	7	4	61	75	156	31	5.2
503	7	4	35	75	155	38	4.6
504	7	4	82	75	**158**	25	6.0

Table B3 - Predicted Temperatures and Temperature Differences for Concrete Pier Shafts

Case	Concrete Mix No.	Insulation R-Value	Average Air Temp., °F	Initial Concrete Temp., °F	Maximum Concrete Temp., °F	Maximum Temeprature Difference, °F	Time of Maximum Temp. Diff., days
505	8	0	48	45	101	49	3.0
506	8	0	55	45	102	44	3.2
507	8	0	63	45	104	38	3.5
508	8	0	61	45	103	40	3.5
509	8	0	35	45	99	59	2.8
510	8	0	82	45	109	25	4.6
511	8	0	48	55	109	57	2.8
512	8	0	55	55	110	52	3.0
513	8	0	63	55	112	45	3.2
514	8	0	61	55	111	47	3.1
515	8	0	35	55	107	68	2.6
516	8	0	82	55	116	32	4.0
517	8	0	48	65	118	65	2.6
518	8	0	55	65	119	59	2.8
519	8	0	63	65	120	53	2.9
520	8	0	61	65	119	55	2.9
521	8	0	35	65	116	76	2.4
522	8	0	82	65	123	39	3.5
523	8	0	48	75	127	73	2.4
524	8	0	55	75	127	68	2.6
525	8	0	63	75	128	61	2.7
526	8	0	61	75	128	63	2.6
527	8	0	35	75	125	84	2.3
528	8	0	82	75	131	46	3.2

Table B3 - Predicted Temperatures and Temperature Differences for Concrete Pier Shafts

Case	Concrete Mix No.	Insulation R-Value	Average Air Temp., °F	Initial Concrete Temp., °F	Maximum Concrete Temp., °F	Maximum Temeprature Difference, °F	Time of Maximum Temp. Diff., days
529	8	2	48	45	107	29	5.0
530	8	2	55	45	108	27	5.4
531	8	2	63	45	110	23	5.8
532	8	2	61	45	109	24	5.7
533	8	2	35	45	106	34	4.5
534	8	2	82	45	113	16	7.8
535	8	2	48	55	116	33	4.6
536	8	2	55	55	117	30	4.9
537	8	2	63	55	118	27	5.3
538	8	2	61	55	118	28	5.2
539	8	2	35	55	115	38	4.2
540	8	2	82	55	121	20	6.6
541	8	2	48	65	125	37	4.3
542	8	2	55	65	126	34	4.5
543	8	2	63	65	127	31	4.8
544	8	2	61	65	126	32	4.7
545	8	2	35	65	124	42	3.9
546	8	2	82	65	129	24	5.8
547	8	2	48	75	134	41	4.0
548	8	2	55	75	135	38	4.2
549	8	2	63	75	136	35	4.4
550	8	2	61	75	135	36	4.4
551	8	2	35	75	133	46	3.7
552	8	2	82	75	138	28	5.2

Table B3 - Predicted Temperatures and Temperature Differences for Concrete Pier Shafts

Case	Concrete Mix No.	Insulation R-Value	Average Air Temp., °F	Initial Concrete Temp., °F	Maximum Concrete Temp., °F	Maximum Temeprature Difference, °F	Time of Maximum Temp. Diff., days
553	8	4	48	45	110	21	6.8
554	8	4	55	45	111	20	7.3
555	8	4	63	45	112	17	8.1
556	8	4	61	45	112	18	7.9
557	8	4	35	45	109	25	6.0
558	8	4	82	45	116	13	11.1
559	8	4	48	55	119	24	6.1
560	8	4	55	55	120	22	6.6
561	8	4	63	55	121	20	7.1
562	8	4	61	55	121	21	7.0
563	8	4	35	55	118	27	5.5
564	8	4	82	55	124	15	9.2
565	8	4	48	65	128	27	5.7
566	8	4	55	65	129	25	6.0
567	8	4	63	65	130	23	6.4
568	8	4	61	65	130	23	6.3
569	8	4	35	65	127	30	5.2
570	8	4	82	65	132	18	8.0
571	8	4	48	75	137	29	5.3
572	8	4	55	75	138	27	5.5
573	8	4	63	75	139	25	5.9
574	8	4	61	75	138	26	5.8
575	8	4	35	75	136	32	4.8
576	8	4	82	75	141	20	7.0

Table B3 - Predicted Temperatures and Temperature Differences for Concrete Pier Shafts

Case	Concrete Mix No.	Insulation R-Value	Average Air Temp., °F	Initial Concrete Temp., °F	Maximum Concrete Temp., °F	Maximum Temeprature Difference, °F	Time of Maximum Temp. Diff., days
577	9	0	48	45	126	73	2.8
578	9	0	55	45	127	67	2.9
579	9	0	63	45	128	61	3.1
580	9	0	61	45	128	62	3.0
581	9	0	35	45	124	83	2.6
582	9	0	82	45	132	47	3.6
583	9	0	48	55	134	81	2.7
584	9	0	55	55	135	75	2.8
585	9	0	63	55	136	69	2.9
586	9	0	61	55	136	70	2.8
587	9	0	35	55	133	91	2.5
588	9	0	82	55	140	54	3.3
589	9	0	48	65	143	89	2.5
590	9	0	55	65	144	83	2.6
591	9	0	63	65	145	76	2.7
592	9	0	61	65	145	78	2.7
593	9	0	35	65	142	99	2.4
594	9	0	82	65	148	62	3.1
595	9	0	48	75	152	97	2.4
596	9	0	55	75	153	91	2.5
597	9	0	63	75	154	85	2.6
598	9	0	61	75	153	86	2.6
599	9	0	35	75	151	108	2.3
600	9	0	82	75	156	69	2.9

Table B3 - Predicted Temperatures and Temperature Differences for Concrete Pier Shafts

Case	Concrete Mix No.	Insulation R-Value	Average Air Temp., °F	Initial Concrete Temp., °F	Maximum Concrete Temp., °F	Maximum Temeprature Difference, °F	Time of Maximum Temp. Diff., days
601	9	2	48	45	134	41	4.5
602	9	2	55	45	135	39	4.7
603	9	2	63	45	135	35	4.9
604	9	2	61	45	135	36	4.8
605	9	2	35	45	132	47	4.2
606	9	2	82	45	138	28	5.7
607	9	2	48	55	143	45	4.2
608	9	2	55	55	143	43	4.4
609	9	2	63	55	144	39	4.6
610	9	2	61	55	144	40	4.6
611	9	2	35	55	142	51	4.0
612	9	2	82	55	147	32	5.3
613	9	2	48	65	152	49	4.0
614	9	2	55	65	152	47	4.2
615	9	2	63	65	153	43	4.3
616	9	2	61	65	153	44	4.3
617	9	2	35	65	151	55	3.8
618	9	2	82	65	155	36	4.9
619	9	2	48	75	**161**	53	3.8
620	9	2	55	75	**162**	51	4.0
621	9	2	63	75	**162**	47	4.1
622	9	2	61	75	**162**	48	4.1
623	9	2	35	75	**160**	59	3.7
624	9	2	82	75	**164**	40	4.6

Table B3 - Predicted Temperatures and Temperature Differences for Concrete Pier Shafts

Case	Concrete Mix No.	Insulation R-Value	Average Air Temp., °F	Initial Concrete Temp., °F	Maximum Concrete Temp., °F	Maximum Temeprature Difference, °F	Time of Maximum Temp. Diff., days
625	9	4	48	45	137	29	5.8
626	9	4	55	45	138	28	6.1
627	9	4	63	45	139	25	6.4
628	9	4	61	45	139	26	6.3
629	9	4	35	45	136	33	5.4
630	9	4	82	45	141	20	7.5
631	9	4	48	55	146	32	5.5
632	9	4	55	55	147	30	5.7
633	9	4	63	55	148	28	6.0
634	9	4	61	55	148	29	5.9
635	9	4	35	55	145	35	5.1
636	9	4	82	55	150	23	6.9
637	9	4	48	65	156	35	5.2
638	9	4	55	65	156	33	5.4
639	9	4	63	65	157	31	5.6
640	9	4	61	65	157	31	5.6
641	9	4	35	65	155	38	4.9
642	9	4	82	65	**159**	26	6.3
643	9	4	48	75	**165**	37	4.9
644	9	4	55	75	**165**	35	5.1
645	9	4	63	75	**166**	33	5.3
646	9	4	61	75	**166**	34	5.3
647	9	4	35	75	**164**	41	4.7
648	9	4	82	75	**168**	28	5.9

Table B3 - Predicted Temperatures and Temperature Differences for Concrete Pier Shafts

Case	Concrete Mix No.	Insulation R-Value	Average Air Temp., °F	Initial Concrete Temp., °F	Maximum Concrete Temp., °F	Maximum Temeprature Difference, °F	Time of Maximum Temp. Diff., days
649	10	0	48	45	107	55	3.0
650	10	0	55	45	108	50	3.2
651	10	0	63	45	110	44	3.5
652	10	0	61	45	109	45	3.4
653	10	0	35	45	105	65	2.8
654	10	0	82	45	115	31	4.3
655	10	0	48	55	115	63	2.8
656	10	0	55	55	116	57	3.0
657	10	0	63	55	118	51	3.2
658	10	0	61	55	117	53	3.1
659	10	0	35	55	113	73	2.6
660	10	0	82	55	122	37	3.8
661	10	0	48	65	124	71	2.6
662	10	0	55	65	125	65	2.8
663	10	0	63	65	126	59	2.9
664	10	0	61	65	126	61	2.9
665	10	0	35	65	122	82	2.4
666	10	0	82	65	130	45	3.4
667	10	0	48	75	133	79	2.5
668	10	0	55	75	133	73	2.6
669	10	0	63	75	135	67	2.7
670	10	0	61	75	134	68	2.7
671	10	0	35	75	131	90	2.3
672	10	0	82	75	138	52	3.2

Table B3 - Predicted Temperatures and Temperature Differences for Concrete Pier Shafts

Case	Concrete Mix No.	Insulation R-Value	Average Air Temp., °F	Initial Concrete Temp., °F	Maximum Concrete Temp., °F	Maximum Temeprature Difference, °F	Time of Maximum Temp. Diff., days
673	10	2	48	45	114	33	5.0
674	10	2	55	45	115	30	5.3
675	10	2	63	45	116	27	5.7
676	10	2	61	45	116	28	5.6
677	10	2	35	45	113	38	4.5
678	10	2	82	45	120	20	7.3
679	10	2	48	55	123	37	4.6
680	10	2	55	55	124	34	4.9
681	10	2	63	55	125	31	5.2
682	10	2	61	55	125	31	5.1
683	10	2	35	55	122	42	4.3
684	10	2	82	55	128	23	6.3
685	10	2	48	65	132	41	4.3
686	10	2	55	65	133	38	4.5
687	10	2	63	65	134	35	4.8
688	10	2	61	65	133	35	4.8
689	10	2	35	65	131	46	4.0
690	10	2	82	65	136	27	5.7
691	10	2	48	75	141	44	4.0
692	10	2	55	75	142	42	4.3
693	10	2	63	75	142	39	4.5
694	10	2	61	75	142	39	4.4
695	10	2	35	75	140	50	3.8
696	10	2	82	75	145	31	5.2

Table B3 - Predicted Temperatures and Temperature Differences for Concrete Pier Shafts

Case	Concrete Mix No.	Insulation R-Value	Average Air Temp., °F	Initial Concrete Temp., °F	Maximum Concrete Temp., °F	Maximum Temeprature Difference, °F	Time of Maximum Temp. Diff., days
697	10	4	48	45	118	24	6.8
698	10	4	55	45	119	22	7.2
699	10	4	63	45	120	20	7.9
700	10	4	61	45	119	20	7.7
701	10	4	35	45	116	27	6.0
702	10	4	82	45	123	15	10.3
703	10	4	48	55	126	26	6.2
704	10	4	55	55	127	25	6.6
705	10	4	63	55	128	23	7.1
706	10	4	61	55	128	23	6.9
707	10	4	35	55	125	30	5.6
708	10	4	82	55	131	18	8.8
709	10	4	48	65	135	29	5.7
710	10	4	55	65	136	27	6.0
711	10	4	63	65	137	25	6.5
712	10	4	61	65	137	26	6.3
713	10	4	35	65	134	32	5.3
714	10	4	82	65	140	20	7.8
715	10	4	48	75	145	32	5.4
716	10	4	55	75	145	30	5.6
717	10	4	63	75	146	28	5.9
718	10	4	61	75	146	28	5.8
719	10	4	35	75	144	35	4.9
720	10	4	82	75	148	23	7.0

Table B3 - Predicted Temperatures and Temperature Differences for Concrete Pier Shafts

Case	Concrete Mix No.	Insulation R-Value	Average Air Temp., °F	Initial Concrete Temp., °F	Maximum Concrete Temp., °F	Maximum Temeprature Difference, °F	Time of Maximum Temp. Diff., days
721	11	0	48	45	134	80	2.8
722	11	0	55	45	135	74	2.9
723	11	0	63	45	136	68	3.0
724	11	0	61	45	136	70	3.0
725	11	0	35	45	132	90	2.6
726	11	0	82	45	140	54	3.5
727	11	0	48	55	142	88	2.7
728	11	0	55	55	143	82	2.8
729	11	0	63	55	144	76	2.9
730	11	0	61	55	144	78	2.8
731	11	0	35	55	141	99	2.5
732	11	0	82	55	148	61	3.2
733	11	0	48	65	151	96	2.6
734	11	0	55	65	152	90	2.6
735	11	0	63	65	153	84	2.8
736	11	0	61	65	153	86	2.7
737	11	0	35	65	149	107	2.4
738	11	0	82	65	156	69	3.0
739	11	0	48	75	**160**	104	2.4
740	11	0	55	75	**161**	99	2.5
741	11	0	63	75	**162**	92	2.6
742	11	0	61	75	**161**	94	2.6
743	11	0	35	75	**158**	115	2.3
744	11	0	82	75	**164**	77	2.8

Table B3 - Predicted Temperatures and Temperature Differences for Concrete Pier Shafts

Case	Concrete Mix No.	Insulation R-Value	Average Air Temp., °F	Initial Concrete Temp., °F	Maximum Concrete Temp., °F	Maximum Temeprature Difference, °F	Time of Maximum Temp. Diff., days
745	11	2	48	45	143	46	4.5
746	11	2	55	45	143	43	4.7
747	11	2	63	45	144	40	4.9
748	11	2	61	45	144	40	4.8
749	11	2	35	45	141	51	4.2
750	11	2	82	45	147	32	5.6
751	11	2	48	55	152	50	4.2
752	11	2	55	55	152	47	4.4
753	11	2	63	55	153	44	4.6
754	11	2	61	55	153	44	4.5
755	11	2	35	55	150	55	4.0
756	11	2	82	55	155	36	5.2
757	11	2	48	65	**161**	54	4.0
758	11	2	55	65	**161**	51	4.2
759	11	2	63	65	**162**	48	4.3
760	11	2	61	65	**162**	48	4.3
761	11	2	35	65	**160**	59	3.8
762	11	2	82	65	**164**	40	4.8
763	11	2	48	75	**170**	58	3.9
764	11	2	55	75	**170**	55	4.0
765	11	2	63	75	**171**	52	4.1
766	11	2	61	75	**171**	52	4.1
767	11	2	35	75	**169**	63	3.7
768	11	2	82	75	**173**	44	4.6

Table B3 - Predicted Temperatures and Temperature Differences for Concrete Pier Shafts

Case	Concrete Mix No.	Insulation R-Value	Average Air Temp., °F	Initial Concrete Temp., °F	Maximum Concrete Temp., °F	Maximum Temeprature Difference, °F	Time of Maximum Temp. Diff., days
769	11	4	48	45	146	32	5.8
770	11	4	55	45	147	31	6.0
771	11	4	63	45	148	28	6.3
772	11	4	61	45	148	29	6.3
773	11	4	35	45	145	36	5.4
774	11	4	82	45	150	23	7.3
775	11	4	48	55	156	35	5.5
776	11	4	55	55	156	33	5.7
777	11	4	63	55	157	31	5.9
778	11	4	61	55	157	32	5.9
779	11	4	35	55	154	38	5.1
780	11	4	82	55	**159**	26	6.7
781	11	4	48	65	**165**	38	5.2
782	11	4	55	65	**165**	36	5.4
783	11	4	63	65	**166**	34	5.6
784	11	4	61	65	**166**	34	5.6
785	11	4	35	65	**164**	41	4.9
786	11	4	82	65	**168**	29	6.3
787	11	4	48	75	**174**	40	5.0
788	11	4	55	75	**174**	38	5.1
789	11	4	63	75	**175**	36	5.4
790	11	4	61	75	**175**	37	5.3
791	11	4	35	75	**173**	44	4.8
792	11	4	82	75	**177**	31	5.9

Table B3 - Predicted Temperatures and Temperature Differences for Concrete Pier Shafts

Case	Concrete Mix No.	Insulation R-Value	Average Air Temp., °F	Initial Concrete Temp., °F	Maximum Concrete Temp., °F	Maximum Temeprature Difference, °F	Time of Maximum Temp. Diff., days
793	12	0	48	45	113	61	3.0
794	12	0	55	45	114	55	3.2
795	12	0	63	45	116	50	3.4
796	12	0	61	45	115	51	3.3
797	12	0	35	45	111	71	2.8
798	12	0	82	45	121	36	4.2
799	12	0	48	55	121	69	2.8
800	12	0	55	55	122	63	3.0
801	12	0	63	55	124	57	3.2
802	12	0	61	55	123	58	3.1
803	12	0	35	55	120	79	2.6
804	12	0	82	55	128	43	3.7
805	12	0	48	65	130	77	2.7
806	12	0	55	65	131	71	2.8
807	12	0	63	65	132	65	2.9
808	12	0	61	65	132	66	2.9
809	12	0	35	65	128	87	2.5
810	12	0	82	65	136	50	3.4
811	12	0	48	75	139	85	2.5
812	12	0	55	75	140	79	2.6
813	12	0	63	75	141	73	2.8
814	12	0	61	75	140	74	2.7
815	12	0	35	75	137	96	2.4
816	12	0	82	75	144	58	3.1

Table B3 - Predicted Temperatures and Temperature Differences for Concrete Pier Shafts

Case	Concrete Mix No.	Insulation R-Value	Average Air Temp., °F	Initial Concrete Temp., °F	Maximum Concrete Temp., °F	Maximum Temeprature Difference, °F	Time of Maximum Temp. Diff., days
817	12	2	48	45	121	36	5.0
818	12	2	55	45	122	33	5.3
819	12	2	63	45	123	30	5.7
820	12	2	61	45	123	31	5.5
821	12	2	35	45	120	41	4.6
822	12	2	82	45	127	23	7.0
823	12	2	48	55	130	40	4.7
824	12	2	55	55	131	37	4.9
825	12	2	63	55	132	34	5.2
826	12	2	61	55	131	35	5.1
827	12	2	35	55	128	45	4.3
828	12	2	82	55	135	27	6.2
829	12	2	48	65	139	44	4.4
830	12	2	55	65	140	41	4.6
831	12	2	63	65	140	38	4.8
832	12	2	61	65	140	39	4.8
833	12	2	35	65	138	49	4.0
834	12	2	82	65	143	31	5.6
835	12	2	48	75	148	48	4.1
836	12	2	55	75	148	45	4.3
837	12	2	63	75	149	42	4.5
838	12	2	61	75	149	43	4.4
839	12	2	35	75	147	53	3.8
840	12	2	82	75	152	34	5.2

Table B3 - Predicted Temperatures and Temperature Differences for Concrete Pier Shafts

Case	Concrete Mix No.	Insulation R-Value	Average Air Temp., °F	Initial Concrete Temp., °F	Maximum Concrete Temp., °F	Maximum Temeprature Difference, °F	Time of Maximum Temp. Diff., days
841	12	4	48	45	125	26	6.7
842	12	4	55	45	126	24	7.1
843	12	4	63	45	127	22	7.8
844	12	4	61	45	127	23	7.5
845	12	4	35	45	123	30	6.1
846	12	4	82	45	130	18	9.7
847	12	4	48	55	134	29	6.2
848	12	4	55	55	134	27	6.6
849	12	4	63	55	135	25	7.0
850	12	4	61	55	135	25	6.9
851	12	4	35	55	132	32	5.7
852	12	4	82	55	138	20	8.5
853	12	4	48	65	143	31	5.8
854	12	4	55	65	143	30	6.1
855	12	4	63	65	144	28	6.5
856	12	4	61	65	144	28	6.3
857	12	4	35	65	141	35	5.4
858	12	4	82	65	147	23	7.6
859	12	4	48	75	152	34	5.5
860	12	4	55	75	152	32	5.7
861	12	4	63	75	153	30	6.0
862	12	4	61	75	153	31	5.9
863	12	4	35	75	151	37	5.1
864	12	4	82	75	155	25	6.9

Table B4 - Predicted Temperatures and Temperature Differences for the Pier Table and Box Girder Bottom Slabs

Case	Concrete Mix No.	Insulation R-Value	Average Air Temp., °F	Initial Concrete Temp., °F	Normal Weight Concrete at Pier Shaft			Lightweight Concrete at Location 1N			Lightweight Concrete at Location 7N		
					Maximum Concrete Temp., °F	Maximum Temeprature Difference, °F	Time of Maximum Temp. Diff., days	Maximum Concrete Temp., °F	Maximum Temeprature Difference, °F	Time of Maximum Temp. Diff., days	Maximum Concrete Temp., °F	Maximum Temeprature Difference, °F	Time of Maximum Temp. Diff., days
1	1	0	48	45	95	46	3.0	97	48	3.7	89	40	2.2
2	1	0	55	45	96	40	3.3	98	42	3.9	92	35	2.3
3	1	0	63	45	98	34	3.6	100	36	4.3	95	31	2.7
4	1	0	61	45	97	35	3.5	99	38	4.3	94	32	2.5
5	1	0	35	45	93	56	2.7	95	59	3.3	86	48	1.9
6	1	0	82	45	103	21	4.7	105	22	5.8	103	21	3.6
7	1	0	48	55	103	54	2.8	106	57	3.3	96	46	1.9
8	1	0	55	55	104	48	2.9	107	51	3.6	98	42	2.1
9	1	0	63	55	105	42	3.2	108	44	3.9	101	37	2.3
10	1	0	61	55	105	43	3.1	107	46	3.8	100	38	2.3
11	1	0	35	55	101	65	2.5	104	68	3.0	93	55	1.7
12	1	0	82	55	110	27	4.0	112	29	4.9	109	26	3.0
13	1	0	48	65	112	62	2.5	114	65	3.1	104	53	1.8
14	1	0	55	65	113	56	2.7	115	59	3.3	106	48	1.9
15	1	0	63	65	114	50	2.9	116	52	3.5	108	43	2.0
16	1	0	61	65	113	51	2.8	116	54	3.4	107	44	2.0
17	1	0	35	65	110	73	2.3	113	77	2.8	101	63	1.5
18	1	0	82	65	117	35	3.5	119	37	4.3	114	31	2.6
19	1	0	48	75	120	71	2.3	123	74	2.9	111	61	1.6
20	1	0	55	75	121	65	2.5	124	68	3.0	113	55	1.7
21	1	0	63	75	122	58	2.6	125	61	3.2	115	50	1.8
22	1	0	61	75	122	60	2.6	125	63	3.2	114	51	1.8
23	1	0	35	75	119	82	2.2	122	86	2.7	109	70	1.4
24	1	0	82	75	125	42	3.1	128	45	3.8	121	37	2.3

Table B4 - Predicted Temperatures and Temperature Differences for the Pier Table and Box Girder Bottom Slabs

Case	Concrete Mix No.	Insulation R-Value	Average Air Temp., °F	Initial Concrete Temp., °F	Normal Weight Concrete at Pier Shaft			Lightweight Concrete at Location 1N			Lightweight Concrete at Location 7N		
					Maximum Concrete Temp., °F	Maximum Temeprature Difference, °F	Time of Maximum Temp. Diff., days	Maximum Concrete Temp., °F	Maximum Temeprature Difference, °F	Time of Maximum Temp. Diff., days	Maximum Concrete Temp., °F	Maximum Temeprature Difference, °F	Time of Maximum Temp. Diff., days
25	1	2	48	45	98	30	4.5	100	33	5.3	94	22	3.2
26	1	2	55	45	99	27	4.9	101	29	5.8	96	20	3.5
27	1	2	63	45	101	24	5.5	102	26	6.4	98	18	3.9
28	1	2	61	45	101	24	5.3	102	27	6.2	97	18	3.8
29	1	2	35	45	97	36	4.1	98	39	4.7	91	25	2.7
30	1	2	82	45	106	16	7.4	107	17	8.8	105	14	5.8
31	1	2	48	55	107	34	4.2	109	37	4.8	102	25	2.8
32	1	2	55	55	108	31	4.4	110	34	5.1	103	22	3.0
33	1	2	63	55	109	28	4.8	111	30	5.6	105	20	3.4
34	1	2	61	55	109	29	4.7	110	31	5.4	105	21	3.3
35	1	2	35	55	106	41	3.8	108	44	4.3	99	29	2.5
36	1	2	82	55	113	20	6.2	114	22	7.3	111	16	4.7
37	1	2	48	65	116	39	3.8	118	42	4.4	110	27	2.5
38	1	2	55	65	117	36	4.1	118	39	4.7	111	25	2.7
39	1	2	63	65	118	32	4.3	119	35	5.0	113	23	3.0
40	1	2	61	65	117	33	4.2	119	36	4.9	112	24	2.9
41	1	2	35	65	115	45	3.5	117	49	4.1	108	33	2.3
42	1	2	82	65	121	24	5.4	122	26	6.3	118	18	3.9
43	1	2	48	75	125	44	3.6	127	47	4.1	118	32	2.3
44	1	2	55	75	126	41	3.8	128	44	4.3	119	29	2.5
45	1	2	63	75	127	37	4.0	128	40	4.6	121	26	2.7
46	1	2	61	75	126	38	3.9	128	41	4.5	120	26	2.6
47	1	2	35	75	124	50	3.3	127	54	3.8	117	38	2.1
48	1	2	82	75	129	28	4.7	131	31	5.5	125	21	3.3

Table B4 - Predicted Temperatures and Temperature Differences for the Pier Table and Box Girder Bottom Slabs

Case	Concrete Mix No.	Insulation R-Value	Average Air Temp., °F	Initial Concrete Temp., °F	Normal Weight Concrete at Pier Shaft			Lightweight Concrete at Location 1N			Lightweight Concrete at Location 7N		
					Maximum Concrete Temp., °F	Maximum Temeprature Difference, °F	Time of Maximum Temp. Diff., days	Maximum Concrete Temp., °F	Maximum Temeprature Difference, °F	Time of Maximum Temp. Diff., days	Maximum Concrete Temp., °F	Maximum Temeprature Difference, °F	Time of Maximum Temp. Diff., days
49	1	4	48	45	100	23	6.2	102	25	6.9	96	16	3.8
50	1	4	55	45	101	21	6.7	102	22	7.5	97	13	4.3
51	1	4	63	45	102	18	7.1	104	19	8.0	99	12	4.9
52	1	4	61	45	102	19	7.0	103	20	7.8	99	12	4.7
53	1	4	35	45	99	28	5.4	101	29	6.1	93	21	3.3
54	1	4	82	45	107	13	9.7	108	14	11.2	106	10	7.4
55	1	4	48	55	109	26	5.5	111	28	6.3	104	20	3.4
56	1	4	55	55	110	24	5.9	111	26	6.7	105	17	3.7
57	1	4	63	55	111	21	6.5	112	23	7.3	107	14	4.1
58	1	4	61	55	111	22	6.4	112	24	7.2	106	15	4.0
59	1	4	35	55	108	33	5.0	110	34	5.6	102	25	3.3
60	1	4	82	55	114	15	8.1	115	17	9.2	112	11	5.8
61	1	4	48	65	119	31	5.1	120	33	5.8	113	24	3.3
62	1	4	55	65	119	28	5.4	121	29	6.1	113	21	3.3
63	1	4	63	65	120	25	5.8	121	27	6.6	115	18	3.6
64	1	4	61	65	120	25	5.7	121	27	6.4	114	19	3.5
65	1	4	35	65	118	38	4.6	119	40	5.3	111	30	3.0
66	1	4	82	65	122	18	7.0	123	20	7.9	119	12	4.8
67	1	4	48	75	128	36	4.7	130	38	5.3	121	29	3.1
68	1	4	55	75	128	33	5.0	130	34	5.6	122	25	3.3
69	1	4	63	75	129	29	5.3	131	30	6.0	123	22	3.3
70	1	4	61	75	129	30	5.2	130	31	5.9	123	23	3.4
71	1	4	35	75	127	43	4.3	129	45	4.9	120	35	2.8
72	1	4	82	75	131	22	6.4	132	23	7.2	127	14	4.1

Table B4 - Predicted Temperatures and Temperature Differences for the Pier Table and Box Girder Bottom Slabs

Case	Concrete Mix No.	Insulation R-Value	Average Air Temp., °F	Initial Concrete Temp., °F	Normal Weight Concrete at Pier Shaft			Lightweight Concrete at Location 1N			Lightweight Concrete at Location 7N		
					Maximum Concrete Temp., °F	Maximum Temeprature Difference, °F	Time of Maximum Temp. Diff., days	Maximum Concrete Temp., °F	Maximum Temeprature Difference, °F	Time of Maximum Temp. Diff., days	Maximum Concrete Temp., °F	Maximum Temeprature Difference, °F	Time of Maximum Temp. Diff., days
73	2	0	48	45	84	35	3.3	86	37	4.1	80	31	2.4
74	2	0	55	45	85	30	3.7	87	32	4.5	83	27	2.7
75	2	0	63	45	87	24	4.1	89	26	5.1	87	23	3.1
76	2	0	61	45	87	25	4.0	89	27	4.9	86	24	3.0
77	2	0	35	45	81	45	2.8	84	48	3.5	76	39	2.0
78	2	0	82	45	95	13	5.8	96	14	6.6	97	15	4.3
79	2	0	48	55	92	43	2.9	94	45	3.6	87	37	2.1
80	2	0	55	55	93	37	3.2	95	40	3.9	89	33	2.3
81	2	0	63	55	95	31	3.6	97	33	4.4	92	28	2.7
82	2	0	61	55	94	33	3.4	96	35	4.2	92	29	2.6
83	2	0	35	55	90	54	2.6	92	56	3.2	83	46	1.8
84	2	0	82	55	100	18	4.8	102	20	5.9	101	19	3.7
85	2	0	48	65	100	51	2.6	103	54	3.3	94	44	1.8
86	2	0	55	65	101	45	2.8	104	48	3.5	96	39	2.0
87	2	0	63	65	103	39	3.1	105	41	3.8	99	34	2.3
88	2	0	61	65	102	40	3.0	105	43	3.8	98	36	2.2
89	2	0	35	65	99	62	2.3	101	65	2.9	91	53	1.6
90	2	0	82	65	107	25	4.1	109	27	5.0	106	23	3.1
91	2	0	48	75	109	60	2.4	112	63	3.0	102	51	1.6
92	2	0	55	75	110	54	2.6	112	56	3.2	103	46	1.8
93	2	0	63	75	111	47	2.8	113	50	3.4	105	41	2.0
94	2	0	61	75	111	49	2.7	113	51	3.3	105	42	1.9
95	2	0	35	75	108	71	2.2	111	74	2.7	99	61	1.4
96	2	0	82	75	114	32	3.5	117	34	4.3	112	29	2.6

Table B4 - Predicted Temperatures and Temperature Differences for the Pier Table and Box Girder Bottom Slabs

Case	Concrete Mix No.	Insulation R-Value	Average Air Temp., °F	Initial Concrete Temp., °F	Normal Weight Concrete at Pier Shaft			Lightweight Concrete at Location 1N			Lightweight Concrete at Location 7N		
					Maximum Concrete Temp., °F	Maximum Temeprature Difference, °F	Time of Maximum Temp. Diff., days	Maximum Concrete Temp., °F	Maximum Temeprature Difference, °F	Time of Maximum Temp. Diff., days	Maximum Concrete Temp., °F	Maximum Temeprature Difference, °F	Time of Maximum Temp. Diff., days
97	2	2	48	45	87	24	5.2	89	27	6.2	84	18	3.7
98	2	2	55	45	89	22	5.9	90	24	6.9	86	17	4.3
99	2	2	63	45	91	18	6.8	92	20	8.1	89	15	5.1
100	2	2	61	45	90	19	6.5	91	21	7.7	88	15	4.9
101	2	2	35	45	85	30	4.4	87	33	5.1	80	22	3.0
102	2	2	82	45	97	10	9.5	99	12	11.3	99	11	7.3
103	2	2	48	55	96	29	4.6	97	31	5.3	91	21	3.1
104	2	2	55	55	97	26	5.0	98	28	5.9	93	19	3.5
105	2	2	63	55	98	22	5.7	100	25	6.7	95	17	4.1
106	2	2	61	55	98	23	5.5	99	25	6.4	95	17	3.9
107	2	2	35	55	94	34	4.0	96	37	4.6	88	24	2.6
108	2	2	82	55	103	15	8.2	105	16	9.5	103	13	6.2
109	2	2	48	65	104	33	4.1	106	36	4.7	99	23	2.7
110	2	2	55	65	105	30	4.4	107	33	5.1	100	22	3.0
111	2	2	63	65	106	26	4.8	108	29	5.7	102	19	3.4
112	2	2	61	65	106	27	4.8	108	30	5.6	102	20	3.3
113	2	2	35	65	103	39	3.7	105	42	4.2	97	27	2.3
114	2	2	82	65	110	19	6.7	112	21	7.9	109	15	4.9
115	2	2	48	75	113	38	3.8	115	41	4.3	107	26	2.4
116	2	2	55	75	114	34	4.0	116	37	4.6	108	24	2.6
117	2	2	63	75	115	31	4.3	117	33	5.0	110	22	2.9
118	2	2	61	75	115	32	4.2	116	34	4.9	110	23	2.8
119	2	2	35	75	112	44	3.4	114	47	3.9	106	32	2.1
120	2	2	82	75	118	23	5.6	119	25	6.6	115	17	4.0

Table B4 - Predicted Temperatures and Temperature Differences for the Pier Table and Box Girder Bottom Slabs

Case	Concrete Mix No.	Insulation R-Value	Average Air Temp., °F	Initial Concrete Temp., °F	Normal Weight Concrete at Pier Shaft			Lightweight Concrete at Location 1N			Lightweight Concrete at Location 7N		
					Maximum Concrete Temp., °F	Maximum Temeprature Difference, °F	Time of Maximum Temp. Diff., days	Maximum Concrete Temp., °F	Maximum Temeprature Difference, °F	Time of Maximum Temp. Diff., days	Maximum Concrete Temp., °F	Maximum Temeprature Difference, °F	Time of Maximum Temp. Diff., days
121	2	4	48	45	89	19	7.2	90	20	7.9	85	12	4.6
122	2	4	55	45	90	17	7.8	91	18	9.0	87	12	5.4
123	2	4	63	45	92	15	9.1	93	16	10.5	90	11	6.6
124	2	4	61	45	92	15	8.8	93	17	10.0	90	11	6.2
125	2	4	35	45	87	23	6.1	89	25	6.9	82	16	3.7
126	2	4	82	45	99	9	13.5	100	11	15.4	99	10	10.1
127	2	4	48	55	98	22	6.3	99	24	7.2	93	14	3.8
128	2	4	55	55	98	20	7.0	100	22	7.9	95	13	4.3
129	2	4	63	55	100	17	7.5	101	19	8.6	97	12	5.2
130	2	4	61	55	99	18	7.3	101	19	8.3	96	12	5.0
131	2	4	35	55	96	26	5.4	98	28	6.2	91	20	3.3
132	2	4	82	55	105	12	11.1	106	14	12.7	104	10	8.3
133	2	4	48	65	107	25	5.6	108	27	6.3	101	18	3.3
134	2	4	55	65	107	23	6.1	109	25	6.9	102	16	3.7
135	2	4	63	65	108	21	6.8	109	22	7.7	104	13	4.2
136	2	4	61	65	108	21	6.6	109	23	7.4	104	13	4.1
137	2	4	35	65	106	31	4.9	107	33	5.6	100	24	3.1
138	2	4	82	65	112	15	8.9	113	16	10.3	110	11	6.4
139	2	4	48	75	116	29	5.1	117	31	5.8	110	23	3.2
140	2	4	55	75	116	26	5.4	118	28	6.2	111	20	3.3
141	2	4	63	75	117	24	5.9	118	26	6.7	112	16	3.6
142	2	4	61	75	117	24	5.8	118	26	6.6	112	17	3.5
143	2	4	35	75	115	36	4.5	116	38	5.2	108	29	2.9
144	2	4	82	75	120	18	7.4	121	19	8.5	117	12	5.0

Table B4 - Predicted Temperatures and Temperature Differences for the Pier Table and Box Girder Bottom Slabs

Case	Concrete Mix No.	Insulation R-Value	Average Air Temp., °F	Initial Concrete Temp., °F	Normal Weight Concrete at Pier Shaft			Lightweight Concrete at Location 1N			Lightweight Concrete at Location 7N		
					Maximum Concrete Temp., °F	Maximum Temeprature Difference, °F	Time of Maximum Temp. Diff., days	Maximum Concrete Temp., °F	Maximum Temeprature Difference, °F	Time of Maximum Temp. Diff., days	Maximum Concrete Temp., °F	Maximum Temeprature Difference, °F	Time of Maximum Temp. Diff., days
145	3	0	48	45	102	53	2.9	105	56	3.6	96	46	2.1
146	3	0	55	45	104	48	3.2	106	51	3.9	98	41	2.3
147	3	0	63	45	105	41	3.4	108	44	4.2	101	36	2.5
148	3	0	61	45	105	43	3.4	107	46	4.1	100	38	2.5
149	3	0	35	45	100	64	2.7	104	67	3.3	92	55	1.9
150	3	0	82	45	110	28	4.4	112	30	5.3	109	26	3.3
151	3	0	48	55	111	61	2.8	114	65	3.3	103	53	1.9
152	3	0	55	55	112	56	2.9	115	59	3.5	105	48	2.0
153	3	0	63	55	113	49	3.1	116	52	3.8	107	43	2.2
154	3	0	61	55	113	51	3.1	116	54	3.7	107	44	2.2
155	3	0	35	55	109	72	2.5	112	76	3.0	100	62	1.7
156	3	0	82	55	118	35	3.8	120	37	4.6	114	31	2.8
157	3	0	48	65	120	70	2.6	123	73	3.1	110	60	1.8
158	3	0	55	65	120	64	2.7	124	67	3.3	112	55	1.9
159	3	0	63	65	122	57	2.9	125	61	3.5	114	49	2.0
160	3	0	61	65	121	59	2.8	124	62	3.4	114	50	2.0
161	3	0	35	65	118	81	2.4	122	85	2.9	107	69	1.5
162	3	0	82	65	125	42	3.4	128	45	4.1	121	37	2.5
163	3	0	48	75	128	78	2.4	132	82	2.9	118	67	1.6
164	3	0	55	75	129	72	2.5	132	76	3.0	120	62	1.7
165	3	0	63	75	130	66	2.6	133	69	3.2	122	56	1.8
166	3	0	61	75	130	67	2.6	133	71	3.2	121	57	1.8
167	3	0	35	75	127	90	2.3	131	94	2.7	116	77	1.5
168	3	0	82	75	133	50	3.1	136	53	3.8	127	43	2.2

Table B4 - Predicted Temperatures and Temperature Differences for the Pier Table and Box Girder Bottom Slabs

Case	Concrete Mix No.	Insulation R-Value	Average Air Temp., °F	Initial Concrete Temp., °F	Normal Weight Concrete at Pier Shaft			Lightweight Concrete at Location 1N			Lightweight Concrete at Location 7N		
					Maximum Concrete Temp., °F	Maximum Temeprature Difference, °F	Time of Maximum Temp. Diff., days	Maximum Concrete Temp., °F	Maximum Temeprature Difference, °F	Time of Maximum Temp. Diff., days	Maximum Concrete Temp., °F	Maximum Temeprature Difference, °F	Time of Maximum Temp. Diff., days
169	3	2	48	45	107	35	4.5	109	38	5.2	101	25	3.1
170	3	2	55	45	108	32	4.8	110	35	5.6	103	23	3.3
171	3	2	63	45	109	28	5.3	111	31	6.1	105	21	3.7
172	3	2	61	45	109	29	5.1	111	32	5.9	105	21	3.6
173	3	2	35	45	106	41	4.1	108	44	4.7	99	29	2.7
174	3	2	82	45	113	20	6.8	115	22	7.9	111	16	5.1
175	3	2	48	55	116	40	4.2	118	43	4.8	109	28	2.8
176	3	2	55	55	117	36	4.4	118	39	5.0	111	26	3.0
177	3	2	63	55	118	33	4.7	119	36	5.4	112	23	3.3
178	3	2	61	55	117	33	4.6	119	37	5.3	112	24	3.2
179	3	2	35	55	115	46	3.8	117	49	4.4	107	33	2.5
180	3	2	82	55	121	24	5.9	123	27	6.8	118	18	4.3
181	3	2	48	65	125	44	3.9	127	48	4.5	117	32	2.5
182	3	2	55	65	126	41	4.1	128	44	4.7	119	29	2.7
183	3	2	63	65	126	37	4.4	128	40	5.0	120	26	2.9
184	3	2	61	65	126	38	4.3	128	41	4.9	120	27	2.9
185	3	2	35	65	124	51	3.6	126	54	4.2	116	38	2.3
186	3	2	82	65	129	29	5.2	131	31	6.0	125	21	3.6
187	3	2	48	75	134	49	3.7	136	53	4.2	126	36	2.3
188	3	2	55	75	135	46	3.8	137	49	4.4	127	33	2.5
189	3	2	63	75	135	42	4.1	137	45	4.6	128	29	2.7
190	3	2	61	75	135	43	4.0	137	46	4.6	128	30	2.6
191	3	2	35	75	133	55	3.4	135	59	3.9	124	42	2.2
192	3	2	82	75	138	33	4.7	139	36	5.4	132	24	3.2

Table B4 - Predicted Temperatures and Temperature Differences for the Pier Table and Box Girder Bottom Slabs

Case	Concrete Mix No.	Insulation R-Value	Average Air Temp., °F	Initial Concrete Temp., °F	Normal Weight Concrete at Pier Shaft			Lightweight Concrete at Location 1N			Lightweight Concrete at Location 7N		
					Maximum Concrete Temp., °F	Maximum Temeprature Difference, °F	Time of Maximum Temp. Diff., days	Maximum Concrete Temp., °F	Maximum Temeprature Difference, °F	Time of Maximum Temp. Diff., days	Maximum Concrete Temp., °F	Maximum Temeprature Difference, °F	Time of Maximum Temp. Diff., days
193	3	4	48	45	110	27	6.1	111	29	6.9	104	20	3.8
194	3	4	55	45	110	25	6.6	112	27	7.4	105	17	4.1
195	3	4	63	45	111	22	7.2	113	24	8.1	107	14	4.6
196	3	4	61	45	111	23	7.0	112	25	7.9	106	15	4.4
197	3	4	35	45	108	33	5.5	110	35	6.2	102	25	3.6
198	3	4	82	45	115	16	8.8	116	17	10.1	113	11	6.3
199	3	4	48	55	119	31	5.6	120	33	6.3	112	24	3.7
200	3	4	55	55	119	28	5.9	121	30	6.7	113	21	3.7
201	3	4	63	55	120	25	6.4	122	27	7.2	115	18	4.0
202	3	4	61	55	120	26	6.3	121	28	7.1	114	19	3.9
203	3	4	35	55	118	38	5.1	119	40	5.8	110	30	3.3
204	3	4	82	55	123	19	7.8	124	20	8.6	119	13	5.2
205	3	4	48	65	128	36	5.2	130	38	5.9	121	28	3.4
206	3	4	55	65	128	33	5.5	130	35	6.2	122	25	3.6
207	3	4	63	65	129	29	5.8	131	31	6.6	123	22	3.6
208	3	4	61	65	129	30	5.8	131	32	6.5	123	23	3.6
209	3	4	35	65	127	43	4.8	129	45	5.4	119	34	3.1
210	3	4	82	65	131	23	7.1	133	24	8.0	127	14	4.5
211	3	4	48	75	137	41	4.8	139	44	5.5	130	33	3.2
212	3	4	55	75	138	38	5.1	139	40	5.8	130	30	3.3
213	3	4	63	75	138	34	5.4	140	36	6.1	131	26	3.6
214	3	4	61	75	138	35	5.3	140	37	6.0	131	27	3.5
215	3	4	35	75	136	48	4.5	138	50	5.1	128	39	2.9
216	3	4	82	75	140	26	6.4	142	28	7.2	135	18	4.0

Table B4 - Predicted Temperatures and Temperature Differences for the Pier Table and Box Girder Bottom Slabs

Case	Concrete Mix No.	Insulation R-Value	Average Air Temp., °F	Initial Concrete Temp., °F	Normal Weight Concrete at Pier Shaft			Lightweight Concrete at Location 1N			Lightweight Concrete at Location 7N		
					Maximum Concrete Temp., °F	Maximum Temeprature Difference, °F	Time of Maximum Temp. Diff., days	Maximum Concrete Temp., °F	Maximum Temeprature Difference, °F	Time of Maximum Temp. Diff., days	Maximum Concrete Temp., °F	Maximum Temeprature Difference, °F	Time of Maximum Temp. Diff., days
217	4	0	48	45	90	41	3.3	92	43	4.0	85	36	2.4
218	4	0	55	45	91	35	3.6	94	38	4.4	88	32	2.6
219	4	0	63	45	93	30	4.0	95	32	4.9	91	27	3.0
220	4	0	61	45	93	31	3.9	95	33	4.8	90	28	2.9
221	4	0	35	45	87	51	2.8	90	54	3.5	81	44	2.0
222	4	0	82	45	100	18	5.6	102	19	6.8	101	18	4.1
223	4	0	48	55	98	49	2.9	101	52	3.6	92	42	2.1
224	4	0	55	55	99	43	3.1	102	46	3.9	94	38	2.3
225	4	0	63	55	101	37	3.4	103	40	4.3	97	33	2.5
226	4	0	61	55	100	38	3.4	103	41	4.2	96	34	2.5
227	4	0	35	55	96	59	2.6	99	63	3.2	88	51	1.8
228	4	0	82	55	106	24	4.6	108	26	5.6	105	23	3.5
229	4	0	48	65	106	57	2.7	109	60	3.3	99	49	1.9
230	4	0	55	65	107	51	2.8	110	54	3.5	101	44	2.0
231	4	0	63	65	109	45	3.1	111	48	3.8	103	39	2.2
232	4	0	61	65	108	46	3.0	111	49	3.7	103	40	2.2
233	4	0	35	65	105	68	2.4	108	71	3.0	96	58	1.6
234	4	0	82	65	113	30	3.9	115	33	4.8	111	28	3.0
235	4	0	48	75	115	65	2.5	118	69	3.0	106	56	1.7
236	4	0	55	75	116	59	2.6	119	63	3.2	108	51	1.8
237	4	0	63	75	117	53	2.8	120	56	3.4	110	45	1.9
238	4	0	61	75	117	54	2.8	120	58	3.4	110	47	1.9
239	4	0	35	75	114	77	2.3	117	80	2.8	104	65	1.5
240	4	0	82	75	120	38	3.4	123	40	4.2	117	33	2.5

Table B4 - Predicted Temperatures and Temperature Differences for the Pier Table and Box Girder Bottom Slabs

Case	Concrete Mix No.	Insulation R-Value	Average Air Temp., °F	Initial Concrete Temp., °F	Normal Weight Concrete at Pier Shaft			Lightweight Concrete at Location 1N			Lightweight Concrete at Location 7N		
					Maximum Concrete Temp., °F	Maximum Temeprature Difference, °F	Time of Maximum Temp. Diff., days	Maximum Concrete Temp., °F	Maximum Temeprature Difference, °F	Time of Maximum Temp. Diff., days	Maximum Concrete Temp., °F	Maximum Temeprature Difference, °F	Time of Maximum Temp. Diff., days
241	4	2	48	45	94	28	5.1	96	31	6.0	89	20	3.6
242	4	2	55	45	95	25	5.7	97	28	6.7	91	19	4.0
243	4	2	63	45	97	22	6.5	98	24	7.6	94	17	4.7
244	4	2	61	45	96	23	6.2	98	25	7.3	93	17	4.5
245	4	2	35	45	92	34	4.4	94	37	5.2	86	24	3.0
246	4	2	82	45	103	14	9.3	104	16	11.1	103	13	7.0
247	4	2	48	55	102	32	4.5	104	35	5.3	97	23	3.1
248	4	2	55	55	103	29	4.9	105	32	5.8	99	21	3.4
249	4	2	63	55	105	26	5.5	106	29	6.5	101	19	3.9
250	4	2	61	55	104	27	5.4	106	30	6.3	100	20	3.8
251	4	2	35	55	101	39	4.1	103	42	4.7	94	27	2.7
252	4	2	82	55	109	18	7.5	111	20	9.0	108	15	5.6
253	4	2	48	65	111	37	4.2	113	40	4.8	105	26	2.8
254	4	2	55	65	112	34	4.4	114	37	5.2	106	24	3.0
255	4	2	63	65	113	30	4.8	115	33	5.6	108	22	3.3
256	4	2	61	65	113	31	4.7	114	34	5.5	108	22	3.2
257	4	2	35	65	110	43	3.8	112	47	4.4	103	30	2.4
258	4	2	82	65	117	22	6.3	118	25	7.4	114	17	4.6
259	4	2	48	75	120	42	3.9	122	45	4.5	113	29	2.5
260	4	2	55	75	121	39	4.1	123	42	4.7	114	27	2.7
261	4	2	63	75	122	35	4.4	123	38	5.0	116	24	2.9
262	4	2	61	75	121	36	4.3	123	39	4.9	115	25	2.8
263	4	2	35	75	119	48	3.5	121	52	4.1	111	35	2.2
264	4	2	82	75	125	26	5.4	126	29	6.4	121	19	3.8

Table B4 - Predicted Temperatures and Temperature Differences for the Pier Table and Box Girder Bottom Slabs

Case	Concrete Mix No.	Insulation R-Value	Average Air Temp., °F	Initial Concrete Temp., °F	Normal Weight Concrete at Pier Shaft			Lightweight Concrete at Location 1N			Lightweight Concrete at Location 7N		
					Maximum Concrete Temp., °F	Maximum Temeprature Difference, °F	Time of Maximum Temp. Diff., days	Maximum Concrete Temp., °F	Maximum Temeprature Difference, °F	Time of Maximum Temp. Diff., days	Maximum Concrete Temp., °F	Maximum Temeprature Difference, °F	Time of Maximum Temp. Diff., days
265	4	4	48	45	96	22	7.3	97	24	8.2	91	14	4.4
266	4	4	55	45	97	20	8.0	98	22	9.0	93	13	5.0
267	4	4	63	45	99	17	8.7	100	19	9.9	96	12	6.0
268	4	4	61	45	98	18	8.4	100	20	9.6	95	12	5.7
269	4	4	35	45	95	27	6.2	96	29	7.0	89	19	3.7
270	4	4	82	45	104	12	12.7	106	14	14.8	104	10	9.4
271	4	4	48	55	105	26	6.4	106	28	7.3	99	17	3.9
272	4	4	55	55	106	23	7.0	107	25	7.9	101	15	4.3
273	4	4	63	55	107	21	7.8	108	23	8.8	103	13	4.8
274	4	4	61	55	106	21	7.6	108	23	8.6	102	13	4.7
275	4	4	35	55	104	30	5.6	105	32	6.3	97	23	3.6
276	4	4	82	55	111	15	10.3	112	17	11.8	109	11	7.4
277	4	4	48	65	114	29	5.7	115	31	6.5	107	22	3.7
278	4	4	55	65	115	27	6.2	116	29	7.0	109	19	3.7
279	4	4	63	65	115	24	6.8	117	26	7.7	110	16	4.1
280	4	4	61	65	115	25	6.6	117	27	7.5	110	16	4.0
281	4	4	35	65	113	35	5.1	114	37	5.8	106	27	3.3
282	4	4	82	65	118	18	8.6	120	19	9.8	115	12	5.8
283	4	4	48	75	123	34	5.3	125	36	6.0	116	26	3.3
284	4	4	55	75	124	30	5.6	125	32	6.3	117	23	3.6
285	4	4	63	75	124	27	6.0	126	29	6.8	118	19	3.6
286	4	4	61	75	124	28	5.9	126	30	6.7	118	20	3.6
287	4	4	35	75	122	40	4.8	124	42	5.4	115	32	3.0
288	4	4	82	75	127	21	7.7	128	23	8.7	122	13	4.8

Table B4 - Predicted Temperatures and Temperature Differences for the Pier Table and Box Girder Bottom Slabs

Case	Concrete Mix No.	Insulation R-Value	Average Air Temp., °F	Initial Concrete Temp., °F	Normal Weight Concrete at Pier Shaft			Lightweight Concrete at Location 1N			Lightweight Concrete at Location 7N		
					Maximum Concrete Temp., °F	Maximum Temeprature Difference, °F	Time of Maximum Temp. Diff., days	Maximum Concrete Temp., °F	Maximum Temeprature Difference, °F	Time of Maximum Temp. Diff., days	Maximum Concrete Temp., °F	Maximum Temeprature Difference, °F	Time of Maximum Temp. Diff., days
289	5	0	48	45	110	61	2.9	114	64	3.6	102	52	2.1
290	5	0	55	45	112	55	3.1	115	59	3.8	104	47	2.2
291	5	0	63	45	113	49	3.3	116	52	4.1	107	42	2.4
292	5	0	61	45	113	51	3.3	116	54	4.0	106	44	2.3
293	5	0	35	45	108	72	2.7	112	76	3.3	99	61	1.9
294	5	0	82	45	118	35	4.1	120	38	4.9	115	31	3.0
295	5	0	48	55	119	69	2.8	122	73	3.3	109	59	1.9
296	5	0	55	55	120	63	2.9	123	67	3.5	111	54	2.0
297	5	0	63	55	121	57	3.1	124	60	3.8	114	49	2.2
298	5	0	61	55	121	59	3.0	124	62	3.7	113	50	2.2
299	5	0	35	55	117	80	2.5	121	84	3.1	106	68	1.7
300	5	0	82	55	125	42	3.6	128	45	4.4	121	37	2.7
301	5	0	48	65	127	78	2.6	131	82	3.1	117	66	1.8
302	5	0	55	65	128	72	2.7	132	76	3.3	119	61	1.9
303	5	0	63	65	130	65	2.8	133	69	3.5	121	55	2.0
304	5	0	61	65	129	67	2.8	133	70	3.4	120	57	2.0
305	5	0	35	65	126	89	2.4	130	93	2.9	114	75	1.5
306	5	0	82	65	133	50	3.3	136	53	4.0	127	43	2.3
307	5	0	48	75	136	86	2.4	140	90	3.0	125	73	1.6
308	5	0	55	75	137	80	2.5	141	84	3.1	126	68	1.7
309	5	0	63	75	138	73	2.7	142	77	3.3	128	62	1.8
310	5	0	61	75	138	75	2.6	141	79	3.2	128	64	1.8
311	5	0	35	75	135	97	2.3	139	102	2.8	122	83	1.5
312	5	0	82	75	141	58	3.1	144	61	3.7	134	49	2.2

Table B4 - Predicted Temperatures and Temperature Differences for the Pier Table and Box Girder Bottom Slabs

Case	Concrete Mix No.	Insulation R-Value	Average Air Temp., °F	Initial Concrete Temp., °F	Normal Weight Concrete at Pier Shaft			Lightweight Concrete at Location 1N			Lightweight Concrete at Location 7N		
					Maximum Concrete Temp., °F	Maximum Temeprature Difference, °F	Time of Maximum Temp. Diff., days	Maximum Concrete Temp., °F	Maximum Temeprature Difference, °F	Time of Maximum Temp. Diff., days	Maximum Concrete Temp., °F	Maximum Temeprature Difference, °F	Time of Maximum Temp. Diff., days
313	5	2	48	45	116	40	4.6	118	43	5.2	109	28	3.0
314	5	2	55	45	117	37	4.8	119	40	5.5	110	26	3.3
315	5	2	63	45	118	33	5.1	120	36	5.9	112	24	3.6
316	5	2	61	45	117	34	5.0	119	37	5.8	112	24	3.4
317	5	2	35	45	114	46	4.2	117	50	4.8	106	33	2.7
318	5	2	82	45	122	25	6.3	123	27	7.3	118	19	4.6
319	5	2	48	55	125	45	4.3	127	49	4.8	117	31	2.8
320	5	2	55	55	125	42	4.4	127	45	5.1	118	29	2.9
321	5	2	63	55	126	38	4.8	128	41	5.3	120	26	3.2
322	5	2	61	55	126	39	4.7	128	42	5.3	120	27	3.1
323	5	2	35	55	123	51	3.9	126	55	4.5	115	37	2.5
324	5	2	82	55	129	29	5.6	131	32	6.5	125	21	3.9
325	5	2	48	65	134	50	4.0	136	53	4.5	125	36	2.6
326	5	2	55	65	134	46	4.2	137	50	4.8	126	33	2.7
327	5	2	63	65	135	43	4.4	137	46	5.0	128	29	2.9
328	5	2	61	65	135	43	4.3	137	47	4.9	127	30	2.8
329	5	2	35	65	133	56	3.7	135	60	4.3	123	42	2.3
330	5	2	82	65	138	34	5.0	140	37	5.8	132	24	3.5
331	5	2	48	75	143	54	3.8	145	59	4.3	134	40	2.4
332	5	2	55	75	143	51	3.9	146	55	4.5	135	37	2.5
333	5	2	63	75	144	47	4.1	146	51	4.7	136	34	2.7
334	5	2	61	75	144	48	4.1	146	52	4.6	136	35	2.6
335	5	2	35	75	142	60	3.5	144	65	4.1	132	47	2.2
336	5	2	82	75	146	38	4.7	148	41	5.3	140	27	3.1

Table B4 - Predicted Temperatures and Temperature Differences for the Pier Table and Box Girder Bottom Slabs

Case	Concrete Mix No.	Insulation R-Value	Average Air Temp., °F	Initial Concrete Temp., °F	Normal Weight Concrete at Pier Shaft			Lightweight Concrete at Location 1N			Lightweight Concrete at Location 7N		
					Maximum Concrete Temp., °F	Maximum Temeprature Difference, °F	Time of Maximum Temp. Diff., days	Maximum Concrete Temp., °F	Maximum Temeprature Difference, °F	Time of Maximum Temp. Diff., days	Maximum Concrete Temp., °F	Maximum Temeprature Difference, °F	Time of Maximum Temp. Diff., days
337	5	4	48	45	119	31	6.1	121	33	6.8	112	24	4.1
338	5	4	55	45	120	29	6.5	121	31	7.3	113	21	4.0
339	5	4	63	45	120	26	7.0	122	28	7.8	115	18	4.4
340	5	4	61	45	120	27	6.9	122	29	7.7	114	19	4.3
341	5	4	35	45	118	38	5.5	119	40	6.2	110	30	3.7
342	5	4	82	45	123	20	8.5	125	21	9.3	120	13	5.7
343	5	4	48	55	128	36	5.6	130	39	6.3	120	28	3.8
344	5	4	55	55	128	33	5.9	130	35	6.7	121	25	4.0
345	5	4	63	55	129	29	6.4	131	32	7.2	123	22	3.9
346	5	4	61	55	129	30	6.3	131	32	7.0	122	23	3.9
347	5	4	35	55	127	43	5.2	129	45	5.8	119	34	3.4
348	5	4	82	55	132	23	7.8	133	25	8.6	127	15	4.9
349	5	4	48	65	137	41	5.3	139	44	5.9	129	33	3.5
350	5	4	55	65	138	38	5.5	139	40	6.2	130	30	3.7
351	5	4	63	65	138	34	5.8	140	36	6.6	131	26	3.9
352	5	4	61	65	138	35	5.8	140	37	6.5	131	27	3.8
353	5	4	35	65	136	48	4.9	138	51	5.5	127	39	3.2
354	5	4	82	65	140	27	6.9	142	29	7.8	135	18	4.3
355	5	4	48	75	146	47	5.0	148	49	5.6	138	37	3.3
356	5	4	55	75	147	43	5.2	149	45	5.8	139	34	3.4
357	5	4	63	75	147	39	5.4	149	41	6.2	140	31	3.6
358	5	4	61	75	147	40	5.4	149	42	6.1	139	31	3.6
359	5	4	35	75	145	53	4.6	147	56	5.3	136	43	3.0
360	5	4	82	75	149	30	6.3	151	32	7.1	143	22	3.9

Table B4 - Predicted Temperatures and Temperature Differences for the Pier Table and Box Girder Bottom Slabs

Case	Concrete Mix No.	Insulation R-Value	Average Air Temp., °F	Initial Concrete Temp., °F	Normal Weight Concrete at Pier Shaft			Lightweight Concrete at Location 1N			Lightweight Concrete at Location 7N		
					Maximum Concrete Temp., °F	Maximum Temeprature Difference, °F	Time of Maximum Temp. Diff., days	Maximum Concrete Temp., °F	Maximum Temeprature Difference, °F	Time of Maximum Temp. Diff., days	Maximum Concrete Temp., °F	Maximum Temeprature Difference, °F	Time of Maximum Temp. Diff., days
361	6	0	48	45	96	47	3.3	99	50	3.9	90	40	2.3
362	6	0	55	45	97	41	3.5	100	44	4.3	92	36	2.5
363	6	0	63	45	99	35	3.9	102	38	4.8	96	31	2.8
364	6	0	61	45	99	37	3.8	101	40	4.6	95	33	2.7
365	6	0	35	45	93	57	2.9	97	60	3.5	86	49	2.0
366	6	0	82	45	105	23	5.1	107	25	6.3	105	22	3.8
367	6	0	48	55	104	55	2.9	107	58	3.6	97	47	2.1
368	6	0	55	55	105	49	3.1	108	52	3.9	99	42	2.3
369	6	0	63	55	107	43	3.4	110	46	4.2	102	37	2.5
370	6	0	61	55	106	44	3.3	109	47	4.1	101	38	2.4
371	6	0	35	55	102	65	2.6	105	69	3.3	93	56	1.8
372	6	0	82	55	112	29	4.4	114	31	5.3	110	27	3.3
373	6	0	48	65	112	63	2.7	116	66	3.3	104	53	1.9
374	6	0	55	65	113	57	2.9	117	60	3.5	106	49	2.0
375	6	0	63	65	115	51	3.1	118	54	3.8	108	43	2.2
376	6	0	61	65	114	52	3.0	117	55	3.7	108	45	2.1
377	6	0	35	65	111	74	2.5	114	78	3.0	101	63	1.7
378	6	0	82	65	119	36	3.8	121	39	4.7	115	32	2.8
379	6	0	48	75	121	71	2.5	124	75	3.1	111	61	1.7
380	6	0	55	75	122	65	2.6	125	69	3.3	113	56	1.8
381	6	0	63	75	123	59	2.8	126	62	3.4	115	50	2.0
382	6	0	61	75	123	60	2.8	126	64	3.4	115	51	1.9
383	6	0	35	75	120	83	2.3	123	87	2.8	108	70	1.5
384	6	0	82	75	127	44	3.4	129	47	4.1	121	38	2.5

Table B4 - Predicted Temperatures and Temperature Differences for the Pier Table and Box Girder Bottom Slabs

Case	Concrete Mix No.	Insulation R-Value	Average Air Temp., °F	Initial Concrete Temp., °F	Normal Weight Concrete at Pier Shaft			Lightweight Concrete at Location 1N			Lightweight Concrete at Location 7N		
					Maximum Concrete Temp., °F	Maximum Temeprature Difference, °F	Time of Maximum Temp. Diff., days	Maximum Concrete Temp., °F	Maximum Temeprature Difference, °F	Time of Maximum Temp. Diff., days	Maximum Concrete Temp., °F	Maximum Temeprature Difference, °F	Time of Maximum Temp. Diff., days
385	6	2	48	45	100	32	5.1	102	35	6.0	95	23	3.5
386	6	2	55	45	102	29	5.6	104	32	6.4	97	21	3.8
387	6	2	63	45	103	26	6.2	105	28	7.2	100	19	4.4
388	6	2	61	45	103	27	6.0	105	29	7.0	99	19	4.3
389	6	2	35	45	99	38	4.5	101	41	5.2	92	26	3.0
390	6	2	82	45	109	18	8.5	110	20	10.0	107	15	6.3
391	6	2	48	55	109	37	4.7	111	40	5.3	103	25	3.1
392	6	2	55	55	110	33	4.9	112	36	5.7	104	23	3.3
393	6	2	63	55	111	30	5.4	113	33	6.3	106	21	3.8
394	6	2	61	55	111	31	5.3	113	34	6.2	106	22	3.6
395	6	2	35	55	108	43	4.2	110	46	4.8	100	29	2.7
396	6	2	82	55	116	22	7.2	117	24	8.4	113	17	5.2
397	6	2	48	65	118	41	4.3	120	45	4.9	111	28	2.8
398	6	2	55	65	119	38	4.5	121	41	5.2	112	26	3.0
399	6	2	63	65	120	34	4.8	122	37	5.6	114	24	3.3
400	6	2	61	65	119	35	4.8	121	38	5.5	113	25	3.2
401	6	2	35	65	117	47	3.9	119	51	4.5	108	34	2.5
402	6	2	82	65	123	26	6.0	125	29	7.2	119	19	4.3
403	6	2	48	75	127	46	4.0	129	50	4.6	119	32	2.5
404	6	2	55	75	128	43	4.2	130	46	4.8	120	29	2.7
405	6	2	63	75	128	39	4.5	130	42	5.1	122	27	2.9
406	6	2	61	75	128	40	4.4	130	43	5.0	121	28	2.8
407	6	2	35	75	126	52	3.7	128	56	4.2	117	38	2.3
408	6	2	82	75	131	30	5.3	133	33	6.2	126	22	3.7

Table B4 - Predicted Temperatures and Temperature Differences for the Pier Table and Box Girder Bottom Slabs

Case	Concrete Mix No.	Insulation R-Value	Average Air Temp., °F	Initial Concrete Temp., °F	Normal Weight Concrete at Pier Shaft			Lightweight Concrete at Location 1N			Lightweight Concrete at Location 7N		
					Maximum Concrete Temp., °F	Maximum Temeprature Difference, °F	Time of Maximum Temp. Diff., days	Maximum Concrete Temp., °F	Maximum Temeprature Difference, °F	Time of Maximum Temp. Diff., days	Maximum Concrete Temp., °F	Maximum Temeprature Difference, °F	Time of Maximum Temp. Diff., days
409	6	4	48	45	103	26	7.2	105	28	8.2	97	17	4.4
410	6	4	55	45	104	24	7.9	106	25	8.9	99	14	4.8
411	6	4	63	45	106	21	8.8	107	23	10.0	101	13	5.5
412	6	4	61	45	105	22	8.6	107	23	9.7	101	13	5.3
413	6	4	35	45	102	30	6.3	103	32	7.1	95	22	4.1
414	6	4	82	45	110	15	11.6	112	17	13.4	109	11	8.3
415	6	4	48	55	112	29	6.4	114	31	7.3	105	21	3.9
416	6	4	55	55	113	27	7.0	114	29	7.9	107	18	4.2
417	6	4	63	55	114	24	7.7	115	26	8.7	109	15	4.6
418	6	4	61	55	114	25	7.5	115	27	8.5	108	16	4.5
419	6	4	35	55	111	34	5.7	113	36	6.5	103	26	3.7
420	6	4	82	55	118	18	9.8	119	20	11.1	115	12	6.6
421	6	4	48	65	121	33	5.8	123	35	6.7	114	25	3.8
422	6	4	55	65	122	30	6.3	123	32	7.1	115	22	4.1
423	6	4	63	65	123	27	6.8	124	30	7.7	116	19	4.1
424	6	4	61	65	122	28	6.7	124	30	7.5	116	19	4.0
425	6	4	35	65	120	39	5.3	122	41	6.0	112	31	3.4
426	6	4	82	65	125	21	8.7	127	23	9.8	121	13	5.4
427	6	4	48	75	130	38	5.4	132	40	6.2	123	29	3.5
428	6	4	55	75	131	34	5.7	133	36	6.5	123	26	3.7
429	6	4	63	75	132	30	6.1	133	33	7.0	125	23	4.0
430	6	4	61	75	131	31	6.0	133	34	6.8	124	24	3.9
431	6	4	35	75	129	44	4.9	131	47	5.6	121	35	3.1
432	6	4	82	75	134	25	7.6	135	27	8.6	128	15	4.6

Table B4 - Predicted Temperatures and Temperature Differences for the Pier Table and Box Girder Bottom Slabs

Case	Concrete Mix No.	Insulation R-Value	Average Air Temp., °F	Initial Concrete Temp., °F	Normal Weight Concrete at Pier Shaft			Lightweight Concrete at Location 1N			Lightweight Concrete at Location 7N		
					Maximum Concrete Temp., °F	Maximum Temeprature Difference, °F	Time of Maximum Temp. Diff., days	Maximum Concrete Temp., °F	Maximum Temeprature Difference, °F	Time of Maximum Temp. Diff., days	Maximum Concrete Temp., °F	Maximum Temeprature Difference, °F	Time of Maximum Temp. Diff., days
433	7	0	48	45	118	69	2.9	122	73	3.6	109	58	2.1
434	7	0	55	45	119	63	3.1	123	67	3.8	111	54	2.2
435	7	0	63	45	121	57	3.3	124	60	3.9	114	49	2.3
436	7	0	61	45	121	58	3.2	124	62	3.9	113	50	2.3
437	7	0	35	45	116	79	2.7	120	84	3.3	105	67	1.9
438	7	0	82	45	125	42	3.9	128	45	4.7	121	37	2.8
439	7	0	48	55	127	77	2.8	131	81	3.3	116	65	1.9
440	7	0	55	55	128	71	2.9	132	75	3.5	118	60	2.0
441	7	0	63	55	129	65	3.0	133	68	3.7	120	55	2.2
442	7	0	61	55	129	66	3.0	132	70	3.6	120	56	2.1
443	7	0	35	55	125	88	2.6	129	92	3.1	113	74	1.7
444	7	0	82	55	133	50	3.5	136	53	4.3	127	43	2.5
445	7	0	48	65	135	85	2.6	139	90	3.2	123	72	1.8
446	7	0	55	65	136	79	2.7	140	84	3.3	125	67	1.9
447	7	0	63	65	138	73	2.9	141	77	3.4	127	62	2.0
448	7	0	61	65	137	74	2.8	141	79	3.4	127	63	2.0
449	7	0	35	65	134	96	2.4	138	101	3.0	121	81	1.6
450	7	0	82	65	141	58	3.3	144	61	3.9	133	49	2.3
451	7	0	48	75	144	94	2.5	148	99	3.0	131	79	1.7
452	7	0	55	75	145	88	2.6	149	92	3.1	133	74	1.7
453	7	0	63	75	146	81	2.7	150	85	3.3	135	68	1.8
454	7	0	61	75	146	83	2.6	150	87	3.2	134	70	1.8
455	7	0	35	75	143	105	2.3	147	110	2.8	129	89	1.5
456	7	0	82	75	149	65	3.0	152	69	3.7	140	56	2.1

Table B4 - Predicted Temperatures and Temperature Differences for the Pier Table and Box Girder Bottom Slabs

Case	Concrete Mix No.	Insulation R-Value	Average Air Temp., °F	Initial Concrete Temp., °F	Normal Weight Concrete at Pier Shaft			Lightweight Concrete at Location 1N			Lightweight Concrete at Location 7N		
					Maximum Concrete Temp., °F	Maximum Temeprature Difference, °F	Time of Maximum Temp. Diff., days	Maximum Concrete Temp., °F	Maximum Temeprature Difference, °F	Time of Maximum Temp. Diff., days	Maximum Concrete Temp., °F	Maximum Temeprature Difference, °F	Time of Maximum Temp. Diff., days
457	7	2	48	45	124	45	4.5	127	49	5.2	116	31	3.0
458	7	2	55	45	125	42	4.8	127	46	5.4	118	29	3.2
459	7	2	63	45	126	38	5.1	128	41	5.7	120	27	3.4
460	7	2	61	45	126	39	5.0	128	42	5.6	119	27	3.3
461	7	2	35	45	123	52	4.2	126	56	4.8	114	37	2.7
462	7	2	82	45	130	30	6.0	132	33	6.9	125	21	4.2
463	7	2	48	55	133	50	4.3	136	54	4.8	125	36	2.8
464	7	2	55	55	134	47	4.4	136	51	5.1	126	33	2.9
465	7	2	63	55	135	43	4.7	137	46	5.3	127	30	3.1
466	7	2	61	55	135	44	4.7	137	48	5.3	127	30	3.1
467	7	2	35	55	132	56	4.0	135	61	4.5	122	42	2.5
468	7	2	82	55	138	34	5.4	140	37	6.2	132	24	3.8
469	7	2	48	65	142	55	4.0	145	59	4.6	133	40	2.6
470	7	2	55	65	143	52	4.2	146	56	4.8	134	37	2.7
471	7	2	63	65	144	48	4.4	146	52	5.0	135	33	2.9
472	7	2	61	65	144	49	4.3	146	53	4.9	135	34	2.8
473	7	2	35	65	141	61	3.8	144	66	4.3	131	46	2.4
474	7	2	82	65	146	39	5.1	148	42	5.7	140	27	3.4
475	7	2	48	75	152	59	3.8	154	64	4.4	141	45	2.4
476	7	2	55	75	152	56	4.0	155	61	4.5	142	42	2.5
477	7	2	63	75	153	52	4.1	155	57	4.7	144	38	2.7
478	7	2	61	75	153	53	4.1	155	58	4.7	143	39	2.6
479	7	2	35	75	151	66	3.6	153	71	4.1	139	51	2.3
480	7	2	82	75	155	44	4.7	157	47	5.3	147	30	3.1

Table B4 - Predicted Temperatures and Temperature Differences for the Pier Table and Box Girder Bottom Slabs

Case	Concrete Mix No.	Insulation R-Value	Average Air Temp., °F	Initial Concrete Temp., °F	Normal Weight Concrete at Pier Shaft			Lightweight Concrete at Location 1N			Lightweight Concrete at Location 7N		
					Maximum Concrete Temp., °F	Maximum Temeprature Difference, °F	Time of Maximum Temp. Diff., days	Maximum Concrete Temp., °F	Maximum Temeprature Difference, °F	Time of Maximum Temp. Diff., days	Maximum Concrete Temp., °F	Maximum Temeprature Difference, °F	Time of Maximum Temp. Diff., days
481	7	4	48	45	128	37	6.1	130	39	6.8	120	28	4.1
482	7	4	55	45	129	33	6.4	131	35	7.2	121	25	4.3
483	7	4	63	45	130	30	6.9	131	33	7.7	123	22	4.3
484	7	4	61	45	129	31	6.8	131	33	7.6	122	23	4.2
485	7	4	35	45	127	43	5.6	129	46	6.3	118	34	3.7
486	7	4	82	45	132	24	8.3	134	26	9.3	127	15	5.2
487	7	4	48	55	137	42	5.7	139	44	6.4	129	33	3.8
488	7	4	55	55	138	38	5.9	140	40	6.7	130	30	4.0
489	7	4	63	55	138	34	6.3	140	36	7.1	131	26	4.3
490	7	4	61	55	138	35	6.2	140	37	7.0	131	27	4.2
491	7	4	35	55	136	48	5.3	138	51	5.9	127	38	3.5
492	7	4	82	55	141	27	7.5	142	29	8.4	135	18	4.7
493	7	4	48	65	146	47	5.3	148	49	6.0	137	37	3.5
494	7	4	55	65	147	43	5.6	149	46	6.3	138	34	3.7
495	7	4	63	65	147	39	5.9	149	41	6.6	139	30	3.9
496	7	4	61	65	144	36	3.2	149	43	6.5	139	31	3.8
497	7	4	35	65	145	53	5.0	147	56	5.6	136	43	3.3
498	7	4	82	65	150	31	6.8	151	33	7.6	142	22	4.2
499	7	4	48	75	155	52	5.0	158	54	5.7	146	42	3.3
500	7	4	55	75	156	48	5.3	158	51	5.9	147	38	3.5
501	7	4	63	75	157	44	5.5	159	47	6.2	148	35	3.7
502	7	4	61	75	156	45	5.4	159	48	6.1	148	36	3.6
503	7	4	35	75	154	58	4.7	157	61	5.4	145	47	3.1
504	7	4	82	75	158	35	6.3	160	37	7.0	151	26	4.2

Table B4 - Predicted Temperatures and Temperature Differences for the Pier Table and Box Girder Bottom Slabs

Case	Concrete Mix No.	Insulation R-Value	Average Air Temp., °F	Initial Concrete Temp., °F	Normal Weight Concrete at Pier Shaft			Lightweight Concrete at Location 1N			Lightweight Concrete at Location 7N		
					Maximum Concrete Temp., °F	Maximum Temeprature Difference, °F	Time of Maximum Temp. Diff., days	Maximum Concrete Temp., °F	Maximum Temeprature Difference, °F	Time of Maximum Temp. Diff., days	Maximum Concrete Temp., °F	Maximum Temeprature Difference, °F	Time of Maximum Temp. Diff., days
505	8	0	48	45	102	53	3.2	105	56	3.9	95	45	2.3
506	8	0	55	45	103	47	3.4	106	50	4.2	97	41	2.5
507	8	0	63	45	105	41	3.8	108	44	4.6	100	36	2.7
508	8	0	61	45	105	43	3.6	107	46	4.5	99	37	2.7
509	8	0	35	45	99	63	2.9	103	67	3.5	91	53	2.0
510	8	0	82	45	111	28	4.8	113	31	5.9	109	26	3.6
511	8	0	48	55	110	61	3.0	113	64	3.6	102	51	2.1
512	8	0	55	55	111	55	3.1	114	58	3.8	104	47	2.2
513	8	0	63	55	113	49	3.4	116	52	4.1	106	42	2.5
514	8	0	61	55	112	50	3.3	116	54	4.1	106	43	2.4
515	8	0	35	55	108	71	2.7	112	75	3.3	98	60	1.9
516	8	0	82	55	118	35	4.2	120	38	5.1	114	31	3.0
517	8	0	48	65	118	69	2.8	122	73	3.3	109	58	1.9
518	8	0	55	65	119	63	2.9	123	67	3.5	111	53	2.0
519	8	0	63	65	121	57	3.1	124	60	3.8	113	48	2.2
520	8	0	61	65	120	58	3.0	124	62	3.7	112	49	2.1
521	8	0	35	65	117	80	2.5	121	84	3.1	105	67	1.7
522	8	0	82	65	125	42	3.7	128	45	4.5	120	36	2.7
523	8	0	48	75	127	77	2.6	131	81	3.1	116	65	1.8
524	8	0	55	75	128	71	2.7	132	75	3.3	118	60	1.9
525	8	0	63	75	129	65	2.8	133	68	3.5	120	55	2.0
526	8	0	61	75	129	66	2.8	132	70	3.4	120	56	1.9
527	8	0	35	75	126	88	2.4	130	93	2.9	113	75	1.5
528	8	0	82	75	133	49	3.3	136	53	4.1	126	42	2.4

Table B4 - Predicted Temperatures and Temperature Differences for the Pier Table and Box Girder Bottom Slabs

Case	Concrete Mix No.	Insulation R-Value	Average Air Temp., °F	Initial Concrete Temp., °F	Normal Weight Concrete at Pier Shaft			Lightweight Concrete at Location 1N			Lightweight Concrete at Location 7N		
					Maximum Concrete Temp., °F	Maximum Temeprature Difference, °F	Time of Maximum Temp. Diff., days	Maximum Concrete Temp., °F	Maximum Temeprature Difference, °F	Time of Maximum Temp. Diff., days	Maximum Concrete Temp., °F	Maximum Temeprature Difference, °F	Time of Maximum Temp. Diff., days
529	8	2	48	45	107	36	5.1	109	39	5.8	101	25	3.4
530	8	2	55	45	108	33	5.4	110	36	6.3	103	23	3.8
531	8	2	63	45	110	30	6.0	112	33	7.0	105	21	4.1
532	8	2	61	45	109	30	5.8	111	33	6.8	104	22	4.1
533	8	2	35	45	105	42	4.6	108	46	5.3	98	29	3.0
534	8	2	82	45	115	22	7.9	116	24	9.3	112	17	5.8
535	8	2	48	55	116	41	4.7	118	44	5.4	108	28	3.1
536	8	2	55	55	117	38	5.0	119	41	5.7	110	26	3.3
537	8	2	63	55	118	34	5.3	120	37	6.2	112	24	3.6
538	8	2	61	55	118	35	5.3	120	38	6.0	112	24	3.5
539	8	2	35	55	114	47	4.3	117	51	4.9	106	33	2.7
540	8	2	82	55	122	26	6.8	124	28	7.9	118	19	4.8
541	8	2	48	65	125	46	4.3	127	49	5.0	116	31	2.8
542	8	2	55	65	125	42	4.6	128	46	5.3	118	29	3.0
543	8	2	63	65	126	39	4.9	129	42	5.6	120	26	3.2
544	8	2	61	65	126	39	4.8	128	43	5.5	119	27	3.2
545	8	2	35	65	123	52	4.0	126	56	4.6	114	37	2.5
546	8	2	82	65	130	30	5.9	132	33	6.9	125	21	4.1
547	8	2	48	75	134	50	4.1	136	54	4.7	125	36	2.6
548	8	2	55	75	134	47	4.3	137	51	4.9	126	33	2.7
549	8	2	63	75	135	43	4.5	137	47	5.2	127	29	2.9
550	8	2	61	75	135	44	4.4	137	48	5.1	127	30	2.8
551	8	2	35	75	133	56	3.8	135	61	4.3	123	42	2.3
552	8	2	82	75	138	34	5.3	140	38	6.2	132	24	3.6

Table B4 - Predicted Temperatures and Temperature Differences for the Pier Table and Box Girder Bottom Slabs

Case	Concrete Mix No.	Insulation R-Value	Average Air Temp., °F	Initial Concrete Temp., °F	Normal Weight Concrete at Pier Shaft			Lightweight Concrete at Location 1N			Lightweight Concrete at Location 7N		
					Maximum Concrete Temp., °F	Maximum Temeprature Difference, °F	Time of Maximum Temp. Diff., days	Maximum Concrete Temp., °F	Maximum Temeprature Difference, °F	Time of Maximum Temp. Diff., days	Maximum Concrete Temp., °F	Maximum Temeprature Difference, °F	Time of Maximum Temp. Diff., days
553	8	4	48	45	110	29	7.2	112	31	8.1	104	20	4.3
554	8	4	55	45	111	27	7.8	113	29	8.8	105	17	4.7
555	8	4	63	45	113	24	8.6	114	26	9.8	107	14	5.2
556	8	4	61	45	112	25	8.4	114	27	9.5	107	15	5.1
557	8	4	35	45	109	33	6.3	111	36	7.2	101	25	4.1
558	8	4	82	45	117	18	11.0	118	20	12.5	114	12	7.4
559	8	4	48	55	119	32	6.5	121	35	7.4	112	24	4.2
560	8	4	55	55	120	30	7.0	122	32	7.9	113	21	4.5
561	8	4	63	55	121	28	7.6	123	30	8.6	115	18	4.6
562	8	4	61	55	121	28	7.4	123	30	8.4	114	19	4.4
563	8	4	35	55	118	38	5.8	120	41	6.6	110	30	3.8
564	8	4	82	55	124	21	9.8	126	23	11.0	120	13	6.1
565	8	4	48	65	128	37	6.0	130	39	6.8	120	28	3.8
566	8	4	55	65	129	33	6.3	131	36	7.2	121	25	4.1
567	8	4	63	65	130	31	6.8	132	33	7.7	123	22	4.4
568	8	4	61	65	130	31	6.7	131	34	7.6	122	23	4.3
569	8	4	35	65	127	43	5.4	129	46	6.2	119	34	3.5
570	8	4	82	65	132	25	8.5	134	27	9.6	127	15	5.1
571	8	4	48	75	137	42	5.5	139	44	6.3	129	33	3.6
572	8	4	55	75	138	38	5.8	140	41	6.6	130	30	3.8
573	8	4	63	75	139	34	6.2	141	37	7.1	131	26	4.0
574	8	4	61	75	139	35	6.1	140	38	6.9	131	27	3.9
575	8	4	35	75	136	48	5.1	138	51	5.8	127	39	3.3
576	8	4	82	75	141	28	7.5	143	30	8.5	134	18	4.5

Table B4 - Predicted Temperatures and Temperature Differences for the Pier Table and Box Girder Bottom Slabs

Case	Concrete Mix No.	Insulation R-Value	Average Air Temp., °F	Initial Concrete Temp., °F	Normal Weight Concrete at Pier Shaft			Lightweight Concrete at Location 1N			Lightweight Concrete at Location 7N		
					Maximum Concrete Temp., °F	Maximum Temeprature Difference, °F	Time of Maximum Temp. Diff., days	Maximum Concrete Temp., °F	Maximum Temeprature Difference, °F	Time of Maximum Temp. Diff., days	Maximum Concrete Temp., °F	Maximum Temeprature Difference, °F	Time of Maximum Temp. Diff., days
577	9	0	48	45	126	77	2.9	130	81	3.6	115	65	2.0
578	9	0	55	45	128	71	3.1	131	75	3.7	118	60	2.2
579	9	0	63	45	129	64	3.2	133	68	3.9	120	55	2.3
580	9	0	61	45	129	66	3.2	132	70	3.8	119	56	2.2
581	9	0	35	45	124	87	2.7	129	92	3.3	112	73	1.8
582	9	0	82	45	133	50	3.8	136	53	4.5	127	43	2.7
583	9	0	48	55	135	85	2.8	139	89	3.3	123	71	1.9
584	9	0	55	55	136	79	2.9	140	83	3.5	125	67	2.0
585	9	0	63	55	137	72	3.0	141	77	3.6	127	61	2.1
586	9	0	61	55	137	74	3.0	141	78	3.6	126	63	2.1
587	9	0	35	55	133	96	2.6	138	101	3.1	119	81	1.8
588	9	0	82	55	141	58	3.4	144	61	4.2	133	49	2.5
589	9	0	48	65	144	93	2.6	148	98	3.2	130	78	1.8
590	9	0	55	65	144	87	2.7	149	92	3.3	132	73	1.8
591	9	0	63	65	146	81	2.8	150	85	3.4	134	68	2.0
592	9	0	61	65	145	82	2.8	149	87	3.4	133	69	1.9
593	9	0	35	65	142	104	2.5	147	109	3.0	127	88	1.6
594	9	0	82	65	149	65	3.2	152	69	3.9	140	55	2.3
595	9	0	48	75	152	102	2.5	157	107	3.0	138	86	1.7
596	9	0	55	75	153	96	2.6	158	101	3.1	139	81	1.8
597	9	0	63	75	154	89	2.7	**159**	94	3.3	141	75	1.8
598	9	0	61	75	154	91	2.7	**158**	95	3.2	141	76	1.8
599	9	0	35	75	151	113	2.4	156	118	2.9	135	95	1.5
600	9	0	82	75	157	73	3.0	**161**	78	3.6	147	62	2.1

Table B4 - Predicted Temperatures and Temperature Differences for the Pier Table and Box Girder Bottom Slabs

Case	Concrete Mix No.	Insulation R-Value	Average Air Temp., °F	Initial Concrete Temp., °F	Normal Weight Concrete at Pier Shaft			Lightweight Concrete at Location 1N			Lightweight Concrete at Location 7N		
					Maximum Concrete Temp., °F	Maximum Temeprature Difference, °F	Time of Maximum Temp. Diff., days	Maximum Concrete Temp., °F	Maximum Temeprature Difference, °F	Time of Maximum Temp. Diff., days	Maximum Concrete Temp., °F	Maximum Temeprature Difference, °F	Time of Maximum Temp. Diff., days
601	9	2	48	45	133	51	4.5	136	55	5.2	124	36	2.9
602	9	2	55	45	134	47	4.8	137	51	5.4	126	33	3.1
603	9	2	63	45	135	44	5.0	138	47	5.7	127	30	3.3
604	9	2	61	45	135	45	4.9	137	48	5.6	127	30	3.3
605	9	2	35	45	132	57	4.2	135	61	4.8	122	41	2.7
606	9	2	82	45	138	35	5.8	140	38	6.6	132	24	4.0
607	9	2	48	55	142	55	4.3	145	60	4.9	132	40	2.8
608	9	2	55	55	143	52	4.4	146	56	5.1	134	37	2.9
609	9	2	63	55	144	48	4.7	146	52	5.3	135	33	3.1
610	9	2	61	55	144	49	4.6	146	53	5.3	135	34	3.0
611	9	2	35	55	141	61	4.0	144	66	4.6	130	46	2.6
612	9	2	82	55	146	39	5.4	149	43	6.0	140	27	3.6
613	9	2	48	65	151	60	4.1	154	65	4.6	141	45	2.6
614	9	2	55	65	152	57	4.2	155	61	4.8	142	41	2.7
615	9	2	63	65	153	53	4.4	155	57	5.0	143	38	2.8
616	9	2	61	65	153	54	4.3	155	58	5.0	143	39	2.8
617	9	2	35	65	150	66	3.8	153	71	4.4	138	50	2.4
618	9	2	82	65	155	44	5.0	157	48	5.7	147	30	3.3
619	9	2	48	75	**160**	65	3.9	**163**	70	4.4	149	49	2.5
620	9	2	55	75	**161**	61	4.0	**164**	66	4.6	150	46	2.6
621	9	2	63	75	**162**	58	4.2	**165**	62	4.8	151	42	2.7
622	9	2	61	75	**162**	59	4.1	**164**	63	4.7	151	43	2.7
623	9	2	35	75	**159**	71	3.7	**162**	76	4.2	147	55	2.3
624	9	2	82	75	**164**	49	4.7	**166**	53	5.3	155	34	3.0

Table B4 - Predicted Temperatures and Temperature Differences for the Pier Table and Box Girder Bottom Slabs

Case	Concrete Mix No.	Insulation R-Value	Average Air Temp., °F	Initial Concrete Temp., °F	Normal Weight Concrete at Pier Shaft			Lightweight Concrete at Location 1N			Lightweight Concrete at Location 7N		
					Maximum Concrete Temp., °F	Maximum Temeprature Difference, °F	Time of Maximum Temp. Diff., days	Maximum Concrete Temp., °F	Maximum Temeprature Difference, °F	Time of Maximum Temp. Diff., days	Maximum Concrete Temp., °F	Maximum Temeprature Difference, °F	Time of Maximum Temp. Diff., days
625	9	4	48	45	137	42	6.1	139	44	6.8	129	33	4.1
626	9	4	55	45	138	39	6.4	140	41	7.2	130	30	4.3
627	9	4	63	45	139	35	6.8	141	37	7.6	131	26	4.6
628	9	4	61	45	139	36	6.7	141	38	7.5	131	27	4.5
629	9	4	35	45	136	48	5.6	138	51	6.3	127	38	3.7
630	9	4	82	45	141	28	8.0	143	30	8.9	135	19	5.0
631	9	4	48	55	146	47	5.7	149	50	6.4	137	37	3.8
632	9	4	55	55	147	43	5.9	149	46	6.7	138	34	4.0
633	9	4	63	55	148	39	6.3	150	42	7.1	139	30	4.2
634	9	4	61	55	148	40	6.2	150	43	7.0	139	31	4.2
635	9	4	35	55	145	54	5.3	148	56	6.0	135	43	3.5
636	9	4	82	55	150	31	7.3	152	34	8.2	143	22	4.5
637	9	4	48	65	155	52	5.4	158	55	6.1	146	41	3.6
638	9	4	55	65	156	48	5.6	158	51	6.3	147	38	3.7
639	9	4	63	65	157	44	5.9	159	47	6.6	148	35	3.9
640	9	4	61	65	157	45	5.8	159	48	6.5	147	36	3.9
641	9	4	35	65	154	59	5.0	157	62	5.7	144	47	3.3
642	9	4	82	65	159	35	6.7	161	37	7.5	151	27	4.5
643	9	4	48	75	165	57	5.1	167	60	5.8	154	46	3.4
644	9	4	55	75	165	54	5.3	168	56	6.0	155	43	3.5
645	9	4	63	75	166	49	5.5	168	52	6.3	156	39	3.7
646	9	4	61	75	166	50	5.5	168	53	6.2	156	40	3.6
647	9	4	35	75	164	64	4.8	166	67	5.5	153	52	3.2
648	9	4	82	75	168	40	6.2	170	42	7.0	159	31	4.2

Table B4 - Predicted Temperatures and Temperature Differences for the Pier Table and Box Girder Bottom Slabs

Case	Concrete Mix No.	Insulation R-Value	Average Air Temp., °F	Initial Concrete Temp., °F	Normal Weight Concrete at Pier Shaft			Lightweight Concrete at Location 1N			Lightweight Concrete at Location 7N		
					Maximum Concrete Temp., °F	Maximum Temeprature Difference, °F	Time of Maximum Temp. Diff., days	Maximum Concrete Temp., °F	Maximum Temeprature Difference, °F	Time of Maximum Temp. Diff., days	Maximum Concrete Temp., °F	Maximum Temeprature Difference, °F	Time of Maximum Temp. Diff., days
649	10	0	48	45	108	59	3.2	111	62	3.9	100	50	2.3
650	10	0	55	45	109	53	3.4	113	57	4.1	102	45	2.4
651	10	0	63	45	111	47	3.6	114	50	4.4	105	40	2.7
652	10	0	61	45	111	49	3.6	114	52	4.4	104	42	2.6
653	10	0	35	45	106	69	2.9	109	73	3.6	96	58	2.0
654	10	0	82	45	116	34	4.5	119	37	5.6	113	30	3.3
655	10	0	48	55	116	67	3.0	120	71	3.6	107	56	2.1
656	10	0	55	55	117	61	3.2	121	65	3.8	109	52	2.2
657	10	0	63	55	119	55	3.3	122	58	4.1	111	46	2.3
658	10	0	61	55	118	56	3.3	122	60	4.0	111	48	2.3
659	10	0	35	55	114	77	2.7	118	82	3.3	103	65	1.9
660	10	0	82	55	123	41	4.0	126	44	4.9	119	35	3.0
661	10	0	48	65	125	75	2.8	129	79	3.4	114	63	1.9
662	10	0	55	65	126	69	2.9	129	73	3.6	116	58	2.0
663	10	0	63	65	127	63	3.1	131	66	3.8	118	53	2.2
664	10	0	61	65	127	64	3.0	130	68	3.7	117	54	2.1
665	10	0	35	65	123	86	2.6	127	90	3.1	110	72	1.7
666	10	0	82	65	131	48	3.6	134	51	4.4	125	41	2.7
667	10	0	48	75	133	83	2.6	137	88	3.2	121	70	1.8
668	10	0	55	75	134	77	2.7	138	82	3.3	123	65	1.9
669	10	0	63	75	135	71	2.9	139	75	3.5	125	60	2.0
670	10	0	61	75	135	72	2.8	139	77	3.4	125	61	1.9
671	10	0	35	75	132	94	2.4	136	99	3.0	118	79	1.6
672	10	0	82	75	139	55	3.3	142	59	4.1	131	47	2.3

Table B4 - Predicted Temperatures and Temperature Differences for the Pier Table and Box Girder Bottom Slabs

Case	Concrete Mix No.	Insulation R-Value	Average Air Temp., °F	Initial Concrete Temp., °F	Normal Weight Concrete at Pier Shaft			Lightweight Concrete at Location 1N			Lightweight Concrete at Location 7N		
					Maximum Concrete Temp., °F	Maximum Temeprature Difference, °F	Time of Maximum Temp. Diff., days	Maximum Concrete Temp., °F	Maximum Temeprature Difference, °F	Time of Maximum Temp. Diff., days	Maximum Concrete Temp., °F	Maximum Temeprature Difference, °F	Time of Maximum Temp. Diff., days
673	10	2	48	45	114	40	5.1	116	44	5.9	107	28	3.4
674	10	2	55	45	115	37	5.4	117	40	6.3	108	26	3.6
675	10	2	63	45	117	34	5.9	119	37	6.8	111	23	4.0
676	10	2	61	45	116	34	5.8	118	38	6.7	110	24	3.9
677	10	2	35	45	112	47	4.6	115	50	5.3	104	31	3.0
678	10	2	82	45	121	26	7.4	123	28	8.7	117	19	5.3
679	10	2	48	55	123	45	4.7	125	49	5.4	114	30	3.0
680	10	2	55	55	124	42	5.0	126	45	5.7	116	28	3.3
681	10	2	63	55	125	38	5.3	127	41	6.1	118	26	3.5
682	10	2	61	55	124	39	5.3	127	42	6.0	117	27	3.5
683	10	2	35	55	121	51	4.3	124	55	4.9	112	36	2.7
684	10	2	82	55	128	30	6.5	131	33	7.6	124	21	4.5
685	10	2	48	65	132	50	4.4	134	54	5.1	122	35	2.8
686	10	2	55	65	132	47	4.6	135	50	5.3	124	31	3.0
687	10	2	63	65	133	43	4.9	136	46	5.6	125	29	3.2
688	10	2	61	65	133	44	4.8	135	47	5.5	125	30	3.1
689	10	2	35	65	130	56	4.1	133	60	4.7	120	40	2.5
690	10	2	82	65	136	34	5.8	139	37	6.7	130	24	3.9
691	10	2	48	75	141	54	4.1	143	59	4.8	131	39	2.6
692	10	2	55	75	141	51	4.3	144	55	4.9	132	36	2.7
693	10	2	63	75	142	47	4.6	145	51	5.2	133	32	2.9
694	10	2	61	75	142	48	4.5	144	52	5.2	133	33	2.9
695	10	2	35	75	139	60	3.8	142	65	4.4	129	45	2.4
696	10	2	82	75	145	39	5.3	147	42	6.1	138	26	3.5

Table B4 - Predicted Temperatures and Temperature Differences for the Pier Table and Box Girder Bottom Slabs

Case	Concrete Mix No.	Insulation R-Value	Average Air Temp., °F	Initial Concrete Temp., °F	Normal Weight Concrete at Pier Shaft			Lightweight Concrete at Location 1N			Lightweight Concrete at Location 7N		
					Maximum Concrete Temp., °F	Maximum Temeprature Difference, °F	Time of Maximum Temp. Diff., days	Maximum Concrete Temp., °F	Maximum Temeprature Difference, °F	Time of Maximum Temp. Diff., days	Maximum Concrete Temp., °F	Maximum Temeprature Difference, °F	Time of Maximum Temp. Diff., days
697	10	4	48	45	118	33	7.2	120	35	8.1	110	23	4.7
698	10	4	55	45	119	30	7.7	121	33	8.7	111	20	4.6
699	10	4	63	45	120	28	8.4	122	30	9.5	113	17	5.0
700	10	4	61	45	120	28	8.3	121	31	9.3	113	18	4.9
701	10	4	35	45	116	38	6.4	118	40	7.3	108	29	4.1
702	10	4	82	45	124	22	10.8	125	23	11.9	119	13	6.7
703	10	4	48	55	127	36	6.5	129	38	7.4	118	27	4.3
704	10	4	55	55	127	33	7.0	129	36	7.9	120	24	4.5
705	10	4	63	55	128	31	7.5	130	33	8.5	121	21	4.9
706	10	4	61	55	128	32	7.4	130	34	8.3	121	22	4.8
707	10	4	35	55	125	42	5.9	127	45	6.7	116	33	3.8
708	10	4	82	55	132	25	9.4	133	27	10.7	126	15	5.7
709	10	4	48	65	135	41	6.0	138	43	6.9	127	32	3.9
710	10	4	55	65	136	38	6.4	138	40	7.3	128	29	4.1
711	10	4	63	65	137	34	6.8	139	37	7.8	129	25	4.4
712	10	4	61	65	137	35	6.7	139	38	7.6	129	26	4.4
713	10	4	35	65	134	47	5.5	137	50	6.3	125	37	3.6
714	10	4	82	65	140	28	8.3	142	30	9.4	133	18	5.0
715	10	4	48	75	145	46	5.6	147	49	6.4	135	36	3.6
716	10	4	55	75	145	42	5.9	147	45	6.7	136	33	3.8
717	10	4	63	75	146	39	6.3	148	41	7.1	138	29	4.1
718	10	4	61	75	146	39	6.2	148	42	7.0	137	30	4.0
719	10	4	35	75	143	53	5.2	146	55	5.9	134	42	3.3
720	10	4	82	75	148	31	7.5	150	34	8.4	141	21	4.9

Table B4 - Predicted Temperatures and Temperature Differences for the Pier Table and Box Girder Bottom Slabs

Case	Concrete Mix No.	Insulation R-Value	Average Air Temp., °F	Initial Concrete Temp., °F	Normal Weight Concrete at Pier Shaft			Lightweight Concrete at Location 1N			Lightweight Concrete at Location 7N		
					Maximum Concrete Temp., °F	Maximum Temeprature Difference, °F	Time of Maximum Temp. Diff., days	Maximum Concrete Temp., °F	Maximum Temeprature Difference, °F	Time of Maximum Temp. Diff., days	Maximum Concrete Temp., °F	Maximum Temeprature Difference, °F	Time of Maximum Temp. Diff., days
721	11	0	48	45	134	84	2.9	139	89	3.5	122	71	2.0
722	11	0	55	45	135	79	3.1	140	83	3.7	124	66	2.1
723	11	0	63	45	137	72	3.2	141	77	3.8	127	61	2.2
724	11	0	61	45	137	74	3.1	141	78	3.8	126	62	2.2
725	11	0	35	45	132	95	2.8	137	100	3.3	119	80	1.8
726	11	0	82	45	141	58	3.6	144	61	4.4	133	49	2.6
727	11	0	48	55	143	93	2.8	147	98	3.3	129	78	1.9
728	11	0	55	55	144	87	2.9	148	92	3.4	131	73	1.9
729	11	0	63	55	145	80	3.0	149	85	3.6	133	67	2.1
730	11	0	61	55	145	82	2.9	149	87	3.6	133	69	2.1
731	11	0	35	55	141	104	2.6	146	109	3.2	126	87	1.8
732	11	0	82	55	149	65	3.4	152	69	4.1	140	55	2.4
733	11	0	48	65	151	101	2.6	156	106	3.2	137	85	1.8
734	11	0	55	65	152	95	2.8	157	100	3.3	139	80	1.8
735	11	0	63	65	154	88	2.8	158	93	3.4	141	74	1.9
736	11	0	61	65	153	90	2.8	158	95	3.4	140	75	1.9
737	11	0	35	65	150	112	2.5	155	118	3.0	134	94	1.7
738	11	0	82	65	157	73	3.2	161	77	3.8	146	62	2.2
739	11	0	48	75	160	110	2.5	165	115	3.1	144	92	1.7
740	11	0	55	75	161	104	2.6	166	109	3.2	146	87	1.8
741	11	0	63	75	162	97	2.7	167	102	3.3	148	81	1.8
742	11	0	61	75	162	98	2.7	167	104	3.3	148	83	1.8
743	11	0	35	75	159	121	2.4	164	127	2.9	142	101	1.5
744	11	0	82	75	165	81	3.0	169	86	3.6	153	68	2.1

Table B4 - Predicted Temperatures and Temperature Differences for the Pier Table and Box Girder Bottom Slabs

Case	Concrete Mix No.	Insulation R-Value	Average Air Temp., °F	Initial Concrete Temp., °F	Normal Weight Concrete at Pier Shaft			Lightweight Concrete at Location 1N			Lightweight Concrete at Location 7N		
					Maximum Concrete Temp., °F	Maximum Temeprature Difference, °F	Time of Maximum Temp. Diff., days	Maximum Concrete Temp., °F	Maximum Temeprature Difference, °F	Time of Maximum Temp. Diff., days	Maximum Concrete Temp., °F	Maximum Temeprature Difference, °F	Time of Maximum Temp. Diff., days
745	11	2	48	45	142	56	4.5	145	60	5.2	132	40	2.9
746	11	2	55	45	143	53	4.7	146	57	5.4	133	37	3.1
747	11	2	63	45	144	49	5.0	147	53	5.6	135	33	3.3
748	11	2	61	45	144	50	4.9	146	54	5.6	135	34	3.2
749	11	2	35	45	141	62	4.2	144	67	4.8	129	46	2.7
750	11	2	82	45	147	40	5.6	149	43	6.4	140	27	3.8
751	11	2	48	55	151	60	4.3	154	65	4.9	140	44	2.8
752	11	2	55	55	152	57	4.5	155	62	5.1	141	41	2.9
753	11	2	63	55	153	53	4.7	155	58	5.3	143	38	3.0
754	11	2	61	55	152	54	4.6	155	59	5.3	142	39	3.0
755	11	2	35	55	150	67	4.0	153	72	4.6	138	50	2.6
756	11	2	82	55	155	45	5.3	158	48	6.0	147	30	3.5
757	11	2	48	65	**160**	65	4.1	**163**	71	4.7	148	49	2.6
758	11	2	55	65	**161**	62	4.2	**164**	67	4.8	149	46	2.7
759	11	2	63	65	**162**	58	4.4	**164**	63	5.0	151	42	2.8
760	11	2	61	65	**161**	59	4.3	**164**	64	5.0	150	43	2.8
761	11	2	35	65	**159**	71	3.9	**162**	77	4.4	146	55	2.4
762	11	2	82	65	**164**	49	4.9	**166**	53	5.6	155	34	3.2
763	11	2	48	75	**169**	70	3.9	**172**	75	4.5	157	53	2.5
764	11	2	55	75	**170**	67	4.0	**173**	72	4.6	158	50	2.6
765	11	2	63	75	**171**	63	4.2	**174**	68	4.8	**159**	47	2.7
766	11	2	61	75	**170**	64	4.2	**173**	69	4.8	**159**	47	2.7
767	11	2	35	75	**168**	76	3.7	**171**	82	4.3	155	60	2.3
768	11	2	82	75	**173**	54	4.6	**175**	58	5.3	**163**	38	3.0

Table B4 - Predicted Temperatures and Temperature Differences for the Pier Table and Box Girder Bottom Slabs

Case	Concrete Mix No.	Insulation R-Value	Average Air Temp., °F	Initial Concrete Temp., °F	Normal Weight Concrete at Pier Shaft			Lightweight Concrete at Location 1N			Lightweight Concrete at Location 7N		
					Maximum Concrete Temp., °F	Maximum Temeprature Difference, °F	Time of Maximum Temp. Diff., days	Maximum Concrete Temp., °F	Maximum Temeprature Difference, °F	Time of Maximum Temp. Diff., days	Maximum Concrete Temp., °F	Maximum Temeprature Difference, °F	Time of Maximum Temp. Diff., days
769	11	4	48	45	146	47	6.1	149	50	6.8	137	37	4.1
770	11	4	55	45	147	44	6.3	149	46	7.1	138	34	4.3
771	11	4	63	45	148	40	6.7	150	42	7.5	139	30	4.5
772	11	4	61	45	148	41	6.6	150	43	7.4	139	31	4.4
773	11	4	35	45	145	54	5.6	148	57	6.3	135	43	3.8
774	11	4	82	45	151	32	7.8	153	35	8.7	143	23	4.8
775	11	4	48	55	155	52	5.7	158	55	6.4	145	41	3.8
776	11	4	55	55	156	49	5.9	159	51	6.7	146	38	4.0
777	11	4	63	55	157	45	6.3	159	47	7.0	148	35	4.2
778	11	4	61	55	157	46	6.2	159	48	6.9	147	36	4.1
779	11	4	35	55	154	59	5.3	157	62	6.0	144	47	3.5
780	11	4	82	55	159	35	7.1	161	38	8.0	151	27	4.8
781	11	4	48	65	165	57	5.4	167	60	6.1	154	46	3.6
782	11	4	55	65	165	54	5.6	168	57	6.3	155	43	3.8
783	11	4	63	65	166	50	5.9	168	52	6.6	156	39	3.9
784	11	4	61	65	166	51	5.8	168	53	6.6	156	40	3.9
785	11	4	35	65	164	64	5.1	166	67	5.8	152	52	3.4
786	11	4	82	65	168	40	6.6	170	43	7.4	159	31	4.5
787	11	4	48	75	174	62	5.2	176	65	5.8	163	50	3.4
788	11	4	55	75	174	59	5.3	177	62	6.0	164	47	3.5
789	11	4	63	75	175	55	5.6	178	58	6.3	165	43	3.7
790	11	4	61	75	175	56	5.5	177	59	6.2	164	44	3.7
791	11	4	35	75	173	69	4.9	176	72	5.6	161	56	3.2
792	11	4	82	75	177	45	6.2	179	48	7.0	167	35	4.2

Table B4 - Predicted Temperatures and Temperature Differences for the Pier Table and Box Girder Bottom Slabs

Case	Concrete Mix No.	Insulation R-Value	Average Air Temp., °F	Initial Concrete Temp., °F	Normal Weight Concrete at Pier Shaft			Lightweight Concrete at Location 1N			Lightweight Concrete at Location 7N		
					Maximum Concrete Temp., °F	Maximum Temeprature Difference, °F	Time of Maximum Temp. Diff., days	Maximum Concrete Temp., °F	Maximum Temeprature Difference, °F	Time of Maximum Temp. Diff., days	Maximum Concrete Temp., °F	Maximum Temeprature Difference, °F	Time of Maximum Temp. Diff., days
793	12	0	48	45	114	65	3.2	118	69	3.9	105	54	2.2
794	12	0	55	45	115	59	3.3	119	63	4.1	107	50	2.3
795	12	0	63	45	117	53	3.6	121	57	4.4	110	45	2.5
796	12	0	61	45	117	54	3.5	120	58	4.3	109	46	2.5
797	12	0	35	45	112	75	2.9	116	80	3.6	101	63	2.0
798	12	0	82	45	122	39	4.3	125	43	5.3	118	34	3.2
799	12	0	48	55	122	73	2.9	126	77	3.6	112	61	2.1
800	12	0	55	55	123	67	3.1	127	71	3.8	114	56	2.2
801	12	0	63	55	125	61	3.3	129	65	4.0	116	51	2.3
802	12	0	61	55	125	62	3.3	128	66	3.9	116	52	2.3
803	12	0	35	55	120	83	2.8	125	88	3.3	108	70	1.9
804	12	0	82	55	129	46	3.9	133	50	4.8	123	40	2.8
805	12	0	48	65	131	81	2.8	135	85	3.4	119	68	1.9
806	12	0	55	65	132	75	2.9	136	80	3.6	121	63	2.0
807	12	0	63	65	133	68	3.1	137	73	3.8	123	58	2.2
808	12	0	61	65	133	70	3.0	137	74	3.7	122	59	2.1
809	12	0	35	65	129	92	2.6	133	97	3.2	115	77	1.7
810	12	0	82	65	137	54	3.6	140	57	4.3	129	46	2.5
811	12	0	48	75	139	89	2.6	144	94	3.2	126	75	1.8
812	12	0	55	75	140	83	2.8	145	88	3.3	128	70	1.9
813	12	0	63	75	141	77	2.9	146	81	3.5	130	64	2.0
814	12	0	61	75	141	78	2.8	145	83	3.4	129	66	1.9
815	12	0	35	75	138	100	2.5	142	105	3.0	123	84	1.6
816	12	0	82	75	145	61	3.3	149	65	4.0	136	52	2.3

Table B4 - Predicted Temperatures and Temperature Differences for the Pier Table and Box Girder Bottom Slabs

Case	Concrete Mix No.	Insulation R-Value	Average Air Temp., °F	Initial Concrete Temp., °F	Normal Weight Concrete at Pier Shaft			Lightweight Concrete at Location 1N			Lightweight Concrete at Location 7N		
					Maximum Concrete Temp., °F	Maximum Temeprature Difference, °F	Time of Maximum Temp. Diff., days	Maximum Concrete Temp., °F	Maximum Temeprature Difference, °F	Time of Maximum Temp. Diff., days	Maximum Concrete Temp., °F	Maximum Temeprature Difference, °F	Time of Maximum Temp. Diff., days
817	12	2	48	45	121	45	5.1	123	48	5.8	112	30	3.3
818	12	2	55	45	122	41	5.4	124	45	6.2	114	28	3.6
819	12	2	63	45	123	37	5.7	126	41	6.6	116	26	3.9
820	12	2	61	45	123	38	5.7	125	42	6.5	116	26	3.8
821	12	2	35	45	119	51	4.7	122	55	5.3	110	35	3.0
822	12	2	82	45	127	29	7.1	130	32	8.3	122	21	4.9
823	12	2	48	55	130	49	4.8	132	53	5.4	120	33	3.0
824	12	2	55	55	130	46	5.0	133	50	5.7	122	31	3.2
825	12	2	63	55	132	42	5.3	134	46	6.1	124	29	3.5
826	12	2	61	55	131	43	5.3	134	47	6.0	123	29	3.4
827	12	2	35	55	128	55	4.3	131	60	5.0	118	39	2.8
828	12	2	82	55	135	34	6.3	137	37	7.3	129	23	4.3
829	12	2	48	65	138	54	4.4	141	58	5.1	128	38	2.8
830	12	2	55	65	139	51	4.7	142	55	5.3	130	35	3.0
831	12	2	63	65	140	47	4.9	143	51	5.7	131	31	3.2
832	12	2	61	65	140	48	4.8	143	52	5.6	131	32	3.1
833	12	2	35	65	137	60	4.1	140	65	4.8	126	44	2.6
834	12	2	82	65	143	38	5.7	145	41	6.6	136	26	3.8
835	12	2	48	75	147	59	4.2	150	63	4.8	136	42	2.6
836	12	2	55	75	148	55	4.3	151	60	5.0	138	39	2.8
837	12	2	63	75	149	52	4.6	152	56	5.3	139	36	2.9
838	12	2	61	75	149	53	4.5	151	57	5.2	139	36	2.9
839	12	2	35	75	146	65	3.9	149	70	4.5	134	48	2.4
840	12	2	82	75	151	43	5.3	154	46	6.1	143	29	3.4

Table B4 - Predicted Temperatures and Temperature Differences for the Pier Table and Box Girder Bottom Slabs

Case	Concrete Mix No.	Insulation R-Value	Average Air Temp., °F	Initial Concrete Temp., °F	Normal Weight Concrete at Pier Shaft			Lightweight Concrete at Location 1N			Lightweight Concrete at Location 7N		
					Maximum Concrete Temp., °F	Maximum Temeprature Difference, °F	Time of Maximum Temp. Diff., days	Maximum Concrete Temp., °F	Maximum Temeprature Difference, °F	Time of Maximum Temp. Diff., days	Maximum Concrete Temp., °F	Maximum Temeprature Difference, °F	Time of Maximum Temp. Diff., days
841	12	4	48	45	125	36	7.2	127	39	8.1	116	26	4.7
842	12	4	55	45	126	34	7.6	128	36	8.6	118	23	5.0
843	12	4	63	45	127	31	8.3	129	34	9.3	119	20	4.9
844	12	4	61	45	127	32	8.1	129	34	9.2	119	21	4.8
845	12	4	35	45	123	42	6.4	126	44	7.3	114	32	4.2
846	12	4	82	45	131	25	10.4	132	27	11.8	125	15	6.3
847	12	4	48	55	134	40	6.6	136	43	7.5	125	31	4.3
848	12	4	55	55	135	37	7.0	137	40	7.9	126	28	4.5
849	12	4	63	55	136	34	7.5	138	37	8.5	127	24	4.9
850	12	4	61	55	135	35	7.3	138	38	8.3	127	25	4.8
851	12	4	35	55	132	47	6.0	135	49	6.8	123	36	3.9
852	12	4	82	55	139	28	9.2	141	31	10.3	132	17	5.5
853	12	4	48	65	143	45	6.1	145	48	6.9	133	35	4.0
854	12	4	55	65	143	42	6.4	146	44	7.3	134	32	4.2
855	12	4	63	65	144	38	6.8	147	40	7.8	136	28	4.5
856	12	4	61	65	144	39	6.8	146	41	7.6	135	29	4.4
857	12	4	35	65	141	52	5.6	144	54	6.4	131	41	3.6
858	12	4	82	65	147	31	8.2	149	34	9.3	139	21	4.8
859	12	4	48	75	152	50	5.7	154	53	6.5	142	39	3.7
860	12	4	55	75	152	47	6.0	155	49	6.8	143	36	3.9
861	12	4	63	75	153	43	6.3	156	45	7.2	144	33	4.1
862	12	4	61	75	153	44	6.3	155	46	7.1	144	34	4.0
863	12	4	35	75	151	57	5.3	153	60	6.1	140	45	3.4
864	12	4	82	75	156	35	7.4	158	37	8.4	147	25	4.8

- FHWA Guidelines for Instrumentation

FHWA-SA-96-075

U.S. Department
of Transportation
Federal Highway
Administration

Implementation Program on High Performance Concrete

Guidelines for Instrumentation of Bridges

August 1996

TECHNOLOGY APPLICATIONS

Technical Report Documentation Page

1. Report No.	2. Government Accession No.	3. Recipient's Catalog No.
FHWA-SA-96-075		

4. Title and Subtitle	5. Report Date
Implementation Program on High Performance Concrete Guidelines for Instrumentation of Bridges	August 1996
	6. Performing Organization Code
7. Author(s)	8. Performing Organization Report No.
Henry Russell	
9. Performing Organization Name and Address	10. Work Unit No. (TRAIS)
Henry G. Russell, Inc. Engineering Consultant 720 Coronet Road Glenview, IL 60025-4457	11. Contract or Grant No. DTFH61-94-P-01730
12. Sponsoring Agency Name and Address	13. Type of Report and Period Covered
Office of Engineering Office of Technology Applications Federal Highway Administration 400 Seventh Street, NW Washington, DC 20590	Final Report 1994 to February 1996
	14. Sponsoring Agency Code

15. Supplementary Notes

Technical Contact: Terry Halkyard, HTA-20

16. Abstract

This report provides an outline for the instrumentation of bridges being constructed under the Federal Highway Administration's (FHWA's) Strategic Highway Research Program (SHRP) implementation effort in High Performance Concrete (HPC). The report describes the various types of measurements that can be made and the appropriate types of instrumentation that should be used. A basic instrumentation program is described that should be implemented on all demonstration bridges. Optional items that may be included at the discretion of each State are also suggested.

17. Key Words	18. Distribution Statement
bridge, instrumentation, high performance concrete, strains, thermocouples, end slip, deflectons	No restriction. This document is available to the public through the National Technical Information Services, Springfield, VA 22161

19. Security Classification (of this report)	20. Security Classification (of this page)	21. No. of Pages	22. Price
unclassified	unclassified	21	

Form DOT F 1700.7 (12-92) Reproduction of completed page authorized

CONTENTS

SECTION	PAGE
BACKGROUND	1
OBJECTIVE	1
TYPES OF MEASUREMENTS	1
Temperatures	1
Strains	2
Length Changes	4
Deflections	4
Slopes	5
Prestressing Forces	5
Strand End Slip	5
DATA ACQUISITION	5
DATA INTERPRETATION	6
SAMPLE INSTRUMENTATION PROGRAM	6
Basic Instrumentation Program	6
Optional Additional Instrumentation Program	8
APPENDIX A—PHOTOGRAPHS OF ACTUAL INSTALLATIONS	11
APPENDIX B—TYPES OF INSTRUMENTATION	17
Thermocouples	17
Electrical Resistance Strain Gages	17
Vibrating Wire Gages	17
Carlson Strain Meters	18
Mechanical Strain Gages	18
Tiltmeters	18
Caliper for Strand Slip	18
Data Acquisition Systems	19
APPENDIX C—INFORMATION SOURCES	21

BACKGROUND

High performance concrete has been used in the building industry for many years. Although its application in highway structures has been limited, it is now receiving increased attention. As part of a program to further the implementation of high performance concrete, the Federal Highway Administration (FHWA) is developing a showcase package. The package will include demonstrations, workshops, and field assistance. Several demonstration high performance concrete bridges will be built and the results described at the workshops. The bridges will have different types of superstructures, will be built in different climatic regions, and will be examples of the practical application of high performance concretes. Construction of these bridges will provide opportunities to learn more about the placement of high performance concrete as well as the actual behavior of high performance concrete bridges. It is anticipated that each bridge will be instrumented to monitor its performance over a period of several years. Similar instrumen-tation will be used on each structure so that performance comparisons can be made among these demonstration bridges.

OBJECTIVE

The objective of this report is to provide an outline for the instrumentation program of the demonstration bridges. The report describes various types of measurements that can be made and the appropriate types of instrumentation that should be used. A basic instrumentation program is described that should be implemented on all demonstration bridges. Optional items that may be included at the discretion of each State are also suggested. The optional items are not intended to restrict the use of innovative ideas and States may want to try other types of instrumentation not described in this report.

TYPES OF MEASUREMENTS

This section of the report describes several types of measurements for which the technology is well established. However, successful instrumentation depends on the abilities and skills of the individuals doing the work. In-plant or on-site installation should not be considered a training ground for students or technicians. Training should be completed prior to any installation and collection of data.

Temperatures

Temperatures are measured to determine:

- Heat of hydration.
- Temperature for match-cured cylinders.
- Temperature of quality control cylinders.
- Temperature gradients.
- Temperature corrections for other measurements.

Temperatures are measured using thermocouples that can be purchased assembled or can be made from thermocouple wire. They are best positioned prior to concrete placement by attachment to either the reinforcement or a special fixture that is then tied to the reinforcement. The latter method is preferred when temperature gradients over a short distance such as a slab thickness are required.

Thermocouple wires must be carefully positioned to avoid damage during concrete placement and vibration. The lead wires from a group of thermocouples should be bundled together and tied to the reinforcement so that they exit the concrete at a single and convenient location. Whenever possible, the wires should be tied to the underside of reinforcement to protect the wires from falling concrete. Wires may also be protected by using plastic sheathing.

When strains are measured with electrical resistance strain gages or mechanical strain gages, temperatures should be measured at the gage locations. When strains are measured with Carlson strain meters or vibrating wire gages, the gages include a built-in system for determining temperatures at the gage.

Strains

For purposes of instrumentation, strains can be divided into two types—short-term and long-term. Short-term strains are those changes that occur over a period of hours whereas long-term strains are those occurring over months or years. Short-term strains are generally caused by changes in dead and live loads, daily temperature cycles, or wind loading. Long-term strains are caused by seasonal temperature changes and creep and shrinkage in concrete structures.

Short-Term Strains

Short-term strains should be measured using electrical resistance strain gages. Although these gages can be attached directly to reinforcing steel in the field, this method requires attachment under field conditions and is very difficult. Consequently, the gages should be attached to separate lengths of reinforcement such as a 10- or 15-mm-diameter bar about 600 mm long. This allows the gages to be attached to the bars under laboratory conditions and permits proper attachment of leads and waterproofing. Waterproofing should be done according to the manufacturer's recommendations and should be verified before gages are cast in concrete. The gaged bars can be tied directly to the reinforcement cage in the plant or at the site with minimum interruption to construction. Lead wires from groups of strain gages should be bundled together and tied to the reinforcement so that they exit the concrete at a single and convenient location. Whenever possible, the wires should be protected from damage from falling concrete by tieing to the underside of the reinforcement and, if necessary, protecting them in plastic sheathing. Electrical resistance strain gages should not be attached to prestressing strands, as this requires a special technique of attaching the gages along the spiral of individual wires and is difficult to accomplish. It is also likely that the gages will be damaged during stressing.

Electrical resistance strain gages can be applied to hardened concrete surfaces. For surfaces cast against steel forms, this is relatively easy provided access to the surface is possible and the weather is suitable. For troweled or grooved surfaces, special techniques are needed to prepare the surface prior to application of the gages.

Weldable electrical resistance strain gages are available for use on steel structures and large size reinforcing bars. These gages are produced with leads and waterproofing attached and only require spot welding to the steel. With practice, they can be installed under adverse site conditions.

Electrical resistance strain gages are available as temperature-compensated gages. These gages are designed so that when attached to a material with the specified coefficient of thermal expansion, the

measured strain will not change as a result of temperature changes when length changes of the material are unrestrained. However, it must be remembered that the temperature compensation is not perfect because of the following:

- The coefficient of expansion of the material will not exactly match the specified coefficient of expansion of the gage.
- Any restraint to the free expansion or contraction of the material will result in an apparent strain.

Interpretation of measured strains under varying temperature conditions should consider the above factors.

Long-Term Strains

Long-term strains should be measured with gages designed specifically for this purpose. Two types are available for measurements inside concrete.

- Carlson strain meters.
- Vibrating wire gages.

These two types operate on different principles. However, they are both designed to have long-term stability, are robust for installation on site, and are provided with leads already attached. The lead wires are durable and may be tied directly to the underside of reinforcement for protection. Additional protection is not generally needed. The gages can be attached directly to the reinforcement although the vibrating wire gage may require a special mounting fixture. It is also possible to cast these gages in concrete blocks and then cast the blocks in the concretestructure. Use of this method is discouraged because of doubts about the effect of differential creep and shrinkage between the block and the concrete.

Output from these gages is affected by temperature changes, and the output data need to be corrected for both temperature changes of the gage and temperature changes of the structure. In most cases, the temperature of the gage and structure will be the same though the coefficients of thermal expansion will be different.

Long-term strain measurements are generally used to determine prestress losses. For this purpose, the gages are best positioned at the centroid of the prestressing force. Since strands are often draped or debonded in prestressed girders, the measurements are best made near midspan of the girders. If measurements near the ends of girders are required, the gages should be placed to avoid any effect on the strand transfer length.

Long-term strains have been measured using electrical resistance strain gages. However, attachment of the gages requires special care and this technique is not recommended.

Mechanical Strain Gage Measurements

Both short-term and long-term surface strains can be measured using mechanical strain gages. In this method, the distance between two points on the concrete surface is compared with the length of a standard invar reference bar. This approach requires the installation of special points on the concrete

surface, is labor intensive, and cannot be used easily with an automated data acquisition system. It is particularly suitable for measurements of strand transfer length and as back-up for long-term strain measurements by other means. In some applications, the sensitivity of the mechanical strain gage measurements will not be sufficient to provide reliable data. Measurements of concrete surface temperatures and standard reference bar temperatures are also needed when using a mechanical strain gage. To maintain the accuracy of this method, frequent comparisons with the reference bar are needed.

Length Changes

Measurements of overall length changes of a bridge or portions of a bridge can be comparedwith calculated length changes from creep and shrinkage or seasonal temperature changes. Length change measurements require a reference rod with a very low coefficient of thermal expansion. The rod must be fixed to the bridge at one end and relative movement between the rod and the bridge measured at the other end with a dial gage, linear potentiometer, or linear variable differential transformer. Care must be taken to ensure that the rod is protected from damage or changes in alignment. When electrical transducers are used to measure length changes, they must be electrically stable over the duration and temperature range of the observation period.

Deflections

No simple automated method exists for measuring vertical deflections of long-span girders. However, two simple manual methods are available. The first method involves the use of precise surveying equipment to measure the deflection at various points along the span relative to the ends of the girder. Reference pins can be located in the tops of girders for this purpose. The reference pins need to be relocated to the top of the slab when the deck is placed.

In the second method, a taut wire is stretched between two reference locations at the ends of a girder and the relative movement measured at locations along the span. The reference locations may be two bolts fixed rigidly to the sides of the girder, and the taut wire may be removed when not in use. However, it is important that the same tension be applied to the wire each time by using a pulley and weights at one end. A fixed reference, such as a scale on the side of the girder, is needed at each measurement location. Parallax errors can be eliminated by mounting a mirror adjacent to the scale. On box girders with easy access to the inside, deflections relative to the wire can be measured on the underside of the top slab inside the box. Non-corroding steel plates can be attached to the slab and measurements made with a digital sliding ruler on a magnetic base.

In some situations, a combination of the taut wire and surveying methods may be needed, depending on plant and site conditions and the construction timing.

Vertical deflections can be measured with electrical transducers such as potentiometers and linear variable differential transformers. This method requires a stable accessible reference location for each measurement and, for most bridges, is not practical.

When monitoring deflections, it is important to remember that temperature gradients can have a large effect on camber changes. Ideally, all deflection measurements should be taken just before sunrise when the temperature gradient is a minimum.

Slopes

Changes in slope can be measured with tiltmeters. Both uniaxial and biaxial tiltmeters are available. Biaxial tiltmeters measure rotations in two orthogonal directions. Tiltmeters can be mounted on either vertical or horizontal surfaces and can be read manually or with an automated data acquisition system. They may be used for both short-term and long-term measurements.

Prestressing Forces

The most accurate method to determine prestressing forces prior to transfer is with load cells. Load cells can be positioned on strand at either the dead end or jacking end in the prestressing bed. Although calibrated hydraulic jacks are used to stress strands, they only provide the force before their release. For pretensioned members, load cells provide the force after release of the jack, during curing, and immediately prior to detensioning of the strand.

Load cells may also be used on the ends of unbonded post-tensioning tendons and stay cables to measure the changes of force with time. In this application, a means to verify the "zero" reading of the load cell is needed. This is generally done using a lift-off procedure where the force in the load cell is removed by pulling on the end of the tendons and reacting directly against the concrete member. The load cell "zero" reading is verified when all the load is carried by the jack. Load cells are available as stock items from several manufacturers or can be custom built.

Strand End Slip

Slip of strand at the ends of girders can be measured using a technique developed by FHWA andillustrated in appendix A. A small channel-shaped fixture is attached to a strand at the end of the member. Holes in the legs of the fixture accept a digital depth gage or caliper which measures the distance from the outer leg of the fixture to the concrete surface. An initial measurement must be made prior to detensioning. Subsequent changes in the distance correspond to strand slip. Strand slip can be measured at detensioning, during the subsequent life of the girder, and during load tests. If it is necessary to cut the strand flush with the end of the girder, subsequent slip can be determined by measuring the relative movement between the end of strand and the end of the girder using a depth gage.

DATA ACQUISITION

Output from the sensing elements described in the previous sections can generally be measured using manual-read-out boxes or automated data-acquisition systems (ADAS). The two exceptions are deflections and mechanical strain gages, which can only be measured manually.

For instrumentation of precast girders, it is recommended that measurements prior to erection of the girders be measured manually. An ADAS may be necessary to facilitate frequent temperature measurements during the curing process. After erection, measurements may be taken manually or with an ADAS depending on the frequency of measurements. An ADAS requires an investment in equipment and installation time but greatly facilitates data acquisition particularly where a lot of readings are required in a short time. Data reduction is also a lot easier and more timely. Manual readings are labor intensive to obtain and still require input into a computer for data reduction and analysis.

For instrumentation of cast-in-place construction, the measurements may be taken manually or with an ADAS. For cast-in-place construction, installation of an ADAS is much easier and the sensing elements can be connected to the ADAS prior to concrete placement. Manual readout boxes will still be necessary in case the ADAS cannot be connected in time or in the event of failure of the ADAS. It should be noted that, with instrumentation during construction, there is no opportunity to put the experiment "on-hold" while the instrumentation is fixed. It is, therefore, essential to have a back-up plan particularly as it relates to obtaining "initialreadings."

DATA INTERPRETATION

Installation of sensing elements and data acquisition is only the start of monitoring field performance. Interpretation of data is equally important. Measurements of strains must be corrected for the coefficient of thermal expansion of the gages and the concrete if measurement of long-term strains is the objective. This requires a determination of the coefficient of thermal expansion of the concrete and, in some cases, the coefficient of thermal expansion of the gage. Determination of stresses from short-term strains requires a determination of the modulus of elasticity of the concrete or steel. Determination of stresses from long-term strains is considerably more complex and requires information about creep and shrinkage of the concrete. The determination of creep properties requires special loading equipment.

Consequently, accurate interpretation of the measured data requires information about the coefficients of thermal expansion of the gages and concrete, moduli of elasticity of concrete and steel, and creep and shrinkage of concrete. These data can be calculated or may be available from previous projects. However, it is recommended that the properties be determined from measurements on the actual concretes used in the instrumented portions of the structure. This requires the manufacturing of separate test specimens—usually 150- by 300-mm cylinders. These specimens should be cured and stored as long as practical with the actual structure prior to test.

SAMPLE INSTRUMENTATION PROGRAM

Many variations of instrumentation programs are possible depending on the specific interest of individual States. However, it is recommended that all States implement the basic program described in the next section. This will provide a basis for comparison between bridges in the different States. An optional program is also provided for States that wish to obtain additional information. It should be noted that the incremental costs for some parts of the optional program will be small compared to the extra information obtained.

Basic Instrumentation Program

The basic program consists of measurements of temperatures, long-term strains, and long-term deflections.

Temperatures

Temperature measurements are required to determine:

- Effects of heat of hydration on the properties of high performance concretes.

- Temperature gradients for superstructures at different locations in the United States.
- Number of freeze-thaw cycles experienced by the bridges at each location.
- Temperature correction for other measurements.

Measurements of temperature to determine the effects of the heat of hydration, must be made during the concrete curing period. Measurements of temperature gradients are only needed for the completed bridge. However, one set of thermocouples can be used for both measurements.

For measurements of thermal gradients, thermocouples should be placed along the vertical center line of the girder at the following depths:

- Top surface of the deck.
- 100 mm below top surface of the deck.
- 200 mm below top surface of the deck if deck is greater than 200 mm thick.
- Bottom surface of the deck.
- Approximate location of center of gravity of the top flange of the girder.
- Mid-depth of the girder.
- Approximate location of center of gravity of the bottom flange of the girder.
- Bottom surface of girder.
- Outside girder for measurement of air shade temperature.

At least three girders of each structure should be instrumented. The instrumentation should be placed near midspan in each girder. For measurements of heat of hydration, additionalthermocouples at the same depths but near the concrete surface may be included to determine transverse thermal gradients. Thermocouples should be placed near each end of the girders to measure the variation of temperature along the girders. Temperatures of match-cured cylinders and quality control cylinders cured in the prestressing bed should also be measured.

Data acquisition for heat of hydration requires that measurements must begin as soon as the concrete is placed and continue until the concrete temperatures fall to near ambient. Temperatures should be recorded at 30-minute intervals during the first 24 hours to ensure measurement of the maximum temperature. Data acquisition for temperature gradients need not begin until the bridge is complete and need only be made in summer and winter. Temperature readings at hourly intervals will provide sufficient information. Data acquisition for freeze-thaw cycles need only be made from late fall to early spring depending on geographic location. Temperature readings at 30-minute intervals should provide sufficient information.

Long-Term Strains

Long-term strains are required to determine prestress losses from elastic shortening, creep and shrinkage. Gages should be placed at the center of gravity of the prestressing force close to midspan and parallel to the strand. At least three gages should be provided in at least three girders. The three gages in each girder may be spaced longitudinally along the center line or transversely at one longitudinal section. The use of three gages provides some redundancy in case a gage is damaged and provides an indication of scatter in the data.

Measurements of long-term strains should begin as soon as the concrete is placed, although readings in fresh concrete may not be appropriate for the "initial readings" for data reduction. Initial readings should be taken before and after every significant event that affects the stress in the girder (such as before and after detensioning). After completion of the structure, it may only be necessary to obtain data every few months. Sufficient readings should be obtained so that trends in the data are clearly discernable. Readings should continue for the duration of the project.

Deflections

Measurements of deflection are necessary to determine changes of camber with time. Since high performance concrete is likely to be used in longer span bridges, absolute camber will be greater than in shorter span structures. However, changes in camber may not be as significant due to the higher modulus of elasticity and lower creep properties of the high performance concrete. At least three girders in every structure should be monitored although measurements on more girders are desirable. Mid-span deflection relative to the ends of the girder is the minimum amount of information needed. Measurements of deflection must begin prior to detensioning and be obtained before and after every significant event that affects the girder. Frequency of readings after completion of the structure should be selected so that trends in the data are clearly discernable. Readings should continue for the duration of the project.

Since changes in temperature gradients and live loads influence measured deflections, it is important to eliminate or minimize their effects. The effect of temperature gradients can be minimized by taking readings early in the morning just before sunrise. Temperature gradients should be measured at the same time, and, if necessary, a correction can be made for the temperature induced deflections. Live load effects can be eliminated or minimized by closing the bridge to traffic, if practical, or taking readings when the traffic volume is light. Failure to minimize these extraneous effects will increase scatter in the data.

Optional Additional Instrumentation Program

The basic program described above included the instrumentation of three girders to measure temperatures, long-term strains, and deflections. This program can be extended as described in Option No 1. Option No 2 describes additional types of measurements that can be made to supplement the basic program. Option No 3 discusses instrumentation for use with live load tests.

Option No 1 - Extension of Basic Instrumentation Program

Additional girders and additional cross sections of the same girder can be instrumented to measure temperatures, long-term strains, and deflections. Additional thermocouples can beplaced to measure

the variations of concrete temperatures along individual girders and along the prestressing bed during curing. Since previous research has shown that temperature gradients in completed bridges do not vary much along the length of a bridge, a smaller array of thermocouples can be located at the ends and quarter points of the girders at the following depths:

- Approximate location of center of gravity of the top flange of the girder.
- Mid-depth of the girder.
- Approximate location of center of gravity of the bottom flange of the girder.

Temperature gradients in the deck can be measured at locations midway between girders. Due to the exposed underside of the deck, gradients at these locations will be different from those at locations directly above girders.

Strains can be measured at the quarter or third points of girder. The vertical distribution of longitudinal strain can also be measured to verify a linear strain gradient.

Deflection profiles along individual girders can be determined from measurements at 8 to 10 locations.

Option No 2 - Additional Types of Measurements

End slip of prestressing strands can be measured using the technique described previously. If feasible, the slip of all strands at both ends of three girders should be measured. For girders with a large number of strands, at least 20 strands should be instrumented. Access to the ends of girders will be needed prior to detensioning.

Strand transfer lengths at the ends of girders can be determined from the variation of strains along the length of girders. These strains are generally measured with a mechanical strain gage. Access to the outside faces of the girders is needed prior to detensioning for installation of strain gage points and initial readings. The alignment of strain gage points must be parallel to the prestressing strand. Special techniques are needed to ensure rapid installation of strain gage points.

Longitudinal slopes at the ends of simply supported girders can be measured for comparison with calculated values. Longitudinal slopes of continuous girders can be measured at the section of maximum rotation. It is recommended that not more than three girders be instrumented in this manner. The instrumentation may be installed prior to detensioning or after the girders are erected.

For precise measurement of prestressing force prior to release, several prestressing strands at the end of the prestressing bed can be instrumented with load cells. It is recommended that at least three strands be instrumented at one end of the bed. As a minimum, readings should be taken before and after stressing every strand and before and after detensioning every strand. Readings at other times will indicate how the forces vary during concrete placement and curing.

Measurements of length changes are appropriate for long bridges without joints. However, little benefit will be obtained by measuring length changes of individual girders because of the complications of installing the reference rod.

In addition to the well established and proven types of instrumentation, States should consider including instrumentation that might be considered "experimental" in nature. For example, the use of fiber optic sensors has been identified as a new technique for instrumentation of civil engineering structures. The technique may offer several advantages over conventional type sensors and has the potential for establishment of "smart" structures. Lasers might also be used for measurement of deflections.

Option No 3 - Instrumentation for Live Load Tests

Many of the design provisions in the AASHTO Standard Specifications for Highway Bridges are based on knowledge and experience with normal concretes. With the introduction of high performance concrete, the applicability of these provisions needs to be reassessed. Items that can be investigated with live load tests include impact factors, lateral load distribution, shear lag, and vertical deflections.

Since a live load test is essentially designed to investigate a bridge response under short-termloading, instrumentation should be selected that will respond accordingly. In addition, strains from live loads are likely to be relatively small (less than 100 microstrain) and the instrumentation must have the required sensitivity.

For static load tests, manual reading of data is possible provided all instrumentation can be read in a time that is short enough to eliminate strain changes caused by temperature changes and creep. For dynamic load tests, a data acquisition system with a very short scanning time is required.

Depending on the objectives of the live load test, some of the instrumentation described under the Basic Instrumentation Program will be appropriate. However, it is likely that additional instrumentation in the form of strain gages will be needed. As discussed previously, it is recommended that the majority of short-term strains be measured with electrical resistance gages attached to reinforcing bars cast in the concrete. Surface mounted strain gages can also be used to measure live load response and may be necessary to achieve certain objectives. The number and layout of gages will be dependent on the objectives of the load test. Specific types of gages for these measurements are given in Appendix B.

APPENDIX A
PHOTOGRAPHS OF ACTUAL INSTALLATIONS

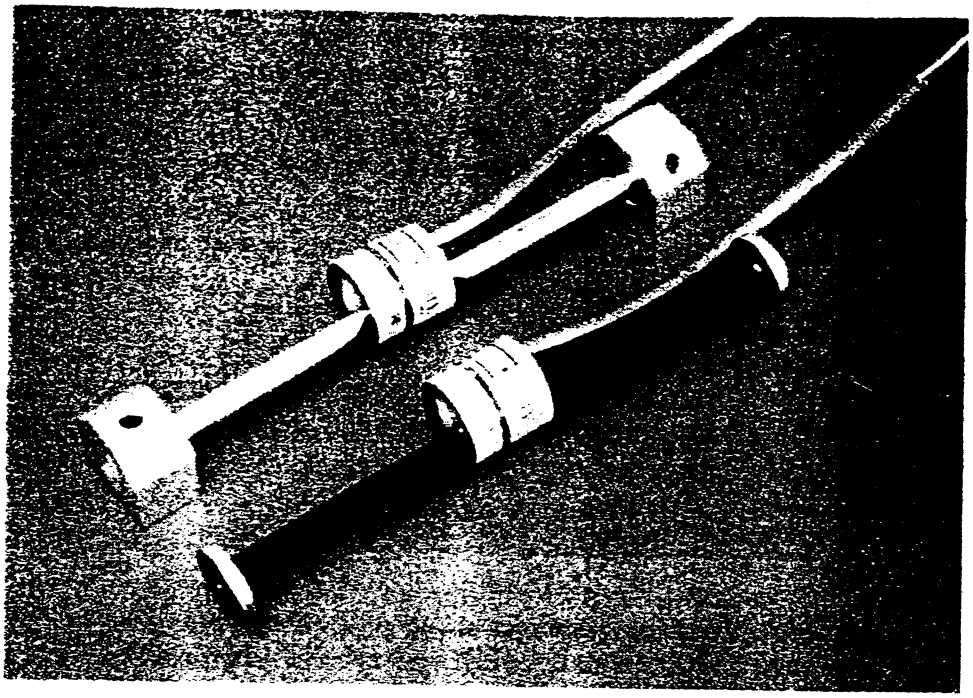

Figure 1. Vibrating wire strain gages prior to installation.

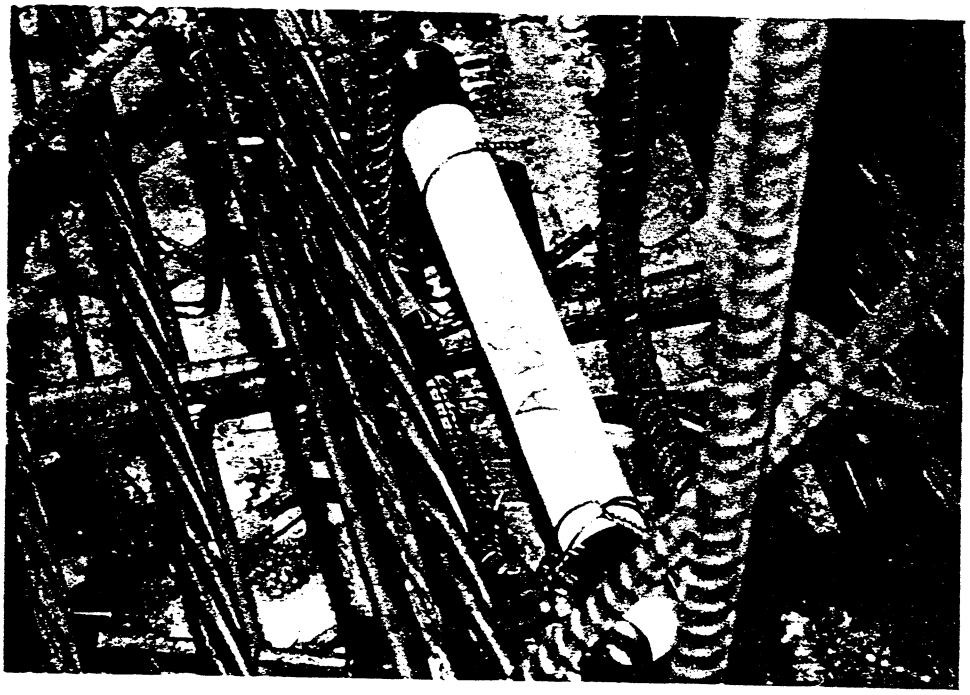

Figure 2. Carlson Strain Meter.
The gage is located in the bottom flange of a prestressed concrete girder.

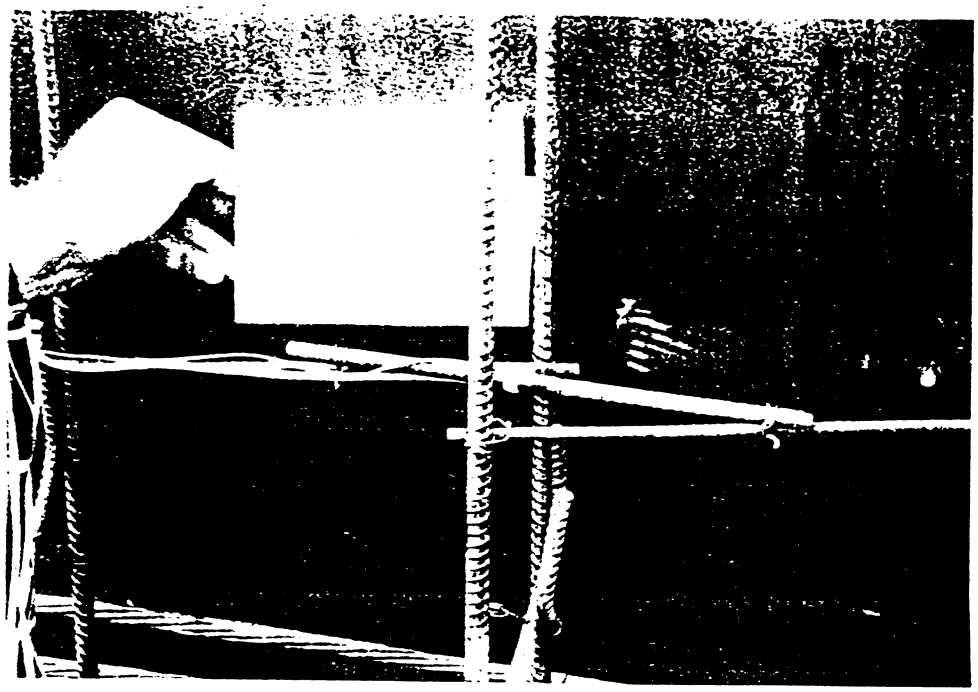

Figure 3. Electrical resistance strain gage on reinforcement. The gage is attached to a short length of steel reinforcement and located in the web of a prestressed concrete girder.

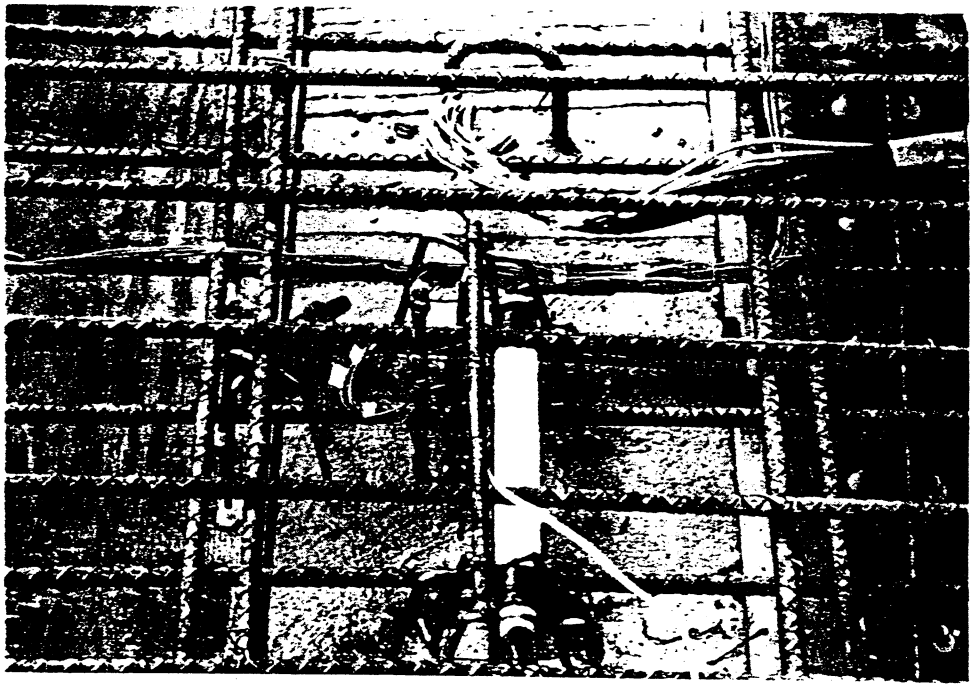

Figure 4. Electrical resistance strain gage and Carlson Strain Meter. Both gages are located in the deck slab above a prestressed concrete girder.

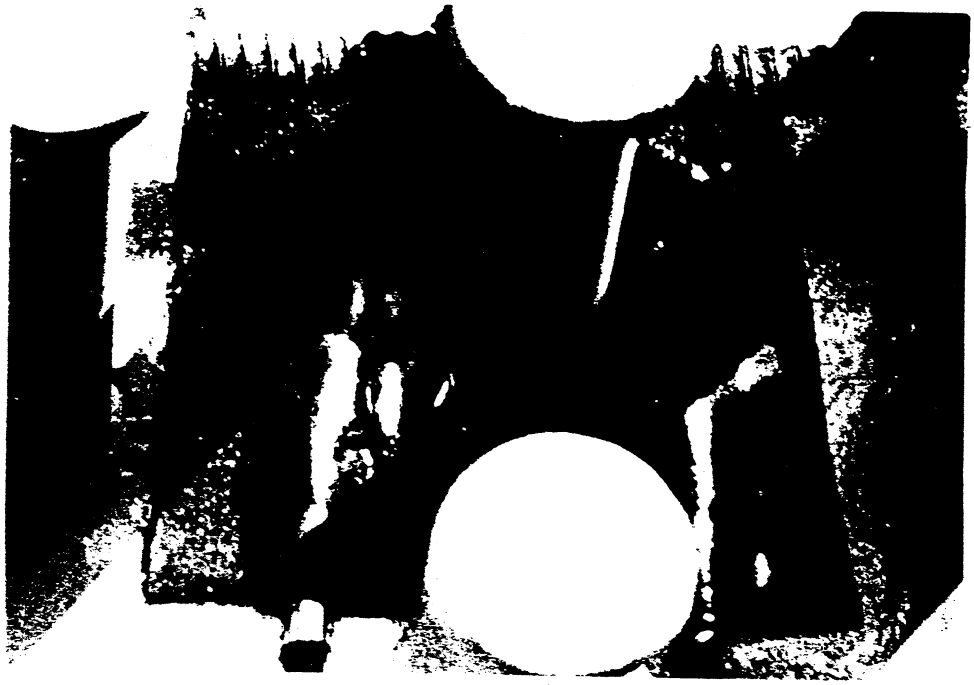

Figure 5. Weldable electrical resistance gages on a steel girder. The gages are located on the top flange between the studs.

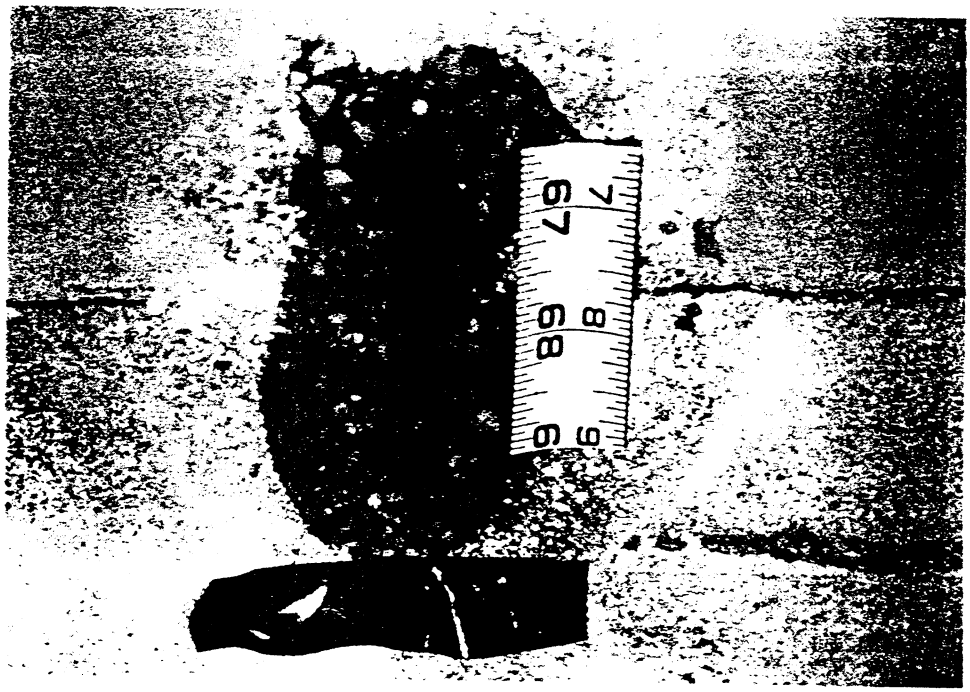

Figure 6. Electrical resistance strain gage on concrete surface. Special preparation on the surface was needed prior to application of the gage.

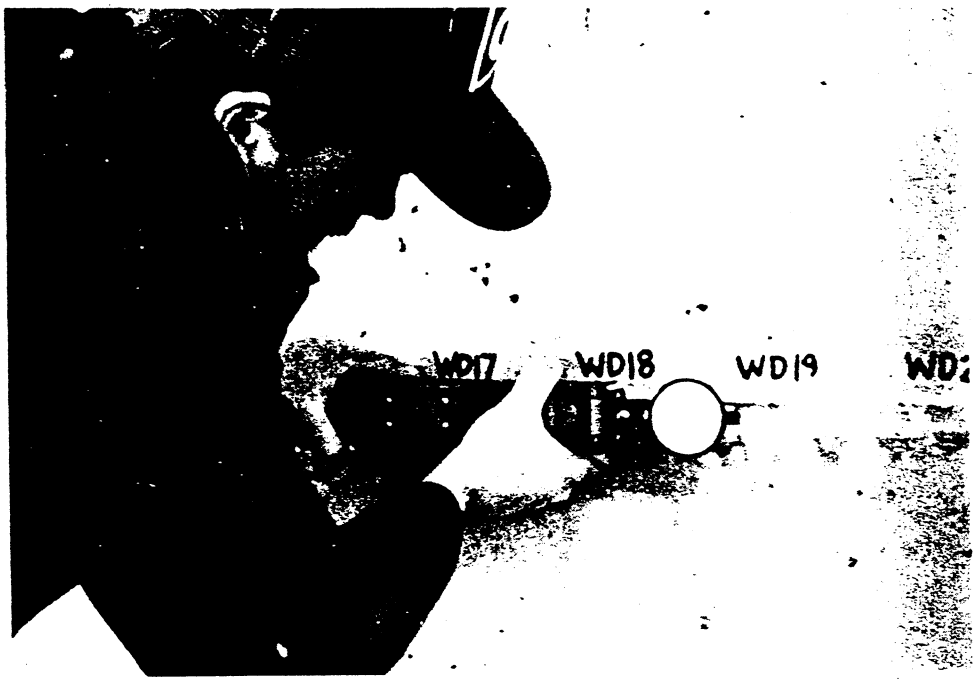

Figure 7. Surface strains.
A Whittemore mechanical strain gage is being used to measure transfer length in a prestressed concrete girder.

Figure 8. Deflection measurement relative to a taut wire.

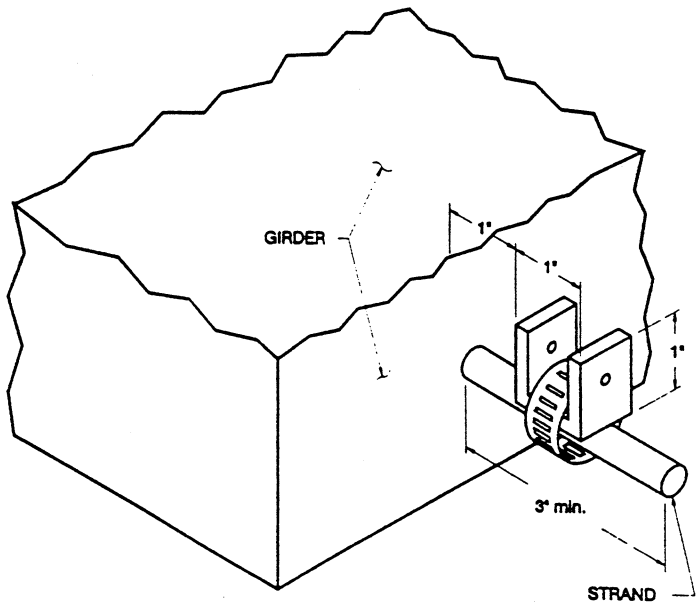

Figure 9. End slip instrumentation.

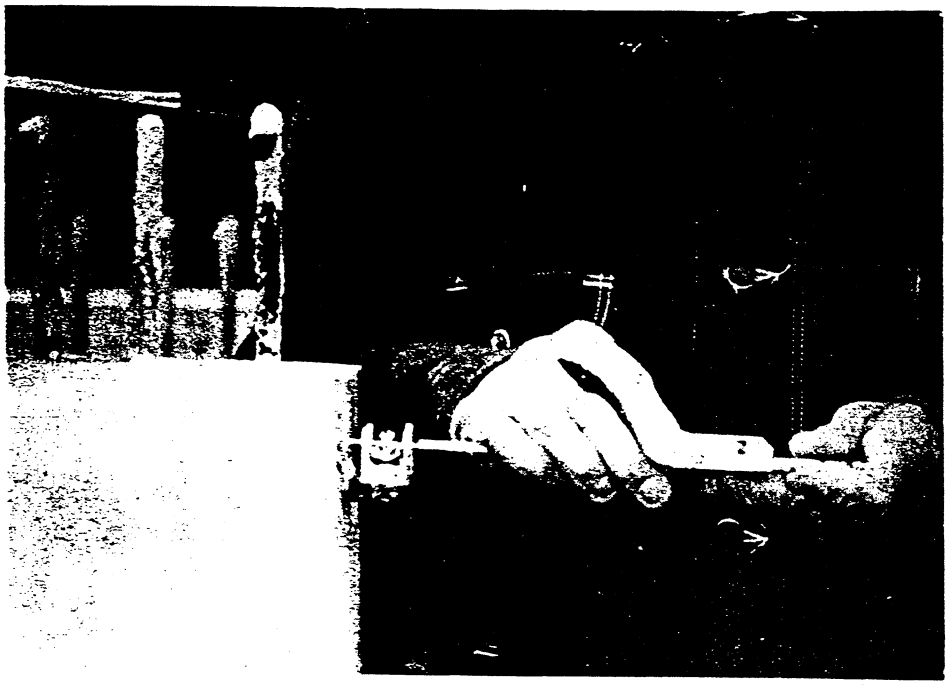

Figure 10. Measurement of strand end slip using a caliper.

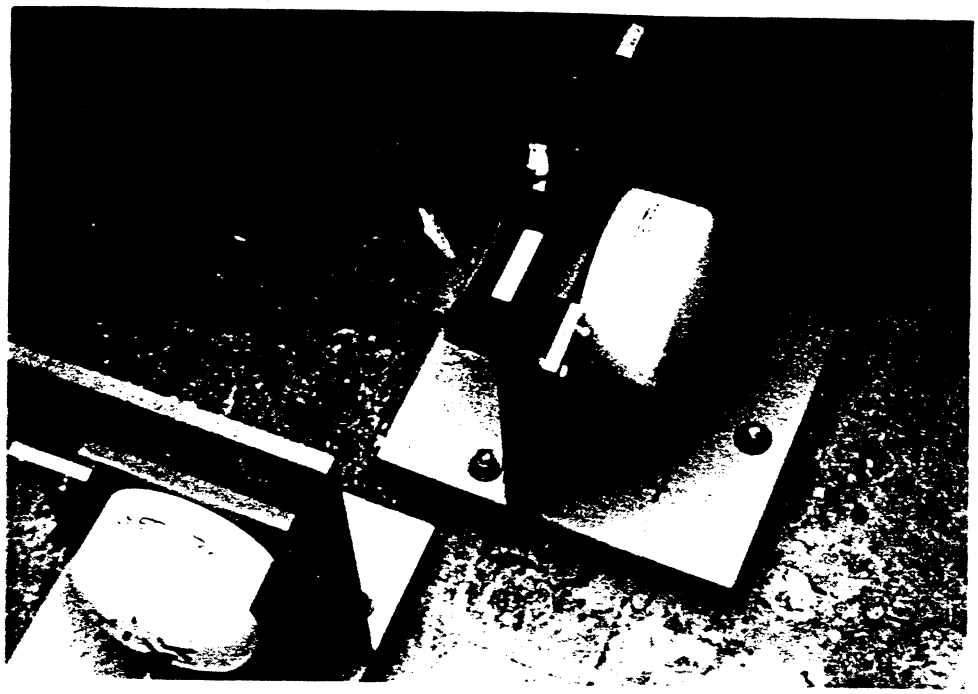

Figure 11. Tiltmeters.
The meters are arranged to measure changes in slope in two orthogonal directions.

APPENDIX B - TYPES OF INSTRUMENTATION

This appendix identifies specific sensors that can be used for bridge instrumentation. Although alternatives are available from different suppliers, the listed sensors have been used in the past and have worked successfully. The use of these sensors should be verified with the manufacturer to ensure that they are appropriate for the specific applications.

Thermocouples

- Copper-Constantan Type T (Minimum temperature range (-50° F to +250° F)

Electrical Resistance Strain Gages

For reinforcing bars:

- Designation CEA - 06 - 250UW - 350
- Designation CEA - 06 - 250UW - 120
- Designation EA - 06 - 250AE - 350

  The CEA series features large, rugged copper-coated tabs for ease in soldering leadwires directly to the gage. The above three designations indicate a gage length of 0.25 in. (6.4 mm), self temperature compensation of 6.0 ppm /°F and a resistance of either 350 or 120 ohms. The gages are available from Measurements Group, Inc.

For concrete surfaces:

- Designation EA - 05 - 20CBW - 120
- Designation EA - 06 - 20CBW - 120
- Designation EA - 05 - 40CBY - 120
- Designation EA - 06 - 40CBY - 120

  The above gages are self temperature compensated for either 5.0 or 6.0 ppm /°F and have a gage length of either 2 or 4 in. (51 or 102 mm). The gages are available from Measurements Group, Inc.

For structural steel:

- TML AWC - 8B

  This weldable gage is available from Texas Measurements, Inc.

Vibrating Wire Gages

- Model VCE - 4200 with a 6-in (152-mm) gage length.

- Model VCE - 4210 with a 10-in (254-mm) gage length.

  The Model VCE - 4210 is more rugged to resist bending. Both gages are available from Geokon, Incorporated.

- Model EM-5 with a 168 mm gage length.

  The gage is available from Roctest, Inc.

Carlson Strain Meters

- Model No. A8 with a gage length of 8 in. (203 mm).
- Model No. A10 with a gage length of 10 in. (254 mm).

  The A8 and A10 models have resolutions of 3.6 and 2.9 x 10^{6} respectively. Both meters are available from Carlson/R. S. T. Instruments, Inc.

Mechanical Strain Gages

- Demec mechanical strain gage with a gage length of 8 in. (203 mm).

  The gage is available from Mayes Instruments Limited.

- Model No. C 6981 (English) or C 6991 (Metric) plus accessories and spare parts.

  The gage is available from Hogentogler & Co., Inc.

- Model No. H-3230 (English) or H-3231 (Metric) plus replacement parts.

  The gage is available from Humboldt Mfg. Co.

- Model No. CT-171 (English) or CT-171M (Metric) plus accessories and replacement parts.

  The gage is available from ELE International, Soiltest Products Division.

- Whittemore mechanical strain gage with a gage length of 10 in. (254 mm).

  Although this gage is no longer produced, it is available at several testing facilities.

Tiltmeters

- Model 800

  This uniaxial tiltmeter has a resolution of 0.0001 degrees and an angular range of ± 0.5 degrees. The model is available from Applied Geomechanics, Incorporated.

Caliper for Strand Slip

- Digit-Cal plus Model No. 599-571-3

The caliper is manufactured by Brown & Sharpe and is available from McMaster-Carr Supply Company.

Data Acquisition Systems

Data acquisition systems need to be selected based on the types and quantity of sensors. Manual readout boxes are generally available from the sensor suppliers. Automated data acquisition systems are available from a variety of suppliers including Geokon, Incorporated; Campbell Scientific; Measurements Group; Roctest, Inc; and Texas Measurements, Inc.

APPENDIX C - INFORMATION SOURCES

Applied Geomechanics, Incorporated
1336 Brommer Street
Santa Cruz, CA 95062
Tel: (408) 462-2801
Fax: (408) 462-4418

Brown & Sharpe
1701 Howard Street, Suite F
Elk Grove Village, IL 60007-2447
Tel: (847) 593-5950
Fax: (847) 593-6619

Campbell Scientific, Inc.
815 W 1800 N.
Logan, UT 84321-1784
Tel: (801) 753-2342
Fax: (801) 752-3268

Carlton/R. S. T. Instruments, Inc.
241 Lynch Road
Yakima, WA 98908
Tel: (509) 966-1254
Fax: (509) 965-0857

ELE International, Inc.
Soiltest Products Division
P. O. Box 8004
Lake Bluff, IL 60044-8004
Tel: (800) 323-1242
Fax: (847) 295-9414

Geokon, Incorporated
48 Spencer Street
Lebanon, NH 03766
Tel: (603) 448-1562
Fax: (603) 448-3216

Hogentogler & Co., Inc.
P. O. Box 2219
Columbia, MD 21045
Tel: (800) 638-8582
Fax: (410) 381-2398

Humboldt Mfg. Co.
7300 W. Agatite Ave.
Norridge, IL 60656
Tel: (800) 544-7220
Fax: (708) 456-0137

Mayes Instruments Limited
Vansittart Estate
Arthur Road
Windsor, Berkshire SL4 1SD
UK
Tel: 011-44-1753-620237
Fax: 011-44-1753-832430

McMaster-Carr Supply Company
P. O. Box 4355
Chicago, IL 60680-4355
Tel: (708) 833-0300
Fax: (708) 834-9427

Measurements Group, Inc.
P. O. Box 27777
Raleigh, NC 27611
Tel: (919) 365-3800
Fax: (919) 365-3945

Roctest, Inc.
94 Industrial Blvd.,
Plattsburgh, NY 12901-2016
Tel: (518) 561-3300
Fax: (518) 561-1192

Texas Measurements, Inc.
P. O. Box 2618
College Station, TX 77841
Tel: (409) 764-0442
Fax: (409) 696-2390

Instrumentation
Tech. Memo

- Instrumentation Tech Memo

T·Y·LIN INTERNATIONAL / CH2M HILL

A JOINT VENTURE

To: Steve Thoman/CH2M HILL/Sac

From: Scott Hunter

Date: December 14, 1999

Subject: Instrumentation of the new Benicia Martinez Bridge, Bridge No. 28-0153R EA 04-6031

Cc: Mirek Olmer/TYLI/SF, Sajid Abbas/TYLI/SF

TECHNICAL MEMORANDUM

The State has requested that the joint venture develop plans, specifications and a cost estimate to instrument the new Benicia-Martinez Bridge for health monitoring. This memo outlines the tasks including defining goals; types of information sought and the instrumentation required; locations of instruments; supplementary data collection; data collection, and evaluation of the instrumentation; and a program schedule and team. It is to be used with the memo on the cost estimate dated Dec.14, 1999 , the Instrumentation Specifications dated Dec.14,1999 and the 100% plans sheet "Health Monitoring System, Shipping Channel Spans"

GOALS

Ongoing monitoring and instrumentation of the new Benicia-Martinez Bridge is useful both in understanding and assessing the condition of the bridge throughout its life and in evaluating the unique features of this bridge for future bridge designs in California and elsewhere.

While the safety of the bridge under quasi-static loading is well established by the design methods, the service performance over time and the details of the response of the structure to seismic forces are less precisely known. It is the joint venture's understanding that CALTRANS is designing a seismic monitoring system for the bridge. Therefore seismic monitoring is not included in this technical memorandum. This program concentrates on the service performance over time. Unusual features of the bridge include: Main spans of 200 meters, superstructure of lightweight concrete, near midspan hinges between frames that carry moment and shear, large single cell box design for concrete box girder, and ribs supporting wide deck overhangs.

Accordingly the goals of the health monitoring instrumentation study are:

1. Monitor and assess bridge deflections and rotations and concrete strains of the main span superstructure over time. Assessment is made by calibrating and modifying the design computer model for the bridge for the actual material properties, temperature distribution, tendon forces, deflections, strains and environmental conditions. This "best fit model" is then studied to understand how creep, shrinkage and consequent moment redistribution have affected the bridge response. This

understanding is used to make the best possible rational assessment of the present condition and to forecast the future condition of the bridge.

2. Monitor and assess condition of the post-tensioning in the bridge over its service life. This is accomplished by monitoring the relaxation of representative tendons and possibly by the installation of sensors to "listen" for wire breaks in the post-tensioning.

3. Monitor and assess temperature distribution and history of different bridge elements both during construction and during service. For bridges of this type, temperature gradient loading is a significant and often a governing load. Because the dimensions of the subject box girder are outside the range of most of the bridges where data has been collected it is advisable to collect temperature data for this bridge.

4. Collect supplementary information as necessary for the above assessments i. e. concrete material data, ambient temperature and relative humidity in and around the box girder.

INSTRUMENTATION AND DATA COLLECTION

Deflections and Rotations

While optical survey can be used to record deflection history, we would recommend the use of a base-line system consisting of a piano wire strung at constant tension from pier to pier for recording deflections. This system, which has been used successfully on several projects, offers the following benefits:

It is simple to set up and read and can be used by personnel untrained in surveying such as university students.

Since it is setup inside the bridge, the personnel are safe from traffic.

It can be read at any time e.g. before dawn when traffic vibration is minimal. Using optical survey equipment on the bridge deck would be difficult and hazardous at this time. It is important to obtain the deflections simultaneously with other data for correlation.

It is possible to read the piano wire electronically by installing displacement transducers at intervals along the span. This greatly simplifies and reduces costs for data collection.

We would also recommend installing tiltmeters and extensometers at pier tables. Tiltmeters are reliable and highly accurate spirit levels that are monitored electrically to determine rotations at a point. The tiltmeter results give the rotations at the top of pier due to both girder moments and bending and deflection in the column. Our experience in a study of the Parrotts Ferry Bridge was that tiltmeters offer accurate reliable information quickly and can be read electronically. The tiltmeters, the piano wire deflection measurements and any survey results are used to compare with the analytic model results in the effort to assess the long term deflections.

Extensometers are displacement transducers that record the change in length of the span relative to an unstressed graphite rod placed in the cell of the box girder. The change in length of the span after the initial construction is the sum of the shrinkage, creep, relaxation moment redistribution and temperature effects over the time period studied. It is an important first check on the analytical modeling.

For the substructure, we recommend incorporating 3 permanent benchmarks into every footing top surface. Records should be kept at regular intervals to allow assessment of horizontal and vertical movements and rotations of the footings over time as well as before and after seismic events.

Strains

Long term concrete strains can be measured reliably by use of vibrating wire strain gauges. The strain gauge would be placed in the concrete at the time of casting with wires leading to a data collector for periodic downloading. Because the strain in the gauge is measured by monitoring changes in frequency of the wire element they are not sensitive to the length of the recording wires or connection quality or other sources of resistance. Locations within the section for the strain gauges and other instruments can be seen in figure 2. In the past, vibrating wire gauges have been backed up by Demec strain gauges at the surface of the concrete. Our perception at this time is that the vibrating wire gauges are sufficiently reliable and that money is better spent on providing some redundancy in the vibrating wire gauges.

Alternative means of measuring concrete strains include Carlson strain meters, fiber optics and resistance strain gauges attached to rebar. Carlson strain meters are significantly more costly than the vibrating wire gauges. Fiber optics are still a research tool at this time and resistance strain gauges attached to rebar are more appropriate to short term laboratory experiments. They have problems with calibration, zeroing the gauge and the fundamental problem that, over time, the rebar strain diverges from the surrounding concrete due to creep and shrinkage.

Forces

Load cells will be used to monitor forces over time of two selected span tendons and at the hinge bearings for both beams of span 8. Load cells for the tendons will have a doughnut shape and be inserted around the strand between the anchor plate containing the wedges and the concrete build out that it bears on. Load cells at hinge bearings must be incorporated in the bearing between the bearing surface and the support area in the web of the box girder.

Tendon forces are used in determining the actual tendon relaxation and actual tendon force over time. The load cells at the hinge bearings are used to directly measure the moment redistribution at the hinge over time due to creep and shrinkage.

Temperature

Temperature data is of interest on three accounts:

1. Temperatures are needed to correctly interpret deflections and strain data. The temperature information needed includes the temperature gradient information in item 3. The gradient temperature strains must be known and backed out correctly in order to accurately determine what strains are due to elastic forces, creep, and shrinkage. If the temperature gradient is not known accurately, the strain measures must be made when the temperature gradient effects are negligible. Sufficient temperature information must be available to assess when the gradient is minimal.
2. During construction, thick elements subject to strains due to differential temperature, can be monitored to determine the actual temperature distribution. This is important for bridge elements are sensitive to mass concrete temperature effects. For this bridge, these elements include: Pier tables, girder soffit slabs, piers and footings.
3. In service the actual temperature gradient over the depth of the box girder can monitored. The temperature gradient is of particular interest since group IV loadings usually control design of some aspects for long span concrete box girders. While there have been a number of studies of temperature gradients in box girders, this bridge is wider, deeper, and has thicker elements than the bridges in the completed studies. Moreover, the box girder is composed of lightweight concrete composed in part of lightweight aggregate which may affect the temperature gradient.

Condition of Post-tensioning tendons.

Recently it has become possible to continuously acoustically monitor post-tensioned concrete structures in order to detect and locate wires breaks in bonded and unbonded post-tensioning tendons. Detection is accomplished by filtering and analysing the ambient vibration of the structure. The wire break event has a distinctive signature and the method has achieved excellent results in full scale tests and on a grouted post-tensioned bridge in service. The sensors for this technology are externally mounted.

In between the cases of not monitoring (and not knowing) the condition of the post-tensioning and the case of deploying a comprehensive network of monitors over all the bridge elements which contain post-tensioning lies the possibility of monitoring selected areas for significant periods of time. The areas would be selected based on concern due to relative exposure (the deck is usually more susceptible to corrosion than the webs or bottom slab for a box girder, the areas near joints are also more susceptible) or by being representative of typical conditions. Towards the end of the service life of the bridge more comprehensive monitoring could be installed when the limited monitoring, structure age or visual inspection makes the condition of the structure a matter of concern.

We do not expect that there will be breaking wires in the post-tensioning during the initial part of the service life of the new Benicia-Martinez bridge. Given this condition, the acoustic sensing information would still be useful in establishing a record of the bridge in its healthy state. However, this instrumentation is not integral to the evaluation of the strain and deflection data described above.

Corrosion

This bridge is constructed with large diameter steel cased piles filled with concrete supporting a concrete footing reinforced with mild steel and post-tensioning. For steel and reinforced concrete exposed to salt water corrosion is a serious issue. Sensors are available which measure the electric potential at the surface of the steel. This can be interpreted to determine the likelihood of corrosion. This method is useful even when the rebar is epoxy –coated. It indicates the potential for corrosion if there are nicks or gaps in the epoxy coating.

Supplementary Data

Concrete Material Data

Our experience is that there can be significant differences between the lab mix material properties and the properties of the concrete placed in the bridge. In order to correctly assess the time dependent response of the bridge and to "back out" the strains due to the different phenomena, cylinders need to be taken from the concrete placed in the bridge and tested for strength, elastic modulus, temperature coefficient, creep and shrinkage under standard lab conditions.

The contractor is also required to conduct various property tests on the lightweight concrete placed in the box girder as part of the verification and quality control for the job. We examined the tests required for verification to see if there was overlap and duplication. Eliminating duplication would result in cost savings. However we found that:

1. The strength and Young's modulus tests as per ASTM469 are called for by both series. For verification only E_c at 3 days is required. For the instrumentation program E_c is tested at 3, 7,28,56,91 and 180 days.

2. Creep and shrinkage tests are called for by both series. The verification tests only require creep for loading at 28 days, the instrumentation program requires loading at 3, 28 and 180 days.

It is reasonable that the tests are treated differently, after all, they have different purposes. Other considerations are:

- It is important that all the data for any one property be taken from the same source. It is preferable that all the material property data for the program be taken from one source. This eliminates extraneous differences in interpretation and lab conditions. It offers the best conditions for obtaining reliable data.

- It is logistically cleaner and simpler to keep the programs separate.

- The most likely candidate for combination, strength and Young's modulus testing are also the least costly.

In our view, the best use of the job site field mix data is for concrete weight and for a cross check on concrete strength, stiffness and variability.

It may also be desirable to conduct creep and shrinkage tests under field conditions by placing creep frames in the cell of the box girder. We are currently reviewing this item.

Ambient Temperature and Relative Humidity
In order to assess the deflection, concrete strains and in situ temperature, data ambient temperature data is needed. In order to assess how the actual creep and shrinkage compares to a constitutive model (e.g. the model used in design or a new proposed model) the relative humidity history is needed.

Data Collection

Data from the instruments is collected on site in data loggers within the bridge. Two dataloggers may be necessary given the construction sequence and the locations of the sensors. One type of data acquisition system has all the sensors at a section being routed to a multiplexer (automatic switch box) then a single cable runs from the multiplexer to the datalogger. Power for the system may be supplied from house current or solar panels. It is possible and cost effective to set up the instrumentation system for remote download and instructions via phone lines and modems. A hard wired phone line is recommended over a cell phone for long term reliability. Data processing can be automated and reports generated automatically. If a database is used, queries and specialty reports are easily generated. Continuous access to the health monitoring results can be made available via the internet.

PROGRAM

Our experience is that an instrumentation project is well served by using a team consisting of the bridge designer, an engineering lab experienced in instrumentation, and a local university. For this project, local universities that might participate include UC Berkeley or UC Davis. However, in this case, CALTRANS is not only the client but actively conducts investigations on many aspects of bridge design, construction and performance. Therefore we assume that CALTRANS will be taking an active role in all phases of the health monitoring instrumentation, particularly data collection and evaluation.

Program Planning

This memorandum represents a milestone in the task of planning the instrumentation project. CALTRANS reviewed the first draft of this technical memorandum and a first draft of the specifications for the instrumentation. They asked for background information on our instrumentation work in Hawaii, and a fuller description of the goals and usefulness of the different elements of the instrumentation program. This memorandum is part of our response to those requests. CALTRANS made it clear that they want to have the contractor responsible for the installation and the initial monitoring of the instrumentation during construction. The functioning system will then be handed over to CALTRANS and further monitoring and evaluation will be paid for as part of maintenance. They also indicated that they are open to the participation of a local university at this stage. The next step should be a review by

CALTRANS of the current memo, estimate and specifications and a meeting to discuss precise goals and scope for the instrumentation, a budget and the program for carrying out the study. The program which follows from the current thinking is described below.

Installation

The general contractor is responsible for the installation and initial monitoring (during construction) of the instrumentation. The specifications require that an experienced engineering laboratory be retained for the detailed design and installation of the system. Three competent companies are given in Appendix A to this memorandum. A modified version of this memorandum including the short list of recommended contractors can be given to the bidding general contractors to aid in their understanding the task and in selecting an appropriate subcontractor for it. A kickoff meeting specifically for the instrumentation can be used to establish communication and familiarity between the installer and CALTRANS and the other members of the instrumentation team. The University team should be on board by this time and the construction schedule should be in shape to allow tentative dates to be set for different installation tasks. Shop drawing review will be coordinated with the designer. The remaining details of the sensors, cabling and ADAS system will be reviewed and determined before installation begins. Field inspection by the designer will be required for all installations but especially those with instruments placed in the concrete. The university team should be present for some of the installation in order to be familiar with the details and nature of the sensors and the system producing the data. The engineering lab and the CALTRANS/university team should meet with the bridge designer to determine the monitoring schedule.

The instrumentation installation team should meet with the resident engineer and contractor to determine the installation schedule and clarify details of the installation. During the installation, close coordination with the resident engineer and the contractor are vital.

Different checks are performed on the data beginning immediately after casting of the concrete in order to assure that the instruments are functioning correctly and that baseline data is collected in order to correctly evaluate the long term strains.

Data Collection

We would recommend getting the data from both the bridge site and the material property tests into a database with minimum prior handling. Then the programming features of the database (e.g. Microsoft Access) can be used to manipulate, filter, search, summarize and extract statistics from the data. A single location must be determined for the data with access for all team members. The university team or CALTRANS can take the lead on data collection, reduction, documentation of all aspects of the instrumentation and dissemination of the results over the 5 to 20 years of the project life. The university is geared to research and publishing. The best faculty team member for this project is one with experience with bridge design and instrumentation. Someone local to the Bay area or Sacramento will have less difficulty with access and will have the stimulus of the constant presence of the structure to pursue the investigation to a useful conclusion. This project can also be an opportunity for students to

get first hand experience with the design and construction of a major structure. Alternatively the bridge designer can fulfill a large part of this task.

Evaluation

The bridge design team and CALTRANS should take the lead in the interpretation and evaluation of the data coming from the instrumentation. The designer understands the bridge and has analytic models already developed that can be compared with the actual results. The actual material properties from the field mix tests and any changes in construction sequence or prestressing must be incorporated in the model to be used for comparison with recorded deflections and strains. Reports should be written on a yearly basis for the first five years to keep on top of any trends that show up in the bridge response.

APPENDIX A

As discussed, it is important that the instrumentation be installed by an experienced, qualified, and interested contractor. The following is a list of three contractors who have previous experience in this activity:

Construction Technology Laboratories, Inc.
5420 Old Orchard Road,
Skokie, IL 60077-1030
Phone: 800-522-2285

Wiss Janney Elstner Associates
330 Pfingsten Road
Northbrook, IL 60062
Phone: 847-272-7400

RocTest
94 Industrial Blvd
Plattsburg, NY 12901
Phone: 518-561-3300

- Sep 98 H3 Report

Instrumentation of the North Halawa Valley Viaduct Oahu, Hawaii

Progress Report

by

Kenneth W. Shushkewich
Nhan T. Vo
T. Y. Lin International
825 Battery Street
San Francisco, CA 94111
(415) 291-3700

and

Ian N. Robertson
University of Hawaii at Manoa
2540 Dole Street
Honolulu, HI 96822
(808) 956-6536

funding provided by

Hawaii Department of Transportation
and
Federal Highway Administration

September 1998

Table of Contents

Executive Summary

Acknowledgements

Chapter 1 - Introduction

Chapter 2 - Description of the North Halawa Valley Viaduct

Chapter 3 - Field Instrumentation

Chapter 4 - Concrete Material Properties

Chapter 5 - Mathematical Models for Creep and Shrinkage

Chapter 6 - Comparison of Creep and Shrinkage Models with Field Observations

Chapter 7 - Time-Dependent Analysis

Chapter 8 - Thermal Behavior

Chapter 9 - Load Test

Chapter 10 - Conclusions

Appendix A - Design of Segmental Bridges for Thermal Gradient - Shushkewich

Appendix B - Long-Term Monitoring of the North Halawa Valley Viaduct - Robertson

Appendix C - Calibration and Verification of Load Cell Data - Russell & Hunter

Appendix D - CTL Creep and Shrinkage Data

Appendix E - Field Creep and Shrinkage Data

EXECUTIVE SUMMARY

The North Halawa Valley Viaduct instrumentation program has been a tremendous success. An excellent database of instrumentation results has been recorded. This progress report includes results to the end of 1997. The report will be updated as additional results are recorded, and a final report will be issued at the end of 1999.

Field instrumentation has been placed at seven sections on the North Halawa Valley Viaduct to measure concrete strain, prestressing stress, deflection, and temperature. Concrete material properties have been determined. Short-term properties (compressive strength, modulus of elasticity, and coefficient of thermal expansion) have been determined in the laboratory. Long-term properties (creep and shrinkage) have been determined in the laboratory as well as in the field.

Mathematical models for creep and shrinkage have been compared with the experimental results. A comparison between creep and shrinkage test data and four current prediction models has been made. The Bazant creep model and Gardner shrinkage model have been shown to yield the best results. A procedure to predict long-term creep and shrinkage based on 28 day test results has been presented. This is a significant breakthrough, since one month of testing can now be used to predict the creep and shrinkage models to be used in the design, rather than one year of testing which was required when the bridge was originally designed. A comparison has been made between the field measured data and results predicted by the computer program SFRAME.

Thermocouple readings have been systematically reduced to determine critical positive and negative thermal gradients. These gradients have been shown to compare favorably with those recommended in the 1998 proposed AASHTO segmental guide specifications. This information is particularly timely since it validates the reduction of the negative thermal gradient by 40% from the 1994 AASHTO LRFD bridge design specifications.

The authors believe that practising engineers will find the results of this study to be very useful (creep and shrinkage models, time-dependent analysis, thermal behavior, load test, etc.). The results will also be most valuable for those wishing to conduct further research utilizing this data, or those planning future instrumentation projects based on the knowledge gained from this study. With this in mind, it is intended to make a CD-ROM available in the future for easy access to the data.

ACKNOWLEDGEMENTS

The instrumentation program of the North Halawa Valley Viaduct was conducted under the sponsorship of the Hawaii Department of Transportation and the Federal Highway Administration. The authors would like to acknowledge the following individuals:

James Hoblitzell and Roland Nimis of FHWA for their interest and encouragement. Raymond McCormick of FHWA for his assistance in obtaining funding, and general support of the program. Donald Ornellas of HDOT for his support of the program. Diana Lee of HDOT for her assistance with administrative issues.

Henry Russell and Tom Weinmann of CTL for input during the instrumentation plan development stage. Scott Hunter and Jose Sanchez of TYLin who were extremely helpful from both planning and technical standpoints. Kirk Wellington of Kiewit Pacific without whose cooperation the instruments could not have been installed. Tom Weinmann and Scott Kostakos of CTL for assistance with installation of some of the instruments. Andre Lee of SSFM Engineers who assisted with the installation of all of the instrumentation while a graduate student at UH.

UH technicians Andrew Oshita and Miles Wagner for assistance in fabrication of some of the components for the instrumentation. UH graduate students Michael Durbin for his considerable effort in compiling and processing the immense amount of data collected during the first two years. UH graduate students Todd Dwight, Eric Matsumoto, Chun Dong and Weng Ao for contributing to various elements of the analysis and reporting of the results.

CHAPTER 1

INTRODUCTION

Segmentally constructed concrete bridges have become a mainstay in North American Highway construction. Since their introduction in 1964, more than 360,700 lineal feet of segmental bridge have been built, with a trend toward increasing popularity. Their versatility, durability, aesthetically-pleasing appearance and relative economy make them the best choice in many situations. These bridges are generally long-span post-tensioned structures which are subject to the same prestress losses as all other prestressed structures. However, these prestress losses have a greater impact on the long-term performance of long-span structures than is the case with shorter span prestressed bridge and building elements, particularly if the bridge is continuous over several spans, as in this case.

The North Halawa Valley Viaduct is a segmental cast-in-place concrete box girder bridge built by the cantilever construction method. It utilized a truss supporting the form travellers, launched without dismantling from pier to pier. Inbound and outbound viaducts are separate structures, each consisting of three continuous units totaling approximately 5500 feet. Deck width is 41 feet and the single cell box width is 21 feet; box depth varies from 8 feet at mid-span to 18 feet at the piers. Spans are typically 360 feet with shorter end spans and accommodations to avoid placing piers in the stream.

Since it is a major project, both the initial design and construction history are well documented. The final design was done with a state-of-the-art SFRAME computer model that has been thoroughly checked and updated consistent with the actual history. The analysis program can use any of several concrete constitutive models to model time-dependent response of the structure, and modification of the modular-based program to test other constitutive models is straightforward. A good basis exists for a study to investigate and compare the stresses recorded in a bridge under service with the estimates of the time-dependent response of a major structure by a state-of-the-art analysis program.

The viaduct is a CIP box girder unusual in several respects. The concrete aggregates used in Hawaii are known to result in a concrete with higher values of creep and shrinkage than most concrete used elsewhere in the United States. As a consequence, there is some concern that long-span prestressed structures such as the Halawa Valley Viaduct will suffer from higher than anticipated prestress losses and long-term deflections. The design of this structure was required to provide a "no-tension" condition in the concrete after all losses and under full live loading. As a precaution against failure to meet this criterion, the bridge has been provided with the capability of installing additional prestressing tendons at a later date. These tendons could also be used to upgrade the bridge's rating capacity if higher live loads or additional overlay were ever applied to the structure. The more knowledge found from the instrumentation study of the bridge would allow for a better the assessment of the bridge's remaining capacity required for the additional loads.

The objectives of the study are as follows:

1. Evaluate the longitudinal strain history at critical locations (mid-span and adjacent to piers of selected spans). Measurements began immediately after construction in March '94 and continued for the first 5 years of service life. Temperature gradients at mid-spans were also recorded and used to evaluate stresses due to daily and seasonal temperature variations.

2. Evaluate the deflection response of the structure. Selected spans have been monitored to record deflections along the span and rotation at piers. Measurements began immediately after construction and continue for five years.

3. Collect concrete shrinkage and creep data from as-placed concrete samples, and evaluate the resulting parameters.

4. Compare the stress and deflection histories with the estimates from the SFRAME computer model using selected concrete constitutive models (CEB1, Bazant-Panula or refinements of these).

Seven sections of the inbound Viaduct were selected for instrumentation to provide an adequate representation of the Viaduct behavior. The measurements required to achieve the project objectives are concrete strain, span shortening, concrete creep and shrinkage strains, concrete and ambient temperatures, tendon forces, span deflections and support rotations. The instrumentation system used to make the above measurements includes vibrating wire gages, electrical resistance strain gages, demec strain gages, extensometers, thermocouples, load cells, a base-line system, tiltmeters, and an automated monitoring system. During the construction of the bridge, all instrumentations were installed by personnel from the University of Hawaii (UH) and Construction Technology Laboratories (CTL) of Skokie, Illinois. CTL also performed concrete testing to determine the compressive strength, static modulus of elasticity, and coefficient of thermal expansion of the concrete used in the instrumented sections.

Standard creep and shrinkage tests are being performed in the laboratory conditions, in accordance with the American Society for Testing and Materials (ASTM), and on-site in atmospheric conditions similar to those of the structure. The laboratory testing is being conducted by CTL, while the on-site tests are located inside and outside of the box girder bridge in the Halawa Valley.

Based on the above discussion, the benefits of the instrumentation project are as follows:

<u>For the State of Hawaii:</u> This study allows assessment of the performance and condition of this 140 million dollar structure based on field measurement of the bridge in service. The knowledge gained will be useful in the design of any viaducts and rail structures in the future. What is learned about the creep and shrinkage of local concrete will be useful in design of future prestressed structures in Hawaii. A realistic assessment of typical local temperature effects on bridge structures has been made. Since the University of Hawaii, Manoa is an important part of the team conducting the project, the state has benefit both by the participation and newly-acquired knowledge of this institution and by the increased quality of the education provided to Hawaii's engineers.

For the Nation: This study increases our knowledge of the performance of this bridge type. By comparing long-term performance with the theoretical values generated from the computer models, it will allow modification and refinement of the design process and contribute to the selection of a concrete constitutive model that will allow future segmental designs to be neither overly conservative nor unduly risky.

For the profession: This study is the necessary next step in improving the analysis and design of long-span and segmental concrete bridge structures. The estimates of long-term stresses and deflection made in the design of this project are the best available and are superior to evaluations made before the use of computer modeling. Nonetheless, comparison with the field data of a major structure in service will stimulate the development of the appropriate constitutive model for the concrete and encourage a look at the modeling details to determine what is crucial to a good model. The involvement of the bridge designer in the project will ensure access to all the data accumulated in the original design and construction phases of the project and the rapid transfer of the results back to the design office with a consequent advance in the state of the art.

Chapter 2 - Description of the North Halawa Valley Viaduct

Design and Construction of North Halawa Valley Viaduct

Tim J. Ingham, Rafael Manzanarez, and Karen Cormier,
T. Y Lin International

The North Halawa Valley Viaduct is a 2-km-long prestressed concrete box girder bridge on the island of Oahu, Hawaii. It is the first cast-in-place cantilever segmental bridge in the United States to be built from an overhead erection gantry. The design features of the project are described, and the reasons for choosing that construction method are given. The main features of the operation of an erection gantry are described, and some of the problems arising during the construction of the bridge are discussed. Finally, the instrumentation of the structure to monitor its long-term performance is detailed.

The North Halawa Valley Viaduct is a part of the so-called Interstate route H-3 project on the island of Oahu, Hawaii. As shown in Figure 1, the project runs from the Halawa interchange on H-1, north of Honolulu, across the Koolau Mountains (which form the backbone of Oahu), to Kaneohe, on the windward side of the island. The project is intended to relieve congestion on the existing Pali and Likelike highways, connect the Pearl Harbor naval station with the Marine Corps station at Kaneohe, and provide for future trans-Koolau travel demand.

Project Description

The H-3 project, besides including several miles of at-grade highway, includes three major structures: the trans-Koolau tunnel, which runs approximately a mil beneath the crest of the island; the recently complete Windward Viaduct immediately to the east of the tun nel; and the North Halawa Valley Viaduct immediatel to the west of the tunnel. The North Halawa Valle Viaduct was designed by Nakamura & Tyau, of Hono lulu, Hawaii, and T. Y. Lin International, of San Fran cisco, California.

Site Conditions

The bridge runs through the upper North Halaw Valley, which is typical of the deep erosional valleys tha have formed on the flanks of the ancient Koolau vol cano. The valley is generally V-shaped, with irregula side valleys and ridges extending to the valley bottom slopes along the project alignment are frequently a steep as 2h:1v to 1h:1v.

The viaduct design reflects the fact that the Nort Halawa Valley is an environmentally sensitive site. Sev eral native Hawaiian burial sites have been found in th valley; these are now the subject of archaeological in vestigation. The valley is also a watershed area and wil be closed to the general public after the H-3 project i completed. The viaduct has been designed and con structed so as to minimize disturbance to the site.

The North Halawa Stream meanders along the via duct alignment as shown in Figure 2. The stream is sub

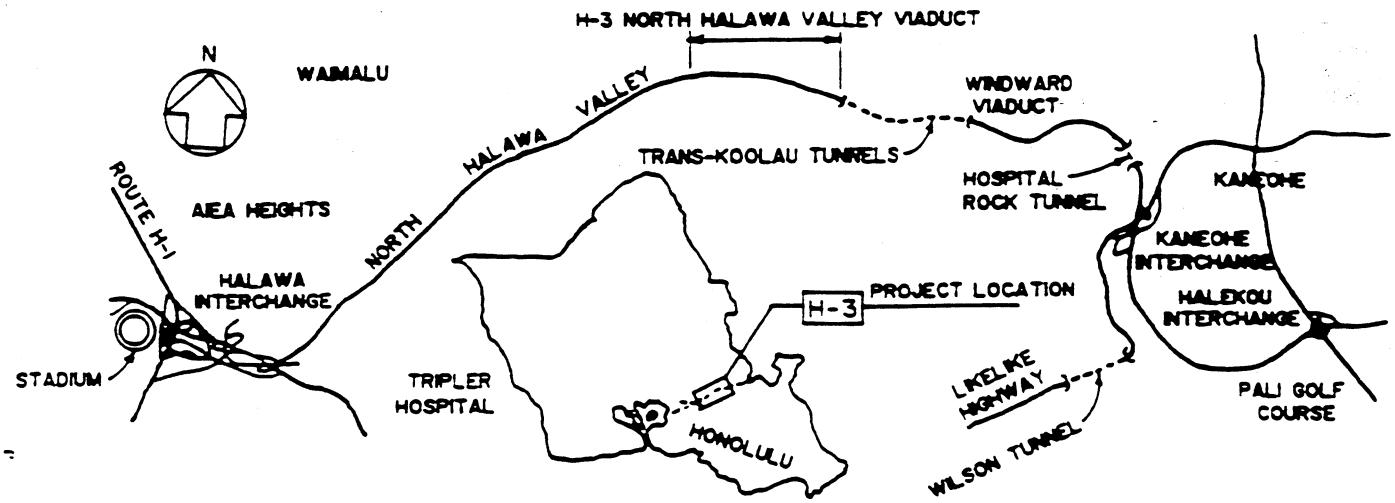

FIGURE 1 Project location.

ject to frequent floods because of an average of 150 in. of rain annually at the top of the valley. An important part of the project involves improving the stream to protect the viaduct foundations from scour.

Description of Structure

A general plan and elevation of the bridge are shown in Figure 2. The project actually consists of two parallel viaducts, one carrying two lanes of traffic inbound to Honolulu and one carrying two lanes of outbound traffic. The inbound viaduct is 1897 m (6,225 ft) long and the outbound viaduct is 1667 m (5,470 ft) long. Both viaducts are aligned horizontally on curves with radii of approximately 1800 m (5,906 ft) at the lower end of the valley and 2900 m (9,514 ft) at the upper end of the valley. The viaducts are on a nearly constant 6 percent grade sloping up toward the mountains (the vertical scale is exaggerated by a factor of two in Figure 2). The typical (and maximum) span length is 109.728 m (360 ft), with some span lengths as small as 91.44 m (300 ft) to accommodate the vagaries of the terrain and the stream in the valley bottom.

Figure 2 shows the viaducts to be divided into three structural units each, averaging 565 m (1,854 ft) in length between expansion joints. Each unit has two fixed piers toward its center and two or three flanking expansion piers on either side. Each unit was constructed by the segmental cantilever method using an overhead erection gantry.

The expansion joints between the units are located at the top of so-called end piers. This was done to avoid the excessive deflections that sometimes accompany midspan hinges and the construction problems that often accompany cantilever construction past a quarter-point hinge. The fact that the end piers, located at what would otherwise appear to be the middle of a span, are perhaps unattractive was discounted because the valley will eventually be closed to the public. The rather large movement ratings of the expansion joints, up to 21 in., combined with the steep 6 percent grade of the bridge led to an unusual design detail. At each end pier the bearings were aligned along the grade of the stru[illegible] in order to constrain the movement of the bridge t[illegible]e parallel to the expansion joint. If the bearings had been set horizontally, as is done normally, the movement of the bridge would have had a component perpendicular to the expansion joint, causing a jog in the roadway surface of 1¼ in. Of course, inclining the bearings induces a slope load into the pier and footing, equal to the grade of the bridge times its dead load. But the dead load reactions on the end piers are relatively small, and, fortuitously, most of the end piers are fairly short.

The viaduct cross section is shown in Figure 3. The out-to-out width of the bridge is 12.497 m (41 ft), which accommodates two lanes of traffic plus shoulders. The cross section varies in depth from 2.438 m (8 ft) at midspan to 5.468 m (18 ft) near the piers. These dimensions are typical of cast-in-place structures of about 100-m (328-ft) span length.

Piers

The bridge piers are designed conventionally. They are of hollow construction with a wall thickness of 457 mm (1 ft 6 in.) and exterior dimensions of 3.048 × 7.010 m (10 × 23 ft). They vary in height from 8.336 to 31.766 m (27 ft 4 in. to 104 ft 3 in.). The piers [illegible] built in tall lifts of concrete, up to 12.192 m (4[illegible]), using flying forms. The construction took place without incident.

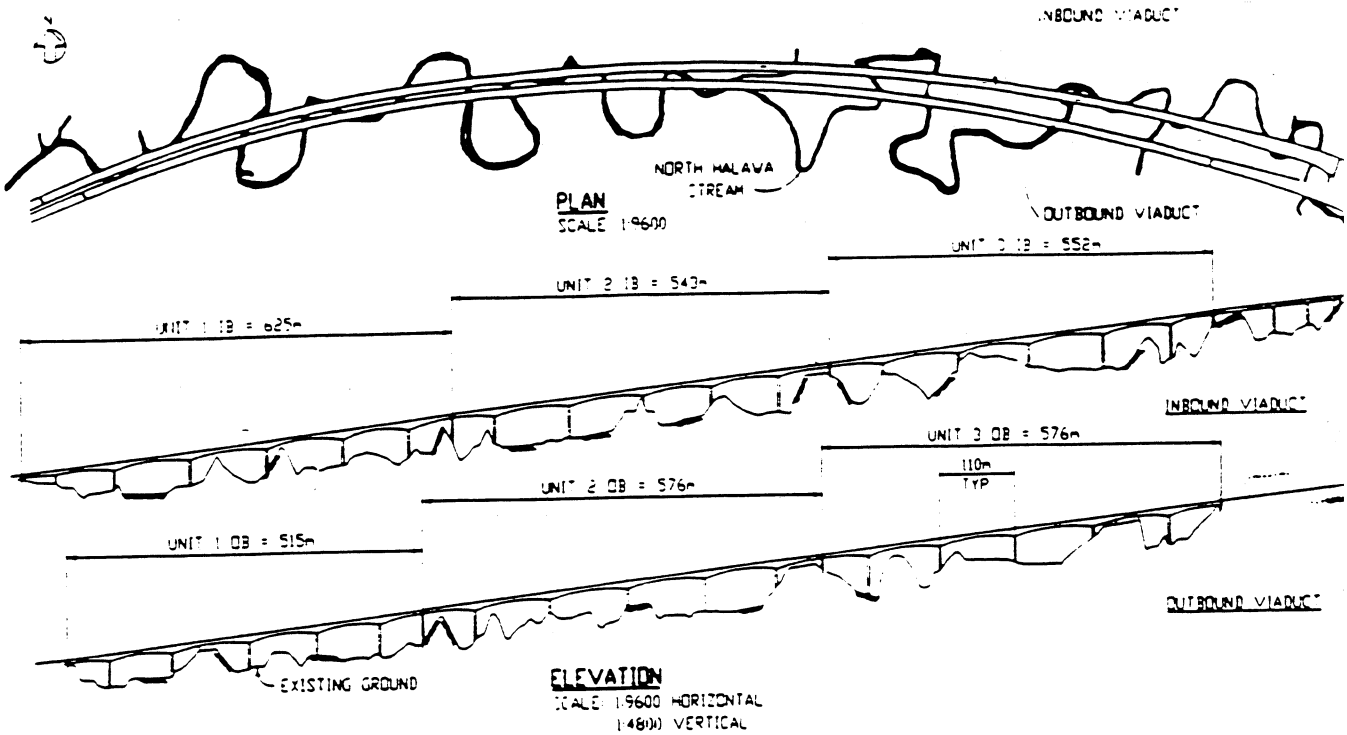

FIGURE 2 General plan and elevation of viaduct.

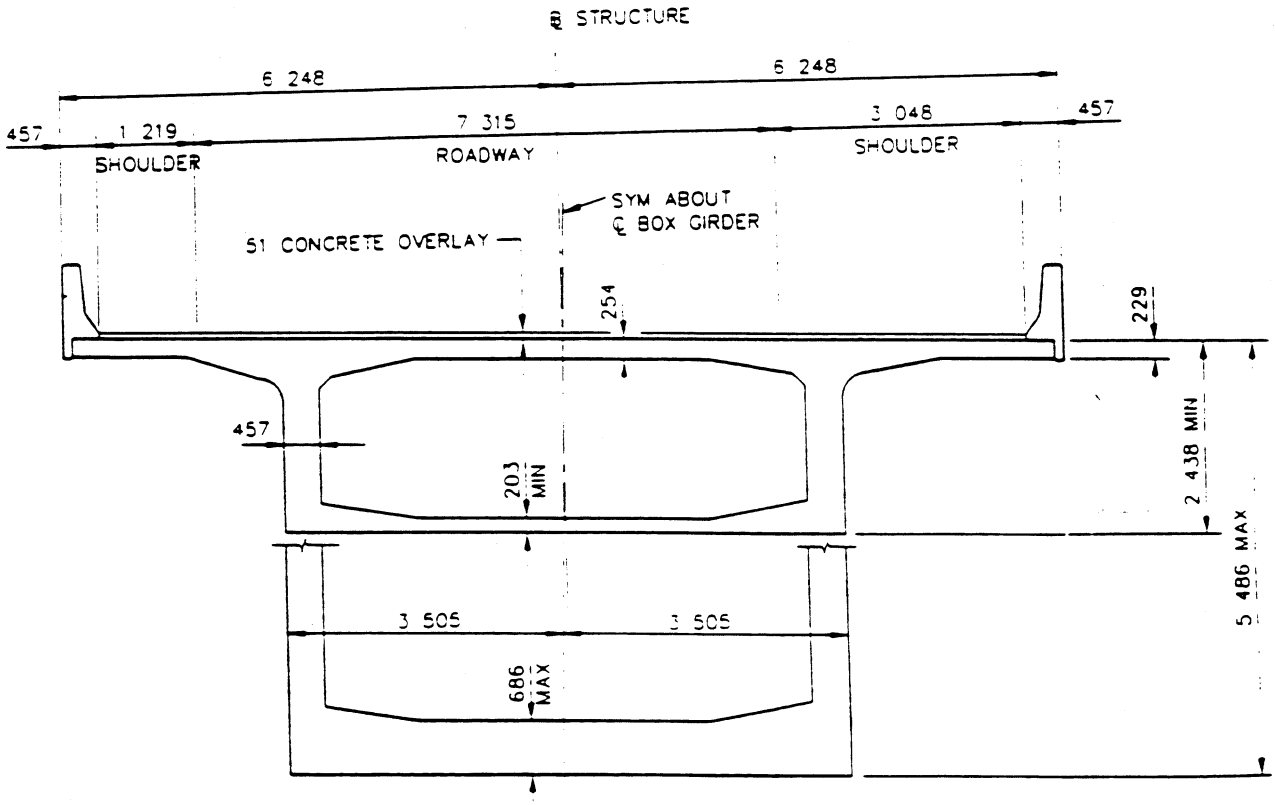

FIGURE 3 Bridge cross section.

Foundations

The soils along the bridge alignment consist of surficial layers of alluvium and colluvium underlain by thick layers of residual soils and saprolite decomposed from basalt. At depths approaching 30.480 m (100 ft), the saprolite gradually gives way to slightly weathered and unweathered basalt rock.

Both prestressed concrete pile and drilled shaft foundations were designed and fully detailed and bid as alternatives. A typical pile foundation consisted of octagonal piles 70 508 mm (20 in.) in diameter. Because at depth the ground is fairly hard, it was anticipated that these piles would be driven through predrilled holes 457 mm (18 in.) in diameter to depths ranging from 15.240 to 30.480 m (50 to 100 ft). Not surprisingly, no contractor bid the pile alternative—it probably does not make sense to predrill piles if one can just make a drilled shaft.

The successful drilled shaft alternative was only the second application of this construction method in Hawaii. A 3 × 3 pattern of drilled shafts 1.524 m (5 ft 0 in.) in diameter is typically used, with one or two shafts occasionally omitted from the pattern. The shafts vary in length from 24.384 to 36.576 m (80 to 120 ft). Further details are given later in the paper.

Three site factors complicated the foundation work. The construction of drilled shafts near the stream had to contend with large fields of boulders. These boulders were deposited over the years as the stream meandered back and forth over the valley bottom. (The boulders were another reason that drilled shafts were favored over piles.) Footings near the stream had to be constructed in cofferdams to protect them from scour, because flooding was a possibility at any time of the year. And several of the viaduct foundations fall on the ridges that intersect the valley bottom; each of these required a large excavation.

Transition Area Box Girder

In addition to the three segmentally constructed units, the inbound viaduct also has a portion 178.308 m (585 ft) long that is built on falsework. This is a conventional multicell box girder at which the viaduct widens so rapidly (to accommodate some transition lanes before the trans-Koolau tunnels) that segmental construction was considered impractical.

Bridge Types and Construction Methods Considered

Only segmental construction methods were considered when the bridge type was selected. Both precast and cast-in-place superstructures were considered, with span lengths ranging from 48.768 to 109.728 m (160 to [illegible] ft). Balanced cantilever construction, with either form travelers or erection gantries, was considered for both the precast and cast-in-place alternatives. Span-by-span construction was also considered for the cast-in-place alternative.

The precast alternatives were thought to be relatively expensive because there was no suitable location for a segment precasting yard near the bridge site. The only suitable locations were several miles away, outside of the North Halawa Valley. Unfortunately, the access road to the site was long and narrow and had to be shared with several other construction projects in the valley. The Hawaii Department of Transportation and the bridge designers favored cast-in-place construction over precast for subjective reasons: the greater durability of cast-in-place bridges and their possibly better behavior during earthquakes.

In considering only cast-in-place construction, erection from conventional form travelers was thought to be expensive because of the time-consuming assembly and disassembly of the form travelers on each pier (31 in number). Erection from an overhead gantry (as shown in Figure 4) was thought to offer several advantages with respect to erection from form travelers.

The fundamental advantage of this construction method is that, except for the pier segment, the superstructure construction is independent of the ground; all of the necessary materials, equipment, and personnel can be delivered to the point of work from overhead, along the completed structure and over the gantry. And the difficult topography of the valley and the project's environmental restrictions made it desirable to work from overhead as much as possible.

To be sure, 3564 m (11,695 ft) of viaduct is a lot of bridge. Once mobilization costs are overcome, construction with an erection gantry is inherently fast, because large segments are possible and because the launch of the gantry from one pier to another can be quick. Savings are also possible in piers and foundations because the gantry can absorb some of the unbalanced moment of the cantilever. And although the erection gantries themselves are expensive, there are offsetting savings in auxiliary equipment, which is not required to service cantilever construction at each pier, and in spur roads and lay-down areas at each pier, which are not required to service the same volume of material as for conventional construction with form travelers.

The typical span length of 109.728 m (360 ft) is thought to be about the maximum practical span length for this method of construction. The maximum span length was chosen in order to minimize the number of piers and foundations to be built in the difficult terrain. The North Halawa Valley Viaduct is the first cantilever

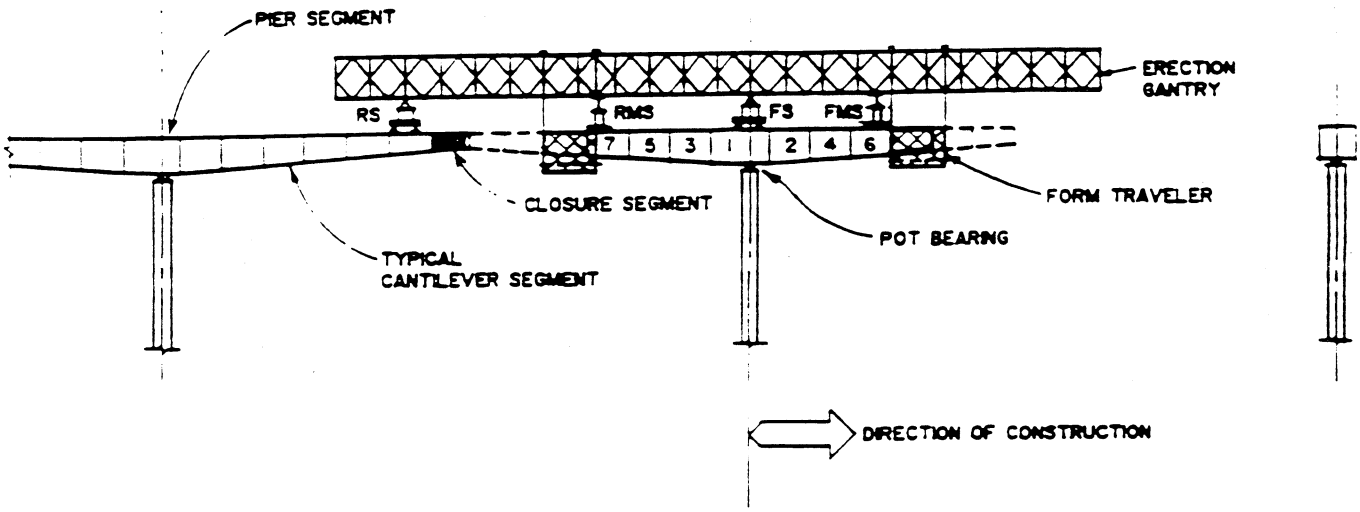

FIGURE 4 Operation of erection gantry.

segmental bridge in the United States to be cast in place from an overhead gantry. The method has been used several times in Europe, however.

Construction

After a very competitive bidding process, a contract for construction of the viaduct was awarded to the Kiewit Pacific Company on December 19, 1991, with a notice to proceed on February 21, 1992. The bid price was approximately $141 million, for the viaducts and the ancillary site work; the viaduct itself cost about $105 million. Nine hundred ninety calendar days were allowed for the construction of the viaducts and for the site work. Major subcontractors to Kiewit Pacific included the VSL Corporation, for erection gantry design and superstructure construction engineering, and the Malcolm Drilling Company, for drilled shaft construction.

Foundations

Drilling the shafts was the first construction activity on the site. They were constructed both in the dry and by tremie inside a casing near the stream. The boulder fields were found to be a significant obstacle to the drilling. In fact, the drilling subcontractor filed a successful claim against the state, charging that the boulders were larger and more densely packed than indicated by the test borings. Boulders smaller than one shaft diameter were usually removed with a choker; the subcontractor was generally able to drill through larger boulders, but some shafts were cut off when very large boulders were encountered. Aside from this problem, however, the construction of the drilled shafts was straightforward. The drilling subcontractor was able to drill about one shaft a day, on average. A total of 6781 m (22,429 ft) of shaft 1.524 m (5 ft) in diameter and 2856 m (9,370 ft) of shaft 914 mm (3 ft) in diameter were drilled and cast in just over a year.

Superstructure

Cantilever Construction

The superstructure was built by cantilever construction about each pier. Each cantilever (or pair of cantilevers) was cast in place in segments using an erection gantry, as shown in Figure 4. At each pier, the construction was started by casting a pier segment directly on top of the pier; this was actually cast in place in formwork supported on the pier shaft. In each case, the pier segment was eccentric with respect to the centerline of the pier, thus applying an unbalanced moment to the pier shaft. The eccentric length of the pier segment was equal to half of the typical segment length.

After casting the pier segment, the typical cantilever segments were cast in place in formwork supported

from the erection gantry. The segments were cast alternately to either side of the pier, starting from the side opposite the pier segment cantilever. When released from the formwork, each segment potentially applied a net unbalanced moment to the pier shaft corresponding to half of the segment length times the remainder of the cantilever length minus a quarter of the segment length.

The cantilever construction at each pier was concluded by casting a closure segment between the rear cantilever segment (relative to the direction of construction) and the tip of the previously completed cantilever. The closure segments were cast using the same formwork as for the cantilever segments (with some revisions to the support of the interior formwork).

Because the end spans in each structural unit are longer than a typical cantilever length, often 76.200 m (250 ft) versus about half the span length, or 54.864 m (180 ft), a portion of each end span was cast in place in formwork supported on the ground. These supported segments were typically 12.192 to 18.288 m (40 to 60 ft) long.

Contractor Modifications

Although segmental construction using an erection gantry was anticipated in the design of the viaducts and shown on the contract plans, the actual construction involved two important modifications to the original design. Each of these modifications was made to increase the rate of construction, relative to the conservative assumptions made by the designers of the bridge. One modification made by the contractor was to increase the segment length from the 6.401-m (21-ft) length assumed in the original design to 7.315 m (24 ft). (The original design would have allowed construction with conventional form travelers.) Another modification was to increase the rate of casting of segments from an assumed 5-day cycle (in effect a weekly cycle without working on the weekends) to a 4-day cycle.

Taken together these modifications allowed the contractor to build the bridge with three erection gantries rather than the four shown on the contract plans. One gantry was used on each of the inbound and outbound viaducts, moving uphill from the abutments to construct Units 1 and 2. The third gantry (actually the first to be launched since it was on the critical path) was used to construct Unit 3 of both viaducts; it started on the outbound viaduct, moving downhill from the abutment toward one of the other gantries. When Unit 3 of the outbound viaduct had been completed, this gantry was pushed back up the completed structure and then sideways onto the transition area box girder. It was then launched downhill again, to build Unit 3 of the inbound viaduct.

The posttensioning layout was also revised by the contractor to accommodate the revised segment length; the overall posttensioning scheme was maintained, however. The changes to the segment and posttensioning layouts, and particularly the increased rate of construction of the bridge, made it necessary for the contractor and the designer to reanalyze the bridge, because the creep and shrinkage of concrete renders the behavior of the bridge time-dependent.

Casting Cycle

As mentioned previously, a 4-day cycle was used for casting cantilever segments (indeed, occasionally the contractor was able to build a segment in 3 days). The daily operations in the typical cycle were as follows:

- Day 1: Install the reinforcing and posttensioning in the bottom slab of the cross section.
- Day 2: Install the reinforcing and posttensioning in the webs and the top slab, adjust the forms, and perform a button-up survey.
- Day 3: Perform a prepour survey and cast the segment.
- Day 4: Stress the posttensioning tendons anchored in the segment, break down and move the forms forward, and perform an as-built survey.

The superstructure concrete mix designed by the contractor was an important factor in the success of the 4-day cycle. A strength of 24 MPa (3,500 psi) (70 percent of the design concrete strength) was required for posttensioning of the structure. The mix used had a high cement content, low ratio of water to cement, and superplasticizers. In the insulated forms used, the required strength routinely was reached at about 18 hr after casting. [The 28-day strength of the mix is about 48 MPa (7,000 psi).] Frequently, when the required strength for full posttensioning was not achieved on schedule, partial posttensioning at 17 MPa (2,500 psi) strength was used to allow the forms to be moved forward.

Creep and Shrinkage Testing

As required by the specifications, the contractor performed creep and shrinkage testing of his proposed superstructure concrete mix, both to prove the suitability of the mix for construction and to confirm the characteristics used in the design. Although the creep and shrinkage properties of Hawaiian concrete were researched by the designers of the bridge, such tests are always necessary because of the high variability of concrete as a material.

The original research suggested that the shrinkage of Hawaiian concrete (in general) was much larger than

predicted by the CEB-FIP model of the creep and shrinkage of concrete (commonly used for bridge design). The designers assumed the shrinkage of concrete to be 2½ times that predicted by the model, and this factor was confirmed by the shrinkage testing. (Hawaiian aggregates are of volcanic origin, which is not common elsewhere.) The original research did not reveal any systematic difference between the creep of Hawaiian concrete (considering materials from several sources) and that predicted by the CEB-FIP model, but this particular assumption was not confirmed by the testing, which showed the mix proposed by the contractor to have about 25 percent higher creep than predicted. Consequently, the reanalysis of the bridge, made necessary by the contractor's increased rate of construction, used this higher creep coefficient. From the testing, the ultimate shrinkage strain of the superstructure concrete mix was taken to be 0.000449 and the ultimate creep coefficient was taken to be 2.47, for 28-day loading.

Increased Continuity Posttensioning

The increased rate of construction of the bridge and the higher creep coefficient both led to a small increase in the amount of continuity posttensioning needed in the bridge. The so-called continuity tendons are draped tendons in the webs in each span. They are an important factor in eliminating tension in the bottom fibers of the bridge at midspan; the design criteria did not allow any tensile stress in the structure under combinations of live load and temperature gradient. The aforementioned factors both cause tensile stress at midspan. The additional continuity posttensioning needed to compensate for this stress took the form of additional strands placed in the existing ducts; no additional tendons were required. The contractor was compensated for the additional posttensioning required to offset the higher creep coefficient but not for that required to offset the increased rate of construction, since that was his choice relative to the contract plans.

Gantry Design and Operations

The erection gantries, illustrated in Figure 4, were designed and built by the contractor. Each gantry had a crane rail and two cranes of 5.9-ton (13-kip) capacity running along its soffit. The cranes were used to deliver reinforcing bars and other materials to the point of work. Each gantry also had a 480V power line running along its soffit to power equipment at the point of work. Each gantry was 140 m (450 ft) long, weighed about 613 tons (1,350 kips), and cost about $2.5 million, including the form travelers and auxiliary equipment.

As can be seen in Figure 4, the form travelers were suspended from the gantry rather than from "horses" supported on the cantilever, as in conventional cantilever construction. The form travelers themselves were fairly conventional (except in one respect to be discussed later). During cantilever construction, each gantry was balanced on a front main support (FS) on the forward pier (in the direction of construction) and a rear main support (RS) on the tip of the previously completed cantilever. The sequence of casting concrete, stressing tendons, and moving the form travelers was the same as for conventional cantilever construction.

An important feature of the gantry operation was the use of struts between each gantry and the viaduct—the front mobile support (FMS) and rear mobile support (RMS) shown in Figure 4. These were jacks placed immediately behind the form travelers to support the gantry on the bridge deck. They took advantage of the inherent strength and stiffness of the structure to help the gantry carry the load of freshly cast segments. They were moved with the form travelers so as to be always just behind the segment being cast.

Also, at expansion piers, where the superstructure is supported on pot bearings, the struts were used to balance the cantilever on top of the pier. One strut, at least, was always maintained in compression between the gantry and the structure to react the weight of the unbalanced segment on the opposite side of the cantilever. Form travelers and struts being moved to the next segment were always on the heavy side of the cantilever (where a segment had just been cast), so that the strut on the opposite side was compressed naturally by the unbalanced moment. When the form travelers were stationary, both struts were maintained in compression. This scheme enabled the contractor to avoid a complicated moment restraint to stabilize the cantilever against the pier shaft.

Geometrical Control

Because struts were used to share loads between the gantry and the structure, they formed a system that had to be analyzed to determine its behavior under load. This use made the geometrical control of the structure more complicated than it is for conventional cantilever construction. But using the gantries to stabilize the cantilevers at expansion piers (by using the struts just described) allowed those cantilevers to be "rocked" in order to compensate for geometrical errors, in effect providing an additional variable for solving geometrical control problems.

In accordance with the specifications, the contractor wrote a geometry control plan that subsequently was reviewed by the designer. The goal of the plan was to compensate for the deflection and movement of the

bridge during construction (due to the method of construction and construction operations) and for the creep and shrinkage of the bridge after construction (up to 20 years). In accordance with the geometry control plan, the bridge was cast to a cambered "control line" so that it would eventually deflect into the required vertical alignment. The plan also contained provisions to compensate for errors in construction (differences from the control line) of more than 25.4 mm (1 in.).

The successful geometrical control of the structure was due to a cooperative effort between the contractor and the designer. Both the contractor and the state of Hawaii maintained a team of bridge surveyors in the field, who independently monitored the position of the bridge at each stage of construction as well as the loads in the gantry front and rear mobile supports (struts). Both the contractor's engineer and the designers ran detailed computer simulations of the construction of the bridge, using the measured mobile support loads at each step. These simulations were compared with each other and with the measured geometry of the bridge before and after the casting of each segment. For each segment, the contractor and the designer agreed to a preset elevation of the segment to meet the control line.

A difficult part of the geometrical control of the bridge was compensating for the deflection of the tip of the previous cantilever, because of creep of the bridge under the gantry rear main support reaction. This deflection was as much as 50 mm (1.97 in.) because of the large lever arm of the reaction. Any deviations from the planned construction schedule led to relatively large deviations from the control line as well.

Closure Segments

Another interesting challenge was the geometrical control of the closure segments between the cantilever under construction and the previous cantilever. The closure segments were usually 7.315 m (24 ft) long, and occasionally 8.534 m (28 ft) long. It was found necessary to place struts on both sides of the closure segments in order to minimize the relative displacements between the tips of the cantilevers during casting. Even with struts on both sides of the closure segments, small relative displacements required compensation by an opposing camber.

Gantry Launching

Subsequent to the closure of each cantilever to the tip of the previous cantilever, the gantry was launched to the next pier, carrying the form travelers with it. The form traveler bottom platforms could split open so that they could pass around the piers.

Each gantry was launched by hydraulic rams mounted on the rear main support. The rams w[illegible] either push the gantry uphill or lower it downhill, according to its overall direction of motion. Each gantry was held in position by toothed grippers acting between its bottom flange and the rear main support while the rams were recycled. These grippers were used to hold the gantry firmly in position during cantilever construction also.

The launching of a gantry was a complicated operation requiring many steps. Three basic operations were involved. The most basic of these was moving the gantry forward over the front and rear main supports by pushing against the rear main support. The gantries moved over Hilman rollers on the main supports. Another basic operation was the temporary support of each gantry on either the front or the rear mobile support (strut), which relieved the load of the gantry on the corresponding main support and allowed that support to be moved. The third basic operation was moving the form travelers to reposition the center of gravity of the gantry/form traveler system to change the reactions on the gantry supports.

At each pier, a sequence of these operations was planned to simultaneously maintain the equilibrium of the gantry and avoid any overstress of the structure. The launch sequence was summarized by the contrac[illegible] in a launch manual that was carefully reviewed by the designer.

Perhaps the most critical step in the launch procedure was the relocation of the front main support to the next pier for cantilever construction. This relocation was accomplished by launching the gantry tip as far the next pier, in steps as described earlier. The front main support was then moved to the next pier while the gantry tip was supported temporarily on that pier by the front mobile support. Similarly, the rear main support was relocated to the tip of the just-completed cantilever; it was then posttensioned to the bridge to carry uplift forces.

The typical launch of a gantry involved about 100 steps. Despite this evident complexity, the typical launch took only $2^1/_2$ days once the contractor gained experience. This speed was possible because each of the steps was simple and the operations of the gantry were highly automated.

INSTRUMENTATION

An unusual aspect of the project is the instrumentation of one of the structural units, specifically, Unit 2 of t[illegible] inbound viaduct (the last unit to be completed). T[illegible] instrumentation program will gather data on the behavior of the structure for comparison with the design

assumptions and the predicted behavior. The instrumentation program was a joint effort between T.Y. Lin International; the Construction Technologies Laboratory, Chicago, Illinois; and the University of Hawaii, Manoa. It will continue for 5 years after the completion of the bridge. The measurements include:

1. The forces in six posttensioning tendons will be measured by load cells placed behind the anchor heads.
2. At instrumented sections of the bridge, the strains in the concrete will be measured by cast-in-situ vibrating wire strain gauges and mechanical extensometers. There are four instrumented sections: two at midspan locations and two near piers.
3. At instrumented sections, the strains in some of the reinforcing bars will be measured by resistance strain gauges, adjacent to the concrete strain gauges.
4. At instrumented sections, the average temperature of the concrete and the temperature gradients over the depths of the section and the top slab will be measured by thermocouples placed around the perimeter of the box.
5. The vertical deflections of the bridge will be measured by reference to a high-strength piano wire stretched over the length of the unit and supported inside the cross section at the piers.
6. The rotations of the bridge over the piers will be measured by tiltmeters.
7. The horizontal displacements of the bridge will be measured at the joints by linear variable differential transformers spanning between the soffit of the box and the tops of the piers.
8. Any lateral displacements of the bridge will be surveyed from the ground.
9. The creep and shrinkage properties of the concrete used in the instrumented sections will be determined by testing under laboratory and site conditions.

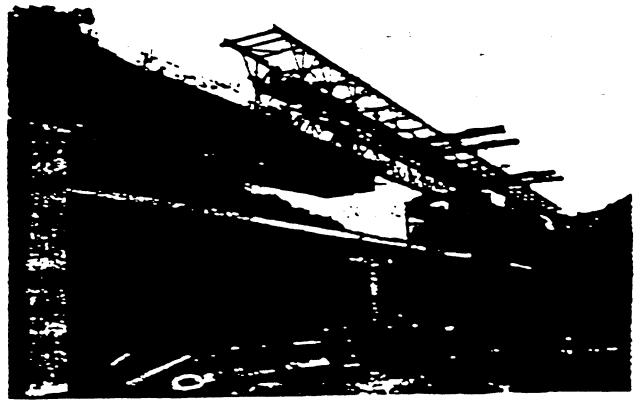

FIGURE 5 Partly completed structure.

Hopefully, comparison of the collected data with the design assumptions and the predicted behavior of the bridge will lead to an improved understanding of long-span posttensioned bridges in general, as well as to improved design methodologies.

Conclusions

Figure 5 shows a photograph of the two viaducts, one of them completed and one of them with an erection gantry in place. When this paper was written, the construction of the superstructure had been completed. Only the deck overlay and expansion joints and some site work remained to be completed. A total of 445 superstructure segments were cast in place in just over 2 years. The successful use of the overhead gantries shows the viability of this construction method where conditions make other methods unsuitable.

CHAPTER 3

FIELD INSTRUMENTATION

3.1 Introduction

This chapter describes the various types of instrumentation used in this project. More detailed information is presented in the report "Instrumentation of the H3 Halawa Valley Viaduct", by Lee and Robertson (1995).

All of the instrumentation was placed in Unit 2 of the inbound Viaduct (traffic flow toward Pearl Harbor). Seven sections were selected for instrumentation in order to provide an adequate representation of the Viaduct behavior. These sections, titled A through G are shown in Figure 3.1. The number of instruments installed at each section is shown in Table 3.1. Sections A, D, E, and G are at, or close to, midspan (termed *midspan sections*) while B, C, and F are close to the ends of the *instrumented spans* (termed *support sections*).

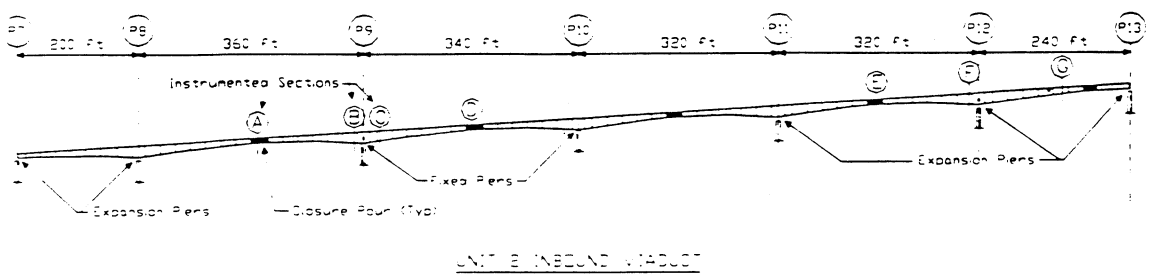

Figure 3.1: Location of Instrumented Sections.

Table 3.1: Instruments at each Section.

INSTR. SECTION	VIBRATING WIRE STRAIN GAGES	ELECTRICAL RESISTANCE STRAIN GAGES	DEMEC STRAIN GAGES	LOAD CELLS	THERMO-COUPLES	EXTENSO-METERS	TILT-METERS	BASE-LINE SYSTEMS	RELATIVE HUMIDITY METERS	DATA CHANNELS REQUIRED
A	8	0	8	2	0	1	1 (P8)	1	0	12
B	10	0	10	0	0	0	1 (P9)	0	2	23 (B & C)
C	10	0	10	0	0	0	0	0	0	-
D	8	0	8	2	0	1	1 (P10)	1	0	12
E	8	31	8	1	32	1	1 (P11)	1	0	74
F	10	32	10	0	32	0	1 (P12)	0	0	75
G	8	0	8	1	0	1	1 (P13)	1	0	11
TOTAL	62	63	62	6	64	4	6	4	2	207

All intrumentation was installed by personnel from the University of Hawaii (UH), Construction Technology Laboratories (CTL), and VSL Corporation as presented in Table 3.2.

Table 3.2: Instrument Installation

INSTR. SECTION	V. W. STRAIN GAGES	E. R. STRAIN GAGES	DEMEC STRAIN GAGES	LOAD CELLS	THERMO-COUPLES	EXTENSO-METERS	TILT-METERS	BASE-LINE SYSTEMS	RELATIVE HUMIDITY METERS	DATA-LOGGER SYSTEMS	CREEP AND SHRINKAGE TESTS
A	UH/CTL		UH	VSL/UH			UH	UH		UH	CTL*
B	UH/CTL		UH			UH	UH		UH	UH	CTL*
C	UH/CTL		UH							UH	CTL*
D	UH		UH	VSL/UH			UH	UH		UH	CTL*
E	UH/CTL	UH/CTL	UH	VSL/UH	UH/CTL		UH	UH		UH/CTL	UH/CTL*
F	UH/CTL	UH/CTL	UH		UH/CTL	UH	UH			UH/CTL	UH/CTL*
G	UH		UH	VSL/UH			UH	UH		UH	UH/CTL*

* - Creep and shrinkage tests performed in laboratory by CTL and on site by UH.

3.2 Concrete Strain Measurements

3.2.1 Vibrating Wire Strain Gages

3.2.1.1 Description

Vibrating Wire (VW) Strain Gages are designed for direct embedment in the concrete at the critical sections. Geokon model VCE-4200 gages were selected for this project (Fig. 3.2). Actual dimensions are shown in Figure 3.3. The vibrating wire strain gages have excellent long-term zero stability and automatic monitoring of both compressive and tensile concrete strains. The advantage of the vibrating wire strain gages over more conventional electrical resistance gages lies mainly in the use of a frequency measurement, rather than a resistance, as the output signal from the gage. Changes in lead wire length and resistance at lead connections do not affect the frequency of the vibrating wire, and therefore do not impact the reading.

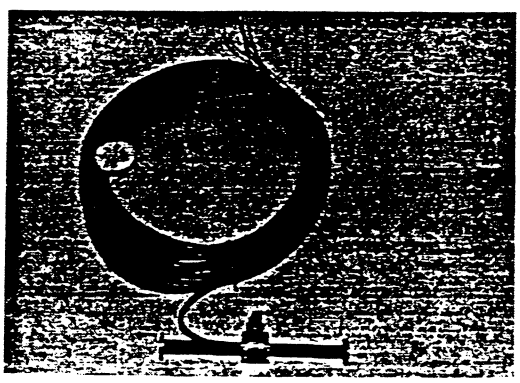

Figure 3.2: Vibrating Wire Strain Gage.

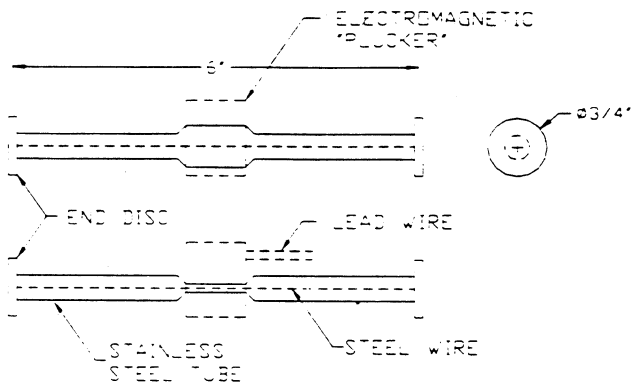

Figure 3.3: VW Gage Dimensions.

3.2.1.2 Layout and Installation

Vibrating wire strain gages were installed at all seven instrumented sections. All gages were oriented along the length of the viaduct. Typical locations at midspan sections and support sections are shown in Figures 3.4 and 3.5 respectively. Midspan sections A, D, E, and G have 8 vibrating wire gages each as shown in Figure 3.4. Support sections have 10 vibrating wire strain gages each as shown in Figure 3.5. The as-built locations of the Vibrating Wire gages at all sections are recorded in Lee and Robertson (1995).

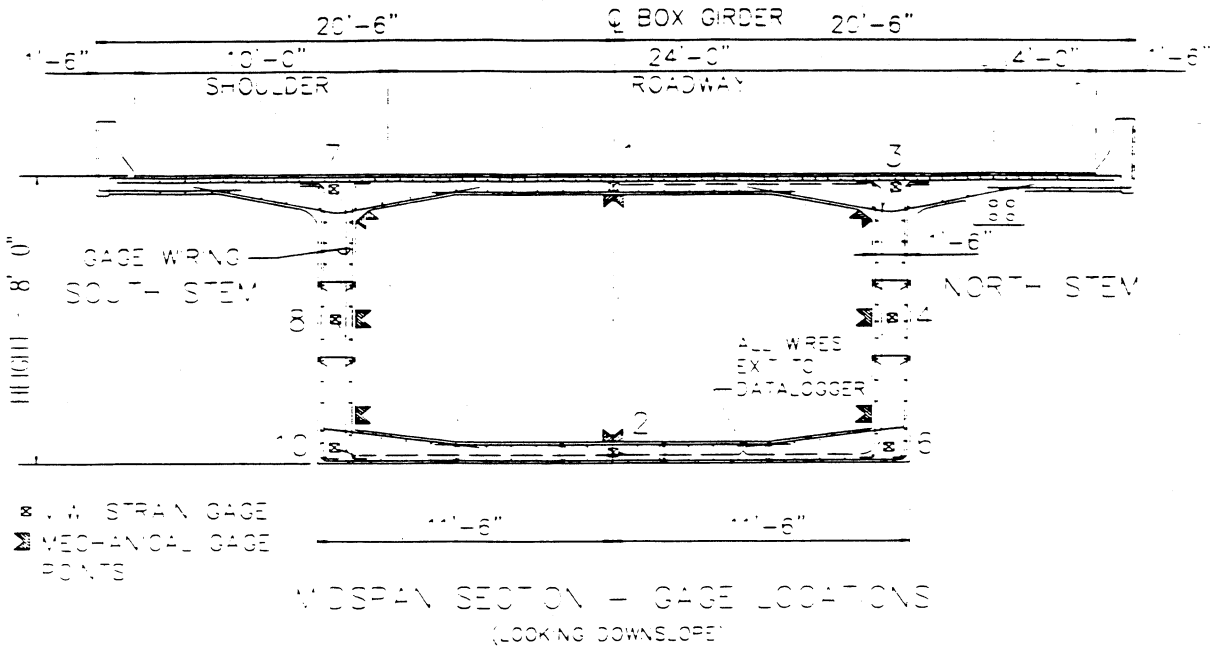

Figure 3.4: Vibrating Wire Strain Gages and Demec Points at Midspan Section.

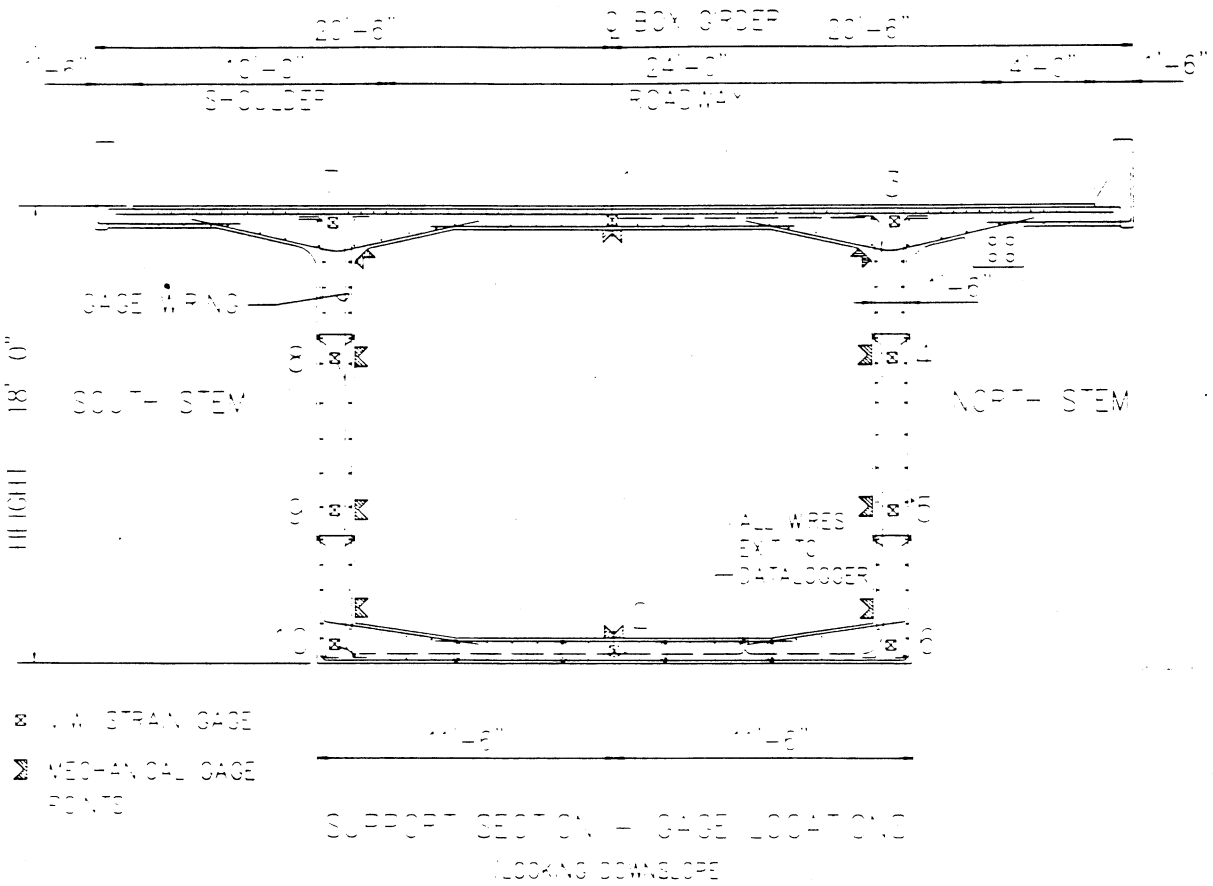

Figure 3.5: Vibrating Wire Gages and Demec Points at Support Section.

During installation of the vibrating wire strain gages, it was important to maintain proper orientation and location of the gages while pouring concrete. A bracket was designed and fabricated to support each gage and assure proper orientation after concrete placement (Figures 3.6 and 3.7). The bracket must withstand impacts from falling concrete during pouring and have no influence on the gage readings. The bracket consists of a 1 inch square standard steel tube and a light gauge sheet-metal holder.

The brackets were installed during placement of the steel reinforcement. They were designed so that the vibrating wire strain gage could be added immediately prior to closing the stem formwork or pouring concrete, so as to reduce the potential for damage to the gage (Figure 3.6, Detail C).

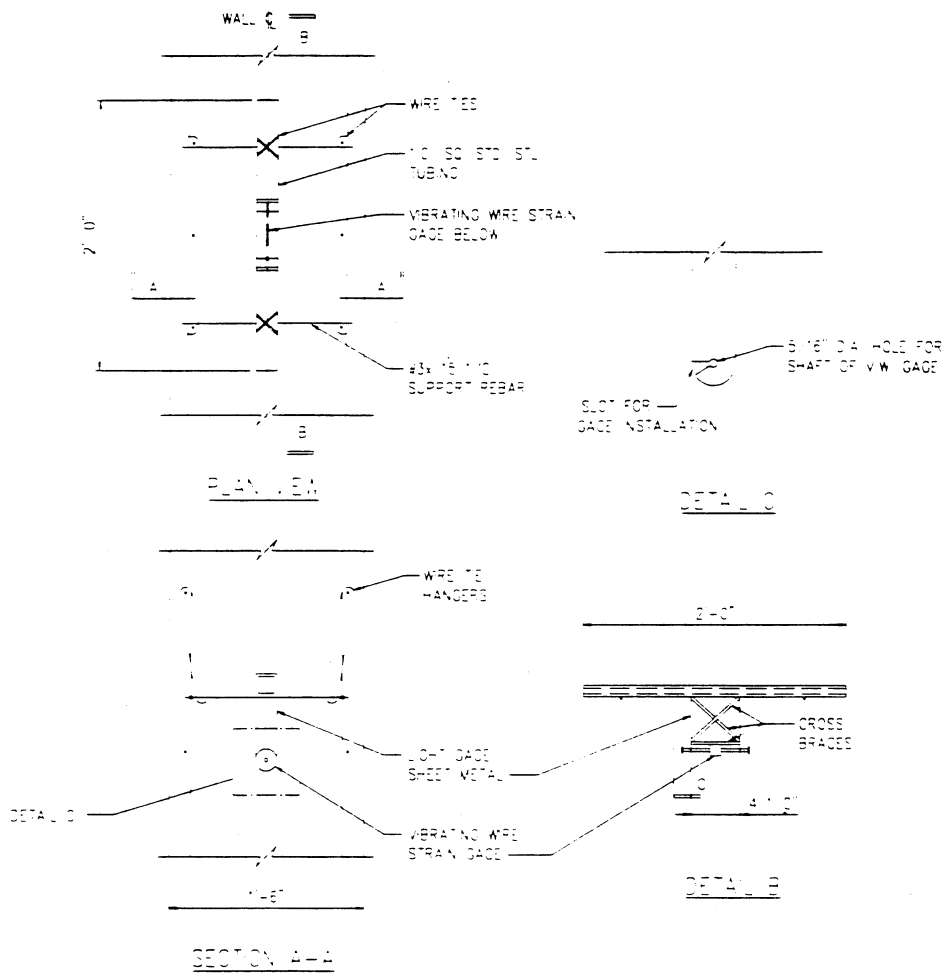

Figure 3.6: Vibrating Wire Gage Support Bracket in Box Girder Stem

Figure 3.7 shows a typical stem gage support. In top and bottom slabs, reinforcement support chairs were used to support the vibrating wire strain gage as shown in Figure 3.8.

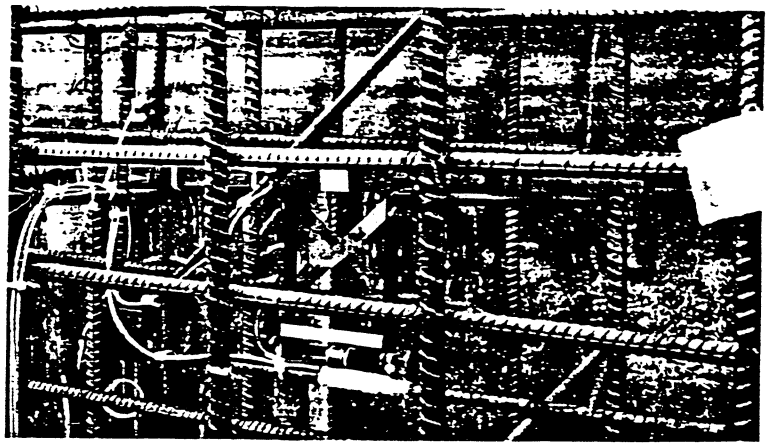

Figure 3.7: Instrumentation in Stem.

A spirit level and tape measure were used to ensure proper location, orientation, and alignment of the gages. All vibrating wire strain gages were oriented in the viaduct longitudinal direction. Gages in the top slab and stems were sloped parallel with the top slab, while those in the bottom slab were oriented parallel with the bottom slab.

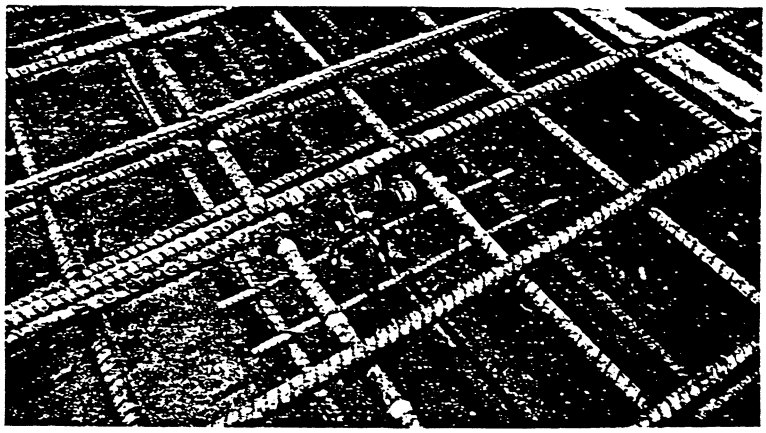

Figure 3.8: V.W. Gage in Top Slab.

3.2.1.3 Data Collection

Strain in the concrete is computed from the difference between the initial and subsequent readings, R_o and R_t respectively. When the concrete is subjected to compression, the readings will decrease such that R_t is less than R_o. In tension, the readings will increase such that R_t is greater than R_o. These readings must be adjusted for changes in the temperature at the gage location, since the wire used in the gage has a different coefficient of thermal expansion than the surrounding concrete. A complete discussion of the vibrating wire gage data reduction is presented in "Report on Vibrating Wire Strain Gage Instrumentation" (Robertson, 1995).

3.2.2 Electrical Resistance Strain Gages

3.2.2.1 Description

The electrical resistance strain gages used in this project are Micro Measurements CEA-06-250UW-120 gages. These gages consist of a polymide-encapsulated constantan foil grid with large copper-coated tabs. The gages were bonded to the center of Number 4 deformed bar coupons (1/2 in. diameter by 2.0 feet long) in the laboratory using M10/15 adhesive following the manufacturer's instructions. Prior to bonding, the contact surface of the reinforcing bar was sanded and polished using 300 grit abrasive paper in accordance with the gage manufacturer's recommendation.

Each gage was supplied with lead wires and fully encapsulated in a water-proof coating. The gages were then covered with a layer of wax and shrink-wrap tubing prior to placement in the formwork to fully protect them from water seepage and abrasion damage during pouring of the concrete. Gage preparation is described in detail in Lee and Robertson, 1995.

At certain locations, three instrumented coupons were assembled to form a 45 degree strain rosette as shown in Figures 3.7 and 3.9. The rosettes will be used to determine principal stresses in the top slab and stems of the box girder.

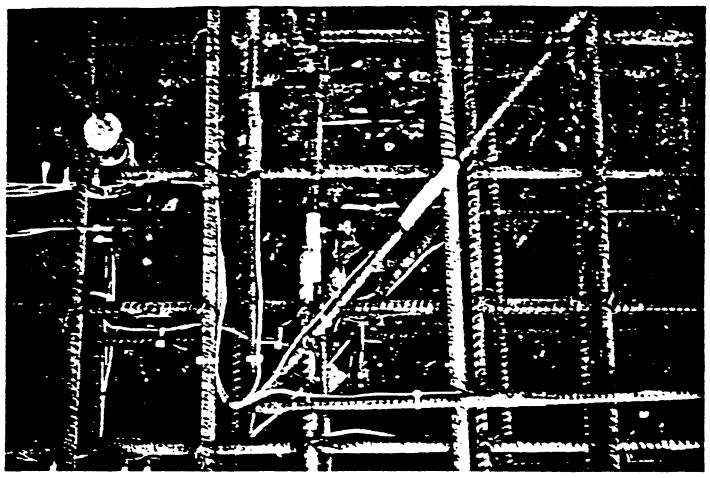

Figure 3.9: Instruments in top slab.

3.2.2.2 Layout and Installation

Two sections were selected for extensive instrumentation with electrical resistance strain gages. Midspan section E contains ten longitudinal gages and six 45 degree gage rosettes as shown in Figure 3.10. Support section F contains eleven longitudinal gages and six 45 degree gage rosettes as shown in Figure 3.11.

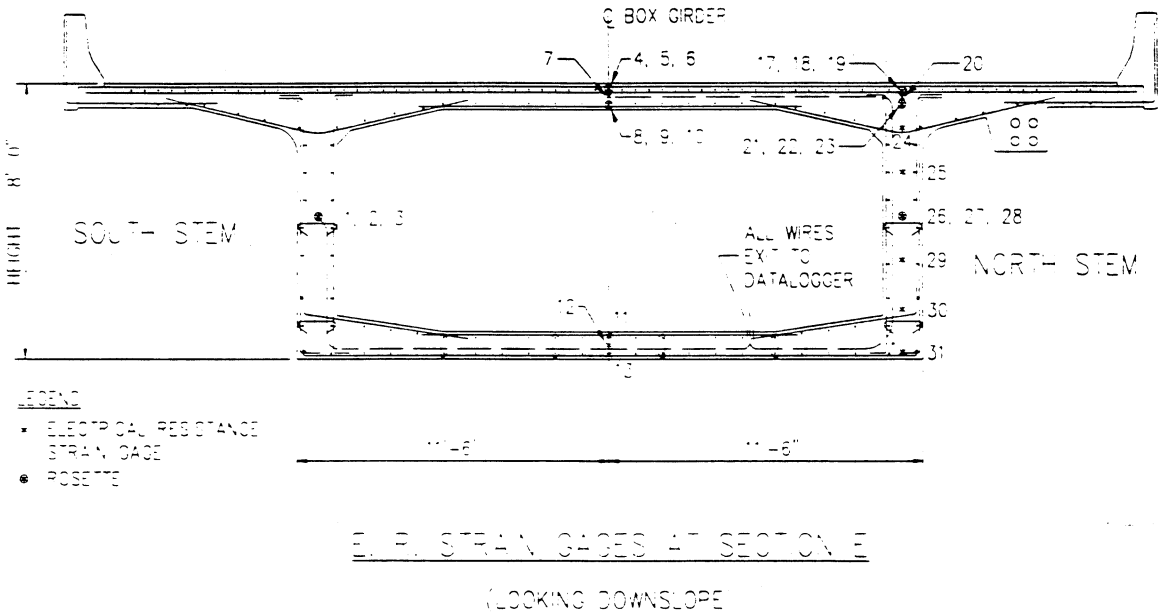

Figure 3.10: Electrical Resistance Strain Gages at Section E.

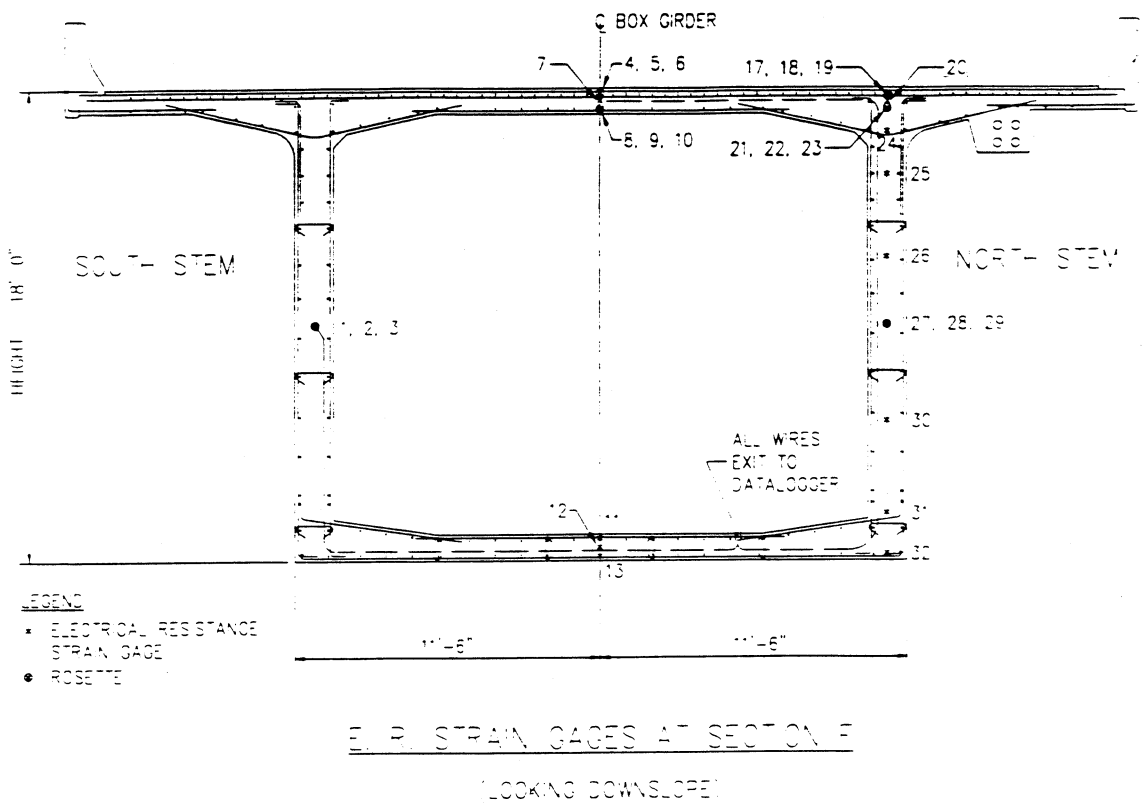

Figure 3.11: Electrical Resistance Strain Gages at Section F.

3.2.2.3 Data Collection

Immediately after casting the segment, a full set of manual readings was recorded. Each gage was calibrated to adjust for the resistance of the lead wires. The modified gage factors will be used for subsequent data reduction. Information on the gage factors and data reduction is presented in Lee and Robertson, 1995. The lead wires were then connected to the datalogger for automated data collection.

3.2.3 Mechanical Strain Measurements

3.2.3.1 Description

In order to verify the long-term stability of the vibrating wire strain gages, mechanical strain gage points were installed inside the box girder. A precision extensometer (Figure 3.12) is a mechanical device which measures the relative movement of locating points permanently attached to the concrete surface. A gage length of 8 inches was used at each monitoring location.

3.2.3.2 Layout and Installation

Mechanical gage points were installed inside the box girder on the concrete surface, as close as possible to the location of the vibrating wire gages inside the concrete. As with the VW gages, the mechanical gage points were oriented along the length of the viaduct. Figures 3.4 and 3.5 show the location of the gage points at typical instrumented sections.

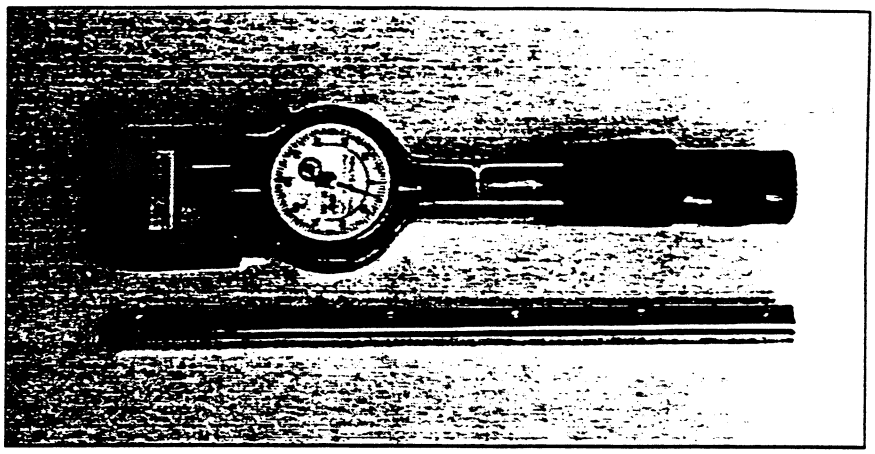

Figure 3.12: Mechanical Strain Gage.

Hilti hit anchors were used as locating points. Each anchor consists of a receptacle and a nail insert. To ensure correct placement, a drilling guide was used to drill holes in the concrete at a gage length of 8 inches. A conical hole was machined into the head of the hit anchor as the extensometer locating point.

3.3 Tendon Prestress - Load Cells

3.3.1 Description

The load cells used to measure the tendon forces were custom designed and manufactured by Construction Technology Laboratories. They are cylindrical load cells with a 700 kip compressive capacity. The load cells were placed directly below the stressing anchor block prior to stressing of the tendons as shown in Figure 3.13.

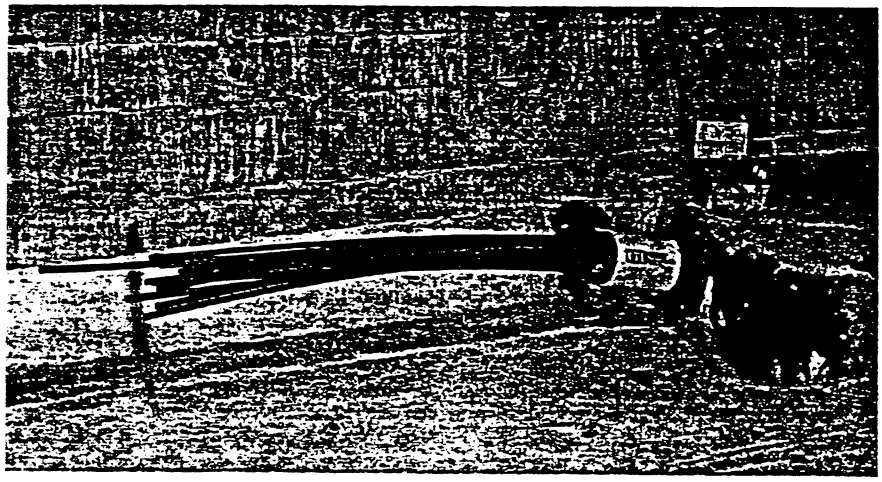

Figure 3.13: Prestress Tendon Load Cell

3.3.2 Layout and Installation

Six span tendons were fitted with load cells. At each of the long span conditions from piers P8 to P9 and P9 to P10, two span tendons were fitted with load cells, one in each stem as shown in Figure 3.14. One of these tendons was a long tendon while the other was a short tendon. The remaining two load cells were installed on span tendons in the spans from pier P11 to P12 and P12 to P13 as shown in Figure 3.15.

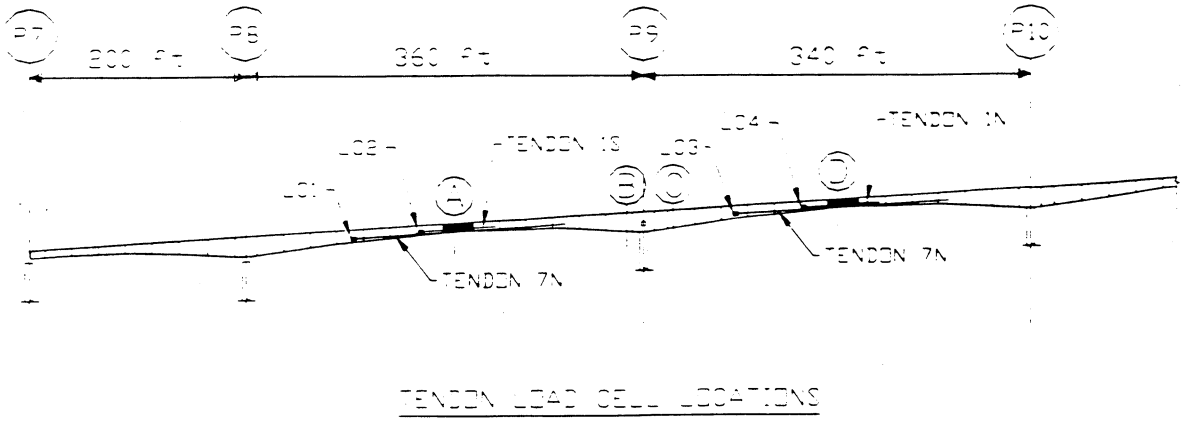

Figure 3.14: Tendon Load Cell Locations - Spans P8 to P10

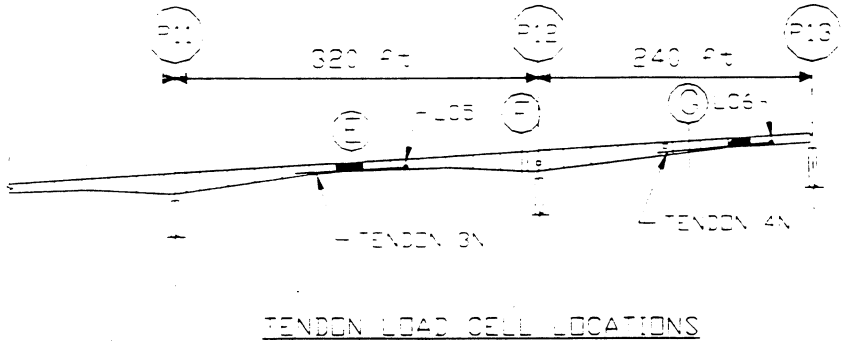

Figure 3.15: Tendon Load Cell Locations - Spans P11 to P13

Stressing of the tendons was conducted by VSL Corporation employees. The stressing was monitored at all times by University of Hawaii and T. Y. Lin International personnel. Unexpected load cell readings during stressing of the tendons prompted an investigation of the CTL load cells, and the load cell used to calibrate the prestressing pump and ram used in the stressing operation. The results of this investigation will be presented in a separate report by T.Y. Lin International and Henry Russell of CTL.

The tendons monitored by load cells were left ungrouted. They are being protected from corrosion by means of Dichan 100, a powder corrosion inhibitor. Each load cell was calibrated at CTL laboratories prior to shipping to site. During tendon stressing, the load cell readings were recorded using a manual readout box. Subsequently, the load cell lead wires were connected to the nearest datalogger with available data channels for automated reading.

3.4 Temperature and Humidity

3.4.1 Ambient Temperature and Relative Humidity

Two electronic relative humidity meters were installed at Pier P9. Each meter records the relative humidity and ambient temperature. One meter was located inside the box girder adjacent to Datalogger B. The other meter monitors the humidity and temperature outside of the box girder. It is attached to the side of Pier P9, about 3 feet below the bottom of the box girder. It is permanently in the shadow of the box girder, and is protected from direct rainfall. Both meters are connected to Datalogger B for continuous monitoring of both relative humidity and ambient temperature.

3.4.2 Concrete Temperature

3.4.2.1 Thermistors

Each vibrating wire strain gage is equipped with a thermistor to monitor temperature of the concrete at the gage location. This temperature measurement is required for thermal adjustment of the strain gage readings. Thermistors are also located in each of the datalogger enclosures to monitor the ambient temperature at the datalogger.

3.4.2.2 Thermocouples

3.4.2.2.1 Description

Thermocouples used in the instrumentation were made using Teflon/Neoflon FEP insulated copper/constantan type-T wire obtained from Omega Measurements. To assist in maintaining the correct location for the thermocouples during pouring, thermocouple "trees" were fabricated in the laboratory. A typical "tree" consists of a length of 1/2 inch diameter PVC pipe with predetermined holes drilled along the length of the pipe. A thermocouple was then inserted into each hole and set in position with a drop of epoxy. This allowed easy installation and exact location of the thermocouples as shown in Figure 3.16. The "trees" ensured correct placement throughout the duration of the concrete pour.

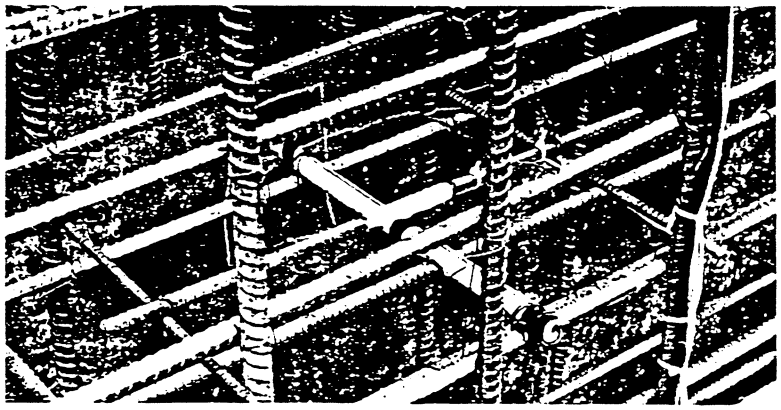

Figure 3.16: Thermocouple tree through stem.

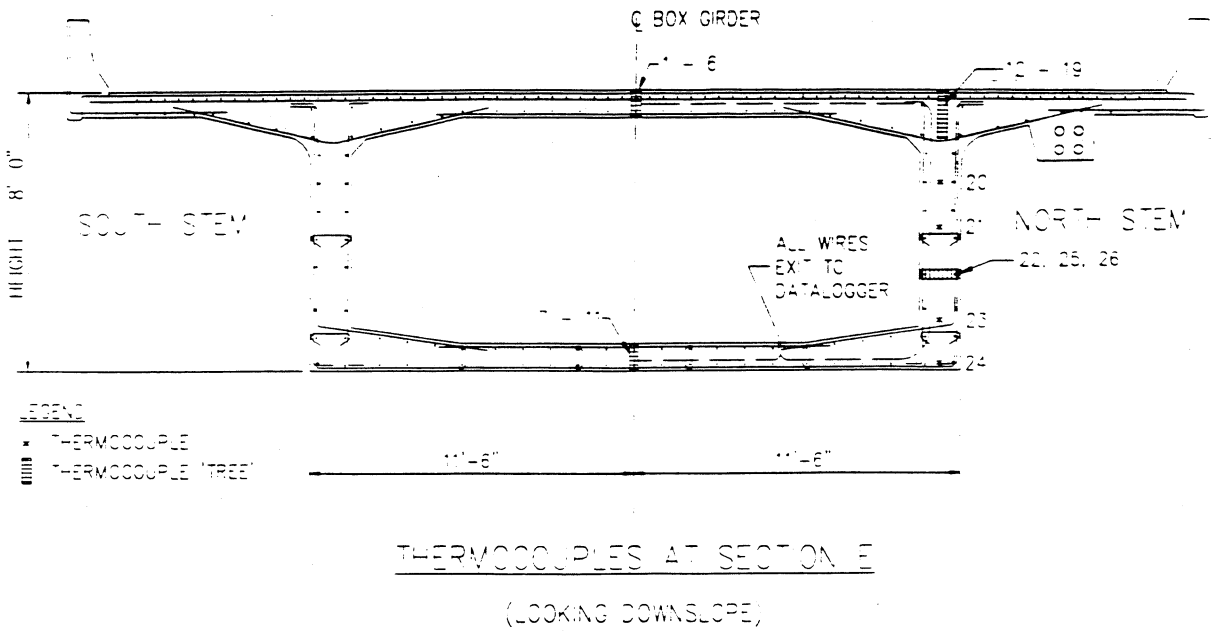

Figure 3.17: Thermocouple locations at section E.

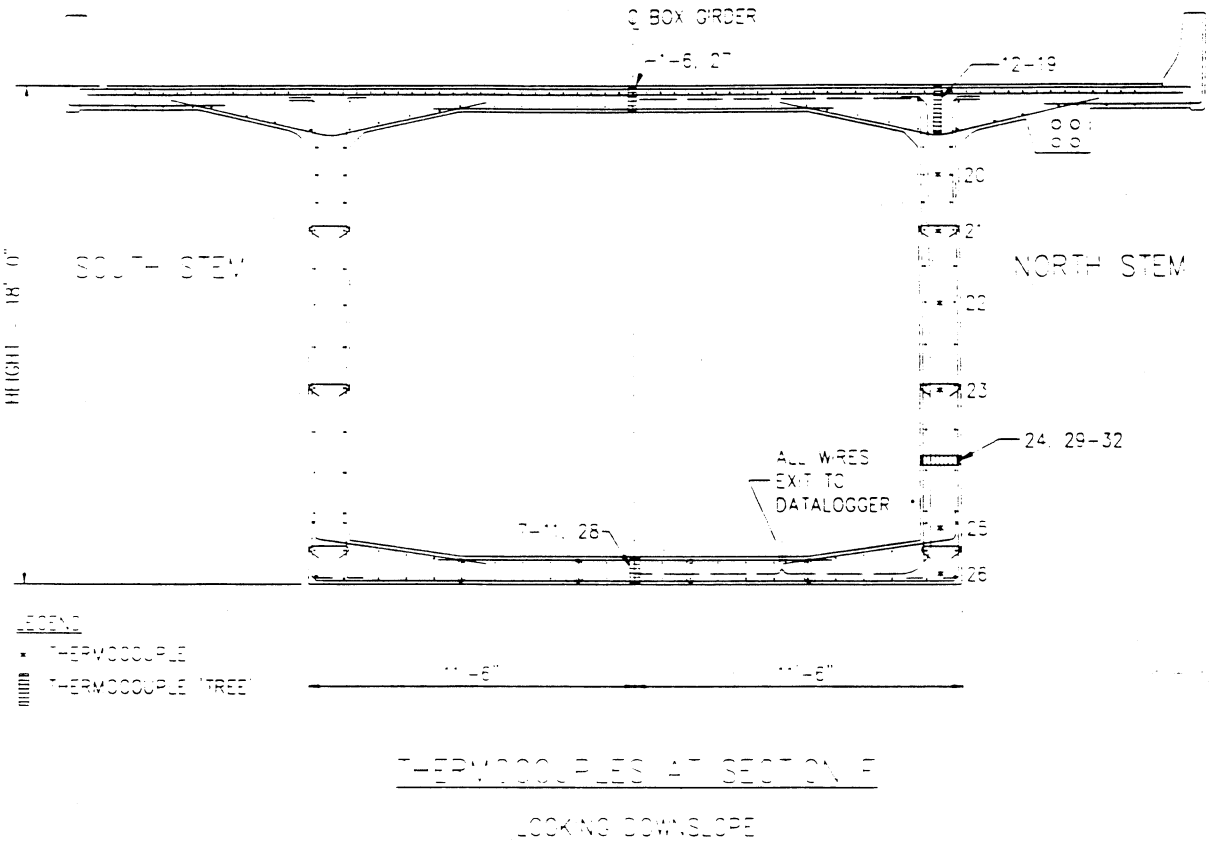

Figure 3.18: Thermocouple locations at section F.

3.4.2.2.2 Layout and Installation

Sections E and F were extensively instrumented with thermocouples as shown in Figures 3.17 and 3.18 respectively. For top and bottom slabs, thermocouple trees were used through the thickness of the slab. Trees were also used for thermal monitoring through the thickness of the North stem. Individual thermocouples were also taped to the shrink tubing surrounding the electrical resistance strain gages

3.4.2.2.3 Data Collection

A reference thermistor is provided in the datalogger multiplexer box to calibrate the thermocouple readings. The datalogger records the temperature directly in degrees Celsius.

3.5 Deflection Measurement

The deflected shape of the Viaduct was recorded by a number of methods. During construction, the deflected shape of the cantilevers and backspans were monitored by optical surveys. After completion of construction, a base-line system was installed in the instrumented spans. Tiltmeters were installed at each support in the instrumented viaduct. The following sections describe these measurement systems.

3.5.1 Optical Surveys

During construction, optical surveys were made of the viaduct top surface to ensure construction progressed at the correct elevations. Subsequent to construction, optical surveys have been undertaken for barrier elevation and topping elevation purposes. These and any future optical surveys will be used to confirm the observations based on the permanent monitoring systems described below.

3.5.2 Base-Line System

3.5.2.1 Description

A taut-wire base-line system was installed in all four instrumented spans for deflection measurements. This system consists of a high-strength piano wire strung at constant tension inside the box girder from one pier to the next to act as a reference line. Precision measurements between this base-line and plates attached to the underside of the top slab provide accurate deflection measurements.

3.5.2.2 Layout and Installation

Four spans are equipped with base-line systems. The instrumented spans are from piers P8 to P9, P9 to P10, P11 to P12, and P12 to P13. The deflection measurements are taken at locations shown in Figures 3.19.

The base line system consists of a piano wire as a reference line, two end brackets (live and dead), base plates, and a caliper. The arrangement is shown schematically in Figure 3.20.

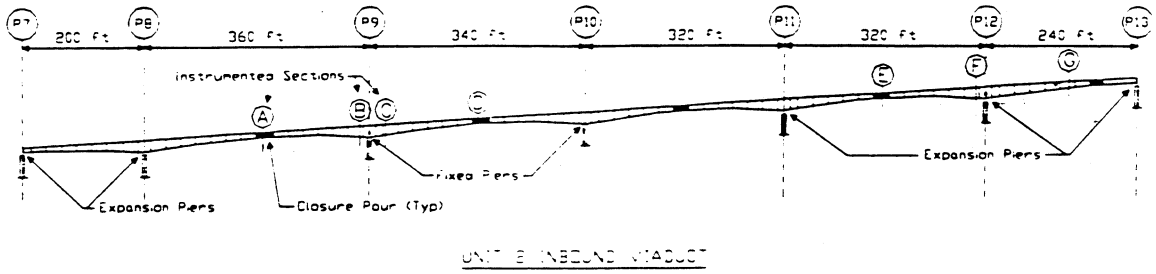

Figure 3.19: Base-line deflection monitoring points.

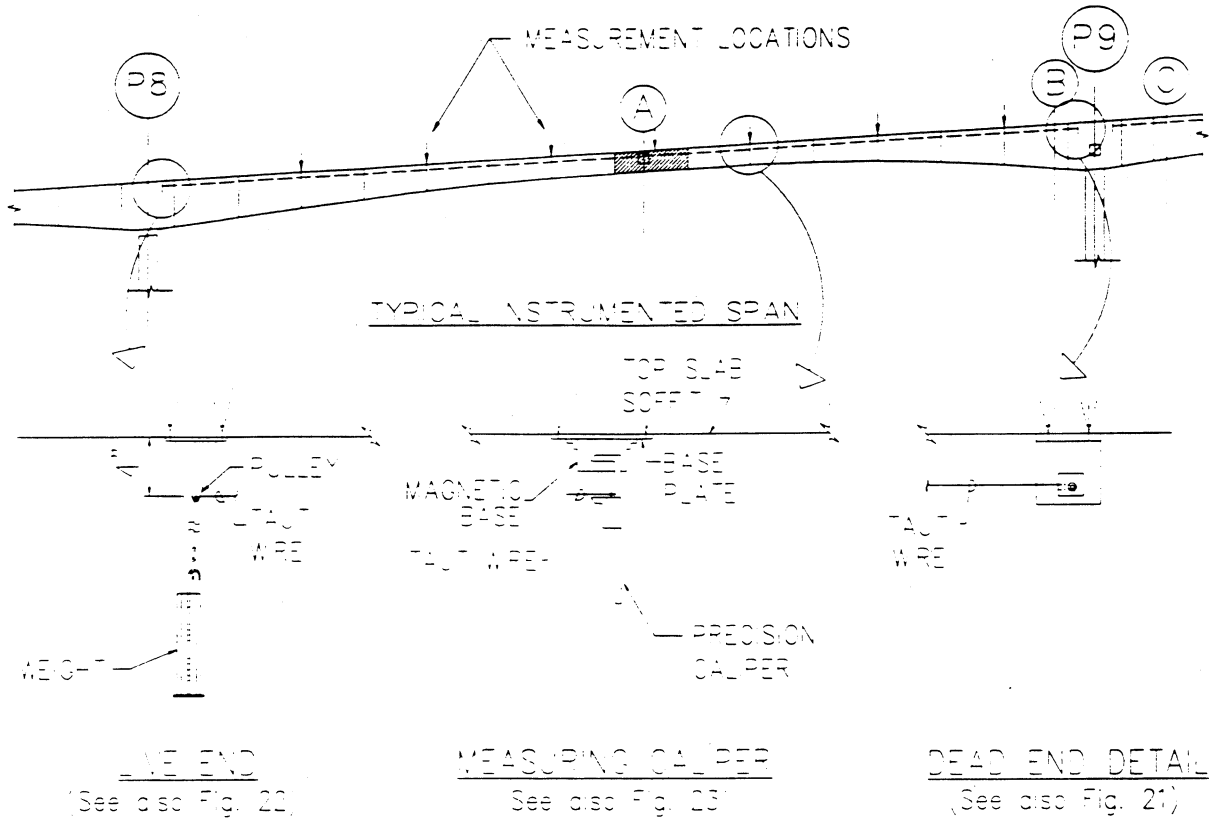

Figure 3.20: Base-line Deflection Measurement System.

The number 8 piano wire was stressed to approximately 80 % of its breaking strength to avoid any appreciable variations in the catenary shape of the free length of the piano wire. To create this tension in the piano wire, one end of the wire is fixed (Figure 3.21) while the other end runs over a pulley and supports an 80 pound weight (Figure 3.22). The wires were coated with Linseed oil to reduce corrosion.

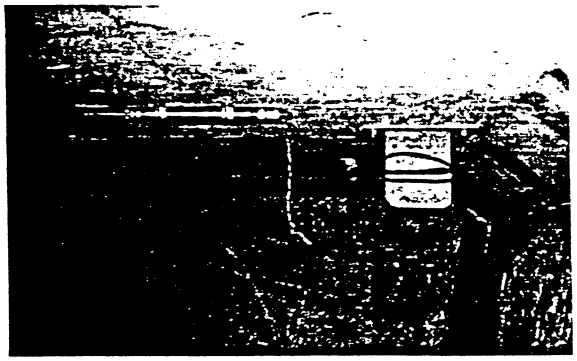

Figure 3.21: Base-line Fixed End

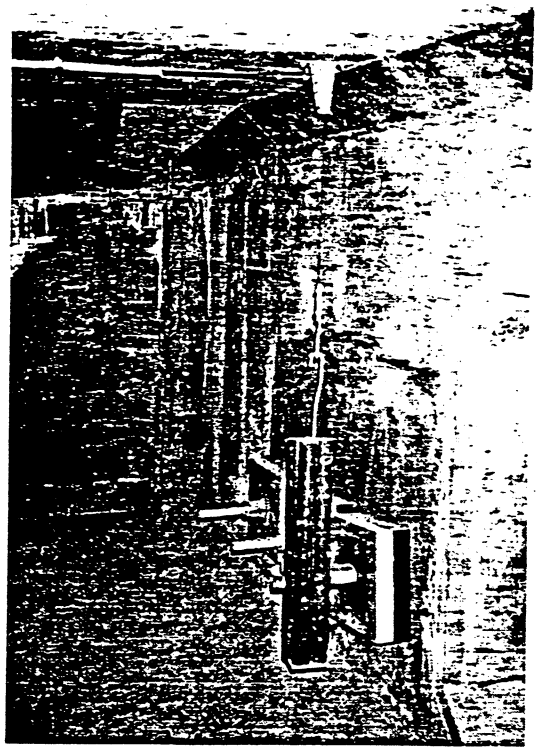

Figure 3.22: Base-line Tension End

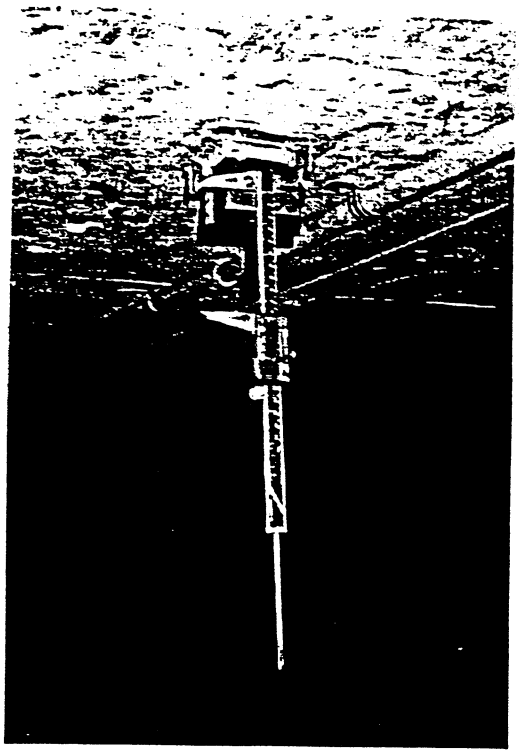

Figure 3.23: Base-line Caliper.

The exact location of the dead and live end brackets for each base-line are given in Lee and Robertson (1995).

Note that the piano-wire represents a straight line in a curved viaduct. The end brackets were positioned such that the wire came as close as possible to the centerline of the box girder at midspan. To do this, the end brackets were positioned to the North of the girder centerline at each end of the span. In addition, access openings in the top slab near the ends of certain spans had to be avoided, resulting in further offsets of the end brackets in these spans.

Deflection measurement points along the span are located at alternate construction joints. Steel base plates were installed at each of these locations using expansion anchor bolts. Three small angles were welded to each base plate as guide bars. This ensures consistent positioning of the measuring caliper on the base plate.

The measuring caliper is a modified 8 in. range Mitutoyo digital caliper. The caliper is attached to a magnetic base which is used to secure its position on the base plates. The magnetic base is equipped with a on/off switch allowing easy attachment to and removal from the base plates. Once the magnetic base is secured to a base plate, the caliper is used to read the location of the piano-wire relative to the top slab of the viaduct box (Fig. 3.23).

3.5.2.3 Data Collection

Once the piano wire and base plates were installed, the modified caliper was used to read the distance between the bottom surface of the top slab and the reference line. The difference between the initial reading and all subsequent measurements is the girder deflection relative to the ends of the span. Measurements are taken early in the morning to reduce the thermal effects. The readings are recorded monthly.

In order to relate the base-line deflection readings to prior optical surveys performed on the viaduct roadway, a tie-in survey was performed. An optical survey of the Unit 2 IB roadway was made simultaneously with a full set of piano-wire readings. The results of these surveys and the prior optical surveys will be presented in a subsequent report.

3.5.3 Tiltmeters

3.5.3.1 Description

For support rotation measurement, Applied Geomechanic Instruments (AGI) Uniaxial Tiltmeters Model 800 were installed in the box girder above piers P8 through P13 (See Figure 3.24). These tiltmeters incorporate a high-precision electrolytic tilt transducer as the internal sensing element. They measure rotational movement with respect to the unchanging vertical gravity vector.

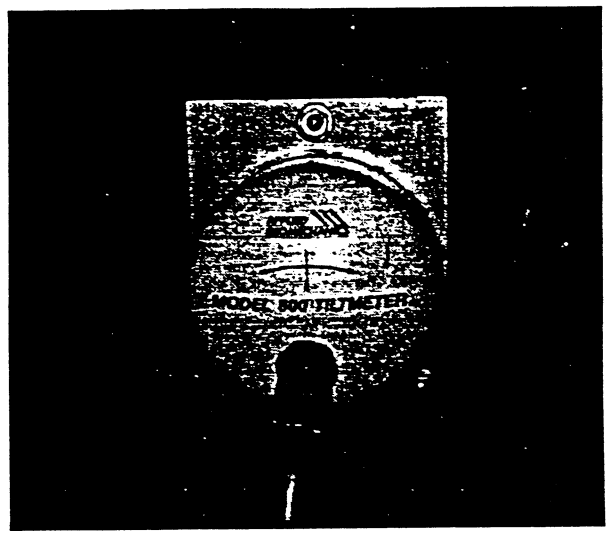

Figure 3.24: AGI Uniaxial Tiltmeter

3.5.3.2 Layout and Installation

Tiltmeters were installed at piers 8, 9, 10, 11, 12, and 13. They were mounted on a smooth vertical surface. The as-built locations of each tiltmeter are recorded in Lee and Robertson (1995). Clockwise rotations are represented by a positive tiltmeter output. All of the tiltmeters were installed on South facing vertical surfaces except at pier 12, where the tiltmeter faces North.

3.5.3.3 Data Collection

Each tiltmeter is connected to the nearest datalogger. Rotation measurements are recorded in angle units. The tiltmeters, and DC to DC voltage inverters required to provide the tiltmeter excitation, represented a significant drain on the datalogger battery if monitored continously. Since the tiltmeter readings will be used in conjuction with the base-line deflection measurements, the tiltmeters are switched off except while recording base-line deflections.

3.6 Span Shortening Measurements

Measurement of the overall shortening of each of the instrumented spans provides a valuable check of the behavior observed at the localized instrumented sections. The ability to extrapolate the strain measured at midspan and support sections to the overall span shortening

is a fundamental component of the comparison between analytical and measured behavior. The overall span shortening measurements provide a reference for these comparisons.

The span shortening is measured in two ways. Extensometers have been installed over the full length of each of the four instrumented spans. In addition, measurement of the movement of the slide bearings at the expansion piers provides a measure of the shortening of the intervening span.

3.6.1 Extensometers

3.6.1.1 Description

To measure the overall shortening of the box girder, extensometers were installed in the four instrumented spans (Fig. 3.25).

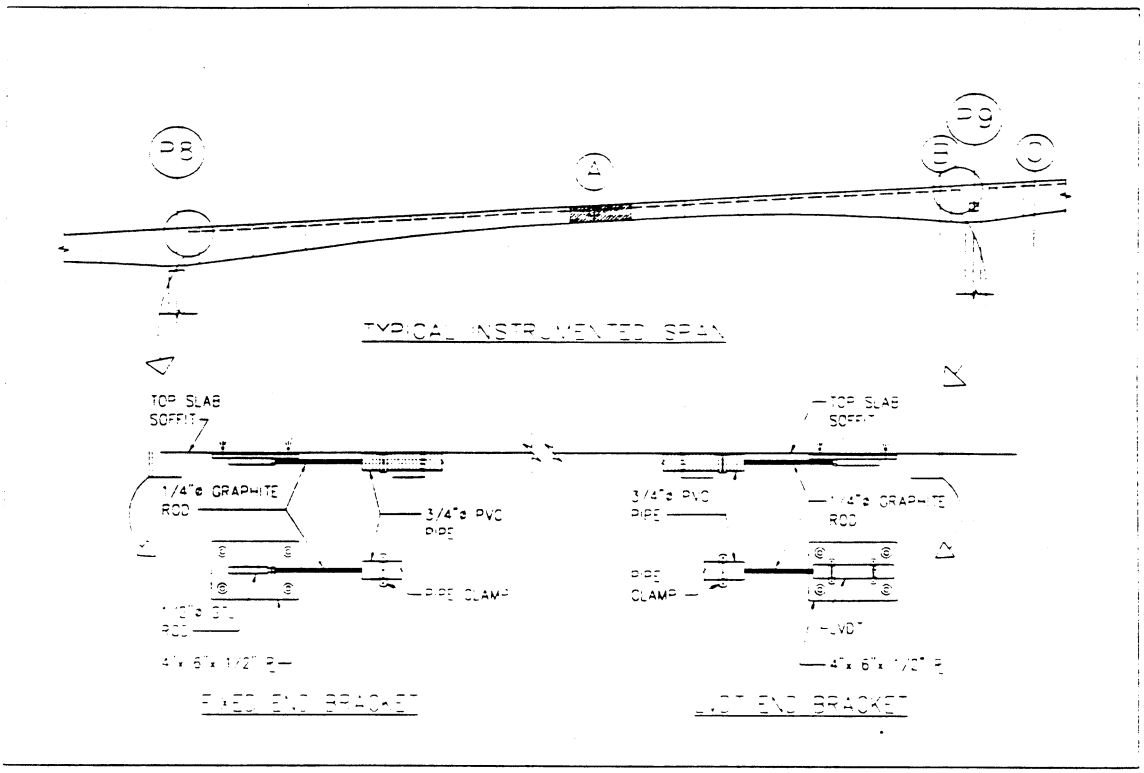

Figure 3.25: Span Extensometer Details

Each span extensometer consists of a series of graphite rods (1/4 inch diameter by 20 feet long) spliced together to span from pier to pier inside the box girder. The graphite rods are connected with rigid couplers and inserted into a 3/4 inch diameter PVC conduit attached to the underside of the girder top slab. One end of the rod is fixed (Fig. 3.26), while the other end is coupled to a Linear Variable Displacement Transducer (LVDT) shown in Figure 3.27.

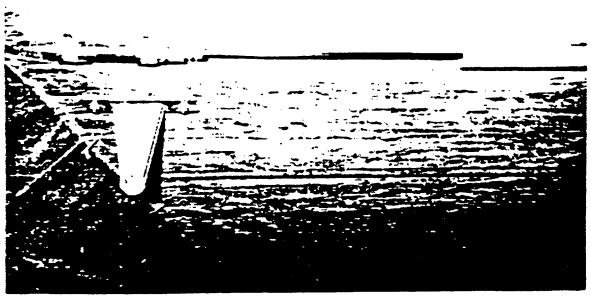

Figure 3.26: Extensometer Fixed End.

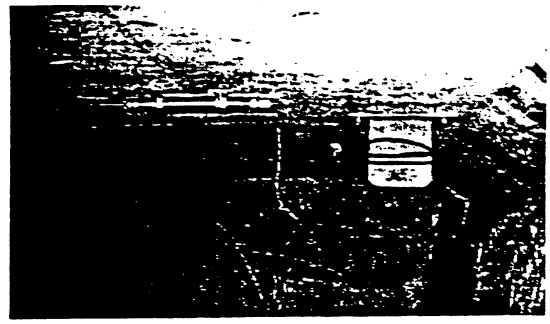

Figure 3.27: Extensometer LVDT End.

The relative displacement of the two ends of the extensometer is measured by the LVDT. The LVDTs were manufactured by Geokon and operate on the vibrating wire principle. One of the LVDTs has a six inch stroke, while the others have two inch strokes. Once this limit is reached, they will be repositioned so as to continue monitoring the span shortening.

3.6.1.2 Layout and Installation

Extensometers were installed in all four instrumented spans, that is, between piers P8 and P9, P9 and P10, P11 and P12, and P12 and P13, as shown in Figure 3.28. The as-built locations of the extensometer end brackets in each span are recorded in Lee and Robertson (1995).

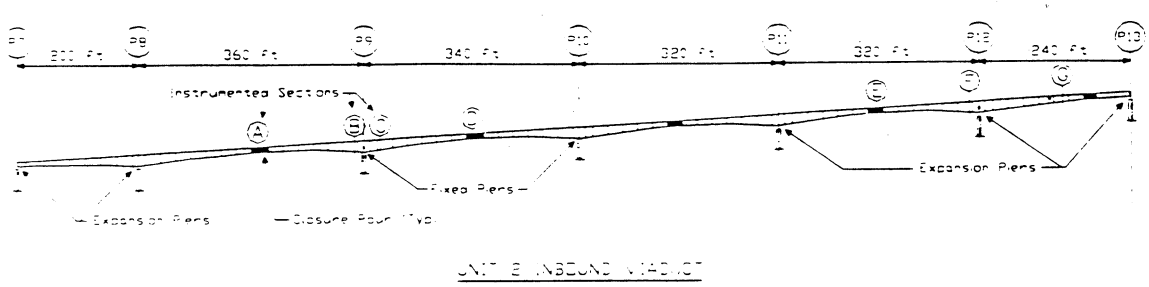

Figure 3.28: Span Extensometer locations.

3.6.1.3 Data Collection

The extensometer lead wires were connected to dataloggers B and F for automated data recording.

3.6.2 Bearing Movement Measurement

In addition to the extensometers, relative displacements are measured between the box girder and the top of the expansion piers (P8, P11, and P12), and movement of each end of the bridge unit relative to the supporting piers (P7 and P13).

3.7 Monitoring System

3.7.1 Description

All of the electrical gages used in this project are permanently connected to battery operated Data Acquisition systems as shown in Figure 3.29. All data acquisition systems consist of Micro-10 Dataloggers and multiplexers assembled by Geokon Incorporated. Battery operated systems were used since there is no power supply to the Viaduct. Solar panels have been installed at each datalogger to continually charge the batteries. The dataloggers are housed in water resistant metal enclosures inside the box girder. Each Micro-10 Datalogger contains a Campbell Scientific CR10 Measurement and Control Unit (MCU). The CR10 consists of a microcomputer, clock, multimeter, calibrator, scanner, frequency counter, storage module. The dataloggers are programmed be means of a laptop computer. The laptop is also used to download the data from the storage module at regular intervals.

Figure 3.29: Typical Data Acquisition System.

3.7.2 Layout and Installation

Six data acquisition systems were located at the instrumented sections as shown in Figure 3.1. Because of time constraints at the start of this project, the first datalogger at sections B and C could only be installed subsequent to the section pours. Manual readings of all instruments were taken until the datalogger was installed. All subsequent systems were installed and connected to the gages prior to casting of the instrumented sections.

During special events such as concrete hydration and stressing of tendons, the datalogger at the section in question was set to read all instruments at between 5 and 30 minute intervals. Once all stressing was completed at a particular section, the datalogger scan interval was set to a standard 2 hours. After the first year of monitoring, the scan interval was set to four readings per day, at 6:00 am, 12:00 noon, 6:00 pm and 12:00 midnight. This greatly reduces the amount of data recorded, and increases the time period between downloading from the dataloggers. The processing, presentation and storage of this data is performed on a regular basis by UH personnel using Excel Spreadsheets and Graphs.

3.8 Instrumentation Performance

Overall, the instrumentation of the North Halawa Valley Viaduct is performing extremely well. All instrumentation was successfully installed prior to concrete pouring. Figure 3.30 shows a typical viaduct segment immediately prior to pouring. The top slab gages are partially visible near the left edge of the pour. Each concrete pour was monitored carefully to try to reduce damage to the gages from falling concrete and contact with concrete vibrators.

Of the 207 electronic instruments installed in this project, only 12 are no longer functioning correctly. A few vibrating wire strain gages at Section C were damaged during the concrete pour. Three north stem gages (gages #4, #5, and #6) and one south stem gage (gage #9) are no longer working. Section C was the second instrumented segment poured. The brackets supporting the vibrating wire gages were not provided with the cross braces shown in Figure 3.6 Detail B. During casting, the concrete flow pulled the two flanges of the gage apart, so stretching the internal wire and rendering the gages useless. The problem was discovered and corrected for subsequent sections.

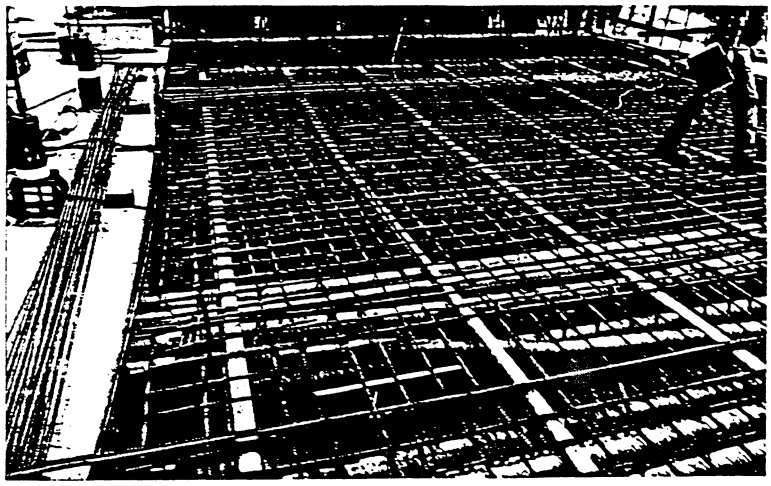

Figure 3.30: Top slab prior to concrete pour.

Two other vibrating wire gages (#5 at section F, and #2 at section G) are recording unrealistic values. The data from these gages has been ignored. Two thermocouples at section F failed to work after the concrete pour. Another thermocouple appears to have failed subsequently. A few electrical resistance strain gages are also no longer functioning properly. The remaining 195 gages are performing well after three years of embeddment in concrete or field exposure.

The dataloggers have also performed extremely well. Initial problems with loss of battery charge have been solved by the installation of the solar panels. Occasional gaps in the data resulted from overflow of the logger storage module if data was not downloaded in a timely manner. This was particularily critical when short reading intervals were used, since the amount of data soon exceeded the logger storage capacity. Moisture leakage into some of the multiplexer enclosures at Logger F resulted in some erroneous readings from the thermocouples and some of the electrical resistance gages at this section. These multiplexers were replaced and all gages at this section are again being monitored correctly.

4.2 Data Analysis

All data collection is being performed on a regular basis by University of Hawaii personnel. The data is then processed on a continual basis at UH using Excel Spreadsheets and Graphs. This processed data is then distributed to the other participants in the project for analysis.

A number of studies have been performed both at the University of Hawaii and by T. Y. Lin International based on the data collected from the instrumentation. The results of these studies are presented in subsequent chapters of this report. Results of some of these studies have also been presented at various national and international conferences. Future presentations are planned for further dissemination of the results of this instrumentation program.

CHAPTER 4

CONCRETE MATERIAL PROPERTIES

4.1 Introduction

In order to establish the material properties of the concrete used in the instrumented sections, concrete samples were taken from each instrumented section. The following tests were performed on these samples;

Compressive Strength, f'_c, ASTM C39

Modulus of Elasticity, E_c, ASTM C469

Coefficient of Thermal Expansion, α, CRD C39, and

Creep and Shrinkage, ASTM C512

These tests were all performed by CTL at their laboratory in Skokie, Illinois. Tests were performed at a concrete age of 3, 28 and 90 days (Concrete age is the number of days after the section was poured).

4.2 Concrete Sample Collection

Concrete samples were collected at each instrumented section for testing (Figure 4.1). Standard 6 in. diameter by 12 in. long concrete cylinders were used for all tests. Thirty three cylinders were collected at each section and shipped to CTL. Additional cylinders were made at sections E, F and G for creep and shrinkage tests performed on site as described later in this chapter. All samples were made in plastic cylinder molds in accordance with ASTM C192 procedures. The molds were capped to ensure sealed conditions during shipping of the cylinders to CTL.

The samples were collected at ten different locations in the cross section and throughout the pour to obtain a complete representation of the concrete at the instrumented segment. The sample locations are bottom slab middle (BSM), south stem bottom (SSB), south stem middle (SSM), south stem top (SST), north stem bottom (NSB), north stem middle (NSM), north stem top (NST), top slab south (TSS), top slab north (TSN), and top slab middle (TSM) as shown in Figure 4.2. A log was prepared listing the time, location, and delivery truck number for each cylinder specimen. The cylinder logs for each section are given in Lee and Robertson (1995).

4.3 Concrete Sample Shipping

The day after the pour, eleven of the cylinders were shipped overnight to Construction Technology Laboratories (CTL) in Skokie, Illinois, so as to arrive in time for 3-day tests. Cylinders 1, 4, 7,...etc were used for the 3-day tests. Another twenty two cylinders were shipped by surface transportation for 28-day and 90-day tests. Cylinders 2, 5, 8, ... etc were used for the 28-day tests, while the remaining cylinders 3, 6, 9, ... etc were used for 90-day tests.

Figure 4.1: Concrete Sampling at pump discharge.

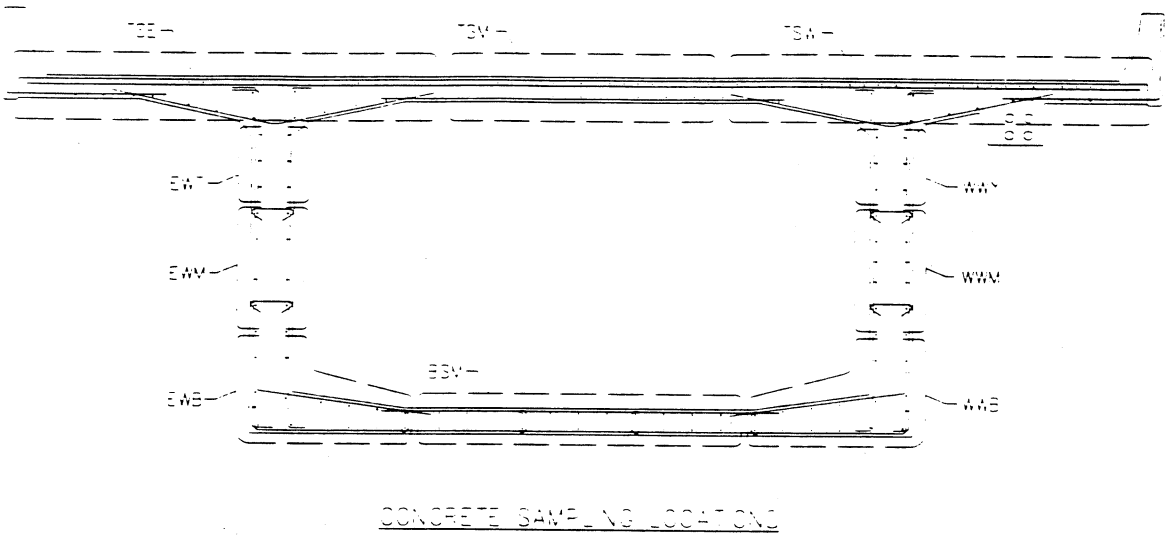

Figure 4.2: Concrete Sampling Locations in typical Cross Section.

All cylinders were shipped in the capped plastic molds to preserve 100 percent moisture conditions. They were packed individually in styrofoam filled cardboard boxes. No damage was evident on any of the cylinders upon arrival at the test laboratory.

4.4 Concrete Test Results

4.4.1 Compressive Strength

The compressive strength tests were performed in accordance with ASTM C39. Table 4.1 presents the test results at 3, 28, and 90 days at each section. Each result is an average of three concrete cylinders.

Table 4.1: Compressive Strength, f'_c (psi)*

	Age at Test (days)		
Section	**3**	**28**	**90**
A	4260	6140	7700
B	3780	6770	7910
C	3780	6740	7650
D	4290	6640	7630
E	4210	6530	7430
F	3880	5850	7060
G	3830	5990	6510
Average	**4004**	**6380**	**7413**
Standard Deviation	**237**	**379**	**478**

* Each result is the average of 3 cylinder tests.

4.4.2 Modulus of Elasticity

The Modulus of Elasticity tests were performed in accordance with ASTM C469. Table 4.2 presents the test results at 3, 28, and 90 days at each section. Each result is an average of two concrete cylinders.

Table 4.2: Static Modulus of Elasticity, E_c (psi)*

	Age at Test (days)		
Section	**3**	**28**	**90**
A	3.07×10^6	3.51×10^6	3.93×10^6
B	3.23×10^6	3.98×10^6	3.93×10^6
C	3.23×10^6	3.54×10^6	3.95×10^6
D	3.21×10^6	3.59×10^6	4.12×10^6
E	3.27×10^6	3.81×10^6	3.54×10^6
F	3.48×10^6	3.57×10^6	3.88×10^6
G	3.05×10^6	3.45×10^6	3.58×10^6
Average	**3.22×10^6**	**3.64×10^6**	**3.85×10^6**
Standard Deviation	**0.142×10^6**	**0.189×10^6**	**0.210×10^6**

* Each result is the average of 2 cylinder tests.

4.4.3 Coefficient of Thermal Expansion

The coefficient of thermal expansion tests were performed in accordance with CRD C39. Tables 4.3 and 4.4 present the test results at 3, 28, and 90 days at each section, per degree farenheit and per degree celsius respectively. Each result is an average of three concrete cylinders.

Table 4.3: Concrete Coefficient of Thermal Expansion, α (10^{-6} per ^{o}F)*

	Age at Test (days)		
Section	**3**	**28**	**90**
A	5.55	4.86	5.38
B	4.80	4.77	5.23
C	6.04	4.86	5.52
D	4.09	5.34	4.34
E	3.85	4.10	6.53
F	3.92	4.21	4.06
G	3.78	4.34	6.24
Average	**4.58**	**4.64**	**5.33**
Standard Deviation	**0.91**	**0.44**	**0.90**

* Each result is the average of 3 cylinder tests.

Table 4.4: Concrete Coefficient of Thermal Expansion, α (10^{-6} per ^{o}C)*

	Age at Test (days)		
Section	**3**	**28**	**90**
A	9.99	8.75	9.68
B	8.64	8.59	9.41
C	10.87	8.75	9.94
D	7.36	9.61	7.81
E	6.93	7.38	11.75
F	7.06	7.58	7.31
G	6.80	7.81	11.23
Average	**8.24**	**8.35**	**9.59**
Standard Deviation	**1.64**	**0.79**	**1.63**

* Each result is the average of 3 cylinder tests.

More detailed records of the CTL test data is presented in Table 4.5.

Table 4.5: CTL Concrete Material Property Test Summary

Section	Description	Date Started	Date Completed	Days Loaded	Applied Stress	f'c (psi)	Ec (psi)	α (per °F)
A	casting date	5/25/98						
	3 day loading	5/28/98	5/27/99	364	1700	4260	3.07E+06	5.55E-06
	28 day loading	6/22/98	6/22/99	365	2500	6140	3.51E+06	4.86E-06
	90 day loading	8/23/98	8/23/99	365	2500	7700	3.93E+06	5.38E-06
B	casting date	4/27/98						
	3 day loading	4/30/98	4/30/99	365	1510	3780	3.23E+06	4.80E-06
	28 day loading	5/25/98	5/25/99	365	2500	6770	3.98E+06	4.77E-06
	90 day loading	7/26/98	7/26/99	365	2500	7910	3.93E+06	5.23E-06
C	casting date	4/29/98						
	3 day loading	5/2/98	6/2/99	396	1880	3780	3.23E+06	6.04E-06
	28 day loading	5/27/98	5/27/99	365	2500	6740	3.54E+06	4.86E-06
	90 day loading	7/28/98	7/28/99	365	2500	7650	3.95E+06	5.52E-06
D	casting date	7/2/98						
	3 day loading	7/5/98	1/5/01	915	1720	4290	3.21E+06	4.09E-06
	28 day loading	7/30/98	1/30/01	915	2480	6640	3.59E+06	5.34E-06
	90 day loading	9/30/98	1/30/01	853	2500	7630	4.12E+06	4.34E-06
E	casting date	9/21/98						
	3 day loading	9/24/98	1/24/01	853	1660	4210	3.27E+06	3.85E-06
	28 day loading	10/19/98	1/20/01	824	2480	6530	3.81E+06	4.10E-06
	90 day loading	12/20/98	1/20/01	762	2480	7430	3.54E+06	6.53E-06
F	casting date	8/18/98						
	3 day loading	8/21/98	1/21/01	884	1550	3880	3.48E+06	3.92E-06
	28 day loading	9/15/98	1/15/01	853	2290	5850	3.57E+06	4.21E-06
	90 day loading	11/16/98	1/16/01	792	2480	7060	3.88E+06	4.06E-06
G	casting date	9/11/98						
	3 day loading	9/14/98	9/14/99	365	1530	3830	3.05E+06	3.78E-06
	28 day loading	10/9/98	10/9/99	365	2380	5990	3.45E+06	4.34E-06
	90 day loading	12/10/98	12/10/99	365	2480	6510	3.58E+06	6.24E-06

4.4.4 Creep and Shrinkage Tests

Parallel creep and shrinkage tests were performed at CTL under controlled laboratory conditions, and at the site under field conditions. Each creep test consists of a single creep frame containing two creep cylinders accompanied by two shrinkage cylinders alongside the frame. The two creep cylinders are loaded into the creep frame with dummy cylinders above and below the instrumented cylinders as shown in Figure 4.3.

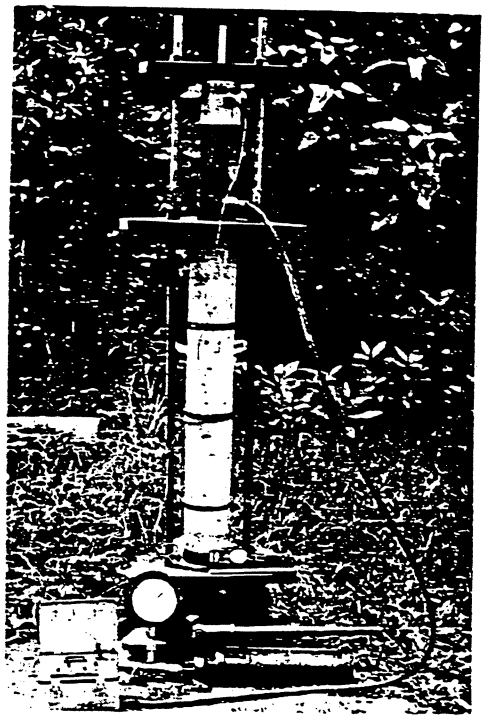

Figure 4.3: Field creep frame.

The creep frame consists of header plates bearing on the ends of the loaded specimens, a load-maintaining element (double steel coil springs), and threaded rods to take the reaction of the loaded system. The coil springs are needed to ensure consistant long-term loading. The load on each frame was checked on a regular basis.

At CTL laboratories, tests were conducted following the recommendations of ASTM C512. The laboratory tests were performed on concrete samples from each of the seven instrumented sections. For each of the seven instrumented sections, three creep frames were loaded, one each at 3 days, 28 days and 90 days age after pouring. There are therefore 21 laboratory creep frames each containing two creep cylinders and each accompanied by two shrinkage cylinders.

The creep and shrinkage results from the CTL tests are presented in Figures 4.4 through 4.24. These plots present the Load Induced Deformation, which includes the elastic and creep strains, and the Drying Shrinkage. All tests were performed for at least one year of loading, with tests for sections D, E and F continuing for over 800 days. The raw data on which these plots are based is presented in the Appendix.

Parallel field creep tests were performed on concrete cylinders from sections E, F and G. Three creep frames were loaded with cylinders from each of sections E and G, while 2 frames were loaded with cylinders from section F. These creep frames are located in or near the North Halawa Valley Viaduct. Companion shrinkage cylinders made from the same concrete as the creep cylinders are stored alongside the creep frames. A full discussion of the field creep tests is presented in Lee and Robertson (1995). The creep and shrinkage results from the field tests are presented in Figures 4.25 through 4.32. The raw data on which these plots are based is presented in the Appendix.

Load Induced Deformation and Drying Shrinkage for Section A Loaded After 3 Days

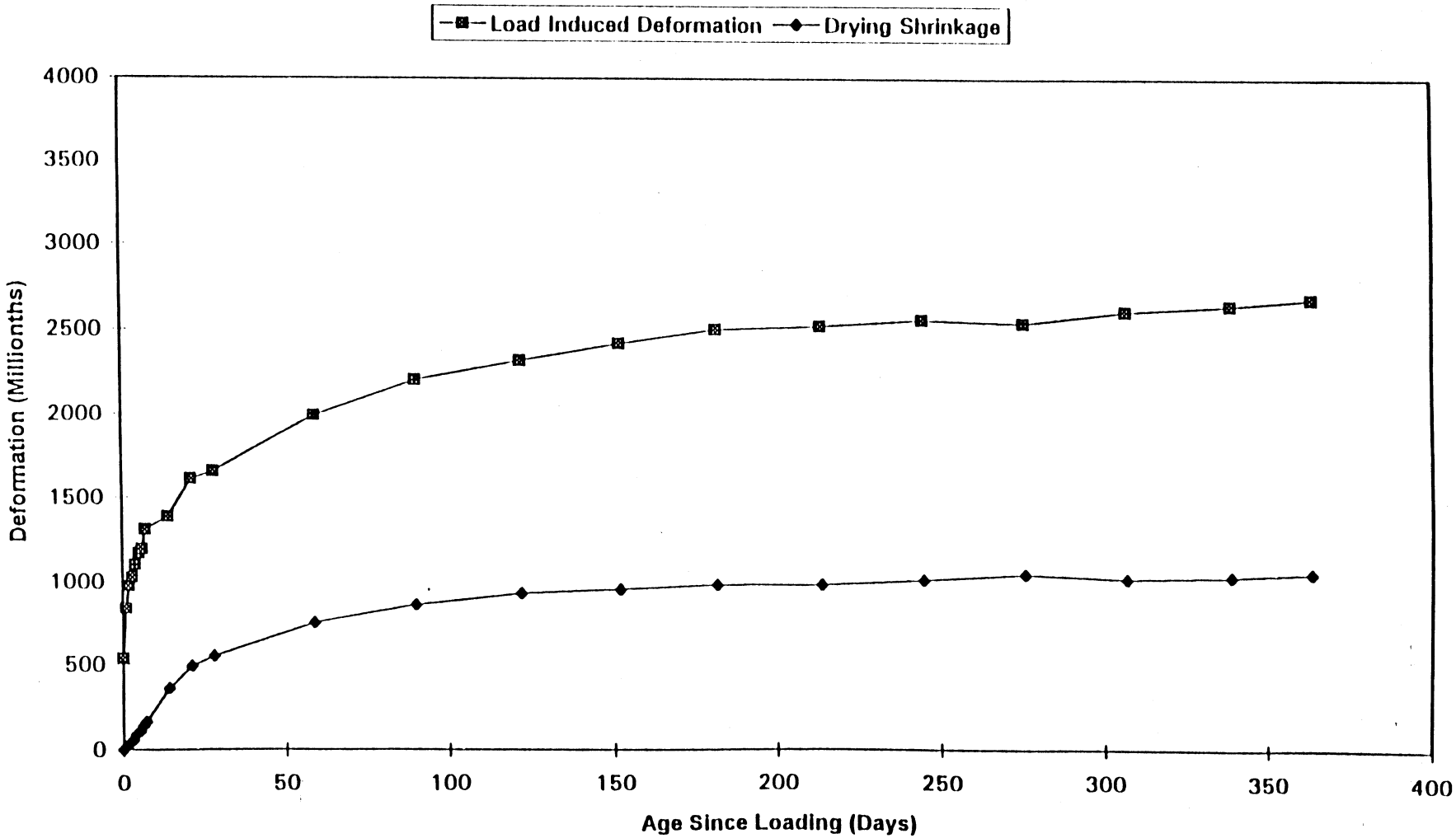

Load Induced Deformation and Drying Shrinkage for Section A Loaded After 28 Days

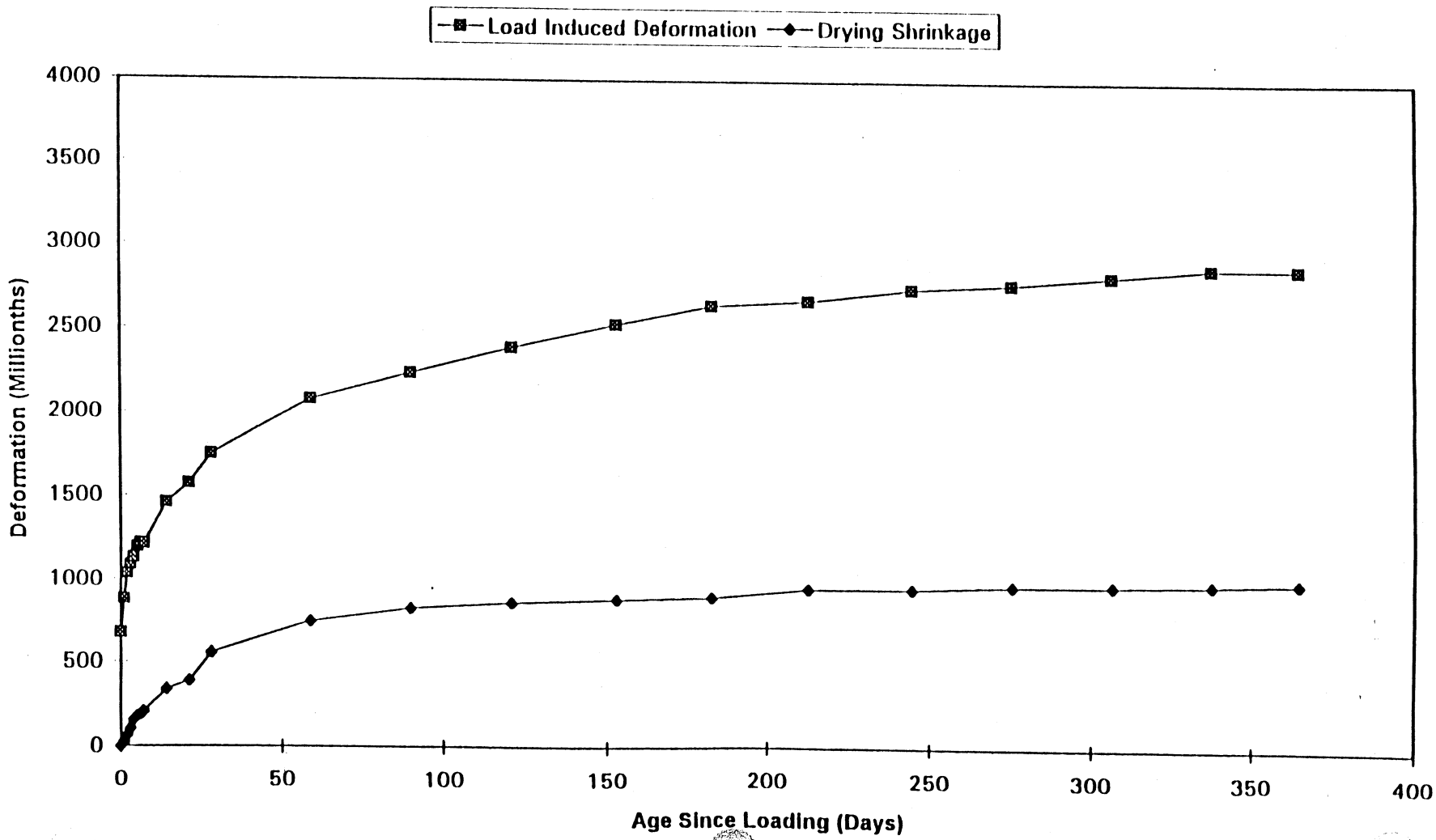

Load Induced Deformation and Drying Shrinkage for Section A Loaded After 90 Days

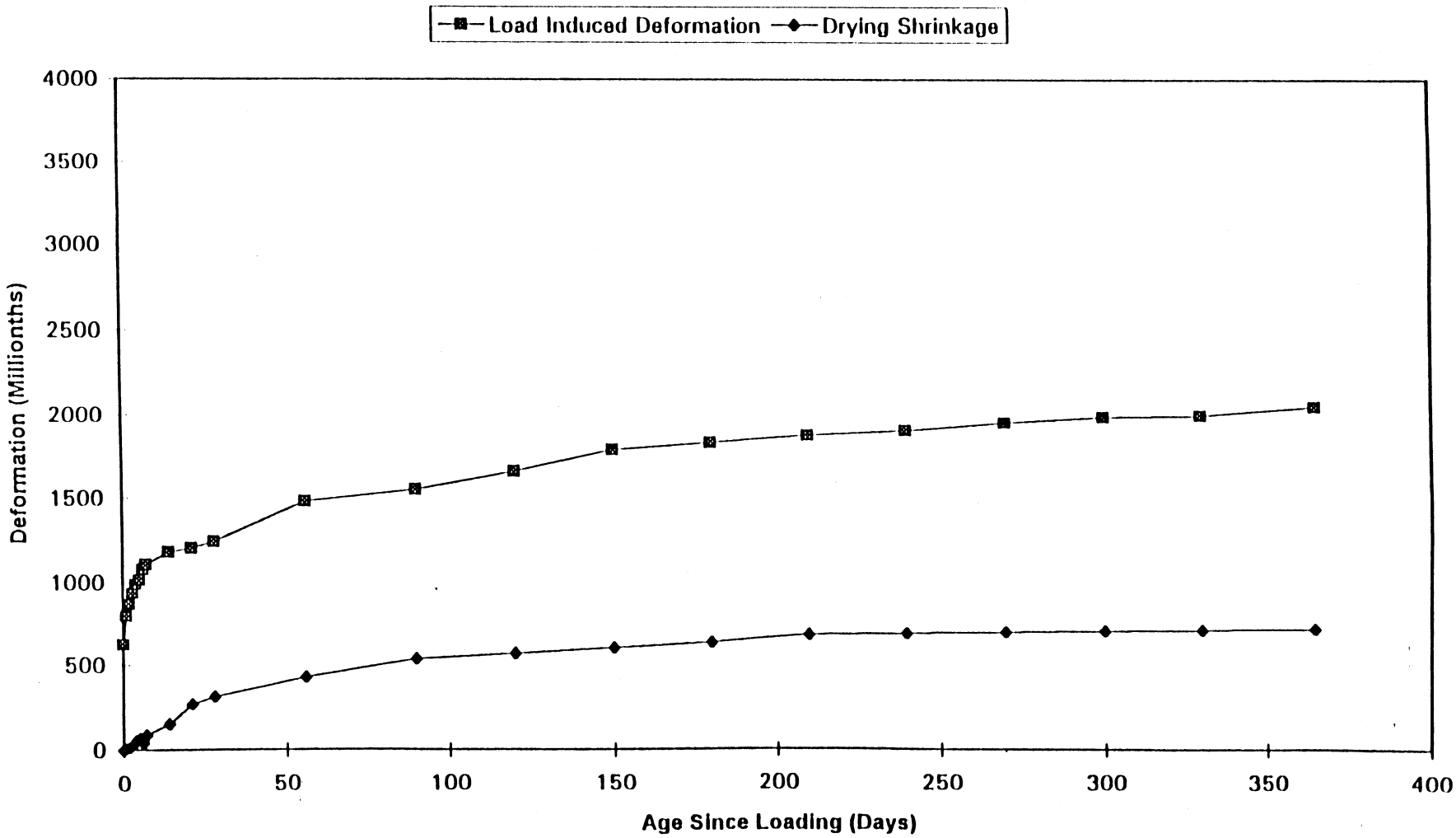

Load Induced Deformation and Drying Shrinkage for Section B Loaded After 3 Days

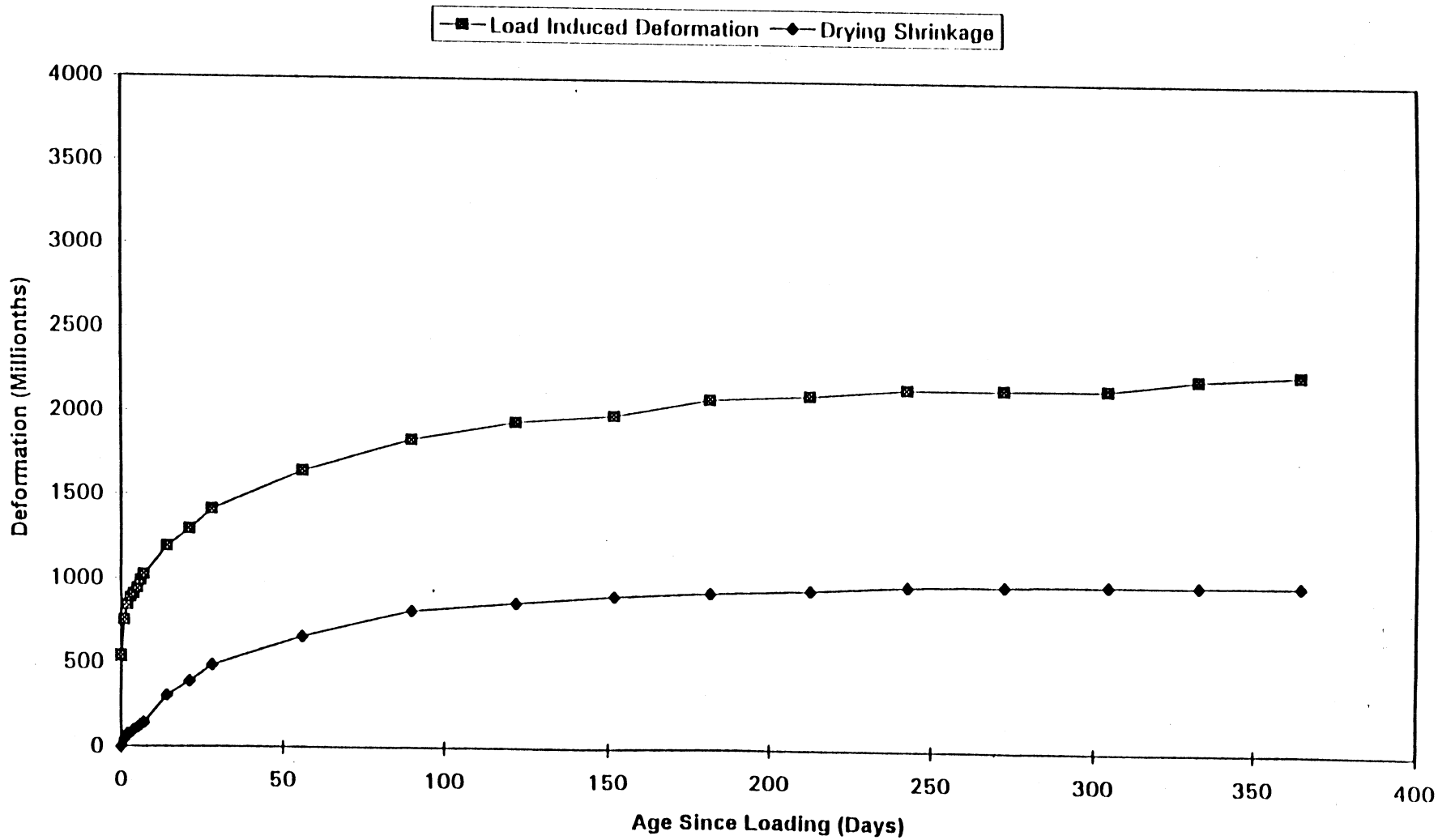

Load Induced Deformation and Drying Shrinkage for Section B Loaded After 28 Days

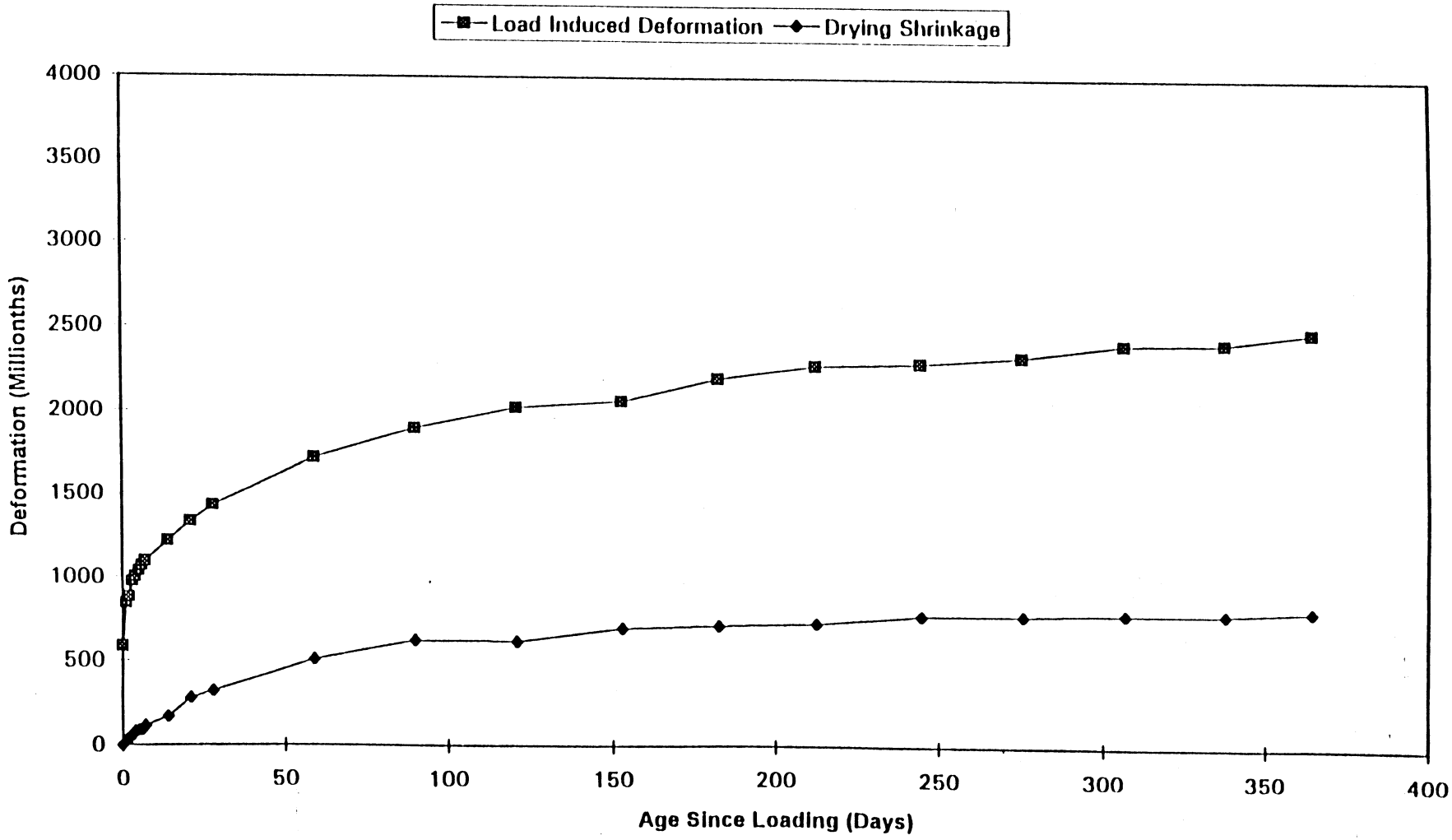

Load Induced Deformation and Drying Shrinkage for Section B Loaded After 90 Days

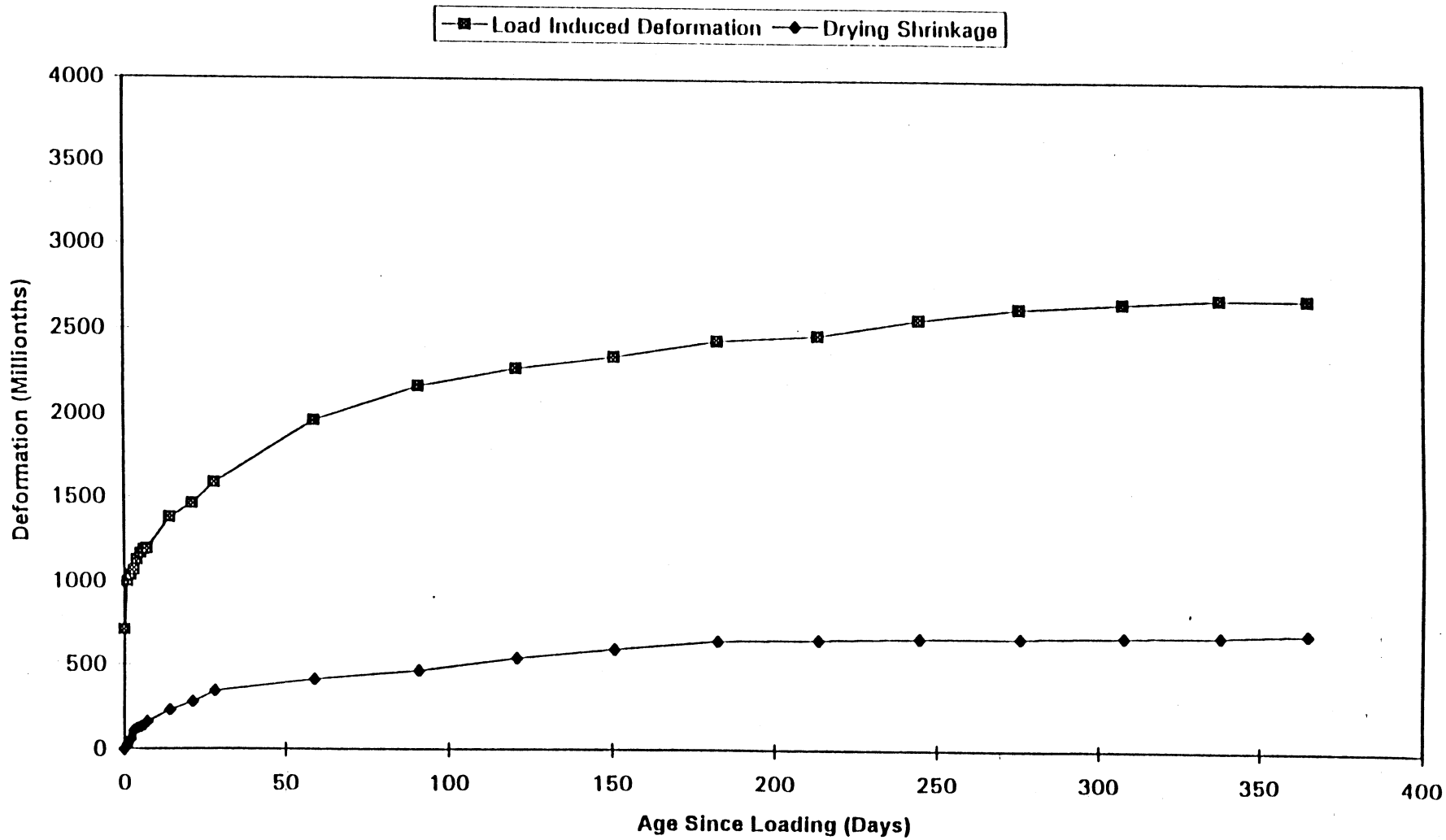

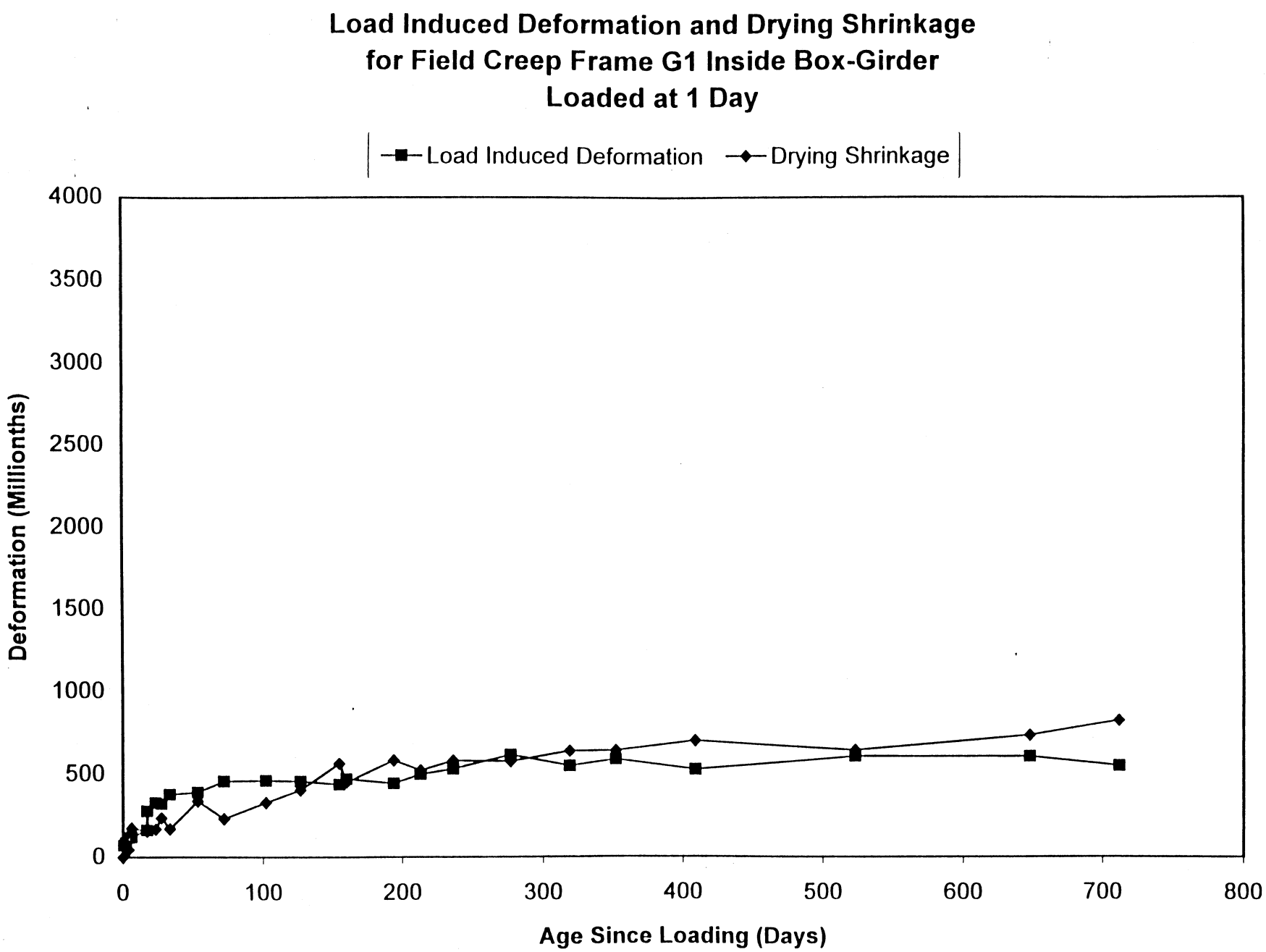
Load Induced Deformation and Drying Shrinkage
for Field Creep Frame G1 Inside Box-Girder
Loaded at 1 Day
Load Induced Deformation
Drying Shrinkage
Deformation (Millionths)
4000
3500
3000
2500
2000
1500
1000
500
0
0
100
200
300
400
500
600
700
800
Age Since Loading (Days)

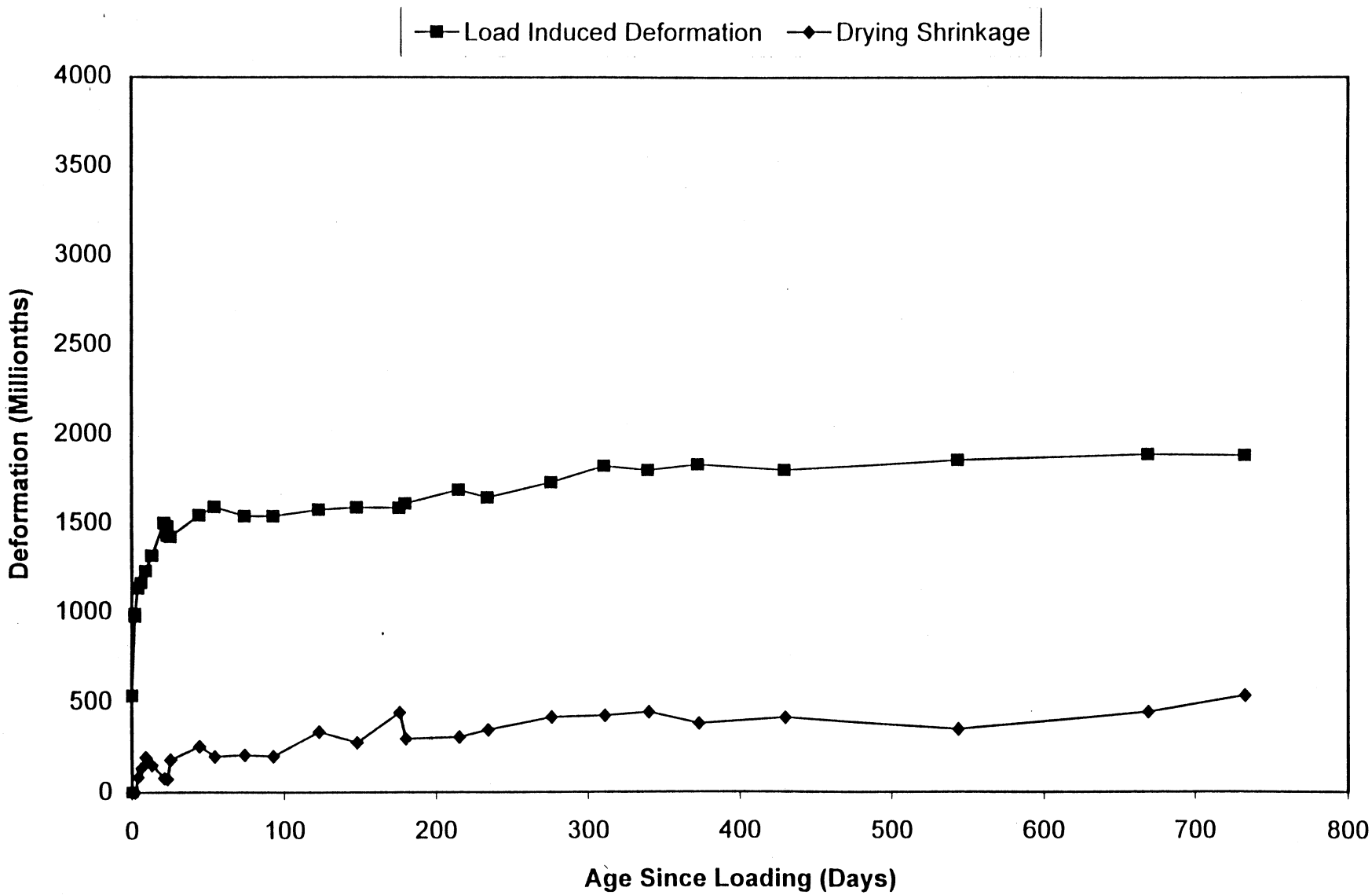
Load Induced Deformation and Drying Shrinkage
for Field Creep Frame F3 Outside Box-Girder
Loaded at 4 Days
Load Induced Deformation
Drying Shrinkage
Deformation (Millionths)
4000
3500
3000
2500
2000
1500
1000
500
0
0
100
200
300
400
500
600
700
800
Age Since Loading (Days)

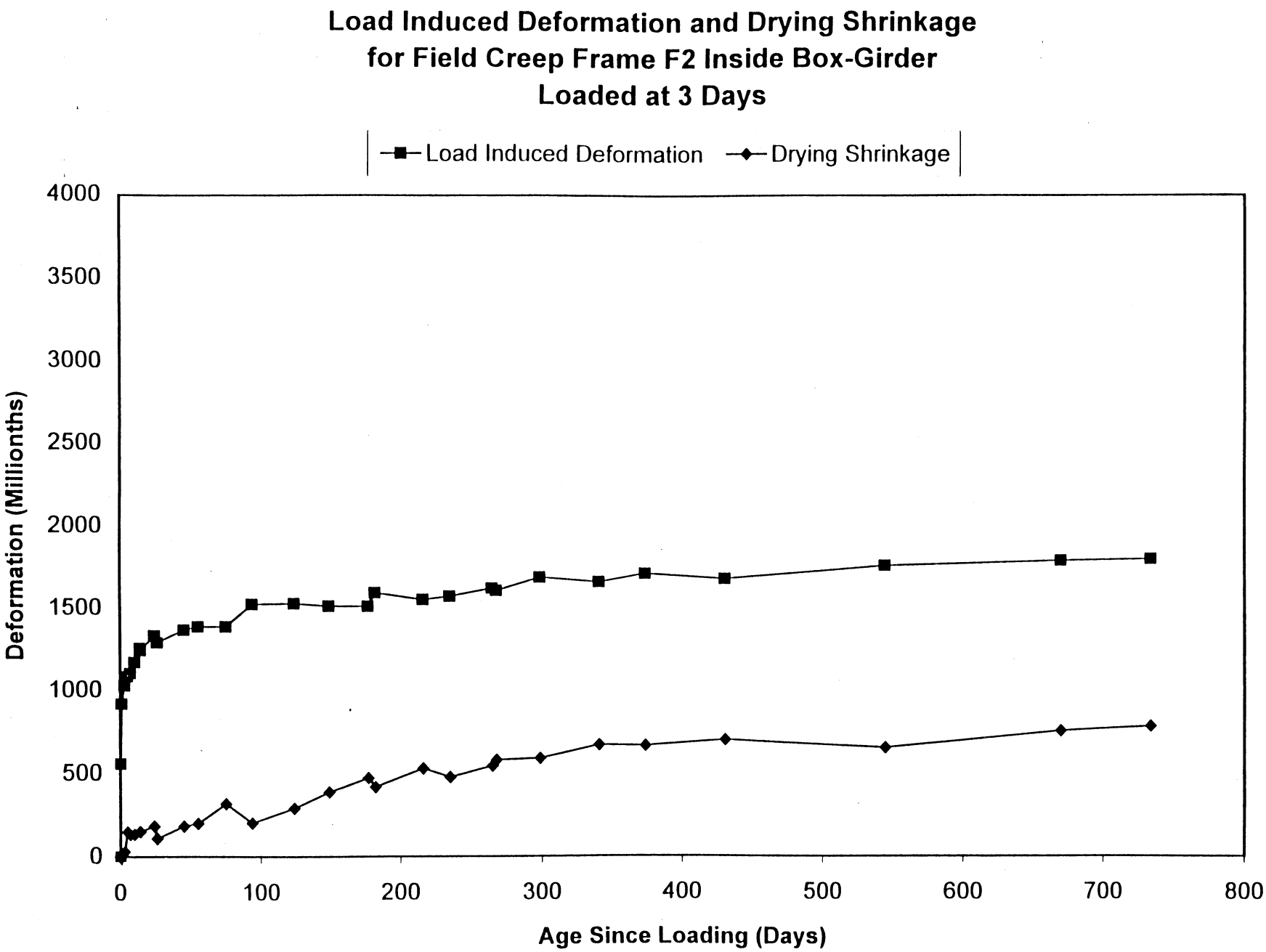
Load Induced Deformation and Drying Shrinkage
for Field Creep Frame F2 Inside Box-Girder
Loaded at 3 Days
Load Induced Deformation
Drying Shrinkage
Deformation (Millionths)
4000
3500
3000
2500
2000
1500
1000
500
0
0
100
200
300
400
500
600
700
800
Age Since Loading (Days)

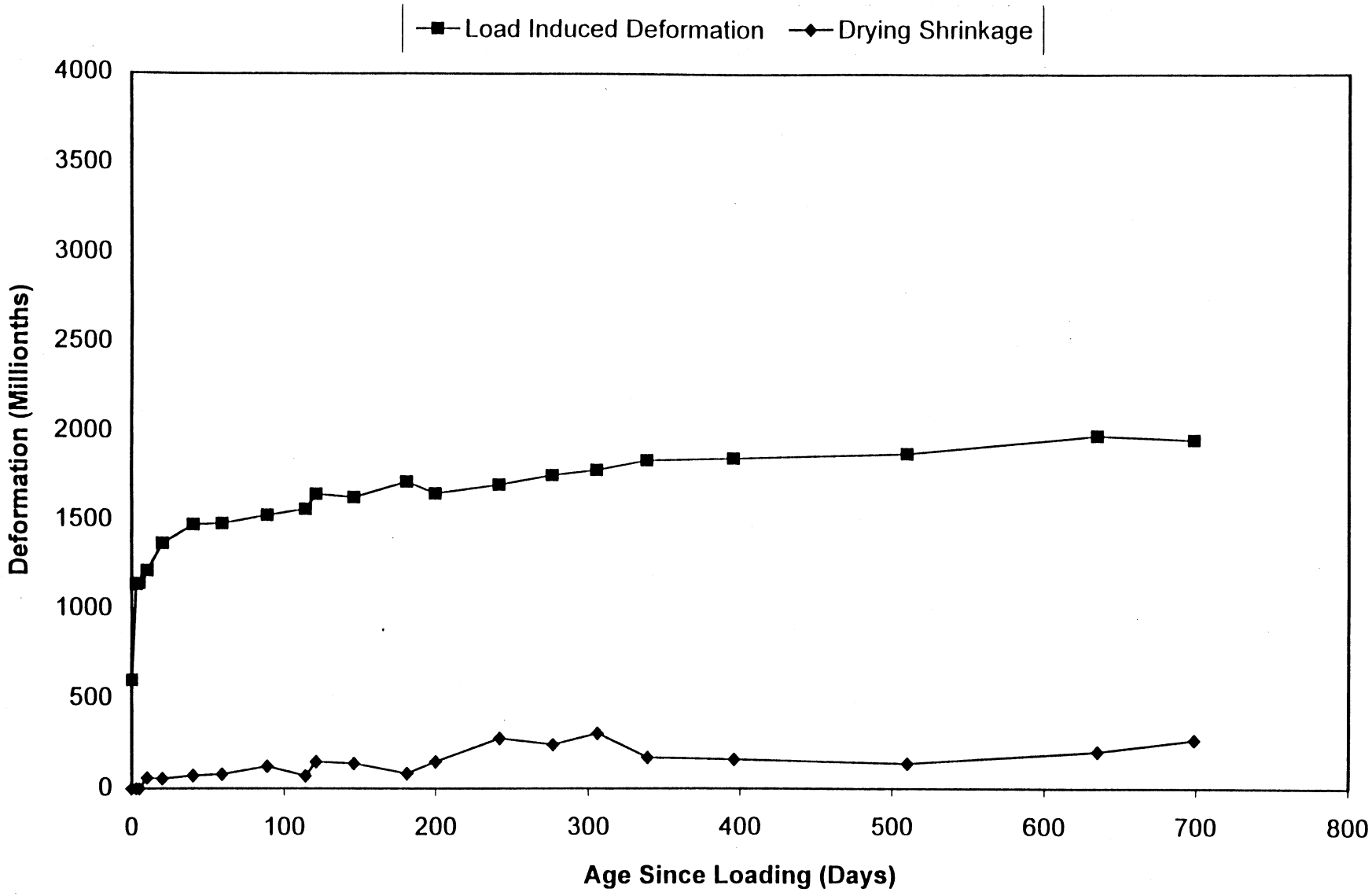
Load Induced Deformation and Drying Shrinkage
for Field Creep Frame E3 Outside Box-Girder
Loaded at 4 Days
Load Induced Deformation
Drying Shrinkage
Deformation (Millionths)
4000
3500
3000
2500
2000
1500
1000
500
0
0
100
200
300
400
500
600
700
800
Age Since Loading (Days)

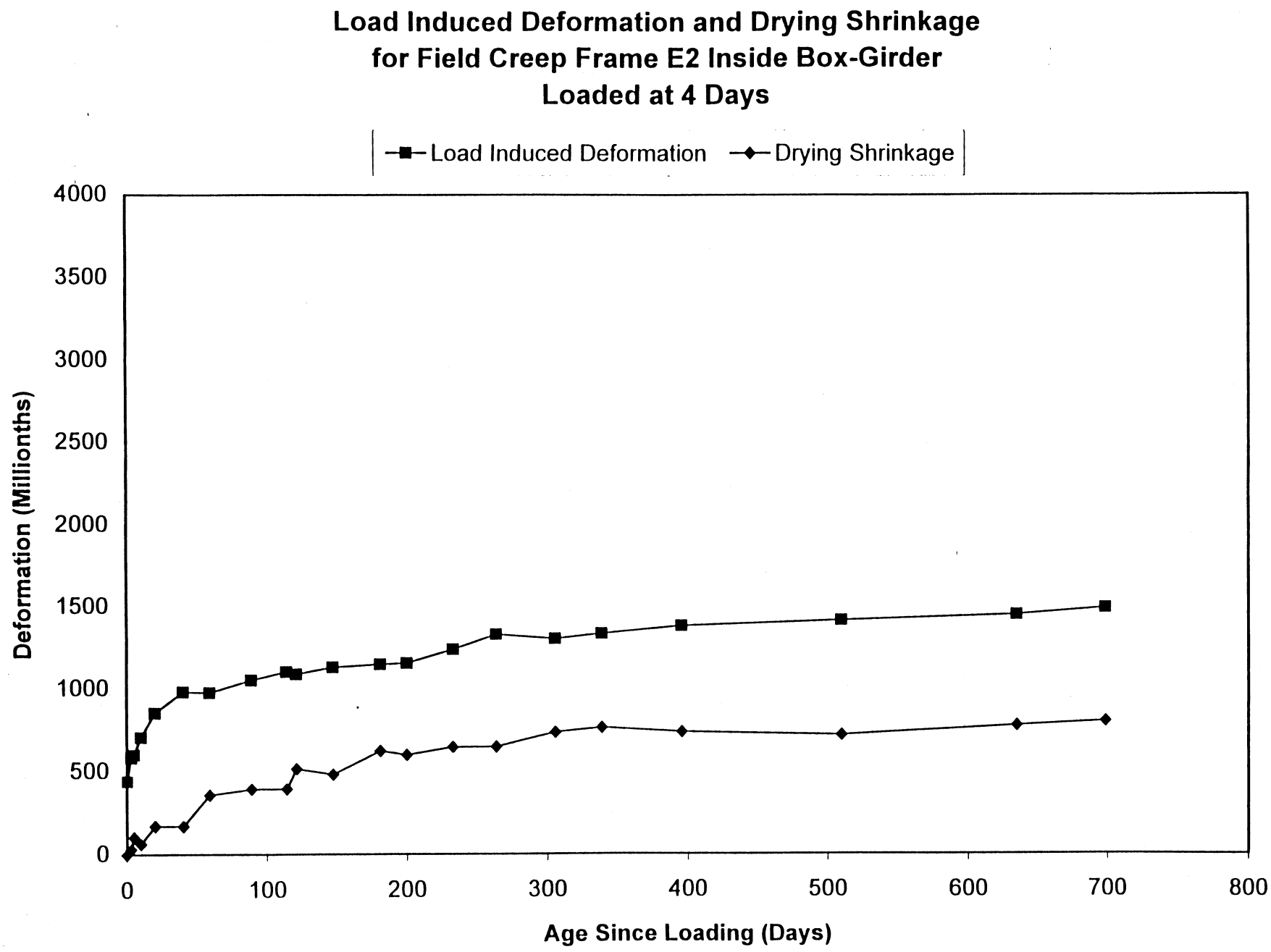
Load Induced Deformation and Drying Shrinkage
for Field Creep Frame E2 Inside Box-Girder
Loaded at 4 Days
Load Induced Deformation
Drying Shrinkage
Deformation (Millionths)
4000
3500
3000
2500
2000
1500
1000
500
0
0
100
200
300
400
500
600
700
800
Age Since Loading (Days)

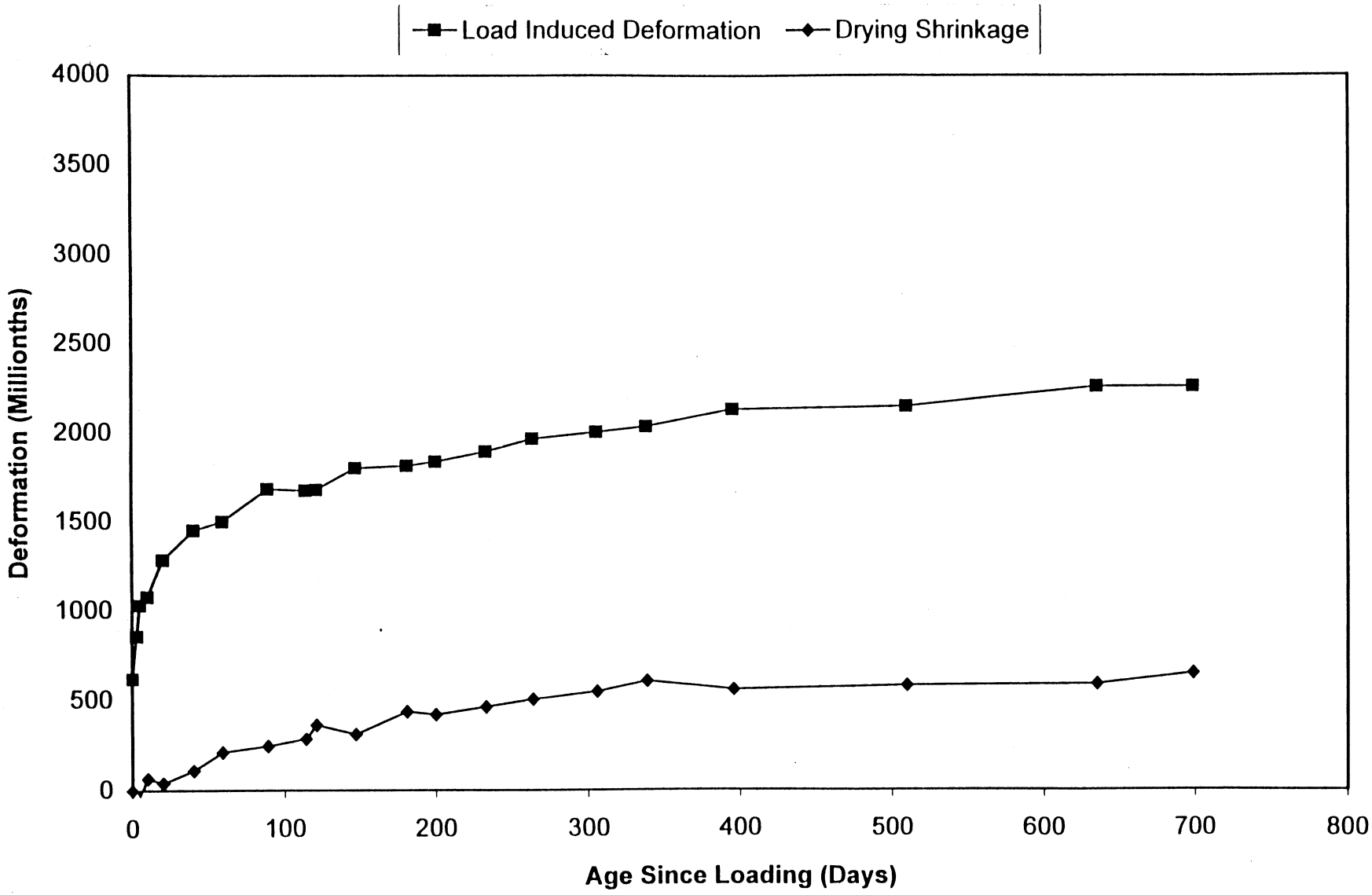
Load Induced Deformation and Drying Shrinkage
for Field Creep Frame E1 Inside Box-Girder
Loaded at 4 Days
Load Induced Deformation
Drying Shrinkage
Deformation (Millionths)
4000
3500
3000
2500
2000
1500
1000
500
0
0
100
200
300
400
500
600
700
800
Age Since Loading (Days)

Load Induced Deformation and Drying Shrinkage for Section G Loaded After 90 Days

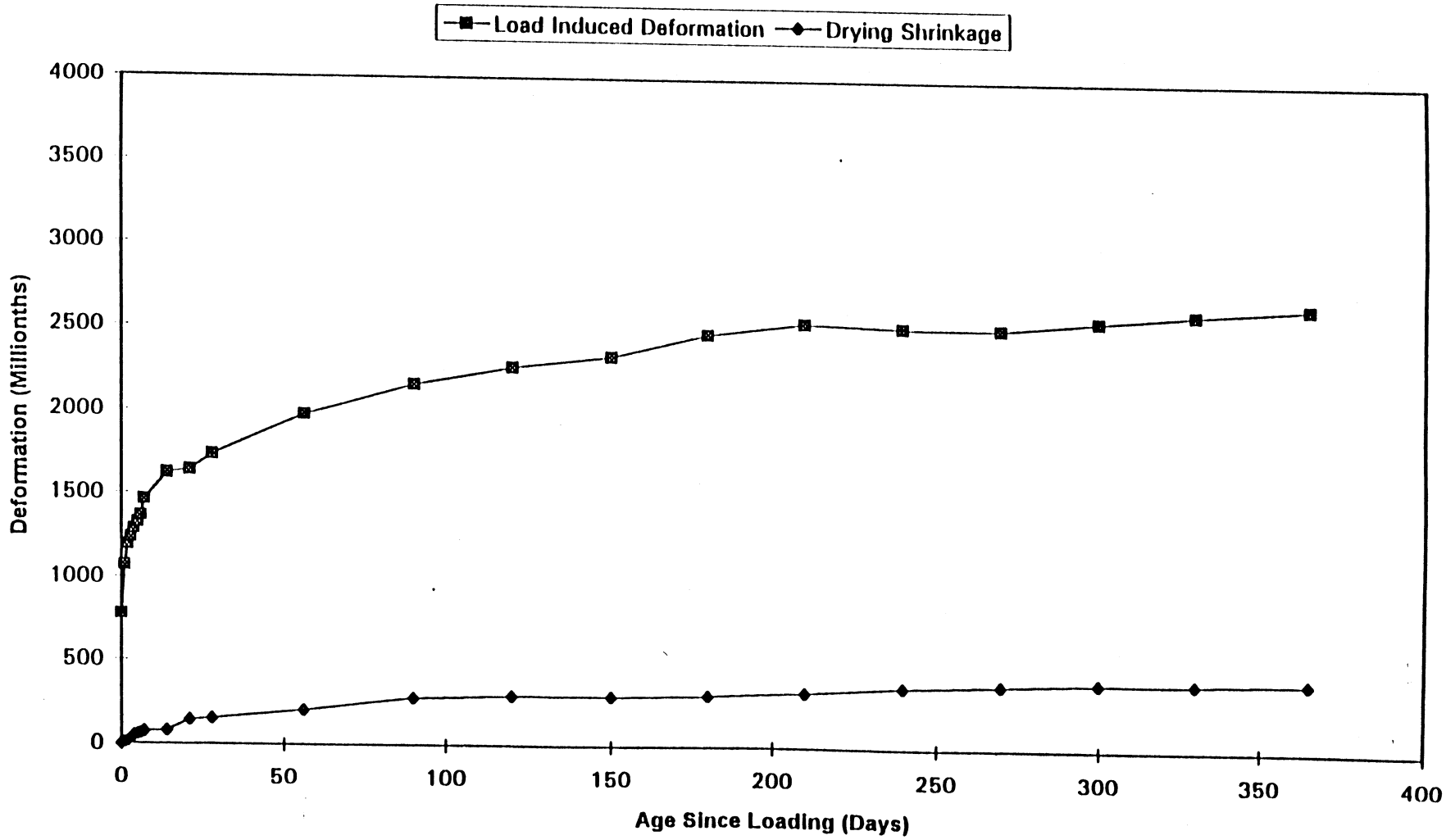

Load Induced Deformation and Drying Shrinkage for Section G Loaded After 28 Days

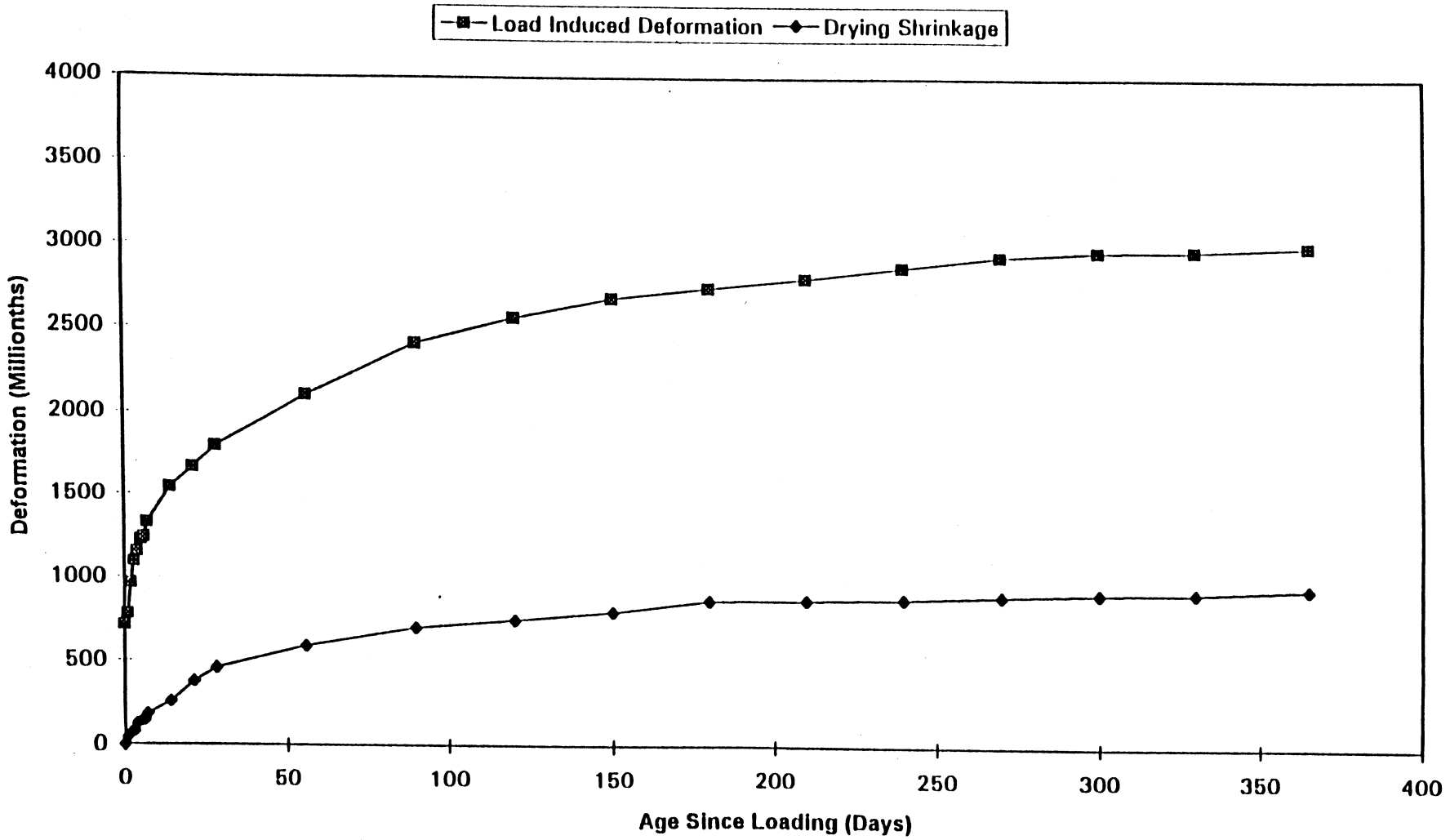

Load Induced Deformation and Drying Shrinkage for Section G Loaded After 3 Days

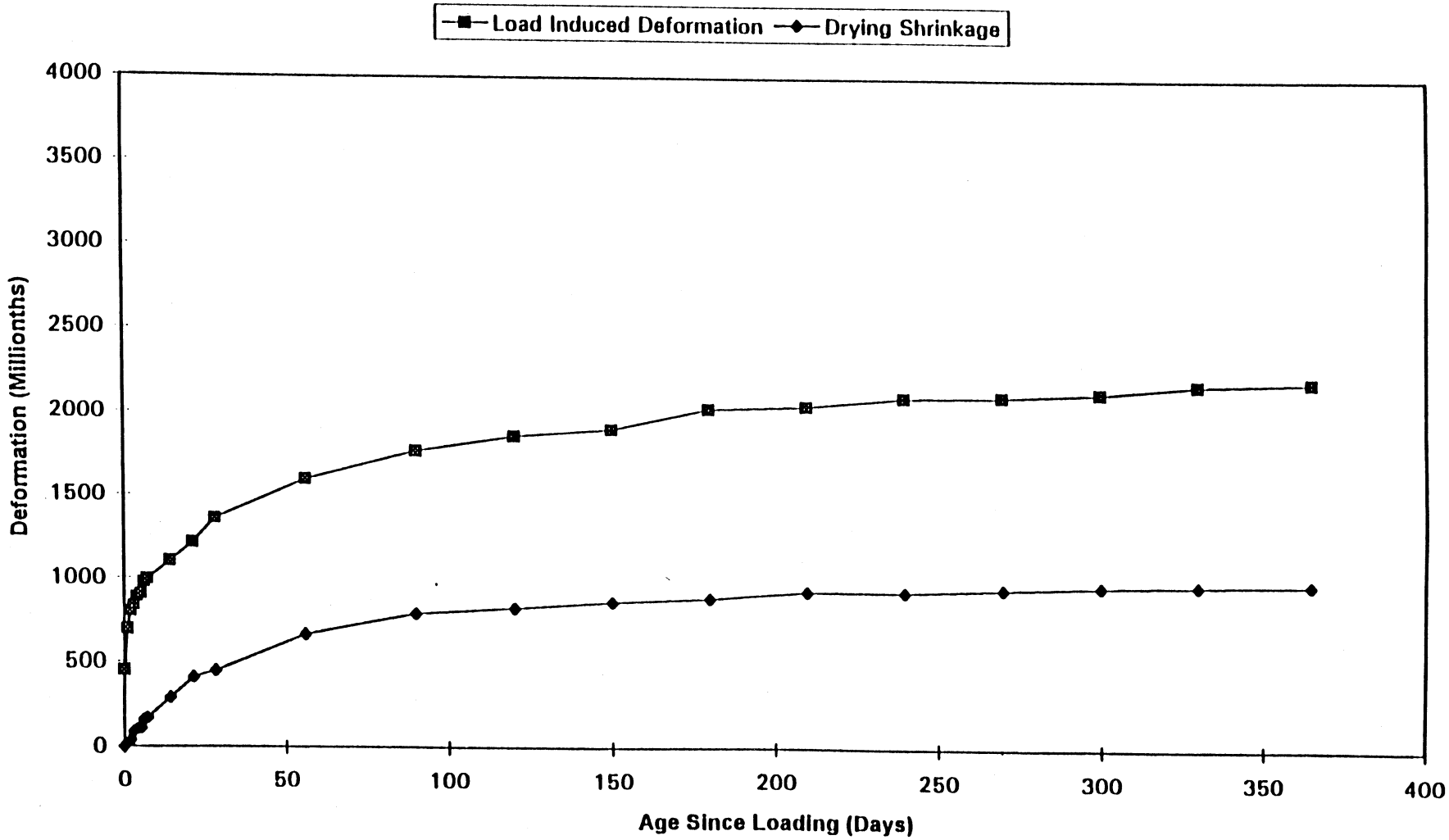

Load Induced Deformation and Drying Shrinkage for Section F Loaded After 90 Days

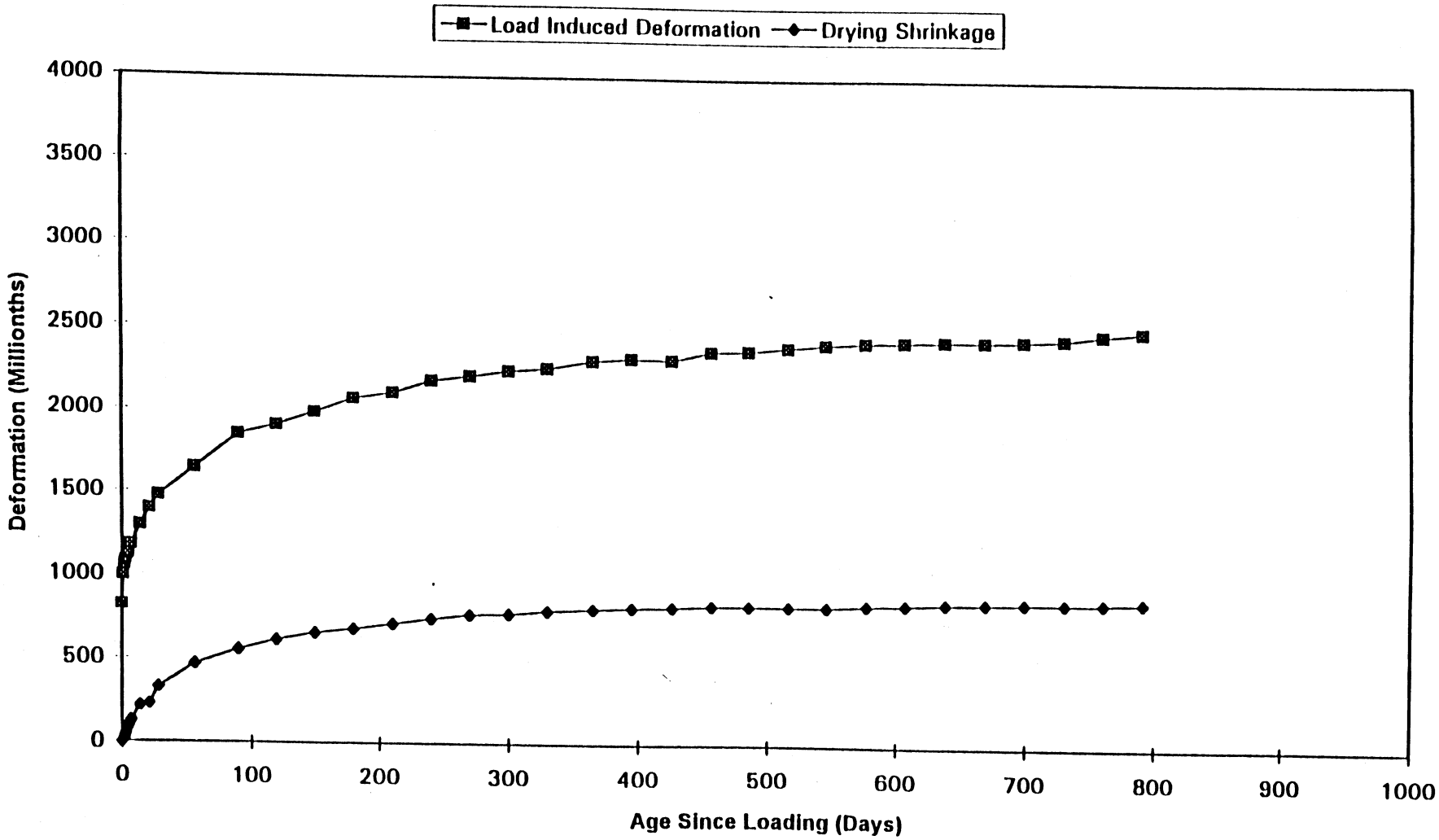

Load Induced Deformation and Drying Shrinkage for Section F Loaded After 28 Days

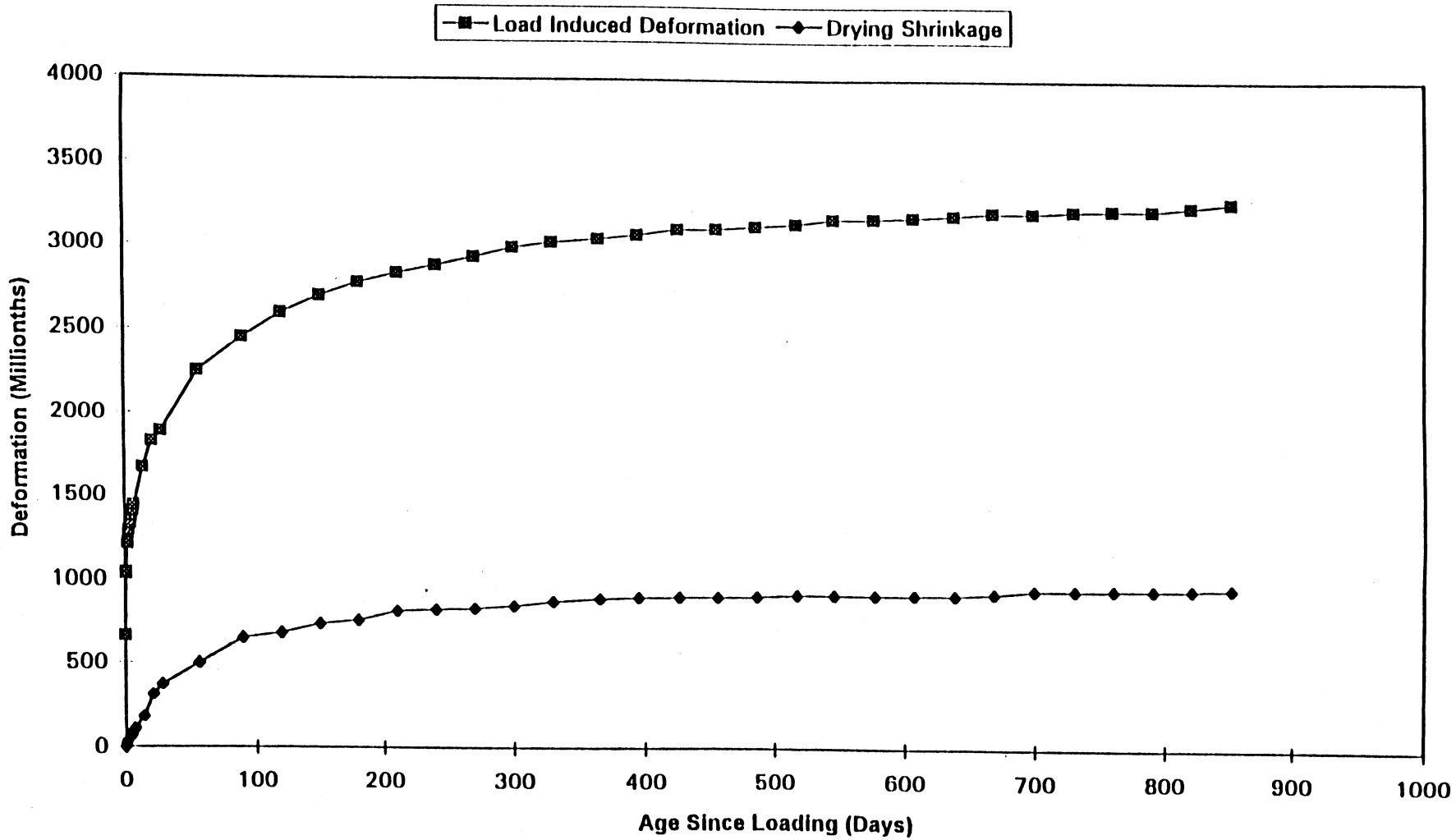

Load Induced Deformation and Drying Shrinkage for Section F Loaded After 3 Days

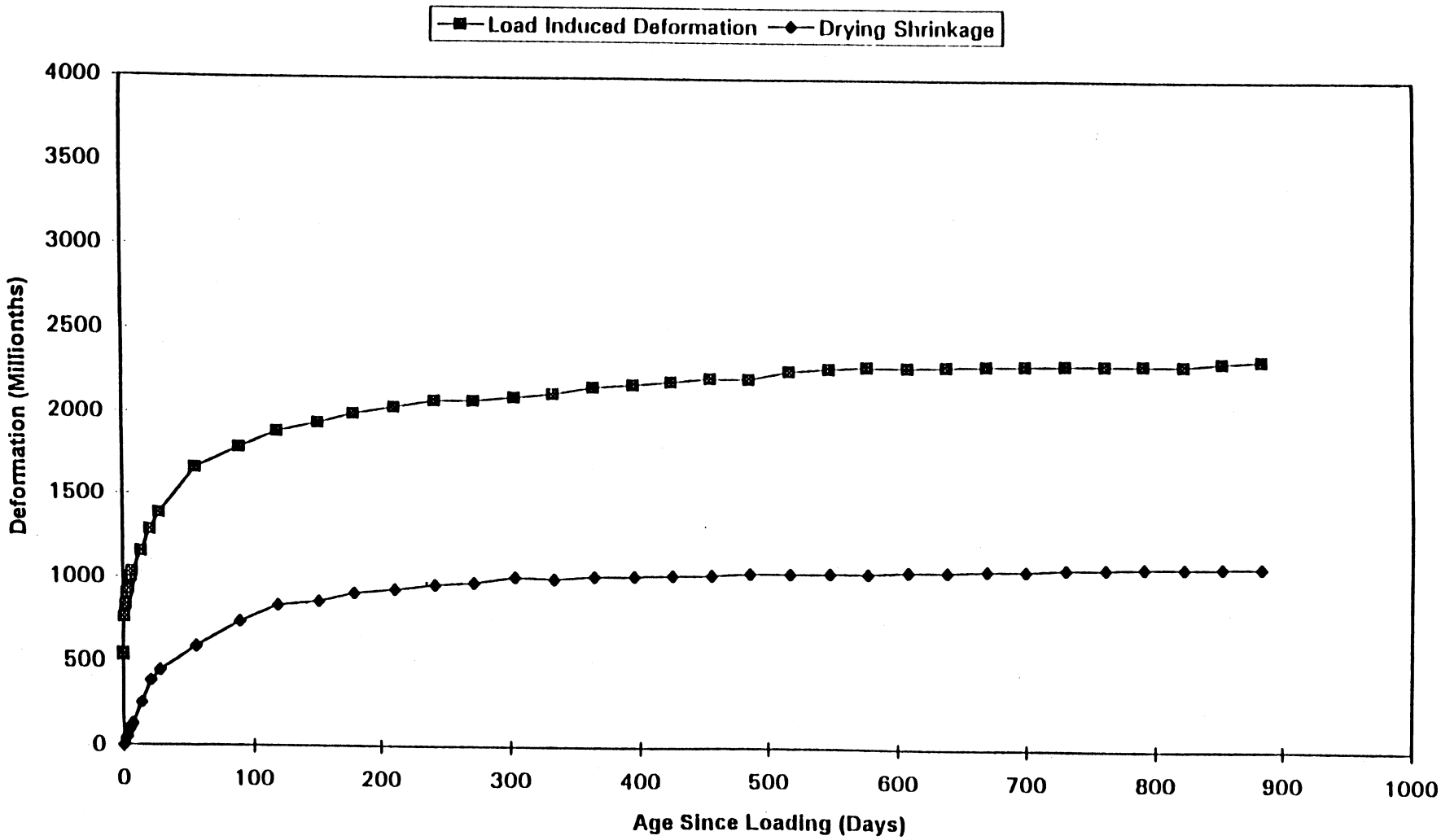

Load Induced Deformation and Drying Shrinkage for Section E Loaded After 90 Days

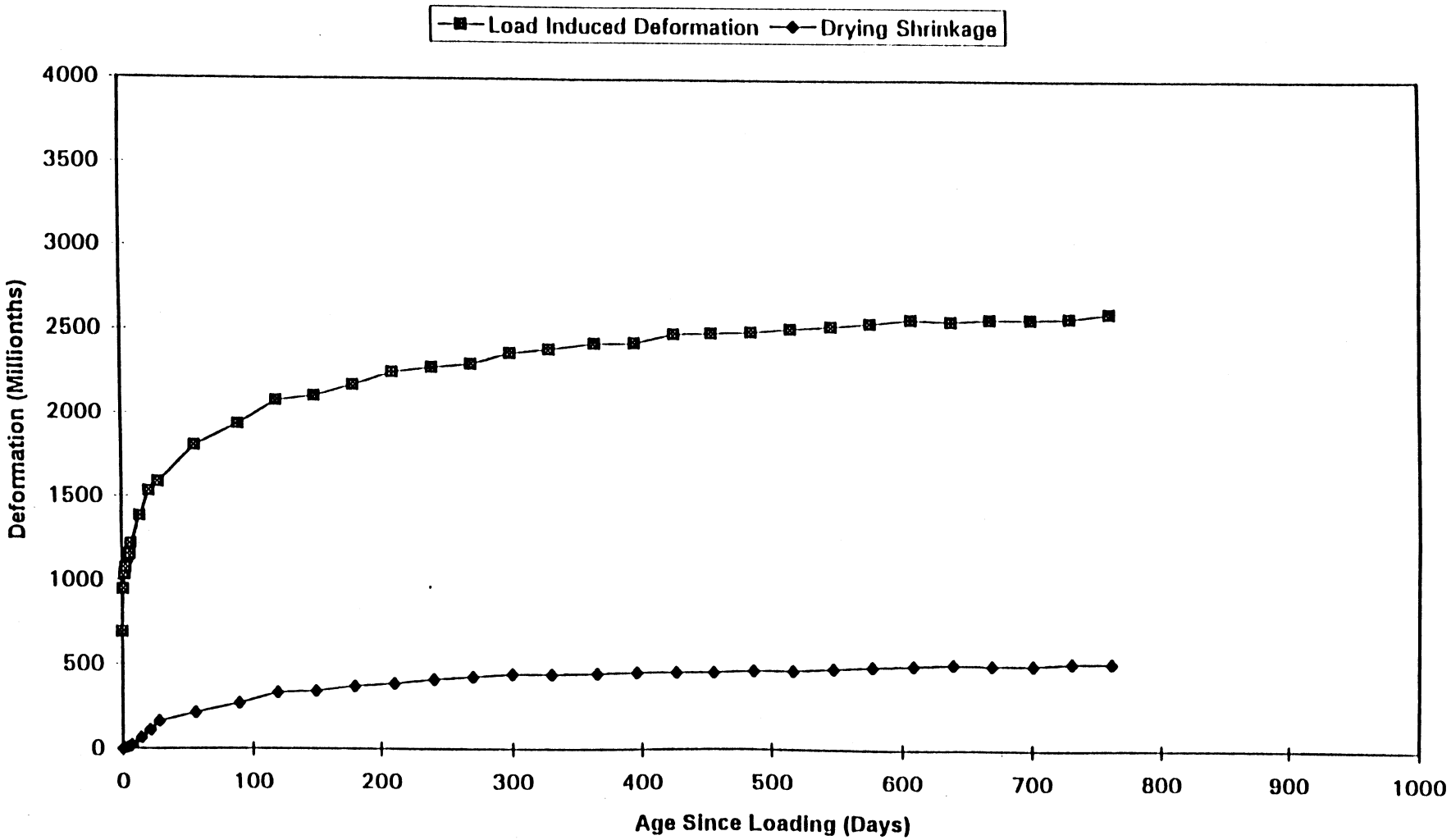

Load Induced Deformation and Drying Shrinkage for Section E Loaded After 28 Days

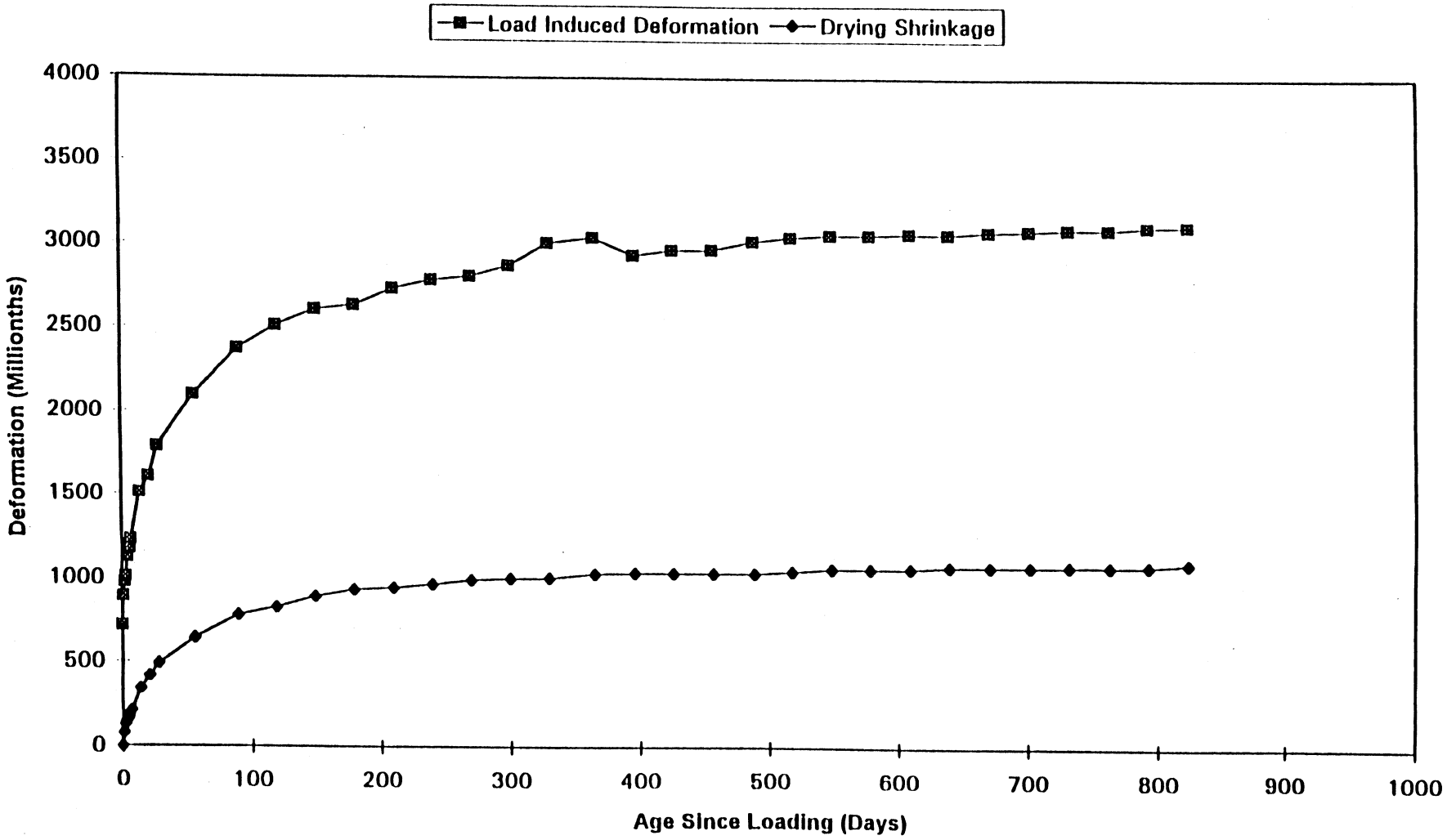

Load Induced Deformation and Drying Shrinkage for Section E Loaded After 3 Days

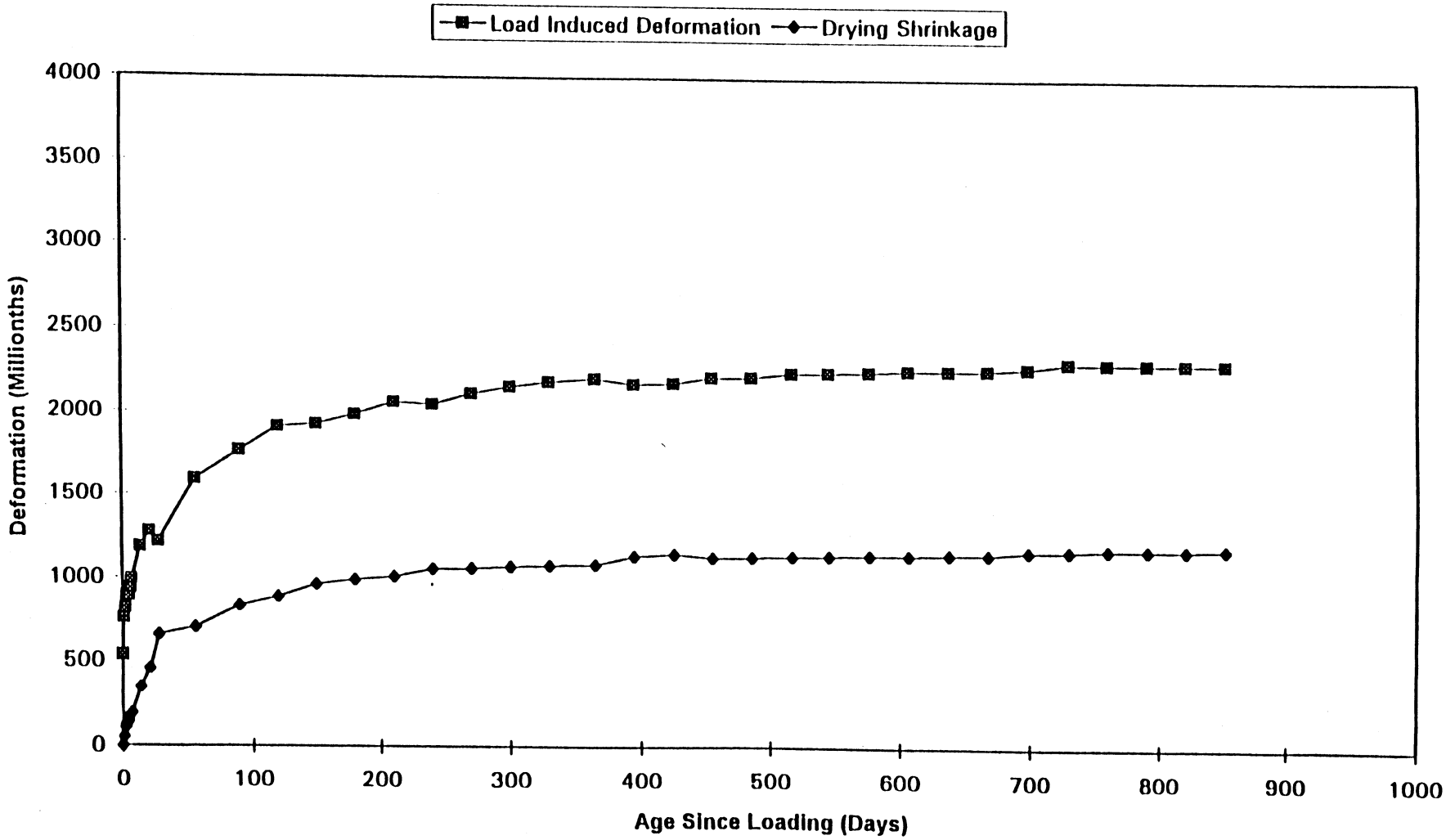

Load Induced Deformation and Drying Shrinkage for Section D Loaded After 90 Days

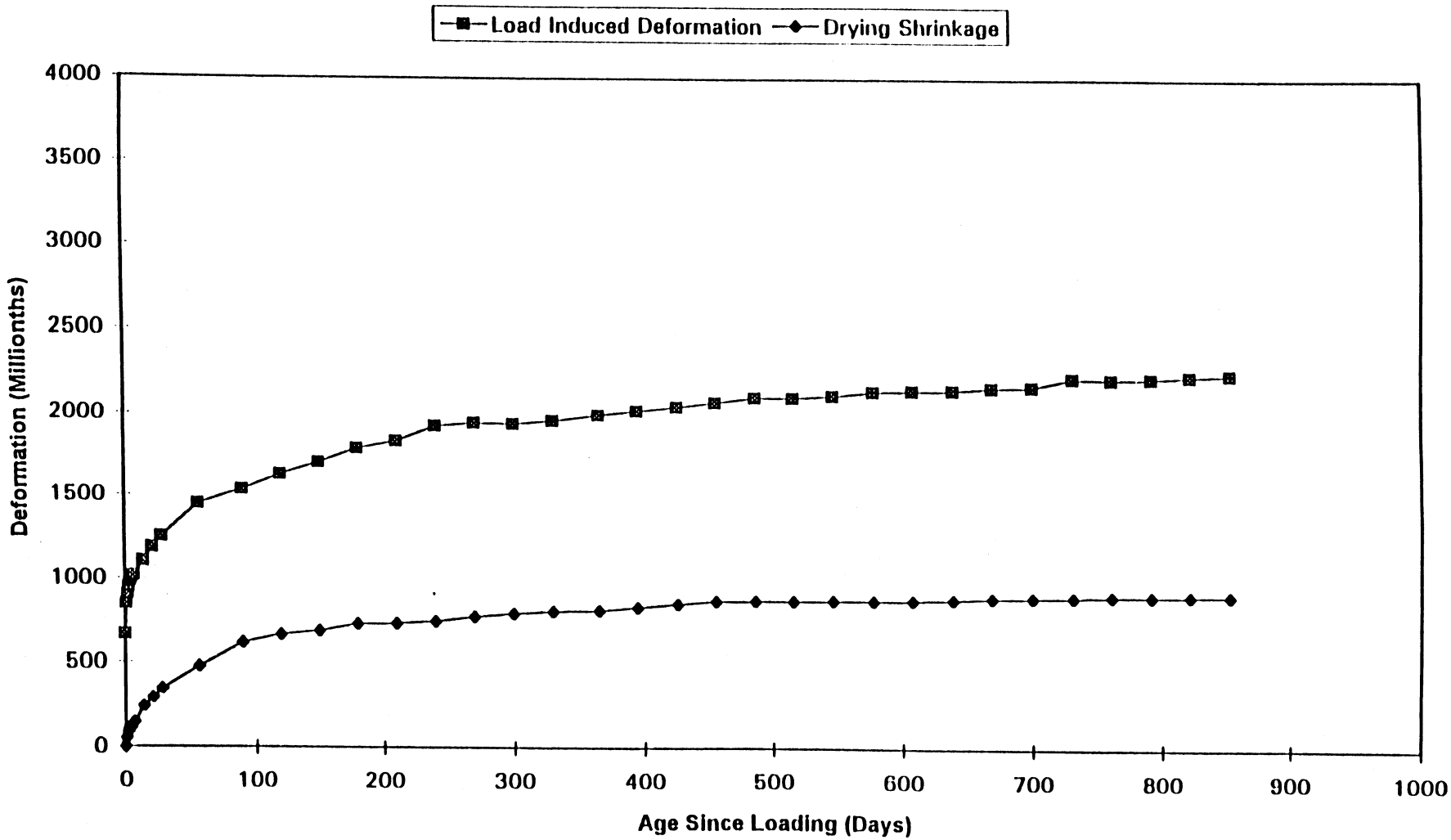

Load Induced Deformation and Drying Shrinkage for Section D Loaded After 28 Days

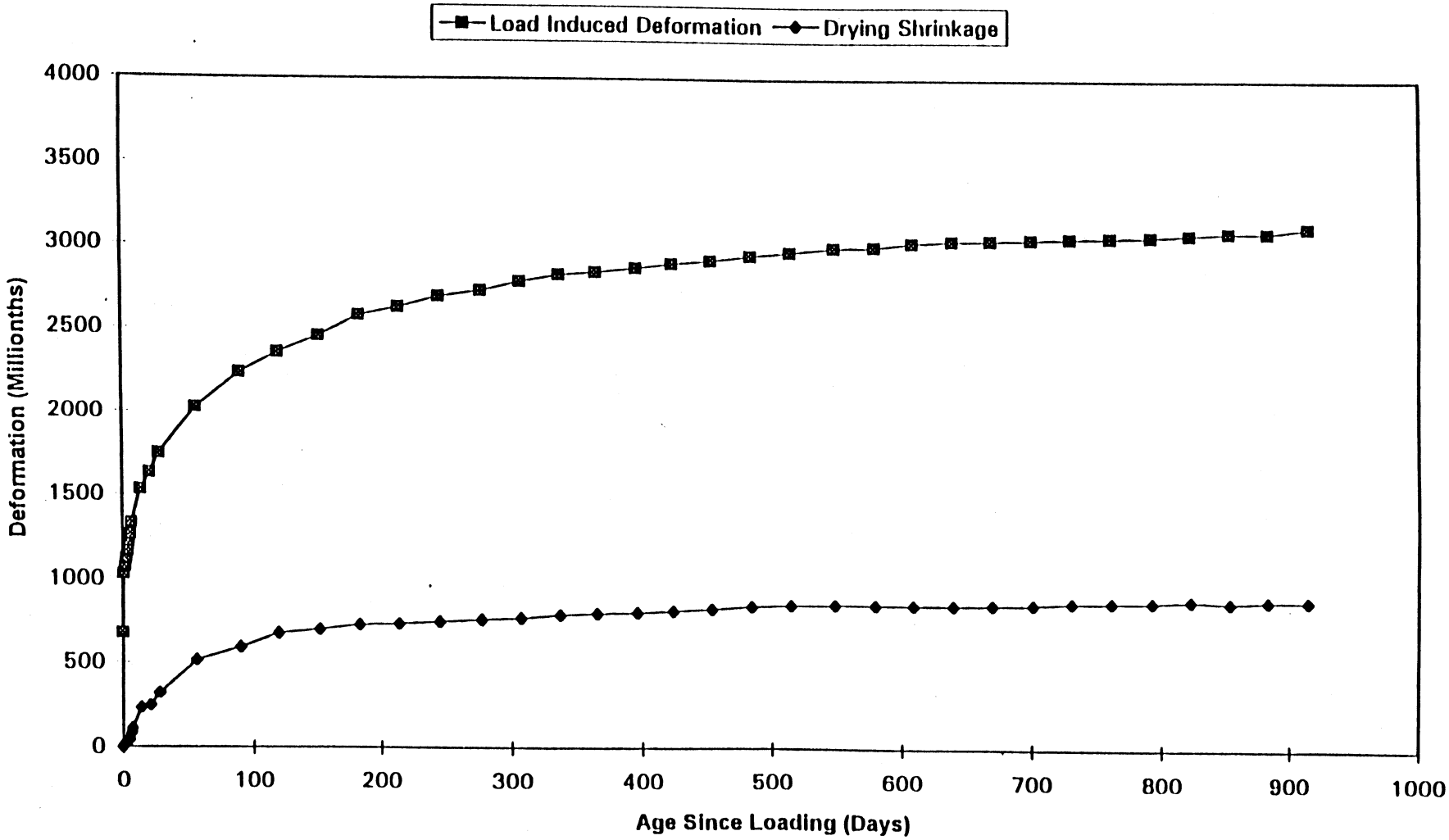

Load Induced Deformation and Drying Shrinkage for Section D Loaded After 3 Days

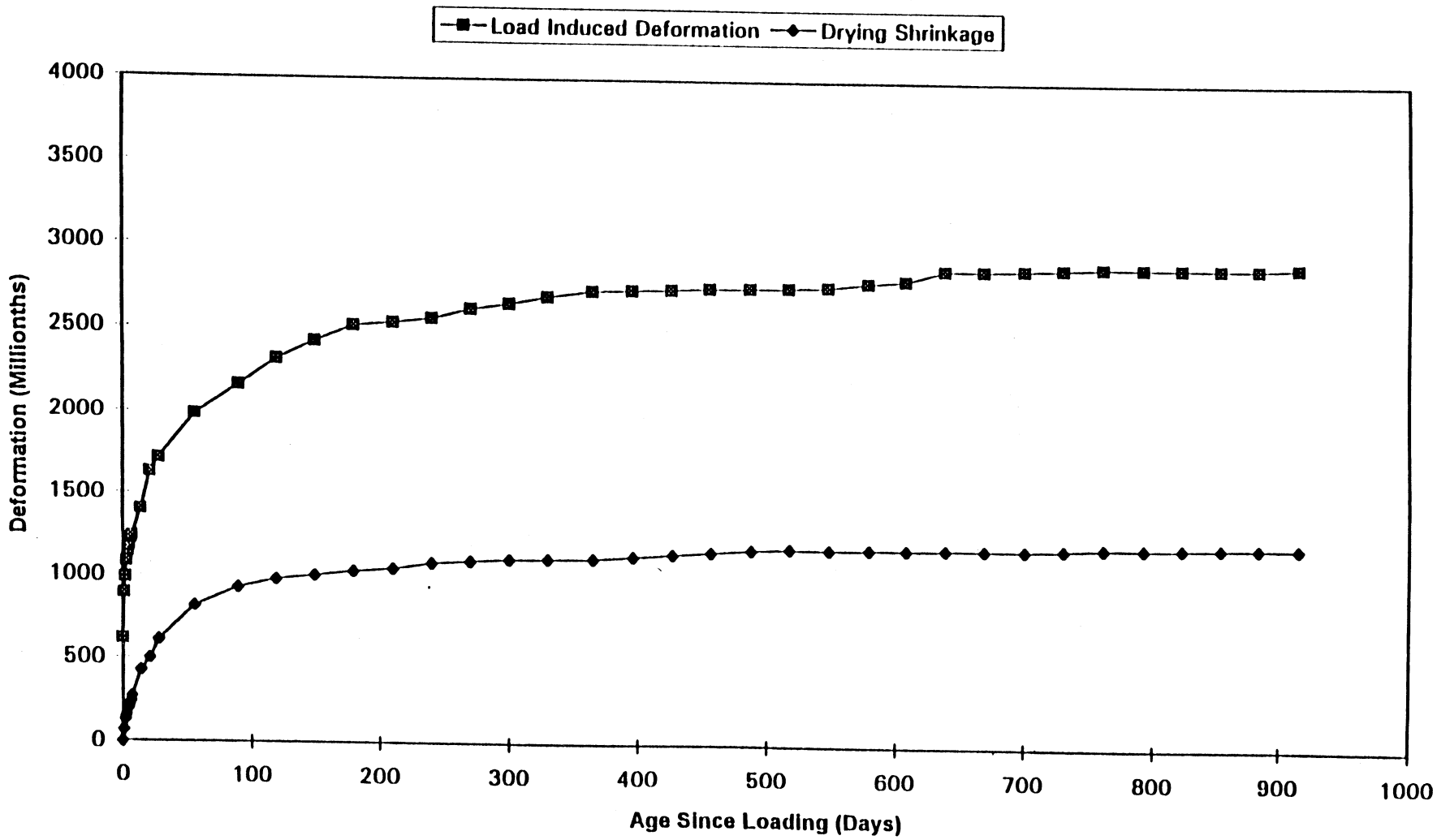

Load Induced Deformation and Drying Shrinkage for Section C Loaded After 90 Days

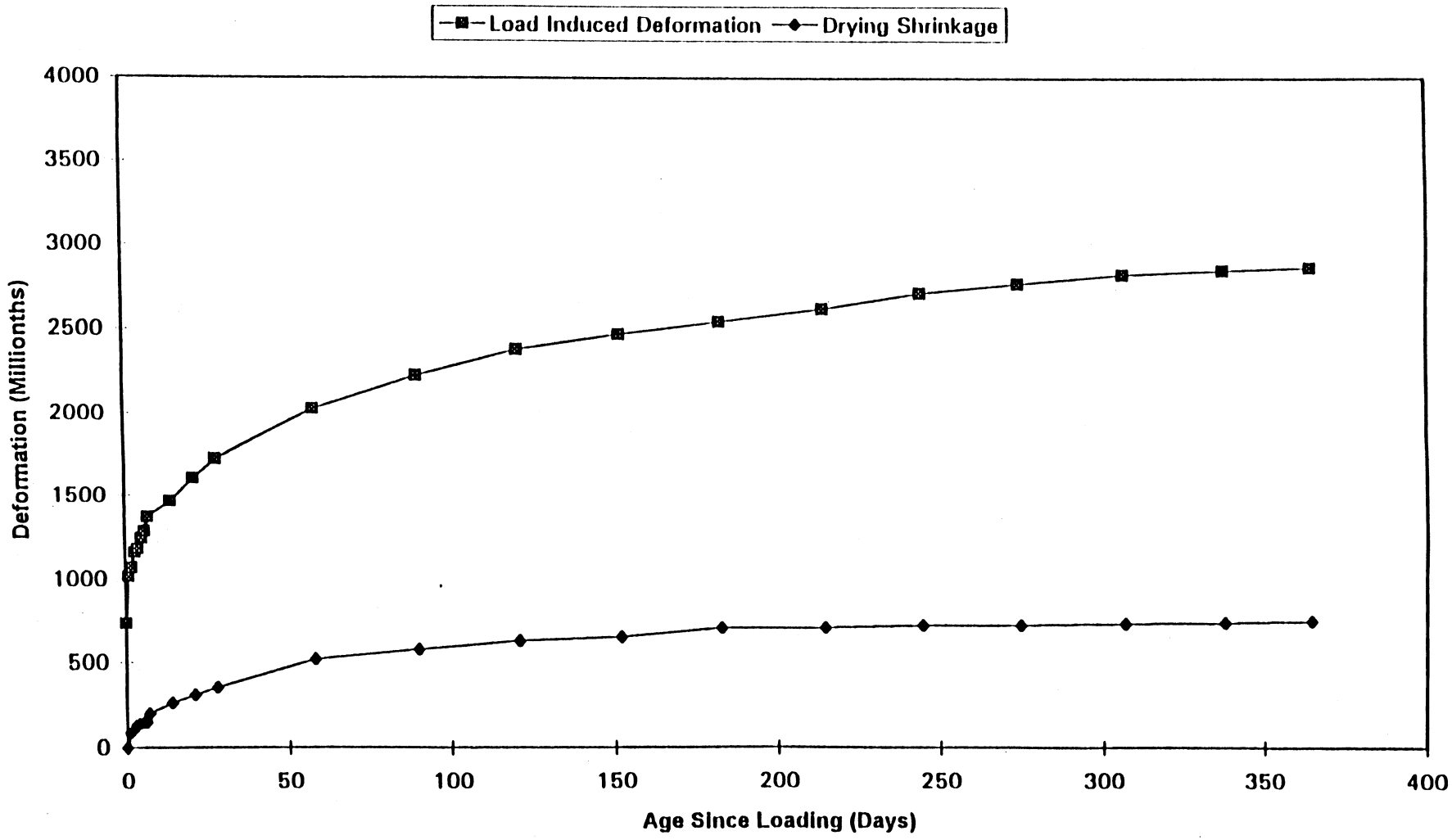

Load Induced Deformation and Drying Shrinkage for Section C Loaded After 28 Days

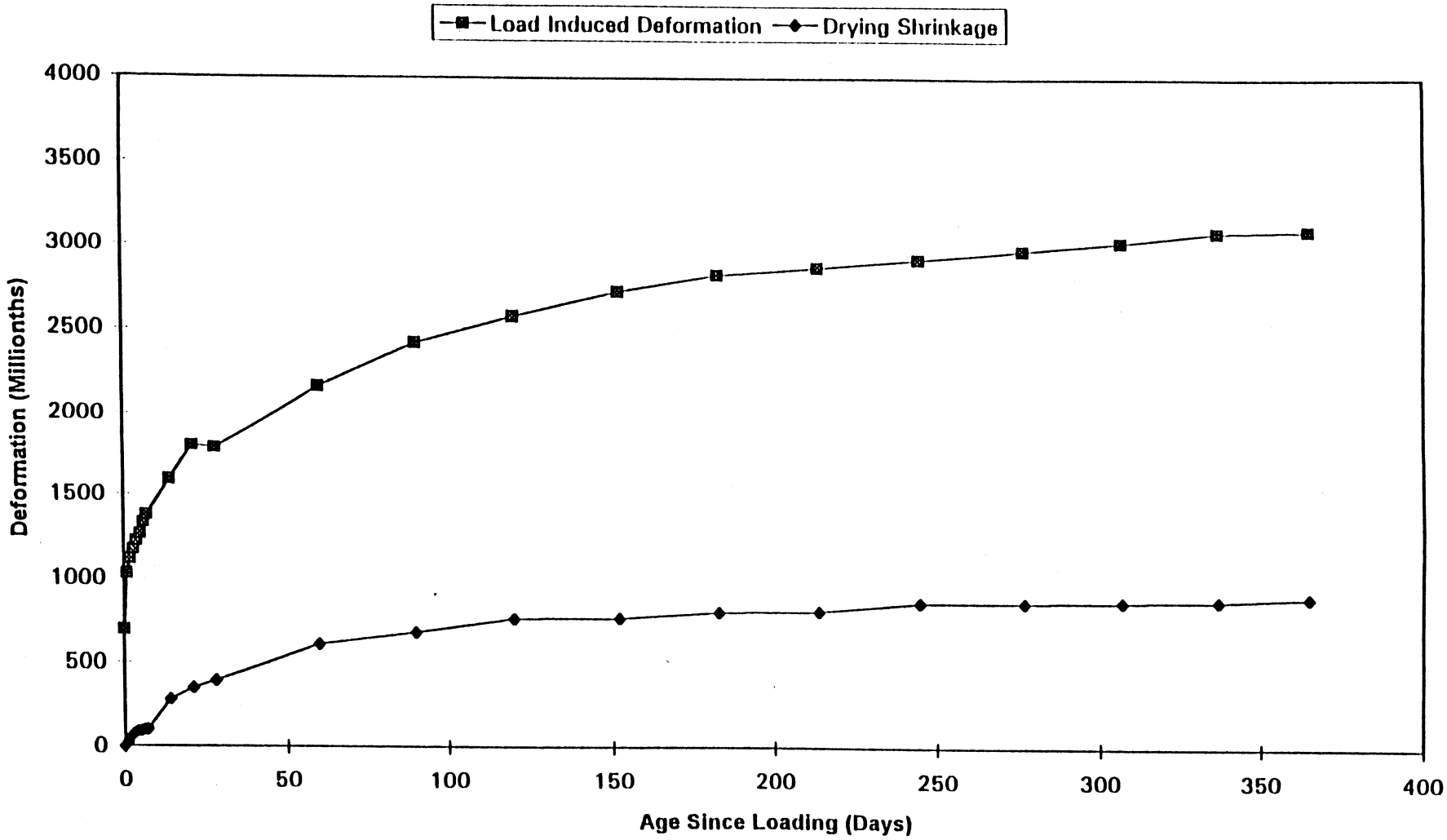

Load Induced Deformation and Drying Shrinkage for Section C Loaded After 3 Days

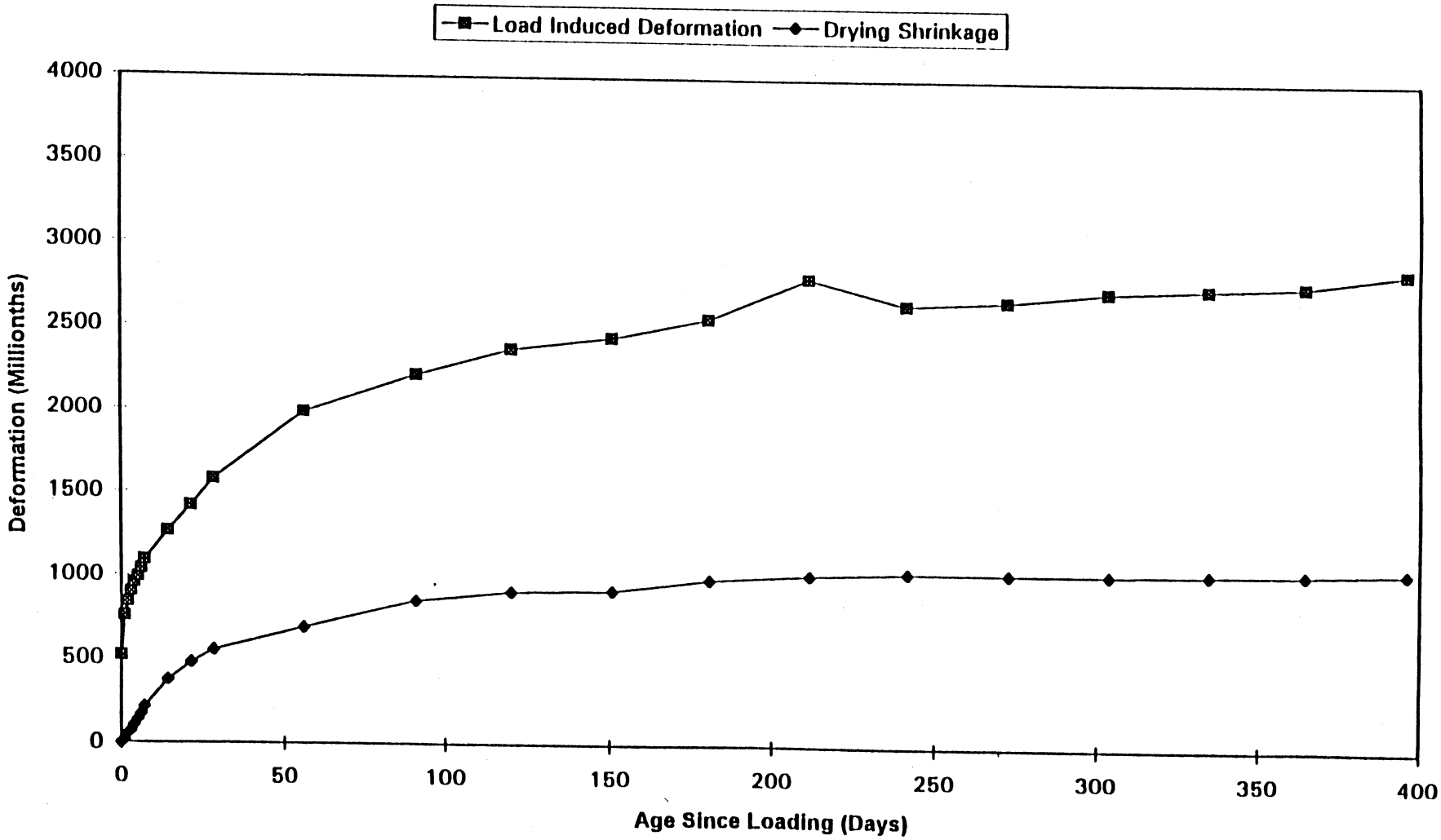

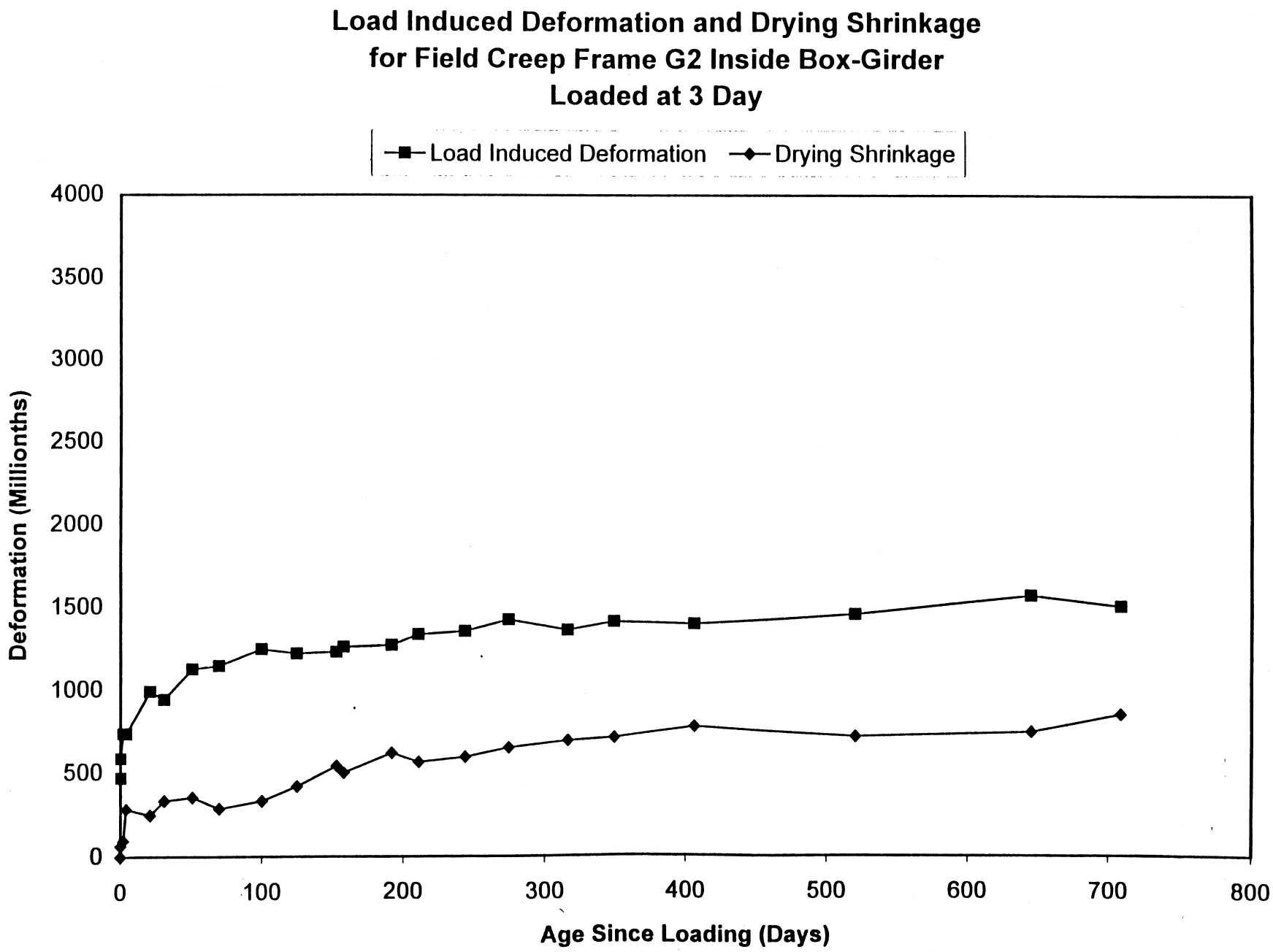
Load Induced Deformation and Drying Shrinkage
for Field Creep Frame G2 Inside Box-Girder
Loaded at 3 Day
Load Induced Deformation
Drying Shrinkage
Deformation (Millionths)
4000
3500
3000
2500
2000
1500
1000
500
0
0
100
200
300
400
500
600
700
800
Age Since Loading (Days)

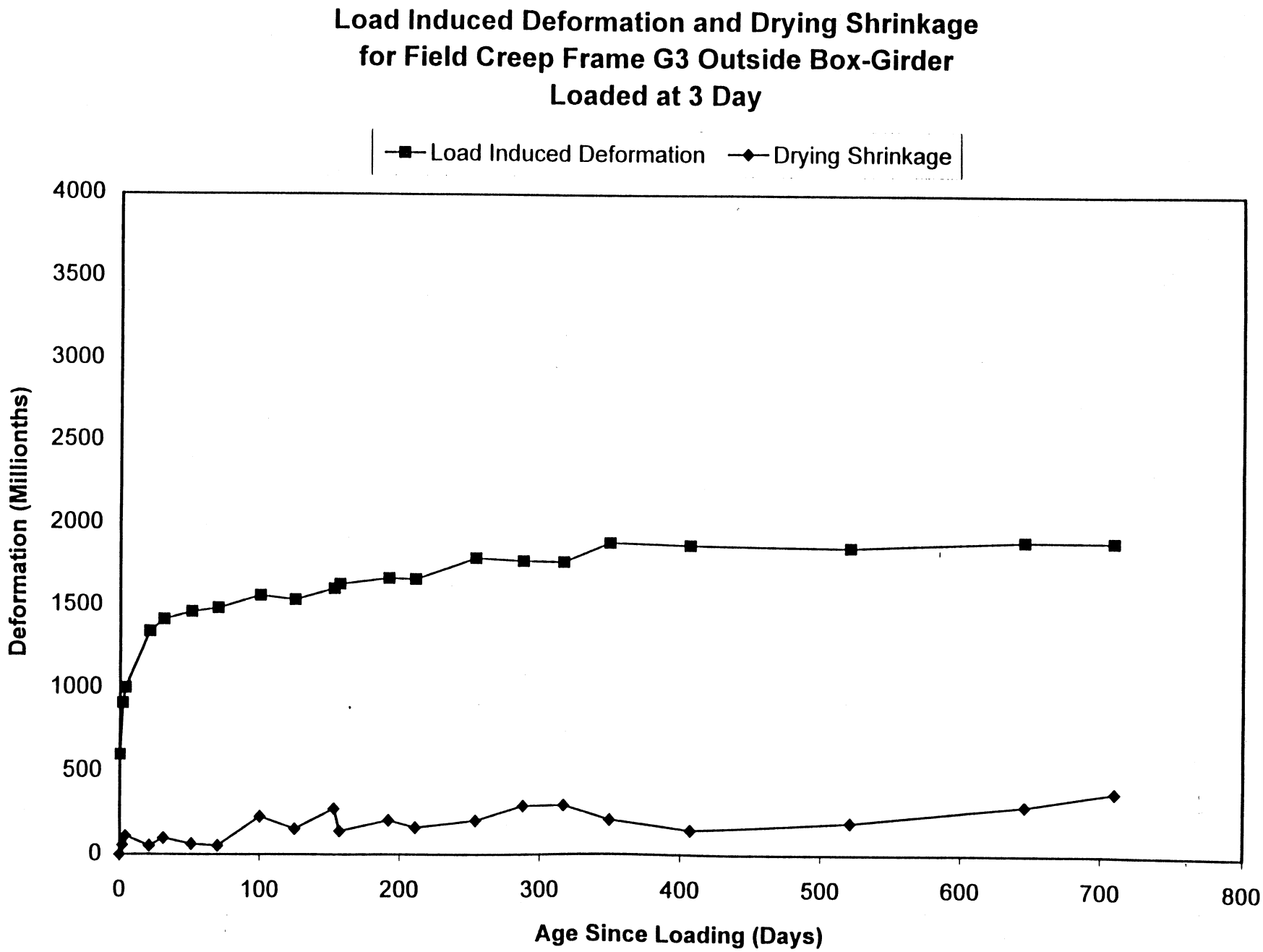
Load Induced Deformation and Drying Shrinkage
for Field Creep Frame G3 Outside Box-Girder
Loaded at 3 Day
Load Induced Deformation
Drying Shrinkage
Deformation (Millionths)
4000
3500
3000
2500
2000
1500
1000
500
0
0
100
200
300
400
500
600
700
800
Age Since Loading (Days)

CHAPTER 5

MATHEMATICAL MODELS FOR CREEP AND SHRINKAGE

5.1 Introduction

A number of material property tests were performed on the concrete used in this project. These tests included creep and shrinkage tests in the Construction Technology Laboratory (CTL). Tests were performed on concrete samples from each of the seven instrumented sections, with creep frames loaded at 3, 28 and 90 days age. Hence a total of 21 creep frames and associated shrinkage cylinders were established and maintained for one year. Certain of these frames were monitored for an additional two years.

This chapter presents the results of a comparison between the creep and shrinkage test data and four current prediction models. A procedure to predict long-term creep and shrinkage based on short-term laboratory test results is presented and evaluated using the CTL test results. A more extensive presentation of the models, comparison, and prediction procedure is available in Durbin and Robertson (1998).

5.2 Laboratory Test Results

5.2.1 Creep Results

Figures 5.1 through 5.3 present the CTL measured creep values for concrete samples loaded at 3 days, 28 days and 90 days of age, respectively. Each figure displays creep values for sections A through G, as well as the average value. Sections A, B, C, and G have been plotted for a period of 1 year, at which time these tests were discontinued. Sections D, E, and F have been plotted for approximately 800 days.

Creep values are expressed as specific creep (creep strain per unit stress). Table 5.1 lists the value of average specific creep for the 3 day, 28 day, and 90 day samples along with the corresponding creep coefficients after one year of loading.

Table 5.1: Average creep values for one year of loading

Age at Loading	Age (days)	Days Loaded	Creep/psi (Ave.) ($in^2/lb \times 10^6$)	Creep Coefft. (Ave)
3 Days	368	365	1.147	3.654
28 Days	393	365	0.917	3.324
90Days	455	365	0.686	2.633

For a loading age of 365 days, it can be seen from Table 5.1 that the average creep coefficient for the 3-day loaded samples is 3.654. This value decreases by 9% for the 28-day loaded samples, and by 28% for the 90-day loaded samples.

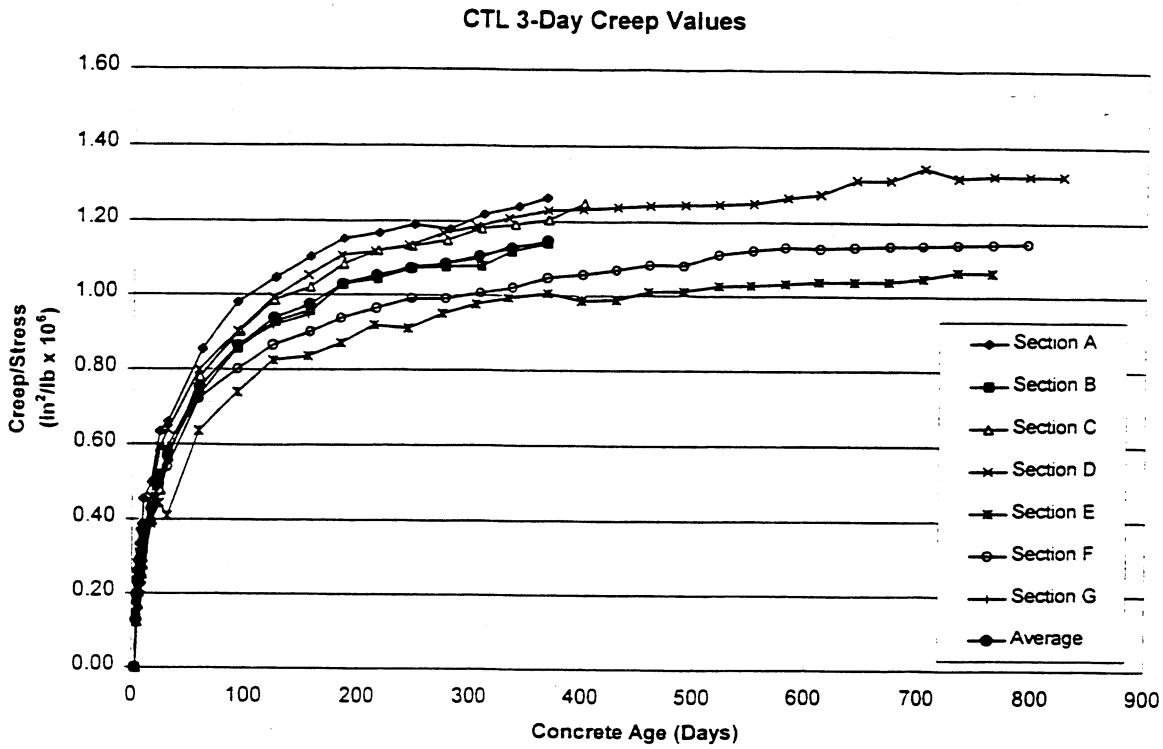

Figure 5.1: CTL laboratory creep for 3-day loading.

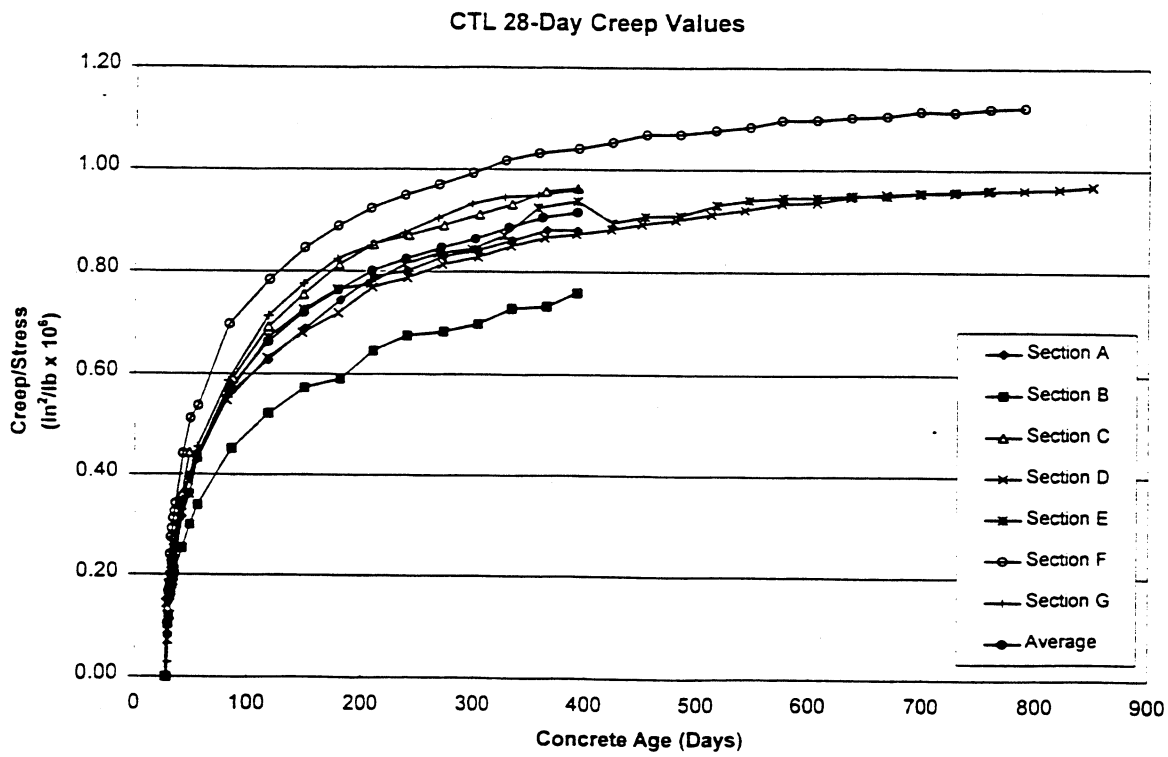

Figure 5.2: CTL laboratory creep for 28-day loading

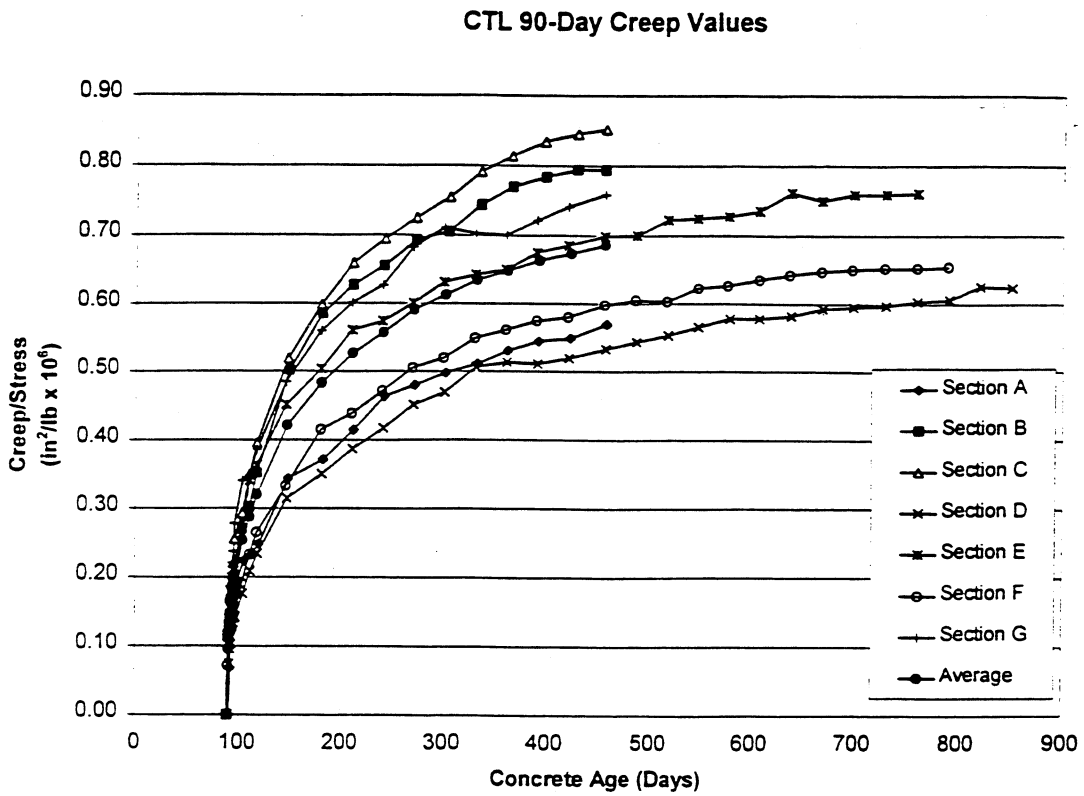

Figure 5.3: CTL laboratory creep for 90-day loading

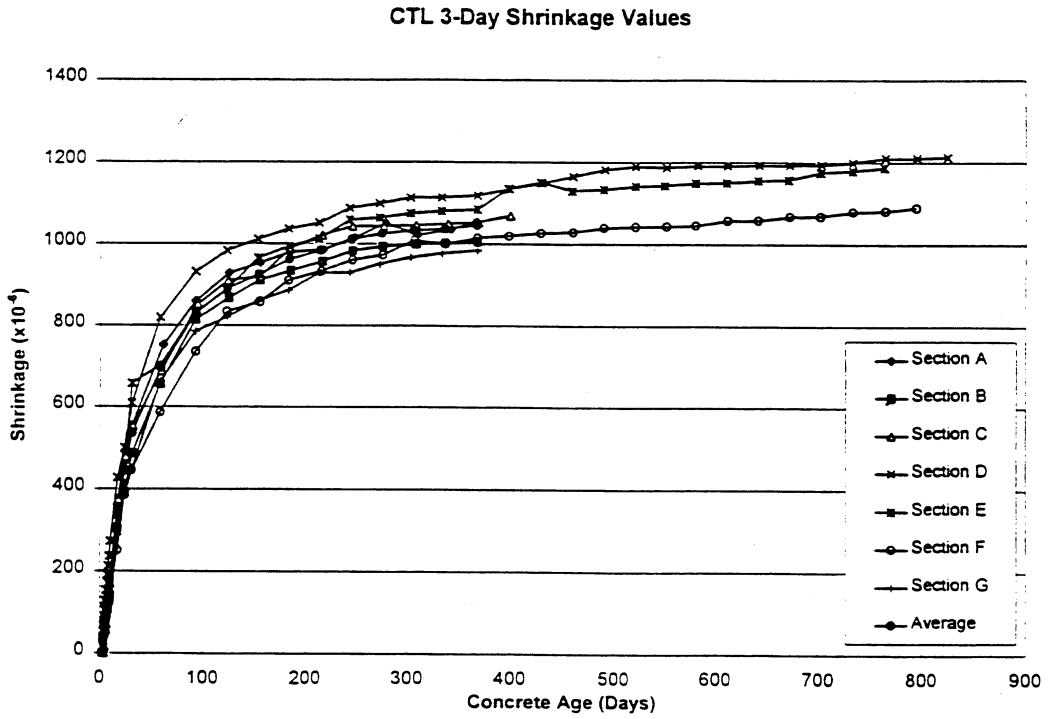

Figure 5.4: CTL laboratory Shrinkage for drying from 3-days

5.2.2 Shrinkage Results

Figure 5.4 presents the CTL measured shrinkage values of the companion shrinkage cylinders corresponding to the 3-day creep cylinders. Only these shrinkage results are reported, since the initial start of drying for the 28-day and 90-day shrinkage companion cylinders was not recorded.

The plot shows shrinkage values for sections A through G, as well as the average value. As with the creep cylinders, sections A, B, C, and G have been recorded for a period of one year, while sections D, E, and F have been recorded for approximately 800 days.

Shrinkage values are expressed in microstrain. Table 5.2 lists the average value of shrinkage for the 3-day cylinders.

Table 5.2: Average 3-day shrinkage value for one year of drying.

Age at Loading	Age (days)	Days Drying	Shrinkage ($\mu\varepsilon$)
3 Days	368	365	1045

5.3 Creep and Shrinkage Prediction Models

Numerous analytical models have been developed to predict the long-term creep and shrinkage of plain concrete. In this study, four analytical models are investigated and compared with the results of the CTL tests. These four models are the current ACI 209 model (ACI 209R-92, 1992), the CEB-FIP Model Code 90 (CEB, 1993), the Bazant Model BP (Short Form) (Bazant and Baweja, 1996), and the Gardner Model (Gardner and Zhou, 1993). The Bazant and Gardner models are currently under consideration by ACI committee 209 as possible replacements for the current ACI 209 model.

Figures 5.5 through 5.7 compare the CTL average values and the predictive model values for concrete samples loaded at 3 days, 28 days, and 90 days, respectively. Each figure displays creep values for loading periods of one year.

5.3.1 Creep Comparison for 3-day loading

Referring to Figure 5.5 and Table 5.3, it is seen that all of the predictive models fall well short of estimating creep values over the period of loading. At one year of loading, the Gardner model best approaches the test data values, followed by the CEB-FIP and Bazant models. ACI 209 produces the lowest results.

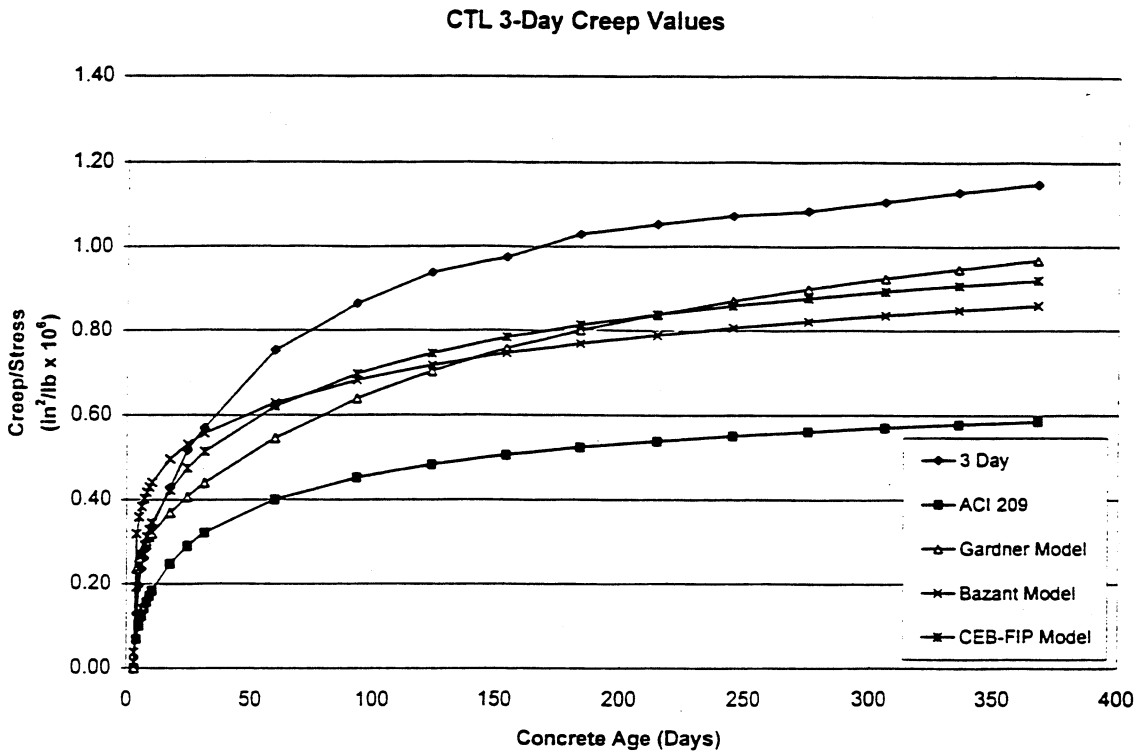

Figure 5.5: Creep Predictive Models for 3-day loading

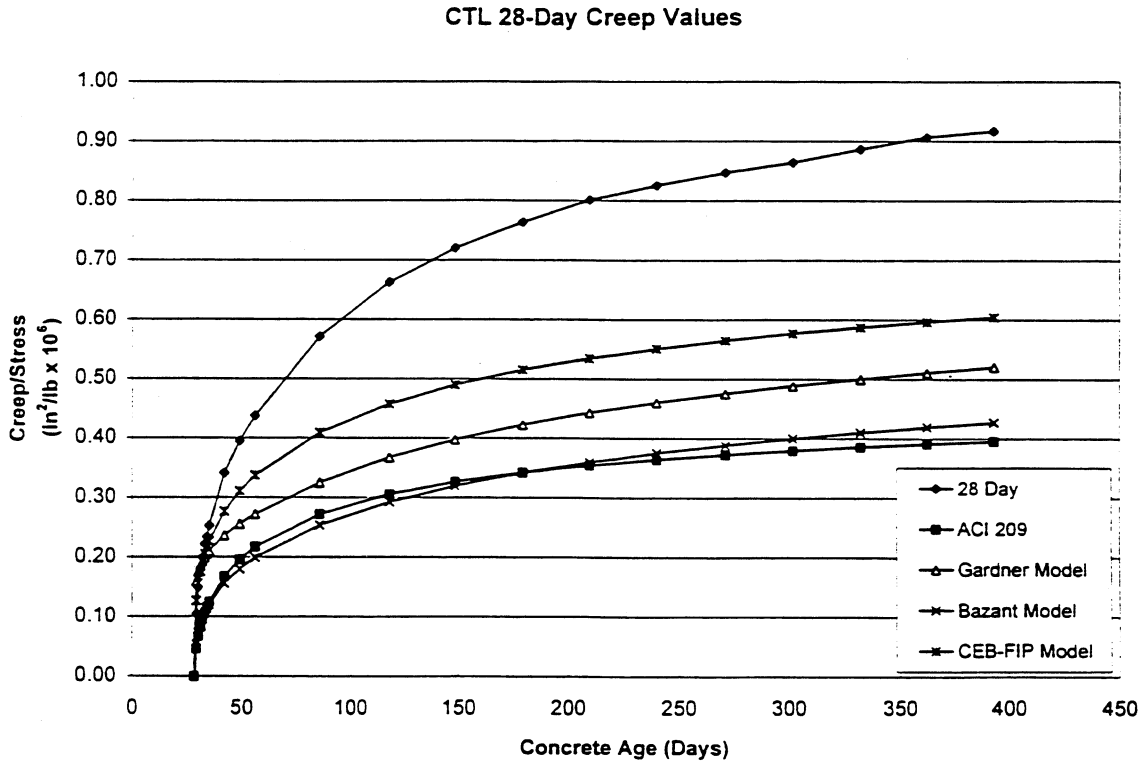

Figure 5.6: Creep Prediction Models for 28-day loading

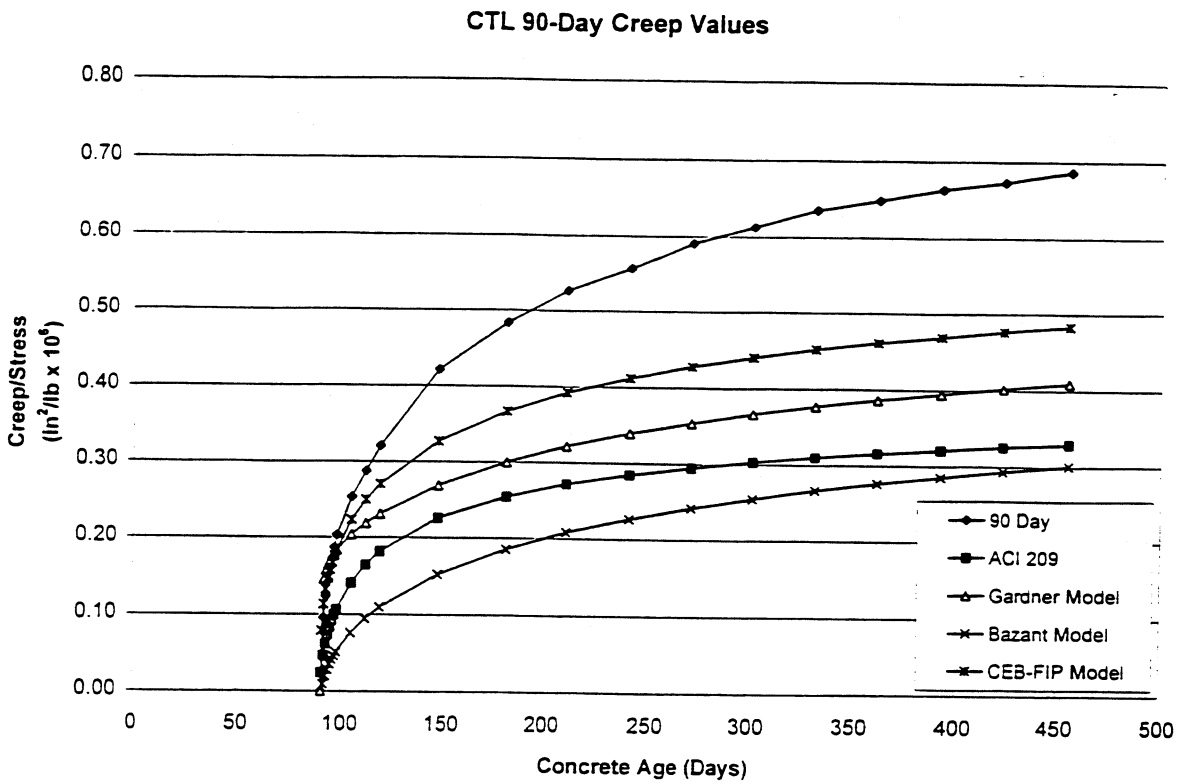

Figure 5.7: Creep Prediction Models for 90-day loading

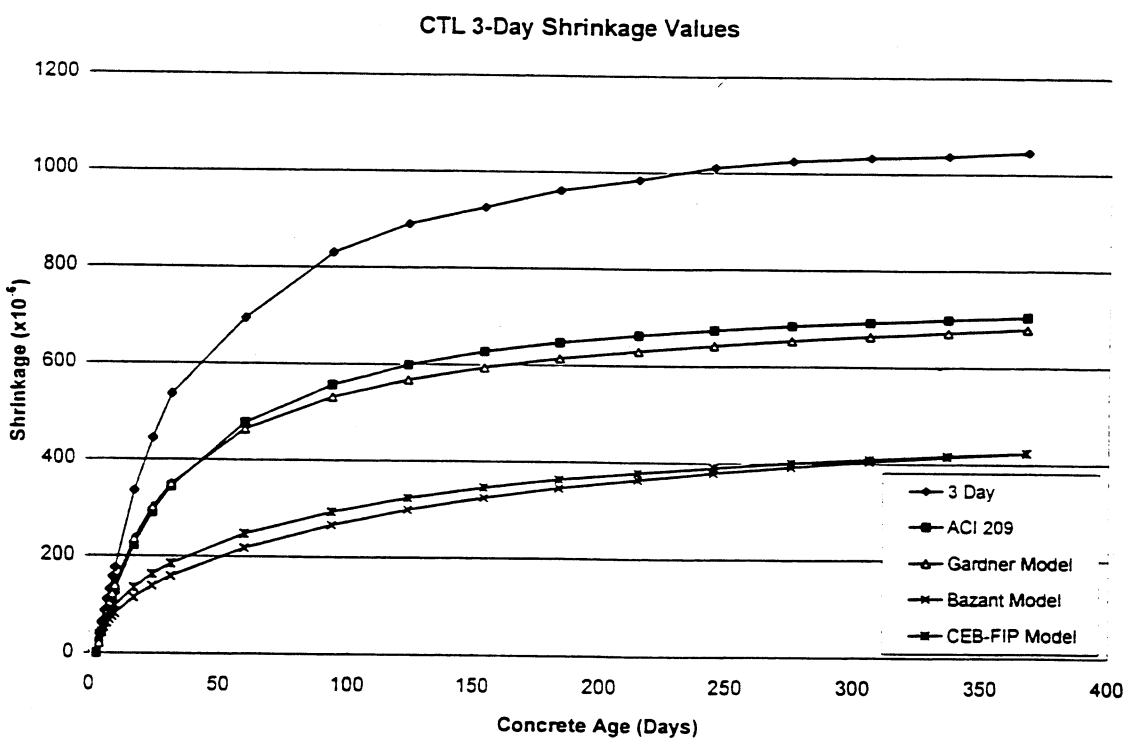

Figure 5.8: Shrinkage Prediction Models for 3-day drying age

Table 5.3: 3-Day Creep values for one year of loading

Data Type	Age (Days)	Days Loaded	Creep/psi ($in^2/lb \times 10^6$)	Creep Coefficient
CTL Data	368	365	1.147	3.654
ACI 209	368	365	0.585	1.882
CEB-FIP	368	365	0.919	2.956
Bazant Model	368	365	0.859	2.763
Gardner Model	368	365	0.967	3.110

5.3.2 Creep Comparison for 28-day loading

Referring to Figure 5.6 and Table 5.4, it is seen that the difference between the test data and the predictive models is even greater for the 28-day loading age. While both the test data and the predictive models yield lower creep values than the 3-day results, as expected, the test data creep values are still far higher than the values predicted by the various models. The CEB-FIP model most closely approximates the test data, followed by the Gardner, Bazant and ACI 209 models.

Table 5.4: 28-Day Creep values for one year of loading

Data Type	Age (Days)	Days Loaded	Creep/psi ($in^2/lb \times 10^6$)	Creep Coefficient
CTL Data	393	365	0.917	3.324
ACI 209	393	365	0.396	1.438
CEB-FIP	393	365	0.604	2.193
Bazant Model	393	365	0.427	1.550
Gardner Model	393	365	0.520	1.888

5.3.3 Creep Comparison for 90-day loading

As in the case of the 3-day and 28-day tests, none of the predictive models produce results that closely approximate the 90-day test data as shown in Figure 5.7 and Table 5.5. As for the 28-day data, the CEB-FIP model most closely approximates the test data, followed by the Gardner, ACI 209, and Bazant models.

Table 5.5: 90-Day Creep values for one year of loading

Data Type	Age (Days)	Days Loaded	Creep/psi ($in^2/lb \times 10^6$)	Creep Coefficient
CTL Data	455	365	0.686	2.633
ACI 209	455	365	0.329	1.263
CEB-FIP	455	365	0.483	1.854
Bazant Model	455	365	0.300	1.151
Gardner Model	455	365	0.409	1.570

5.3.4 Shrinkage Comparison for 3-day age at drying

Figure 5.8 and Table 5.6 compare the CTL average 3-day shrinkage values with the predictive models. All of the predictive models fall well short of the test data. The curves for the ACI 209 and Gardner models are similar, as are the Bazant and CEB-FIP model curves. The ACI 209 and Gardner models are closer to the test data while still underestimating considerably.

Table 5.6: 3-Day Shrinkage values after one year of drying

Data Type	Age (Days)	Days Drying	Shrinkage ($\mu\varepsilon$)
CTL Data	368	365	1045
ACI 209	368	365	705
CEB-FIP	368	365	424
Bazant Model	368	365	423
Gardner Model	368	365	679

5.4 Updating Predictive Models Using 28 Day Test Data

5.4.1 Introduction

The largest source of uncertainty of creep and shrinkage prediction models is the dependence of model parameters on the composition and strength of concrete (ACI-209, 1996). Because this effect is very complicated, and because a satisfactory mathematical theory has yet to be developed, the problem may be handled empirically by conducting short-term creep and shrinkage tests and using the results obtained to adjust the long-term parameters accordingly. This may be done on a parameter-by-parameter basis, although trying to account empirically for

the effects of each model parameter individually would be difficult due to the many parameters and their combinations.

The overall model prediction may also be modified in a more gross sense, by comparing the short-term test data results for creep and shrinkage to the predictive model results over the same time period, and adjusting the predictive model results to improve the correlation between the two. This procedure, outlined by Bazant (ACI-209, 1996), is examined in section 5.4.2.

5.4.2 Regression Analysis

Modified prediction values for creep and shrinkage may be obtained by comparing actual short-term data points against the values obtained by using one of the predictive models. These values are plotted against each other on a graph, such as Figure 5.9. Determination of a modified creep coefficient is used as an example. If the model data, $\phi'(t)$, corresponded exactly to the test data, $\phi(t)$, a plot of $\phi'(t)$ vs. $\phi(t)$ would be a single straight line passing through the origin. In reality, these values do not correspond exactly (as shown in Figure 5.9). To obtain the least deviation between the test data and the model, a least-squares regression is calculated. This results in the regression line

$$\phi''(t) = p_2\phi(t) + p_1 \tag{5.1}$$

where

$p_1 =$	The intercept of the regression line
$p_2 =$	The slope of the regression line
$\phi(t) =$	Creep coefficients from the short-term (first 28 days) test data
$\phi'(t) =$	Creep coefficients from the original model
$\phi''(t) =$	Modified creep coefficients using the short-term test data

The regression coefficients p_1 and p_2 are determined as follows:

$$p_2 = \left[\frac{n\sum(\phi_i\phi_i') - \left(\sum\phi_i\right)\left(\sum\phi_i'\right)}{n\sum\left(\phi_i^2\right) - \left(\sum\phi_i\right)^2}\right] \tag{5.2}$$

$$p_1 = \overline{\phi'} - \overline{\phi} \tag{5.3}$$

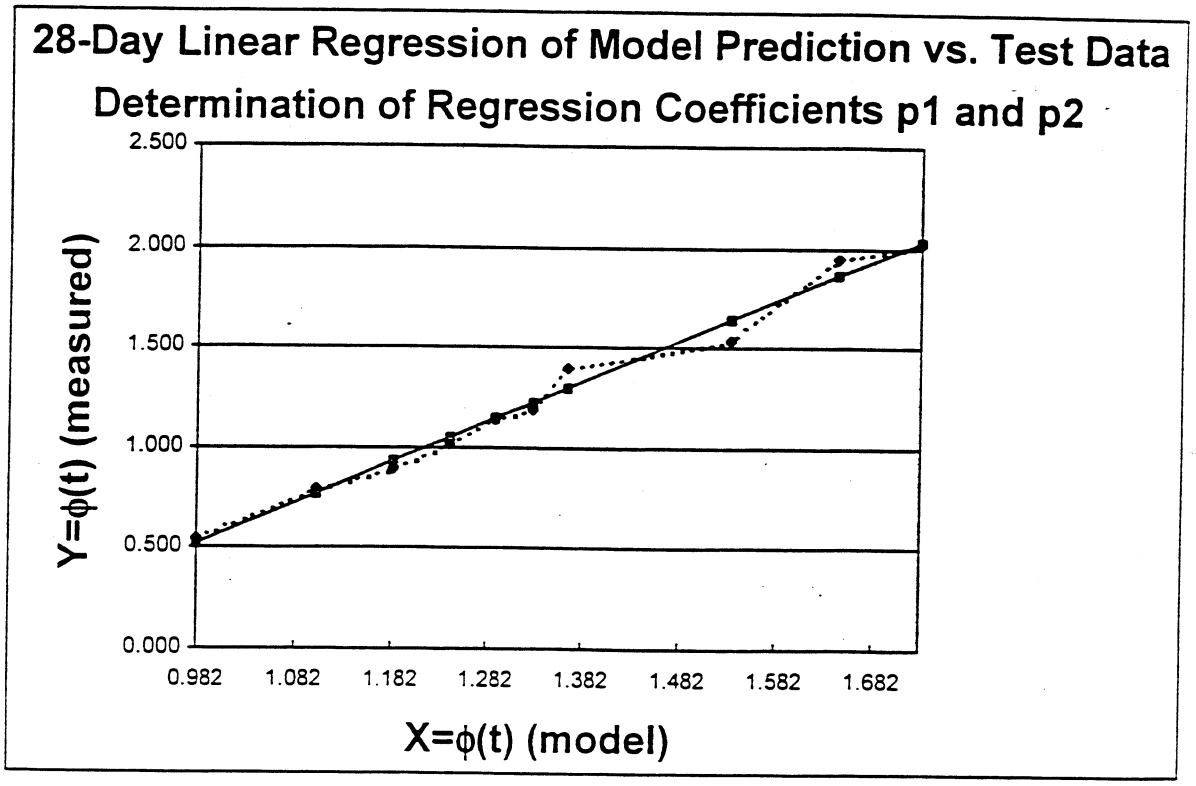

Figure 5.9: Linear Regression of 28 Day Test Data

where

$n =$ The number of data points in the short-term (first 28 days) test data

$\phi_i =$ The ith creep coefficient from the short-term data

$\phi_i' =$ The ith creep coefficient from the predictive model

$\bar{\phi} =$ The average value of the short-term test data creep coefficients

$\bar{\phi}' =$ The average value of the predictive model creep coefficients

Modified values of creep and shrinkage for each predictive model were calculated using equations 5.1 through 5.3 and the results are discussed in the following sections.

5.4.3 Creep Results

Figures 6.10 through 6.12 compare the CTL average creep values vs. predictive model values for concrete samples loaded at 3 days, 28 days, and 90 days, respectively. The predictive models have been modified using the short-term test data as described in section 6.4.2. Each chart displays creep values for loading periods of one year.

5.4.3.1 Creep Comparison (3 Day)

Figure 5.10 and Table 5.7 illustrate the effect of using the short-term test data to modify the creep predictions of the various models. Data from Table 5.3 (unmodified values) has been incorporated into Table 5.7 for comparison purposes. With the exception of the Gardner model, both the shapes and data values of the predictive curves are in much closer agreement to the test data than they were using the unmodified predictive models. The Gardner model appears to diverge from the test data points (Figure 5.10), while the CEB-FIP and Bazant models give very close results. The ACI model is also greatly improved, although the results are not as close as the Bazant and CEB-FIP models.

Table 5.7: Average 3 Day Creep Values Using Corrected Predictive Models

Data Type	Age (Days)	Days Loaded	Creep/psi (Ave) Orig.	Creep/psi (Ave) New	Creep Coeff. Orig.	Creep Coeff. New	Error Reduction
CTL Data	368	365	1.147	1.147	3.654	3.654	-
ACI 209	368	365	.585	.996	1.882	3.203	73.1%
CEB-FIP	368	365	.919	1.094	2.956	3.519	76.8%
Bazant Model	368	365	.859	1.094	2.763	3.519	81.6%
Gardner Model	368	365	.967	1.678	3.110	5.397	-

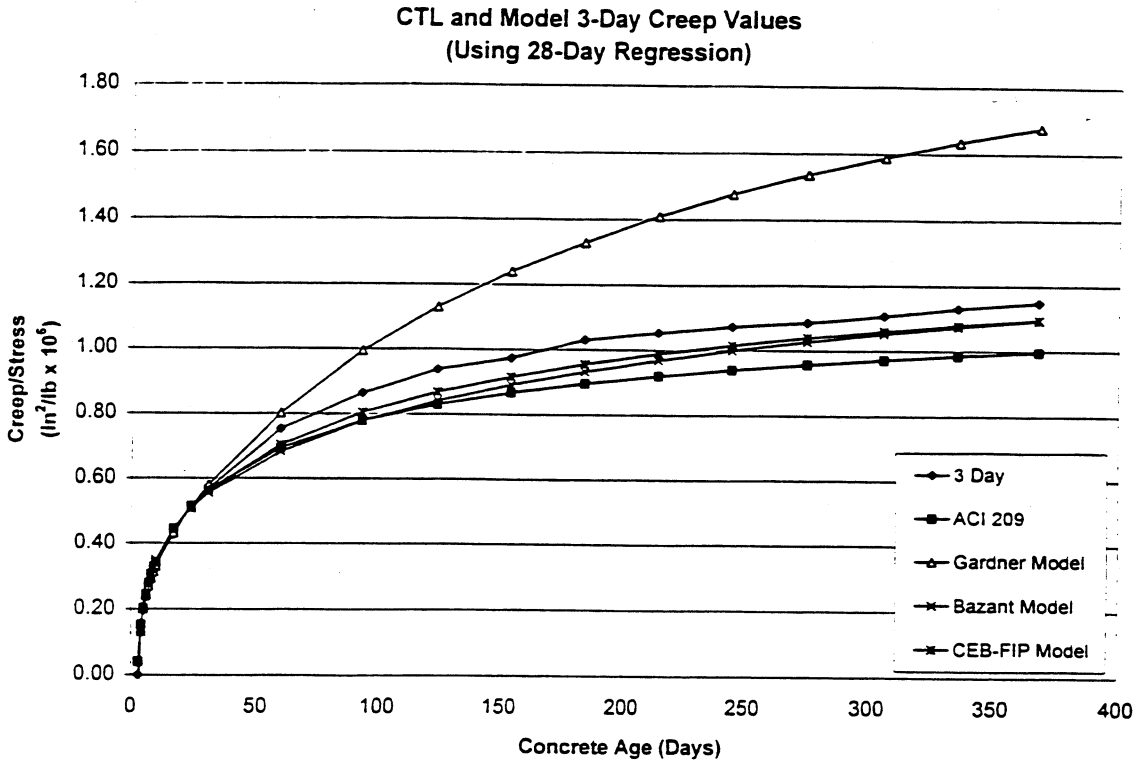

Figure 5.10: Modified Predictive Models for 3-day Creep

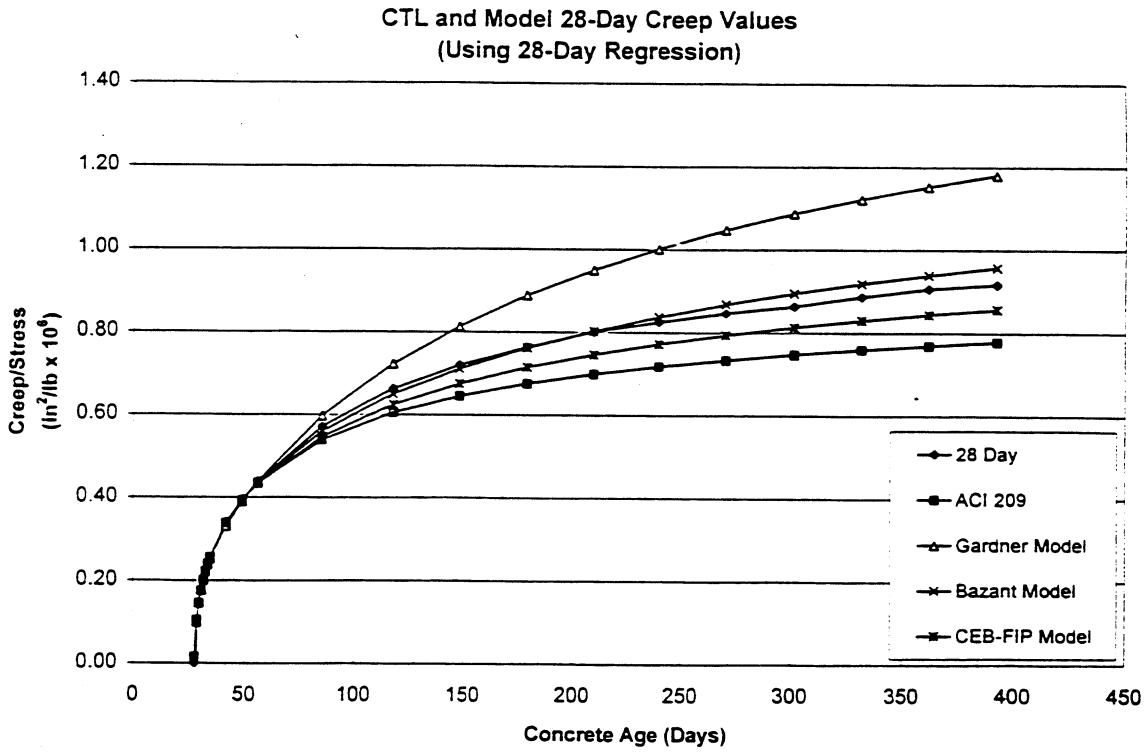

Figure 5.11: Modified Predictive Models for 28-day Creep

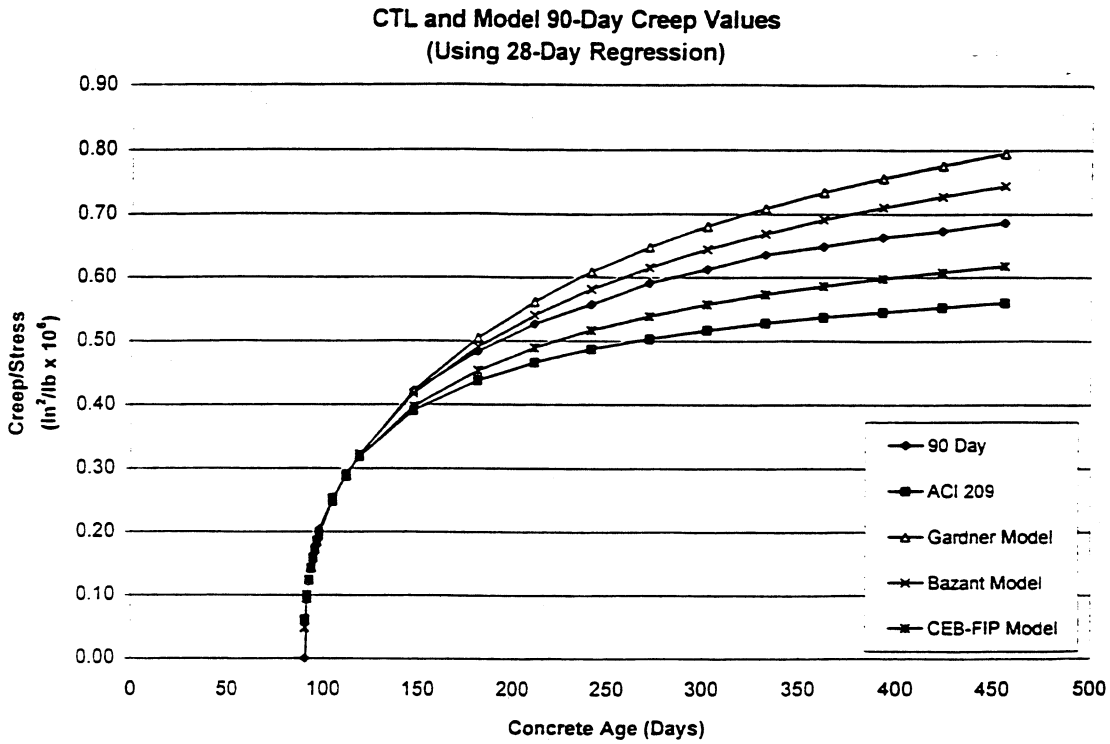

Figure 5.12: Modified Predictive Models for 90-day Creep

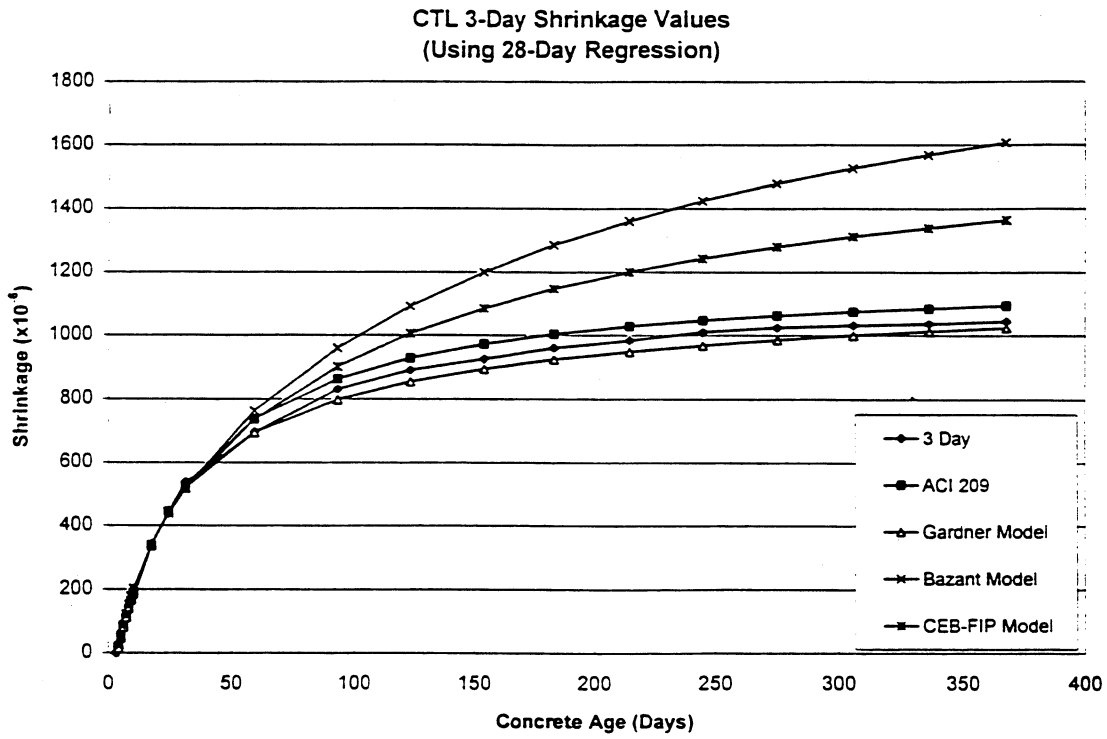

Figure 5.13: Modified Predictive Models for 3-day Shrinkage

5.4.3.2 Creep Comparison (28 Day)

Figure 5.11 and Table 5.8 show the results for 28 day creep chart. Data from Table 5.4 has been incorporated into Table 5.8 for comparative purposes. For the 28 day creep, a significant improvement is achieved by using the short-term test data. The exception is the Gardner model, which diverges from the test data. The Bazant model appears to give the best results, followed by the CEB-FIP and ACI models.

Table 5.8: Average 28 Day Creep Values Using Corrected Predictive Models

Data Type	Age (Days)	Days Loaded	Creep/psi (Ave) Orig.	Creep/psi (Ave) New	Creep Coeff. Orig.	Creep Coeff. New	Error Reduction
CTL Data	393	365	.917	.917	3.324	3.324	-
ACI 209	393	365	.396	.779	1.438	2.828	73.5%
CEB-FIP	393	365	.604	.857	2.193	3.111	80.8%
Bazant Model	393	365	.427	.958	1.550	3.478	91.6%
Gardner Model	393	365	.520	1.181	1.888	4.288	33.5%

5.4.3.3 Creep Comparison (90 Day)

Figure 5.12 and Table 5.9 give the results for the 90 day creep chart. Data from Table 5.5 has been incorporated into Table 5.9 for comparative purposes. Both the Gardner and Bazant models appear to overestimate the test data, while the CEB-FIP and ACI models appear to underestimate the test data. It is difficult to determine whether or not the Gardner model is diverging from the test data, as was the case for the 3 day and 28 day charts. However, in comparison to Figure 5.5, the use of the short-term test data to update the predictive models still produces desirable results.

Table 5.5: Average 90-Day Creep Values Using Modified Predictive Models

Data Type	Age (Days)	Days Loaded	Creep/psi Orig.	Creep/psi New	Creep Coefficient Orig.	Creep Coefficient New	Error Reduction
CTL Data	455	365	0.686	0.686	2.633	2.633	-
ACI 209	455	365	0.329	0.560	1.263	2.149	64.7%
CEB-FIP	455	365	0.483	0.618	1.854	2.372	66.5%
Bazant Model	455	365	0.300	0.744	1.151	2.856	85.0%
Gardner Model	455	365	0.409	0.795	1.570	3.051	60.7%

5.4.4 Shrinkage Results

Figure 5.13 compares the CTL average 3-day shrinkage values with the predictive model values. The predictive model values have been modified using the short-term test data as described in section 5.4.2. Figure 5.13 shows that over the period of one year, the updated ACI 209 and Gardner models correspond well with the CTL test data, while the Bazant and CEB-FIP models diverge from the CTL data. Table 5.6 compares the CTL test data with the modified predictive model results at one year of drying.

Table 5.6: Average 3-Day Shrinkage Values (modified) for One Year of Drying

Data Type	Age (Days)	Days Drying	Shrinkage ($\mu\varepsilon$)
CTL Data	368	365	1045
ACI 209	368	365	1095
CEB-FIP	368	365	1363
Bazant Model	368	365	1606
Gardner Model	368	365	1025

It can be seen from Figure 5.13 and Table 5.6 that the modified ACI 209 and Gardner models are in close agreement with the test data, and show a great improvement over the unmodified predictive model results. The modified Bazant and CEB-FIP models also show an improvement, however, Figure 5.13 shows a divergence between the test data and these models that indicates that the modification procedure applied to these models is unreliable. For the Bazant shrinkage model, this is further supported by Bazant himself who has found that the previously described method using short-term test data to update predictive models is effective for the Bazant creep model, but is ineffective for the Bazant shrinkage model.

5.5 General Observations

5.5.1 Hawaiian Concrete

This research was conducted on test cylinders made using Hawaiian concrete made from locally obtained aggregates. Based on the results of the creep and shrinkage tests preformed at CTL, the following observations can be made:

- As expected, creep strains decreased with an increase in age at loading.
- The concrete creep exhibited greater scatter with an increase in age at loading.
- The scatter in concrete creep values after one year of loading varied between approximately 10% and 20%.
- The scatter in shrinkage values after one year of drying was approximately 8%.

5.5.2 Predictive Creep and Shrinkage Models

Based on the results of this study, none of the four predictive models considered was able to predict the test creep and shrinkage adequately. All of the models underestimate both creep and shrinkage of the Hawaiian concrete. Because none of the models fit the test data, it is reasonable to conclude that these and any other predictive models should be used with caution when applied to Hawaiian concretes.

5.5.3 Use of Short-Term Test Data to Modify the Predictive Models

This study suggests that the appropriate use of short-term data for modifying the predictive models can be quite effective. Using the method outlined earlier in this chapter, significant improvements in the prediction of creep and shrinkage were obtained. However, not all of the models showed an improvement from the modifications.

For creep prediction, the use of short-term test data to update the predictive models worked very well for all models except the Gardner model, which showed a clear divergence from the test data.

For shrinkage prediction, the method used to update the predictive models was effective for two of the four models, namely the ACI 209 and Gardner models. The Bazant and CEB-FIP models clearly diverge from the test data and should not be modified using this approach.

CHAPTER 6

COMPARISON OF CREEP AND SHRINKAGE MODELS WITH FIELD OBSERVATIONS

6.1 Introduction

This chapter presents a comparison between laboratory creep and shrinkage data and the performance of the NHVV. Results from the concrete strain measurements using vibrating wire strain gages, and the span shortening measured by extensometers, are presented. A correlation is made between the laboratory creep and shrinkage results and the field conditions. Using only the first 28 days of creep and shrinkage data from the laboratory tests to modify current predictive models, as described in Chapter 5, it is shown that the field measured strains and span shortening can be simulated with reasonable accuracy.

In order to size the expansion bearings for a long-span bridge structure, it is necessary to predict the overall span shortening due to all effects, including elastic shortening, creep and shrinkage, and thermal changes. This prediction, along with deflection and prestress loss calculations, is commonly performed using a time-step computer program, such as SFRAME (Ketchum, 1986), which models the construction procedure and all subsequent factors affecting the long-term performance of the structure. These computer models require considerable input data including the expected creep and shrinkage performance of the concrete used in the structure.

This chapter presents the results of a simplified prediction of the overall span shortening of the NHVV. This prediction is based on information generally available to a design engineer at the start of a project, including 28 days of creep and shrinkage data from tests performed on the concrete to be used in the structure. The success of this simplified prediction indicates that computer predictions will also be successful using the creep and shrinkage data obtained from the 28 days of testing.

6.2 Description of Instrumentation

A detailed description of all instrumentation in this project is given in Chapter 3. The following is a brief description of the strain and span shortening measurement systems pertaining to the results presented in this chapter.

6.2.1 Concrete Strain Measurements

The primary instruments for measuring concrete strain are Vibrating Wire Strain Gages. These gages were embedded in the concrete to measure longitudinal strain. Eight to ten vibrating wire strain gages were placed around the box-girder cross-section at each instrumented section as described in Chapter 3.

6.2.2 Span Shortening Measurements

Extensometers were installed in the four instrumented spans to monitor the overall shortening of the box-girder as described in Chapter 3. One end of an extensometer is fixed at one end of the span, while the other end is coupled to a Linear Variable Displacement Transducer (LVDT) at the other end of the span. The relative displacement of the concrete at the two ends of the extensometer is measured by the LVDT. The span shortening measured by each extensometer is converted to a strain by dividing by the corresponding span length.

6.3 Axial Shortening Results

6.3.1 Axial strains recorded by VW gages

Figure 6.1 presents the axial strains measured by the 8 vibrating wire strain gages at section A for a period of 30 months after construction. The average strain at the mid-height of this section is also shown. Similar results were recorded for the 10 VW gages at section B. These sections represent the midspan and endspan conditions respectively for span P8 to P9. Figure 6.2 shows these two average strain plots, as well as the overall average for the two sections. This overall average should give an approximate indication of the overall shortening of the entire span as shown by the extensometer strains plotted in Figure 6.2.

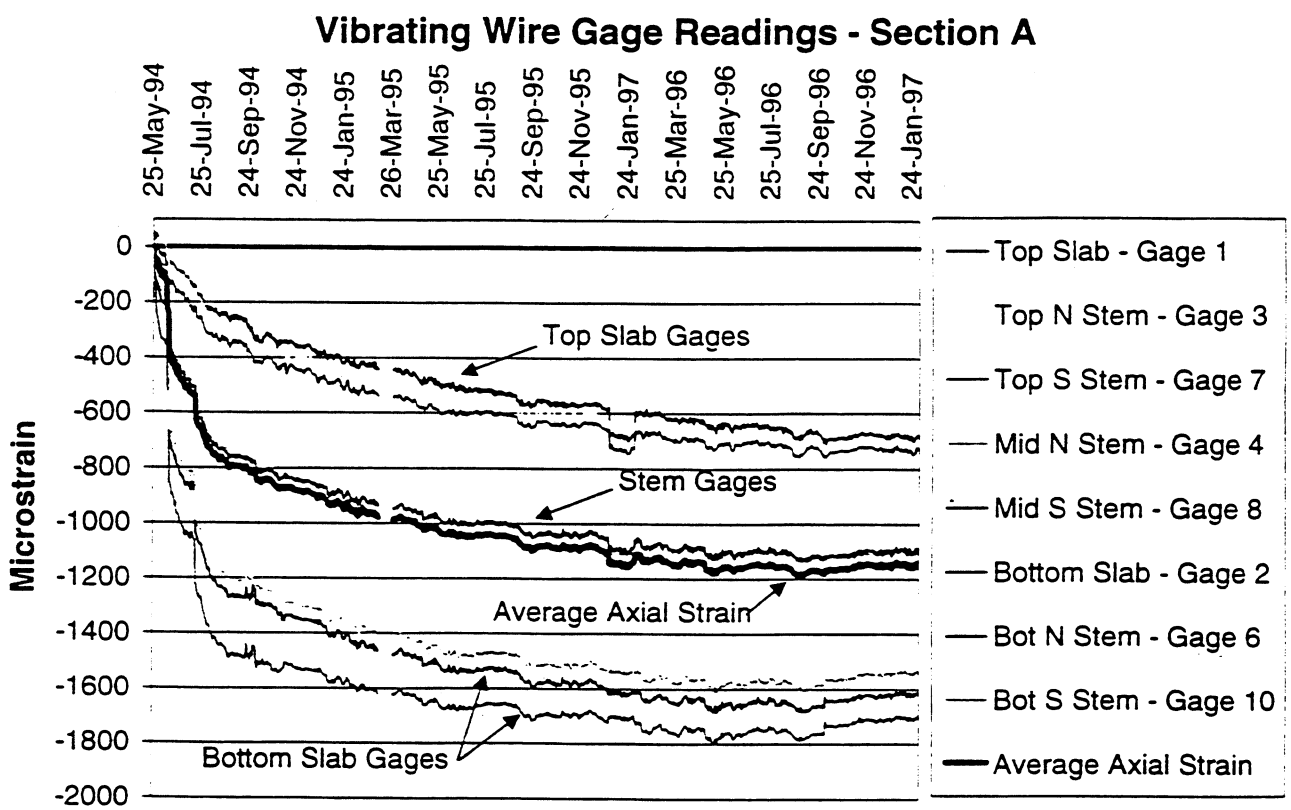

Figure 6.1: Axial strains recorded by the VW gages at section A

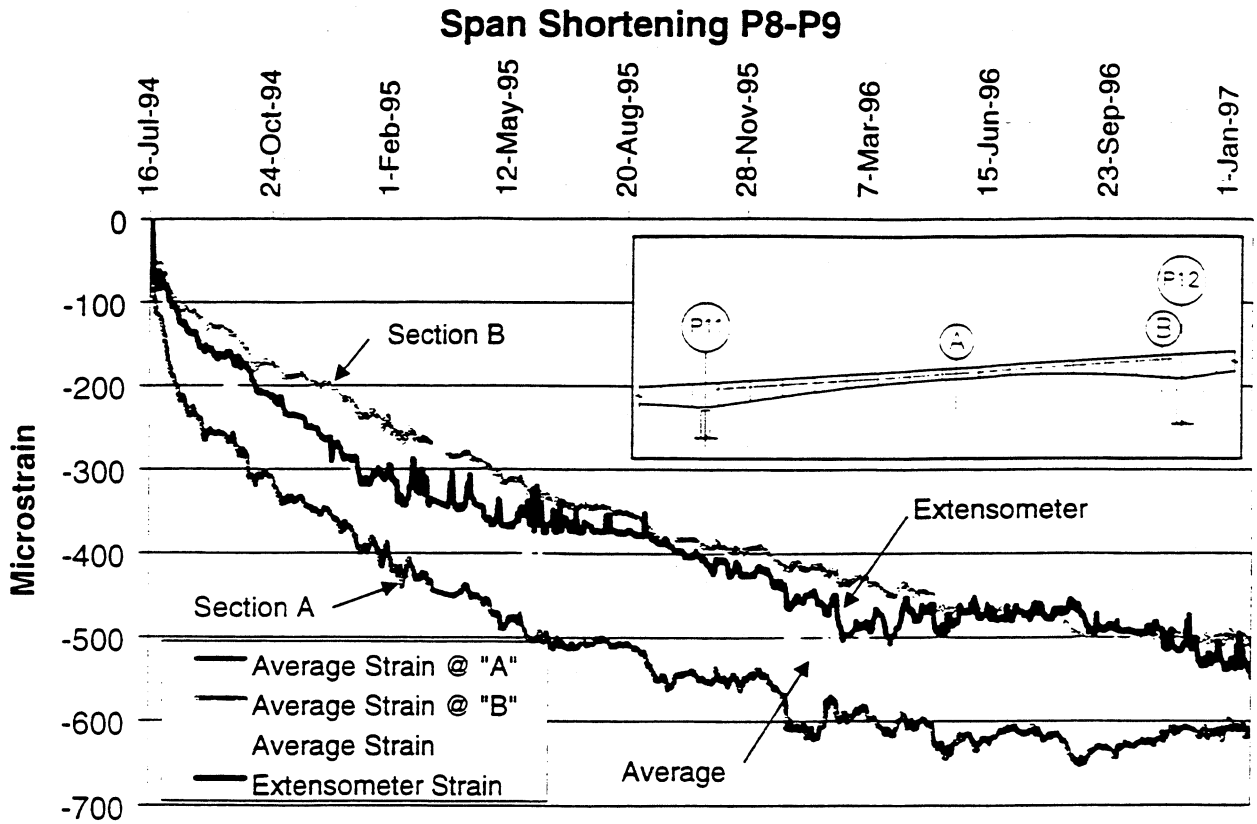

Figure 6.2: Span shortening from P8 to P9 based on extensometer and VW gages.

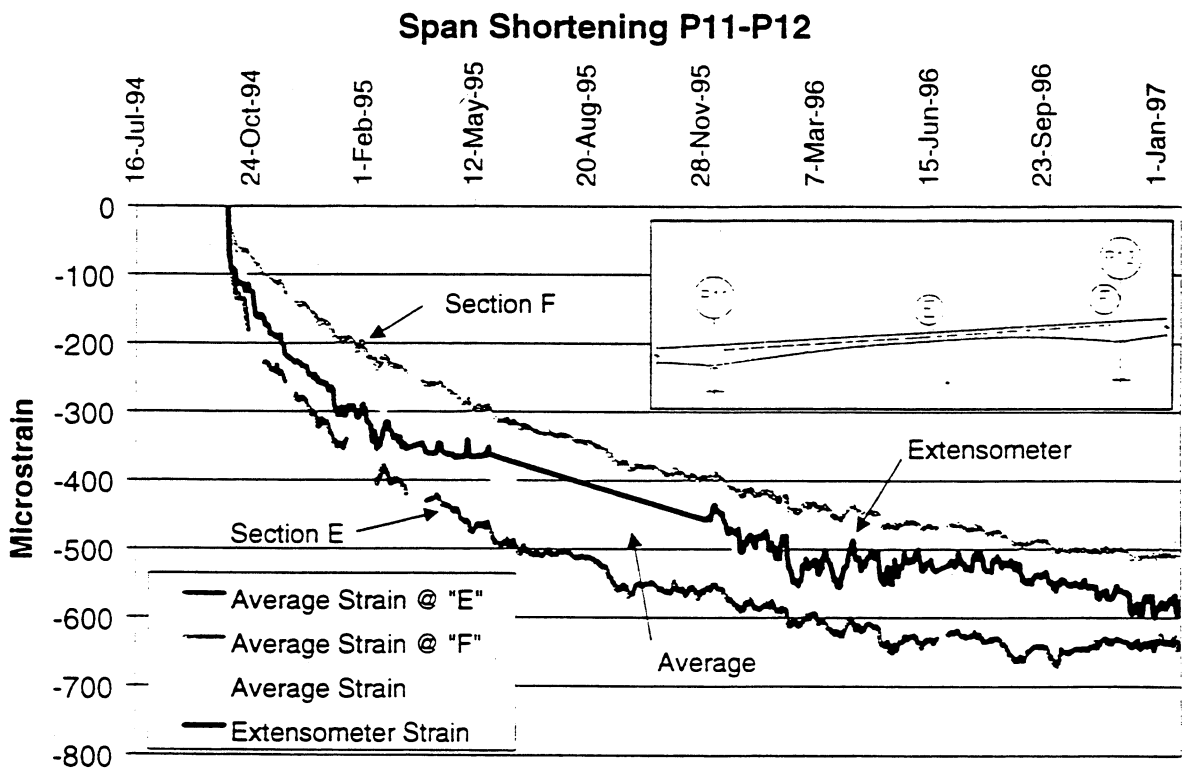

Figure 6.3: Span shortening from P11 to P12 based on extensometer and VW gages.

Figure 6.3 shows the same plot for span P11 to P12 (Sections E and F). These plots indicate that the vibrating wire strain readings at only two sections along the span were able to provide a good indication of the overall span shortening. If it is possible to predict the strains at these two sections, or preferably more sections, it would be possible to deduce the overall span shortening.

Enlarging the strain measurements in Figure 6.1 for the first two months after construction of section A results in Figure 6.4. The average strain at mid-height of the section is also shown. The rapid changes in strain are the result of prestressing events, either of the span tendons or the continuity tendons. Isolating the changes in average strain produces the step-function stress history shown in Figure 6.5.

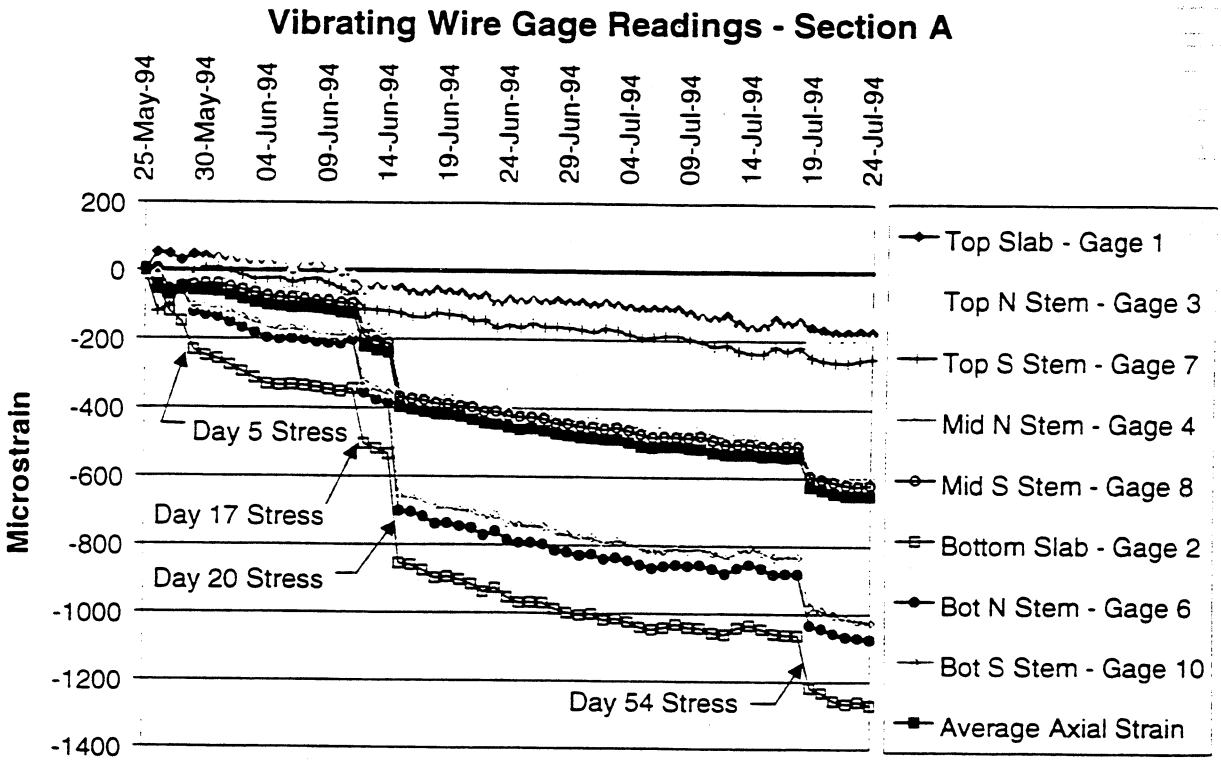

Figure 6.4: Initial axial strains at section A.

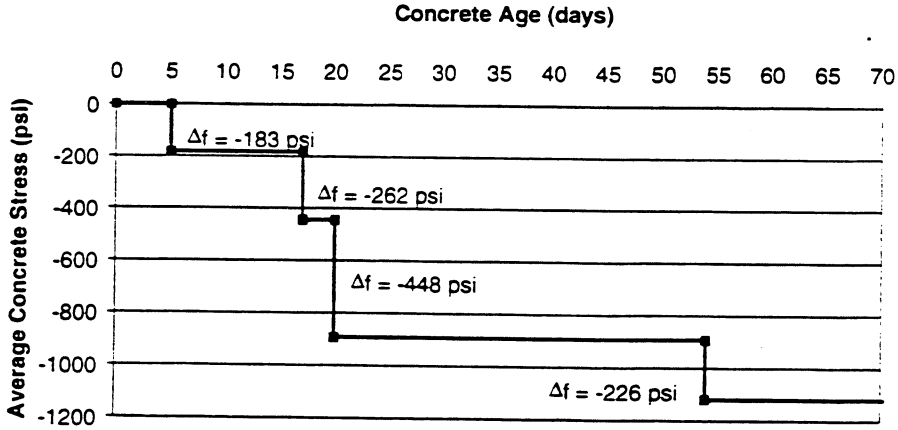

Figure 6.5: Stress history for section A.

6.4 Material Properties

Testing at CTL laboratories performed on concrete samples taken from each of the seven sections produced the material properties reported in Chapter 4. In addition, 21 creep frames with associated shrinkage cylinders were established at CTL under standard ASTM C512 conditions. For each of the seven instrumented sections, one creep frame was loaded at each of 3, 28 and 90 days concrete age.

The results of these creep and shrinkage tests are compared with various predictive models in Chapter 5. All of these models underestimated both the creep and shrinkage observed in the laboratory tests. A simple linearization approach is presented whereby the predictions of some of the models can be substantially improved based on the first 28 days of test data. In particular, the Gardner model for shrinkage responds well to this linearization approach, as does the Bazant model for creep prediction. These modified models will be used in this chapter as a starting point for correlation of the short-term laboratory data with the long-term viaduct response.

Figure 6.6 shows the shrinkage prediction using the Gardner model for section A. Using the linearization approach, the Gardner model is adjusted for the first 28 days of laboratory shrinkage data for section A. The extrapolated shrinkage over the first year shows excellent agreement with the measured shrinkage (Fig. 6.6).

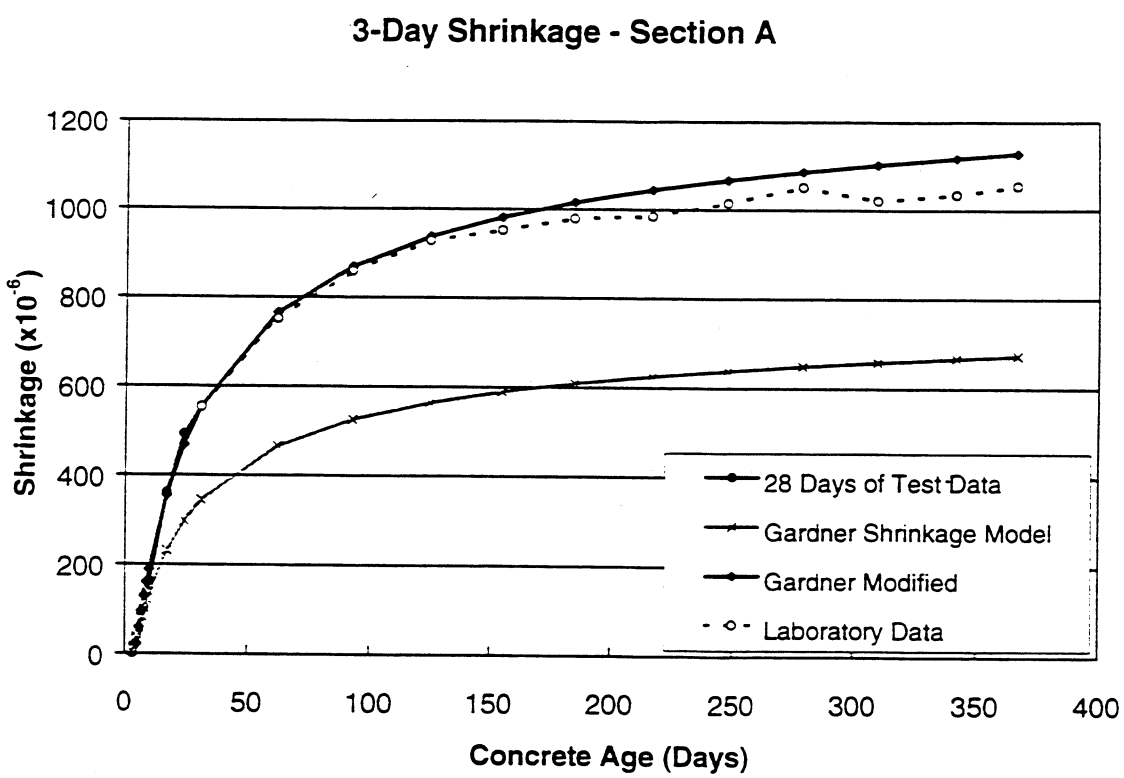

Figure 6.6: Adjustment of Gardner shrinkage prediction based on 28 days of test data.

Similarly, Figure 6.7 shows the creep prediction for 3-day loading using the Bazant model adjusted for the first 28 days of laboratory creep data. Again, excellent agreement is noted for

the first year of loading. Similar adjusted creep predictions were developed for creep tests loaded at 28 and 90 days concrete age as shown in Figures 6.8 and 6.9.

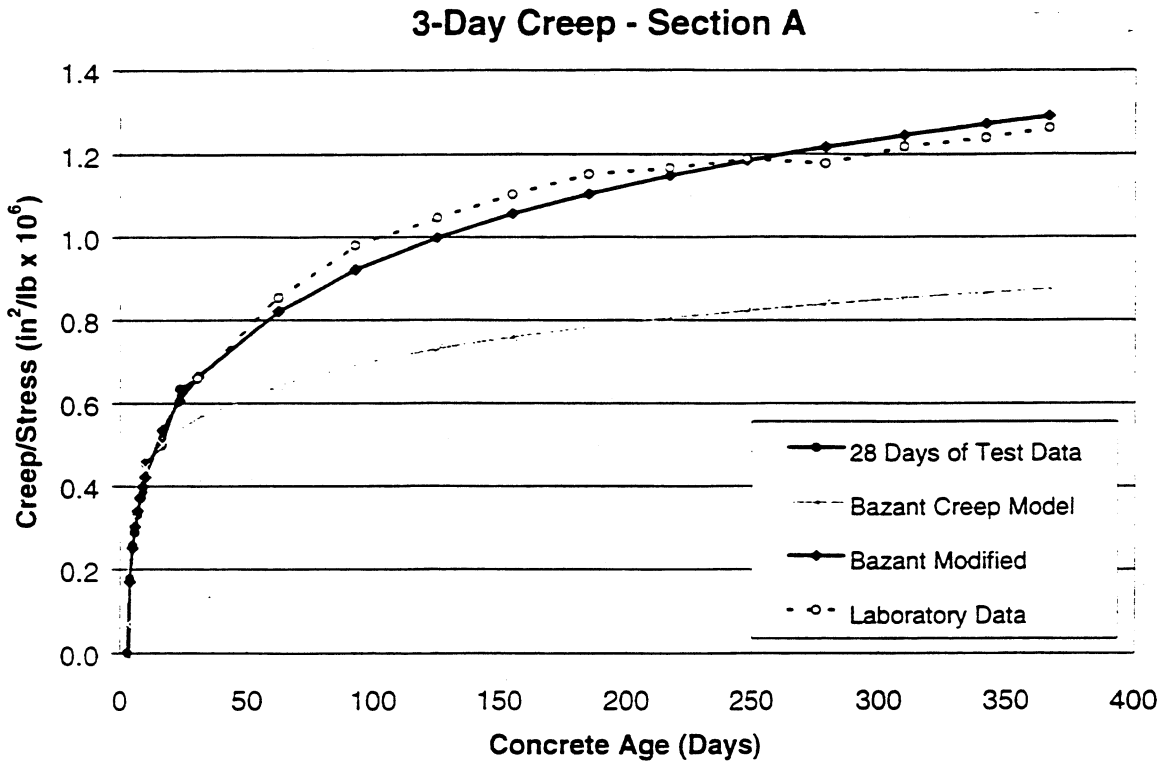

Figure 6.7: Adjustment of Bazant 3-day creep prediction based on 28 days of test data.

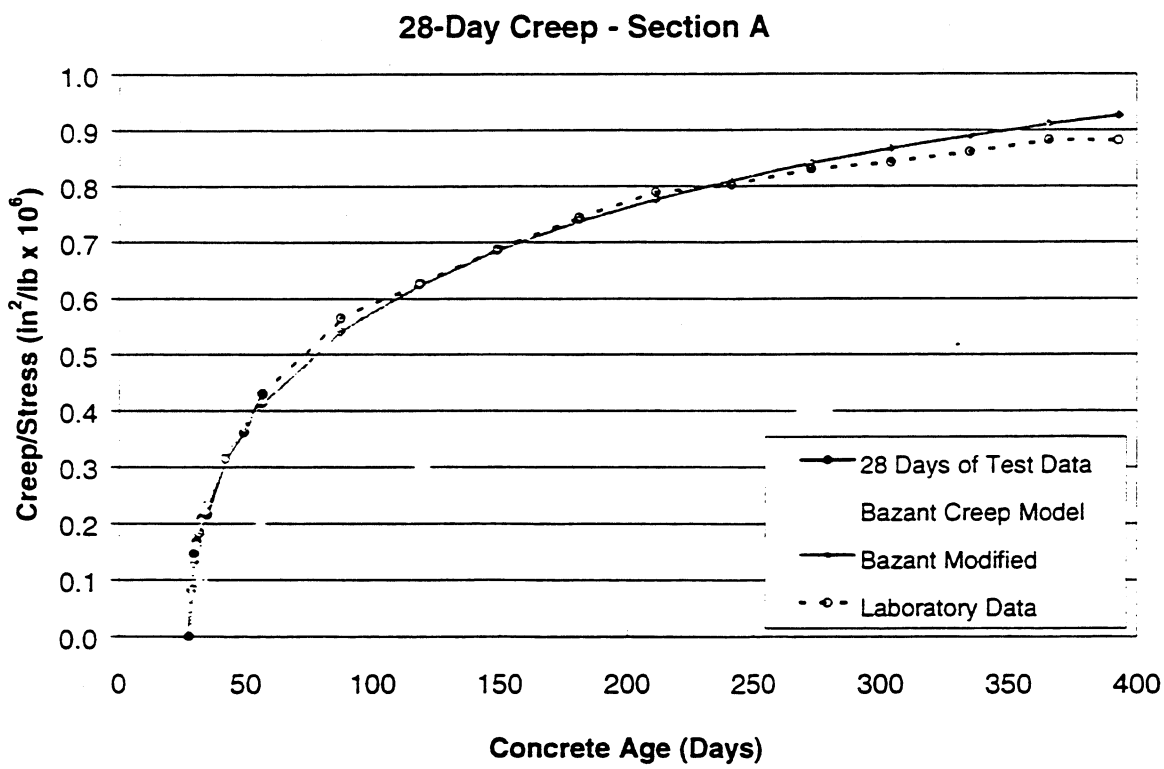

Figure 6.8: Adjustment of Bazant 28-day creep prediction based on 28 days of test data.

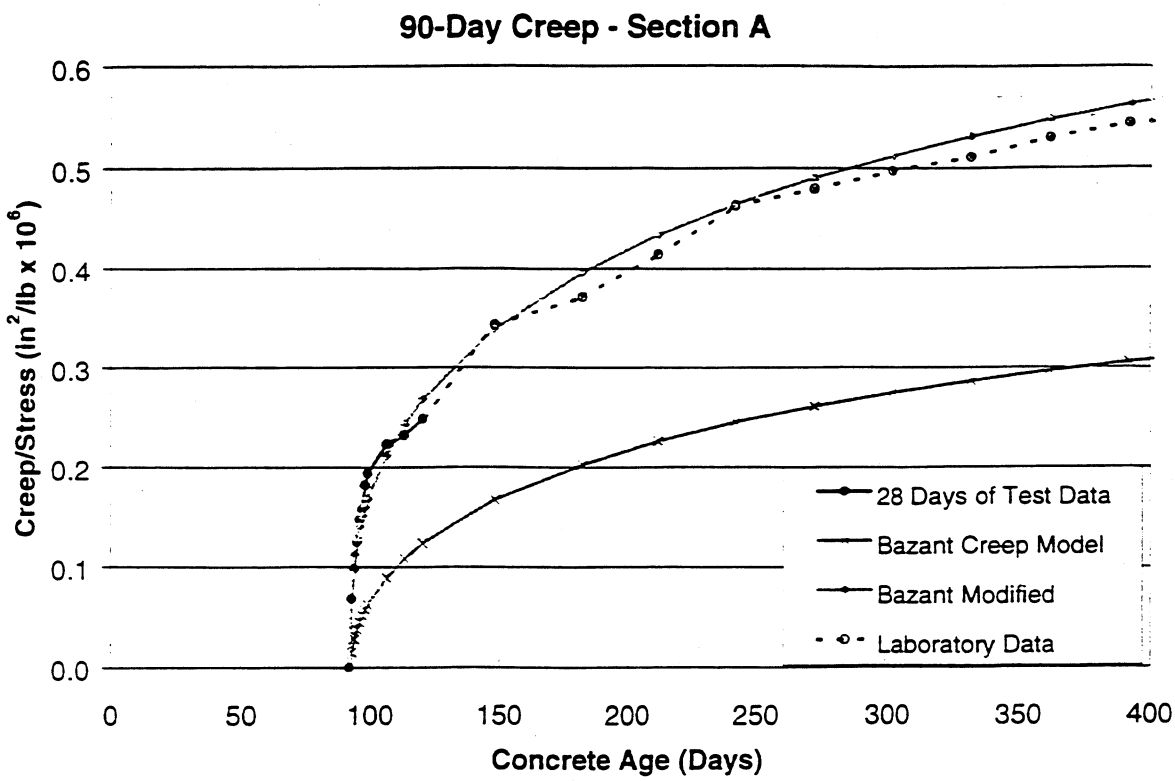

Figure 6.9: Adjustment of Bazant 90-day creep prediction based on 28 days of test data.

6.5 Correlation with Field Conditions

6.5.1 Factors Affecting Field Behavior

In order to utilize laboratory test results in predicting field behavior, it is necessary to adjust for differences between the laboratory test specimens and the actual structural elements. The following adjustments were made in this correlation.

Relative Humidity -- The laboratory relative humidity was a constant 50% while instruments in the field recorded humidity variations from 70% to 95%. Over a one-year period, the average relative humidity inside the box girder was 83.3% while outside the box-girder it was 86.0%. For this study, the laboratory results were modified from 50% to 85% relative humidity. The resulting effect on the 3-day shrinkage and creep predictions is shown in Figures 6.10 and 6.11. The effect on the 28 and 90-day creep predictions is shown in Figures 6.12 and 6.13.

Ambient Temperature -- The laboratory ambient temperature was held constant at 23 $\pm$ 1 °C. The range of field ambient temperature was from 19°C to 27°C with one-year averages of 23.7°C and 23.5°C inside and outside the box girder respectively. Hence, no adjustment was made for ambient temperature.

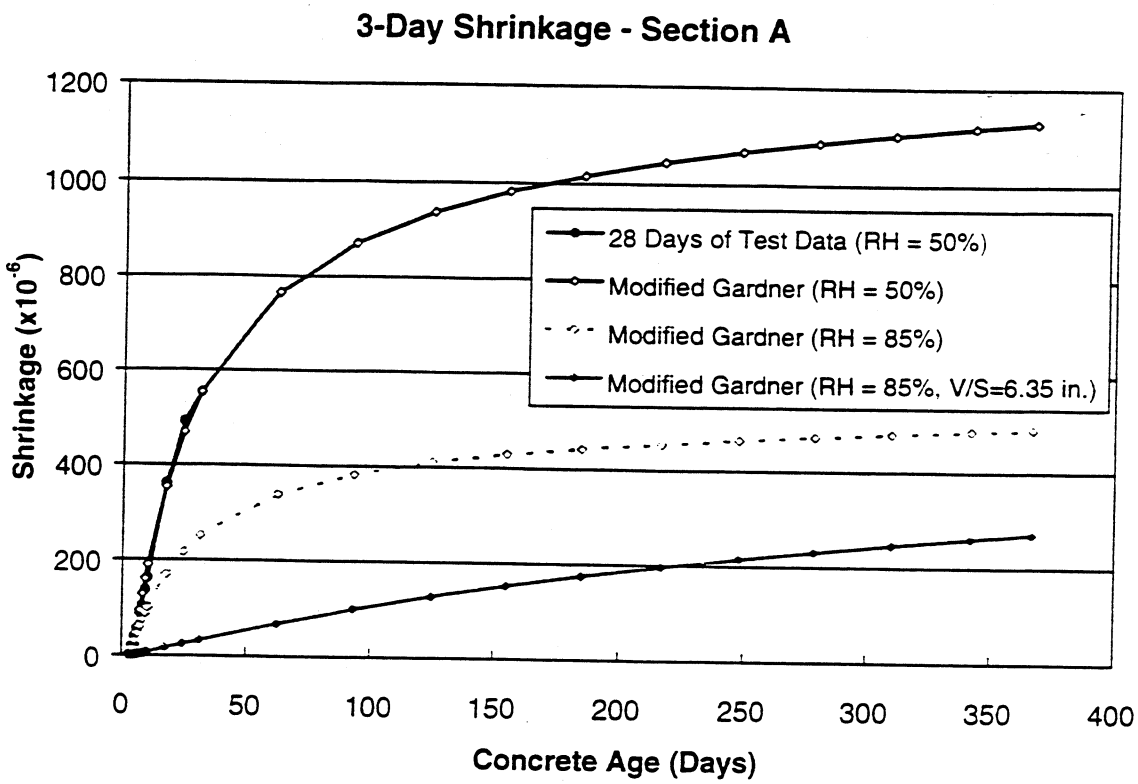

Figure 6.10: Adjustment of shrinkage prediction for relative humidity and V/S ratio.

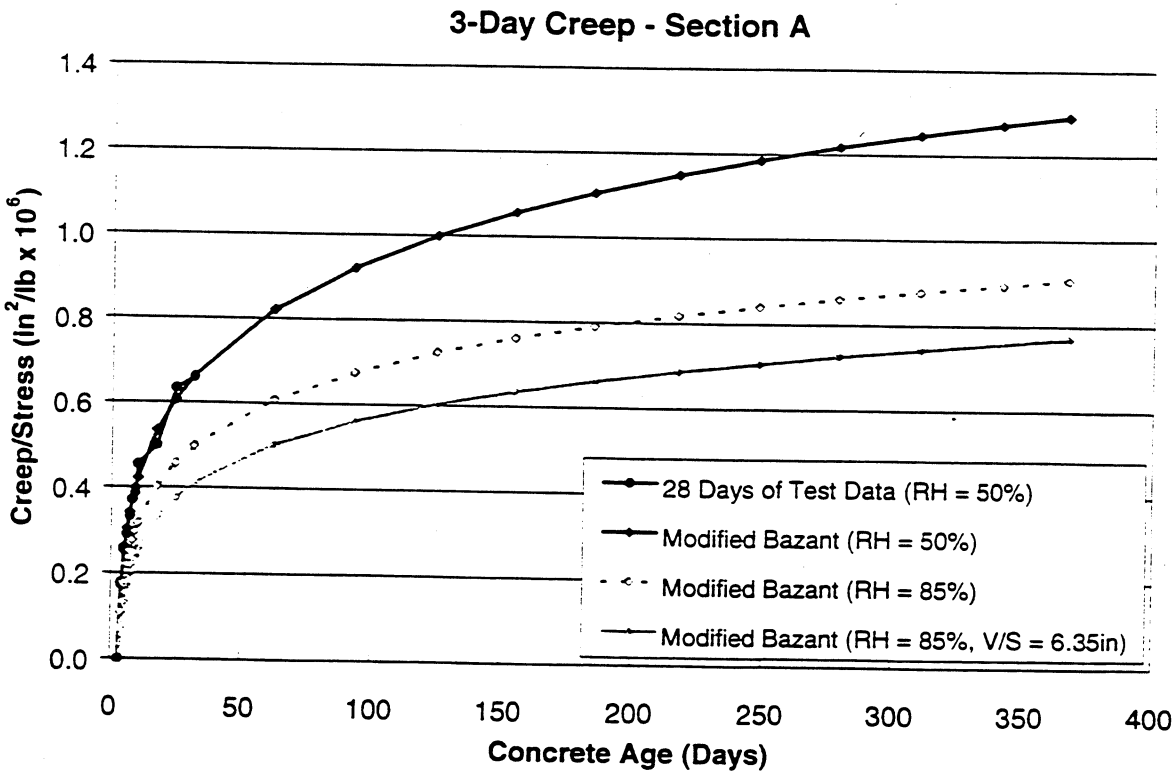

Figure 6.11: Adjustment of 3-day creep prediction for relative humidity and V/S ratio.

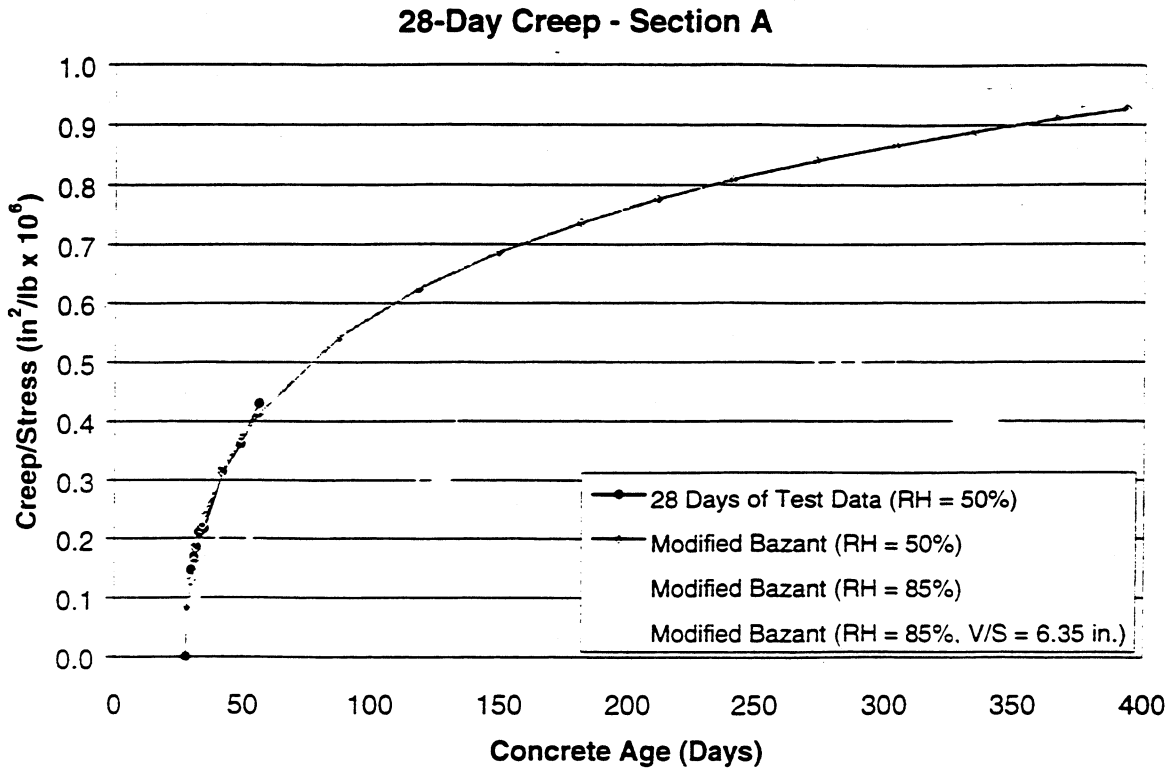

Figure 6.12: Adjustment of 28-day creep prediction for relative humidity and V/S ratio.

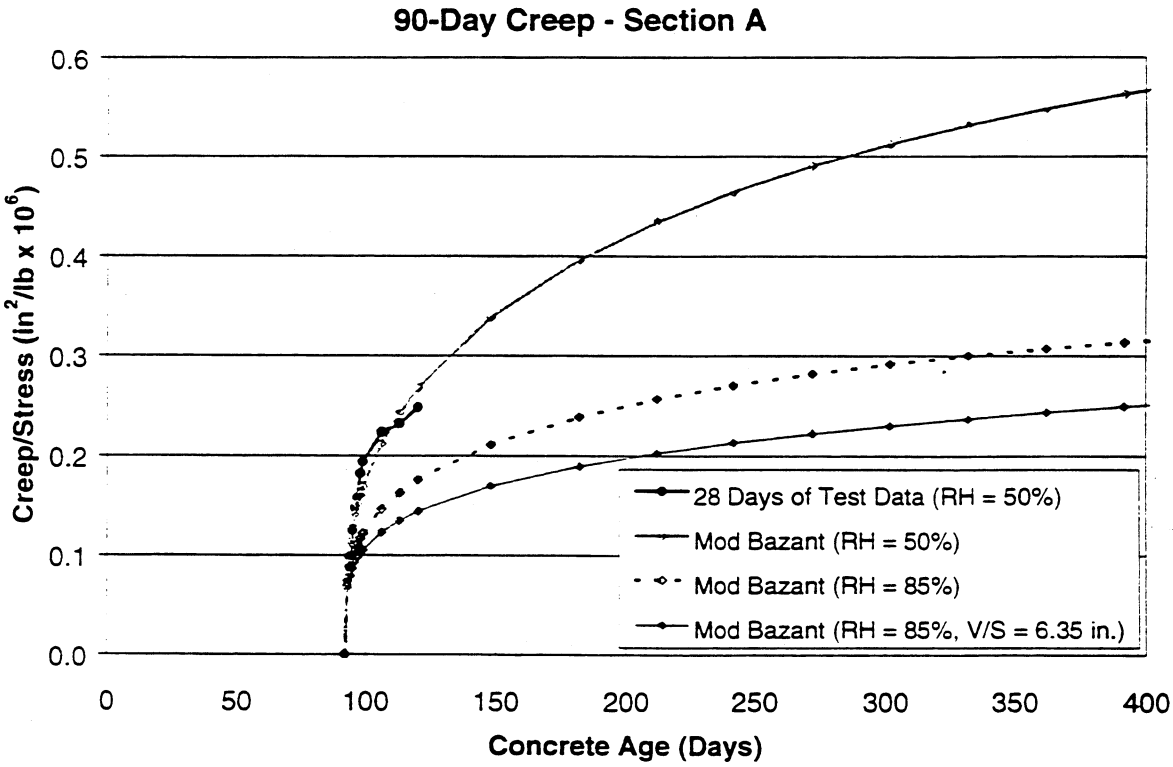

Figure 6.13: Adjustment of 90-day creep prediction for relative humidity and V/S ratio.

Volume-to-Surface Area ratio -- The volume-to-surface area (V/S) ratio for the laboratory cylinders (152 x 305 mm [6"x12"]) is 38 mm (1.5"). The corresponding ratio for the viaduct varies with the variation in cross-section shape. At section A, a typical midspan section, the V/S ratio is 161 mm (6.35"). The shrinkage and creep prediction models were adjusted accordingly as shown in Figures 6.10 through 6.13.

Stress History -- The stress history for the section being considered is required so as to compute elastic and creep strains. Generally, a stress history would be developed during the bridge design. The actual field implementation of this stressing procedure may vary somewhat based on the construction scheduling and concrete strength gain, however, the total stress applied will be the same as the design required value. Any construction related variation in stress history is unlikely to have a significant effect on the long-term structural response. For this study, the concrete stress induced by the prestressing at mid-height of section A is shown in Figure 6.5.

Age at Loading -- Prestressing of section A was performed in four increments at concrete ages of 5, 17, 20 and 54 days as shown in Figure 6.5. In order to model correctly the creep resulting from each of these stressing operations, it is necessary to interpolate between the laboratory generated creep curves as shown in Figure 6.14.

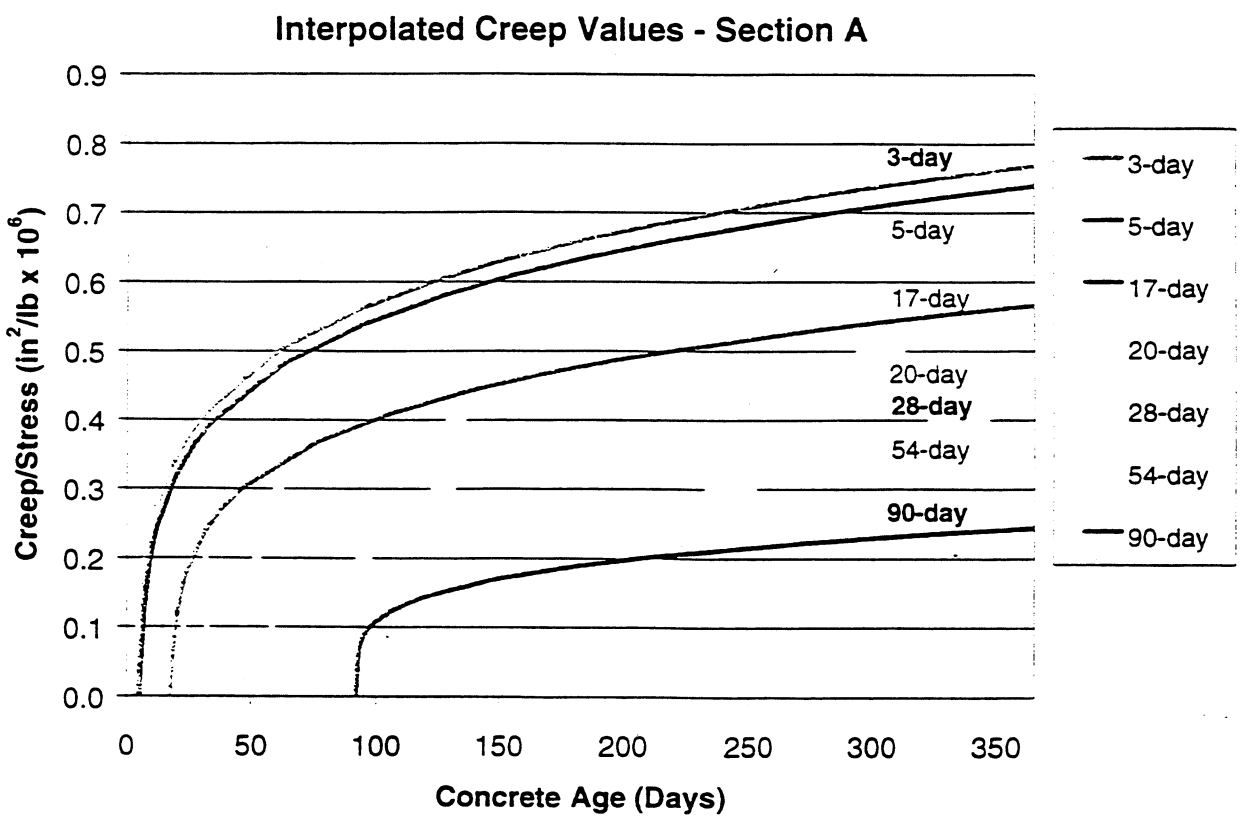

Figure 6.14: Interpolation of creep curves.

Longitudinal Reinforcement -- The presence of non-prestressed longitudinal reinforcement reduces the creep and shrinkage predicted for plain concrete. As the concrete creeps and shrinks, the steel is compressed and so accepts more of the prestress force. The resulting decreased stress on the concrete causes less creep. A step-by-step strain compatibility approach was used to compensate for this effect considering the actual longitudinal steel ratio at section A of 0.008.

Prestress Loss -- The time-dependent loss of prestress also results in a decrease in the concrete stress. Consequently there is a reduction in both elastic strains and creep strains. This effect was incorporated by a step-by-step procedure accounting for a daily reduction in prestress on the section. The total prestress loss for the first year of loading was estimated as 15% of the initial prestress.

6.5 Prediction of Axial Shortening

Using the laboratory test results for compressive strength and modulus of elasticity, along with the adjusted shrinkage and interpolated creep predictions, it was possible to predict the axial shortening at section A as shown in Figure 6.15. Shrinkage strains are applied from day 5 after stripping of the formwork. The axial strain resulting from each stressing event is evaluated using the age appropriate modulus of elasticity. The subsequent creep strains are computed based on the creep curve for that particular age of loading. The cumulative elastic, shrinkage and creep strains for each stressing increment are summed. The effect of longitudinal reinforcement and prestress loss are incorporated as described above. The resulting strain plot compares well with the observed average strain at section A, also shown in Figure 6.15.

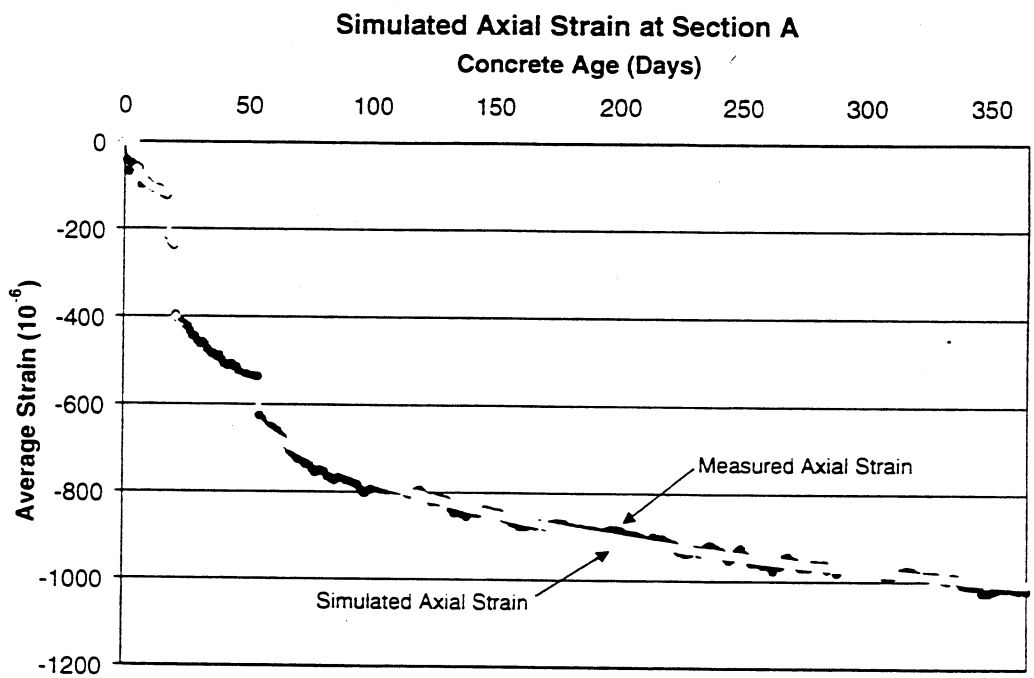

Figure 6.15: Predicted and measured axial strain for section A.

A similar procedure was applied to the other instrumented sections. The first 28 days of laboratory creep and shrinkage data for concrete taken from each section was used to predict the axial shortening at the respective section. At section C, a number of the vibrating wire strain gages were damaged during pouring, so this section was not used in this study. The results for the other five sections (B, D, E, F and G) are shown in Figures 6.16 to 6.20. As with section A, the predicted axial strains compare well with the average measured strains at each section.

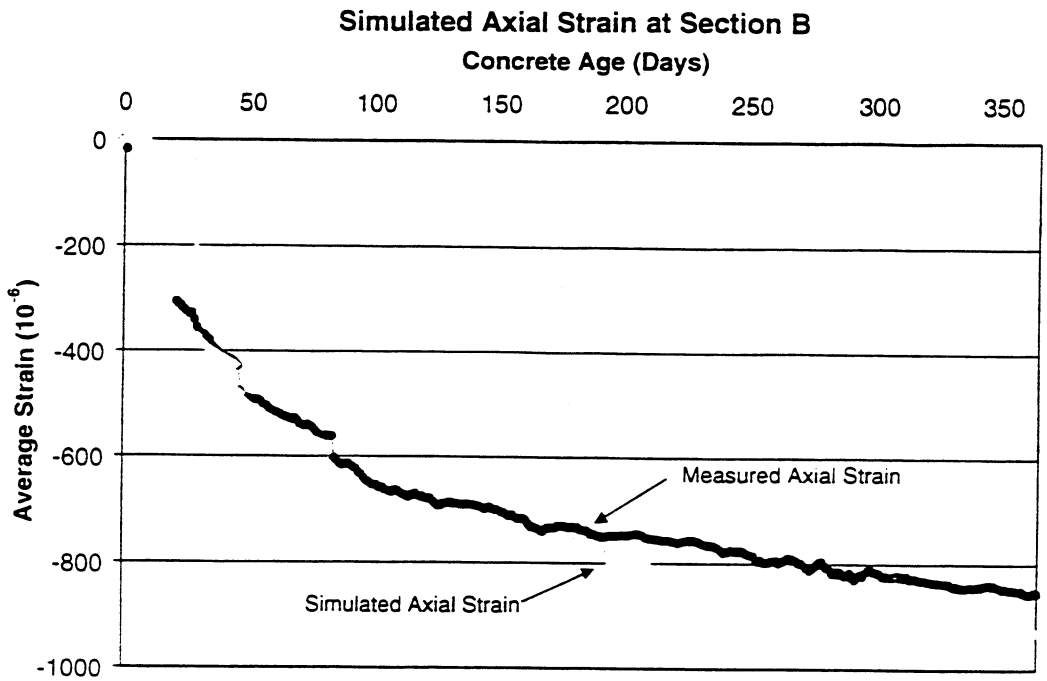

Figure 6.16: Predicted and measured axial strain for section B.

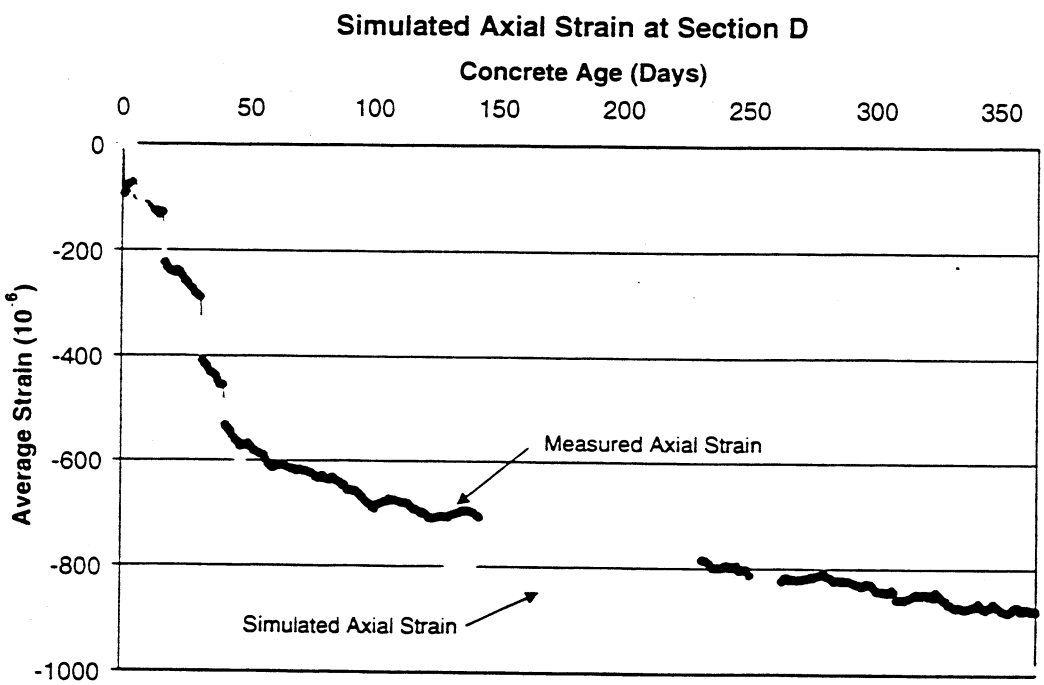

Figure 6.17: Predicted and measured axial strain for section D.

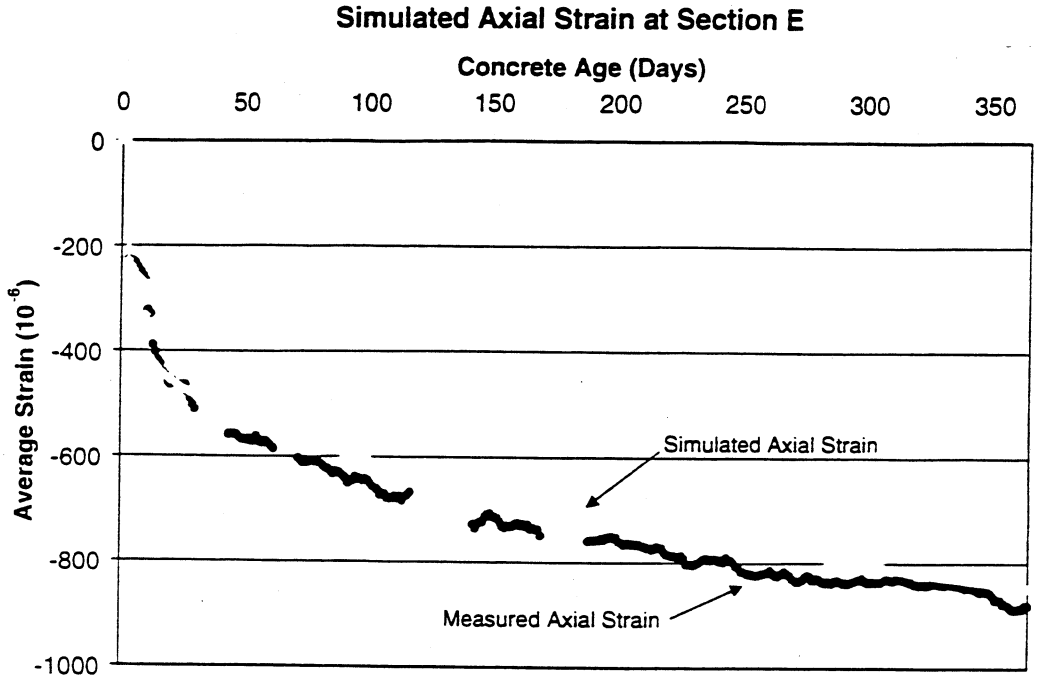

Figure 6.18: Predicted and measured axial strain for section E.

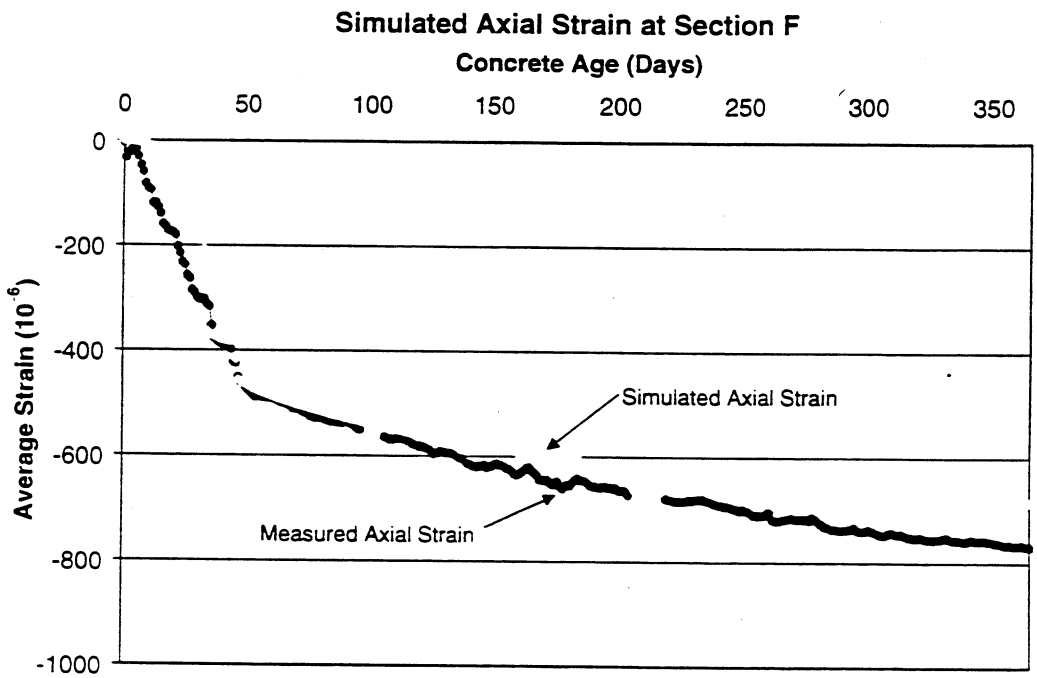

Figure 6.19: Predicted and measured axial strain for section F.

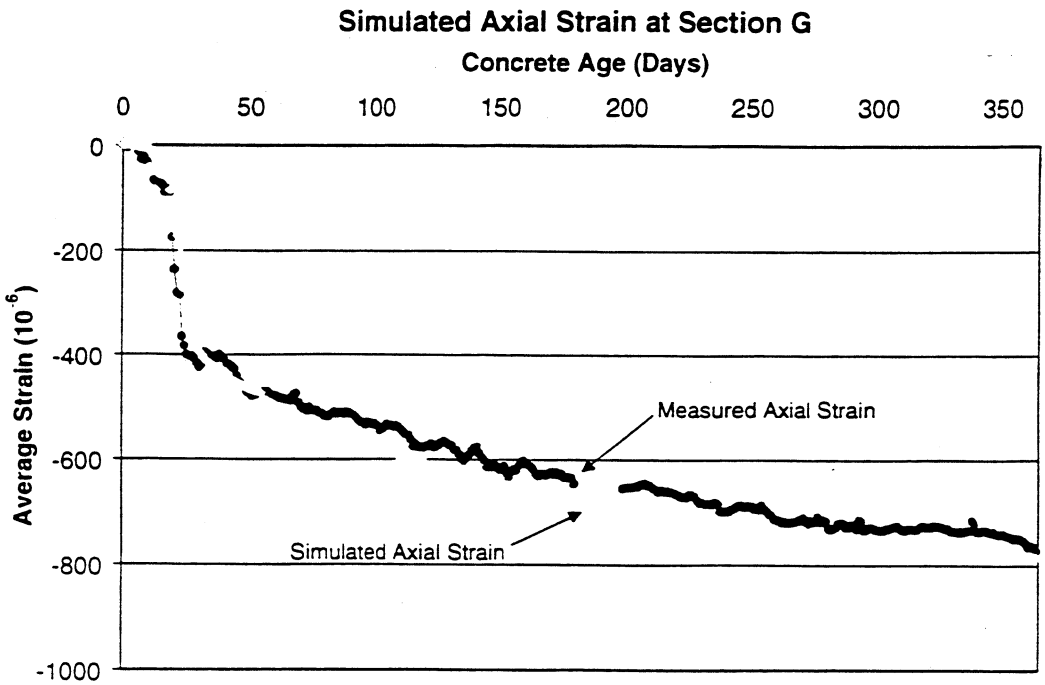

Figure 6.20: Predicted and measured axial strain for section G.

6.6 Conclusions

1. Based on 28 days of laboratory creep and shrinkage, and the modified prediction models presented in Chapter 5, the axial strain at any section in the NHVV box girder can be predicted using the approach presented in this chapter.

2. These predicted axial strains compare well with the average strains measured by the vibrating wire strain gages at each of the instrumented sections.

3. By predicting the strains at midspan and endspan conditions, the average strain over the full span can be estimated. This span shortening strain compares well with the strain measured by the extensometers installed to monitor span shortening.

CHAPTER 7

TIME-DEPENDENT ANALYSIS

7.1 Introduction

In this chapter, comparisons are made between field-measured data with predicted results by the computer program SFRAME. Two sets of predicted results were generated: The first set with the CEB/FIP-78 that was used in the original design, and the second set with the proposed Bazant creep and Gardner shrinkage as presented in chapter 5. SFRAME is a structural analysis program specifically developed for the time-dependent analysis of segmentally erected prestressed concrete plane frame structures and bridges.

In order for the comparison to be accurate, the SFRAME model must reflect the actual structure in the field. The original design model was modified to incorporate the as-built conditions, including:

- As-built construction sequence
- As-built tendon stress profile (revised coefficient of friction)
- Actual no. of strands in each tendon (broken or slipped strands are discounted)
- Activation of future tendons
- Actual date of overlay application

For the design of the North Halawa Valley Viaducts, the CEB/FIP-78 was chosen for the creep and shrinkage model. The CEB model is widely used for the time-dependent analysis of segmental concrete bridges, and it is one of the built-in models in SFRAME. At the beginning of the design process, creep and shrinkage test were performed by Construction Technology Laboratories (CTL) of Skokie, Illinois. The tests were carried out for 3-day, 28-day, and 90-day specimens, and the results were compared to the CEB model. The CEB model underestimated both the creep and shrinkage recorded in the lab tests. In order to best match the test results (minimizing the sum-of-the-error squared for all three curves), "fudge factors" were incorporated

into the CEB model. The design utilized the CEB/FIP-78 model with a fudge factor of 1.50 for creep and 2.50 for shrinkage. Figures 7.1 and 7.2 illustrate the comparison of the CEB model with fudge factors to the lab data for creep and shrinkage respectively.

7.2 Comparison of Measured Data with Predicted Results

Comparisons were made for three parameters: Extensometers and bearings for horizontal movement, and base-line system (piano wire) for vertical deflection. These instrumentation systems are presented in detail in chapter 3. Of the three parameters being compared, the extensometer readings represent the most direct indicator of the creep of the structure under sustained prestressing axial force.

7.2.1 Extensometers

The purpose of the extensometers was to measure axial shortening of the instrumented spans. Readings were recorded once a day at 6:00 AM. Axial strain for a given date was calculated by taking the displacement (difference between initial and given date reading), divided by the extensometer length (span length) and multiplied by 1E6 to give unit of micro-strain. In SFRAME, the predicted axial strain for a given date was calculated by taking the difference between the initial and given date relative displacement (of the two bearing nodes at the ends of the span), divided by the span length and multiplied by 1E6 to give unit of micro-strain. Figures 7.3 to 7.6 illustrate the extensometer comparison for spans 9, 10, 12, and 13 respectively. Both the original CEB model (with fudge factors) and the new proposed Bazant/Gardner model overestimated the creep and shrinkage, with the Bazant/Gardner model to a larger degree. The comparison shows good correlation between measured and CEB predicted axial strain. It should be noted that SFRAME predicted axial strain is purely from the sustained axial stress of the prestressing force. Thermal effects were not considered because SFRAME assumed a constant ambient temperature. However, the extensometer recorded the change in span length caused by any source, including thermal effects. This might explain for the jagged appearance of the extensometer readings.

7.2.2 Bearing Movements

As a backup to the extensometer readings, bearing movement measurements were also taken. The initial readings were taken on 3/29/95, and two subsequent readings on 9/22/95 and 7/7/97. The difference between the initial and subsequent readings represents the bearing movement during each time period. For the predicted movements, the dates of the readings were converted to equivalent dates in the time domain of SFRAME. The difference in the x-position (of the bearing nodes) between the initial and subsequent dates represents the predicted movement during each time period. Figure 7.7 and table 7.1 illustrate the comparison of measured and predicted bearing movements. Consistent with the extensometer results, the predicted movements overestimated the actual movements. It should be noted that the measurements were taken using a plumb-bob and tape measure in a confined space, which was not conducive to very accurate readings. These measurements should be seen as backup to the extensometer readings, which are far more reliable and accurate.

7.2.3 Base-Line System (Piano Wire)

The purpose of the base-line system was to monitor span deflections. The initial readings were taken on 3/29/95, with seven subsequent readings from 5/5/95 to 8/23/96. The difference between the initial and subsequent readings represents the span deflection during each time period. For the predicted deflections, the dates of the readings were converted to equivalent dates in the time domain of SFRAME. For any given time period, SFRAME gives the change in global positions of the structure. To isolate pure span deflection, the y-position of the nodes in a span must first be normalized along a straight line joining the two ends of the span. Normalization along this straight line removes the effect of pier shortening and settlement, and pure span deflection can be isolated and monitored. The difference of the normalized y-position between the initial and subsequent dates represents the predicted deflection during each time period. Figure 7.8 illustrates the span deflection comparison for instrumented spans 9, 10, 12, and 13 for the time period from 3/29/95 to 8/23/96. Correlation is marginally acceptable for span 10 and poor for the other spans. It is not known at this time the reason for the drastic difference in the

span deflection. Because the focus of the time-dependent analysis was on the extensometers, no further investigations were made on the predicted span deflections.

7.3 Comparison of Camber

Figure 7.9 illustrates the comparison of camber of Unit 2 Inbound using the original CEB and the proposed Bazant/Gardner model. As expected, the Bazant/Gardner model produced larger camber values since it predicted larger creep and shrinkage.

7.4 Field Data

This section contains field-measured data for bearing movements and piano wire readings.

Figure 7.1 Superstructure Creep Results (C=1.50)

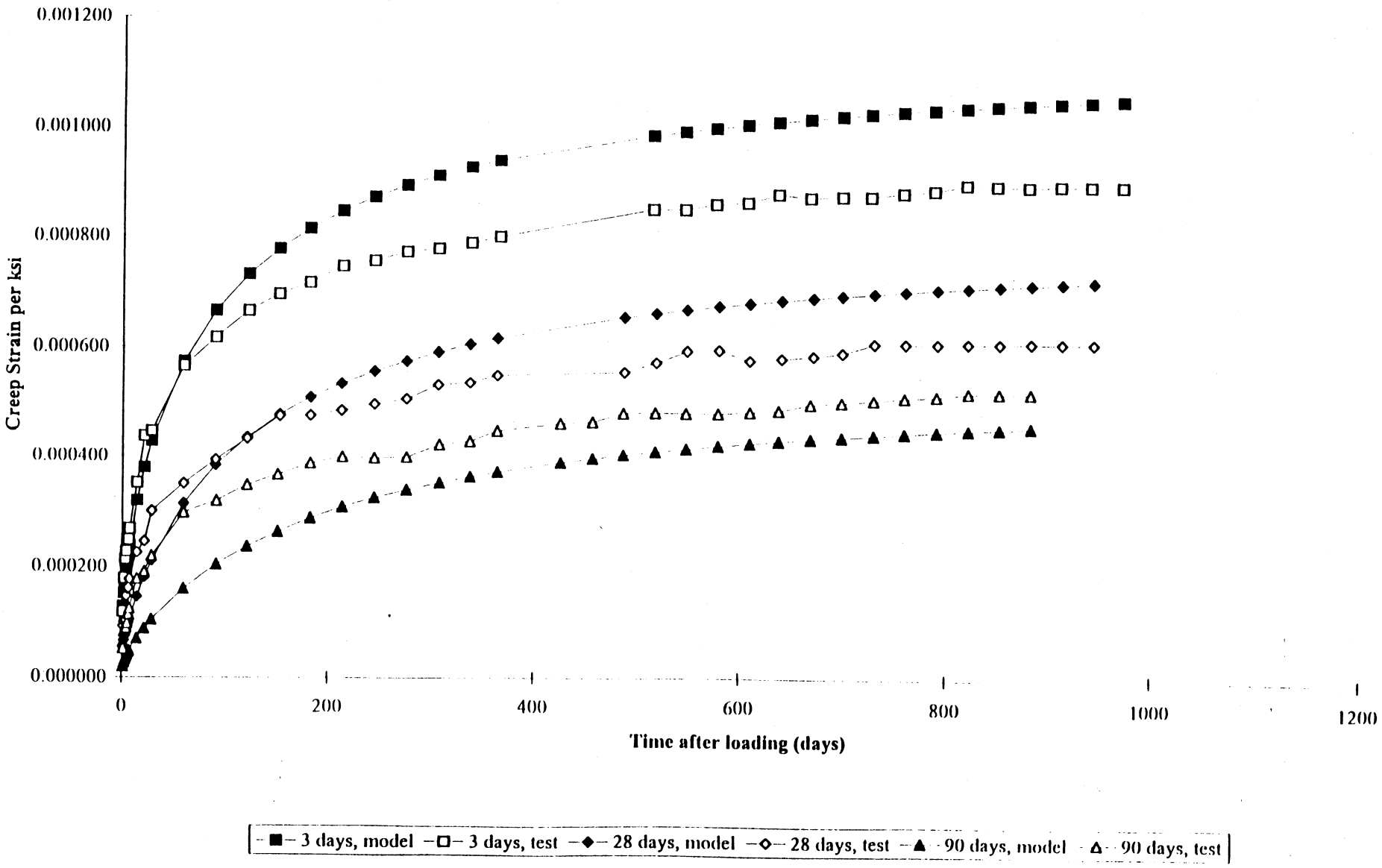

Figure 7.2 Superstructure Shrinkage Results (S=2.50)

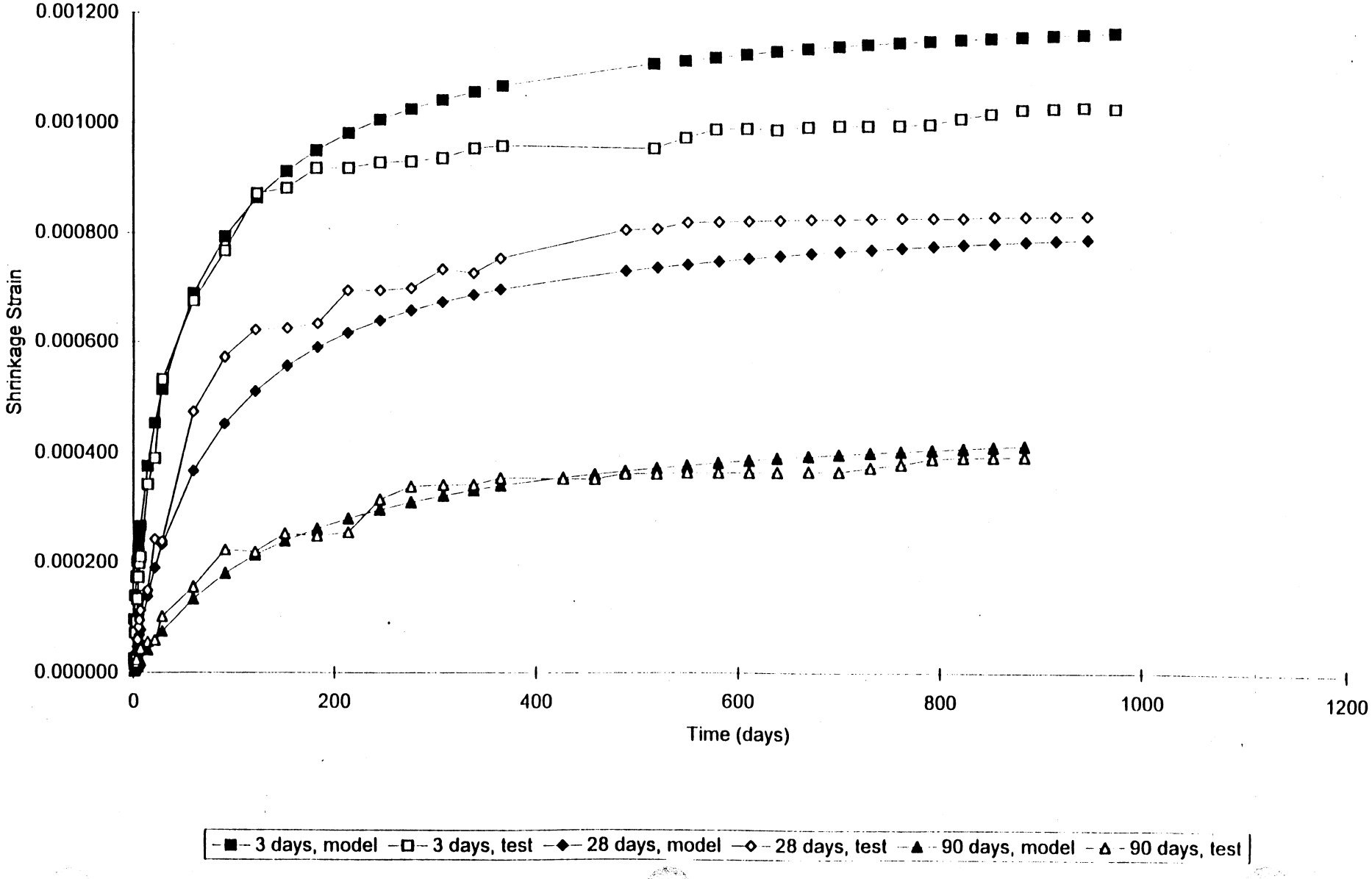

Figure 7.3 - Span 9 Extensometer Readings

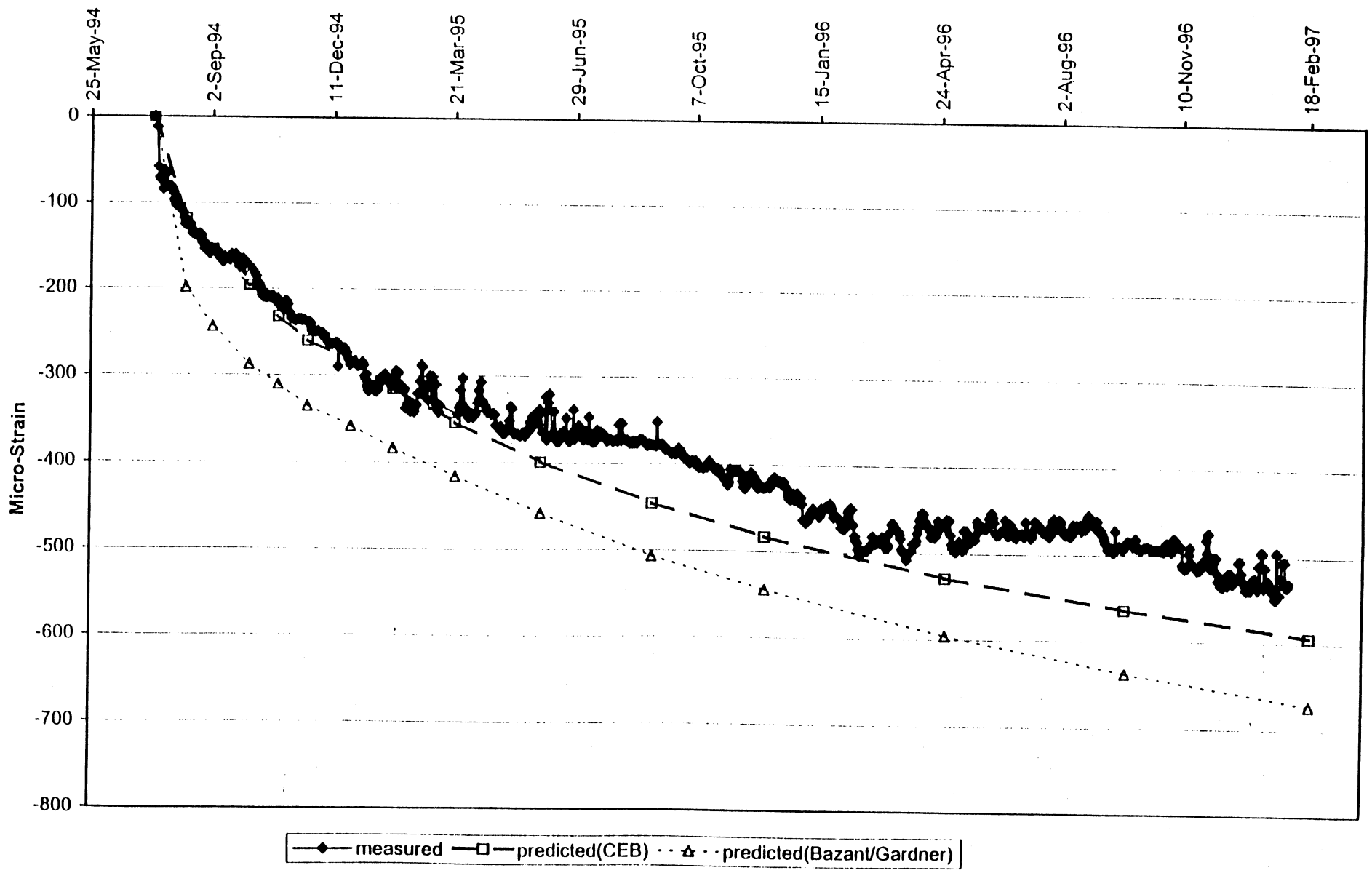

Figure 7.4 - Span 10 Extensometer Readings

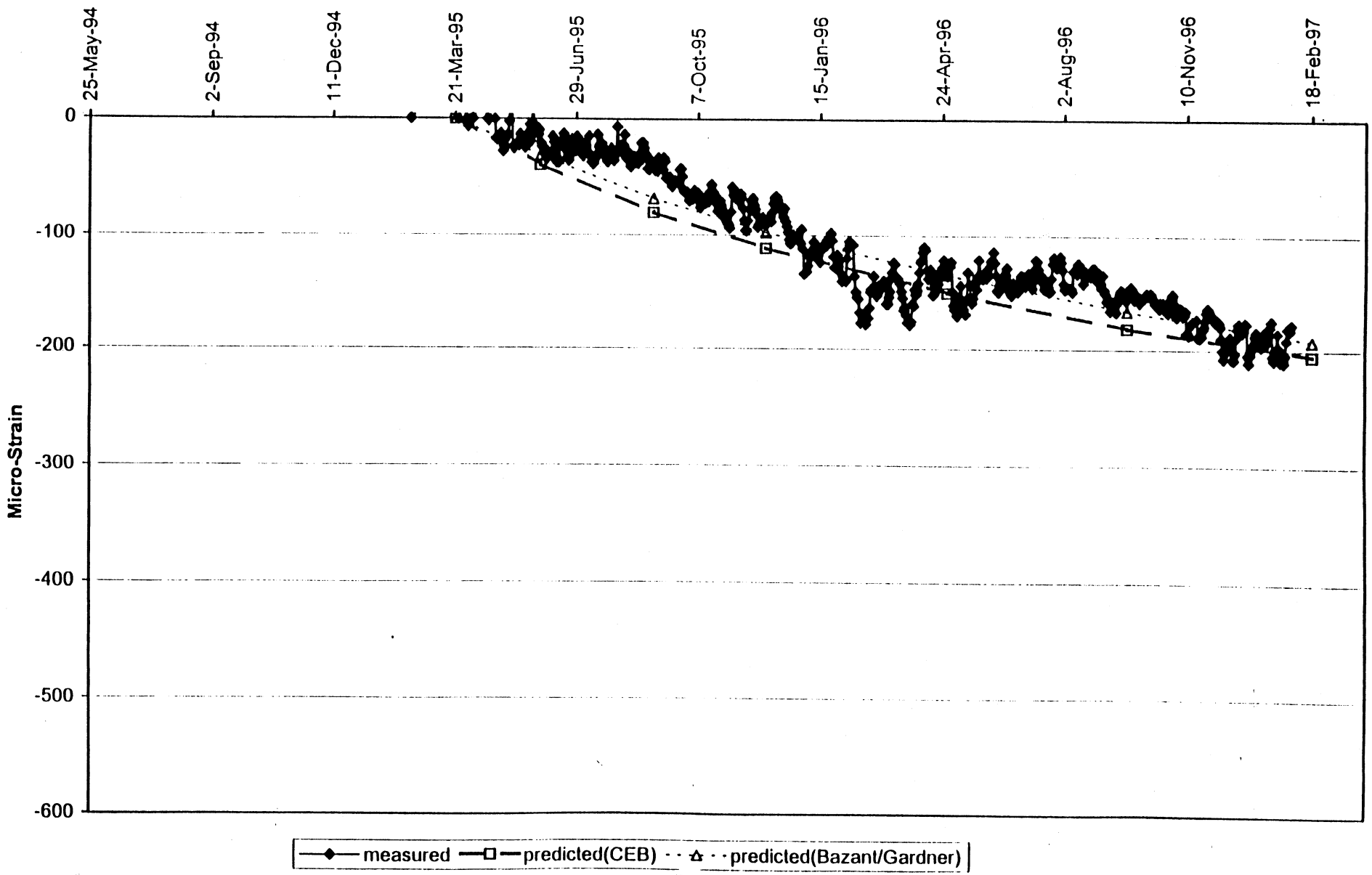

Figure 7.5 - Span 12 Extensometer Readings

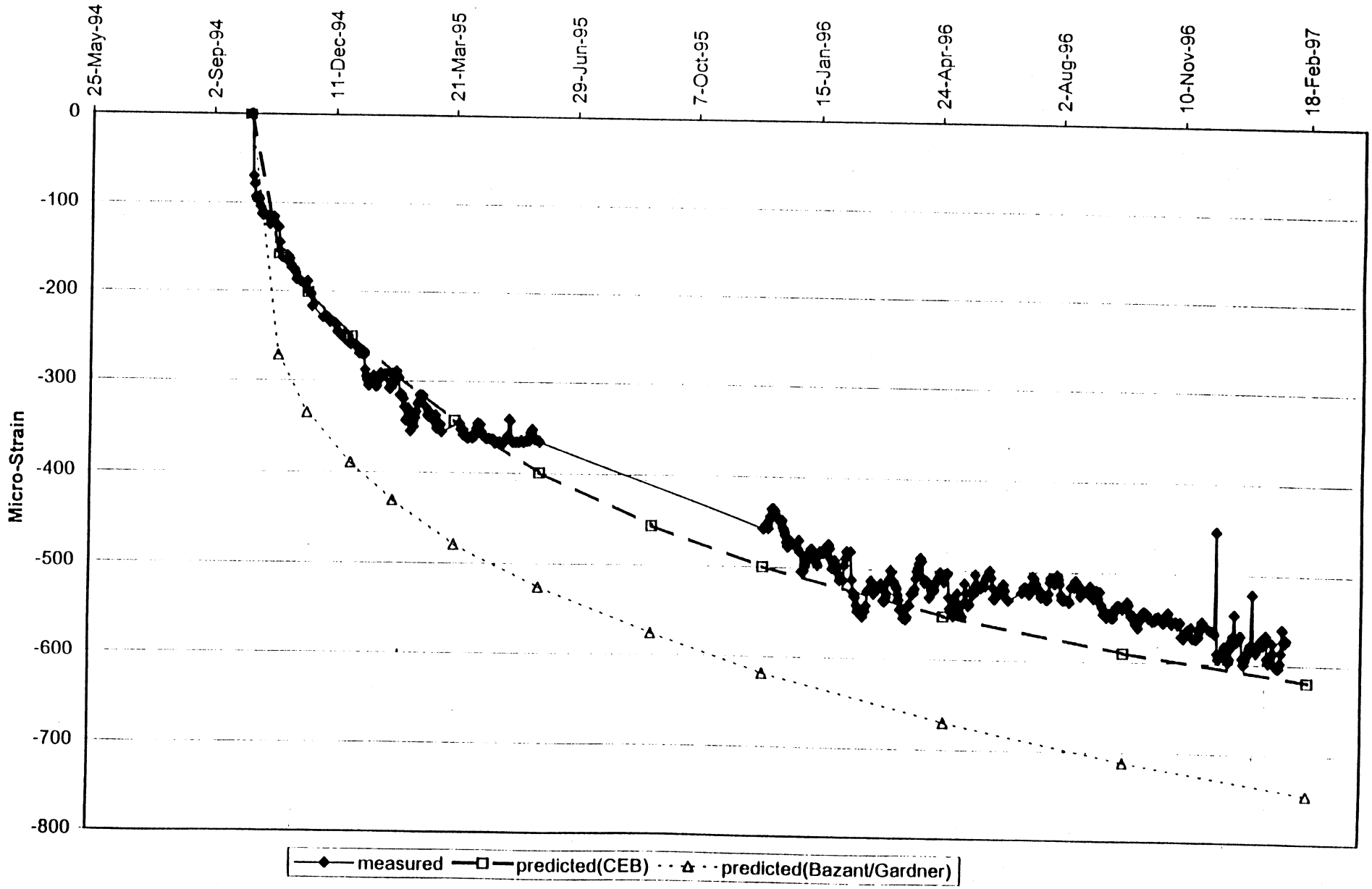

Figure 7.6 - Span 13 Extensometer Readings

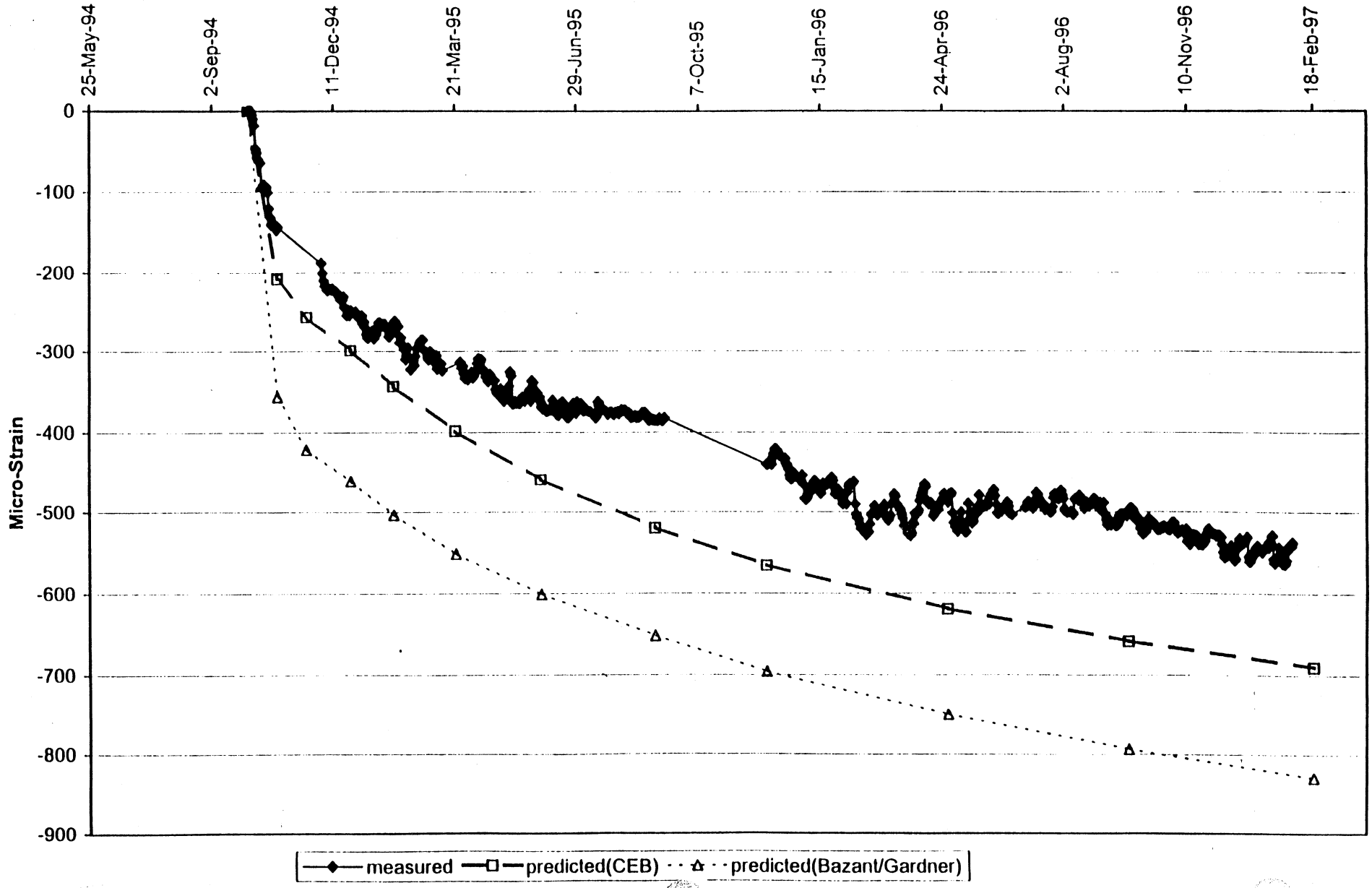

Figure 7.7 - Bearing Movement

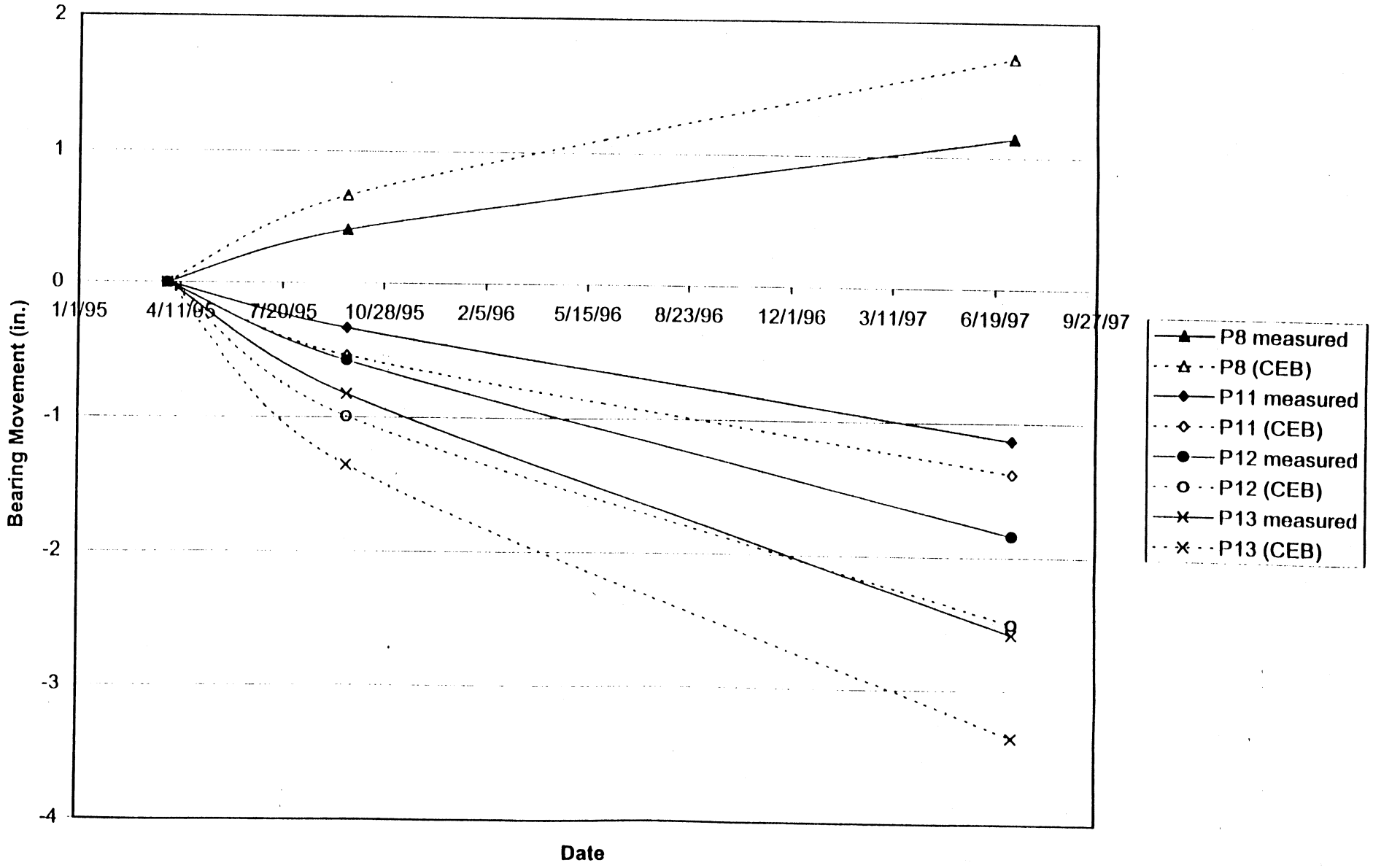

Table 7.1 - Bearing Movements

Date	Unit Inch	Pier 7	Pier 8	Pier 9	Pier 10	Pier 11	Pier 12	Pier 13
3/29/95		------	0.000	Initial Readings*		0.000	0.000	0.000
9/22/95	Measured	0.000	0.406	Movement between 3/29/95 and 9/22/95		-0.336	-0.578	-0.828
	Predicted	------	0.667			-0.540	-0.994	-1.354
	Ratio	------	0.61			0.62	0.58	0.61
7/7/97	Measured	0.828	1.141	Movement between 3/29/95 and 7/7/97		-1.133	-1.844	-2.578
	Predicted	1.403	1.727			-1.382	-2.500	-3.356
	Ratio	0.59	0.66			0.82	0.74	0.77

* Pier 7 was initialized on 9/22/95.

Figure 7.8 - Plano Wire Readings

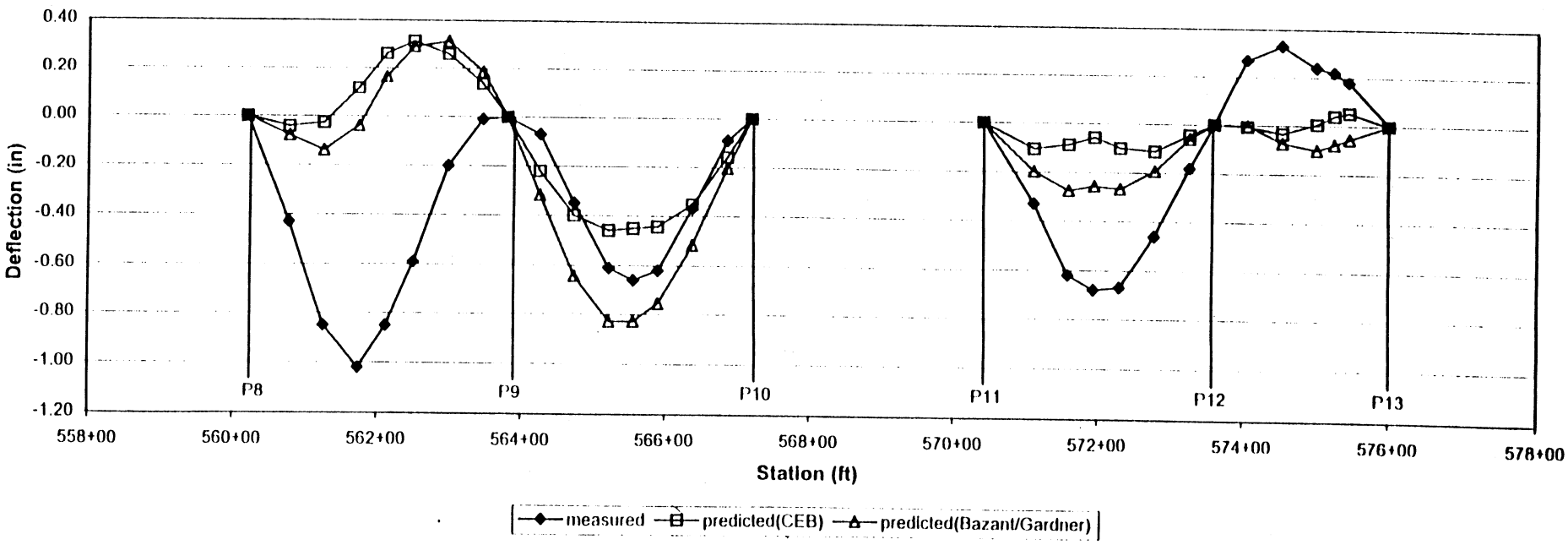

Figure 7.9 - Unit 2IB Camber

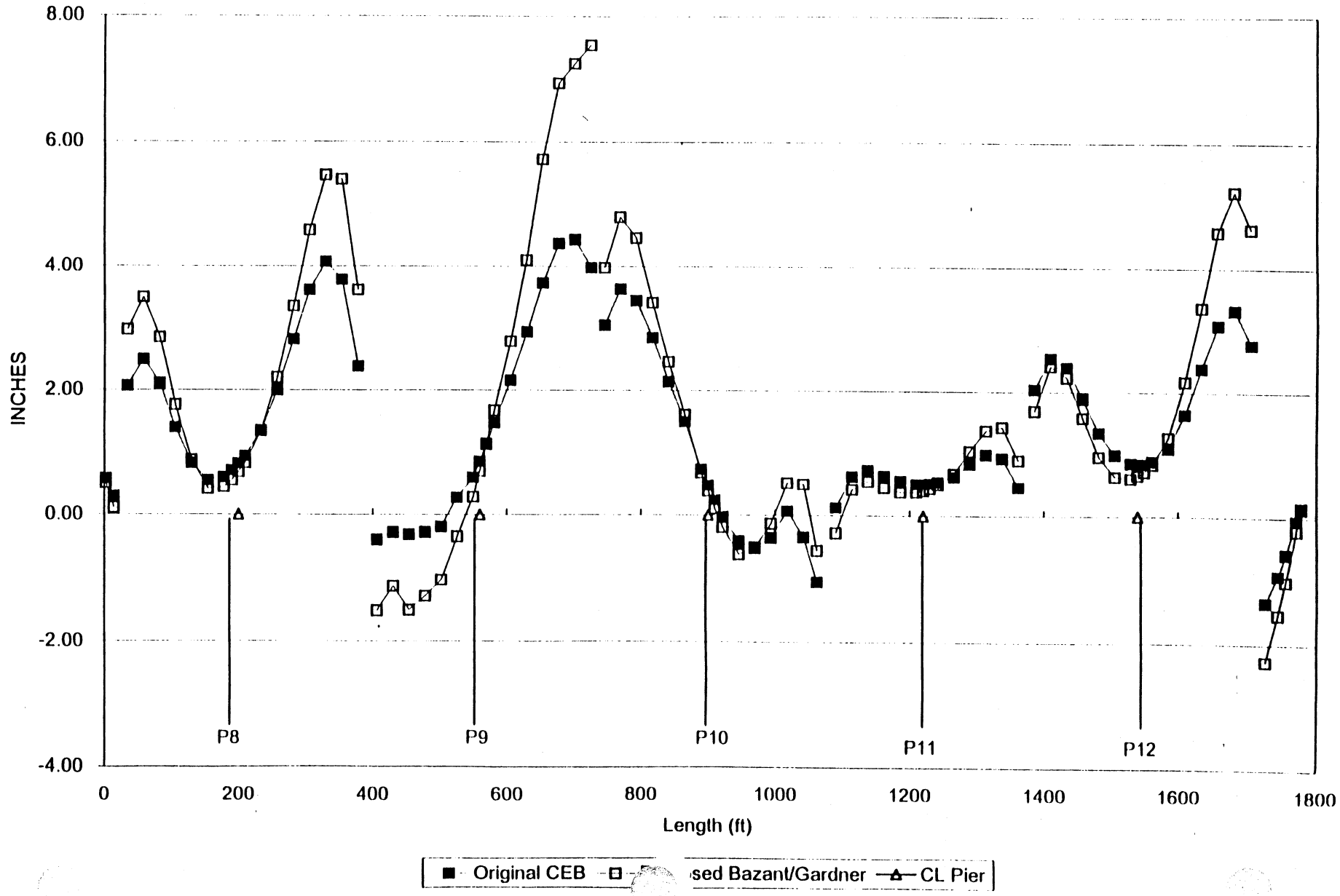

BEARING MOVEMENT READINGS

PIER: 7 IB

BEARING	DATE	TIME	TEMP (C) IN / OUT	READER	READING		DELTA			OVERALL AVERAGE
					UPSLOPE	DOWNSLOPE	UPSLOPE	DOWNSLOPE	AVERAGE	
SOUTH	3/29/95		22	INITIAL			-	-	-	-
	9/13/95	10:30	25.7/26.8	IAN			0.000	0.000	0.000	-
	9/22/95	9:10		IAN	3.438	3.313				-
	7/7/97	9:07		IAN	4.250	2.375	0.813	0.938	0.875	-
										-
										-
										-
										-
										-
										-
NORTH	3/29/95		22	INITIAL			-	-	-	-
	9/13/95	10:00	25.7/26.8	IAN			0.000	0.000	0.000	0.000
	9/22/95	9:10		IAN	3.000	3.625				
	7/7/97	9:07		IAN	3.813	2.875	0.813	0.750	0.781	0.828

BEARING MOVEMENT READINGS

PIER: 8 IB

BEARING	DATE	TIME	TEMP (C) IN / OUT	READER	READING		DELTA			OVERALL AVERAGE
					UPSLOPE	DOWNSLOPE	UPSLOPE	DOWNSLOPE	AVERAGE	
SOUTH	3/29/95		22	INITIAL	6.188	3.688	-	-	-	-
	9/13/95	11:00	25.7/26.8	IAN	6.688	3.438	0.500	0.250	0.375	-
	9/22/95	9:20		IAN	6.750	3.375	0.563	0.313	0.438	-
	7/7/97	9:10		IAN	7.438	2.625	1.250	1.063	1.156	-
										-
										-
										-
										-
										-
										-
NORTH	3/29/95		22	INITIAL	6.250	3.813	-	-	-	-
	9/13/95	10:00	25.7/26.8	IAN	6.688	3.563	0.438	0.250	0.344	0.359
	9/22/95	9:20		IAN	6.688	3.500	0.438	0.313	0.375	0.406
	7/7/97	9:10		IAN	7.438	2.750	1.188	1.063	1.125	1.141

BEARING MOVEMENT READINGS

PIER: 11 IB

BEARING	DATE	TIME	TEMP (C) IN / OUT	READER	READING		DELTA (+ Up, - Down)			OVERALL AVERAGE
					UPSLOPE	DOWNSLOPE	UPSLOPE	DOWNSLOPE	AVERAGE	
SOUTH	3/29/95		22	INITIAL	3.844	2.688	-	-	-	-
	9/13/95	11:15	25.7/26.8	IAN	3.563	3.188	-0.281	-0.500	-0.391	-
	9/22/95	9:25		IAN	3.563	3.125	-0.281	-0.438	-0.359	-
	7/7/97	9:15		IAN	2.750	3.938	-1.094	-1.250	-1.172	-
										-
										-
										-
										-
										-
										-
NORTH	3/29/95		22	INITIAL	3.625	3.000	-	-	-	-
	9/13/95	10:00	25.7/26.8	IAN	3.375	3.375	-0.250	-0.375	-0.313	-0.352
	9/22/95	9:25		IAN	3.375	3.375	-0.250	-0.375	-0.313	-0.336
	7/7/97	9:15		IAN	2.563	4.125	-1.063	-1.125	-1.094	-1.133

BEARING MOVEMENT READINGS

PIER: 12 IB

BEARING	DATE	TIME	TEMP (C) IN / OUT	READER	READING		DELTA (+ Up, - Down)			OVERALL AVERAGE
					UPSLOPE	DOWNSLOPE	UPSLOPE	DOWNSLOPE	AVERAGE	
SOUTH	3/29/95		22	INITIAL	8.063	5.813	-	-	-	-
	9/13/95	11:30	25.7/26.8	IAN	7.500	6.500	-0.563	-0.688	-0.625	-
	9/22/95	9:30		IAN	7.563	6.438	-0.500	-0.625	-0.563	-
	7/7/97	9:30		IAN	6.250	7.688	-1.813	-1.875	-1.844	-
										-
										-
										-
										-
										-
										-
NORTH	3/29/95		22	INITIAL	8.438	5.500	-	-	-	-
	9/13/95	10:00	25.7/26.8	IAN	7.875	6.188	-0.563	-0.688	-0.625	-0.625
	9/22/95	9:30		IAN	7.875	6.125	-0.563	-0.625	-0.594	-0.578
	7/7/97	9:30		IAN	6.625	7.375	-1.813	-1.875	-1.844	-1.844

BEARING MOVEMENT READINGS

PIER: 13 IB

BEARING	DATE	TIME	TEMP (C) IN / OUT	READER	READING		DELTA (+ Up, - Down)			OVERALL AVERAGE
					UPSLOPE	DOWNSLOPE	UPSLOPE	DOWNSLOPE	AVERAGE	
SOUTH	3/29/95		22	INITIAL	6.375	5.500	-	-	-	-
	9/13/95	11:45	25.7/26.8	IAN	5.563	6.313	-0.813	-0.813	-0.813	-
	9/22/95	10:20		IAN	5.625	6.313	-0.750	-0.813	-0.781	-
	7/7/97	9:35		IAN	3.875	8.125	-2.500	-2.625	-2.563	-
										-
										-
										-
										-
										-
										-
NORTH	3/29/95		22	INITIAL	6.500	5.313	-	-	-	-
	9/13/95	10:00	25.7/26.8	IAN	5.688	6.188	-0.813	-0.875	-0.844	-0.828
	9/22/95	10:20		IAN	5.688	6.250	-0.813	-0.938	-0.875	-0.828
	7/7/97	9:35		IAN	3.938	7.938	-2.563	-2.625	-2.594	-2.578

H3 HALAWA VALLEY VIADUCT
PIANO WIRE READINGS

P8 to P9

DATE

STATION	3/29/95	5/5/95	6/15/95	8/11/95	9/22/95	1/17/96	5/11/96	8/23/96
560+20	0.00	0.00	0.00	0.00	0.00	0.00	0.00	0.00
560+78	3.72	3.6	3.59	3.51	3.49	3.38	3.44	3.29
561+26	5.55	5.33	5.33	5.16	5.17	5.13	5.01	4.7
561+74	5.99	5.72	5.75	5.5	5.52	5.5	5.38	4.97
562+12	5.72	5.45	5.52	5.32	5.33	5.35	5.26	4.87
562+50	3.76	3.53	3.5	3.45	3.48	3.52	3.47	3.17
562+98	2.74	2.6	2.57	2.61	2.64	2.7	2.7	2.54
563+46	1.41	1.36	1.36	1.39	1.39	1.43	1.44	1.4
563+80	0	0	0	0	0	0	0	0
Midspan	0	-0.27	-0.24	-0.49	-0.47	-0.49	-0.61	-1.02

P9 to P10

DATE

STATION	3/29/95	5/5/95	6/15/95	8/11/95	9/22/95	1/17/96	5/11/96	8/23/96
563+80	0.00	0.00	0.00	0.00	0.00	0.00	0.00	0.00
564+26	2.36	2.36	2.34	2.32	2.31	2.26	2.23	2.29
564+74	3.94	3.91	3.84	3.81	3.77	3.65	3.55	3.59
565+22	5.23	5.16	5.07	4.99	4.96	4.78	4.62	4.62
565+56	5.79	5.72	5.62	5.53	5.5	5.31	5.15	5.13
565+90	4.9	4.83	4.72	4.65	4.62	4.46	4.29	4.28
566+38	3.52	3.47	3.4	3.36	3.34	3.24	3.13	3.15
566+86	2.32	2.31	2.28	2.27	2.27	2.24	2.2	2.23
567+20	0	0	0	0	0	0	0	0
Midspan	0	-0.07	-0.17	-0.26	-0.29	-0.48	-0.64	-0.66

P11 to P12

DATE

STATION	3/29/95	5/5/95	6/15/95	8/11/95	9/22/95	1/17/96	5/11/96	8/23/96
570+40	0	0	0	0	0	0	0	0
571+10	3.26	3.22	3.19	3.13	3.14	3.08	3.01	2.93
571+58	4.31	4.22	4.15	4.04	4.06	3.95	3.83	3.69
571+94	5.21	5.1	5.01	4.89	4.91	4.79	4.67	4.53
572+30	4.4	4.3	4.22	4.09	4.1	3.98	3.87	3.73
572+78	3	2.92	2.87	2.78	2.79	2.71	2.64	2.54
573+26	1.33	1.3	1.3	1.26	1.27	1.24	1.21	1.15
573+60	0	0	0	0	0	0	0	0
Midspan	0	-0.11	-0.2	-0.32	-0.3	-0.42	-0.54	-0.68

P12 to P13

DATE

STATION	3/29/95	5/5/95	6/15/95	8/11/95	9/22/95	1/17/96	5/11/96	8/23/96
573+60	0	0	0	0	0	0	0	0
574+06	2.06	2.1	2.13	2.19	2.18	2.24	2.27	2.33
574+54	2.35	2.41	2.42	2.54	2.53	2.57	2.61	2.68
575+02	2.43	2.49	2.48	2.6	2.57	2.59	2.61	2.67
575+26	2.53	2.58	2.58	2.69	2.65	2.67	2.67	2.75
575+47	2.43	2.47	2.46	2.56	2.53	2.64	2.54	2.61
576+01	0	0	0	0	0	0	0	0
Midspan	0	0.05	0.05	0.16	0.12	0.14	0.14	0.22

DEFLECTIONS P8 TO P9

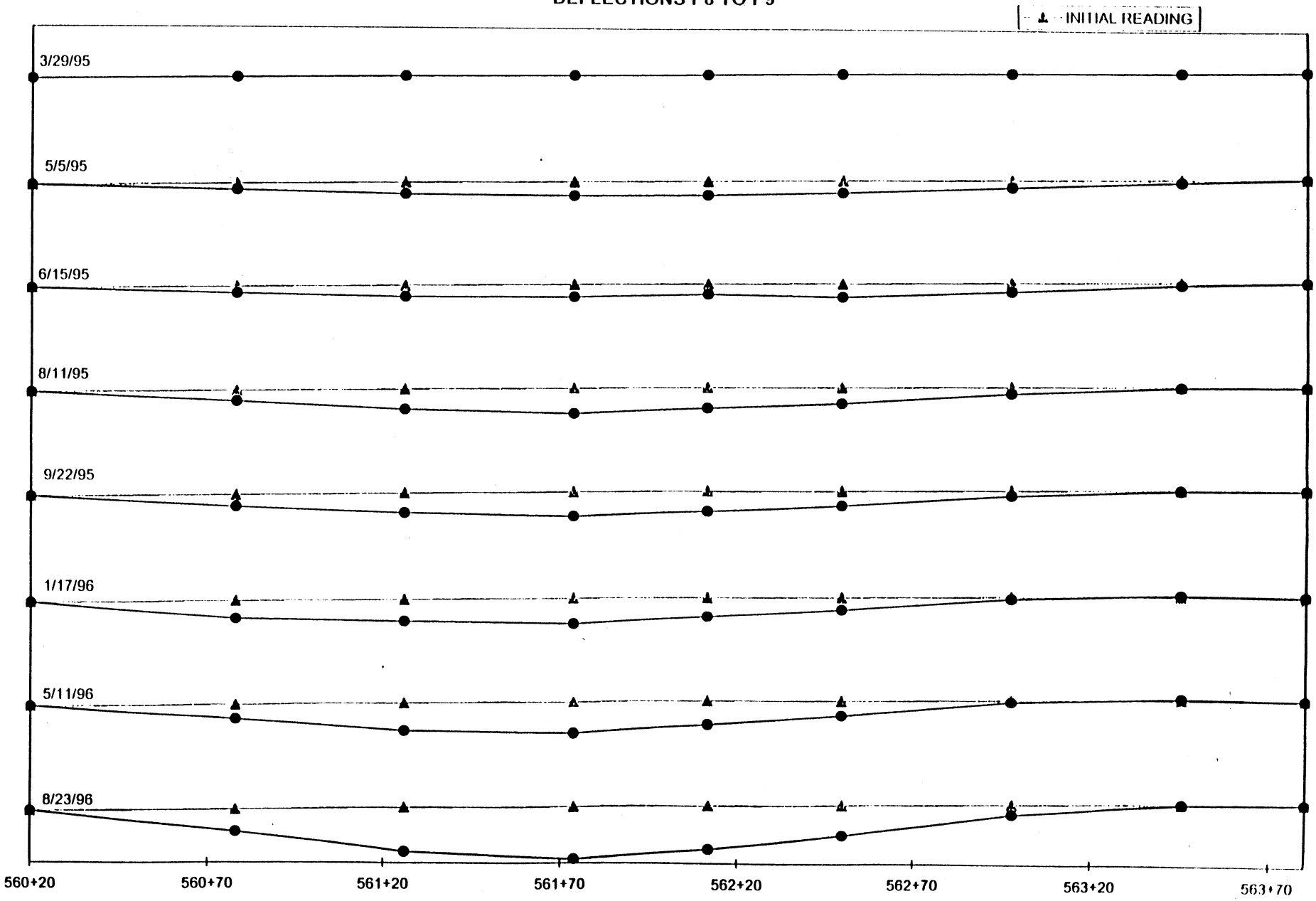

Field Data 7.4.7

DEFLECTIONS P9 TO P10

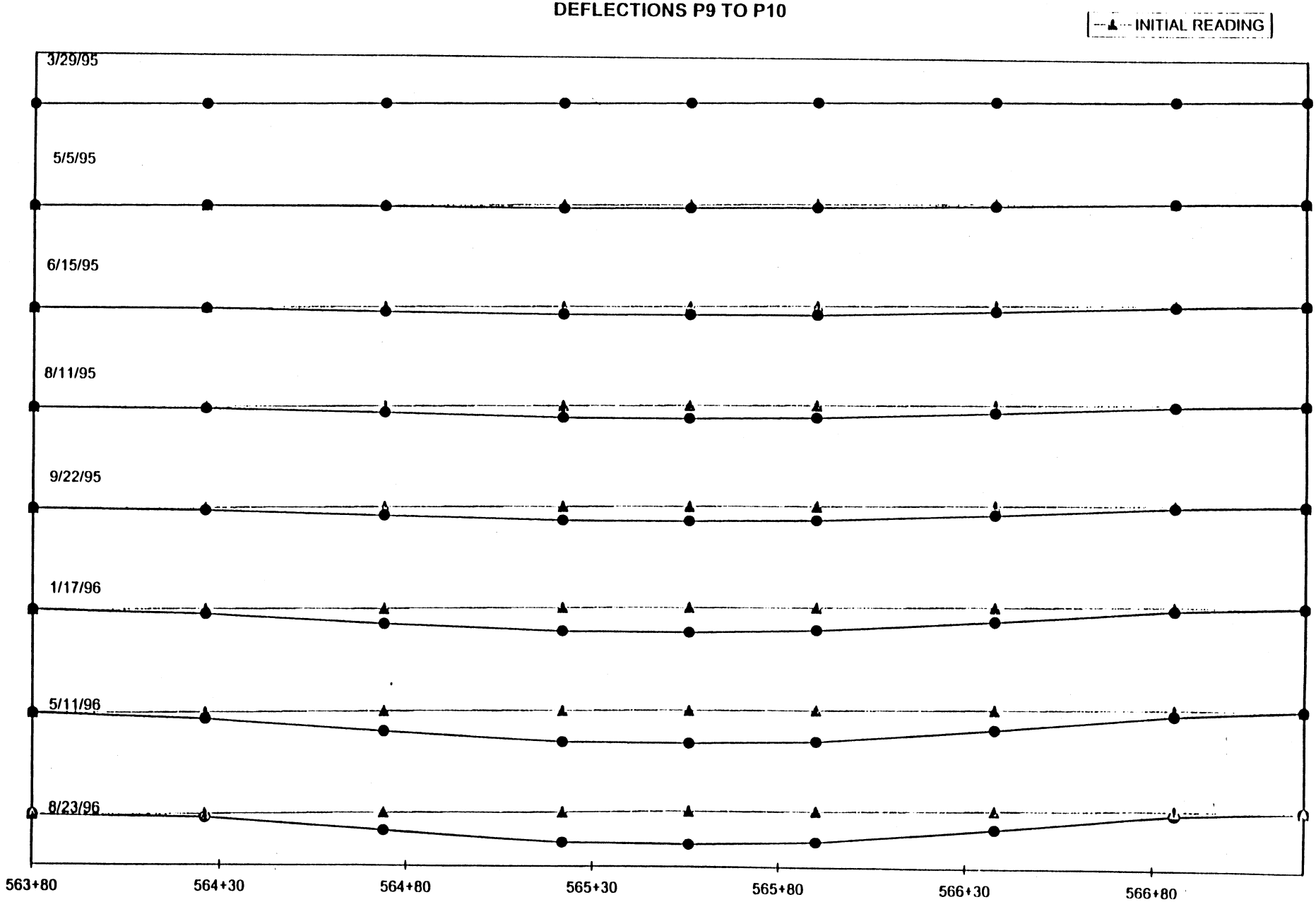

Field [illegible].4.8

DEFLECTIONS P11 TO P12

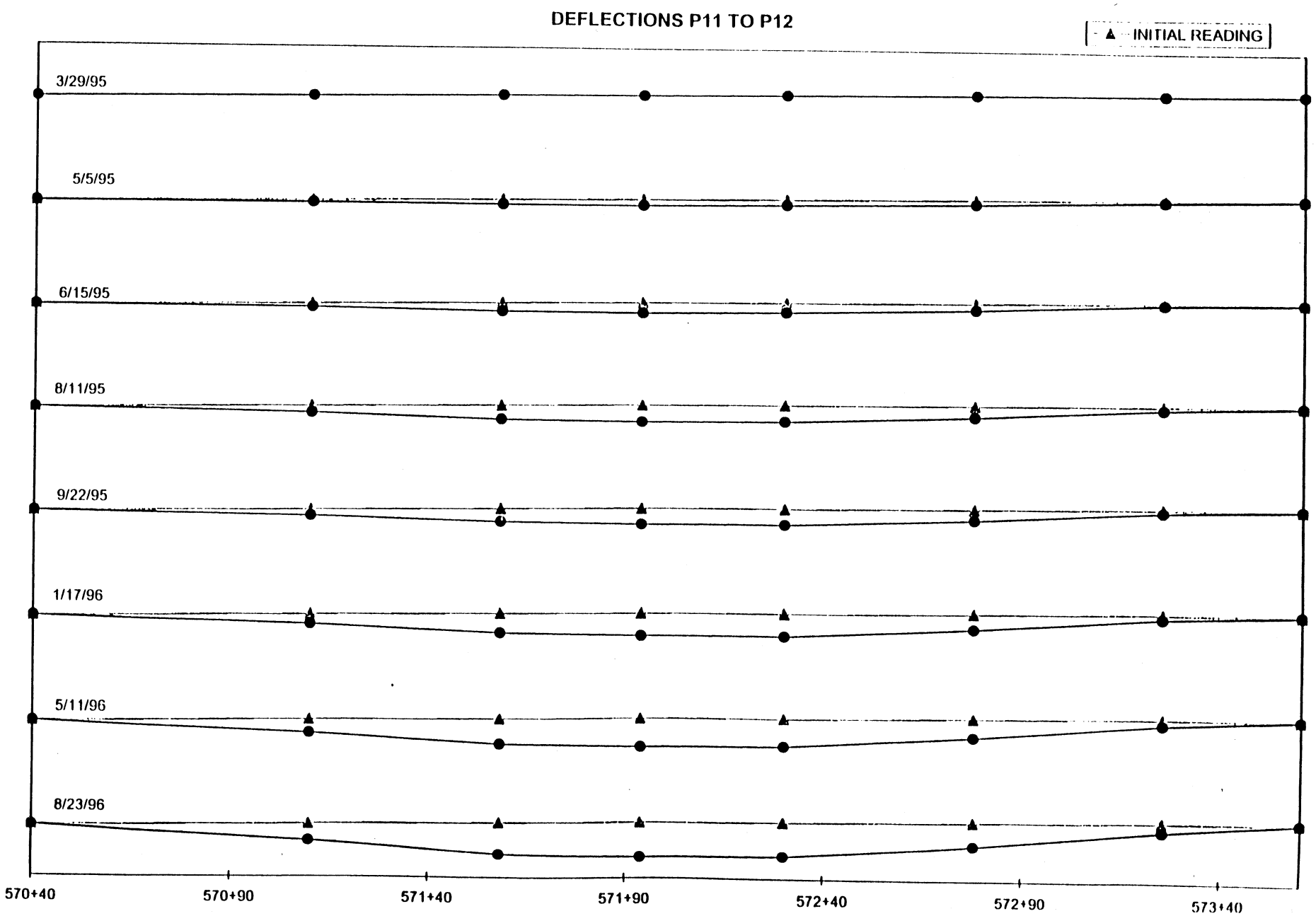

Field Data 7.4.9

DEFLECTIONS P12 TO P13

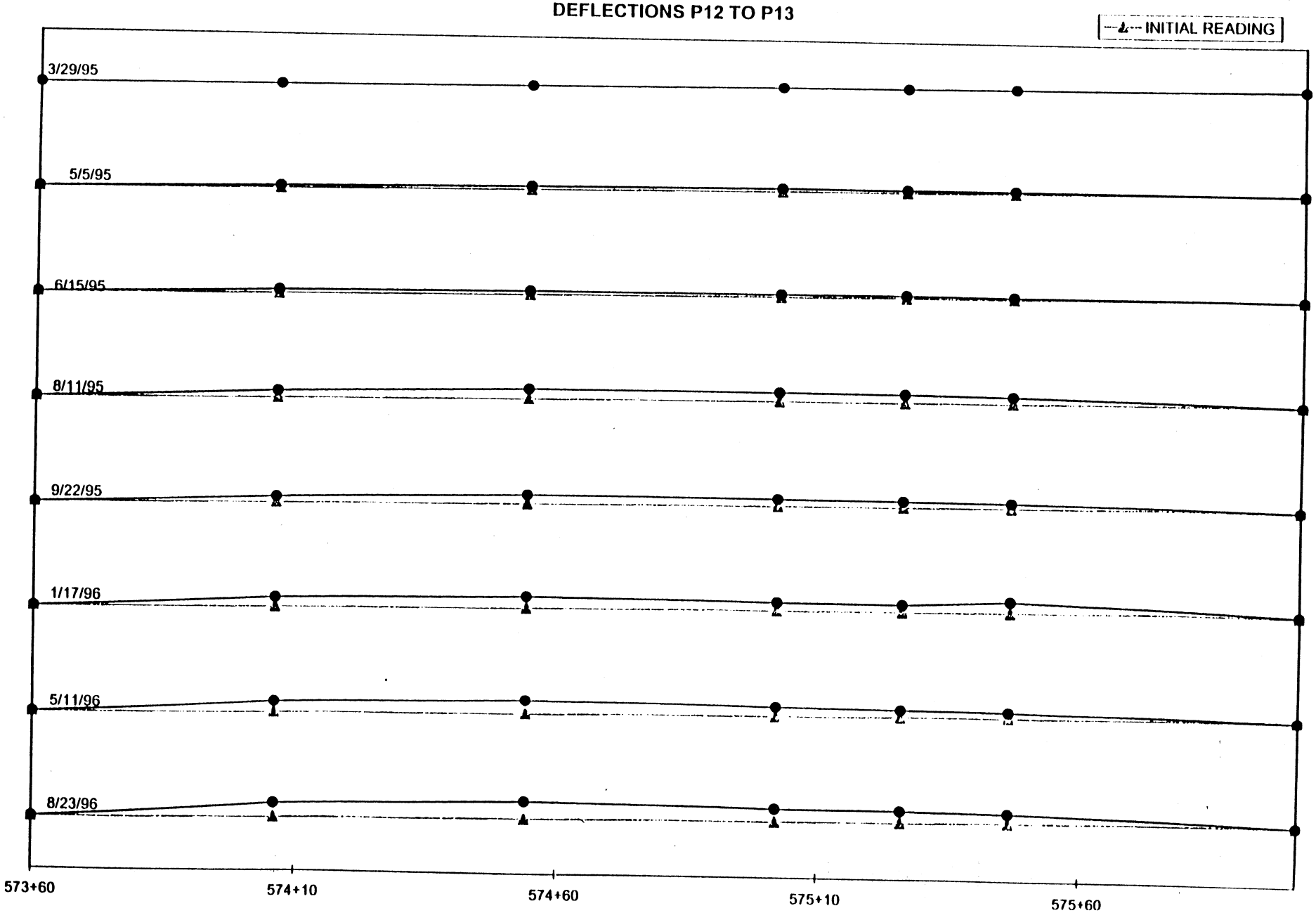

Field D[illegible] 4.10

CHAPTER 8

THERMAL BEHAVIOR

In this chapter, thermocouple readings are systematically reduced to determine critical positive and negative thermal gradients. These critical gradients are shown to compare favorably with those recommended in the new proposed AASHTO segmental guide specifications. A detailed discussion of the thermal behavior of the North Halawa Valley Viaduct is included in the referenced PCI Journal article given in Appendix A.

Although seven sections of the North Halawa Valley Viaduct have been instrumented (Figure 8.1), only Section E and Section F have thermocouples (Figure 8.2). Section E has 26 gages while Section F has 32 gages. Gages 1 to 6 and 7 to 11 are at the centerline of the box girder in the top and bottom slab respectively. Gages 12 to 24 (or 26) are at the centerline of the web. Additional gages are across the width of the web (gages 25 and 26 for Section E and gages 29 to 32 for Section F). Table 8.1 gives the thermocouple locations as a function of the distance from the top slab.

Vast amounts of thermocouple data have to be processed in an efficient manner to obtain critical positive and negative thermal gradients. This is because readings are generally taken every two hours for a five year period at 58 gages. The method selected to reduce the data has been to graphically review thermocouple readings on a (1) annual basis, (2) monthly basis, (3) daily basis and (4) critical positive and negative gradient basis.

Thermocouple readings were first recorded in late 1994 and will be recorded through the end of 1999. Readings were taken at two hour intervals from the beginning of the study until August 22, 1995. The frequency of readings was then changed to six hour intervals since it was felt at that time that too much information was being collected (readings from all instrumentation were taken at the same two hour intervals). The readings reverted back to two hour intervals on October 14, 1997 when it was realized that the peak critical positive thermal gradient was being underestimated by taking readings at six hour intervals.

Two inches of concrete topping were placed on October 7, 1996. The net effect of placing topping is to shift the gage readings down by two inches and give additional thermocouple readings at the top, middle and bottom of the overlay. Note that asphalt topping was not used on this project and consequently the effects of asphalt topping on the thermal gradient cannot be discussed in this report.

Table 8.2 gives a summary of the large number of thermocouple plots included in this report. Each figure shows thermocouple readings at Section E and Section F together for comparison purposes. The present report includes plots from January 1995 to December 1997. The final report will include plots for the entire five year period (January 1995 to December 1999).

Annual plots are given in Figures 8.3 to 8.7 while monthly plots are given in Figures 8.8 to 8.67. These are followed by daily and gradient (positive and negative) plots for each year. The 1995 daily plots are given in Figures 8.68 to 8.82 (note that the September plots miss the peak critical positive gradient due to the change to six hour intervals). The 1995 to 1997 critical positive and negative gradients are given in Figures 8.83 to 8.140. The 1998 and 1999 critical positive and negative gradients will be included in the final report.

Annual readings are reviewed at gage 14 which is 2.5 inches below the deck surface. This gives an overall picture of the thermocouple readings. This also helps to spot areas where there are spurious results (moisture in the datalogger) and no results (power failure). Monthly readings are reviewed at gage 14 and 22. Whereas gage 14 is near the deck surface and gives the daily peaks and valleys, gage 22 is in the middle of the section and is less influenced by daily fluctuations. Daily readings are reviewed at gages 14, 15 and 16 (which are 2.5, 5.0 and 7.5 inches respectively from the deck surface) as well as gage 22. The maximum positive gradient can be seen to occur at 4 PM, while the maximum negative gradient can be seen to occur at 6 AM. Thermal gradients are plotted along the centerline of the web as well as the centerline of the top and bottom slab, and compared to those in the 1998 proposed AASHTO segmental guide specifications (AASHTO 98).

Critical negative gradients from 1995 to 1997 are extremely close to the gradient proposed in the AASHTO 98 recommendations. This is extremely important because the negative gradient in the AASHTO 98 recommendations is taken as -0.3 times the positive gradient. This is a 40% reduction from the AASHTO LRFD bridge design specifications (AASHTO 94) where the negative gradient is taken as -0.5 times the same positive gradient. This study definitely validates the proposed reduction of the negative thermal gradient.

Critical positive gradients from 1995 to 1997 are also extremely close to the gradient proposed in the AASHTO 98 recommendations. The critical 1995 positive gradient occurs on July 1, 1995 (Figure 8.89). The slab and web values correlate very well with the AASHTO 98 recommendations. The critical 1996 positive gradient occurs on June 1, 1996 (Figure 8.103). The critical 1997 positive gradient occurs on July 20, 1997 (Figure 8.123). Although the slab and web values slightly exceed those of the AASHTO 98 recommendations, the peak value is less and hence the overall effect of this gradient should be less severe than the design gradient.

Reference:

Shushkewich, K. W., "Design of Segmental Bridges for Thermal Gradient," PCI JOURNAL, V. 43, No. 4, July-August 1998, pp.120-137.

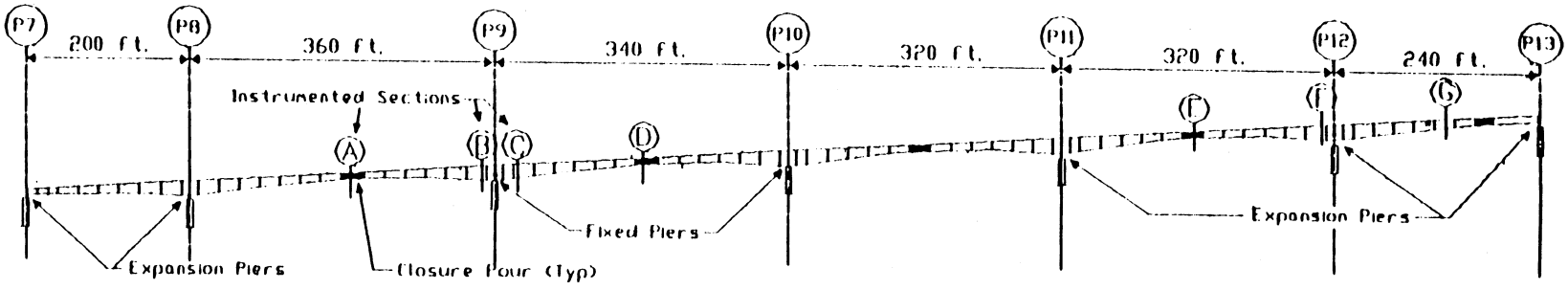

UNIT 2 INBOUND VIADUCT

Figure 8.1

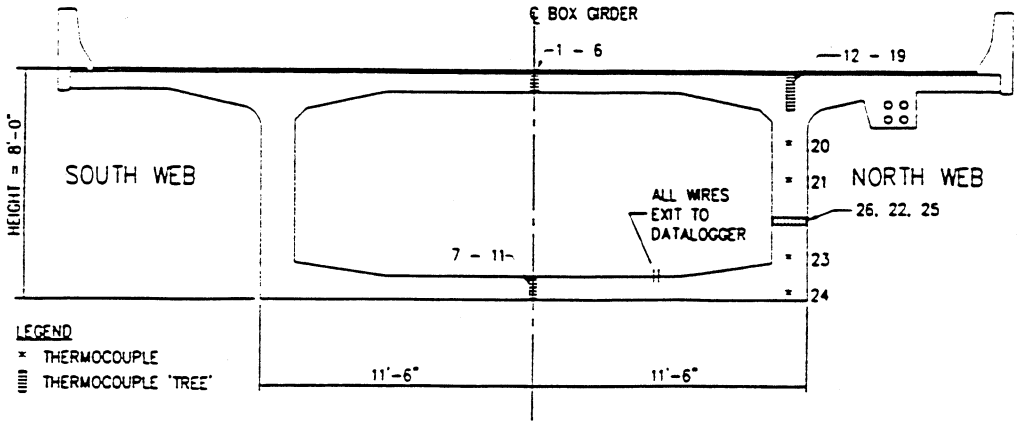

THERMOCOUPLES AT SECTION E

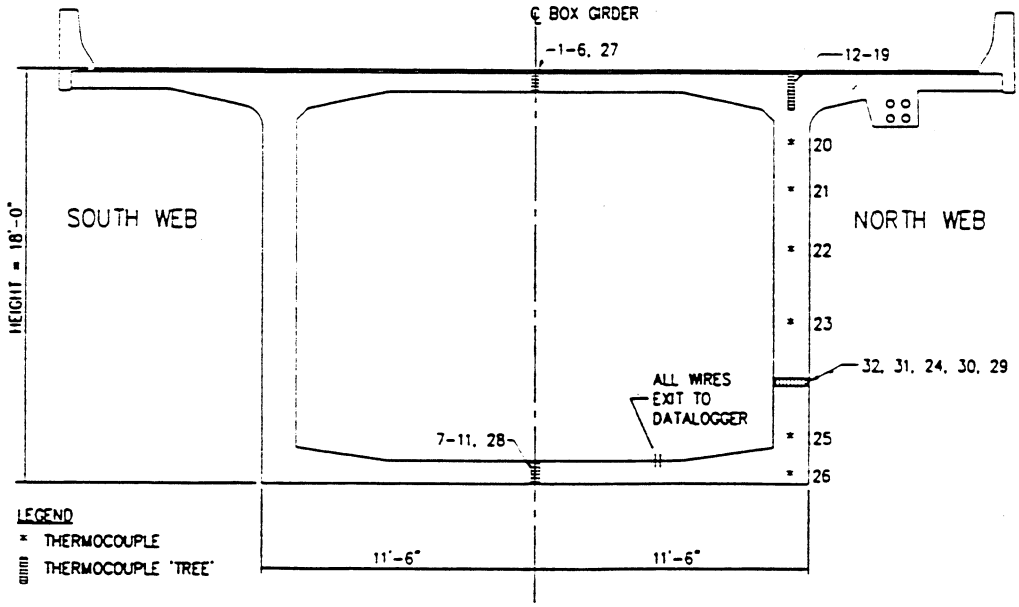

THERMOCOUPLES AT SECTION F

Figure 8.2

Section E				Section F			
gage at midspan	distance from top	gage at web	distance from top	gage at midspan	distance from top	gage at web	distance from top
1E	-2.0	12E	-2.0	1F	-2.0	12F	-2.0
2E	0.0	13E	0.0	2F	0.0	13F	0.0
3E	2.5	14E	2.5	3F	2.5	14F	2.5
4E	5.0	15E	5.0	4F	5.0	15F	5.0
5E	7.5	16E	7.5	5F	7.5	16F	7.5
6E	10.0	17E	10.0	6F	10.0	17F	10.0
7E	88.0	18E	14.0	7F	196.0	18F	14.0
8E	90.5	19E	18.0	8F	198.5	19F	18.0
9E	92.0	20E	22.5	9F	206.0	20F	51.0
10E	93.5	21E	36.5	10F	213.5	21F	82.0
11E	96.0	22E	54.0	11F	216.0	22F	100.5
		23E	71.0			23F	143.0
		24E	86.5			24F	172.0
						25F	202.5
						26F	214.0

Table 8.1 - Thermocouple Locations Measured from Top of Section

figure	annual	8.45	Feb 98	8.85	26 May 95		97 positive
		8.46	Mar 98	8.86	16 Jun 95	figure	gradient
8.3	1995	8.47	Apr 98	8.87	17 Jun 95		
8.4	1996	8.48	May 98	8.88	28 Jun 95	8.119	17 Apr 97
8.5	1997	8.49	Jun 98	8.89	1 Jul 95	8.120	30 May 97
8.6	1998	8.50	Jul 98	8.90	15 Jul 95	8.121	13 June 97
8.7	1999	8.51	Aug 98	8.91	18 Jul 95	8.122	14 July 97
		8.52	Sep 98	8.92	2 Aug 95	8.123	20 July 97
figure	monthly	8.53	Oct 98	8.93	3 Aug 95	8.124	9 Aug 97
		8.54	Nov 98	8.94	16 Aug 95	8.125	14 Aug 97
8.8	Jan 95	8.55	Dec 98			8.126	18 Aug 97
8.9	Feb 95	8.56	Jan 99		95 negative	8.127	1 Sep 97
8.10	Mar 95	8.57	Feb 99	figure	gradient	8.128	13 Sep 97
8.11	Apr 95	8.58	Mar 99			8.129	24 Sep 97
8.12	May 95	8.59	Apr 99	8.95	7 Jan 95	8.130	1 Oct 97
8.13	Jun 95	8.60	May 99	8.96	8 Jan 95		
8.14	Jul 95	8.61	Jun 99	8.97	12 Feb 95		97 negative
8.15	Aug 95	8.62	Jul 99	8.98	15 Feb 95	figure	gradient
8.16	Sep 95	8.63	Aug 99	8.99	6 Mar 95		
8.17	Oct 95	8.64	Sep 99	8.100	7 May 95	8.131	6 Jan 97
8.18	Nov 95	8.65	Oct 99	8.101	20 Dec 95	8.132	17 Jan 97
8.19	Dec 95	8.66	Nov 99	8.102	21 Dec 95	8.133	22 Jan 97
8.20	Jan 96	8.67	Dec 99			8.134	23 Jan 97
8.21	Feb 96				96 positive	8.135	23 Feb 97
8.22	Mar 96	figure	95 daily	figure	gradient	8.136	19 Nov 97
8.23	Apr 96					8.137	25 Nov 97
8.24	May 96	8.68	4 May 95	8.103	1 Jun 96	8.138	11 Dec 97
8.25	Jun 96	8.69	22 May 95	8.104	3 Jun 96	8.139	29 Dec 97
8.26	Jul 96	8.70	26 May 95	8.105	9 Jul 96	8.140	31 Dec 97
8.27	Aug 96	8.71	16 Jun 95	8.106	29 Jul 96		
8.28	Sep 96	8.72	17 Jun 95	8.107	9 Aug 96		
8.29	Oct 96	8.73	28 Jun 95	8.108	23 Aug 96		
8.30	Nov 96	8.74	1 Jul 95	8.109	24 Aug 96		
8.31	Dec 96	8.75	15 Jul 95	8.110	2 Sep 96		
8.32	Jan 97	8.76	18 Jul 95				
8.33	Feb 97	8.77	2 Aug 95		96 negative		
8.34	Mar 97	8.78	3 Aug 95	figure	gradient		
8.35	Apr 97	8.79	16 Aug 95				
8.36	May 97	8.80	7 Sep 95	8.111	2 Jan 96		
8.37	Jun 97	8.81	20 Sep 95	8.112	11 Jan 96		
8.38	Jul 97	8.82	21 Sep 95	8.113	9 Mar 96		
8.39	Aug 97			8.114	27 Mar 96		
8.40	Sep 97		95 positive	8.115	15 Apr 96		
8.41	Oct 97	figure	gradient	8.116	27 Apr 96		
8.42	Nov 97			8.117	5 May 96		
8.43	Dec 97	8.83	4 May 95	8.118	9 May 96		
8.44	Jan 98	8.84	22 May 95				

Table 8.2 - Summary of Thermocouple Figures

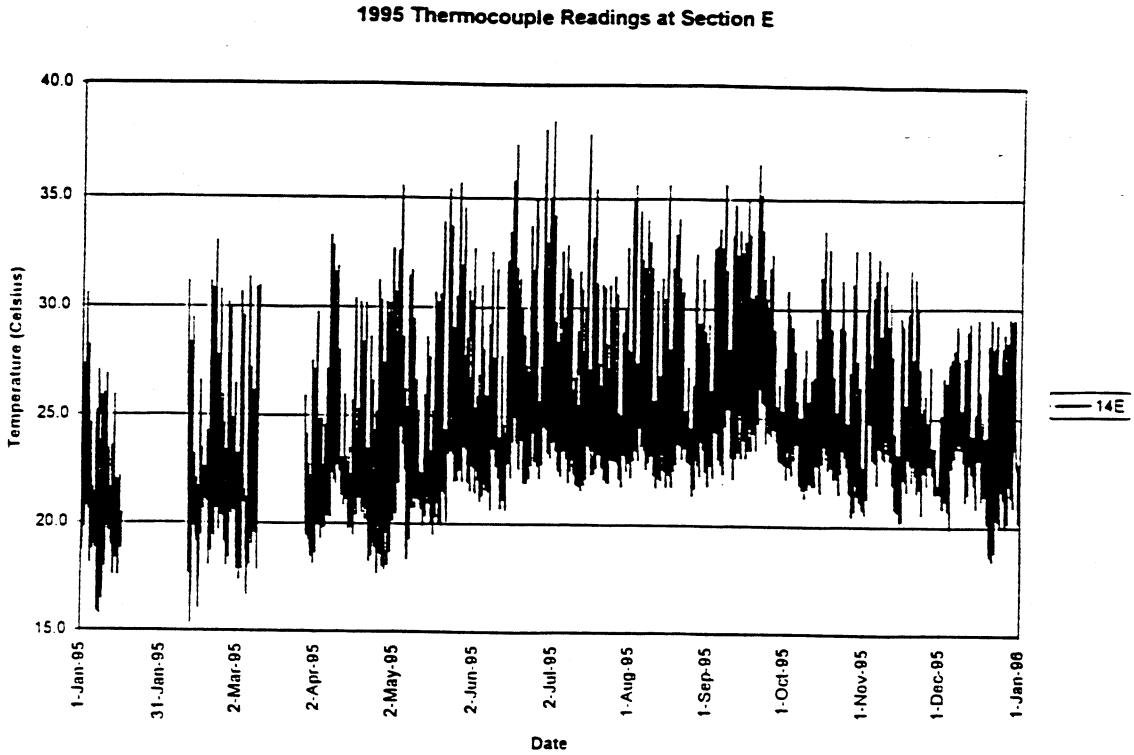
1995 Thermocouple Readings at Section E
40.0
35.0
30.0
25.0
20.0
15.0
Temperature (Celsius)
1-Jan-95
31-Jan-95
2-Mar-95
2-Apr-95
2-May-95
2-Jun-95
2-Jul-95
1-Aug-95
1-Sep-95
1-Oct-95
1-Nov-95
1-Dec-95
1-Jan-96
Date
14E

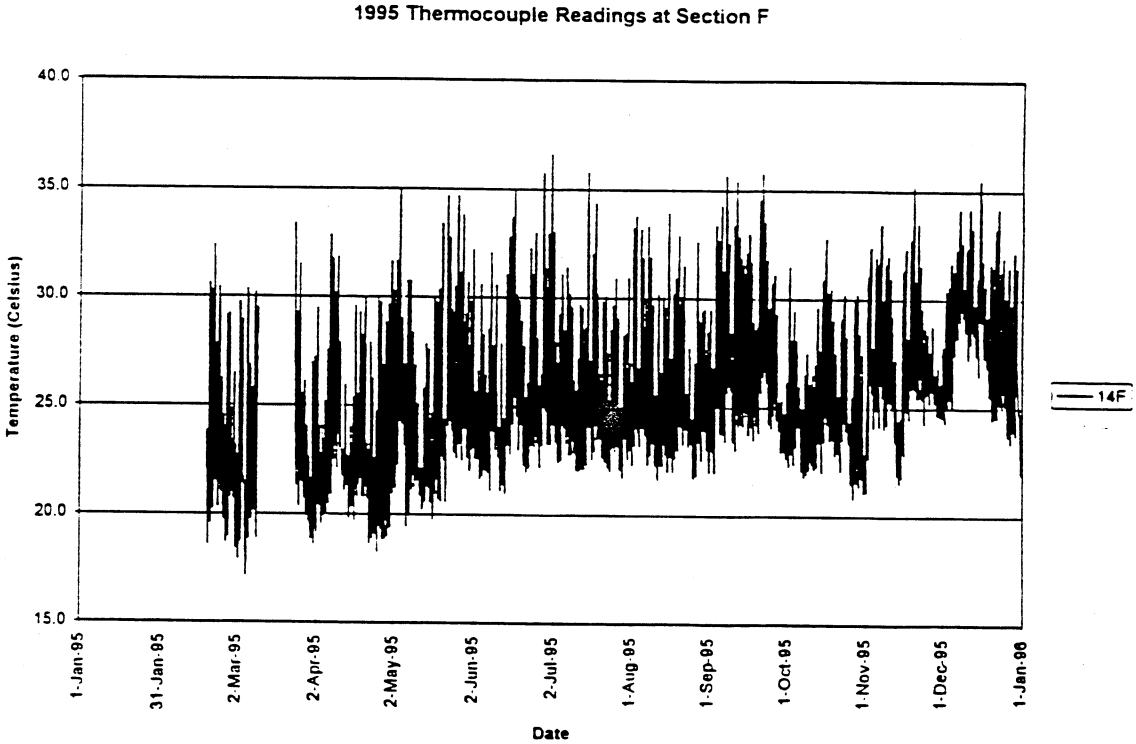
1995 Thermocouple Readings at Section F
40.0
35.0
30.0
25.0
20.0
15.0
Temperature (Celsius)
1-Jan-95
31-Jan-95
2-Mar-95
2-Apr-95
2-May-95
2-Jun-95
2-Jul-95
1-Aug-95
1-Sep-95
1-Oct-95
1-Nov-95
1-Dec-95
1-Jan-96
Date
14F

Figure 8.3

1996 Thermocouple Readings at Section E

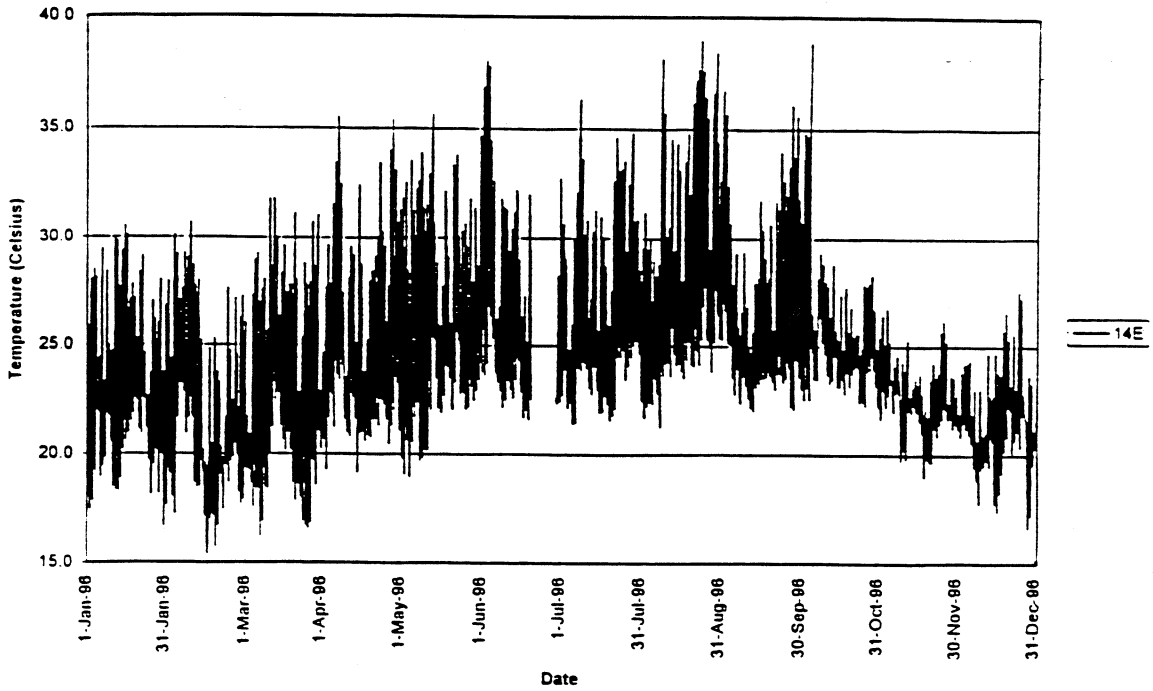

H3 Instrumentation Report

TYLin International

1996 Thermocouple Readings at Section F

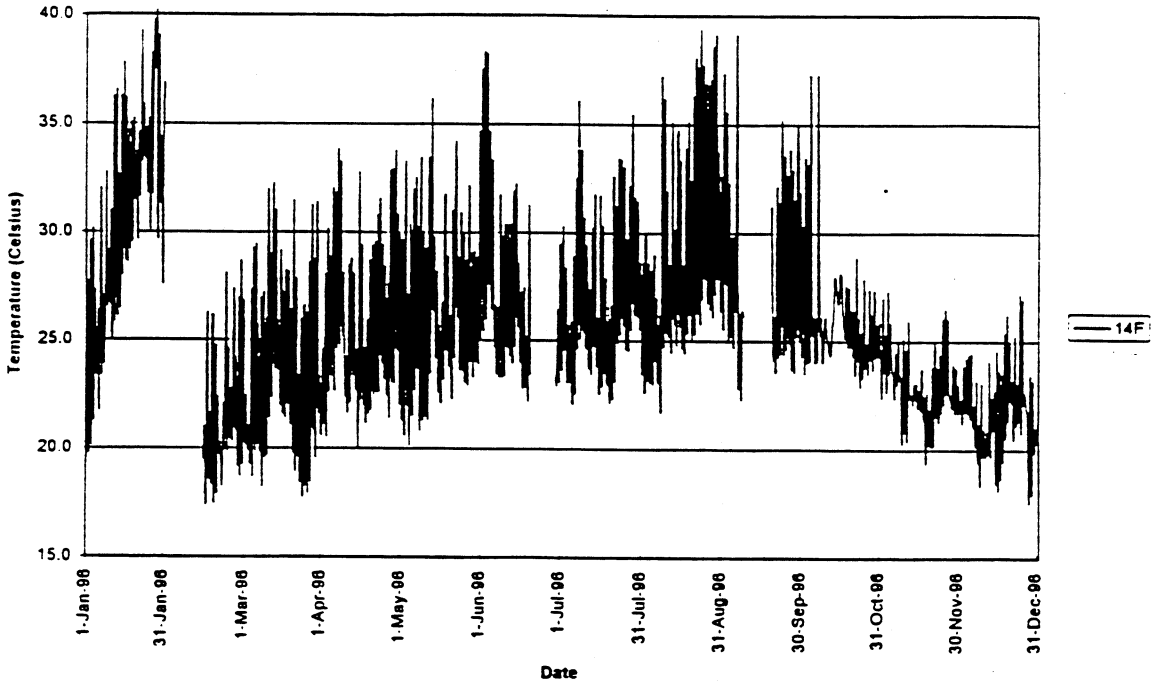

Figure 8.4

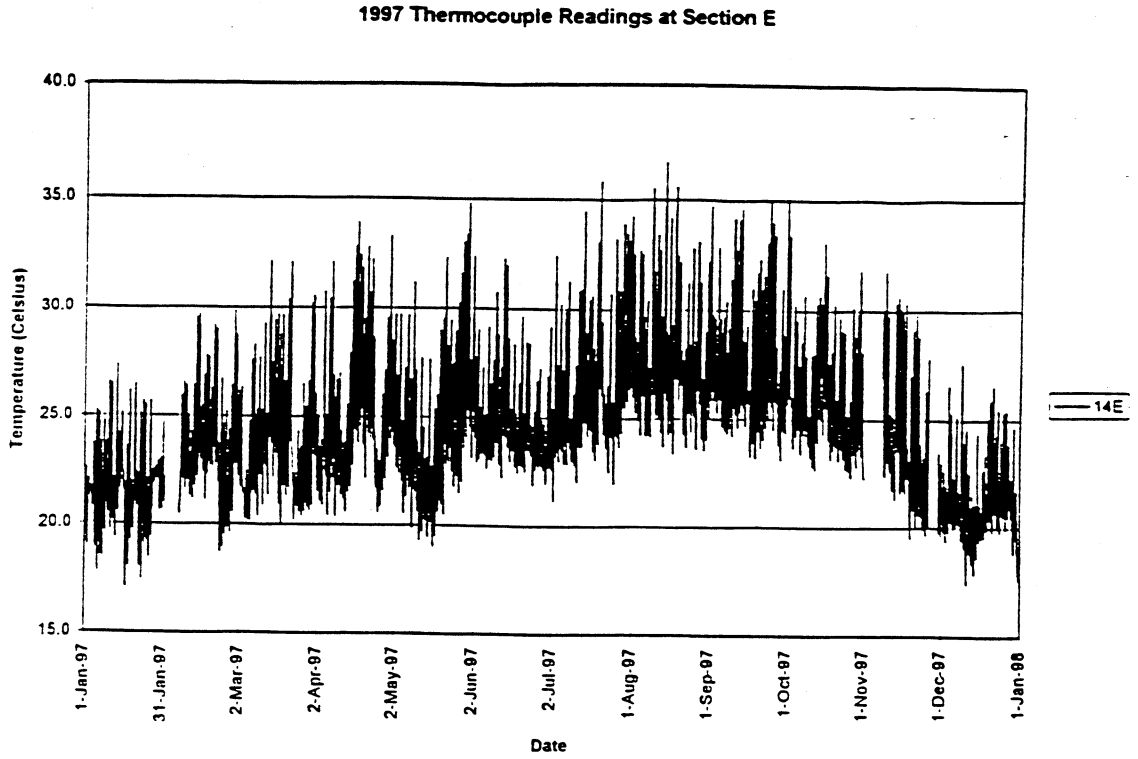
1997 Thermocouple Readings at Section E
40.0
35.0
30.0
25.0
20.0
15.0
Temperature (Celsius)
1-Jan-97
31-Jan-97
2-Mar-97
2-Apr-97
2-May-97
2-Jun-97
2-Jul-97
1-Aug-97
1-Sep-97
1-Oct-97
1-Nov-97
1-Dec-97
1-Jan-98
Date
14E

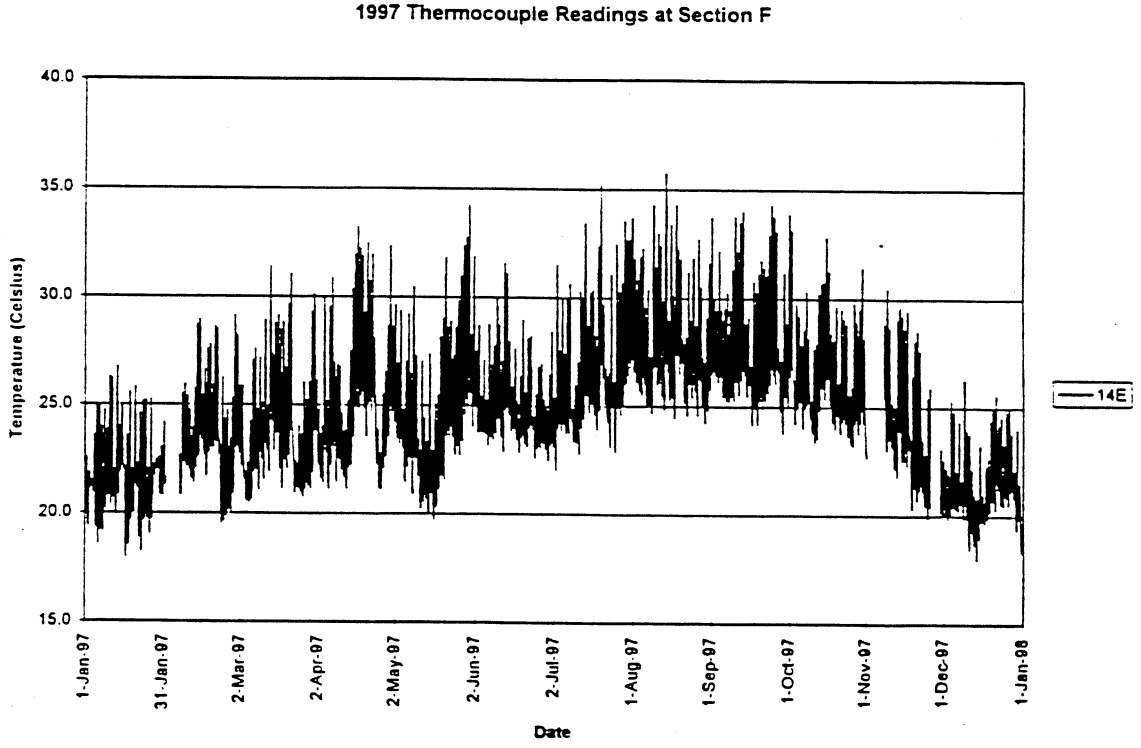
1997 Thermocouple Readings at Section F
40.0
35.0
30.0
25.0
20.0
15.0
Temperature (Celsius)
1-Jan-97
31-Jan-97
2-Mar-97
2-Apr-97
2-May-97
2-Jun-97
2-Jul-97
1-Aug-97
1-Sep-97
1-Oct-97
1-Nov-97
1-Dec-97
1-Jan-98
Date
14E

Figure 8.5

1998 Thermocouple Readings at Section E

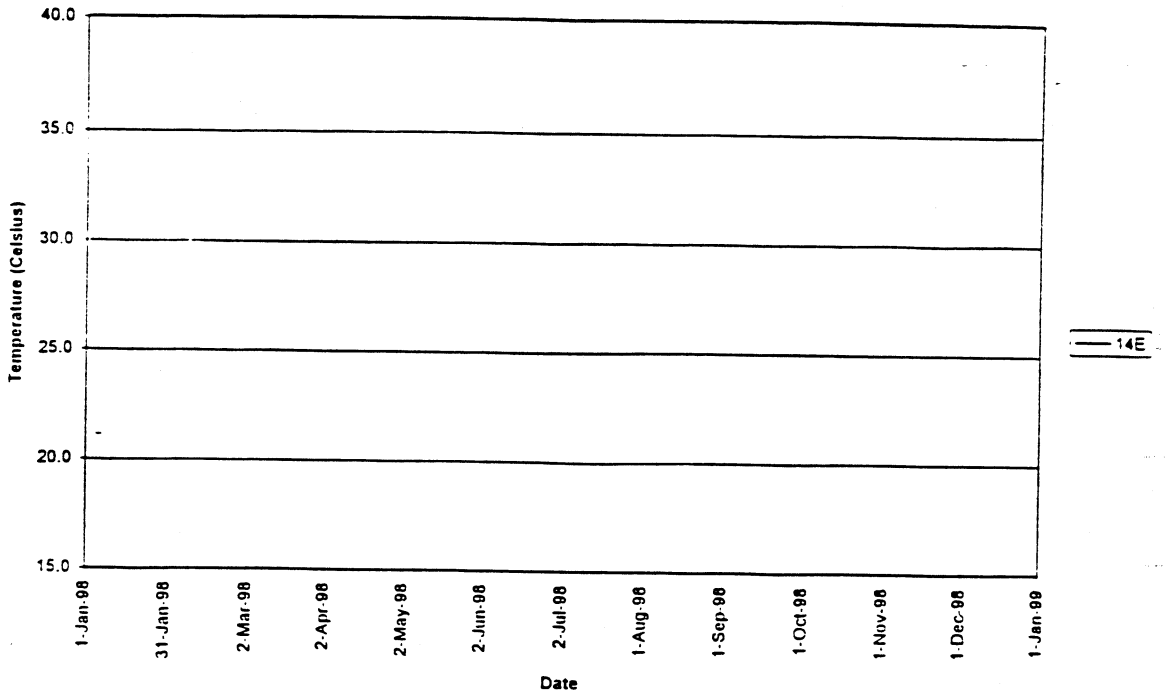

1998 Thermocouple Readings at Section F

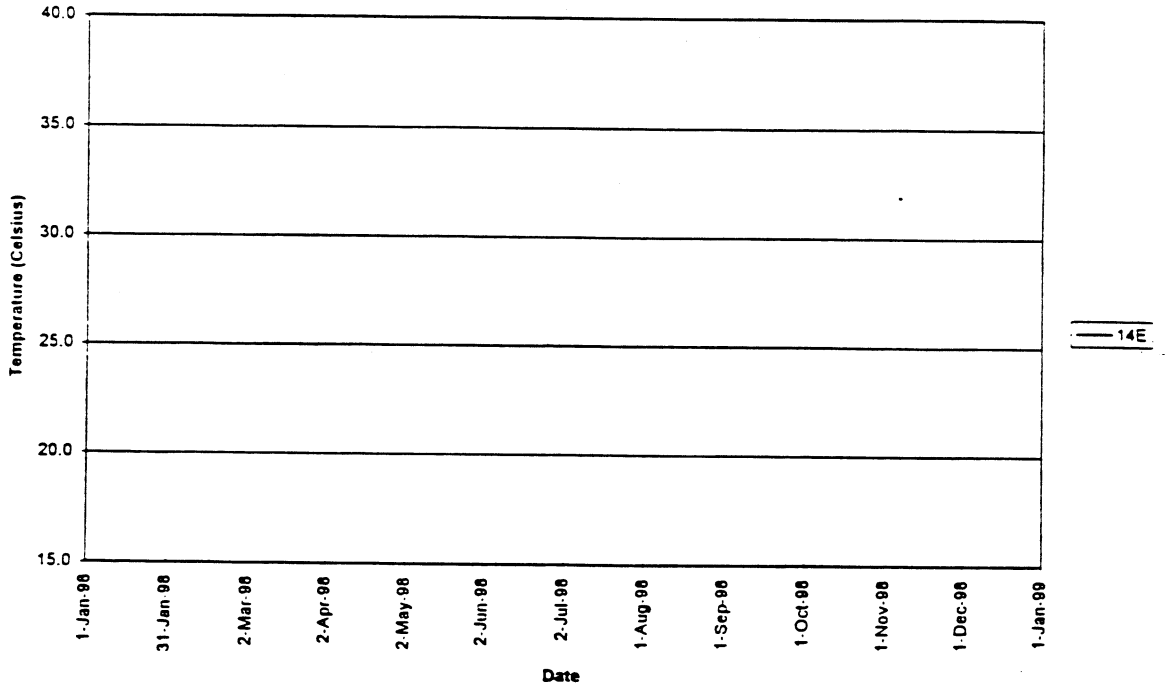

Figure 8.6

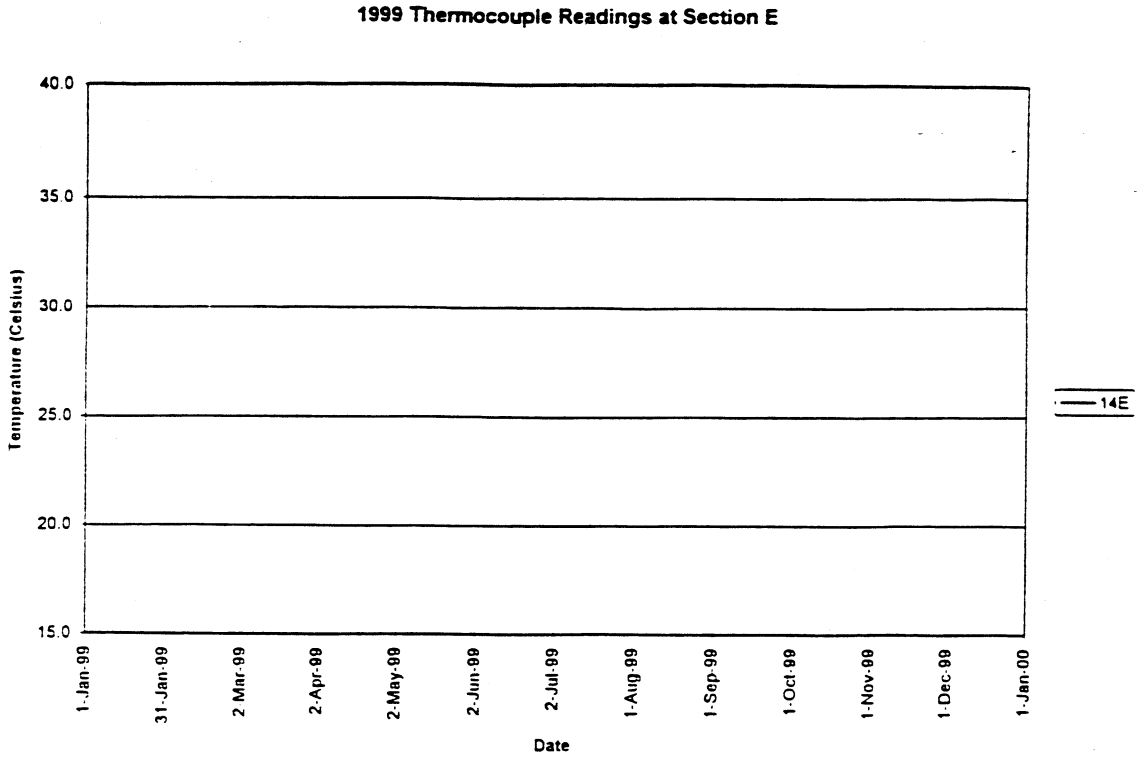
1999 Thermocouple Readings at Section E
40.0
35.0
30.0
25.0
20.0
15.0
Temperature (Celsius)
1-Jan-99
31-Jan-99
2-Mar-99
2-Apr-99
2-May-99
2-Jun-99
2-Jul-99
1-Aug-99
1-Sep-99
1-Oct-99
1-Nov-99
1-Dec-99
1-Jan-00
Date
14E

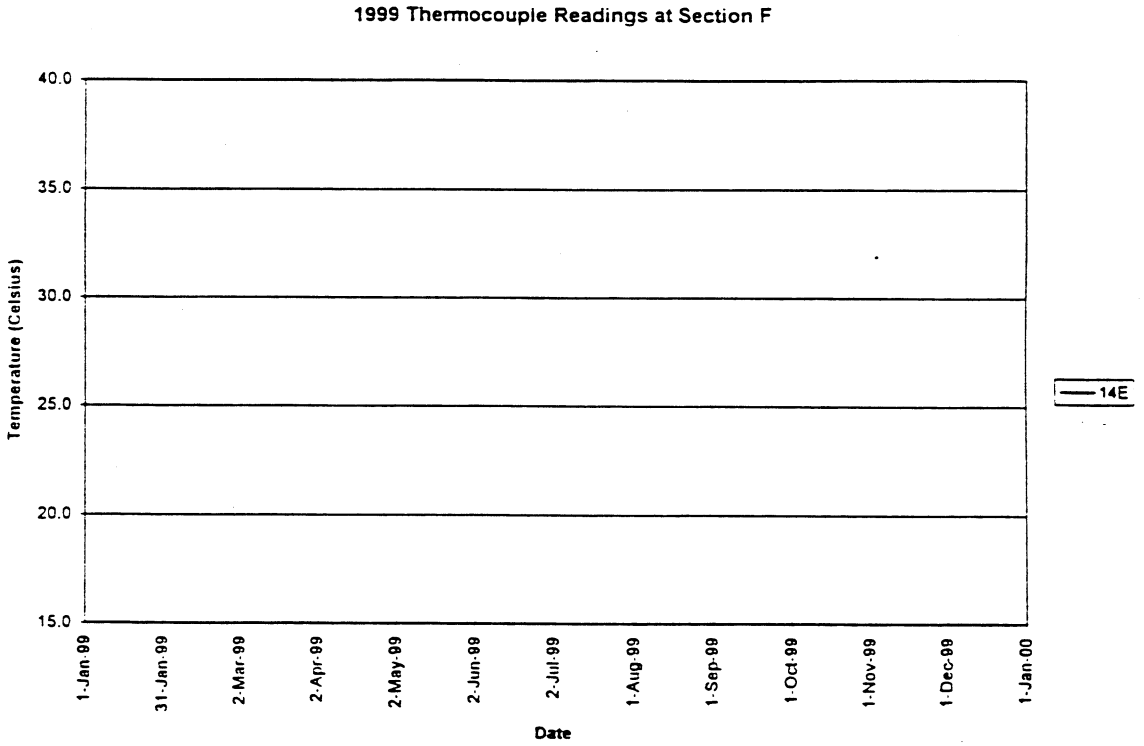
1999 Thermocouple Readings at Section F
40.0
35.0
30.0
25.0
20.0
15.0
Temperature (Celsius)
1-Jan-99
31-Jan-99
2-Mar-99
2-Apr-99
2-May-99
2-Jun-99
2-Jul-99
1-Aug-99
1-Sep-99
1-Oct-99
1-Nov-99
1-Dec-99
1-Jan-00
Date
14E

Figure 8.7

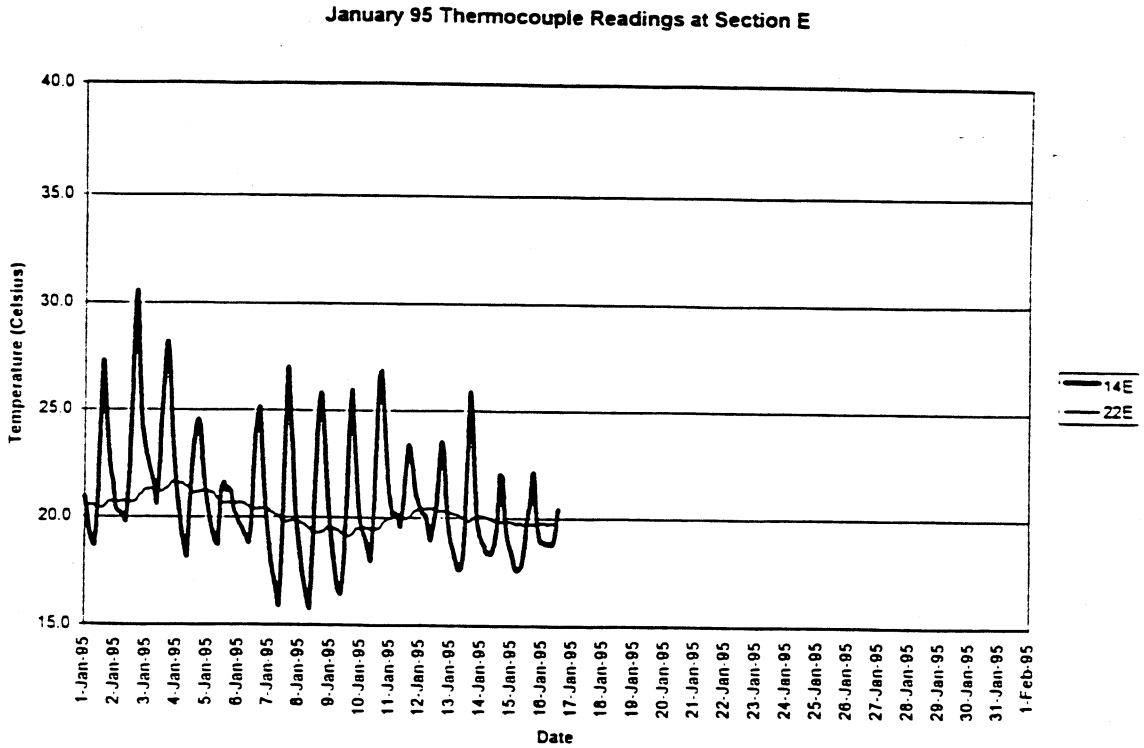
January 95 Thermocouple Readings at Section E
Temperature (Celsius)
40.0
35.0
30.0
25.0
20.0
15.0
1-Jan-95
2-Jan-95
3-Jan-95
4-Jan-95
5-Jan-95
6-Jan-95
7-Jan-95
8-Jan-95
9-Jan-95
10-Jan-95
11-Jan-95
12-Jan-95
13-Jan-95
14-Jan-95
15-Jan-95
16-Jan-95
17-Jan-95
18-Jan-95
19-Jan-95
20-Jan-95
21-Jan-95
22-Jan-95
23-Jan-95
24-Jan-95
25-Jan-95
26-Jan-95
27-Jan-95
28-Jan-95
29-Jan-95
30-Jan-95
31-Jan-95
1-Feb-95
Date
14E
22E

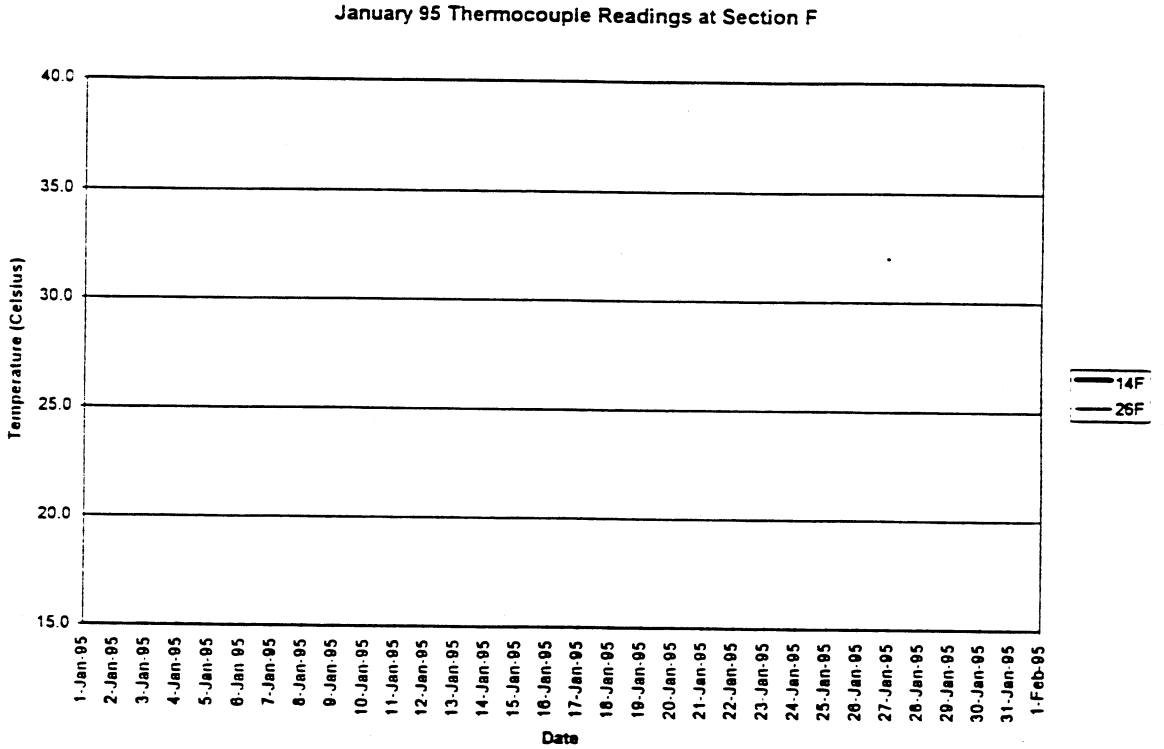
January 95 Thermocouple Readings at Section F
Temperature (Celsius)
40.0
35.0
30.0
25.0
20.0
15.0
1-Jan-95
2-Jan-95
3-Jan-95
4-Jan-95
5-Jan-95
6-Jan-95
7-Jan-95
8-Jan-95
9-Jan-95
10-Jan-95
11-Jan-95
12-Jan-95
13-Jan-95
14-Jan-95
15-Jan-95
16-Jan-95
17-Jan-95
18-Jan-95
19-Jan-95
20-Jan-95
21-Jan-95
22-Jan-95
23-Jan-95
24-Jan-95
25-Jan-95
26-Jan-95
27-Jan-95
28-Jan-95
29-Jan-95
30-Jan-95
31-Jan-95
1-Feb-95
Date
14F
26F

Figure 8.8

February 95 Thermocouple Readings at Section E

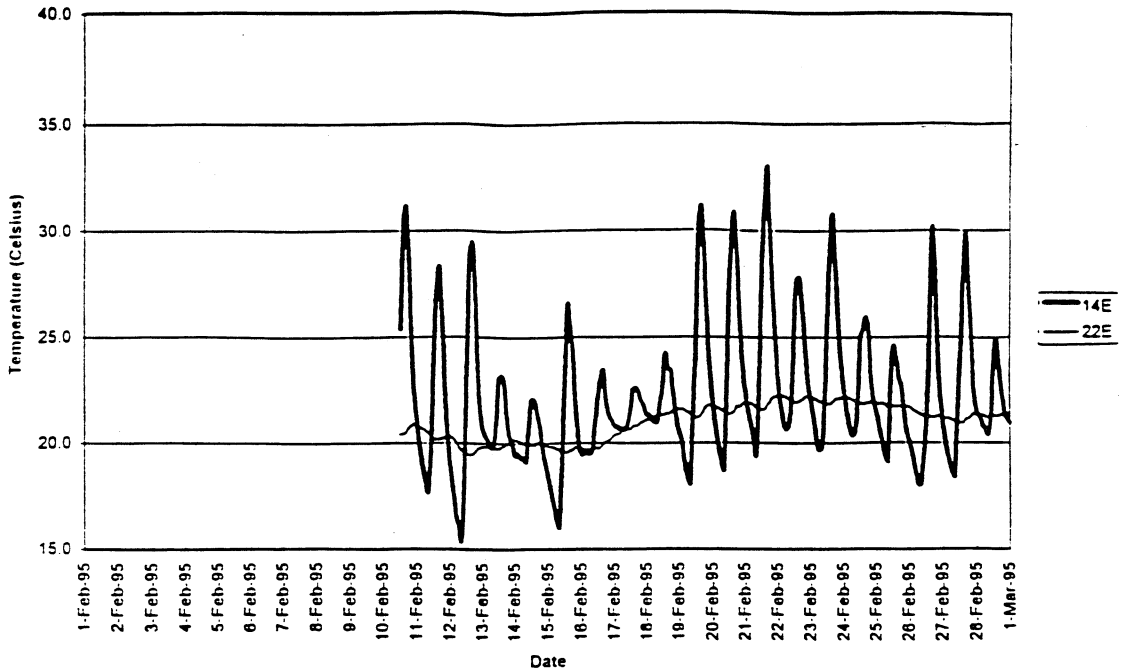

February 95 Thermocouple Readings at Section F

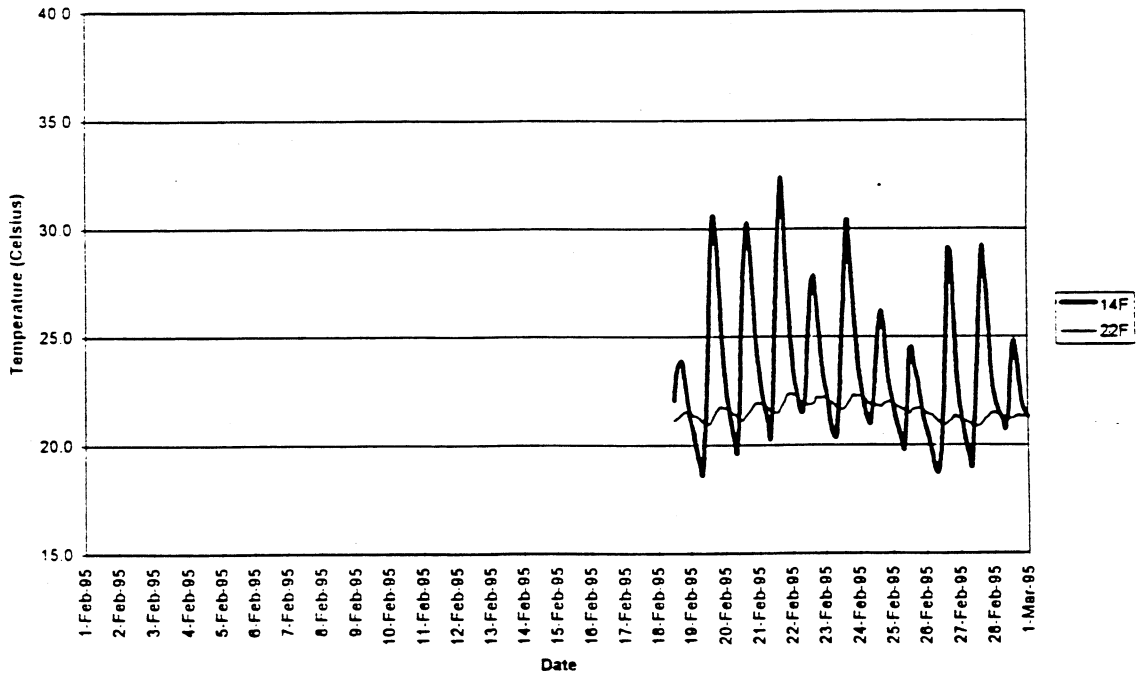

Figure 8.9

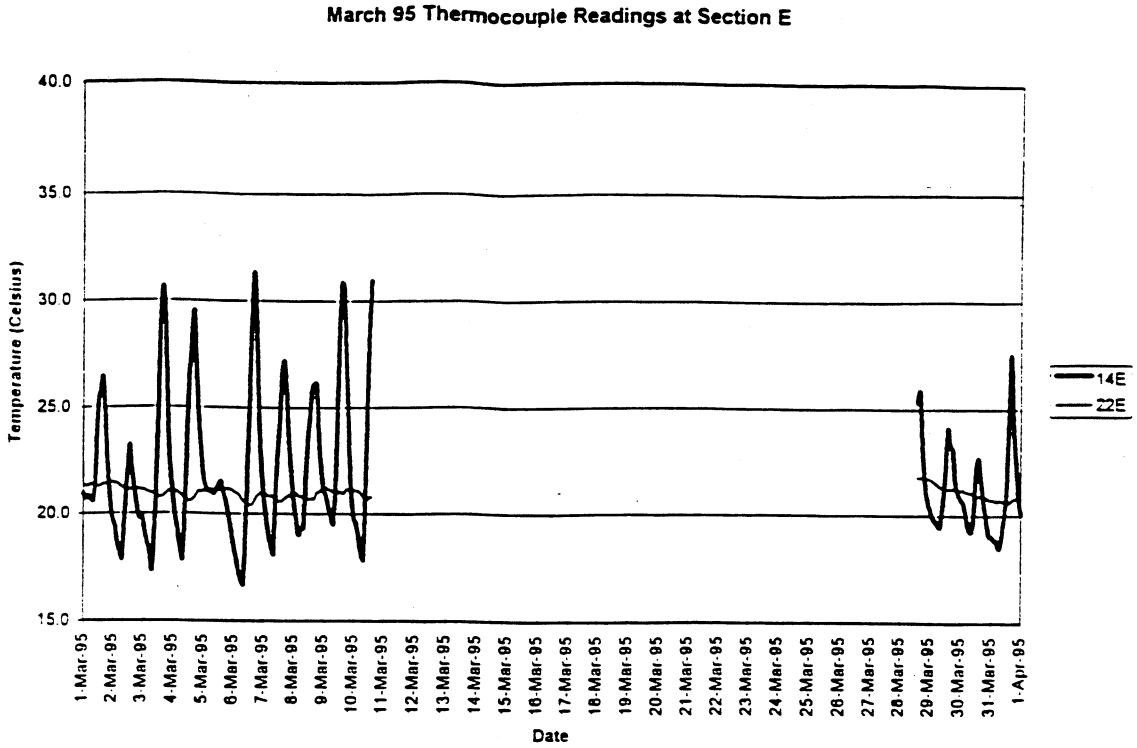
March 95 Thermocouple Readings at Section E
Temperature (Celsius)
40.0
35.0
30.0
25.0
20.0
15.0
1-Mar-95
2-Mar-95
3-Mar-95
4-Mar-95
5-Mar-95
6-Mar-95
7-Mar-95
8-Mar-95
9-Mar-95
10-Mar-95
11-Mar-95
12-Mar-95
13-Mar-95
14-Mar-95
15-Mar-95
16-Mar-95
17-Mar-95
18-Mar-95
19-Mar-95
20-Mar-95
21-Mar-95
22-Mar-95
23-Mar-95
24-Mar-95
25-Mar-95
26-Mar-95
27-Mar-95
28-Mar-95
29-Mar-95
30-Mar-95
31-Mar-95
1-Apr-95
Date
14E
22E

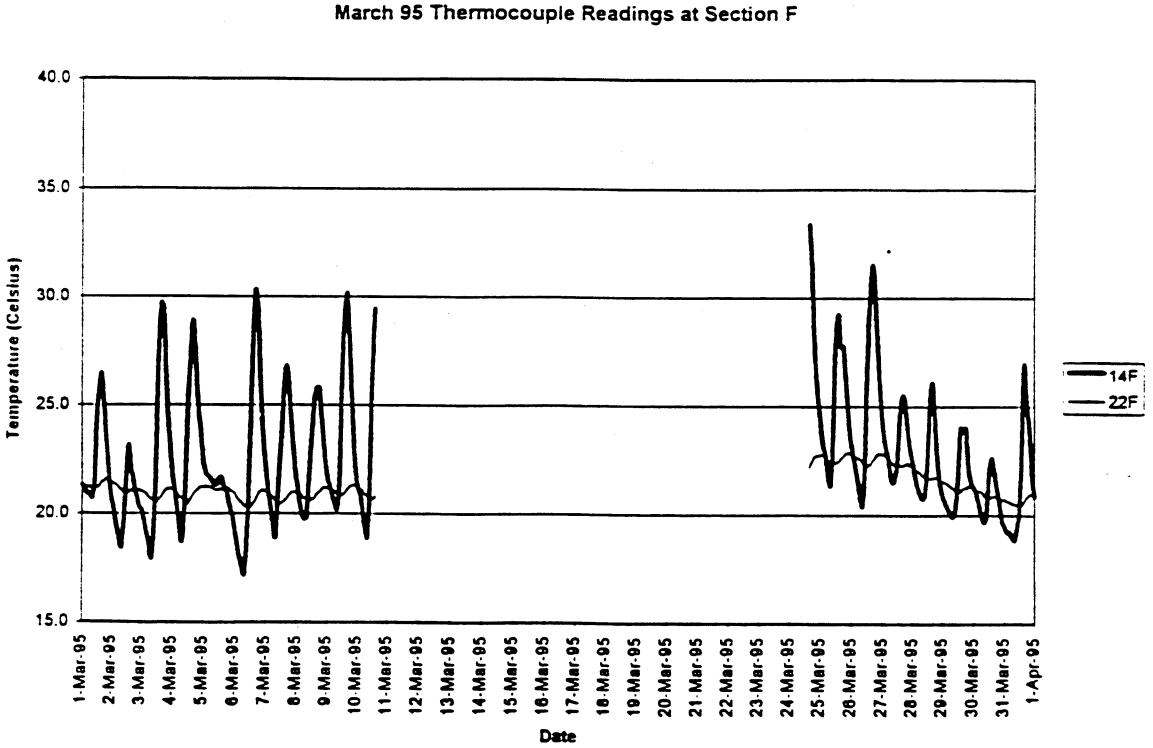
March 95 Thermocouple Readings at Section F
Temperature (Celsius)
40.0
35.0
30.0
25.0
20.0
15.0
1-Mar-95
2-Mar-95
3-Mar-95
4-Mar-95
5-Mar-95
6-Mar-95
7-Mar-95
8-Mar-95
9-Mar-95
10-Mar-95
11-Mar-95
12-Mar-95
13-Mar-95
14-Mar-95
15-Mar-95
16-Mar-95
17-Mar-95
18-Mar-95
19-Mar-95
20-Mar-95
21-Mar-95
22-Mar-95
23-Mar-95
24-Mar-95
25-Mar-95
26-Mar-95
27-Mar-95
28-Mar-95
29-Mar-95
30-Mar-95
31-Mar-95
1-Apr-95
Date
14F
22F

Figure 8.10

April 95 Thermocouple Readings at Section E

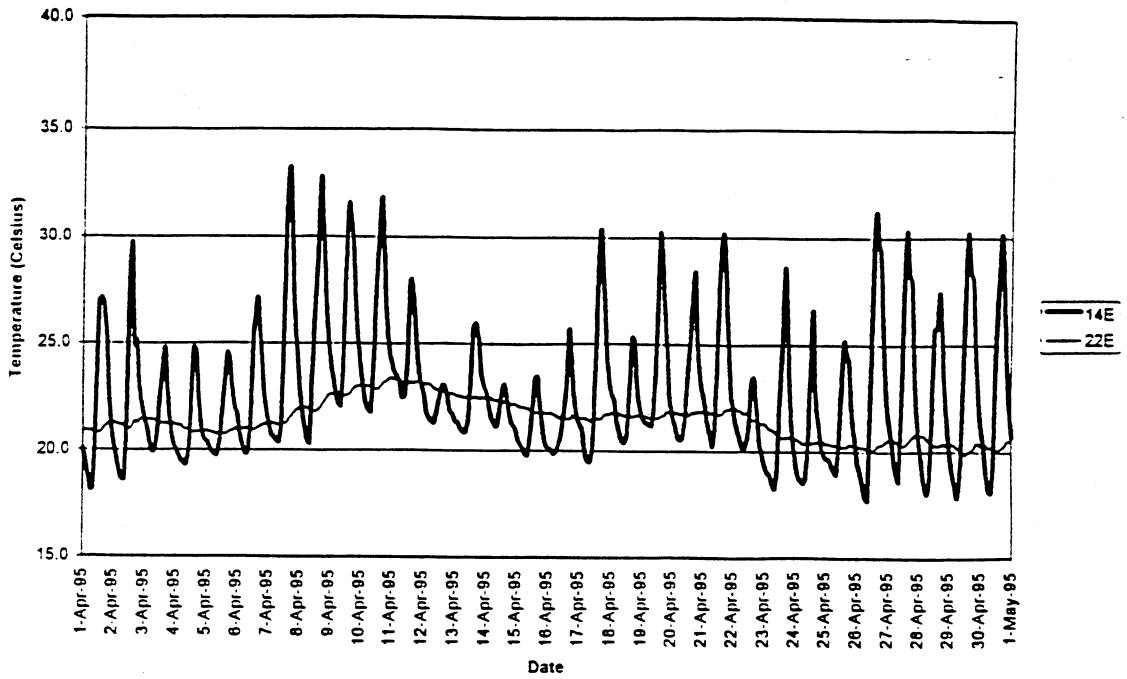

April 95 Thermocouple Readings at Section F

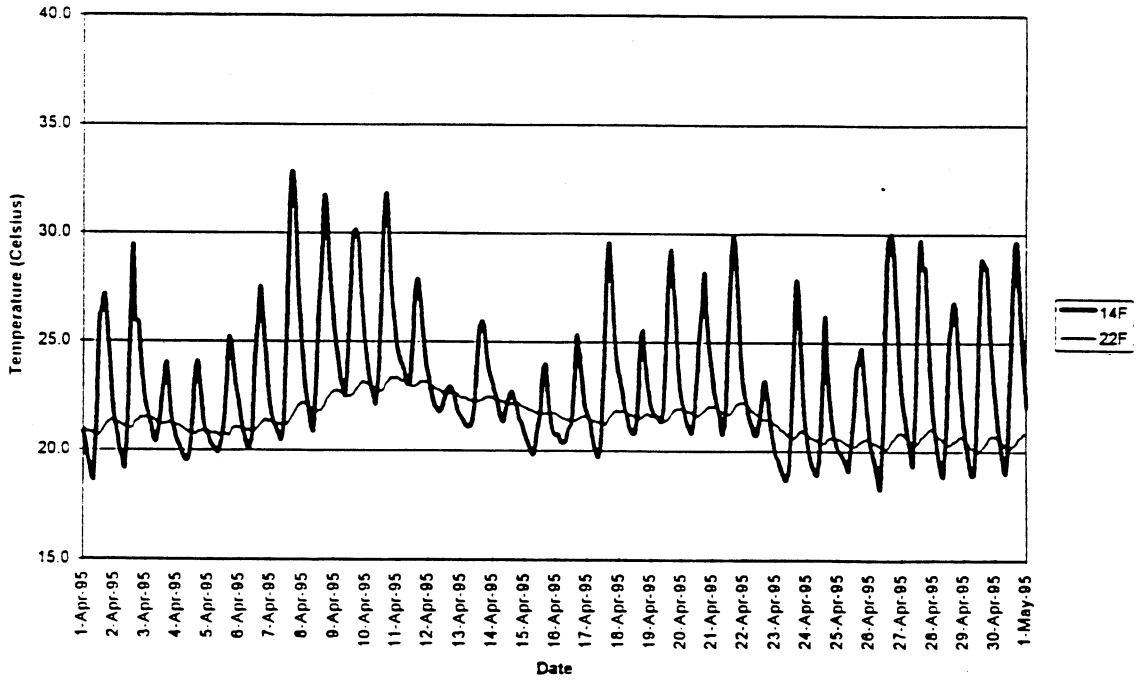

Figure 8.11

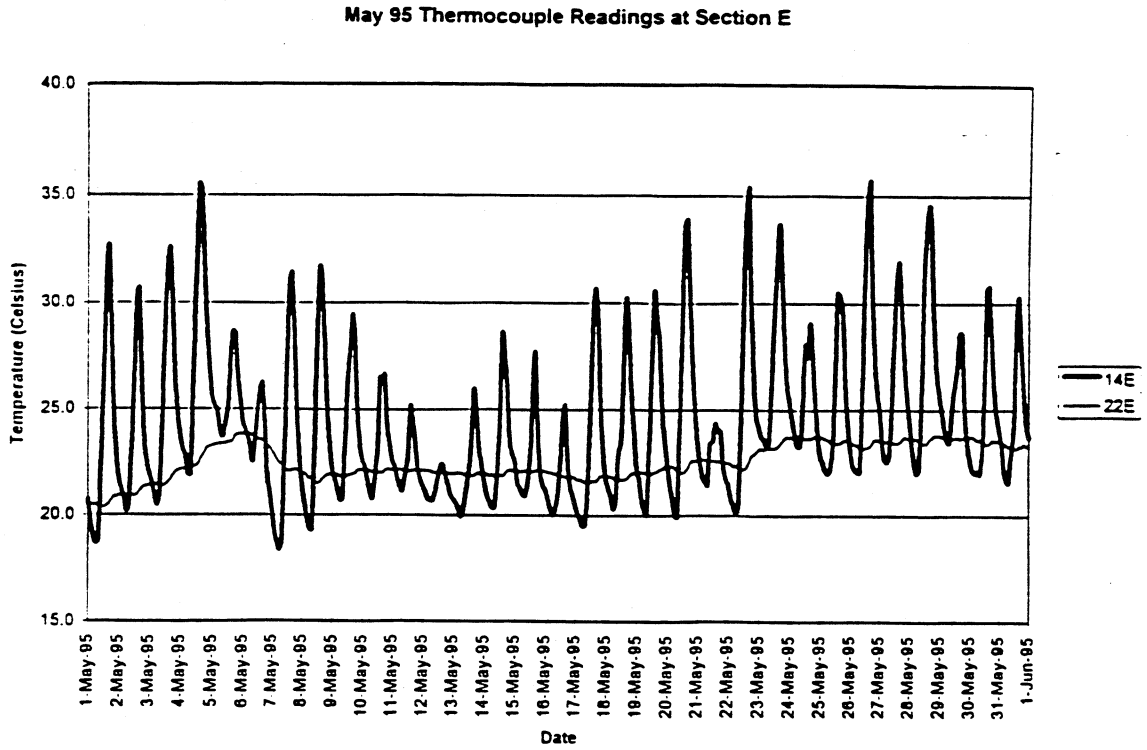
May 95 Thermocouple Readings at Section E
Temperature (Celsius)
40.0
35.0
30.0
25.0
20.0
15.0
1-May-95
2-May-95
3-May-95
4-May-95
5-May-95
6-May-95
7-May-95
8-May-95
9-May-95
10-May-95
11-May-95
12-May-95
13-May-95
14-May-95
15-May-95
16-May-95
17-May-95
18-May-95
19-May-95
20-May-95
21-May-95
22-May-95
23-May-95
24-May-95
25-May-95
26-May-95
27-May-95
28-May-95
29-May-95
30-May-95
31-May-95
1-Jun-95
Date
14E
22E

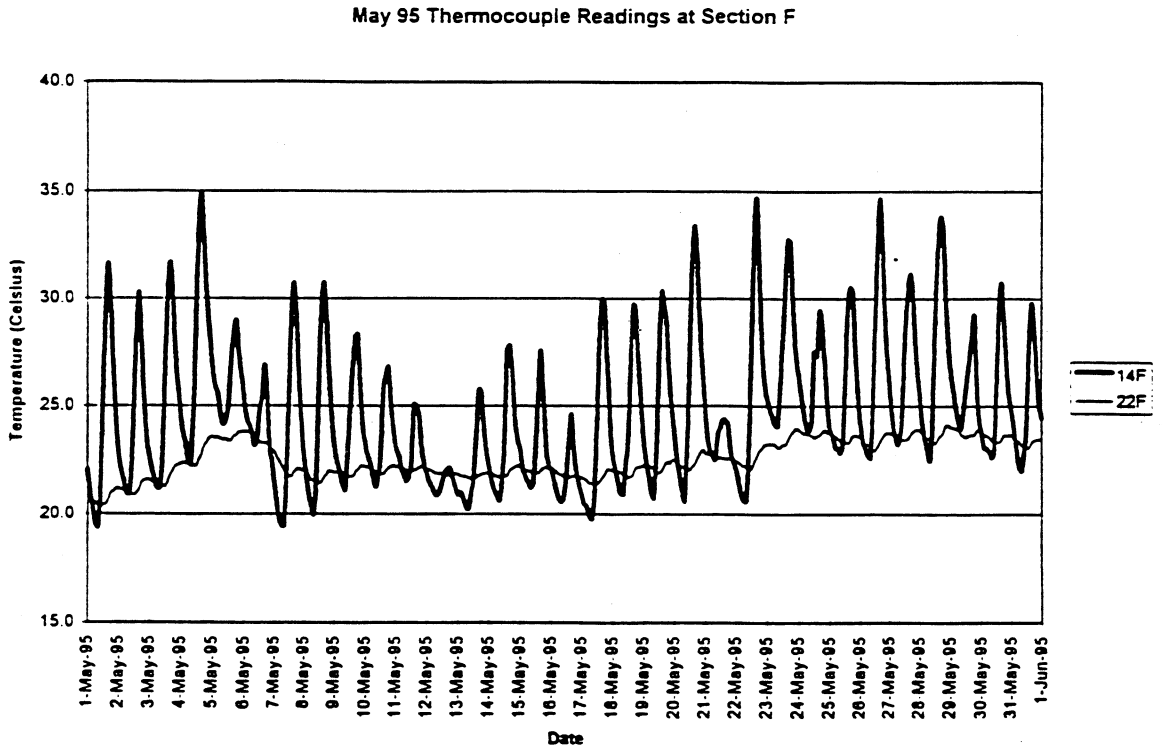
May 95 Thermocouple Readings at Section F
Temperature (Celsius)
40.0
35.0
30.0
25.0
20.0
15.0
1-May-95
2-May-95
3-May-95
4-May-95
5-May-95
6-May-95
7-May-95
8-May-95
9-May-95
10-May-95
11-May-95
12-May-95
13-May-95
14-May-95
15-May-95
16-May-95
17-May-95
18-May-95
19-May-95
20-May-95
21-May-95
22-May-95
23-May-95
24-May-95
25-May-95
26-May-95
27-May-95
28-May-95
29-May-95
30-May-95
31-May-95
1-Jun-95
Date
14F
22F

Figure 8.12

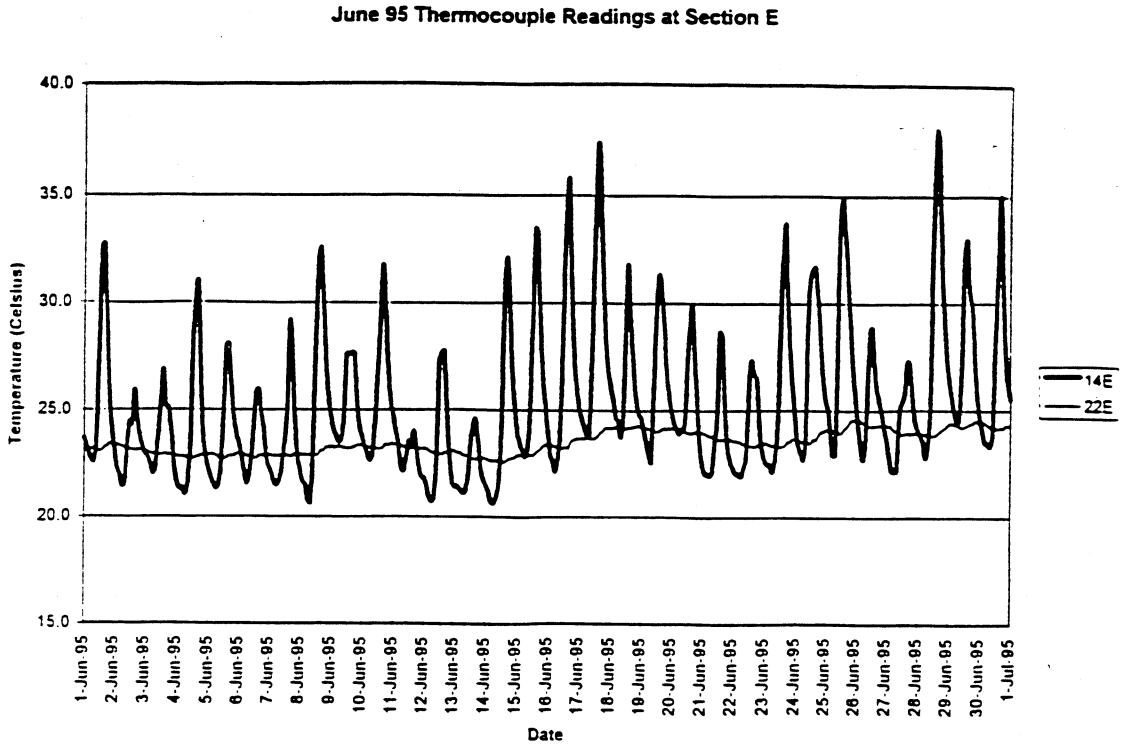
June 95 Thermocouple Readings at Section E
Temperature (Celsius)
40.0
35.0
30.0
25.0
20.0
15.0
1-Jun-95
2-Jun-95
3-Jun-95
4-Jun-95
5-Jun-95
6-Jun-95
7-Jun-95
8-Jun-95
9-Jun-95
10-Jun-95
11-Jun-95
12-Jun-95
13-Jun-95
14-Jun-95
15-Jun-95
16-Jun-95
17-Jun-95
18-Jun-95
19-Jun-95
20-Jun-95
21-Jun-95
22-Jun-95
23-Jun-95
24-Jun-95
25-Jun-95
26-Jun-95
27-Jun-95
28-Jun-95
29-Jun-95
30-Jun-95
1-Jul-95
Date
14E
22E

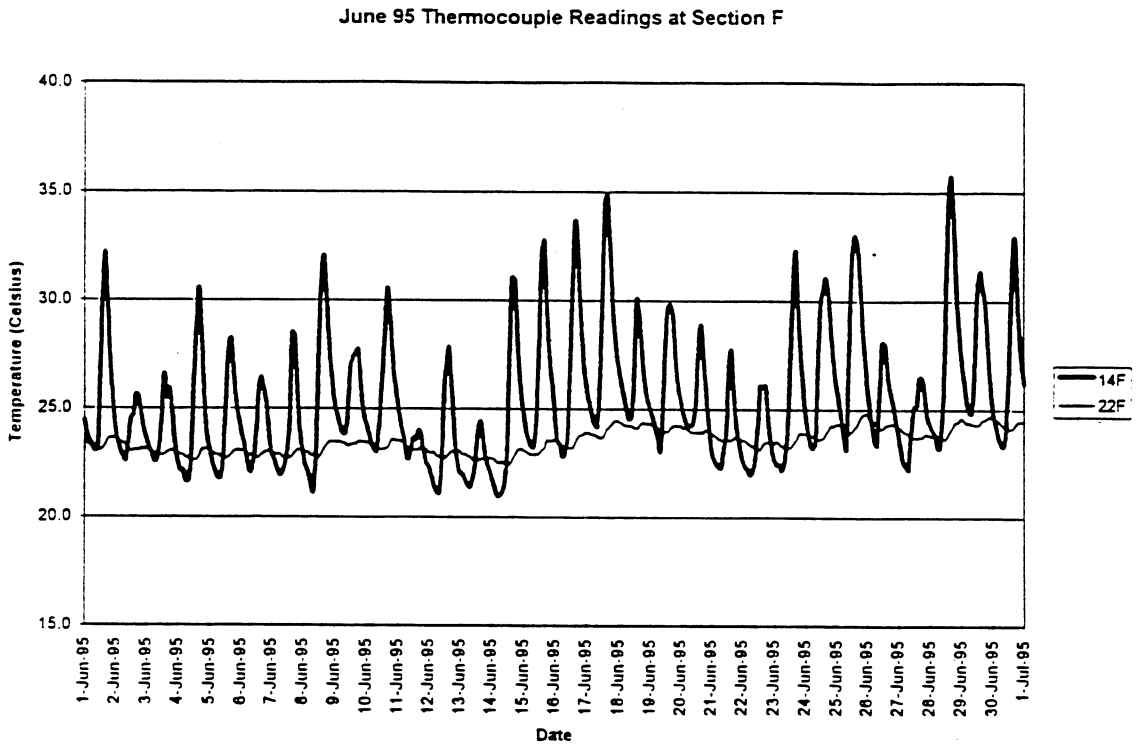
June 95 Thermocouple Readings at Section F
Temperature (Celsius)
40.0
35.0
30.0
25.0
20.0
15.0
1-Jun-95
2-Jun-95
3-Jun-95
4-Jun-95
5-Jun-95
6-Jun-95
7-Jun-95
8-Jun-95
9-Jun-95
10-Jun-95
11-Jun-95
12-Jun-95
13-Jun-95
14-Jun-95
15-Jun-95
16-Jun-95
17-Jun-95
18-Jun-95
19-Jun-95
20-Jun-95
21-Jun-95
22-Jun-95
23-Jun-95
24-Jun-95
25-Jun-95
26-Jun-95
27-Jun-95
28-Jun-95
29-Jun-95
30-Jun-95
1-Jul-95
Date
14F
22F

Figure 8.13

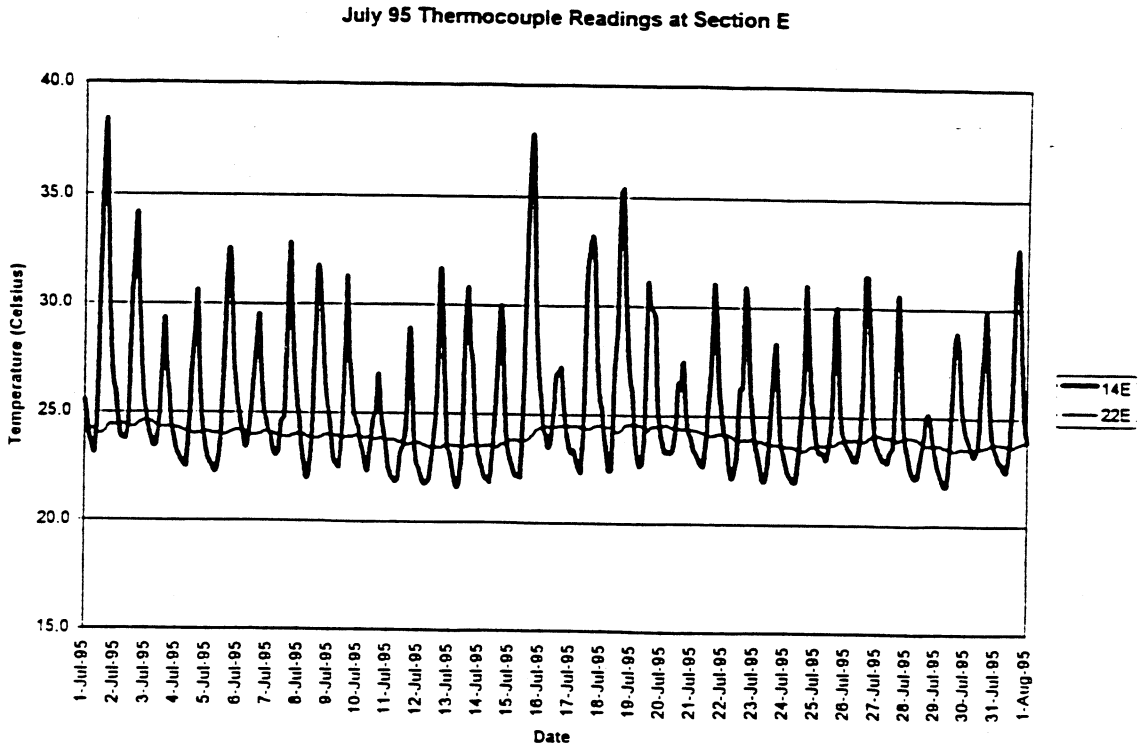
July 95 Thermocouple Readings at Section E
Temperature (Celsius)
40.0
35.0
30.0
25.0
20.0
15.0
1-Jul-95
2-Jul-95
3-Jul-95
4-Jul-95
5-Jul-95
6-Jul-95
7-Jul-95
8-Jul-95
9-Jul-95
10-Jul-95
11-Jul-95
12-Jul-95
13-Jul-95
14-Jul-95
15-Jul-95
16-Jul-95
17-Jul-95
18-Jul-95
19-Jul-95
20-Jul-95
21-Jul-95
22-Jul-95
23-Jul-95
24-Jul-95
25-Jul-95
26-Jul-95
27-Jul-95
28-Jul-95
29-Jul-95
30-Jul-95
31-Jul-95
1-Aug-95
Date
14E
22E

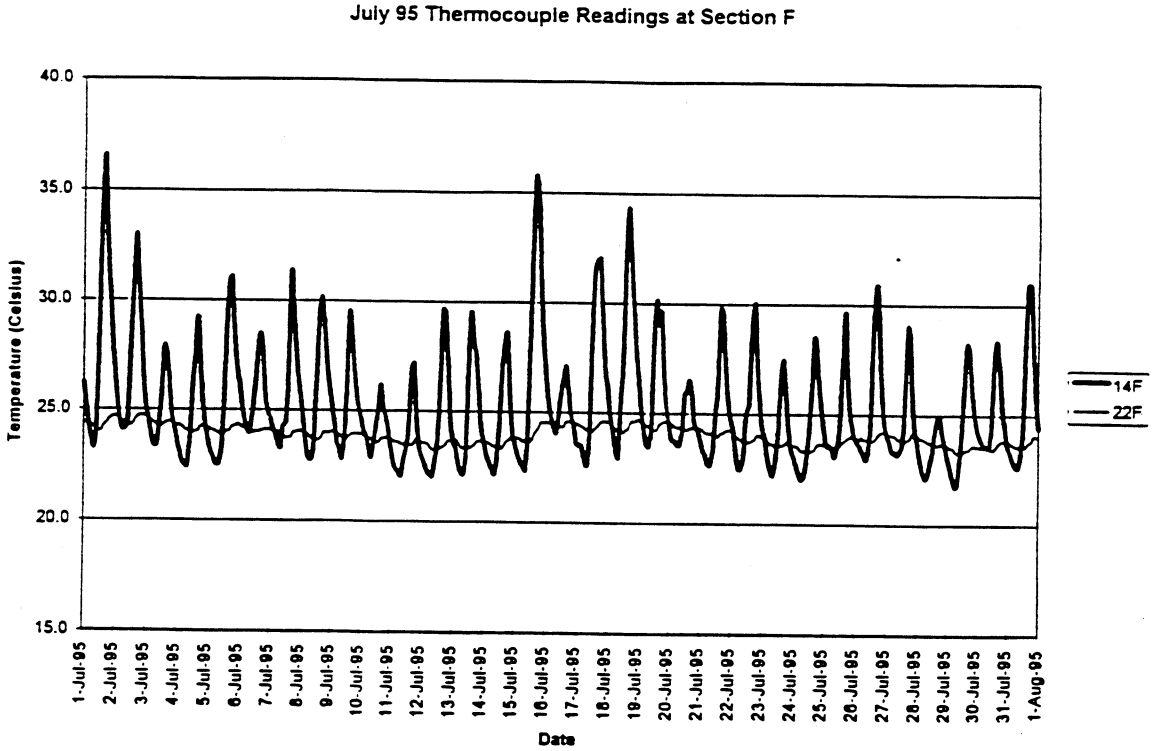
July 95 Thermocouple Readings at Section F
Temperature (Celsius)
40.0
35.0
30.0
25.0
20.0
15.0
1-Jul-95
2-Jul-95
3-Jul-95
4-Jul-95
5-Jul-95
6-Jul-95
7-Jul-95
8-Jul-95
9-Jul-95
10-Jul-95
11-Jul-95
12-Jul-95
13-Jul-95
14-Jul-95
15-Jul-95
16-Jul-95
17-Jul-95
18-Jul-95
19-Jul-95
20-Jul-95
21-Jul-95
22-Jul-95
23-Jul-95
24-Jul-95
25-Jul-95
26-Jul-95
27-Jul-95
28-Jul-95
29-Jul-95
30-Jul-95
31-Jul-95
1-Aug-95
Date
14F
22F

Figure 8.14

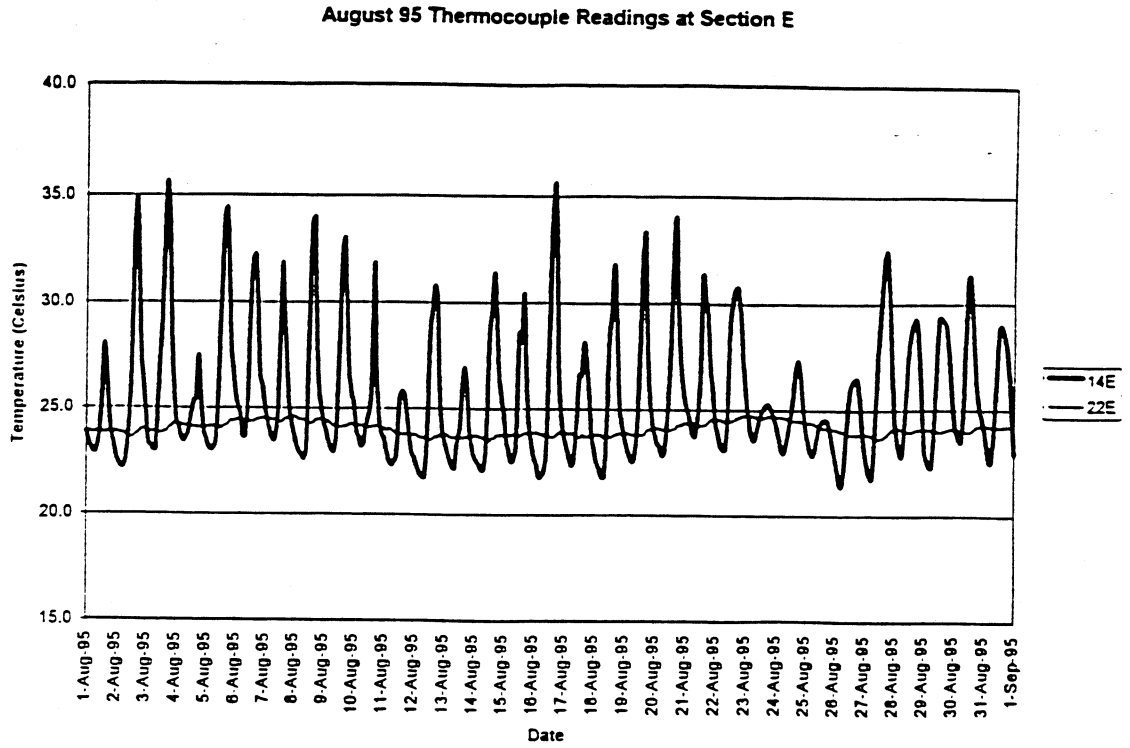

H3 Instrumentation Report

TYLin International

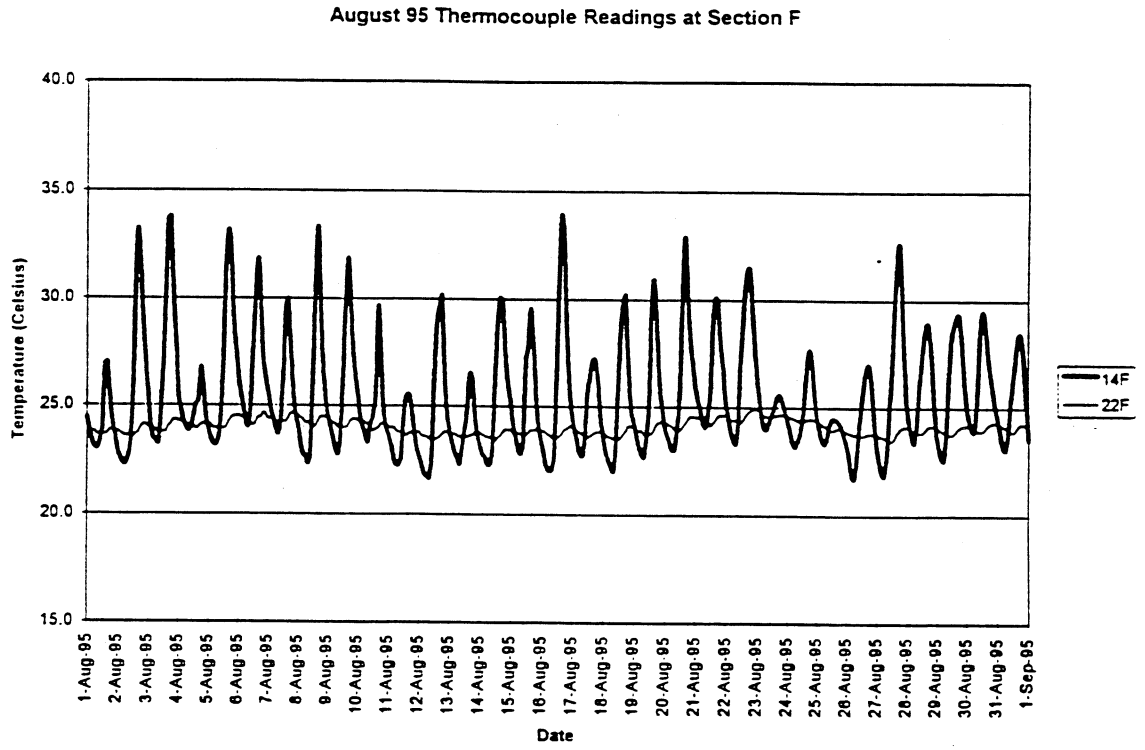

Figure 8.15

September 95 Thermocouple Readings at Section E

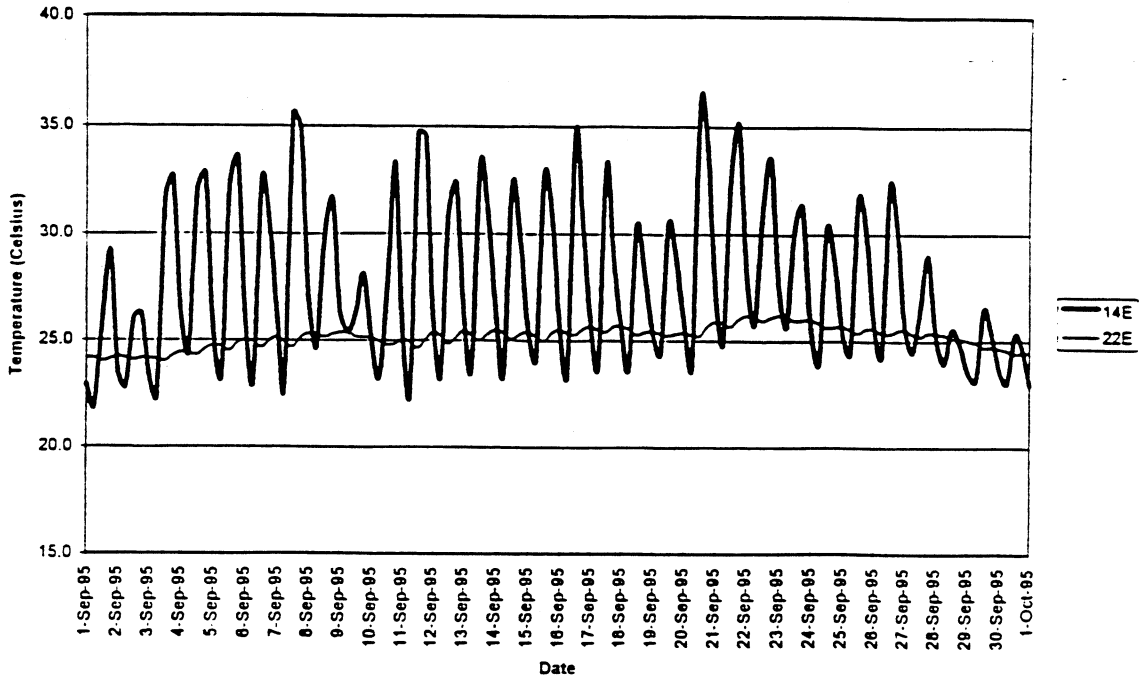

September 95 Thermocouple Readings at Section F

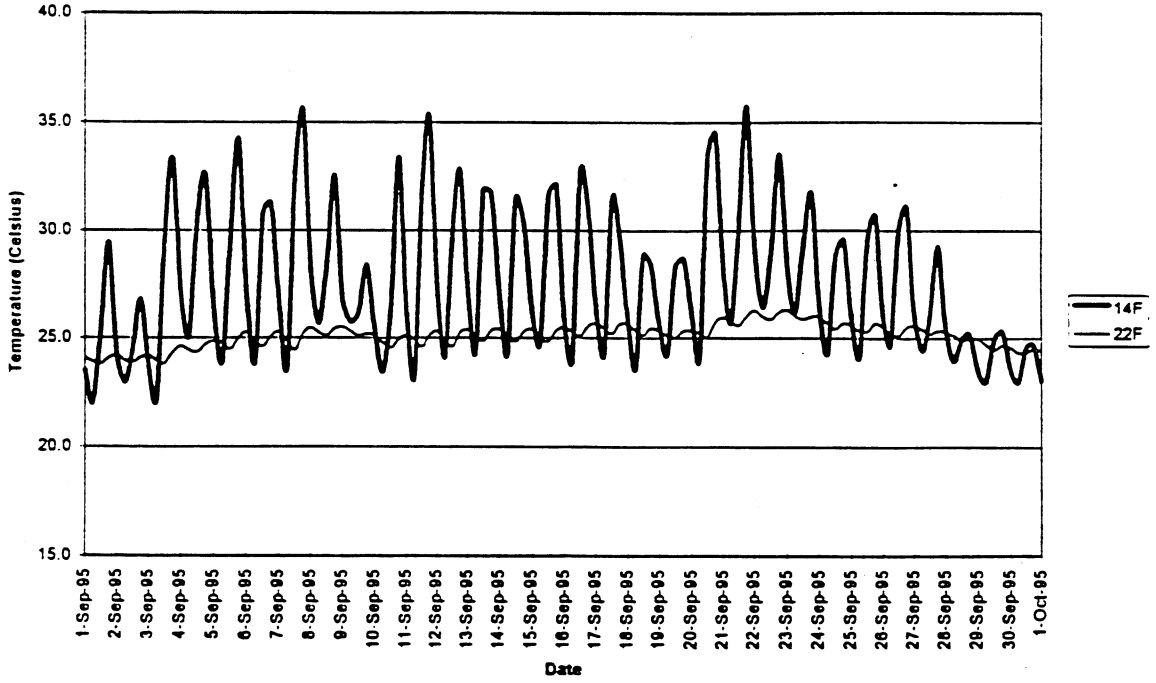

Figure 8.16

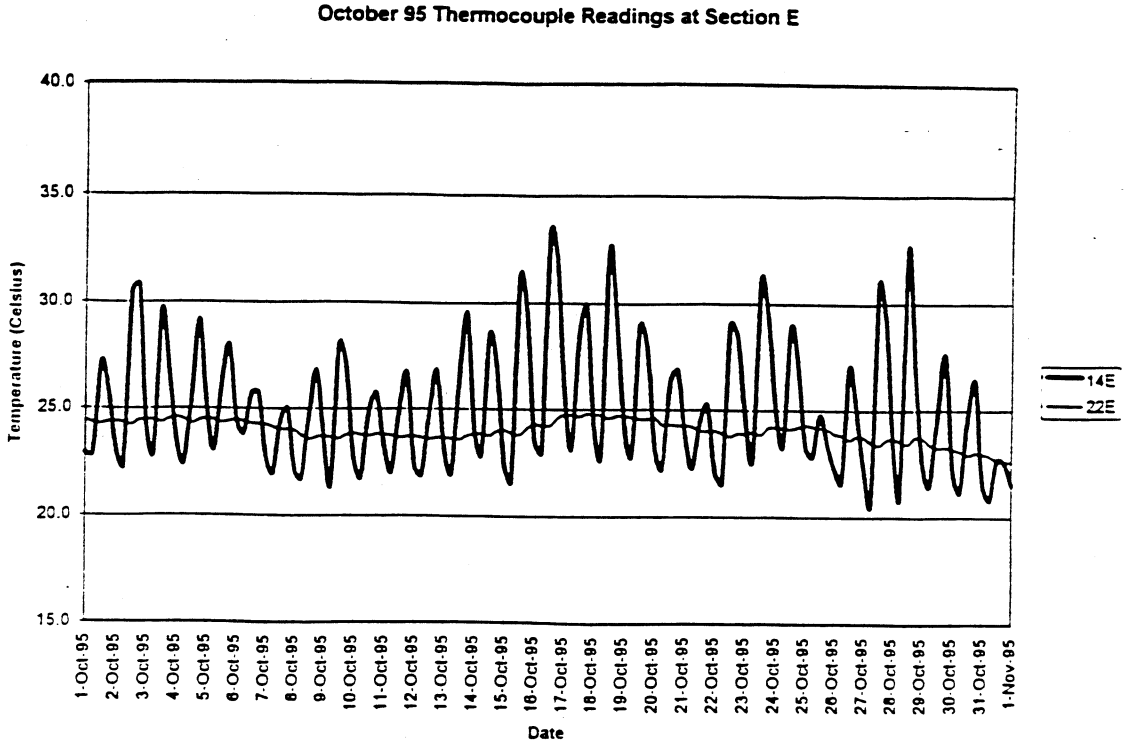
October 95 Thermocouple Readings at Section E
40.0
35.0
30.0
25.0
20.0
15.0
Temperature (Celsius)
1-Oct-95
2-Oct-95
3-Oct-95
4-Oct-95
5-Oct-95
6-Oct-95
7-Oct-95
8-Oct-95
9-Oct-95
10-Oct-95
11-Oct-95
12-Oct-95
13-Oct-95
14-Oct-95
15-Oct-95
16-Oct-95
17-Oct-95
18-Oct-95
19-Oct-95
20-Oct-95
21-Oct-95
22-Oct-95
23-Oct-95
24-Oct-95
25-Oct-95
26-Oct-95
27-Oct-95
28-Oct-95
29-Oct-95
30-Oct-95
31-Oct-95
1-Nov-95
Date
14E
22E

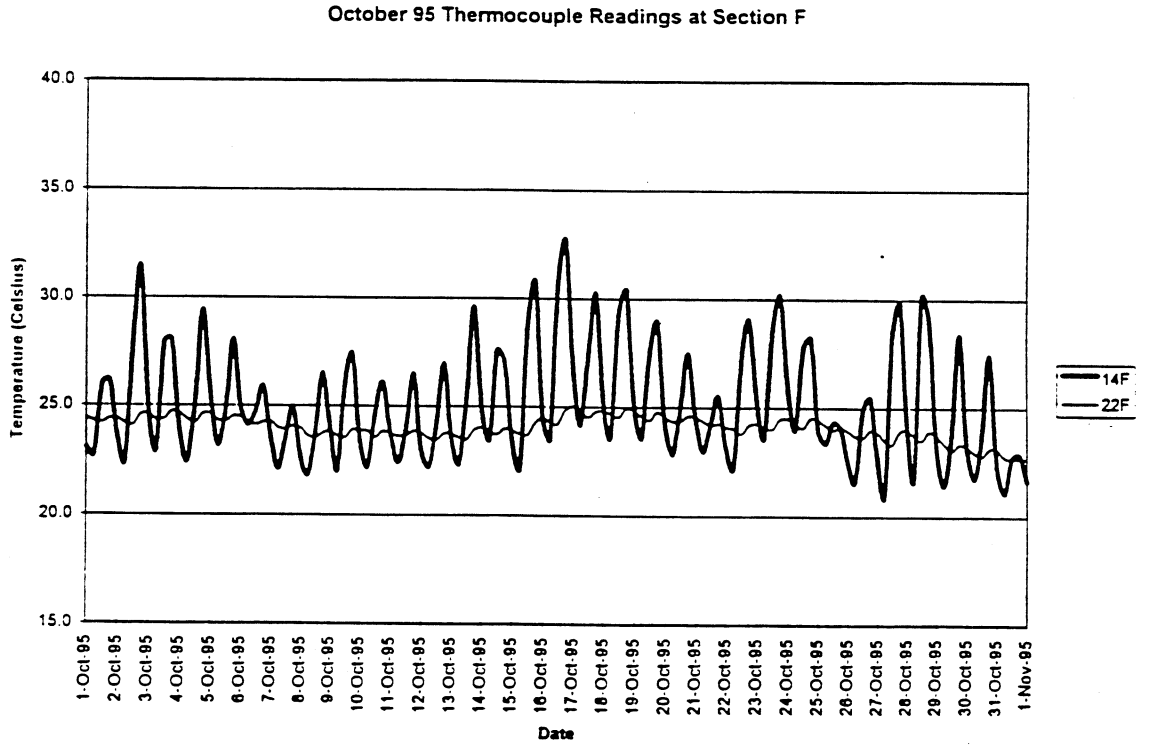
October 95 Thermocouple Readings at Section F
40.0
35.0
30.0
25.0
20.0
15.0
Temperature (Celsius)
1-Oct-95
2-Oct-95
3-Oct-95
4-Oct-95
5-Oct-95
6-Oct-95
7-Oct-95
8-Oct-95
9-Oct-95
10-Oct-95
11-Oct-95
12-Oct-95
13-Oct-95
14-Oct-95
15-Oct-95
16-Oct-95
17-Oct-95
18-Oct-95
19-Oct-95
20-Oct-95
21-Oct-95
22-Oct-95
23-Oct-95
24-Oct-95
25-Oct-95
26-Oct-95
27-Oct-95
28-Oct-95
29-Oct-95
30-Oct-95
31-Oct-95
1-Nov-95
Date
14F
22F

Figure 8.17

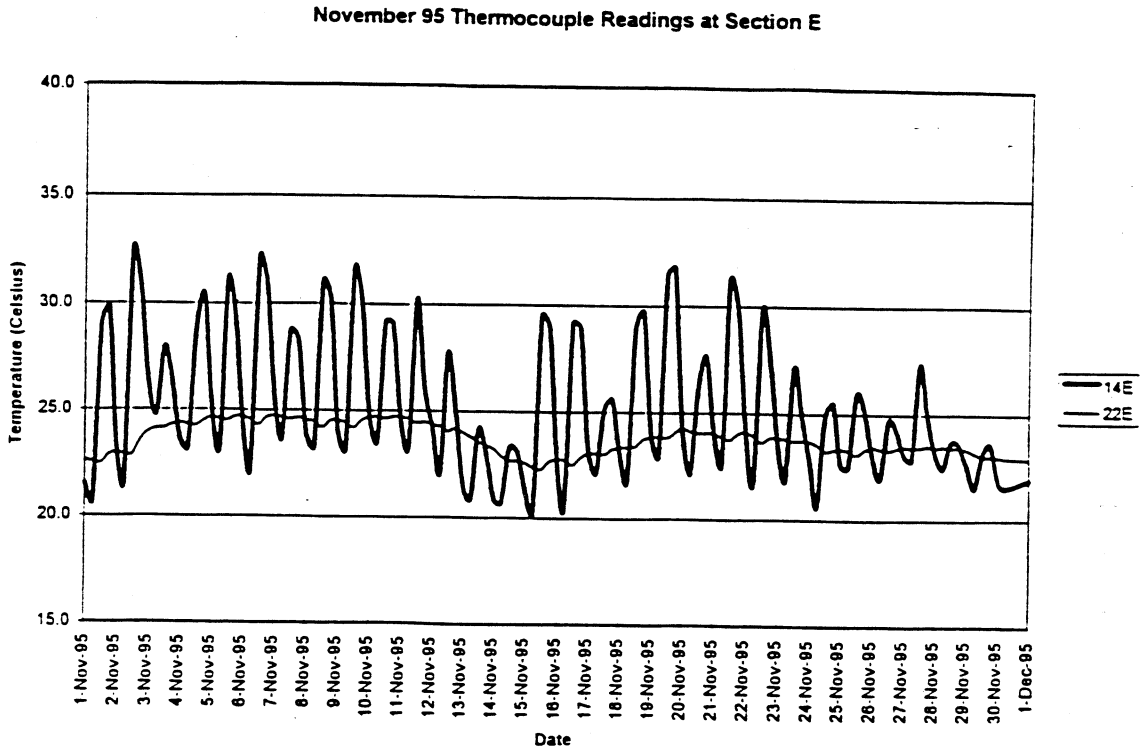
November 95 Thermocouple Readings at Section E
Temperature (Celsius)
40.0
35.0
30.0
25.0
20.0
15.0
1-Nov-95
2-Nov-95
3-Nov-95
4-Nov-95
5-Nov-95
6-Nov-95
7-Nov-95
8-Nov-95
9-Nov-95
10-Nov-95
11-Nov-95
12-Nov-95
13-Nov-95
14-Nov-95
15-Nov-95
16-Nov-95
17-Nov-95
18-Nov-95
19-Nov-95
20-Nov-95
21-Nov-95
22-Nov-95
23-Nov-95
24-Nov-95
25-Nov-95
26-Nov-95
27-Nov-95
28-Nov-95
29-Nov-95
30-Nov-95
1-Dec-95
Date
14E
22E

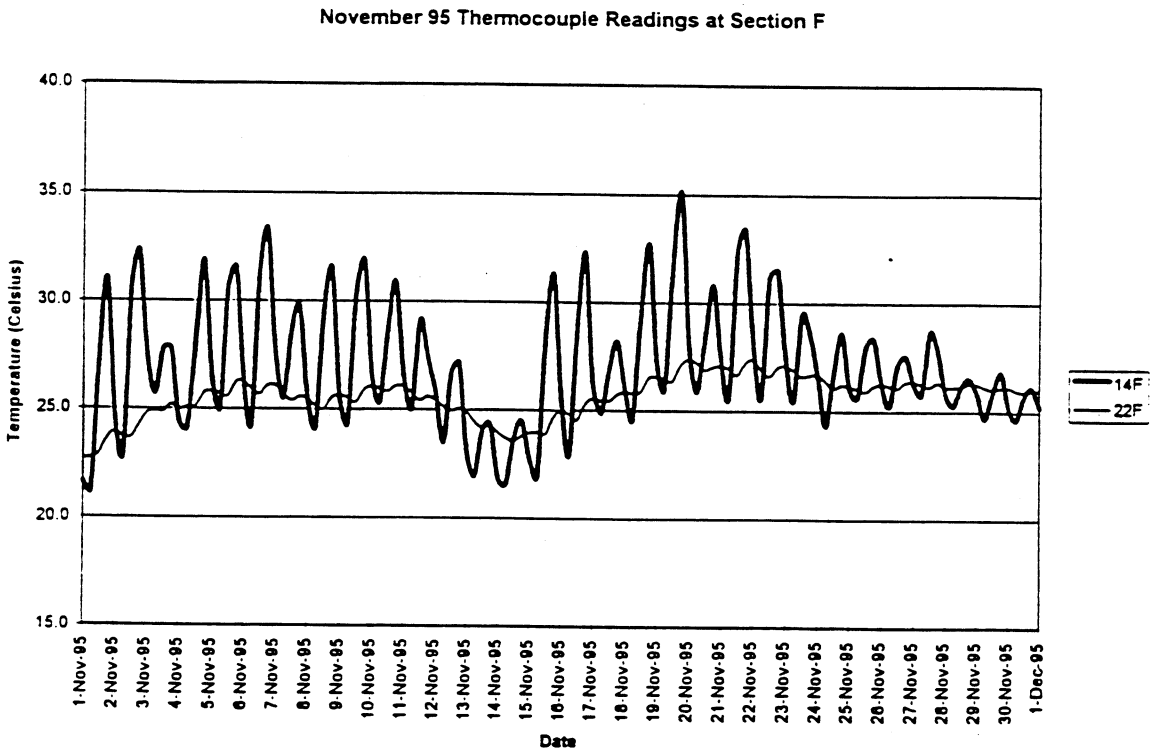
November 95 Thermocouple Readings at Section F
Temperature (Celsius)
40.0
35.0
30.0
25.0
20.0
15.0
1-Nov-95
2-Nov-95
3-Nov-95
4-Nov-95
5-Nov-95
6-Nov-95
7-Nov-95
8-Nov-95
9-Nov-95
10-Nov-95
11-Nov-95
12-Nov-95
13-Nov-95
14-Nov-95
15-Nov-95
16-Nov-95
17-Nov-95
18-Nov-95
19-Nov-95
20-Nov-95
21-Nov-95
22-Nov-95
23-Nov-95
24-Nov-95
25-Nov-95
26-Nov-95
27-Nov-95
28-Nov-95
29-Nov-95
30-Nov-95
1-Dec-95
Date
14F
22F

Figure 8.18

December 95 Thermocouple Readings at Section E

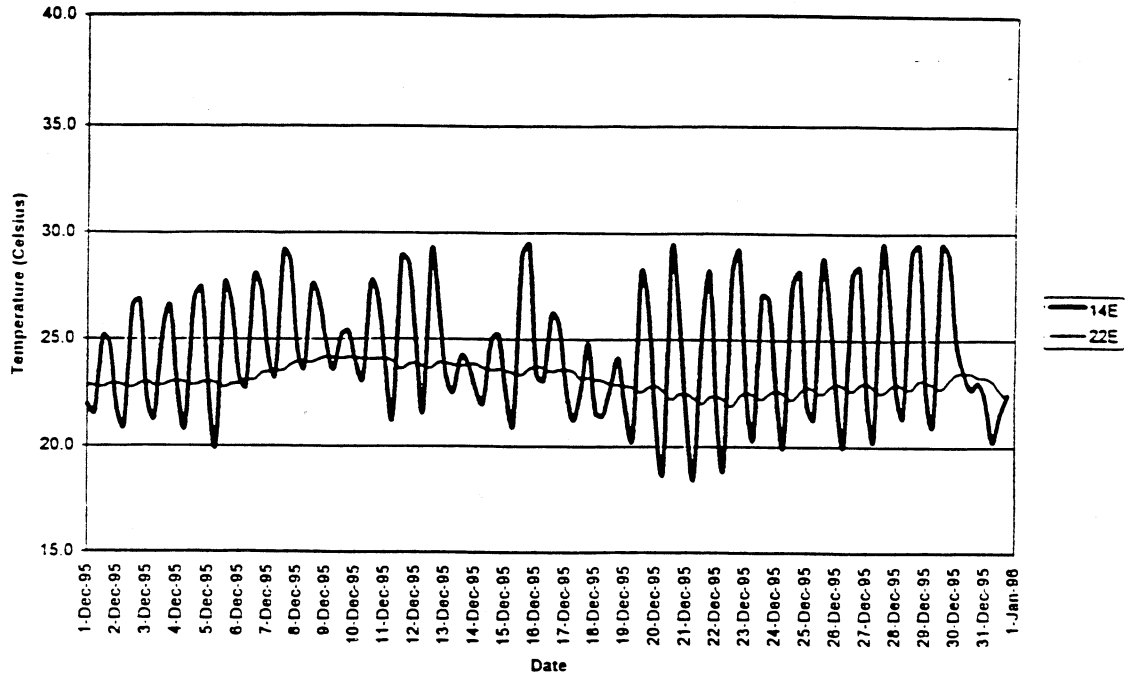

December 95 Thermocouple Readings at Section F

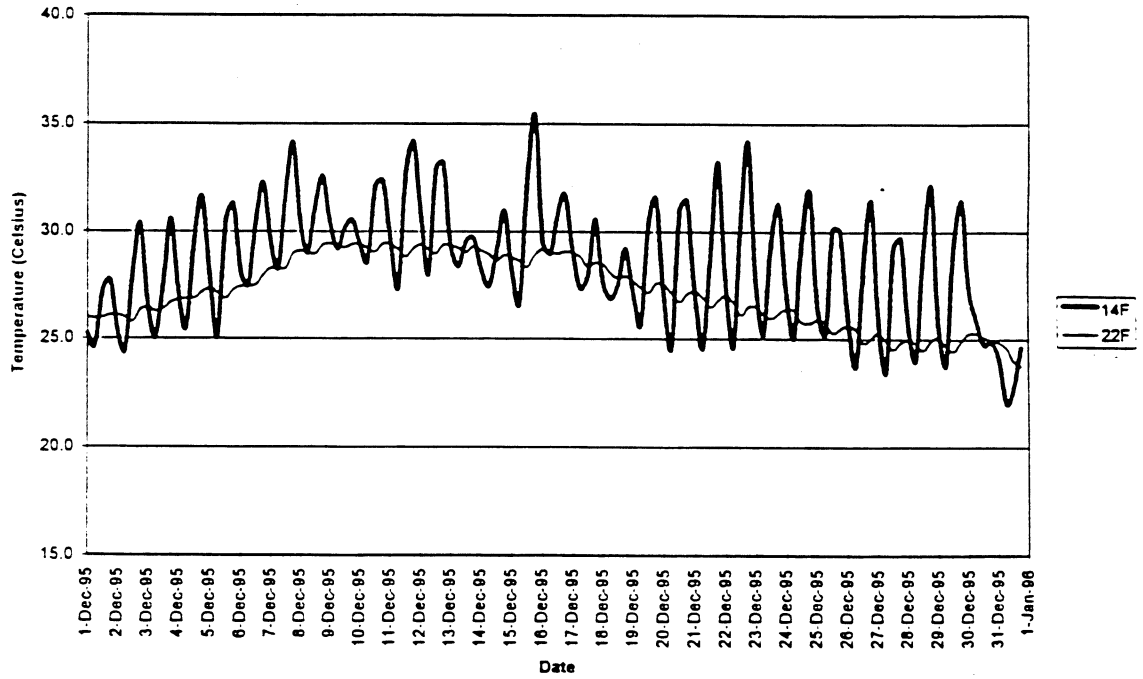

Figure 8.19

January 96 Thermocouple Readings at Section E

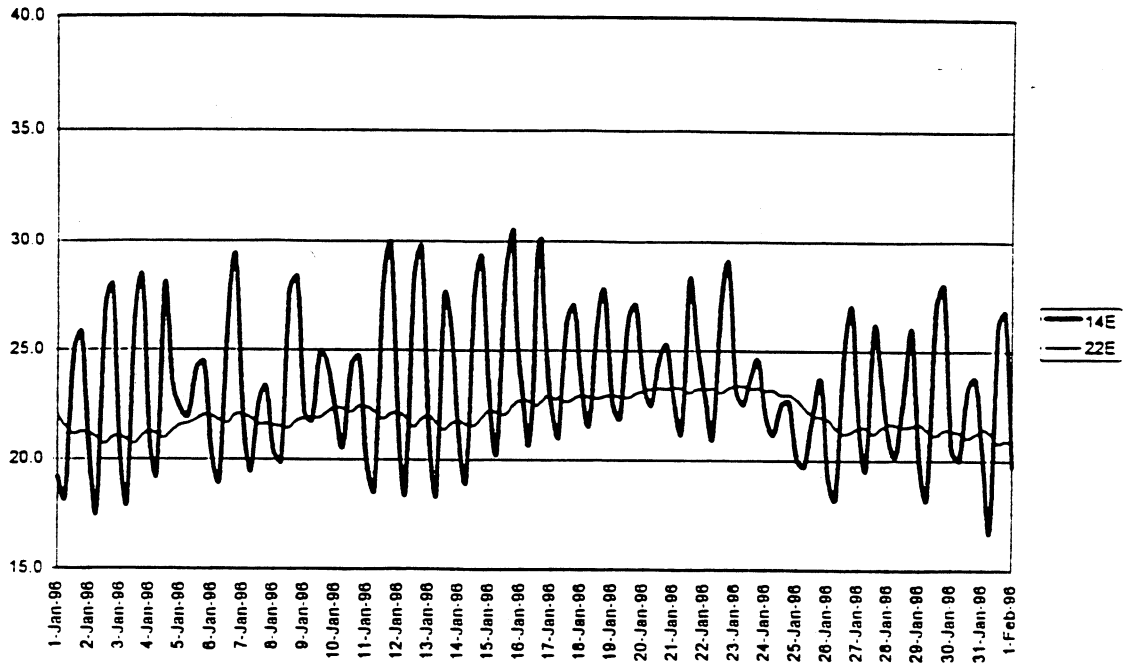

January 96 Thermocouple Readings at Section F

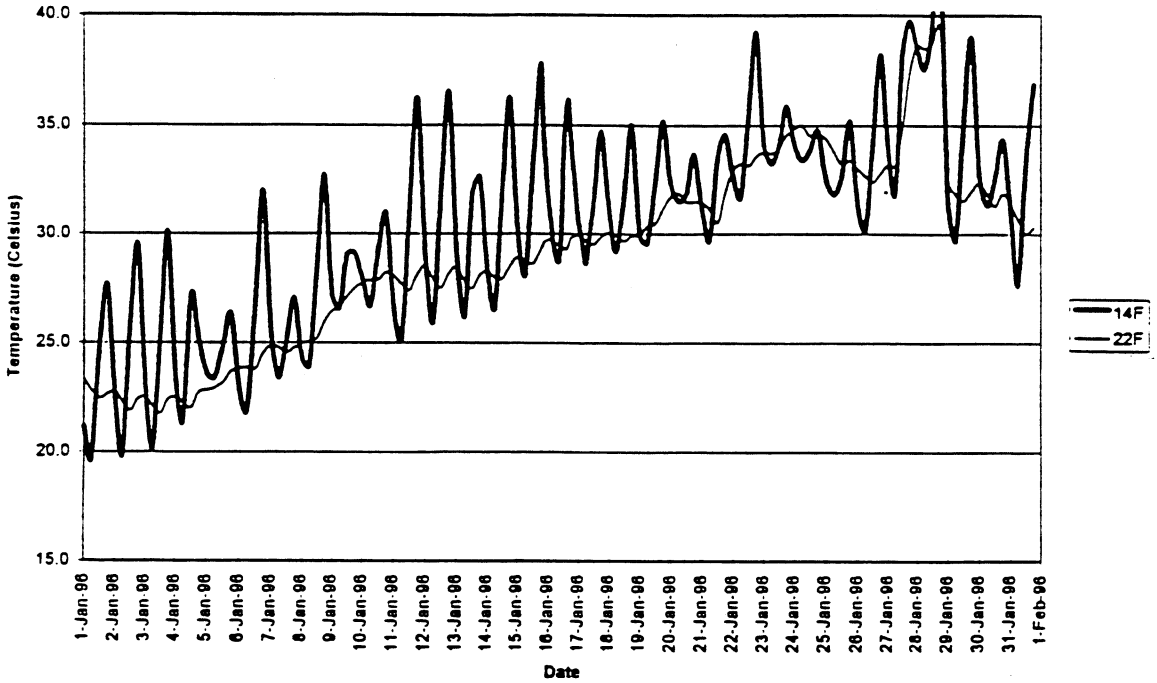

Figure 8.20

February 96 Thermocouple Readings at Section E

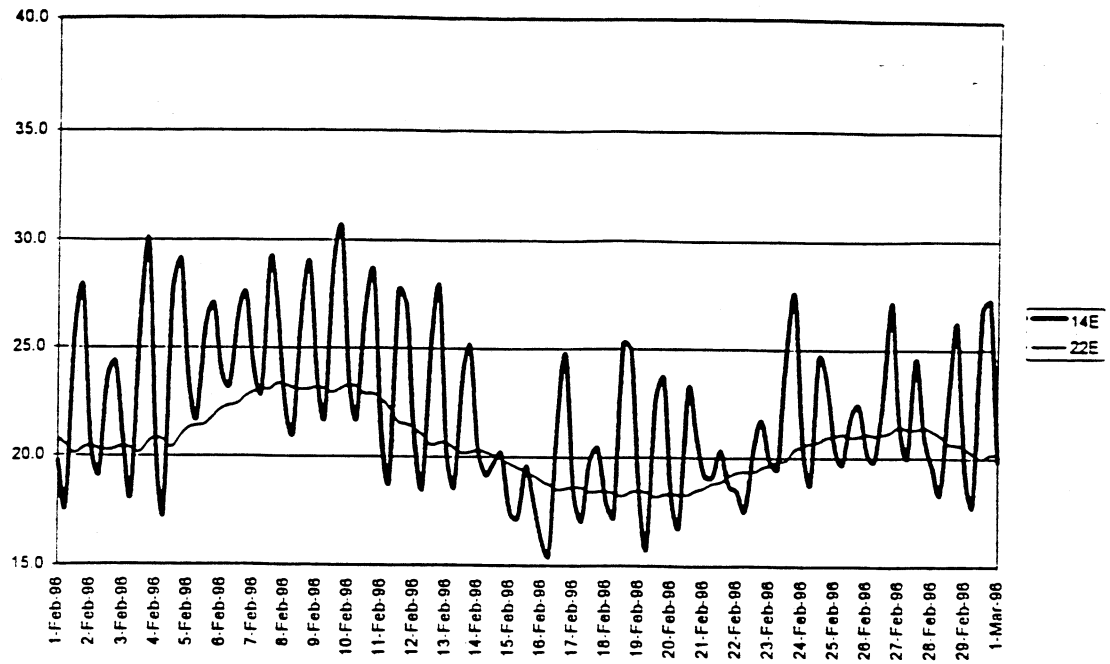

H3 Instrumentation Report

TYLin International

February 96 Thermocouple Readings at Section F

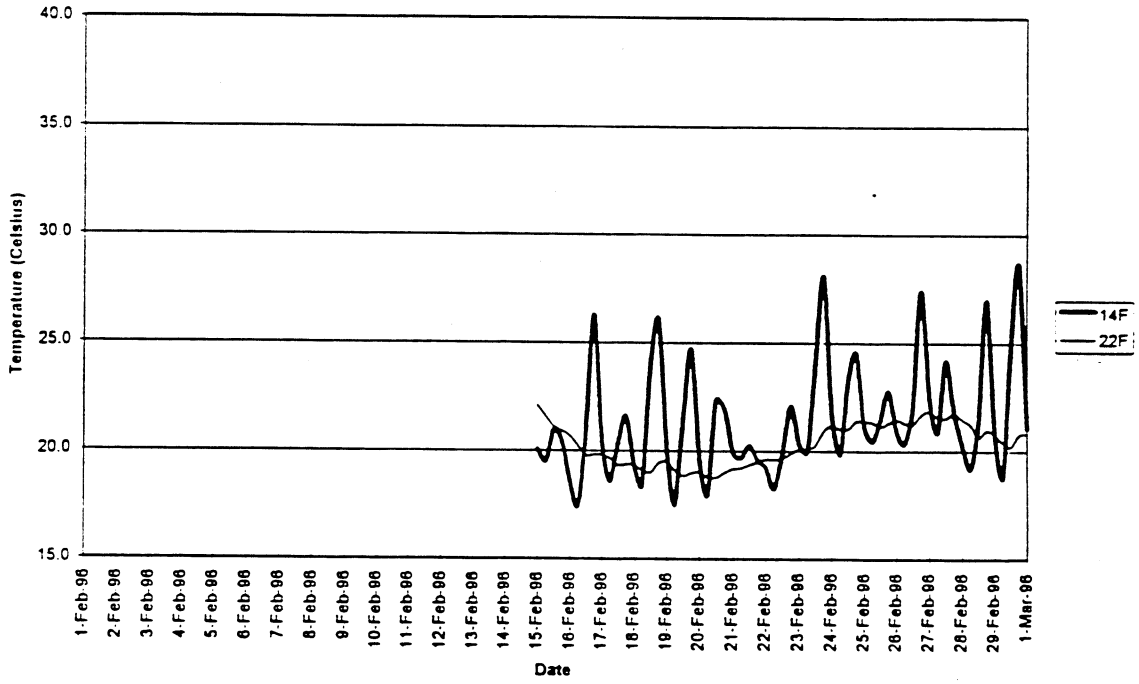

Figure 8.21

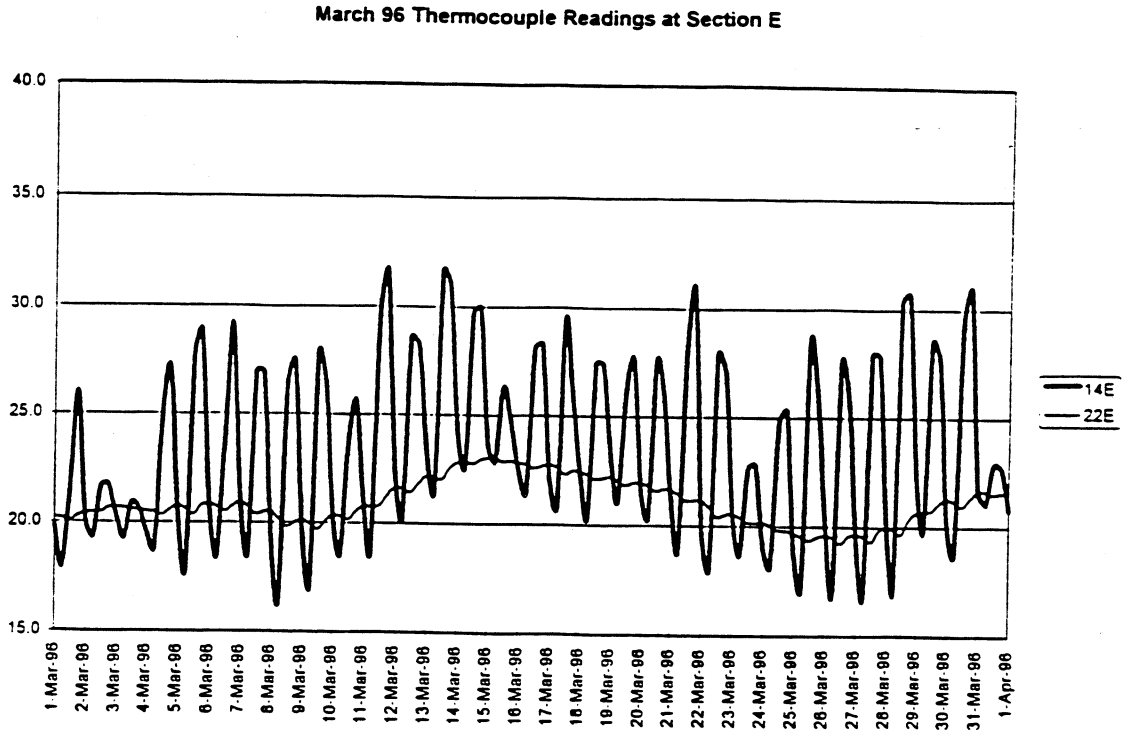
March 96 Thermocouple Readings at Section E
40.0
35.0
30.0
25.0
20.0
15.0
1-Mar-96
2-Mar-96
3-Mar-96
4-Mar-96
5-Mar-96
6-Mar-96
7-Mar-96
8-Mar-96
9-Mar-96
10-Mar-96
11-Mar-96
12-Mar-96
13-Mar-96
14-Mar-96
15-Mar-96
16-Mar-96
17-Mar-96
18-Mar-96
19-Mar-96
20-Mar-96
21-Mar-96
22-Mar-96
23-Mar-96
24-Mar-96
25-Mar-96
26-Mar-96
27-Mar-96
28-Mar-96
29-Mar-96
30-Mar-96
31-Mar-96
1-Apr-96
14E
22E

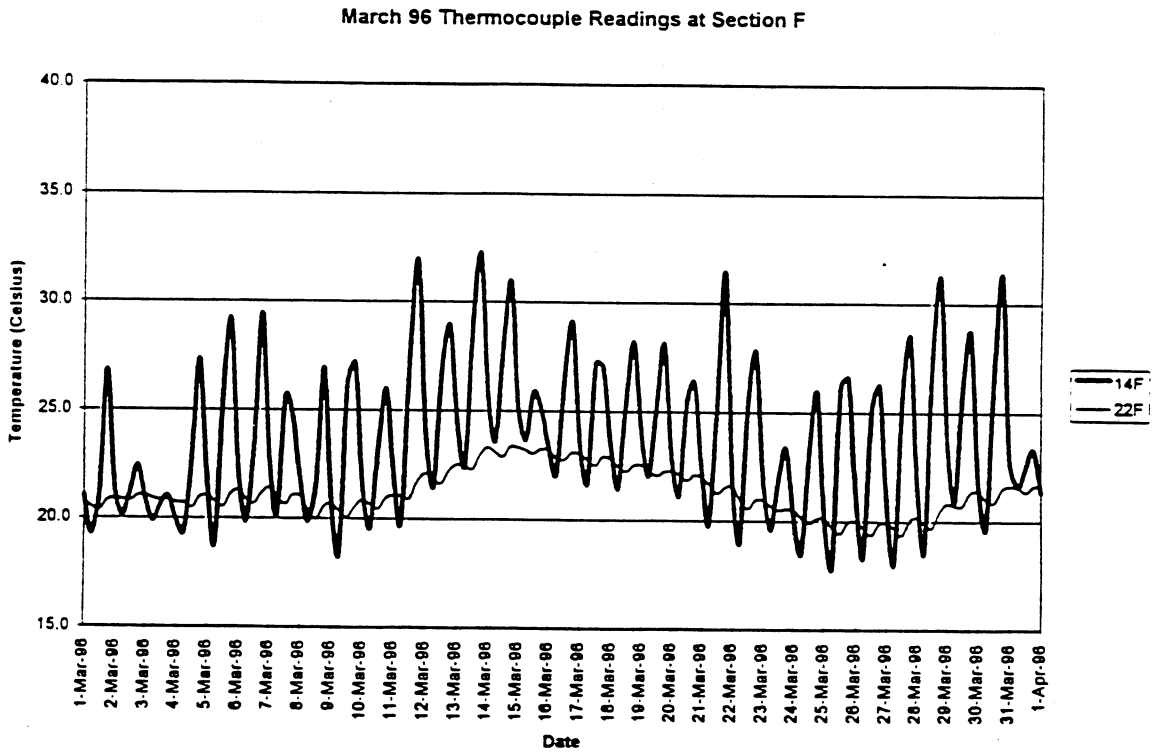
March 96 Thermocouple Readings at Section F
Temperature (Celsius)
40.0
35.0
30.0
25.0
20.0
15.0
1-Mar-96
2-Mar-96
3-Mar-96
4-Mar-96
5-Mar-96
6-Mar-96
7-Mar-96
8-Mar-96
9-Mar-96
10-Mar-96
11-Mar-96
12-Mar-96
13-Mar-96
14-Mar-96
15-Mar-96
16-Mar-96
17-Mar-96
18-Mar-96
19-Mar-96
20-Mar-96
21-Mar-96
22-Mar-96
23-Mar-96
24-Mar-96
25-Mar-96
26-Mar-96
27-Mar-96
28-Mar-96
29-Mar-96
30-Mar-96
31-Mar-96
1-Apr-96
Date
14F
22F

Figure 8.22

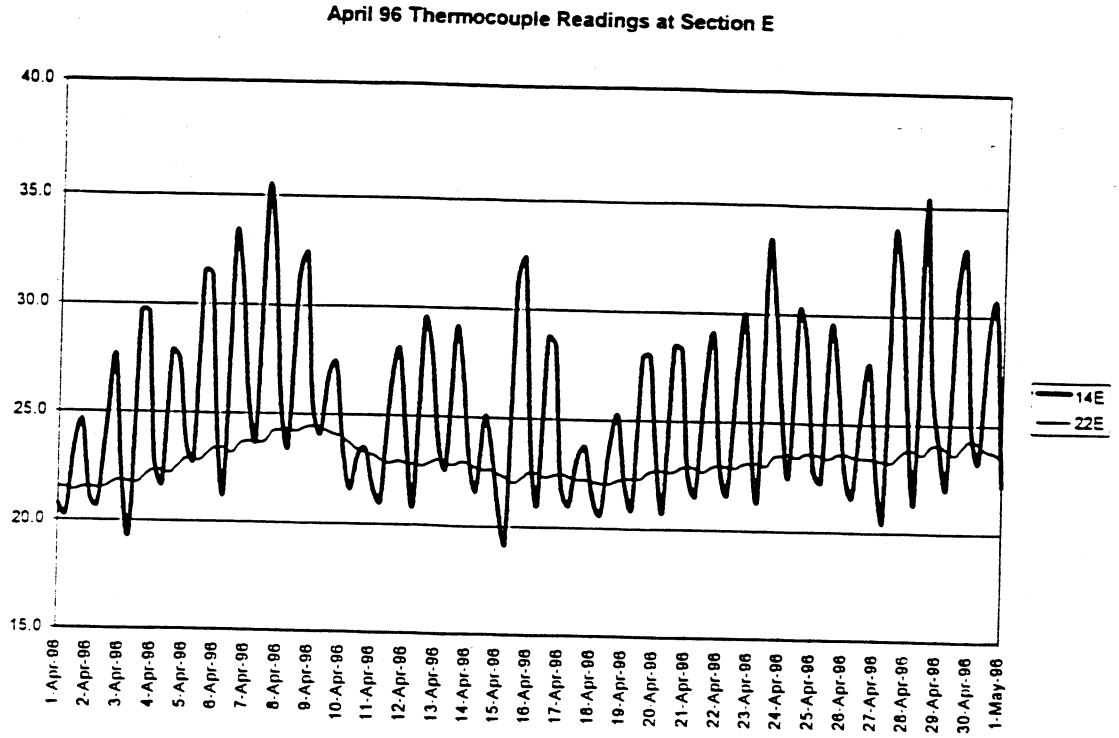
April 96 Thermocouple Readings at Section E
40.0
35.0
30.0
25.0
20.0
15.0
1-Apr-96
2-Apr-96
3-Apr-96
4-Apr-96
5-Apr-96
6-Apr-96
7-Apr-96
8-Apr-96
9-Apr-96
10-Apr-96
11-Apr-96
12-Apr-96
13-Apr-96
14-Apr-96
15-Apr-96
16-Apr-96
17-Apr-96
18-Apr-96
19-Apr-96
20-Apr-96
21-Apr-96
22-Apr-96
23-Apr-96
24-Apr-96
25-Apr-96
26-Apr-96
27-Apr-96
28-Apr-96
29-Apr-96
30-Apr-96
1-May-96
14E
22E

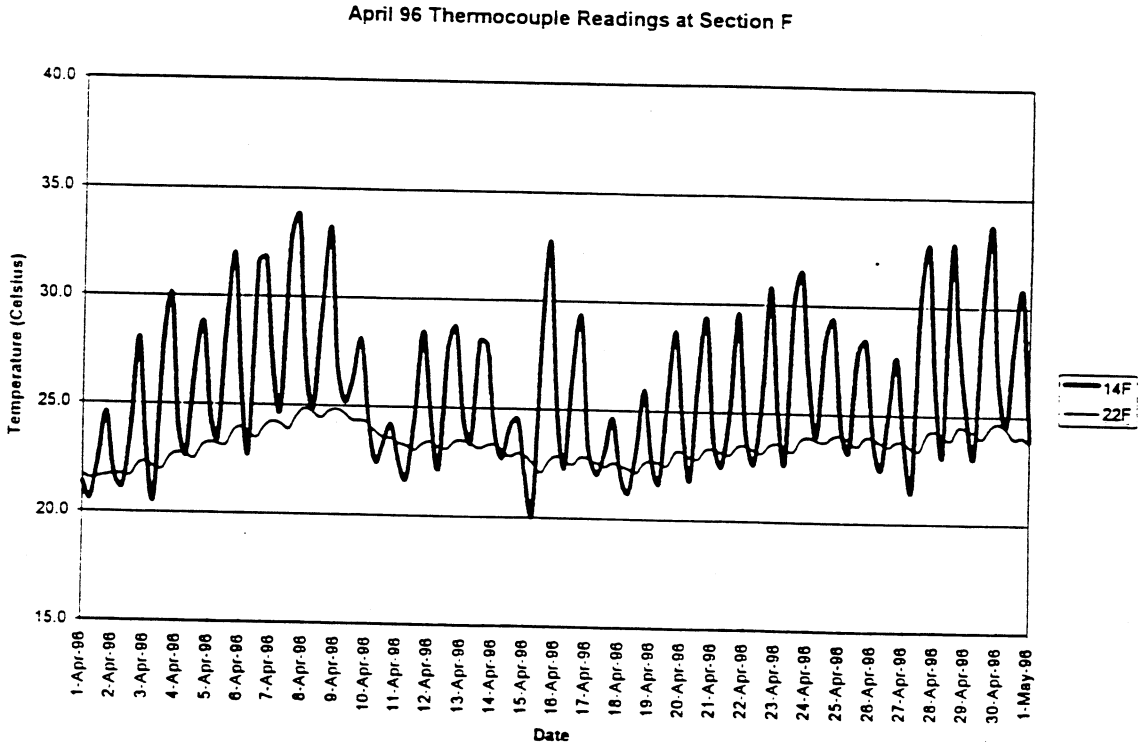
April 96 Thermocouple Readings at Section F
Temperature (Celsius)
40.0
35.0
30.0
25.0
20.0
15.0
1-Apr-96
2-Apr-96
3-Apr-96
4-Apr-96
5-Apr-96
6-Apr-96
7-Apr-96
8-Apr-96
9-Apr-96
10-Apr-96
11-Apr-96
12-Apr-96
13-Apr-96
14-Apr-96
15-Apr-96
16-Apr-96
17-Apr-96
18-Apr-96
19-Apr-96
20-Apr-96
21-Apr-96
22-Apr-96
23-Apr-96
24-Apr-96
25-Apr-96
26-Apr-96
27-Apr-96
28-Apr-96
29-Apr-96
30-Apr-96
1-May-96
Date
14F
22F

Figure 8.23

May 96 Thermocouple Readings at Section E

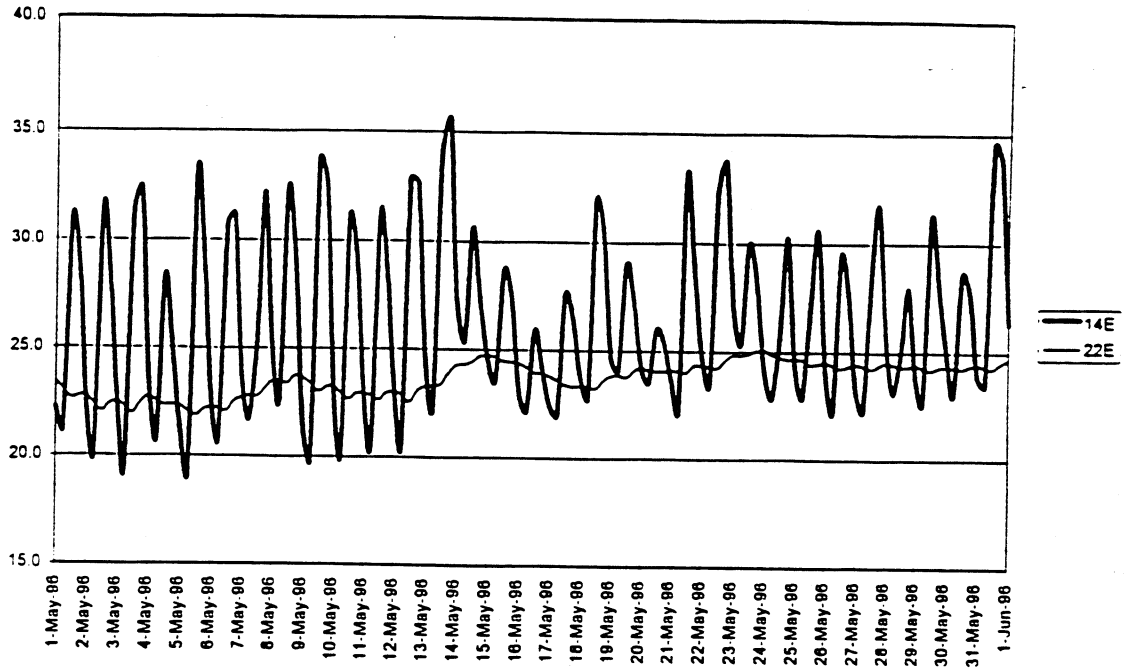

May 96 Thermocouple Readings at Section F

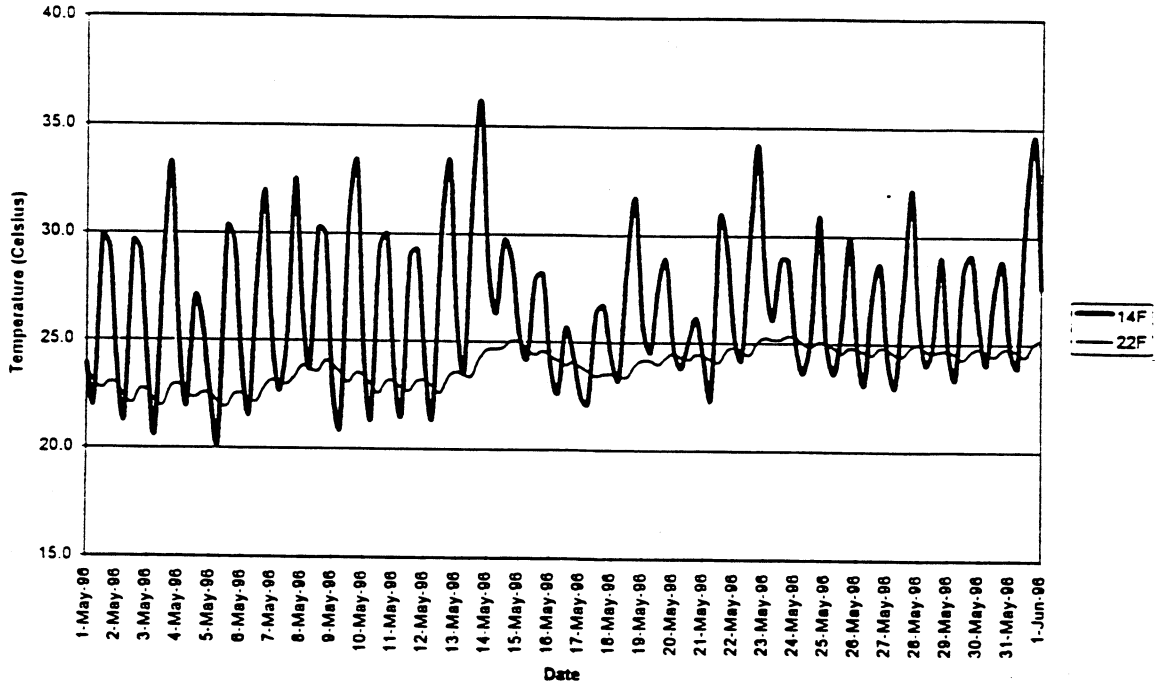

Figure 8.24

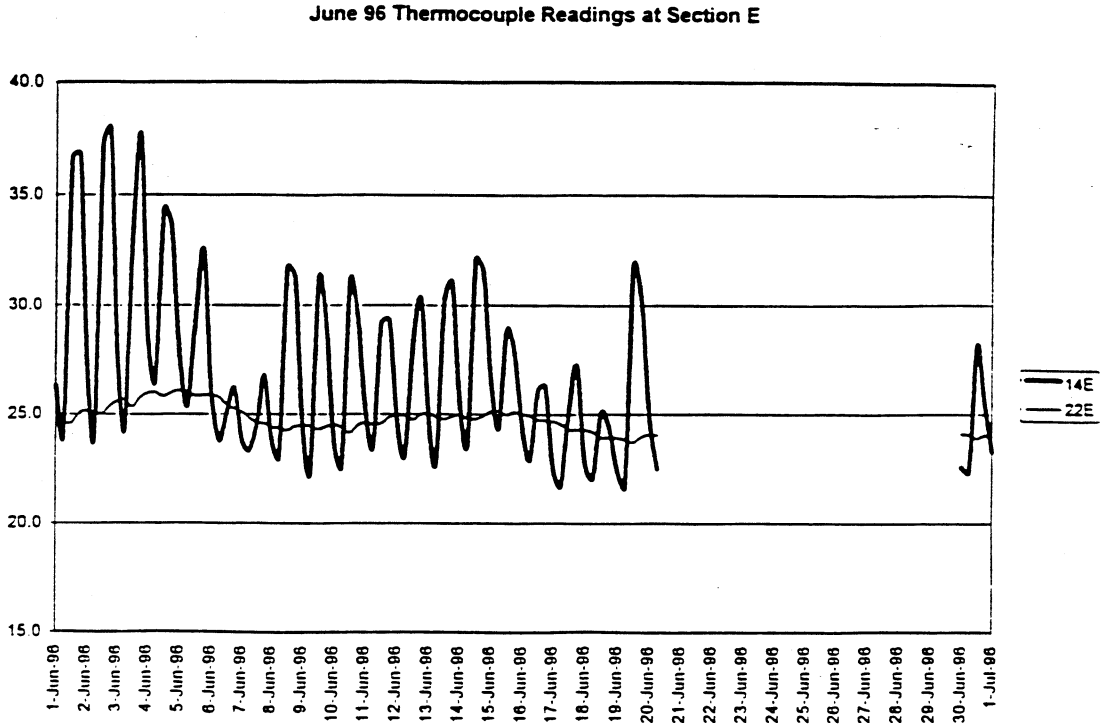
June 96 Thermocouple Readings at Section E
40.0
35.0
30.0
25.0
20.0
15.0
1-Jun-96
2-Jun-96
3-Jun-96
4-Jun-96
5-Jun-96
6-Jun-96
7-Jun-96
8-Jun-96
9-Jun-96
10-Jun-96
11-Jun-96
12-Jun-96
13-Jun-96
14-Jun-96
15-Jun-96
16-Jun-96
17-Jun-96
18-Jun-96
19-Jun-96
20-Jun-96
21-Jun-96
22-Jun-96
23-Jun-96
24-Jun-96
25-Jun-96
26-Jun-96
27-Jun-96
28-Jun-96
29-Jun-96
30-Jun-96
1-Jul-96
14E
22E

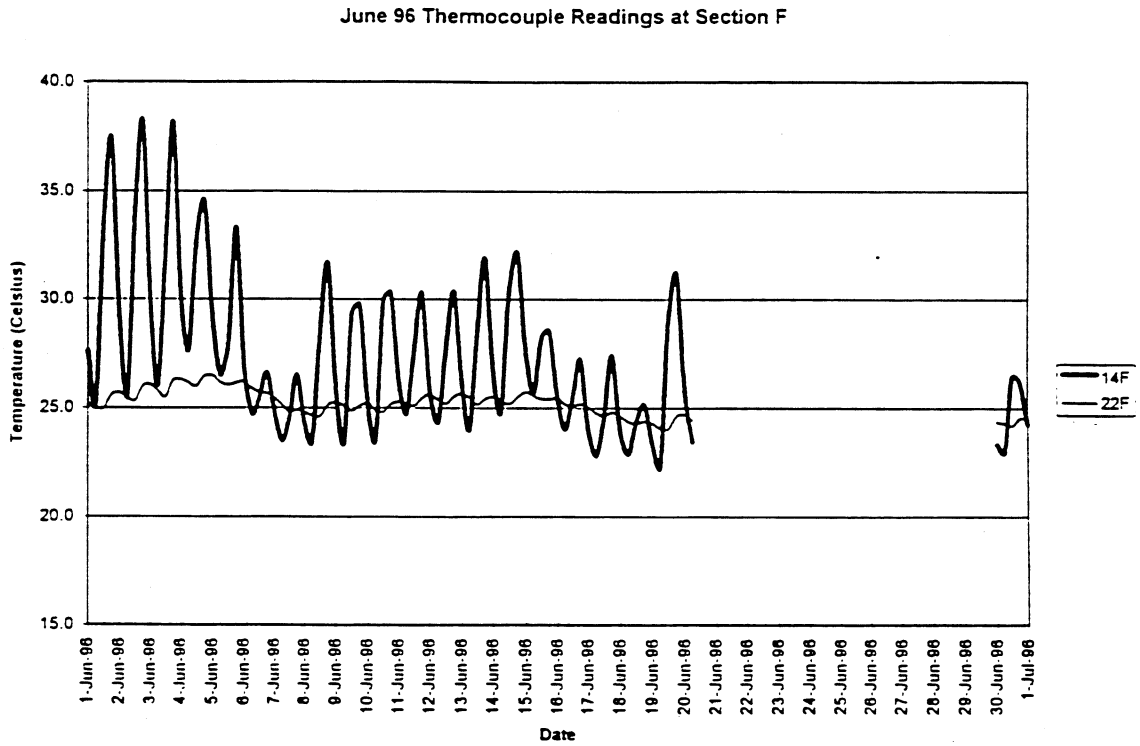
June 96 Thermocouple Readings at Section F
Temperature (Celsius)
40.0
35.0
30.0
25.0
20.0
15.0
1-Jun-96
2-Jun-96
3-Jun-96
4-Jun-96
5-Jun-96
6-Jun-96
7-Jun-96
8-Jun-96
9-Jun-96
10-Jun-96
11-Jun-96
12-Jun-96
13-Jun-96
14-Jun-96
15-Jun-96
16-Jun-96
17-Jun-96
18-Jun-96
19-Jun-96
20-Jun-96
21-Jun-96
22-Jun-96
23-Jun-96
24-Jun-96
25-Jun-96
26-Jun-96
27-Jun-96
28-Jun-96
29-Jun-96
30-Jun-96
1-Jul-96
Date
14F
22F

Figure 8.25

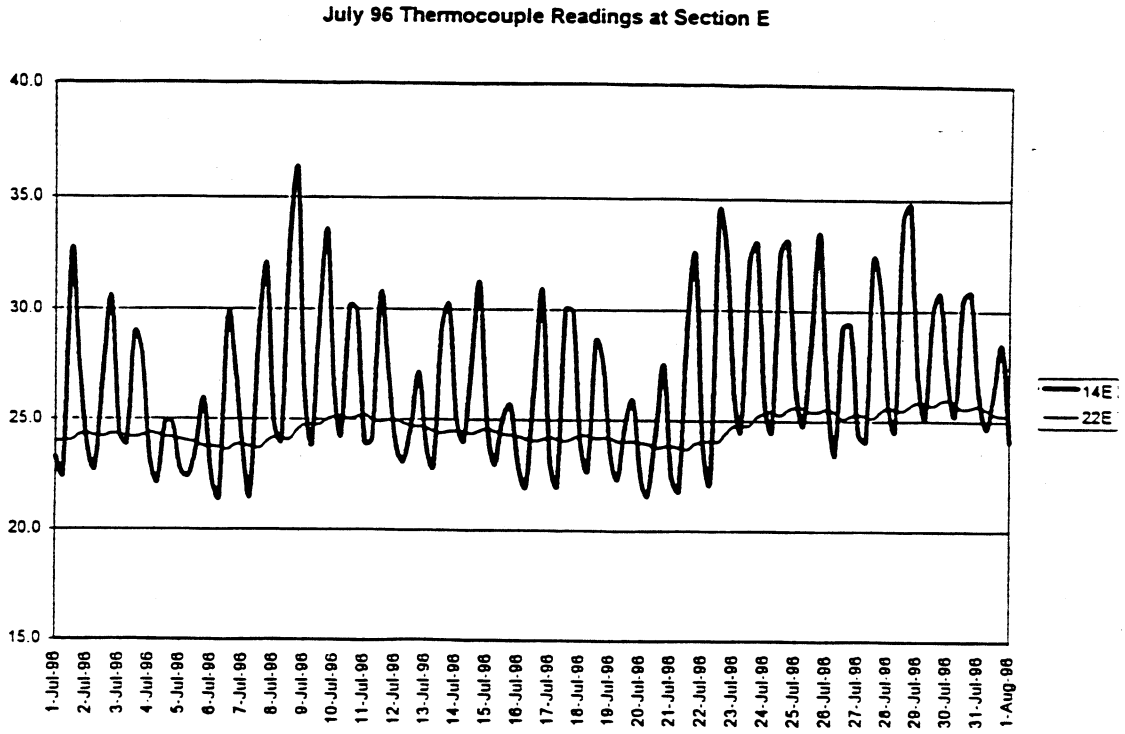
July 96 Thermocouple Readings at Section E
40.0
35.0
30.0
25.0
20.0
15.0
1-Jul-96
2-Jul-96
3-Jul-96
4-Jul-96
5-Jul-96
6-Jul-96
7-Jul-96
8-Jul-96
9-Jul-96
10-Jul-96
11-Jul-96
12-Jul-96
13-Jul-96
14-Jul-96
15-Jul-96
16-Jul-96
17-Jul-96
18-Jul-96
19-Jul-96
20-Jul-96
21-Jul-96
22-Jul-96
23-Jul-96
24-Jul-96
25-Jul-96
26-Jul-96
27-Jul-96
28-Jul-96
29-Jul-96
30-Jul-96
31-Jul-96
1-Aug-96
14E
22E

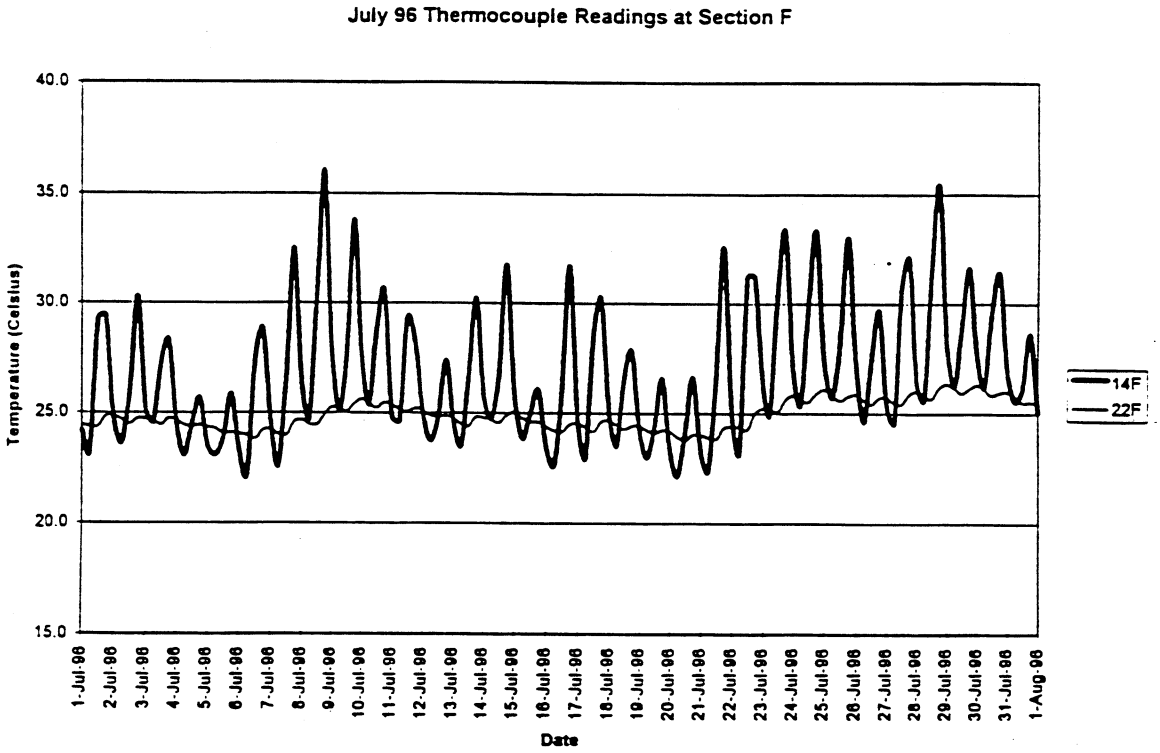
July 96 Thermocouple Readings at Section F
Temperature (Celsius)
40.0
35.0
30.0
25.0
20.0
15.0
1-Jul-96
2-Jul-96
3-Jul-96
4-Jul-96
5-Jul-96
6-Jul-96
7-Jul-96
8-Jul-96
9-Jul-96
10-Jul-96
11-Jul-96
12-Jul-96
13-Jul-96
14-Jul-96
15-Jul-96
16-Jul-96
17-Jul-96
18-Jul-96
19-Jul-96
20-Jul-96
21-Jul-96
22-Jul-96
23-Jul-96
24-Jul-96
25-Jul-96
26-Jul-96
27-Jul-96
28-Jul-96
29-Jul-96
30-Jul-96
31-Jul-96
1-Aug-96
Date
14F
22F

Figure 8.26

August 96 Thermocouple Readings at Section E

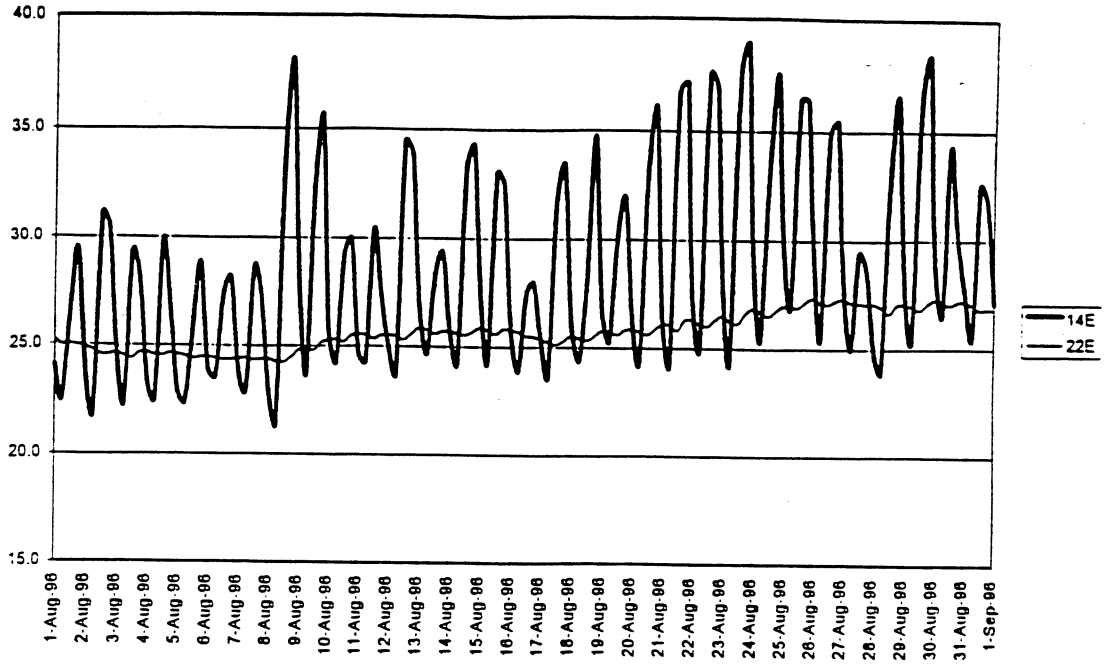

August 96 Thermocouple Readings at Section F

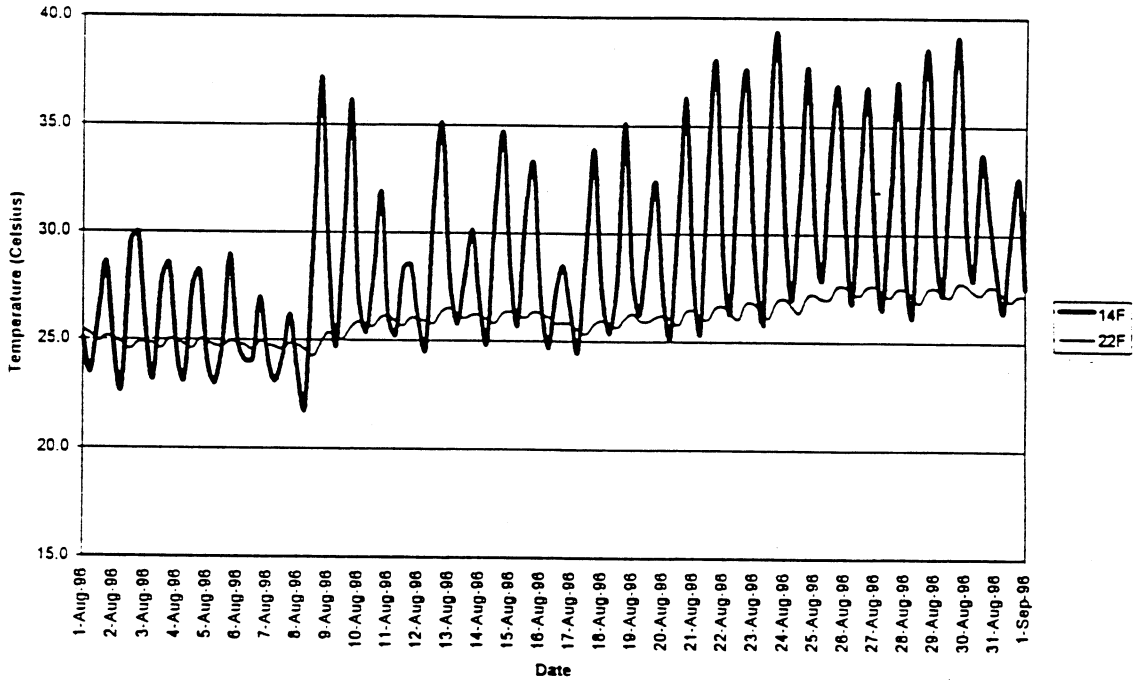

Figure 8.27

September 96 Thermocouple Readings at Section E

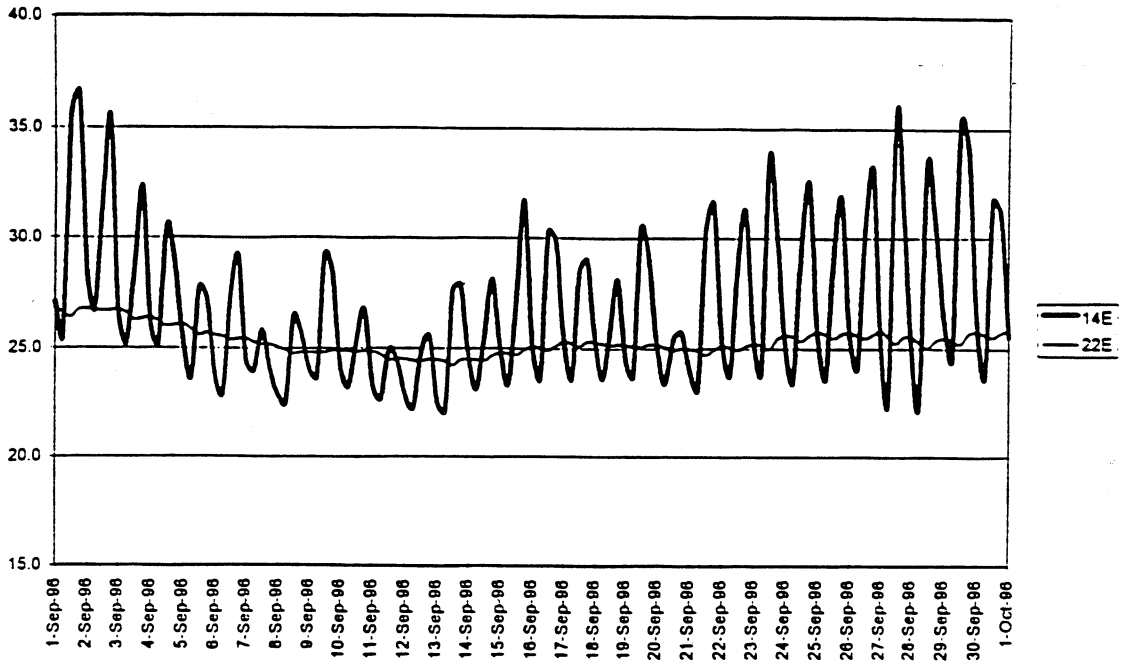

September 96 Thermocouple Readings at Section F

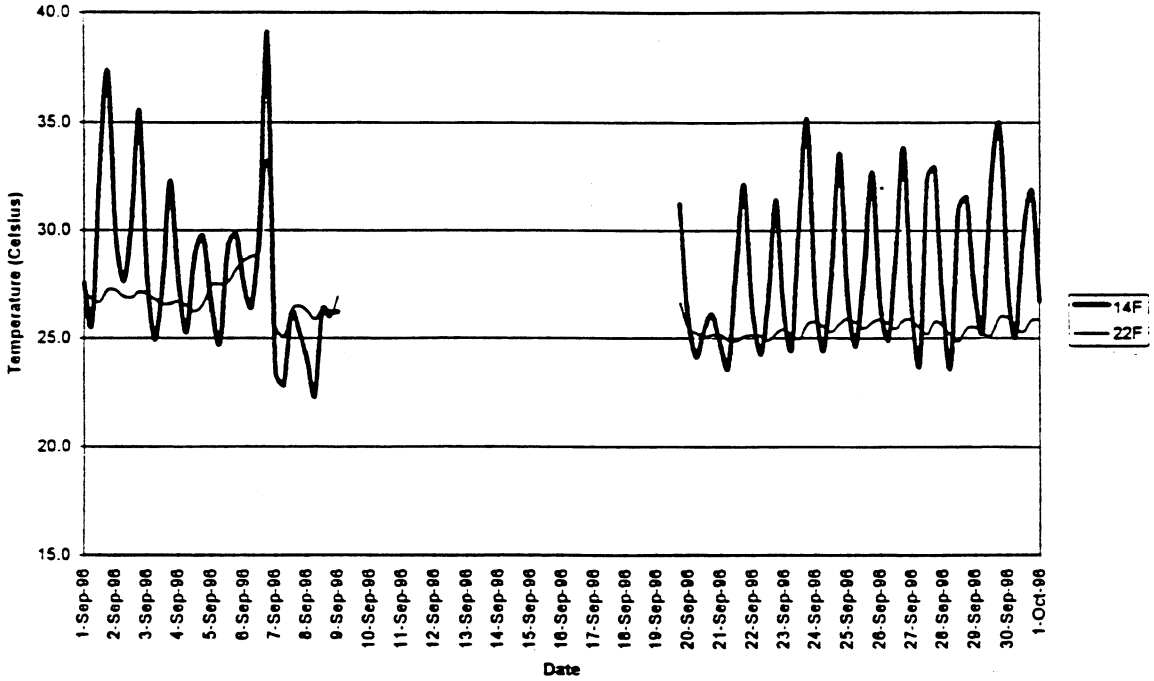

Figure 8.28

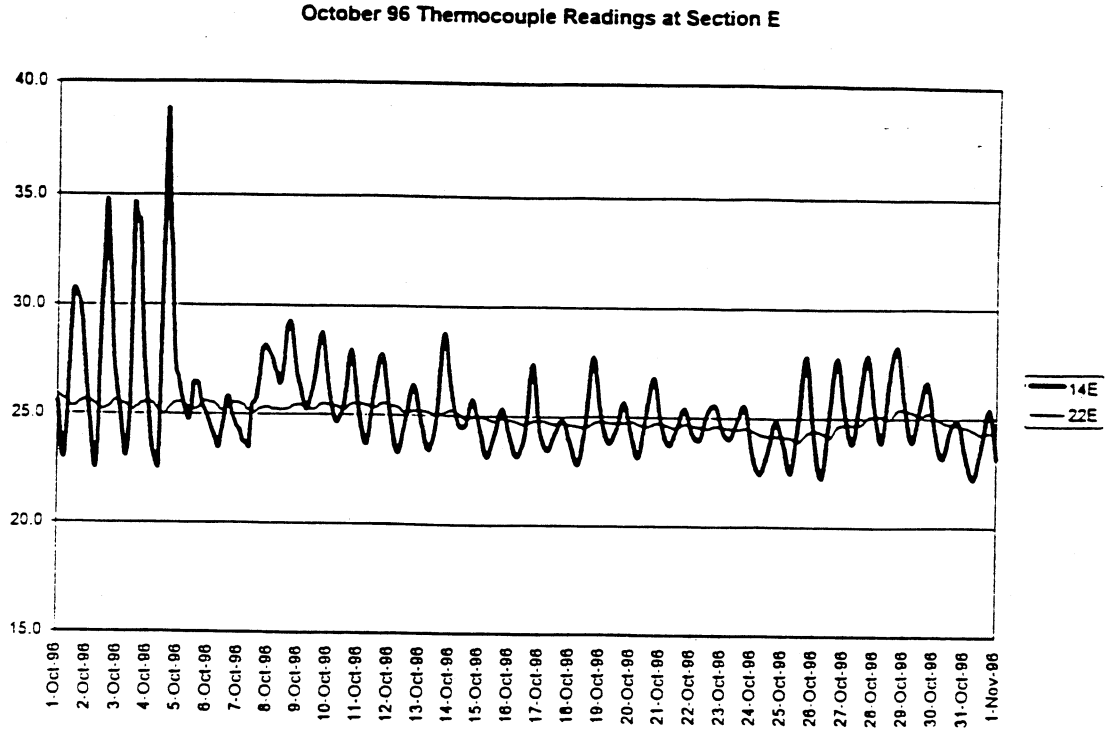
October 96 Thermocouple Readings at Section E
40.0
35.0
30.0
25.0
20.0
15.0
1-Oct-96
2-Oct-96
3-Oct-96
4-Oct-96
5-Oct-96
6-Oct-96
7-Oct-96
8-Oct-96
9-Oct-96
10-Oct-96
11-Oct-96
12-Oct-96
13-Oct-96
14-Oct-96
15-Oct-96
16-Oct-96
17-Oct-96
18-Oct-96
19-Oct-96
20-Oct-96
21-Oct-96
22-Oct-96
23-Oct-96
24-Oct-96
25-Oct-96
26-Oct-96
27-Oct-96
28-Oct-96
29-Oct-96
30-Oct-96
31-Oct-96
1-Nov-96
14E
22E

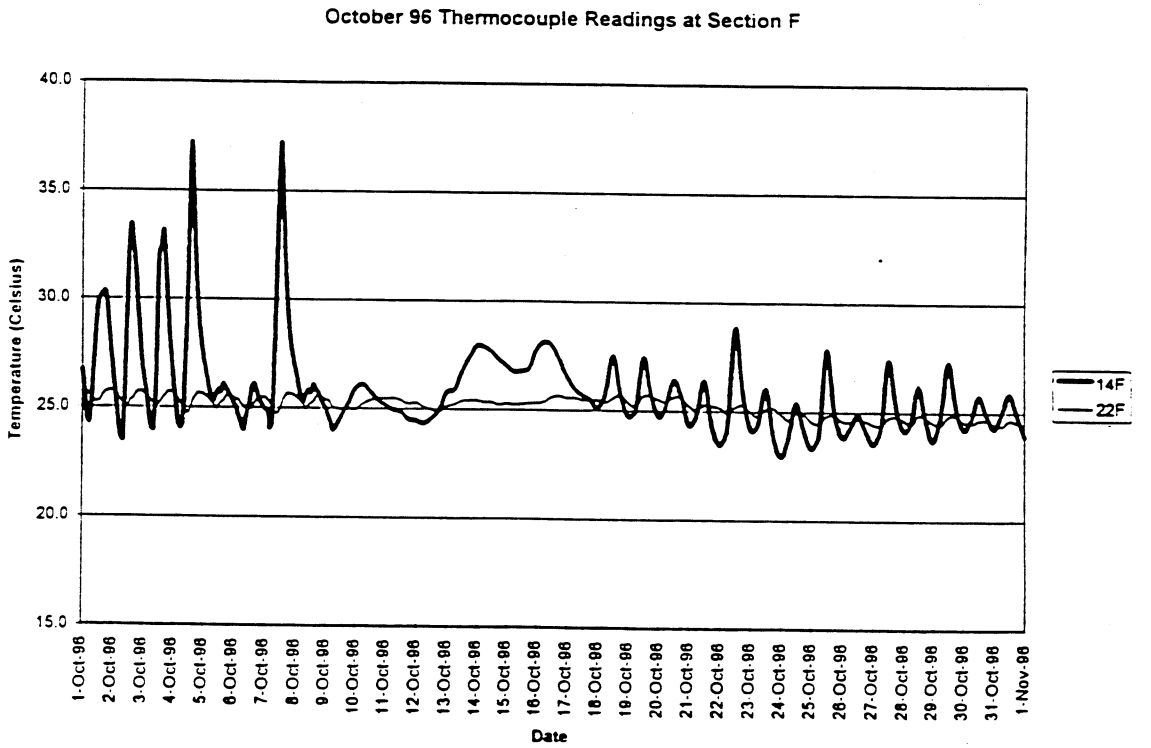
October 96 Thermocouple Readings at Section F
Temperature (Celsius)
40.0
35.0
30.0
25.0
20.0
15.0
1-Oct-96
2-Oct-96
3-Oct-96
4-Oct-96
5-Oct-96
6-Oct-96
7-Oct-96
8-Oct-96
9-Oct-96
10-Oct-96
11-Oct-96
12-Oct-96
13-Oct-96
14-Oct-96
15-Oct-96
16-Oct-96
17-Oct-96
18-Oct-96
19-Oct-96
20-Oct-96
21-Oct-96
22-Oct-96
23-Oct-96
24-Oct-96
25-Oct-96
26-Oct-96
27-Oct-96
28-Oct-96
29-Oct-96
30-Oct-96
31-Oct-96
1-Nov-96
Date
14F
22F

Figure 8.29

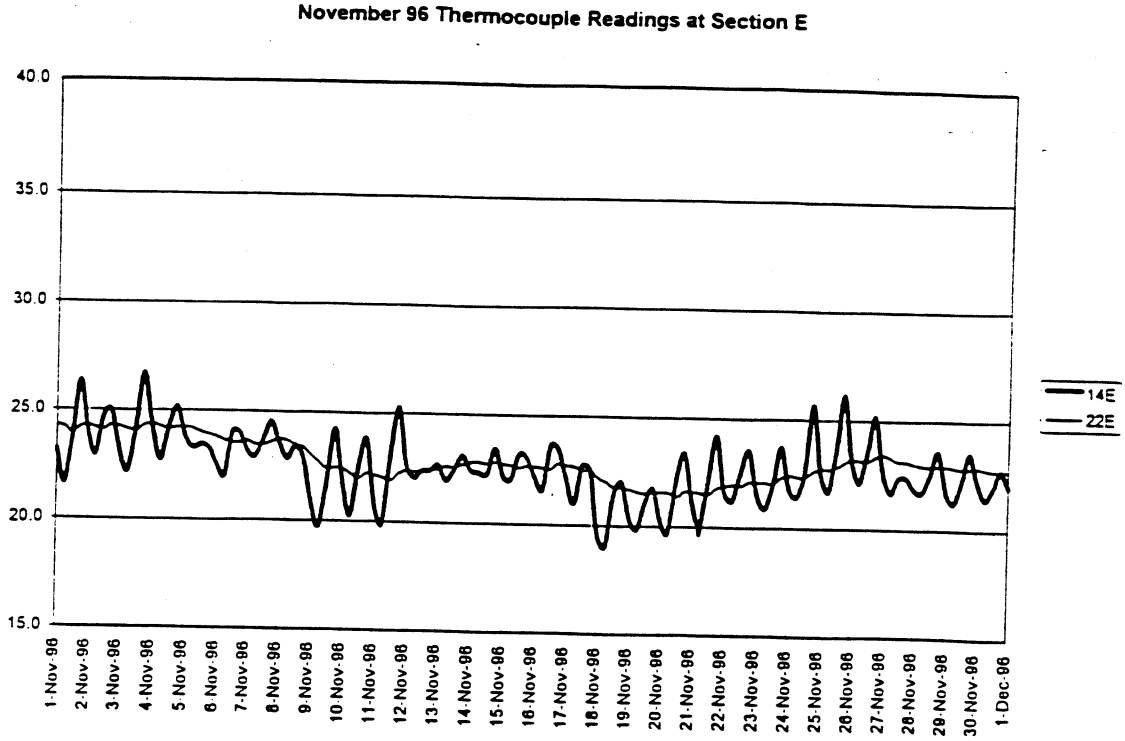
November 96 Thermocouple Readings at Section E
40.0
35.0
30.0
25.0
20.0
15.0
1-Nov-96
2-Nov-96
3-Nov-96
4-Nov-96
5-Nov-96
6-Nov-96
7-Nov-96
8-Nov-96
9-Nov-96
10-Nov-96
11-Nov-96
12-Nov-96
13-Nov-96
14-Nov-96
15-Nov-96
16-Nov-96
17-Nov-96
18-Nov-96
19-Nov-96
20-Nov-96
21-Nov-96
22-Nov-96
23-Nov-96
24-Nov-96
25-Nov-96
26-Nov-96
27-Nov-96
28-Nov-96
29-Nov-96
30-Nov-96
1-Dec-96
14E
22E

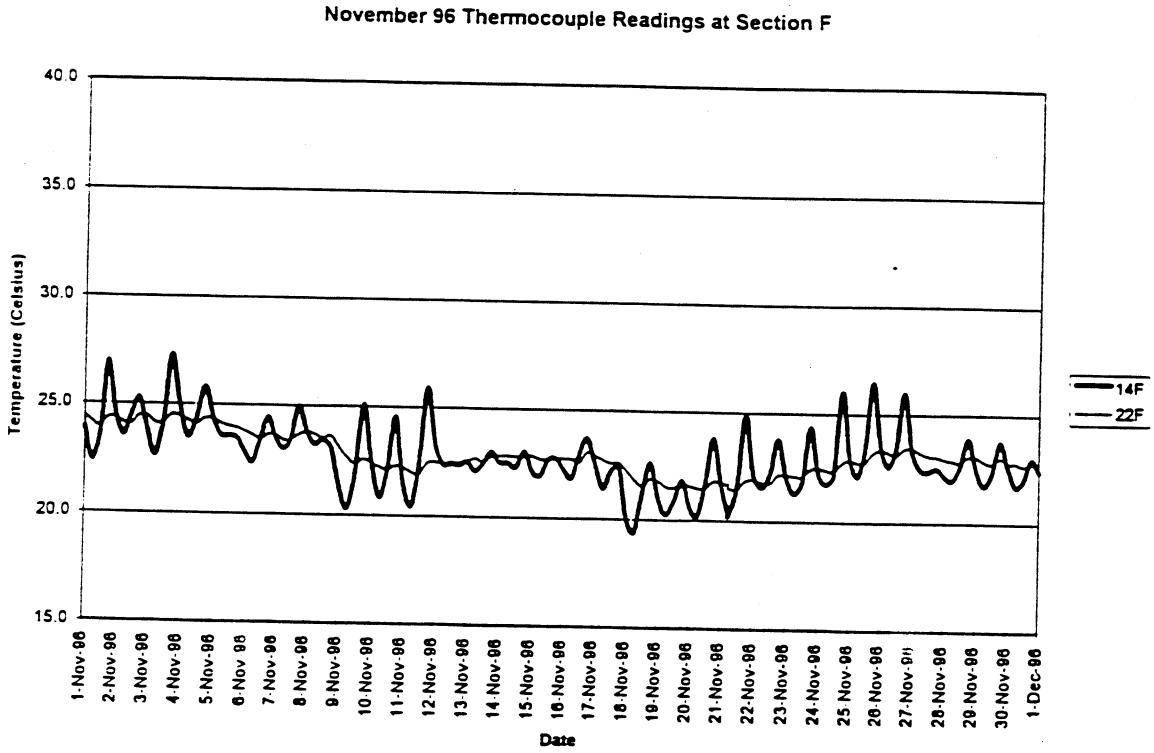
November 96 Thermocouple Readings at Section F
Temperature (Celsius)
40.0
35.0
30.0
25.0
20.0
15.0
1-Nov-96
2-Nov-96
3-Nov-96
4-Nov-96
5-Nov-96
6-Nov-96
7-Nov-96
8-Nov-96
9-Nov-96
10-Nov-96
11-Nov-96
12-Nov-96
13-Nov-96
14-Nov-96
15-Nov-96
16-Nov-96
17-Nov-96
18-Nov-96
19-Nov-96
20-Nov-96
21-Nov-96
22-Nov-96
23-Nov-96
24-Nov-96
25-Nov-96
26-Nov-96
27-Nov-96
28-Nov-96
29-Nov-96
30-Nov-96
1-Dec-96
Date
14F
22F

Figure 8.30

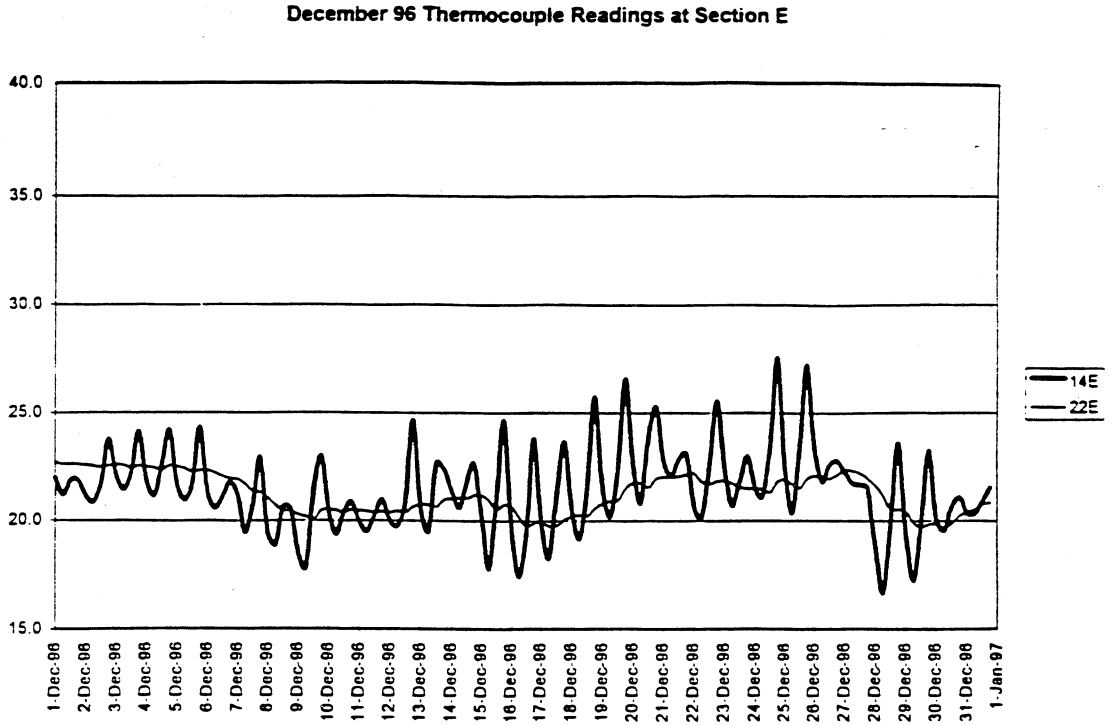
December 96 Thermocouple Readings at Section E
40.0
35.0
30.0
25.0
20.0
15.0
14E
22E
1-Dec-96
2-Dec-96
3-Dec-96
4-Dec-96
5-Dec-96
6-Dec-96
7-Dec-96
8-Dec-96
9-Dec-96
10-Dec-96
11-Dec-96
12-Dec-96
13-Dec-96
14-Dec-96
15-Dec-96
16-Dec-96
17-Dec-96
18-Dec-96
19-Dec-96
20-Dec-96
21-Dec-96
22-Dec-96
23-Dec-96
24-Dec-96
25-Dec-96
26-Dec-96
27-Dec-96
28-Dec-96
29-Dec-96
30-Dec-96
31-Dec-96
1-Jan-97

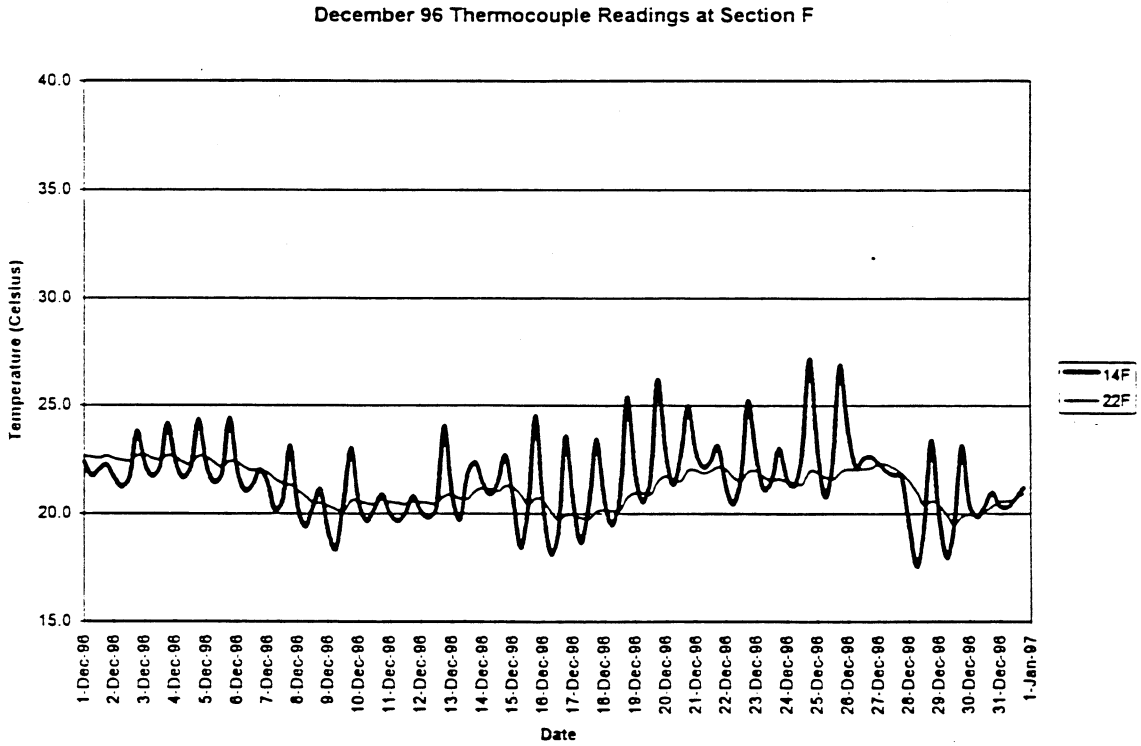
December 96 Thermocouple Readings at Section F
Temperature (Celsius)
40.0
35.0
30.0
25.0
20.0
15.0
14F
22F
1-Dec-96
2-Dec-96
3-Dec-96
4-Dec-96
5-Dec-96
6-Dec-96
7-Dec-96
8-Dec-96
9-Dec-96
10-Dec-96
11-Dec-96
12-Dec-96
13-Dec-96
14-Dec-96
15-Dec-96
16-Dec-96
17-Dec-96
18-Dec-96
19-Dec-96
20-Dec-96
21-Dec-96
22-Dec-96
23-Dec-96
24-Dec-96
25-Dec-96
26-Dec-96
27-Dec-96
28-Dec-96
29-Dec-96
30-Dec-96
31-Dec-96
1-Jan-97
Date

Figure 8.31

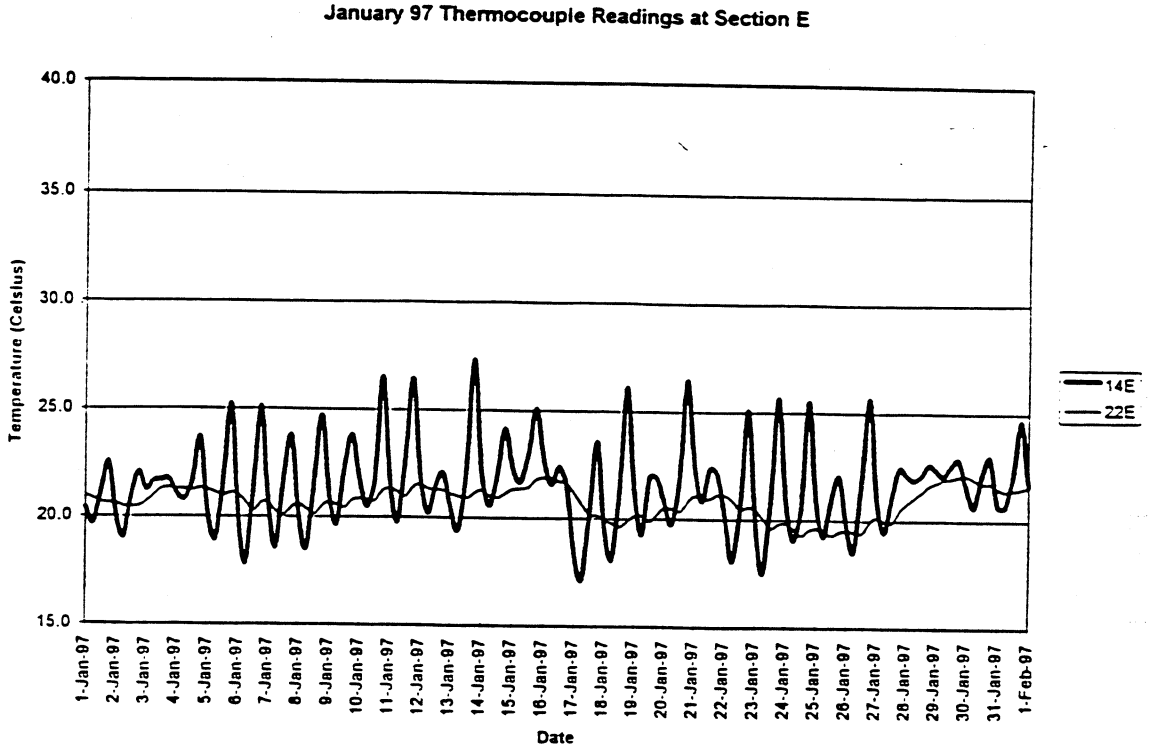
January 97 Thermocouple Readings at Section E
Temperature (Celsius)
40.0
35.0
30.0
25.0
20.0
15.0
1-Jan-97
2-Jan-97
3-Jan-97
4-Jan-97
5-Jan-97
6-Jan-97
7-Jan-97
8-Jan-97
9-Jan-97
10-Jan-97
11-Jan-97
12-Jan-97
13-Jan-97
14-Jan-97
15-Jan-97
16-Jan-97
17-Jan-97
18-Jan-97
19-Jan-97
20-Jan-97
21-Jan-97
22-Jan-97
23-Jan-97
24-Jan-97
25-Jan-97
26-Jan-97
27-Jan-97
28-Jan-97
29-Jan-97
30-Jan-97
31-Jan-97
1-Feb-97
Date
14E
22E

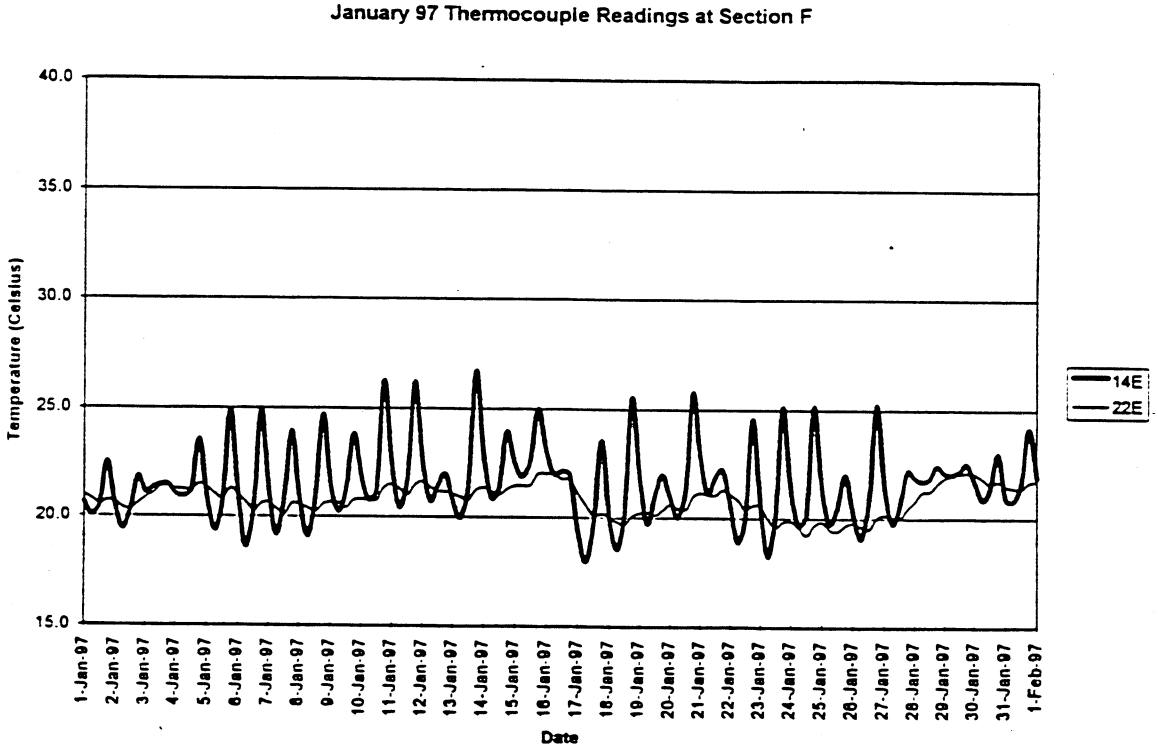
January 97 Thermocouple Readings at Section F
Temperature (Celsius)
40.0
35.0
30.0
25.0
20.0
15.0
1-Jan-97
2-Jan-97
3-Jan-97
4-Jan-97
5-Jan-97
6-Jan-97
7-Jan-97
8-Jan-97
9-Jan-97
10-Jan-97
11-Jan-97
12-Jan-97
13-Jan-97
14-Jan-97
15-Jan-97
16-Jan-97
17-Jan-97
18-Jan-97
19-Jan-97
20-Jan-97
21-Jan-97
22-Jan-97
23-Jan-97
24-Jan-97
25-Jan-97
26-Jan-97
27-Jan-97
28-Jan-97
29-Jan-97
30-Jan-97
31-Jan-97
1-Feb-97
Date
14E
22E

Figure 8.32

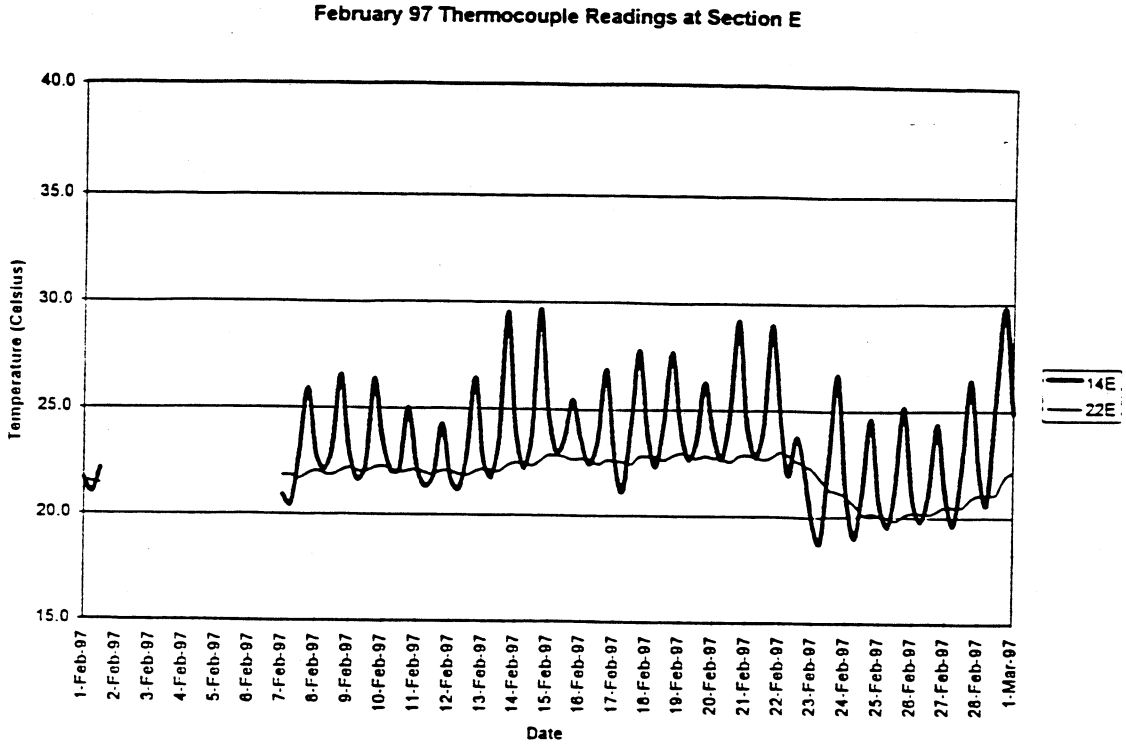
February 97 Thermocouple Readings at Section E
Temperature (Celsius)
40.0
35.0
30.0
25.0
20.0
15.0
1-Feb-97
2-Feb-97
3-Feb-97
4-Feb-97
5-Feb-97
6-Feb-97
7-Feb-97
8-Feb-97
9-Feb-97
10-Feb-97
11-Feb-97
12-Feb-97
13-Feb-97
14-Feb-97
15-Feb-97
16-Feb-97
17-Feb-97
18-Feb-97
19-Feb-97
20-Feb-97
21-Feb-97
22-Feb-97
23-Feb-97
24-Feb-97
25-Feb-97
26-Feb-97
27-Feb-97
28-Feb-97
1-Mar-97
Date
14E
22E

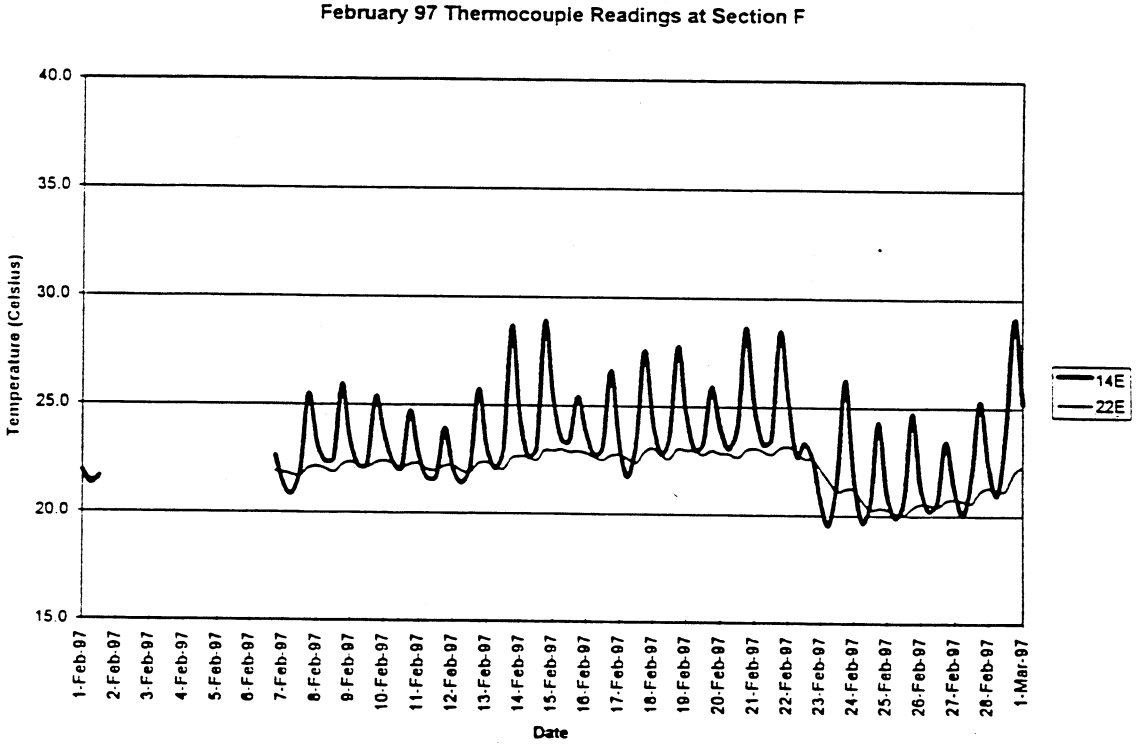
February 97 Thermocouple Readings at Section F
Temperature (Celsius)
40.0
35.0
30.0
25.0
20.0
15.0
1-Feb-97
2-Feb-97
3-Feb-97
4-Feb-97
5-Feb-97
6-Feb-97
7-Feb-97
8-Feb-97
9-Feb-97
10-Feb-97
11-Feb-97
12-Feb-97
13-Feb-97
14-Feb-97
15-Feb-97
16-Feb-97
17-Feb-97
18-Feb-97
19-Feb-97
20-Feb-97
21-Feb-97
22-Feb-97
23-Feb-97
24-Feb-97
25-Feb-97
26-Feb-97
27-Feb-97
28-Feb-97
1-Mar-97
Date
14E
22E

Figure 8.33

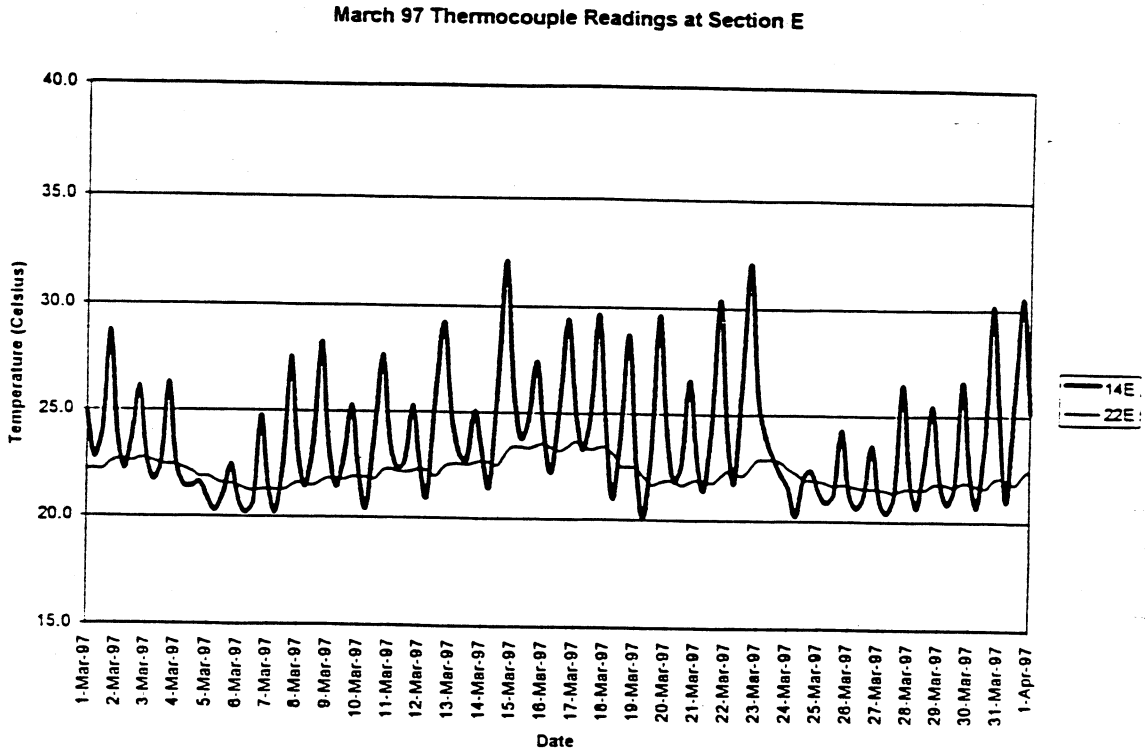
March 97 Thermocouple Readings at Section E
Temperature (Celsius)
40.0
35.0
30.0
25.0
20.0
15.0
1-Mar-97
2-Mar-97
3-Mar-97
4-Mar-97
5-Mar-97
6-Mar-97
7-Mar-97
8-Mar-97
9-Mar-97
10-Mar-97
11-Mar-97
12-Mar-97
13-Mar-97
14-Mar-97
15-Mar-97
16-Mar-97
17-Mar-97
18-Mar-97
19-Mar-97
20-Mar-97
21-Mar-97
22-Mar-97
23-Mar-97
24-Mar-97
25-Mar-97
26-Mar-97
27-Mar-97
28-Mar-97
29-Mar-97
30-Mar-97
31-Mar-97
1-Apr-97
Date
14E
22E

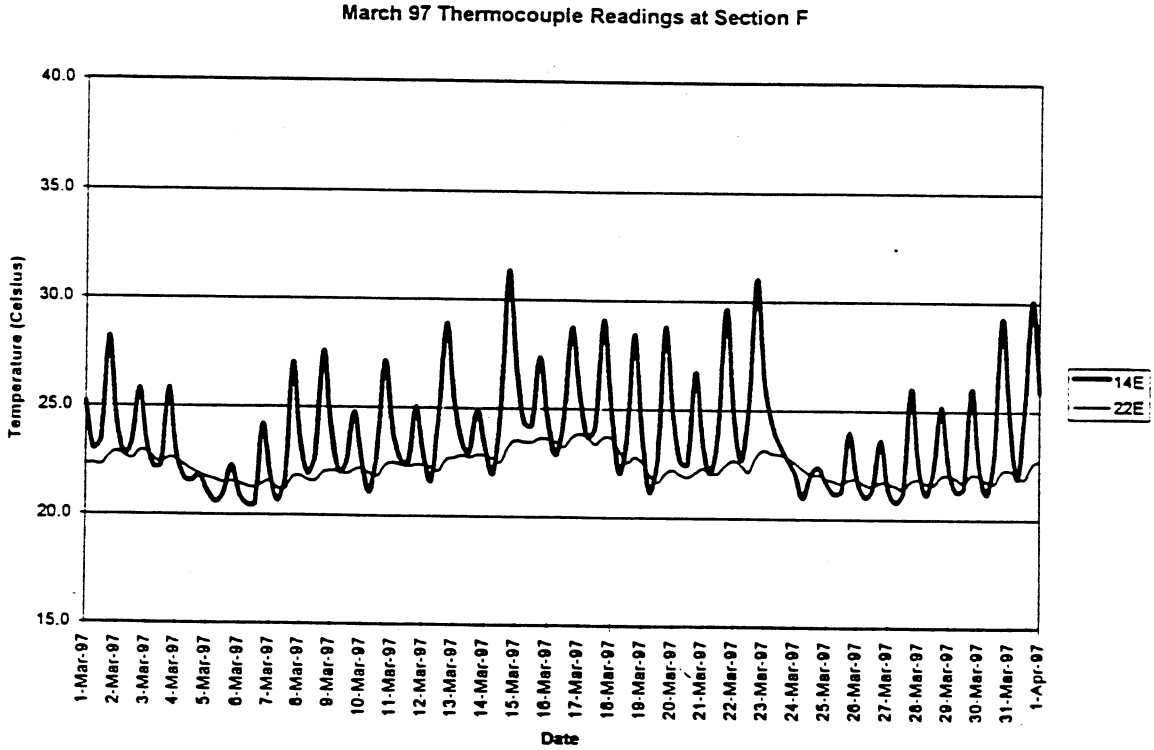
March 97 Thermocouple Readings at Section F
Temperature (Celsius)
40.0
35.0
30.0
25.0
20.0
15.0
1-Mar-97
2-Mar-97
3-Mar-97
4-Mar-97
5-Mar-97
6-Mar-97
7-Mar-97
8-Mar-97
9-Mar-97
10-Mar-97
11-Mar-97
12-Mar-97
13-Mar-97
14-Mar-97
15-Mar-97
16-Mar-97
17-Mar-97
18-Mar-97
19-Mar-97
20-Mar-97
21-Mar-97
22-Mar-97
23-Mar-97
24-Mar-97
25-Mar-97
26-Mar-97
27-Mar-97
28-Mar-97
29-Mar-97
30-Mar-97
31-Mar-97
1-Apr-97
Date
14E
22E

Figure 8.34

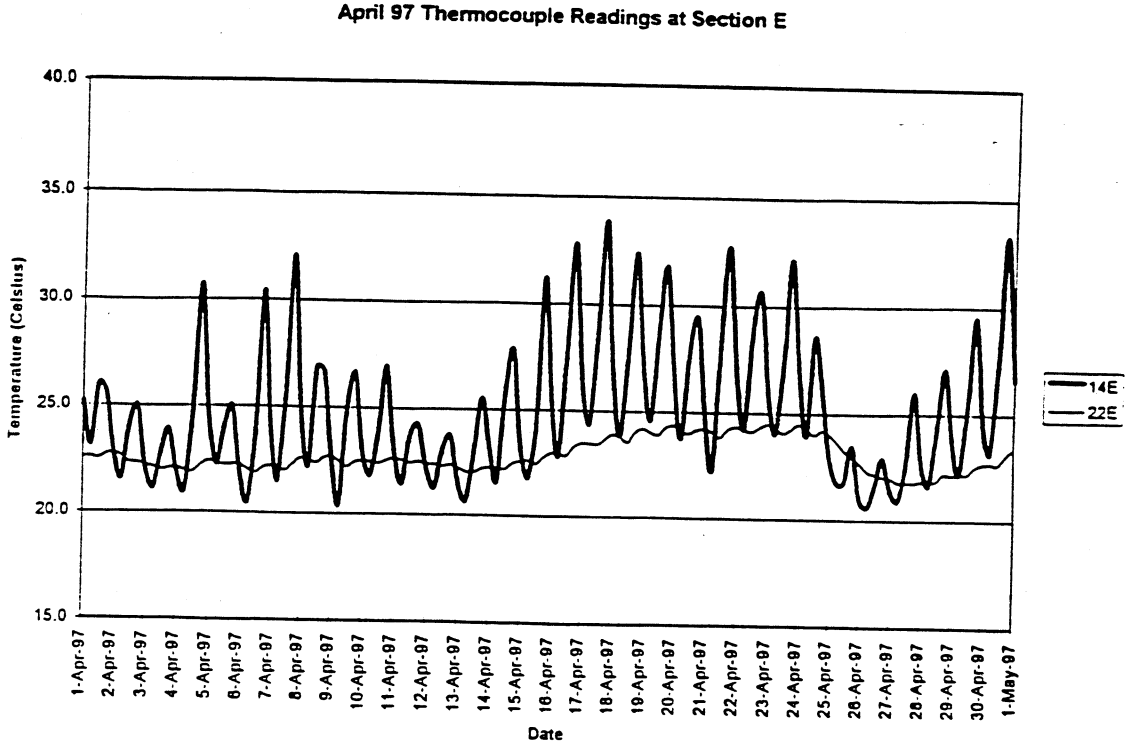
April 97 Thermocouple Readings at Section E
Temperature (Celsius)
40.0
35.0
30.0
25.0
20.0
15.0
1-Apr-97
2-Apr-97
3-Apr-97
4-Apr-97
5-Apr-97
6-Apr-97
7-Apr-97
8-Apr-97
9-Apr-97
10-Apr-97
11-Apr-97
12-Apr-97
13-Apr-97
14-Apr-97
15-Apr-97
16-Apr-97
17-Apr-97
18-Apr-97
19-Apr-97
20-Apr-97
21-Apr-97
22-Apr-97
23-Apr-97
24-Apr-97
25-Apr-97
26-Apr-97
27-Apr-97
28-Apr-97
29-Apr-97
30-Apr-97
1-May-97
Date
14E
22E

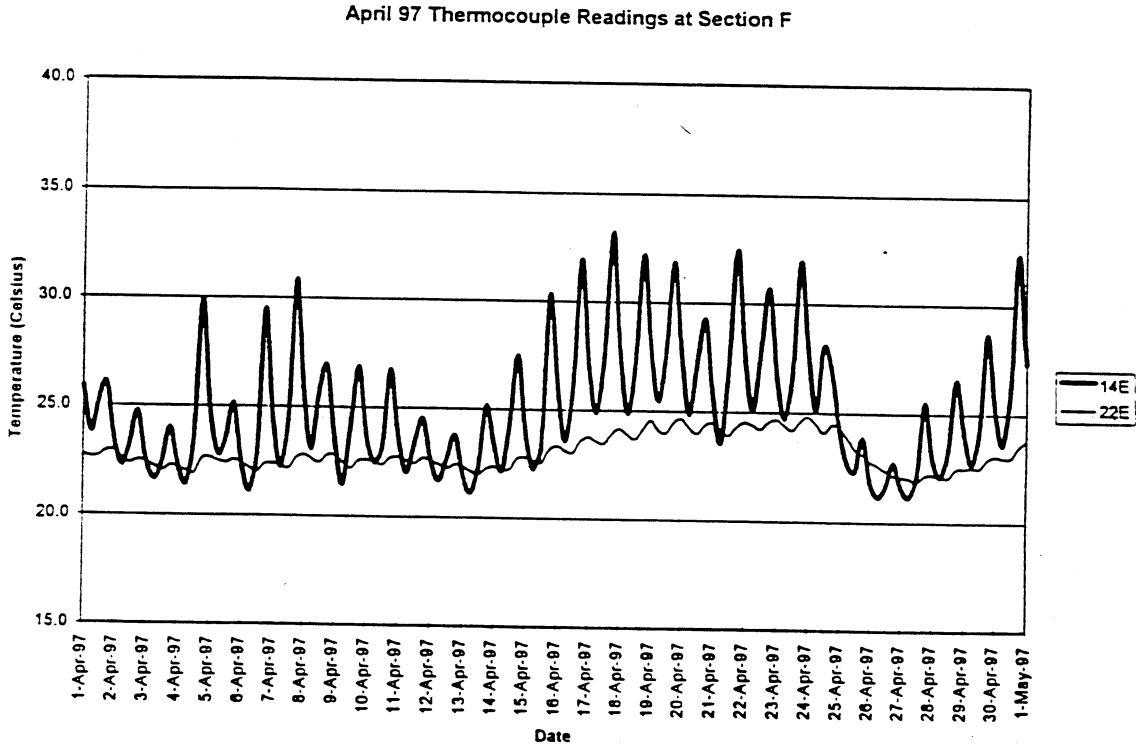
April 97 Thermocouple Readings at Section F
Temperature (Celsius)
40.0
35.0
30.0
25.0
20.0
15.0
1-Apr-97
2-Apr-97
3-Apr-97
4-Apr-97
5-Apr-97
6-Apr-97
7-Apr-97
8-Apr-97
9-Apr-97
10-Apr-97
11-Apr-97
12-Apr-97
13-Apr-97
14-Apr-97
15-Apr-97
16-Apr-97
17-Apr-97
18-Apr-97
19-Apr-97
20-Apr-97
21-Apr-97
22-Apr-97
23-Apr-97
24-Apr-97
25-Apr-97
26-Apr-97
27-Apr-97
28-Apr-97
29-Apr-97
30-Apr-97
1-May-97
Date
14E
22E

Figure 8.35

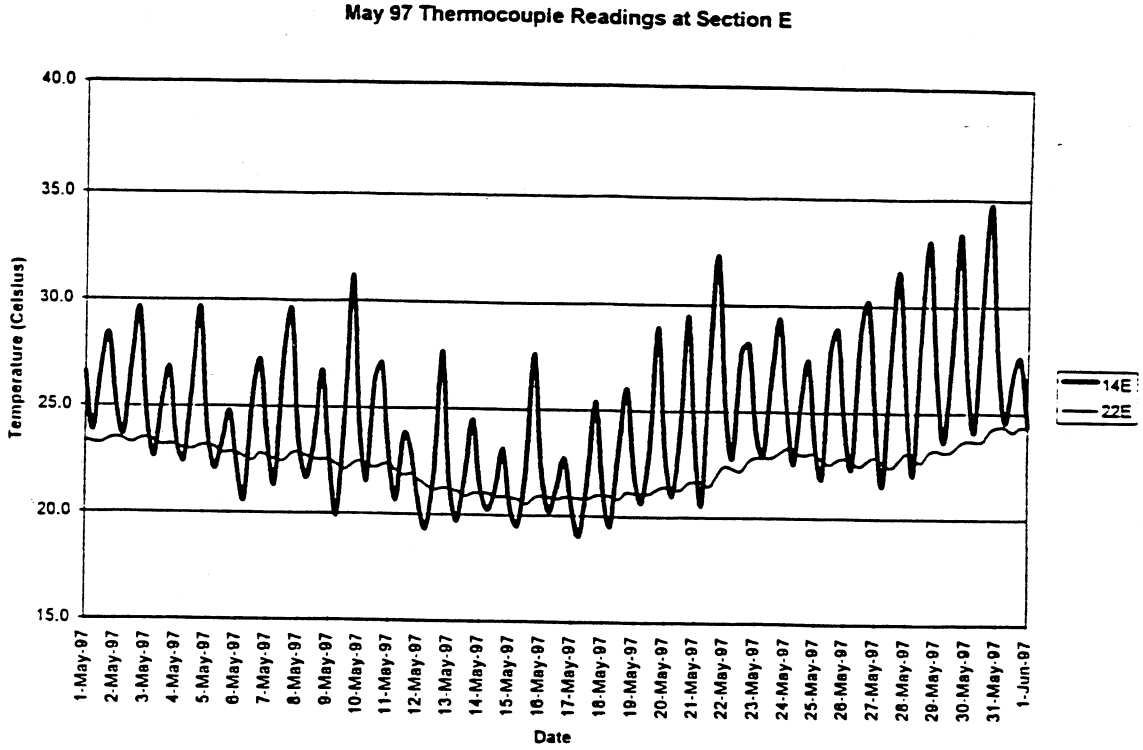

H3 Instrumentation Report

TYLin International

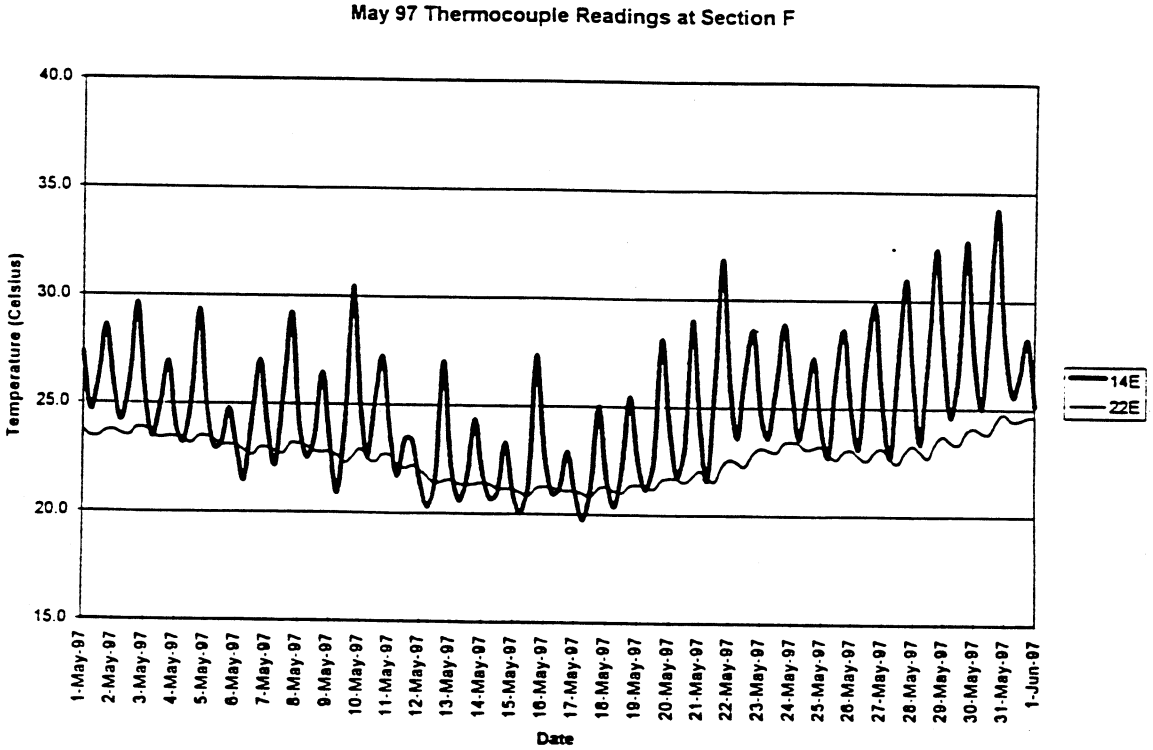

Figure 8.36

June 97 Thermocouple Readings at Section E

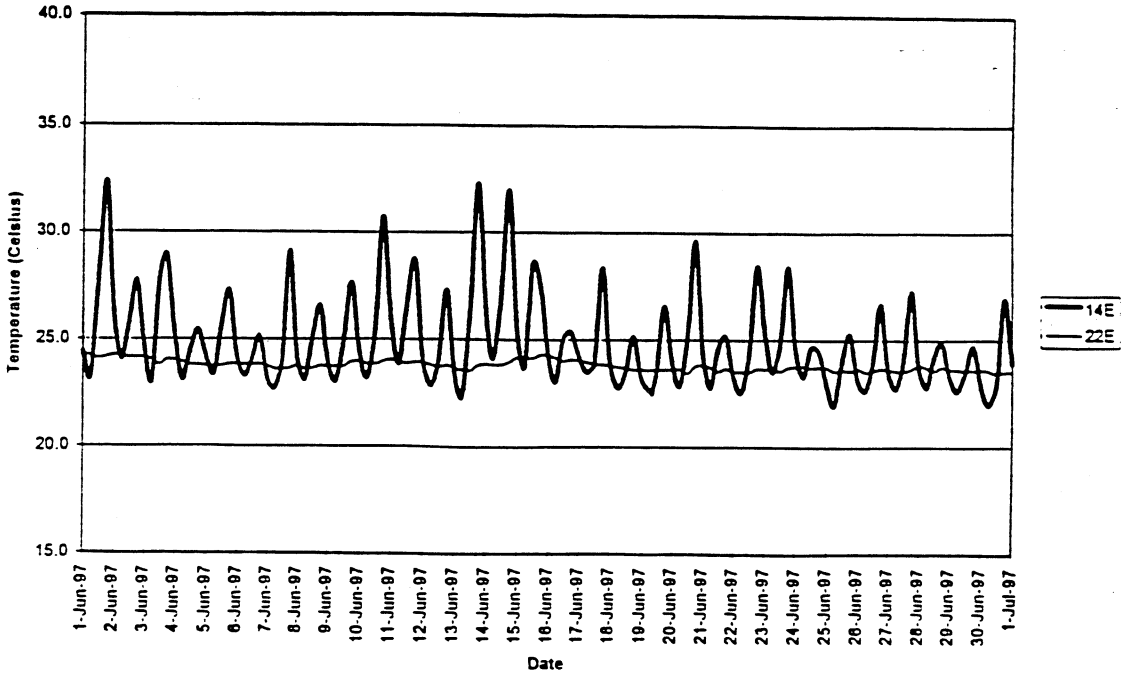

June 97 Thermocouple Readings at Section F

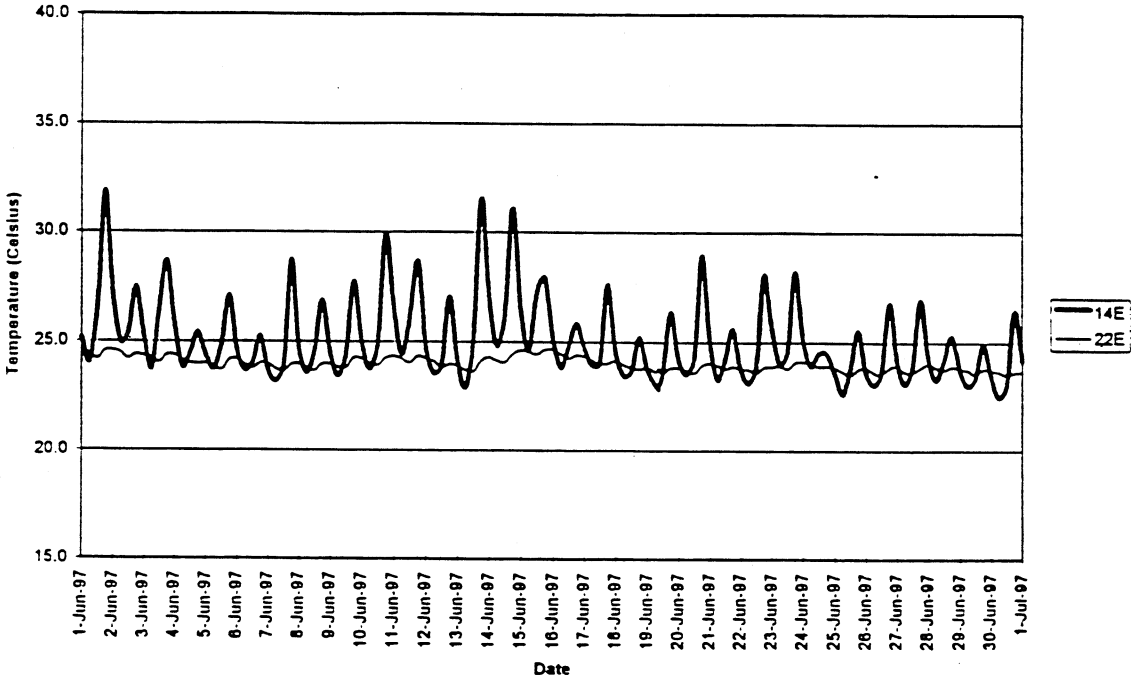

Figure 8.37

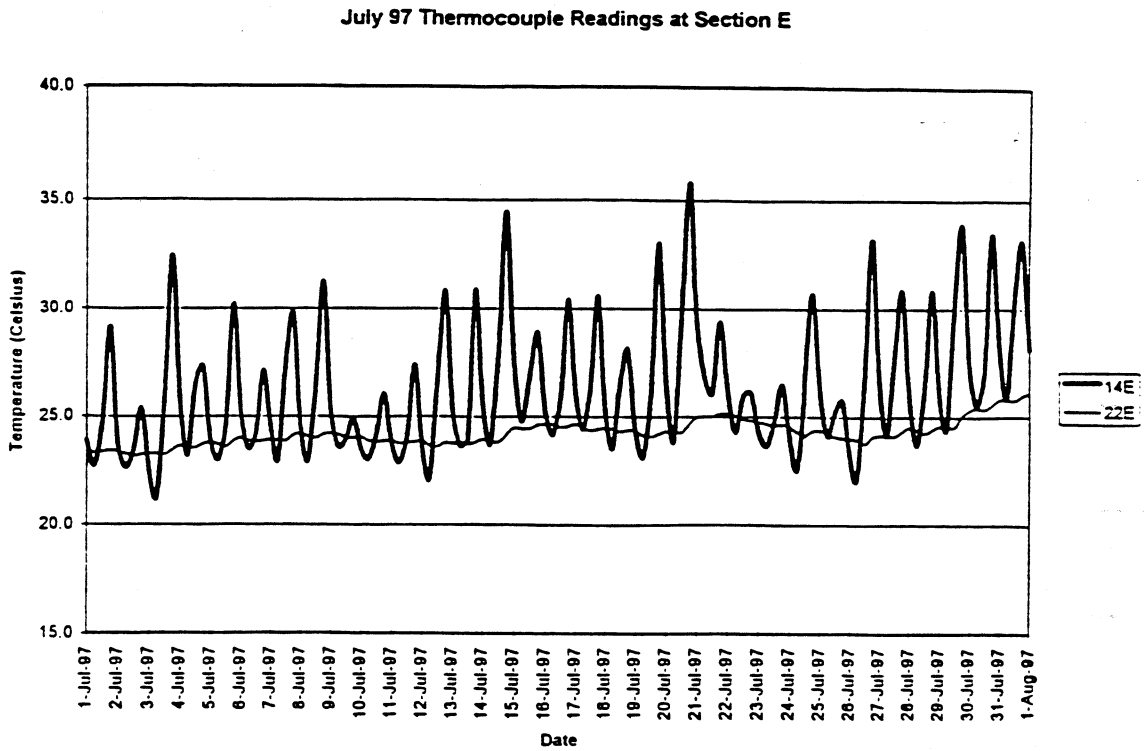
July 97 Thermocouple Readings at Section E
Temperature (Celsius)
40.0
35.0
30.0
25.0
20.0
15.0
1-Jul-97
2-Jul-97
3-Jul-97
4-Jul-97
5-Jul-97
6-Jul-97
7-Jul-97
8-Jul-97
9-Jul-97
10-Jul-97
11-Jul-97
12-Jul-97
13-Jul-97
14-Jul-97
15-Jul-97
16-Jul-97
17-Jul-97
18-Jul-97
19-Jul-97
20-Jul-97
21-Jul-97
22-Jul-97
23-Jul-97
24-Jul-97
25-Jul-97
26-Jul-97
27-Jul-97
28-Jul-97
29-Jul-97
30-Jul-97
31-Jul-97
1-Aug-97
Date
14E
22E

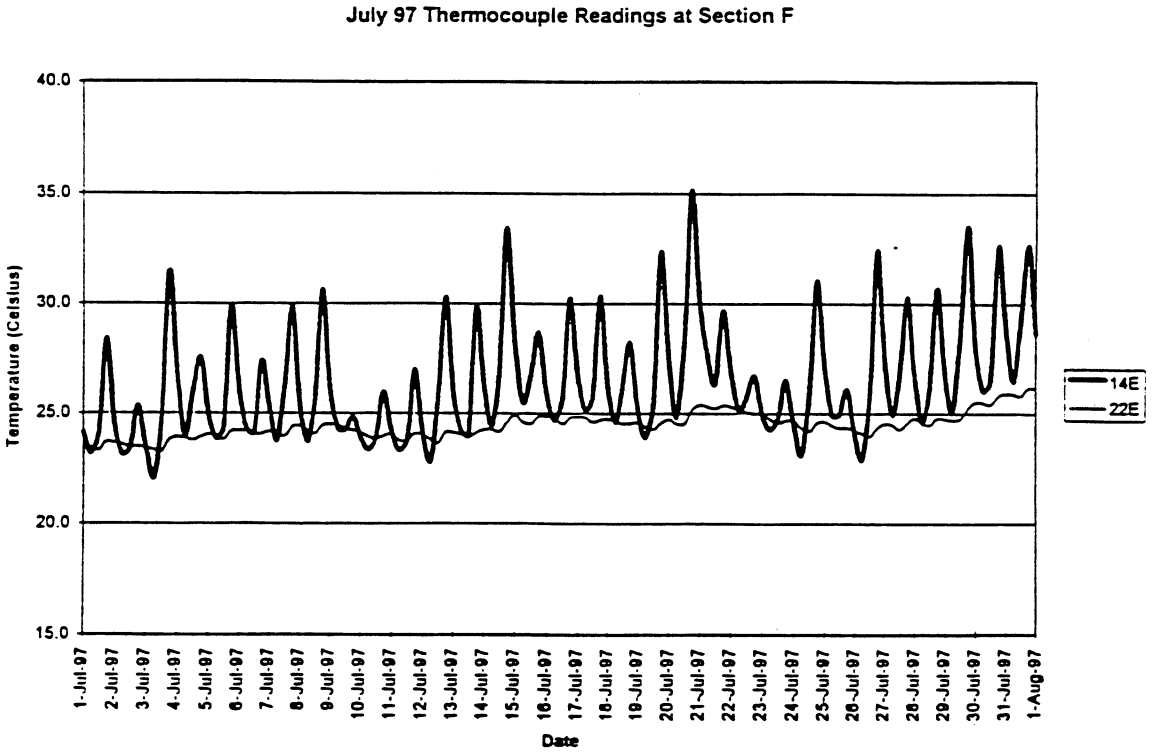
July 97 Thermocouple Readings at Section F
Temperature (Celsius)
40.0
35.0
30.0
25.0
20.0
15.0
1-Jul-97
2-Jul-97
3-Jul-97
4-Jul-97
5-Jul-97
6-Jul-97
7-Jul-97
8-Jul-97
9-Jul-97
10-Jul-97
11-Jul-97
12-Jul-97
13-Jul-97
14-Jul-97
15-Jul-97
16-Jul-97
17-Jul-97
18-Jul-97
19-Jul-97
20-Jul-97
21-Jul-97
22-Jul-97
23-Jul-97
24-Jul-97
25-Jul-97
26-Jul-97
27-Jul-97
28-Jul-97
29-Jul-97
30-Jul-97
31-Jul-97
1-Aug-97
Date
14E
22E

Figure 8.38

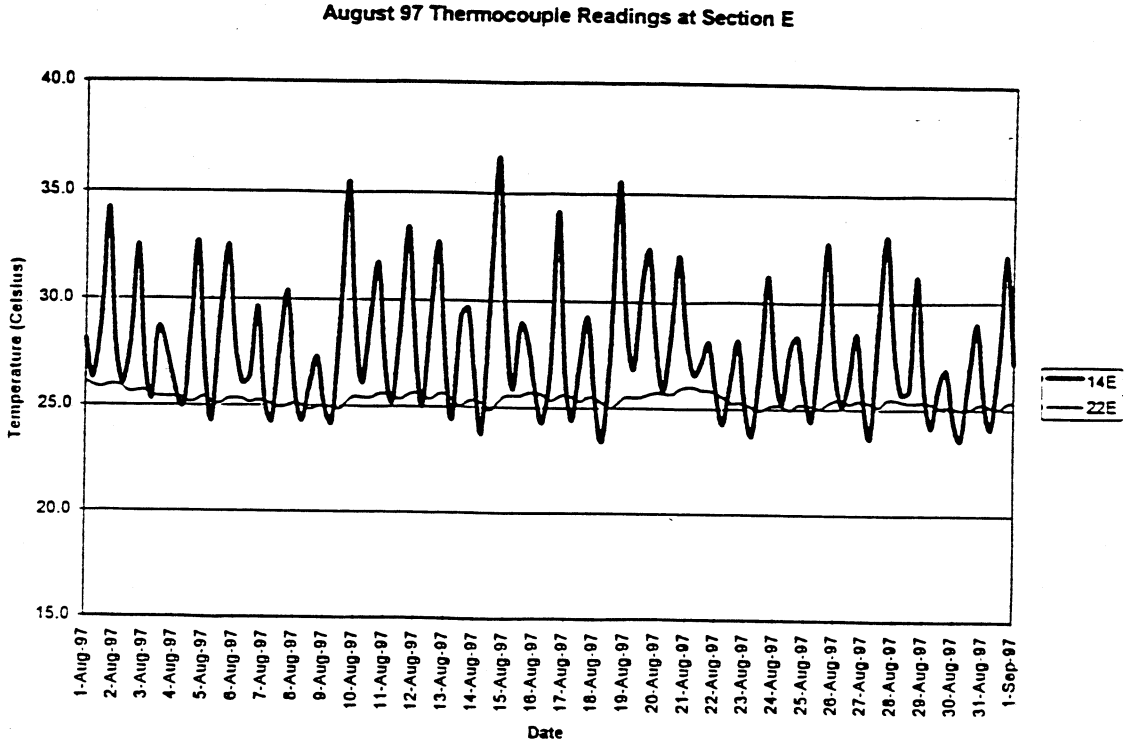
August 97 Thermocouple Readings at Section E
Temperature (Celsius)
40.0
35.0
30.0
25.0
20.0
15.0
1-Aug-97
2-Aug-97
3-Aug-97
4-Aug-97
5-Aug-97
6-Aug-97
7-Aug-97
8-Aug-97
9-Aug-97
10-Aug-97
11-Aug-97
12-Aug-97
13-Aug-97
14-Aug-97
15-Aug-97
16-Aug-97
17-Aug-97
18-Aug-97
19-Aug-97
20-Aug-97
21-Aug-97
22-Aug-97
23-Aug-97
24-Aug-97
25-Aug-97
26-Aug-97
27-Aug-97
28-Aug-97
29-Aug-97
30-Aug-97
31-Aug-97
1-Sep-97
Date
14E
22E

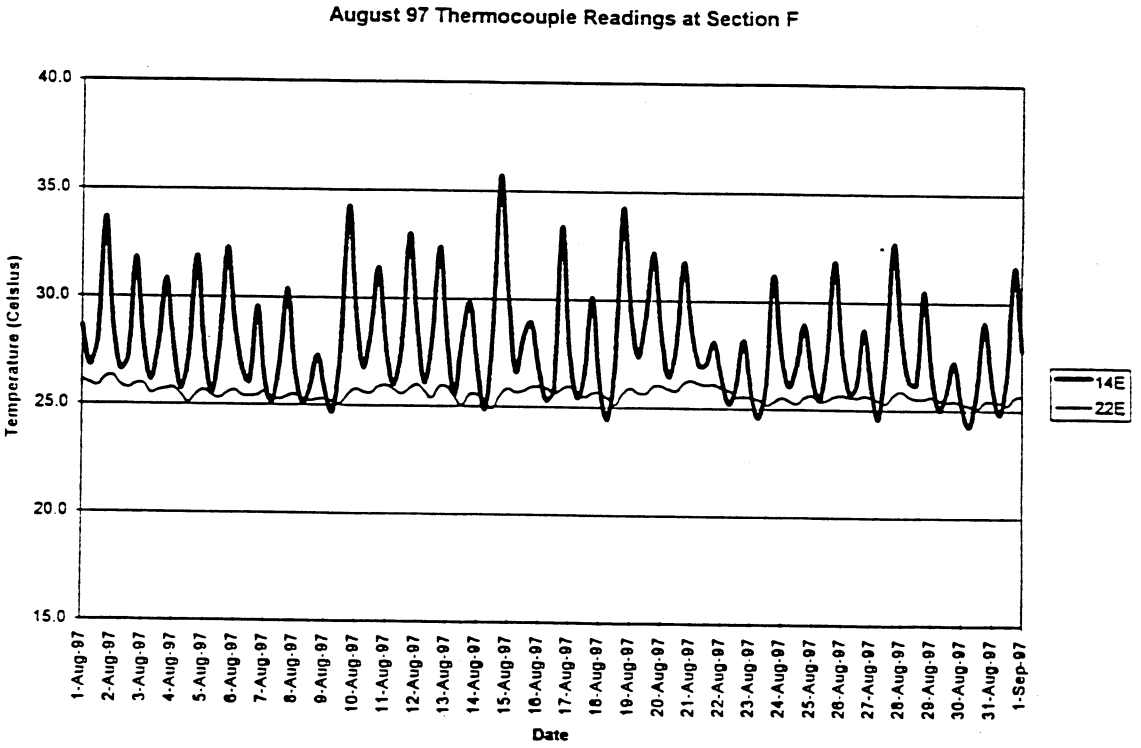
August 97 Thermocouple Readings at Section F
Temperature (Celsius)
40.0
35.0
30.0
25.0
20.0
15.0
1-Aug-97
2-Aug-97
3-Aug-97
4-Aug-97
5-Aug-97
6-Aug-97
7-Aug-97
8-Aug-97
9-Aug-97
10-Aug-97
11-Aug-97
12-Aug-97
13-Aug-97
14-Aug-97
15-Aug-97
16-Aug-97
17-Aug-97
18-Aug-97
19-Aug-97
20-Aug-97
21-Aug-97
22-Aug-97
23-Aug-97
24-Aug-97
25-Aug-97
26-Aug-97
27-Aug-97
28-Aug-97
29-Aug-97
30-Aug-97
31-Aug-97
1-Sep-97
Date
14E
22E

Figure 8.39

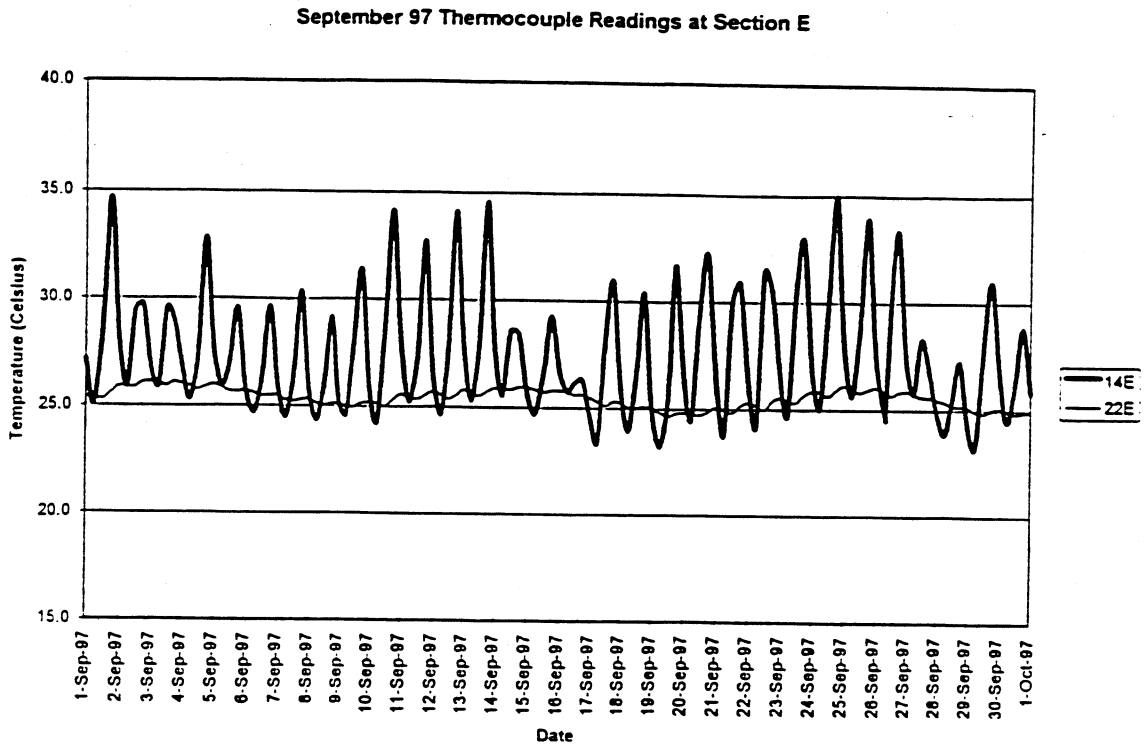
September 97 Thermocouple Readings at Section E
40.0
35.0
30.0
25.0
20.0
15.0
Temperature (Celsius)
1-Sep-97
2-Sep-97
3-Sep-97
4-Sep-97
5-Sep-97
6-Sep-97
7-Sep-97
8-Sep-97
9-Sep-97
10-Sep-97
11-Sep-97
12-Sep-97
13-Sep-97
14-Sep-97
15-Sep-97
16-Sep-97
17-Sep-97
18-Sep-97
19-Sep-97
20-Sep-97
21-Sep-97
22-Sep-97
23-Sep-97
24-Sep-97
25-Sep-97
26-Sep-97
27-Sep-97
28-Sep-97
29-Sep-97
30-Sep-97
1-Oct-97
Date
14E
22E

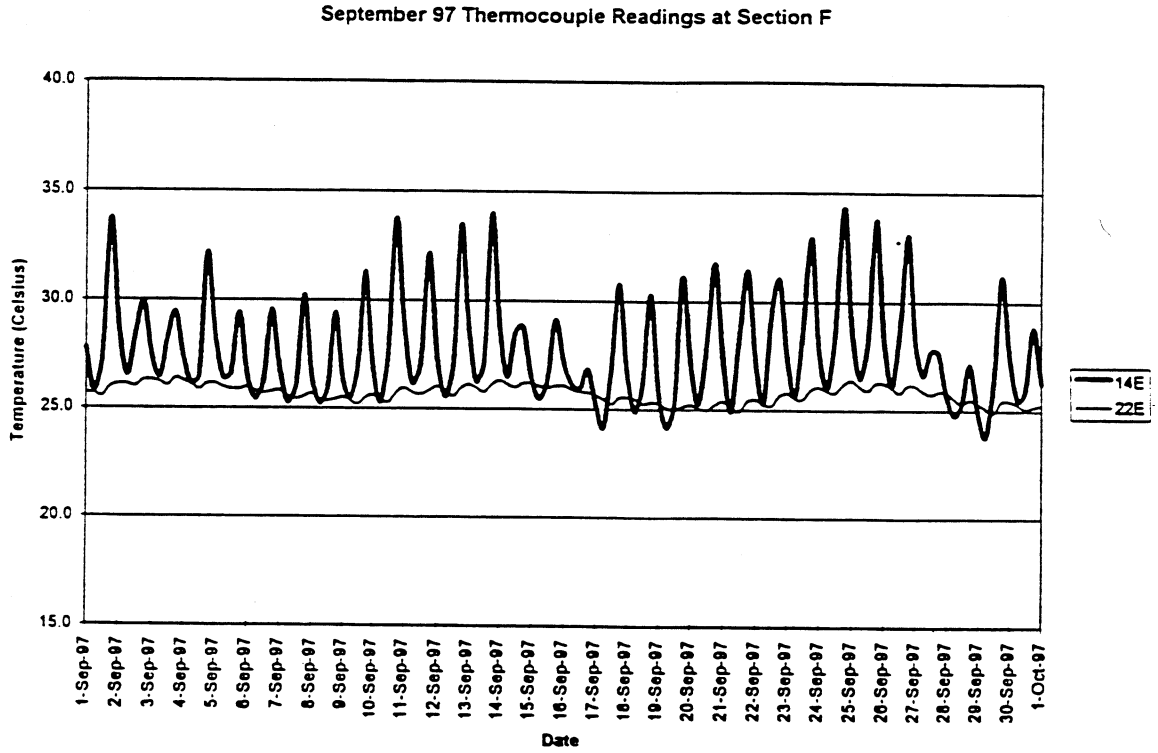
September 97 Thermocouple Readings at Section F
40.0
35.0
30.0
25.0
20.0
15.0
Temperature (Celsius)
1-Sep-97
2-Sep-97
3-Sep-97
4-Sep-97
5-Sep-97
6-Sep-97
7-Sep-97
8-Sep-97
9-Sep-97
10-Sep-97
11-Sep-97
12-Sep-97
13-Sep-97
14-Sep-97
15-Sep-97
16-Sep-97
17-Sep-97
18-Sep-97
19-Sep-97
20-Sep-97
21-Sep-97
22-Sep-97
23-Sep-97
24-Sep-97
25-Sep-97
26-Sep-97
27-Sep-97
28-Sep-97
29-Sep-97
30-Sep-97
1-Oct-97
Date
14E
22E

Figure 8.40

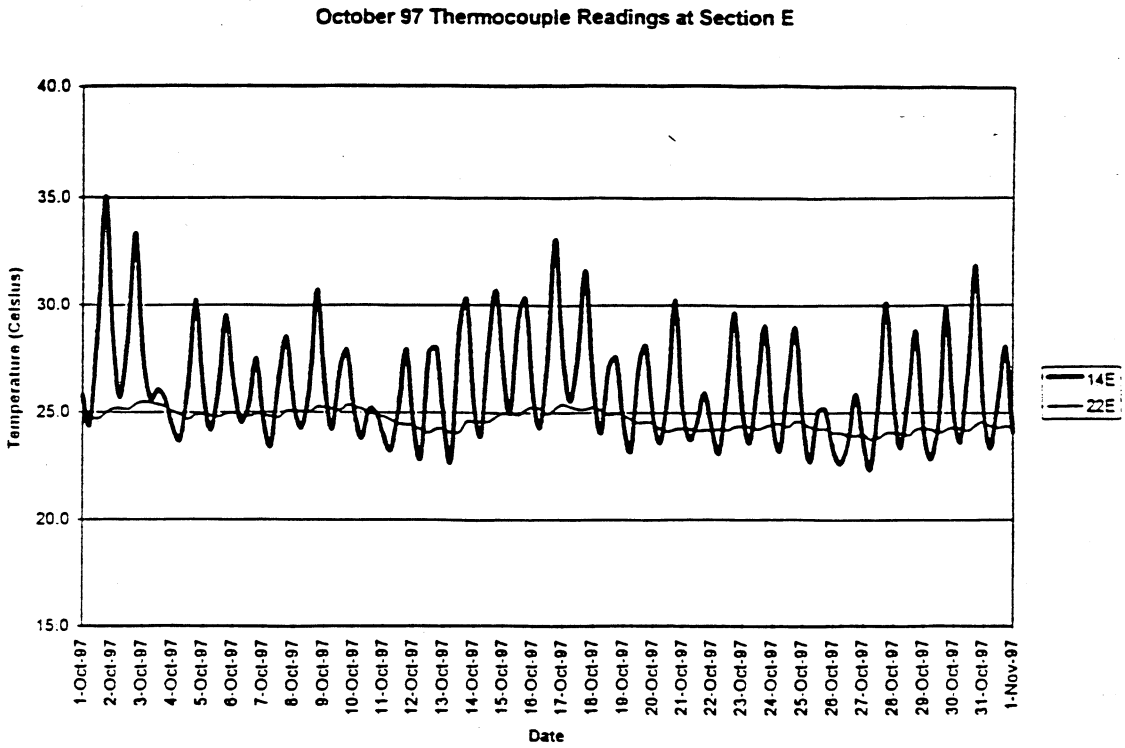

H3 Instrumentation Report TYLin International

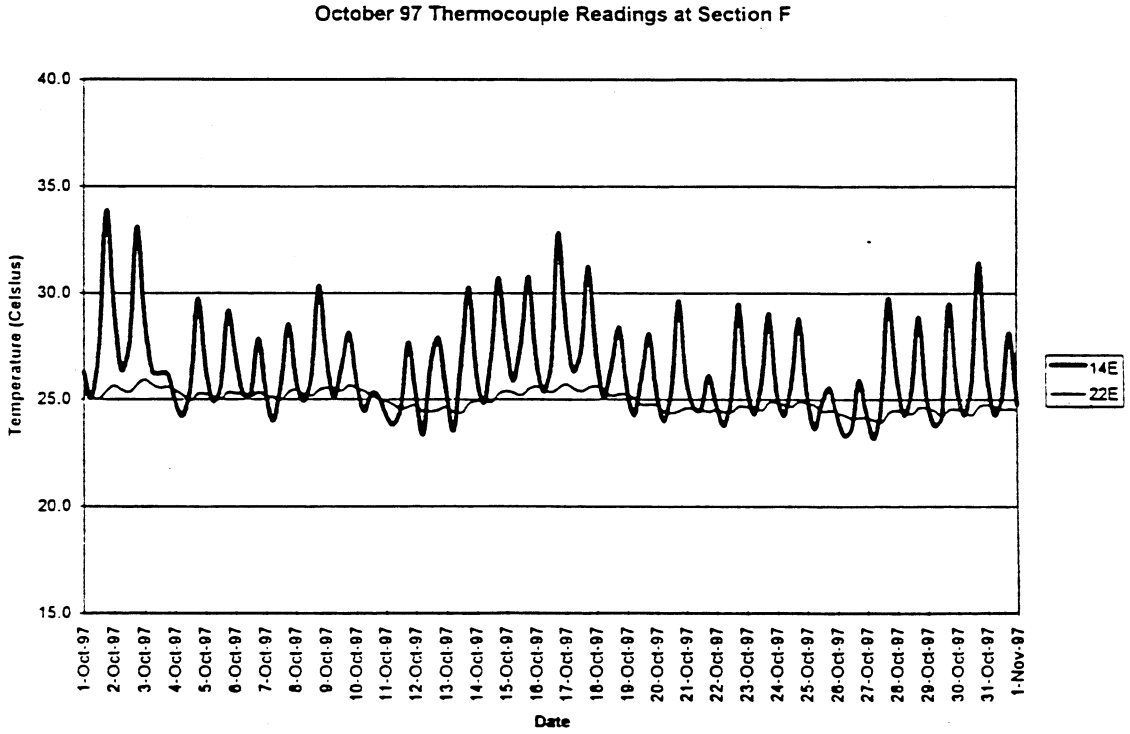

Figure 8.41

November 97 Thermocouple Readings at Section E

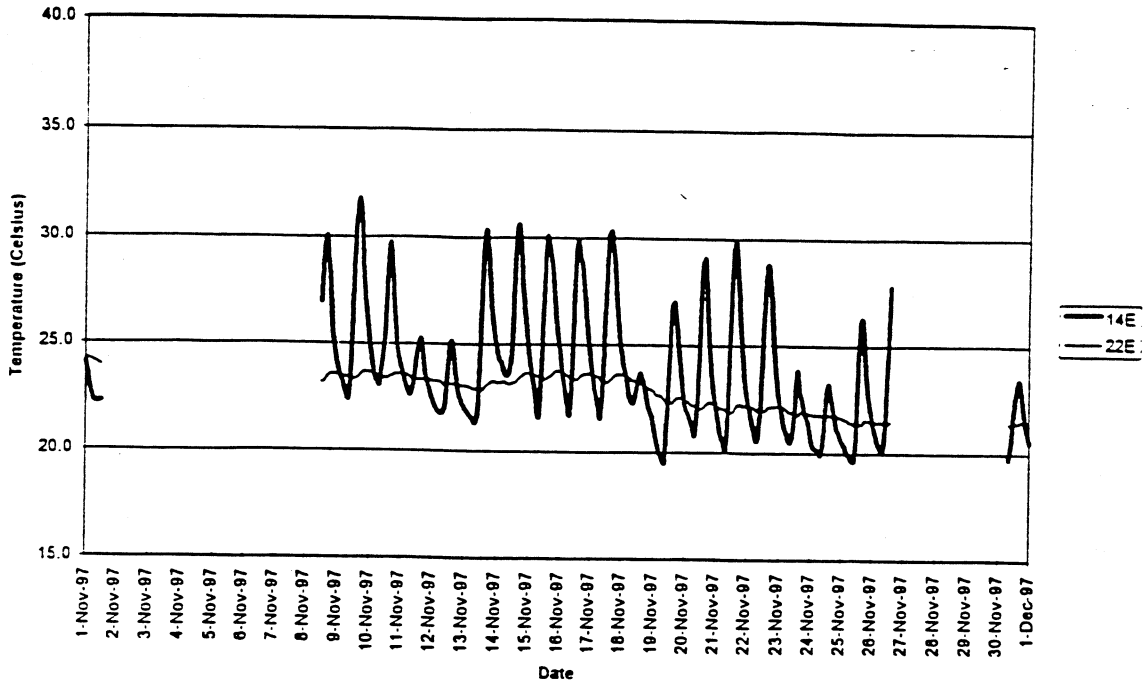

November 97 Thermocouple Readings at Section F

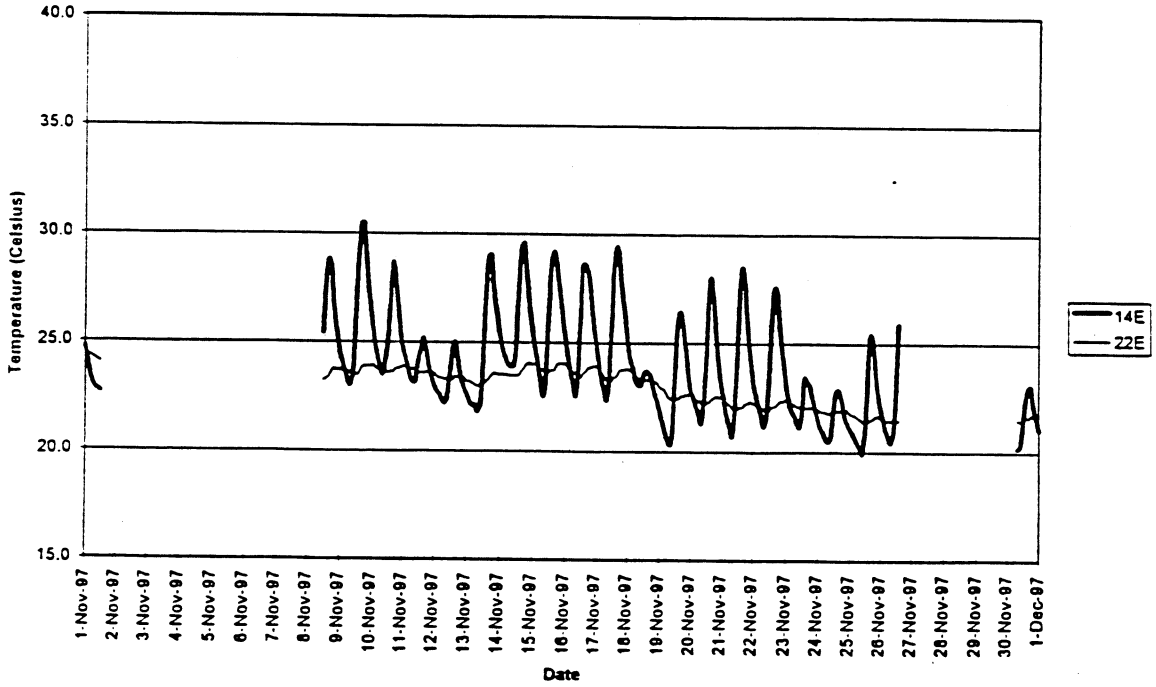

Figure 8.42

December 97 Thermocouple Readings at Section E

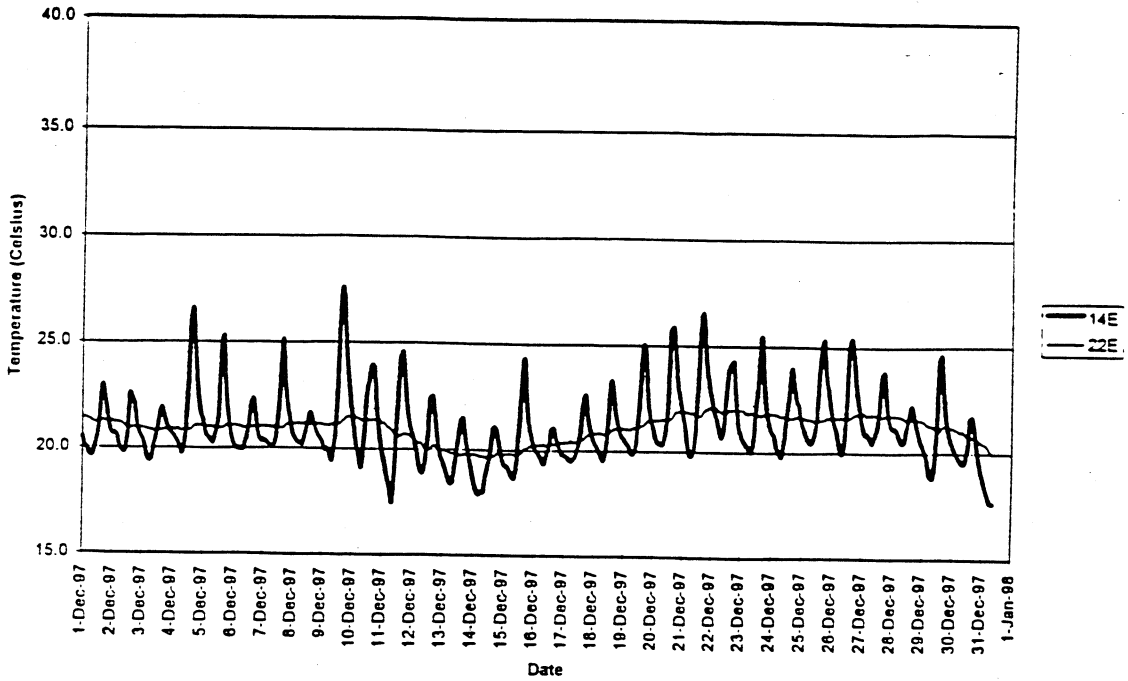

December 97 Thermocouple Readings at Section F

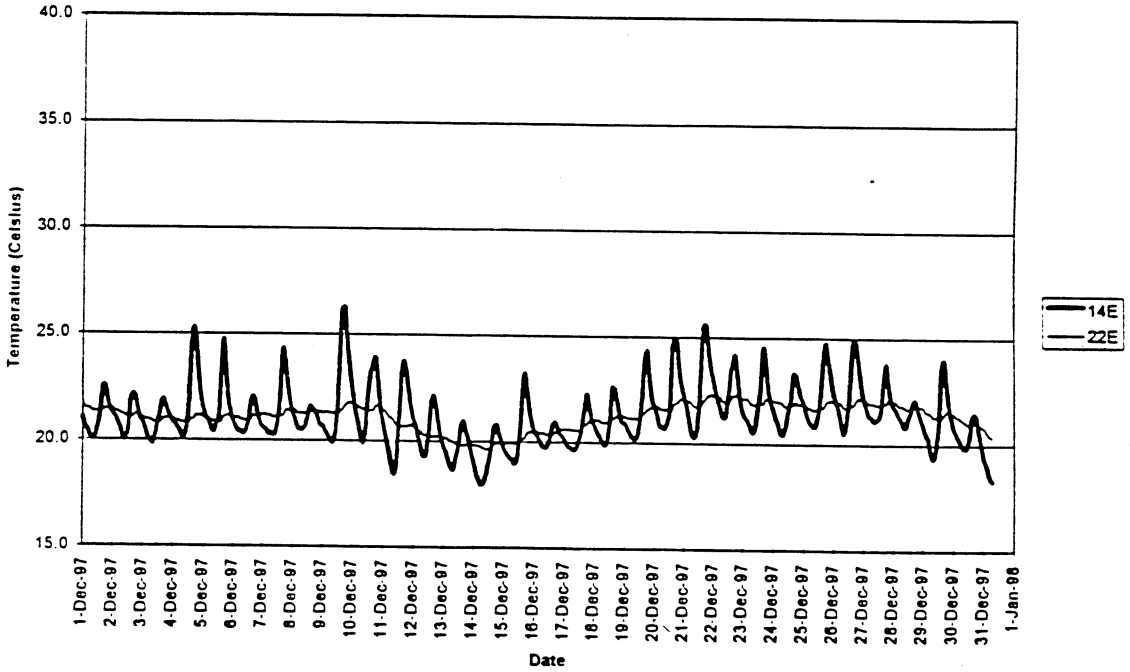

Figure 8.43

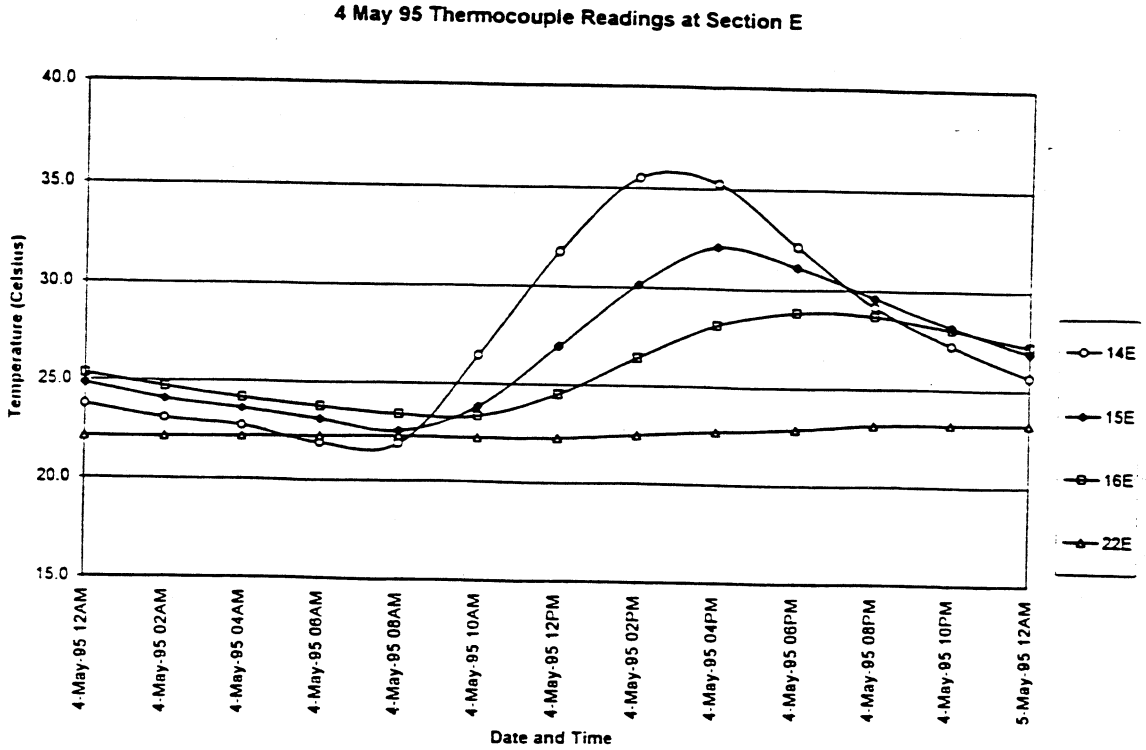

H3 Instrumentation Report

TYLin International

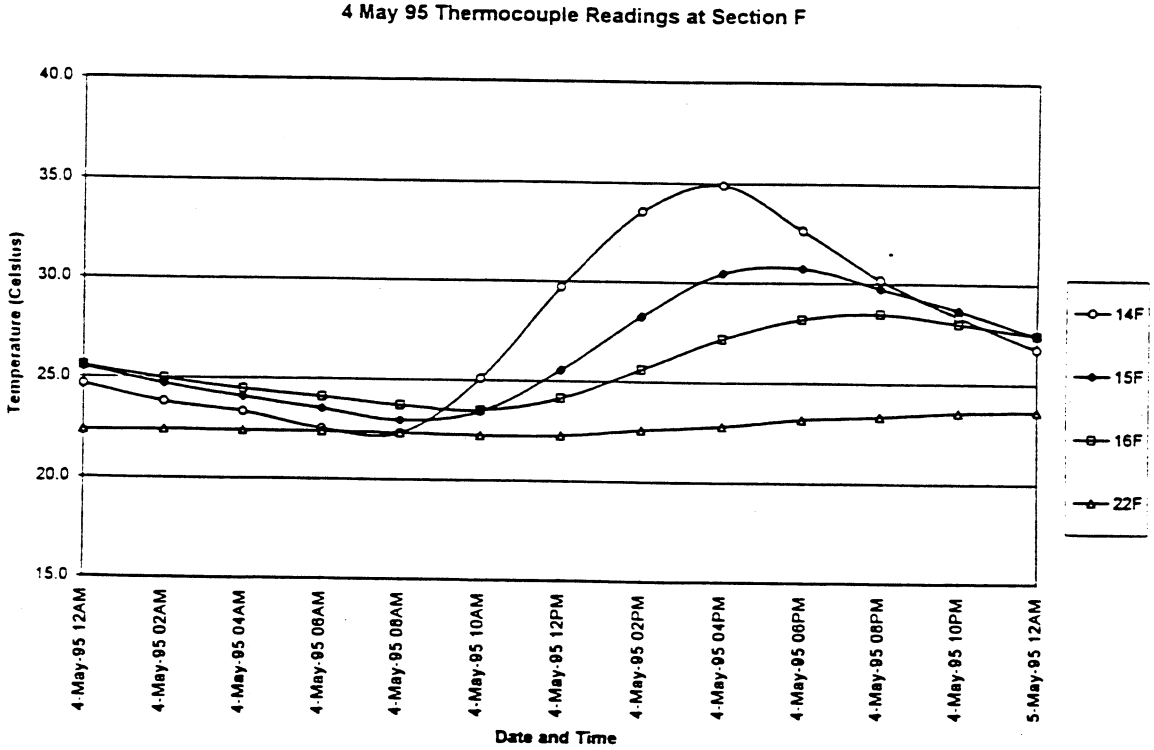

Figure 8.68

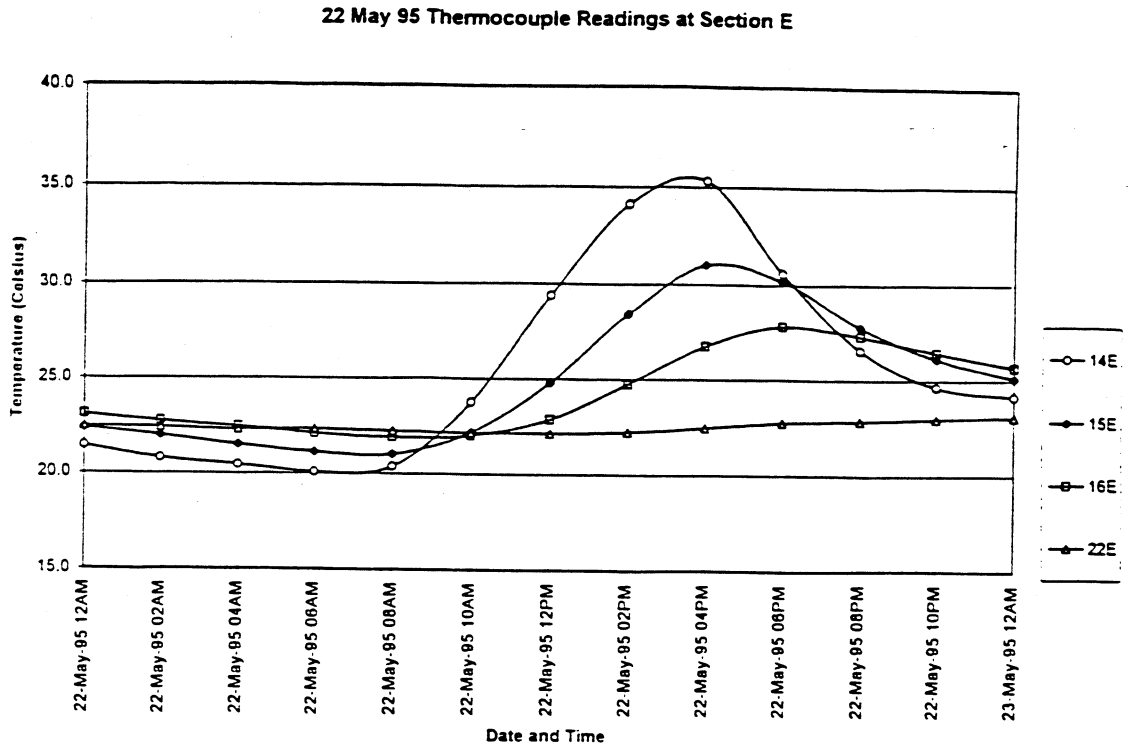
22 May 95 Thermocouple Readings at Section E
Temperature (Celsius)
40.0
35.0
30.0
25.0
20.0
15.0
22-May-95 12AM
22-May-95 02AM
22-May-95 04AM
22-May-95 06AM
22-May-95 08AM
22-May-95 10AM
22-May-95 12PM
22-May-95 02PM
22-May-95 04PM
22-May-95 06PM
22-May-95 08PM
22-May-95 10PM
23-May-95 12AM
Date and Time
14E
15E
16E
22E

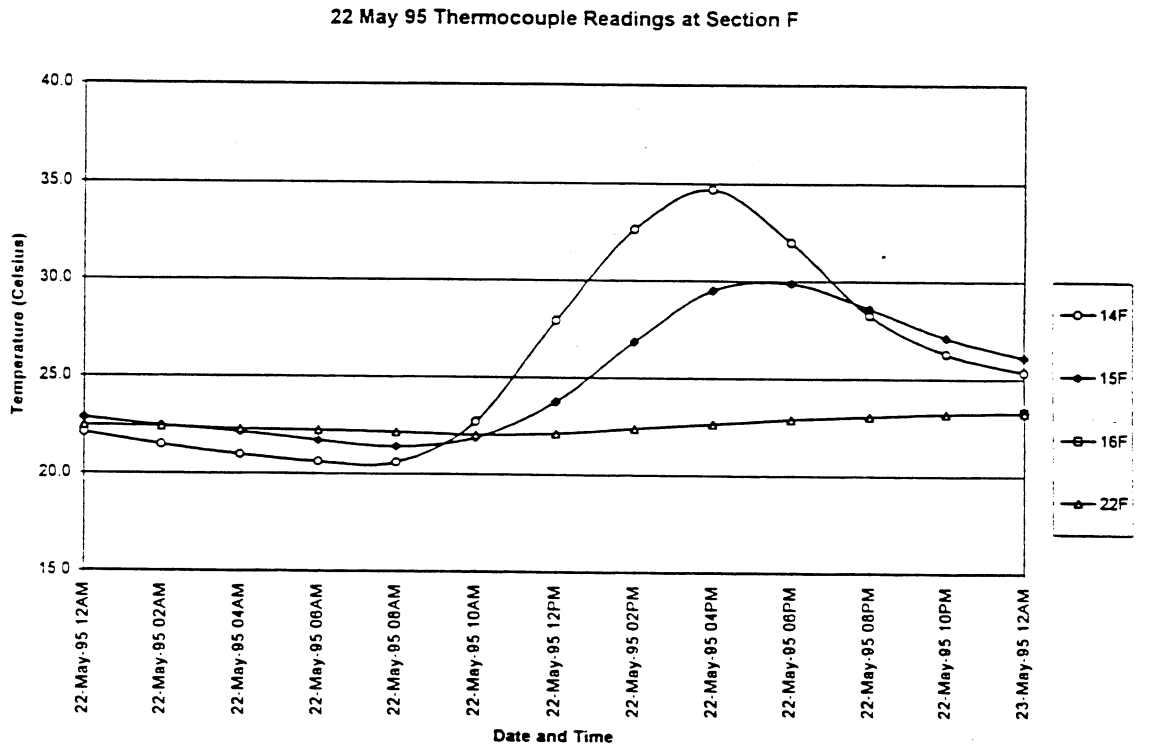
22 May 95 Thermocouple Readings at Section F
Temperature (Celsius)
40.0
35.0
30.0
25.0
20.0
15.0
22-May-95 12AM
22-May-95 02AM
22-May-95 04AM
22-May-95 06AM
22-May-95 08AM
22-May-95 10AM
22-May-95 12PM
22-May-95 02PM
22-May-95 04PM
22-May-95 06PM
22-May-95 08PM
22-May-95 10PM
23-May-95 12AM
Date and Time
14F
15F
16F
22F

Figure 8.69

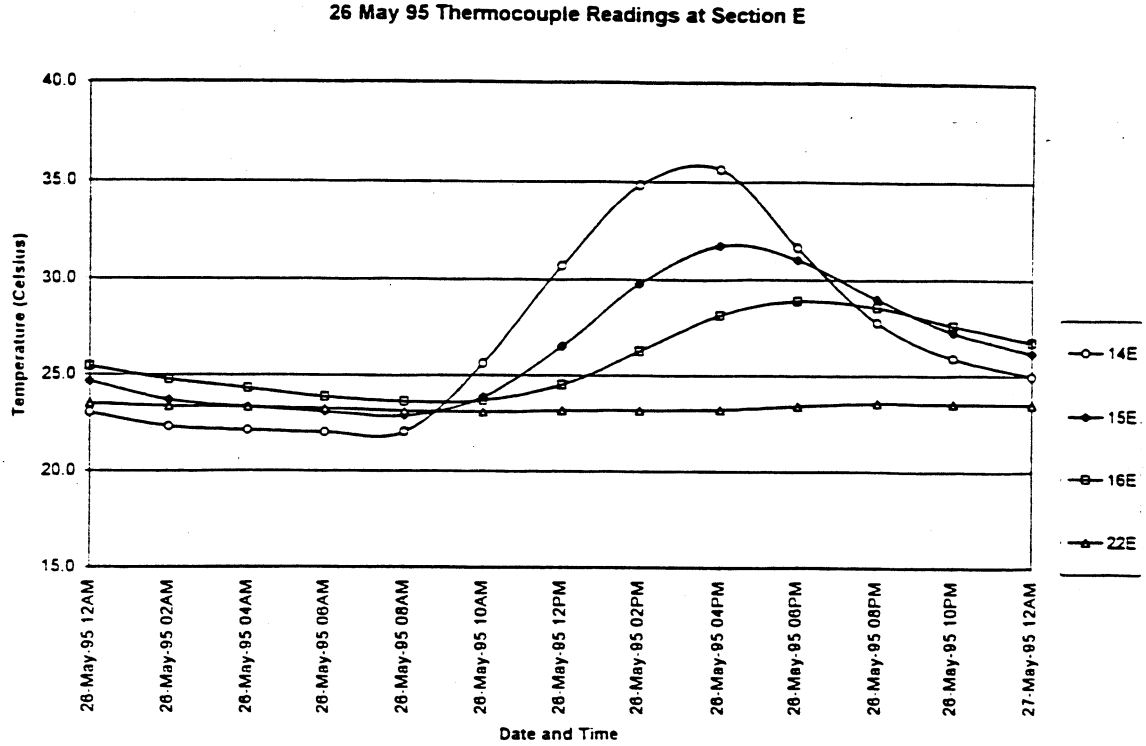
26 May 95 Thermocouple Readings at Section E
Temperature (Celsius)
40.0
35.0
30.0
25.0
20.0
15.0
26-May-95 12AM
26-May-95 02AM
26-May-95 04AM
26-May-95 06AM
26-May-95 08AM
26-May-95 10AM
26-May-95 12PM
26-May-95 02PM
26-May-95 04PM
26-May-95 06PM
26-May-95 08PM
26-May-95 10PM
27-May-95 12AM
Date and Time
14E
15E
16E
22E

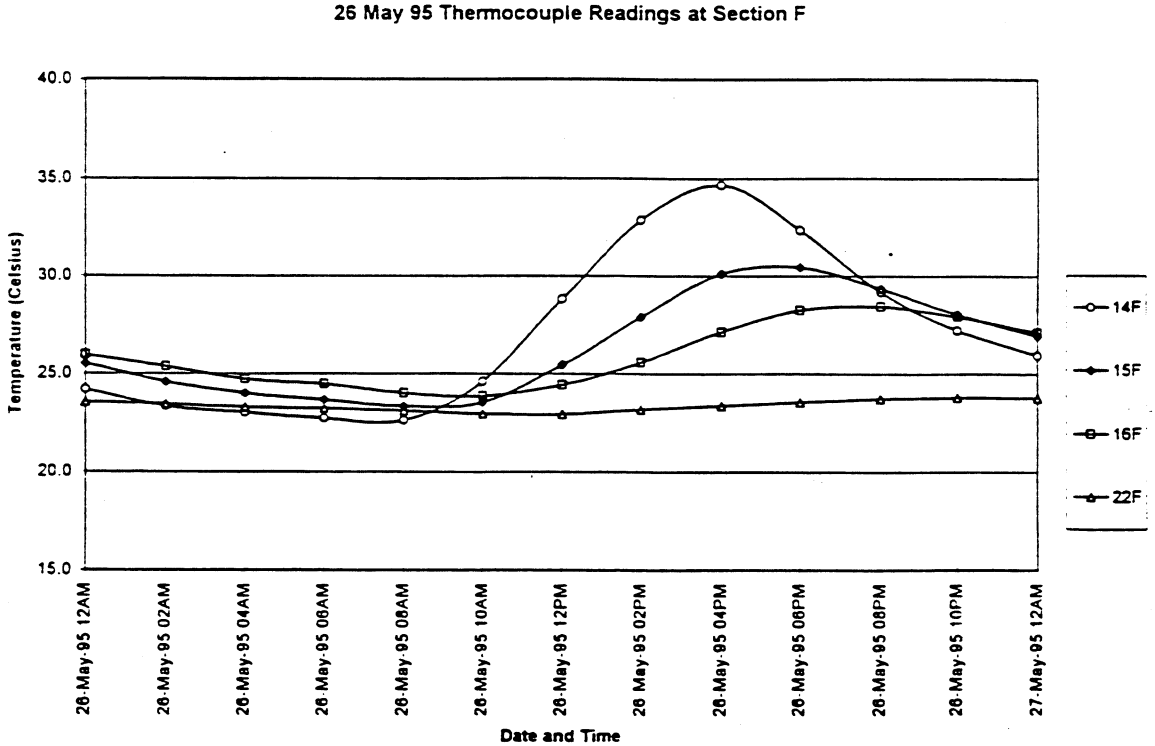
26 May 95 Thermocouple Readings at Section F
Temperature (Celsius)
40.0
35.0
30.0
25.0
20.0
15.0
26-May-95 12AM
26-May-95 02AM
26-May-95 04AM
26-May-95 06AM
26-May-95 08AM
26-May-95 10AM
26-May-95 12PM
26-May-95 02PM
26-May-95 04PM
26-May-95 06PM
26-May-95 08PM
26-May-95 10PM
27-May-95 12AM
Date and Time
14F
15F
16F
22F

Figure 8.70

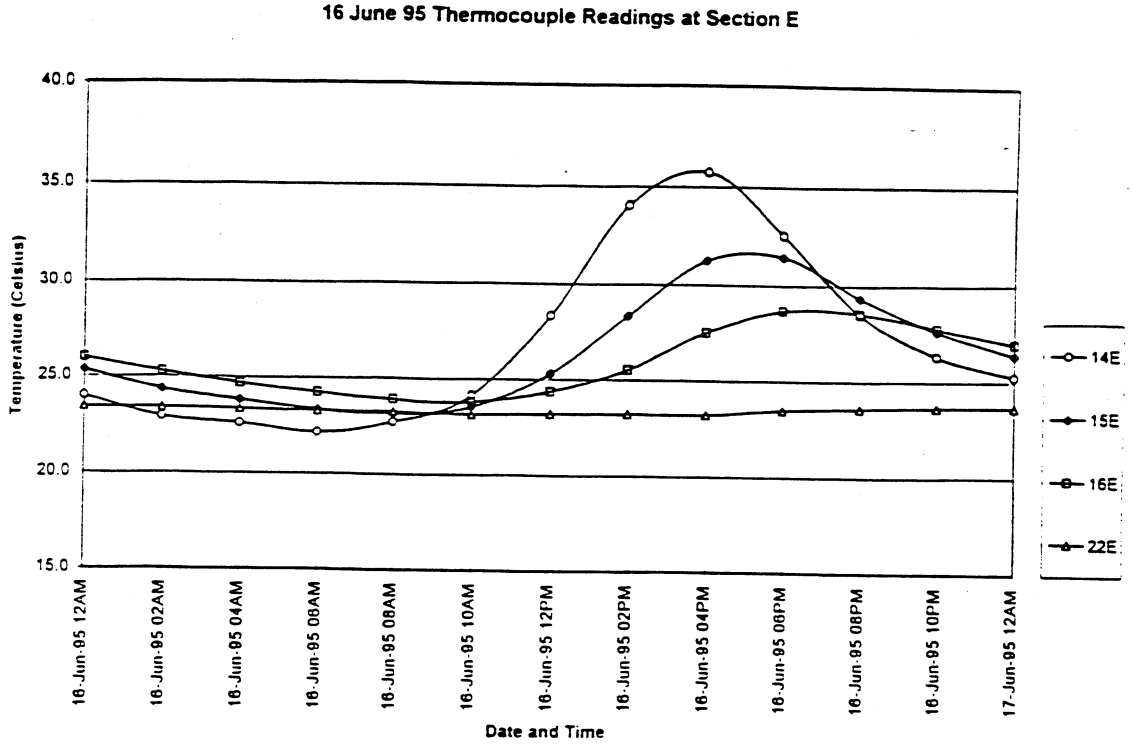

H3 Instrumentation Report

TYLin International

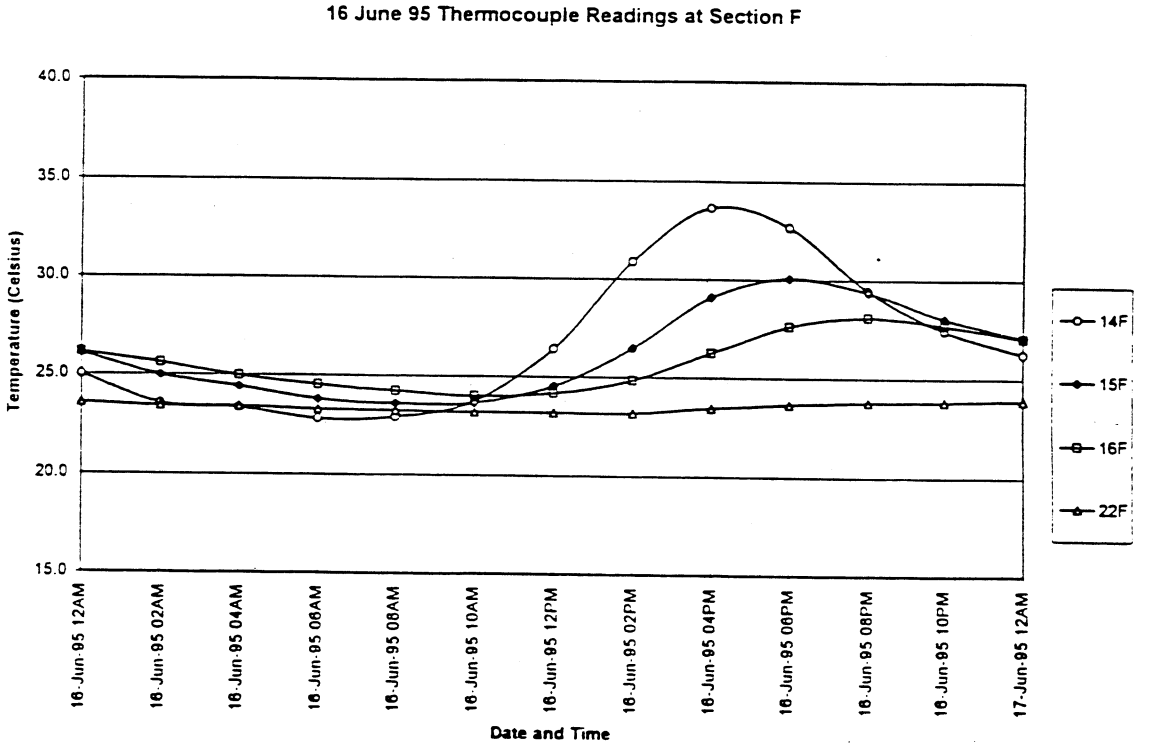

Figure 8.71

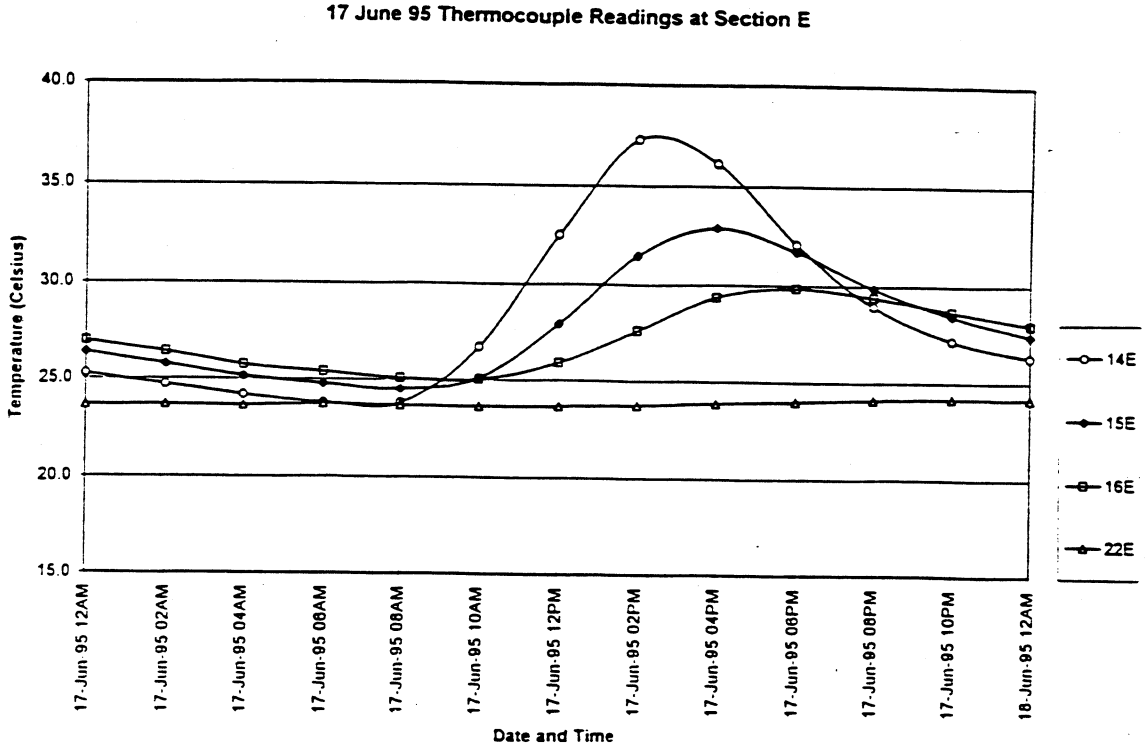

H3 Instrumentation Report

TYLin International

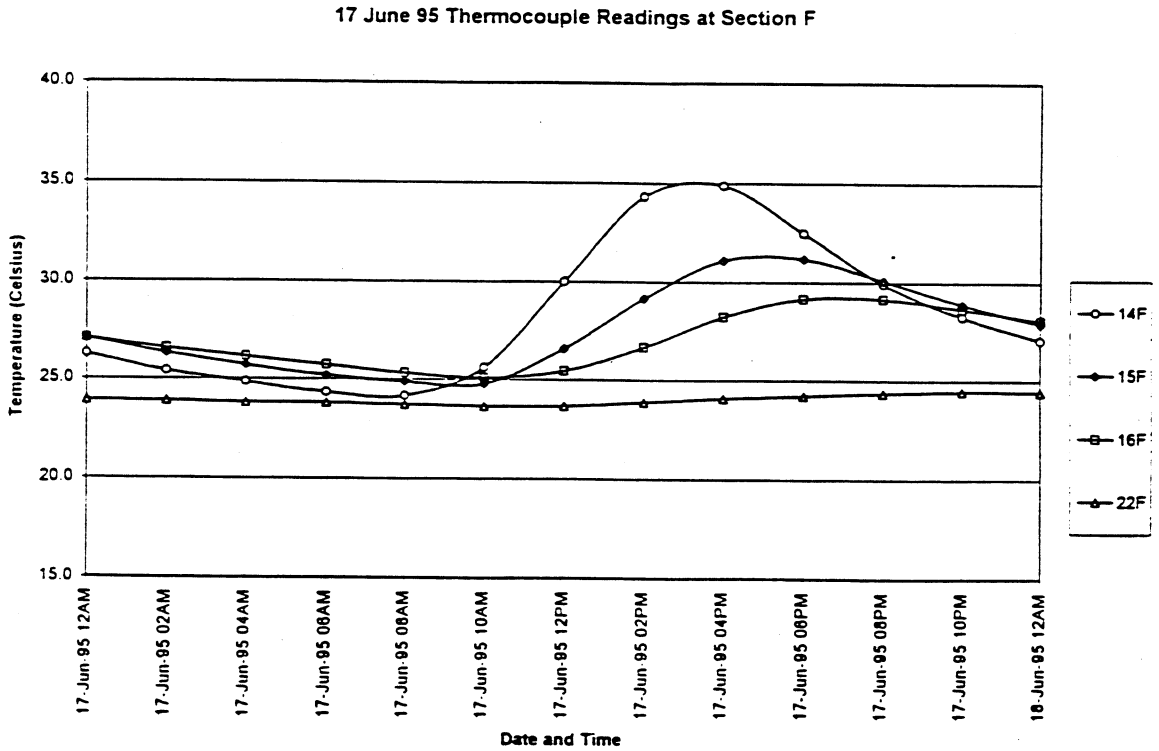

Figure 8.72

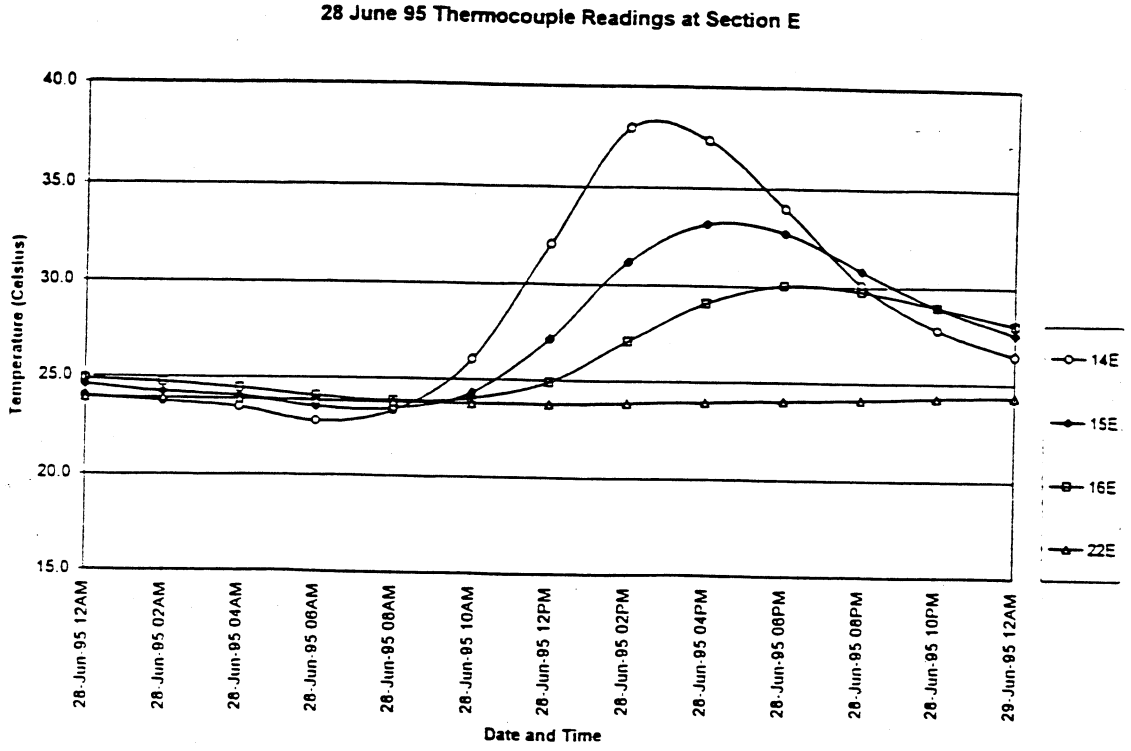
28 June 95 Thermocouple Readings at Section E
40.0
35.0
30.0
25.0
20.0
15.0
Temperature (Celsius)
28-Jun-95 12AM
28-Jun-95 02AM
28-Jun-95 04AM
28-Jun-95 06AM
28-Jun-95 08AM
28-Jun-95 10AM
28-Jun-95 12PM
28-Jun-95 02PM
28-Jun-95 04PM
28-Jun-95 06PM
28-Jun-95 08PM
28-Jun-95 10PM
29-Jun-95 12AM
Date and Time
14E
15E
16E
22E

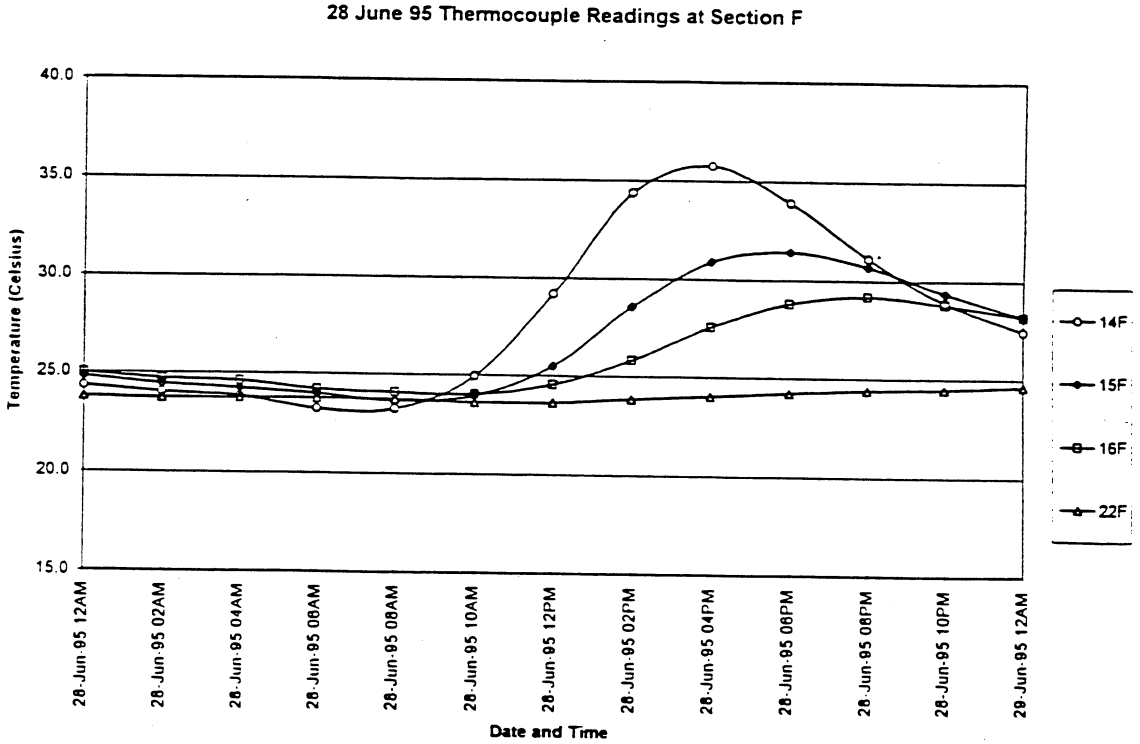
28 June 95 Thermocouple Readings at Section F
40.0
35.0
30.0
25.0
20.0
15.0
Temperature (Celsius)
28-Jun-95 12AM
28-Jun-95 02AM
28-Jun-95 04AM
28-Jun-95 06AM
28-Jun-95 08AM
28-Jun-95 10AM
28-Jun-95 12PM
28-Jun-95 02PM
28-Jun-95 04PM
28-Jun-95 06PM
28-Jun-95 08PM
28-Jun-95 10PM
29-Jun-95 12AM
Date and Time
14F
15F
16F
22F

Figure 8.73

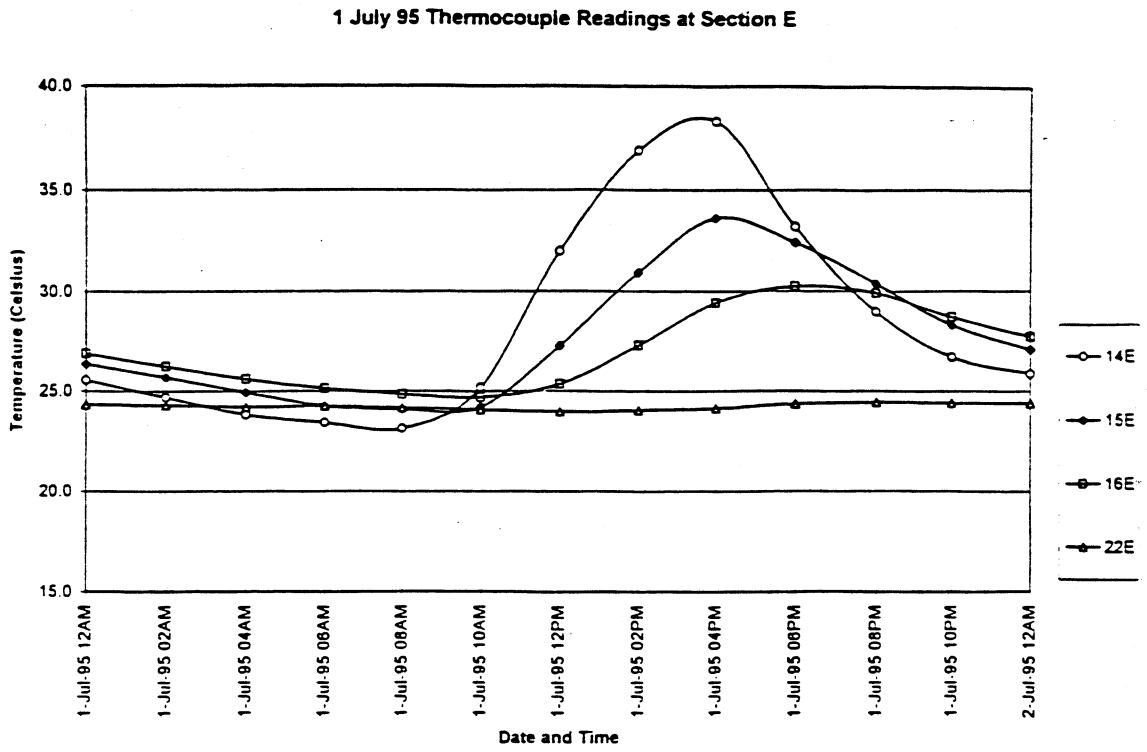

H3 Instrumentation Report TYLin International

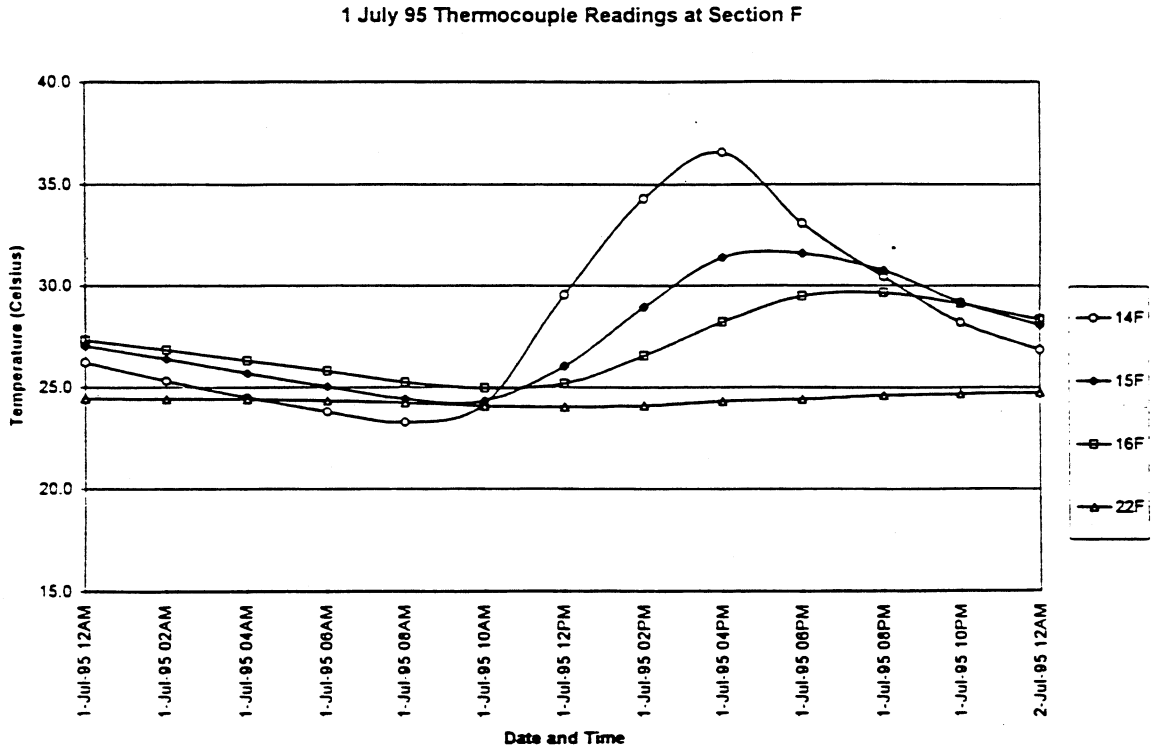

Figure 8.74

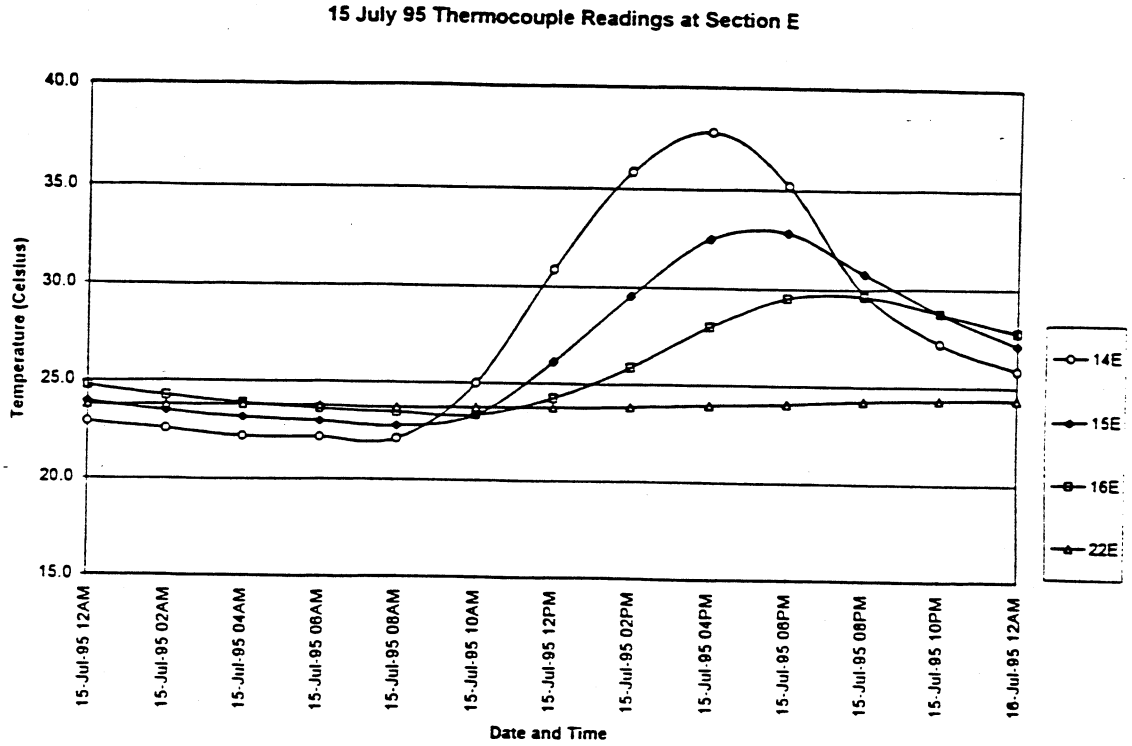

H3 Instrumentation Report

TYLin International

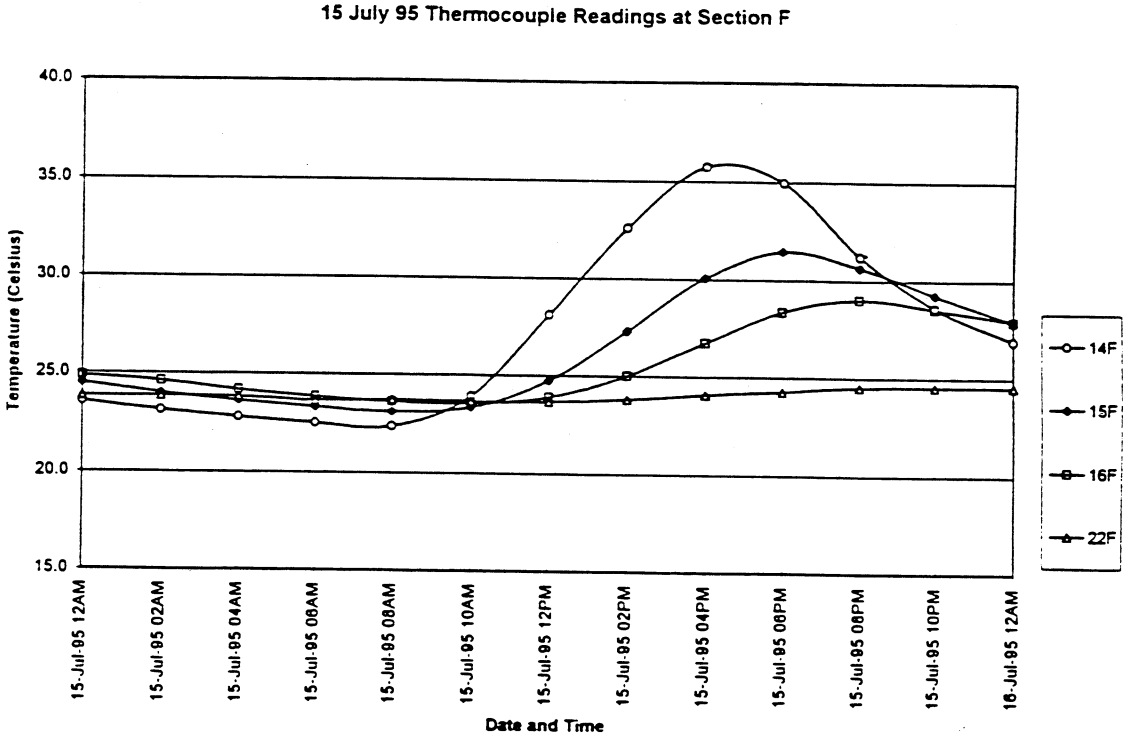

Figure 8.75

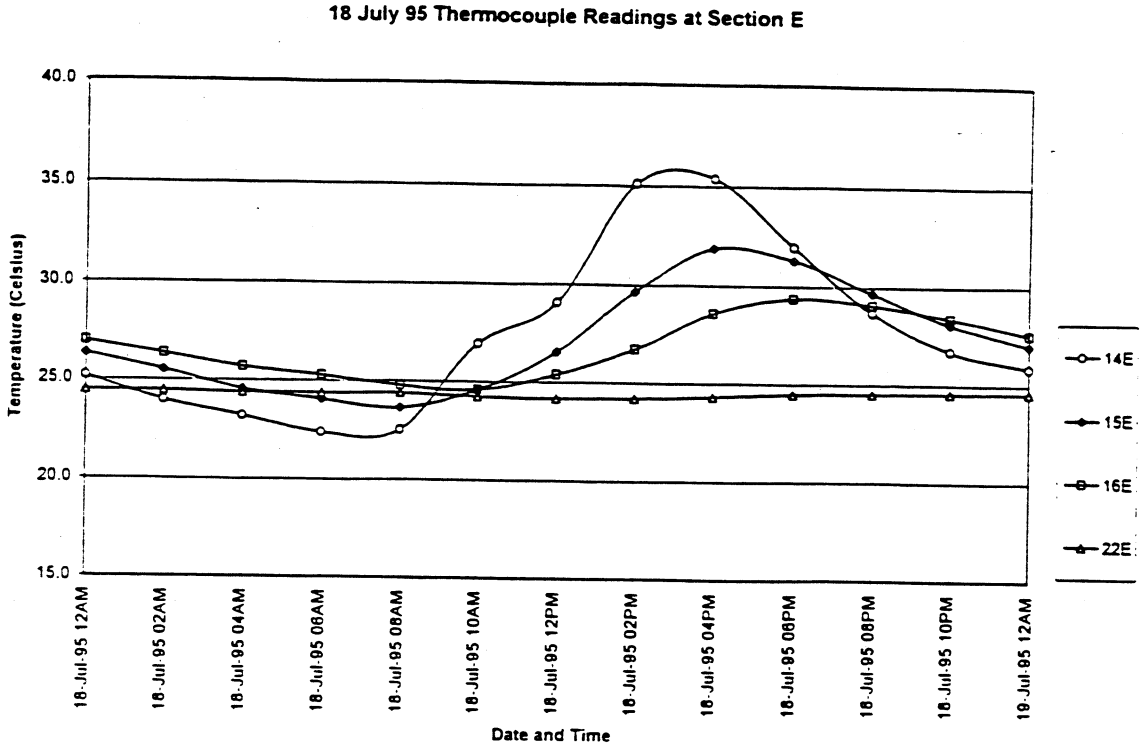

H3 Instrumentation Report

TYLin International

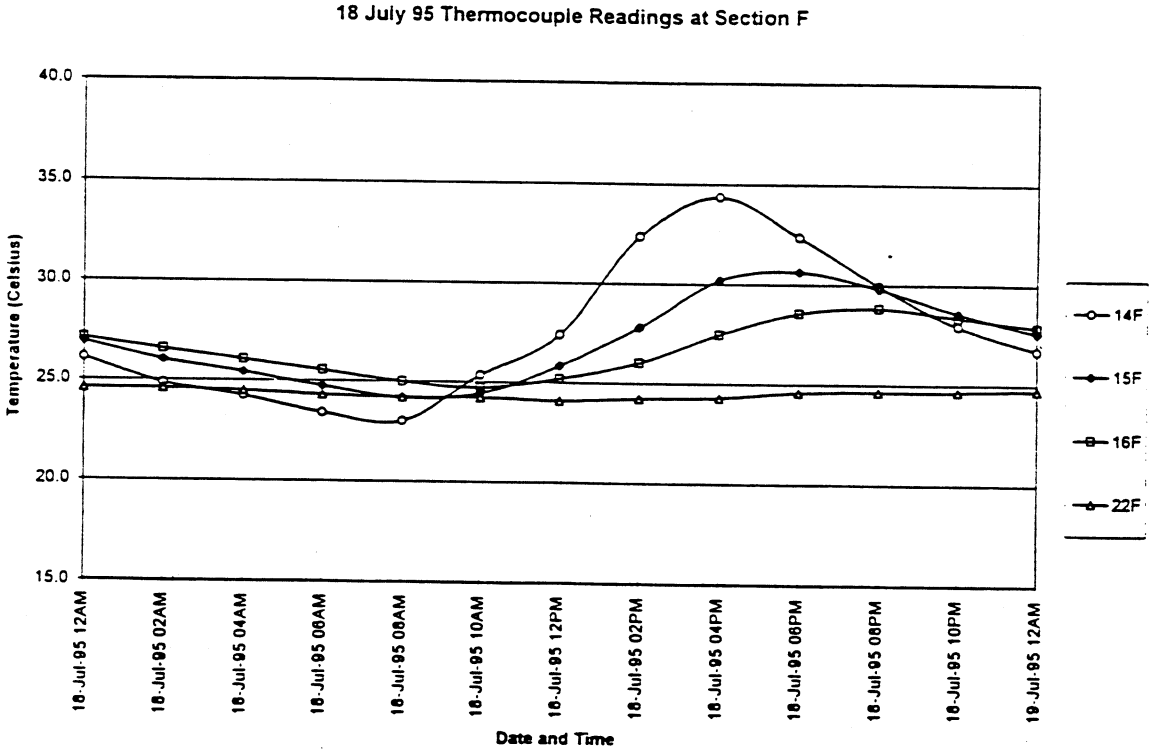

Figure 8.76

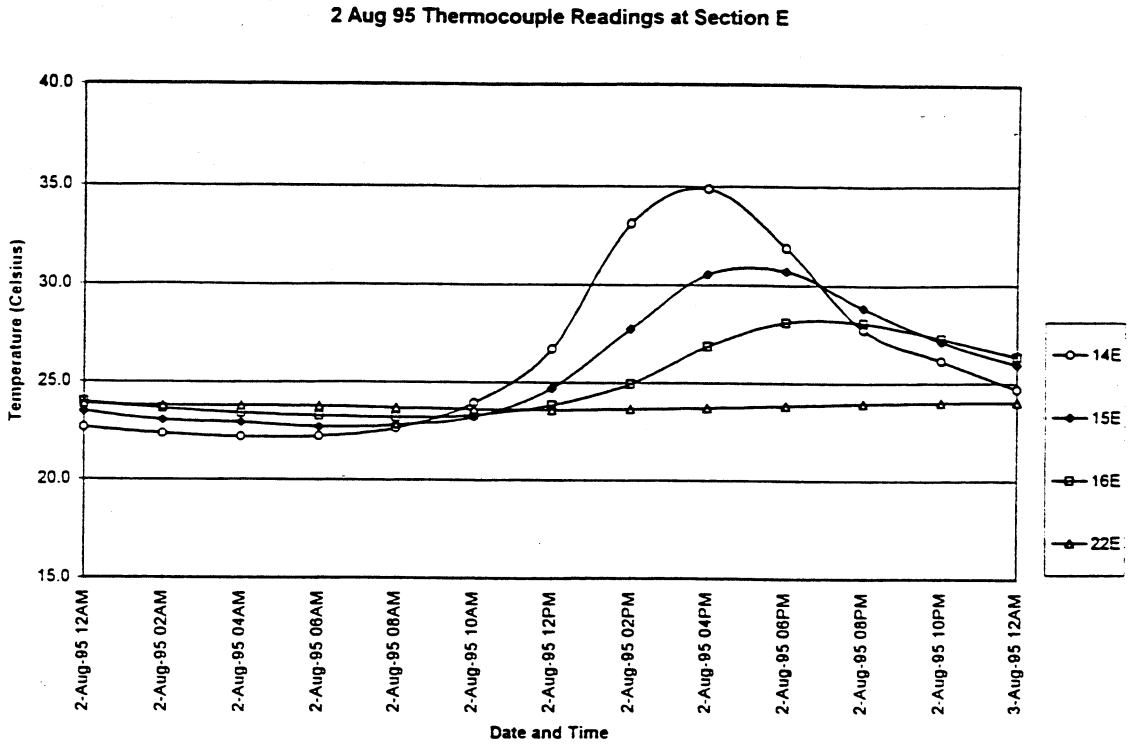
2 Aug 95 Thermocouple Readings at Section E
Temperature (Celsius)
40.0
35.0
30.0
25.0
20.0
15.0
2-Aug-95 12AM
2-Aug-95 02AM
2-Aug-95 04AM
2-Aug-95 06AM
2-Aug-95 08AM
2-Aug-95 10AM
2-Aug-95 12PM
2-Aug-95 02PM
2-Aug-95 04PM
2-Aug-95 06PM
2-Aug-95 08PM
2-Aug-95 10PM
3-Aug-95 12AM
Date and Time
14E
15E
16E
22E

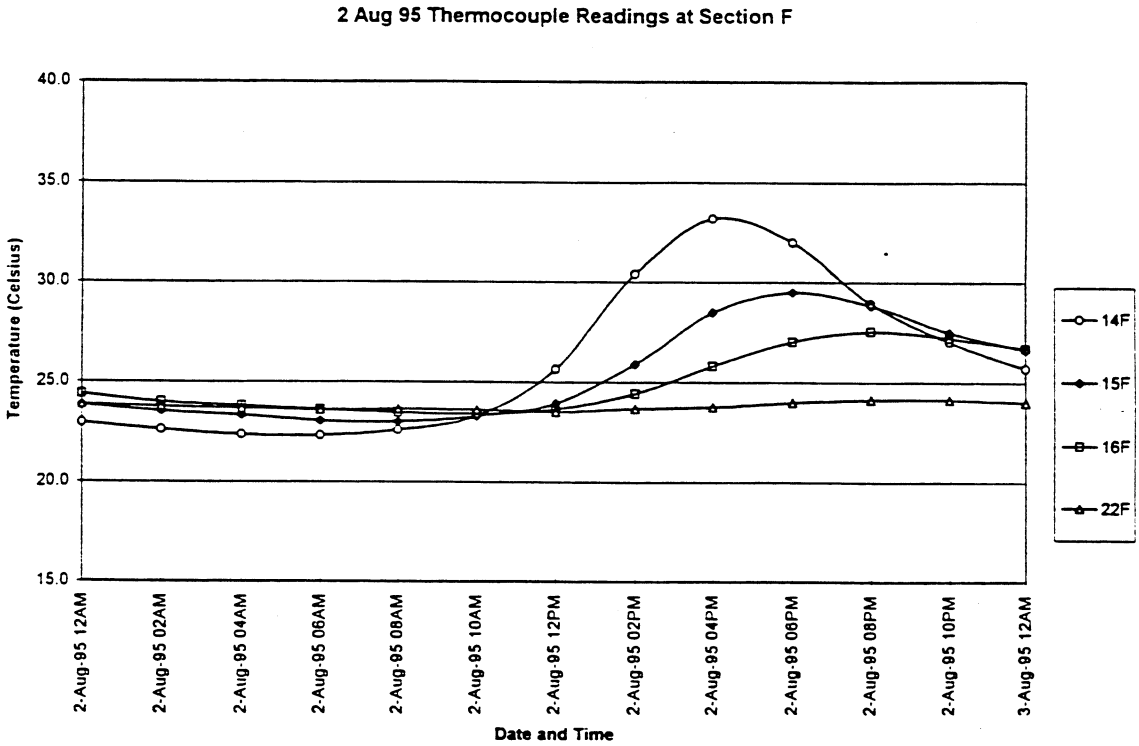
2 Aug 95 Thermocouple Readings at Section F
Temperature (Celsius)
40.0
35.0
30.0
25.0
20.0
15.0
2-Aug-95 12AM
2-Aug-95 02AM
2-Aug-95 04AM
2-Aug-95 06AM
2-Aug-95 08AM
2-Aug-95 10AM
2-Aug-95 12PM
2-Aug-95 02PM
2-Aug-95 04PM
2-Aug-95 06PM
2-Aug-95 08PM
2-Aug-95 10PM
3-Aug-95 12AM
Date and Time
14F
15F
16F
22F

Figure 8.77

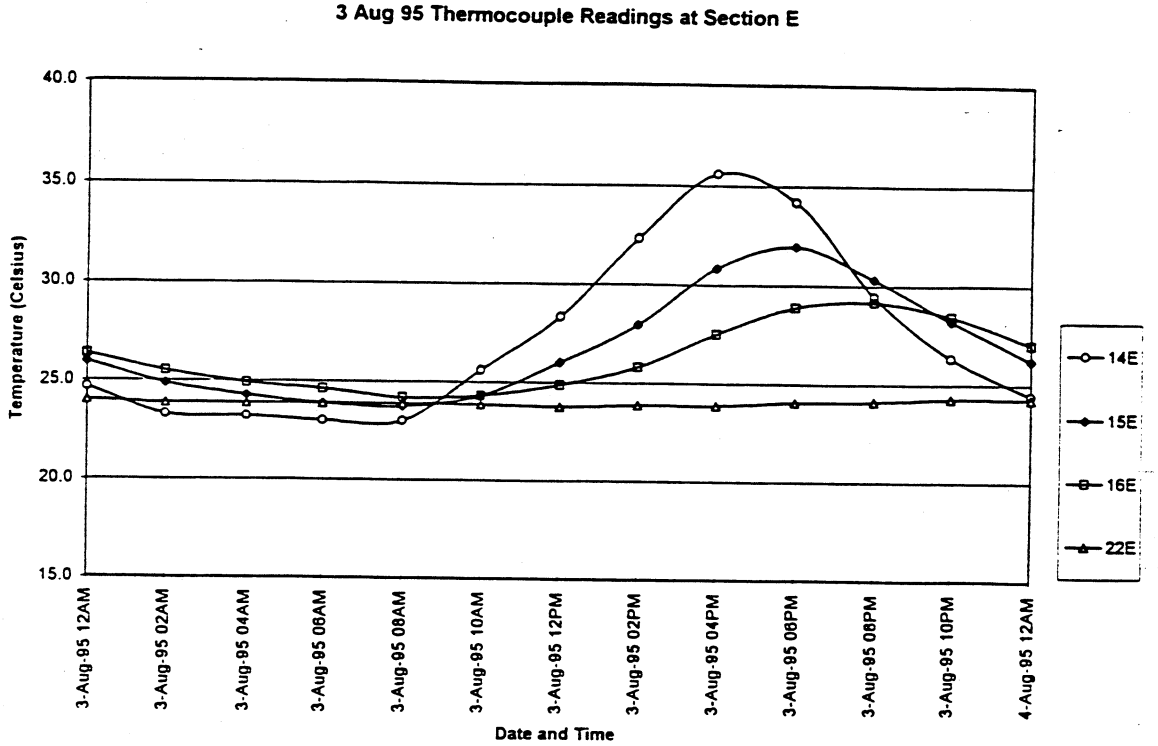
3 Aug 95 Thermocouple Readings at Section E
40.0
35.0
30.0
25.0
20.0
15.0
Temperature (Celsius)
3-Aug-95 12AM
3-Aug-95 02AM
3-Aug-95 04AM
3-Aug-95 06AM
3-Aug-95 08AM
3-Aug-95 10AM
3-Aug-95 12PM
3-Aug-95 02PM
3-Aug-95 04PM
3-Aug-95 06PM
3-Aug-95 08PM
3-Aug-95 10PM
4-Aug-95 12AM
Date and Time
14E
15E
16E
22E

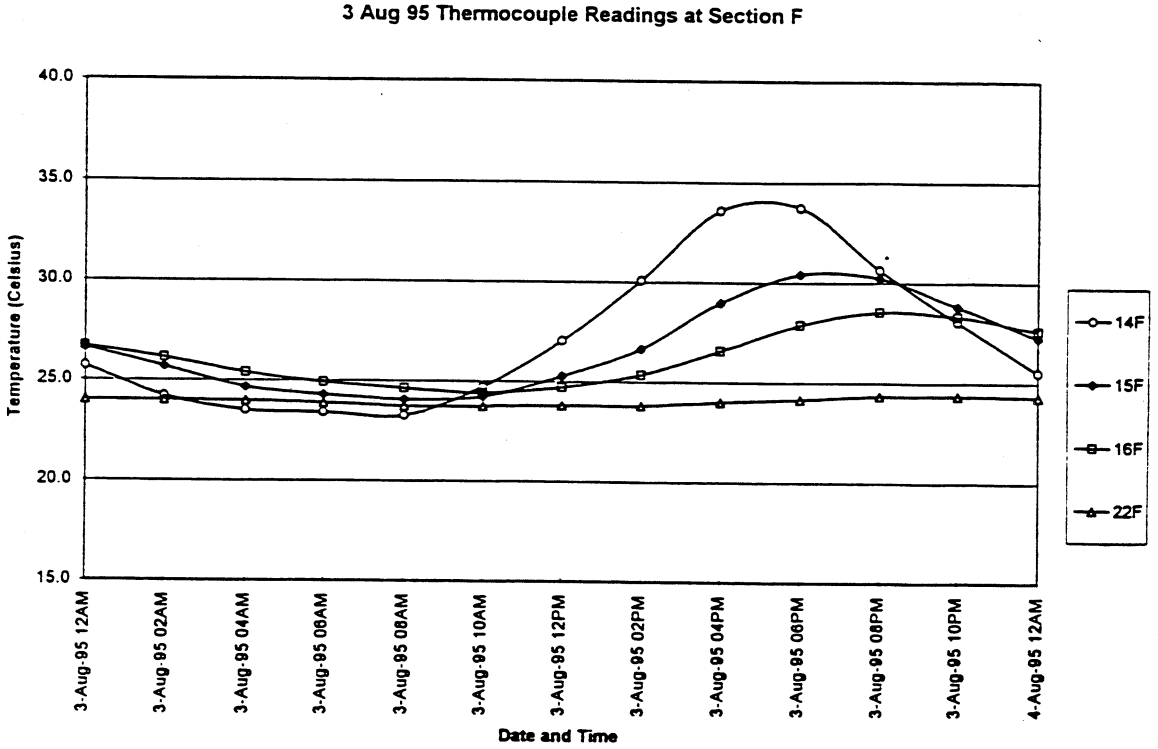
3 Aug 95 Thermocouple Readings at Section F
40.0
35.0
30.0
25.0
20.0
15.0
Temperature (Celsius)
3-Aug-95 12AM
3-Aug-95 02AM
3-Aug-95 04AM
3-Aug-95 06AM
3-Aug-95 08AM
3-Aug-95 10AM
3-Aug-95 12PM
3-Aug-95 02PM
3-Aug-95 04PM
3-Aug-95 06PM
3-Aug-95 08PM
3-Aug-95 10PM
4-Aug-95 12AM
Date and Time
14F
15F
16F
22F

Figure 8.78

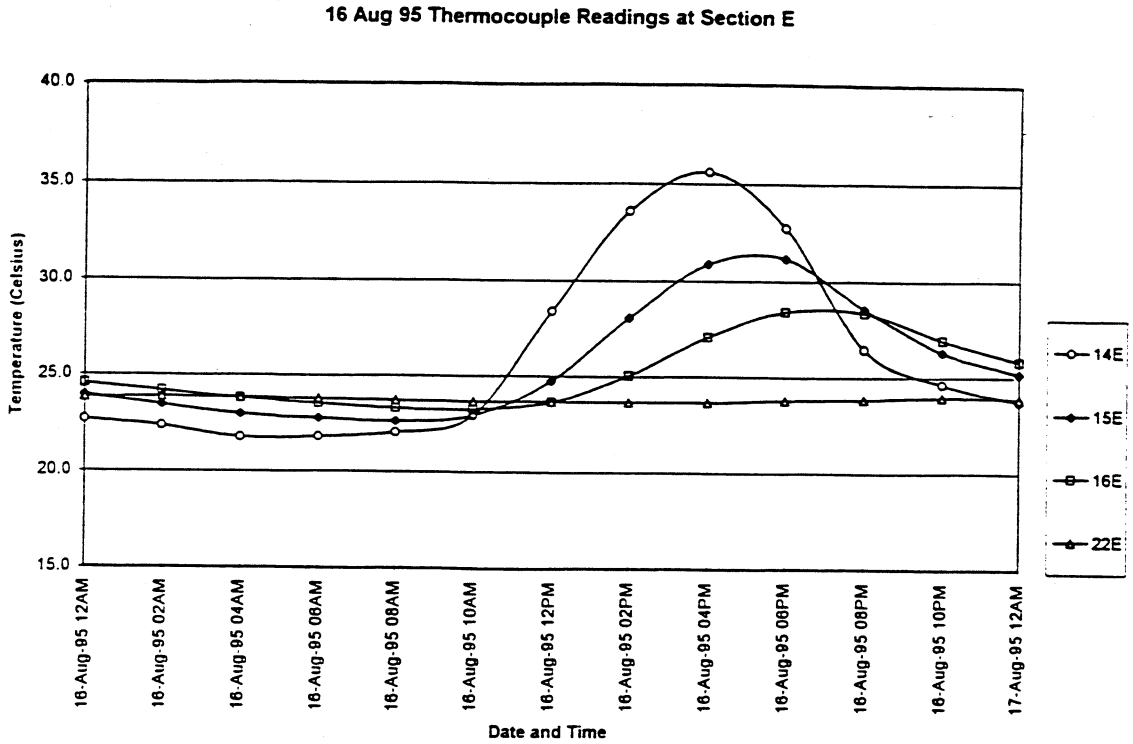
16 Aug 95 Thermocouple Readings at Section E
Temperature (Celsius)
40.0
35.0
30.0
25.0
20.0
15.0
16-Aug-95 12AM
16-Aug-95 02AM
16-Aug-95 04AM
16-Aug-95 06AM
16-Aug-95 08AM
16-Aug-95 10AM
16-Aug-95 12PM
16-Aug-95 02PM
16-Aug-95 04PM
16-Aug-95 06PM
16-Aug-95 08PM
16-Aug-95 10PM
17-Aug-95 12AM
Date and Time
14E
15E
16E
22E

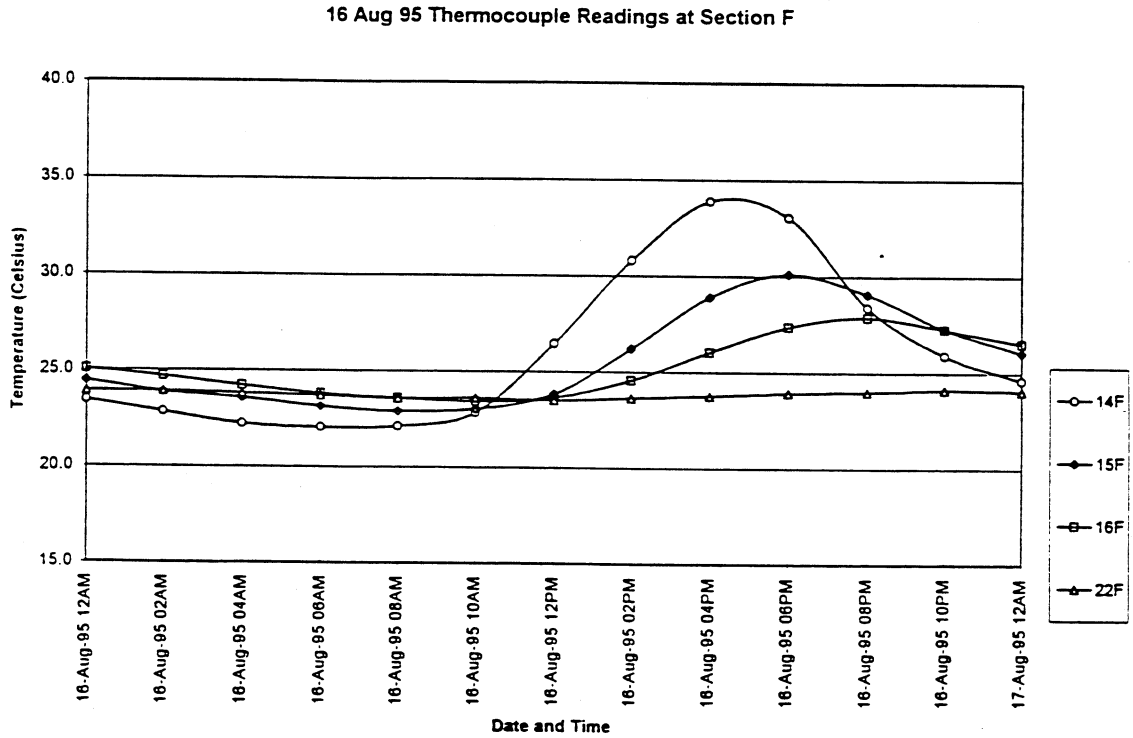
16 Aug 95 Thermocouple Readings at Section F
Temperature (Celsius)
40.0
35.0
30.0
25.0
20.0
15.0
16-Aug-95 12AM
16-Aug-95 02AM
16-Aug-95 04AM
16-Aug-95 06AM
16-Aug-95 08AM
16-Aug-95 10AM
16-Aug-95 12PM
16-Aug-95 02PM
16-Aug-95 04PM
16-Aug-95 06PM
16-Aug-95 08PM
16-Aug-95 10PM
17-Aug-95 12AM
Date and Time
14F
15F
16F
22F

Figure 8.79

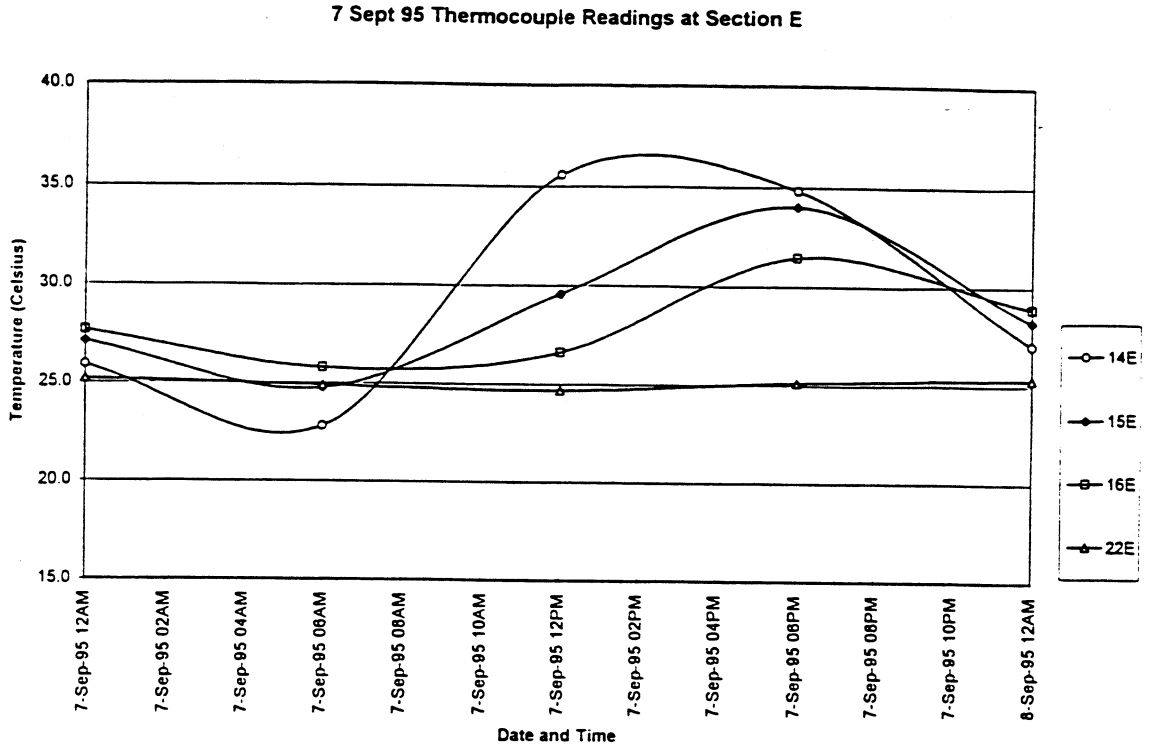
7 Sept 95 Thermocouple Readings at Section E
40.0
35.0
30.0
25.0
20.0
15.0
Temperature (Celsius)
7-Sep-95 12AM
7-Sep-95 02AM
7-Sep-95 04AM
7-Sep-95 06AM
7-Sep-95 08AM
7-Sep-95 10AM
7-Sep-95 12PM
7-Sep-95 02PM
7-Sep-95 04PM
7-Sep-95 06PM
7-Sep-95 08PM
7-Sep-95 10PM
8-Sep-95 12AM
Date and Time
14E
15E
16E
22E

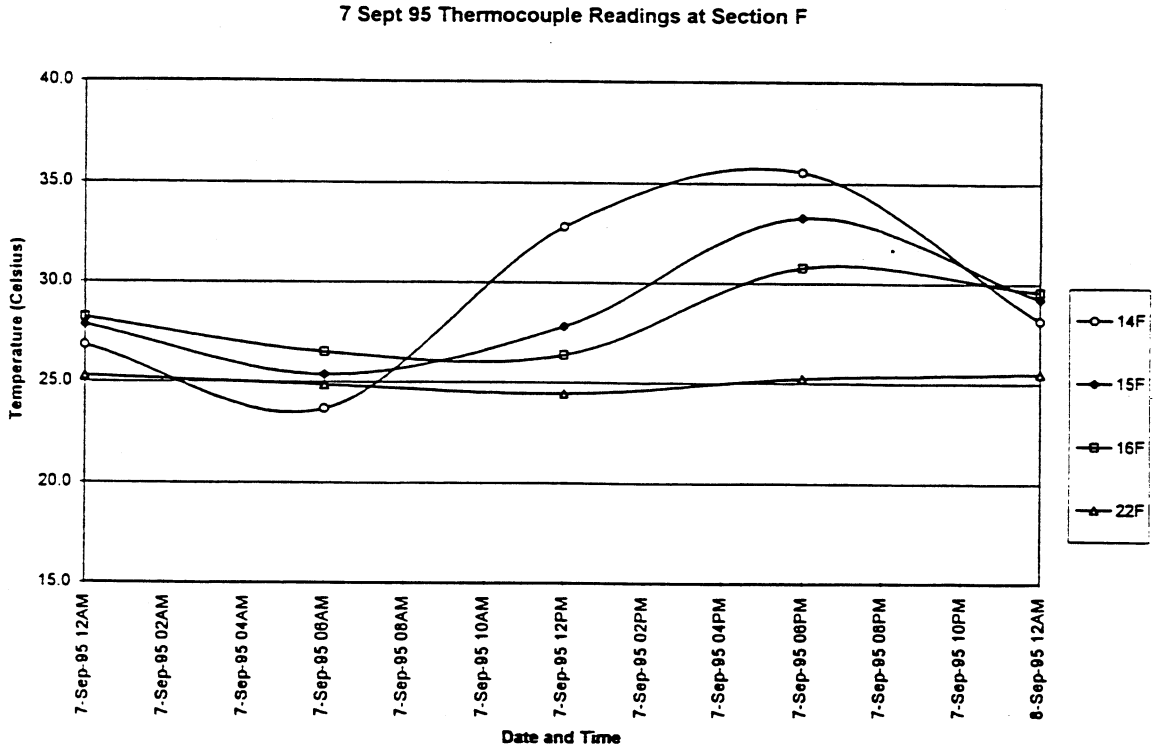
7 Sept 95 Thermocouple Readings at Section F
40.0
35.0
30.0
25.0
20.0
15.0
Temperature (Celsius)
7-Sep-95 12AM
7-Sep-95 02AM
7-Sep-95 04AM
7-Sep-95 06AM
7-Sep-95 08AM
7-Sep-95 10AM
7-Sep-95 12PM
7-Sep-95 02PM
7-Sep-95 04PM
7-Sep-95 06PM
7-Sep-95 08PM
7-Sep-95 10PM
8-Sep-95 12AM
Date and Time
14F
15F
16F
22F

Figure 8.80

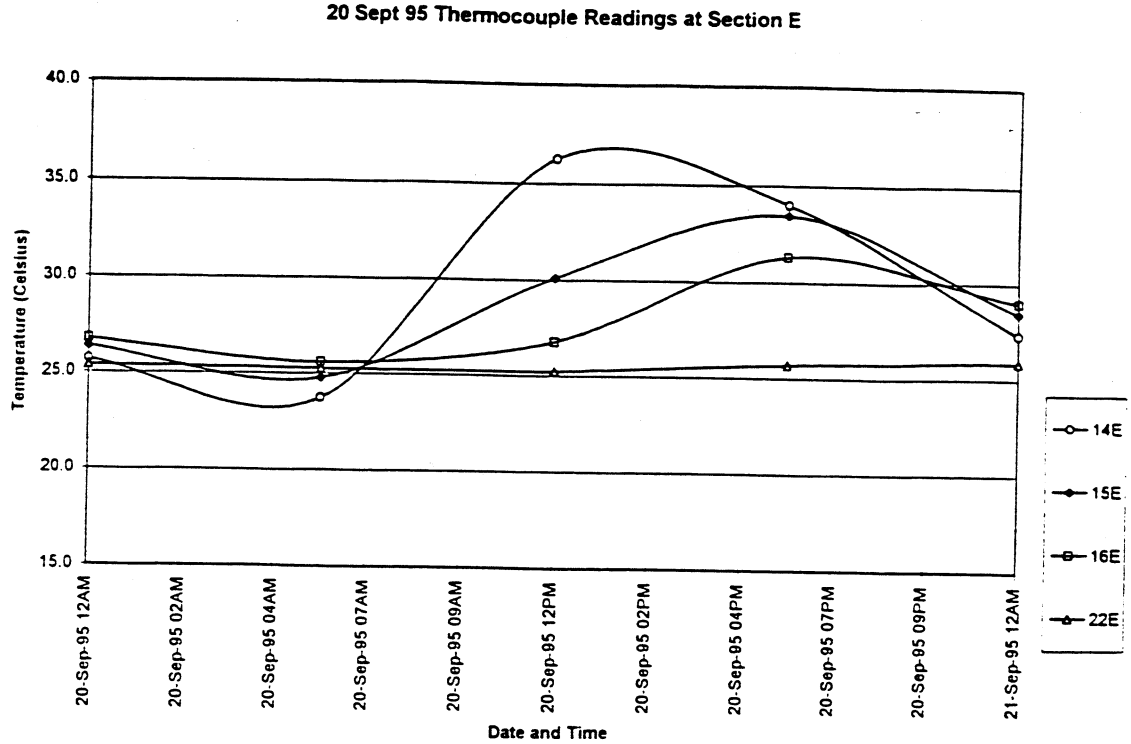
20 Sept 95 Thermocouple Readings at Section E
40.0
35.0
30.0
25.0
20.0
15.0
Temperature (Celsius)
20-Sep-95 12AM
20-Sep-95 02AM
20-Sep-95 04AM
20-Sep-95 07AM
20-Sep-95 09AM
20-Sep-95 12PM
20-Sep-95 02PM
20-Sep-95 04PM
20-Sep-95 07PM
20-Sep-95 09PM
21-Sep-95 12AM
Date and Time
14E
15E
16E
22E

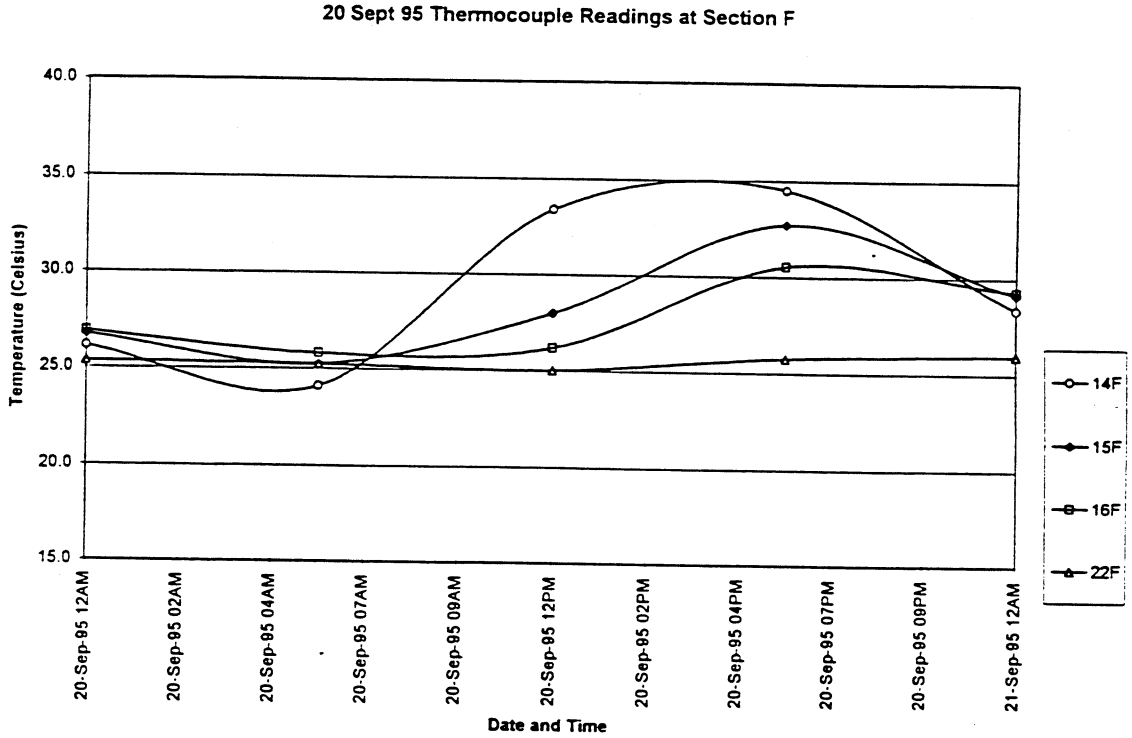
20 Sept 95 Thermocouple Readings at Section F
40.0
35.0
30.0
25.0
20.0
15.0
Temperature (Celsius)
20-Sep-95 12AM
20-Sep-95 02AM
20-Sep-95 04AM
20-Sep-95 07AM
20-Sep-95 09AM
20-Sep-95 12PM
20-Sep-95 02PM
20-Sep-95 04PM
20-Sep-95 07PM
20-Sep-95 09PM
21-Sep-95 12AM
Date and Time
14F
15F
16F
22F

Figure 8.81

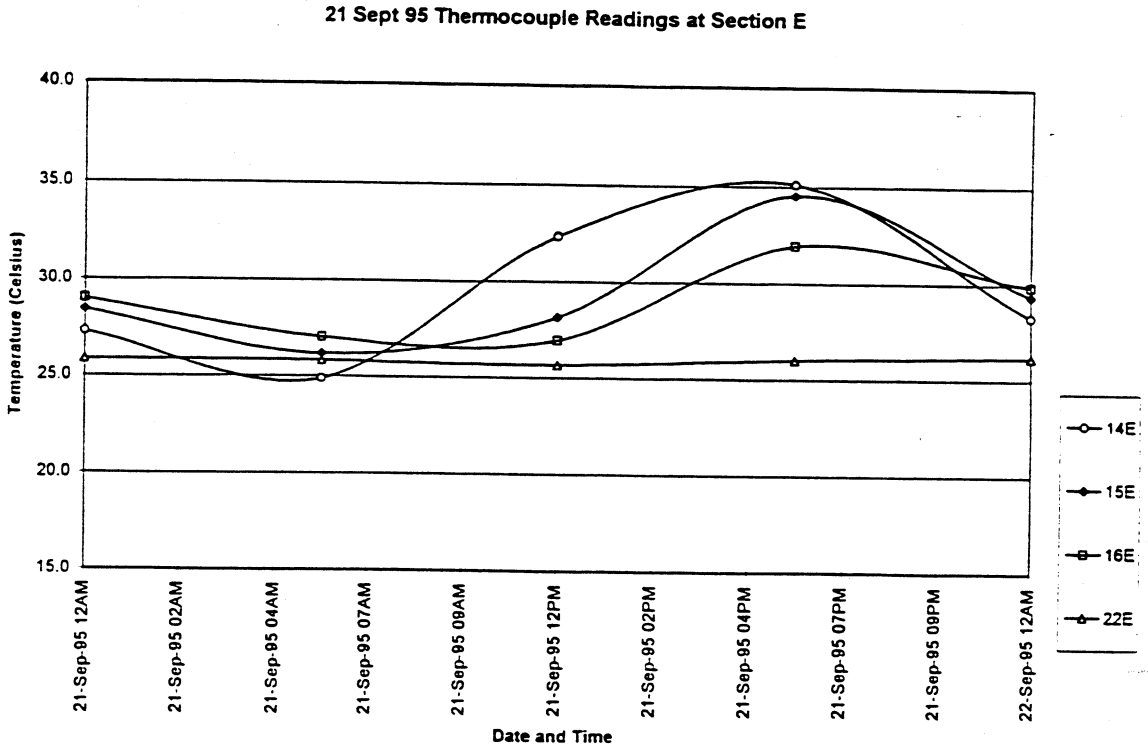

H3 Instrumentation Report

TYLin International

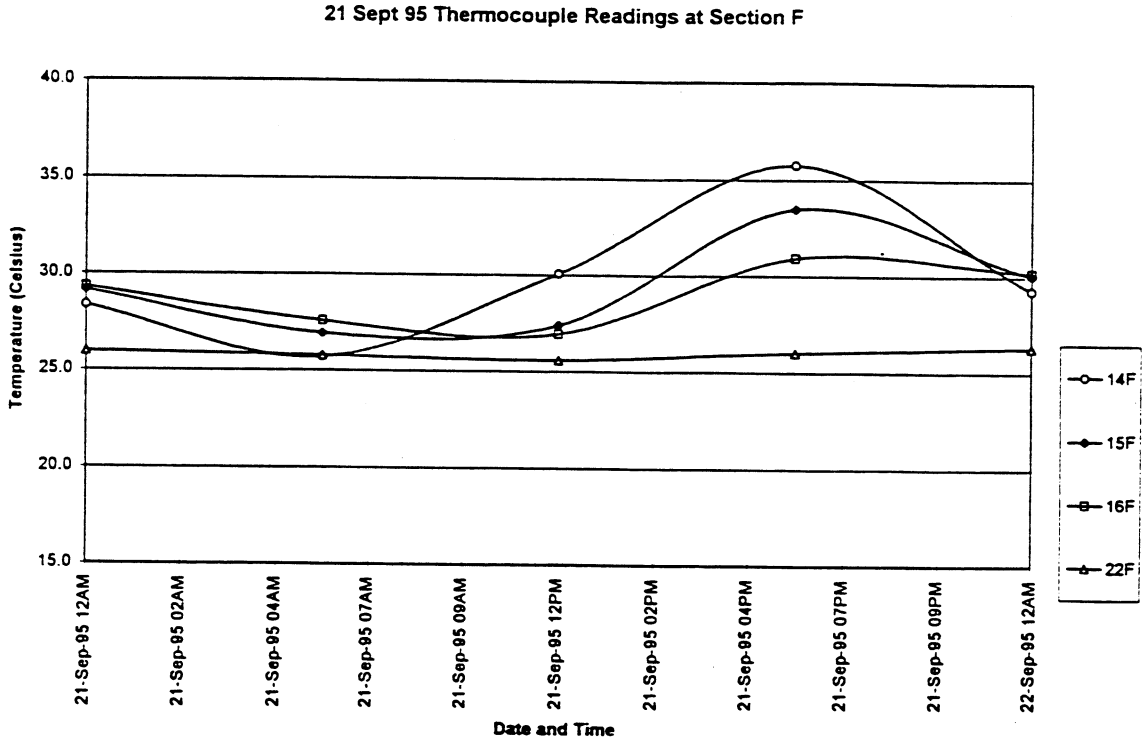

Figure 8.82

Positive Thermal Gradient at Section E

4-May-95 04PM

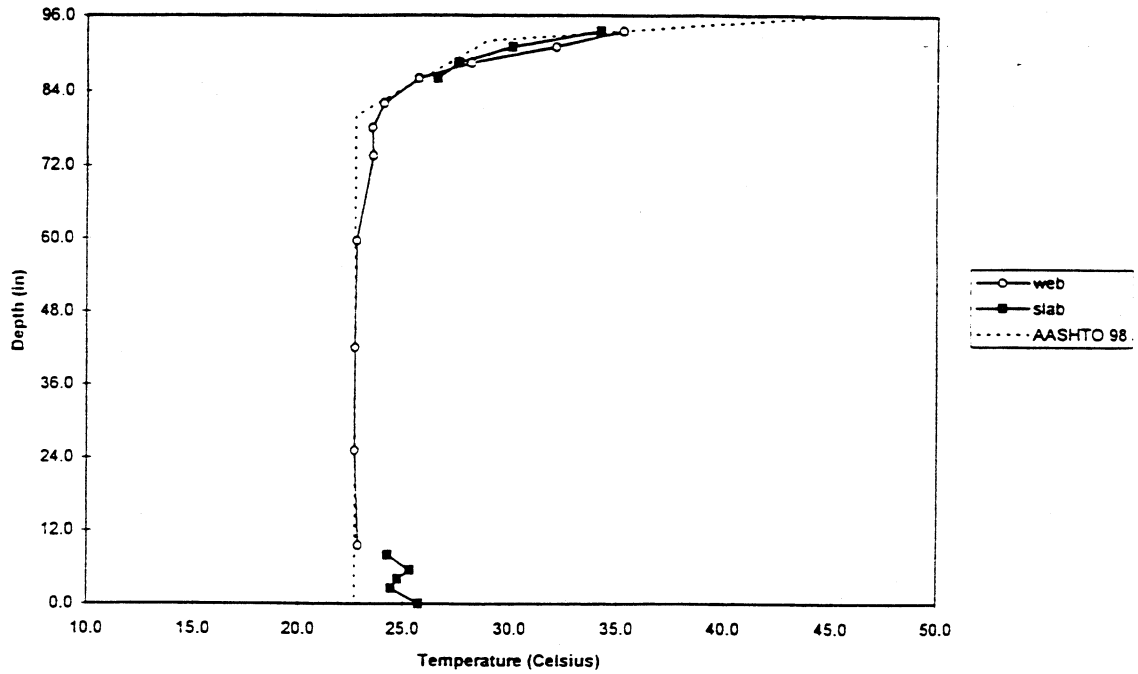

Positive Thermal Gradient at Section F

4-May-95 04PM

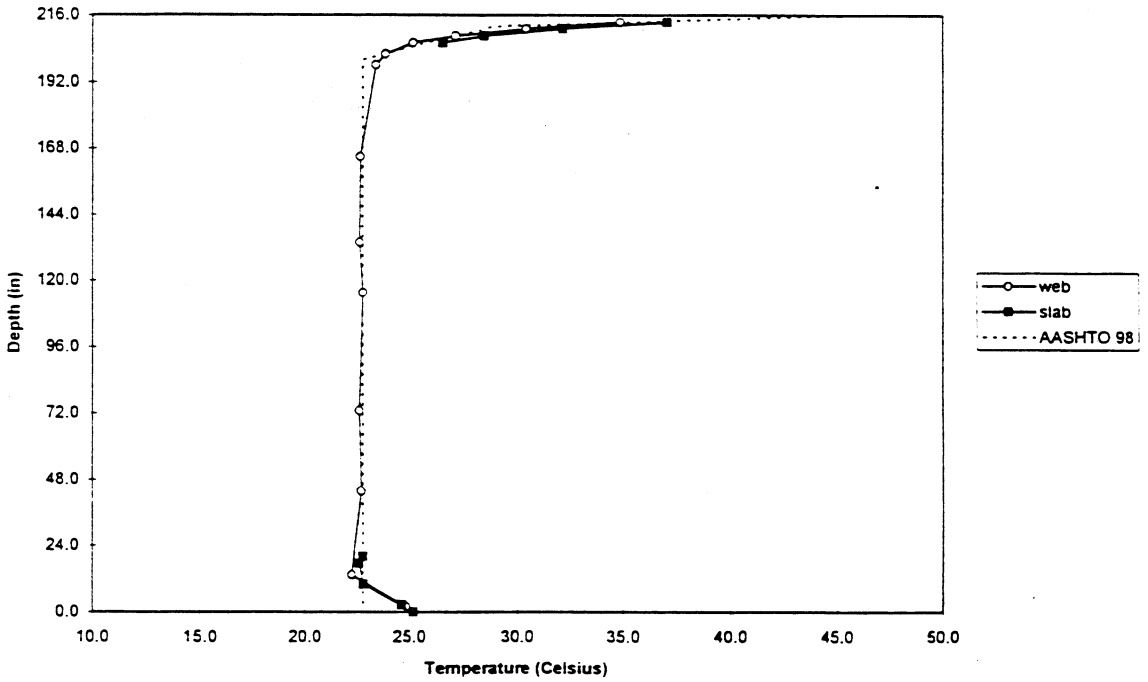

Figure 8.83

Positive Thermal Gradient at Section E

22-May-95 04PM

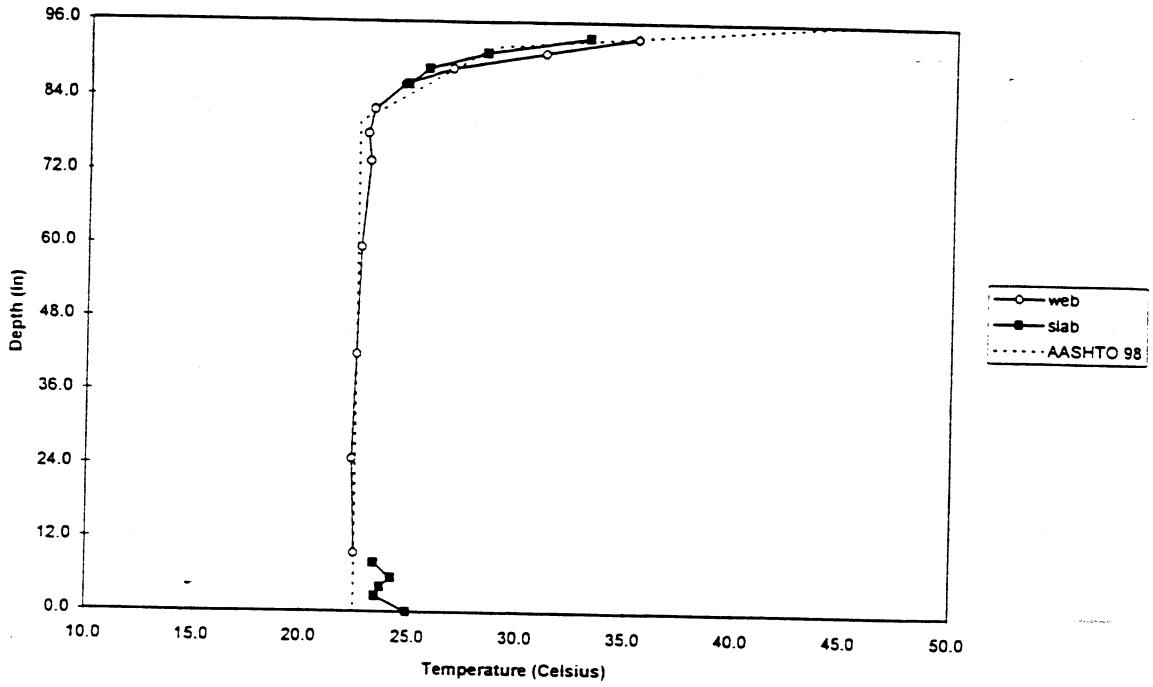

Positive Thermal Gradient at Section F

22-May-95 04PM

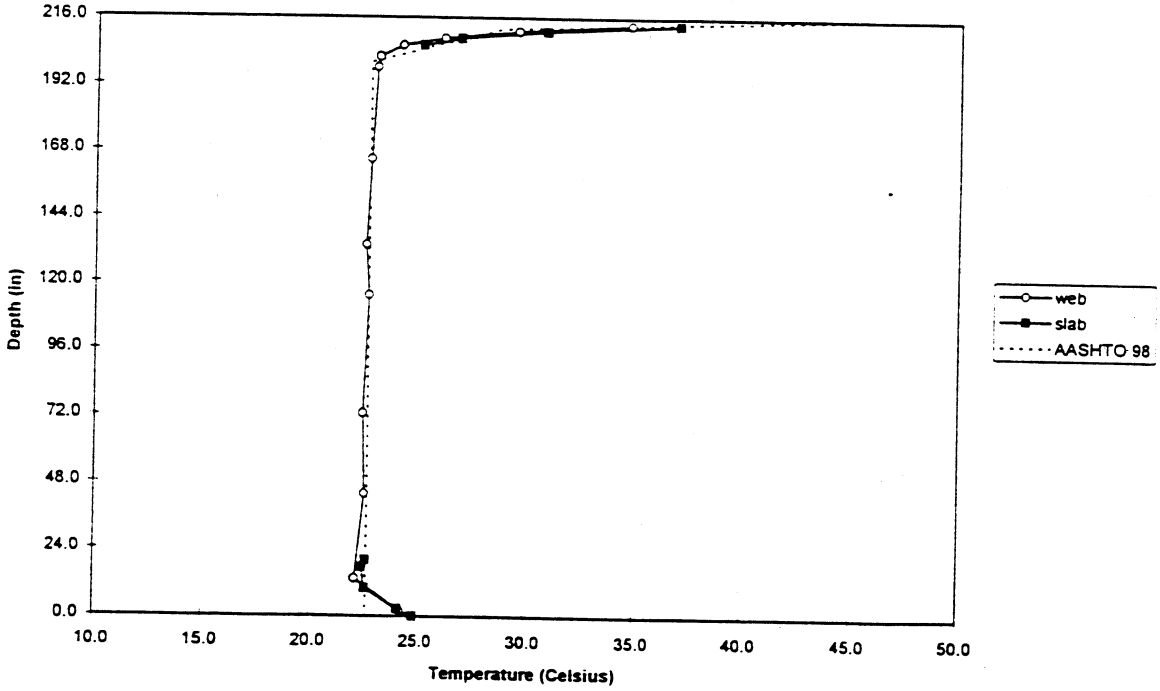

Figure 8.84

26-May-95 04PM

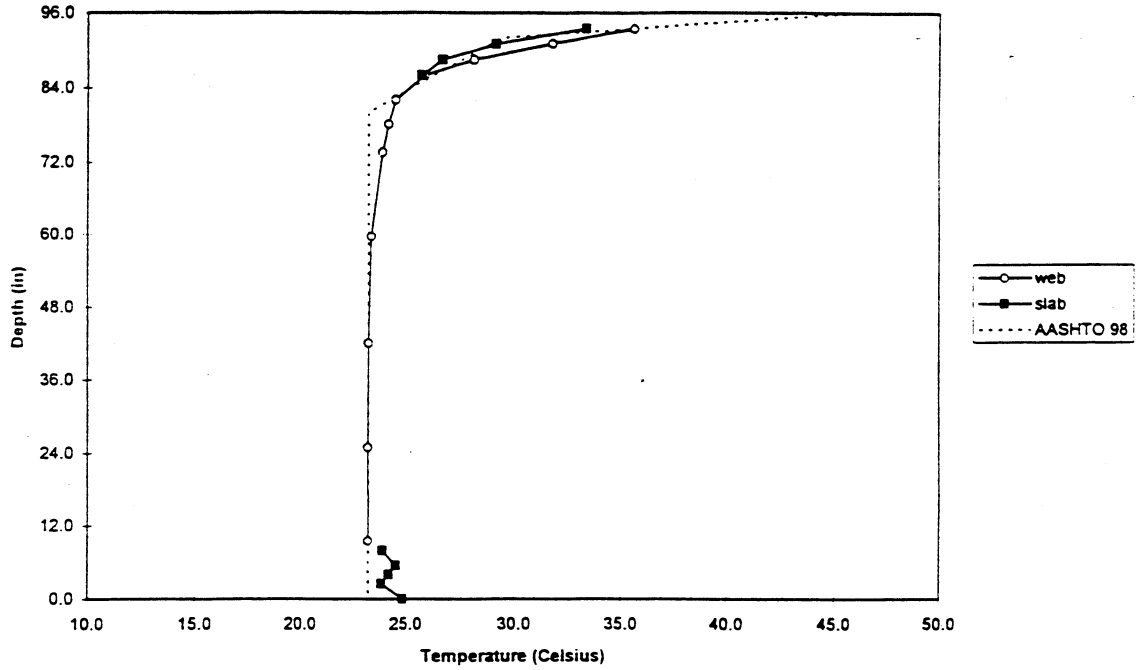

26-May-95 04PM

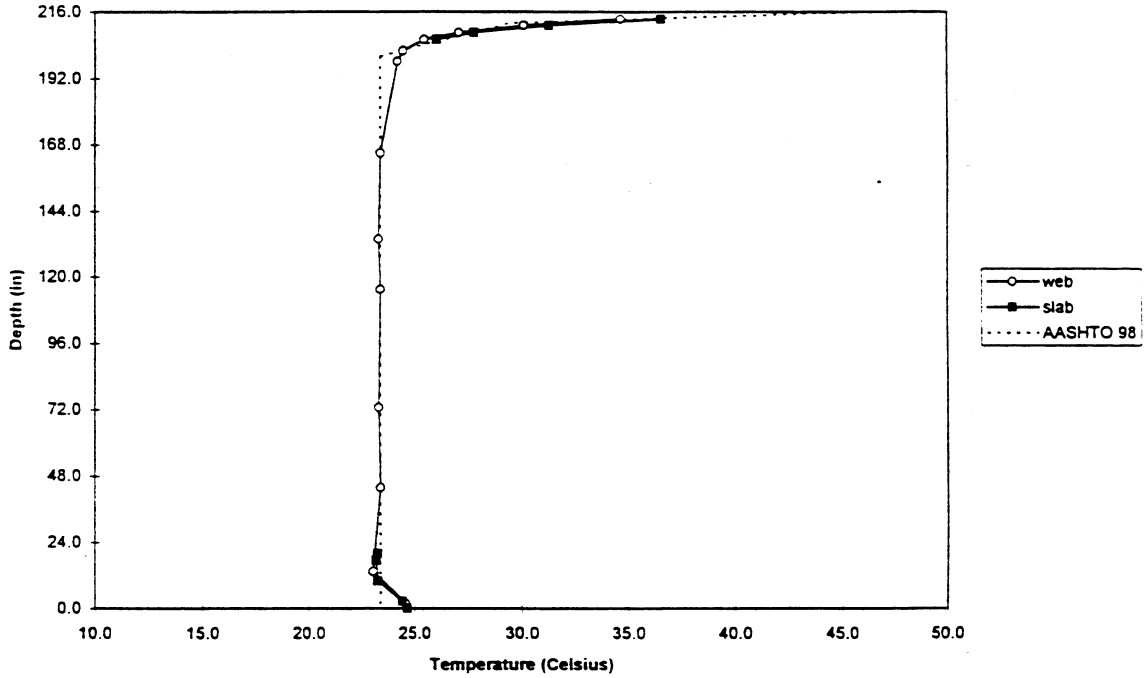

Figure 8.85

Positive Thermal Gradient at Section E

16-Jun-95 04PM

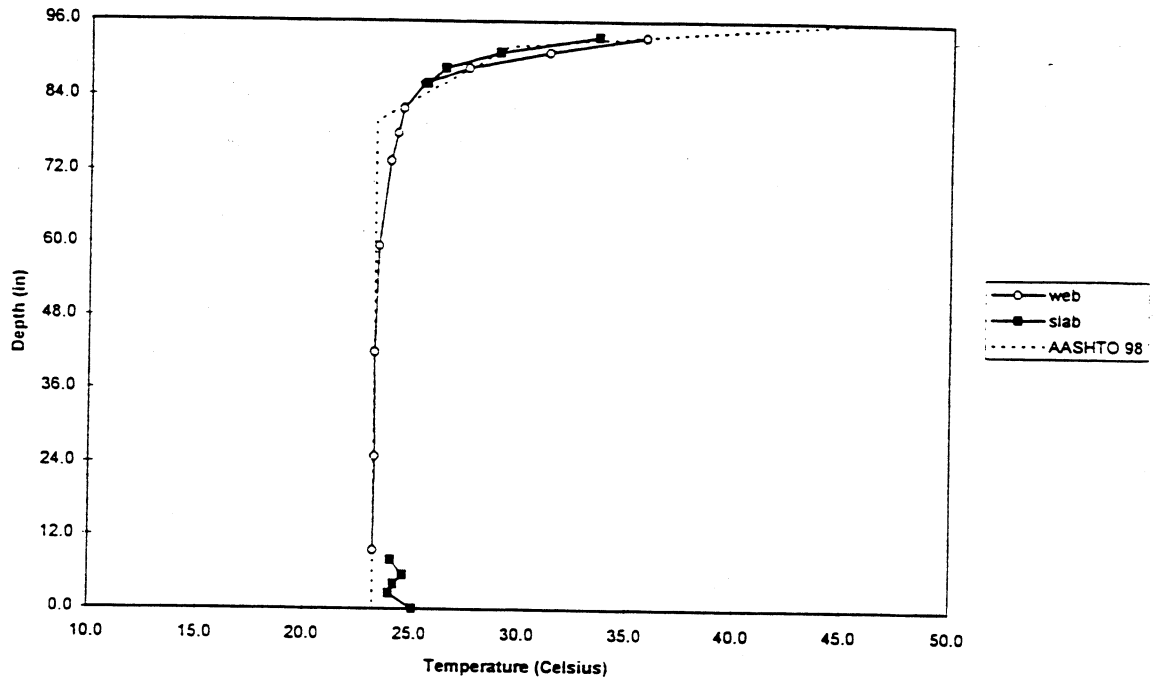

Positive Thermal Gradient at Section F

16-Jun-95 04PM

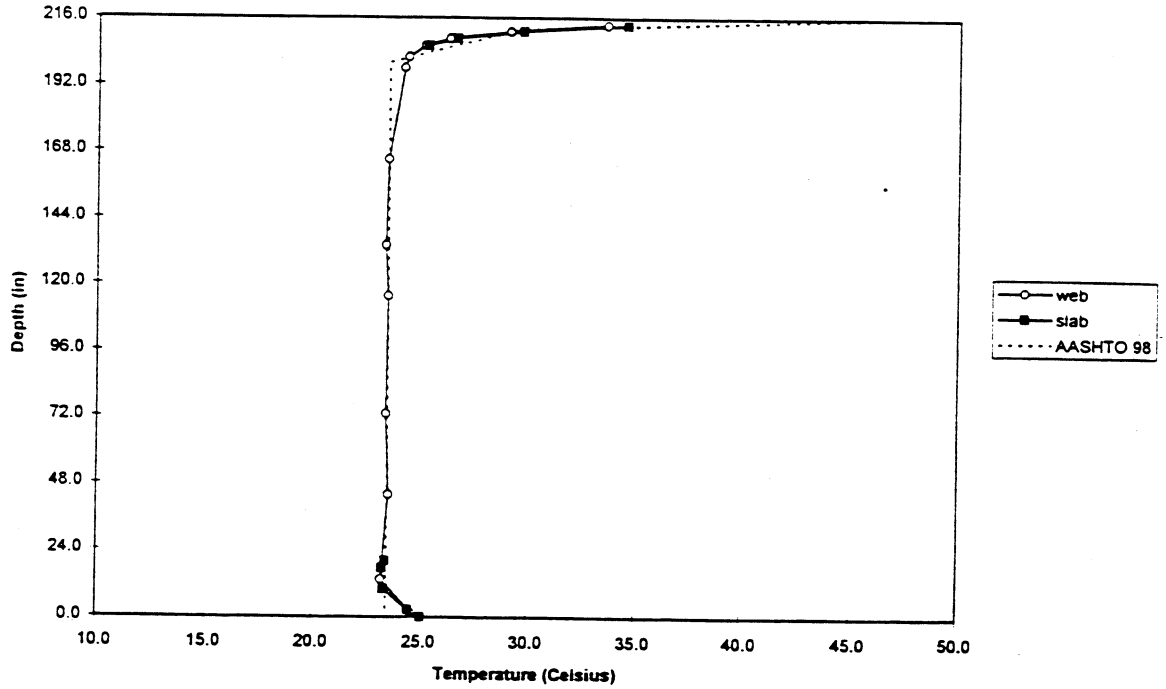

Figure 8.86

Positive Thermal Gradient at Section E

17-Jun-95 04PM

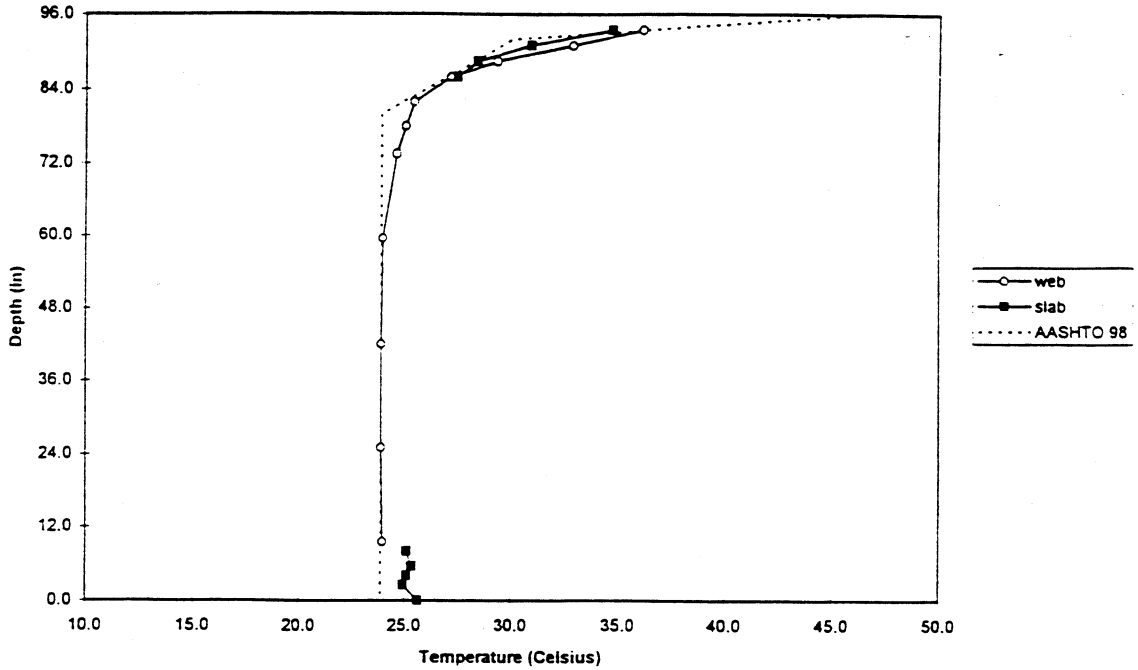

Positive Thermal Gradient at Section F

17-Jun-95 04PM

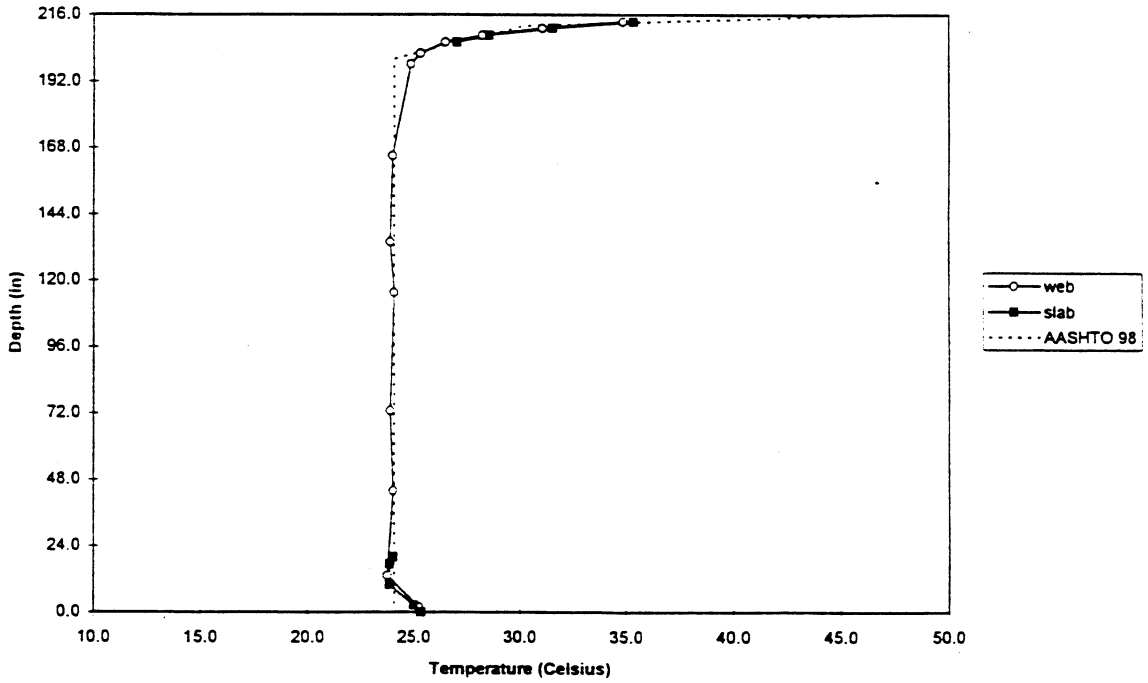

Figure 8.87

Positive Thermal Gradient at Section E

28-Jun-95 04PM

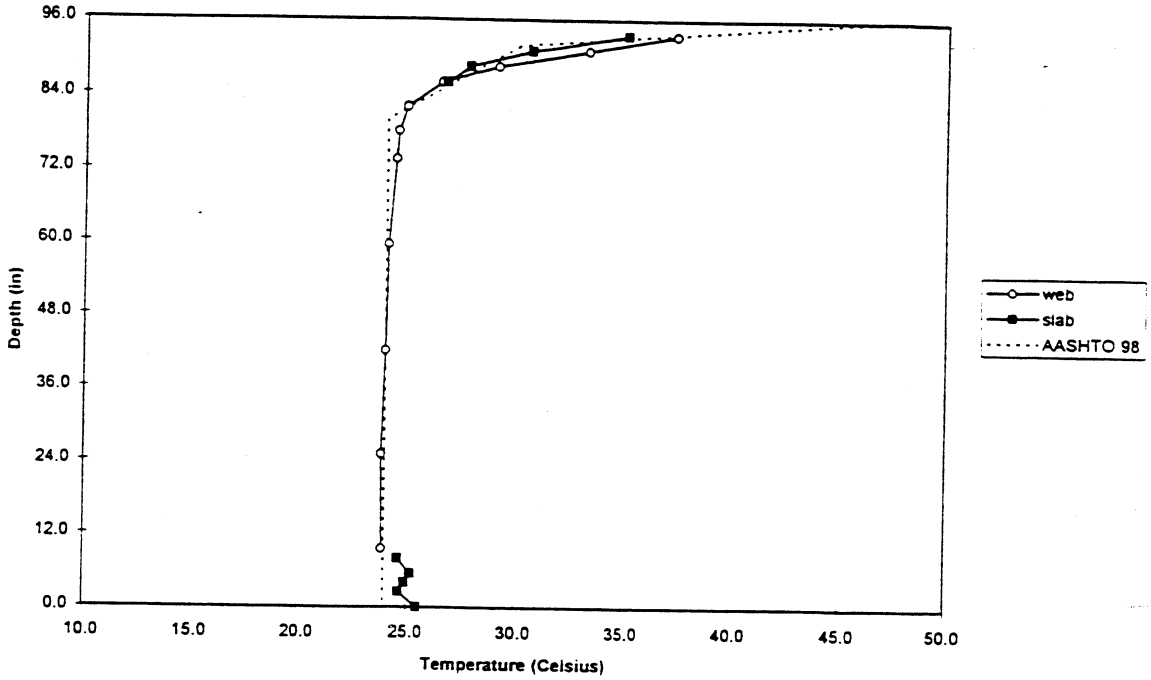

Positive Thermal Gradient at Section F

28-Jun-95 04PM

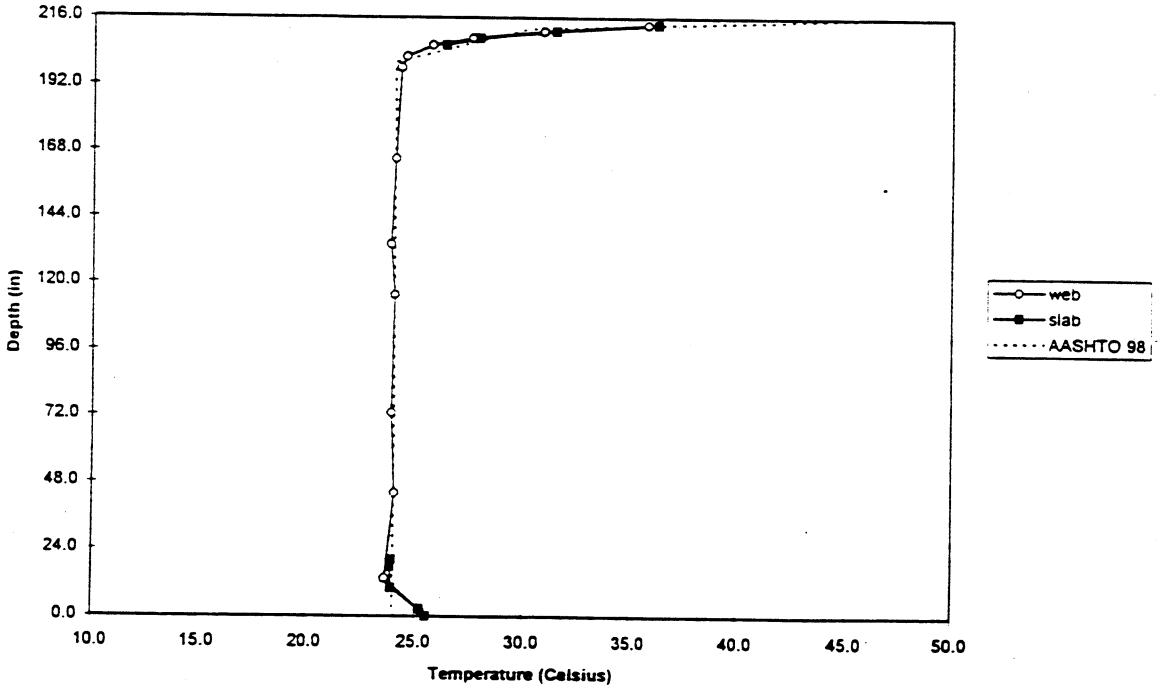

Figure 8.88

1-Jul-95 04PM

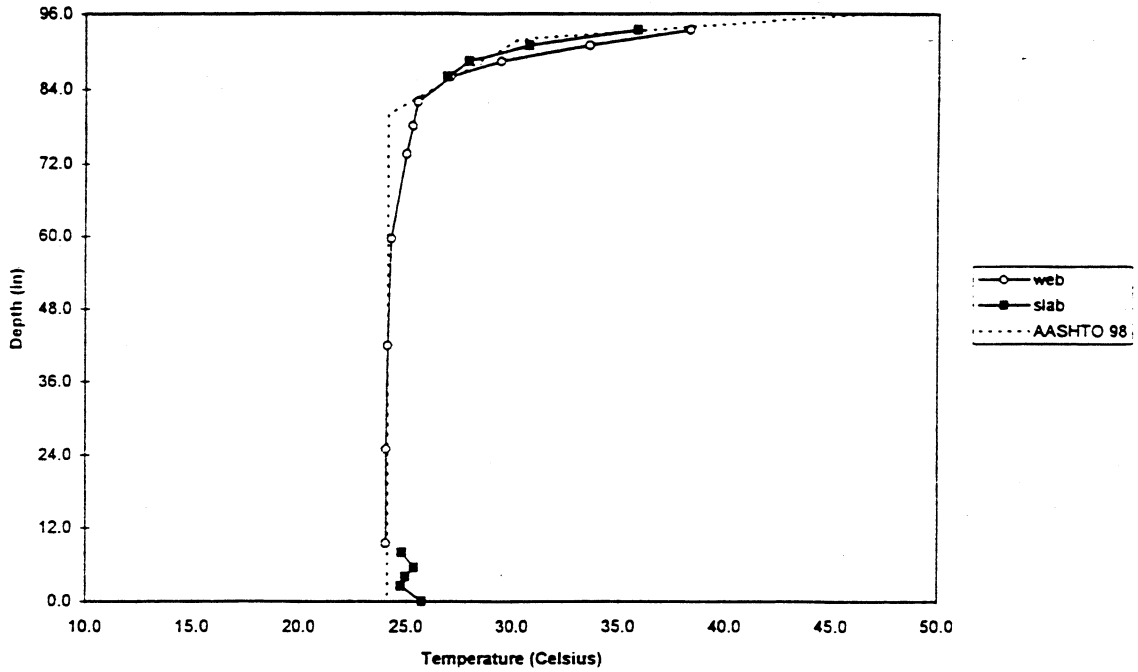

1-Jul-95 04PM

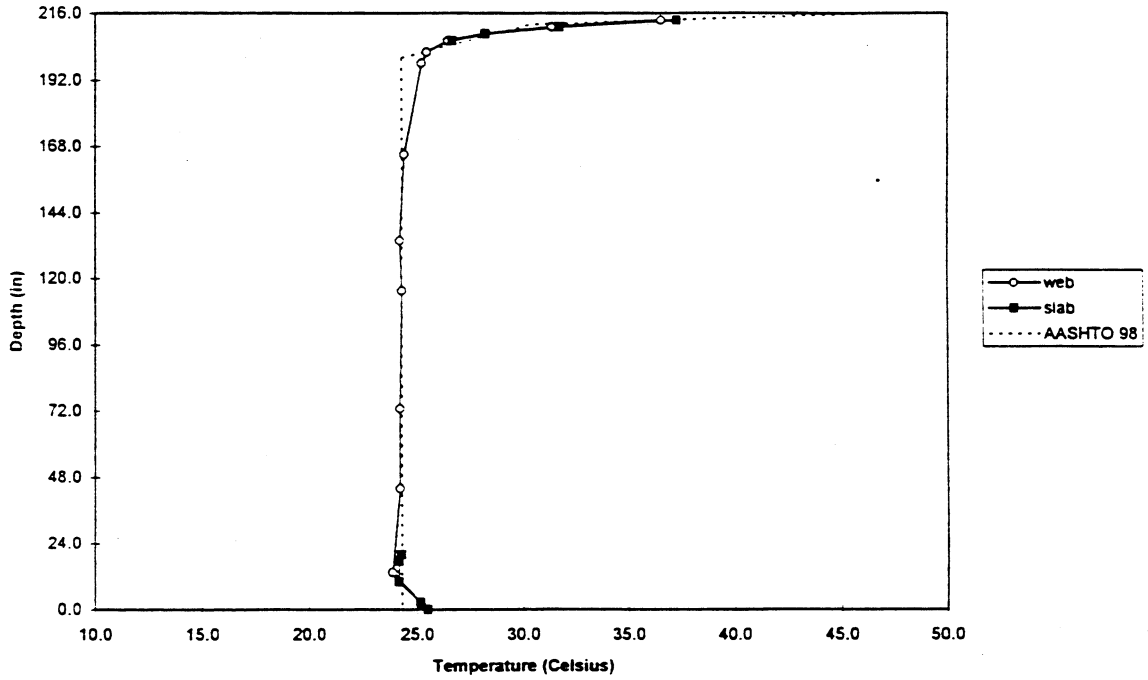

Figure 8.89

Positive Thermal Gradient at Section E

15-Jul-95 04PM

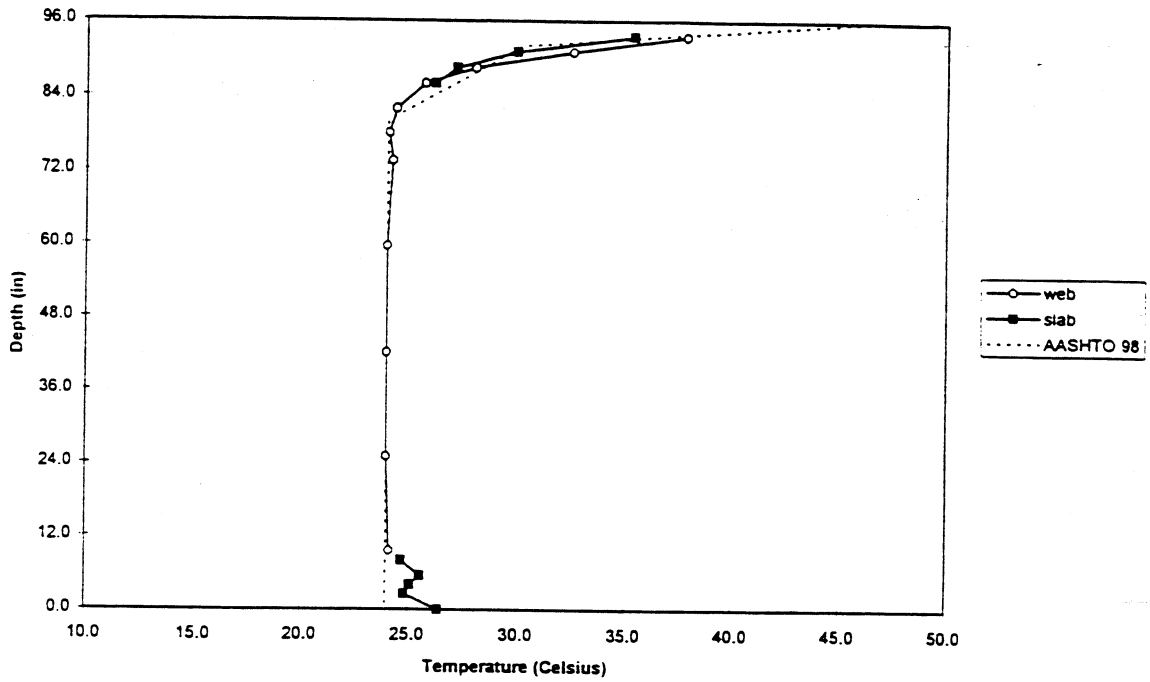

Positive Thermal Gradient at Section F

15-Jul-95 04PM

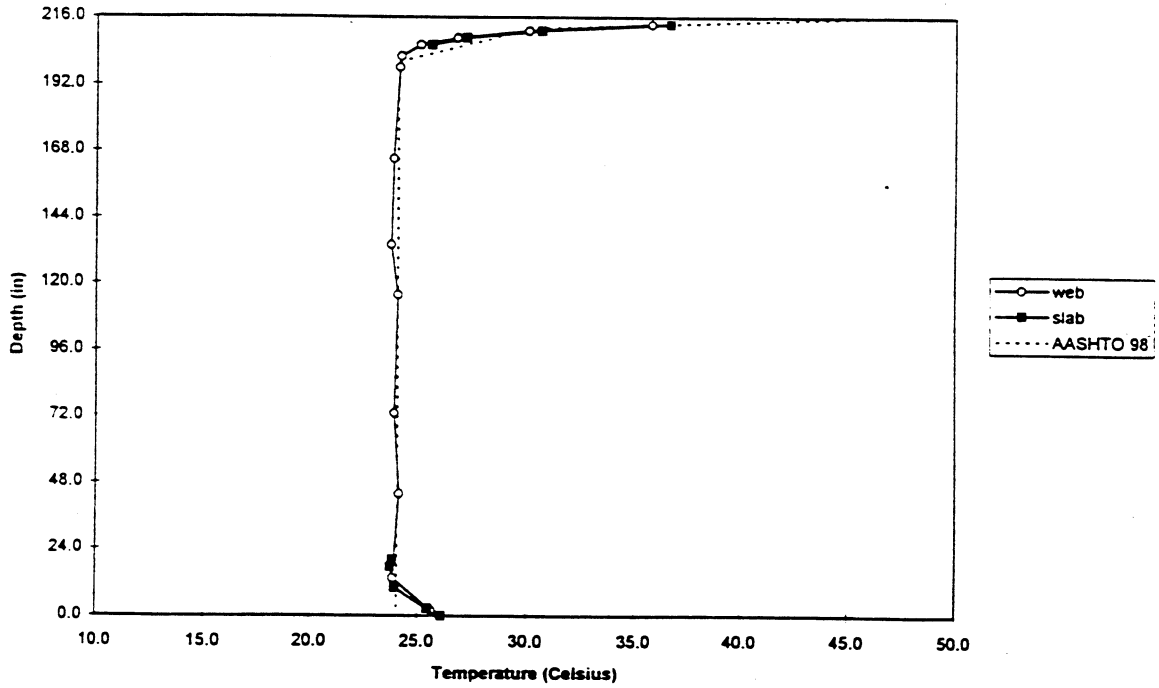

Figure 8.90

Positive Thermal Gradient at Section E

18-Jul-95 04PM

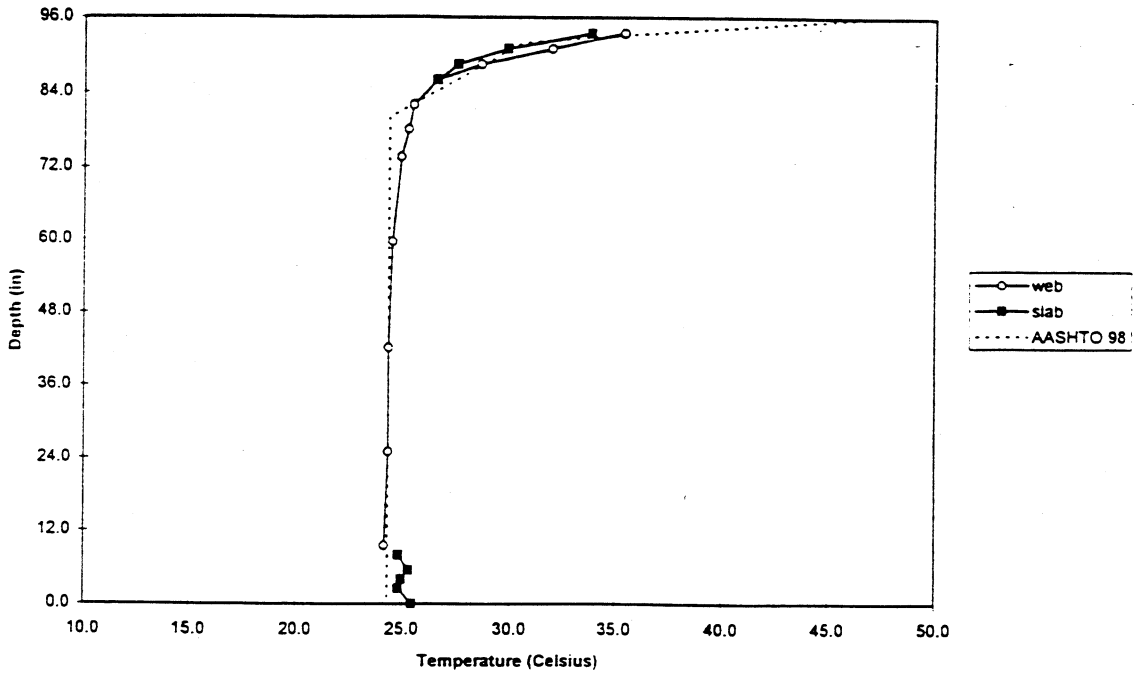

Positive Thermal Gradient at Section F

18-Jul-95 04PM

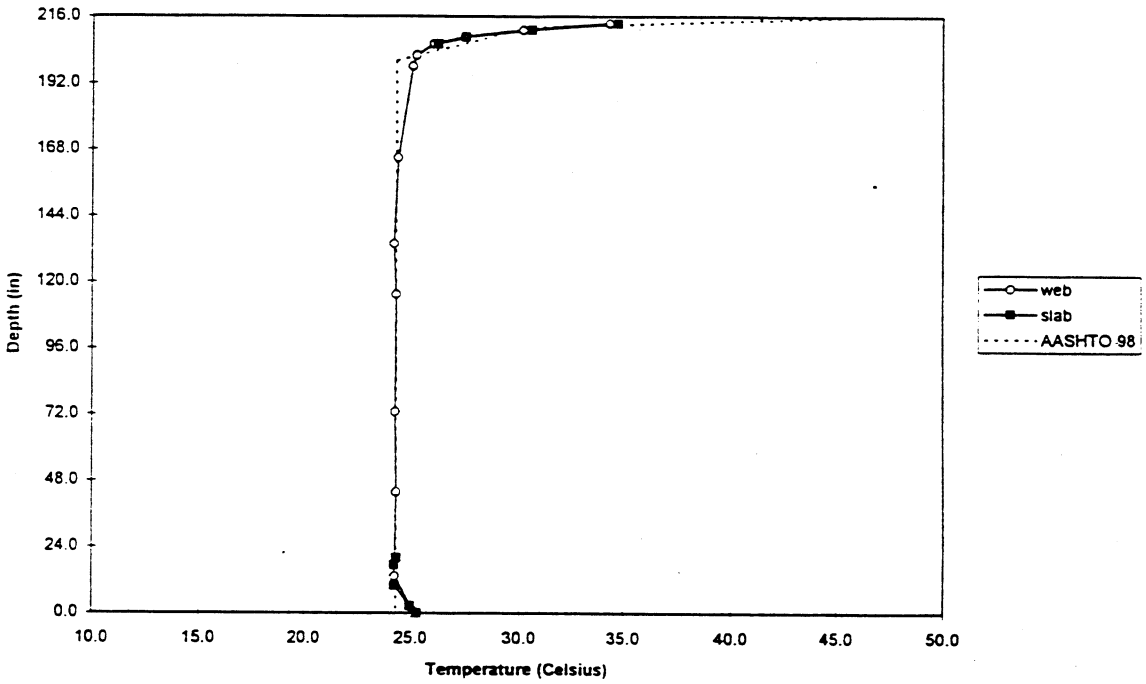

Figure 8.91

Positive Thermal Gradient at Section E

2-Aug-95 04PM

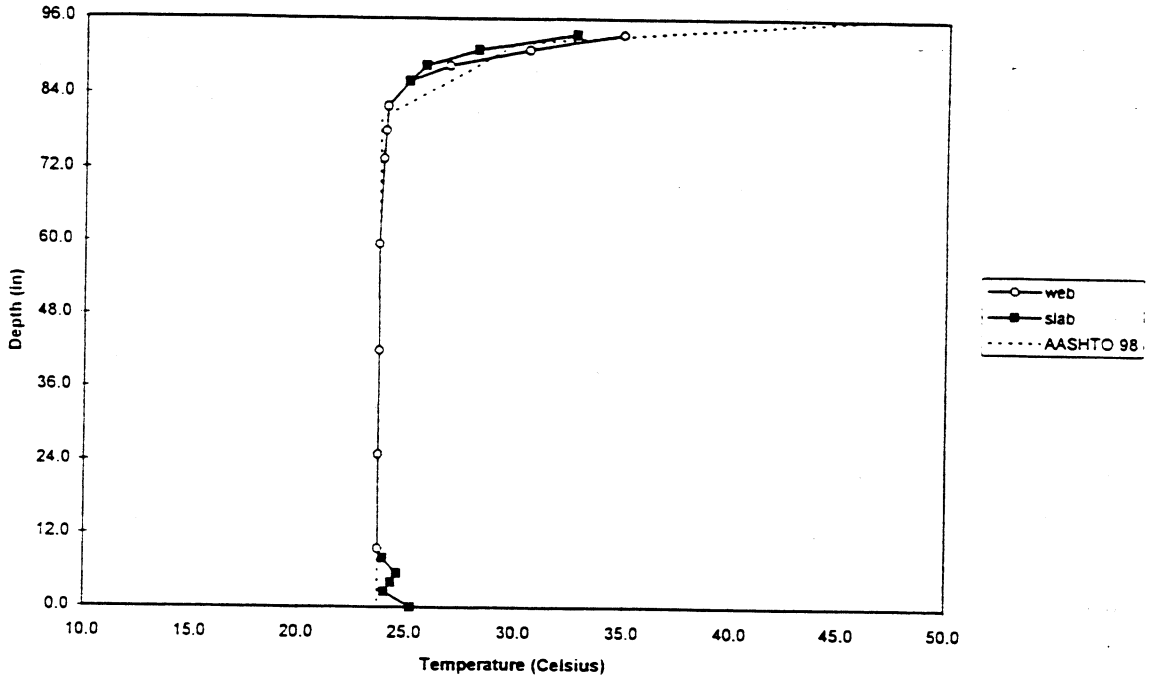

Positive Thermal Gradient at Section F

2-Aug-95 04PM

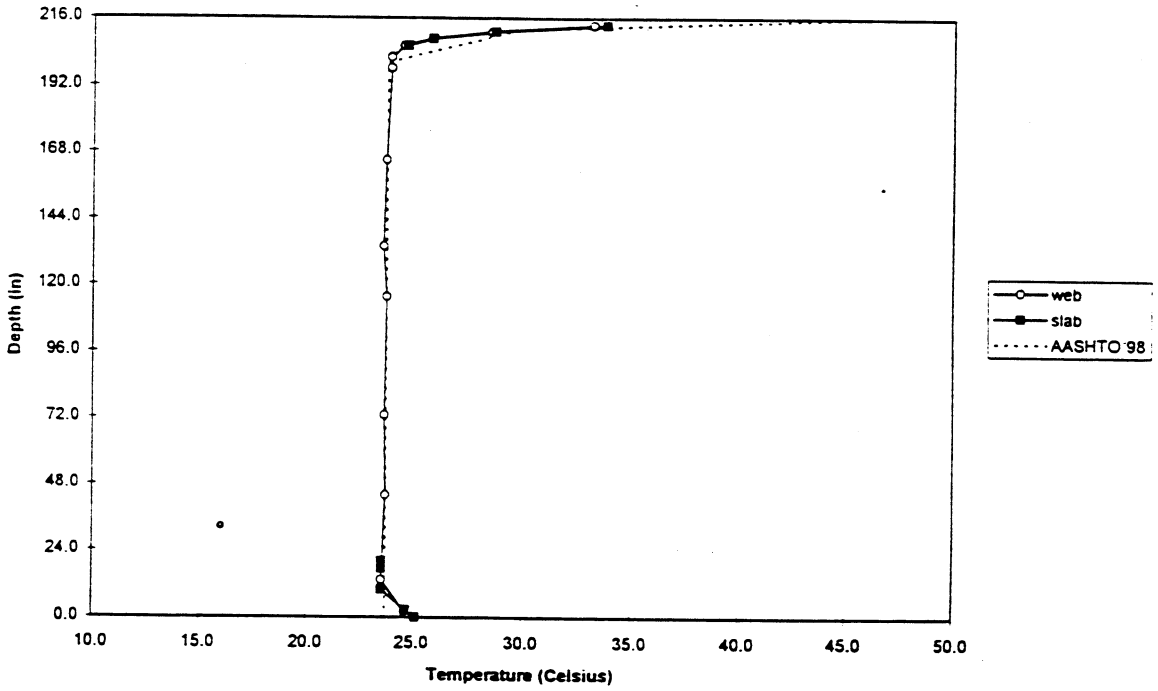

Figure 8.92

Positive Thermal Gradient at Section E

3-Aug-95 04PM

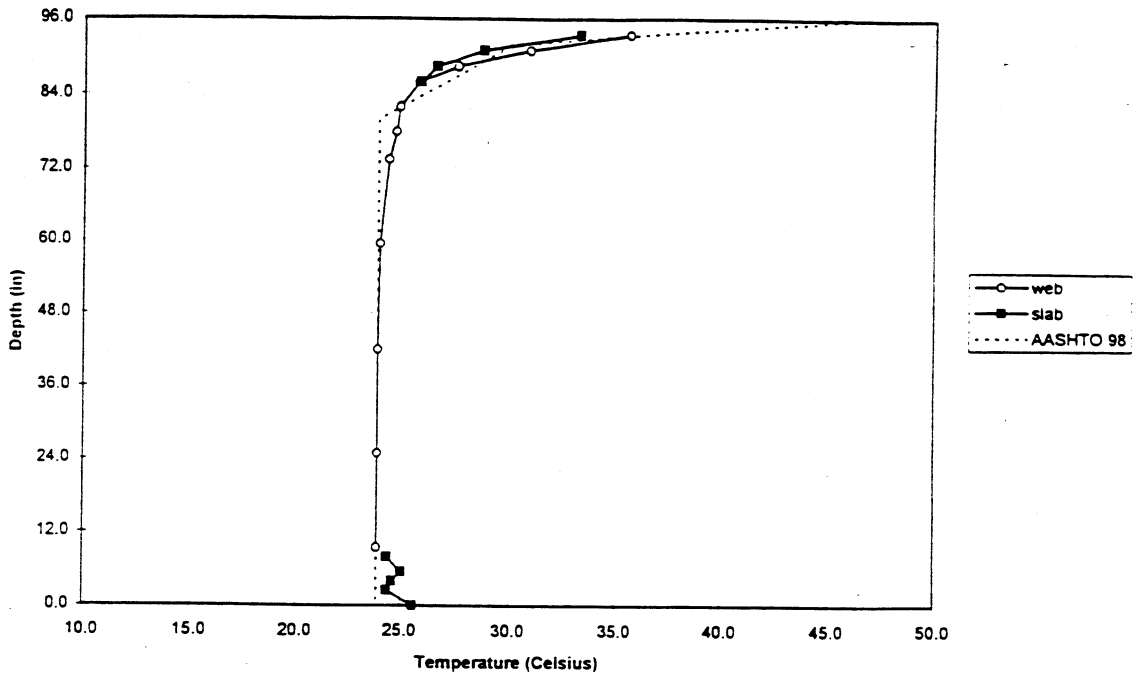

Positive Thermal Gradient at Section F

3-Aug-95 04PM

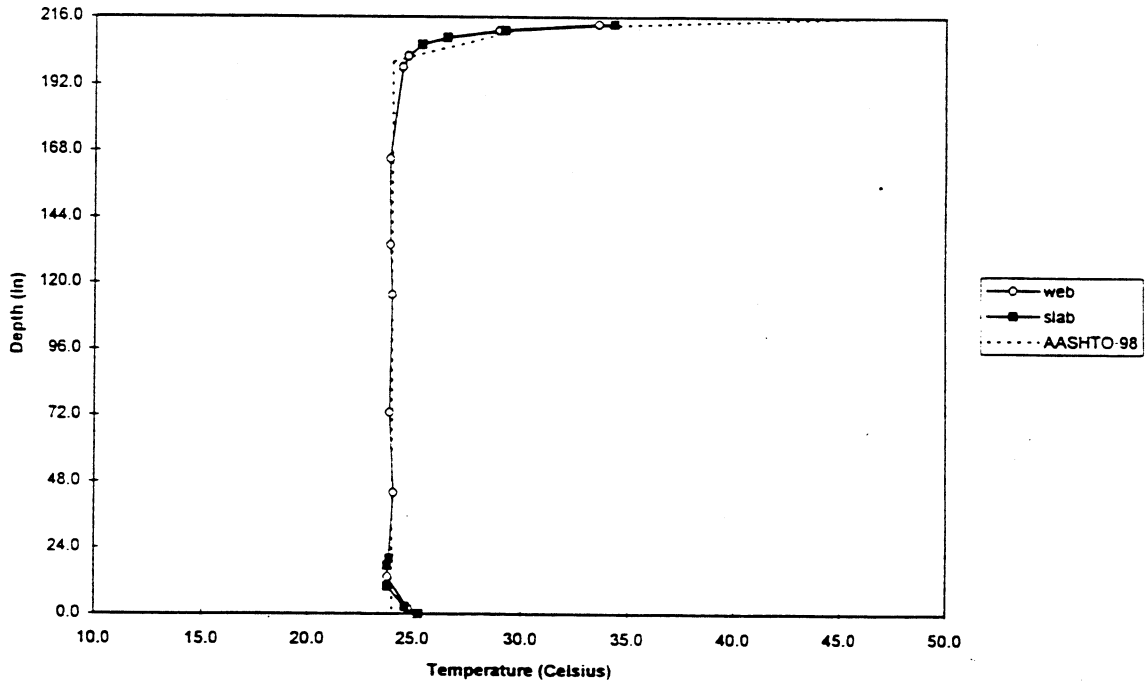

Figure 8.93

H3 Instrumentation Report

Positive Thermal Gradient at Section E

TYLin International

16-Aug-95 04PM

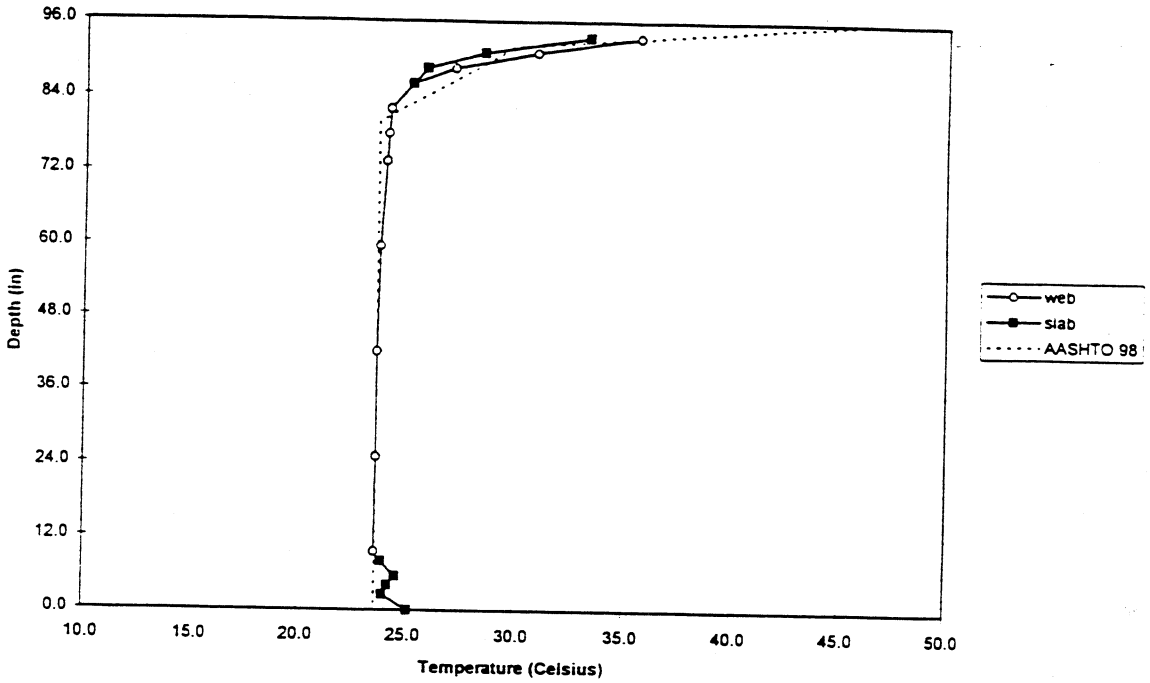

H3 Instrumentation Report

Positive Thermal Gradient at Section F

TYLin International

16-Aug-95 04PM

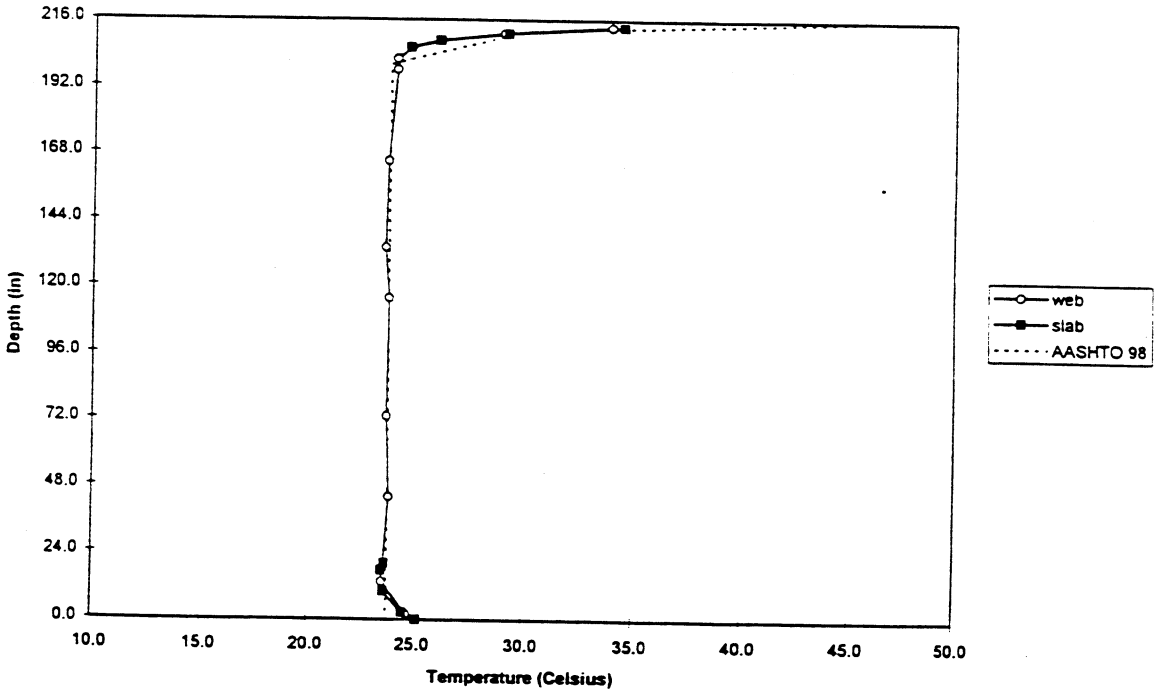

Figure 8.94

Negative Thermal Gradient at Section E

7-Jan-95 06AM

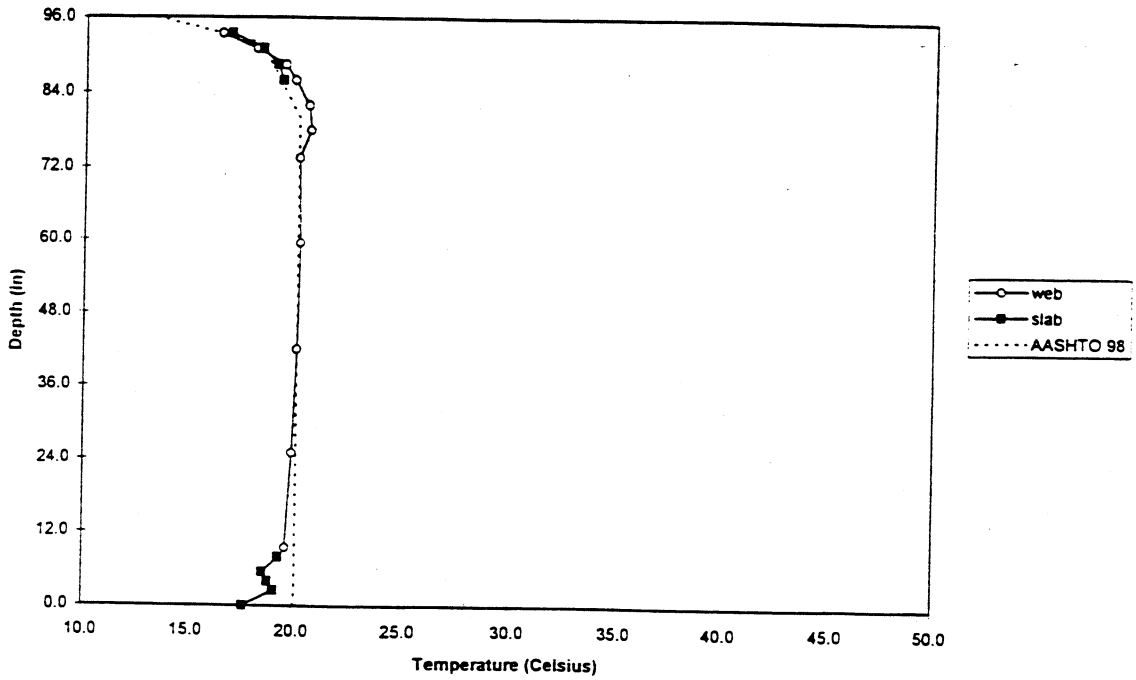

Negative Thermal Gradient at Section F

7-Jan-95 06AM

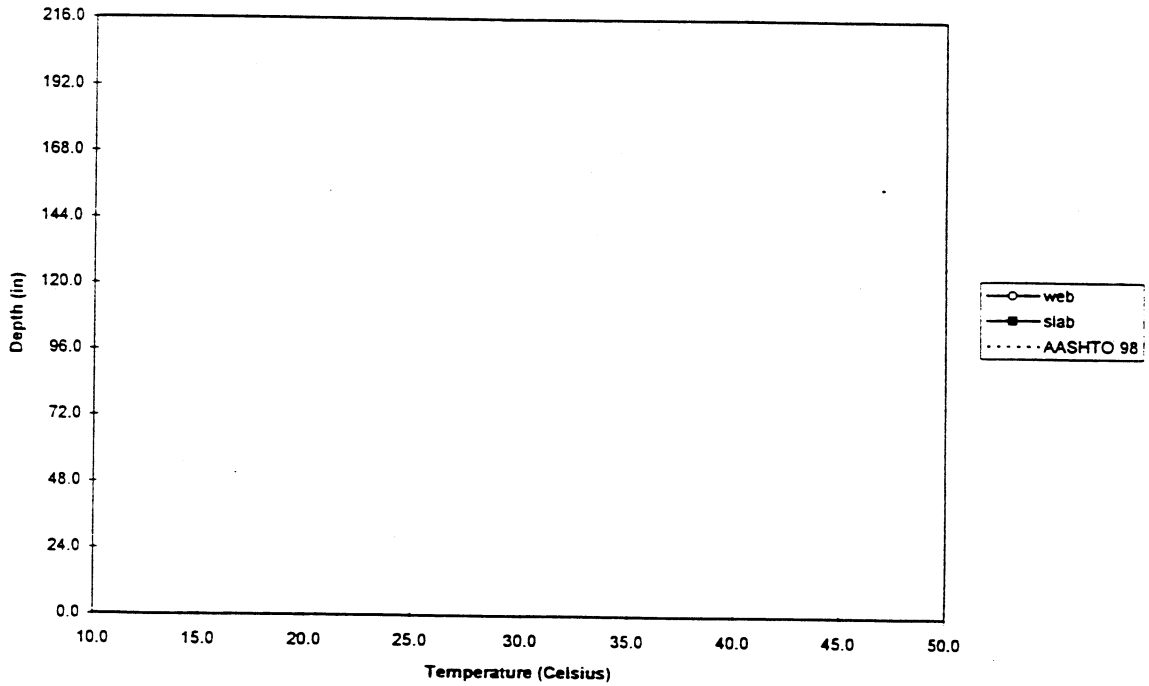

Figure 8.95

Negative Thermal Gradient at Section E

8-Jan-95 06AM

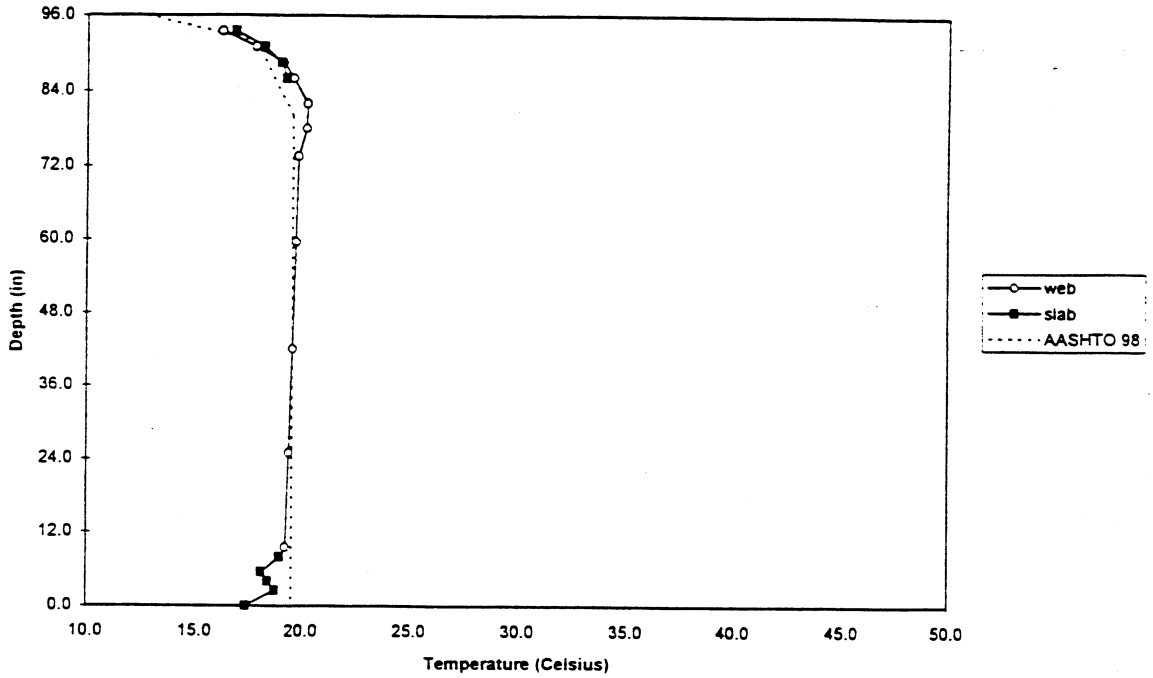

Negative Thermal Gradient at Section F

8-Jan-95 06AM

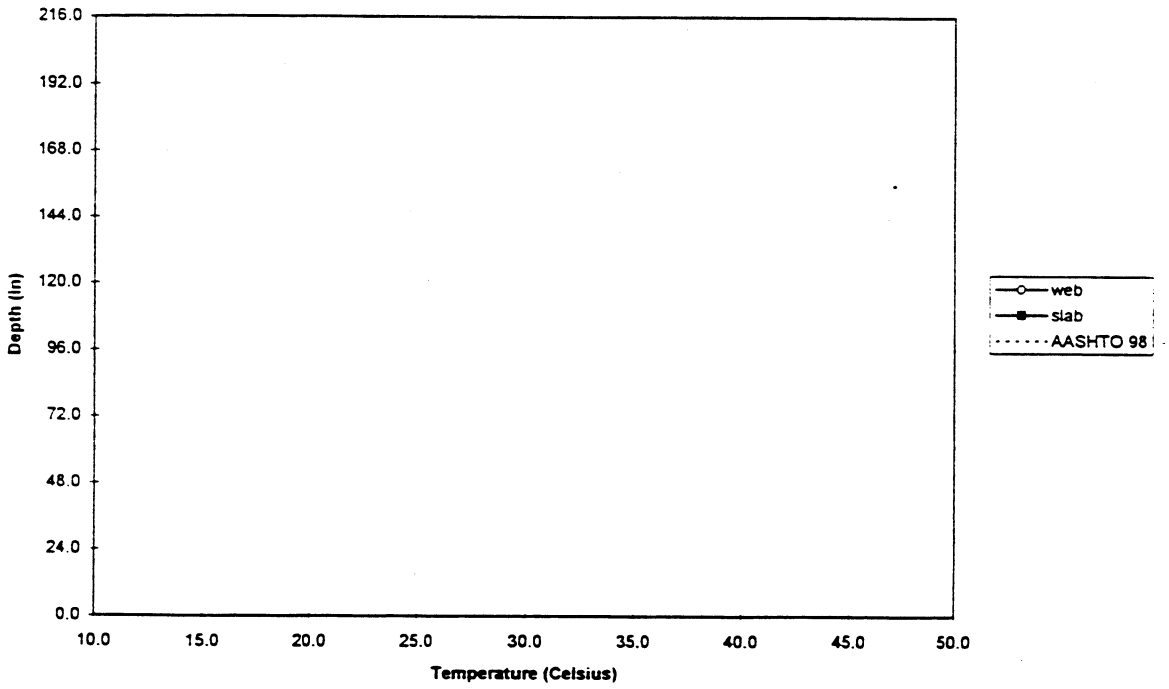

Figure 8.96

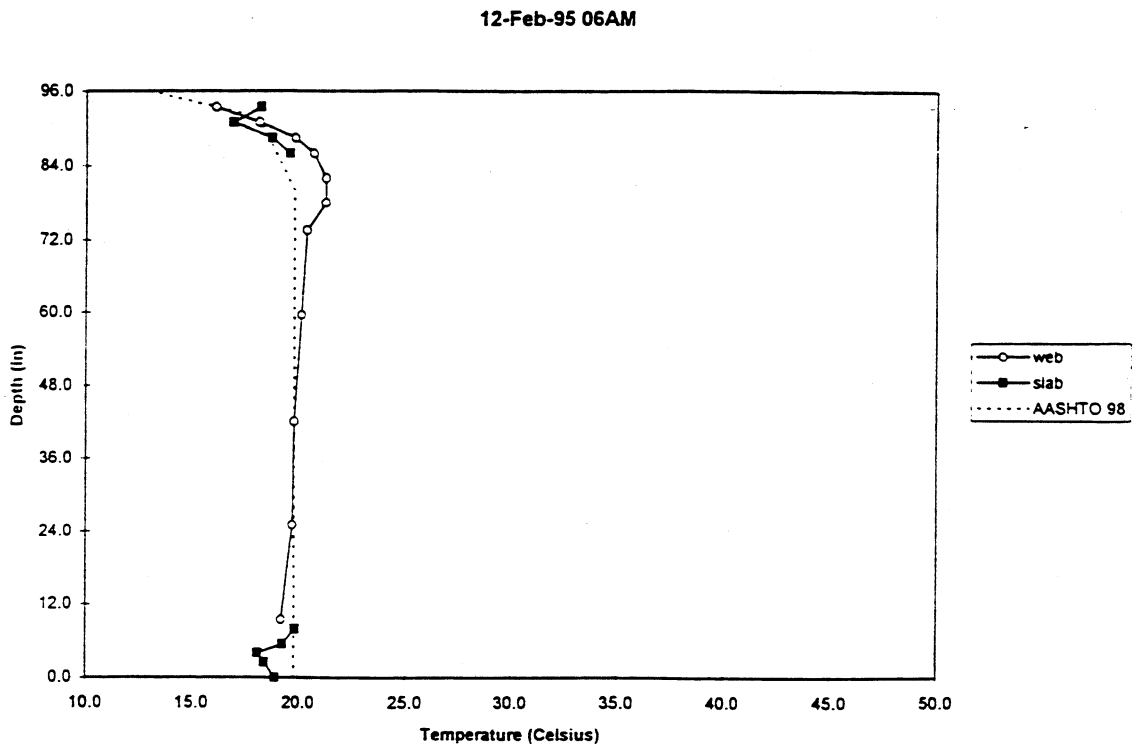
12-Feb-95 06AM
96.0
84.0
72.0
60.0
48.0
36.0
24.0
12.0
0.0
Depth (in)
10.0
15.0
20.0
25.0
30.0
35.0
40.0
45.0
50.0
Temperature (Celsius)
web
slab
AASHTO 98

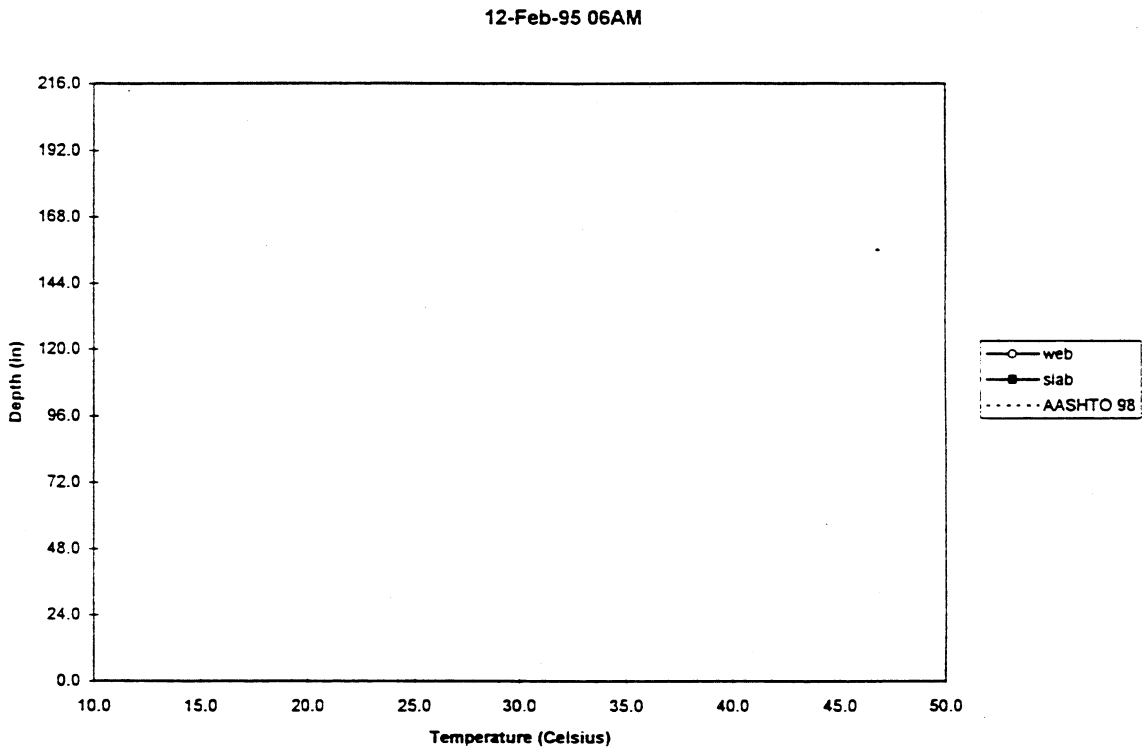
12-Feb-95 06AM
216.0
192.0
168.0
144.0
120.0
96.0
72.0
48.0
24.0
0.0
Depth (in)
10.0
15.0
20.0
25.0
30.0
35.0
40.0
45.0
50.0
Temperature (Celsius)
web
slab
AASHTO 98

Figure 8.97

Negative Thermal Gradient at Section E

15-Feb-95 06AM

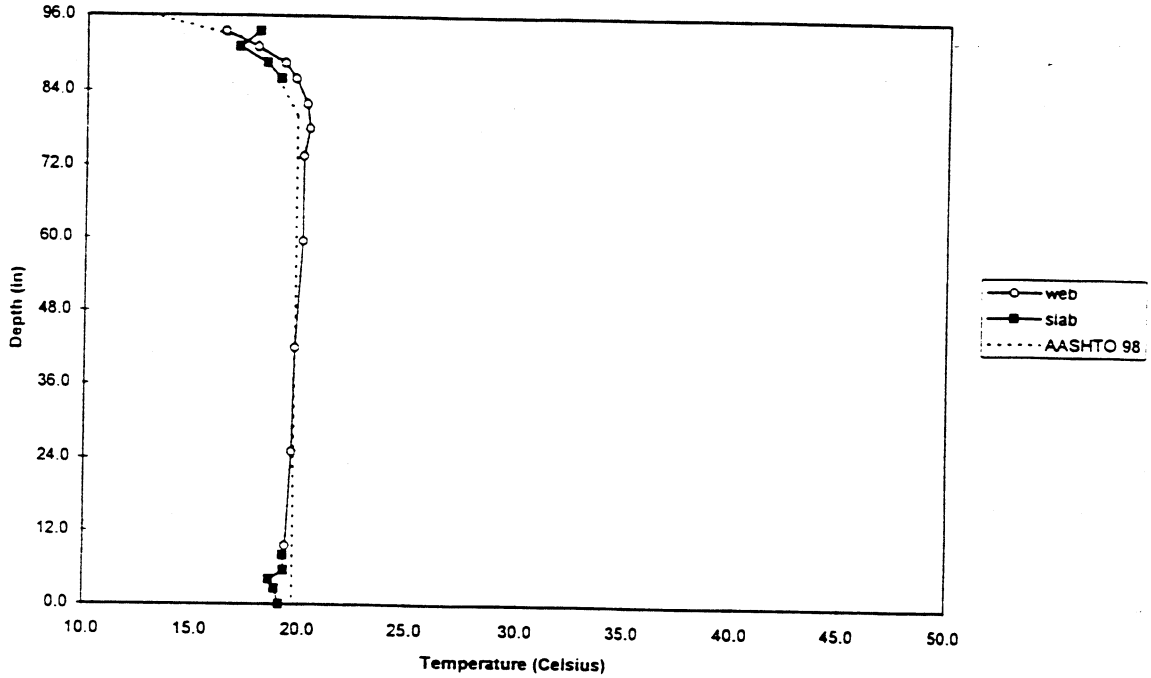

Negative Thermal Gradient at Section F

15-Feb-95 06AM

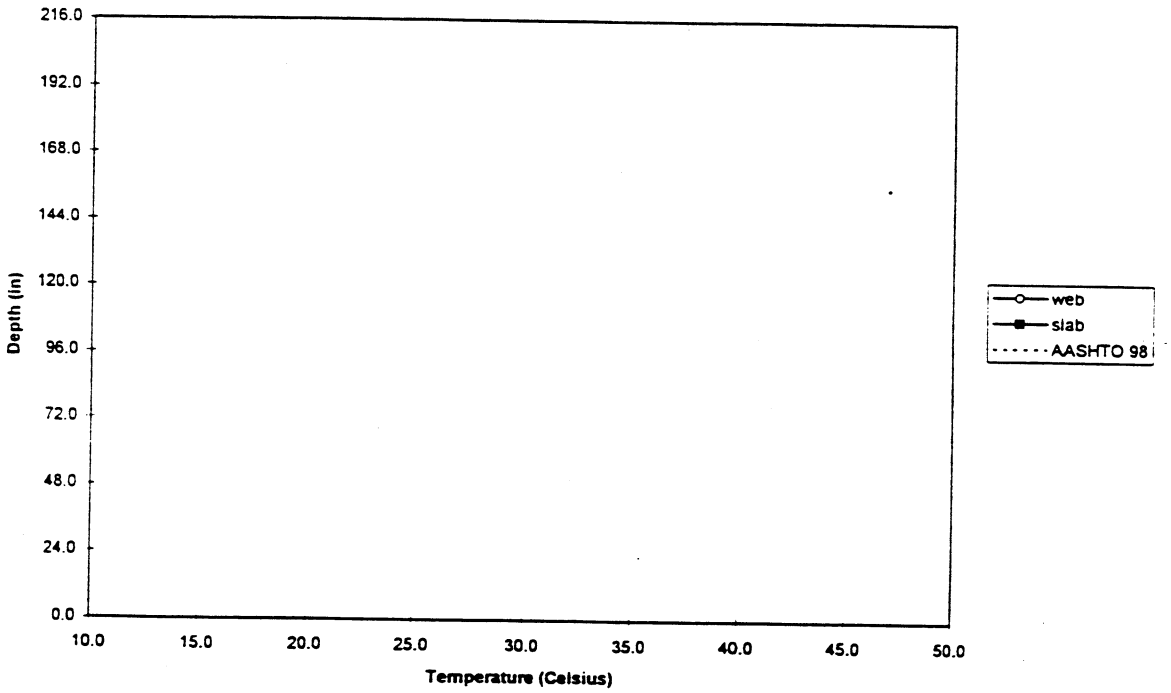

Figure 8.98

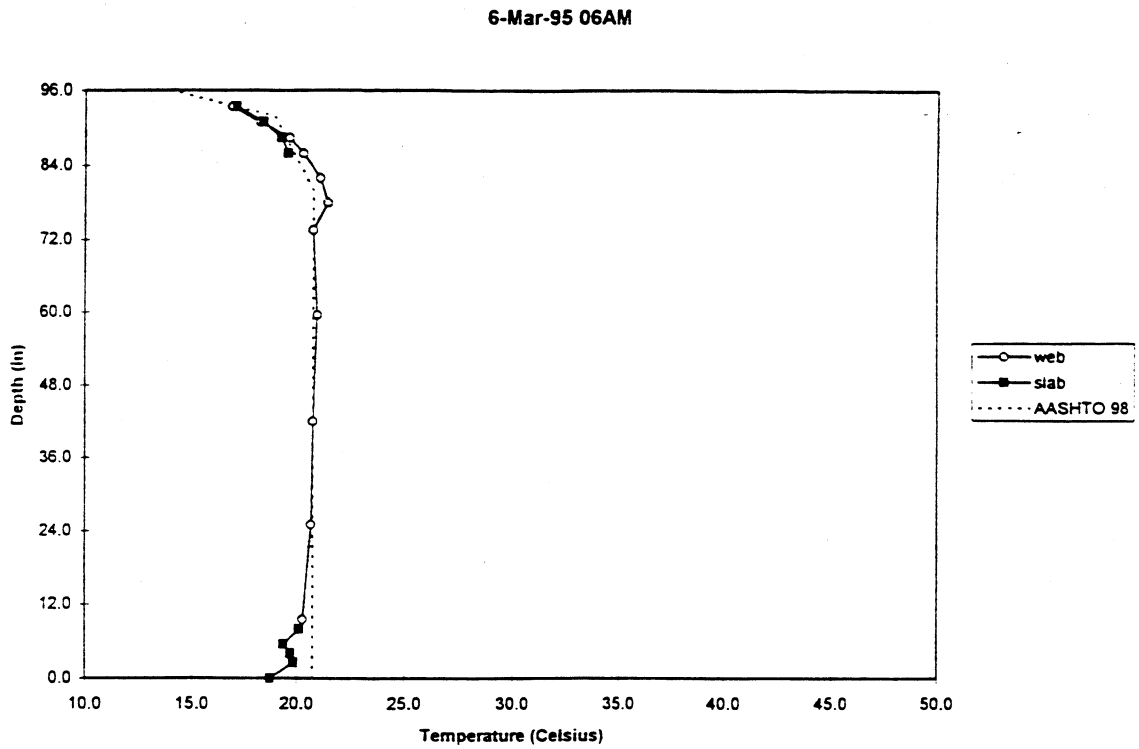
6-Mar-95 06AM
96.0
84.0
72.0
60.0
48.0
36.0
24.0
12.0
0.0
Depth (in)
10.0
15.0
20.0
25.0
30.0
35.0
40.0
45.0
50.0
Temperature (Celsius)
web
slab
AASHTO 98

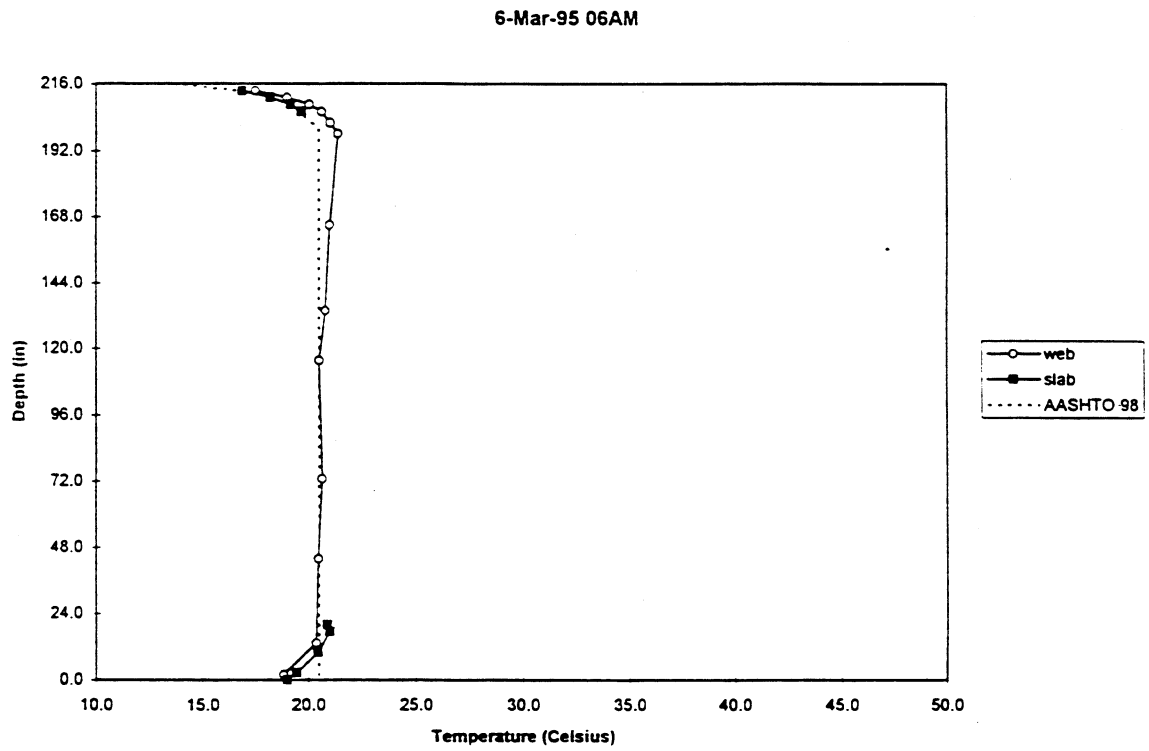
6-Mar-95 06AM
216.0
192.0
168.0
144.0
120.0
96.0
72.0
48.0
24.0
0.0
Depth (in)
10.0
15.0
20.0
25.0
30.0
35.0
40.0
45.0
50.0
Temperature (Celsius)
web
slab
AASHTO 98

Figure 8.99

Negative Thermal Gradient at Section E

7-May-95 06AM

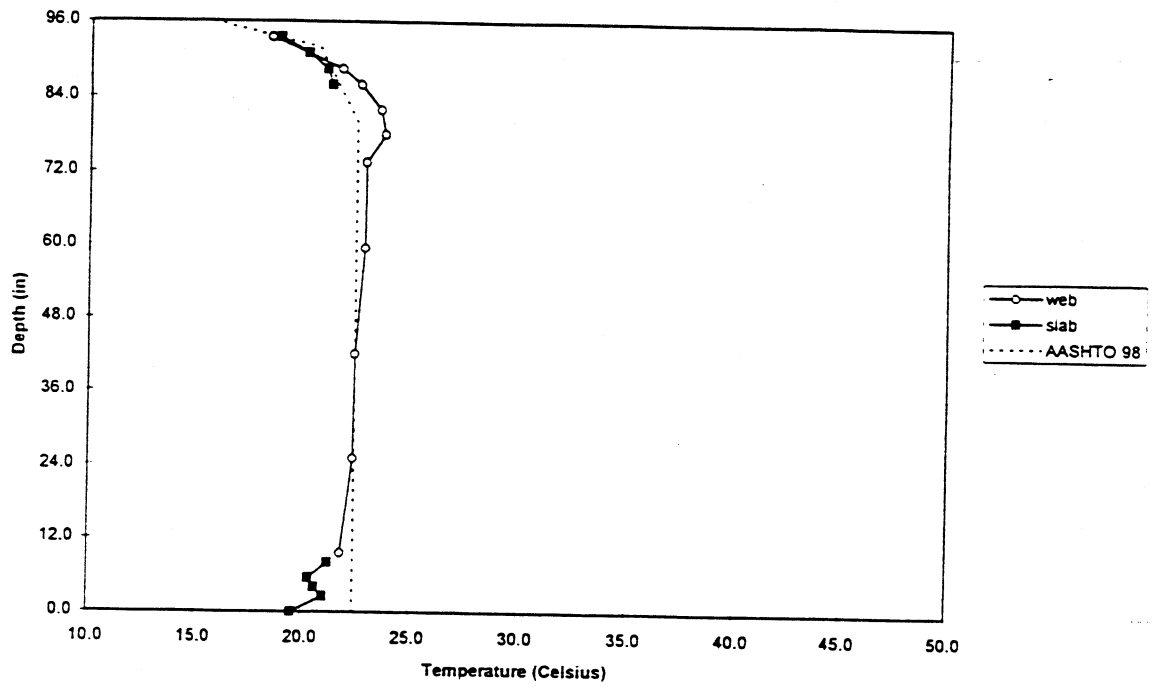

Negative Thermal Gradient at Section F

7-May-95 06AM

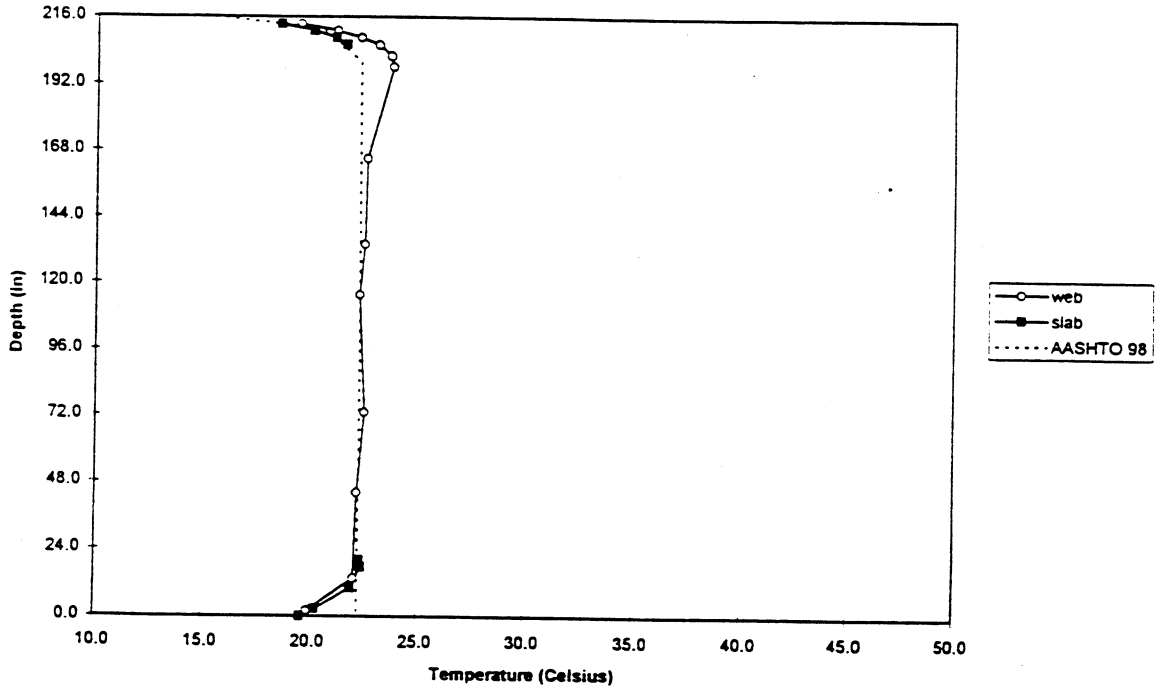

Figure 8.100

Negative Thermal Gradient at Section E

20-Dec-95 06AM

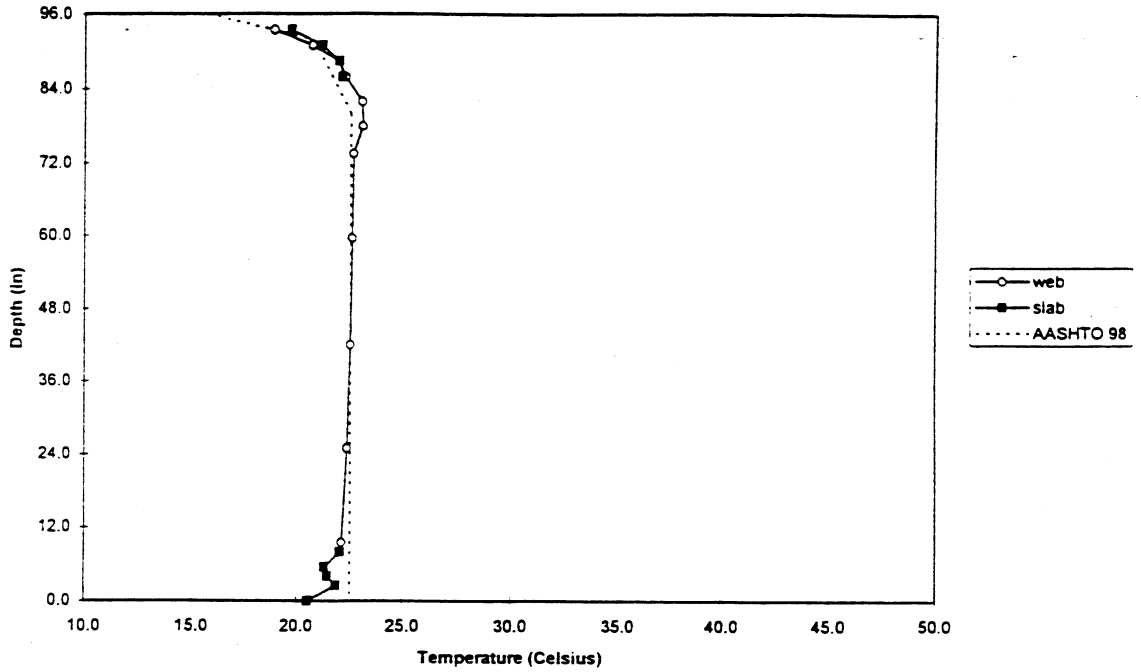

Negative Thermal Gradient at Section F

20-Dec-95 06AM

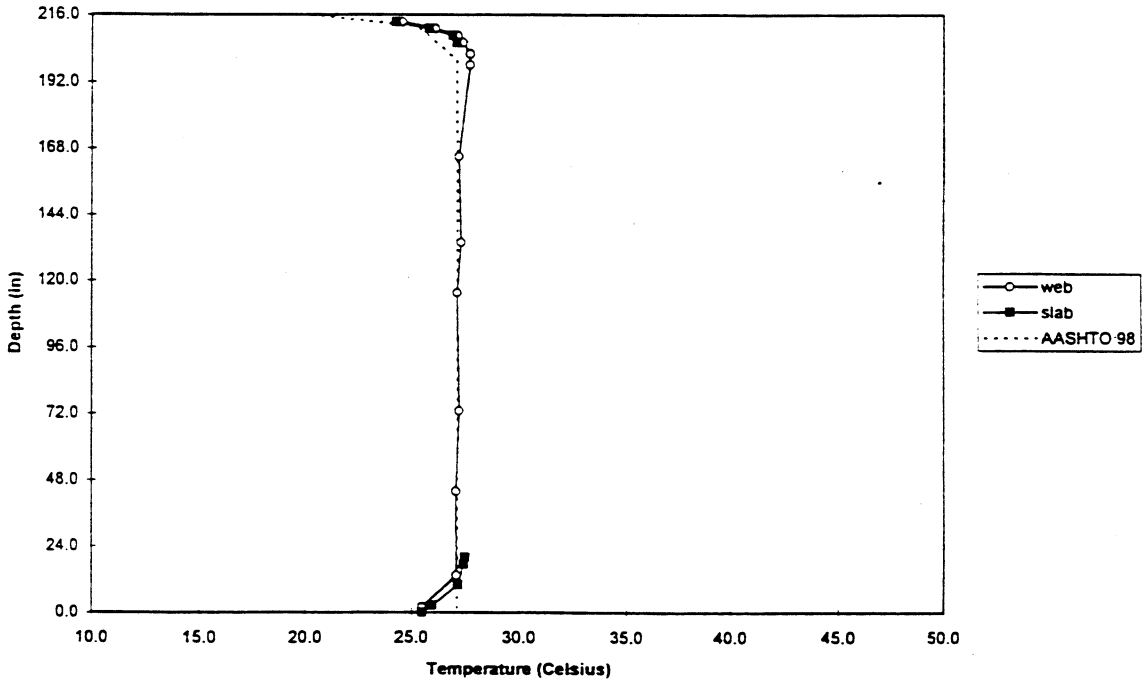

Figure 8.101

Negative Thermal Gradient at Section E

21-Dec-95 06AM

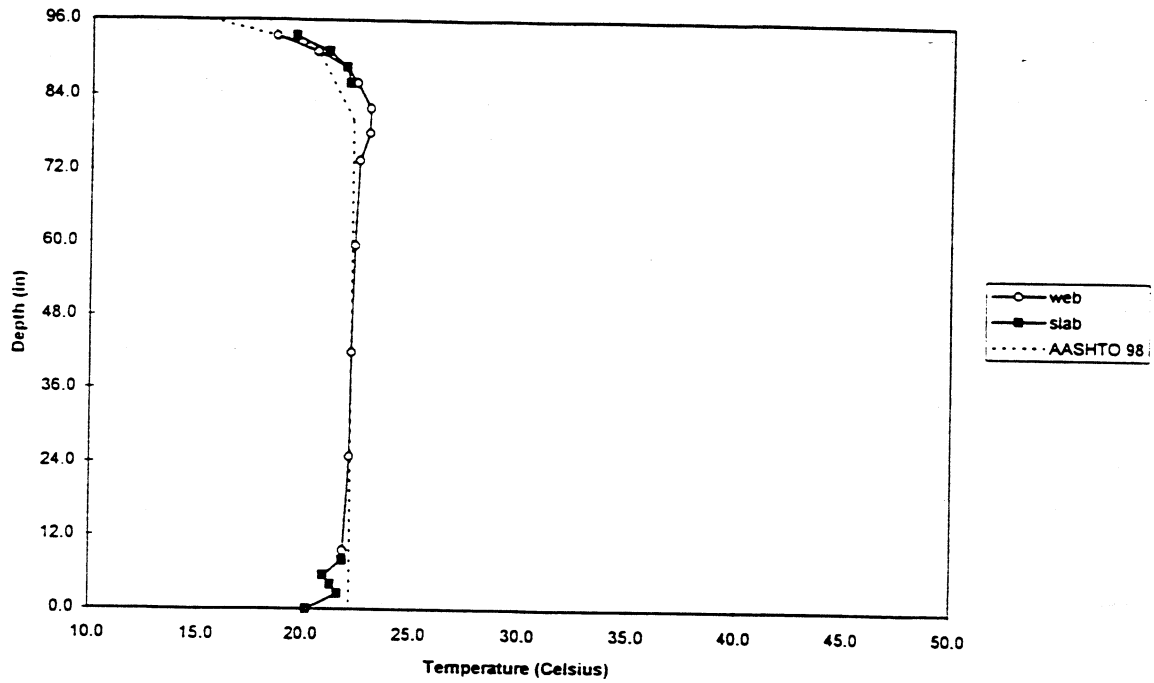

Negative Thermal Gradient at Section F

21-Dec-95 06AM

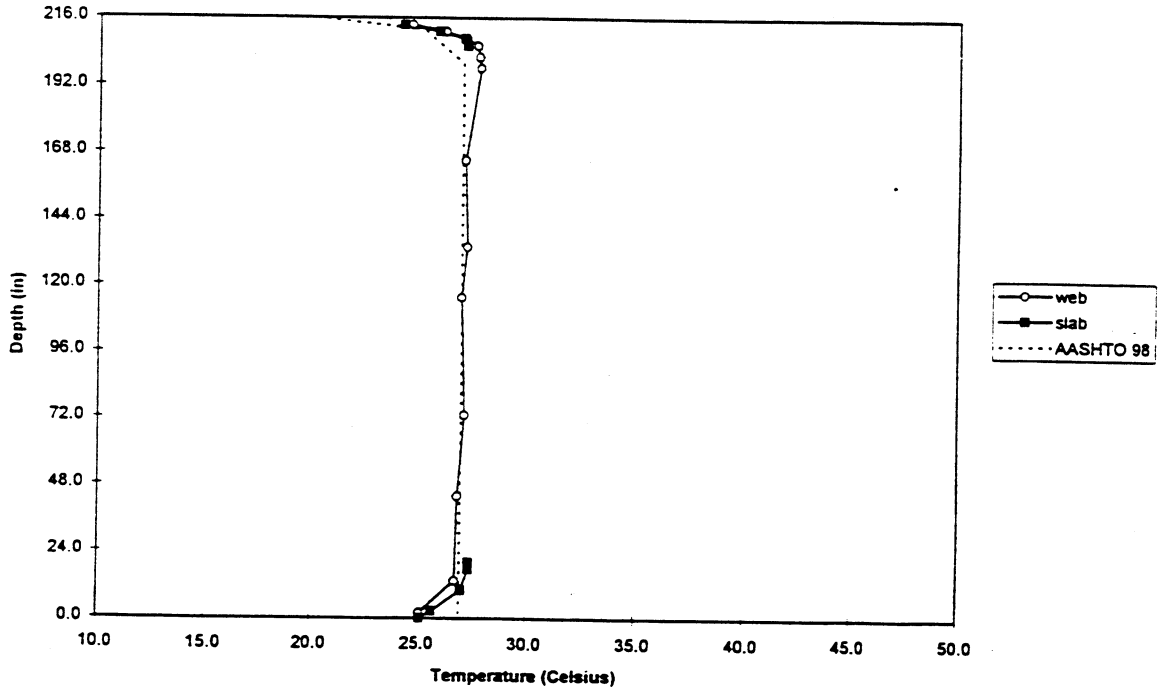

Figure 8.102

Positive Thermal Gradient at Section E

1-Jun-96 06PM

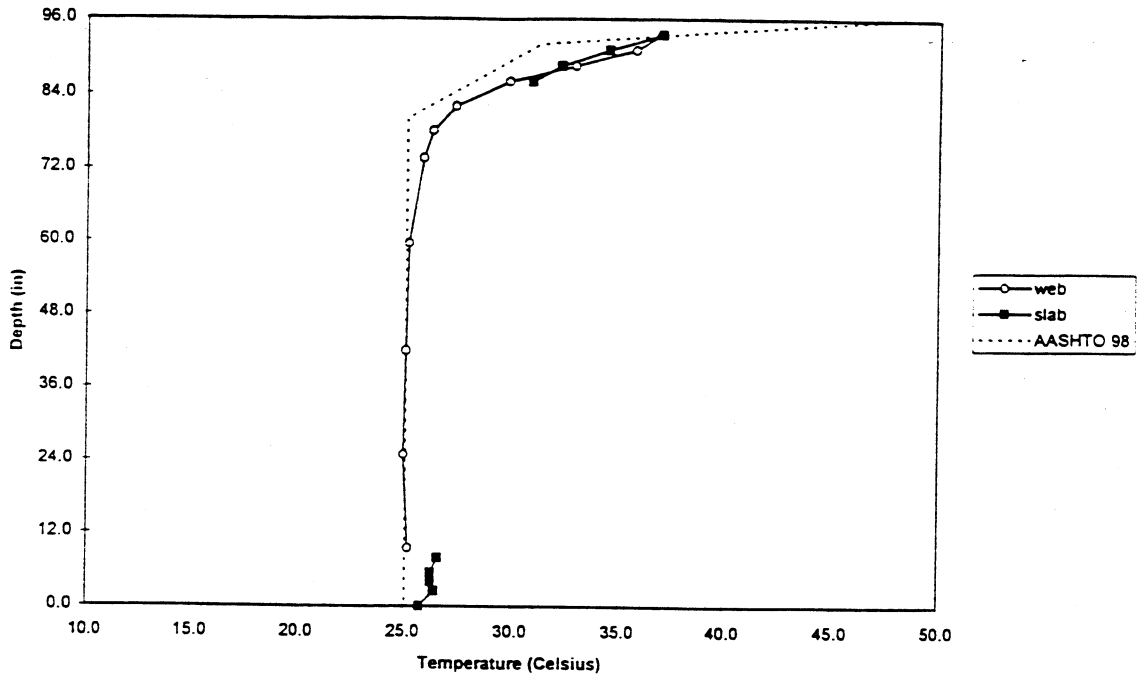

Positive Thermal Gradient at Section F

1-Jun-96 06PM

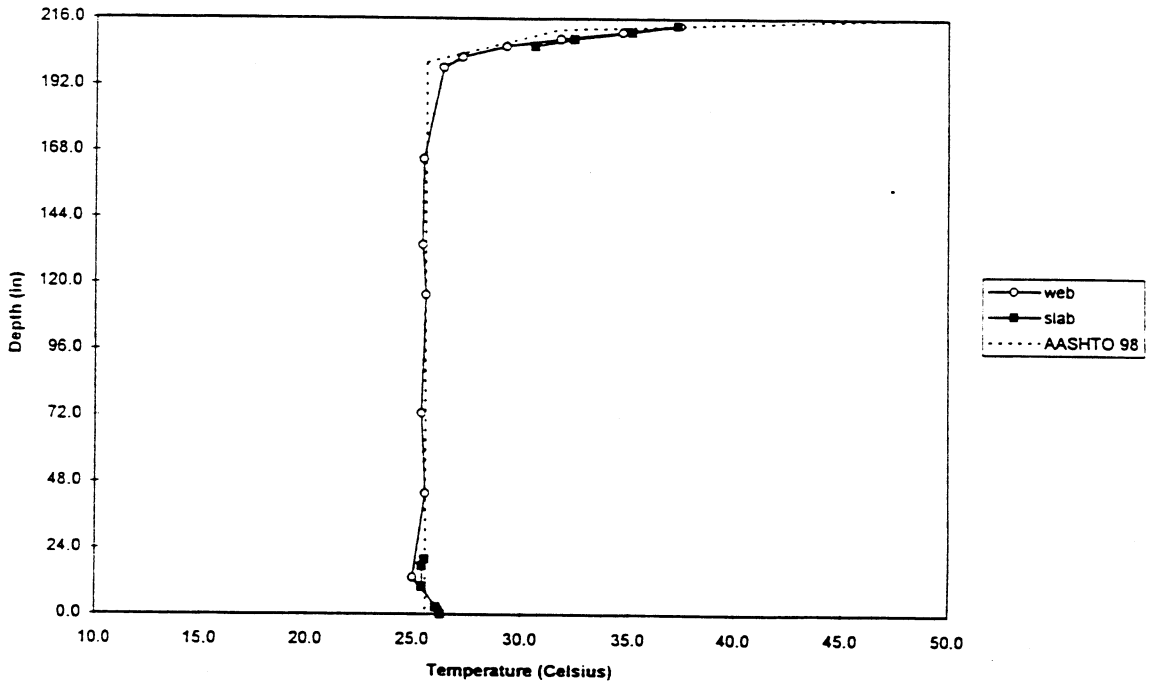

Figure 8.103

Positive Thermal Gradient at Section E

3-Jun-96 06PM

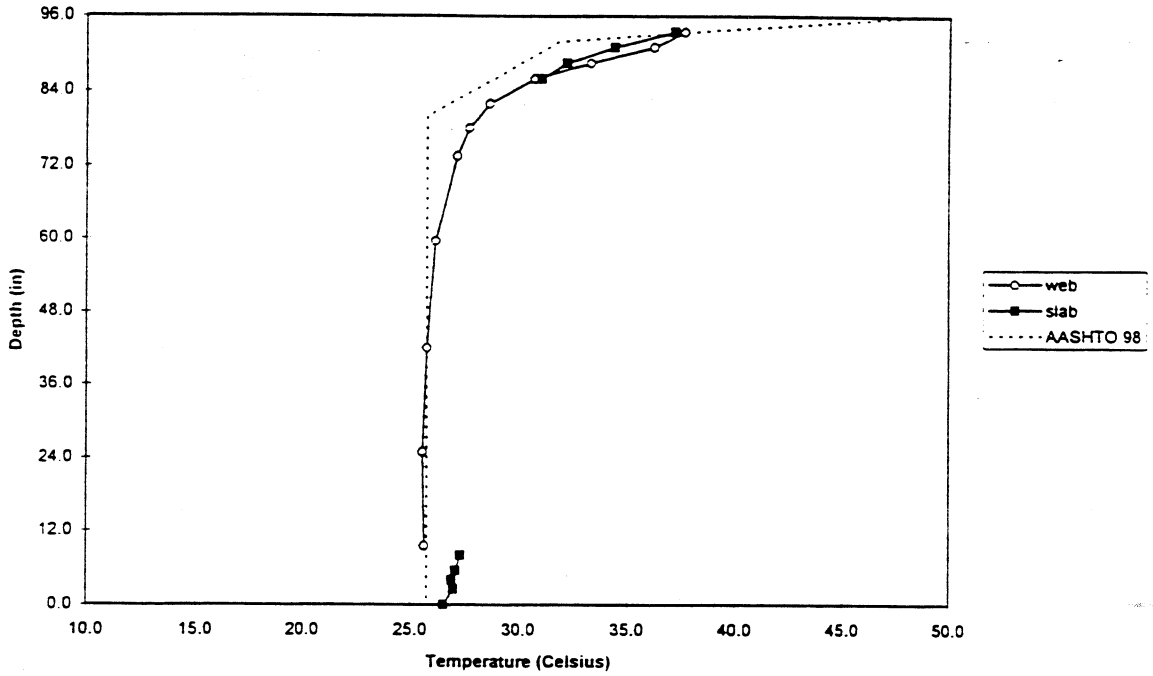

Positive Thermal Gradient at Section F

3-Jun-96 06PM

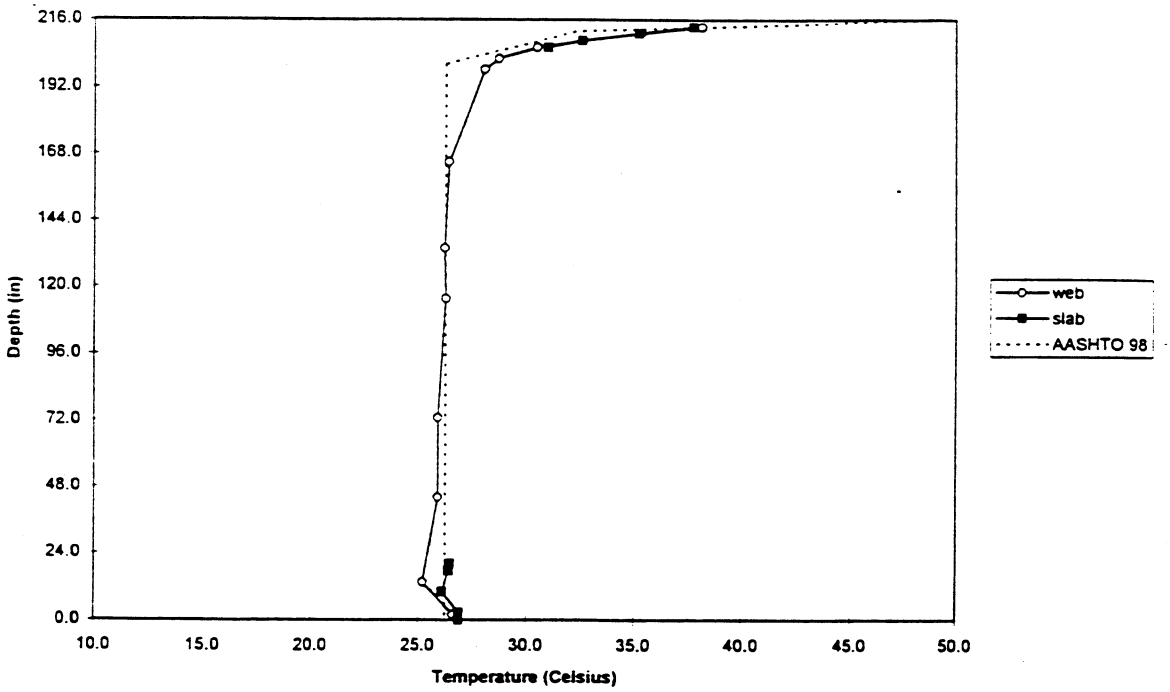

Figure 8.104

Positive Thermal Gradient at Section E

9-Jul-96 06PM

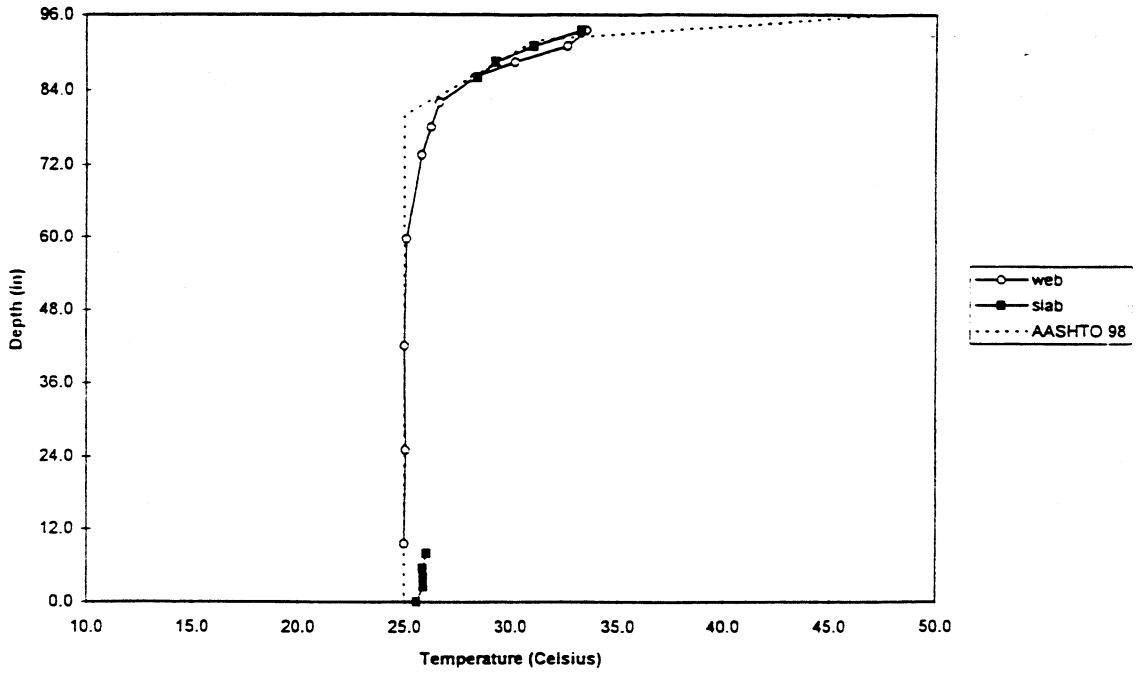

Positive Thermal Gradient at Section F

9-Jul-96 06PM

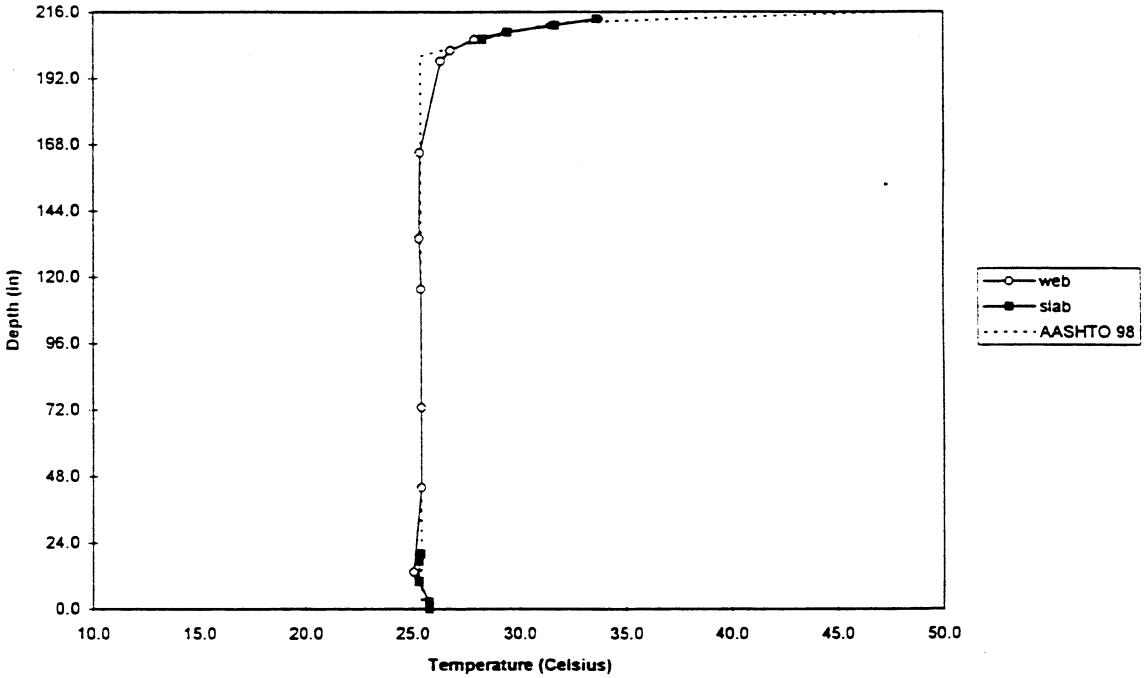

Figure 8.105

Positive Thermal Gradient at Section E

29-Jul-96 06PM

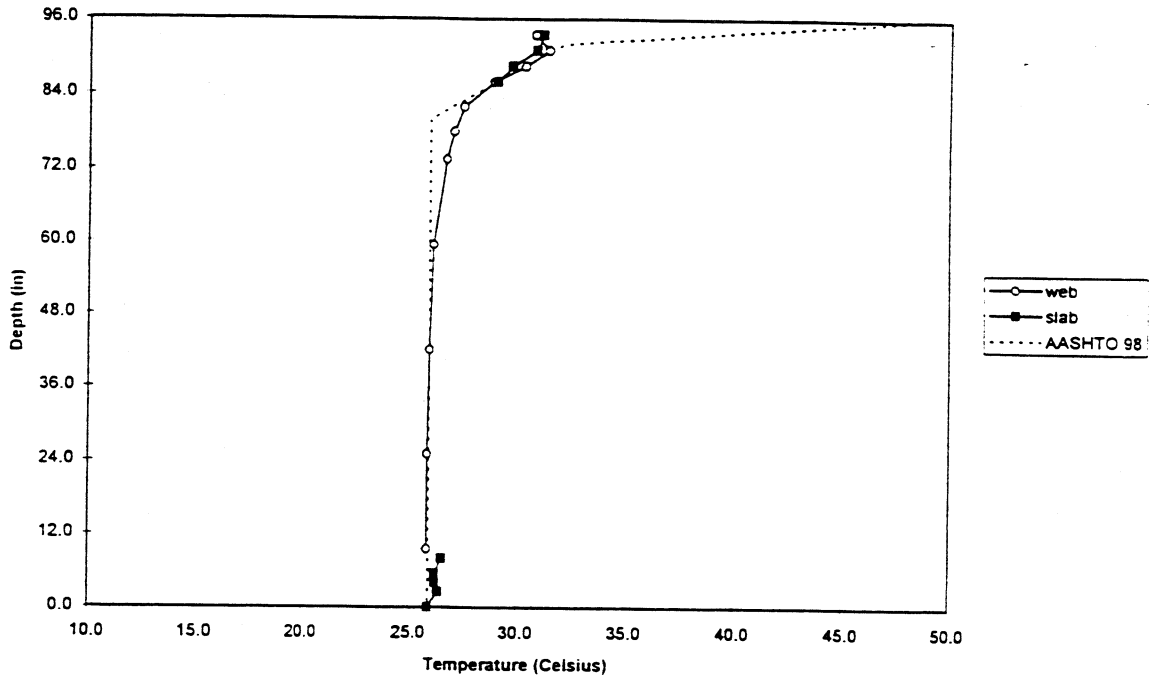

Positive Thermal Gradient at Section F

29-Jul-96 06PM

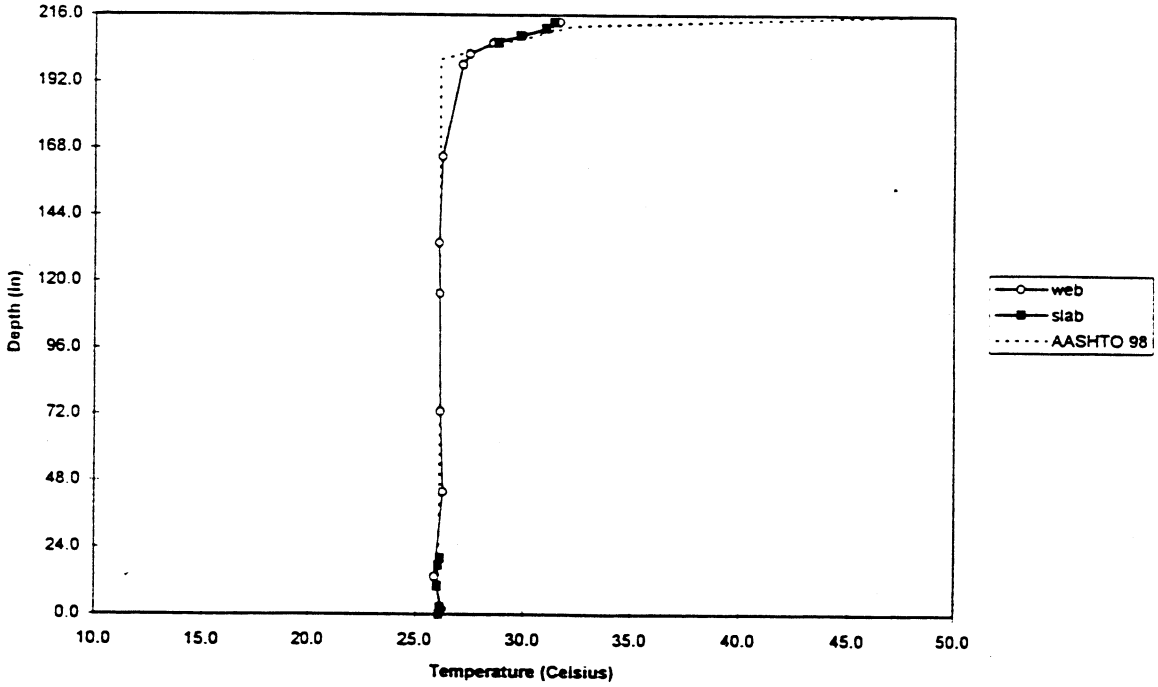

Figure 8.106

9-Aug-96 06PM

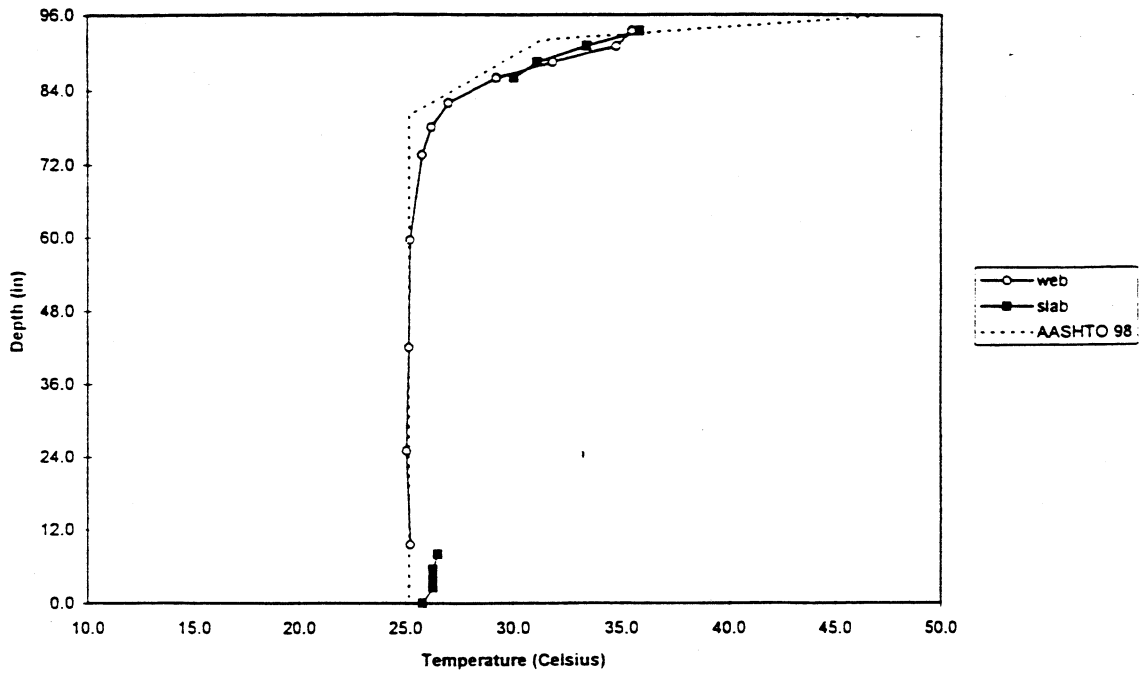

9-Aug-96 06PM

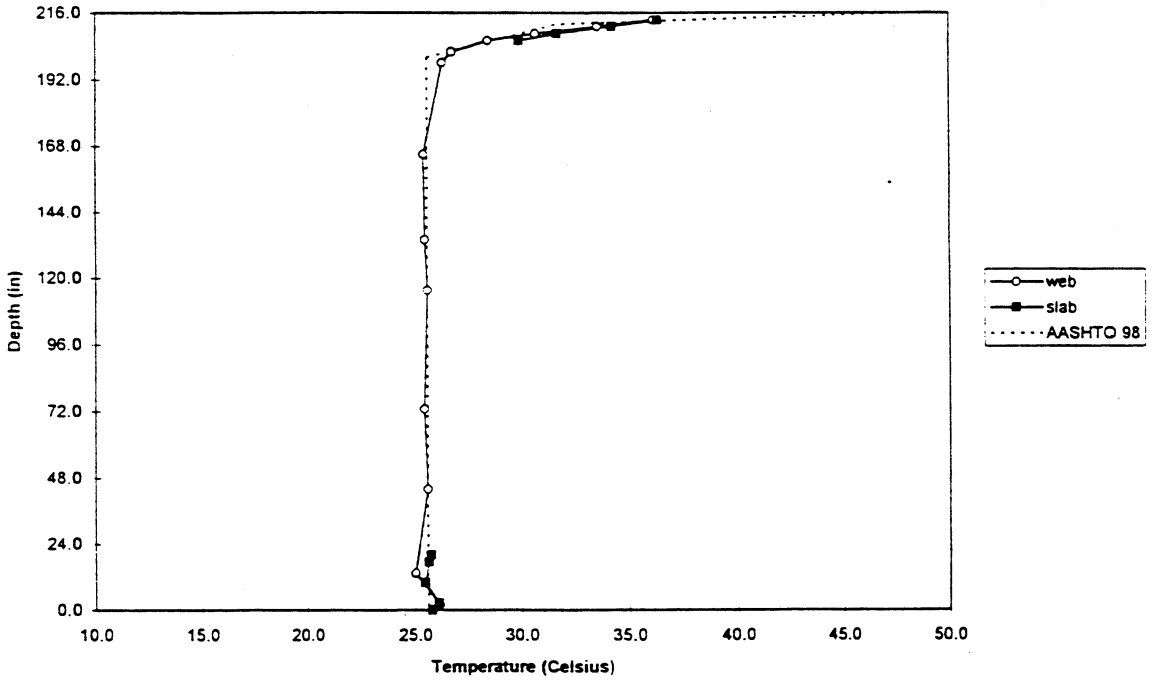

Figure 8.107

Positive Thermal Gradient at Section E

23-Aug-96 06PM

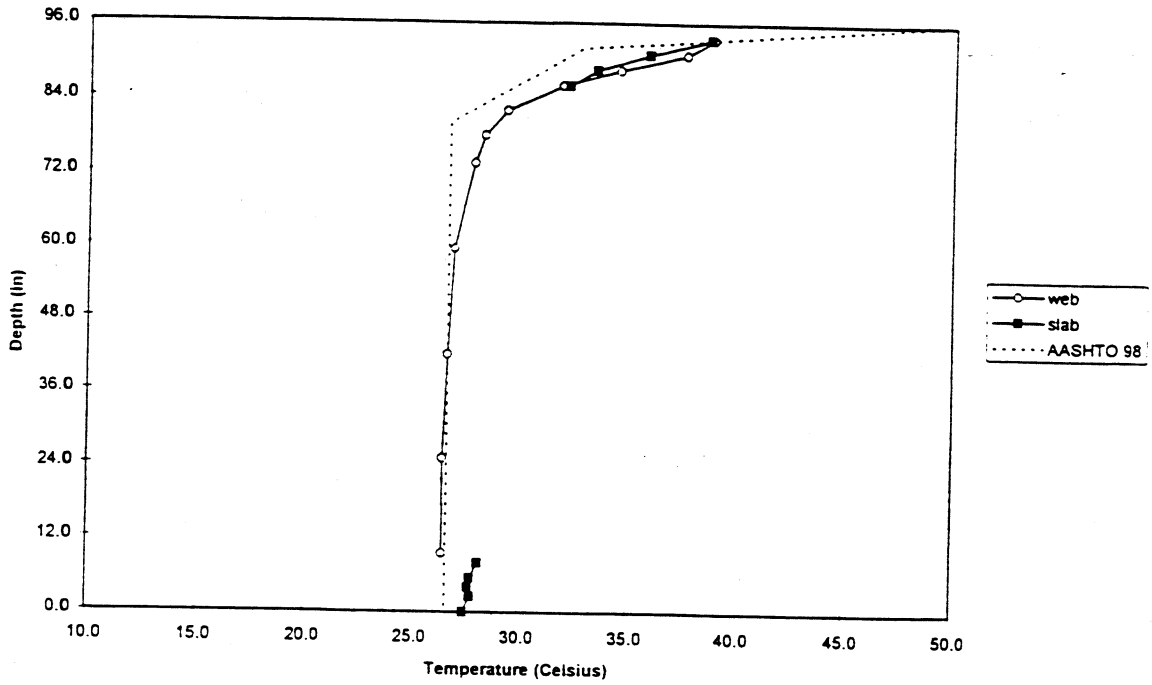

Positive Thermal Gradient at Section F

23-Aug-96 06PM

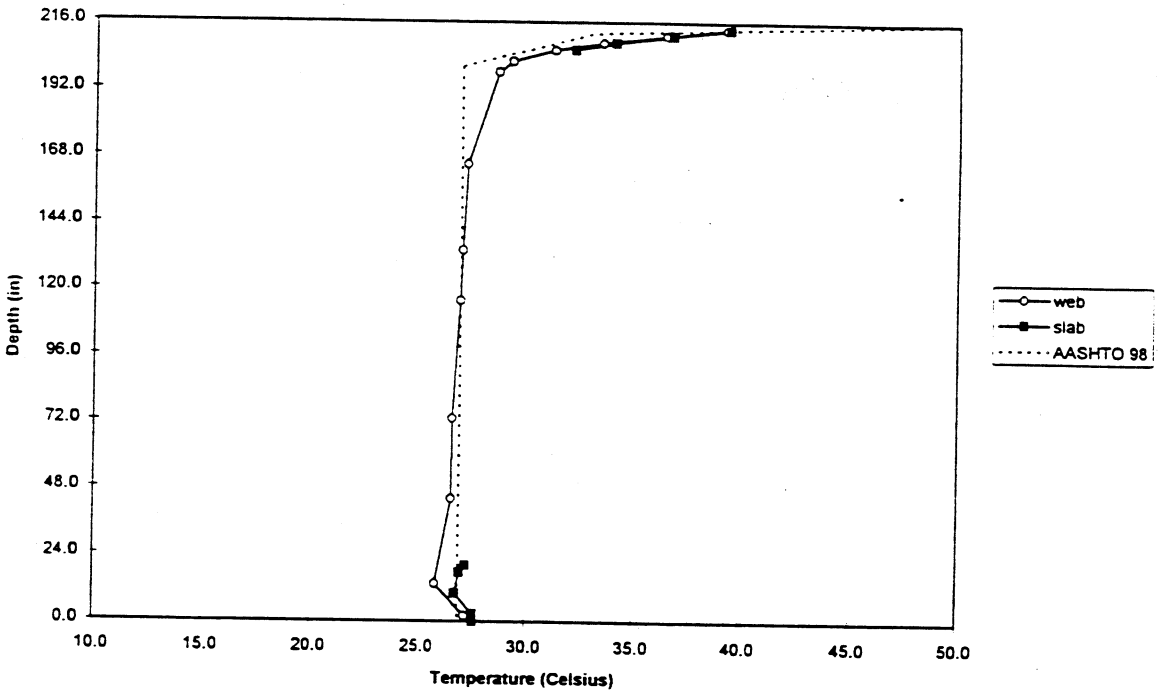

Figure 8.108

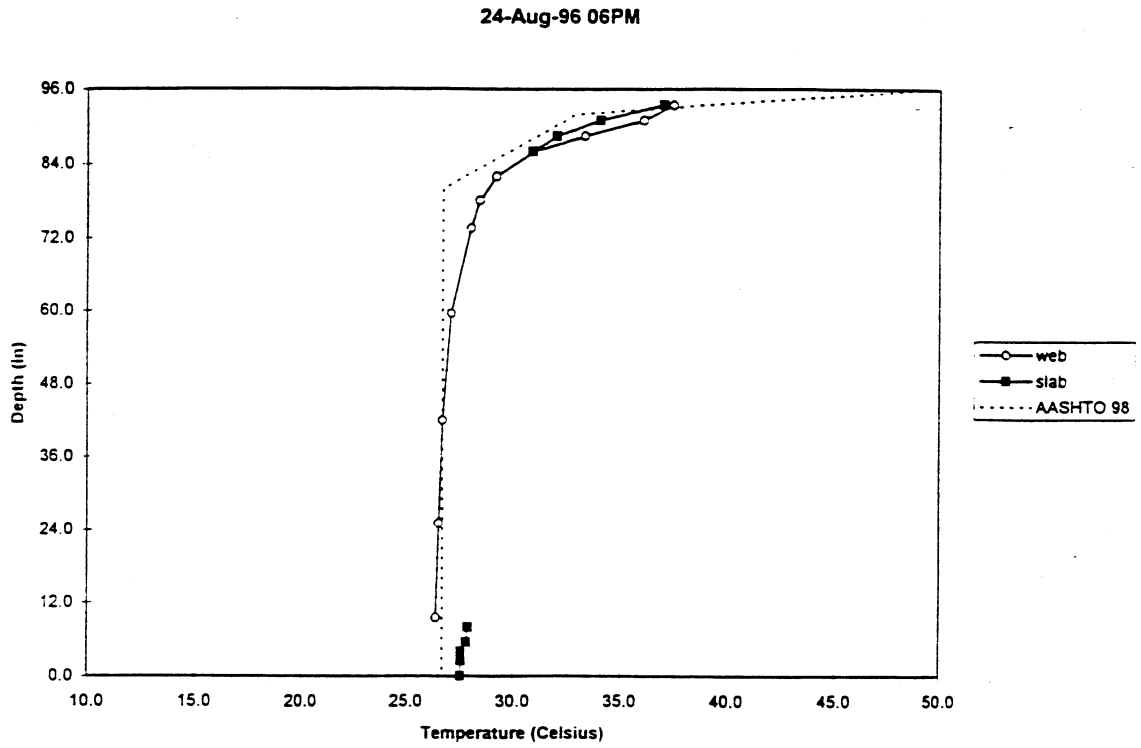
24-Aug-96 06PM
96.0
84.0
72.0
60.0
48.0
36.0
24.0
12.0
0.0
Depth (in)
10.0
15.0
20.0
25.0
30.0
35.0
40.0
45.0
50.0
Temperature (Celsius)
web
slab
AASHTO 98

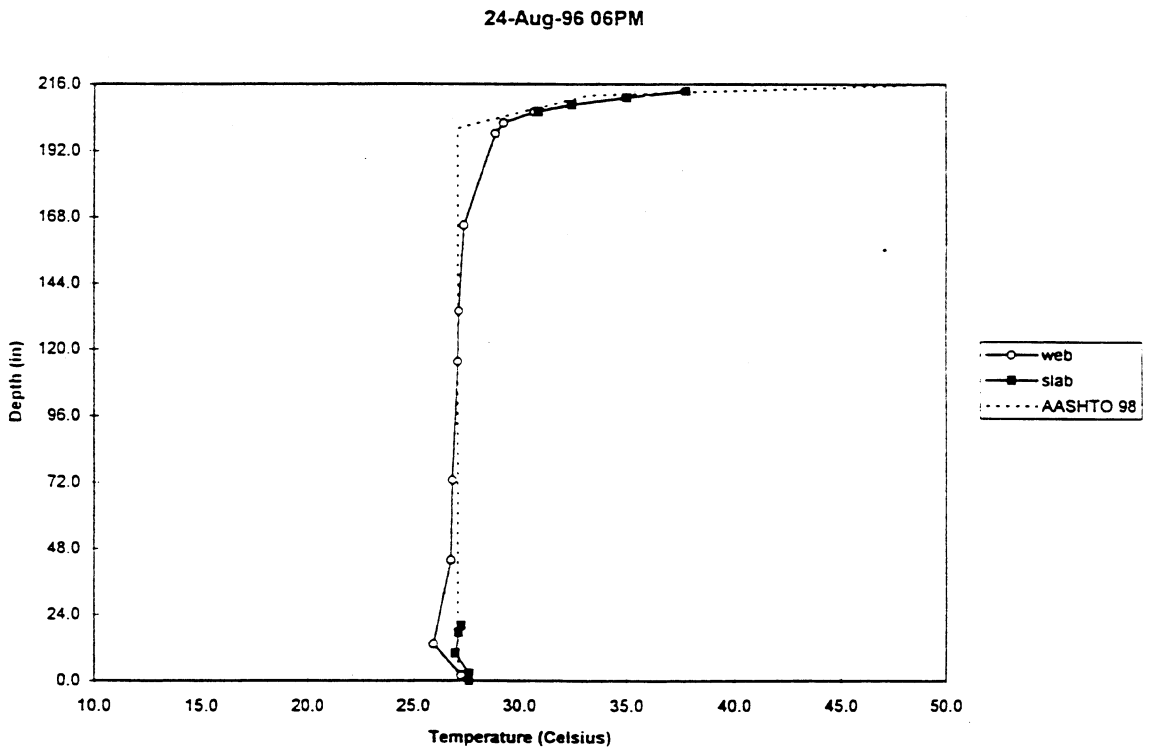
24-Aug-96 06PM
216.0
192.0
168.0
144.0
120.0
96.0
72.0
48.0
24.0
0.0
Depth (in)
10.0
15.0
20.0
25.0
30.0
35.0
40.0
45.0
50.0
Temperature (Celsius)
web
slab
AASHTO 98

Figure 8.109

Positive Thermal Gradient at Section E

2-Sep-96 06PM

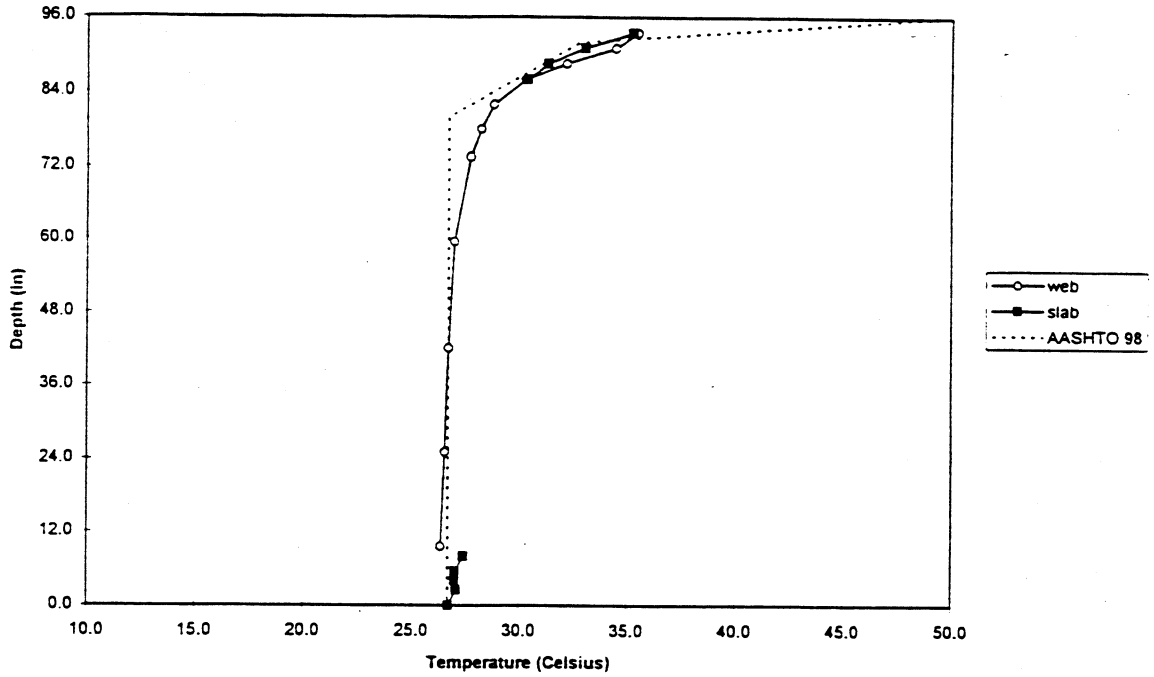

Positive Thermal Gradient at Section F

2-Sep-96 06PM

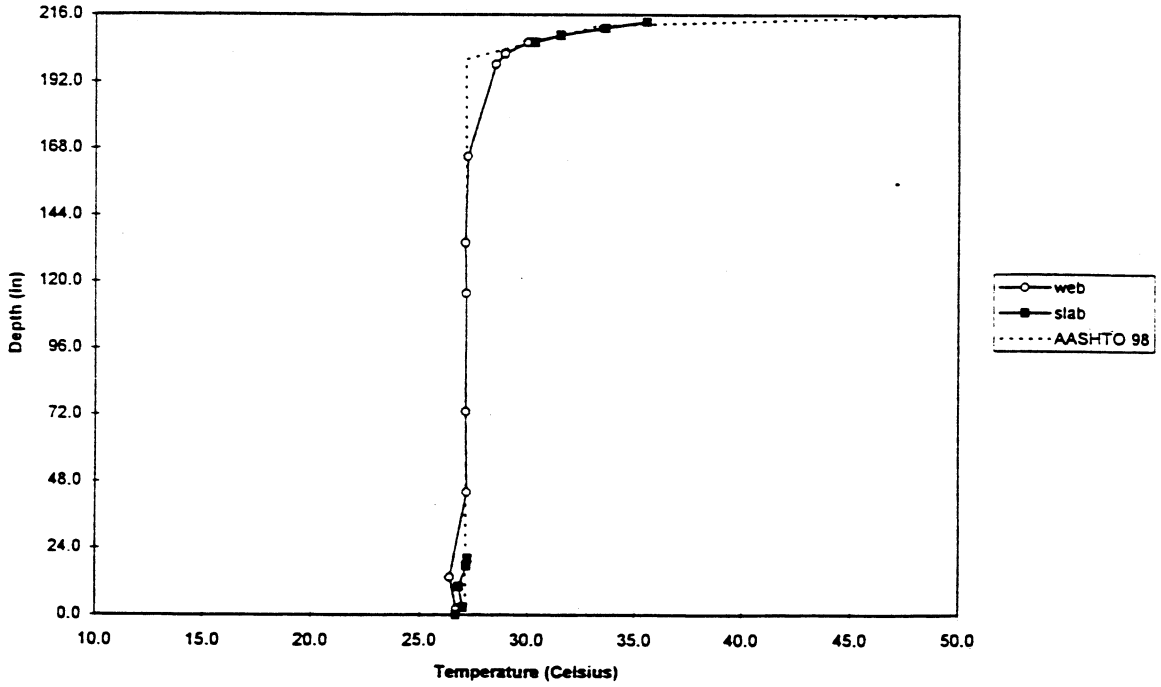

Figure 8.110

Negative Thermal Gradient at Section E

2-Jan-96 06AM

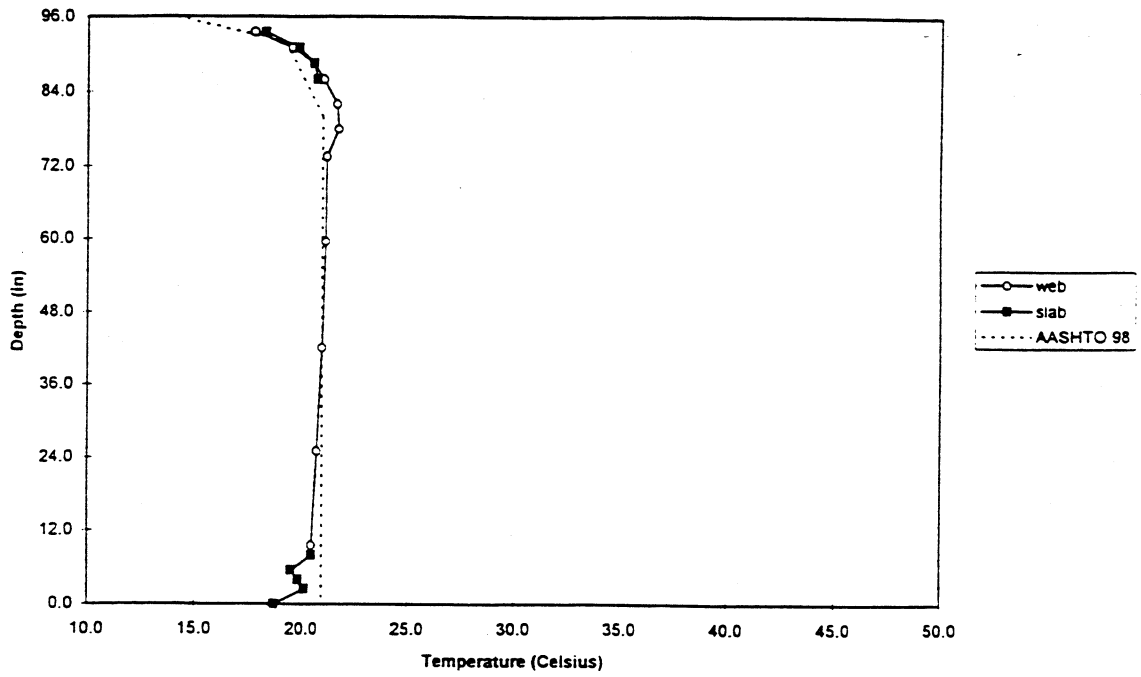

Negative Thermal Gradient at Section F

2-Jan-96 06AM

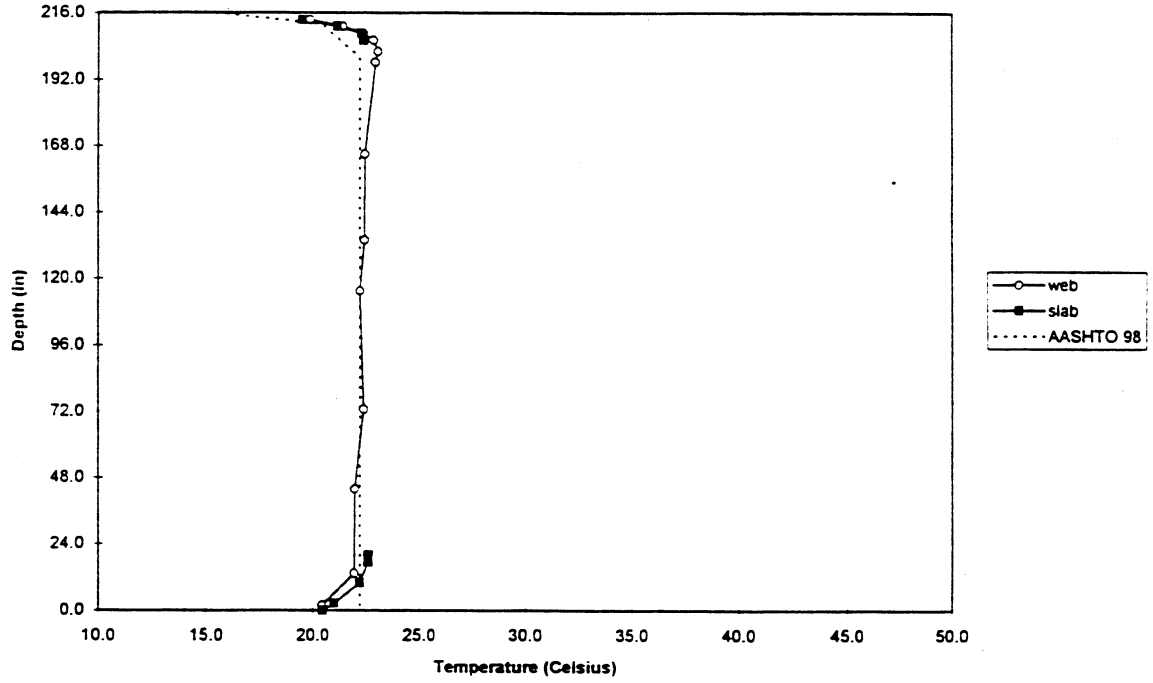

Figure 8.111

Negative Thermal Gradient at Section E

11-Jan-96 06AM

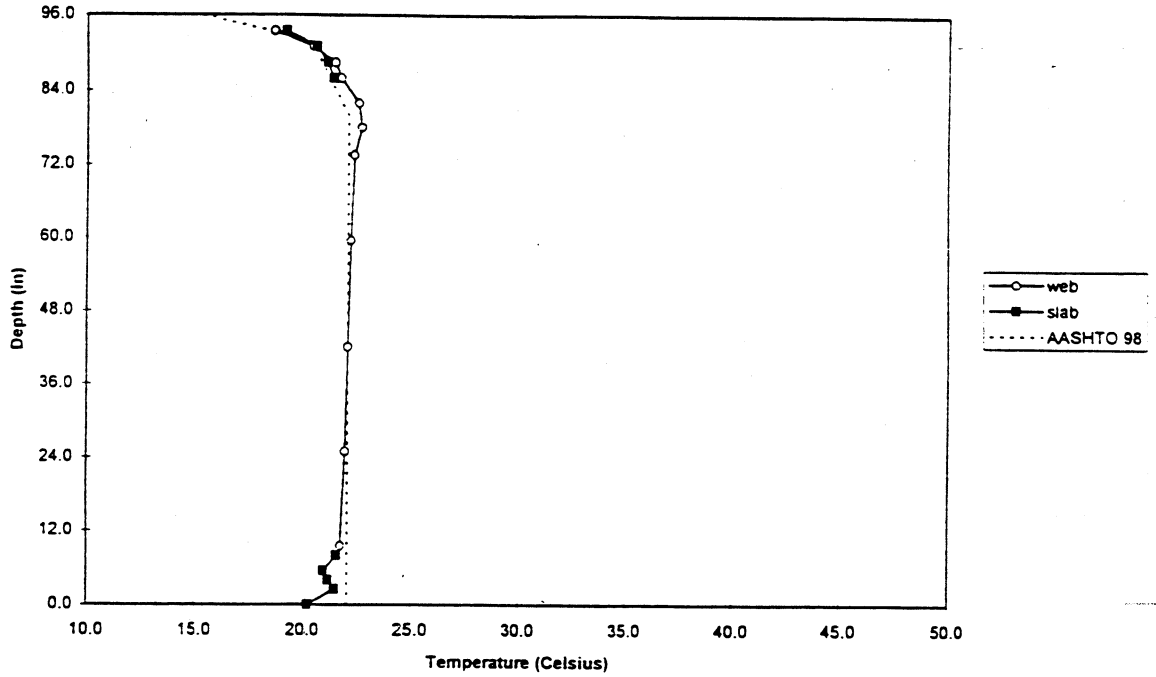

Negative Thermal Gradient at Section F

11-Jan-96 06AM

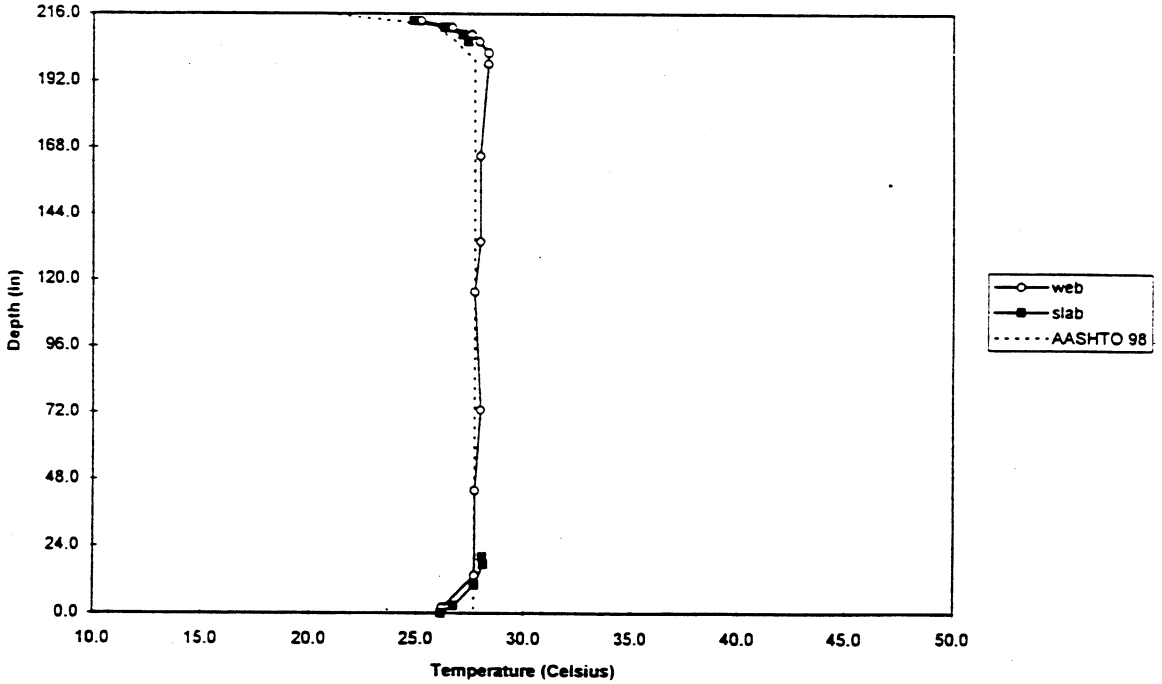

Figure 8.112

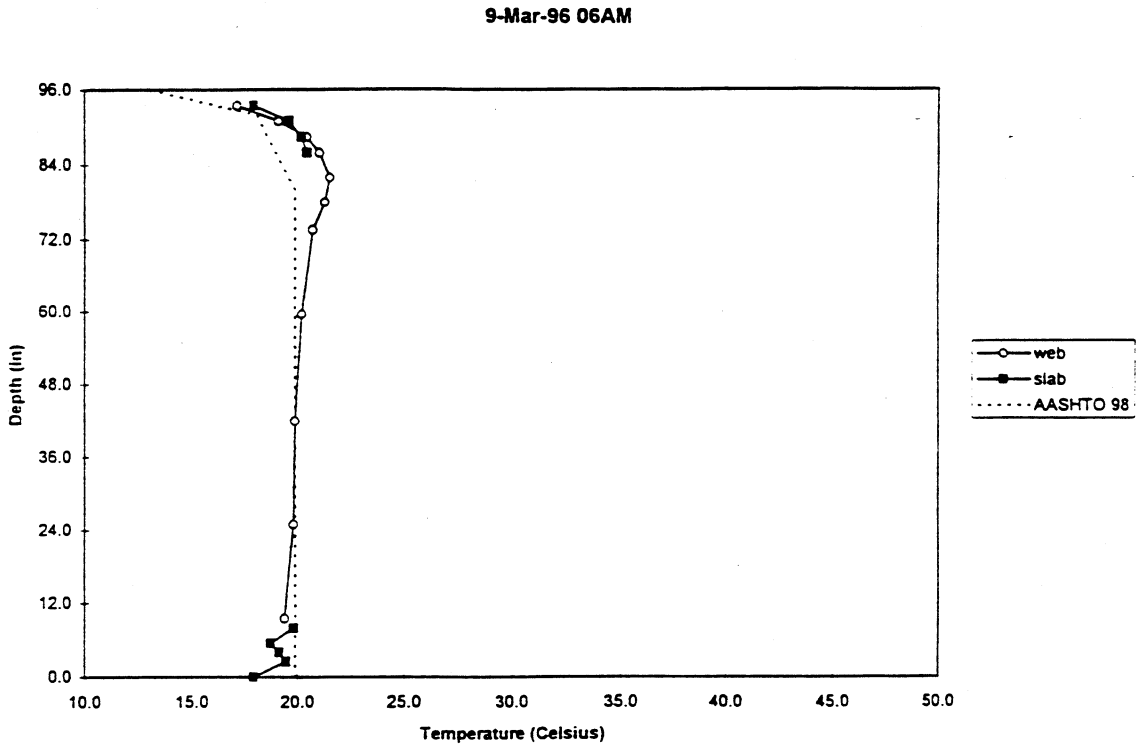
9-Mar-96 06AM
96.0
84.0
72.0
60.0
48.0
36.0
24.0
12.0
0.0
Depth (in)
10.0
15.0
20.0
25.0
30.0
35.0
40.0
45.0
50.0
Temperature (Celsius)
web
slab
AASHTO 98

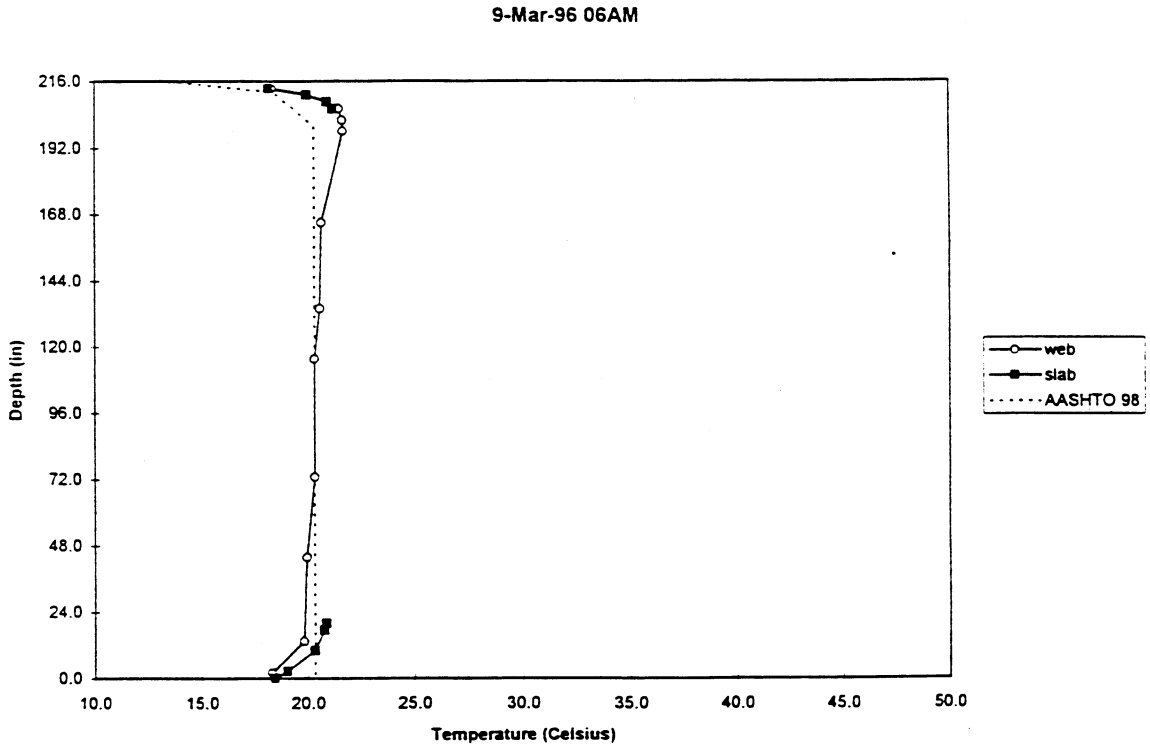
9-Mar-96 06AM
216.0
192.0
168.0
144.0
120.0
96.0
72.0
48.0
24.0
0.0
Depth (in)
10.0
15.0
20.0
25.0
30.0
35.0
40.0
45.0
50.0
Temperature (Celsius)
web
slab
AASHTO 98

Figure 8.113

Negative Thermal Gradient at Section E

27-Mar-96 06AM

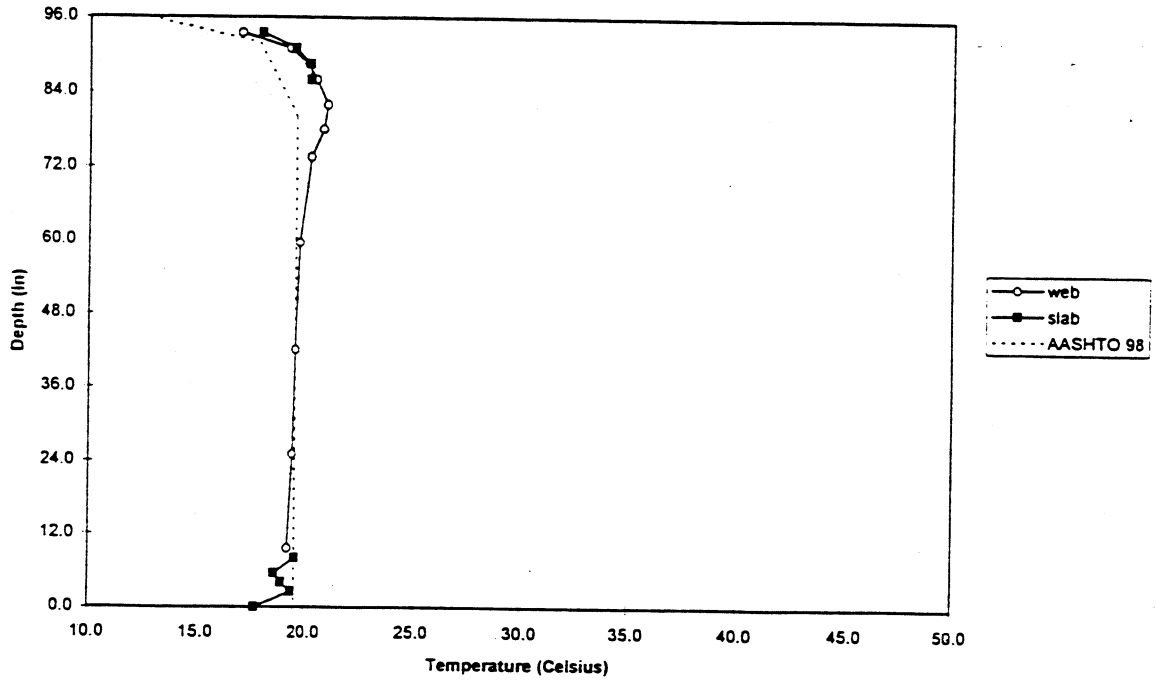

Negative Thermal Gradient at Section F

27-Mar-96 06AM

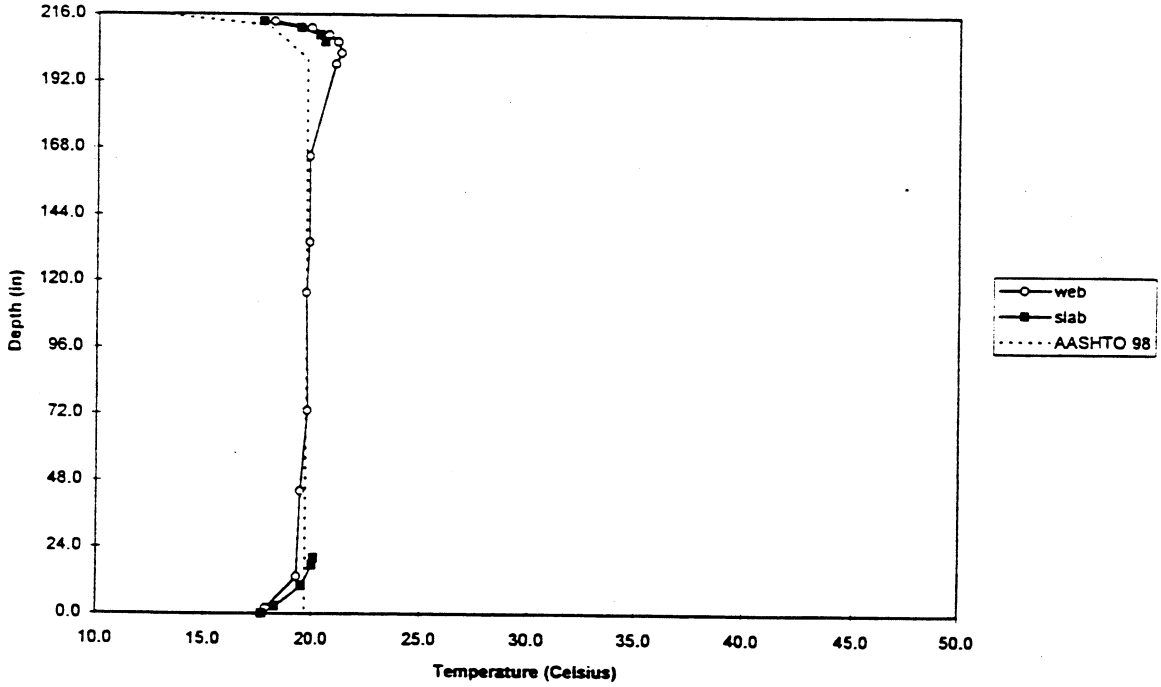

Figure 8.114

Negative Thermal Gradient at Section E

15-Apr-96 06AM

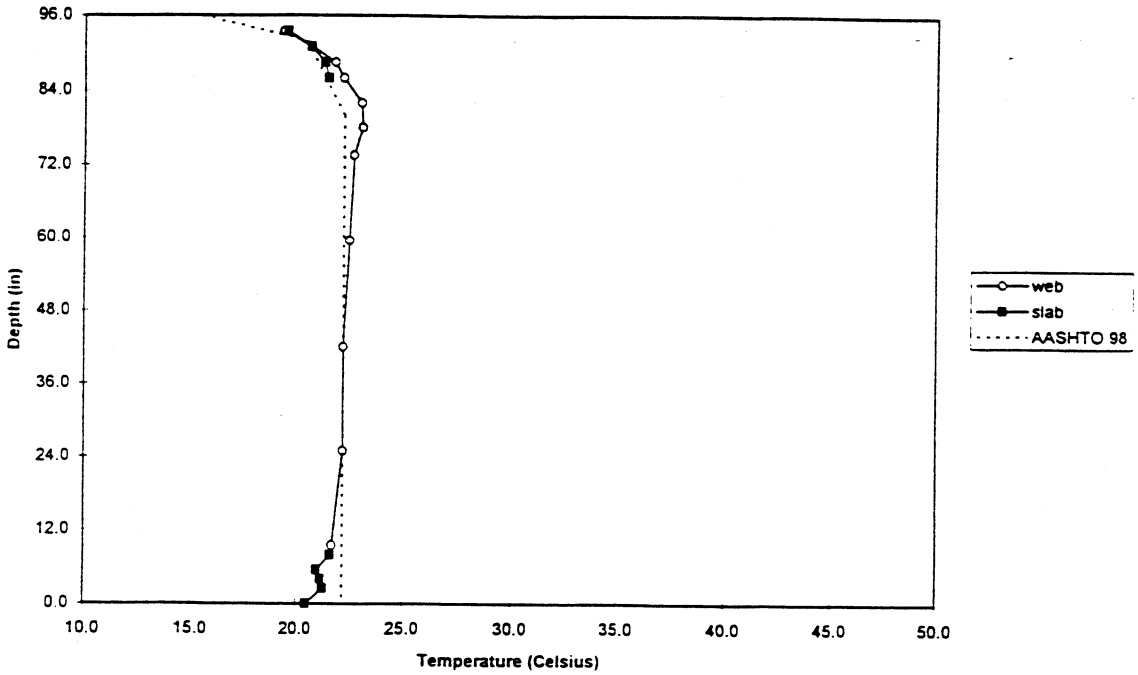

Negative Thermal Gradient at Section F

15-Apr-96 06AM

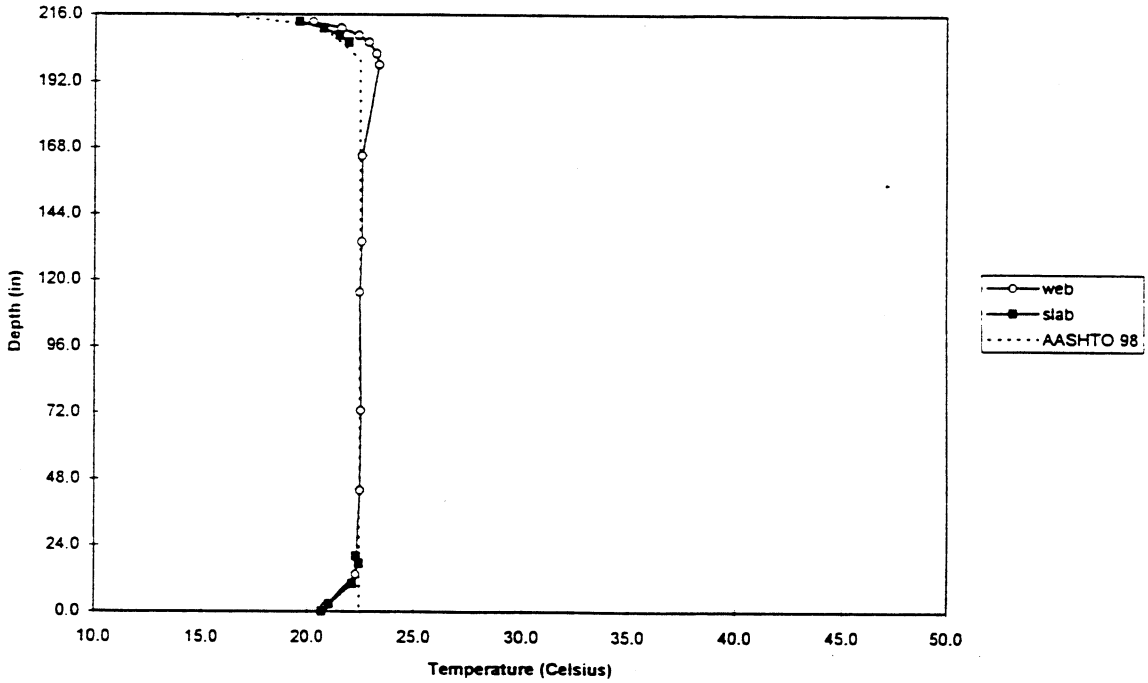

Figure 8.115

Negative Thermal Gradient at Section E

27-Apr-96 06AM

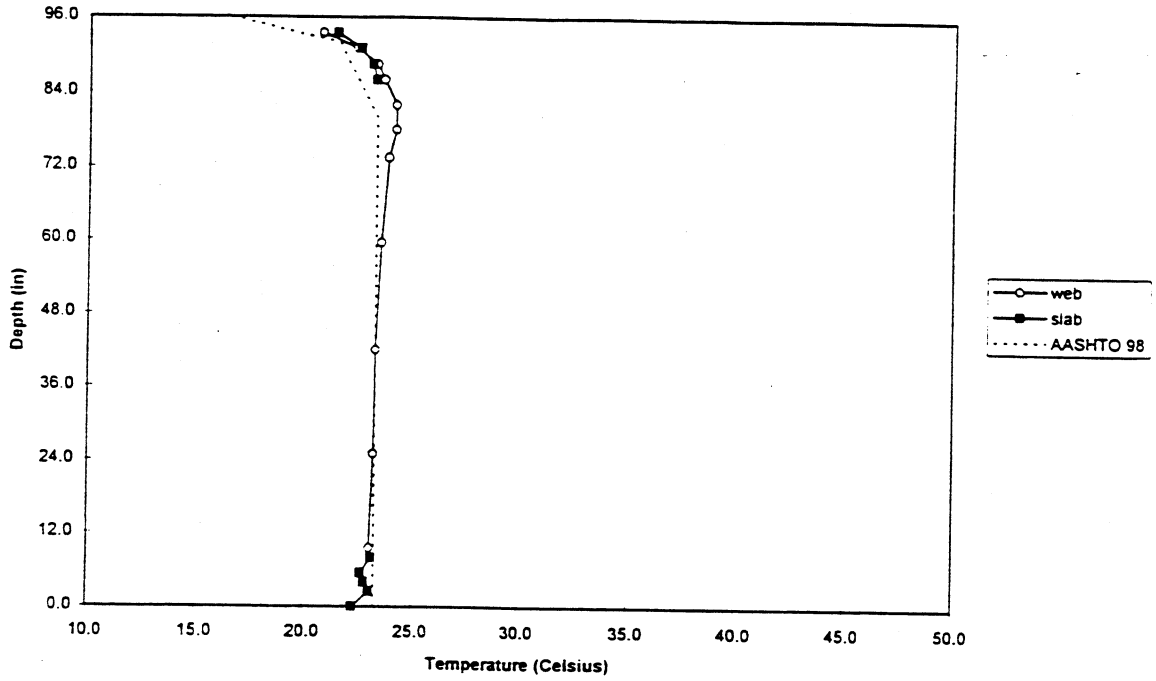

Negative Thermal Gradient at Section F

27-Apr-96 06AM

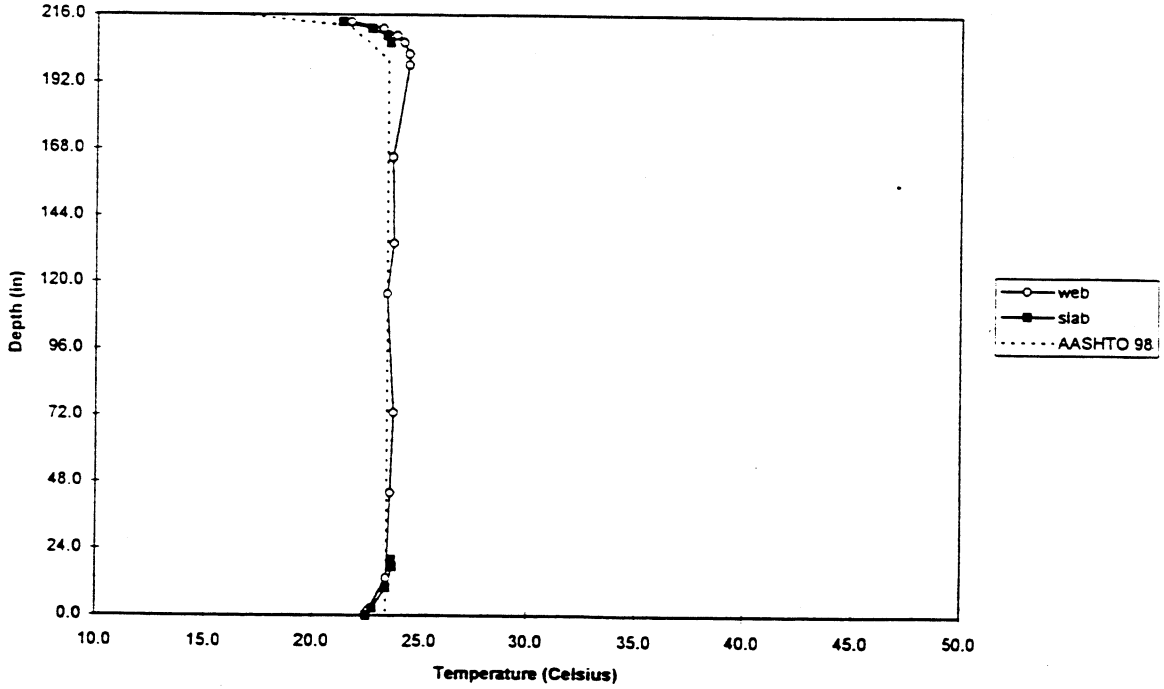

Figure 8.116

5-May-96 06AM

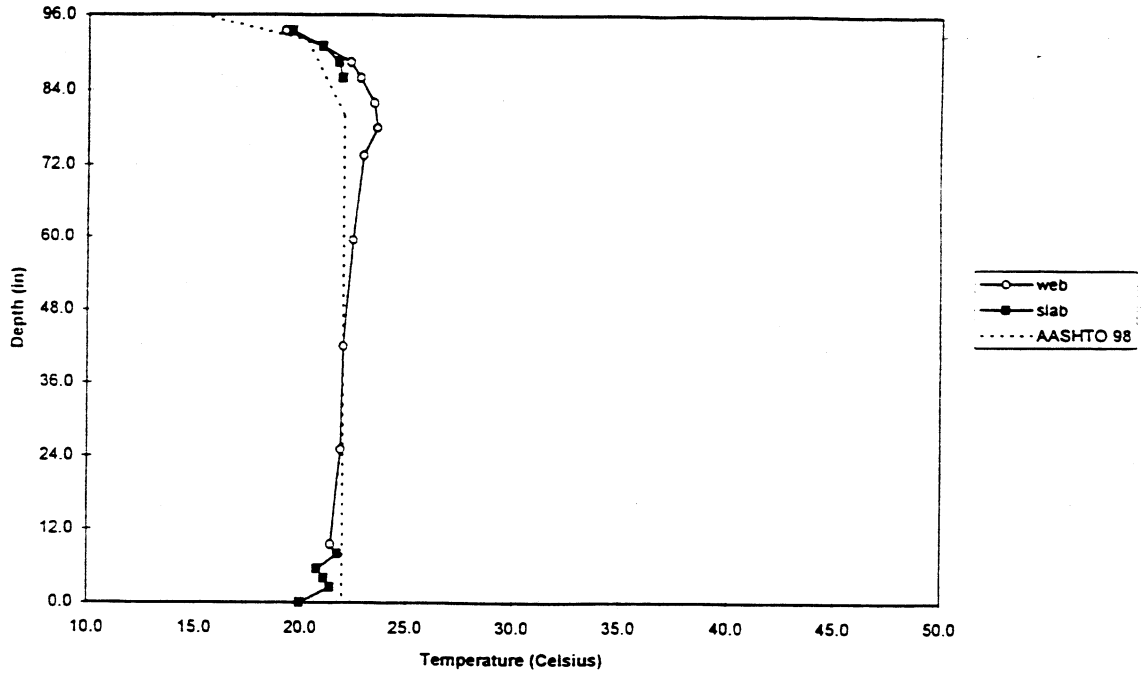

5-May-96 06AM

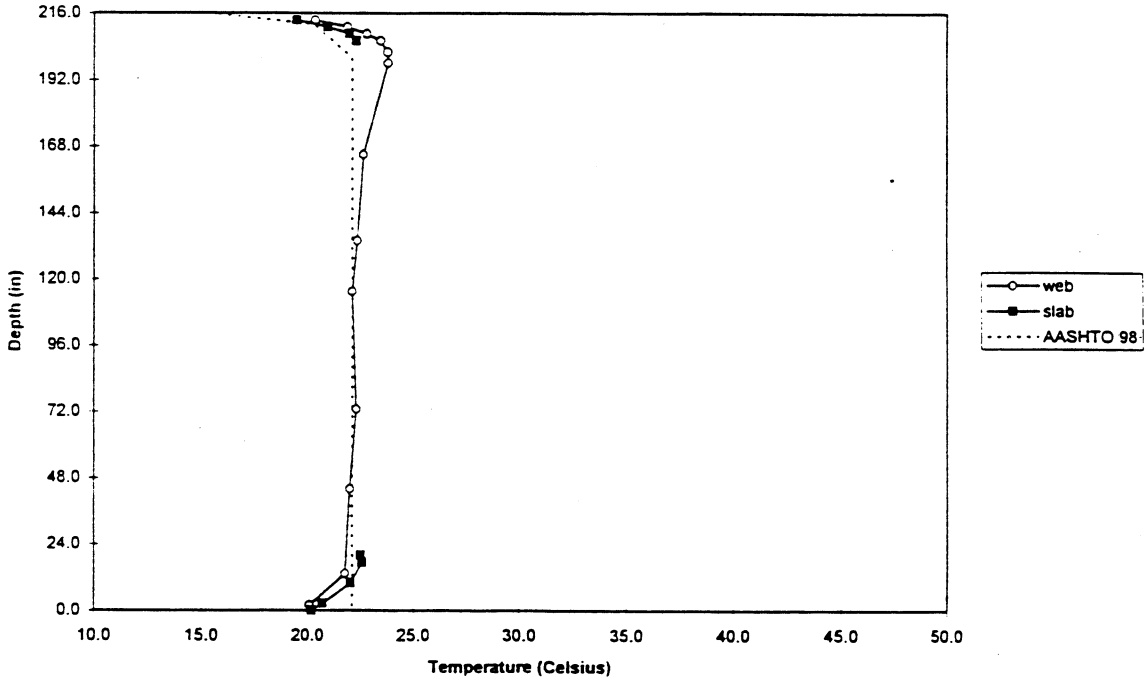

Figure 8.117

Negative Thermal Gradient at Section E

9-May-96 06AM

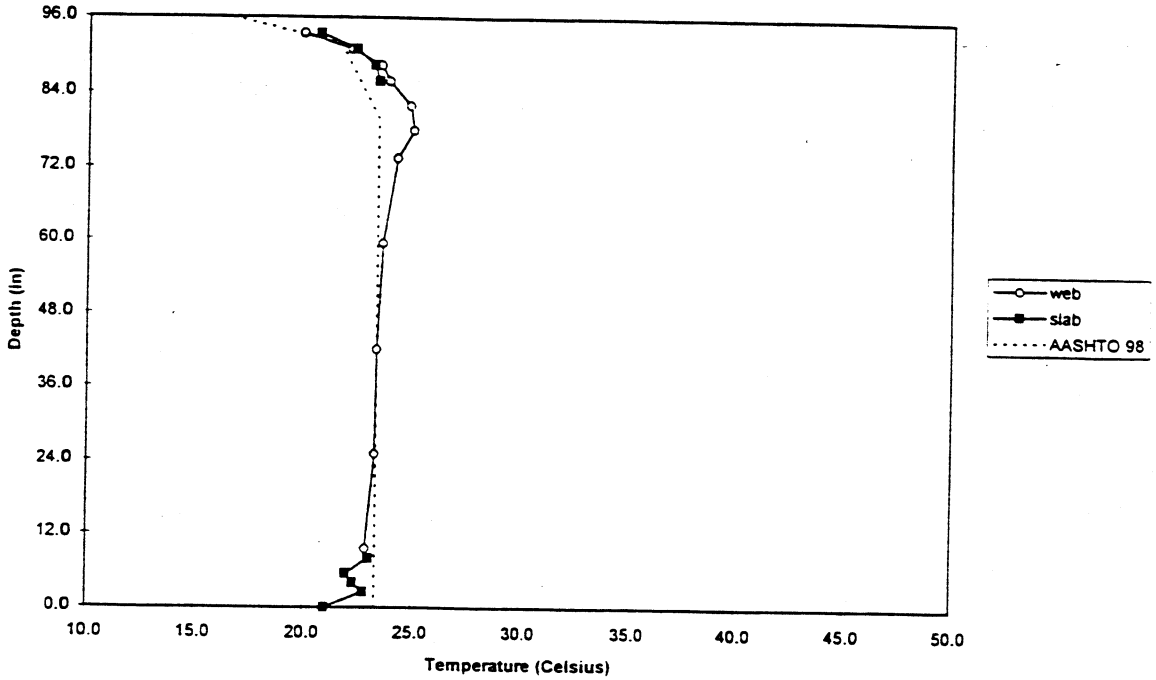

Negative Thermal Gradient at Section F

9-May-96 06AM

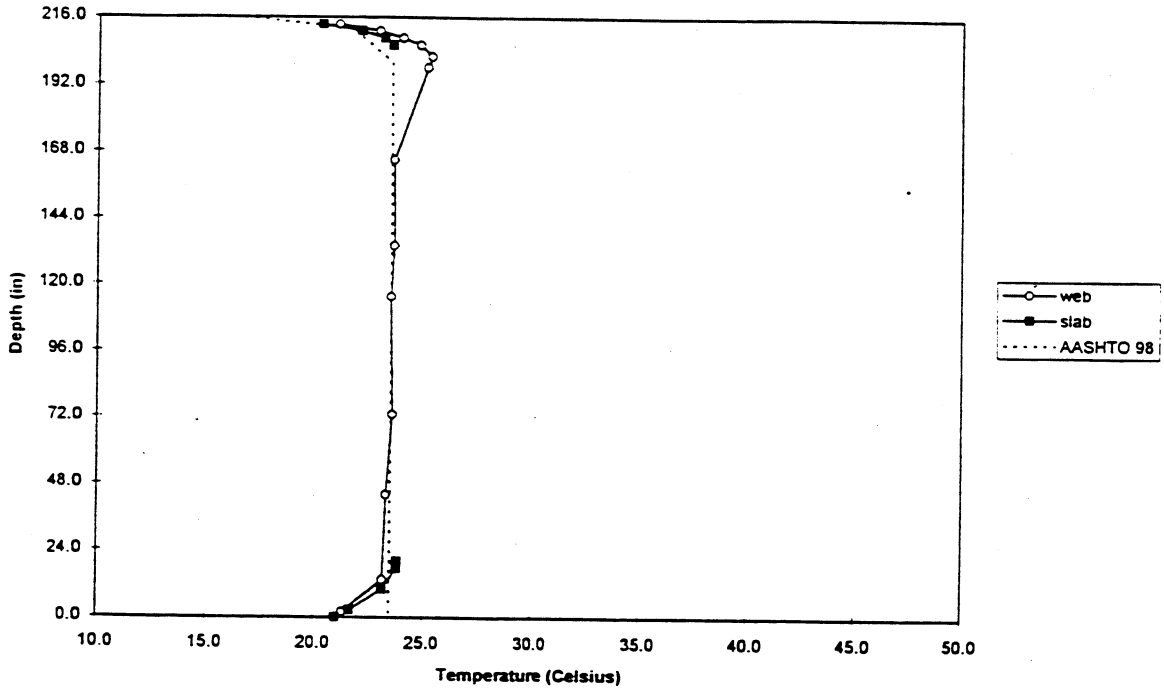

Figure 8.118

H3 Instrumentation Report

Positive Thermal Gradient at Section E

TYLin International

17-Apr-97 06PM

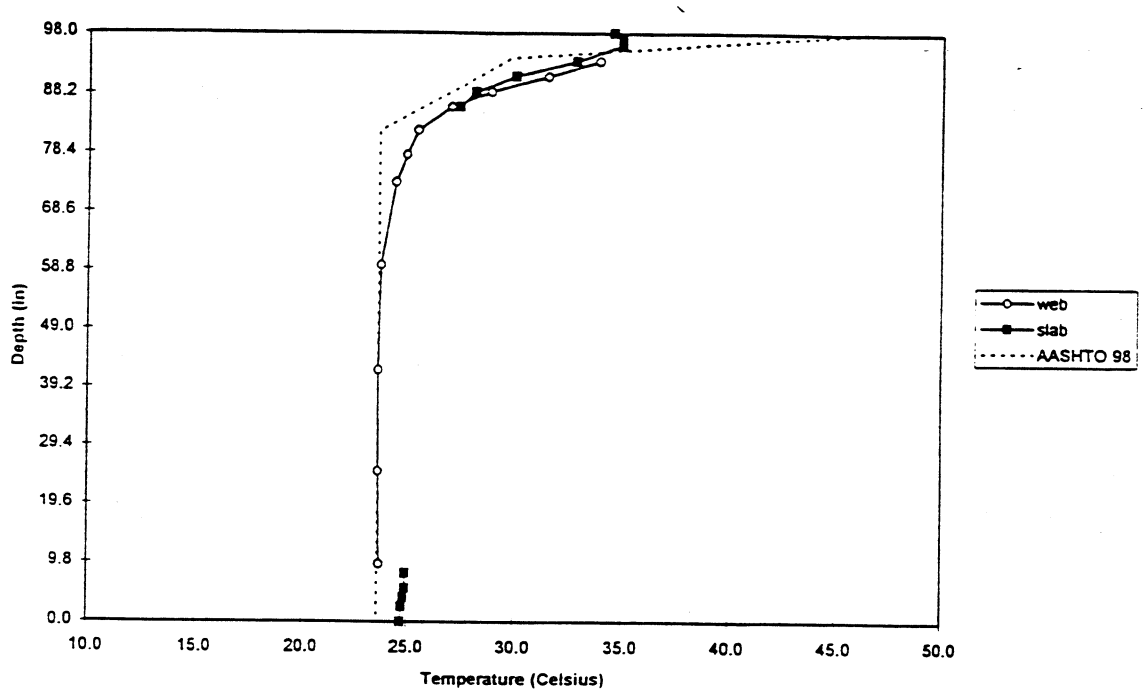

H3 Instrumentation Report

Positive Thermal Gradient at Section F

TYLin International

17-Apr-97 06PM

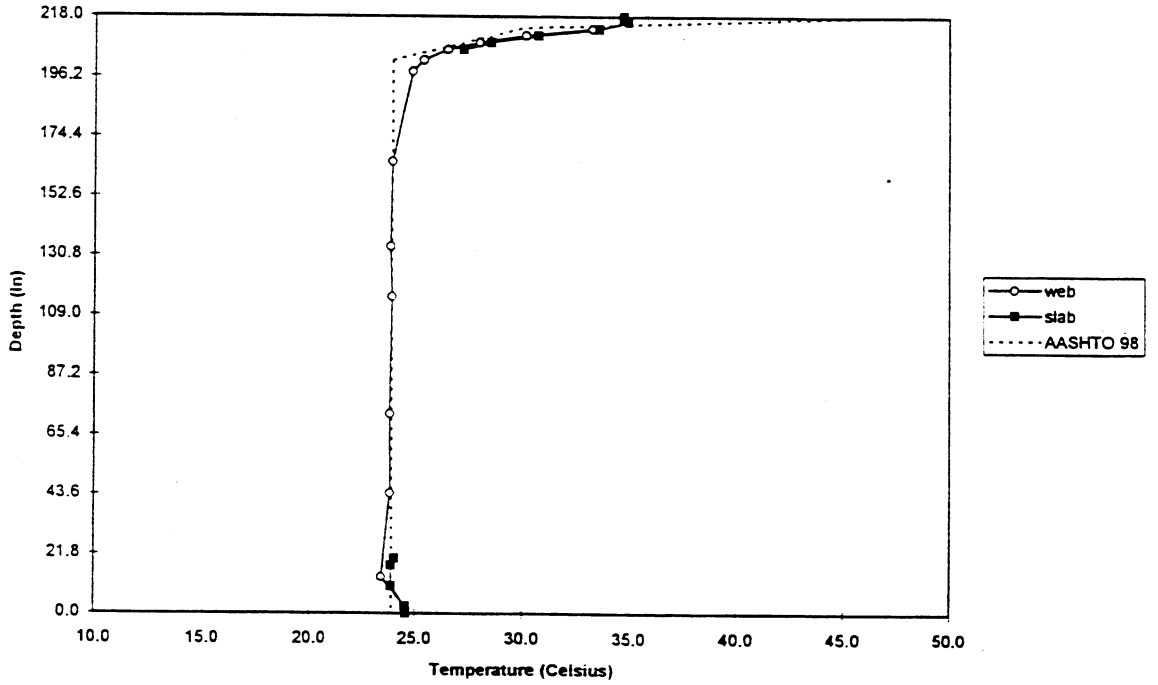

Figure 8.119

H3 Instrumentation Report

Positive Thermal Gradient at Section E

TYLin International

30-May-97 06PM

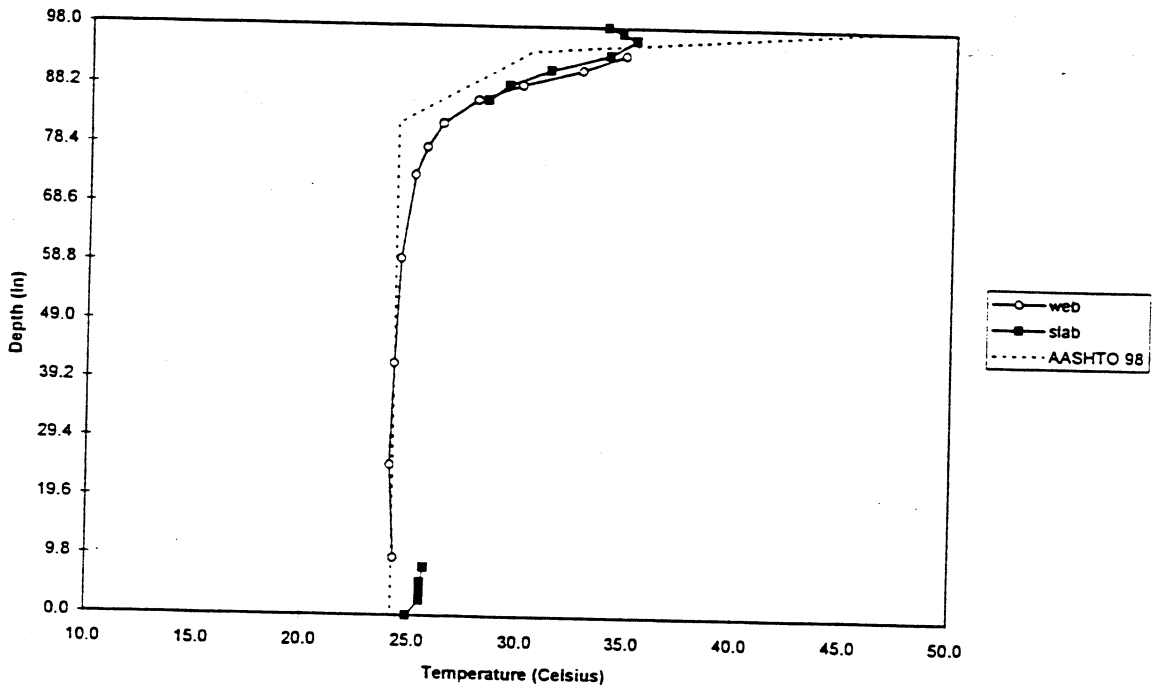

H3 Instrumentation Report

Positive Thermal Gradient at Section F

TYLin International

30-May-97 06PM

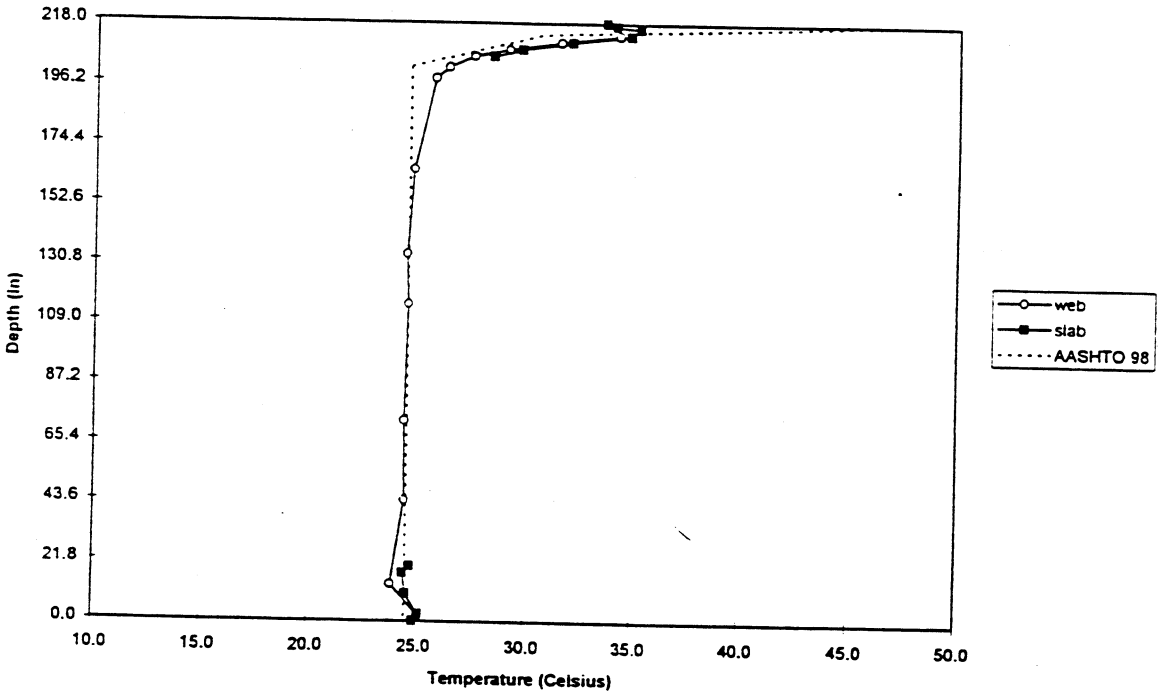

Figure 8.120

Positive Thermal Gradient at Section E

13-Jun-97 06PM

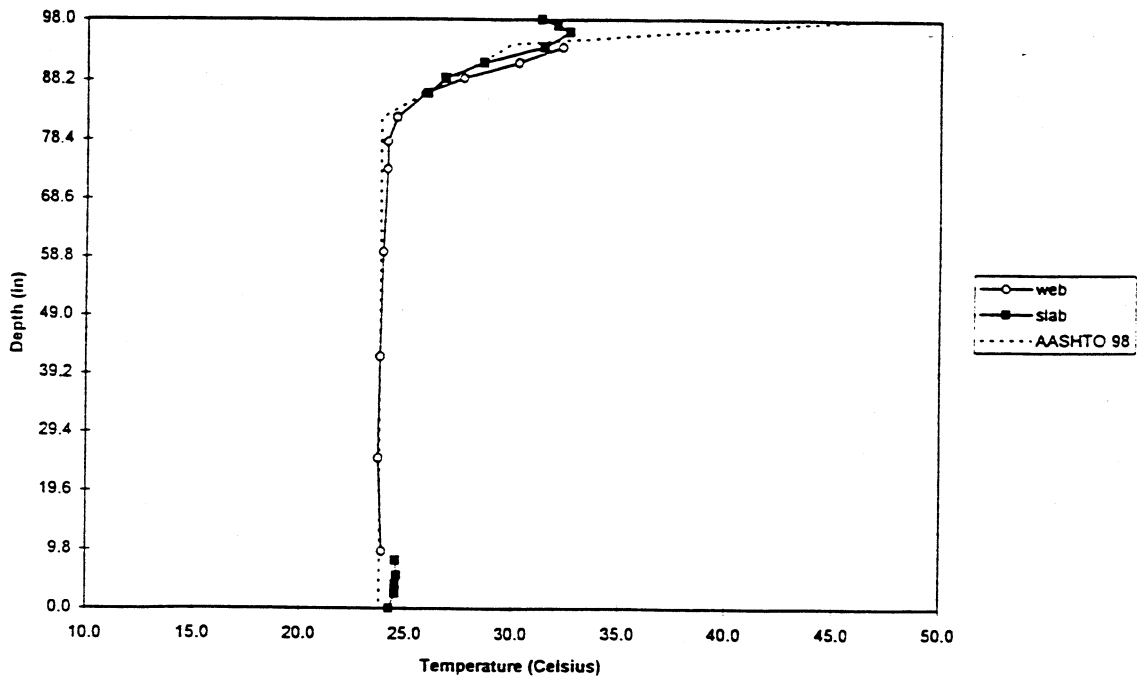

Positive Thermal Gradient at Section F

13-Jun-97 06PM

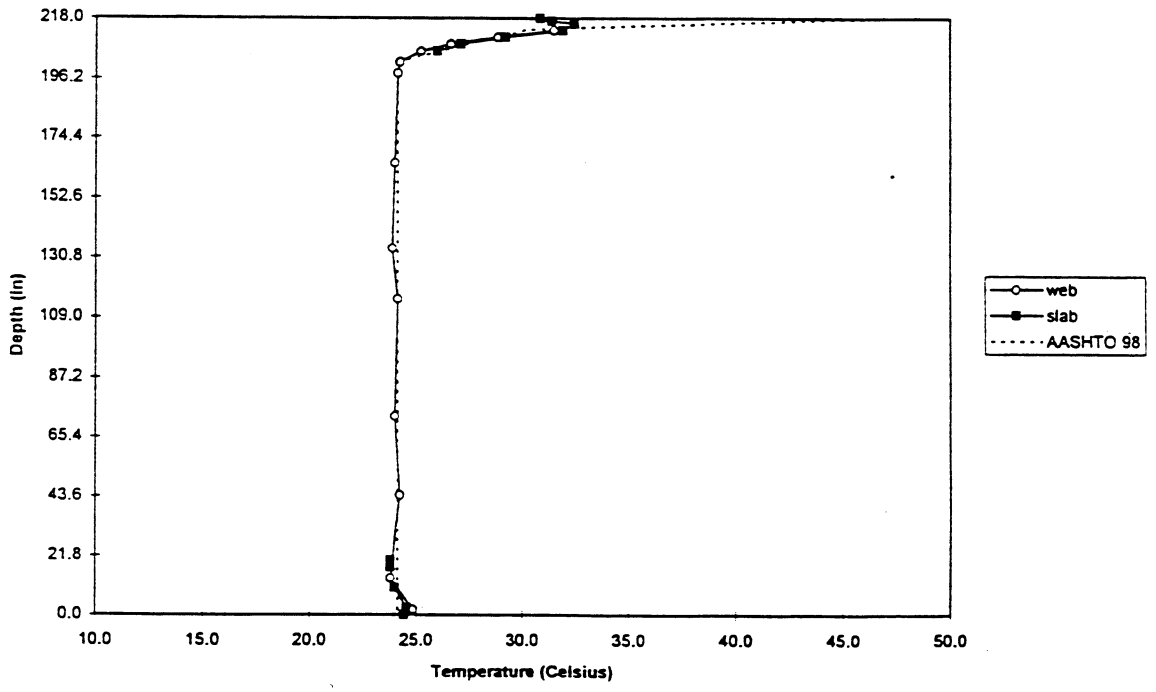

Figure 8.121

H3 Instrumentation Report

Positive Thermal Gradient at Section E

TYLin International

14-Jul-97 06PM

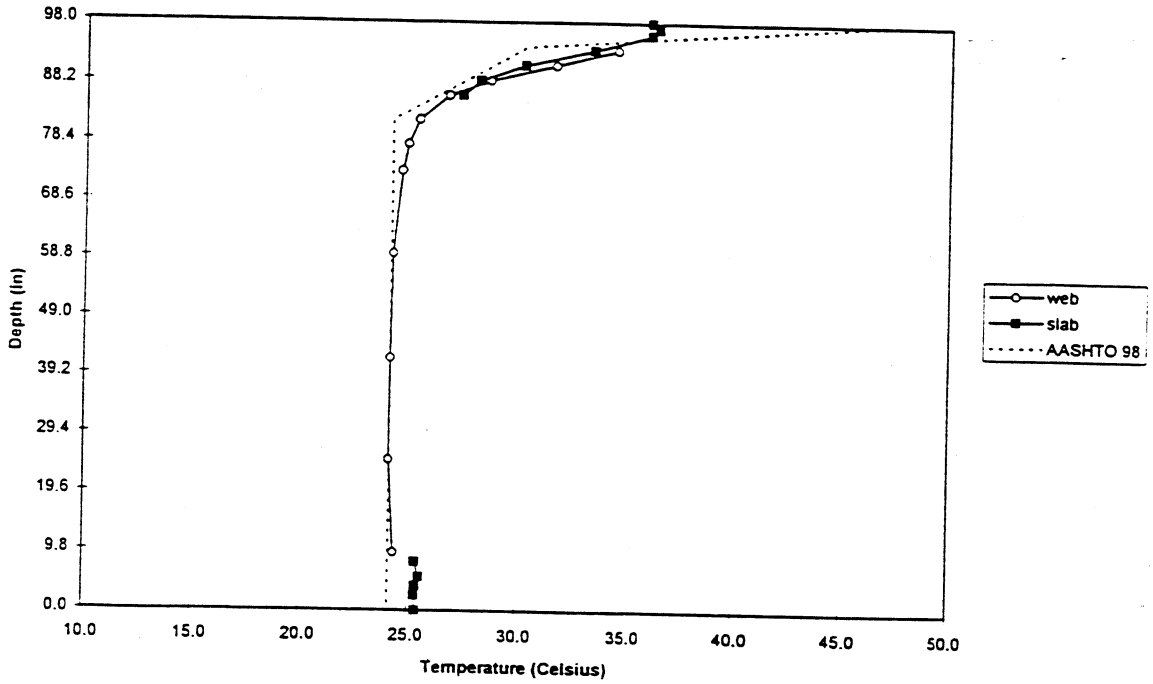

H3 Instrumentation Report

Positive Thermal Gradient at Section F

TYLin International

14-Jul-97 06PM

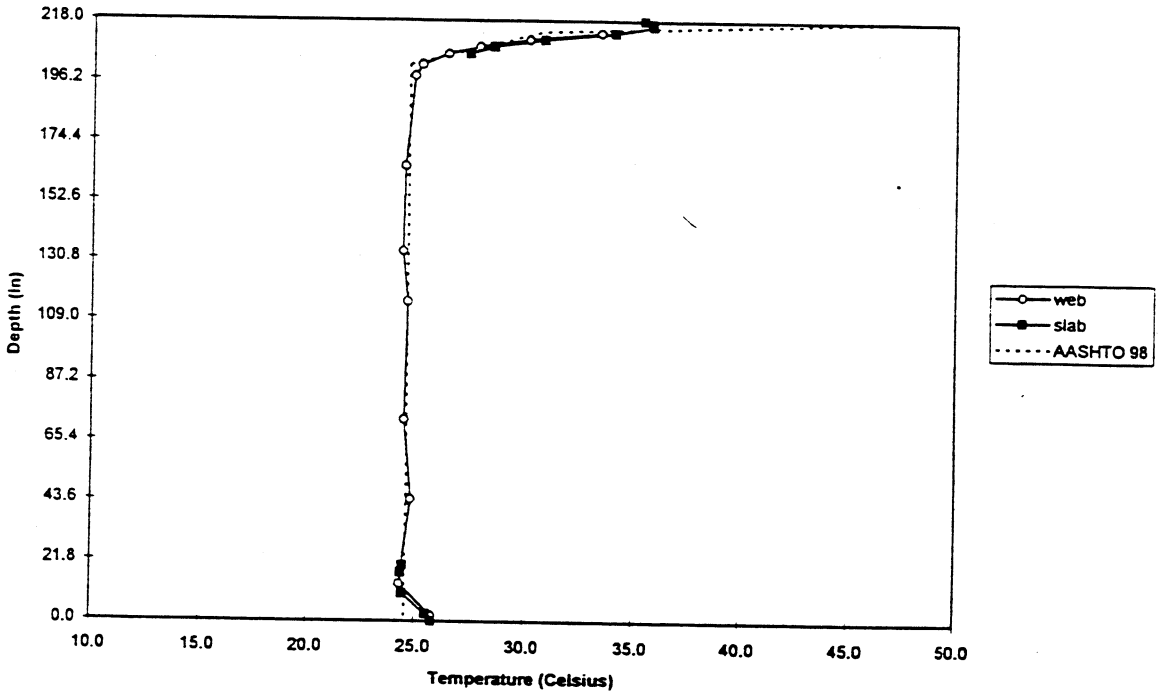

Figure 8.122

20-Jul-97 06PM

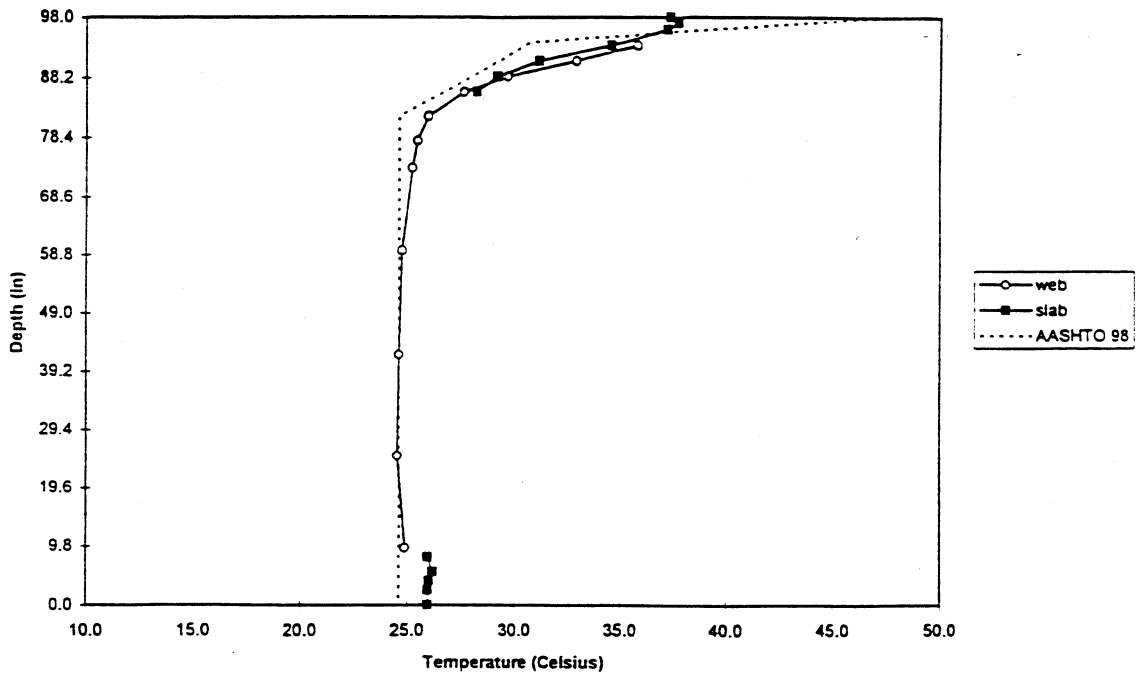

20-Jul-97 06PM

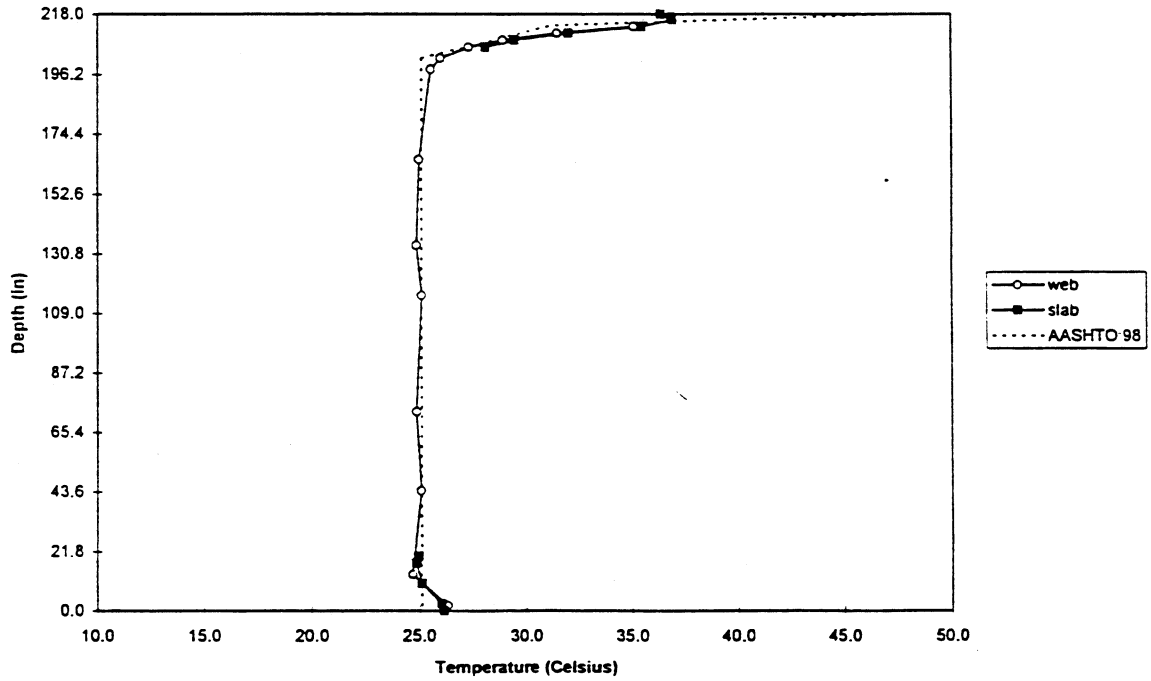

Figure 8.123

Positive Thermal Gradient at Section E

9-Aug-97 06PM

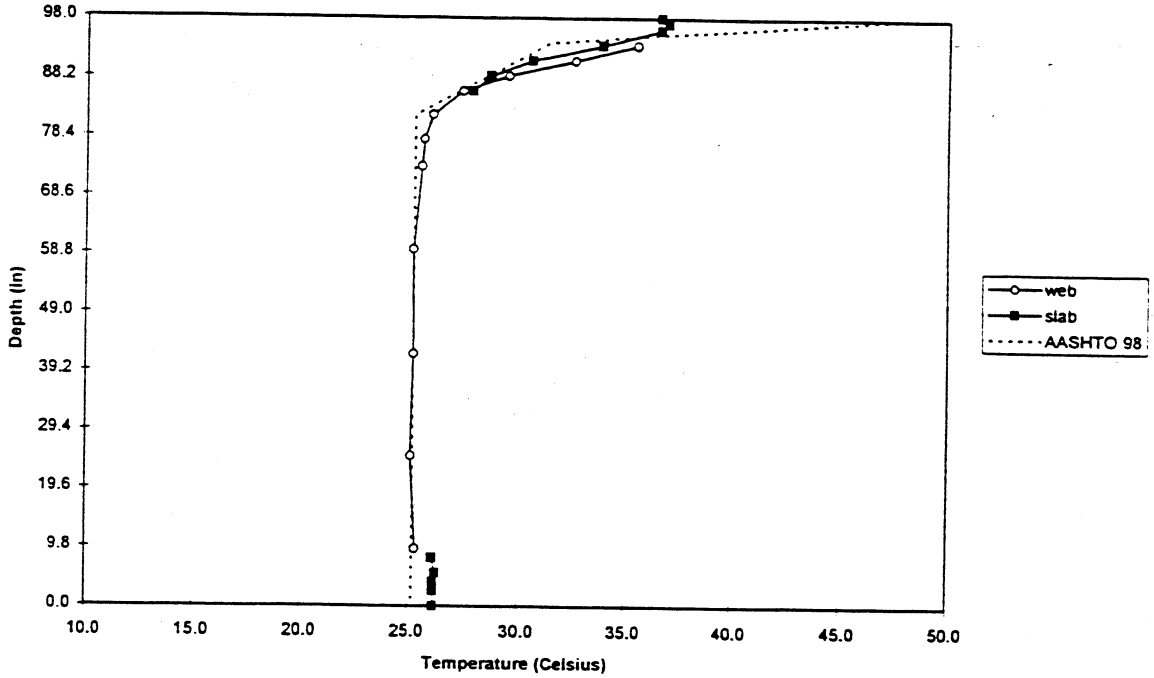

Positive Thermal Gradient at Section F

9-Aug-97 06PM

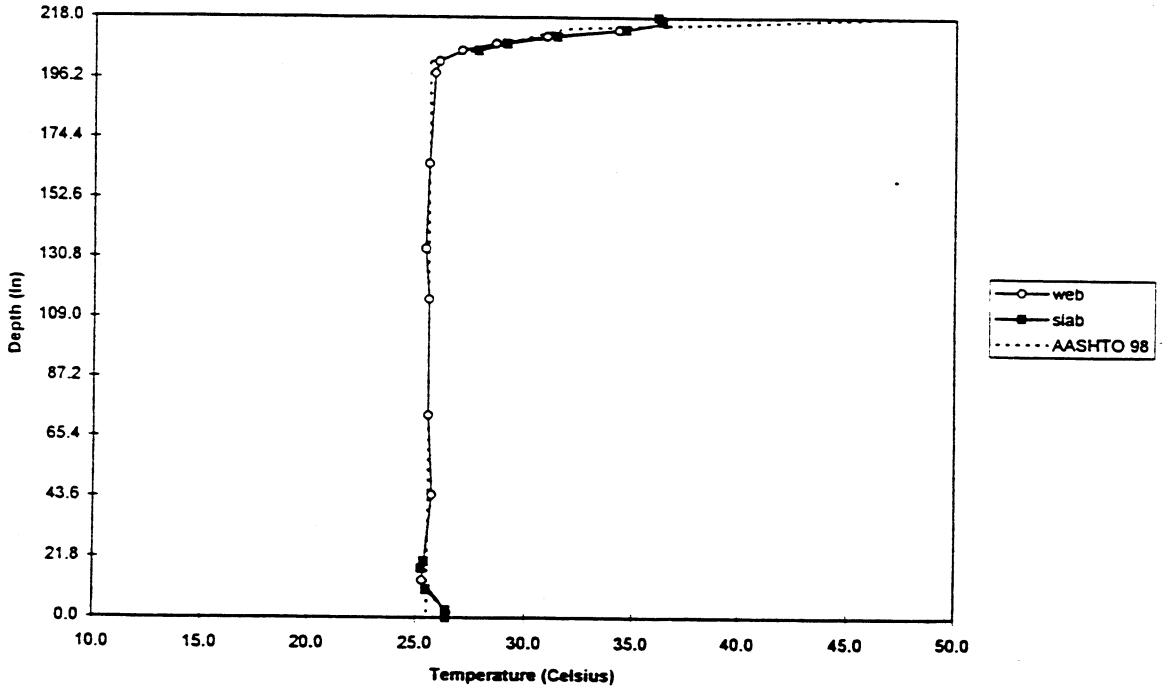

Figure 8.124

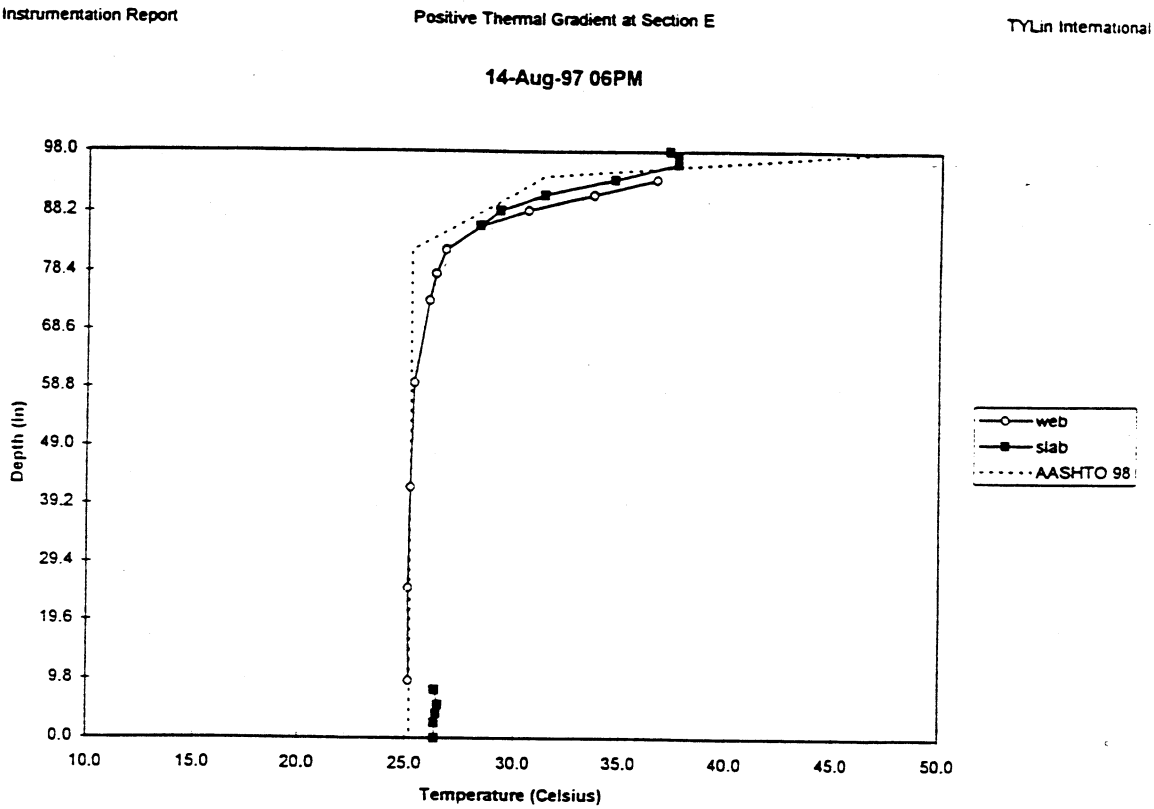
H3 Instrumentation Report
Positive Thermal Gradient at Section E
TYLin International
14-Aug-97 06PM
98.0
88.2
78.4
68.6
58.8
49.0
39.2
29.4
19.6
9.8
0.0
Depth (in)
10.0
15.0
20.0
25.0
30.0
35.0
40.0
45.0
50.0
Temperature (Celsius)
web
slab
AASHTO 98

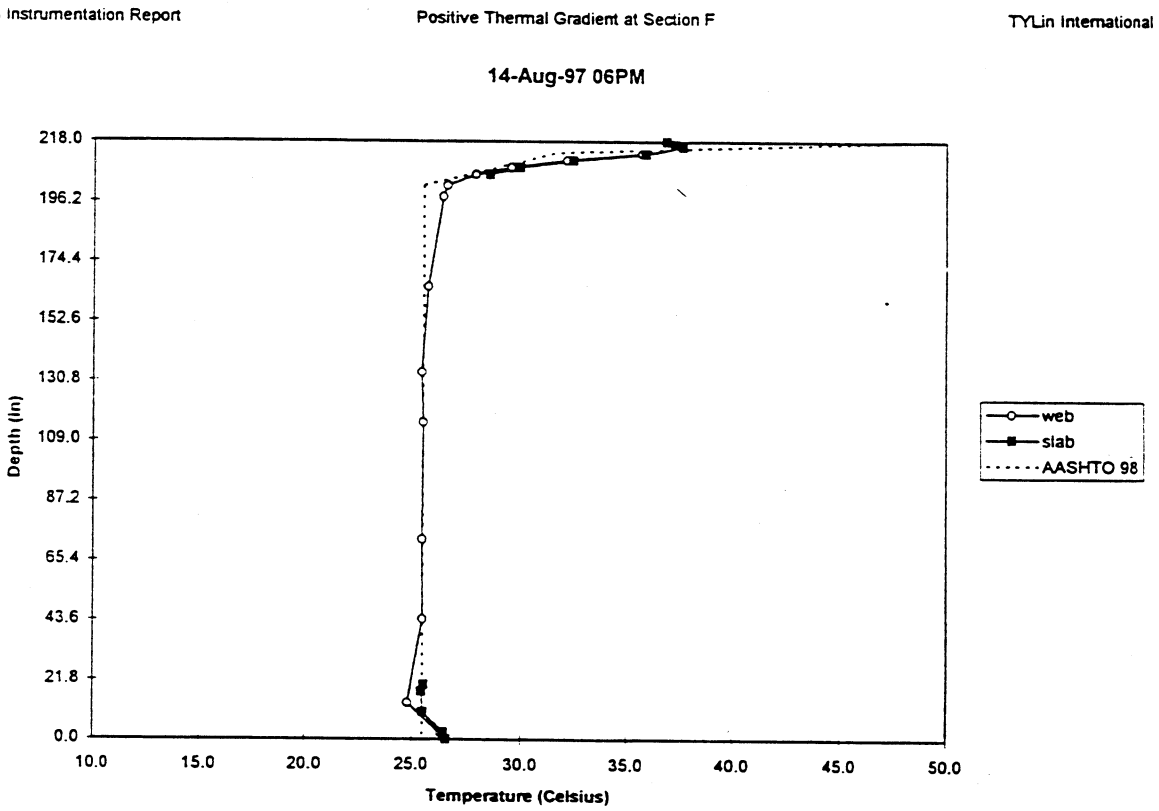
H3 Instrumentation Report
Positive Thermal Gradient at Section F
TYLin International
14-Aug-97 06PM
218.0
196.2
174.4
152.6
130.8
109.0
87.2
65.4
43.6
21.8
0.0
Depth (in)
10.0
15.0
20.0
25.0
30.0
35.0
40.0
45.0
50.0
Temperature (Celsius)
web
slab
AASHTO 98

Figure 8.125

H3 Instrumentation Report

Positive Thermal Gradient at Section E

TYLin International

18-Aug-97 06PM

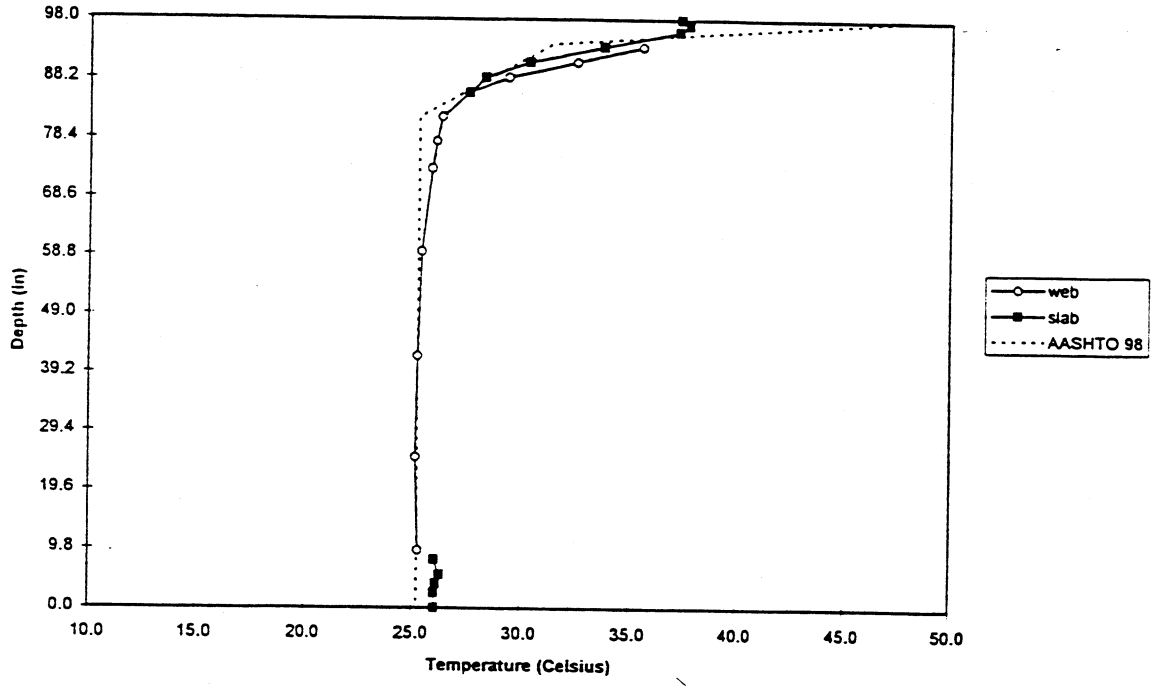

H3 Instrumentation Report

Positive Thermal Gradient at Section F

TYLin International

18-Aug-97 06PM

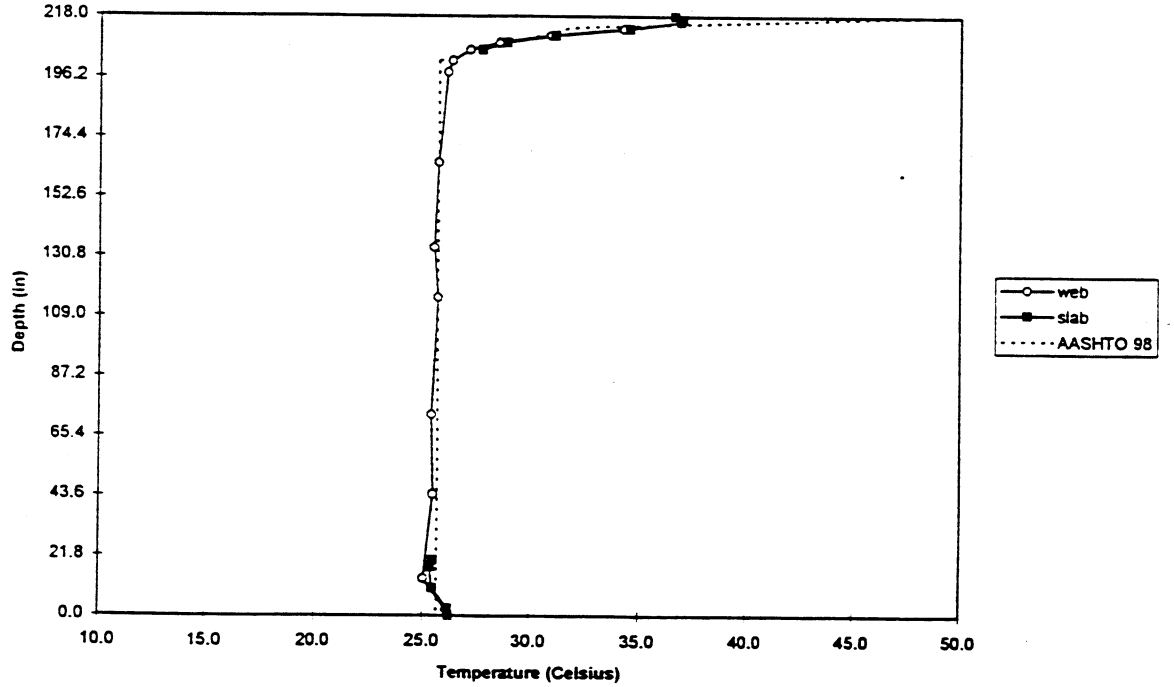

Figure 8.126

Positive Thermal Gradient at Section E

1-Sep-97 06PM

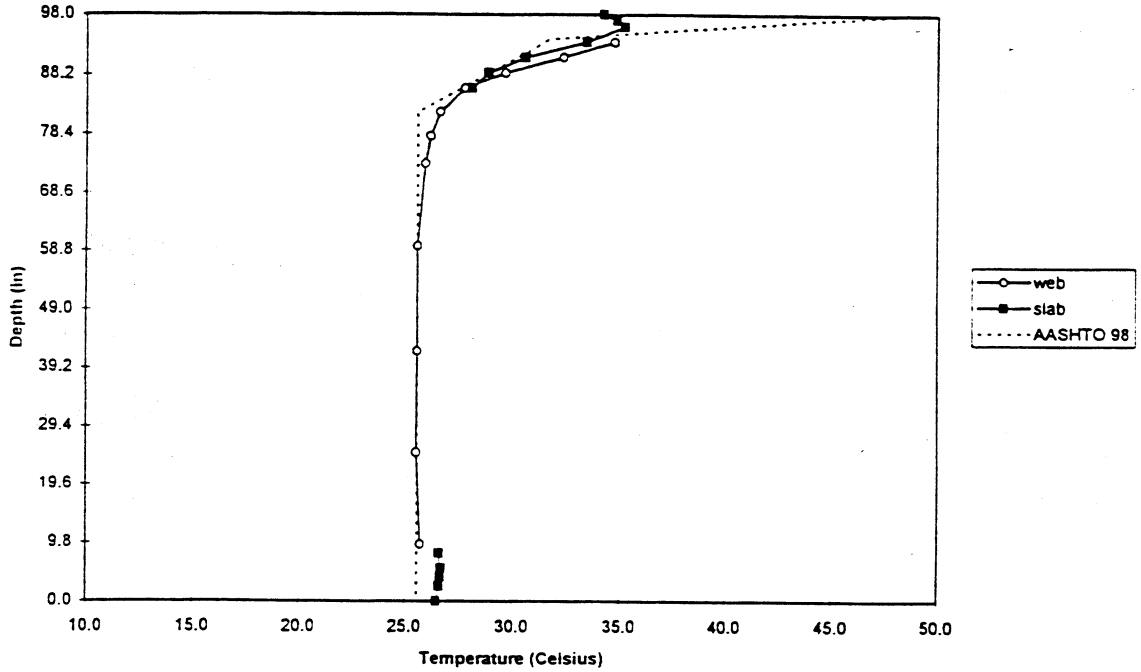

Positive Thermal Gradient at Section F

1-Sep-97 06PM

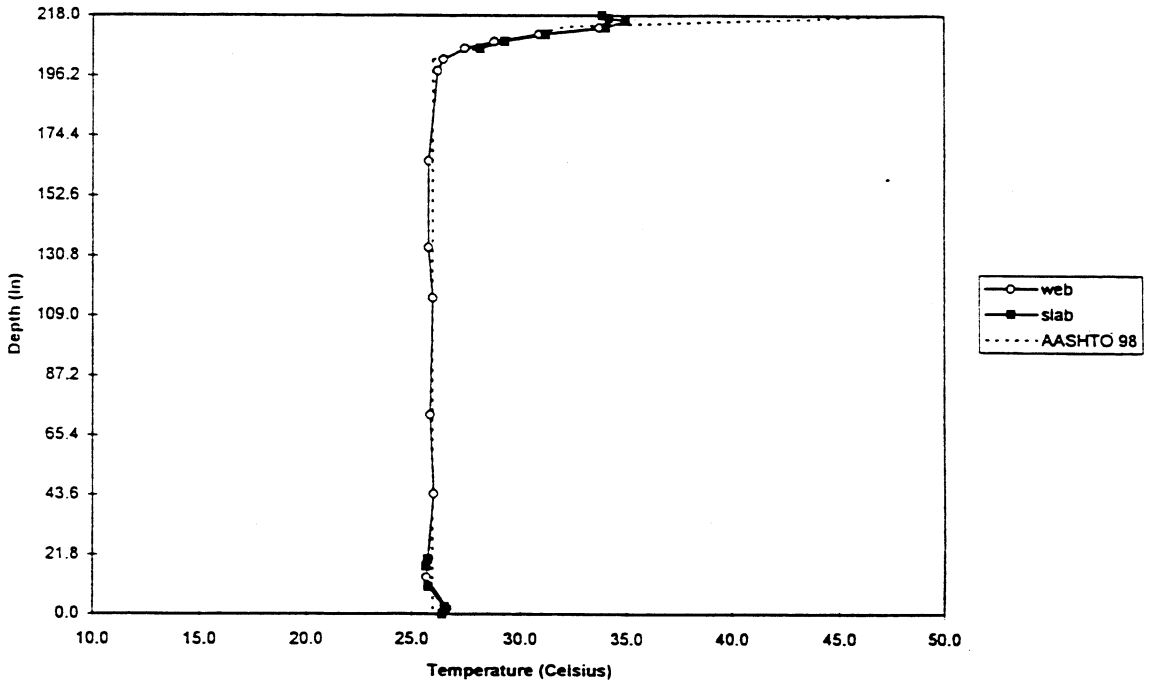

Figure 8.127

Positive Thermal Gradient at Section E

13-Sep-97 06PM

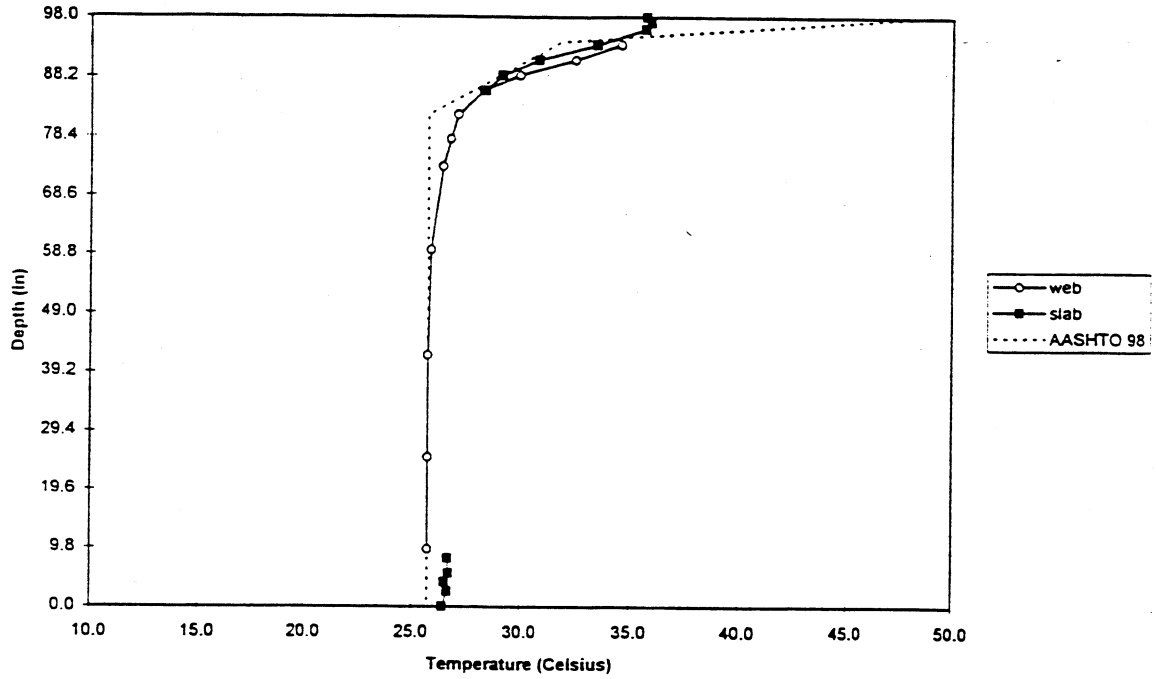

Positive Thermal Gradient at Section F

13-Sep-97 06PM

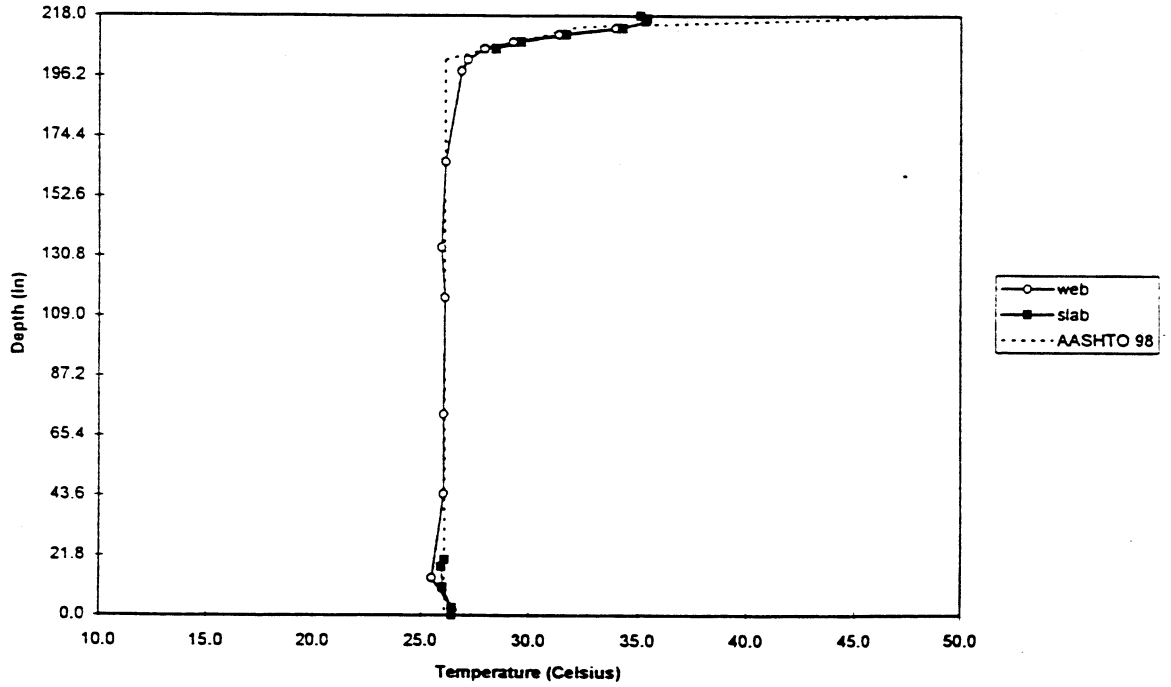

Figure 8.128

Positive Thermal Gradient at Section E

24-Sep-97 06PM

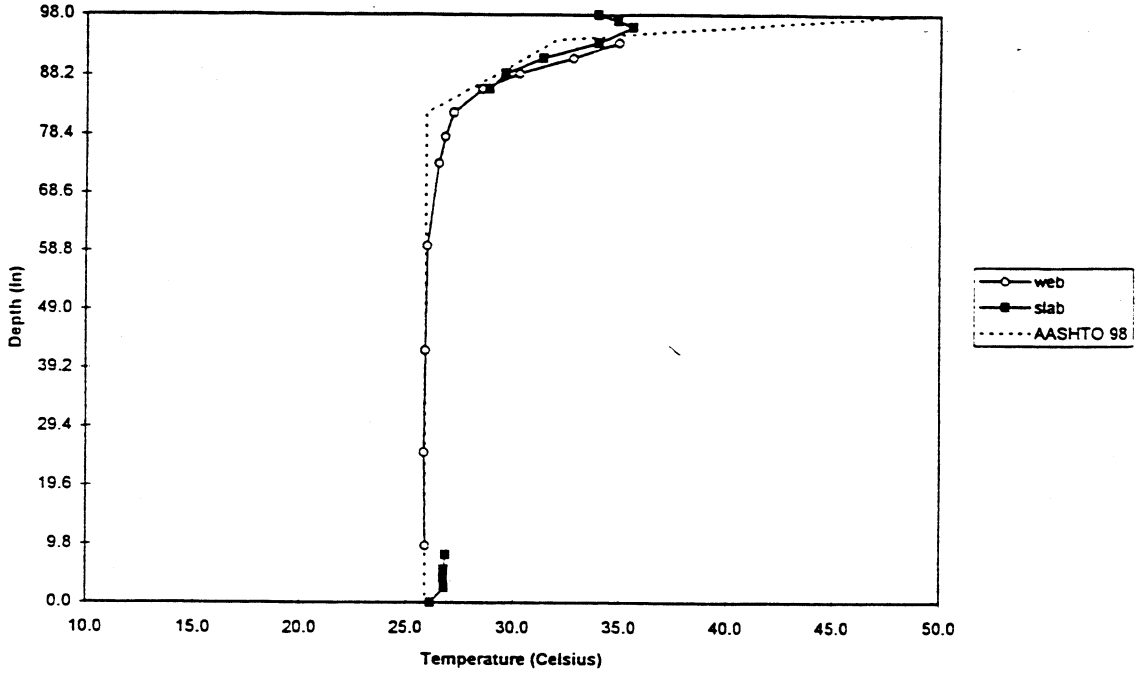

Positive Thermal Gradient at Section F

24-Sep-97 06PM

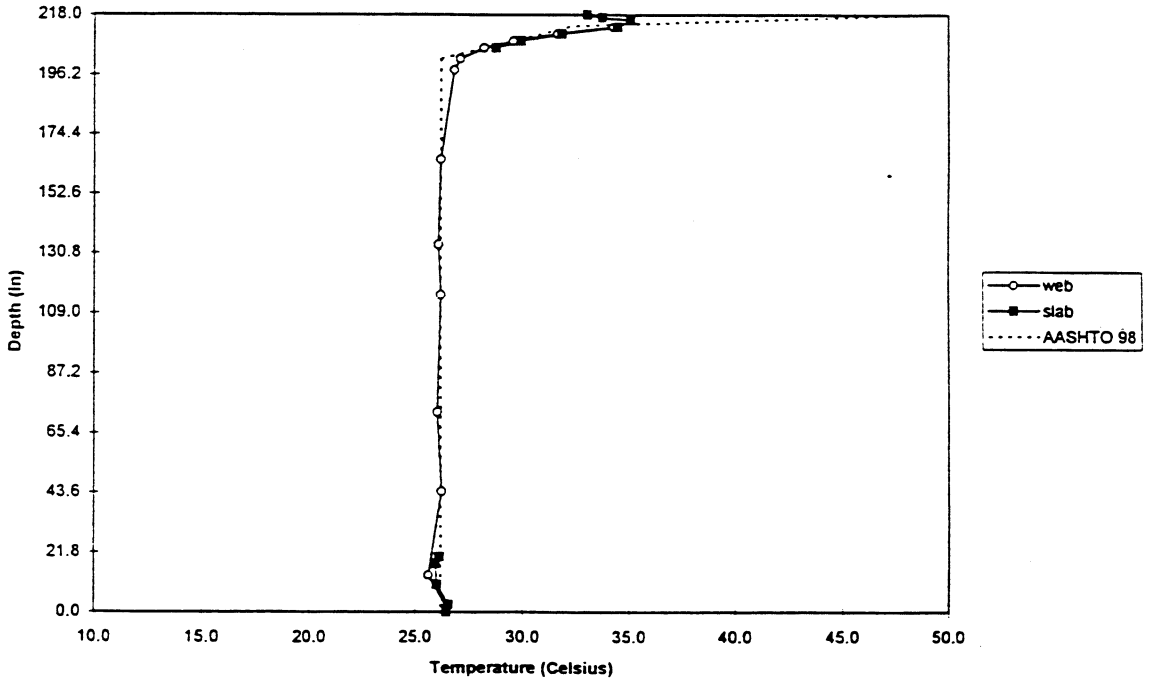

Figure 8.129

H3 Instrumentation Report

Positive Thermal Gradient at Section E

TYLin International

1-Oct-97 06PM

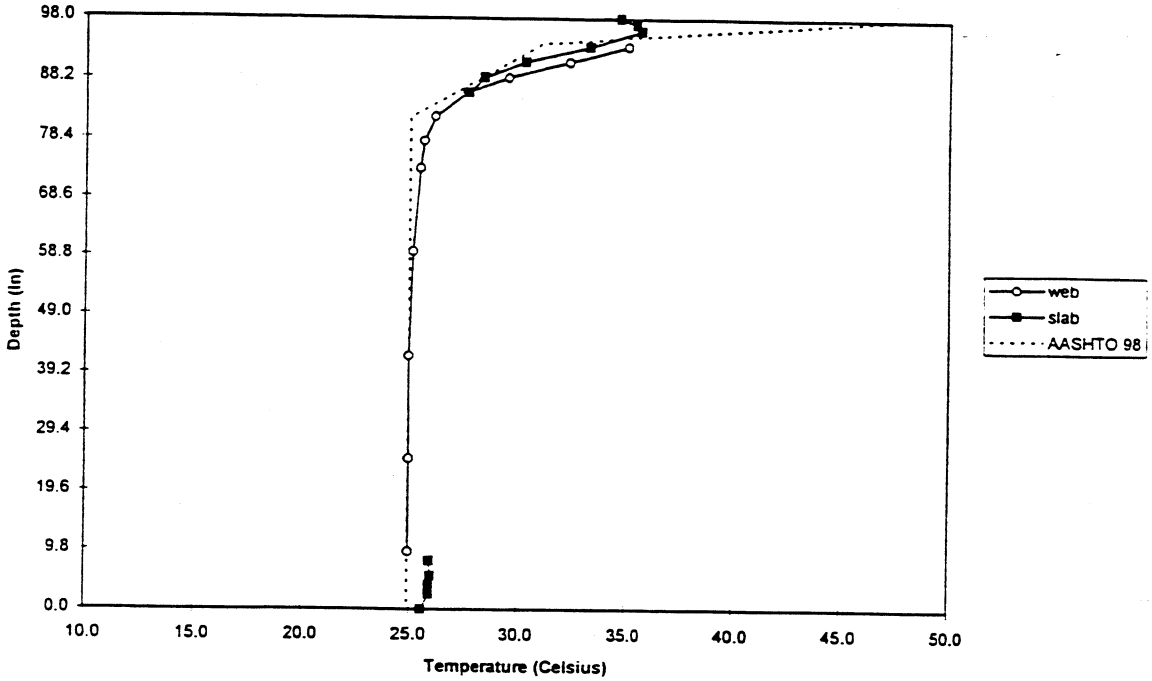

H3 Instrumentation Report

Positive Thermal Gradient at Section F

TYLin International

1-Oct-97 06PM

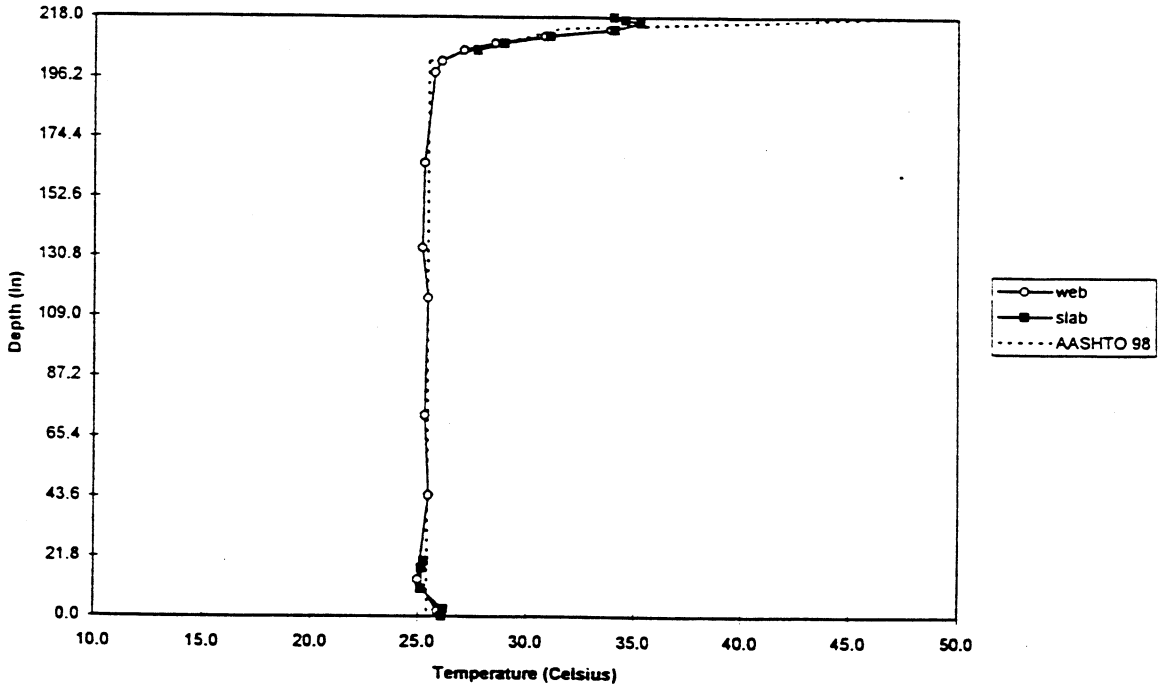

Figure 8.130

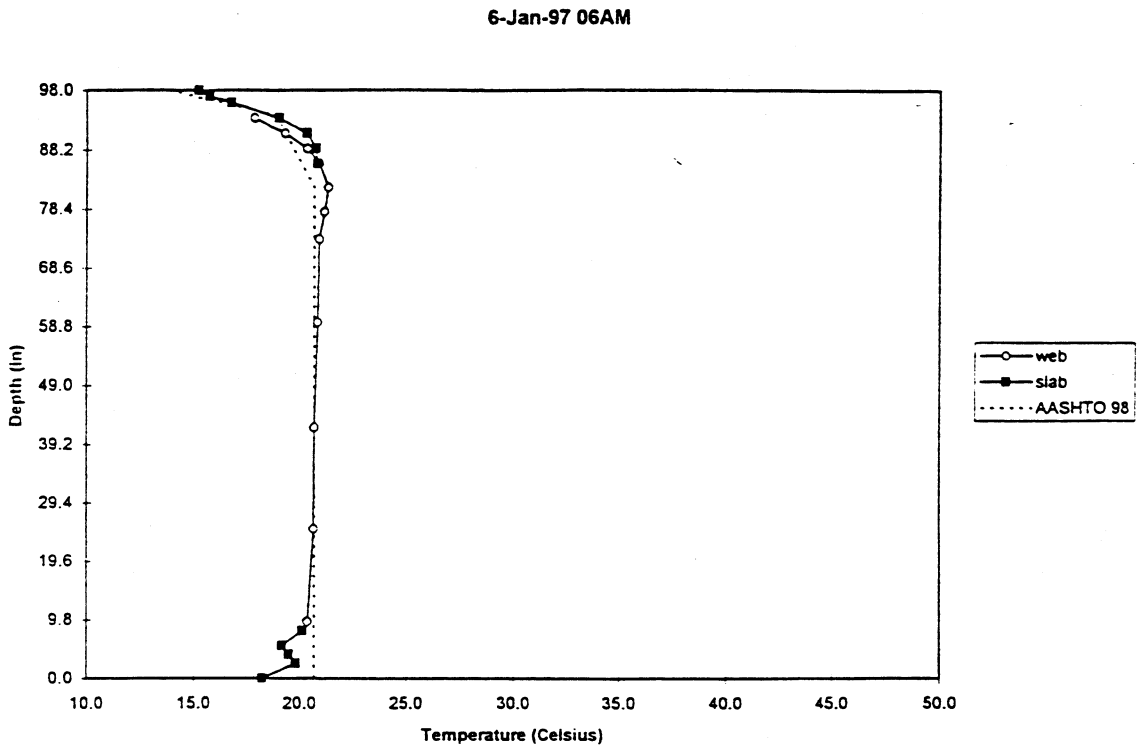
6-Jan-97 06AM
98.0
88.2
78.4
68.6
58.8
49.0
39.2
29.4
19.6
9.8
0.0
Depth (In)
10.0
15.0
20.0
25.0
30.0
35.0
40.0
45.0
50.0
Temperature (Celsius)
web
slab
AASHTO 98

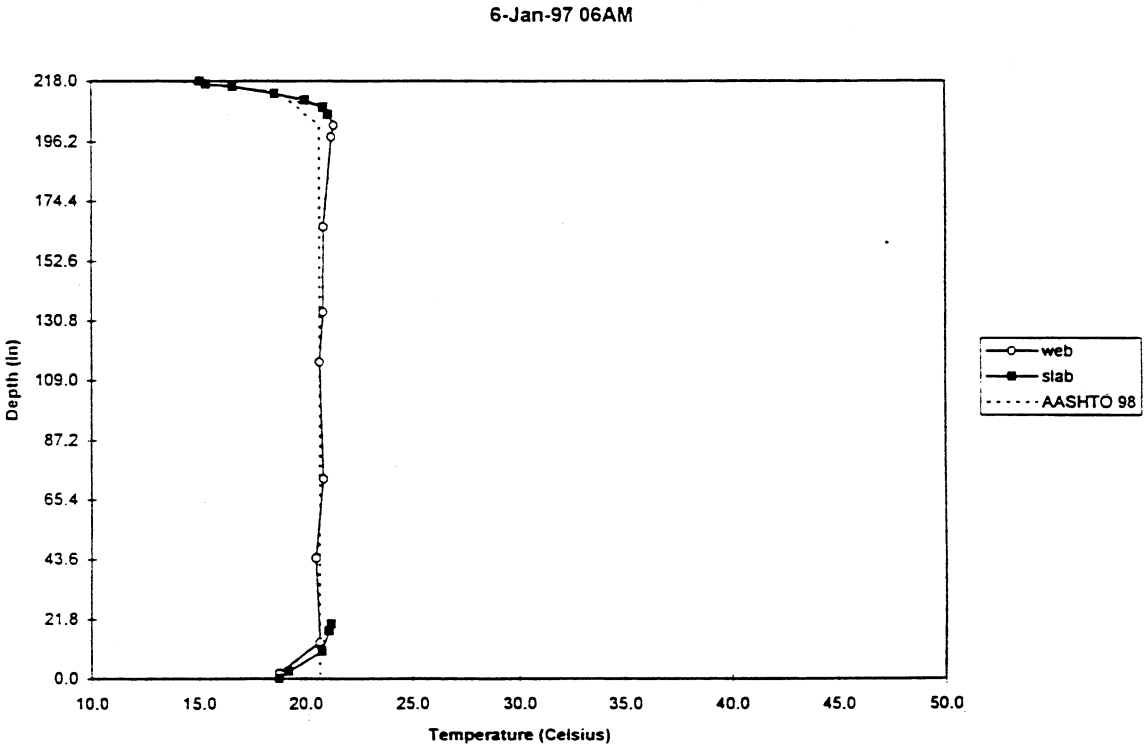
6-Jan-97 06AM
218.0
196.2
174.4
152.6
130.8
109.0
87.2
65.4
43.6
21.8
0.0
Depth (In)
10.0
15.0
20.0
25.0
30.0
35.0
40.0
45.0
50.0
Temperature (Celsius)
web
slab
AASHTO 98

Figure 8.131

Negative Thermal Gradient at Section E

17-Jan-97 06AM

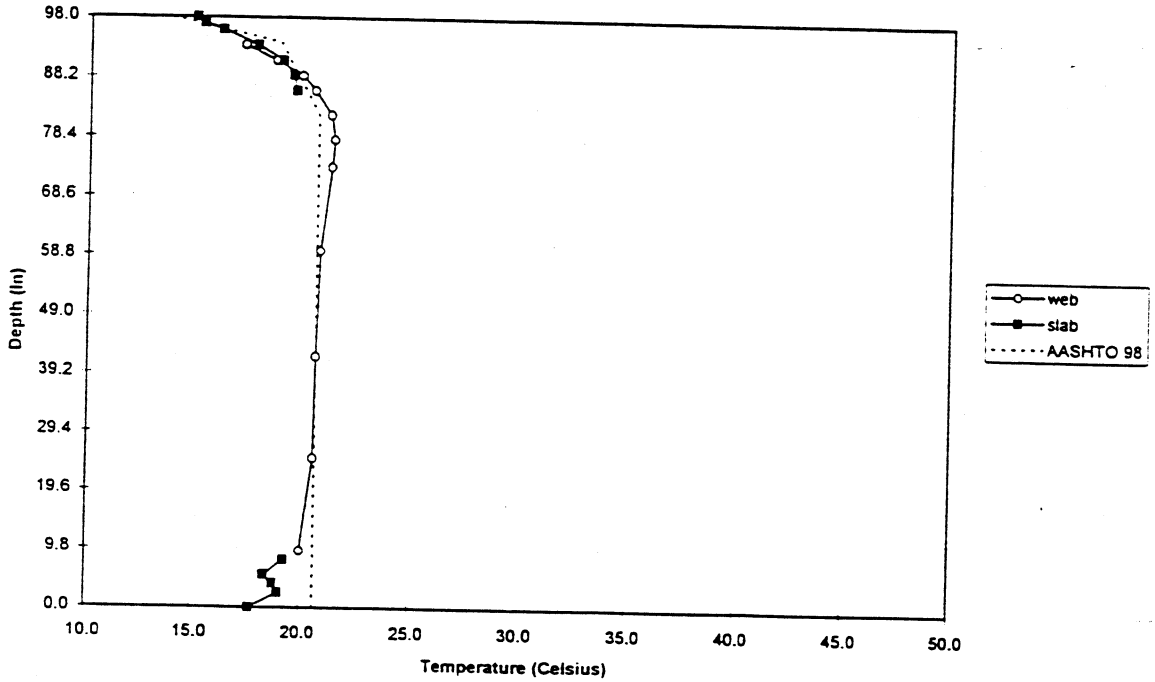

Negative Thermal Gradient at Section F

17-Jan-97 06AM

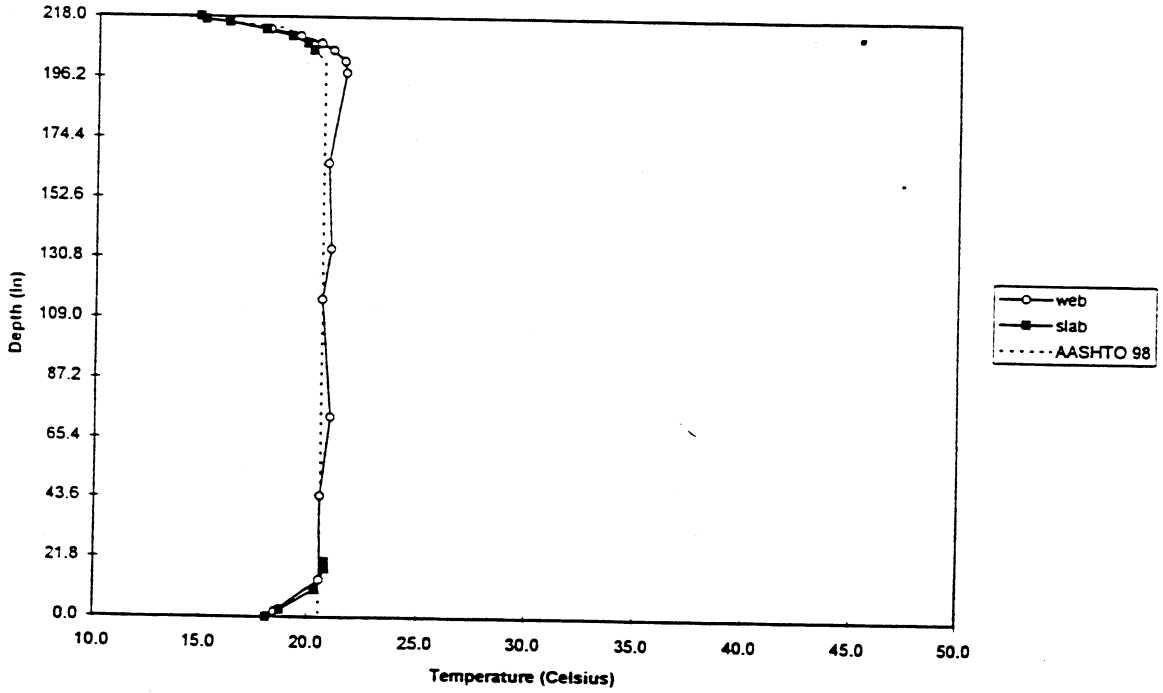

Figure 8.132

Negative Thermal Gradient at Section E

22-Jan-97 06AM

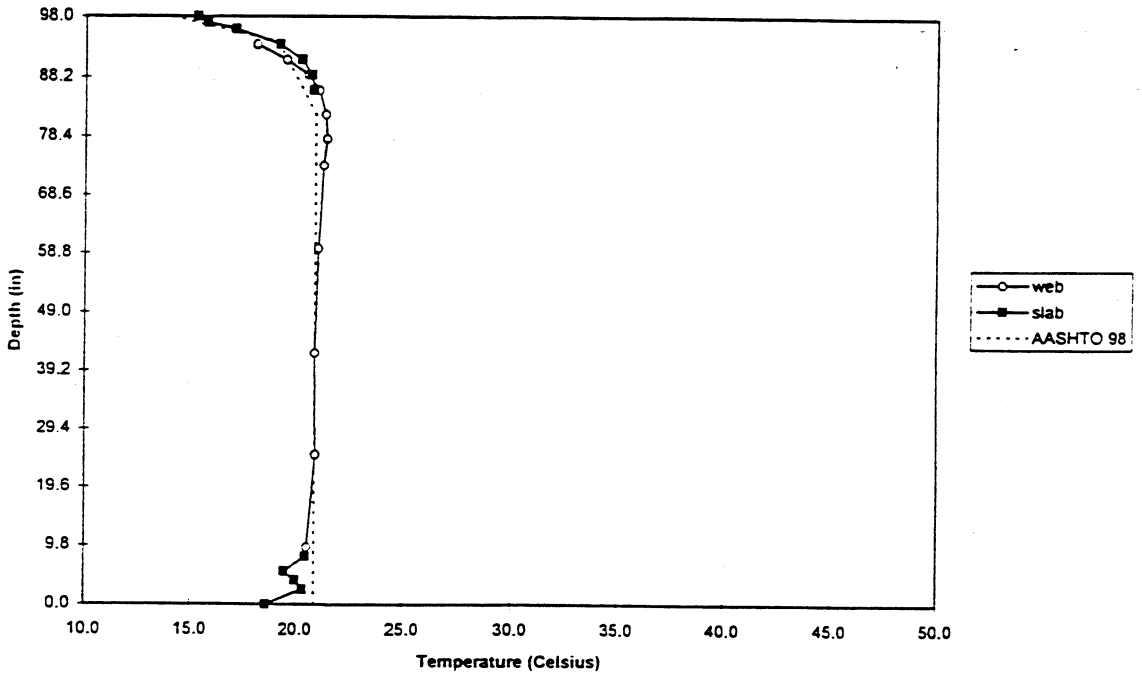

Negative Thermal Gradient at Section F

22-Jan-97 06AM

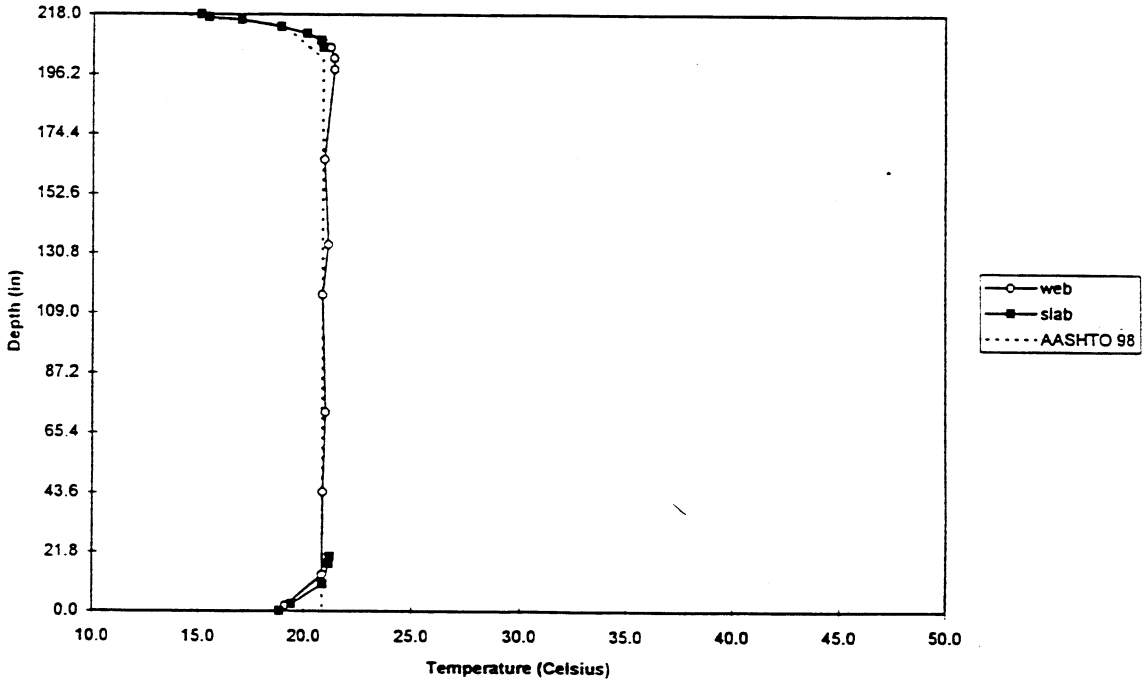

Figure 8.133

H3 Instrumentation Report

Negative Thermal Gradient at Section E

TYLin International

23-Jan-97 06AM

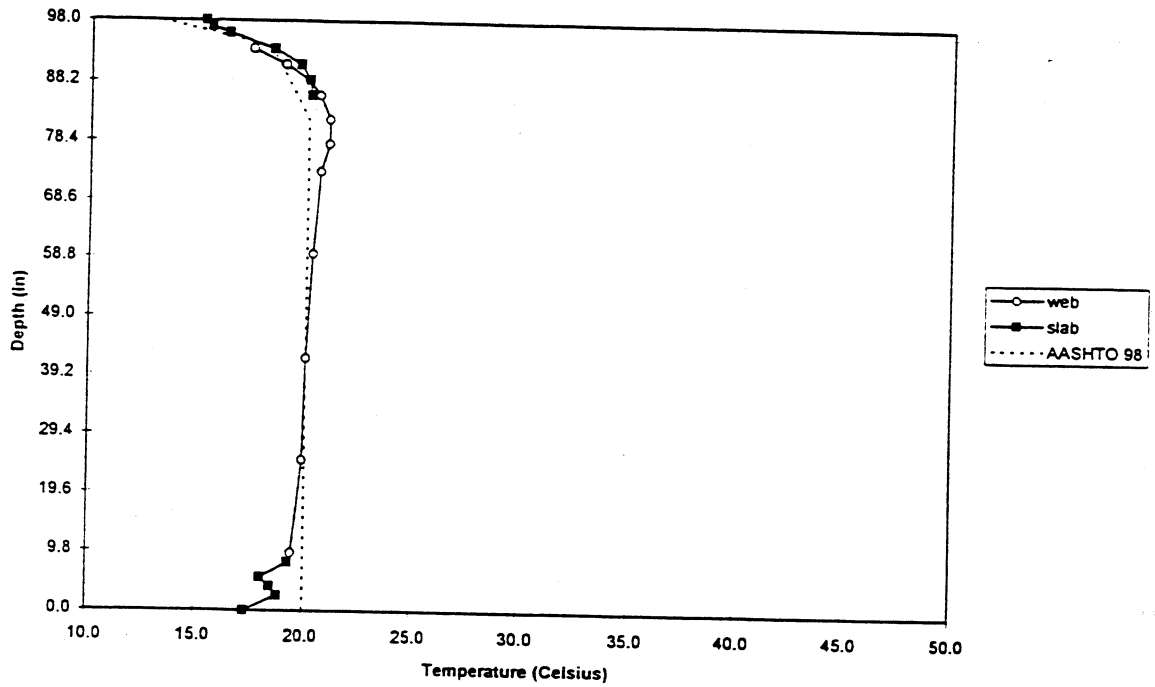

H3 Instrumentation Report

Negative Thermal Gradient at Section F

TYLin International

23-Jan-97 06AM

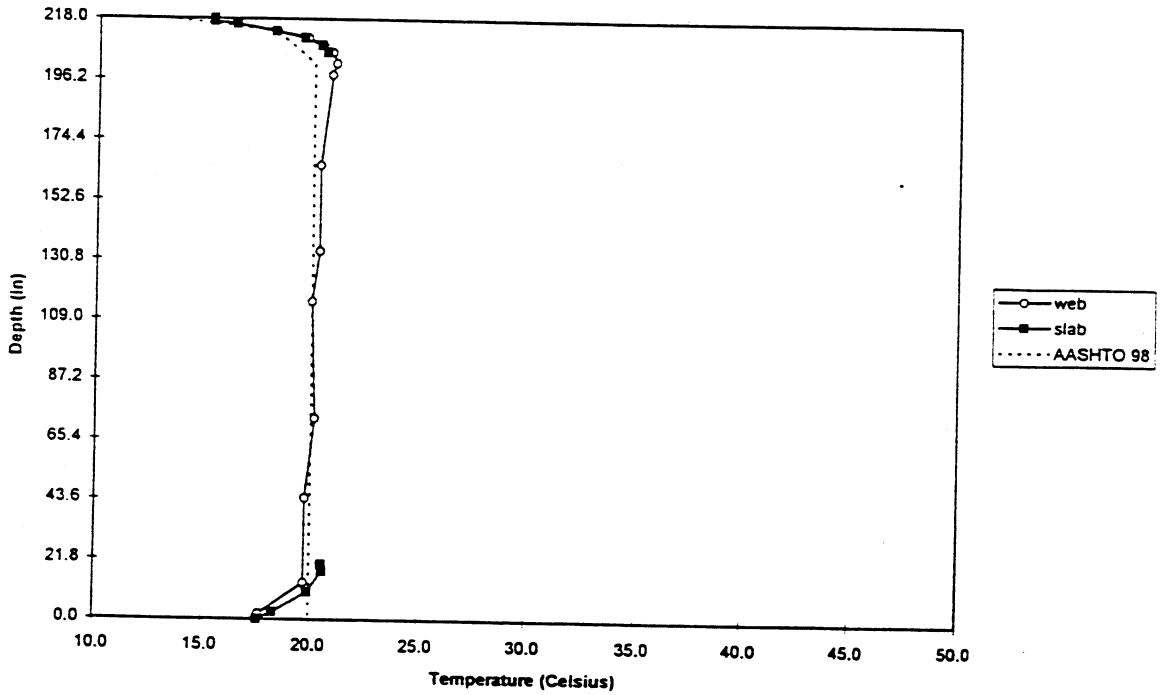

Figure 8.134

Negative Thermal Gradient at Section E

23-Feb-97 06AM

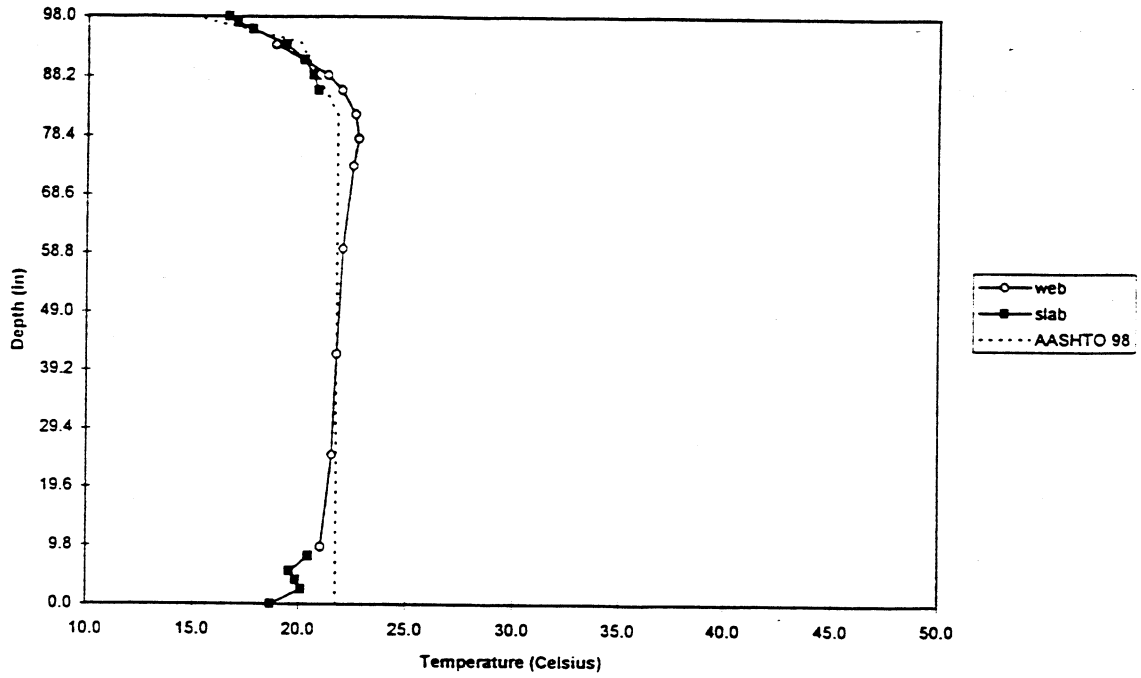

Negative Thermal Gradient at Section F

23-Feb-97 06AM

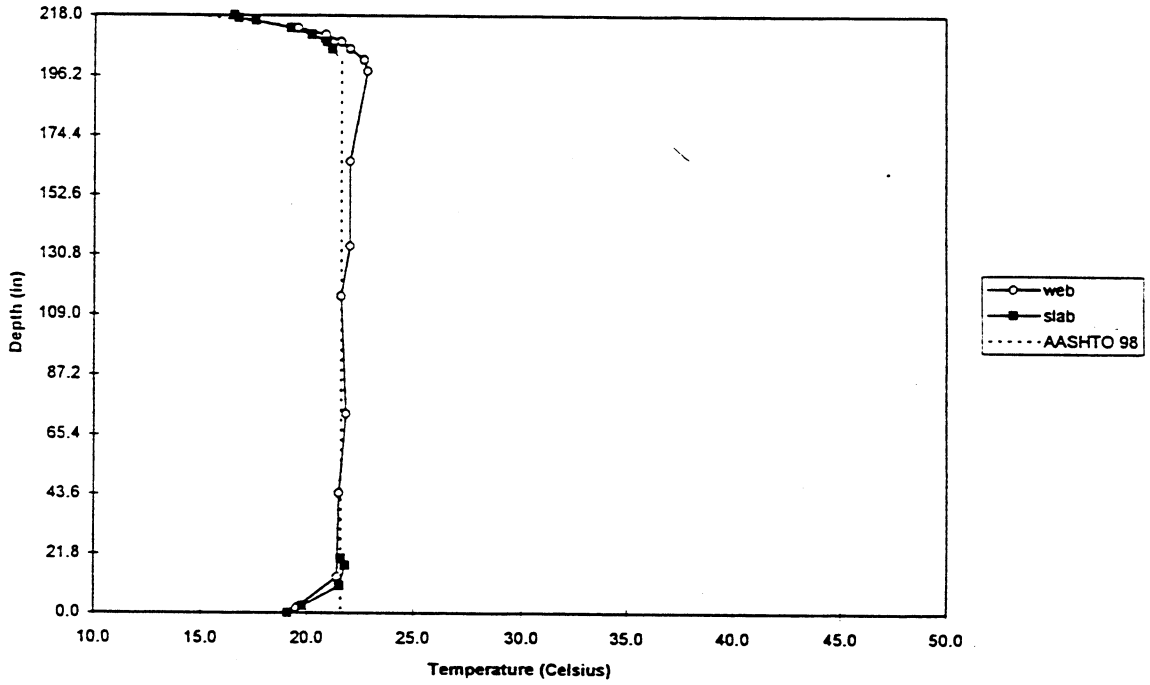

Figure 8.135

Negative Thermal Gradient at Section E

19-Nov-97 06AM

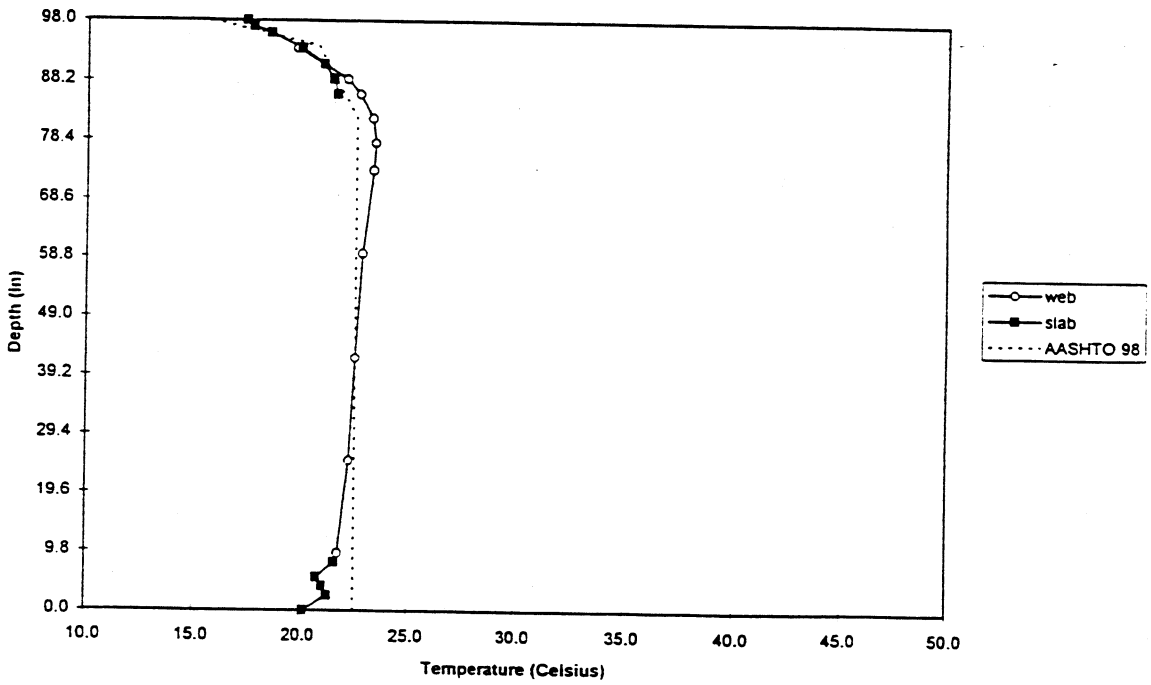

Negative Thermal Gradient at Section F

19-Nov-97 06AM

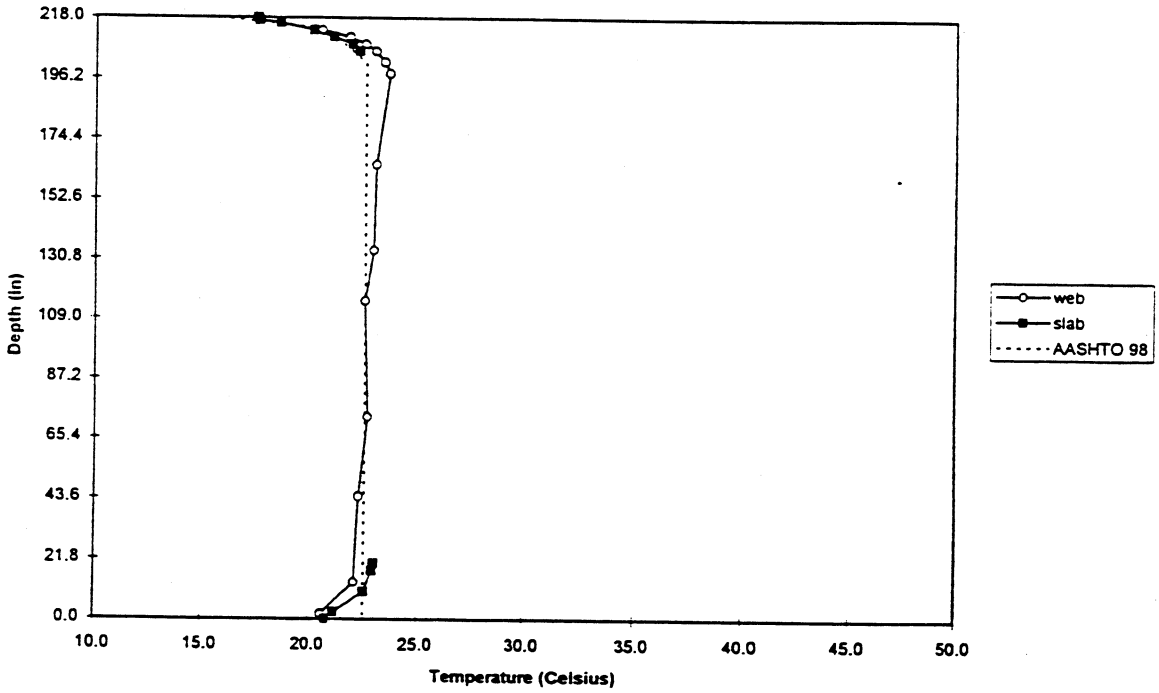

Figure 8.136

Negative Thermal Gradient at Section E

25-Nov-97 06AM

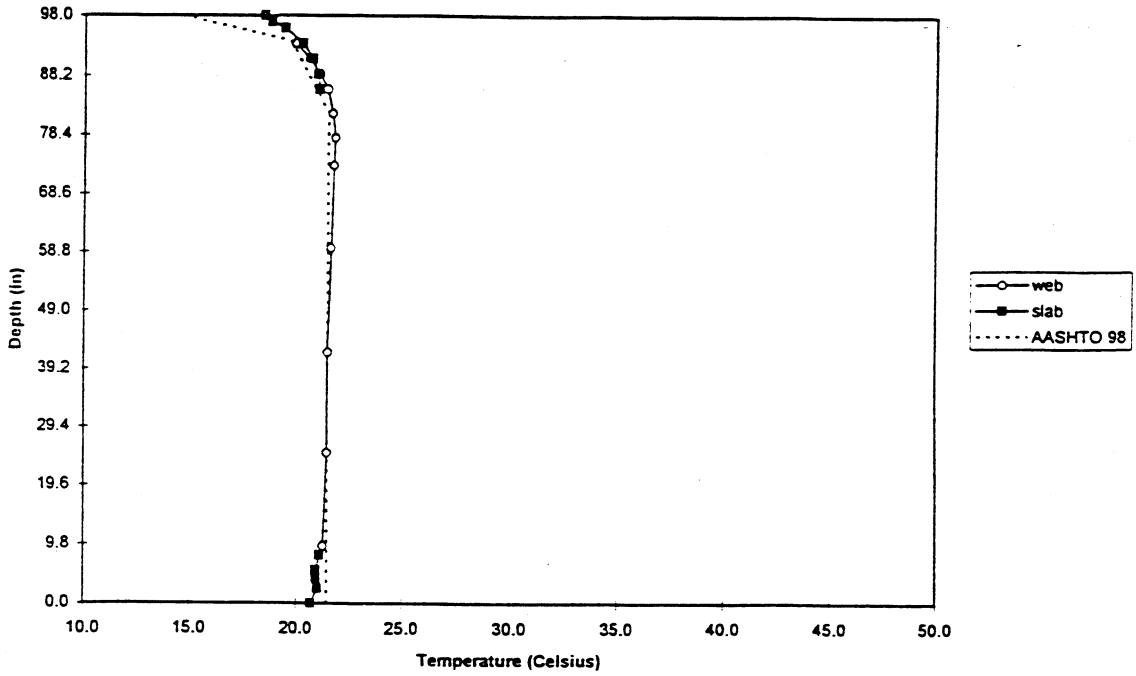

Negative Thermal Gradient at Section F

25-Nov-97 06AM

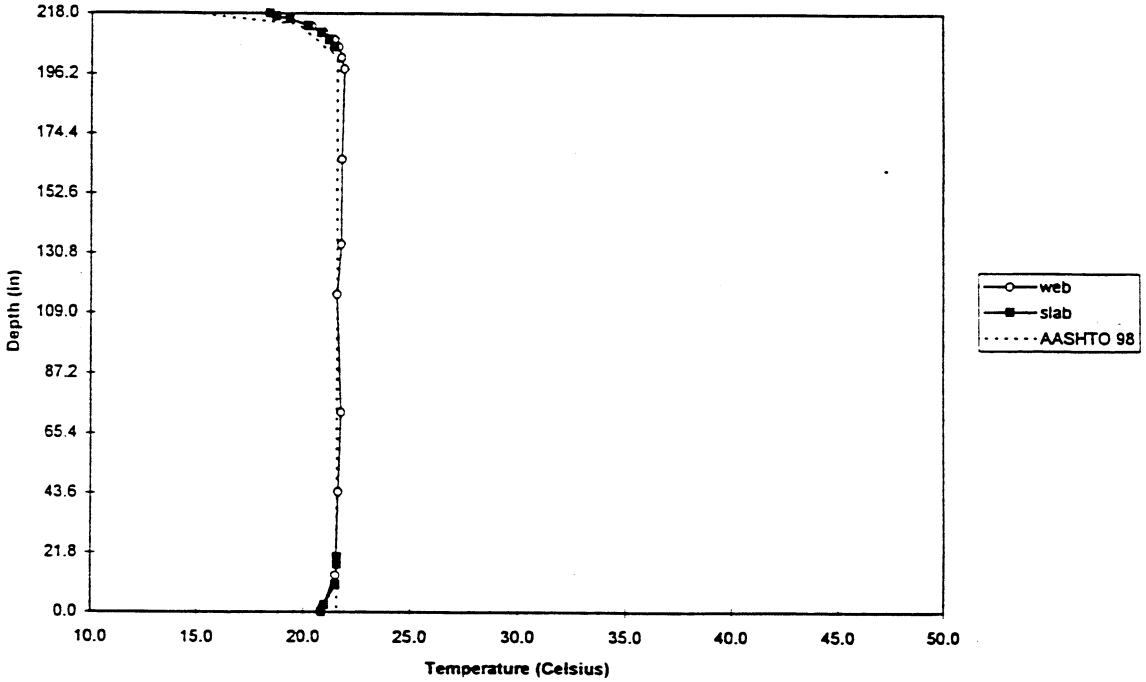

Figure 8.137

Negative Thermal Gradient at Section E

11-Dec-97 06AM

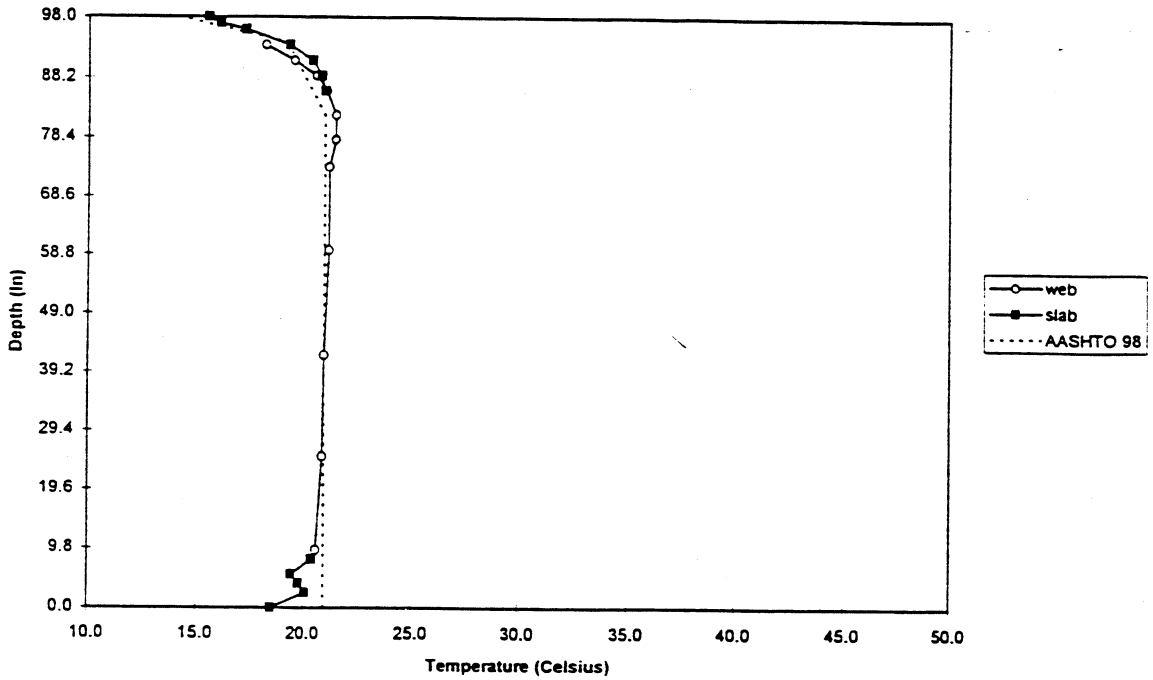

Negative Thermal Gradient at Section F

11-Dec-97 06AM

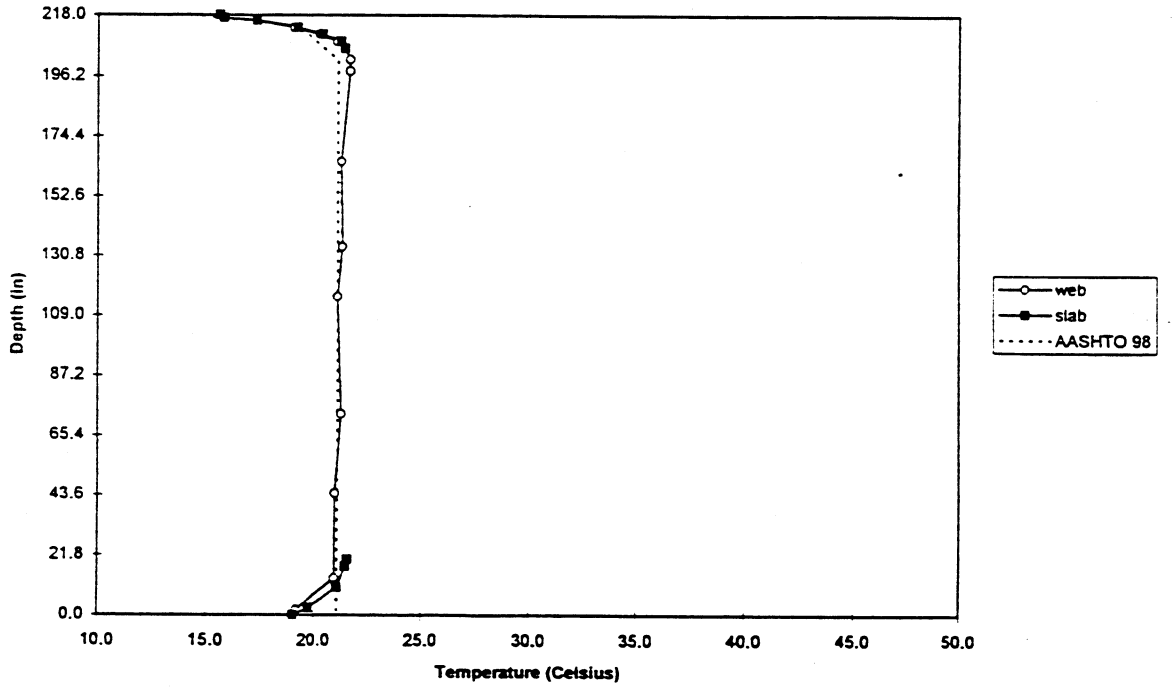

Figure 8.138

29-Dec-97 06AM

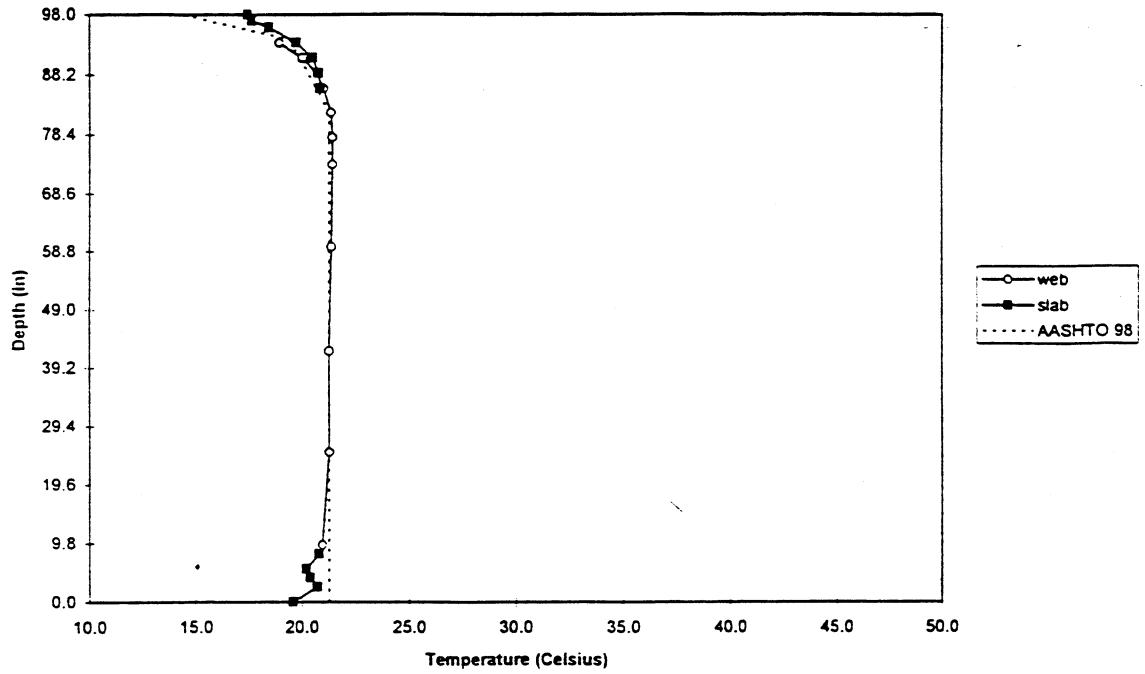

29-Dec-97 06AM

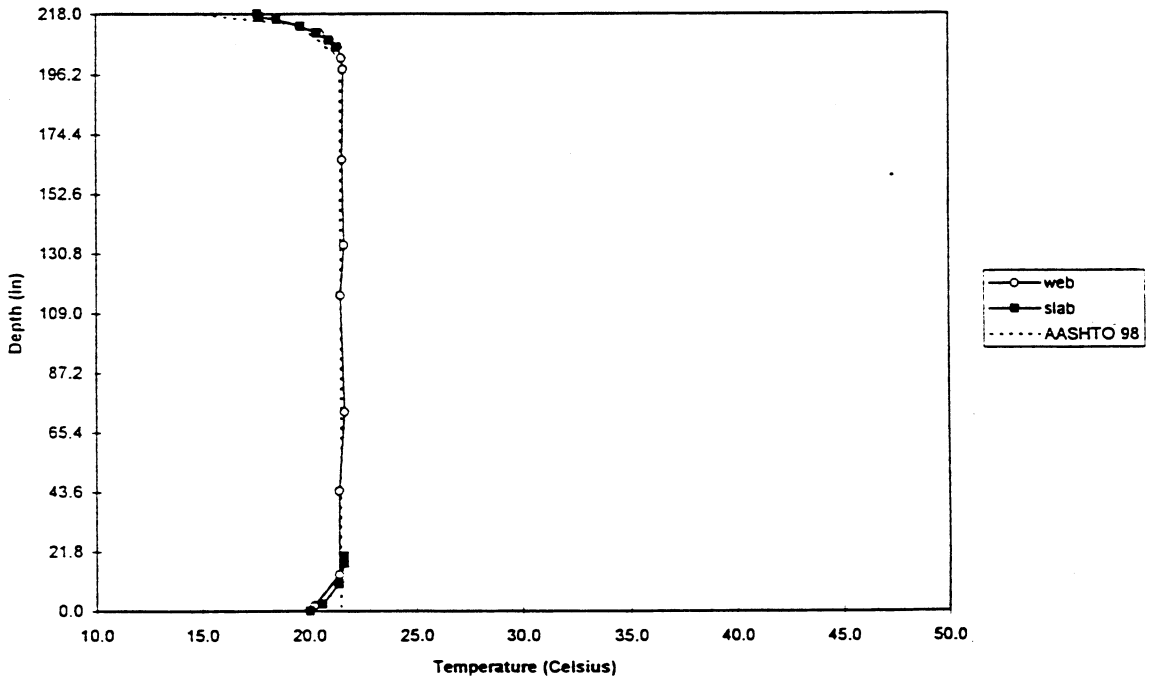

Figure 8.139

Negative Thermal Gradient at Section E

31-Dec-97 06AM

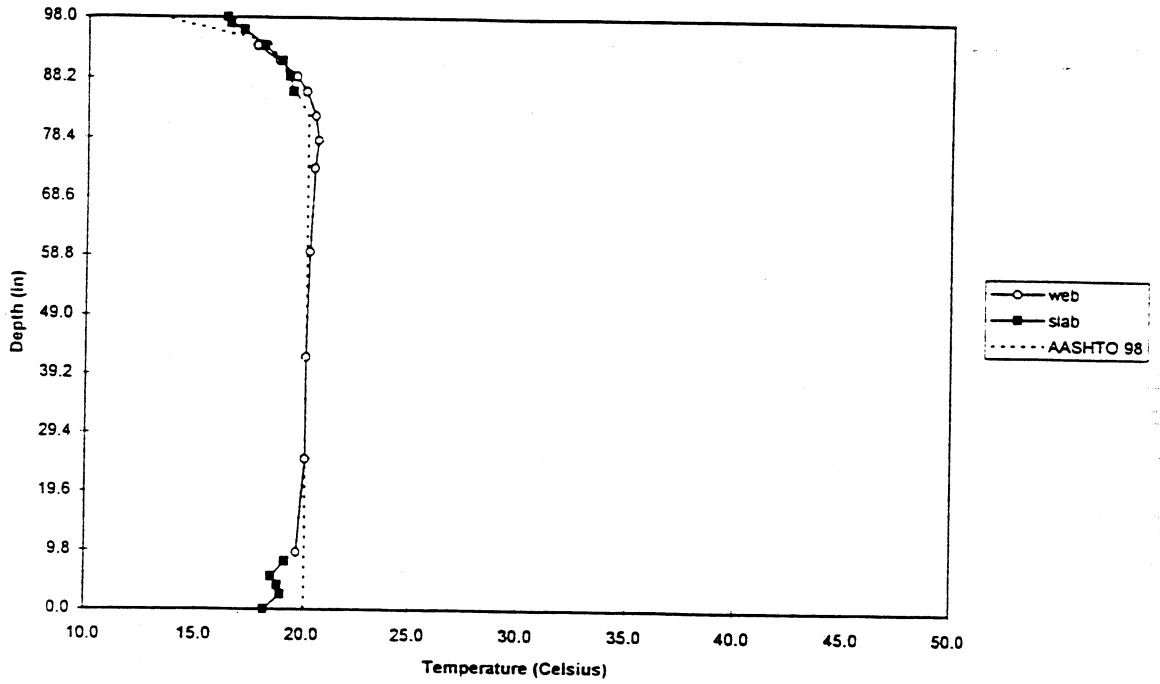

Negative Thermal Gradient at Section F

31-Dec-97 06AM

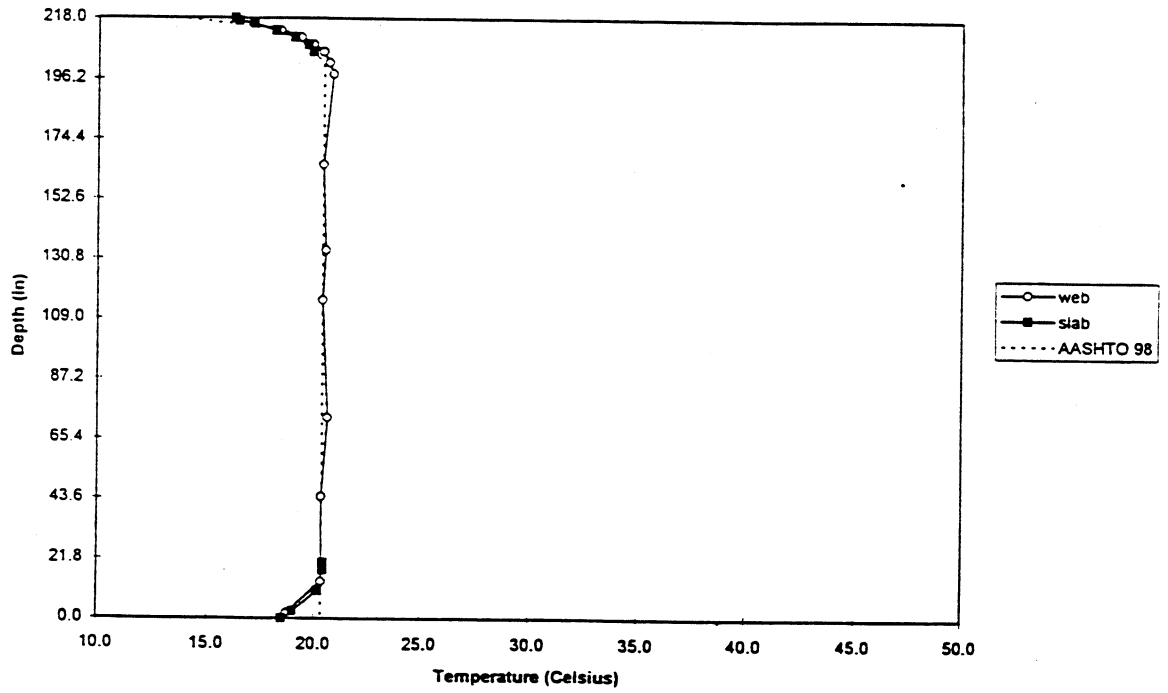

Figure 8.140

CHAPTER 9

LOAD TEST

9.1 Introduction

This chapter presents the observations made during two major loading events on the NHVV. The first event was the addition of a 50 mm (2 in.) thick concrete overlay or topping slab over the entire viaduct roadway. The second event was a planned load test of the instrumented spans of the viaduct. Each of these events was monitored using the instrumentation installed in the viaduct. The observations made regarding vertical deflections and bending stress distributions are compared with analyses using the SAP2000 computer program. Each loading event will be presented and discussed separately. Some common conclusions are drawn regarding the performance of the viaduct and the instrumentation during these events.

9.2 Addition of Overlay

During the first two weeks of October, 1996, a 50 mm (2 in.) thick concrete overlay or topping slab was added to the roadway of Unit 2IB, the instrumented section of the NHVV. The overlay placement was accomplished in seven separate concrete pours each covering approximately 80 meters (260 lineal feet) of viaduct roadway. Short-term vertical deflections were monitored at 5:30 AM each morning immediately prior to the subsequent overlay placement. The deflections were monitored by the taut-wire base-line system and the tiltmeters located at each of the piers supporting Unit 2IB.

The measured deflected shapes are compared with analytical values obtained from SAP2000 (1996) computer analyses. Comparison of the analytical and measured deflections indicates good agreement for this short-term event.

9.2.1 Deflection Monitoring

9.2.1.1 Base-Line System

The taut-wire base-line system was installed in all four instrumented spans for deflection measurements as described in Chapter 3. This system consists of a high-strength piano wire strung at constant tension inside the box-girder from one pier to the next, to act as a reference line. Precision measurements between this base-line and steel plates on the underside of the top slab provide deflection measurements at set locations.

9.2.1.2 Tiltmeters

Tiltmeters located inside the box-girder at each of the supporting piers were monitored during each of the base-line deflection measurements. The tiltmeters are oriented to record the rotation of the box-girder around an axis perpendicular to the longitudinal axis of the viaduct.

9.2.1.3 Data Collection

Initial readings were taken after completion of construction. The difference between the initial reading and all subsequent measurements is the girder deflection relative to the ends of the span. Measurements are taken early in the morning to reduce the effects of diurnal thermal variations.

For deflection measurements during the overlay placement, a series of initial readings were taken immediately before placement of the first section of overlay on Unit 2IB. Subsequent readings taken at 5:30 AM each morning were compared with these initial readings to provide the vertical deflection of the viaduct resulting from the overlay placement. Note that any shortening of the supporting piers is not detected by the base-line system and was therefore also removed from the computer analyses.

9.2.2 Computer Analysis

During the design of the North Halawa Valley Viaduct, T. Y. Lin International utilized the general purpose program SAP90 (1992) for analysis of short-term elastic events. The original SAP90 input file has been updated to an "as-built" SAP2000 (1996) file for use in this study for the analytical prediction of the deflections during pouring of the concrete overlay. This model is a relatively simple two-dimensional model which assumes that the viaduct is horizontal and straight (See Figure 9.1). This model is referred to here as the 2-D model. In addition, a full three-dimensional model of Unit 2IB of the viaduct has been created at the University of Hawaii. This 3-D model includes the 6% slope and horizontal curve of the viaduct (See Figure 9.2). Both analytical models were used to analyze the effect of the overlay pours, and the results are compared with the measured deflections in the following sections.

9.2.3 Short-term Deflections During Overlay Placement

The final driving surface of the Viaduct consists of an unreinforced 50 mm (2 in.) thick concrete overlay. On Unit 2IB, this overlay was poured during October 1996 in approximately 80 meter (260 ft) sections. The base-line deflection system was monitored each morning at 5:30 AM prior to pouring the next section of overlay. SAP2000 analyses, both 2-D and 3-D models, were run for each of the overlay placements for comparison with the field measurements.

The modulus of elasticity of the concrete was based on the average CTL 90-day modulus of elasticity of 26.5 GPa (3850 ksi), modified to an equivalent 3-year modulus of 28.4 GPa (4115 ksi). Gross concrete section properties were assumed for the uncracked prestressed concrete box girder. The analytical results are compared with the measured deflection profiles in Figure 9.3 for spans P7 to P10, and Figure 9.4 for spans P10 to P13. The extent of the overlay is shown above each of the deflection profiles.

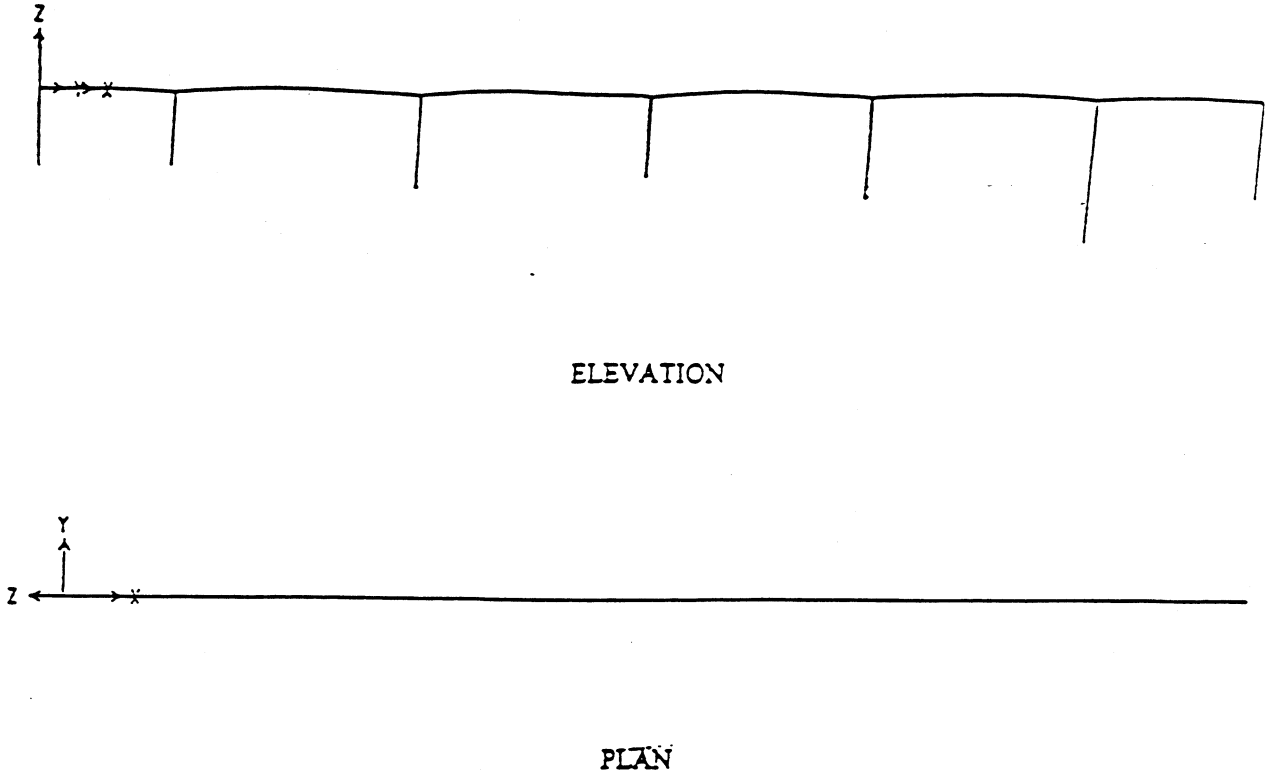

Figure 9.1: SAP2000 Two Dimensional (2-D) Computer Model

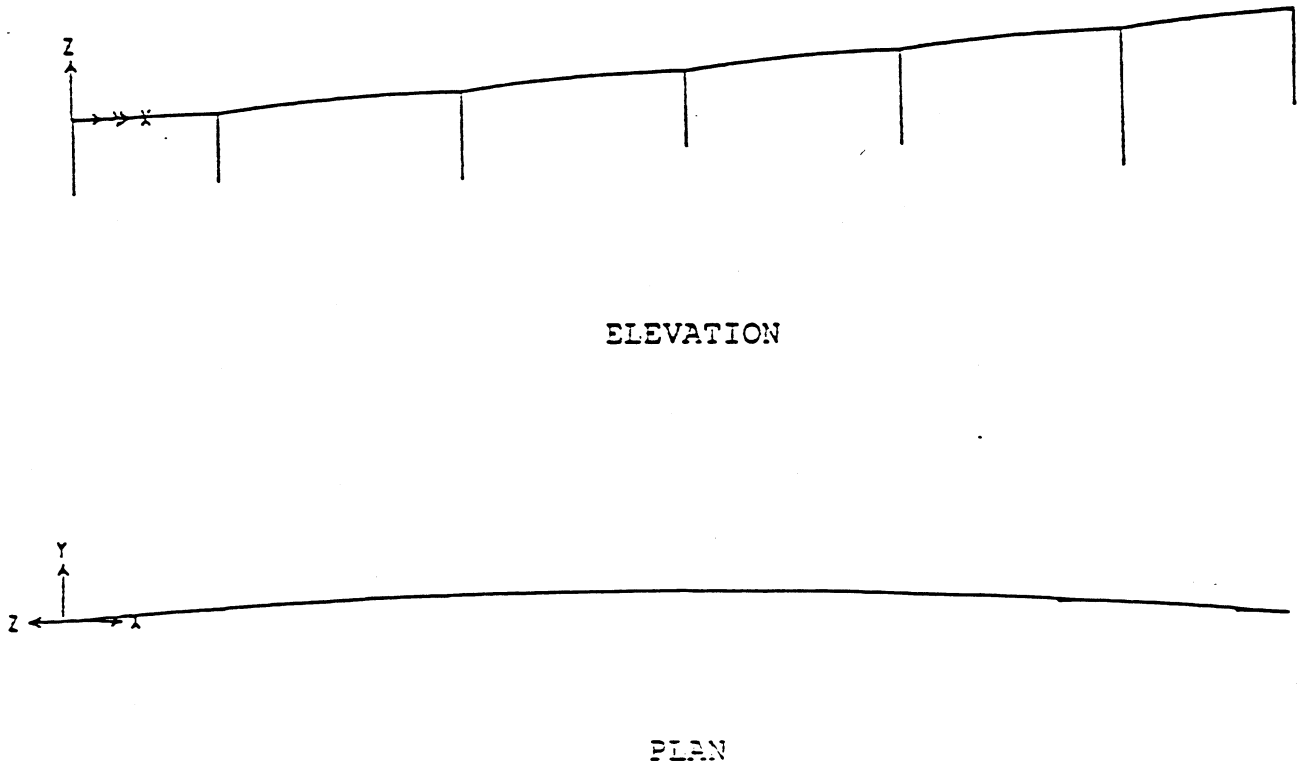

Figure 9.2: SAP2000 Three Dimensional (3-D) Computer Model

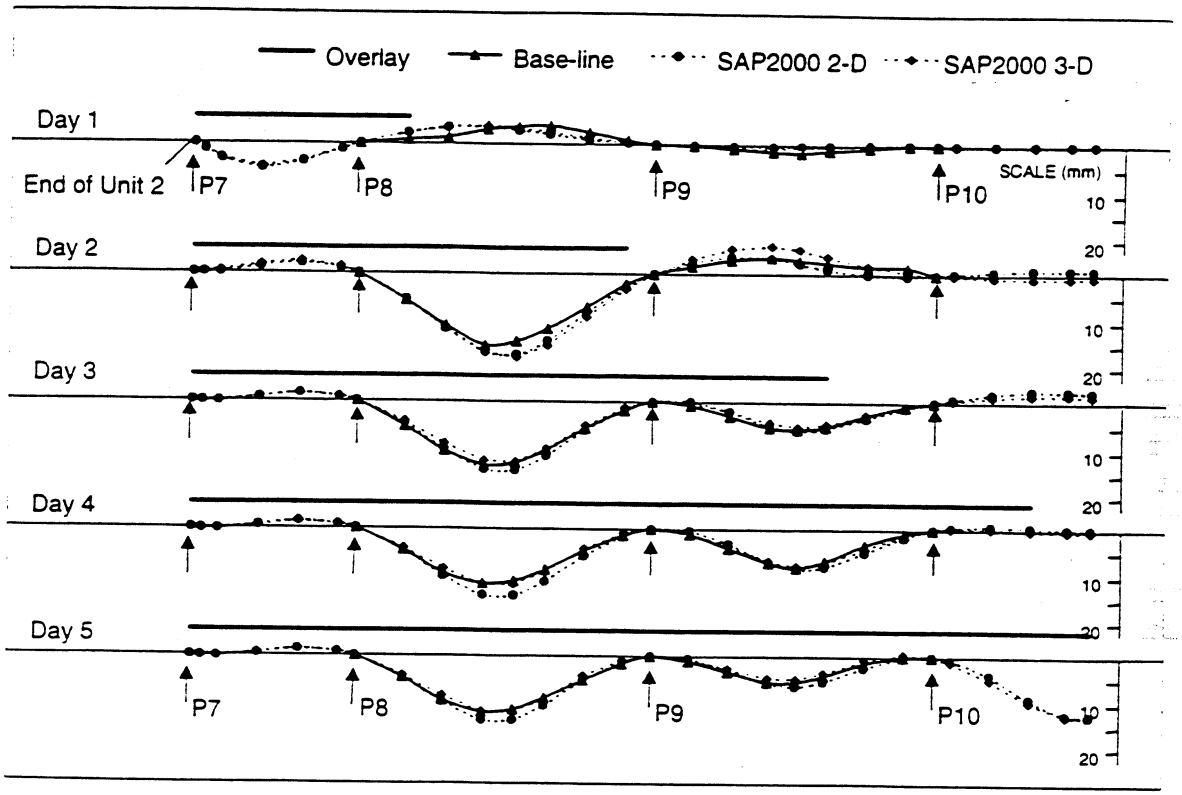

Figure 9.3: Overlay Deflections for Spans P7 to P10

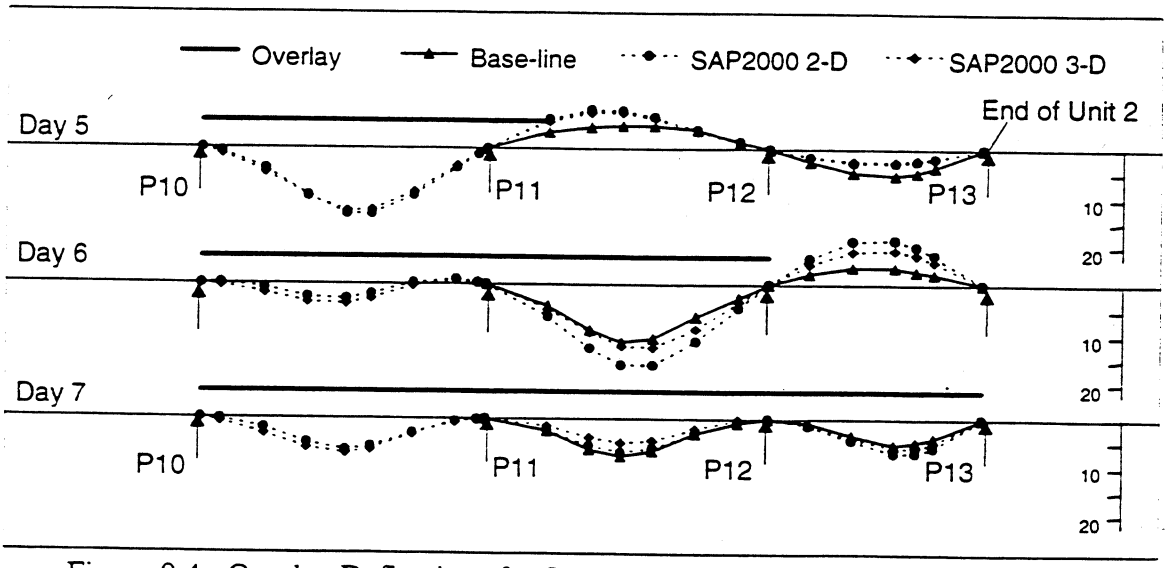

Figure 9.4: Overlay Deflections for Spans P10 to P13

9.2.4 Discussion of Results

The maximum deflection observed during placement of the overlay was 14 mm (9/16") at midspan between piers P8 and P9. The maximum residual deflection after completion of the entire overlay was 11 mm (7/16") also at midspan between piers P8 and P9.

The analytical models used in the SAP2000 analyses assume a uniform 50 mm (2 in.) thick overlay throughout. Because of construction tolerances in the surface of the structural concrete, the overlay thickness as-placed varied somewhat from this design thickness. This variation will affect the comparison between analytical and measured results to some extent, but refinement of the model loading based on actual overlay thickness would only be possible if systematic thickness measurements had been made during overlay placement.

In spite of the uncertainty of the actual loading, good comparison between analytical and measured results is observed for most of the deflection profiles. The SAP2000 2-D analysis appears to overestimate the deflection slightly, particularly for spans P11 to P13 under partial loading conditions. However, under full overlay loading (Day 5 in Figure 9.3 and Day 7 in Figure 9.4) the SAP2000 2-D analytical and measured deflections are in close agreement.

The full three-dimensional analytical model, SAP2000 3-D, generally produces better agreement with the measured deflections than the 2-D model.

The only areas of significant disagreement between the analytical models and the measured results are found in the unloaded spans adjacent to a loaded span. This is particularly noticeable on Day 5 in span P11 to P12 (Figure 9.4) and Day 6 in span P12 to P13 (Figure 9.4). This phenomenon is probably due in part to modeling of the bearing supports as pure pin connections in the SAP2000 analyses, while in reality, the bearing pads provide limited rotational stiffness at the expansion piers.

9.2.5 Conclusions

- Prediction of instantaneous deflections of an uncracked prestressed concrete structure can be achieved with reasonable accuracy utilizing commercially available Finite Element Analysis programs.
- The analytical deflections predicted by SAP2000 2-D and 3-D models for the addition of the 50 mm (2 in.) concrete overlay compared well with the measured deflections.
- The full three dimensional analytical model was generally in closer agreement with the measured deflections than the 2-D analysis. With computer capabilities currently available, it seems appropriate always to utilize full 3-D representation of a structure to produce the best possible estimate of the structural response.
- A simple piano-wire base-line system proved effective as an inexpensive deflection monitoring technique for short-term events.

9.3 Load Test

After placement of the overlay, and effective completion of the NHV Viaduct, a load test was performed on the instrumented spans of Unit 2IB. Analysis of the results of this load test are in progress at the University of Hawaii. A final report will be completed in late 1998 or early 1999. This report will describe the load test in detail, and will present all of the comparisons between observed and analytical results.

At the time of writing this progress report, some of the analytical studies on the load test had been completed. A sampling of the findings to date are included, however this is not a complete description either of the load test or of the results of that study.

9.3.1 Test Objectives

The following were the primary objectives of the load test.

1. To provide an exhaustive comparison between the theoretical short-term elastic computer analysis model (SAP2000) and the behavior of the actual structure.
2. Concrete strain distributions across the various instrumented sections (both deep end-span sections and shallow mid-span sections) were monitored by three types of existing instrumentation; vibrating wire (VW) strain gages, electrical resistance (ER) strain gages on the rebar, and Demec mechanical gage readings on the inside surface of the concrete box girder. Comparison of these observed strains with theoretical strains computed assuming plane-sections-remain-plane would allow verification of this and other analysis assumptions. It would also allow for comparison between the various strain instrument readings.
3. Deflection measurements were made using optical surveys of the roadway barriers, the interior taut-wire deflection system and the tiltmeters installed at each pier. The deflected shape of the viaduct under each load condition could be compared with the deflections anticipated by the SAP2000 computer model.
4. A significant benefit of a load test on the recently completed structure is that this load test would be reproducible in the future. Comparison of the results of two tests, performed five to ten years apart, would yield valuable information on the long-term changes in the bridge properties. Repeating this test every five to ten years would provide valuable confirmation of the results of the long-term monitoring program.
5. In the event that additional external prestressing must be added at a later date to enhance the viaduct performance, a subsequent load test identical to the one proposed here could be compared with the results from this test to validate the improvements introduced by the additional prestress.

9.3.2 Test Program

The load test was performed using four loaded trucks producing axle loads similar to those specified for the HS20 design truck loading. The trucks were loaded with sand to produce a gross weight close to 72,000 lbs. The exact weight of each truck, and the load on each axle, were determined using a load scale at the Hawaiian Cement Ready Mix Plant at Halawa Valley.

The load test consisted of two test series. All four trucks were used for each of the series. Series 1 involved positioning the trucks in two rows of two trucks located side-by-side across the viaduct roadway as shown in Figures 9.5a and 9.6a. Series 2 involved all four trucks immediately behind each other located along the extreme North side of the viaduct roadway as shown in Figures 9.5b and 9.6b.

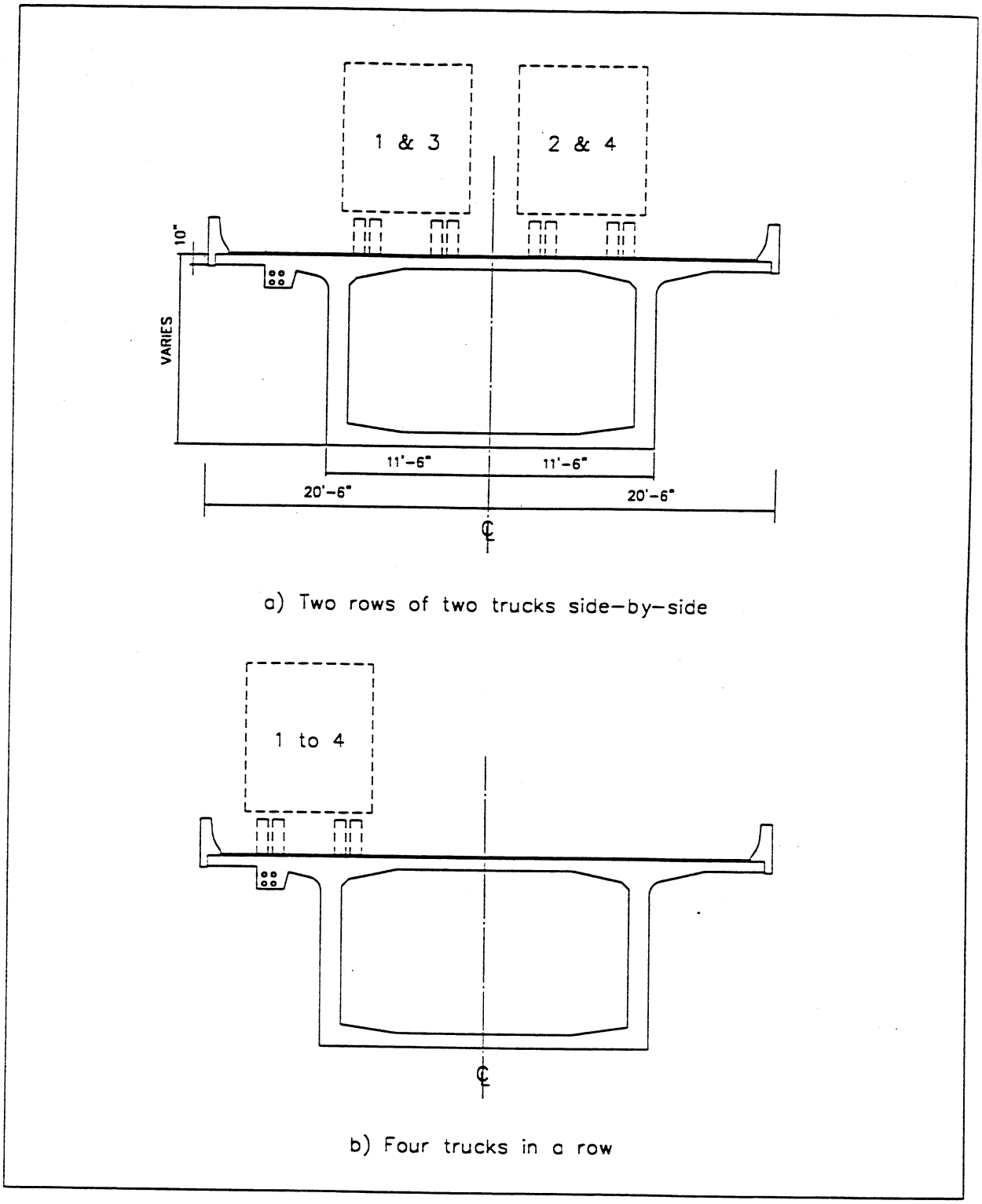

Figure 9.5: Viaduct Section showing Load Test Truck Configurations

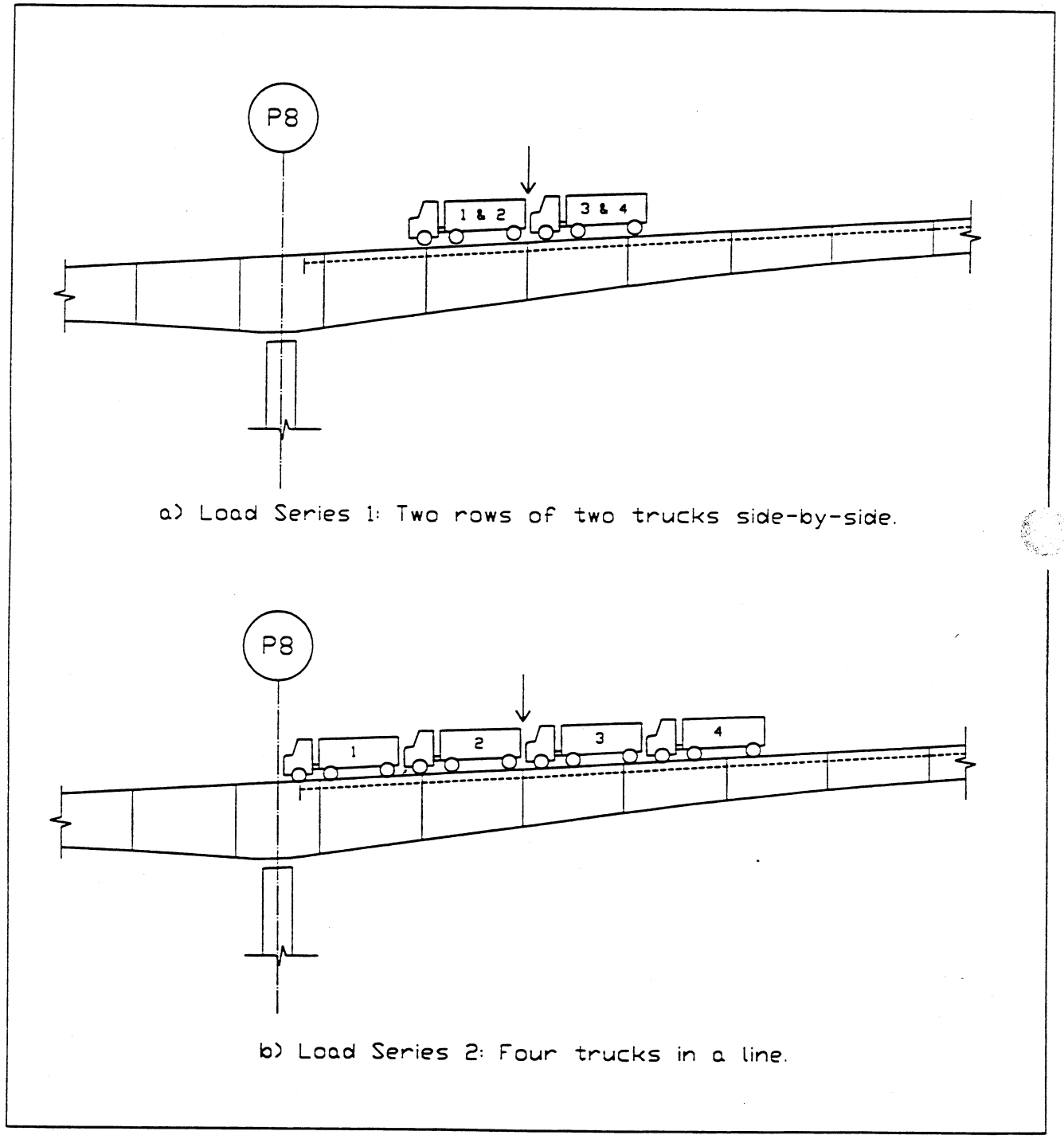

Figure 9-6: Viaduct Elevation showing Load Test Truck Configurations

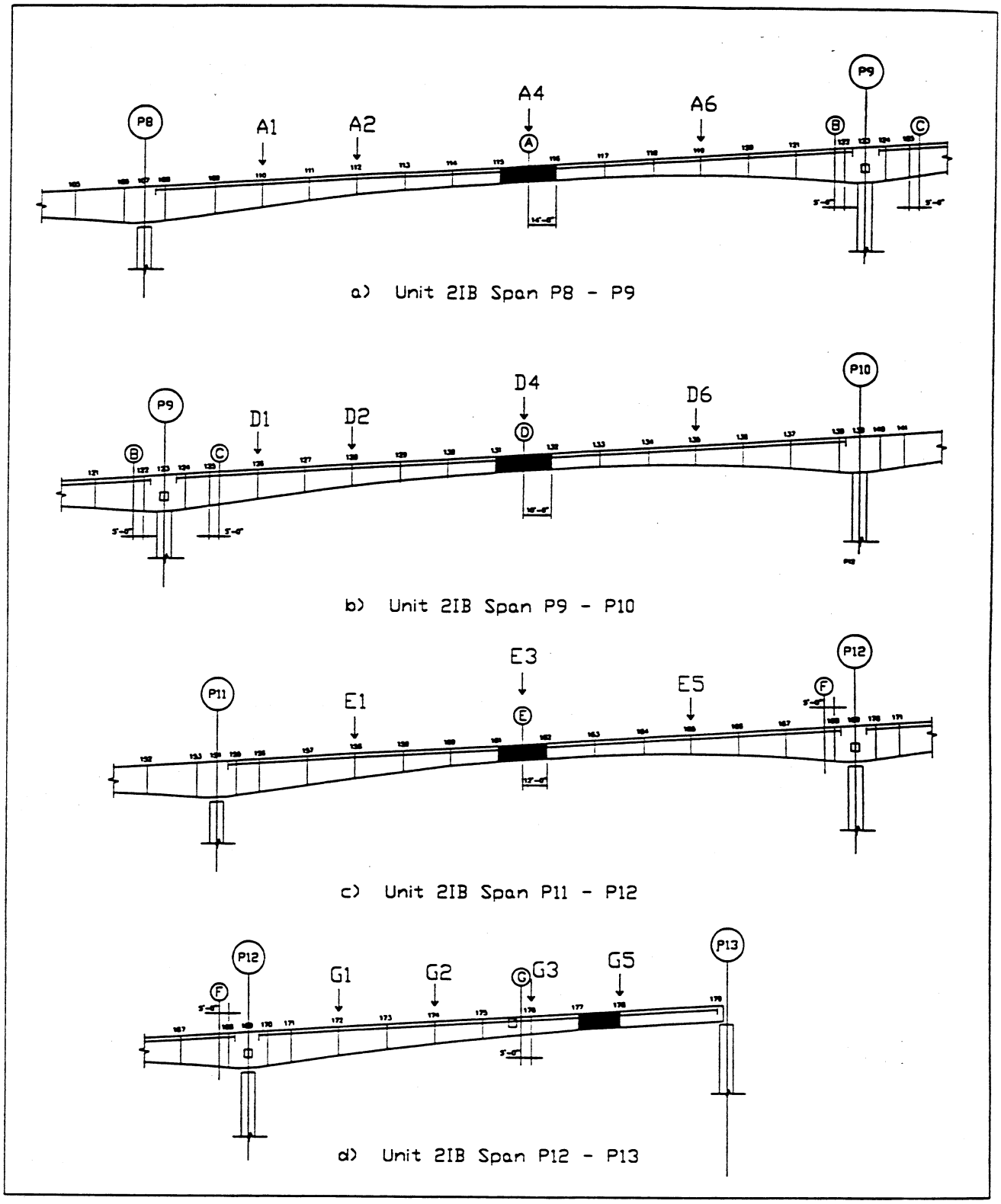

Figure 9-7: Elevation showing Load Test Truck Locations

In each test series, the truck loads were centered over each of the selected joints and a full set of instrument readings taken. The trucks were then moved to the next joint for another set of readings. The various load points are shown in Figure 9.7. This procedure continued until the trucks had been located at all selected joints in the instrumented spans.

9.3.3 Analytical Models

The same SAP2000 models used for the overlay analysis were used in the load test study. These models consist of a simple 2-D model which ignores the slope and curvature of the viaduct. A more accurate 3-D model was also used as described in section 9.2.2. The modulus of elasticity of the concrete was based on the average CTL 90-day modulus of elasticity of 26.5 GPa (3850 ksi), modified to an equivalent 3-year modulus of 28.4 GPa (4115 ksi). This modulus is referred to as E1. In addition, analyses were made using the modulus predicted by the ACI code recommended expression for E_c producing a value of 35.5 GPa (5140 ksi), referred to as E2. Gross concrete section properties were assumed for the uncracked prestressed concrete box girder.

9.3.4 Deflection Comparisons

Field measurements of vertical deflections were made using three systems. The taut-wire baseline system was monitored inside the box girder. Optical surveys of the barriers at each side of the roadway were average to produce a centerline deflection. Tiltmeters at the top of each pier monitored the rotation of the box girder at the supports.

The taut-wire system and tiltmeters proved extremely accurate and reliable, as will be seen in the subsequent comparisons with the analytical results. Unfortunately, the optical survey results were not always as consistent. Windy conditions and line-of-sight problems contributed to less than desirable survey results. Most of the optical survey results are included in the presentation of the results, but in some cases the optical survey results were clearly unreliable and were ignored.

The analytical results are compared with the measured deflection profiles in Figures 9.8 to 9.22. Each plot shows the loaded span and the adjacent instrumented span. The truck load center point is indicated by the load arrow on top of the girder, while the pier supports are indicated by arrows below the girder. All plots are drawn with the same vertical scale for ease of comparison.

9.3.5 Discussion of Deflection Results

As expected, the girder deflections increase as the truck load is located closer to the center of the span. In addition, the backspan upward deflections also increase. The taut-wire or piano wire deflection system agrees well with the optical survey for those surveys that were reliable. For example, in Figure 9.10, when the truck load was at midspan on span P8 to P9, a maximum deflection of 0.93 in. was measured by the piano wire, while the survey measured 0.97 in. In the adjacent backspan, agreement is also good except for some clearly unreliable survey results.

In addition, the tiltmeter readings, indicated by tangent lines drawn at each of the supports, agree very well with the measured deflected shape at the supports. Again referring to Figure 9.10, the tiltmeter readings at each support are almost exactly tangent to the piano wire profiles at the support, thus confirming the accuracy of the taut wire deflection system.

The analytical results are shown as three plots, one for the 2-D SAP2000 model, and two for the 3-D models with different modulus of elasticity values indicated by E1 and E2. Again referring to Figure 9.10 as a typical case, all of the analytical plots indicate the same shape as the measured deflections. However, the 2-D model appears to underestimate the deflection both in the loaded span and the backspan. The 3-D model using a concrete modulus based on the laboratory test results consistently overestimates the deflections.

However, the 3-D model using the ACI code recommended modulus provides good correlation with the measured deflections in the loaded span, though generally overestimates the deflections in the backspan. This overestimation of backspan deflections is often severe, as seen in Figure 9.14 with the truck load at the midspan of P9 to P10. The piano wire measured small backspan deflections, which are confirmed by the good agreement with the tiltmeters at supports P8 and P9. However, the 3-D analytical model significantly overestimated these deflections while correctly predicting the loaded span deflections. The analytical models assume fully pinned conditions at the sliding bearing supports, and rigid connection to the top of the pier at the fixed supports. These assumptions are being reviewed to determine their effect on the deflection predictions.

9.3.6 Stress Comparisons

Preliminary comparisons between strains measured in the instrumented cross-sections and stresses predicted by the SAP2000 computer models show good agreement. These results are only preliminary and so will not be included in this report. However, they will be fully detailed in the final load test program report.

9.3.7 Conclusions

- The analytical deflections predicted by the SAP2000 3-D model for the load test compared well with the measured deflections in the loaded span, but were less accurate in the adjacent backspan. The support conditions assumed in the computer model will be reviewed. The selection of modulus of elasticity of the concrete also will be investigated further.
- The piano-wire base-line system again proved effective as an inexpensive deflection monitoring technique for short-term events. Correlation with the optical surveys and tiltmeter readings at the supports confirm the accuracy of the base-line system.
- Continued studies of both deflection and stress results are required before final reporting on the load test program.

9.4 References

SAP90 (1992). *A Series of Computer Programs for the Finite Element Analysis of Structures*, Computer Software, Computers and Structures, Inc., Berkeley, CA.

SAP2000 (1996). *Integrated Finite Element Analysis and Design of Structures*, Computer Software, Computers and Structures, Inc., Berkeley, CA.

Figure 9.8: Spans P8 - P10 Deflection
Centerline of Truck Load at A1

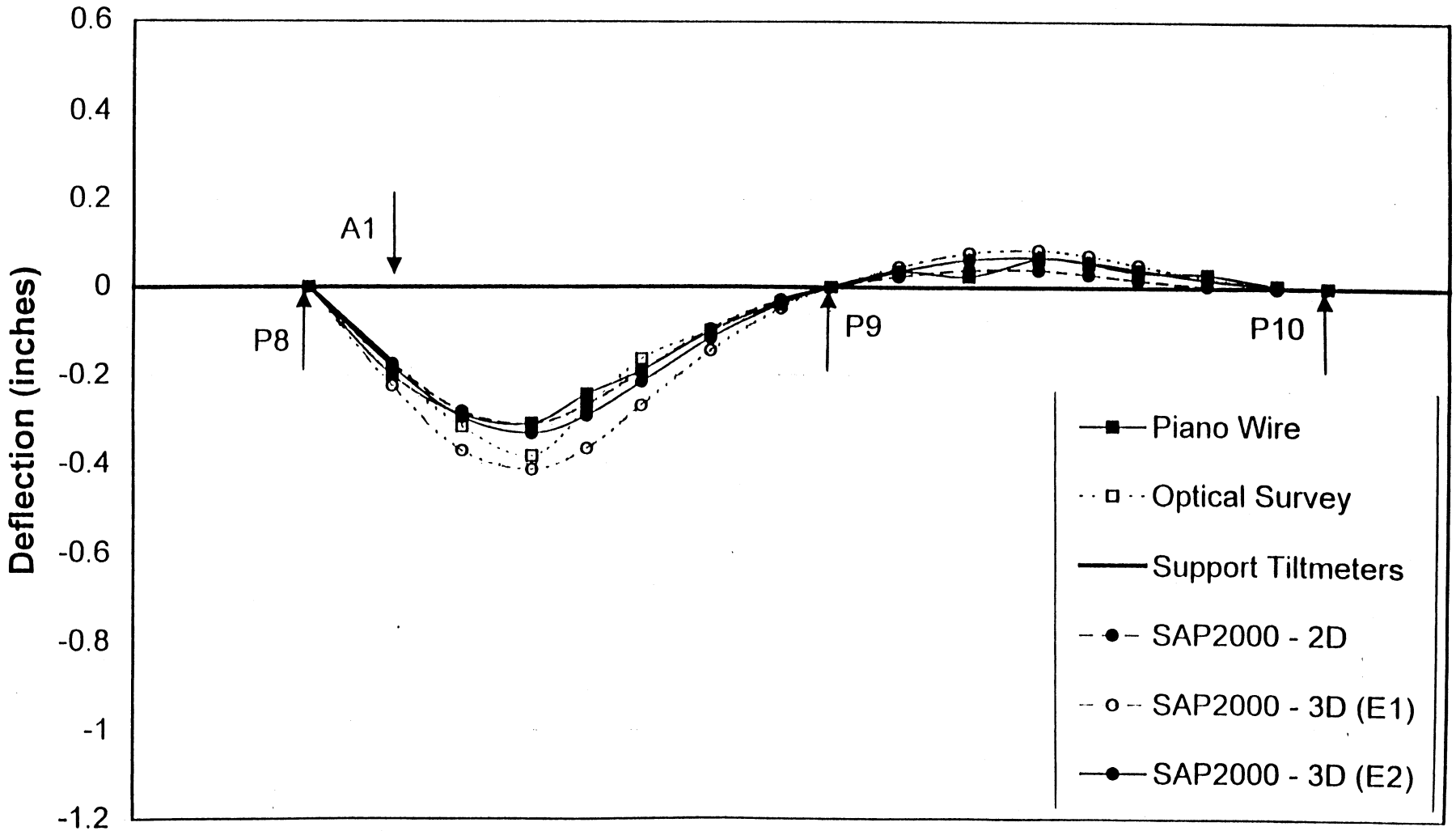

Figure 9.9: Spans P8 - P10 Deflection
Centerline of Truck Load at A2

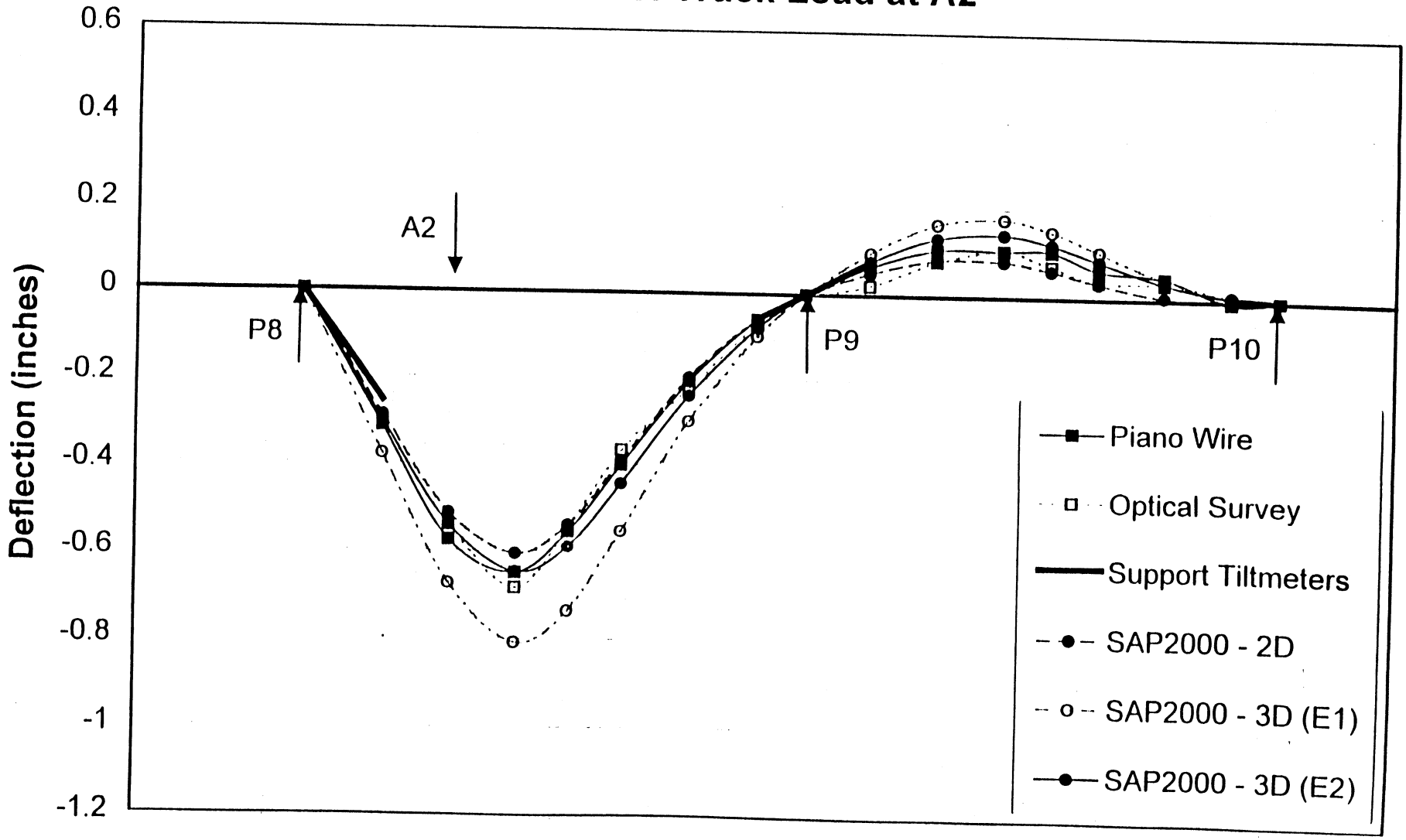

Figure 9.10: Spans P8 - P10 Deflection
Centerline of Truck Load at A4

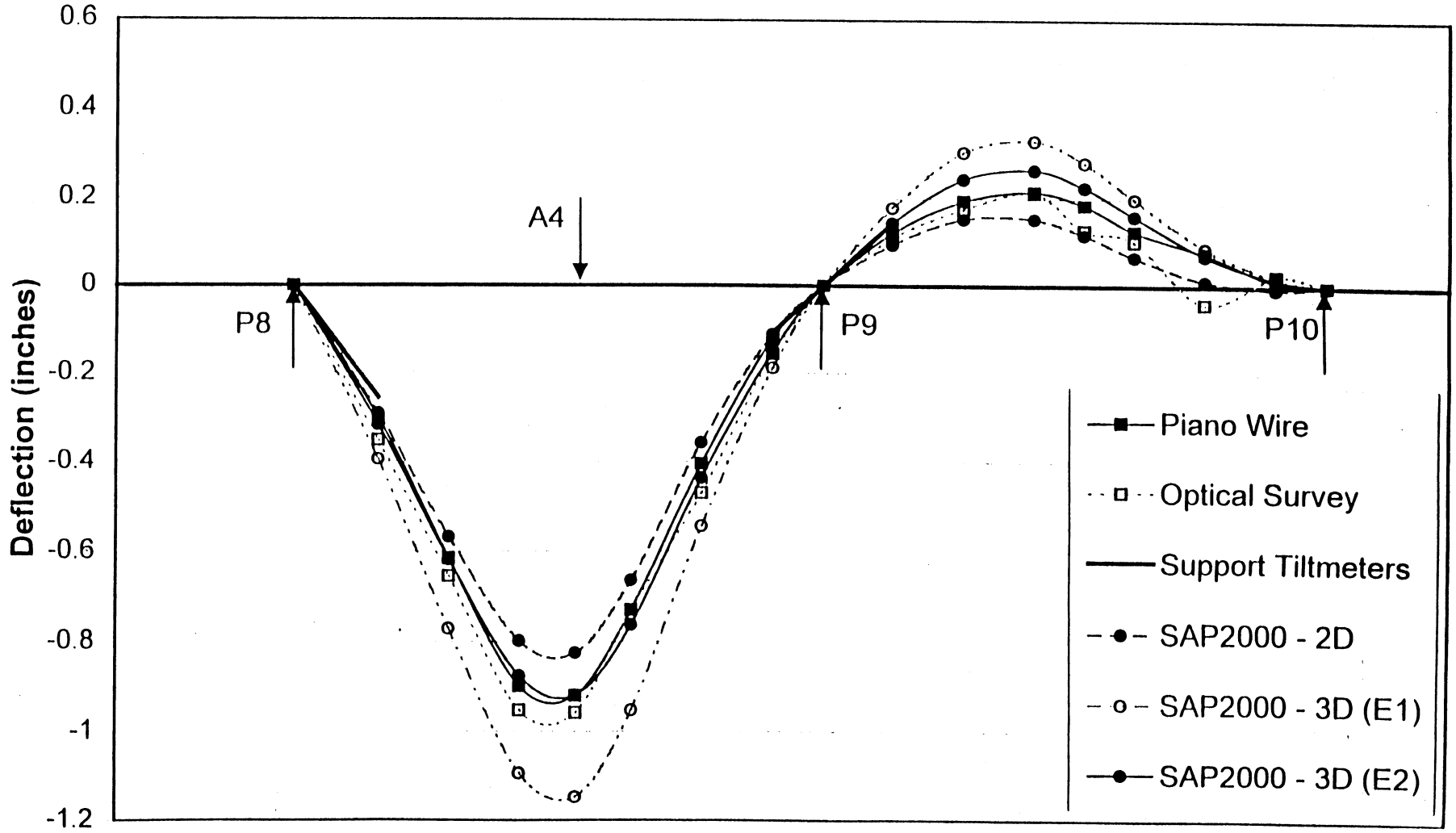

Figure 9.11: Spans P8 - P10 Deflection
Centerline of Truck Load at A6

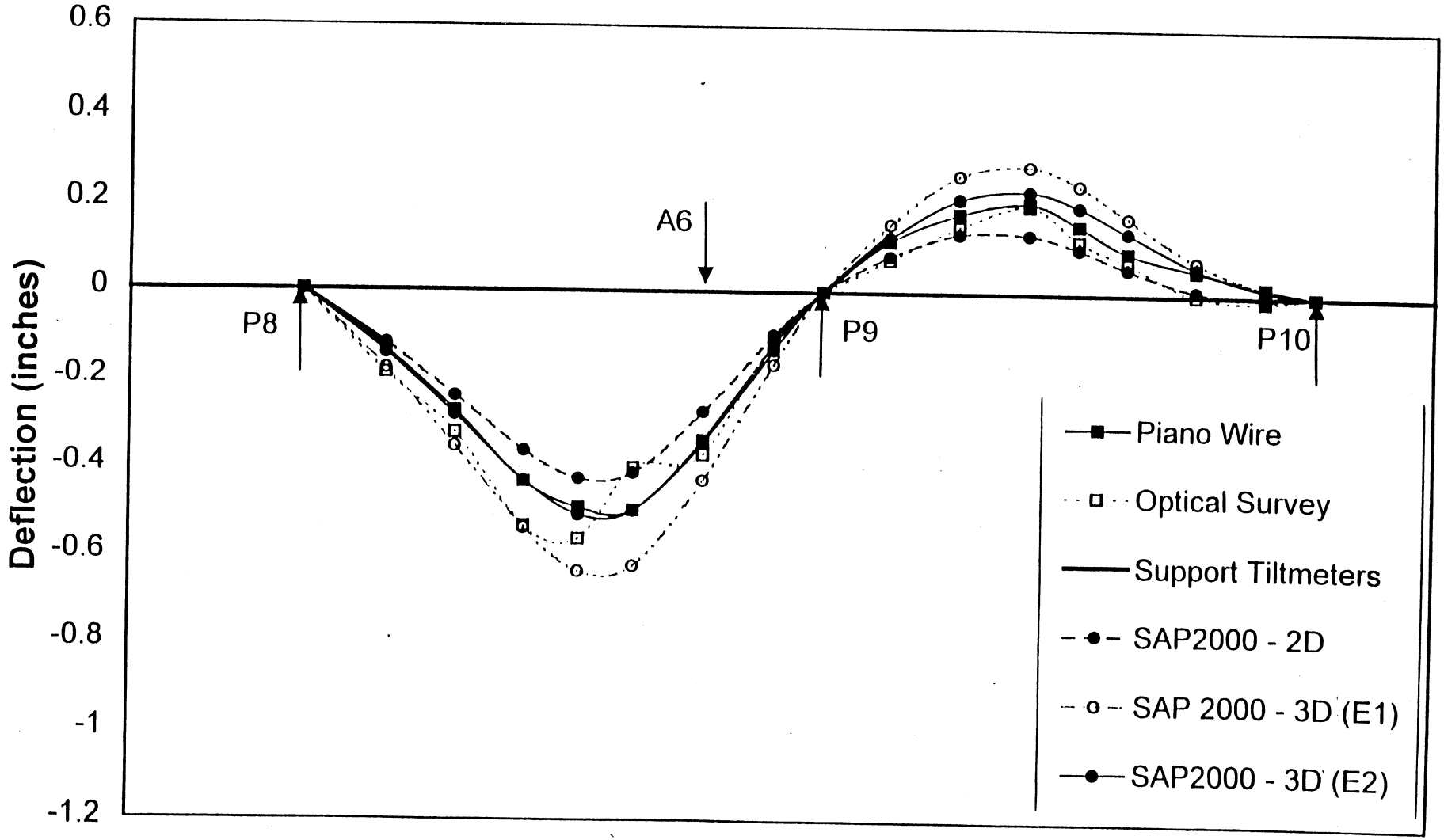

Figure 9.12: Spans P8 - P10 Deflection
Centerline of Truck Load at D1

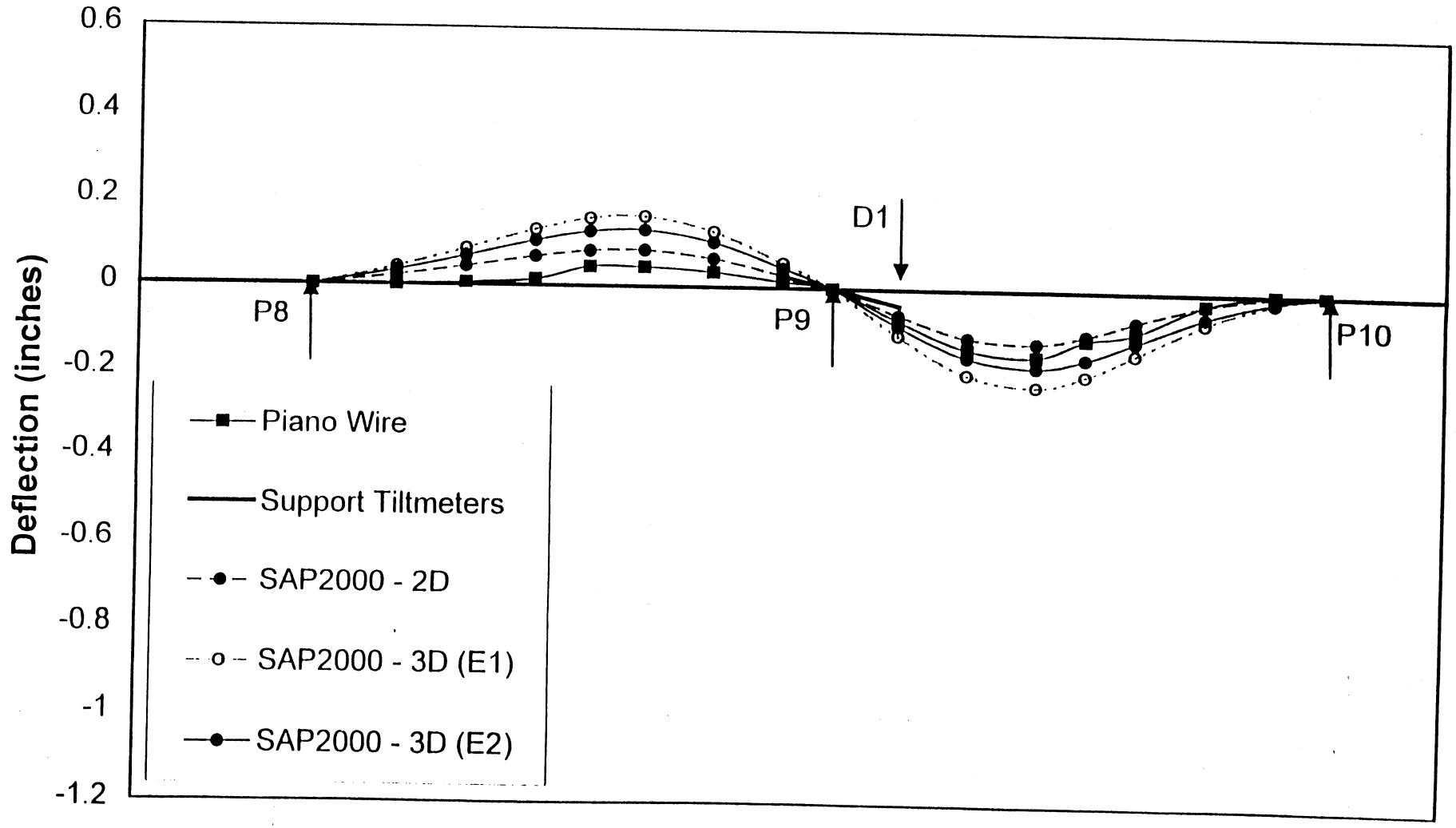

Figure 9.13: Spans P8 - P10 Deflection
Centerline of Truck Load at D2

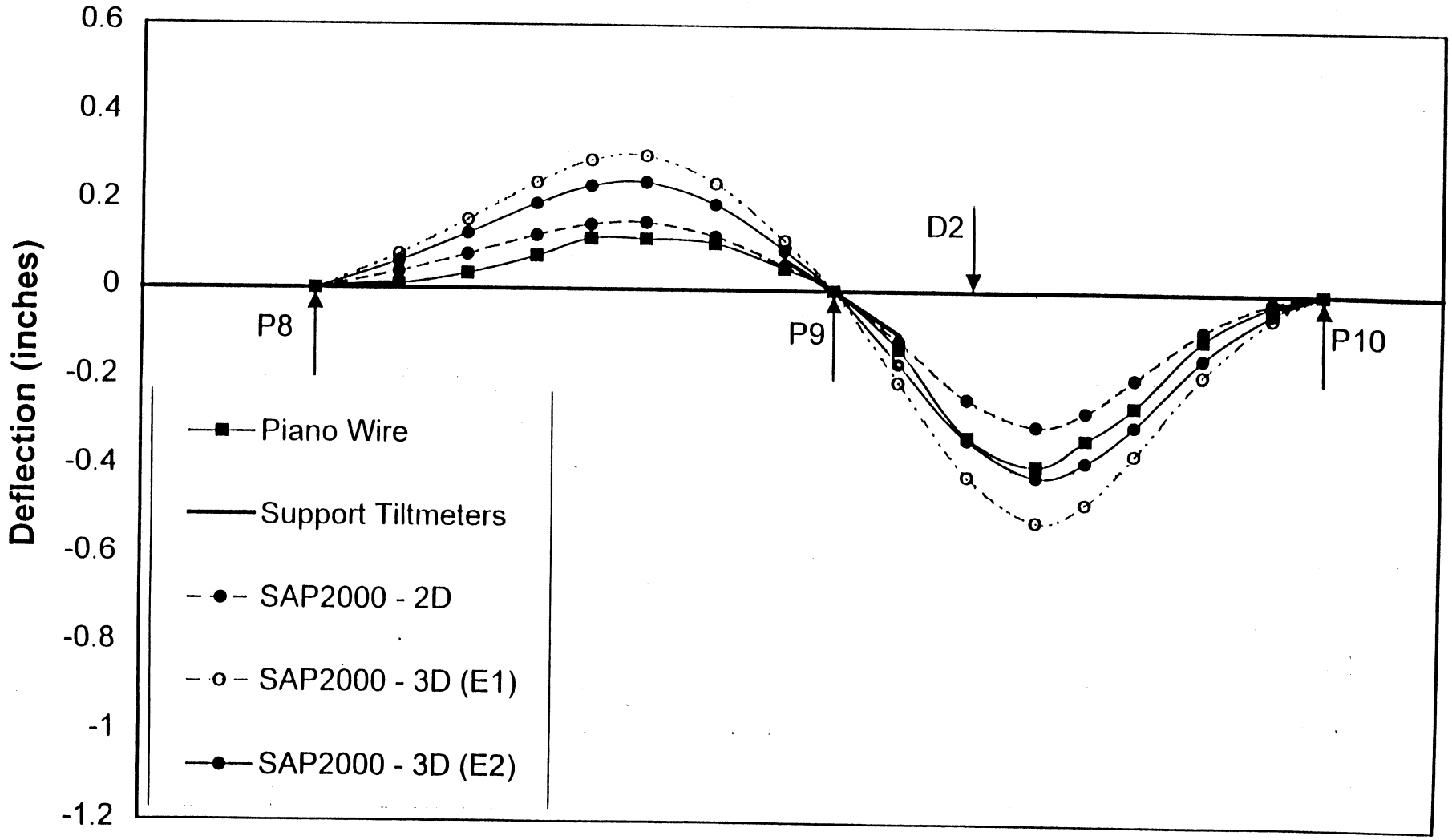

Figure 9.14: Spans P8 - P10 Deflection
Centerline of Truck Load at D4

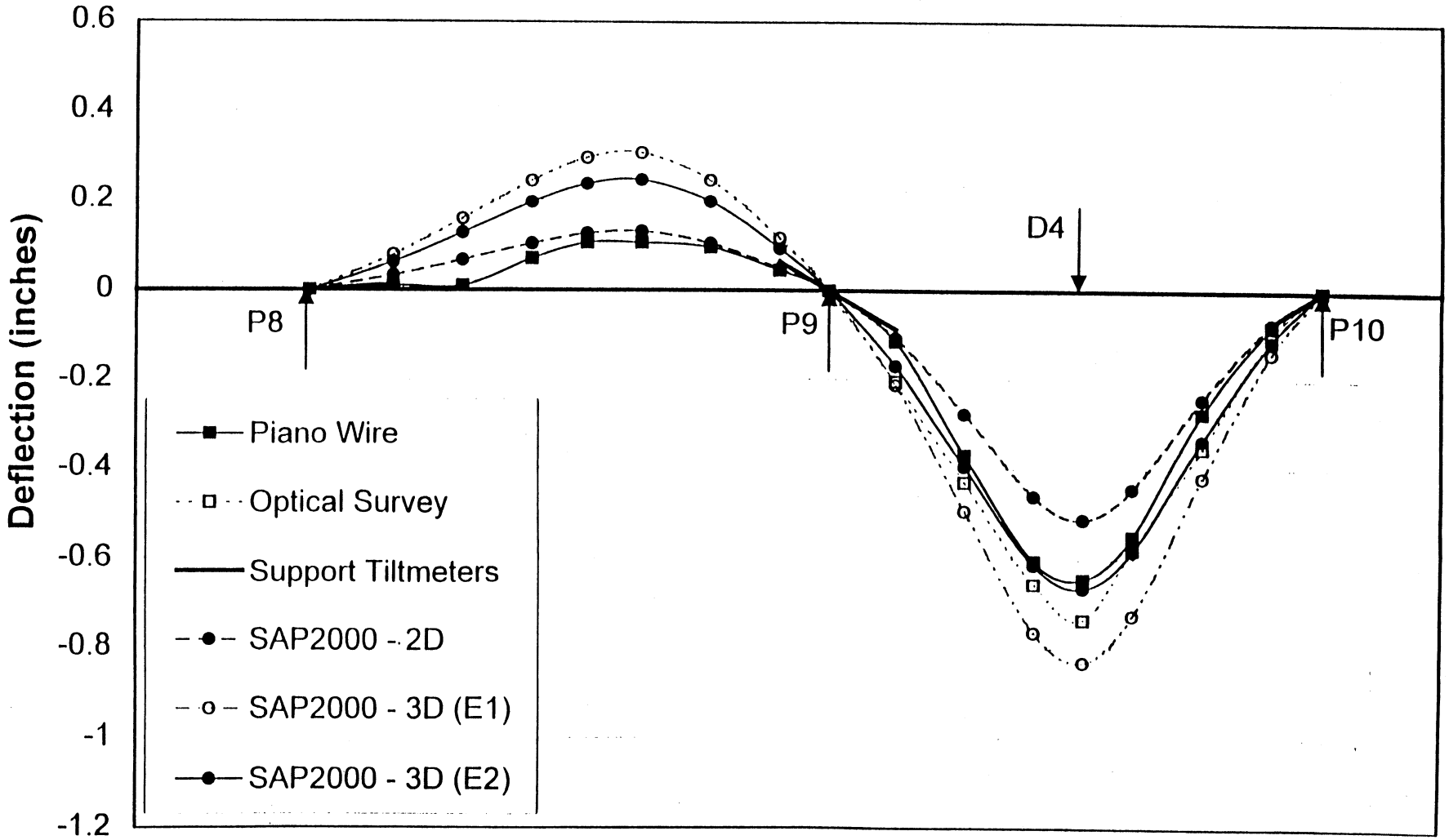

Figure 9.15: Spans P8 - P10 Deflection
Centerline of Truck Load at D6

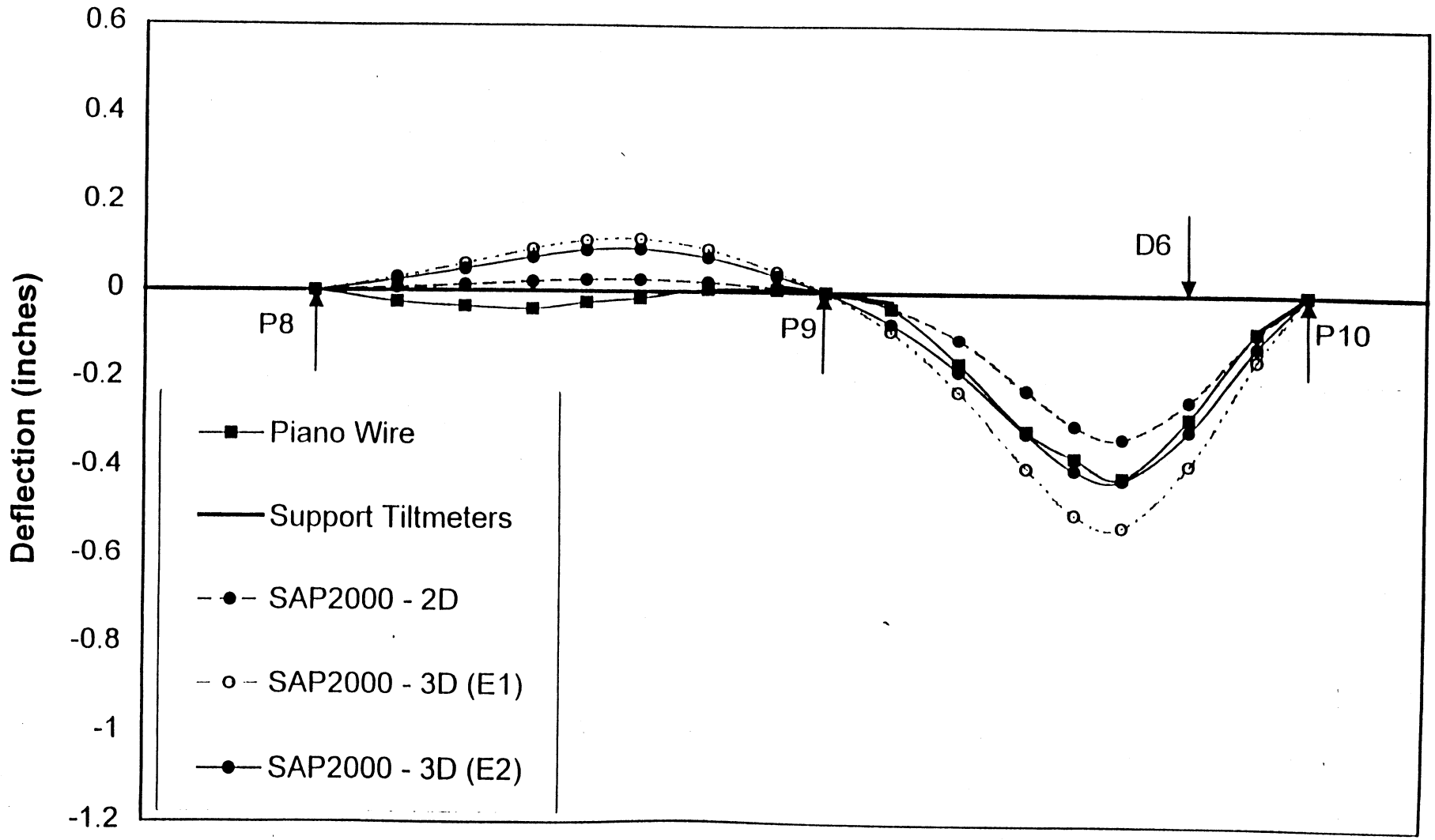

Figure 9.16: Spans P11 - P13 Deflections
Centerline of Truck Load at E1

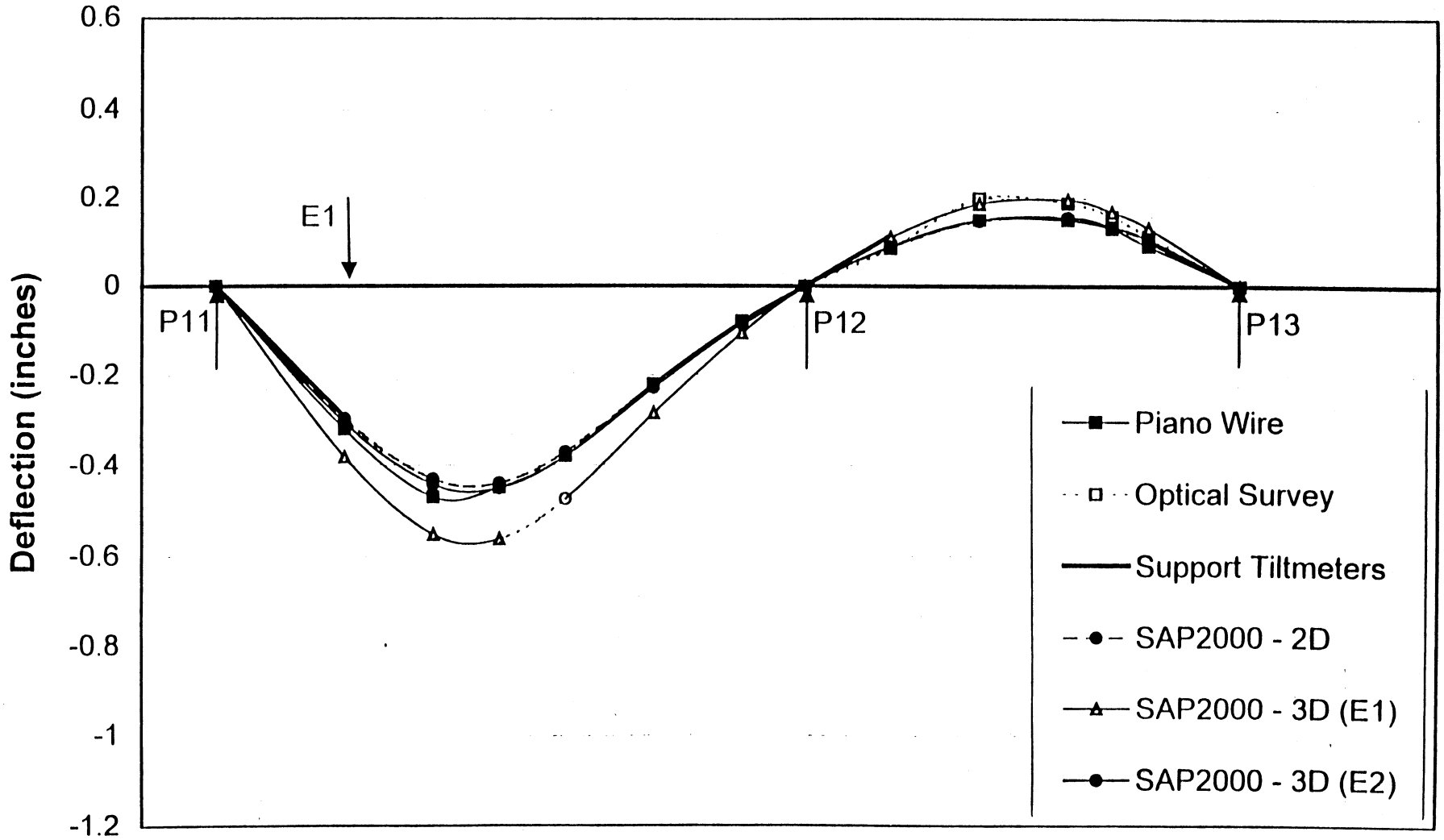

Figure 9.17: Spans P11 - P13 Deflection
Centerline of Truck Load at E3

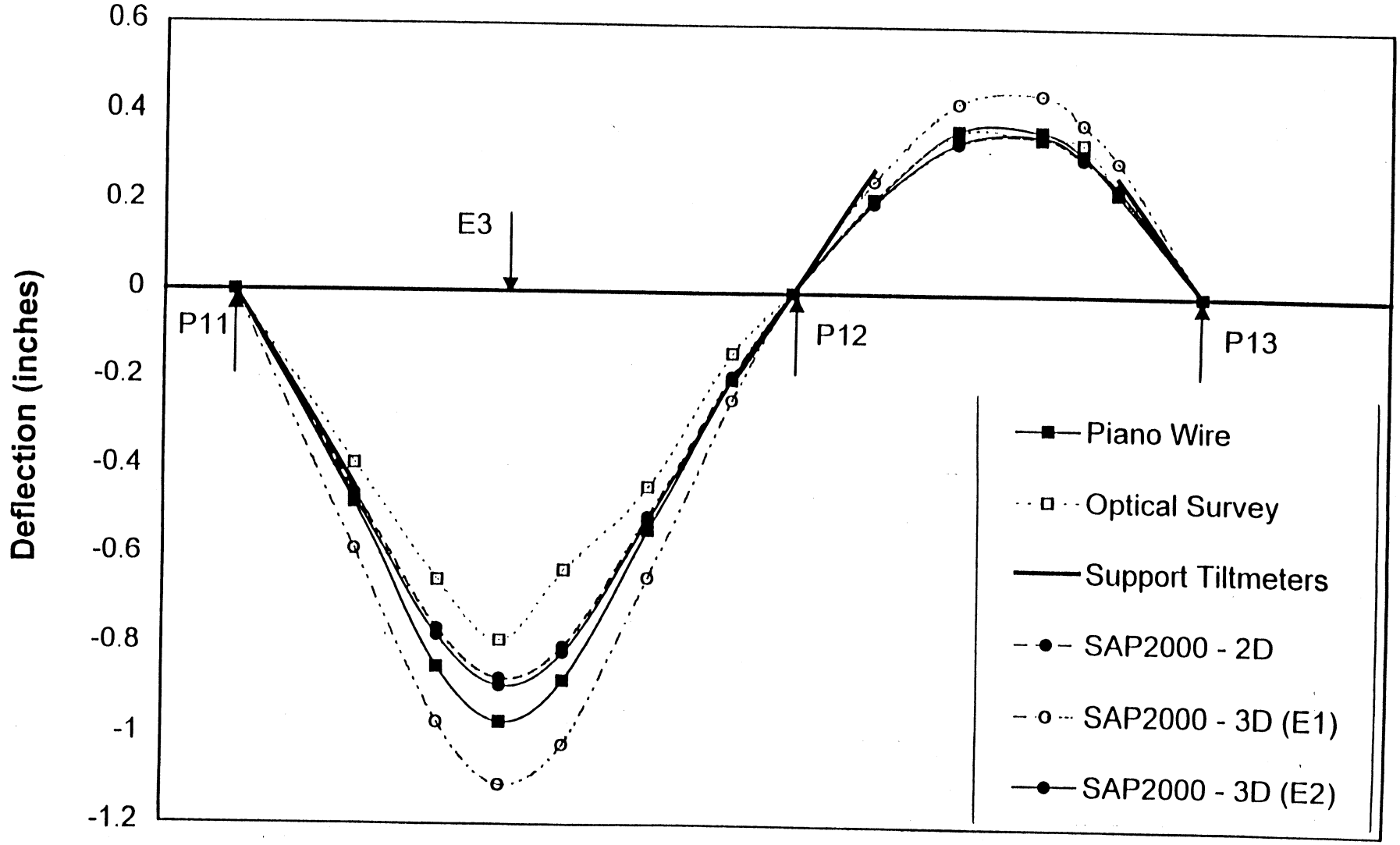

Figure 9.18: Spans P11 - P13 Deflection
Centerline of Truck Load at E5

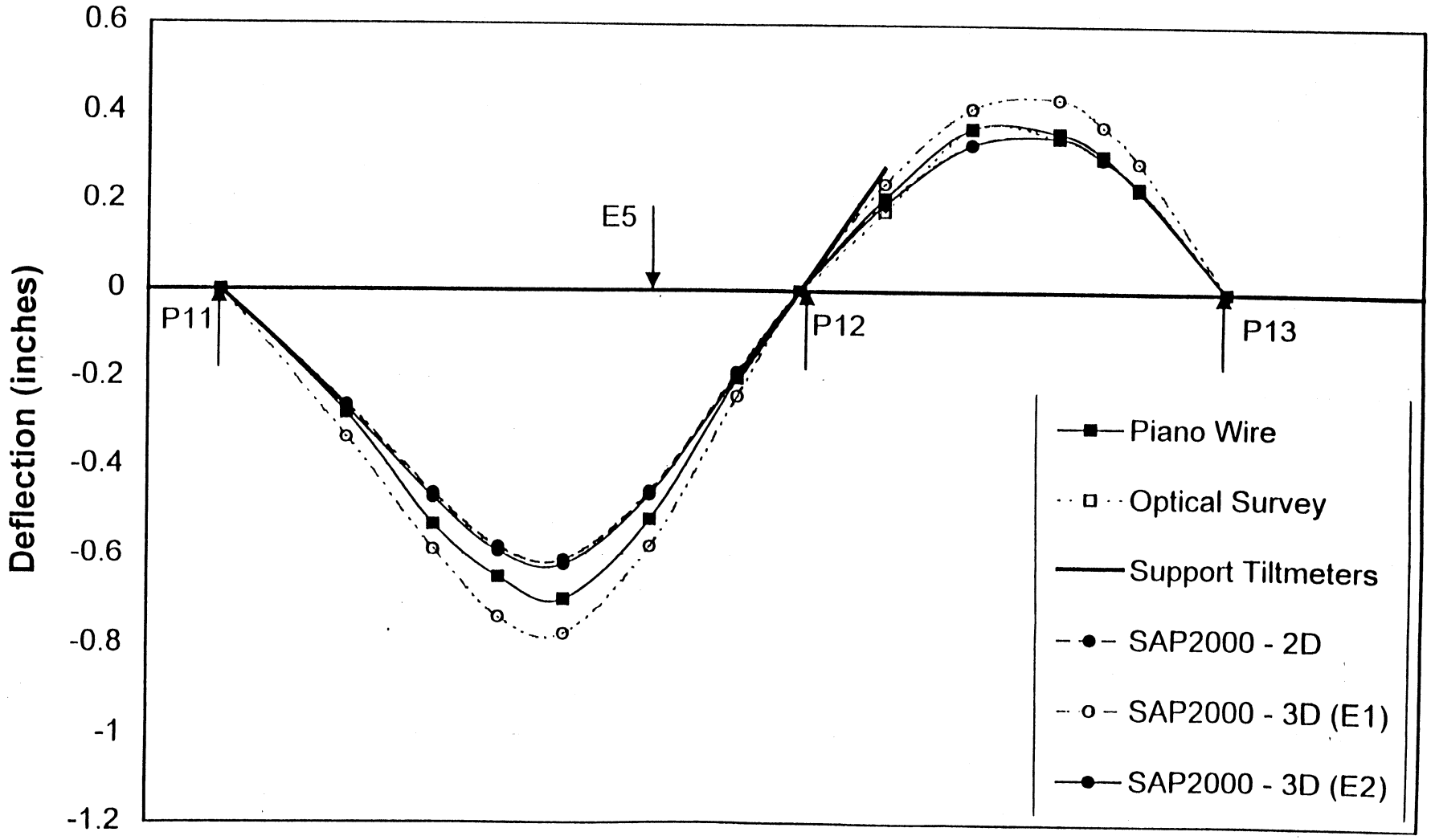

Figure 9.19: Spans P11 - P13 Deflection
Centerline of Truck Load at G1

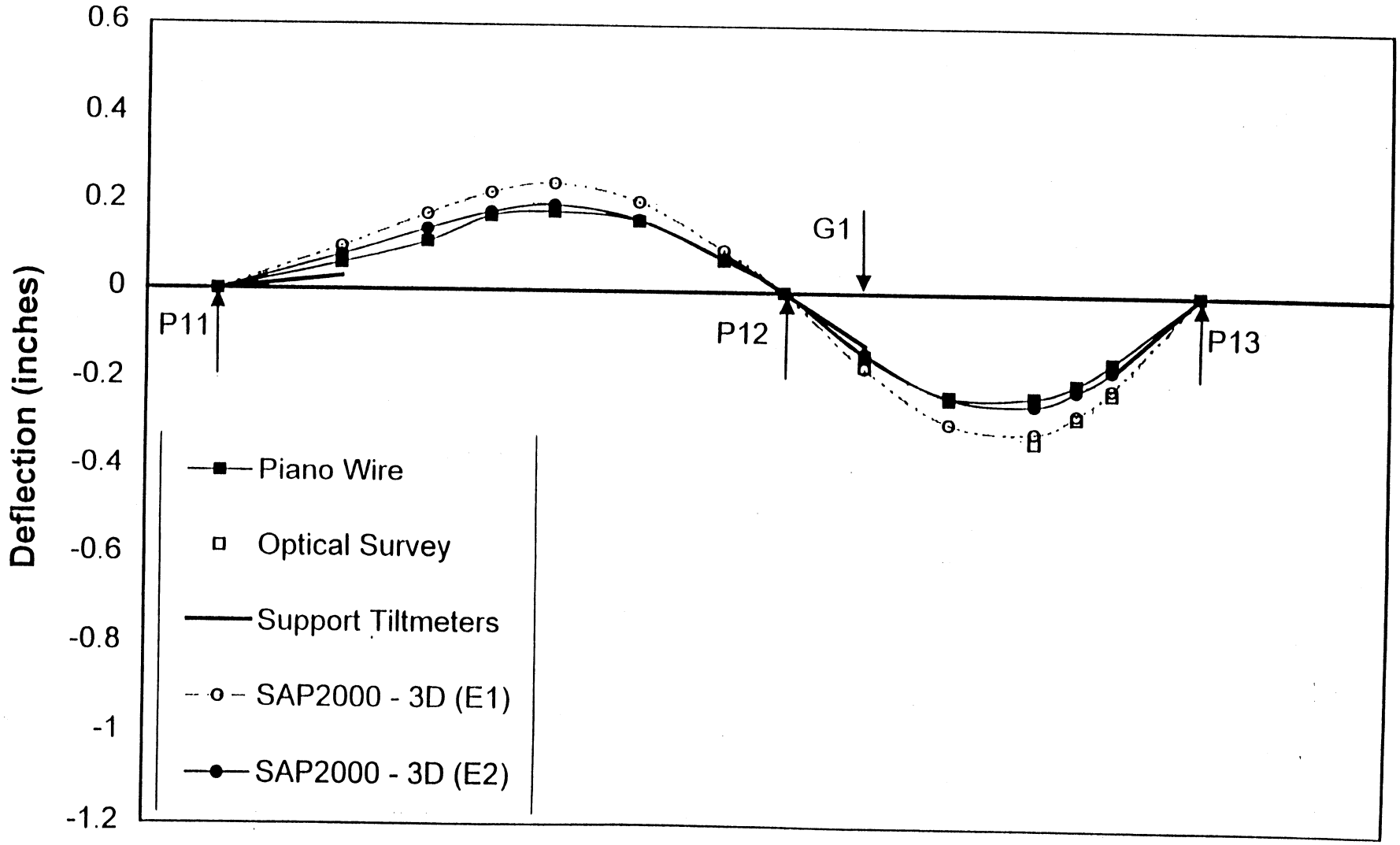

Figure 9.20: Spans P11 - P13 Deflection
Centerline of Truck Load at G2

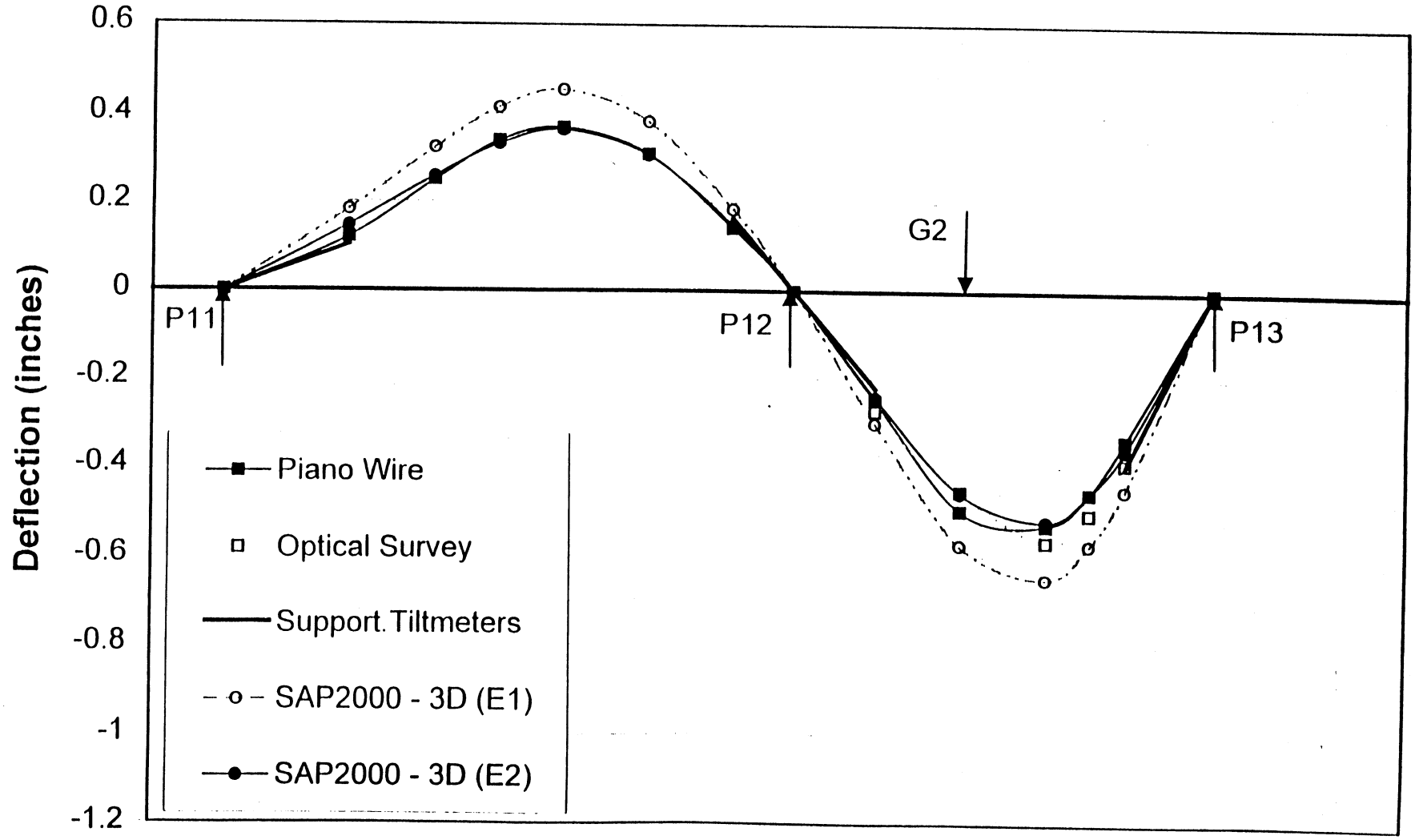

Figure 9.21: Spans P11 - P13 Deflection
Centerline of Truck Load at G3

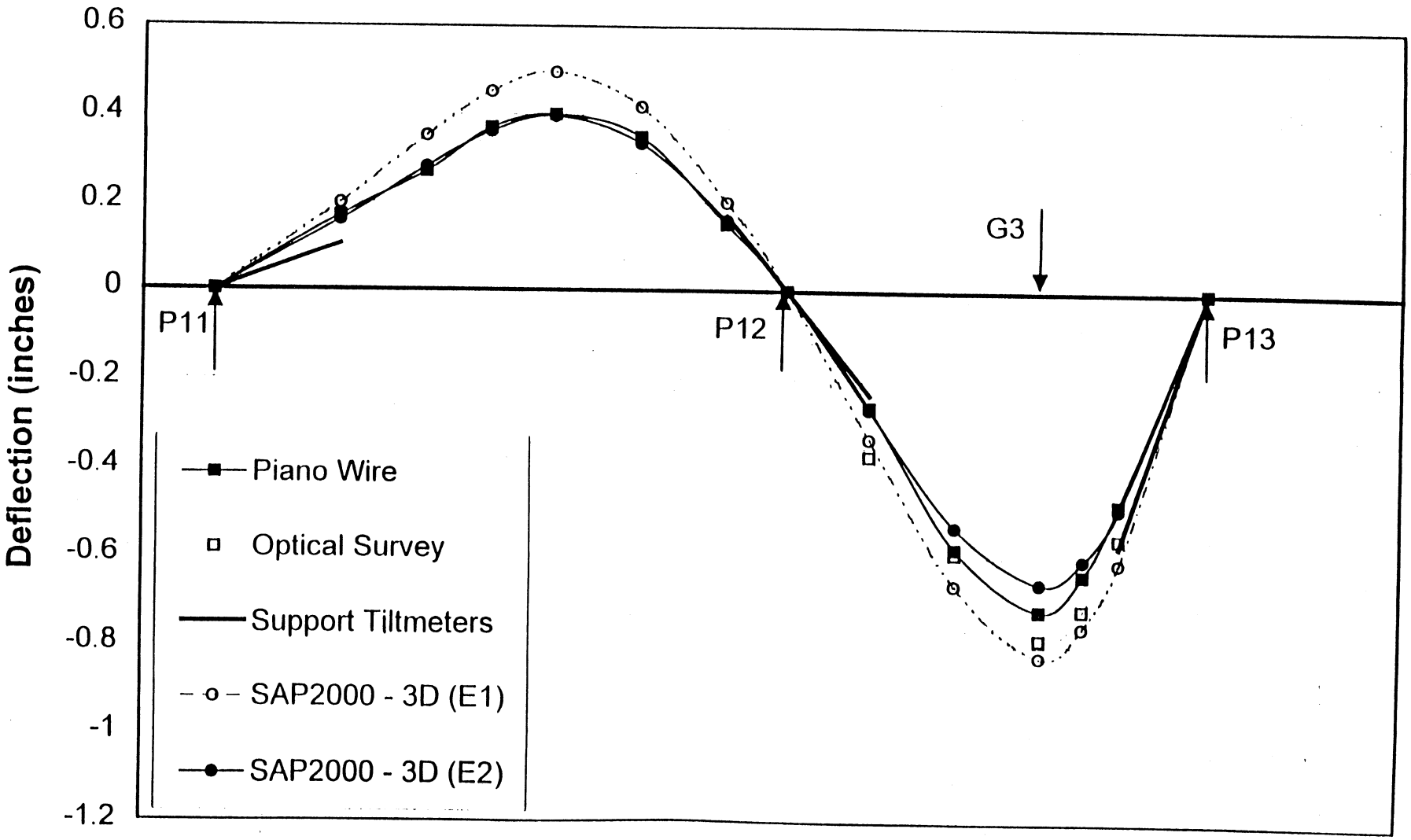

Figure 9.22: Spans P11 - P13 Deflection
Centerline of Truck Load at G5

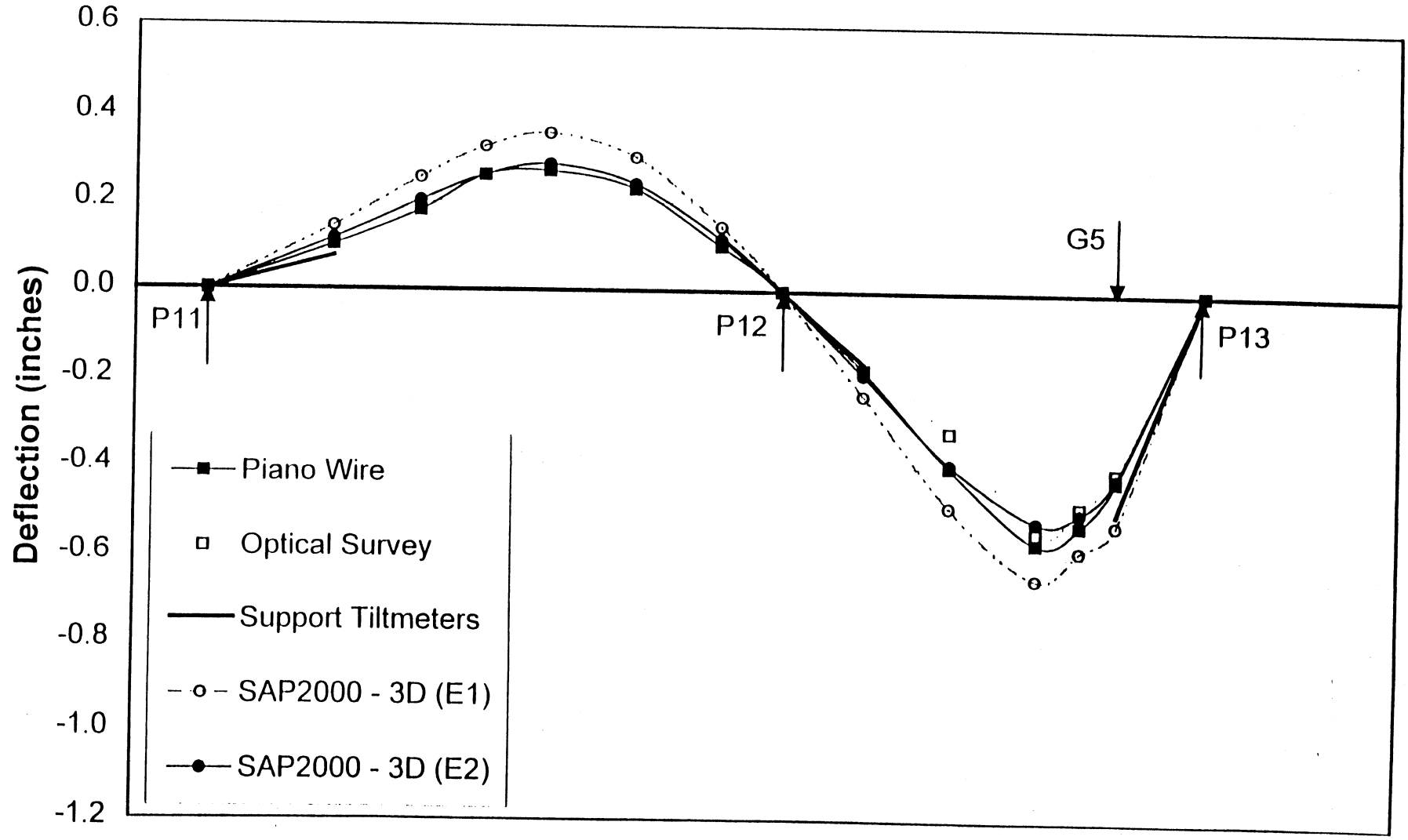

CHAPTER 10

CONCLUSIONS

Field instrumentation has been placed at seven sections on the North Halawa Valley Viaduct to measure concrete strain, prestressing stress, deflection and temperature. In general, the instrumentation is performing extremely well, and there should eventually be a five year database of useful instrumentation readings.

Concrete material properties have been determined. Short-term properties (compressive strength, modulus of elasticity and coefficient of thermal expansion) have been determined in the laboratory. Long-term creep and shrinkage properties have been determined at seven locations for three ages (3, 28 and 90 days) in the laboratory, as well as at three locations in the field.

Mathematical models for creep and shrinkage have been compared with the experimental results. A comparison between creep and shrinkage test data and four current prediction models has been made. The Bazant creep model and Gardner shrinkage model have been shown to yield the best results.

A procedure to predict long-term creep and shrinkage based on short-term (28 day) laboratory test results has been presented and evaluated using the test results. This is a significant breakthrough, since one month of testing can now be used to predict the creep and shrinkage models to be used in the design, rather than one year of testing which was required when the bridge was originally designed.

A comparison has been made between field measured data with results predicted by the computer program SFRAME. In particular, the extensometer readings which measure axial shortening of the instrumented spans compare favorably with values predicted by the program. Both the results of the CEB-FIP 78 model and the Bazant/Gardner model have been compared with the extensometer results. (Additional work is presently being done to improve the correlation between the Bazant/Gardner model and the extensometer results).

Thermocouple readings have been systematically reduced to determine critical positive and negative thermal gradients. These gradients have been shown to compare favorably with those recommended in the 1998 proposed AASHTO segmental guide specifications. This information is particularly timely since it validates the reduction of the negative thermal gradient by 40% from the1994 AASHTO LRFD bridge design specifications.

A load test has been conducted on the instrumented spans. Instrumentation readings obtained for deflection and stress have been found to compare favorably with analysis results obtained with a SAP2000 computer model.

Appendix A - Design of Segmental Bridges for Thermal Gradient - Shushkewich

Design of Segmental Bridges for Thermal Gradient

Kenneth W. Shushkewich Ph.D., P.E.
Project Manager
T.Y. Lin International
San Francisco, California

Thermocouple data from an instrumented prestressed concrete segmental bridge (North Halawa Valley Viaduct) have been efficiently reduced graphically to determine the critical positive and negative thermal gradient. The results are compared with those recommended by various AASHTO specifications. A simplification to the computation procedure for the analysis of segmental bridges for nonlinear thermal gradient is proposed. A fully worked numerical design example is included to demonstrate how the analysis is greatly simplified, and to discuss the impact of the design thermal gradient on the prestressing requirements.

This article presents a state-of-the-art paper on practical segmental bridge design for thermal gradient. The evolution of the design positive and negative thermal gradient in North America over the past 20 years is described. The recommendations given by three current AASHTO specifications are reviewed and compared. The prestressed concrete segmental bridge shown in Fig. 1 (North Halawa Valley Viaduct in Hawaii) has been extensively instrumented with thermocouples at a midspan section and a pier section, and readings are being taken over a five-year period (1995-1999).

The processing of thermocouple readings to-date reveals that the results correlate extremely well with the positive and negative thermal gradients in a proposed revision to an AASHTO specification. These results are particularly timely because they validate the proposed reduction of the negative thermal gradient by 40 percent and substantiate the use of the positive thermal gradient. The general analysis of a segmental bridge for thermal gradient is discussed, and a simplification to the computation procedure is introduced.

A detailed numerical design example (North Halawa Valley Viaduct) is included to demonstrate how the analysis is greatly simplified, and to discuss the impact of thermal gradient on prestressing requirements. Because thermal gradients act on all completed segmental bridges in a similar manner, it should be emphasized that the method advocated in this paper applies equally to precast and cast-in-place

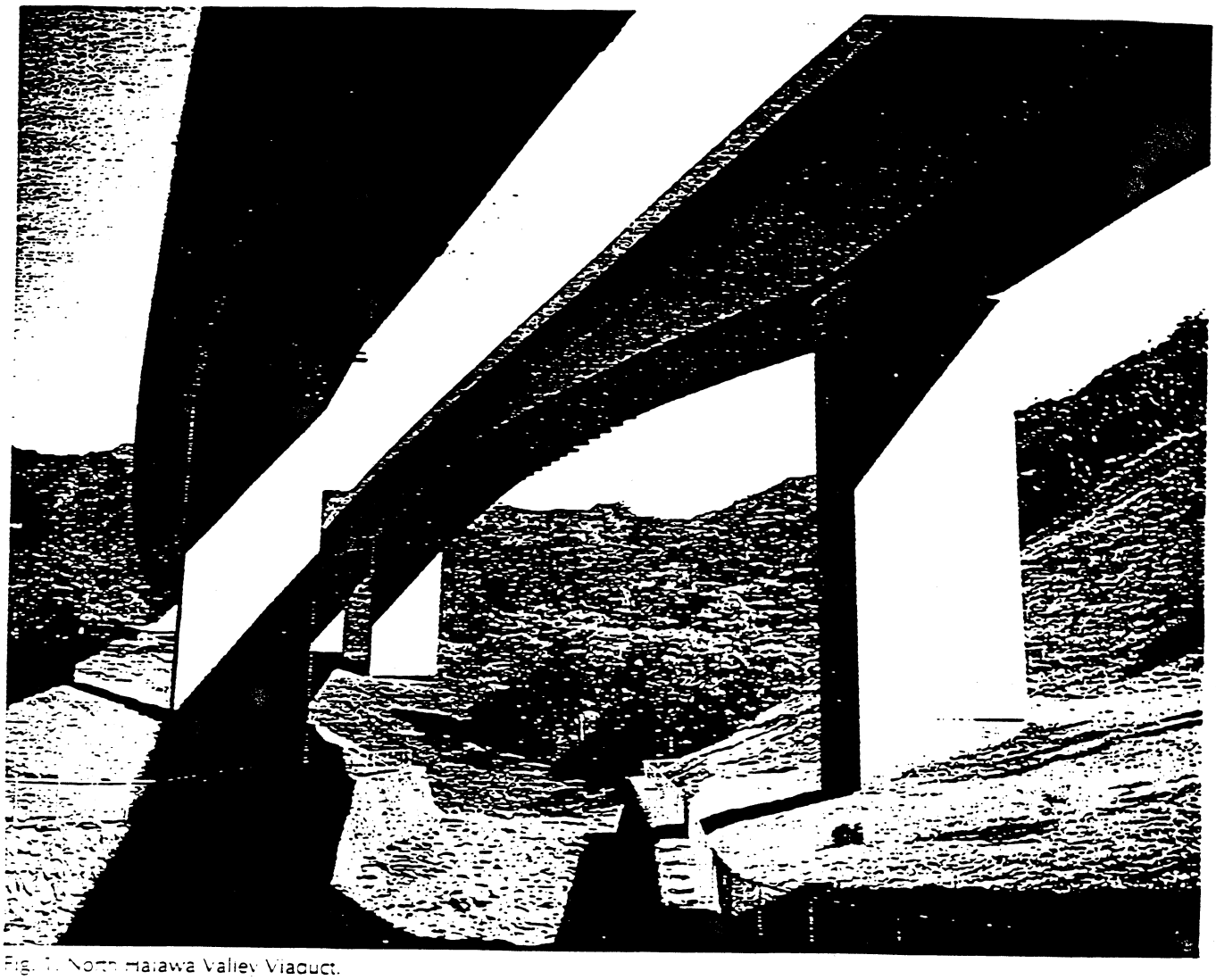

Fig. 1. North Halawa Valley Viaduct.

segmental bridges built by a variety of construction methods (including balanced cantilever, span-by-span, incremental launch, and others).

BACKGROUND

The first breakthrough in the design of segmental bridges for thermal gradient came when the recommendations of the PCI-PTI (Prestressed Concrete Institute-Post-Tensioning Institute) and the New Zealand specification[2] became available 20 years ago. The PCI-PTI suggested a constant gradient over the top slab with a temperature differential of 18°F (10°C). The New Zealand specification considered a fifth order parabola over a depth of 47.2 in. (1200 mm) with a temperature differential of 57.6°F (32°C).

Hoffman, McClure and West conducted a thermal study on an experimental segmental bridge in Pennsylvania. They found that the stresses predicted by the New Zealand specification compared favorably with the experimental results. They also found that the stress at the bottom of the section could be made to agree with the experimental results if a temperature differential of 36°F (20°C) were used with the PCI-PTI recommendations instead of the specified 18°F (10°C).

Elbadry and Ghali[3] developed a finite element computer program to determine the nonlinear temperature distribution in concrete bridges and conducted a parametric study to evaluate the effect of various parameters (solar radiation, wind speed, ambient temperature, deck surface cover) on thermal gradient. Cooke, Priestley and Thurston[4] considered the thermal analysis of partially prestressed concrete bridges. Reasonable agreement was found when experimental results were compared to the theory developed to consider the influence of cracking.

Potgieter and Gamble[5] conducted a comprehensive study of nonlinear thermal gradients at various locations in the United States. A finite difference heat flow computer model was developed and the predicted thermal results showed reasonable agreement with experimental measurements taken from a precast concrete segmental bridge (Kishwaukee River Bridge in Illinois). The computer model was then used to compute probable temperature distributions at 26 SOLMET stations across the United States.

Imbsen, Vandershaf, Schamber and Nutt[6] built on the results of Potgieter and Gamble and produced a state-of-the-art report on thermal effects in concrete bridges. This document formed the basis of the AASHTO guide specification on thermal effects in concrete bridges[7] as well as the AASHTO segmental guide specifications. These documents have been the

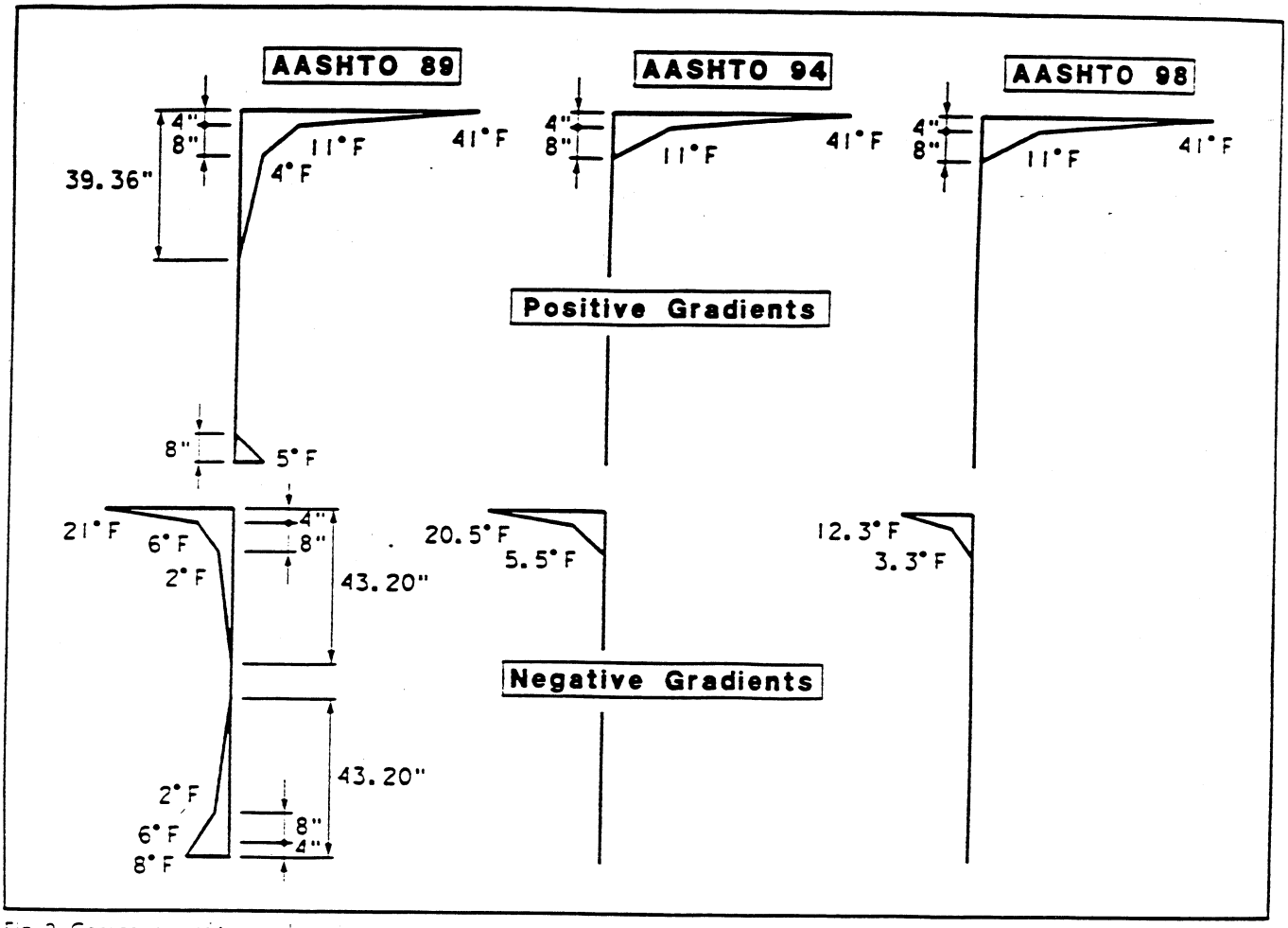

Fig. 2. Comparison of thermal gradients.

basis for the design of segmental bridges for thermal gradient during the past 10 years.

A few refinements have appeared in subsequent specifications. It is interesting to compare the positive and negative thermal gradients (see Fig. 2) in three AASHTO documents (for Zone 3 and plain concrete surface):

1. AASHTO Segmental Guide Specifications[9] (AASHTO 89)
2. AASHTO LRFD Bridge Design Specifications[10] (AASHTO 94)
3. AASHTO proposed Segmental Guide Specifications[11] (AASHTO 98)

The magnitude of the positive gradient is the same for all three gradients [i.e., 41°F, 11°F (22.8°C, 6.1°C)]. The magnitude of the negative gradient is roughly the same for the 89 and 94 gradients [i.e., 21°F, 6°F (11.7°C, 3.3°C)] and reduced by 40 percent for the 98 gradient. Whereas the 89 positive and negative gradients have three pieces at the top and a peak at the bottom, the 94 and 98 gradients have two pieces at the top and no peak at the bottom.

The positive gradient is the same in both the 94 and 98 documents. The negative gradient is -0.50 times the positive gradient in the 94 document, and -0.30 times the positive gradient in the 98 document. Because the results of the instrumentation study validate the 98 gradient, it will be used in the remainder of this paper.

DESCRIPTION OF NORTH HALAWA VALLEY VIADUCT

The North Halawa Valley Viaduct consists of twin prestressed concrete segmental bridges on the island of Oahu in Hawaii (see Fig. 3). The project consists of a 5640 ft (1720 m) inbound viaduct that carries traffic to Honolulu and a 5470 ft (1667 m) outbound viaduct that carries traffic to Kaneohe. The viaducts are on a horizontal curve with a radius of approximately 9500 ft (2900 m), and have a nearly constant grade of 6 percent.

Each viaduct consists of three structural units, with expansion joints at the end of each unit, two fixed piers in the middle of each unit, and expansion piers forming the remainder of the unit. The maximum span length is 360 ft (110 m). The viaduct cross section (see Fig. 4) has a width of 41 ft (12.50 m), which accommodates two lanes of traffic plus shoulders. The depth of the section varies from 18 ft (5.5 m) at the piers to 8 ft (2.4 m) at midspan.

The bridge was designed by T. Y. Lin International of San Francisco, California, in conjunction with Nakamura and Tyau of Honolulu, Hawaii. The bridge design process started in 1988 with the evaluation of seven different alternatives as part of the Major Structures Report. This was followed by the detailed design and construction of the bridge. Kiewit Pacific was awarded the construction contract in early 1992 and given 990 calendar days to complete the project. The bridge (and the entire H-3 Interstate system) opened to traffic in December of 1997.

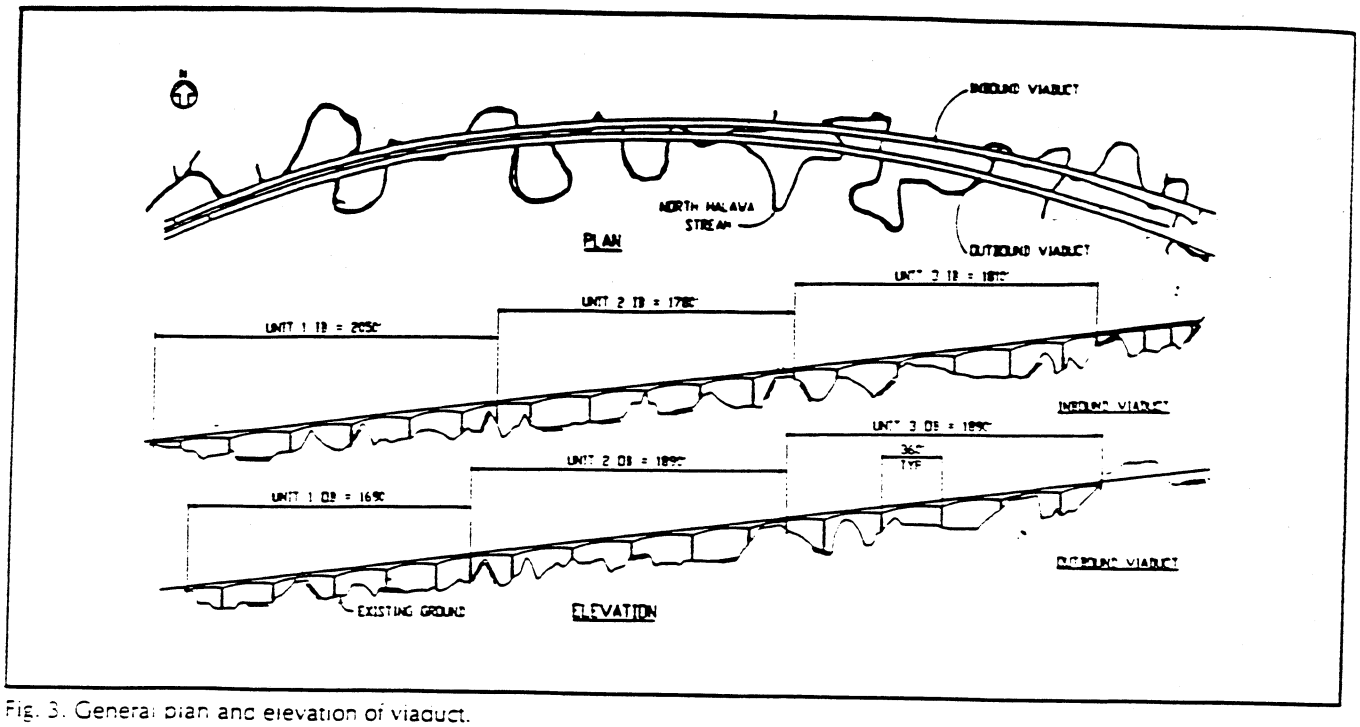

Fig. 3. General plan and elevation of viaduct.

This cast-in-place segmental bridge was built using the balanced cantilever method of construction using form travelers normally associated with cast-in-place segmental construction in combination with launching trusses normally used in precast segmental construction. This project represents the first time in the United States that launching trusses have been used with cast-in-place segmental construction. Additional information on the design and construction of the bridge is given by Ingham, Manzanarez and Cormier.[11]

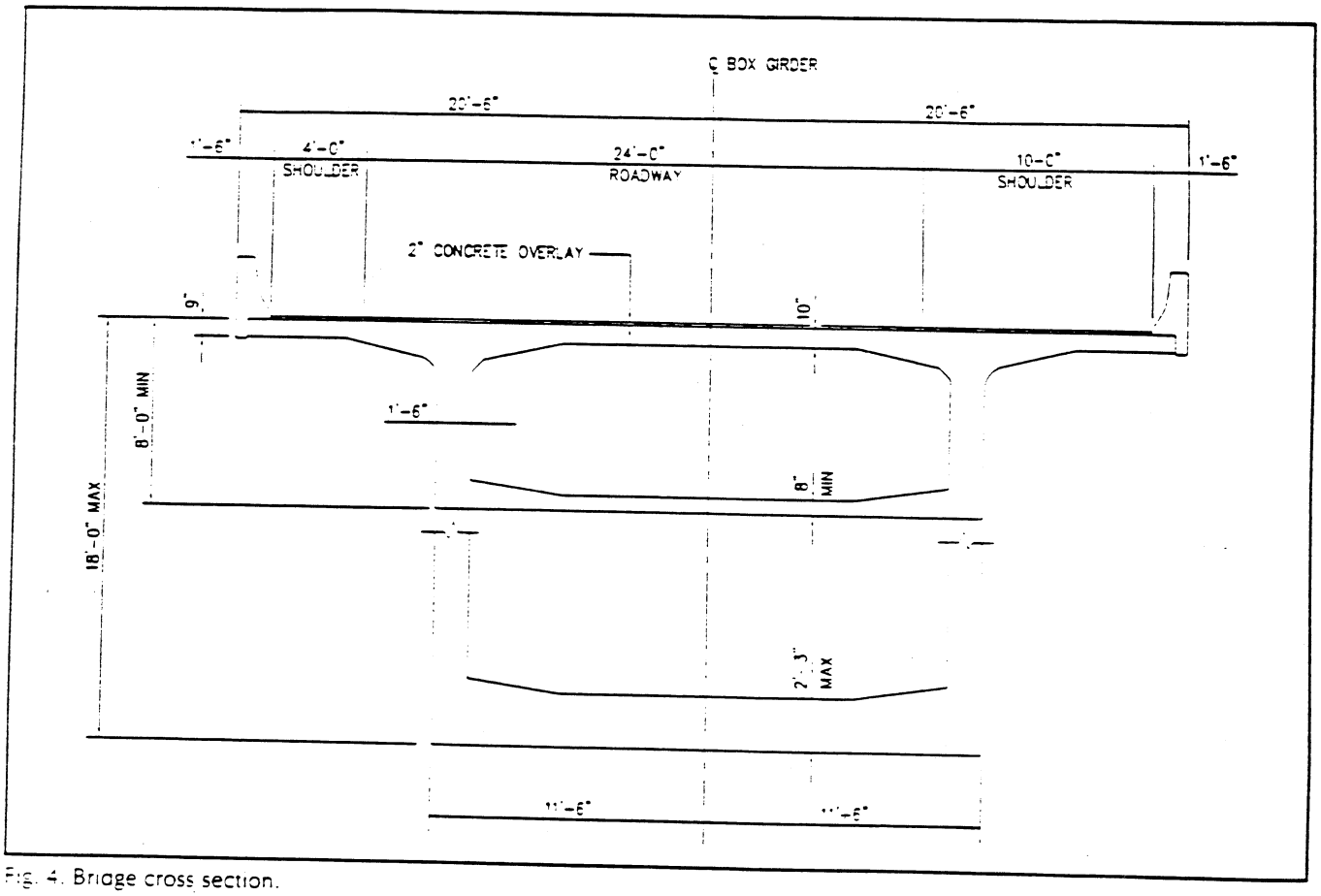

Fig. 4. Bridge cross section.

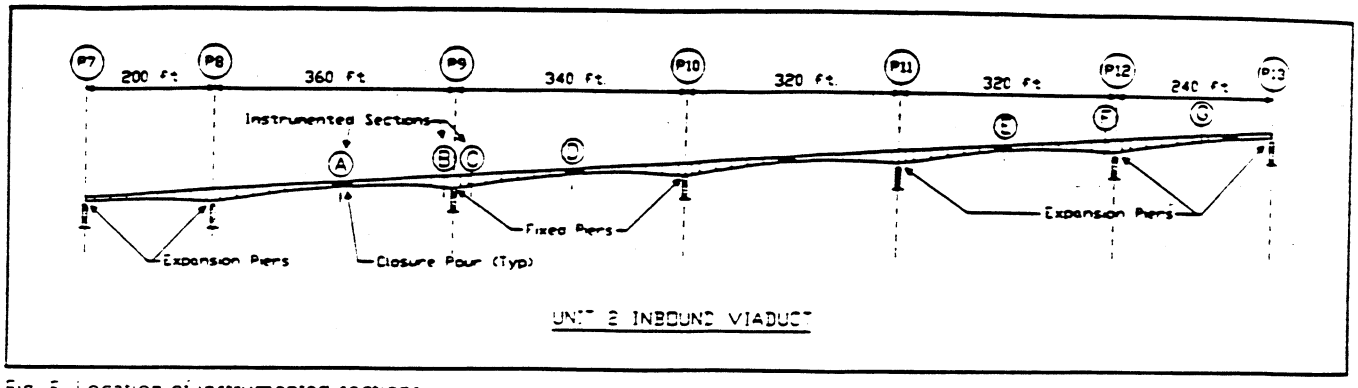

Fig. 5. Location of instrumented sections.

INSTRUMENTATION OF NORTH HALAWA VALLEY VIADUCT

T. Y. Lin International is presently involved in a five-year program (1995-1999) to instrument and monitor the bridge. The participants in this program are T. Y. Lin International, the University of Hawaii at Manoa, and Construction Technology Laboratories. Funding has been obtained from the State of Hawaii Department of Transportation and the Federal Highway Administration. Additional information on the instrumentation and monitoring setup is given by Lee and Robertson.[13] Detailed results from the instrumentation study are given by Shushkewich, Vo and Robertson.[14]

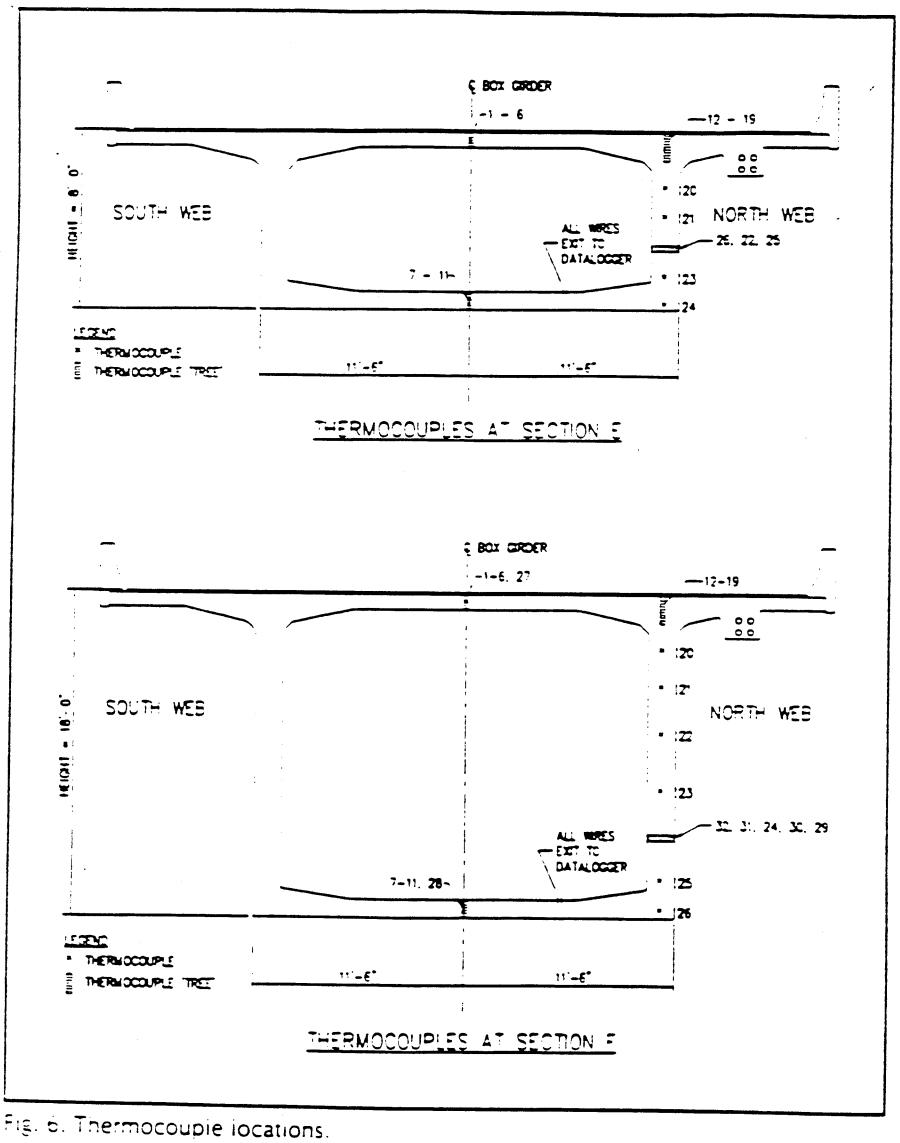

Fig. 6. Thermocouple locations.

Instrumentation Setup

An extensive system of instrumentation was set up in Unit 2 Inbound (see Fig. 5). This unit has span lengths of 200, 360, 340, 320, 320 and 240 ft (61, 110, 104, 98, 98 and 73 m). Instrumentation was placed at seven sections. Sections A, D, E and G are termed midspan sections (because they are near midspan), while Sections B, C and F are termed support sections (because they are near supports).

Instrumentation was placed to measure concrete strains, prestressing forces, deflections and temperatures. Concrete strain was measured with vibrating wire strain gauges, mechanical (DEMEC) strain gauges and electrical resistance strain gauges. Prestressing force was measured with load cells. Horizontal deflections were measured with extensometers, while vertical deflections were measured with baseline (piano wire) systems. Rotations were measured with tiltmeters. Temperatures were measured (at Section E and F only) with thermocouples (as well as with the thermistors that were used to adjust the strain gauge data for temperature effects). Additional information on the instrumentation is given in Ref. 13.

Sections E and F were extensively instrumented with thermocouples (see Fig. 6). Gauges 1 to 6 and 7 to 11 are at the centerline of the box girder in the top and bottom slab, respectively. Gauges 12 to 24 (or 26) are at the centerline of the web and monitor the entire depth of the section. Additional

SECTION G - 3 DAYS			
CREEP FRAME G2 INSIDE BOX GIRDER - STANDARD TEST			
Creep Of Concrete in Compression			
Instantaneous and Long-Term Deformation (Adjusted for Drying Shrinkage)			
	Drying	Load Induced	
Days	Shrinkage	Deformation	
Loaded	(millionths)	(millionths)	Condition
0	0	469	Instantaneous strain
0	65	585	Instantaneous Strain + Creep Strain
2	95	738	Instantaneous Strain + Creep Strain
4	283	733	Instantaneous Strain + Creep Strain
21	248	990	Instantaneous Strain + Creep Strain
31	333	942	Instantaneous Strain + Creep Strain
51	353	1127	Instantaneous Strain + Creep Strain
70	286	1146	Instantaneous Strain + Creep Strain
100	332	1246	Instantaneous Strain + Creep Strain
125	418	1221	Instantaneous Strain + Creep Strain
153	540	1229	Instantaneous Strain + Creep Strain
158	500	1258	Instantaneous Strain + Creep Strain
192	619	1269	Instantaneous Strain + Creep Strain
211	564	1331	Instantaneous Strain + Creep Strain
244	591	1350	Instantaneous Strain + Creep Strain
275	648	1419	Instantaneous Strain + Creep Strain
317	687	1352	Instantaneous Strain + Creep Strain
350	704	1402	Instantaneous Strain + Creep Strain
407	771	1390	Instantaneous Strain + Creep Strain
521	715	1450	Instantaneous Strain + Creep Strain
646	742	1560	Instantaneous Strain + Creep Strain
710	844	1496	Instantaneous Strain + Creep Strain
Applied Stress = 1530 psi			
f'_c @ 3 days = 3830 psi			
Modulus of Elasticity @ 3 days = 3.05 x 10^6			

SECTION G - 3 DAYS			
CREEP FRAME G3 OUTSIDE BOX GIRDER - STANDARD TEST			
Creep Of Concrete in Compression			
Instantaneous and Long-Term Deformation (Adjusted for Drying Shrinkage)			
	Drying	Load Induced	
Days	Shrinkage	Deformation	
Loaded	(millionths)	(millionths)	Condition
0	0	598	Instantaneous strain
2	57	910	Instantaneous Strain + Creep Strain
4	109	1002	Instantaneous Strain + Creep Strain
21	51	1342	Instantaneous Strain + Creep Strain
31	97	1415	Instantaneous Strain + Creep Strain
51	63	1460	Instantaneous Strain + Creep Strain
70	53	1483	Instantaneous Strain + Creep Strain
100	227	1560	Instantaneous Strain + Creep Strain
125	152	1535	Instantaneous Strain + Creep Strain
153	272	1602	Instantaneous Strain + Creep Strain
157	140	1629	Instantaneous Strain + Creep Strain
192	203	1665	Instantaneous Strain + Creep Strain
211	161	1658	Instantaneous Strain + Creep Strain
254	201	1788	Instantaneous Strain + Creep Strain
288	289	1771	Instantaneous Strain + Creep Strain
317	291	1765	Instantaneous Strain + Creep Strain
350	206	1883	Instantaneous Strain + Creep Strain
407	145	1869	Instantaneous Strain + Creep Strain
521	193	1858	Instantaneous Strain + Creep Strain
646	293	1896	Instantaneous Strain + Creep Strain
710	377	1894	Instantaneous Strain + Creep Strain
Applied Stress = 1530 psi			
f_c @ 3 days = 3830 psi			
Modulus of Elasticity @ 3 days = 3.05 x 10°			

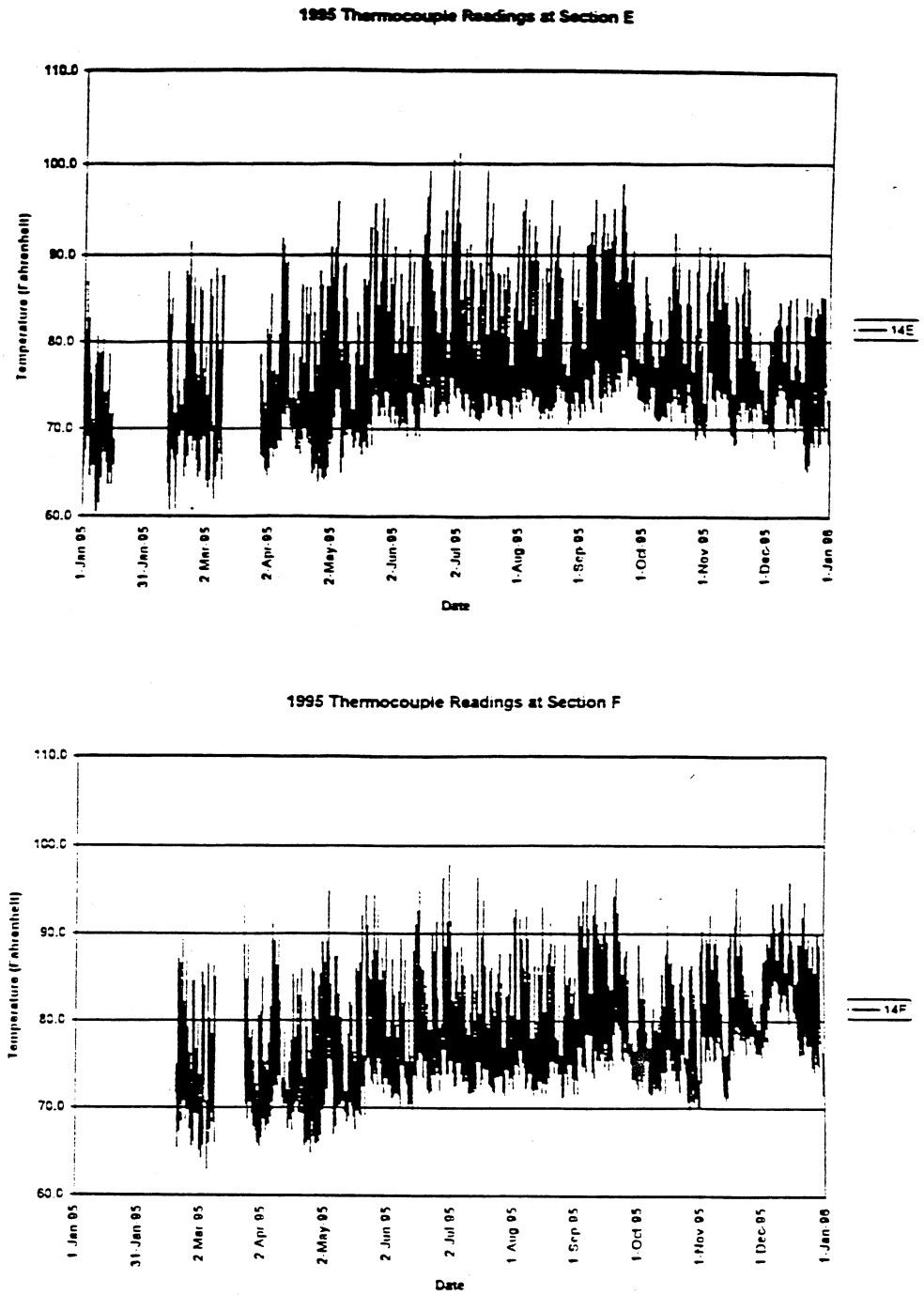

Fig. 7. 1995 thermocouple readings.

gauges are across the width of the web (Gauges 25 and 26 for Section E and Gauges 29 to 32 for Section F).

The thermocouples used in the instrumentation were made using Teflon/Neoflon FEP insulated copper/constantin type-T wire obtained from Omega Measurements. Thermocouple "trees" made of PVC pipe with predrilled holes were used to correctly maintain the location of closely spaced thermocouples during concrete pours. A reference thermistor provided in the datalogger multiplexer box calibrated the thermocouple readings to record the temperatures directly in degrees Celsius. (Note: $°F = 1.8 \times °C - 32$)

Thermocouple readings were first recorded in late 1994 and will be recorded through the end of 1999. The goal of the thermocouple instrumentation is to obtain critical positive and negative thermal gradients. Readings were taken at 2-hour intervals from the beginning of the study until August 22, 1995. At this time, it was felt that too much information was being collected (all instrumentation readings were taken at the same 2-hour intervals), and readings were then changed to 6-hour intervals.

It became apparent on October 14, 1997, that the peak critical positive thermal gradient was being underestimated by taking readings at 6-hour intervals so the readings were then

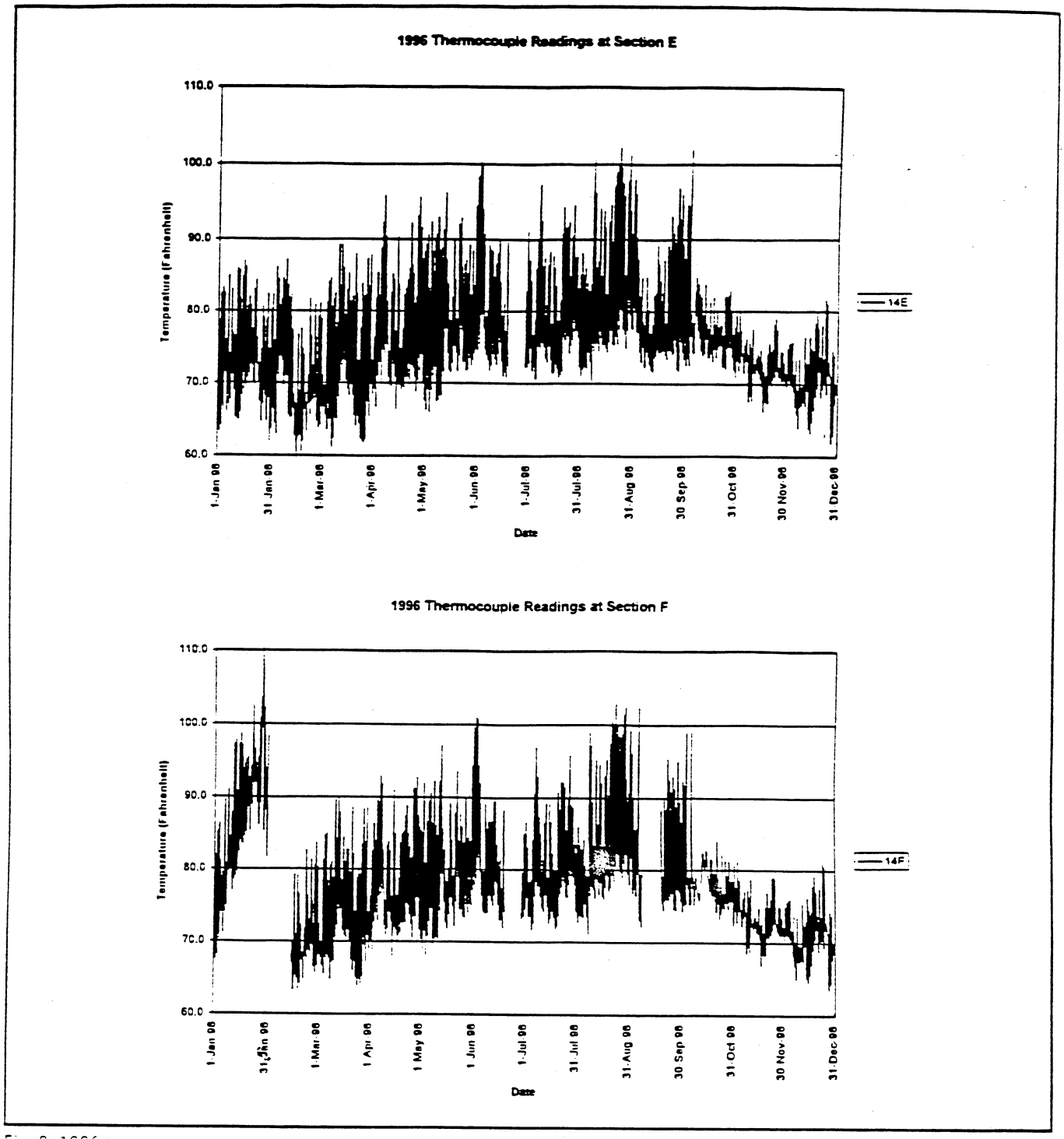

Fig. 8. 1996 thermocouple readings.

changed back to 2-hour intervals for the remainder of the study. Although the positive gradients were underestimated somewhat during the 6-hour interval period, the remainder of the positive gradient readings are informative. Negative gradient readings are not nearly as sensitive to the time interval, so all of the negative gradient readings are useful. The North Halawa Valley Viaduct has an excellent database of thermocouple readings.

A concrete topping 2 in. (50 mm) thick was placed on the instrumented sections on October 7, 1996. (Note that asphalt topping was not used on this project and consequently the effects of asphalt cannot be discussed in this paper.) The net effect of placing the concrete topping on the instrumented sections is to add three additional thermocouple readings at the top, middle and bottom of the overlay and shift the remainder of the gauge readings down by 2 in. (50 mm). This increases the overall number of gauges near the deck surface where gauge readings are desirable.

Instrumentation Results

There is an extremely large amount of data that has to be interpreted in an efficient manner in order to obtain critical positive and negative thermal gradients because the thermocouple

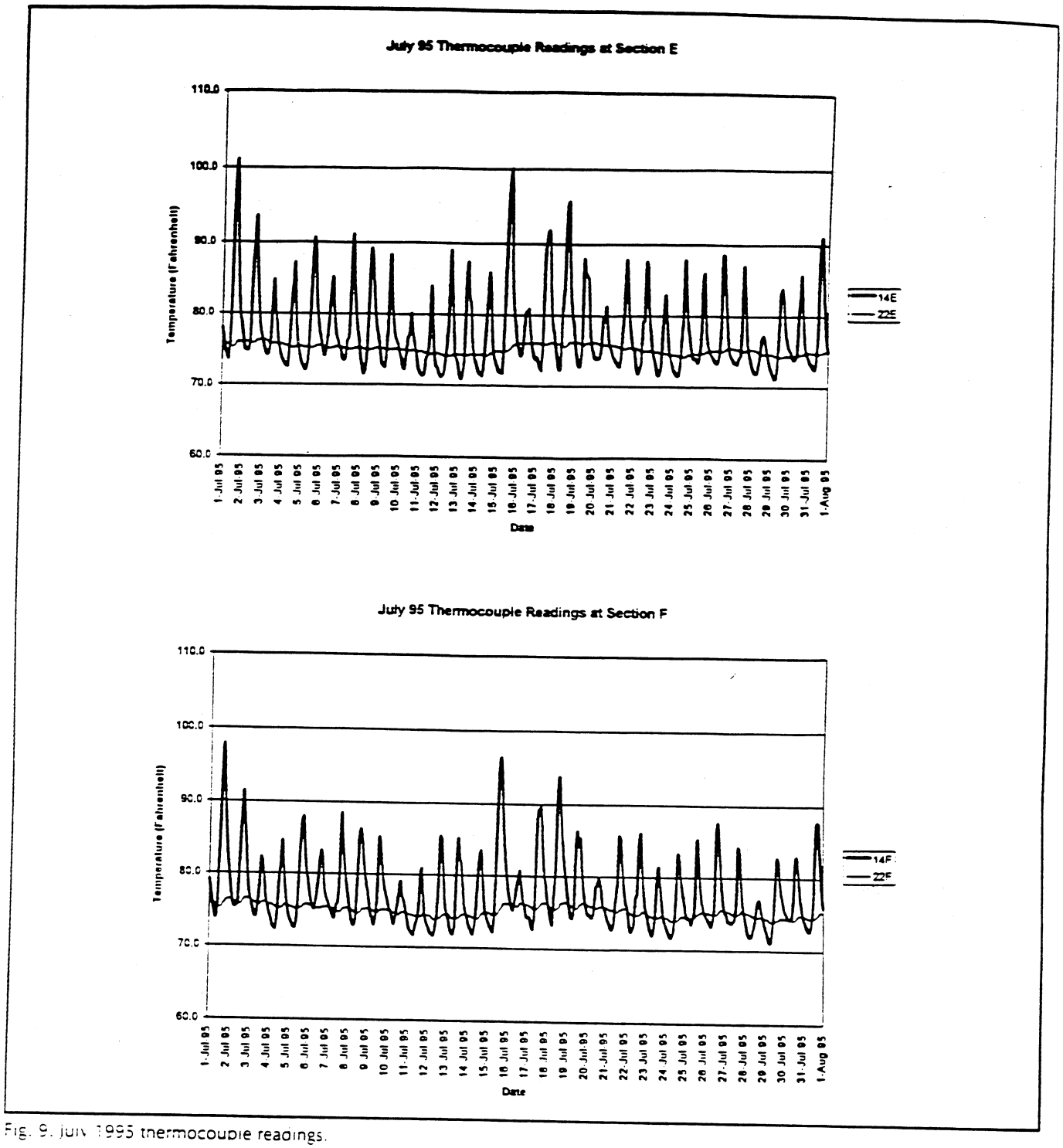

Fig. 9. July 1995 thermocouple readings.

readings are taken every 2 hours for a 5-year period at 58 gauges. (Section E has 26 gauges while Section F has 32 gauges.) The method used to reduce the data has been to graphically review the thermocouple readings on: (1) a year-by-year basis; (2) a month-by-month basis; (3) a day-by-day basis (for critical days); and, (4) a gradient-by-gradient basis (at critical times for critical days). Numerous plots of annual, monthly, daily and critical thermal gradients (positive and negative) are given in Ref. 14 and only representative plots will be discussed here.

Annual readings for 1995 (see Fig. 7) and 1996 (see Fig. 8) are reviewed at Gauge 14 [2.5 in. (63 mm) below the deck surface] for Section E [8 ft (2.4 m) depth] and Section F [18 ft (5.5 m) depth]. This gives the overall picture of the thermocouple readings and what the relative high and low temperatures are in various months. This also helps to spot spurious results (moisture in the datalogger) and no results (power failure). For instance, January 1996 readings at Section F are neglected because there was moisture in the datalogger.

Note that Gauge 14 is plotted because Gauge 13 (at the deck surface) is not reliable. Examination of Fig. 7 reveals that July 1995 appears to have some very high temperatures. Note that the peak readings at Gauge 14

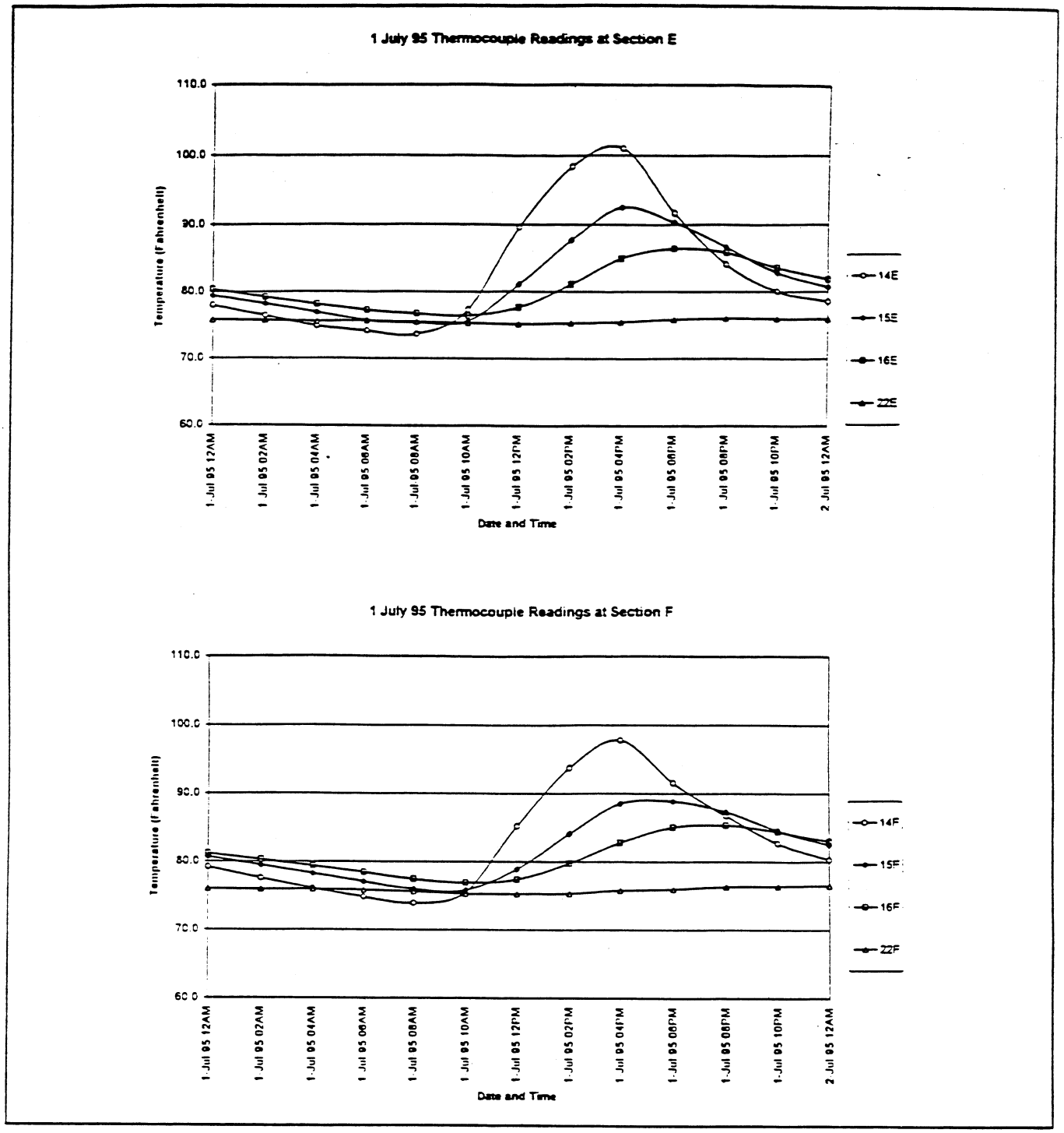

Fig. 10. July 1, 1995, thermocouple readings.

drop after August 22, 1995, due to the fact that the readings were changed from 2-hour intervals to 6-hour intervals. Furthermore, note that the peak readings at Gauge 14 drop even more after October 7, 1996, because the concrete topping has been added and Gauge 14 is now reading a value 2 in. (50 mm) lower on the thermal gradient.

Monthly readings (see Fig. 9) are reviewed at Gauge 14 and at Gauge 22. Gauge 14 is near the deck surface and gives daily peaks and valleys. Gauge 22 is near the middle of the section and is less influenced by daily fluctuations. In general, large thermal gradients occur when the difference (positive or negative) between readings at Gauges 14 and 22 is maximum. Inspection of Fig. 9 indicates that July 1, 15 and 18 should have the largest positive thermal gradients. It is interesting to note that the readings for these days are slightly lower for Section F than for Section E. This is because Section F [18 ft (5.5 m) depth] has a higher thermal inertia than Section E [8 ft (2.4 m) depth].

Daily readings (see Fig. 10) are reviewed at several gauges for July 1, 1995 (which has the highest July reading). Readings are plotted every 2 hours for Gauges 14, 15 and 16, which have respective distances from the deck of 2.5, 5.0 and 7.5 in. (63, 126 and 189

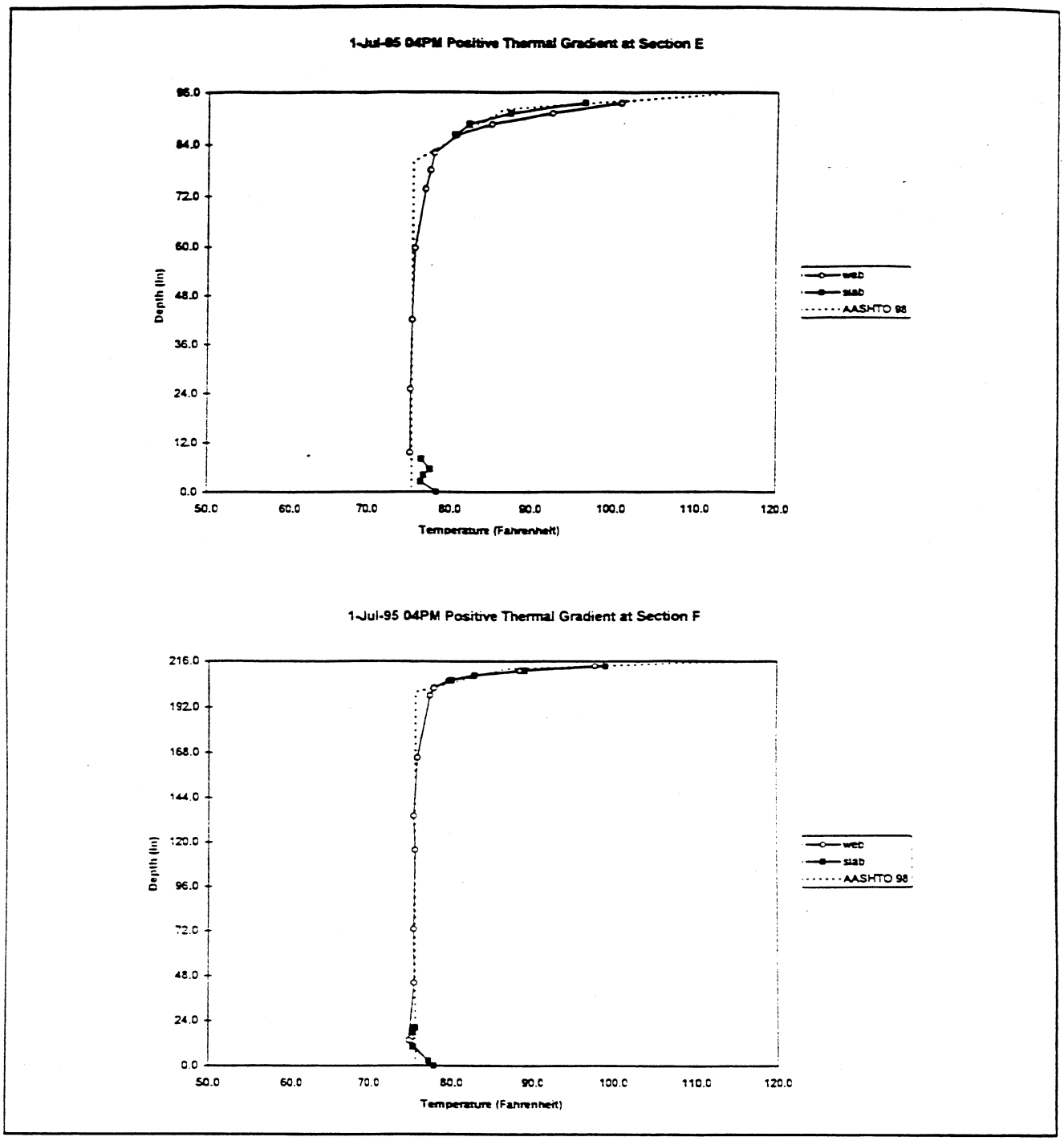

Fig. 11. July 1, 1995, positive thermal gradients.

mm) as well as Gauge 22, which is in the middle of the section. It can be seen that the maximum positive thermal gradient occurs at 4 p.m. and the maximum negative thermal gradient occurs at 8 a.m. Again, note that the maximum positive thermal gradient appears to be slightly lower for Section F than for Section E (because Section F has a higher thermal inertia than Section E).

The critical positive thermal gradients (see Fig. 11) are reviewed at 4 p.m. on July 1, 1995. Readings are plotted for gauges along the centerline of the web as well as along the centerline of the top and bottom slab. These readings are compared to those in the 1998 proposed second edition of the AASHTO segmental guide specifications (AASHTO 98). Similarly, the critical negative thermal gradients (see Fig. 12) are reviewed at 6 a.m. on May 7, 1995.

It is interesting to note that both the web and top slab values are quite close to the design gradient at both Section E and Section F. For the positive and negative thermal gradient, top slab readings are very close to the design gradient, while web readings deviate slightly from the design gradient. However, because there is much more slab area at the deck level than web area, it is very encouraging that the slab values are so close to the proposed design gradient. These values and others in the report[14] should help

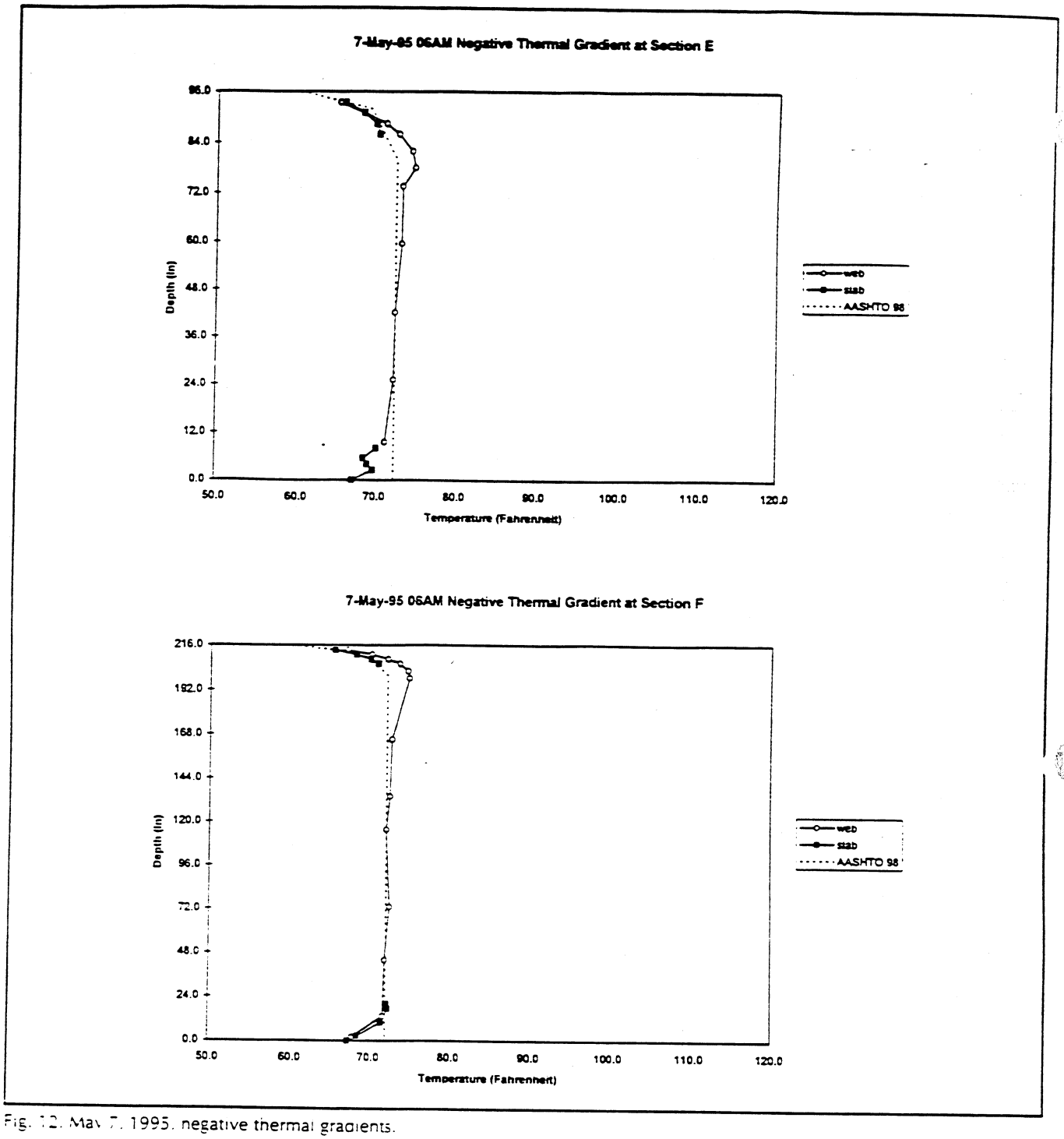

Fig. 12. May 7, 1995, negative thermal gradients.

to validate the use of this proposed design gradient.

Extrapolation should be used to determine the temperatures at the deck level (because readings for Gauge 13 are unreliable). At Section F, the positive and negative thermal gradient both show a peak at the bottom of the section; the web and bottom slab values are quite close to each other. At Section E, the peak at the bottom is less clearly defined; the bottom slab value is jagged (and there is no gauge in the web at the bottom). The proposed design gradients (AASHTO 98) also indicate that peaks at the bottom will occur but that they can be neglected.

ANALYSIS OF NORTH HALAWA VALLEY VIADUCT

Analysis for Thermal Gradient

In general, thermal stresses are induced by restraint to expansion and rotation, and not by temperature changes directly. Restraint is provided by the cross section and the support conditions. The cross section induces primary stresses that vary in the vertical direction but are constant in the longitudinal direction (if the section is constant). The support conditions induce secondary stresses that vary in the longitudinal direction.

For a positive thermal gradient (see Fig. 13), the compressive thermal

stress component can be considered as being equilibrated by a tensile resultant force P at some distance e_{top} from the top of the section. This resultant force is equivalent to a tensile axial force N_p and a negative bending moment M_p at the location of the neutral axis y_{top} from the top of the section.

The primary stress (see Fig. 14) is the superposition of the thermal component $f(y)$ with the axial component N_p/A and the flexural component $M_p y/I$. The support conditions cause redistribution to occur and create compressive axial forces N_s and positive bending moments M_s. The secondary stress (see Fig. 14) is the superposition of the axial component N_s/A and the flexural component $M_s y/I$. The total stress is the superposition of the primary and secondary stresses (see Fig. 14). (For more details see Refs. 7 and 8.)

The calculations can be simplified substantially by recognizing that the resultant axial force P and location from the top e_{top} due to the thermal component are constant for segmental bridges (see Fig. 13). This is due to the fact that the dimensions at the top of a segmental bridge are normally constant and the thermal gradient acts near the top of the section. The net result is that once P and e_{top} have been determined for one section, the primary and secondary effects at any section can be found by a simple manipulation of the section properties.

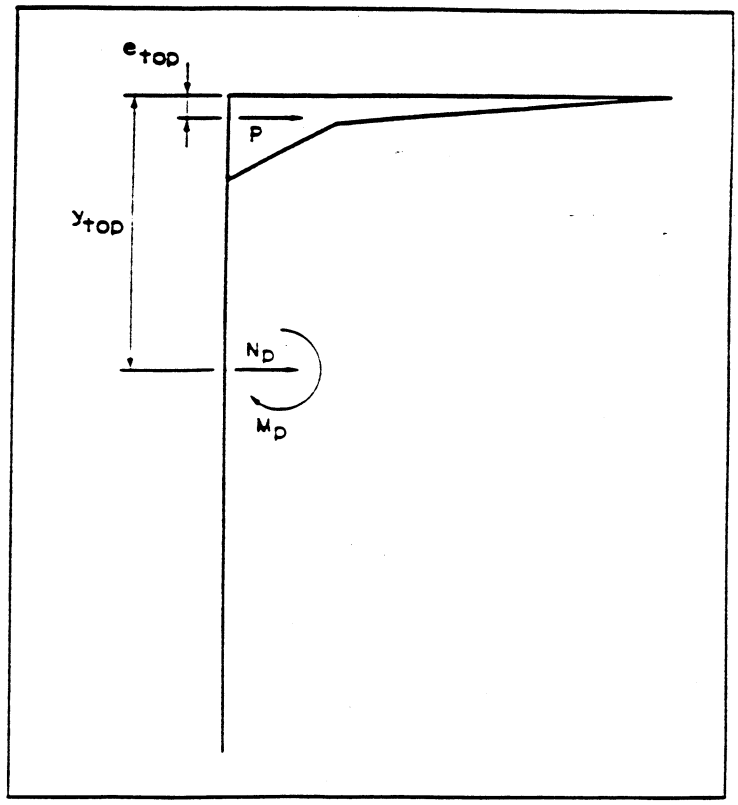

Fig. 13. Positive thermal gradient and equivalent forces.

On the other hand, if the effects of the thermal component are taken about the neutral axis or the bottom of the section (as has commonly been done in the past), a completely new set of calculations has to be made at each location because the depth of the section and/or bottom slab thickness are normally variable.

Expressions for the thermal component $f(y)$, axial force P, bending moment about the top M and eccentricity about the top e_{top} are given as follows:

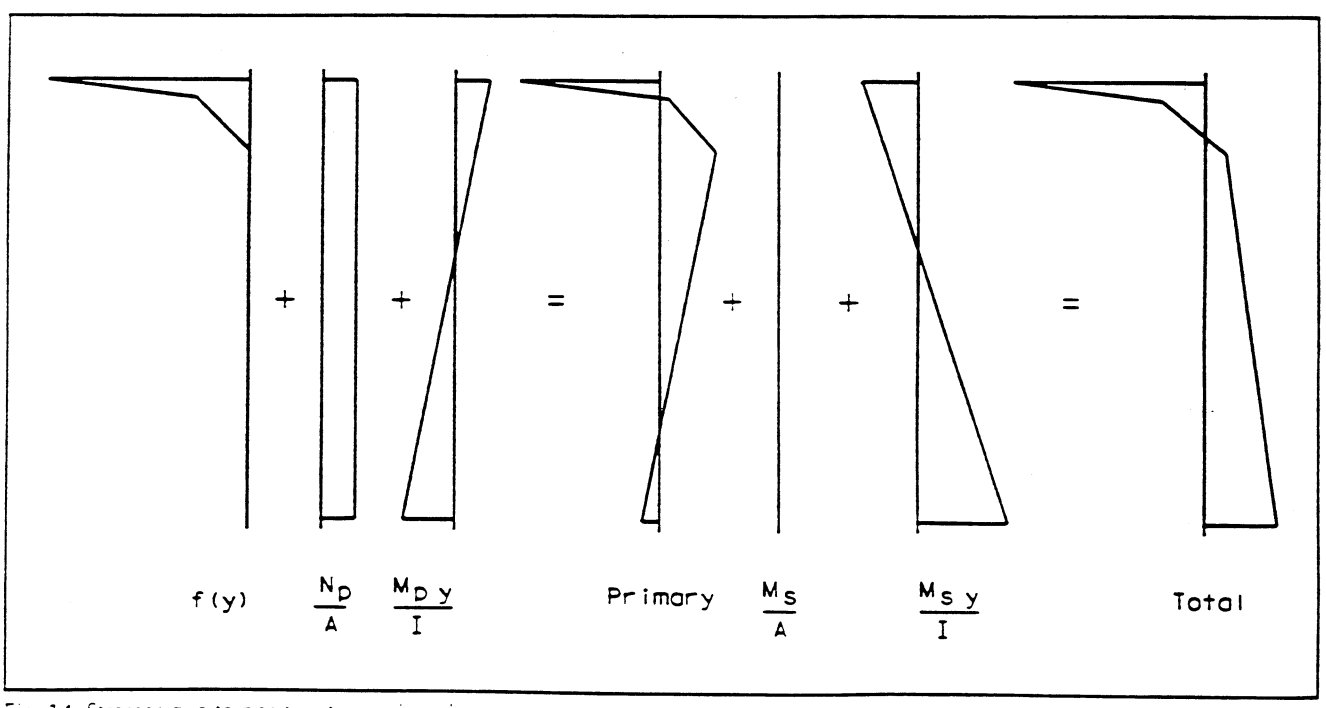

Fig. 14. Stresses due to positive thermal gradient.

$$f(y) = E\alpha t(y) \quad (1)$$

$$P = E\alpha \int t(y)\, b(y)\, dy \quad (2)$$

$$M = E\alpha \int t(y)\, b(y)\, y\, dy \quad (3)$$

$$e_{top} = M/P \quad (4)$$

where E is the modulus of elasticity, α is the coefficient of thermal expansion, and $t(y)$ and $b(y)$ are the thermal gradient and width of the section, respectively, as a function of y which is measured from the top of the section. Once P and e_{top} have been calculated for one section, N_p and M_p can be determined for all sections by simply working with the section properties as follows:

$$N_p = P \quad (5)$$

$$M_p = P(y_{top} - e_{top}) \quad (6)$$

The primary effects at each section can now be determined. The secondary effects can be determined by using a plane frame computer program (or by hand using the flexibility method). Three methods can be used to input thermal data into a plane frame computer program:

1. Axial force and bending moment (N_p and M_p).
2. Equivalent uniform temperature and linear gradient (T_{unif} and T_{grad}).
3. Temperature at the top and bottom of the section (T_{top} and T_{bot}).

The method chosen depends on the capabilities of the program. Expressions for T_{unif}, T_{grad}, T_{top} and T_{bot} are given as follows:

$$T_{unif} = N_p/(E\alpha A) \quad (7)$$

$$T_{grad} = M_p/(E\alpha I) \quad (8)$$

$$T_{top} = T_{unif} + T_{grad} y_{top} \quad (9)$$

$$T_{bot} = T_{unif} - T_{grad} y_{bot} \quad (10)$$

where A and I are the section area and moment of inertia, and y_{top} and y_{bot} are the distances from the neutral axis to the top and bottom of the section, respectively.

Numerical Design Example

The North Halawa Valley Viaduct has been chosen as an example problem. The span layout is shown in Fig. 5 and the cross section is shown in Fig. 4. The AASHTO 98 thermal gradient is used in this example. It should be emphasized again that the methods given in this paper apply equally to precast and cast-in-place segmental bridges.

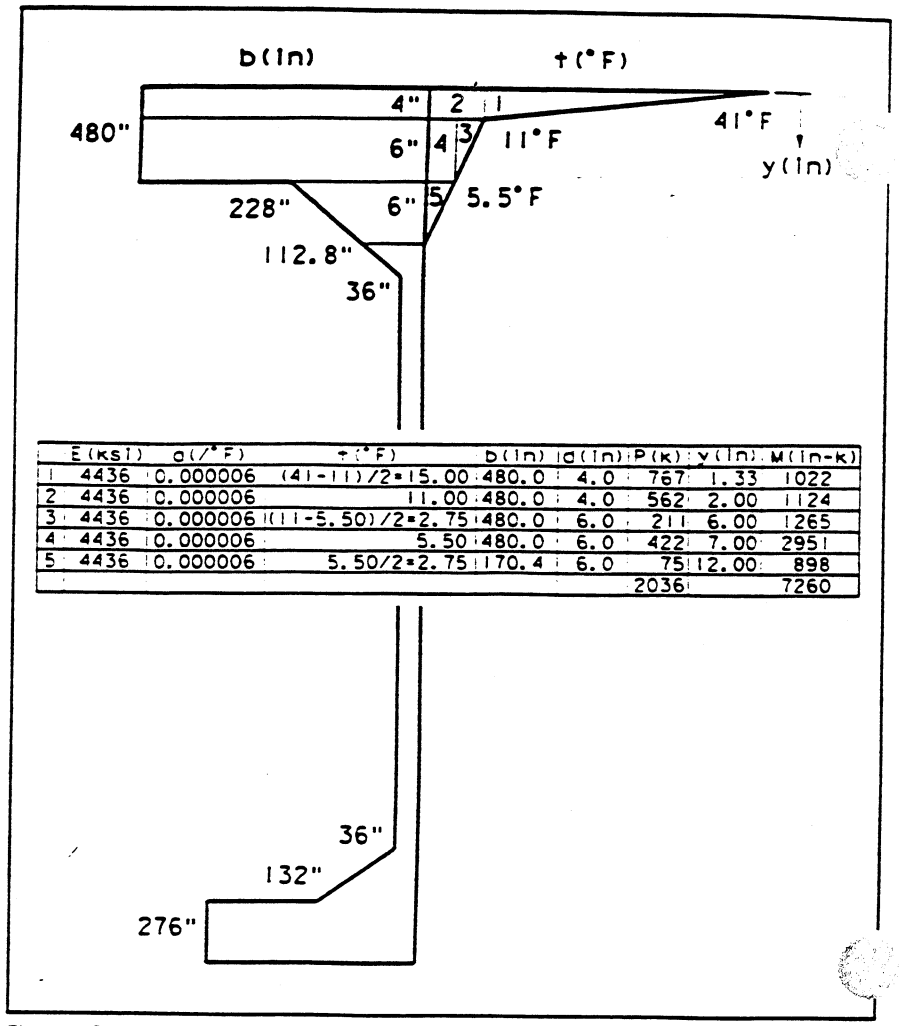

	E(ksi)	α(/°F)	t(°F)	b(in)	d(in)	P(k)	y(in)	M(in-k)
1	4436	0.000006	(41-11)/2=15.00	480.0	4.0	767	1.33	1022
2	4436	0.000006	11.00	480.0	4.0	562	2.00	1124
3	4436	0.000006	(11-5.50)/2=2.75	480.0	6.0	211	6.00	1265
4	4436	0.000006	5.50	480.0	6.0	422	7.00	2951
5	4436	0.000006	5.50/2=2.75	170.4	6.0	75	12.00	898
						2036		7260

Fig. 15. Calculation of P and M.

Eqs. (1) to (4) are used to determine P and e_{top} at the midspan [8 ft (2.4 m)] section. Fig. 15 shows how a simple piecewise integration can be made to determine P and M. The right side of the plot shows $t(y)$ while the left side of the plot shows $b(y)$. The table summarizes the piecewise integration. Eqs. (5) to (10) are then used to determine N_p, M_p, T_{unif}, T_{grad}, T_{top} and T_{bot} at all sections. (Only the section properties at each location along with P and e_{top} are required for this calculation.) Once T_{top} and T_{bot} are determined at each section, the secondary axial force and bending moment can be determined with a plane frame computer program. Temperatures T_{top} and T_{bot} for this bridge are shown in Fig. 16. Note that T_{top} and T_{bot} have larger values at midspan and smaller values at the support.

For the remainder of this study, it is worthwhile to compare thermal gradient with live load because current codes require serviceability to be considered for: (1) 100 percent thermal gradient without live load and (2) 50 percent thermal gradient with live load. The HS20 design live load for this bridge corresponds to three lanes loaded with a reduction factor of 0.9 and an impact factor of 10 percent.

The bending moment diagram and axial force diagram for thermal gradient and live load are shown in Figs. 17 and 18, respectively. The positive thermal gradient (see Fig. 17) produces a positive secondary moment diagram whose maximum values are in the same order as those due to positive live load. The negative thermal gradient produces a negative secondary moment diagram whose values are significantly less than those due to negative live load.

The positive thermal gradient (see Fig. 18) produces a uniform com-

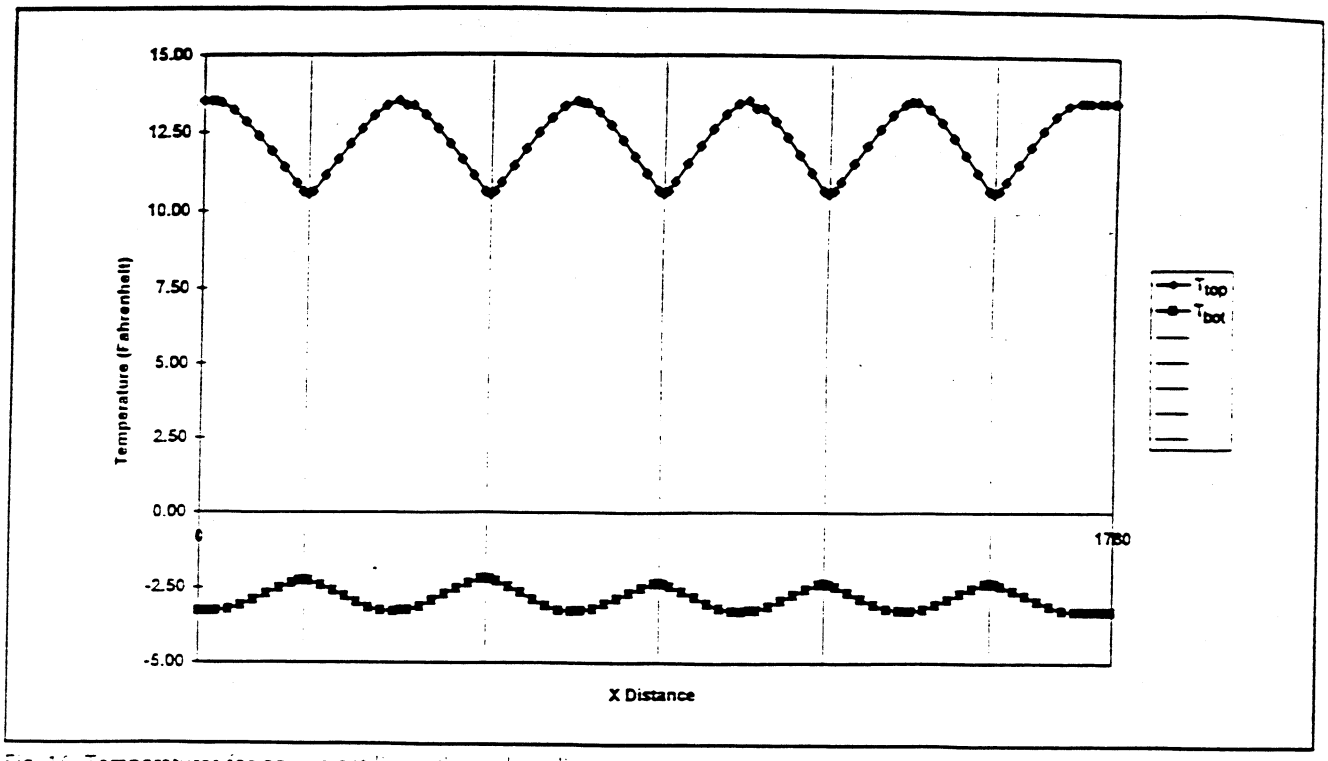

Fig. 16. Temperatures for equivalent linear thermal gradient.

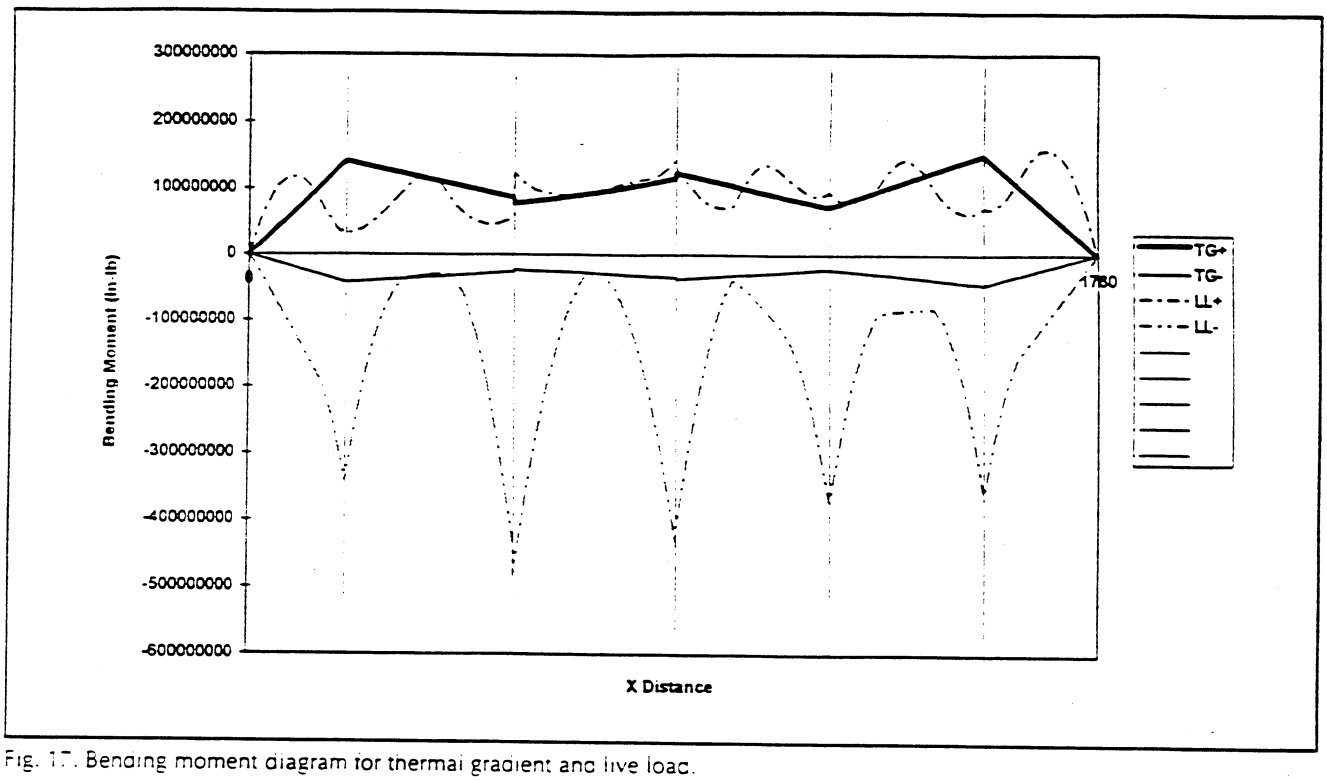

Fig. 17. Bending moment diagram for thermal gradient and live load.

pressive axial force in Span 9-10, which has fixed piers at both ends. The corresponding variable compressive axial force due to positive live load is also shown. The negative thermal gradient and negative live load, respectively, produce a uniform and variable tensile axial force in Span 9-10.

The stresses at the top and bottom of the section due to thermal gradient and live load are shown in Figs. 19 and 20, respectively. Tensile stresses are of primary importance here because additional prestressing is required to keep values within allowable limits; compressive stresses are also of interest but normally not a problem because there is usually a sufficient reserve of compression.

The negative thermal gradient (see Fig. 19) causes approximately uniform

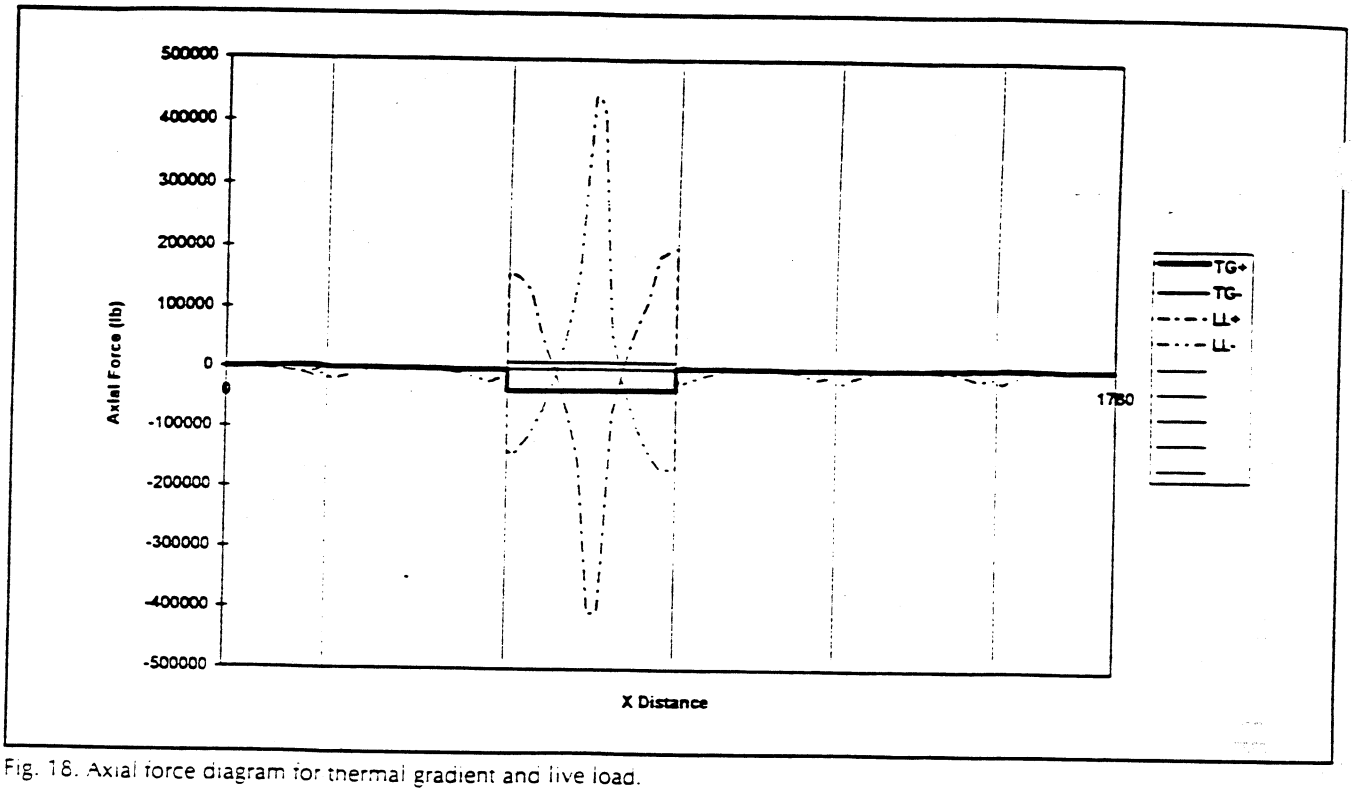

Fig. 18. Axial force diagram for thermal gradient and live load.

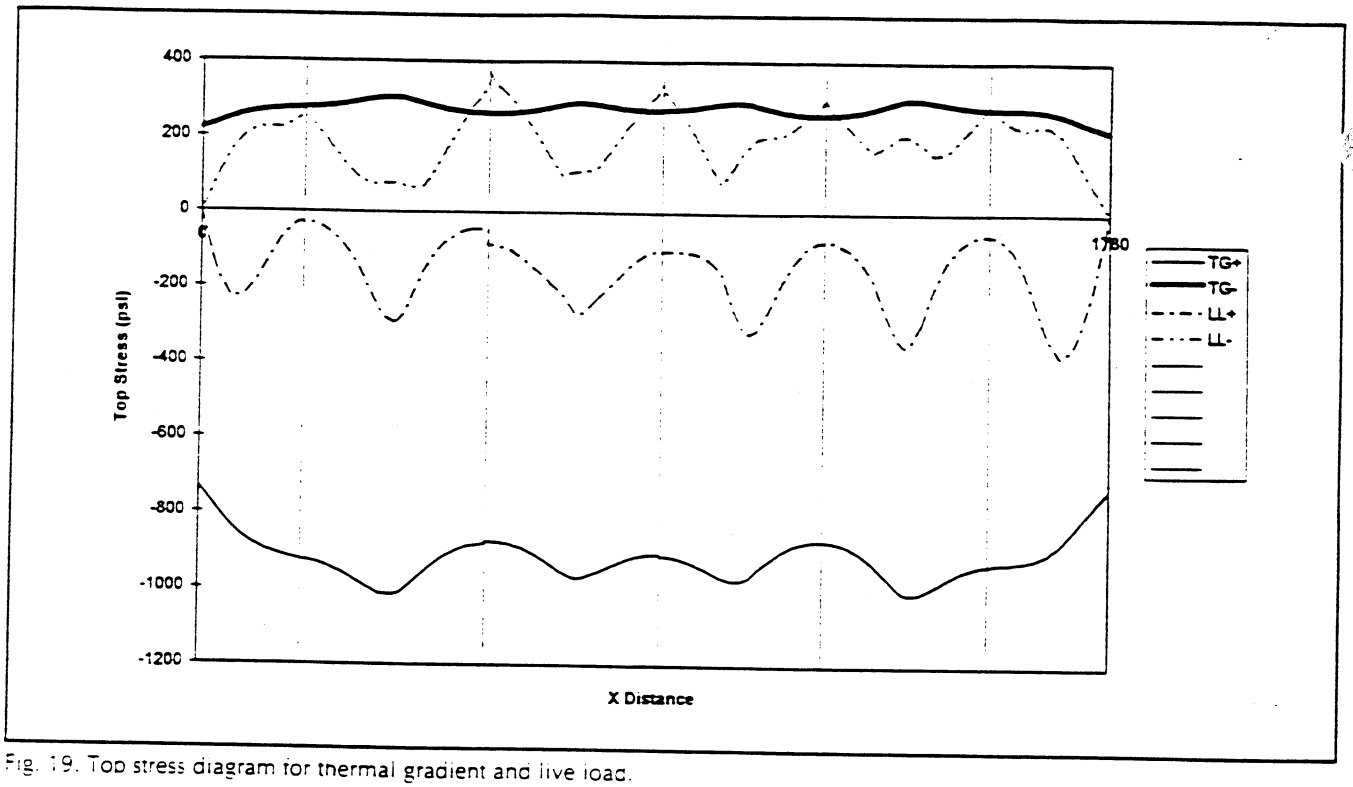

Fig. 19. Top stress diagram for thermal gradient and live load.

tension to occur at the top. The amount of tension varies from a minimum of 220 psi (1.52 MPa) at the ends of the bridge to a maximum of 305 psi (2.10 MPa) at midspan of Span 8-9 [360 ft (110 m) span]. The amount of prestressing (top continuity tendons) may have to be increased at midspan to accommodate this tension.

Both positive thermal gradient (see Fig. 20) and positive live load cause variable tension at the bottom, which is maximum at midspan. For the four interior spans, the ratio of thermal gradient stress to live load stress is 78 percent for Span 8-9, 84 percent for Span 9-10, 60 percent for Span 10-11 and 64 percent for Span 11-12. Thus, the stress due to thermal gradient can be of the same order (60 to 80 percent) as that due to live load. The amount of

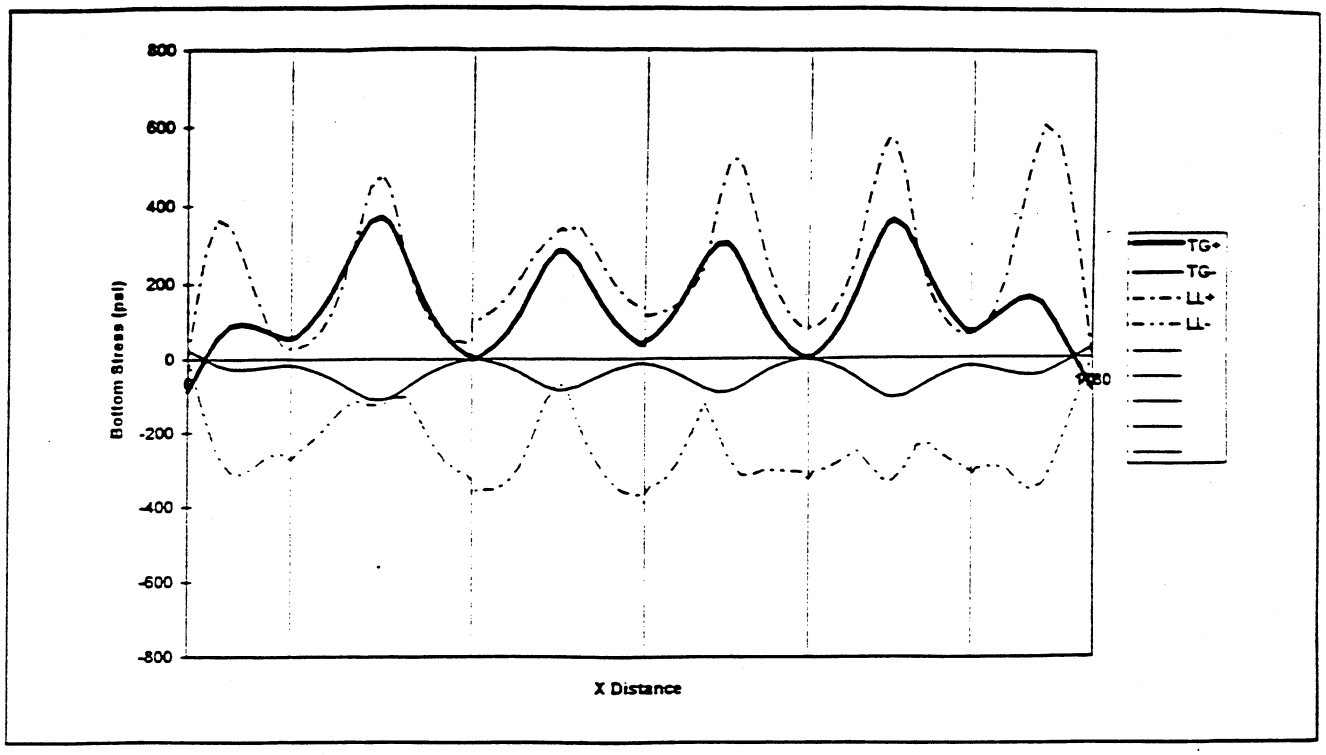

Fig. 20. Bottom stress diagram for thermal gradient and live load.

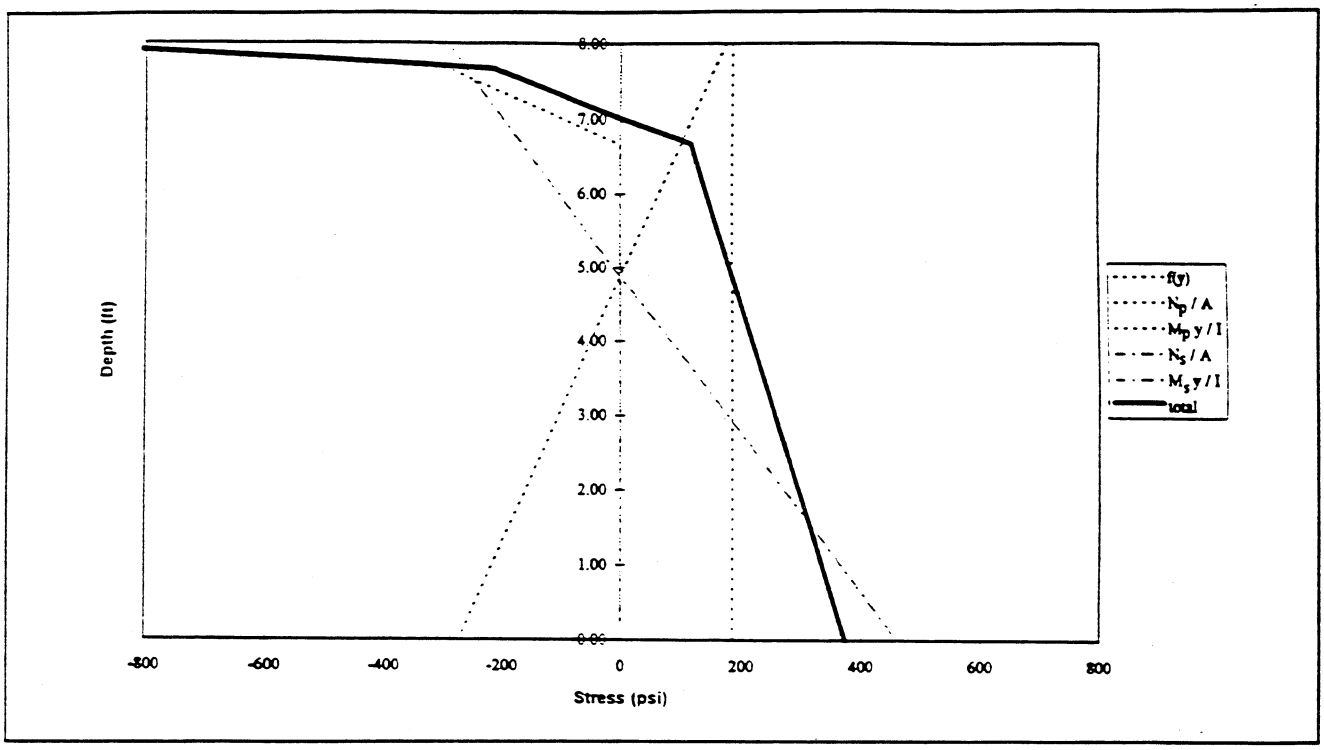

Fig. 21. Thermal stresses at midspan of Span 8-9 for positive thermal gradient.

prestressing (bottom continuity tendons) has to be increased to accommodate the case of live load plus 50 percent thermal gradient.

Thermal stresses at midspan of Span 8-9 [360 ft span (110 m)] for a positive gradient are shown in Fig. 21. The compressive thermal component $f(y)$ is equilibrated by a tensile primary axial force component N_p/A and a negative primary bending moment component $M_p y/I$. Analysis for secondary effects gives a zero secondary axial force component N_s/A and a positive bending moment component $M_s y/I$. The net result of these five effects is a tensile stress of 374 psi (2.58 MPa) at the bottom with a corresponding compressive stress of 1026 psi (7.07 MPa) at the top.

Thermal stresses at Pier 12 for a negative gradient are shown in Fig. 22.

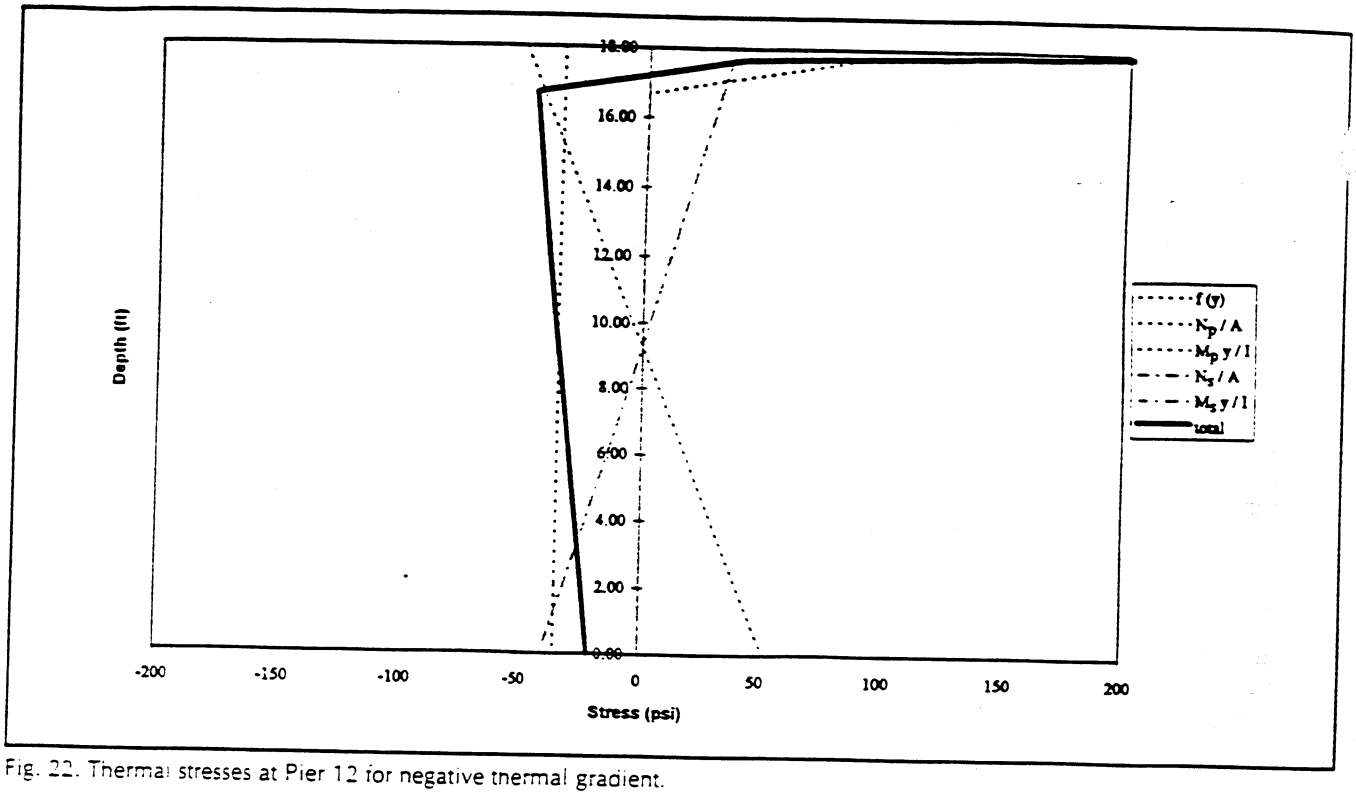

Fig. 22. Thermal stresses at Pier 12 for negative thermal gradient.

The tensile thermal component $f(y)$ is equilibrated by a compressive primary axial force component N_p/A and a positive primary bending moment component $M_p y/I$. Analysis for secondary effects gives a zero secondary axial force component N_s/A and a negative bending moment component $M_s y/I$. The net result of these five effects is a tensile stress of 280 psi (1.93 MPa) at the top with a corresponding compressive stress of 21 psi (0.14 MPa) at the bottom.

SUMMARY OF SIGNIFICANT RESULTS

Large amounts of thermocouple data from an instrumented prestressed concrete segmental bridge (North Halawa Valley Viaduct) have been efficiently reduced graphically to determine the critical positive and negative thermal gradients. The results validate the use of the positive and negative thermal gradient in the proposed 1998 AASHTO Segmental Guide Specifications (which is similar for positive gradient and reduced by 40 percent for negative gradient from the 1994 AASHTO LRFD Bridge Design Specifications).

The computation procedures for a nonlinear thermal gradient are greatly simplified by recognizing that the resultant axial force P and distance from the top e_{top} due to the thermal component are constant for segmental bridges. This is due to the fact that the dimensions at the top of a segmental bridge are normally constant and the thermal gradient acts only near the top of the section. The net result is that once P and e_{top} have been determined for one section, the primary and secondary effects at any section can be found by a simple manipulation of the section properties.

These simplified computation procedures are illustrated using the North Halawa Valley Viaduct as an example problem. A simple hand calculation is used to determine P and e_{top} at one section. This allows the primary and secondary effects to be easily determined at any section. A comparison of the effects of thermal gradient and live load is made with respect to the prestressing requirements. Additional prestressing is required at the bottom near midspan for the case of live load plus 50 percent positive thermal gradient. Additional prestressing may also be required at the top near midspan to accommodate the negative thermal gradient.

CONCLUSIONS

1. A comparison of the positive and negative thermal gradient in various AASHTO documents has been made.

2. A prestressed concrete segmental bridge (North Halawa Valley Viaduct) has been instrumented and large amounts of thermocouple data have been efficiently reduced graphically to determine the critical positive and negative thermal gradient.

3. The results validate the use of the positive and negative thermal gradient in the proposed 1998 AASHTO Segmental Guide Specifications as well as the 1994 AASHTO LRFD Bridge Design Specifications.

4. The results are very timely because they substantiate the reduction of the negative thermal gradient from -0.5 to -0.3 times the positive thermal gradient. This reduction is currently being considered in the proposed 1998 AASHTO Segmental Guide Specifications.

5. The computation procedures for nonlinear thermal gradient have been shown to be greatly simplified by recognizing that the resultant axial force P and location from the top e_{top} due to the thermal component are constant for most segmental bridges. Once P and

e_{top} have been determined for one section, the primary and secondary effects at any section can be found by a simple manipulation of the section properties.

6. A numerical example for the analysis of a segmental bridge for thermal gradient has been included. A simple hand calculation is used to determine P and e_{top} at one section. This allows the primary and secondary effects to be determined at all sections.

7. The numerical example includes a comparison of forces and stresses due to thermal gradient and live load. This allows a comparison of the prestressing requirements. Additional prestressing is required at the bottom near midspan for the case of live load plus 50 percent positive thermal gradient. Additional prestressing may also be required at the top near midspan to accommodate the negative thermal gradient.

ACKNOWLEDGMENTS

The instrumentation program of the North Halawa Valley Viaduct was conducted under the sponsorship of the Hawaii Department of Transportation and the Federal Highway Administration. The interest and encouragement of the sponsors, and especially James Hoblitzell and Roland Nimis of the Federal Highway Administration, is greatly appreciated.

The author also wishes to acknowledge Scott Hunter of T. Y. Lin International and Ian Robertson of the University of Hawaii at Manoa who initiated the instrumentation study and were responsible for its successful execution. The overall guidance of Karen Cormier of T. Y. Lin International and Henry Russell, Engineering Consultant, during the course of the instrumentation program has been extremely valuable.

The contents of this paper reflect the views of the author and do not necessarily reflect the views or policies of the sponsors.

REFERENCES

1. *Precast Segmental Box Girder Bridge Manual*. Published jointly by the Prestressed Concrete Institute, Chicago, Illinois, and Post-Tensioning Institute, Phoenix, AZ, 1978, pp. 41–44.
2. Priestley, M. J. N., "Design of Concrete Bridges for Temperature Gradients," *ACI Journal*, V. 75, No. 5, May 1978, pp. 209-217.
3. Hoffman, P. C., McClure, R. M., and West, H. H., "Temperature Study of an Experimental Segmental Bridge," PCI JOURNAL, V. 28, No. 2, March-April 1983, pp. 78-97.
4. Elbadry, M. M., and Ghali, A., "Temperature Variations in Concrete Bridges," *Journal of Structural Engineering*, V. 20, No. 10, October 1983, pp. 2355-2374.
5. Cooke, N., Priestley, M. J. N., and Thurston, S. J., "Analysis and Design of Partially Prestressed Concrete Bridges Under Thermal Loading," PCI JOURNAL, V. 29, No. 3, May-June 1984, pp. 94-115.
6. Potgieter, I. C., and Gamble, W. L., "Nonlinear Temperature Distributions in Bridges at Different Locations in the United States," PCI JOURNAL, V. 34, No. 4, July-August 1989, pp. 80-103.
7. Imbsen, R. A., Vandershaf, D. E., Schamber, R. A., and Nutt R. V., "Thermal Effects in Concrete Bridge Superstructures," National Cooperative Highway Research Program Report 276, Transportation Research Board, Washington, D.C., September 1985, 99 pp.
8. AASHTO, *Guide Specifications — Thermal Effects in Concrete Bridge Superstructures*, First Edition, American Association of State Highway and Transportation Officials, Washington, D.C., 1989.
9. AASHTO, *Guide Specifications for Design and Construction of Segmental Concrete Bridges*, First Edition, American Association of State Highway and Transportation Officials, Washington, D.C., 1989.
10. AASHTO, *LRFD Bridge Design Specifications*, First Edition, American Association of State Highway and Transportation Officials, Washington, D.C., 1994.
11. AASHTO, *Guide Specifications for Design and Construction of Segmental Concrete Bridges*, Proposed Second Edition, American Association of State Highway and Transportation Officials, Washington, D.C., 1998.
12. Ingham, T. J., Manzanarez, R., and Cormier, K., "Design and Construction of North Halawa Valley Viaduct," Proceedings of Fourth International Bridge Engineering Conference, San Francisco, CA, 1995, pp. 176-184.
13. Lee, A., and Robertson, I. N., "Instrumentation and Long-Term Monitoring of the North Halawa Valley Viaduct," University of Hawaii at Manoa, Department of Civil Engineering Report UHM/CE/95-08, 1995.
14. Shushkewich, K. W., Vo, N. T., and Robertson, I. N., "Instrumentation of the North Halawa Valley Viaduct — Oahu, Hawaii," Progress Report to Hawaii Department of Transportation and Federal Highway Administration, 1998.

APPENDIX — NOTATION

α = coefficient of thermal expansion
A = section area
$b(y)$ = width of section as a function of y
E = modulus of elasticity
e_{top} = eccentricity of thermal stress component about top
$f(y)$ = thermal stress component as a function of y
I = section moment of inertia
M = bending moment resisting thermal stress component
M_p = primary bending moment
M_s = secondary bending moment
N_p = primary axial force
N_s = secondary axial force
P = axial force resisting thermal stress component
T_{bot} = temperature at bottom of section
T_{grad} = linear gradient
T_{top} = temperature at top of section
T_{unif} = uniform temperature
$t(y)$ = thermal gradient as a function of y
y = distance measured from top of section
y_{bot} = distance from neutral axis to bottom of section
y_{top} = distance from neutral axis to top of section

Appendix B - Long-Term Monitoring of the North Halawa Valley Viaduct - Robertson

LONG-TERM MONITORING OF THE NORTH HALAWA VALLEY VIADUCT

Ian N. Robertson

Department of Civil Engineering, University of Hawaii,
Honolulu, Hawaii, 96822, USA

Presented at Structural Engineers World Congress (SEWC '98)
San Francisco, July 1998

ABSTRACT

This paper presents preliminary results of a long-term bridge monitoring program after three years of data collection. The North Halawa Valley Viaduct on the Hawaiian island of Oahu was extensively instrumented during the second half of 1994. The objective of the instrumentation program is to monitor the long-term behavior of the Viaduct. The instrumentation program was designed for an initial five year monitoring period. The primary instruments used for concrete strain and deflection monitoring are described, and their performance over the first three years is discussed. Results are presented for both short-term and long-term events to show the effectiveness of these instruments. These results are compared with analytical predictions using two finite element computer programs.

INTRODUCTION

The North Halawa Valley Viaduct is a 1.5 km box-girder viaduct with span lengths up to 110 m (Figure 9). It is part of the new H-3 highway on the island of Oahu in Hawaii. The viaduct was built by means of post-tensioned in-situ balanced cantilever construction as described by Banchik *et al* (1994) (Figure 10). Four spans of the box-girder viaduct (70 to 110 m spans) were selected for instrumentation to provide an adequate representation of the long-term viaduct behavior. The instrumentation program was developed in conjunction with T.Y. Lin International, structural engineers for the viaduct. During construction, all instruments were installed by personnel from the University of Hawaii (UH) and Construction Technology Laboratories (CTL) in Skokie, Illinois.

The instrumentation used in this project was designed to provide long-term monitoring of the structural performance of the viaduct. The measurements required to achieve the project

objectives include concrete strains, concrete and ambient temperatures, concrete creep and shrinkage strains, span shortening, tendon forces, span deflections, and support rotations. The following instrumentation was selected and installed to perform these measurements: vibrating wire gages, electrical resistance strain gages, demec strain gage points, thermocouples, extensometers, tendon load cells, base-line deflection systems, tiltmeters, and datalogger recording systems.

This paper presents results from the concrete strain and deflection measurements and compares them with analytical predictions for both short-term and long-term events. The finite element computer programs used for the short-term events is SAP2000 (1996), while the long-term events are modeled using SFRAME (Ketchum, 1986), a time-dependent step-wise analysis program written specifically for analysis of incrementally constructed bridges.

DESCRIPTION OF INSTRUMENTATION

A detailed description of all instrumentation and the installation procedures used in this project is given by Lee and Robertson (1995). The following is a brief description of the strain and deflection measurement systems pertaining to the results presented in this paper.

Instrument Locations

Seven sections were selected for instrumentation in order to provide an adequate representation of the viaduct behavior. Sections A, D, E and G are at, or close to midspan, while B, C and F are close to the ends of the instrumented spans as shown in Figure 1.

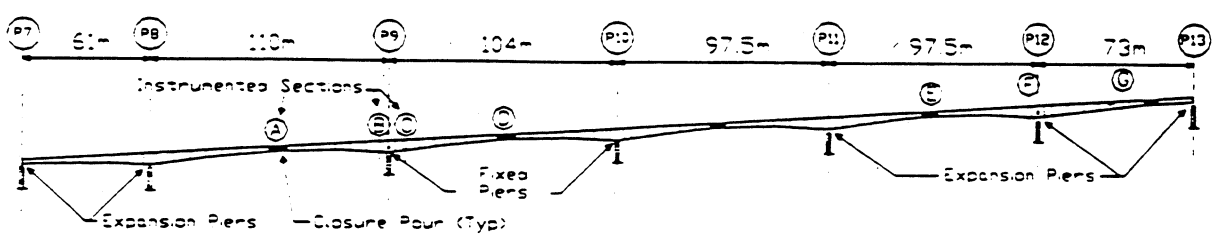

Figure 1: Viaduct elevation showing instrumented sections, A to G

Concrete Strain Measurements

The primary instruments for measuring concrete strain are Vibrating Wire Strain Gages. These gages were embedded in the concrete to measure longitudinal strain. Eight to ten vibrating wire strain gages were placed around the box-girder cross-section at each instrumented section as shown in Figure 2 for section B.

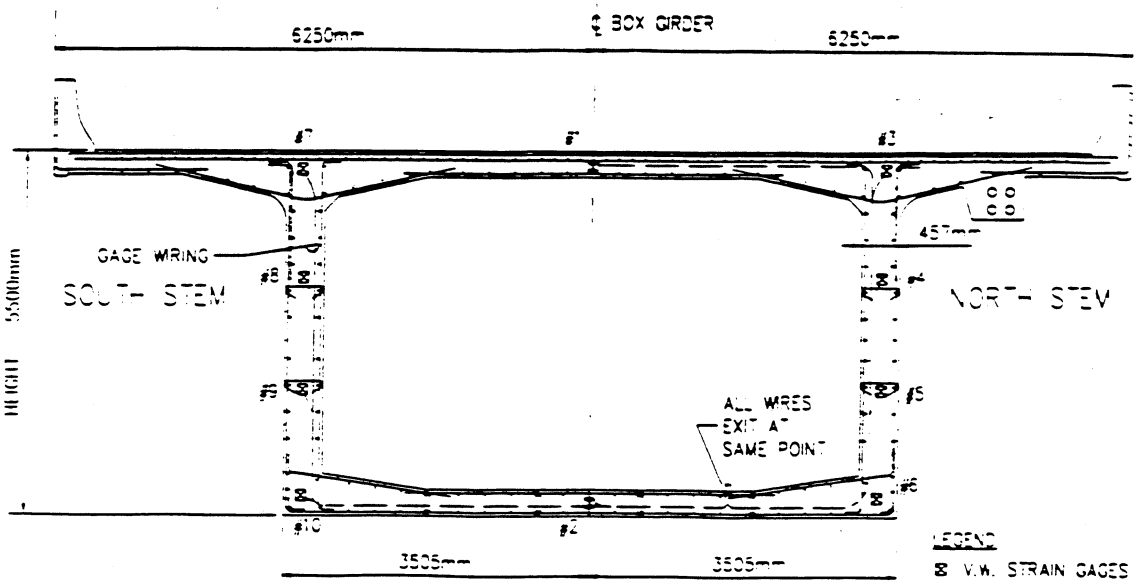

Figure 2: Vibrating wire strain gage locations at section B

At sections E and F, additional concrete strain measurements were made with electrical resistance strain gages attached to reinforcing bar coupons embedded in the concrete. In order to confirm the long-term stability of the electronic strain measurements, backup manual strain gage readings were made using Demec strain gage points attached to the concrete surface inside the box-girder.

Span Shortening

Extensometers were installed in the four instrumented spans to monitor the overall shortening of the box-girder. Each extensometer consists of a series of graphite rods (6mm diameter by 6m long) spliced together to span from pier to pier inside the box girder. The rods are coupled together and inserted into a 20mm diameter PVC pipe attached to the underside of the girder top slab. One end of the rod is fixed to the top slab soffit, while the other end is coupled to a Linear Variable Displacement Transducer (LVDT). The relative displacement of the concrete at the two ends of the extensometer is measured by the LVDT.

Bearing movements were also made at the sliding bearings, but these readings are distorted by any lateral deflection in the supporting piers due to temperature or bearing friction effects.

Span Deflections

A taut-wire base-line system was installed in each of the instrumented spans to monitor vertical deflection of the box-girders. This system consists of a high-strength piano wire strung at constant tension from one pier to the next, inside the box girder, to act as a reference line as shown in Figure 3. A digital caliper is used to measure the distance between the base-

line and plates attached to the underside of the top slab (Figure 12). Changes in the caliper readings indicate the vertical deflection of the box girder relative to the ends of the span.

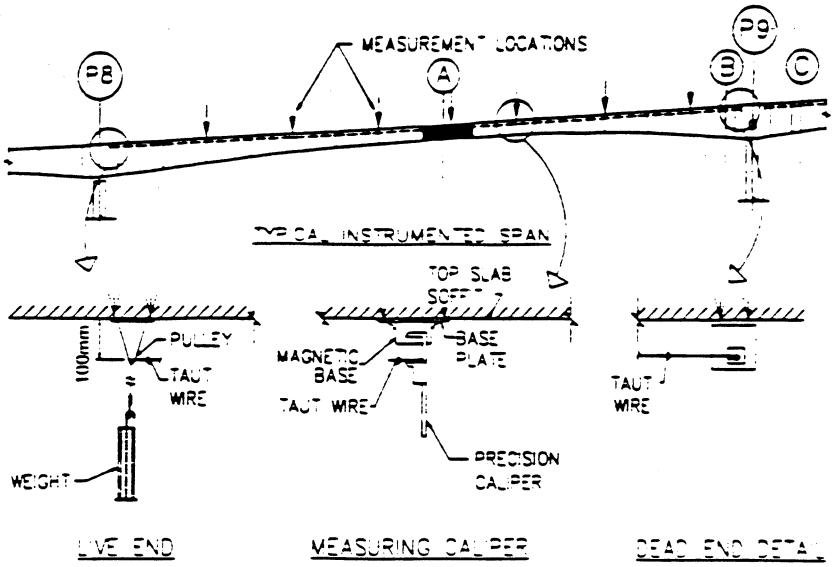

Figure 3: Taut-wire Deflection System

SHORT-TERM EVENT RESULTS

Initial Application of Prestress

The vibrating wire strain gages monitored the longitudinal strain around each instrumented section. A sample of the 6:00 AM strain readings from the 8 gages at section E is shown in Figure 13. These readings represent the first two years of data collected at this section. Enlarging the first 30 days after pouring results in Figure 14. The sudden changes in the strain readings indicate either an application of prestress across this section, or the movement of the gantry truss reaction points on the top of the structure.

The strain gradient across the depth of section E for one particular prestressing event on September 23, 1994 is shown in Figure 4. Both vibrating wire strain gages and electrical resistance gages provide a straight line strain gradient through the depth of the section. Analysis of this prestress event using the computer program SFRAME (Ketchum, 1986) yields slightly different results. This is attributed in part to the lack of precision in the field measurement of the applied prestress force.

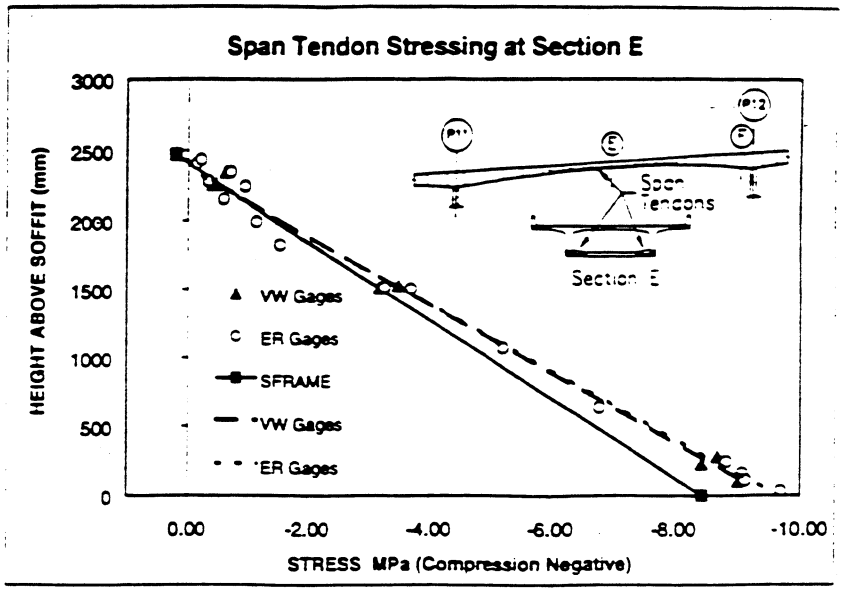

Figure 4: Section E Stresses during Span Tendon Prestressing

Deflection during load test on viaduct

In August 1997, a load test was performed on the instrumented spans of the viaduct using four trucks loaded with sand (Figure 11). Each truck approximated an HS-20 design vehicle. Deflections were monitored using the base-line system and optical surveys of the top surface of the viaduct.

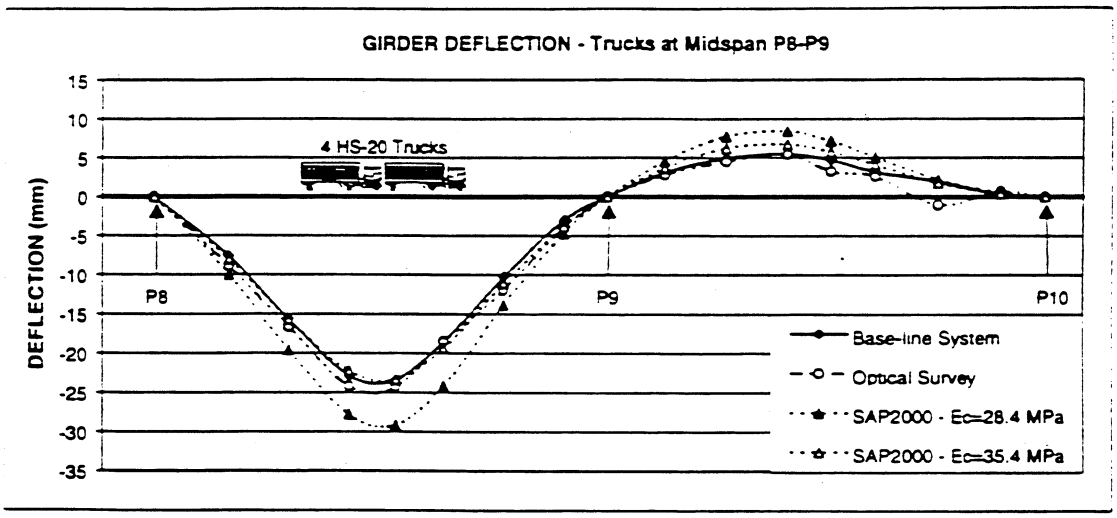

Figure 5: Comparison of Load Test Deflections.

The structure was modeled using SAP2000 (1996) and subjected to the same truck loading. The resulting comparison between measured and analytical deflected shapes for spans P8 to P10 is shown in Figure 5. On the whole, there is excellent agreement between the base-line system and the optical survey. However, because of the windy conditions and reading inaccuracies, the optical survey was somewhat less reliable than the base-line system as can be seen from some of the survey readings adjacent to Pier P10. The SAP2000 analysis was performed with two values of modulus of elasticity for the concrete, E_c. Based on compressive strength tests at 28- and 90-days, extrapolated to a concrete age of 3 years, the modulus of elasticity was obtained from Eqn. 1.

$$E_c = 4700\sqrt{f_c'}$$

$$E_c = 4700\sqrt{f_c'} = 35.4MPa \tag{1}$$

Alternatively, using the modulus of elasticity tests performed at 28- and 90-days, the 3 year modulus of elasticity was extrapolated as E_c = 28.4 MPa. The analytical results from the SAP2000 model using the value of E_c = 35.4 MPa show good agreement with the observed deflections.

Strain readings during load test

The Vibrating Wire Strain Gage readings taken every 5 minutes during the load test are shown in Figure 15. The trucks were located at four different positions on Span P8-P9, indicated by locations L1 through L4. The distinct steps in the strain readings indicate the movement of the trucks to the next loading location. Figure 6 shows the stress distribution through the depth of Section A (at midspan) for each of the truck locations. Note the excellent linearity of the stress gradients, and the consistent location of the neutral axis. Even at relatively small strain readings, the vibrating wire strain gages were extremely accurate and consistent.

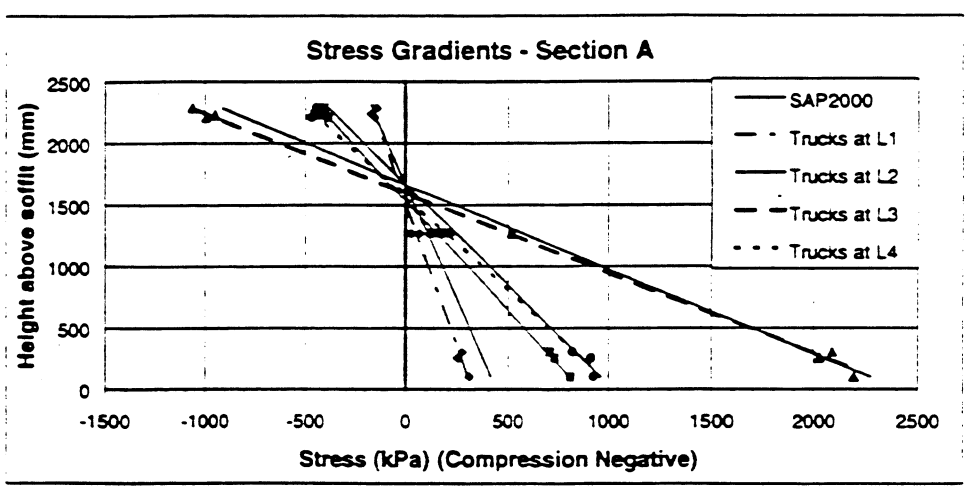

Figure 6: Stress gradients at section A during load test

The stress distributions obtained from SAP2000 analyses using E_c = 35.4 MPa are added for comparison. As with the deflected shape, the analytical model provides good agreement with the observed stresses, particularly for loading at midspan (L3) when the stresses are highest.

LONG-TERM RESULTS

Long-term axial strains

Figure 13 shows the long-term strains measured by the 8 vibrating wire strain gages at section E. Similar results were recorded for the 10 gages at section F. These sections represent the midspan and endspan conditions respectively for span P11 to P12. An average of the strains at these sections should indicate the overall shortening of the entire span. This span shortening has also been monitored by an extensometer installed after the prestressing of this span. Figure 7 shows a comparison between the strains measured at sections E and F, the average of these two sections, and the extensometer results. The resulting plots indicate that the vibrating wire strain readings provide a very good indication of the overall span shortening.

Long-term deflections

For long-term structural behavior, the program SFRAME (Ketchum, 1986) is used to account for all material properties, particularly creep and shrinkage of the concrete. Based on the initial assumptions regarding material properties, prestress and anticipated loading and construction sequence, this program was used to estimate the long-term deflection anticipated for the structure.

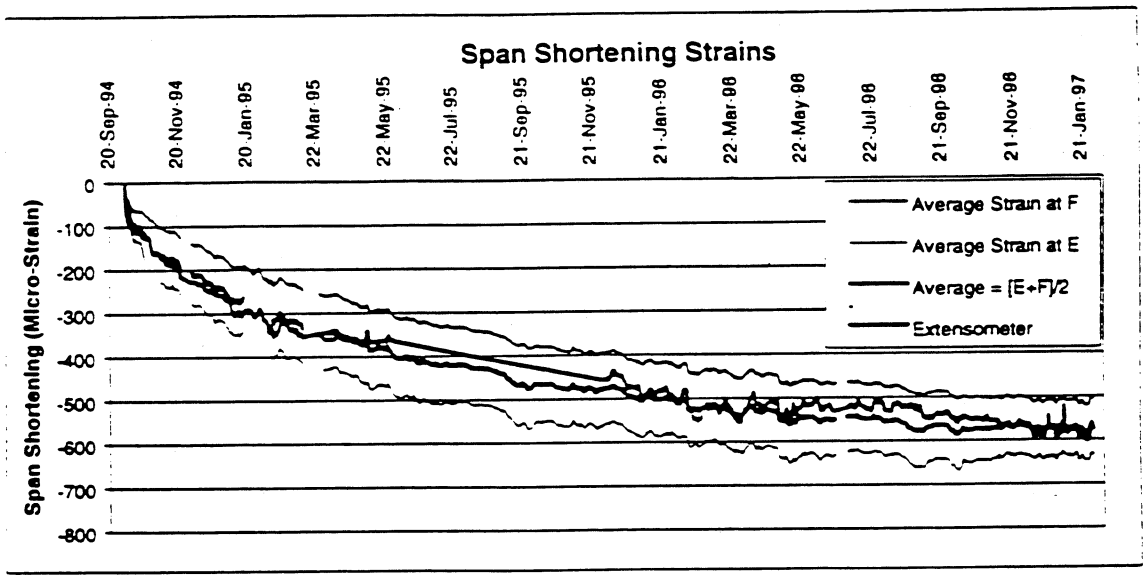

Figure 7: Span shortening strain comparison

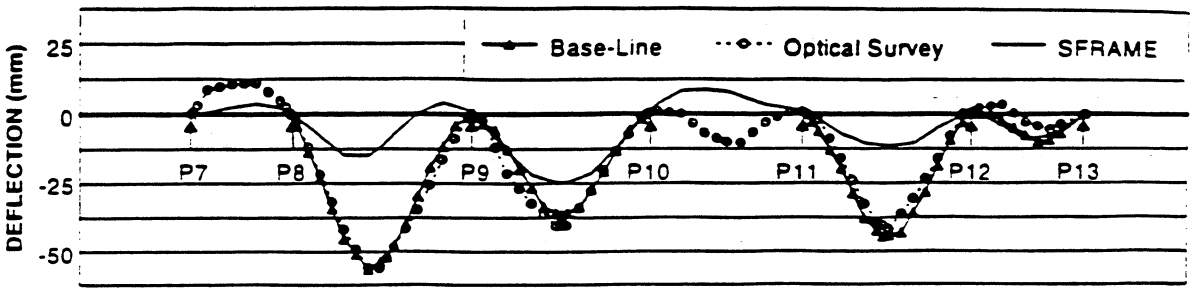

Figure 8: Long-term deflections (1995-1997)

In the field, deflections were monitored by means of the base-line system and optical surveys. The resulting deflections for the first two years after completion of construction are compared with the initial SFRAME predictions in Figure 8. As for the short-term events, there is excellent agreement between the base-line system and the optical survey.

However, the SFRAME prediction substantially underestimates the actual deflection. This disagreement between the analytical and observed deflections is attributed to the assumptions made at the design phase regarding the anticipated concrete material properties. Work is currently in progress at the University of Hawaii and T.Y. Lin International to update the SFRAME model with the material behavior observed during the monitoring program. It is anticipated that this will lead to improved comparisons between analytical and observed deflections.

CONCLUSIONS

1. The Vibrating Wire strain gages used in this instrumentation program proved extremely reliable for both short-term and long-term monitoring. The resulting strain distributions compare well with electrical resistance gages and with analytical modeling using finite element computer analyses (SAP2000 and SFRAME).

2. The span extensometers were able to confirm the overall span shortening indicated by the strains measured at midspan and endspan sections.

3. The base-line system used for deflection measurements was extremely reliable and accurate, both for short-term and long-term events. Prediction of short-term deflections using SAP2000 agreed well with the observed results. Prediction of long-term deflections using SFRAME underestimated the observed deflections. This is attributed to increased creep and shrinkage compared with that anticipated during the design phase.

ACKNOWLEDGEMENT

The author wishes to acknowledge the considerable assistance received during this instrumentation program. The input of Scott Hunter and Jose Sanchez of T. Y. Lin International and Henry Russell and Tom Weinmann of Construction Technology Laboratories was crucial to the successful implementation of this program. The assistance of a number of graduate students at the University of Hawaii is also greatly appreciated. In particular, Andre Lee's tireless efforts during instrument installation, and Michael Durbin's attention to detail during data processing. This project is supported by funds from the U. S. Federal Highway Administration and the Hawaii Department of Transportation. This support is gratefully acknowledged.

References

Banchik, Carlos, and Khaled, Nahlawi, North Halawa Valley Viaduct Design and Construction. *Concrete International*, 1994, **16**(3), 39–43

Ketchum, M. A. (1986), *Redistribution of Stresses in Segmentally Erected Prestressed Concrete Bridges (SFRAME), Report UCB/SESM-86/07,* University of California, Berkeley, California

Lee, Andre, and Robertson, Ian N. (1995), *Instrumentation and Long-Term Monitoring of the North Halawa Valley Viaduct, Report UHM/CE/95-08*, University of Hawaii, Honolulu, Hawaii

SAP2000 (1996), *Integrated Finite Element Analysis and Design of Structures,* Computers and Structures, Inc., Berkeley, California

Figure 9: North Halawa Valley Viaduct.

Figure 10: Viaduct under construction.

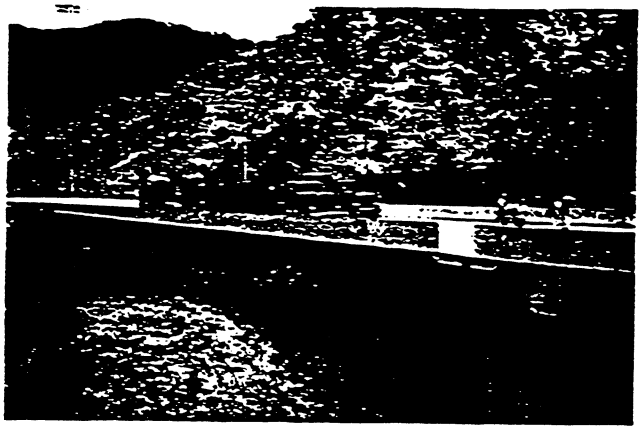

Figure 11: Viaduct load test.

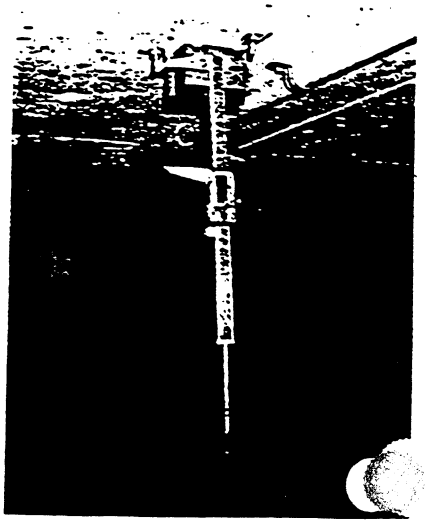

Figure 12: Base-line caliper

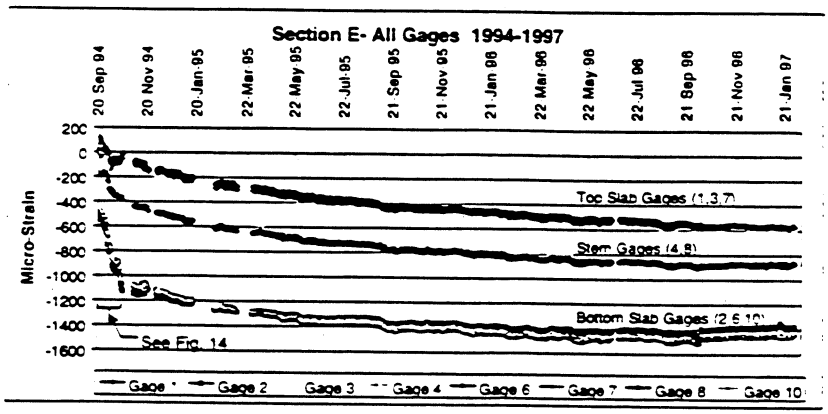

Figure 13: Vibrating wire strain gage readings at section E

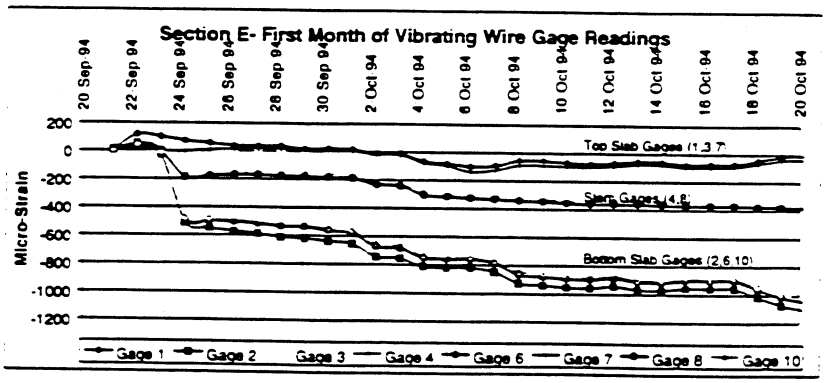

Figure 14: First month VW strain gage readings at section E

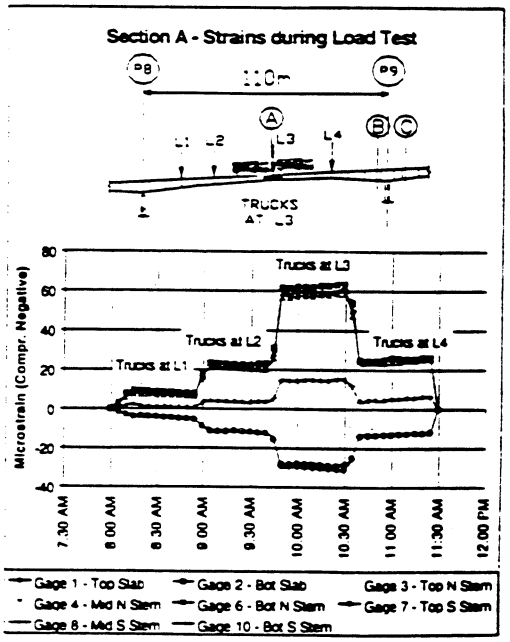

Figure 15: Section A strains dur load test

Appendix C - Calibration and Verification of Load Cell Data - Russell & Hunter

CALIBRATION AND VERIFICATION OF LOAD CELL DATA

by

H. G. Russell

S. Hunter

March, 1995

TABLE OF CONTENTS

BACKGROUND 1

ORIGINAL CALIBRATION PROCEDURE 2

VERIFICATION TESTS 3

- Equipment 3
- Test Procedures 3
- Test Results 4

CONCLUSIONS 5

TABLES 6

FIGURES 8

CALIBRATION AND VERIFICATION OF LOAD CELL DATA

by

H. G. Russell and S. Hunter*

BACKGROUND

As part of the instrumentation program of the H3 Halawa Valley Viaduct, load cells were installed on six span tendons to measure tendon forces. The purpose of the load cells was to monitor the change in tendon force over time in representative tendons. With these data, a more precise calculation of the variation of stresses in the bridge superstructure with time will be possible. Thus, the instrumented tendons will remain ungrouted for five years. Span tendons were selected for instrumentation because they were accessible and well protected. The load cells were located at the fixed end on four tendons and at the stressing end on two tendons. The six tendons varied in length from 44 to 196 ft.

To gain confidence in the method, comparisons were made between the forces from the calibrated hydraulic rams, forces measured on the load cells, measured elongations, theoretical forces and theoretical elongations for the instrumented tendons. The four load cells on the fixed ends indicated forces that were 82 to 89% of the theoretical values. The two load cells at the stressing end indicated forces after anchoring that generally agreed with the specified forces. Measured and theoretical elongations gave reasonable agreement.

A seventh load cell was used at the jacking end during the stressing of some tendons and during several lift-off tests to compare the forces determined from load cell data and the calibrated hydraulic ram. In addition, forces from the two load cells at the stressing end were compared with forces from the calibrated ram. These comparisons indicated that the forces determined from the load cells varied between 90 and 95% of the forces determined from the calibrated ram.

One final test was performed in which the seventh load cell was placed in series with the contractor's load cell and both were loaded using a calibrated ram and a 19 1/2-in. strand tendon. This test indicated that loads measured by the seventh load cell differed from the loads measured by the contractor's load cell by 5 to 13%. The contractor's load cell had been used since July

* Respectively, Engineering Consultant, Henry G. Russell, Inc. and Structural Engineer, T. Y. Lin International.

1994 to calibrate the stressing rams.

Based on the above data, it appeared that the load cells were giving inconsistent data and that further evaluation was needed to verify the source of the differences in the forces.

ORIGINAL CALIBRATION PROCEDURE

Seven center hole load cells were custom designed and built by Construction Technology Laboratories, Inc. (CTL) for use in the instrumentation program. Six load cells were installed on tendons. One cell, identified as No. 7, was retained as a spare. The load cells were designed to have a capacity in excess of the maximum tendon force and to fit the end anchorage details of the post-tensioning system with a center hole as small as possible. The load cells were also designed for high sensitivity.

Prior to installation, each load cell was calibrated in CTL's one million pound capacity testing machine using the following procedure:

1. The load on the load cell was increased from zero to 700 kips and returned to zero. This was repeated three times to verify repeatability of strain output.
2. The load on the load cell was then increased from zero to 700 kips in increments of 100 kips. The load was then reduced in increments of 100 kips to zero. Readings of strain were taken at each 100 kip increment using strain indicator No. 60343.
3. A linear regression analysis of the data was used to obtain the best fit straight line. The slope of the straight line was defined as the calibration factor.

Shortly after the discrepancies were noticed, it was decided to recalibrate the contractor's Geokon load cell and CTL load cell No. 7 using the above procedure. The new calibration factor for the CTL load cell was determined to be 102.2 lb/microstrain compared to the original factor of 101.9 lb/microstrain. The Geokon load cell gave a factor of 157.4 lb/digit over a range of 0 to 1000 kips compared to the manufacturer's supplied factor of 149.8 lb/digit. The Geokon load cell exhibited noticeable non-linearity at the lower loads.

In addition to the standard calibration of the CTL load cell, tests were made to distort the calibration by loading the load cell near its inside or outside edges rather than uniformly over the whole end. This was accomplished by placing sheet metal rings between the load cell and the

head of the testing machine. A variation of ±1% in the calibration factor was obtained. Results from these tests did not yield information about the cause of the differences in the loads observed in the field. Consequently, it was decided to conduct verification tests.

VERIFICATION TESTS

A series of verification tests was performed on March 1, 1995, to identify the cause of differences in forces determined from the hydraulic rams, CTL load cells and the contractor's load cell supplied by Geokon.

Equipment

The following equipment was used in the verification tests:

1. VSL Ram No. 5-4-20 with Gage B which was calibrated with VSL Load Cell No. 8068/83657 on February 18, 1995.
2. Geokon Load Cell with Readout Box GK 501, Serial No. 154 on Range x1.
3. CTL Load Cell No. 7 with Strain Indicator P3500, Serial No. 60343.
4. VSL Load Cell 8068/83657, which was calibrated at the University of Washington on January 19, 1995.
5. Miscellaneous plates and anchor heads.
6. Tendon consisting of 19 1/2-in. dia. 7-wire strands.

Test Procedures

A photograph of one test configuration is shown in Fig 1. A total of eight test configurations as defined in Table 1 and shown in Fig. 2 was used.

The test procedure consisted of pressurizing the VSL ram until a target reading on the CTL load cell was obtained. Readings from the other load cells and the hydraulic pressure in the ram were then recorded. The target readings from the CTL load cells were selected to provide increments of 100 kips as determined from the CTL load cell. The goal was to obtain all readings at the moment when the peak reading from the CTL load cell was reached.

For each test configuration, two calibration runs were made with increasing pressure only.

Measured data were consistent between runs. For the first run of Test No. 1, readings during decreasing pressure were also recorded. This procedure was not used again because of diff in controlling the load.

Measured data at each load increment were averaged for the two runs. Data from the Geokon load cell, the VSL load cell and the hydraulic pressure were then converted to loads using linear interpolation between measured calibration points. This partially corrected for any non-linearity in the calibration. For the Geokon load cell, the CTL calibration data were used. Linear regression analyses of the data were performed to obtain relationships between the loads determined from the Geokon load cell, the VSL load cell and the hydraulic ram and the loads determined from the CTL load cell.

Test Results

The calculated loads for each test configuration are given in Table 2 together with the slope of the best fit straight line determined by linear regression. The slope gives the relationship between the load determined by the Geokon load cell, the VSL load cell or the ram and the load determined from the CTL load cell. The same data are shown graphically in Figs. 3 through 10.

A comparison of the results from Tests 1 and 2 shows that the load determined from the Geokon load cell changed from 111.9% to 93.1% of the load determined from the CTL load cells when additional plates were placed between the Geokon and CTL load cells. A comparison of the results from Tests 4 and 5 shows that the load determined from the Geokon load cell changed from 91.3% to 94.6% of the load determined from the CTL load cell when an additional plate was placed between the ram and the Geokon load cell.

For all test configurations, the load determined from the hydraulic pressure varied from 101.7% to 99.7% of the load determined from the CTL load cell. For the three test configurations with a VSL load cell, the load determined from the VSL load cell was 2.5% lower than the load determined from the hydraulic pressure even though the hydraulic ram had been previously calibrated against the load cell in a reaction frame.

A comparison of the results from Tests 5 and 6 shows that loading the CTL load cell directly with an anchor lead produced a change in calibration of less than 1%. A comparison of the results from Tests 6 and 7 shows that moving the head to a maximum eccentricity produced no chang

the calibration of the CTL load cell. A comparison of the results from Tests 6 and 8 shows that rotating the head changed the calibration factor by a maximum of 1.0%

CONCLUSIONS

Based on the above procedures and results, the following conclusions are made.

1. Geokon load cell output is sensitive to the type of end plates through which the load is applied to the load cell. At low loads, the load cell output responds in a non-linear manner when compared to the applied loads. The calibration factor based on linear regression varies from +12% to −9%.

2. For all test conditions, the hydraulic ram and CTL load cell showed agreement within 0 to 2% with the ram showing the higher readings.

3. For all test conditions, the CTL load cell and VSL load cell showed agreement within 0 to −3% with VSL load cell showing lower readings.

4. Loads determined by the CTL load cell should be considered to be very reliable within ±3% for all conditions similar to those in the tests including:

   a. Use of a 19 1/2-in. strand anchor head bearing on the CTL load cell.

   b. Conditions where strand might try to twist the load cell.

5. Data from the CTL load cells on the Halawa Valley project should be reduced using the CTL calibration factors.

TABLE 1 SUMMARY OF TEST CONFIGURATIONS

Test No.	Ram	Plate Thickness In.	Geokon Load Cell	Plate Thickness In.	CTL Load Cell	Plate Thickness In.	VSL Load Cell	Plate Thickness In.	Anchor Type	Notes
1	yes		yes	1-1/2*	yes				Plate	
2	yes		yes	1-1/2*,1-3/4,1-3/4	yes				Plate	
3	yes		yes	1-1/2*,1-1/2,1-3/4	yes	1-3/4,1-1/2	yes		Plate	
4	yes		yes	1-1/2*,1-1/2,1-3/4	yes	1-3/4,1-1/2	yes	2-1/4	Plate	
5	yes	3	yes	1-1/2*,1-1/2,1-3/4	yes	1-3/4,1-1/2	yes	2-1/4	Plate	
6	yes	3	yes	1-1/2*,1-1/2,1-3/4	yes				Head	
7	yes	3	yes	1-1/2*,1-1/2,1-3/4	yes				Head	Anchor head at max. eccentricity
8	yes	3	yes	1-1/2*,1-1/2,1-3/4	yes				Head	Anchor head rotated by 1 in.

* Plate with individual holes for strand.
All other plates had one single hole for the bundle

TABLE 2 CALCULATED LOADS

All	Test 1			Test 2			Test 3			Test 4			Test 5			Test 6			Test 7			Test 8		
CTL	GEO.	VSL	RAM	GEO.	VSL	RAM	GEO.	VSL	RAM	GEO.	VSL	RAM	GEO.	VSL	RAM	GEO.	VSL	RAM	GEO.	VSL	RAM	GEO.	VSL	RAM
0	0		0	0		0	0	0	0	0	0	0	0	0	0	0		0	0		0	0		0
100	100			85			85	99		84	97		83	97		83			82			82		
200	213		192	176		195	173	197	189	171	195	189	175	195	189	175		192	173		192	175		192
300	330		302	272		303	265	294	297	264	293	294	273	293	295	273		299	273		297	278		300
400	445		406	368		408	360	390	400	359	389	400	373	388	400	374		403	371		400	375		406
500	563		509	467		511	460	486	500	456	485	500	476	487	500	477		503	475		503	481		509
600	678		611	568		611	558	582	602	562	583	602	581	583	603	583		606	580		606	586		613
Slope	1.119		1.014	0.931		1.017	0.914	0.973	0.998	0.913	0.972	0.997	0.946	0.973	0.998	0.948		1.005	0.944		1.003	0.955		1.015

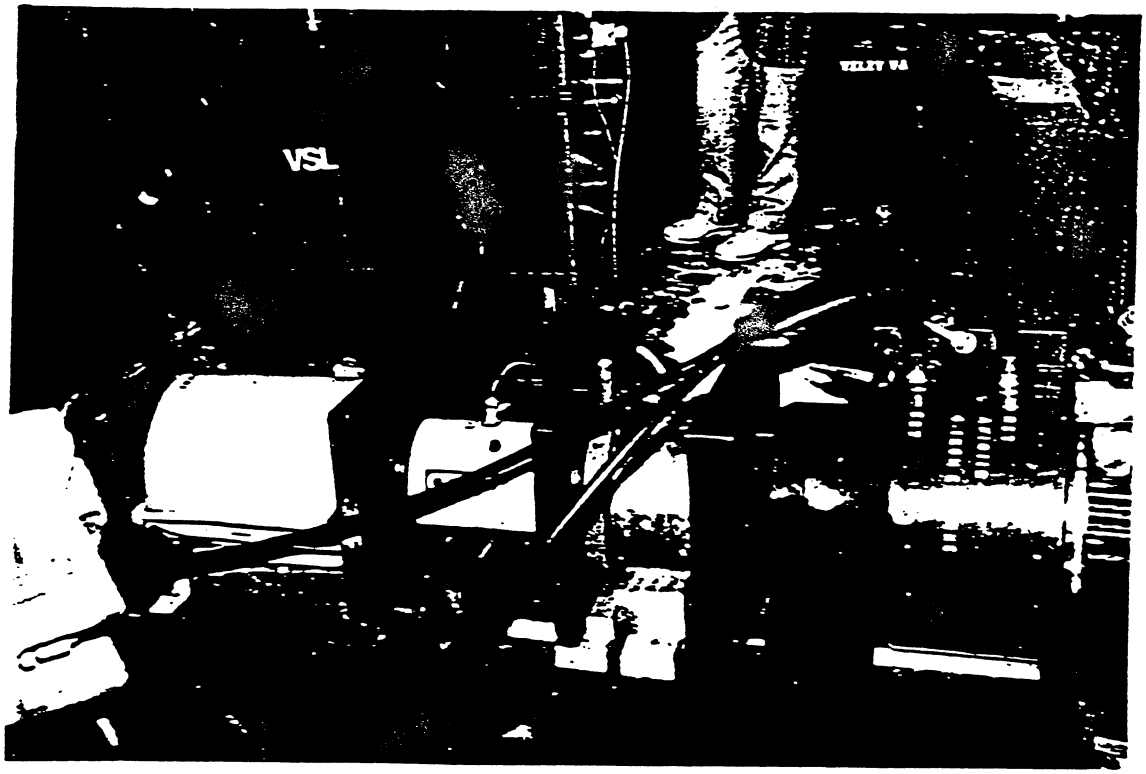

Fig. 1 Test Configuration

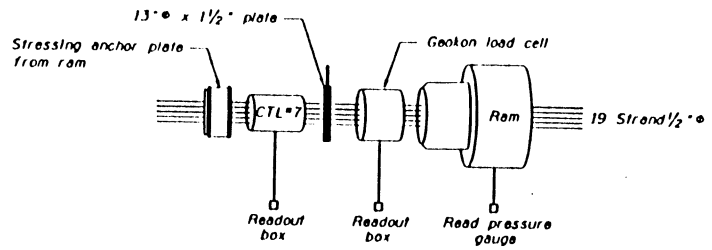

Test 1

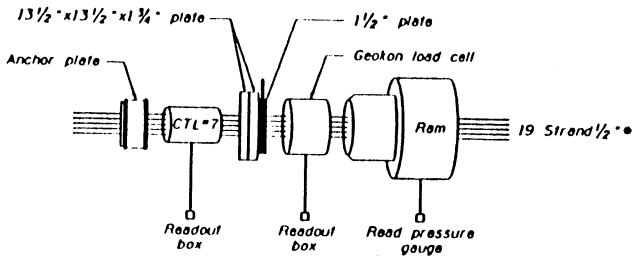

Test 2

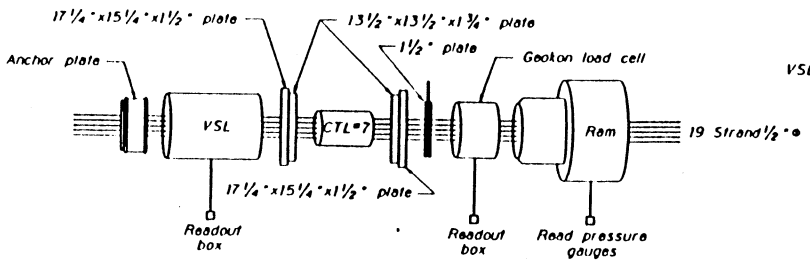

Test 3

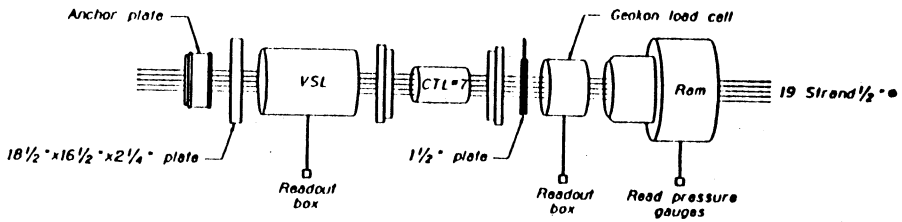

Test 4

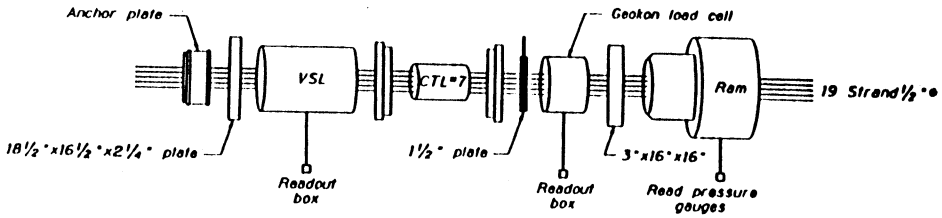

Test 5

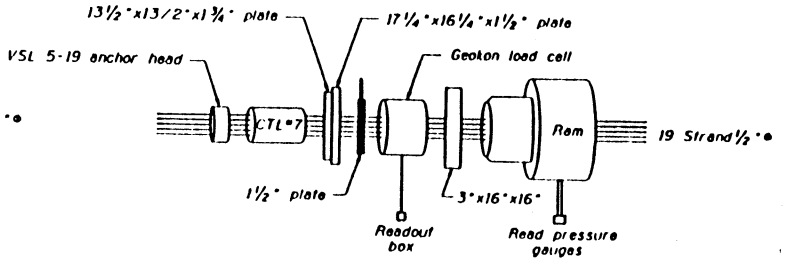

Test 6

Test 7 — ¼" shifted anchor head with same setting as Test 6

Test 8 — Twisted tendon with same setting as Test 6

Figure 2 - Configurations for Verification Tests

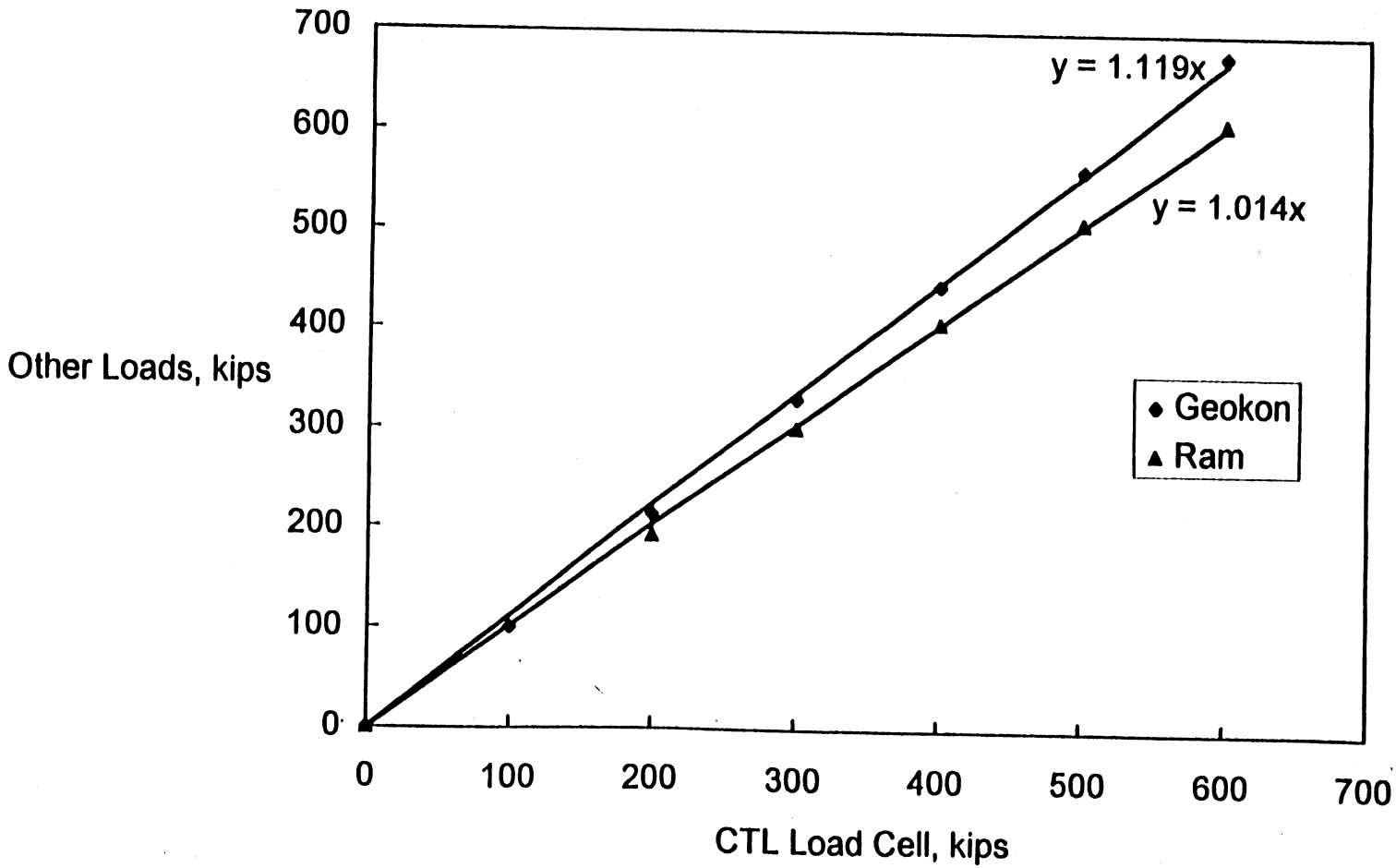

Fig. 3. Calculat[illegible] Loads for Test No. 1

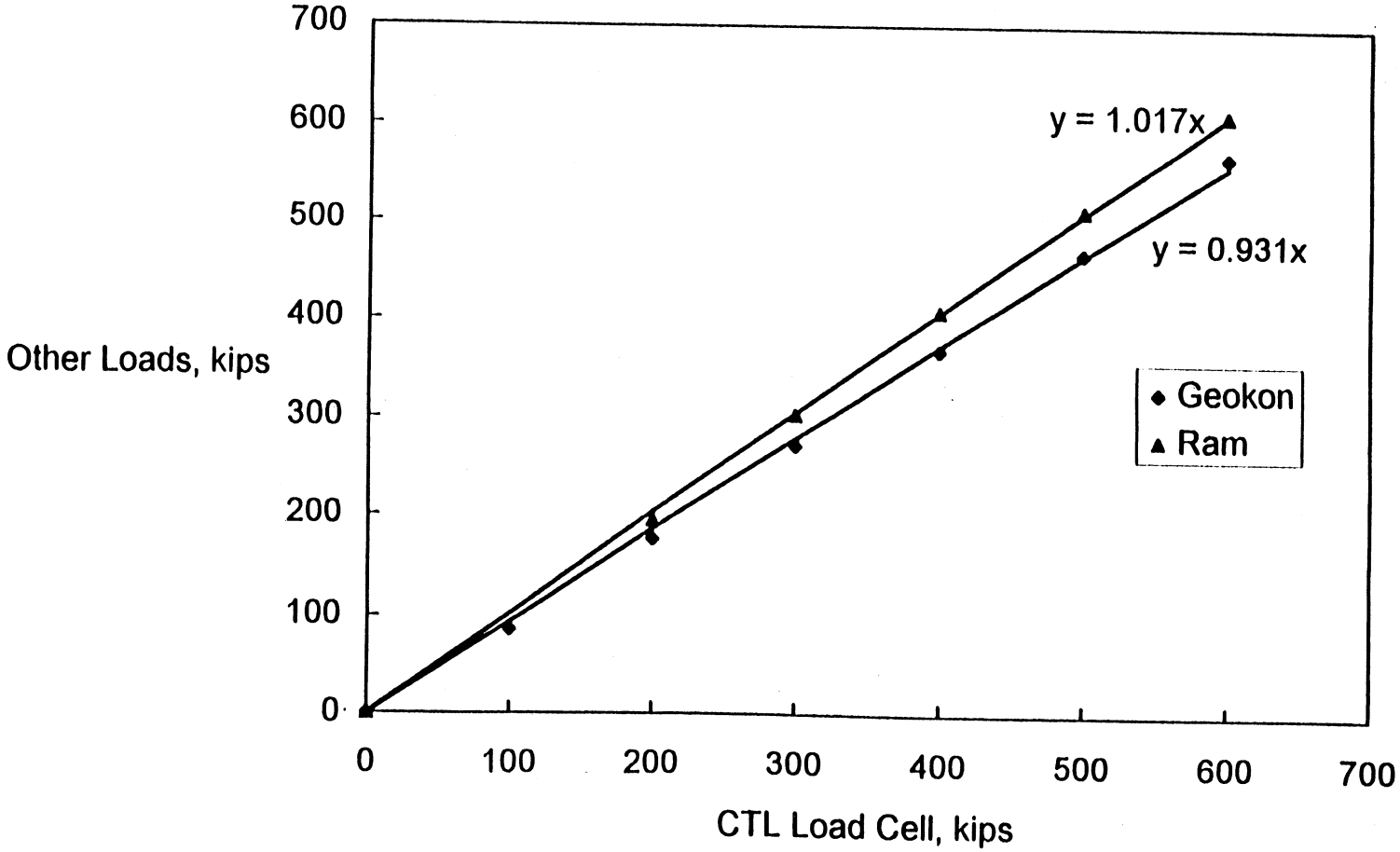

Fig. 4. Calculated Loads for Test No. 2

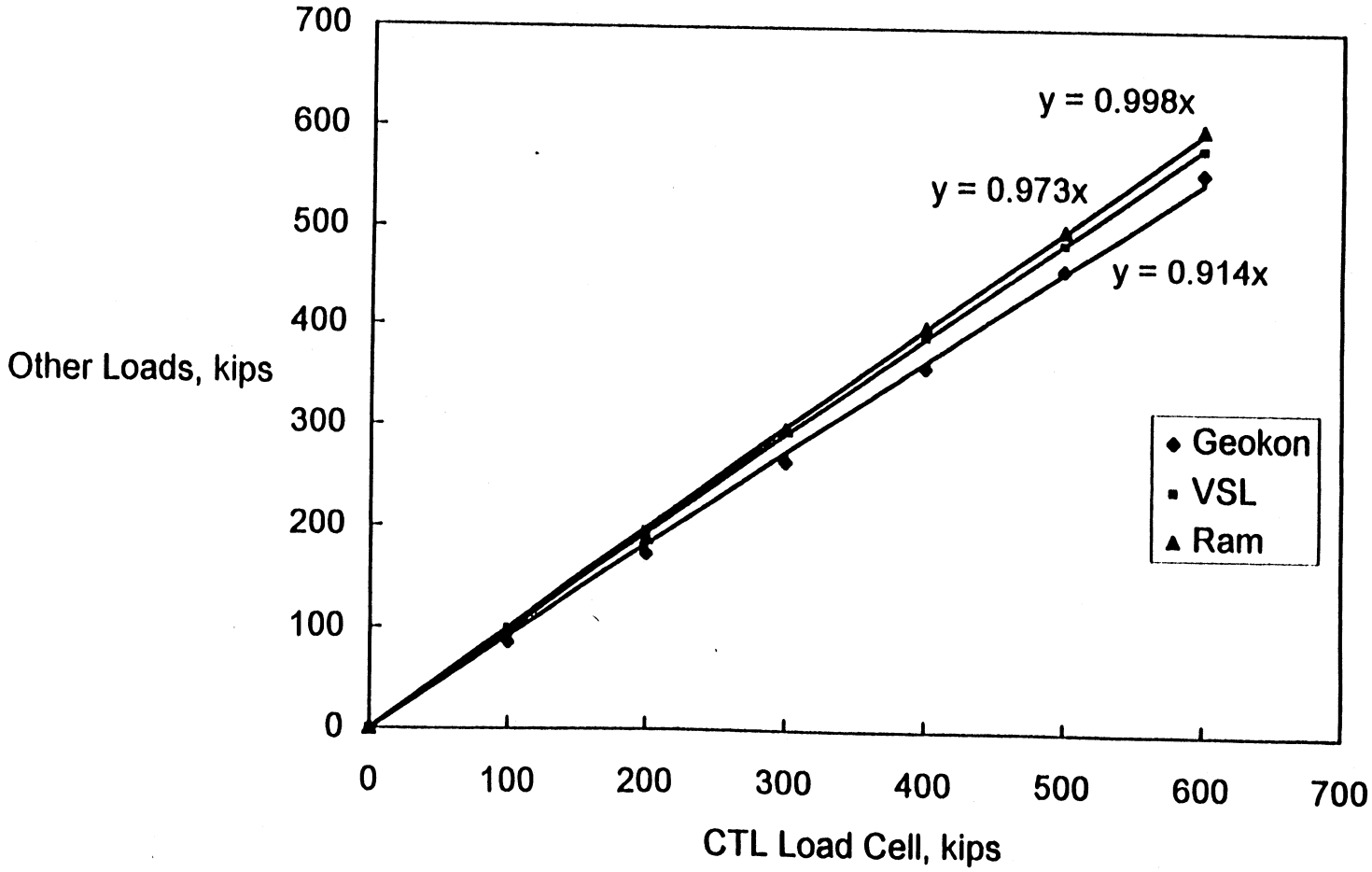

Fig 5. Calculat oads for Test No. 3

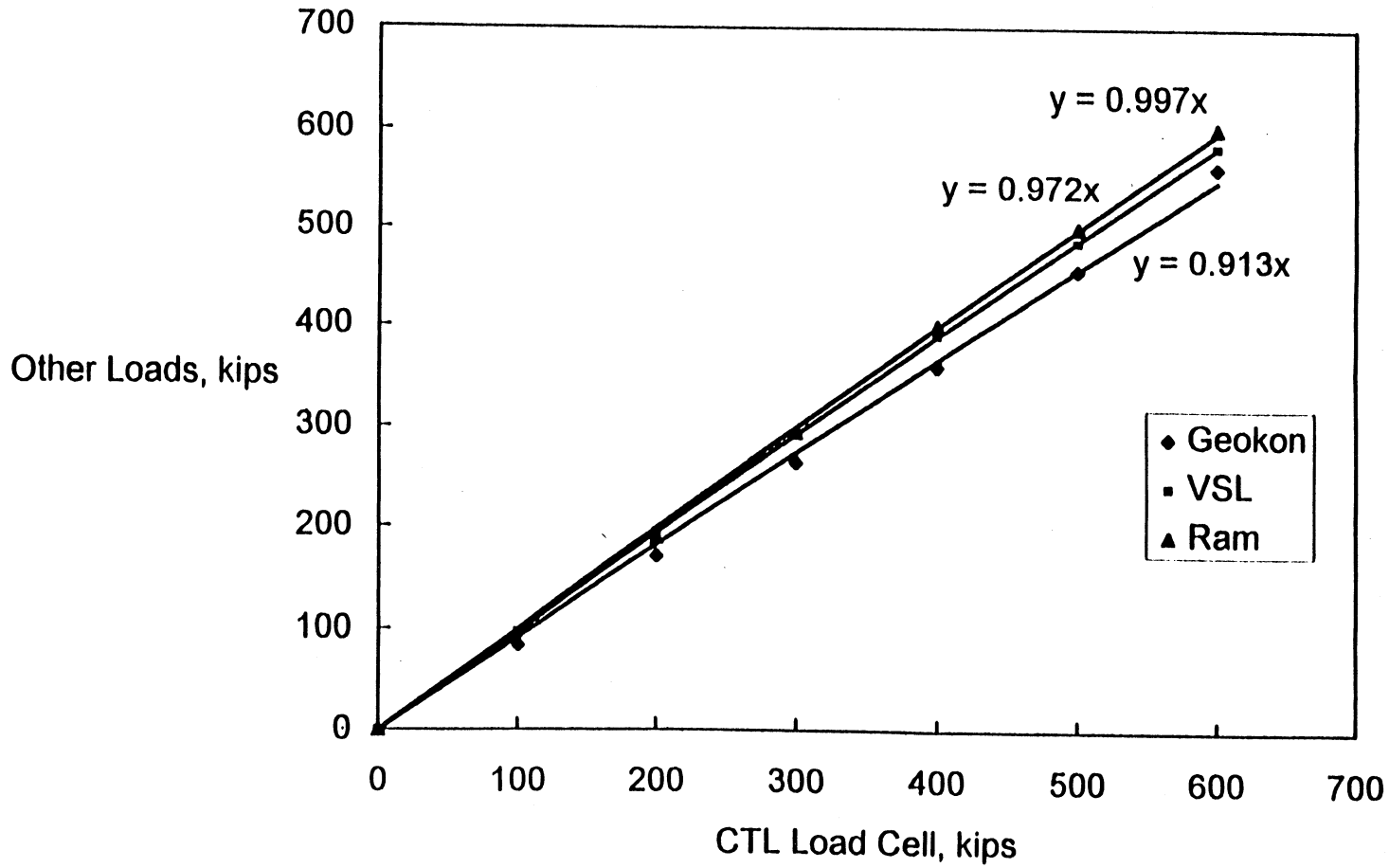

Fig 6. Calculated Loads for Test No. 4

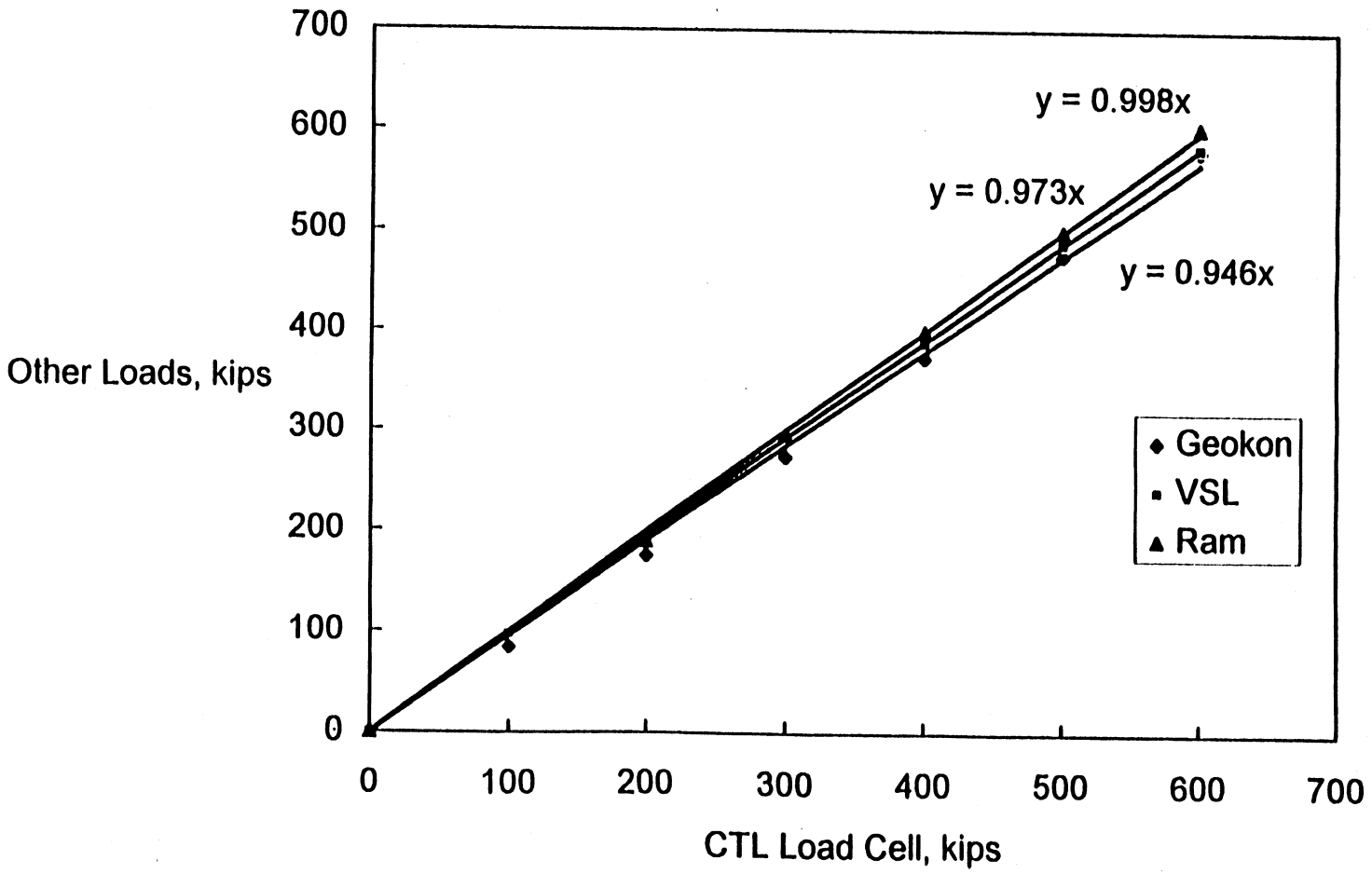

Fig 7. Calcula oads for Test No. 5

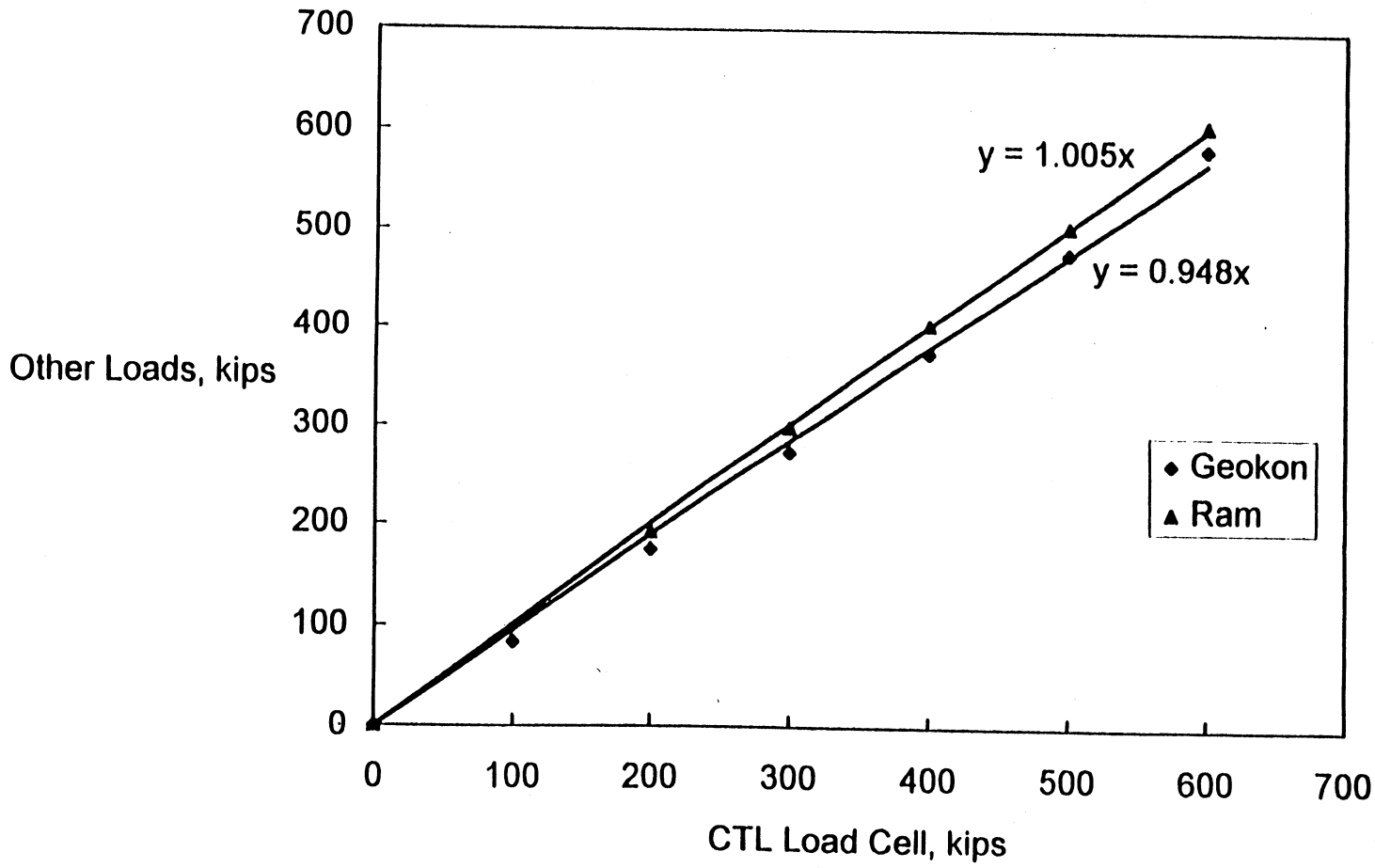

Fig. 8. Calculated Loads for Test No. 6

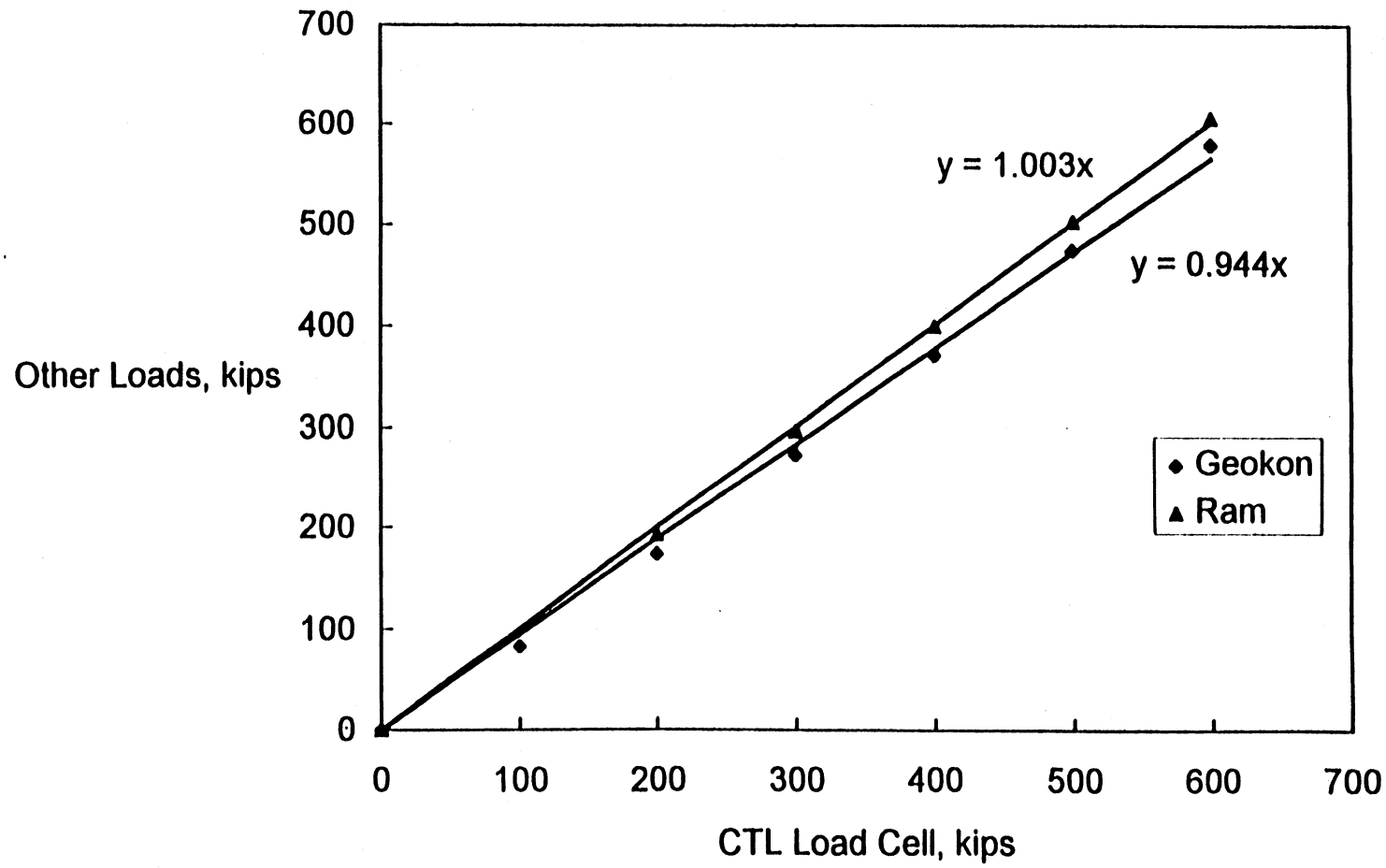

Fig. 9. Calcu Loads for Test No. 7

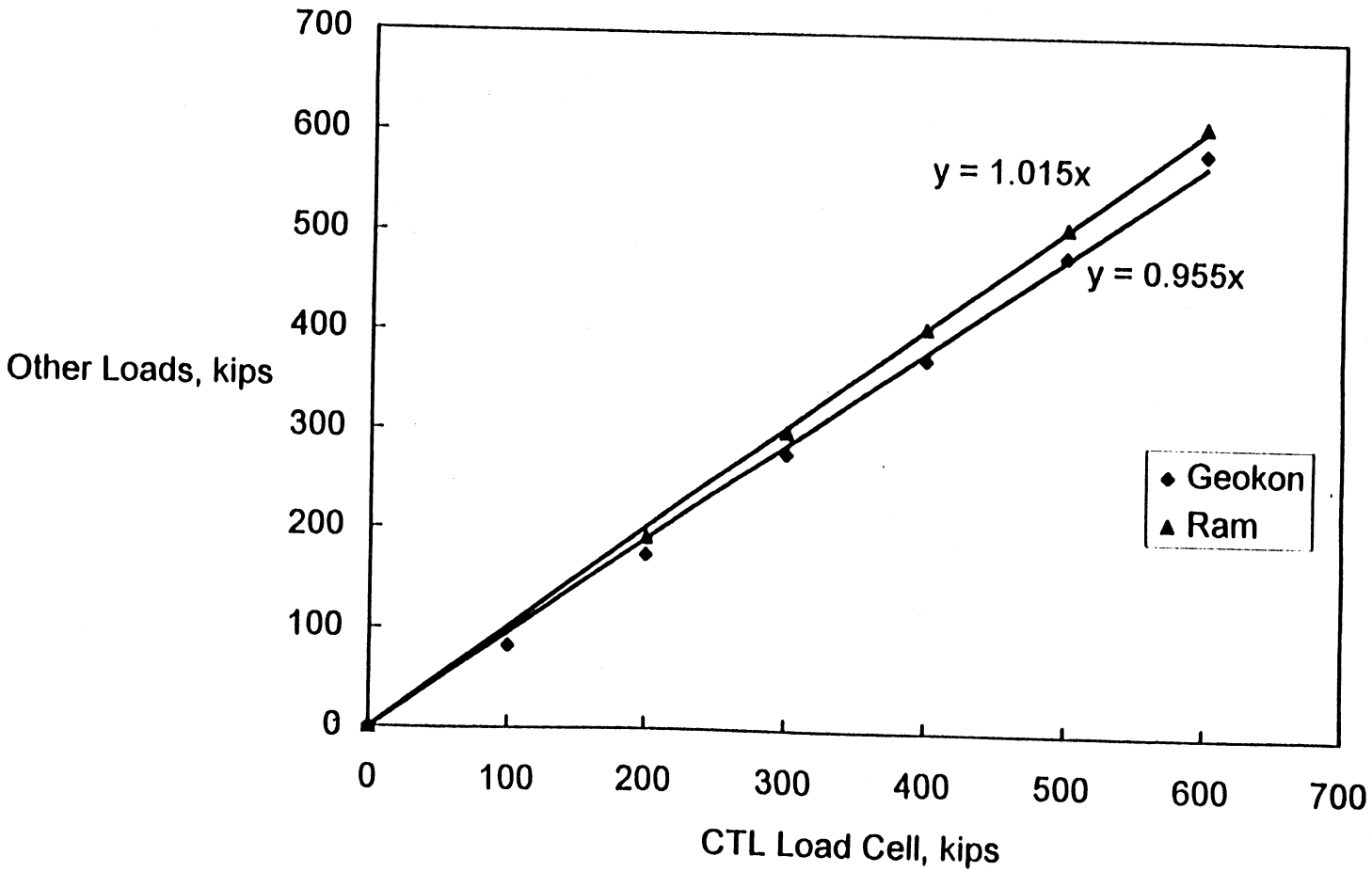

Fig 10. Calculated Loads for Test No. 8

Appendix D - CTL Creep and Shrinkage Data

SECTION A - 3 DAYS

Creep Of Concrete in Compression (ASTM C 512)

Instantaneous and Long-Term Deformation (Adjusted for Drying Shrinkage)

Days Loaded	Drying Shrinkage (millionths)	Load Induced Deformation (millionths)	Condition
0	0	537	Instantaneous Strain
1	21	838	Instantaneous Strain + Creep Strain
2	41	975	Instantaneous Strain + Creep Strain
3	54	1029	Instantaneous Strain + Creep Strain
4	91	1101	Instantaneous Strain + Creep Strain
5	104	1168	Instantaneous Strain + Creep Strain
6	138	1194	Instantaneous Strain + Creep Strain
7	162	1309	Instantaneous Strain + Creep Strain
14	361	1385	Instantaneous Strain + Creep Strain
21	492	1613	Instantaneous Strain + Creep Strain
28	553	1658	Instantaneous Strain + Creep Strain
59	752	1988	Instantaneous Strain + Creep Strain
90	859	2202	Instantaneous Strain + Creep Strain
122	928	2315	Instantaneous Strain + Creep Strain
152	953	2413	Instantaneous Strain + Creep Strain
182	979	2495	Instantaneous Strain + Creep Strain
214	985	2519	Instantaneous Strain + Creep Strain
245	1015	2558	Instantaneous Strain + Creep Strain
276	1051	2538	Instantaneous Strain + Creep Strain
307	1021	2607	Instantaneous Strain + Creep Strain
339	1035	2643	Instantaneous Strain + Creep Strain
364	1054	2683	Instantaneous Strain + Creep Strain

Applied Stress = 1700 psi

f'c @ 3 days = 4260 psi

Modulus of Elasticity @ 3 days = 3.07 x 10^6

SECTION A - 28 DAYS

Creep Of Concrete in Compression (ASTM C 512)

Instantaneous and Long-Term Deformation (Adjusted for Drying Shrinkage)

Days Loaded	Drying Shrinkage (millionths)	Load Induced Deformation (millionths)	Condition
0	0	670	Instantaneous Strain
1	24	879	Instantaneous Strain + Creep Strain
2	63	1035	Instantaneous Strain + Creep Strain
3	101	1089	Instantaneous Strain + Creep Strain
4	152	1130	Instantaneous Strain + Creep Strain
5	176	1192	Instantaneous Strain + Creep Strain
6	185	1213	Instantaneous Strain + Creep Strain
7	206	1210	Instantaneous Strain + Creep Strain
14	338	1458	Instantaneous Strain + Creep Strain
21	391	1574	Instantaneous Strain + Creep Strain
28	556	1745	Instantaneous Strain + Creep Strain
59	743	2081	Instantaneous Strain + Creep Strain
90	827	2237	Instantaneous Strain + Creep Strain
121	862	2388	Instantaneous Strain + Creep Strain
153	884	2528	Instantaneous Strain + Creep Strain
183	899	2643	Instantaneous Strain + Creep Strain
213	959	2674	Instantaneous Strain + Creep Strain
245	958	2744	Instantaneous Strain + Creep Strain
276	981	2775	Instantaneous Strain + Creep Strain
307	983	2823	Instantaneous Strain + Creep Strain
338	993	2874	Instantaneous Strain + Creep Strain
365	1005	2873	Instantaneous Strain + Creep Strain

Applied Stress= 2500 psi

f'c @ 28 days = 6140 psi

Modulus of Elasticity @ 28 days = 3.51 x 10^6

SECTION A - 90 DAYS

Creep Of Concrete in Compression (ASTM C 512)

Instantaneous and Long-Term Deformation (Adjusted for Drying Shrinkage)

Days Loaded	Drying Shrinkage (millionths)	Load Induced Deformation (millionths)	Condition
0	0	623	Instantaneous Strain
1	11	793	Instantaneous Strain + Creep Strain
2	18	868	Instantaneous Strain + Creep Strain
3	32	936	Instantaneous Strain + Creep Strain
4	55	991	Instantaneous Strain + Creep Strain
5	66	1017	Instantaneous Strain + Creep Strain
6	40	1078	Instantaneous Strain + Creep Strain
7	87	1108	Instantaneous Strain + Creep Strain
14	151	1181	Instantaneous Strain + Creep Strain
21	268	1203	Instantaneous Strain + Creep Strain
28	313	1243	Instantaneous Strain + Creep Strain
56	428	1480	Instantaneous Strain + Creep Strain
90	538	1551	Instantaneous Strain + Creep Strain
120	568	1658	Instantaneous Strain + Creep Strain
150	599	1780	Instantaneous Strain + Creep Strain
180	628	1822	Instantaneous Strain + Creep Strain
210	676	1867	Instantaneous Strain + Creep Strain
240	685	1900	Instantaneous Strain + Creep Strain
270	693	1948	Instantaneous Strain + Creep Strain
300	703	1983	Instantaneous Strain + Creep Strain
330	708	1993	Instantaneous Strain + Creep Strain
365	714	2047	Instantaneous Strain + Creep Strain

Applied Stress= 2500 psi

f'c @ 90 days = 7700 psi

Modulus of Elasticity @ 90 days = 3.93 x 10^6

SECTION B - 3 DAYS

Creep Of Concrete in Compression (ASTM C 512)

Instantaneous and Long-Term Deformation (Adjusted for Drying Shrinkage)

Days Loaded	Drying Shrinkage (millionths)	Load Induced Deformation (millionths)	Condition
0	0	540	Instantaneous Strain
1	40	748	Instantaneous Strain + Creep Strain
2	77	839	Instantaneous Strain + Creep Strain
3	81	883	Instantaneous Strain + Creep Strain
4	98	907	Instantaneous Strain + Creep Strain
5	112	941	Instantaneous Strain + Creep Strain
6	128	986	Instantaneous Strain + Creep Strain
7	141	1021	Instantaneous Strain + Creep Strain
14	304	1191	Instantaneous Strain + Creep Strain
21	391	1293	Instantaneous Strain + Creep Strain
28	487	1412	Instantaneous Strain + Creep Strain
56	655	1643	Instantaneous Strain + Creep Strain
90	813	1833	Instantaneous Strain + Creep Strain
122	867	1943	Instantaneous Strain + Creep Strain
152	910	1987	Instantaneous Strain + Creep Strain
182	934	2093	Instantaneous Strain + Creep Strain
213	956	2115	Instantaneous Strain + Creep Strain
243	983	2160	Instantaneous Strain + Creep Strain
273	993	2166	Instantaneous Strain + Creep Strain
305	998	2169	Instantaneous Strain + Creep Strain
333	1002	2230	Instantaneous Strain + Creep Strain
365	1005	2263	Instantaneous Strain + Creep Strain

Applied Stress= 1510 psi

f'c @ 3 days = 3780 psi

Modulus of Elasticity @ 3 days = 3.23 x 10^6

SECTION B - 28 DAYS

Creep Of Concrete in Compression (ASTM C 512)

Instantaneous and Long-Term Deformation (Adjusted for Drying Shrinkage)

Days Loaded	Drying Shrinkage (millionths)	Load Induced Deformation (millionths)	Condition
0	0	585	Instantaneous Strain
1	19	841	Instantaneous Strain + Creep Strain
2	46	877	Instantaneous Strain + Creep Strain
3	56	975	Instantaneous Strain + Creep Strain
4	81	1002	Instantaneous Strain + Creep Strain
5	87	1037	Instantaneous Strain + Creep Strain
6	88	1070	Instantaneous Strain + Creep Strain
7	111	1095	Instantaneous Strain + Creep Strain
14	166	1217	Instantaneous Strain + Creep Strain
21	279	1333	Instantaneous Strain + Creep Strain
28	319	1431	Instantaneous Strain + Creep Strain
59	509	1714	Instantaneous Strain + Creep Strain
90	619	1889	Instantaneous Strain + Creep Strain
121	612	2016	Instantaneous Strain + Creep Strain
153	692	2060	Instantaneous Strain + Creep Strain
183	710	2197	Instantaneous Strain + Creep Strain
213	725	2273	Instantaneous Strain + Creep Strain
245	776	2292	Instantaneous Strain + Creep Strain
276	776	2329	Instantaneous Strain + Creep Strain
307	790	2406	Instantaneous Strain + Creep Strain
338	792	2416	Instantaneous Strain + Creep Strain
365	810	2483	Instantaneous Strain + Creep Strain

Applied Stress= 2500 psi

f'c @ 28 days = 6770 psi

Modulus of Elasticity @ 28 days = 3.98 x 10^6

SECTION B - 90 DAYS

Creep Of Concrete in Compression (ASTM C 512)

Instantaneous and Long-Term Deformation (Adjusted for Drying Shrinkage)

Days Loaded	Drying Shrinkage (millionths)	Load Induced Deformation (millionths)	Condition
0	0	705	Instantaneous Strain
1	29	996	Instantaneous Strain + Creep Strain
2	58	1035	Instantaneous Strain + Creep Strain
3	107	1068	Instantaneous Strain + Creep Strain
4	117	1127	Instantaneous Strain + Creep Strain
5	128	1164	Instantaneous Strain + Creep Strain
6	138	1188	Instantaneous Strain + Creep Strain
7	157	1193	Instantaneous Strain + Creep Strain
14	226	1380	Instantaneous Strain + Creep Strain
21	278	1461	Instantaneous Strain + Creep Strain
28	345	1586	Instantaneous Strain + Creep Strain
59	415	1959	Instantaneous Strain + Creep Strain
91	468	2168	Instantaneous Strain + Creep Strain
121	542	2272	Instantaneous Strain + Creep Strain
151	593	2342	Instantaneous Strain + Creep Strain
183	641	2437	Instantaneous Strain + Creep Strain
214	651	2467	Instantaneous Strain + Creep Strain
245	663	2564	Instantaneous Strain + Creep Strain
276	666	2629	Instantaneous Strain + Creep Strain
308	678	2664	Instantaneous Strain + Creep Strain
338	684	2691	Instantaneous Strain + Creep Strain
365	698	2690	Instantaneous Strain + Creep Strain

Applied Stress= 2500 psi

f'c @ 90 days = 7910 psi

Modulus of Elasticity @ 90 days = 3.93 x 10^6

SECTION C - 3 DAYS

Creep Of Concrete in Compression (ASTM C 512)

Instantaneous and Long-Term Deformation (Adjusted for Drying Shrinkage)

Days Loaded	Drying Shrinkage (millionths)	Load Induced Deformation (millionths)	Condition
0	0	518	Instantaneous Strain
1	16	750	Instantaneous Strain + Creep Strain
2	56	837	Instantaneous Strain + Creep Strain
3	71	900	Instantaneous Strain + Creep Strain
4	107	956	Instantaneous Strain + Creep Strain
5	137	990	Instantaneous Strain + Creep Strain
6	170	1038	Instantaneous Strain + Creep Strain
7	212	1092	Instantaneous Strain + Creep Strain
14	375	1264	Instantaneous Strain + Creep Strain
21	478	1416	Instantaneous Strain + Creep Strain
28	553	1581	Instantaneous Strain + Creep Strain
56	688	1984	Instantaneous Strain + Creep Strain
91	852	2214	Instantaneous Strain + Creep Strain
120	909	2370	Instantaneous Strain + Creep Strain
151	919	2438	Instantaneous Strain + Creep Strain
181	989	2554	Instantaneous Strain + Creep Strain
212	1021	2801	Instantaneous Strain + Creep Strain
242	1043	2647	Instantaneous Strain + Creep Strain
273	1043	2677	Instantaneous Strain + Creep Strain
304	1045	2737	Instantaneous Strain + Creep Strain
335	1049	2757	Instantaneous Strain + Creep Strain
365	1053	2782	Instantaneous Strain + Creep Strain
396	1069	2865	Instantaneous Strain + Creep Strain

Applied Stress= 1880 psi

f'c @ 3 days = 3780 psi

Modulus of Elasticity @ 3 days = 3.23 x 10^6

SECTION C - 28 DAYS

Creep Of Concrete in Compression (ASTM C 512)

Instantaneous and Long-Term Deformation (Adjusted for Drying Shrinkage)

Days Loaded	Drying Shrinkage (millionths)	Load Induced Deformation (millionths)	Condition
0	0	693	Instantaneous Strain
1	26	1029	Instantaneous Strain + Creep Strain
2	57	1114	Instantaneous Strain + Creep Strain
3	73	1172	Instantaneous Strain + Creep Strain
4	86	1220	Instantaneous Strain + Creep Strain
5	88	1260	Instantaneous Strain + Creep Strain
6	97	1330	Instantaneous Strain + Creep Strain
7	99	1377	Instantaneous Strain + Creep Strain
14	283	1592	Instantaneous Strain + Creep Strain
21	352	1802	Instantaneous Strain + Creep Strain
28	396	1787	Instantaneous Strain + Creep Strain
60	609	2169	Instantaneous Strain + Creep Strain
90	680	2422	Instantaneous Strain + Creep Strain
120	763	2579	Instantaneous Strain + Creep Strain
152	770	2725	Instantaneous Strain + Creep Strain
183	808	2825	Instantaneous Strain + Creep Strain
214	813	2871	Instantaneous Strain + Creep Strain
245	868	2919	Instantaneous Strain + Creep Strain
277	868	2973	Instantaneous Strain + Creep Strain
307	875	3023	Instantaneous Strain + Creep Strain
337	880	3086	Instantaneous Strain + Creep Strain
365	901	3101	Instantaneous Strain + Creep Strain

Applied Stress= 2500 psi

f'c @ 28 days = 6740 psi

Modulus of Elasticity @ 28 days = 3.54 x 10^6

SECTION C - 90 DAYS

Creep Of Concrete in Compression (ASTM C 512)

Instantaneous and Long-Term Deformation (Adjusted for Drying Shrinkage)

Days Loaded	Drying Shrinkage (millionths)	Load Induced Deformation (millionths)	Condition
0	0	732	Instantaneous Strain
1	83	1015	Instantaneous Strain + Creep Strain
2	103	1068	Instantaneous Strain + Creep Strain
3	128	1160	Instantaneous Strain + Creep Strain
4	137	1178	Instantaneous Strain + Creep Strain
5	144	1243	Instantaneous Strain + Creep Strain
6	148	1283	Instantaneous Strain + Creep Strain
7	199	1370	Instantaneous Strain + Creep Strain
14	262	1465	Instantaneous Strain + Creep Strain
21	308	1607	Instantaneous Strain + Creep Strain
28	355	1721	Instantaneous Strain + Creep Strain
58	521	2028	Instantaneous Strain + Creep Strain
90	578	2228	Instantaneous Strain + Creep Strain
121	629	2379	Instantaneous Strain + Creep Strain
152	653	2467	Instantaneous Strain + Creep Strain
183	703	2543	Instantaneous Strain + Creep Strain
215	707	2618	Instantaneous Strain + Creep Strain
245	722	2710	Instantaneous Strain + Creep Strain
275	723	2766	Instantaneous Strain + Creep Strain
307	731	2818	Instantaneous Strain + Creep Strain
338	738	2845	Instantaneous Strain + Creep Strain
365	748	2862	Instantaneous Strain + Creep Strain

Applied Stress= 2500 psi

f'c @ 90 days = 7650 psi

Modulus of Elasticity @ 90 days = 3.95 x 10^6

SECTION D - 3 DAYS

Creep Of Concrete in Compression (ASTM C 512)

Instantaneous and Long-Term Deformation (Adjusted for Drying Shrinkage)

Days Loaded	Drying Shrinkage (millionths)	Load Induced Deformation (millionths)	Condition
0	0	612	Instantaneous Strain
1	68	889	Instantaneous Strain + Creep Strain
2	128	985	Instantaneous Strain + Creep Strain
3	153	1083	Instantaneous Strain + Creep Strain
4	191	1141	Instantaneous Strain + Creep Strain
5	213	1173	Instantaneous Strain + Creep Strain
6	236	1216	Instantaneous Strain + Creep Strain
7	273	1235	Instantaneous Strain + Creep Strain
14	427	1400	Instantaneous Strain + Creep Strain
21	500	1628	Instantaneous Strain + Creep Strain
28	608	1710	Instantaneous Strain + Creep Strain
56	818	1985	Instantaneous Strain + Creep Strain
90	931	2163	Instantaneous Strain + Creep Strain
120	983	2318	Instantaneous Strain + Creep Strain
150	1010	2422	Instantaneous Strain + Creep Strain
180	1036	2516	Instantaneous Strain + Creep Strain
210	1051	2533	Instantaneous Strain + Creep Strain
240	1087	2562	Instantaneous Strain + Creep Strain
270	1098	2619	Instantaneous Strain + Creep Strain
300	1113	2650	Instantaneous Strain + Creep Strain
330	1113	2690	Instantaneous Strain + Creep Strain
365	1118	2726	Instantaneous Strain + Creep Strain
396	1134	2732	Instantaneous Strain + Creep Strain
427	1149	2740	Instantaneous Strain + Creep Strain
457	1165	2748	Instantaneous Strain + Creep Strain
488	1182	2753	Instantaneous Strain + Creep Strain
518	1189	2755	Instantaneous Strain + Creep Strain
549	1187	2760	Instantaneous Strain + Creep Strain
580	1191	2787	Instantaneous Strain + Creep Strain
609	1191	2802	Instantaneous Strain + Creep Strain
640	1193	2868	Instantaneous Strain + Creep Strain
670	1193	2868	Instantaneous Strain + Creep Strain
701	1194	2873	Instantaneous Strain + Creep Strain
731	1199	2880	Instantaneous Strain + Creep Strain
762	1210	2888	Instantaneous Strain + Creep Strain
793	1210	2888	Instantaneous Strain + Creep Strain
823	1213	2888	Instantaneous Strain + Creep Strain
854	1215	2888	Instantaneous Strain + Creep Strain
884	1215	2888	Instantaneous Strain + Creep Strain
915	1215	2898	Instantaneous Strain + Creep Strain

Applied Stress= 1720 psi

f'c @ 3 days = 4290 psi

Modulus of Elasticity @ 3 days = 3.21 x 10^6

SECTION D - 28 DAYS

Creep Of Concrete in Compression (ASTM C 512)

Instantaneous and Long-Term Deformation (Adjusted for Drying Shrinkage)

Days Loaded	Drying Shrinkage (millionths)	Load Induced Deformation (millionths)	Condition
0	0	673	Instantaneous Strain
1	13	1028	Instantaneous Strain + Creep Strain
2	25	1072	Instantaneous Strain + Creep Strain
3	33	1119	Instantaneous Strain + Creep Strain
4	39	1163	Instantaneous Strain + Creep Strain
5	41	1218	Instantaneous Strain + Creep Strain
6	80	1263	Instantaneous Strain + Creep Strain
7	108	1332	Instantaneous Strain + Creep Strain
14	231	1532	Instantaneous Strain + Creep Strain
21	247	1630	Instantaneous Strain + Creep Strain
28	320	1748	Instantaneous Strain + Creep Strain
56	517	2028	Instantaneous Strain + Creep Strain
90	593	2237	Instantaneous Strain + Creep Strain
120	678	2358	Instantaneous Strain + Creep Strain
152	699	2453	Instantaneous Strain + Creep Strain
183	729	2579	Instantaneous Strain + Creep Strain
214	733	2626	Instantaneous Strain + Creep Strain
245	747	2692	Instantaneous Strain + Creep Strain
277	759	2726	Instantaneous Strain + Creep Strain
307	770	2782	Instantaneous Strain + Creep Strain
337	788	2821	Instantaneous Strain + Creep Strain
365	797	2839	Instantaneous Strain + Creep Strain
396	806	2863	Instantaneous Strain + Creep Strain
424	815	2888	Instantaneous Strain + Creep Strain
454	828	2908	Instantaneous Strain + Creep Strain
485	844	2936	Instantaneous Strain + Creep Strain
515	852	2958	Instantaneous Strain + Creep Strain
549	854	2989	Instantaneous Strain + Creep Strain
580	854	2994	Instantaneous Strain + Creep Strain
609	857	3021	Instantaneous Strain + Creep Strain
640	857	3034	Instantaneous Strain + Creep Strain
670	858	3038	Instantaneous Strain + Creep Strain
701	862	3043	Instantaneous Strain + Creep Strain
731	871	3050	Instantaneous Strain + Creep Strain
762	876	3054	Instantaneous Strain + Creep Strain
793	878	3061	Instantaneous Strain + Creep Strain
823	888	3074	Instantaneous Strain + Creep Strain
854	876	3087	Instantaneous Strain + Creep Strain
884	883	3087	Instantaneous Strain + Creep Strain
915	883	3118	Instantaneous Strain + Creep Strain

Applied Stress= 2480 psi

f'c @ 28 days = 6640 psi

Modulus of Elasticity @ 28 days = 3.59 x 10^6

SECTION D - 90 DAYS

Creep Of Concrete in Compression (ASTM C 512)

Instantaneous and Long-Term Deformation (Adjusted for Drying Shrinkage)

Days Loaded	Drying Shrinkage (millionths)	Load Induced Deformation (millionths)	Condition
0	0	663	Instantaneous Strain
1	50	848	Instantaneous Strain + Creep Strain
2	85	903	Instantaneous Strain + Creep Strain
3	108	948	Instantaneous Strain + Creep Strain
4	112	983	Instantaneous Strain + Creep Strain
5	129	999	Instantaneous Strain + Creep Strain
6	140	1014	Instantaneous Strain + Creep Strain
7	143	1019	Instantaneous Strain + Creep Strain
14	240	1103	Instantaneous Strain + Creep Strain
21	290	1184	Instantaneous Strain + Creep Strain
28	343	1248	Instantaneous Strain + Creep Strain
56	478	1451	Instantaneous Strain + Creep Strain
90	618	1539	Instantaneous Strain + Creep Strain
120	666	1630	Instantaneous Strain + Creep Strain
150	690	1705	Instantaneous Strain + Creep Strain
180	731	1791	Instantaneous Strain + Creep Strain
210	735	1837	Instantaneous Strain + Creep Strain
240	747	1928	Instantaneous Strain + Creep Strain
270	775	1947	Instantaneous Strain + Creep Strain
300	793	1940	Instantaneous Strain + Creep Strain
330	808	1962	Instantaneous Strain + Creep Strain
365	814	1996	Instantaneous Strain + Creep Strain
395	833	2022	Instantaneous Strain + Creep Strain
426	855	2045	Instantaneous Strain + Creep Strain
456	873	2076	Instantaneous Strain + Creep Strain
487	879	2106	Instantaneous Strain + Creep Strain
516	879	2108	Instantaneous Strain + Creep Strain
547	882	2118	Instantaneous Strain + Creep Strain
578	882	2144	Instantaneous Strain + Creep Strain
608	885	2151	Instantaneous Strain + Creep Strain
639	892	2156	Instantaneous Strain + Creep Strain
669	899	2171	Instantaneous Strain + Creep Strain
700	903	2178	Instantaneous Strain + Creep Strain
731	906	2227	Instantaneous Strain + Creep Strain
761	913	2222	Instantaneous Strain + Creep Strain
792	913	2227	Instantaneous Strain + Creep Strain
822	916	2243	Instantaneous Strain + Creep Strain
853	916	2252	Instantaneous Strain + Creep Strain

Applied Stress= 2500 psi

f'c @ 90 days = 7630 psi

Modulus of Elasticity @ 90 days = 4.12 x 10^6

SECTION E - 3 DAYS

Creep Of Concrete in Compression (ASTM C 512)

Instantaneous and Long-Term Deformation (Adjusted for Drying Shrinkage)

Days Loaded	Drying Shrinkage (millionths)	Load Induced Deformation (millionths)	Condition
0	0	539	Instantaneous Strain
1	52	755	Instantaneous Strain + Creep Strain
2	104	813	Instantaneous Strain + Creep Strain
3	127	887	Instantaneous Strain + Creep Strain
4	137	889	Instantaneous Strain + Creep Strain
5	170	892	Instantaneous Strain + Creep Strain
6	184	934	Instantaneous Strain + Creep Strain
7	191	994	Instantaneous Strain + Creep Strain
14	343	1183	Instantaneous Strain + Creep Strain
21	455	1275	Instantaneous Strain + Creep Strain
28	657	1217	Instantaneous Strain + Creep Strain
56	702	1594	Instantaneous Strain + Creep Strain
90	832	1767	Instantaneous Strain + Creep Strain
120	888	1908	Instantaneous Strain + Creep Strain
150	964	1926	Instantaneous Strain + Creep Strain
180	993	1984	Instantaneous Strain + Creep Strain
210	1012	2063	Instantaneous Strain + Creep Strain
240	1058	2051	Instantaneous Strain + Creep Strain
270	1063	2118	Instantaneous Strain + Creep Strain
300	1074	2158	Instantaneous Strain + Creep Strain
330	1080	2188	Instantaneous Strain + Creep Strain
365	1084	2208	Instantaneous Strain + Creep Strain
395	1135	2175	Instantaneous Strain + Creep Strain
426	1151	2180	Instantaneous Strain + Creep Strain
456	1130	2217	Instantaneous Strain + Creep Strain
487	1133	2219	Instantaneous Strain + Creep Strain
518	1141	2244	Instantaneous Strain + Creep Strain
547	1143	2247	Instantaneous Strain + Creep Strain
578	1149	2255	Instantaneous Strain + Creep Strain
608	1150	2263	Instantaneous Strain + Creep Strain
639	1155	2264	Instantaneous Strain + Creep Strain
669	1157	2266	Instantaneous Strain + Creep Strain
700	1175	2281	Instantaneous Strain + Creep Strain
731	1179	2311	Instantaneous Strain + Creep Strain
761	1187	2307	Instantaneous Strain + Creep Strain
792	1187	2307	Instantaneous Strain + Creep Strain
822	1188	2307	Instantaneous Strain + Creep Strain
853	1194	2307	Instantaneous Strain + Creep Strain

Applied Stress= 1660 psi

f'c @ 3 days = 4210 psi

Modulus of Elasticity @ 3 days = 3.27 x 10^6

SECTION E - 28 DAYS

Creep Of Concrete in Compression (ASTM C 512)

Instantaneous and Long-Term Deformation (Adjusted for Drying Shrinkage)

Days Loaded	Drying Shrinkage (millionths)	Load Induced Deformation (millionths)	Condition
0	0	713	Instantaneous Strain
1	77	888	Instantaneous Strain + Creep Strain
2	128	975	Instantaneous Strain + Creep Strain
3	146	1010	Instantaneous Strain + Creep Strain
4	158	1123	Instantaneous Strain + Creep Strain
5	181	1189	Instantaneous Strain + Creep Strain
6	206	1176	Instantaneous Strain + Creep Strain
7	210	1228	Instantaneous Strain + Creep Strain
14	342	1509	Instantaneous Strain + Creep Strain
21	418	1606	Instantaneous Strain + Creep Strain
28	493	1783	Instantaneous Strain + Creep Strain
56	643	2102	Instantaneous Strain + Creep Strain
90	780	2377	Instantaneous Strain + Creep Strain
120	828	2511	Instantaneous Strain + Creep Strain
150	893	2609	Instantaneous Strain + Creep Strain
180	936	2635	Instantaneous Strain + Creep Strain
210	947	2733	Instantaneous Strain + Creep Strain
240	970	2784	Instantaneous Strain + Creep Strain
270	997	2807	Instantaneous Strain + Creep Strain
300	1005	2871	Instantaneous Strain + Creep Strain
330	1010	3008	Instantaneous Strain + Creep Strain
365	1034	3039	Instantaneous Strain + Creep Strain
396	1041	2933	Instantaneous Strain + Creep Strain
426	1041	2965	Instantaneous Strain + Creep Strain
457	1041	2969	Instantaneous Strain + Creep Strain
489	1042	3020	Instantaneous Strain + Creep Strain
518	1054	3044	Instantaneous Strain + Creep Strain
549	1068	3058	Instantaneous Strain + Creep Strain
579	1068	3058	Instantaneous Strain + Creep Strain
610	1073	3067	Instantaneous Strain + Creep Strain
640	1084	3066	Instantaneous Strain + Creep Strain
671	1085	3079	Instantaneous Strain + Creep Strain
702	1087	3088	Instantaneous Strain + Creep Strain
732	1088	3095	Instantaneous Strain + Creep Strain
763	1088	3096	Instantaneous Strain + Creep Strain
793	1091	3112	Instantaneous Strain + Creep Strain
824	1108	3120	Instantaneous Strain + Creep Strain

Applied Stress= 2480 psi

f'c @ 28 days = 6530 psi

Modulus of Elasticity @ 28 days = 3.81 x 10^6

SECTION E - 90 DAYS

Creep Of Concrete in Compression (ASTM C 512)

Instantaneous and Long-Term Deformation (Adjusted for Drying Shrinkage)

Days Loaded	Drying Shrinkage (millionths)	Load Induced Deformation (millionths)	Condition
0	0	687	Instantaneous Strain
1	4	946	Instantaneous Strain + Creep Strain
2	6	1033	Instantaneous Strain + Creep Strain
3	8	1076	Instantaneous Strain + Creep Strain
4	11	1128	Instantaneous Strain + Creep Strain
5	14	1144	Instantaneous Strain + Creep Strain
6	15	1153	Instantaneous Strain + Creep Strain
7	23	1216	Instantaneous Strain + Creep Strain
14	63	1383	Instantaneous Strain + Creep Strain
21	108	1532	Instantaneous Strain + Creep Strain
28	159	1588	Instantaneous Strain + Creep Strain
56	210	1805	Instantaneous Strain + Creep Strain
90	267	1935	Instantaneous Strain + Creep Strain
120	331	2077	Instantaneous Strain + Creep Strain
150	340	2108	Instantaneous Strain + Creep Strain
180	372	2175	Instantaneous Strain + Creep Strain
210	387	2252	Instantaneous Strain + Creep Strain
240	413	2280	Instantaneous Strain + Creep Strain
270	427	2300	Instantaneous Strain + Creep Strain
300	443	2361	Instantaneous Strain + Creep Strain
330	443	2386	Instantaneous Strain + Creep Strain
365	452	2420	Instantaneous Strain + Creep Strain
396	455	2423	Instantaneous Strain + Creep Strain
427	456	2478	Instantaneous Strain + Creep Strain
456	457	2483	Instantaneous Strain + Creep Strain
487	467	2490	Instantaneous Strain + Creep Strain
517	468	2510	Instantaneous Strain + Creep Strain
548	479	2524	Instantaneous Strain + Creep Strain
578	491	2545	Instantaneous Strain + Creep Strain
609	501	2569	Instantaneous Strain + Creep Strain
640	512	2559	Instantaneous Strain + Creep Strain
670	504	2573	Instantaneous Strain + Creep Strain
701	504	2573	Instantaneous Strain + Creep Strain
731	517	2581	Instantaneous Strain + Creep Strain
762	517	2608	Instantaneous Strain + Creep Strain

Applied Stress = 2480 psi

f'c @ 90 Days = 7430 psi

Modulus of Elasticity @ 90 days = 3.54 x 10^6

SECTION F - 3 DAYS

Creep Of Concrete in Compression (ASTM C 512)

Instantaneous and Long-Term Deformation (Adjusted for Drying Shrinkage)

Days Loaded	Drying Shrinkage (millionths)	Load Induced Deformation (millionths)	Condition
0	0	542	Instantaneous Strain
1	4	754	Instantaneous Strain + Creep Strain
2	44	826	Instantaneous Strain + Creep Strain
3	49	899	Instantaneous Strain + Creep Strain
4	85	924	Instantaneous Strain + Creep Strain
5	103	982	Instantaneous Strain + Creep Strain
6	119	999	Instantaneous Strain + Creep Strain
7	127	1030	Instantaneous Strain + Creep Strain
14	251	1153	Instantaneous Strain + Creep Strain
21	385	1280	Instantaneous Strain + Creep Strain
28	446	1381	Instantaneous Strain + Creep Strain
56	587	1660	Instantaneous Strain + Creep Strain
90	735	1783	Instantaneous Strain + Creep Strain
120	833	1883	Instantaneous Strain + Creep Strain
152	858	1938	Instantaneous Strain + Creep Strain
180	910	1994	Instantaneous Strain + Creep Strain
212	933	2036	Instantaneous Strain + Creep Strain
243	960	2078	Instantaneous Strain + Creep Strain
273	973	2078	Instantaneous Strain + Creep Strain
304	1008	2101	Instantaneous Strain + Creep Stra
334	998	2124	Instantaneous Strain + Creep Strai
365	1014	2165	Instantaneous Strain + Creep Strain
396	1019	2180	Instantaneous Strain + Creep Strain
426	1026	2199	Instantaneous Strain + Creep Strain
457	1028	2221	Instantaneous Strain + Creep Strain
487	1039	2219	Instantaneous Strain + Creep Strain
518	1042	2266	Instantaneous Strain + Creep Strain
549	1043	2283	Instantaneous Strain + Creep Strain
578	1045	2296	Instantaneous Strain + Creep Strain
609	1057	2292	Instantaneous Strain + Creep Strain
639	1058	2298	Instantaneous Strain + Creep Strain
670	1067	2304	Instantaneous Strain + Creep Strain
700	1067	2307	Instantaneous Strain + Creep Strain
731	1079	2310	Instantaneous Strain + Creep Strain
762	1081	2311	Instantaneous Strain + Creep Strain
792	1089	2315	Instantaneous Strain + Creep Strain
823	1089	2312	Instantaneous Strain + Creep Strain
853	1091	2330	Instantaneous Strain + Creep Strain
884	1093	2342	Instantaneous Strain + Creep Strain

Applied Stress= 1550 psi

f'c @ 3 days = 3880 psi

Modulus of Elasticity @ 3 days = 3.48 x 10^6

SECTION F - 28 DAYS

Creep Of Concrete in Compression (ASTM C 512)

Instantaneous and Long-Term Deformation (Adjusted for Drying Shrinkage)

Days Loaded	Drying Shrinkage (millionths)	Load Induced Deformation (millionths)	Condition
0	0	658	Instantaneous Strain
1	29	1042	Instantaneous Strain + Creep Strain
2	43	1208	Instantaneous Strain + Creep Strain
3	51	1283	Instantaneous Strain + Creep Strain
4	68	1324	Instantaneous Strain + Creep Strain
5	88	1370	Instantaneous Strain + Creep Strain
6	98	1402	Instantaneous Strain + Creep Strain
7	108	1439	Instantaneous Strain + Creep Strain
14	178	1668	Instantaneous Strain + Creep Strain
21	310	1828	Instantaneous Strain + Creep Strain
28	372	1886	Instantaneous Strain + Creep Strain
56	502	2253	Instantaneous Strain + Creep Strain
90	648	2452	Instantaneous Strain + Creep Strain
120	677	2595	Instantaneous Strain + Creep Strain
150	732	2693	Instantaneous Strain + Creep Strain
180	754	2773	Instantaneous Strain + Creep Strain
210	811	2831	Instantaneous Strain + Creep Strain
240	822	2880	Instantaneous Strain + Creep Strain
270	828	2929	Instantaneous Strain + Creep Strain
300	843	2987	Instantaneous Strain + Creep Strain
330	873	3020	Instantaneous Strain + Creep Strain
365	891	3041	Instantaneous Strain + Creep Strain
395	899	3068	Instantaneous Strain + Creep Strain
426	903	3103	Instantaneous Strain + Creep Strain
456	905	3105	Instantaneous Strain + Creep Strain
487	908	3122	Instantaneous Strain + Creep Strain
518	915	3138	Instantaneous Strain + Creep Strain
547	916	3168	Instantaneous Strain + Creep Strain
578	918	3170	Instantaneous Strain + Creep Strain
608	918	3181	Instantaneous Strain + Creep Strain
639	919	3191	Instantaneous Strain + Creep Strain
669	932	3210	Instantaneous Strain + Creep Strain
700	950	3208	Instantaneous Strain + Creep Strain
731	950	3222	Instantaneous Strain + Creep Strain
761	955	3228	Instantaneous Strain + Creep Strain
792	955	3228	Instantaneous Strain + Creep Strain
822	958	3251	Instantaneous Strain + Creep Strain
853	963	3274	Instantaneous Strain + Creep Strain

Applied Stress= 2290 psi

f'c @ 28 days = 5850 psi

Modulus of Elasticity @ 28 days = 3.57 x 10^6

SECTION F - 90 DAYS

Creep Of Concrete in Compression (ASTM C 512)

Instantaneous and Long-Term Deformation (Adjusted for Drying Shrinkage)

Days Loaded	Drying Shrinkage (millionths)	Load Induced Deformation (millionths)	Condition
0	0	818	Instantaneous Strain
1	8	995	Instantaneous Strain + Creep Strain
2	24	1058	Instantaneous Strain + Creep Strain
3	48	1087	Instantaneous Strain + Creep Strain
4	76	1116	Instantaneous Strain + Creep Strain
5	93	1126	Instantaneous Strain + Creep Strain
6	115	1178	Instantaneous Strain + Creep Strain
7	129	1179	Instantaneous Strain + Creep Strain
14	214	1293	Instantaneous Strain + Creep Strain
21	226	1396	Instantaneous Strain + Creep Strain
28	328	1476	Instantaneous Strain + Creep Strain
56	468	1644	Instantaneous Strain + Creep Strain
90	554	1848	Instantaneous Strain + Creep Strain
120	614	1905	Instantaneous Strain + Creep Strain
150	654	1987	Instantaneous Strain + Creep Strain
180	679	2071	Instantaneous Strain + Creep Strain
210	712	2108	Instantaneous Strain + Creep Strain
240	744	2179	Instantaneous Strain + Creep Strain
270	768	2210	Instantaneous Strain + Creep Strain
300	774	2243	Instantaneous Strain + Creep Strain
330	794	2256	Instantaneous Strain + Creep Strain
365	808	2302	Instantaneous Strain + Creep Strain
395	817	2318	Instantaneous Strain + Creep Strain
426	824	2313	Instantaneous Strain + Creep Strain
457	832	2362	Instantaneous Strain + Creep Strain
486	832	2370	Instantaneous Strain + Creep Strain
517	833	2392	Instantaneous Strain + Creep Strain
547	834	2411	Instantaneous Strain + Creep Strain
578	845	2423	Instantaneous Strain + Creep Strain
608	853	2431	Instantaneous Strain + Creep Strain
639	862	2436	Instantaneous Strain + Creep Strain
670	866	2436	Instantaneous Strain + Creep Strain
700	868	2441	Instantaneous Strain + Creep Strain
731	868	2452	Instantaneous Strain + Creep Strain
761	870	2482	Instantaneous Strain + Creep Strain
792	879	2500	Instantaneous Strain + Creep Strain

Applied Stress= 2480 psi

f'c @ 90 days = 7060 psi

Modulus of Elasticity @ 90 days = 3.88 x 10^6

SECTION G - 3 DAYS

Creep Of Concrete in Compression (ASTM C 512)

Instantaneous and Long-Term Deformation (Adjusted for Drying Shrinkage)

Days Loaded	Drying Shrinkage (millionths)	Load Induced Deformation (millionths)	Condition
0	0	449	Instantaneous Strain
1	21	691	Instantaneous Strain + Creep Strain
2	38	794	Instantaneous Strain + Creep Strain
3	88	832	Instantaneous Strain + Creep Strain
4	102	886	Instantaneous Strain + Creep Strain
5	109	905	Instantaneous Strain + Creep Strain
6	158	975	Instantaneous Strain + Creep Strain
7	168	994	Instantaneous Strain + Creep Strain
14	289	1103	Instantaneous Strain + Creep Strain
21	411	1210	Instantaneous Strain + Creep Strain
28	449	1358	Instantaneous Strain + Creep Strain
56	662	1595	Instantaneous Strain + Creep Strain
90	785	1767	Instantaneous Strain + Creep Strain
120	820	1854	Instantaneous Strain + Creep Strain
150	859	1896	Instantaneous Strain + Creep Strain
180	886	2025	Instantaneous Strain + Creep Strain
210	928	2043	Instantaneous Strain + Creep Strain
240	929	2096	Instantaneous Strain + Creep Strain
270	951	2107	Instantaneous Strain + Creep Strain
300	967	2129	Instantaneous Strain + Creep Strain
330	977	2179	Instantaneous Strain + Creep Strain
365	984	2198	Instantaneous Strain + Creep Strain

Applied Stress= 1530 psi

f'c @ 3 days = 3830 psi

Modulus of Elasticity @ 3 days = 3.05 x 10^6

SECTION G - 28 DAYS

Creep Of Concrete in Compression (ASTM C 512)

Instantaneous and Long-Term Deformation (Adjusted for Drying Shrinkage)

Days Loaded	Drying Shrinkage (millionths)	Load Induced Deformation (millionths)	Condition
0	0	713	Instantaneous Strain
1	46	780	Instantaneous Strain + Creep Strain
2	72	964	Instantaneous Strain + Creep Strain
3	78	1092	Instantaneous Strain + Creep Strain
4	123	1151	Instantaneous Strain + Creep Strain
5	138	1219	Instantaneous Strain + Creep Strain
6	145	1237	Instantaneous Strain + Creep Strain
7	183	1325	Instantaneous Strain + Creep Strain
14	258	1543	Instantaneous Strain + Creep Strain
21	378	1663	Instantaneous Strain + Creep Strain
28	458	1795	Instantaneous Strain + Creep Strain
56	589	2108	Instantaneous Strain + Creep Strain
90	703	2411	Instantaneous Strain + Creep Strain
120	749	2560	Instantaneous Strain + Creep Strain
150	800	2676	Instantaneous Strain + Creep Strain
180	870	2739	Instantaneous Strain + Creep Strain
210	878	2798	Instantaneous Strain + Creep Strain
240	889	2868	Instantaneous Strain + Creep Strain
270	908	2933	Instantaneous Strain + Creep Strain
300	922	2965	Instantaneous Strain + Creep Strain
330	929	2973	Instantaneous Strain + Creep Strain
365	953	3001	Instantaneous Strain + Creep Strain

Applied Stress= 2380 psi

f'c @ 28 days = 5990 psi

Modulus of Elasticity @ 28 days = 3.45 x 10^6

SECTION G - 90 DAYS

Creep Of Concrete in Compression (ASTM C 512)

Instantaneous and Long-Term Deformation (Adjusted for Drying Shrinkage)

Days Loaded	Drying Shrinkage (millionths)	Load Induced Deformation (millionths)	Condition
0	0	773	Instantaneous Strain
1	8	1069	Instantaneous Strain + Creep Strain
2	18	1192	Instantaneous Strain + Creep Strain
3	33	1236	Instantaneous Strain + Creep Strain
4	51	1283	Instantaneous Strain + Creep Strain
5	58	1321	Instantaneous Strain + Creep Strain
6	63	1363	Instantaneous Strain + Creep Strain
7	73	1463	Instantaneous Strain + Creep Strain
14	78	1618	Instantaneous Strain + Creep Strain
21	143	1638	Instantaneous Strain + Creep Strain
28	153	1732	Instantaneous Strain + Creep Strain
56	206	1975	Instantaneous Strain + Creep Strain
90	282	2162	Instantaneous Strain + Creep Strain
120	297	2263	Instantaneous Strain + Creep Strain
150	298	2326	Instantaneous Strain + Creep Strain
180	306	2465	Instantaneous Strain + Creep Strain
210	328	2535	Instantaneous Strain + Creep Strain
240	366	2516	Instantaneous Strain + Creep Strain
270	382	2511	Instantaneous Strain + Creep Strain
300	398	2563	Instantaneous Strain + Creep Strain
330	403	2612	Instantaneous Strain + Creep Strain
365	413	2656	Instantaneous Strain + Creep Strain

Applied Stress = 2480 psi

f'c @ 90 days = 6510 psi

Modulus of Elasticity @ 90 days = 3.58 x 10^6

Appendix E - Field Creep and Shrinkage Data

SECTION E - 4 DAYS			
CREEP FRAME E1 INSIDE BOX GIRDER			
Creep Of Concrete in Compression			
Instantaneous and Long-Term Deformation (Adjusted for Drying Shrinkage)			
	Drying	Load Induced	
Days	Shrinkage	Deformation	
Loaded	(millionths)	(millionths)	Condition
0	0	619	Instantaneous strain
3	-3	858	Instantaneous Strain + Creep Strain
5	-25	1031	Instantaneous Strain + Creep Strain
10	65	1077	Instantaneous Strain + Creep Strain
20	39	1285	Instantaneous Strain + Creep Strain
40	110	1452	Instantaneous Strain + Creep Strain
59	212	1502	Instantaneous Strain + Creep Strain
89	246	1685	Instantaneous Strain + Creep Strain
114	285	1677	Instantaneous Strain + Creep Strain
121	363	1681	Instantaneous Strain + Creep Strain
147	312	1804	Instantaneous Strain + Creep Strain
181	437	1817	Instantaneous Strain + Creep Strain
200	420	1840	Instantaneous Strain + Creep Strain
233	462	1896	Instantaneous Strain + Creep Strain
264	504	1967	Instantaneous Strain + Creep Strain
306	546	2004	Instantaneous Strain + Creep Strain
339	604	2035	Instantaneous Strain + Creep Strain
396	558	2131	Instantaneous Strain + Creep Strain
510	581	2148	Instantaneous Strain + Creep Strain
635	589	2258	Instantaneous Strain + Creep Strain
699	647	2258	Instantaneous Strain + Creep Strain
Applied Stress = 2000 psi			
f'_c @ 3 days = 4210 psi			
Modulus of Elasticity @ 3 days = 3.27 x 10°			

SECTION E - 4 DAYS			
CREEP FRAME E2 INSIDE BOX GIRDER			
Creep Of Concrete in Compression			
Instantaneous and Long-Term Deformation (Adjusted for Drying Shrinkage)			
	Drying	Load Induced	
Days	Shrinkage	Deformation	
Loaded	(millionths)	(millionths)	Condition
0	0	442	Instantaneous strain
3	31	581	Instantaneous Strain + Creep Strain
5	102	600	Instantaneous Strain + Creep Strain
10	63	706	Instantaneous Strain + Creep Strain
20	169	854	Instantaneous Strain + Creep Strain
40	168	981	Instantaneous Strain + Creep Strain
59	356	977	Instantaneous Strain + Creep Strain
89	392	1052	Instantaneous Strain + Creep Strain
114	394	1102	Instantaneous Strain + Creep Strain
121	515	1088	Instantaneous Strain + Creep Strain
147	481	1129	Instantaneous Strain + Creep Strain
181	623	1146	Instantaneous Strain + Creep Strain
200	599	1154	Instantaneous Strain + Creep Strain
233	645	1238	Instantaneous Strain + Creep Strain
264	648	1329	Instantaneous Strain + Creep Strain
306	733	1302	Instantaneous Strain + Creep Strain
339	763	1333	Instantaneous Strain + Creep Strain
396	738	1379	Instantaneous Strain + Creep Strain
510	718	1415	Instantaneous Strain + Creep Strain
635	775	1448	Instantaneous Strain + Creep Strain
699	801	1490	Instantaneous Strain + Creep Strain
Applied Stress = 1550 psi			
f'_c @ 3 days = 4210 psi			
Modulus of Elasticity @ 3 days = 3.27×10^6			

SECTION E - 4 DAYS			
CREEP FRAME E3 OUTSIDE BOX GIRDER			
Creep Of Concrete in Compression			
Instantaneous and Long-Term Deformation (Adjusted for Drying Shrinkage)			
	Drying	Load Induced	
Days	Shrinkage	Deformation	
Loaded	(millionths)	(millionths)	Condition
0	0	602	Instantaneous strain
3	0	1137	Instantaneous Strain + Creep Strain
5	0	1144	Instantaneous Strain + Creep Strain
10	58	1215	Instantaneous Strain + Creep Strain
20	53	1369	Instantaneous Strain + Creep Strain
40	72	1475	Instantaneous Strain + Creep Strain
59	78	1481	Instantaneous Strain + Creep Strain
89	123	1527	Instantaneous Strain + Creep Strain
114	69	1563	Instantaneous Strain + Creep Strain
121	148	1648	Instantaneous Strain + Creep Strain
146	138	1629	Instantaneous Strain + Creep Strain
181	83	1717	Instantaneous Strain + Creep Strain
200	148	1650	Instantaneous Strain + Creep Strain
242	277	1700	Instantaneous Strain + Creep Strain
277	241	1754	Instantaneous Strain + Creep Strain
306	304	1783	Instantaneous Strain + Creep Strain
339	170	1840	Instantaneous Strain + Creep Strain
396	160	1850	Instantaneous Strain + Creep Strain
510	137	1877	Instantaneous Strain + Creep Strain
635	204	1979	Instantaneous Strain + Creep Strain
699	267	1956	Instantaneous Strain + Creep Strain
Applied Stress = 1550 psi			
f'_c @ 3 days = 4210 psi			
Modulus of Elasticity @ 3 days = 3.27×10^5			

SECTION F - 3 DAYS			
CREEP FRAME F2 INSIDE BOX GIRDER - STANDARD TEST			
Creep Of Concrete in Compression			
Instantaneous and Long-Term Deformation (Adjusted for Drying Shrinkage)			
	Drying	Load Induced	
Days	Shrinkage	Deformation	
Loaded	(millionths)	(millionths)	Condition
0	0	0	
0	0	558	Instantaneous strain
1	-28	921	Instantaneous Strain + Creep Strain
3	32	1029	Instantaneous Strain + Creep Strain
5	148	1083	Instantaneous Strain + Creep Strain
7	132	1104	Instantaneous Strain + Creep Strain
10	134	1169	Instantaneous Strain + Creep Strain
14	150	1254	Instantaneous Strain + Creep Strain
14	150	1242	Instantaneous Strain + Creep Strain
24	182	1331	Instantaneous Strain + Creep Strain
26	107	1290	Instantaneous Strain + Creep Strain
45	182	1367	Instantaneous Strain + Creep Strain
55	197	1388	Instantaneous Strain + Creep Strain
75	317	1388	Instantaneous Strain + Creep Strain
94	200	1523	Instantaneous Strain + Creep Strain
124	290	1527	Instantaneous Strain + Creep Strain
149	388	1513	Instantaneous Strain + Creep Strain
177	473	1510	Instantaneous Strain + Creep Strain
182	420	1594	Instantaneous Strain + Creep Strain
216	530	1550	Instantaneous Strain + Creep Strain
235	477	1571	Instantaneous Strain + Creep Strain
265	544	1621	Instantaneous Strain + Creep Strain
268	578	1606	Instantaneous Strain + Creep Strain
299	589	1688	Instantaneous Strain + Creep Strain
341	671	1658	Instantaneous Strain + Creep Strain
374	666	1710	Instantaneous Strain + Creep Strain
431	702	1677	Instantaneous Strain + Creep Strain
545	655	1758	Instantaneous Strain + Creep Strain
670	756	1790	Instantaneous Strain + Creep Strain
734	782	1800	Instantaneous Strain + Creep Strain
Applied Stress = 1556 psi			
f'_c @ 3 days = 3880 psi			
Modulus of Elasticity @ 3 days = 3.48 x 10^6			

SECTION F - 4 DAYS			
CREEP FRAME F3 OUTSIDE BOX GIRDER - STANDARD TEST			
Creep Of Concrete in Compression			
Instantaneous and Long-Term Deformation (Adjusted for Drying Shrinkage)			
	Drying	Load Induced	
Days	Shrinkage	Deformation	
Loaded	(millionths)	(millionths)	Condition
0	0	0	
0	0	535	Instantaneous strain
2	-1	977	Instantaneous Strain + Creep Strain
2	-1	992	Instantaneous Strain + Creep Strain
4	84	1135	Instantaneous Strain + Creep Strain
6	133	1167	Instantaneous Strain + Creep Strain
9	195	1231	Instantaneous Strain + Creep Strain
13	151	1319	Instantaneous Strain + Creep Strain
21	78	1502	Instantaneous Strain + Creep Strain
23	74	1483	Instantaneous Strain + Creep Strain
23	74	1431	Instantaneous Strain + Creep Strain
25	179	1425	Instantaneous Strain + Creep Strain
44	254	1546	Instantaneous Strain + Creep Strain
54	198	1594	Instantaneous Strain + Creep Strain
74	206	1542	Instantaneous Strain + Creep Strain
93	199	1542	Instantaneous Strain + Creep Strain
123	335	1579	Instantaneous Strain + Creep Strain
148	276	1592	Instantaneous Strain + Creep Strain
176	443	1590	Instantaneous Strain + Creep Strain
180	297	1613	Instantaneous Strain + Creep Strain
215	306	1690	Instantaneous Strain + Creep Strain
234	346	1646	Instantaneous Strain + Creep Strain
276	415	1731	Instantaneous Strain + Creep Strain
311	424	1823	Instantaneous Strain + Creep Strain
340	442	1800	Instantaneous Strain + Creep Strain
373	380	1831	Instantaneous Strain + Creep Strain
430	413	1800	Instantaneous Strain + Creep Strain
544	348	1858	Instantaneous Strain + Creep Strain
669	444	1890	Instantaneous Strain + Creep Strain
733	533	1883	Instantaneous Strain + Creep Strain
Applied Stress = 1556 psi			
f'_c @ 3 days = 3880 psi			
Modulus of Elasticity @ 3 days = 3.48×10^6			

SECTION G - 1 DAYS			
CREEP FRAME G1 INSIDE BOX GIRDER			
Creep Of Concrete in Compression			
Instantaneous and Long-Term Deformation (Adjusted for Drying Shrinkage)			
	Drying	Load Induced	
Days	Shrinkage	Deformation	
Loaded	(millionths)	(millionths)	Condition
0	0	73	Instantaneous strain
2	53	87	Instantaneous Strain + Creep Strain
2	53	87	Instantaneous Strain + Creep Strain
4	46	117	Instantaneous Strain + Creep Strain
6	175	121	Instantaneous Strain + Creep Strain
17	157	163	Instantaneous Strain + Creep Strain
17	157	277	Instantaneous Strain + Creep Strain
23	168	327	Instantaneous Strain + Creep Strain
27	235	321	Instantaneous Strain + Creep Strain
33	170	377	Instantaneous Strain + Creep Strain
53	337	390	Instantaneous Strain + Creep Strain
72	230	456	Instantaneous Strain + Creep Strain
102	329	460	Instantaneous Strain + Creep Strain
127	405	456	Instantaneous Strain + Creep Strain
155	564	437	Instantaneous Strain + Creep Strain
160	451	471	Instantaneous Strain + Creep Strain
194	582	444	Instantaneous Strain + Creep Strain
213	521	498	Instantaneous Strain + Creep Strain
236	579	529	Instantaneous Strain + Creep Strain
277	574	613	Instantaneous Strain + Creep Strain
319	636	546	Instantaneous Strain + Creep Strain
352	638	585	Instantaneous Strain + Creep Strain
409	699	525	Instantaneous Strain + Creep Strain
523	642	606	Instantaneous Strain + Creep Strain
648	732	604	Instantaneous Strain + Creep Strain
712	822	548	Instantaneous Strain + Creep Strain
Applied Stress = 805 psi			
f'_c @ 3 days = 3830 psi			
Modulus of Elasticity @ 3 days = 3.05×10^6			

9. Design Criteria

NEW BENICIA MARTINEZ BRIDGE

Contract 59S742

DESIGN CRITERIA

(May 17, 2000)

Prepared by T.Y.Lin International/CH2M Hill, A Joint Venture

1. GENERAL **1**

2. DESIGN LOADS **1**
2.1 Structural Dead Loads - DL 1
2.2 Other Permanent Loads- SDL 1
2.3 Live Loads - LL+I 1
2.3.1 Load reductions factor for multiple lane loading 1
2.4 Thermal Effects - T 1
2.4.1 Coefficient of thermal expansion 1
2.4.2 Temperature gradient - DT 2
2.5 Ship Collision - SC 2
2.6 Combination of Loads 2
2.6.1 Service and Ultimate Limit States 2
2.6.2 Additional Thermal Loading Combination 4
2.6.3 Construction Load Combinations 4
2.6.4 Construction Load Combinations, Load Factor Design Check 4
2.6.5 Ship Impact Load Combination 4

3. ALLOWABLE STRESSES **4**
3.1 Prestressing Steel 4
3.2 Prestressed Concrete 4
3.2.1 Temporary stresses before losses at time of application of prestress 4
3.2.2 Stresses at service level after losses - fully prestressed components 5
3.2.3 Cracking stress 5
3.2.4 Bearing stress 5
3.2.5 Shear 5

4. STRENGTH REDUCTION FACTORS **5**
4.1 Superstructure 5
4.1.1 Normal and Sand-Light Weight Concrete 6
4.1.2 Bearing 6
4.2 Substructure 6

5. MATERIALS **6**
5.1 Concrete 6
5.1.1 Superstructure 6
5.1.2 Substructure 6
5.1.3 Creep and shrinkage 6
5.2 Prestressing Steel 6
5.3 Reinforcement 6

6. SEISMIC DESIGN **9**
6.1 Performance Criteria 9
6.2 Seismic Loading 9
6.2.1 Seismic Loading During Construction 9
6.3 Seismic Analysis 9
6.3.1 Elastic dynamic analysis 9
6.3.2 Inelastic static analysis 9
6.3.3 Inelastic dynamic analysis 9

6.4 Combination of Effects 9
6.5 Design Displacements 9
6.6 Design Forces 10
6.7 Capacity Design 10
6.8 Restraining Features 10
6.9 P-Δ Effects 10
6.10 Strength Reduction Factors for Columns 10
6.11 Material Properties for Ductile Columns 10
6.11.1 Design flexural strength 10
6.11.2 Maximum plastic moment 10
6.11.3 Steel strain hardening strains 10
6.12 Displacement Capacity 10
6.13 Allowable Strains 11
6.13.1 Normal Weight Concrete 11
6.13.2 Sand Light Weight Concrete 11
6.13.3 Reinforcing steel 11
6.13.4 Pile casing 11
[illegible] 11

7. GEOTECHNICAL AND FOUNDATION DESIGN 11
7.1 Pile Capacity 11
7.2 Scour 11

8. EXPANSION JOINTS 11

1. GENERAL

The bridge shall be designed in accordance with "Caltrans Bridge Design Specifications Manual" updated April 1995, modified or augmented as detailed in this document.
In addition to bridge and site specific criteria, pertinent sections of the following standards or codes have been employed for such modifications or augmentations.

- "AASHTO Guide Specifications for Design and Construction of Segmental Concrete Bridges", 1989 Edition.
- "Proposed LRFD Guide Specifications for Design of Segmental Concrete Bridges," S. I. Units, 1997.
- "AASHTO Standard Specifications for Highway Bridges", 1992 Edition.
- "San Francisco Bay Area Rapid Transit District Design Criteria." Updated 12/27/91.
- "Guide Specifications and Commentary for Vessel Collision Design of Highway Bridges." Volume I: Final Report. February, 1991.
- "Improved Seismic Design Criteria for California Bridges: Provisional Recommendations." ATC-32 Report, June 30, 1996.

2. DESIGN LOADS

This section covers all design loads except for seismic forces discussed in Section 6.

2.1 Structural Dead Loads - DL

The in-service air dry unit weight of sand light weight concrete including reinforcement will be 2005 kg/m^3.

2.2 Other Permanent Loads- SDL

Permanent Loads are assumed to be applied at the time of construction except for utilities and dead load of BART appurtenances.

2.3 Live Loads - LL+I

Live loads shall be based on:
1. Highway Traffic on the entire roadway.
2. Highway traffic on the roadway plus one track of standard BART train loading. The BART track will be placed adjacent to the West barrier on the bridge deck.

2.3.1 Load reductions factor for multiple lane loading

Load reduction factors for multiple lane loading shall be applied to highway lanes only. Full BART Train Loading shall be combined with the combination of highway lanes to produce the largest stresses in the member.

2.4 Thermal Effects - T

2.4.1 Coefficient of thermal expansion

normal weight concrete	10.8×10^{-6} /°C
sand-lightweight concrete	9.0×10^{-6} /°C

2.4.2 Temperature gradient - DT

Positive and negative temperature gradients shall correspond to the values listed below.

AASHTO Seg 1997 6.4.4

Positive Gradient		Negative Gradient	
T_1 =	30.0 °C	T_1 =	-15.0 °C
T_2 =	7.8 °C	T_2 =	-3.9 °C
T_3 =	0 °C	T_3 =	0 °C
A =	300 mm	A =	300 mm

2.5 Ship Collision - SC

"AASHTO Guide Specifications and Commentary for Vessel Collision Design," Volume I, Final Report, February 1991 will be used to determine the ship impact force.

AASHTO Vessel Collision Design of Highway Bridges

The bridge is classified as "critical bridge" and the acceptable annual frequency of collapse shall be equal to or less than 0.01 in 100 years. The design vessel shall be selected based on Method II.

2.6 Combination of Loads

2.6.1 Service and Ultimate Limit States

Loading combinations shall be in accordance with Caltrans BDS Table 3.22.1A and 3.22.1B, AASHTO "Guide Specifications for Design and Construction of Segmental Concrete Bridges" and "San Francisco Bay Area Rapid Transit District Design Criteria".

Table 2.7.1A and 2.7.1B show the applicable load combination for Service Load Design and Load Factor Design.

AASHTO Seg 8.0

Dead Load - D - includes structural dead loads (DL), other permanent loads (SDL) and erection loads (EL) when applicable.

AASHTO Seg 8.2

Permanent effects of creep and shrinkage are added to all Service Load Design combinations with a load factor of 1.0.

AASHTO Seg 8.1

When checking tensile stresses for Service Load Design the variable load effects shall be divided by the allowable stress increases.

AASHTO Seg 8.0

One half of the temperature gradient is used for load combinations which include full live load plus impact.

Group Loading Combinations for Service Load Design and Load Factor Design are given by:

$$\text{Group (N)} = \gamma \{[\beta_d D + \beta_L (L+I) + \beta_c CF + \beta_E E + \beta_B B + \beta_S SF + \beta_W W + \beta_{PS} PS + \beta_{WL} WL + \beta_L LF + \beta_R (R+S+T+DT) + \beta_{EQ} EQ] + \alpha_B[\beta_{LB} (L_B+I_B) + \beta_{CB} CF_B + \beta_L LF_B + \beta_{WLB} WL_B]\}$$

where

N	Group No.
γ	Load Factor, see Table 2.7.1A and 2.7.1B
β	Coefficient, see Table 2.7.1A and 2.7.1B
D	Dead Load
L	Live Load

I	Live Load Impact
E	Earth Pressure
B	Buoyancy
W	Wind Load on Structure
WL	Wind on Live Load. 100 pounds per linear ft.
LF	Longitudinal Force form Live Load
CF	Centrifugal Force
R	Rib Shortening
S	Shrinkage
T	Temperature
DT	Thermal Gradient
EQ	Earthquake
SF	Stream flow pressure
PS	Prestress
α_B	1 or 0 corresponding to presence or otherwise of Bart Train
L_B	Bart Live Load
I_B	Impact from Bart Live Load
CF_B	Centrifugal Force from Bart Train
LF_B	Longitudinal Force, Bart
WL_B	Wind on Bart Train

2.6.2 Additional Thermal Loading Combination

In addition to Service Load Design Combinations defined in Table 2.7.1A, the following load combination shall apply:

$(DL + SDL + EL) + \beta_E E + B + SF + R + S + T + DT$

where DL is the dead load, SDL is the superimposed dead load and EL is the erection load in the final state.

AASHTO Seg 1996
8.2.2

2.6.3 Construction Load Combinations

Allowable tensile stresses for construction load combinations shall be checked according to AASHTO "Guide Specifications for Design and Construction of Segmental Concrete Bridge," 1989.

AASHTO Seg 1996
8.4
Table 8-1

2.6.4 Construction Load Combinations, Load Factor Design Check

The strength provided shall not be less than required by the following combinations:

For maximum forces and moments:

$1.1\ (DL + DIFF) + 1.3\ CE + 2\ A$

For minimum forces and moments:

$DL + CE + 2\ A$

where DIFF is the 2% differential dead load applied to one cantilever, CE is the load from specialized construction equipment and A is the sudden impact from an otherwise static load.

AASHTO Seg 1996
8.4.1
8.4.3

2.6.5 Ship Impact Load Combination

The vessel collision impact forces are combined with other loads. The group loading combination has the same format as that used in the current BDS for seismic design (Group VII) with all gamma and beta factors equal to 1.0 and the ship impact force replacing the earthquake load.

The ship impact load combination is given by the following expression:

Group Load = $\gamma\ (1.0\ D + 1.0\ P + 1.0\ B + 1.0\ SF + 1.0\ E)$

where
$\gamma = 1.0$ for all design methods
D = Dead Load
P = vessel collison impact force
B = Buoyancy
SF = stream flow pressure
E = earth pressure

AASHTO
Vessel Collision Design of Highway Bridges
3.14

3. ALLOWABLE STRESSES

Allowable Stresses are to follow the AASHTO Guide Specifications for Design and Construction of Segmental Concrete Bridges, as modified below for sand-lightweight concrete:

3.1 Prestressing Steel

AASHTO Seg 9.1

3.2 Prestressed Concrete

3.2.1 Temporary stresses before losses at time of application of prestress

3.2.1.1 Compression

Normal and Sand-Light Weight Concrete $0.55\ f'_{ci}$

AASHTO Seg 9.2.1.1

3.2.1.2 Tension

Longitudinal and transverse stresses in the precompressed tensile zone, with minimum bonded auxiliary reinforcement through the joints sufficient to carry the calculated tensile force at a stress of $0.5\ f_{sy}$; internal tendons:

Normal Weight Concrete	$0.25\sqrt{f'_{ci}}$ (MPa)	AASHTO Seg 9.2.1.2
Sand-Light Weight Concrete	$0.21\sqrt{f'_{ci}}$ (MPa)	
Temporary tension in the precompressed tensile zone during construction:		
Normal Weight Concrete	$0.50\sqrt{f'_{ci}}$ (MPa)	AASHTO Seg Table 8.1
Sand-Light Weight Concrete	$0.42\sqrt{f'_{ci}}$ (MPa)	

3.2.2 Stresses at service level after losses - fully prestressed components

3.2.2.1 Compression

Compressive stress due to effective prestress plus permanent (dead) loads shall not exceed:

Normal and Sand-Light Weight Concrete	$0.40\ f'_c$	AASHTO Seg 9.2.2.1

3.2.2.2 Tension in the precompressed tensile zone

Longitudinal and transverse stresses, with minimum bonded auxiliary reinforcement through the joints sufficient to carry the calculated tensile force at a stress of 0.5 f_{sy}; internal tendons:

Normal Weight Concrete	$0.25\sqrt{f'_c}$ (MPa)	AASHTO Seg 9.2.2.2
Sand-Light Weight Concrete	$0.21\sqrt{f'_c}$ (MPa)	
Under dead load only:		
Normal and Sand-Light Weight Concrete	0.0	BDS 9.15.2.2

3.2.2.3 Tension in other areas

Bonded reinforcement shall be provided to carry the calculated tensile force at a stress of 0.5 f_{sy}:

Normal Weight Concrete	$0.50\sqrt{f'_c}$ (MPa)	AASHTO Seg 9.2.2.2
Sand-Light Weight Concrete	$0.42\sqrt{f'_c}$ (MPa)	

3.2.3 Cracking stress

Modulus of rupture

Normal Weight Concrete	$0.63\sqrt{f'_c}$ (MPa)	BDS 9.15.2.3
Sand-Light Weight Concrete	$0.52\sqrt{f'_c}$ (MPa)	BDS 9.15.2.3

3.2.4 Bearing stress

AASHTO Seg 1989 9.2.3

3.2.5 Shear

Shear design shall follow the 1989 Guide Specifications for Design and Construction of Segmental Concrete Bridges. Shear stress must not exceed the limits in Section 12.3.1 — AASHTO Seg 1989 12.0

For Sand-Light Weight Concrete the torsional cracking moment (T_c) and the nominal shear strength provided by concrete (V_c) must be taken as 0.85 times the formulas specified in Sections 12.2.10 and 12.2.12, respectively, of the 1989 Guide Specifications for Design and Construction of Segmental Concrete Bridges.

4. STRENGTH REDUCTION FACTORS

4.1 Superstructure

Superstructure Strength Reduction Factors, ϕ, shall be taken from the 1989 Guide Specifications for Design and Construction of Segmental Concrete Bridges, and amended as follows:

4.1.1 Normal and Sand-Light Weight Concrete

Fully Bonded Tendons, Type A Joint

Flexure	$\phi_f = 0.95$
Shear and torsion	$\phi_v = 0.85$
Unbonded Tendons, Type A Joint	
Flexure	$\phi_f = 0.90$
Shear and torsion	$\phi_v = 0.80$

4.1.2 Bearing

(all types of construction) $\phi_b = 0.70$

4.2 Substructure

Design using Ultimate Load Factor Design, based on Caltrans BDS 8.16.1.2.2 except for Seismic Load Combinations.

5. MATERIALS

Per 1989 AASHTO Guide Specifications for Construction and Design of Segmental Bridges, and the following:

5.1 Concrete

5.1.1 Superstructure

5.1.1.1 Normal weight concrete

28-day minimum strength	$f'c = 45$ MPa
at time of stressing	$f'c_i = 25$ MPa

5.1.1.2 Sand-lightweight concrete

28-day minimum strength	$f'c = 45$ MPa
at time of stressing	$f'c_i = 25$ MPa

5.1.2 Substructure

5.1.2.1 Drilled shafts

28-day minimum strength	$f'c = 25$ MPa

5.1.2.2 Pier shafts and footings

28-day minimum strength	$f'c = 35$ MPa

5.1.3 Creep and shrinkage

Evaluated in accordance with the provisions of the 1978 CEB-FIP Model Code — AASHTO Seg 1989 7.5

5.2 Prestressing Steel

AASHTO M203 (ASTM A416), Uncoated Seven-Wire Stress-Relieved Strand Grade 270 low-relaxation

Tensile strength	$f_{pu} = 1860$ MPa
Yield strength	$f_{py} = 1674$ MPa
Modulus of Elasticity	E= 197,000 MPa

5.3 Reinforcement

Yield strength $f_y = 415$ MPa

Table 2.7.1A Service Load Design

Group	γ factor	D	L+I	CF	E	B	SF	W	WL	LF	PS	RS	T	DT	α_B L_B+I_B	α_B CF_B	α_B LF_B	α_B (WL_B)	% Allow.
I	1.0	1	1	1	1	1	1	0	0	0	1	1	0	0	1	1	1	0	100
II	1.0	1	0	0	1	1	1	1	0	0	1	1	0	0	0	0	0	0	125
III	1.0	1	1	1	1	1	1	β_{w1}	1	1	1	1	0	0	1	1	1	1	125
IV	1.0	1	1	1	1	1	1	β_{w2}	0	0	1	1	1	0.5	1	1	1	0.5	125
V	1.0	1	0	0	1	1	1	1	0	0	1	1	1	1	0	0	0	0	140
VI	1.0	1	1	1	1	1	1	0.3	1	1	1	1	1	0.5	1	1	1	1	140
A	1.0	1	0	0	1	1	1	0	0	0	1	1	0	1	0	0	0	0	100

AASTHO Seg 8.2.2

where

D	Dead Load
L	Highway Live Load
I	Highway Live Load Impact
E	Earth Pressure
B	Buoyancy
W	Wind Load on Structure
WL	Wind on Live Load. 100 pounds per linear ft.
LF	Longitudinal Force form Live Load
CF	Centrifugal Force
R	Rib Shortening
S	Shrinkage
T	Temperature
DT	Thermal Gradient
EQ	Earthquake
SF	Stream flow pressure
PS	Prestress
α_B	1 or 0 corresponding to presence or otherwise of Bart Train
L_B	Bart Live Load
I_B	Impact from Bart Live Load
CF_B	Centrifugal Force from Bart Train
LF_B	Longitudinal Force, Bart
WL_B	Wind on Bart Train

β_{w1} = 0.3 for highway loads only
β_{w1} = 1.0 for highway and Bart loads
β_{w2} = 0.0 for highway loads only
β_{w2} = 0.5 for highway and Bart loads

Table 2.7.1B Load Factor Design

Group	γ factor	D	(L+I)H	(L+I)P	CF	E	B	SF	W	WL	LF	PS	RS	T	DT	EQ	α_B L_B+I_B	α_B CF_B	α_B LF_B	α_B WL_B
I	1.30	β_D	1.67	0	1	β_E	1	1	0	0	0	0.77	0	0	0	0	1.67	1.67	1.67	0
I_{Pw}	1.30	β_D	1	1.15	1	β_E	1	1	0	0	0	0.77	0	0	0	0	1.67	1.67	1.67	0
I_{P3D}	1.30	β_D	1	1.25	1	β_E	1	1	0	0	0	0.77	0	0	0	0	1.67	1.67	1.67	0
II	1.30	β_D	0	0	0	β_E	1	1	1	0	0	0.77	0	0	0	0	0	0	0	0
III	1.30	β_D	1	0	1	β_E	1	1	β_{w1}	1	1	0.77	0	0	0	0	1	1	1	1
IV	1.30	β_D	1	0	1	β_E	1	1	β_{w2}	0	0	0.77	1	1	0.5	0	1	1	1	0.5
V	1.25	β_D	0	0	0	β_E	1	1	1	0	0	0.80	1	1	1	0	0	0	0	0
VI	1.25	β_D	1	0	1	β_E	1	1	0.3	1	1	0.80	1	1	0.5	0	1	1	1	0
VII	1.00	1.0	0	0	0	β_E	1	1	0	0	0	1	0	0	0	1	1	1	1	0

β_D = 0.75 when checking columns for maximum moment or maximum eccentricities and associated axial load; and when Dead Load effects are of opposite sign to the net effects of other loads in a Group.
β_D =1.00 when checking columns for maximum axial load and associated moment.
β_E = 0.5 for checking positive moments in rigid frames.
β_E = 1.00 for vertical earth pressure.
β_E = 1.30 for lateral earth pressure
β_{w1} = 0.3 for highway loads only
β_{w1} = 1.0 for Bart+highway loads only
β_{w2} = 0.0 for highway loads only
β_{w2} = 0.5 for Bart+highway loads only

D	Dead Load
L	Highway Live Load
I	Highway Live Load Impact
E	Earth Pressure
B	Buoyancy
W	Wind Load on Structure
WL	Wind on Live Load. 100 pounds per linear ft.
LF	Longitudinal Force form Live Load
CF	Centrifugal Force
R	Rib Shortening
S	Shrinkage
T	Temperature
DT	Thermal Gradient
EQ	Earthquake
SF	Stream flow pressure
PS	Prestress
α_B	1 or 0 corresponding to presence or otherwise of Bart Train
L_B	Bart Live Load
I_B	Impact from Bart Live Load
CF_B	Centrifugal Force from Bart Train
LF_B	Longitudinal Force, Bart
WL_B	Wind on Bart Train

6. SEISMIC DESIGN

Seismic design will be performed in accordance with BDS, augmented with pertinent provisions of ATC-32 and project specific criteria as detailed in this document.

6.1 Performance Criteria

The Benicia-Martinez Bridge is classified in the important bridge category. ATC-32 3.21.2
Functional Evaluation: Service Level Immediate, Minimal Damage
Safety Evaluation: Service Level Immediate, Repairable Damage
The intended structural action under seismic loading is that of a Limited-Ductility Structure with potential plastic mechanisms in pier shafts. ATC-32 3.21.3
The performance of piles shall be essentially elastic.

6.2 Seismic Loading

Five-percent-damped site-specific elastic response spectra will be provided by Caltrans for both the safety evaluation and functional evaluation earthquakes. The depth and characteristics of the soil deposits surrounding the piles shall be taken into consideration.
Three sets of time histories will also be provided by Caltrans for the inelastic dynamic analysis.

6.2.1 Seismic Loading During Construction

During normally scheduled construction, the sections of the bridge under construction at that time, shall be designed to withstand a lateral seismic force of 0.1g.
If the construction schedule is interrupted, the structure shall be stabilized against seismic loads.

6.3 Seismic Analysis

6.3.1 Elastic dynamic analysis

6.3.2 Inelastic static analysis ATC-32 3.21.6

6.3.3 Inelastic dynamic analysis ATC-32 3.21.7

ATC-32 3.21.8

6.4 Combination of Effects

Seismic effects from elastic dynamic analysis shall be combined in accordance with the BDS 3.21.1.1.
No highway live load shall be considered on the bridge during the seismic event.
The effect of vertical ground accelerations shall be considered on the superstructure only. These effects shall be based on the site specific vertical response spectrum truncated at spectral acceleration of 0.5g.
For reponse spectrum analysis the vertical effects shall not be combined with lateral effects.

6.5 Design Displacements

ATC-32 3.21.10.3

6.6 Design Forces

ATC-32 3.21.11.1

ATC-32 Fig. R3-13

The force reduction coefficient Z shall be taken as 3 for well confined concrete pier shafts when the structural period is greater than the predominant ground motion period. The force reduction factor for piles would be as follows:

Steel encased portion: 1.5
Rock Socket: 1.0

The method utilizing the Z factor will be used for preliminary design only. Final reinforcement will be designed such that strain demands from elastic or inelastic time history analyses do not exceed the allowable values of section 6.13.

6.7 Capacity Design

ATC-32 3.21.14

6.8 Restraining Features

ATC-32 3.21.12

6.9 P-Δ Effects

P-delta moments may be ignored where the following relation is satisfied:

$$W \delta_u \leq 0.25 M_p$$

where:
W = Weight of the frame
δ_u = maximum displacement of the top of the frame
M_p = plastic capacity of the pier

6.10 Strength Reduction Factors for Columns

ATC-32 8.16.1.2.2

6.11 Material Properties for Ductile Columns

6.11.1 Design flexural strength

ATC-32 8.16.2.4

6.11.2 Maximum plastic moment

ATC-32 8.16.4.4

6.11.3 Steel strain hardening strains

For A706 steel:
ε_{sh} = .0150 #8 and smaller (25M and smaller)
ε_{sh} = .0100 #10 and #11 (30M and 35M)
ε_{sh} = .0075 #14 (45M)
ε_{sh} = .0050 #18 (55M)
Assumed upper bound steel strength, considering the effects of strain hardening: $f_{uo} = 1.4\ f_{yo}$

6.12 Displacement Capacity

The displacement capacity shall be assessed from the plastic hinge length calculated according to ATC-32 8.18.2.4.2 and the plastic rotations

corresponding to the allowable material strains

6.13 Allowable Strains

6.13.1 Normal Weight Concrete

Functional evaluation $\varepsilon_c^{Func} \leq 0.004$

Safety evaluation $\varepsilon_c^{Safety} \leq {}^2/_3\, \varepsilon_{cu}$

Where ε_{cu} is the ultimate concrete strain according to the Mander model

(Mander et. al. J. Struct. Engineering, ASCE, 1988 114(8), p 1804-1849)

6.13.2 Sand Light Weight Concrete

Functional evaluation $\varepsilon_c^{Func} \leq 0.003$

Safety evaluation $\varepsilon_c^{Safety} \leq {}^2/_3\, \varepsilon_{cu}$

Where ε_{cu} is the ultimate concrete strain according to the Mander model

6.13.3 Reinforcing steel

Functional evaluation $\varepsilon_s^{Func} = 0.015$

Safety evaluation $\varepsilon_s^{Safety} = {}^2/_3\, \varepsilon_{su}$

ATC-32 C3.21.11.1

Where ε_{su} is the ultimate steel strain. For Grade 60 (A706) reinforcement ε_{su} maybe taken as:

Main reinforcing steel Bar No. 9 - 18 (30M - 55M) $\varepsilon_{su} = 0.09$

Confinement reinforcing steel Bar No. 3 - 8 (10M -25M) $\varepsilon_{su} = 0.12$

6.13.4 Pile casing

Safety evaluation $\varepsilon_s^{safety} = 0.015$

7. GEOTECHNICAL AND FOUNDATION DESIGN

See Foundation Report

8. EXPANSION JOINTS

The expansion joint assembly will be selected based on the hinge movement rating, MR. MR is defined as follows:

$$MR = 1.5x\partial C + 1.5x\,\partial S + \partial FEE$$

Where,

∂C= expected creep movement from the time of installation of expansion joint.

∂S = expected shrinkage movement from the time of installation of expansion joint.

∂FEE = sum of opening and closing movement due to a functional level earthquake.

Pile Driving Records

T·Y·LIN INTERNATIONAL

Project:	Job No.	Sheet: of
Item:	Designer:	Date:
	Checker:	Date:
		Grid: 1/10"

Attached Separately

as

Log Pile Sheets

Retrofit Project.